Synthesis and Reactivity of Anilidophosphine-Supported Lanthanide Complexes

–

Access to Rare Phosphorus-Containing Ligands in Lanthanide Coordination Chemistry

Dissertation

zur Erlangung des akademischen Grades

Doktor der Naturwissenschaften (Dr. rer. nat.)

vorgelegt von

Fabian Allan Watt

an der

Fakultät für Naturwissenschaften

der Universität Paderborn

April 2021

Promotionskommission

Die vorliegende Dissertation wurde von Dezember 2017 bis April 2021 im Institut für Anorganische und Analytische Chemie am Department Chemie der Universität Paderborn angefertigt.

Prof. Dr.-Ing. Hans-Joachim Warnecke (Universität Paderborn)	Vorsitz
Prof. Dr. Matthias Bauer (Universität Paderborn)	Erstgutachter
Priv.-Doz. Dr. Hans Egold (Universität Paderborn)	Zweitgutachter
Ass.-Prof. Dr. Stephan Hohloch (Universität Innsbruck)	Drittgutachter

Selbstständigkeitserklärung

Hiermit versichere ich, dass die vorliegende Arbeit selbstständig angefertigt wurde. Ich habe dazu keine weiteren als die angegeben Hilfsmittel benutzt und die aus anderen Quellen entnommenen Stellen als solche gekennzeichnet. Die Arbeit ist nicht in gleicher oder ähnlicher Form zuvor zur Prüfung eingereicht worden.

Osnabrück, 19.04.2021 

Fabian Allan Watt

Abstract

The scope and utility of a selected bidentate anilidophosphine (PN) ligand in lanthanide coordination chemistry is examined in this work. The obtained complexes were characterized by multinuclear NMR spectroscopy, IR spectroscopy and X-diffraction analysis.

Chapter 1 gives an overview of accessible lanthanide(III) complexes bearing either one or two PN ligand(s). The halide complexes $(PN)_2LnX$ (Ln = La, Lu; X = Cl, I) were found to be suitable precursors for the series $(PN)_2Ln(EMes)$ (E = O, S, NH, PH).

In **Chapter 2** the insertion chemistry of the La–P bond in $(PN)_2La(PHMes)$ with phenyl iso(thio)cyanate is investigated. The resulting phosphaureate could act as a bridging ligand after deprotonation at the *PH* group and coordination of selected coinage-metal carbene fragments.

Chapter 3 deals with the attempted synthesis of the first terminal lanthanum(III) phosphinidene complex by deprotonation of $(PN)_2La(PHMes)$. Strong evidence for the occurrence of a transient phosphinidene complex prior to the C–H-activation to the final product could be gathered by theoretical calculations and experimental means.

Chapter 4 describes the first stable coordination of 2-phosphaethynthiolate. The side-on η^3-coordination mode in $(PN)_2La(SCP)$ could be rationalized by experimental as well as theoretical investigations. The selective reaction with cyclic alkyl amino carbenes (CAACs) led to unprecedented fulminate-type anions.

Kurzzusammenfassung

Der Anwendungsbereich und Nutzen eines ausgewählten Anilidophosphan(PN)-Liganden in der Lanthanid-Koordinationschemie wird in dieser Arbeitet untersucht. Die erhaltenen Komplexe wurden mittels multinuklearer NMR-Spektroskopie, IR-Spektroskopie und Röntgendiffraktometrie charakterisiert.

Kapitel 1 gibt einen Überblick über die zugänglichen Lanthanid(III)-Komplexe mit einem oder zwei PN-Liganden. Die Halogenidkomplexe $(PN)_2LnX$ (Ln = La, Lu; X = Cl, I) erwiesen sich als geeignete Vorstufen für die Serie $(PN)_2Ln(EMes)$ (E = O, S, NH, PH).

In **Kapitel 2** wird die Insertionschemie der La–P-Bindung in $(PN)_2La(PHMes)$ mit Phenyliso(thio)cyanat untersucht. Das resultierende Phosphaureat konnte nach Deprotonierung an der *PH*-Gruppe und Koordination von ausgewählten Münzmetall-Carben-Fragmenten als Brückenligand fungieren.

Kapitel 3 beschäftigt sich mit der versuchten Synthese des ersten terminalen Lanthan(III)-Phosphiniden-Komplexes durch Deprotonierung von $(PN)_2La(PHMes)$. Starke Indizien für das Auftreten eines transienten Phosphiniden-Komplexes vor der C–H-Aktivierung zum Endprodukt konnten mittels theoretischer Rechnungen und Experimente gesammelt werden.

Kapitel 4 beschreibt die erste stabile Koordination von 2-Phosphaethinthiolat. Der η^3-Koordinationsmodus in $(PN)_2La(SCP)$ konnte durch experimentelle und theoretische Untersuchungen rationalisiert werden. Die selektive Reaktion mit zyklischen Alkylaminocarbenen führte zu noch nicht bekannten fulminat-artigen Anionen.

We make our world significant by the courage of our questions and by the depths of our answers.

Carl Sagan

In loving memory of Trevor Allan Watt

In liebender Erinnerung an Anna, Helmut und Joachim Frielinghaus

A man who says he knows is already dead. But the man who thinks, "I don't know", who is discovering, finding out, who is not seeking an end, not thinking in terms of arriving or becoming – such a man is living, and that living is truth.

Jiddu Krishnamurti

Danksagung

Jede persönliche, wahrhaftig wertvolle Reise in das Ungewisse – auch die wissenschaftliche – braucht Mitmenschen, die einem auf dem Weg begegnen oder einen begleiten. Ob von langer oder kurzer Dauer, jedes Stück Weg, welches ich mit den Menschen, bei denen ich mich im Folgenden bedanken möchte, gegangen bin, hat mich auf verschiedene Weise inspiriert oder positiv beeinflusst, mir eine neue Richtung, Rückhalt oder Kraft gegeben und somit diese Arbeit möglich gemacht.

Dass ich Ende 2017 mit der Promotion in Paderborn beginnen konnte, verdanke ich Herrn Prof. Dr. Stephan Hohloch. Danke, dass Du diesen Weg mit mir gegangen bist, vor allem im ersten Promotionsjahr viel Geduld mit mir und der Themenfindung hattest, und mir stets die Freiheit gegeben hast, eigene Ideen auszuprobieren. Ebenso bin ich Dir für die fachliche Betreuung und die vielen Kristallmessungen sehr dankbar. Ich freue mich sehr, dass aus unserer gemeinsamen Zeit viele schöne Ergebnisse hevorgegangen sind und dass ich meine Promotion in Paderborn mit dem chemisch sehr interessanten Thema zwischen Lanthanid- und schwerer Hauptgruppenelement-Chemie abschließen kann.

Herrn Prof. Dr. Matthias Bauer möchte ich herzlich dafür danken, dass er mir bis zum Ende der Laborzeit einen Arbeitsplatz und alle wichtigen Mittel zum Abschließen der Experimente bereitgestellt hat. Vielen Dank ebenfalls für die Begutachtung meiner Arbeit. Deine Unterstützung sowie die Deiner gesamten Arbeitsgruppe haben mich vor allem in den letzten Monaten der Promotion getragen. Meinen täglichen Laborkolleginnen und –kollegen Tanja Hirschhausen, Pia Rehsies, Anabel Miletic, Marina Huber-Gedert, Yannik Vukadinovic, Steffen Schlicher, Philipp Dierks, Jakob Steube und Lennart Schmitz spreche ich hierbei meinen besonderen Dank aus. Ebenso den regelmäßigen ”Laborgästen-auf-Durchreise-zur-Kaffeepause-und-zurück-ins-Büro“ Lorena Fritsch, Anke Schoch, Patrick Müller, Michal Nowakowski und Sven Wendholt – ihr habt meinem Arbeitsplatz fast jeden Tag frischen Wind und Leben eingehaucht, vielen Dank dafür.

Die letzten eineinhalb Jahre der Laborzeit konnte ich mich sehr glücklich schätzen, Athul Krishna als Laborkollegen zu haben. Danke Athul für deinen positiven Charakter und dein Durchhaltevermögen, die vielen persönlichen Gespräche und die Möglichkeiten, gemeinsam mit dir über mich selber, uns, unsere Chemie oder die Welt zu lachen. Ich bin sehr froh, dich einen guten Freund nennen zu dürfen.

Zwei weitere Mitarbeiter des AK Bauer möchte ich ebenfalls einzeln erwähnen: Roland Schoch danke ich für die geduldige Bearbeitung meiner vielen Anfragen für Kristallmessungen. Ohne deine Ausdauer und Unnachgiebigkeit hätten wir die für meine letzten zwei Publikationen wichtigen Molekülstrukturen sicher nicht mehr rechtzeitig aufklären können. Lukas Burkhardt möchte ich für die Rechnungen zu

$(PN)_2La(SCP)$ danken. Die Zeit und Mühe, die du dir damit gemacht hast, haben meine Ideen zur Folgechemie dieses Komplexes inspiriert und somit letztlich dessen Publikation ermöglicht.

Ich bin vielen anderen Kollegen und Kolleginnen des Chemieinstituts der Universität Paderborn zu Dank verpflichtet – ich habe mich von Anfang an willkommen gefühlt und habe die familiäre Atmosphäre eines überschaubaren Instituts schnell sehr zu schätzen gelernt. Im Besonderen gilt mein Dank Dr. Hans Egold, der mir mit seinem großen Lächeln, seinem Enthusiasmus für die NMR-Abteilung, und seiner Bodenständigkeit sofort eine positive Stimmung und ein heimatliches Gefühl gegeben hat. Du hattest immer ein offenes Ohr für mich und meine Fragen und konntest sozusagen meine gesamte Promotion mitverfolgen – ich freue mich sehr, Dich nun als Gutachter dieser Arbeit zu haben. Ein ganz großes Dankeschön geht ebenso an Christiane Gloger, Maria Busse, Karin Stolte und Andrea Harbarth für die kompetente Lösung von Laborproblemen, die super Absprachen bei Elementaranalysen, die vielen (teils kurzfristigen) NMR-Messungen und natürlich all die netten und schönen Gespräche. Herrn Dr. Adam Neuba danke ich für die Messung von Cyclovoltammogrammen. Aus dem AK Paradies möchte ich besonders Benedikt Sieland, Garrit Wicker, Peng Hou, Arne Stepen, Nikolai Sitte und Alexander Maier für den positiven, kollegialen Umgang und die diversen, kleineren Hilfestellungen danken. Herrn Prof. Dr.-Ing. Hans-Joachim Warnecke sei für den Vorsitz der Promotionskomission gedankt.

Ich hatte Glück, auf meinem Weg auch Waldemar Keil aus dem AK Schmidt getroffen zu haben. Dass sich selbst unter den Anstrengungen einer Promotion so schnell eine gute Freundschaft entwickeln konnte, hat mir neue Kraft und einen mehr positiven Blick auf die Dinge gegeben. Ob beim Wandern oder reinem Gedankenaustausch – mit dir konnte ich viele Momente der Heiterkeit erleben. Meinen Bachelor- und Masterstudenten Nicole Dickmann, Maximilian Henning, Jan Locher, Grigoriy Golovanov, Stephan Berg, Philipp Boos und Shenyu Liu danke ich für die angenehme Zeit und Hilfe im Labor sowie für die erfolgreichen Forschungs- bzw. Abschlussarbeiten. Marc Baltrun bin ich besonders für die gemeinsame Zeit und unsere Gespräche am Anfang der Promotion dankbar. Beides hat mir geholfen, zu reflektieren und den Blick für das Gegenwärtige nicht zu verlieren.

Peter Kluth, Florenz Buß, Kai Fischer, Maximilian Wels, Maurice Schrick und Frederik Hinkelmann danke ich für die wertvollen Dinge, die gute Freundschaften ausmachen. Ihr wart stets eine große Stütze. Jessica Fleming danke ich für all das Glück und die Liebe, die in mein Leben gekommen ist. Für deine ganze Unterstüzung, Geduld und Zuversicht bin ich dir mehr dankbar als es einfache Worte ausdrücken können. Ich freue mich, dich an meiner Seite zu haben und zusammen mit dir neue Lebensschritte wagen zu können. Danke auch an die Familien Fleming und Otto, die mich herzlich aufgenommen haben.

Mein größter Dank geht an meine Eltern Birgit & Paul Allan Watt und meine Geschwister Elena und Nadine. Ihr habt immer an mich geglaubt, egal welche Herausforderungen es zu bewältigen gab. Durch eure Unterstützung konnte ich die Welt entdecken und meine Träume erfüllen. Danke, dass ihr da seid. Ich liebe euch von ganzem Herzen.

List of Publications

1. Watt, F. A.; Burkhardt, L.; Schoch, R.; Mitzinger, S.; Bauer, M.; Weigend, F.; Goicoechea, J. M.; Tambornino, F.; Hohloch, S. η^3-Coordination and Functionalization of the 2-Phosphaethynthiolate Anion at Lanthanum(III), *Angew. Chem. Int. Ed.* **2021**, *60*, 9534–9539. https://doi.org/10.1002/anie.202100559

2. Watt, F. A.; McCabe, K. N.; Schoch, R.; Maron, L.; Hohloch, S. A transient lanthanum phosphinidene complex, *Chem. Commun*. **2020**, *56*, 15410–15413. https://doi.org/10.1039/D0CC06670B

3. Watt, F. A.; Dickmann, N.; Schoch, R.; Hohloch, S. Isocyanate Insertion into a La–P Phosphide Bond: A Versatile Route to Phosphaureate-Bridged Heterobimetallic Lanthanide–Coinage-Metal Complexes, *Inorg. Chem.* **2020**, *59*, 13621–13631. https://doi.org/10.1021/acs.inorgchem.0c01971

4. Watt, F. A.; Krishna, A.; Golovanov, G.; Ott, H.; Schoch, R.; Wölper, C.; Neuba, A. G., Hohloch, S. Monoanionic Anilidoposphine Ligand in Lanthanide Chemistry: Scope, Reactivity, and Electrochemistry, *Inorg. Chem.* **2020**, *59*, 2719–2732. https://doi.org/10.1021/acs.inorgchem.9b03071

5. Pinter, P.; Schüßlbauer, C. M.; Watt, F. A.; Dickmann, N.; Herbst-Irmer, R.; Morgenstern, B.; Gründwald, A.; Ullrich, T.; Zimmer, M.; Hohloch, S.; Guldi, D. M.; Munz, D. Bright Luminescent Lithium and Magnesium Carbene Complexes, *Chem. Sci.* **2021**, *accepted.* https://doi.org/10.1039/D1SC00846C

6. Locher, J.; Watt, F. A.; Neuba, A. G.; Schoch, R.; Munz, D.; Hohloch, S. Molybdenum(VI) bis-imido Complexes of Dipyrromethene Ligands, *Inorg. Chem.* **2020**, *59*, 9847–9856. https://doi.org/10.1021/acs.inorgchem.0c01051

7. Boreen, M. A.; McCabe, K. N.; Lohrey, T. D.; Watt. F. A.; Maron, L.; Hohloch, S.; Arnold, J. Uranium Metallocene Azides, Isocyanates, and Their Borane-Capped Lewis Adducts, *Inorg. Chem.* **2020**, *59*, 8580–8588. https://doi.org/10.1021/acs.inorgchem.0c01038

8. Boreen, M. A.; Rao, G.; Villareal, D. G.; Watt, F. A.; Britt, R. D.; Hohloch, S.; Arnold, J. Lewis acid capping of a uranium(V) nitride *via* a uranium(III) azide molecular square, *Chem. Commun*. **2020**, *56*, 4535–4538. https://doi.org/10.1039/D0CC01356K

9. Boreen, M. A.; Lussier, D. J.; Skeel, B. A.; Lohrey, T. D.; Watt, F. A.; Shuh, D. K.; Long, J. R.; Hohloch, S.; Arnold, J. Structural, Electrochemical, and Magnetic Studies of Bulky Uranium(III) and Uranium(IV) Metallocenes, *Inorg. Chem.* **2019**, *58*, 16629–16641. https://doi.org/10.1021/acs.inorgchem.9b02719

10. Baltrun, M.; Watt, F. A.; Schoch, R.; Hohloch, S. Dioxo-, Oxo-imido-, and Bis-imido-Molybdenum(VI) Complexes with a Bis-phenolate-NHC Ligand, *Organometallics* **2019**, *38*, 3719–3729. https://doi.org/10.1021/acs.organomet.9b00472

11. Baltrun, M.; Watt, F. A.; Schoch, R.; Wölper, C.; Neuba, A. G.; Hohloch, S. A new bis-phenolate mesoionic ligand for early transition metal chemistry, *Dalton Trans.* **2019**, *48*, 14611–14625. https://doi.org/10.1039/C9DT03099A

List of Oral Presentations

1. Watt, F. A.; Hohloch, S. Synthese & Reaktivität von Anilidophosphan-Komplexen der Lanthanide; Inorganic Chemistry Seminar (online), Institute of General, Inorganic and Theoretical Chemistry, University of Innsbruck, AT, March 3, 2021.

2. Watt, F. A.; Hohloch, S. Synthesis and Reactivity of Anilidophosphine Supported Lanthanide Complexes; 16. Koordinationschemie-Treffen (KCT), University of Freiburg, GER, March 2, 2020.

List of Poster Presentations

1. Dickmann, N.; Watt, F. A.; Hohloch, S. Synthese und Charakterisierung von heterobimetallischen Lanthan-Münzmetall-Komplexen; Poster Session of JungChemikerForum Paderborn, Paderborn University, GER, February 26, 2020.

2. Watt, F. A.; Hohloch, S. Synthese und Funktionalisierung von Lanthankomplexen mit PN-Liganden; GDCh Wissenschaftsforum 2019, Aachen, GER, September 16, 2019.

Kooperationen und Hilfsmittel

Die vorliegende Arbeit wurde teilweise in Kooperation mit den Universitäten Innsbruck (Ass.-Prof. Dr. S. Hohloch), Oxford (Prof. Dr. J. M. Goicoechea), Toulouse (Prof. Dr. L. Maron) und Marburg (Prof. Dr. F. Weigend und Dr. F. Tambornino) angefertigt (siehe Deckblätter zu den Publikationen von Kapitel 1–4). Zusätzliche, externe kristallographische Messungen fanden an der Universität Essen-Duisburg (Dr. C. Wölper) und am Standort Karlsruhe der Firma Bruker AXS GmbH (Dr. H. Ott) statt (siehe Kapitel 1). Die Art der Beiträge der Co-Autoren sind in den jeweiligen Kapiteln vermerkt.

Folgende Hilfsmittel wurden für die Erstellung der vorliegenden Arbeit verwendet: Die Arbeit wurde mit Hilfe der Software Microsoft Word 2013 © 2012 Microsoft Corporation verfasst. Die Auswertung der NMR-Spektren wurde mit der Software MestReNova (Version 11.0.4-18998) © 2017 Mestrelab Research S.L. durchgeführt. Die chemischen Strukturen wurden mit der Software ChemDraw Professional (Version 19.0.1.28) © 1998–2019 PerkinElmer Informatics Inc. gezeichnet. Die Molekülstrukturen wurden mit Hilfe der Software Olex2 (Version 1.3.0) © 2004–2021 OlexSys Ltd. als "Oak Ridge Thermal Ellipsoid Plots" (ORTEPs) dargestellt. Für die Erstellung einzelner Grafiken bzw. Diagramme wurden die Software Microsoft PowerPoint 2013 & Microsoft Excel 2013 © 2012 Microsoft Corporation verwendet. Die Literaturverzeichnisse wurden mit Hilfe der Software Citavi (Version 6.4.0.35) © 2020 Swiss Academic Software GmbH erstellt.

Table of Contents

Preface & Aim

The coordination chemistry of the f-block metals has advanced to a very important field of research in modern inorganic chemistry.[1] Especially the lanthanides (Ln), which constitute the 4f row of the periodic table and comprise the fifteen elements from lanthanum (element 57) to lutetium (element 71), have gained increasing attention because of their prominent magnetic and luminescent properties.[2,3] These elements already appear in many technological applications as magnetic components in modern electronic devices and large scale energy production[4] as well as magnetic or luminescent probes for biomedical analyses.[5,6] Because of the high Lewis acidity of the Ln^{3+} ions,[7] their coordination complexes can also show a high performance as catalysts in various polymerization and hydrofunctionalization reactions.[8–10] During the last two decades a lot of effort has been expended on the extraction and separation of the similarly sized lanthanide(III) ions – ionic radii between ≈1.16 Å (La^{3+}) and ≈0.98 Å (Lu^{3+}) – with the aim to increase the availability of lanthanide(III) precursors and improve the sustainability of their production.[11–15]

Apart from the distinguished magnetic and photophysical properties of lanthanide ions, which have led to groundbreaking achievements in single molecule magnet research[16–19] as well as a variety of photophysical applications,[20–22] another impetus for the development of new lanthanide complexes is given by the large size and high Lewis acidity of lanthanide ions which can enable (catalytic) reactions complementing those of transition-metal- and organo-catalysis.[23–25]

However, the development of novel coordination compounds of the lanthanides is also driven by the desire to broaden our fundamental understanding of such systems and their scope of chemical reactivity.[26] Especially complexes featuring heavy main group elements bound to lanthanides are much sought-after target compounds for accessing rare structural motifs and evaluating their reactivity as well as the chemical bonding between lanthanide and heavy main group element.[27–33]

In this context, the development of the chemistry of lanthanide complexes with supporting ligands other than the widely used (substituted) cyclopentadienide[17] or oxygen- and nitrogen-based ligand systems[34–37] is crucial. Ideally, an alternative supporting ligand should be able to (i) tailor the accessibility of the lanthanide ions in order to obtain low coordination numbers (of four or five) for a higher reactivity of the complexes, (ii) thereby influence the reactivity of a bound heavy main group element fragment which is to be functionalized, and (iii) stabilize unusual structures or binding modes of rare or novel types of coordinated heavy main group element fragments.

The combination of nitrogen and phosphorus donor atoms in the supporting ligands is still relatively rare in lanthanide coordination chemistry and thus leaves great room for exploration and discovery. This work therefore aims at the introduction and establishment of a selected monoanionic, bidentate anilidophosphine ligand, namely *N*-(2-diisopropylphosphanyl-4-methylphenyl)-2,4,6-trimethylanilide, in a series of lanthanide(III) complexes. Along the line of the three points listed above the investigation

of the utility of the new anilidophosphine-supported lanthanide(III) complexes – in particular those with lanthanum(III) – for the isolation of rare or hitherto unknown structural motifs containing the heavy main group elements phosphorus and sulfur presents another important objective of this work.

References

(1) Liddle, S. T. International Year of the Periodic Table: Lanthanide and Actinide Chemistry. *Angew. Chem. Int. Ed.* **2019**, *58*, 5140–5141.
(2) Cotton, S. *Lanthanide and Actinide Chemistry*; John Wiley & Sons, Ltd.: Chichester, UK, 2006.
(3) Martinez-Gomez, N. C.; Vu, H. N.; Skovran, E. Lanthanide Chemistry: From Coordination in Chemical Complexes Shaping Our Technology to Coordination in Enzymes Shaping Bacterial Metabolism. *Inorg. Chem.* **2016**, *55*, 10083–10089.
(4) Tesfaye, F.; Peng, H.; Zhang, M. Advances in the Circular Economy of Lanthanides. *JOM* **2021**, *73*, 16–18.
(5) Bünzli, J.-C. G. Lanthanide Luminescence for Biomedical Analyses and Imaging. *Chem. Rev.* **2010**, *110*, 2729–2755.
(6) Debroye, E.; Parac-Vogt, T. N. Towards polymetallic lanthanide complexes as dual contrast agents for magnetic resonance and optical imaging. *Chem. Soc. Rev.* **2014**, *43*, 8178–8192.
(7) Kobayashi, S.; Sugiura, M.; Kitagawa, H.; Lam, W. W.-L. Rare-Earth Metal Triflates in Organic Synthesis. *Chem. Rev.* **2002**, *102*, 2227–2302.
(8) Dicken, R. D.; Motta, A.; Marks, T. J. Homoleptic Lanthanide Amide Catalysts for Organic Synthesis: Experiment and Theory. *ACS Catal.* **2021**, *11*, 2715–2734.
(9) Trifonov, A. A.; Basalov, I. V.; Kissel, A. A. Use of organolanthanides in the catalytic intermolecular hydrophosphination and hydroamination of multiple C–C bonds. *Dalton Trans.* **2016**, *45*, 19172–19193.
(10) Weiss, C. J.; Marks, T. J. Organo-f-element catalysts for efficient and highly selective hydroalkoxylation and hydrothiolation. *Dalton Trans.* **2010**, *39*, 6576–6588.
(11) Werner, E. J.; Biros, S. M. Supramolecular ligands for the extraction of lanthanide and actinide ions. *Org. Chem. Front.* **2019**, *6*, 2067–2094.
(12) Cotruvo, J. A. The Chemistry of Lanthanides in Biology: Recent Discoveries, Emerging Principles, and Technological Applications. *ACS Cent. Sci.* **2019**, *5*, 1496–1506.
(13) Higgins, R. F.; Cheisson, T.; Cole, B. E.; Manor, B. C.; Carroll, P. J.; Schelter, E. J. Magnetic Field Directed Rare-Earth Separations. *Angew. Chem. Int. Ed.* **2020**, *59*, 1851–1856.
(14) Nelson, J. J. M.; Cheisson, T.; Rugh, H. J.; Gau, M. R.; Carroll, P. J.; Schelter, E. J. High-throughput screening for discovery of benchtop separations systems for selected rare earth elements. *Commun. Chem.* **2020**, *3*, 7.
(15) Judge, W. D.; Azimi, G. Recent progress in impurity removal during rare earth element processing: A review. *Hydrometallurgy* **2020**, *196*, 105435.
(16) Goodwin, C. A. P.; Ortu, F.; Reta, D.; Chilton, N. F.; Mills, D. P. Molecular magnetic hysteresis at 60 kelvin in dysprosocenium. *Nature* **2017**, *548*, 439–442.
(17) Day, B. M.; Guo, F.-S.; Layfield, R. A. Cyclopentadienyl Ligands in Lanthanide Single-Molecule Magnets: One Ring To Rule Them All? *Acc. Chem. Res.* **2018**, *51*, 1880–1889.
(18) Guo, F.-S.; Day, B. M.; Chen, Y.-C.; Tong, M.-L.; Mansikkamäki, A.; Layfield, R. A. Magnetic hysteresis up to 80 kelvin in a dysprosium metallocene single-molecule magnet. *Science* **2018**, *362*, 1400–1403.
(19) Gould, C. A.; Darago, L. E.; Gonzalez, M. I.; Demir, S.; Long, J. R. A Trinuclear Radical-Bridged Lanthanide Single-Molecule Magnet. *Angew. Chem. Int. Ed.* **2017**, *56*, 10103–10107.
(20) Kotova, O.; Bradberry, S. J.; Savyasachi, A. J.; Gunnlaugsson, T. Recent advances in the development of luminescent lanthanide-based supramolecular polymers and soft materials. *Dalton Trans.* **2018**, *47*, 16377–16387.
(21) Bodman, S. E.; Butler, S. J. Advances in anion binding and sensing using luminescent lanthanide complexes. *Chem. Sci.* **2021**, *12*, 2716–2734.
(22) Bünzli, J.-C. G. On the design of highly luminescent lanthanide complexes. *Coord. Chem. Rev.* **2015**, *293-294*, 19–47.

(23) Dochain, S.; Vetica, F.; Puttreddy, R.; Rissanen, K.; Enders, D. Combining Organocatalysis and Lanthanide Catalysis: A Sequential One-Pot Quadruple Reaction Sequence/Hetero-Diels-Alder Asymmetric Synthesis of Functionalized Tricycles. *Angew. Chem. Int. Ed.* **2016**, *55*, 16153–16155.
(24) Kluger, R.; Cameron, L. L. Activation of Acyl Phosphate Monoesters by Lanthanide Ions: Enhanced Reactivity of Benzoyl Methyl Phosphate. *J. Am. Chem. Soc.* **2002**, *124*, 3303–3308.
(25) Yajima, H.; Sumaoka, J.; Miyama, S.; Komiyama, M. Lanthanide ions for the first non-enzymatic formation of adenosine 3',5'-cyclic monophosphate from adenosine triphosphate under physiological conditions. *J. Biochem.* **1994**, *115*, 1038–1039.
(26) Bart, S. C.; Schelter, E. J. The Vibrancy and Variety of Modern f-Element Organometallic Chemistry. *Organometallics* **2017**, *36*, 4507–4510.
(27) Ma, Y.-Z.; Bestgen, S.; Gamer, M. T.; Konchenko, S. N.; Roesky, P. W. Polysulfide Coordination Clusters of the Lanthanides. *Angew. Chem. Int. Ed.* **2017**, *56*, 13249–13252.
(28) Schoo, C.; Bestgen, S.; Egeberg, A.; Klementyeva, S.; Feldmann, C.; Konchenko, S. N.; Roesky, P. W. Samarium Polystibides Derived from Highly Activated Nanoscale Antimony. *Angew. Chem. Int. Ed.* **2018**, *57*, 5912–5916.
(29) Schoo, C.; Bestgen, S.; Egeberg, A.; Seibert, J.; Konchenko, S. N.; Feldmann, C.; Roesky, P. W. Samarium Polyarsenides Derived from Nanoscale Arsenic. *Angew. Chem. Int. Ed.* **2019**, *58*, 4386–4389.
(30) Reinfandt, N.; Schoo, C.; Dütsch, L.; Köppe, R.; Konchenko, S. N.; Scheer, M.; Roesky, P. W. Synthesis of Unprecedented 4d/4f-Polypnictogens. *Chem. Eur. J.* **2021**, *27*, 3974–3978.
(31) Goodwin, C. A. P.; Réant, B. L. L.; Vettese, G. F.; Kragskow, J. G. C.; Giansiracusa, M. J.; DiMucci, I. M.; Lancaster, K. M.; Mills, D. P.; Sproules, S. Heteroleptic Samarium(III) Chalcogenide Complexes: Opportunities for Giant Exchange Coupling in Bridging σ- and π-Radical Lanthanide Dichalcogenides. *Inorg. Chem.* **2020**, *59*, 7571–7583.
(32) Mills, D. P.; Evans, P. f-Block Phospholyl and Arsolyl Chemistry. *Chem. Eur. J.* **2021**, *27*, in print. DOI: 10.1002/chem.202005231.
(33) Réant, B. L. L.; Liddle, S. T.; Mills, D. P. f-Element silicon and heavy tetrel chemistry. *Chem. Sci.* **2020**, *11*, 10871–10886.
(34) Kazeminejad, N.; Munzel, D.; Gamer, M. T.; Roesky, P. W. Bis(amidinate) ligands in early lanthanide chemistry - synthesis, structures, and hydroamination catalysis. *Chem. Commun.* **2017**, *53*, 1060–1063.
(35) Adams, F.; Machat, M. R.; Altenbuchner, P. T.; Ehrmaier, J.; Pöthig, A.; Karsili, T. N. V.; Rieger, B. Toolbox of Nonmetallocene Lanthanides: Multifunctional Catalysts in Group-Transfer Polymerization. *Inorg. Chem.* **2017**, *56*, 9754–9764.
(36) Zhou, Y.-X.; Zhao, J.; Peng, L.; Wang, Y.-L.; Tao, X.; Shen, Y.-Z. Heteroleptic lanthanide amide complexes bearing carbon-bridged bis(phenolate) ligands: synthesis, structure and their application in the polymerization of ε-caprolactone. *RSC Adv.* **2016**, *6*, 22269–22276.
(37) Edelmann, F. T. Lanthanide amidinates and guanidinates in catalysis and materials science: a continuing success story. *Chem. Soc. Rev.* **2012**, *41*, 7657–7672.

Chapter 1:

Monoanionic Anilidophosphine Ligand in Lanthanide Chemistry: Scope, Reactivity and Electrochemistry

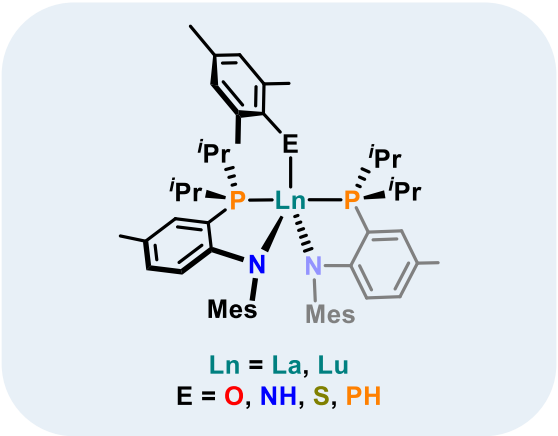

1.1 Introduction: Chelating Ligands with P and N Donor Atoms

Modern coordination chemistry strongly relies on the well conducted design and choice of supporting ligand systems for the isolation of metal complexes with unique coordination motifs, the ability to participate in useful (catalytic) chemical transformations or the possibility of constructing sophisticated systems with other functional (*e.g.*, physical) properties.[1–6]

In this context the vast collection of nitrogen based ligand systems, especially those derived from aniline or *N*-heterocycles such as, *e.g.*, pyridine, pyrrole or carbazole, is predestined to be utilized for the synthesis of phosphanyl-functionalized chelating ligands with P and N donor atoms in varying combinations, many of which have already been employed extensively in the fields of transition metal and main group element chemistry.[2,3,5,7–20]

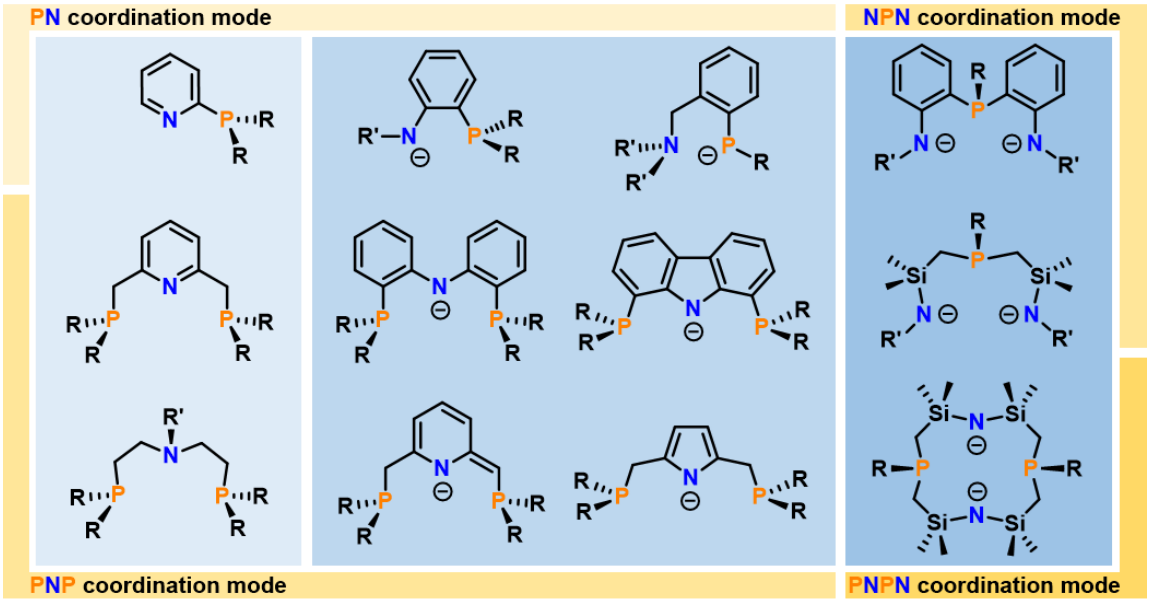

Figure 1.1. Selection of literature reported neutral[3,21–23] (left), monoanionic[4,7,24–34] (middle) and dianionic[35,36] (right) ligand scaffolds with P and N donor atoms (R, R' = alkyl, aryl). The potentially coordinating atoms of the bidentate ligands (upper left), the pincer-type tridentate ligands (upper right and lower left) as well as the macrocyclic tetradentate ligand (lower right) are indicated at the edges, respectively. Note that in some cases additional alkyl substituents on the aryl backbone have been omitted for clarity.

A selection of different ligand scaffolds with P and N donor atoms is shown in Figure 1.1. The selected examples can be classified according to their charge as neutral[3,21–23] (left), monoanionic[4,7,24–34] (middle) and dianionic[35,36] (right) ligand scaffolds. Furthermore, they can be subdivided by the number and spatial arrangement of potentially coordinating P and N atoms into ligand classes with bidentate "PN"[7,21,24–27,34] (upper left), tridentate pincer-type "NPN"[29] (upper right) or "PNP"[3,4,7,20,28,30–33] (lower left) and tetradentate "PNPN"[35,36] (lower right) coordination mode. The straight-forward access to such a large library of these ligands is of great advantage to the organometallic chemist, since the number of anionic (in most cases N) donor atoms, the number and steric profile of the coordinating side arms (*e.g.*, the

phosphanyl groups)[21] as well as the overall geometry and rigidity of the ligand scaffold can be changed according to the size of the metal ion and the synthetic task at hand.[2] Moreover, the phosphanyl groups may be exchanged for other phosphorus(III) containing donors such as more π-accepting phosphinine moieties, which are sterically and electronically quite distinct from the former.[37] Another important factor for the continuing interest in this class of chelating ligands, particularly in the anionic form, is the combination of a "hard" anionic π-base (amido) with a "softer" neutral σ-donor (phosphanyl),[38] for both of which the electronic properties can be tailored to obtain a stronger, weaker or, in the case of phosphanyl, labile binding to the metal ion.[39]

1.1.1 Lanthanide Complexes Featuring Chelating Ligands with P and N Donor Atoms

To date, a comparably small number of chelating ligands with P and N donor atoms have been employed in lanthanide chemistry, even though these ligands have already met with considerable success in the preparation of reactive (terminal or metal-capped) alkylidene, imido, nitride, phosphinidene or oxo complexes of the related rare earth metal scandium,[31,32,40] the early transition metals titanium, zirconium, hafnium and niobium[33,41–49] as well as the actinide uranium.[50]

Fryzuk and co-workers were the first to study lanthanide complexes featuring chelating ligands with P and N donor atoms.[51–55] In 1991, they introduced the PNP ligand framework $[(Me_2PCH_2SiMe_2)_2N]^-$ (with R = Me, ^{i}Pr or Ph) in complexes of the general formula $[\{(Me_2PCH_2SiMe_2)_2N\}_2LnCl]$ (Ln = La or Lu, Scheme 1.1) *via* salt metatheses between the respective lanthanide(III) trichloride and alkali metal salts of the PNP ligand in THF (i).[52]

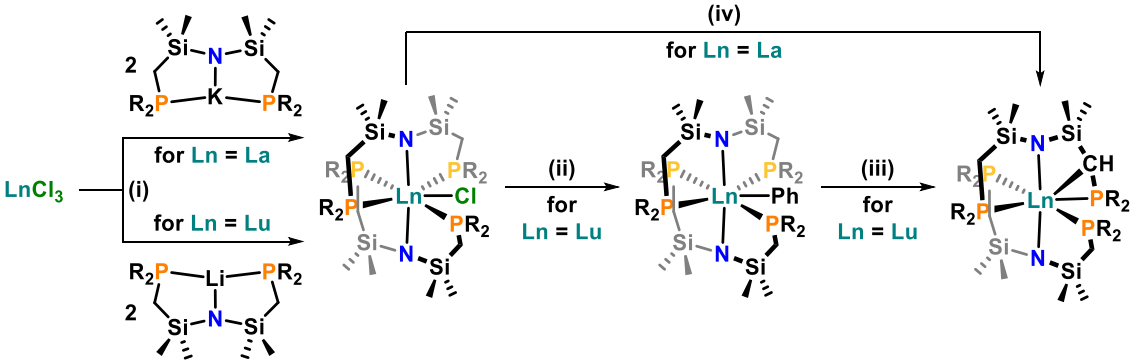

Scheme 1.1. First reported syntheses of lanthanide(III) complexes featuring a chelating ligand with P and N donor atoms by Fryzuk and co-workers (only the selection with R = Me is shown).[52] For the chloride and phenyl complexes only the respective *mer*,*mer* isomers are shown for simplicity. Conditions: (i) THF, rt, 7 d (for Ln = La) or 12 h (for Ln = Lu), – 2 KCl (for Ln = La) or – 2 LiCl (for Ln = Lu); (ii) PhLi (1 equiv), Et_2O, rt, 20 min, – LiCl; (iii) toluene, reflux, – C_6H_6; (iv) $LiCH_2Si(CH_3)_3$ (1 equiv), *n*-hexane, rt, 2 h, – LiCl, – $Si(CH_3)_4$.

Notably, in case of lanthanum(III) the use of the ligand's potassium salt was required, whereas for lutetium(III) the lithium amide had to be used in order to obtain high yields, showing the subtle

differences in reactivity which can occur for early and late lanthanides. The remaining chloride ligand allowed a second metathesis step which resulted in the lutetium(III) phenyl complex [{$(Me_2PCH_2SiMe_2)_2N$}$_2$Lu(Ph)] (ii). The authors inferred a high flexibility of the PNP ligands from the equilibrium between the *fac*,*fac*, the *mer*,*mer* and the *fac*,*mer* isomers of the [{$(Me_2PCH_2SiMe_2)_2N$}$_2$LnX] (X = Cl, Ph) complexes in solution. As a result of this flexibility, the lutetium(III) phenyl complex was thermally unstable and found to undergo a C–H-activation at the methylene unit of the ligand backbone with concomitant elimination of benzene (iii). In case of the larger lanthanum(III) ion the same deprotonation of the ligand backbone took place already at room temperature and no intermediate phenyl complex could be isolated, presumably due to the larger ionic radius of lanthanum(III) and the resulting better ability of the supporting ligand framework to reach the anionic phenyl ligand. However, satisfying yields for the cyclometalated lanthanum(III) complex could only be obtained by switching from phenyl lithium to lithium trimethylsilylmethanide as base (iv).

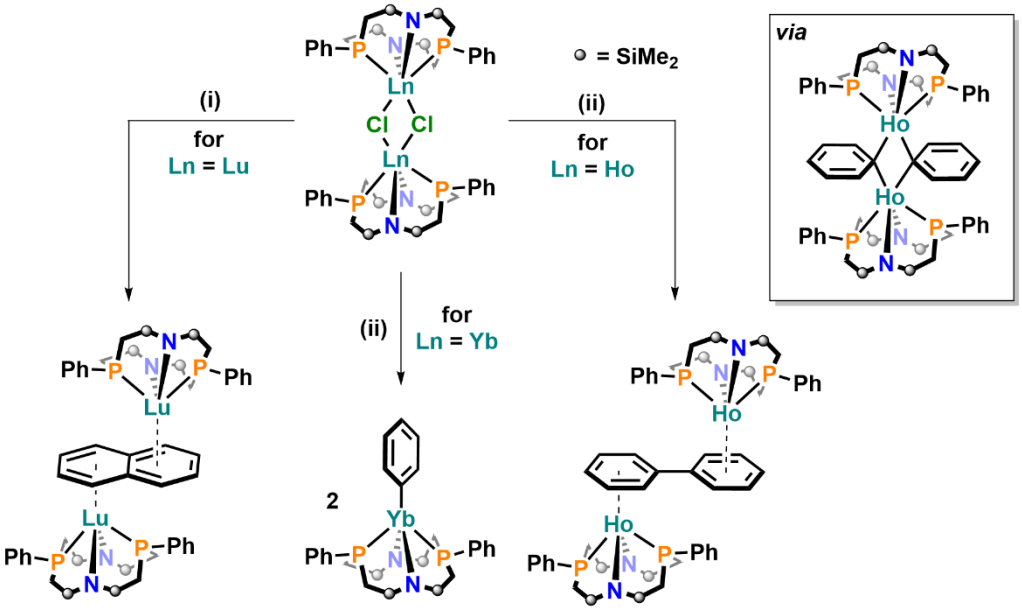

Scheme 1.2. Reactivity of PNPN supported lanthanide(III) chloride complexes by Fryzuk *et al.* towards polycyclic arenes under strongly reducing conditions (left) or aryllithiums (middle and right).[53,55] Conditions: (i) naphthalene (1.5 equiv), KC_8 (2.2 equiv), toluene/diethyl ether (3:1), rt, 4 d, – 2 KCl, – 16 C (graphite), – excess 0.5 naphthalene, – excess 0.2 KC_8; (ii) PhLi (4.4-4.5 equiv), toluene, –78 °C → rt, 18 h, – 2 LiCl.

In the early 2000s, the group of Fryzuk made extensive use of the dianionic, tetradentate PNPN ligand framework $[PhP(CH_2SiMe_2NSiMe_2CH_2)_2PPh]^{2-}$ in lanthanide coordination chemistry and reported that this macrocylic ligand is able to support interesting, strongly colored dinuclear complexes containing dianionic arene bridging ligands.[53,55] The dinuclear systems were accessed either by reduction of suitable polycyclic arenes (*e.g.*, naphthalene) with 2.2 equiv of potassium graphite (KC_8) in the presence of halide precursor complexes such as [{$(PNPN)_2Lu$}$_2$(μ-Cl)$_2$] (Scheme 1.2, left),[55] or by a C–C coupling between two monoanionic arene ligands in the coordination spheres of two lanthanide(III) ions to give, *e.g.*, biphenyldiide complexes of the type [{$(PNPN)_2Ho$}$_2${μ-η^6:$\eta^{6'}$-$(C_6H_5)_2$}] (Scheme 1.2, right).[53]

Significantly, this C–C bond formation process requires no change in the oxidation state of the metal ions. However, it seems to be quite sensitive to changes in the ionic radius of the lanthanide, since the reaction was observed for holmium(III) (1.04 Å), but not for ytterbium(III) (1.01 Å) or lutetium(III) (1.00 Å).[56] Only the monomeric phenyl complex could be identified for ytterbium(III) (Scheme 1.2, middle) or assumed in the case of lutetium(III). Based on these results the authors proposed a mechanism involving a phenyl bridged dimer prior to C–C coupling which should not be favored for the smaller lanthanide(III) ions (see inset in Scheme 1.2, right). In this context it is noteworthy that the biphenyldiide complex of lutetium(III) could still be isolated by applying the reduction route with KC_8.[53]

During the late 1990s and 2000s also other types of chelating ligands with P and N donor atoms appeared in lanthanide coordination chemistry. For instance, Roesky and colleagues described the synthesis of a series of heteroleptic and homoleptic lanthanide complexes featuring between one and three of bis(diphenylphosphanyl)amido[57–61] ligands or bearing four of sterically less encumbering (diphenylphosphanyl)phenylamido[62] ligands (Figure 1.2).

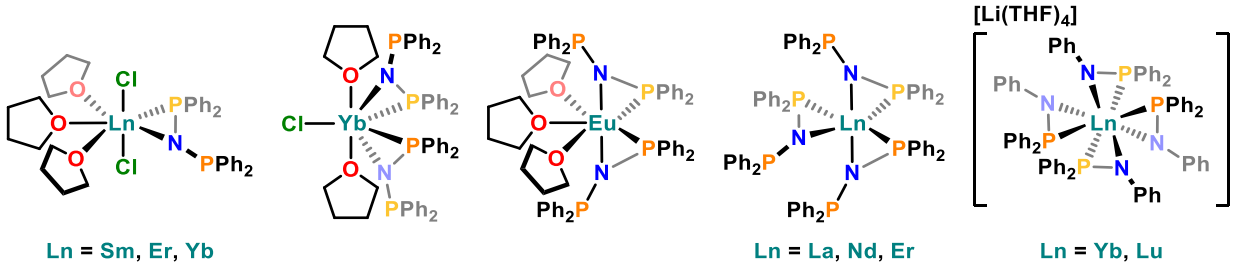

Figure 1.2. Series of lanthanide complexes bearing one,[58] two,[59,61] three,[57] or four[62] phosphanylamido ligands (from left to right), as reported by Roesky and colleagues.

The preparation of the homoleptic ate complexes $[Li(THF)_4][Ln(PhNPPh_2)_4]$ (Ln = Yb, Lu) was accomplished by conventional salt metatheses between the lanthanide(III) trichlorides and lithium (diphenylphosphanyl)phenylamide in THF,[62] whereas for the neutral homoleptic complexes $[Ln\{N(PPh_2)_2\}_3]$ either salt metathesis (Ln = Er) with lithium bis(diphenylphosphanyl)amide in THF or protonolysis of the respective $[Ln\{N(SiMe_3)_2\}_3]$ precursor (Ln = La, Nd) with bis(diphenylphosphanyl)amine in boiling toluene furnished the desired products (Figure 1.2, right).[57] Interestingly, lutetium(III) only yielded the THF solvated heteroleptic complex $[\{(Ph_2P)_2N\}_3Lu(THF)]$ after salt metathesis. In that particular case, the sevenfold coordination can be rationalized by the favored binding of the "hard" O donor atom of THF to lutetium(III), which is the strongest Lewis acid of the lanthanide(III) series. In contrast to the homoleptic complexes, for the heteroleptic lanthanide(III) complexes with two or one phosphanylamido ligand (Figure 1.2, left and middle) the potassium salt of the $[(Ph_2P)_2N]^-$ ligand had to be employed in the metathesis reactions with the lanthanide(III) trichlorides in THF.[58,61] These reactions were found to be sensitive to the molar ratio of the reactands: While treatment of $YbCl_3$ with 2 equiv of $[K(THF)_n][N(PPh_2)_2]$ led to a mixture of $[\{(Ph_2P)_2N\}_2YbCl(THF)_2]$, $[\{(Ph_2P)_2N\}_3Yb]$ and $[\{(Ph_2P)_2N\}YbCl_2(THF)_3]$ from which no pure product could be obtained, a slight excess (2.05 equiv) of the ligand's potassium salt gave mainly

[{$(Ph_2P)_2N$}$_2$YbCl(THF)$_2$] which could be separated from small amounts of homoleptic complex by recrystallization from THF/*n*-pentane.[61] In case of the mono-phosphanylamido complexes [{$(Ph_2P)_2N$}LnCl$_2$(THF)$_3$] (Ln = Sm, Er, Yb) a 1.1 fold excess of lanthanide(III) trichloride was found to be essential to have clean reactions.[58] It is noteworthy at this point that the europium(II) complex [{$(Ph_2P)_2N$}$_2$Eu(THF)$_3$] (Figure 1.2, middle) could be accessed by salt metathesis between EuI$_2$(THF)$_2$ and [K(THF)$_n$][N(PPh_2)$_2$] in an exact 1:2 molar ratio.[59]

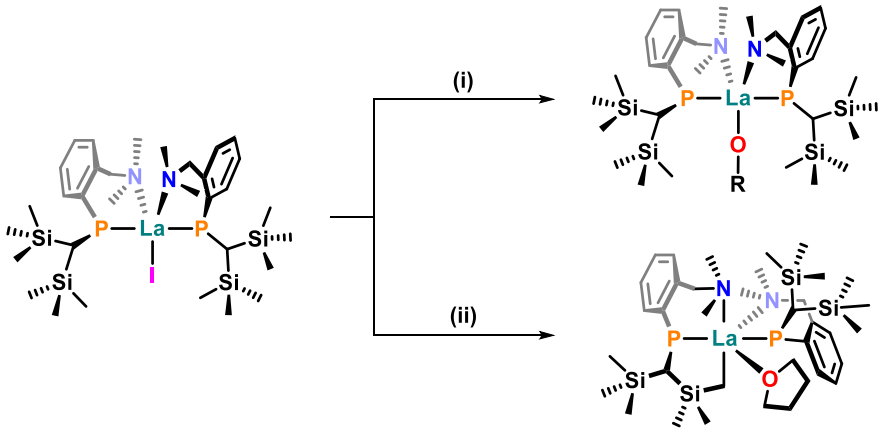

Scheme 1.3. Rare types of heteroleptic lanthanum(III) complexes with amino-functionalized phosphido ligands, prepared by Izod and co-workers (R = ^{i}Pr or ^{t}Bu).[34] Conditions: (i) KO^{i}Pr or KO^{t}Bu (1 equiv), Et_2O, 18-24 h, – KI; (ii) BnK (1 equiv), Et_2O, –196 °C → rt, 20 h, – KI, – C_7H_8. Coordinated THF originates from crude iodide starting complex.

In 2004, Izod and co-workers prepared rare types of heteroleptic lanthanum(III) complexes with a dimethylamino-functionalized phosphido ligand (Scheme 1.3).[34] To coordinate such kind of a ligand with a rather "soft" anionic P donor atom to lanthanum(III), the ligand's potassium salt had to be used in combination with lanthanum(III) triiodide, which lacks the "harder", more strongly bound chloride or triflate anions and therefore favors ligand exchange under formation of potassium iodide. Afterwards the pentacoordinate lanthanum(III) bis(aminophosphido) iodide complex could be reacted in diethyl ether to the respective alkoxide complexes (top) or C–H-activated to give a cyclometallated product (bottom), depending on the strength of the base. In the latter case the coordinated THF molecule originates from the iodide starting complex which was freshly prepared in THF and only used as crude material.

A comprehensive study concerning lanthanum(III) and cerium(III) complexes of a monoanionic, pincer-type bis(2-diisopropylphosphanyl-4-methylphenyl)amido ligand with PNP coordination mode was published in 2017 by Schelter, Ozerov and co-workers.[63] The same ligand had been used by Kiplinger and co-workers to isolate the first phosphinidene bridged dinuclear complex of the lanthanide series (for details see Section 3.1.3).[64] The groups of Schelter and Ozerov first prepared the mono(PNP) ligated complexes [(PNP)Ln{$N(SiMe_3)_2$}$_2$] ((Ln = La or Ce, Scheme 1.4, left) under harsh conditions, *i.e.*, prolonged heating of a mixture of protonated ligand and the [Ln{$N(SiMe_3)_2$}$_3$] precursors in toluene for up to a week. Due to the high steric demand of the PNP and bis(trimethylsilyl)amido ligands, also for

the transamination of the resulting PNP ligated cerium(III) complex in the reaction with 2,6-diisopropylphenylamine harsh conditions (C_6D_6, 120 °C) had to be applied (i). Significantly, the product [(PNP)Ce(NHDipp)$_2$] (Scheme 1.4, top middle) represents the first example of a cerium(III) anilide complex, which underscores the ability of the sterically demanding PNP ligand framework to stabilize rare types of lanthanide coordination compounds.

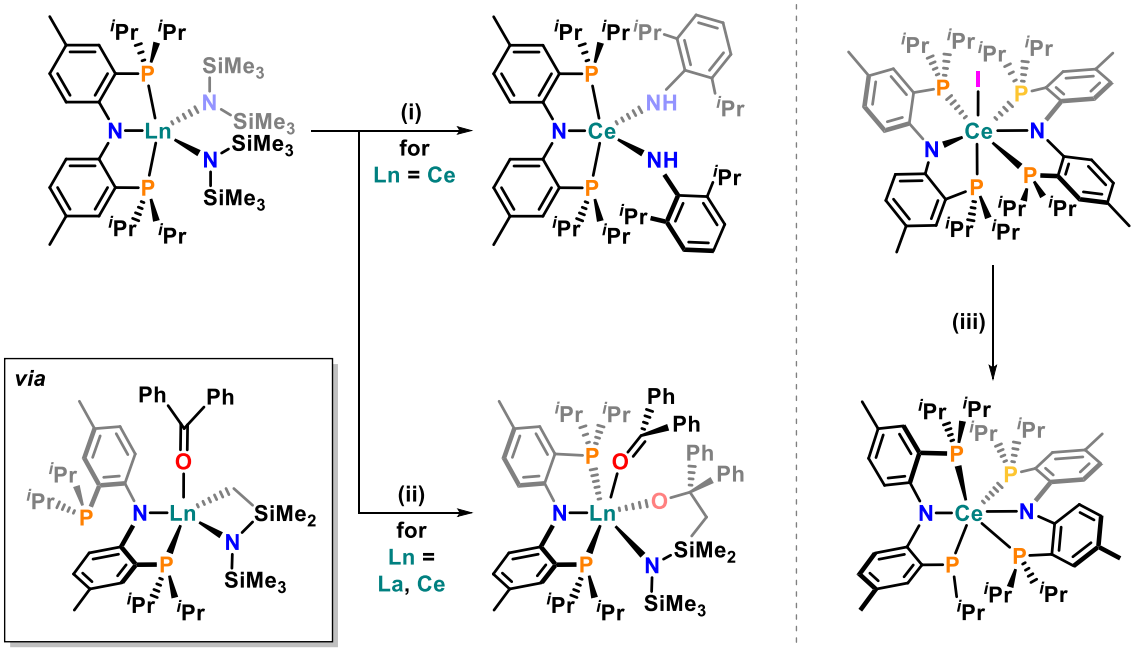

Scheme 1.4. Lanthanum(III) and cerium(III) complexes bearing one (left) or two PNP pincer-type ligands (right), as reported by Schelter and co-workers in 2017.[63] Conditions: (i) 2,6-diisopropylphenylamine (2.42 equiv), C_6D_6, 120 °C, 12 h, – excess 0.42 2,6-diisopropylphenylamine, – 2 HN(SiMe$_3$)$_2$; (ii) benzophenone (2 equiv), C_6D_6, 110 °C, 2 d for Ln = La or 4 d for Ln = Ce, – HN(SiMe$_3$)$_2$; (iii) BnK, toluene, rt, – KI, – C_7H_8, – C_3H_6.

In addition to the transamination reaction with cerium(III), the authors looked more closely into the reaction of [(PNP)Ln{N(SiMe$_3$)$_2$}$_2$] with the O donor ligand benzophenone (ii) for both lanthanum(III) and cerium (III), to see whether one of the phosphanyl groups could be forced to de-coordinate from the oxophilic metal ions as had already been reported for uranium.[65,66] However, a reaction was again only observed after heating the reaction mixture to 110 °C for several days, respectively, and the PNP ligand was found to remain coordinated in a tridentate fashion in the isolated complex. Instead, elimination of bis(trimethylsilyl)amine under an unprecedented functionalization of the second bis(trimethylsilyl)amido ligand had occurred (Scheme 1.4, bottom middle).[63] Based on the control experiment with redox-neutral lanthanum(III), the authors concluded that in the case of cerium(III) no change in redox state of the metal ion is operative. The most likely mechanism involves an initial coordination of one molecule of benzophenone under elimination of bis(trimethylsilyl)amine and de-coordination of one phosphanyl group (see inset in Scheme 1.4, bottom left), followed by the insertion of another benzophenone molecule into the Ln–C bond and re-coordination of the phosphanyl side arm.

For the bis(PNP) ligated cerium(III) iodide complex (Scheme 1.4, top right), which was obtained by salt metathesis between cerium(III) iodide and the ligand's potassium salt in toluene at room temperature, dynamic processes involving de- and re-coordination of the phosphanyl groups and/or conformational changes within the PNP ligands were inferred from variable temperature (VT) ^{1}H NMR spectroscopic studies.[63,65] Notably, the attempt to access bis(PNP) complexes of cerium(III) by protonolysis of the tris(alkyl) precursor complex [Ce{CH(N(CH$_3$)$_2$)C$_6$H$_5$}$_3$] at 75 °C in toluene-d_8 generated a phosphido moiety at one of the PNP ligands (Scheme 1.4, bottom right) through C–H activation and β-elimination[32] of propene, which could be detected *via* ^{1}H NMR spectroscopy. The same first cerium(III) phosphido complex formed as crude product upon treating the iodide complex with benzyl potassium (iii).

The authors further probed the paramagnetic cerium(III) complexes for potentially accessible coordination sites in non-coordinating (C$_6$D$_6$) and coordinating (THF-d_8) solvents, using ^{31}P NMR spectroscopy.[63,67,68] While the complexes [(PNP)Ce{N(SiMe$_3$)$_2$}$_2$] and [(PNP)$_2$CeI] showed no or only very little changes in their ^{31}P NMR shifts, the ^{31}P resonance of [(PNP)Ce(NHDipp)$_2$] experienced a pronounced upfield shift to $\delta = 327.3$ ppm in THF-d_8 compared to $\delta = 436.0$ ppm in C$_6$D$_6$, which strongly suggests the coordination of THF-d_8 solvent molecules to cerium(III). Significant changes in the ^{31}P NMR spectrum were also observed for the mono(PNP) benzophenone complex, in which case two upfield shifted resonances at $\delta \approx 311$ ppm and 243 ppm (ratio 1:1) in THF-d_8 compared to one resonance at $\delta \approx 392$ ppm in C$_6$D$_6$ indicate ligand exchange of benzophenone with THF-d_8 and a lower symmetry of the resulting complex. The intriguing phosphido complex showed upfield shifted ^{31}P resonances in THF-d_8 with differences in shifts of up to ≈52 ppm. Notably, the ^{31}P NMR shifts of the different cerium(III) complexes in C$_6$D$_6$ could be correlated linearly to the crystallographically determined Ce–P interatomic distances (R value of 0.965), which means that the ^{31}P resonances experience a proportionally increasing downfield shift with decreasing Ce–P distance.

Cyclovoltammetric studies of the sterically encumbered complexes [(PNP)Ln{N(SiMe$_3$)$_2$}$_2$] revealed one quasi-reversible and one irreversible redox event in dichloromethane at anodic peak potentials of $E_{pa} = –0.48$ V and –0.13 V for Ln = Ce (*vs* [Fc]/[Fc]$^+$). Since the same electrochemical behavior was also observed for Ln = La, with only minor or no differences in the values of $E_{pa} = –0.54$ V and –0.13 V, the redox processes can be attributed to the oxidation of the PNP ligand, respectively, which is in line with the HOMO of the complexes being mostly centered on the PNP ligand framework (≈83% for Ln = Ce). Thus, taking all the synthetic experiments, electrochemical data and theoretical calculations into account, the authors concluded that the PNP supporting ligand strongly favors the +III over the +IV oxidation state of cerium, which is of general interest to synthetic chemists working with this element.[63]

1.1.2 Ligand Scaffold Used in this Work

The properties of monoanionic, bidentate PN ligands, especially anilidophosphines, should be very favorable for a rich lanthanide coordination chemistry. First of all, this type of ligand scaffold favors a strong binding to the lanthanide ion *via* the anionic "hard" amido group,[52] while the phosphanyl group in 2-position of the rigid aromatic backbone[13] assists in the coordination as a neutral "soft" donor, thereby further increasing the stability of the coordination without adding another negative charge (Figure 1.3, left). As a consequence, the "classical" trivalent lanthanide(III) ion can accommodate up to three supporting ligands of this kind,[69] depending on their steric demand. Secondly, the bidentate PN ligands are in principle less sterically demanding and more weakly bound than the pincer-type PNP ligands and should therefore allow more flexibility in the first coordination sphere of the lanthanide(III) ion, which is beneficial for the introduction and reactivity of other (sterically demanding) ligands.

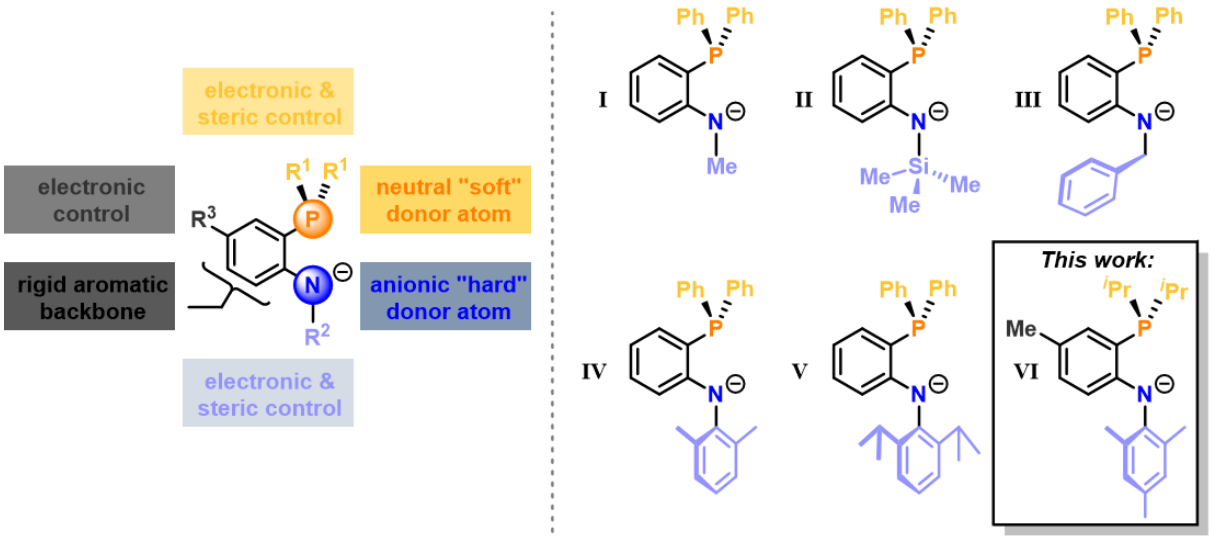

Figure 1.3. Characteristic features of monoanionic, bidentate anilidophosphine (PN) ligands and possibilities for tailoring the electronic and steric properties of such ligands (left). Selection of literature reported PN ligands of this type (right).[7,13,14,25–28,48,69,70] The (2-diisopropylphosphanyl-4-methylphenyl)-2,4,6-trimethylanilide ligand[13] used in this work is highlighted in the lower right corner.

In addition to these primary coordination properties of anilidophosphines, the modular design of the anilido framework and the phosphanyl group facilitates further adjustments of electronic and steric characteristics[32] (Figure 1.3, left) by simply selecting other substituents R^1 at phosphorus, R^2 at nitrogen and R^3 at the aromatic backbone during different steps in the synthesis (*vide infra*). The substituents R^1 at phosphorus are typically phenyl (**I** – **V**, Figure 1.3, right)[14,25–27,48,69,70] or isopropyl (**VI**),[13,26] whereas for the substituent R^2 at nitrogen literature reported examples include alkyl or silyl substituents such as methyl, trimethylsilyl or benzyl (**I** – **III**)[26,27,69,70] and aryl substituents like 2,6-dimethylphenyl, 2,6-diisopropylphenyl or 2,4,6-trimethylphenyl (**IV** – **VI**).[13,14,25,48,69]

The ligand scaffolds **I**, **III** and **IV** have been used as part of lanthanide(III) based catalysts for the polymerization of ethylene to poly(ethylene).[69] This work by Cui and co-workers from 2007 already

underlined the versatility of the modular design of the anilidophosphine framework and how crucial the steric tailoring at nitrogen is to obtain defined lanthanide(III) complexes: While the *N*-methylated or -benzylated versions **I** and **III** only rendered the isolation of the respective bis(anilidophosphine) complexes possible (Figure 1.4, left), of which the latter one slowly reacted to the homoleptic complex (middle) under ligand scrambling, the more sterically demanding 2,6-dimethylphenyl substituent at nitrogen in ligand framework **IV** gave access to a series of mono(anilidophosphine) complexes (right).

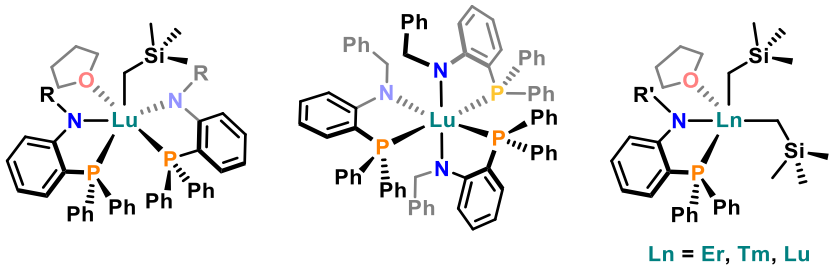

Figure 1.4. Cui and co-workers' series of lanthanide(III) complexes supported by different bidentate anilidophosphine ligands (R = Me, Bn; R' = 2,6-dimethylphenyl).[69]

Due to the favorable NMR spectroscopic features, the *N*-(2-diisopropylphosphanyl-4-methylphenyl)-2,4,6-trimethylanilide system (**VI**)[13] was chosen as supporting ligand for this dissertation. Besides the very practical use of the ^{31}P resonance for the analysis of PN ligands in general (*i.e.*, monoisotopic element and spin ½ of the ^{31}P nucleus result in high sensitivity, less complicated coupling patterns and convenient reaction monitoring),[52] supporting ligand **VI** also has the advantage of showing distinct and quite well separated ^{1}H NMR spectroscopic signatures: (i) In contrast to phenyl groups, the ^{1}H resonances of the isopropyl substituents at phosphorus (R^1) do not overlap with resonances of the aryl groups, thereby significantly reducing the complexity of the aromatic region in the ^{1}H NMR spectrum; (ii) the symmetrical 2,4,6-trimethylphenyl substituent at nitrogen (R^2) typically shows only one singlet in the aromatic region at $\delta \approx 7.0$ ppm; and (iii) because of the methyl substituent in 4-position (R^3), the aromatic backbone gives only three additional resonances between $\delta \approx 5.5$ and 7.0 ppm, of which the resonance of the proton *ortho* to nitrogen is most distinctive with a chemical shift between $\delta \approx 5.5$ and 6.0 ppm.[13]

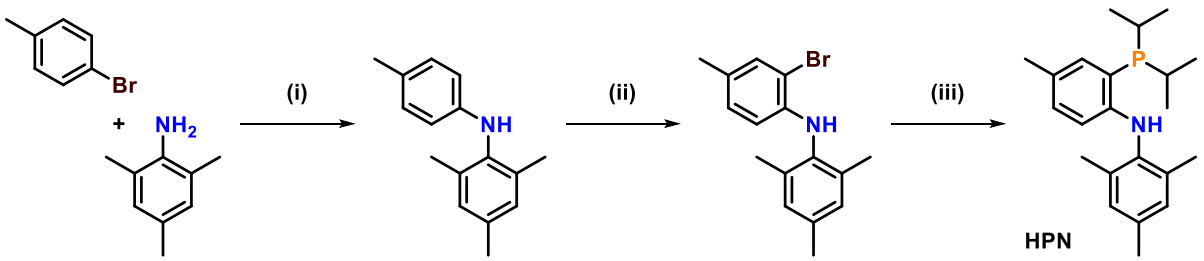

Scheme 1.5. Literature reported, three-step synthesis protocol for the protonated ligand precursor **HPN** used in this work.[13,71] Conditions: (i) $Pd(OAc)_2$ (0.1 equiv), 1,1'-bis(diphenylphosphino)ferrocene (DPPF, 0.2 equiv), sodium *t*-pentoxide (1.7 equiv), toluene, reflux, 4 d, 72%; (ii) NBS (1 equiv), acetonitrile, 12 h, 0 → 30 °C, 94%; (iii) *n*-BuLi (2 equiv), Et_2O, –78 °C, 3 h, then $ClP(^iPr)_2$ (1 equiv), –78 °C → rt, 48 h, then H_2O, 0 °C. Reaction equations not balanced for simplicity.

The protonated form of ligand **VI** (short **HPN**) can be synthesized conveniently in three steps (Scheme 1.5). After construction of the asymmetric diarylamine framework by a Buchwald-Hartwig C–N cross coupling reaction between 4-bromotoluene and 2,4,6-trimethylaniline in the first step (i),[13] a regioselective mono-bromination with *N*-bromosuccinimide (NBS) gives the *ortho*-brominated diarylamine (ii).[71] This substrate is then lithiated at nitrogen and the *ortho*-position, reacted with chlorodiisopropylphosphine and carefully quenched with degassed water to yield crude product **HPN** (iii).[13] Subsequent treatment with suitable strong bases such as alkali metal alkyls or amides in aliphatic solvents results in clean precipitation of the respective alkali metal salts of the ligand which can be used for salt metathesis reactions (see Section 1.2). The overall advantage of this synthesis protocol is the ability to change, *e.g.*, the arylamine or the chlorophosphine in the cross coupling and the nucleophilic aromatic substitution step, respectively (*vide supra*), as well as to enable the decoration of both nitrogen and phosphorus with sterically demanding substituents.[13]

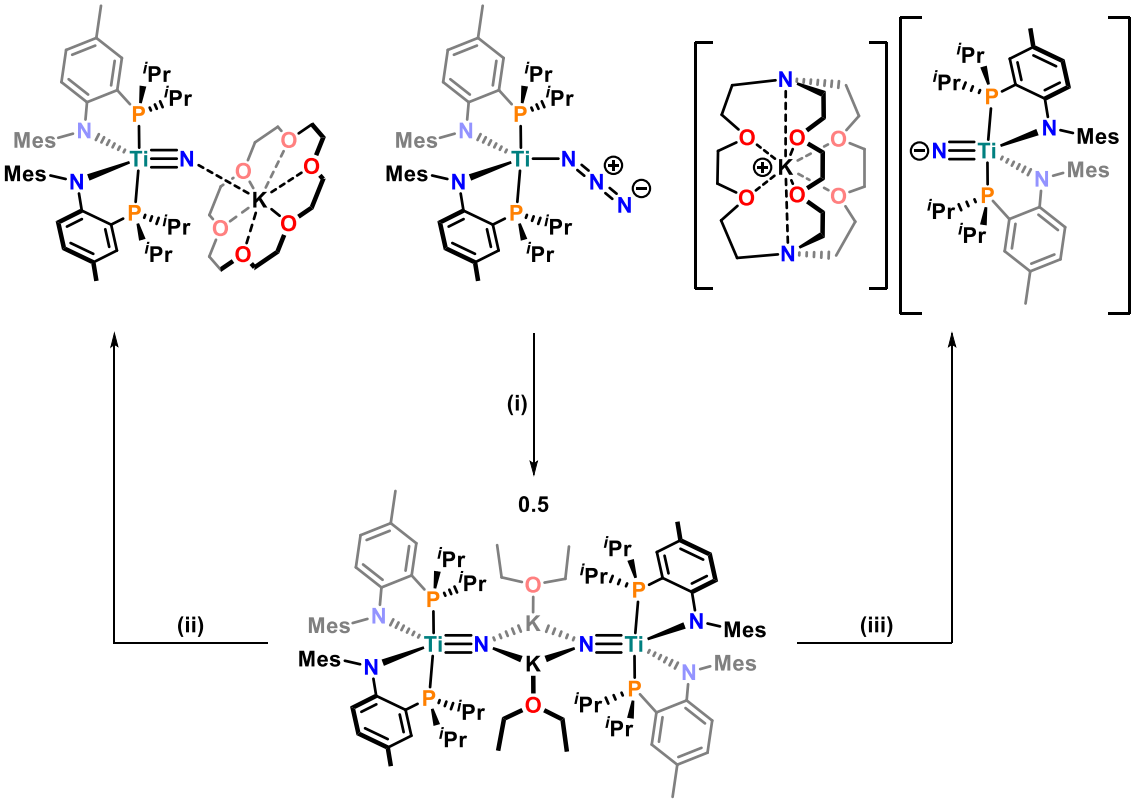

Scheme 1.6. Reaction of a titanium(III) azide complex to a potassium bridged dimeric titanium(IV) nitride complex (middle) supported by anilidophosphine framework **VI**, as reported by Mindiola and co-workers in 2015.[42] Subsequent treatment with the sequestration agents 18-crown-6 (left) or 2.2.2-cryptand (right) affords either a potassium capped (left) or an isolated (right) mononuclear terminal nitride complex. Conditions: (i) KC_8 (1.04 equiv), Et_2O, –35 °C → rt, 1 h, – excess 0.04 KC_8, – N_2; (ii) 18-crown-6 (1 equiv), toluene, rt, 15 min, – Et_2O; (iii) 2.2.2-cryptand (1 equiv), toluene, –35 °C → rt, 15 min, – Et_2O.

The anilidophosphine **VI** has already been proven to be a suitable supporting ligand for highly reactive group IV or uranium methylene, imido and nitride complexes.[42–44,50] In 2015, the group of Mindiola disclosed a route to the first mononuclear terminal titanium(IV) nitride complex using supporting ligand **VI** (Scheme 1.6).[42] Starting from a rare mononuclear, pentacoordinate titanium(III) azide complex of

the composition $[(PN)_2Ti(N_3)]$, treatment with KC_8 in diethyl ether induced the loss of dinitrogen under the formation of the diamagnetic, potassium bridged titanium(IV) nitride dimer $[\mu_2\text{-}K(OEt_2)]_2[N{\equiv}Ti(PN)_2]_2$ (i). The stability of the PN ligand supported titanium(IV) nitride moiety in aromatic solvents allowed a full (heteronuclear) NMR spectroscopic characterization, including the observation of the PN ligand ^{31}P singlet resonance in the typical range at $\delta = 7.2$ ppm.[42] Furthermore, the dimeric structure could be broken by addition of the sequestration agents 18-crown-6 (ii) or 2.2.2-cryptand (iii). Remarkably, both the $[K(18\text{-crown-}6)]^+$-capped or naked (in the case of $[K(2.2.2\text{-cryptand})]^+$) titanium(IV) nitride functionalities did not cannibalize the PN supporting ligands, wherefore very high yields (>90%) were obtained. However, the complex $[K(2.2.2\text{-cryptand})][N{\equiv}Ti(PN)_2]$ is only soluble in coordinating solvents (THF, DME), in which it decomposes within minutes at room temperature to a mixture of products, including the supporting ligand's potassium salt (**KPN**). In a broader context this means that under certain conditions de-coordination of the PN ligand may occur to form, *e.g.*, the thermodynamically stable alkali metal salts or its protonated form.

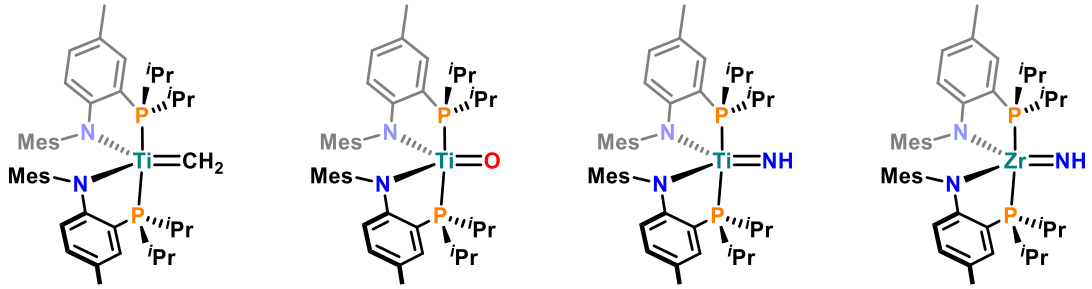

Figure 1.5. Mindiola and co-workers' terminal titanium(IV) methylene,[43] oxo and parent imido[45] complexes as well as the first terminal zirconium(IV) parent imido (from left to right), all supported by the same anilidophosphine used in this work.

Nonetheless, the titanium complexes with anilidophosphine **VI** by Mindiola and co-workers were generally stable to enable the synthesis of other rare and very reactive titanium compounds, including the first terminal titanium(IV) methylene as well as terminal titanium(IV) oxo and parent imido complexes (Figure 1.5, left and middle).[43,45] While the methylene complex could be obtained in up to 75% yield, *e.g.*, by hydrogen abstraction from and concomitant oxidation of the titanium(III) methyl complex $[(PN)_2Ti(CH_3)]$,[43] the terminal oxo and parent imido complexes (yields of >80%) were derived from the previously described dimeric titanium(IV) nitride (Scheme 1.6, bottom).[45] Due to the very reactive nature of $[(PN)_2Ti(CH_2)]$, gradual decomposition at room temperature to the methyl complex, methane and other unidentified products could not be completely suppressed.[43] The flexibility and robustness of the PN ligand was again demonstrated in 2018 with the isolation of the first terminal zirconium(IV) parent imido complex (Figure 1.5, right), which was synthesized in analogy to the titanium(IV) nitride dimer shown in Scheme 1.6 by reduction of the azide precursor $[(PN)_2Zr(N_3)_2]$.[44] However, the isolated yield for the product was comparably low (42%), and reaction control NMR spectroscopic data collected in THF-d_8 indicate that the intermediately formed zirconium(IV) nitride

complex abstracts a hydrogen from another [(PN)$_2$Zr]-fragment, consuming ≈50% of the available [(PN)$_2$Zr]-fragments in the process.

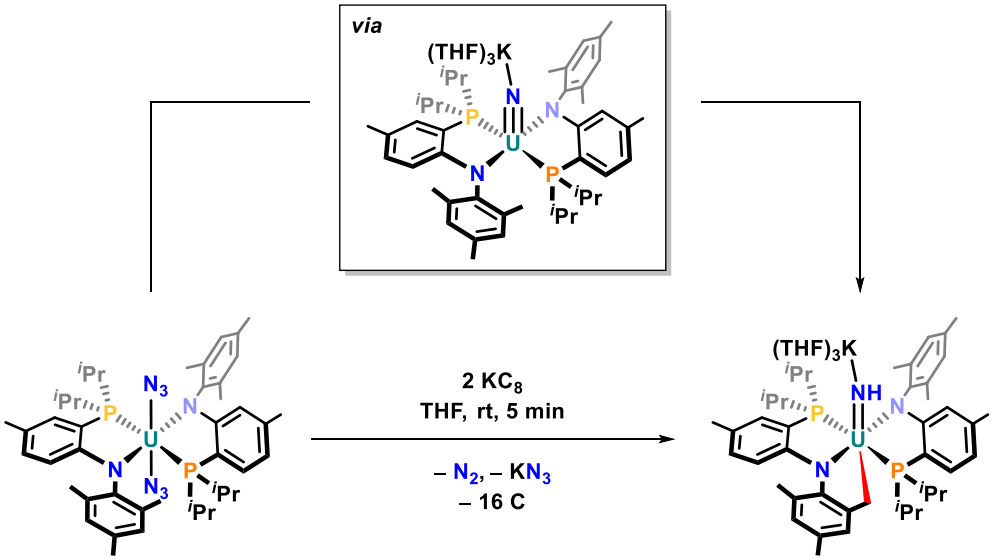

Scheme 1.7. Reaction of an uranium(IV) azide complex to a potassium capped uranium(IV) imido complex supported by anilidophosphine framework **VI**, as reported by Schelter and Mindiola and co-workers in 2018.[50] The transient uranium(IV) nitride complex (top), which is most likely formed during this reaction, undergoes a C–H activation at one of the PN supporting ligands' mesityl-CH_3 groups (new U–C bond highlighted in red, bottom right). Excess of KC_8 (4 equiv) is scaled down for simplifying the reaction equation.

Finally, in 2018 Schelter and Mindiola and co-workers succeeded in isolating a rare uranium(IV) parent imido complex using anilidophosphine **VI** as supporting ligand.[50] Starting from an uranium(IV) diazide complex, the reaction with KC_8 in THF led to the imido functionality instead of the anticipated nitride group (Scheme 1.7, bottom). The formation of the imido group was accompanied by the C–H-activation at one of the mesityl-CH_3 groups of a PN ligand and the formation of a new U–C bond. Based on theoretical calculations the most likely mechanism for this transformation involves the extrusion of dinitrogen to form a transient, highly nucleophilic uranium(IV) nitride (top), which in turn abstracts a proton in an intramolecular fashion from the CH_3 group. This example illustrates that the PN ligand can indeed also stabilize reactive structural motifs of f-elements, and that even though there are some limitations, there are paths such as intramolecular C–H-activation to avoid complete disintegration of the complexes (see also the results presented in Chapter 3).

Considering the examples described above, supporting framework **VI** was employed in this dissertation for the synthesis of two mono(anilidophosphine) and a series of bis(anilidophosphine) lanthanide(III) complexes. The following section describes in detail their syntheses, structural and spectroscopic characteristics as well as their salt metathesis reactivity and electrochemistry in the form of a published manuscript. The results will serve as the starting point for further functionalizations of selected complexes (Chapters 2 and 3) or for the introduction of other ligands (Chapter 4).

1.2 Results and Discussion

Publication: Monoanionic Anilidophosphine Ligand in Lanthanide Chemistry: Scope, Reactivity and Electrochemistry

Fabian A. Watt,[a] Athul Krishna,[a] Grigoriy Golovanov,[a] Holger Ott,[b] Roland Schoch,[a] Christoph Wölper,[c] Adam G. Neuba,[a] and Stephan Hohloch*[d]

* Corresponding author

[a] Paderborn University, Warburger Straße 100, 33098 Paderborn, Germany

[b] Bruker AXS GmbH, Östliche Rheinbrückenstraße 49, 76187 Karlsruhe, Germany

[c] University of Essen-Duisburg, Universitätstraße 5-7, 45117 Essen, Germany

[d] University of Innsbruck, Innrain 80-82, 6020 Innsbruck, Austria

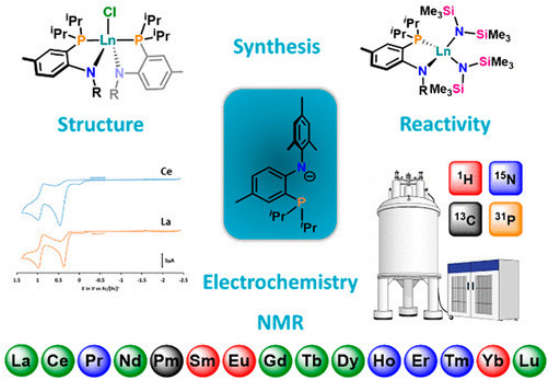

This article was published as follows:

Watt, F. A.; Krishna, A.; Golovanov, G.; Ott, H.; Schoch, R.; Wölper, C.; Neuba, A. G.; Hohloch, S. *Inorg. Chem.* **2020**, *59*, 2719–2732.

DOI: 10.1021/acs.inorgchem.9b03071

https://dx.doi.org/10.1021/acs.inorgchem.9b03071

Synopsis: Two series of lanthanide complexes featuring one or two anilidophosphine ligands have been synthesized and studied towards their electrochemical and structural properties. This contribution shows the potential of monoanionic anilidophosphine ligands as new supporting ligands in rare earth metal chemistry allowing the isolation of various unusual and reactive metal complexes.

Author Contributions: The project was designed by S. Hohloch. Experimental work was carried out by F. A. Watt, A. Krishna, G. Golovanov and S. Hohloch. NMR and IR spectra were recorded by F. A. Watt, A. Krishna and S. Hohloch. CVs were measured by A. G. Neuba and plotted by S. Hohloch. X-ray structure analyses were performed by R. Schoch, H. Ott, C. Wölper and S. Hohloch. The manuscript was written by S. Hohloch and F. A. Watt and proof read by all authors.

Christiane Gloger and Maria Busse are kindly acknowledged for conducting elemental analyses.

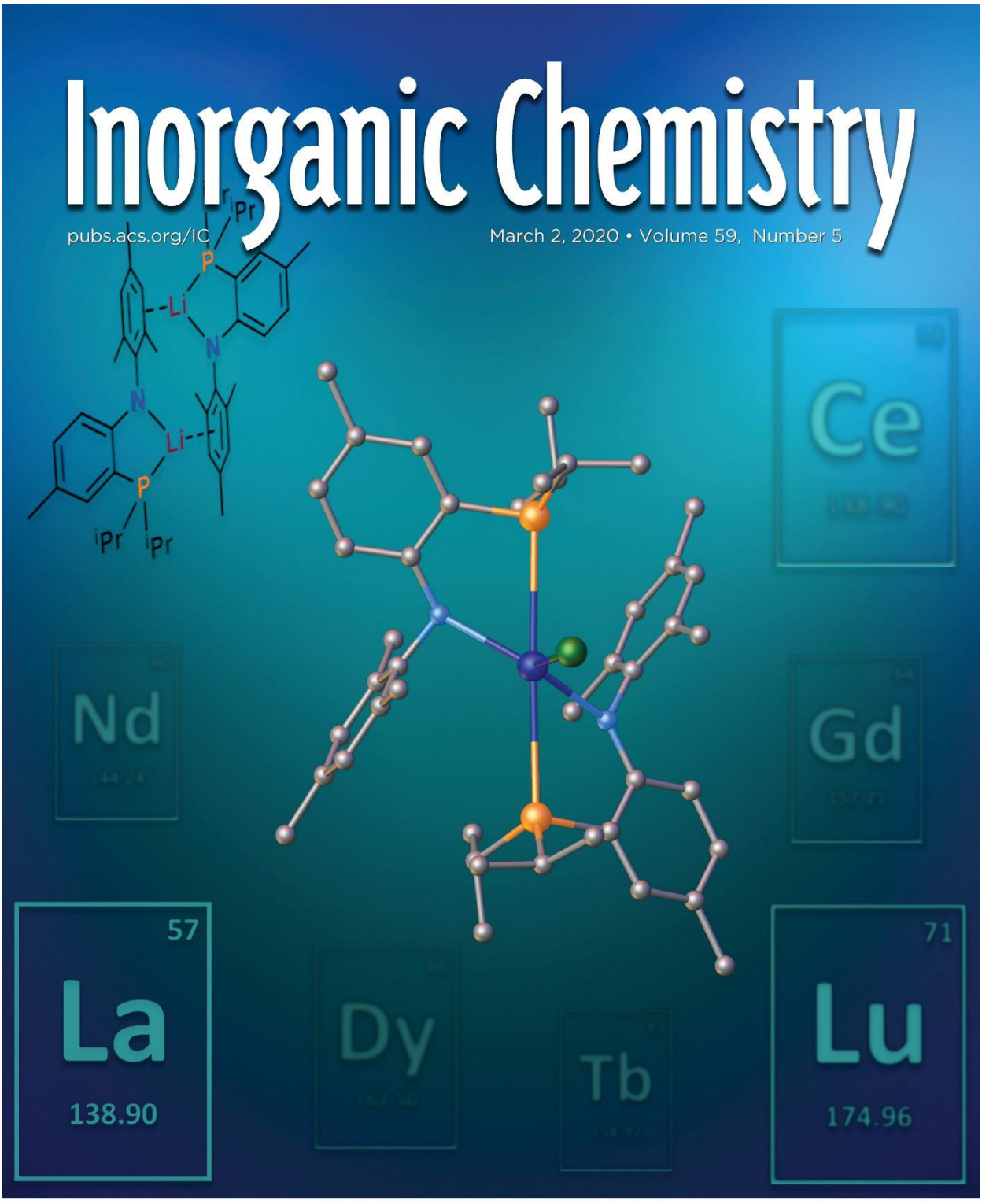
Inorganic Chemistry
pubs.acs.org/IC
March 2, 2020 • Volume 59, Number 5
Li
P
N
iPr
Ce
Nd
Gd
57
La
138.90
Dy
Tb
71
Lu
174.96
ACS Publications
Most Trusted. Most Cited. Most Read.
www.acs.org

Inorganic Chemistry

pubs.acs.org/IC Article

Monoanionic Anilidophosphine Ligand in Lanthanide Chemistry: Scope, Reactivity, and Electrochemistry

Fabian A. Watt, Athul Krishna, Grigoriy Golovanov, Holger Ott, Roland Schoch, Christoph Wölper, Adam G. Neuba, and Stephan Hohloch*

Cite This: *Inorg. Chem.* 2020, 59, 2719−2732 Read Online

ACCESS | Metrics & More | Article Recommendations | Supporting Information

ABSTRACT: We present the synthesis of a series of new lanthanide(III) complexes supported by a monoanionic bidentate anilidophosphine ligand (*N*-(2-(di*iso*propylphosphanyl)-4-methylphenyl)-2,4,6-trimethylanilide, short PN^-). The work comprises the characterization of a variety of heteroleptic complexes containing either one or two PN ligands as well as a study on further functionalization possibilities. The new heteroleptic complexes cover selected examples over the whole lanthanide(III) series including lanthanum, cerium, neodymium, gadolinium, terbium, dysprosium, and lutetium. In case of the two diamagnetic metal cations lanthanum(III) and lutetium(III), we have furthermore studied the influence of the lanthanide ion (early vs. late) on the reactivity of these complexes. Thereby we found that the radius of the lanthanide ion has a major influence on the reactivity. Using sterically demanding, multidentate ligand systems, e.g., cyclopentadienide (Cp^-), we found that the lanthanum complex **La(PN)$_2$Cl** (**1-La**) reacts well to the corresponding cyclopentadienide complex, while for **Lu(PN)$_2$Cl** (**1-Lu**) no reaction was observed under any conditions tested. On the contrary, employing monodentate ligands such as mesitolate, thiomesitolate, 2,4,6-trimethylanilide or 2,4,6-trimethylphenylphosphide, results in the clean formation of the desired complexes for both lanthanum and lutetium. All complexes have been studied by various techniques, including multi nuclear NMR spectroscopy and X-ray crystallography. ^{31}P NMR spectroscopy was furthermore used to evaluate the presence of open coordination sites on the complexes using coordinating and noncoordinating solvents, and as a probe for estimating the Ce−P distance in the corresponding complexes. Additionally, we present cyclic voltammetry (CV) data for **Ce(PN)$_2$Cl** (**1-Ce**), **La(PN)$_2$Cl** (**1-La**), **Ce(PN)(HMDS)$_2$** (**8-Ce**) and **La(PN)(HMDS)$_2$** (**8-La**) (with HMDS = hexamethyldisilazide, $(Me_3Si)_2N^-$) exploring the potential of the anilidophosphane ligand framework to stabilize a potential Ce(IV) ion.

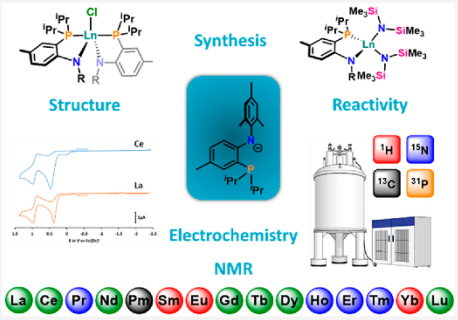

■ INTRODUCTION

The chemistry of the f-elements is one of the fastest developing fields in modern inorganic chemistry.[1−3] Their versatile coordination chemistry, which is owed to their large ionic radii, render these elements the ideal candidates for finding new structural, magnetic, biological, electronic, and spectroscopic properties,[4−13] as well as new modes of reactivity and catalysis.[14−22] Despite this astonishing variety of applications of f-element coordination compounds, the number of supporting ligands used in this field is still relatively limited. In fact, the field is mostly dominated by the ubiquitous cyclopentadienide ligands ($Cp^- = C_5R_5^-$), which were among the first ligands ever used in f-element chemistry.[23,24] Despite the fact, that the use of Cp ligands still reveal a variety of interesting molecules,[25] especially in the field of molecular magnetism,[26−46] it is crucial for other fields, e.g., catalysis, to explore alternative ligand systems in order to design new (catalytic) systems with tailor-made properties in the future.[14,47−53] One archetypical class of ligands in this context is the one of chelating amido- or anilidophosphine ligands with PN(P) coordination mode.[54−56] While PN(P) ligands have been extensively explored in the coordination chemistry of transition metals[57−73] and main group elements,[68,74−77] for the construction of transition metal−main group (multiple) bonds,[63,78−87] transition metal−transition metal bonds,[88−92] and in small molecule activation,[81,93−104] the number of examples of f-block coordination compounds featuring this class of ligands is still limited. This is rather surprising, as pincer type PNP ligands (Figure 1) such as **A** were used not only for the preparation of the first bridging phosphinidene complex of the lanthanides,[105] but also for the preparation of the first terminal scandium imido[106,107] and scandium phosphinidene[108] complexes. Additionally, Schelter et al. have recently published a study on the electronic structure of

Received: October 22, 2019
Published: January 21, 2020

https://dx.doi.org/10.1021/acs.inorgchem.9b03071
Inorg. Chem. 2020, 59, 2719−2732

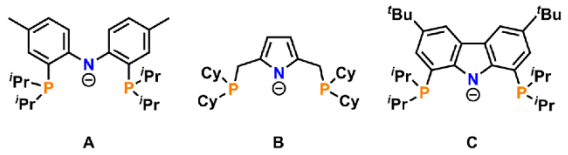

Figure 1. Selection of archetypical monoanionic PNP ligands used in rare earth metal chemistry so far.

cerium PNP complexes featuring ligand **A**, showing the PNP framework to inherently stabilize the "low-valent" cerium(III) oxidation state.[109] Aside from framework **A**, the PNP framework **B** was employed for the activation of sp-, sp^2- and sp^3-C−H bonds and the transient formation of methylidene complexes of scandium and yttrium by Tilley and Andersen et al.,[110,111] while the PNP ligand framework **C** was used recently for the synthesis of highly potent catalysts for the polymerization of ε-caprolactame.[112] Apart from that, framework **A** has also been extensively studied in actinide chemistry.[113] In contrast to the few examples existing for the use of pincer type PNP ligand frameworks, bidentate anilidophosphine ligands have only been employed twice in lanthanide and actinide chemistry yet (Figure 2); by Cui et al.

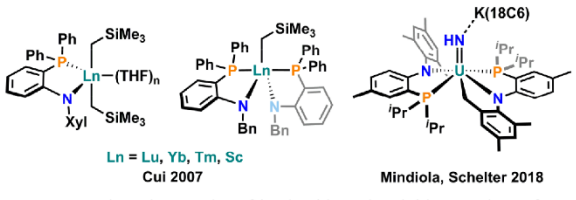

Figure 2. Selected examples of lanthanide and actinide complexes featuring bidentate monoanionic PN ligands.

in lanthanide chemistry for the synthesis of polymerization catalysts[114−117] and by Schelter and Mindiola et al., who isolated a terminal uranium(IV) imido complex, which most likely formed via a transient uranium nitrido complex.[118] Both reports have not only established but also point to promising future applications of bidentate PN ligands in f-element chemistry and lanthanide catalysis as well as in the isolation of unique coordination complexes featuring metal−ligand multiple bonds. Inspired by these findings we were interested in the coordination behavior of the bidentate monoanionic PN ligand, (PN^- = *N*-(2-(di*iso*propylphosphanyl)-4-methylphenyl)-2,4,6-trimethylanilide),[119] which recently has been used by Schelter and Mindiola et al. as stated above, and has also proven its value by stabilizing unique group IV nitride[120−123] and methylidene[124] complexes.

In the following, we will present the synthesis of a variety of heteroleptic lanthanide(III) complexes (with Ln = La, Ce, Nd, Gd, Tb, Dy, and Lu) featuring one or two PN ligands. Their reactivity toward various multidentate as well as monodentate ligands will be examined and the electrochemical properties of the cerium(III) complexes will be compared to their lanthanum(III) congeners to determine, if a potential cerium(IV) complex can be stabilized by the PN ligand used.

■ RESULTS AND DISCUSSION

Lanthanide(III) Complexes Featuring Two PN Ligands. Although the synthesis of the ligand precursor salt **KPN** from **HPN** has been reported earlier,[118] we found a route to isolate **KPN** in high yields and quantities without the need of benzyl potassium, which is especially difficult to handle, in case no glovebox is at hand. Instead of benzyl potassium we used commercially available potassium hexamethyldisilazide (**KHMDS**) in sub stoichiometric amounts (0.95 equiv) for the deprotonation of **HPN** (Scheme 1). Performing the reaction in

Scheme 1. Synthesis of the Ligand Precursor Salts LiPN and KPN

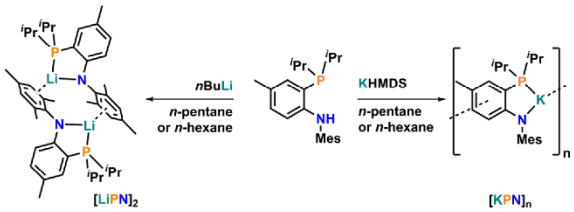

n-pentane or *n*-hexane results in the formation of a thick yellow precipitate, which can be easily filtered and dried under high vacuum to give analytically pure **KPN**. Additionally, we have been able to isolate X-ray quality crystals of **KPN** and **LiPN**. A detailed comparison of their solid state structures and atomic arrangements can be found in the Supporting Information (see Figure S129).

Having the two ligand precursors in hand, we now turned our interest toward the synthesis of new heteroleptic lanthanide(III) complexes with two PN ligands. To our surprise, starting from diamagnetic lanthanum(III) halides $\mathbf{LaCl_3(THF)_x}$ and $\mathbf{LaI_3(THF)_x}$ and following the procedure reported by Schelter et al.,[118] performing salt metathesis in THF at room temperature did only result in small conversions. Instead, we have observed protonation of the **LiPN** or **KPN** salt to form **HPN**. However, this issue can be overcome by performing the reaction between $\mathbf{LaCl_3(THF)_x}$ and **LiPN** in refluxing toluene overnight (Scheme 2). Following this procedure, the desired complex **1-La** can be isolated in good yields of 78% on scales of up to 12 g at once. Most indicative of the successful formation of the desired complex are two features in its NMR spectra: (i) a slightly low-field shifted resonance of the arene proton in *ortho* position of the coordinated nitrogen atom to δ 5.65 ppm compared to that of δ 5.59 ppm for **LiPN** in the ^{1}H NMR spectrum, and (ii) a pronounced low-field shift of the phosphorus resonance from δ −15.2 ppm for **LiPN** to δ 9.2 ppm for **1-La** in the $^{31}P\{^1H\}$ NMR spectrum. In addition, we have observed a slight broadening for the *iso*propyl methine and methyl proton resonances in **1-La**, most likely resulting from a rotation barrier due to steric crowding around the lanthanum atom.

Unambiguous proof for the formation of the desired complex **1-La** was given by X-ray diffraction studies (Figure 3). High quality crystals suitable for X-ray structure analysis could be grown by slow evaporation of a concentrated diethyl ether solution in a *n*-hexane atmosphere at room temperature. The complex crystallizes in the monoclinic space group $P2_1/c$ with one molecule in the asymmetric unit. The lanthanum atom in **1-La** was found to be five-coordinate in a slightly distorted trigonal bipyramidal fashion (τ_5 = 0.874, Figure 3). Therein, the two coordinating phosphorus atoms P1 and P2 are both in axial position, while the chloride and the two amide donors occupy the equatorial positions. The lanthanum−

https://dx.doi.org/10.1021/acs.inorgchem.9b03071
Inorg. Chem. 2020, 59, 2719−2732

Inorganic Chemistry pubs.acs.org/IC Article

Scheme 2. Synthesis of the Heteroleptic Halide Complexes 1-Ln and 2-Ln Starting from either LiPN (Top) or KPN (Bottom) or by Halide Exchange from Chloride to Iodide Using Iodotrimethylsilane (Middle)

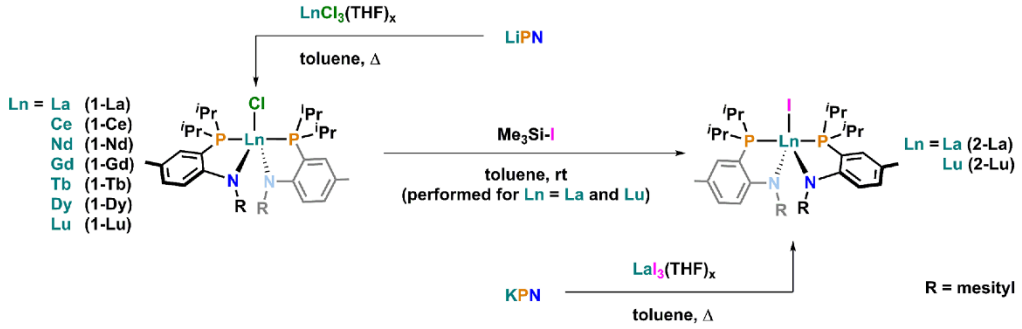

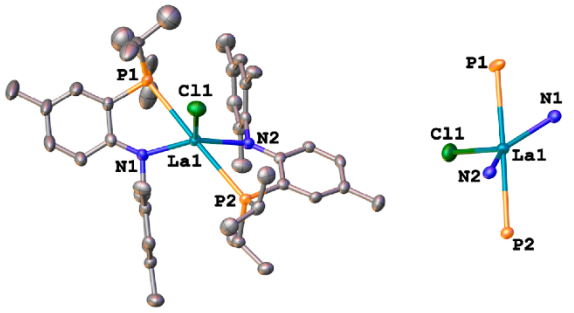

Figure 3. ORTEP plot of **1-La** (left) and simplified representation of the coordination polyhedron (right). Thermal ellipsoids are shown at a probability level of 30%. Hydrogen atoms have been omitted for clarity. The corresponding molecular structures of the complexes **1-Ce**, **1-Nd**, **1-Gd**, **1-Tb**, **1-Dy**, and **1-Lu** can be found in the Supporting Information, as their geometric appearances are similar to the one found in **1-La**.

phosphorus distances were found to be 3.163(1) Å and 3.197(1) Å for La1−P1 and La1−P2, respectively, while the lanthanum−nitrogen distances were found to be much shorter with only 2.373(3) Å for La1−N1 and 2.364(3) Å for La1−N2. The P1−La1−P2 angle was found to be 178.2(1)°, while the N1−La1−N2 angle is only 125.8(1)°. Performing the reaction under similar conditions as used for the preparation of **1-La**, but using **KPN** and $\mathbf{LaI_3(THF)_x}$, works similarly well to yield the corresponding iodide complex **2-La**. However, upscaling of this reaction was found to be more complicated and we found that **2-La** can be prepared more easily by performing a halide exchange reaction between **1-La** and iodotrimethylsilane in toluene at room temperature overnight (Scheme 2). Following this procedure allowed us to prepare the iodide complex **2-La** in scales of at least 1.5 g. Unfortunately, we have not been able to isolate X-ray quality crystals for **2-La** and all methods tested have only yielded strongly twinned crystals. It is also noteworthy at this point, that it is recommendable to use the lithium salt **LiPN** when lanthanide chlorides are used, while for the lanthanide iodides the use of **KPN** as a ligand precursor was found to be more effective (Scheme 2). Using **KPN** for the lanthanide chlorides results in smaller conversions and a more tedious workup. Likewise, this also counts for using **LiPN** in combination with lanthanide iodides. Having found a scalable and well working procedure for the synthesis of **1-La**, we were interested in how this procedure would translate to the other lanthanide elements and repeated the reaction under the same conditions for cerium (**1-Ce**), neodymium (**1-Nd**), samarium, europium, gadolinium (**1-Gd**), terbium (**1-Tb**), dysprosium (**1-Dy**), ytterbium and lutetium (**1-Lu**). We found that for most of the lanthanides, except samarium, europium, and ytterbium, this method gives good conversions and the desired chloride complexes can be obtained in reasonable to good yields of 58% and higher. Unfortunately, for samarium, europium, and ytterbium, we have not been able to isolate any useful products yet. Since these lanthanides have accessible +II oxidation states, we presently assume that the redox properties of these elements interfere with the desired reaction pathway. Except for **1-Ce** (vide infra), we have not been able to record useful NMR data for the paramagnetic complexes **1-Nd**, **1-Gd**, **1-Tb**, and **1-Dy**. However, μ_{eff} has been determined for all these complexes to be lying in the expected range for the corresponding electron configurations of the lanthanide(III) ions (see Table S6 in the Supporting Information and references therein). Additionally, all the paramagnetic complexes have been characterized by X-ray structure determination (see Figure S130) and the expected elemental composition of the isolated material could be confirmed by elemental analysis in each case. For the diamagnetic lutetium complex **1-Lu** we have observed a substantial line broadening of the resonances in the ^{1}H NMR spectrum, probably due to the shorter metal−ligand bonds resulting in much more steric crowding around the metal atom (vide infra). We have tried to overcome this issue by collecting variable temperature (VT) ^{1}H NMR spectra from 298 to 323 K. However, even at 323 K (50 °C) we have not been able to fully resolve the spectra (see Figure S32). X-ray quality crystals for complexes **1-Ce**, **1-Nd**, and **1-Dy** could be grown by slow evaporation of a concentrated diethyl ether solution of the corresponding complexes at room temperature, while X-ray quality crystals of **1-Gd** and **1-Tb** were grown from a very concentrated toluene solution (300 mg in 2 mL) during the reaction workup. Crystals of the lutetium complex **1-Lu** have been obtained by slow evaporation of a concentrated *n*-pentane solution at room temperature. Complexes crystallized by the same method have all been found to crystallize isostructurally in the monoclinic space groups $P2_1/n$ (for **1-Gd** and **1-Tb**), $P2_1/c$ (for **1-La**, **1-Ce**, **1-Nd**, **1-Dy**) or in the triclinic space group $P\bar{1}$ (for **1-Lu**). The general bonding parameters follow the expected trend among the lanthanide series, with decreasing Ln−N as well as Ln−P distances from **1-La** to **1-Lu**. This results in more steric

https://dx.doi.org/10.1021/acs.inorgchem.9b03071
Inorg. Chem. 2020, 59, 2719−2732

Scheme 3. Reactivity of the Complexes 1-La and 1-Lu in Substitution Reactions with π-Aromatic (Left and Middle) and Monodentate, Monoanionic Ligand Systems (Right)

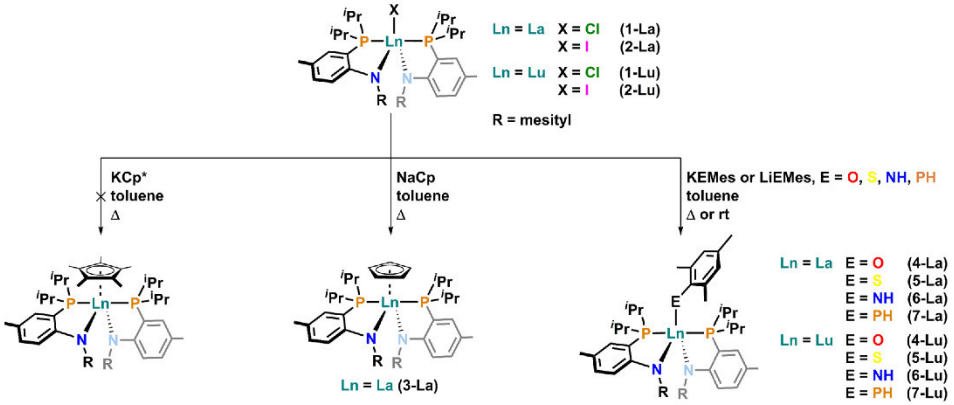

crowding around the metal atom and thus forcing the ligands into a more distorted trigonal bipyramidal coordination environment from **1-La** (τ_5 = 0.874) to **1-Lu** (τ_5 = 0.765) (vide supra). General trends and more information on the crystallographic data for the halide complexes of the general formula **Ln(PN)$_2$Cl** (**Ln** = **La**, **Ce**, **Nd**, **Gd**, **Tb**, **Dy**, and **Lu**) can be found in the Supporting Information (Tables S1−S5). ORTEP plots of **1-Ce**, **1-Nd**, **1-Gd**, **1-Tb**, **1-Dy**, and **1-Lu** can be found in Figure S130.

Salt Metathesis Reactivity of 1-La and 1-Lu. After having established a reliable and general synthesis route for the new halide complexes, we next turned our focus on their reactivity and the possibility to replace the last remaining chloride ligand in these complexes. Due to the NMR spectroscopic advantages of the diamagnetic lanthanum(III) and lutetium(III) complexes, this part will focus only on those compounds. In a first attempt, we prepared a toluene solution of both complexes **1-La** and **1-Lu** and added 1 equiv of **KCp***. To our surprise, we have not found any reaction taking place, even when the reaction mixtures were refluxed at 110 °C for 2 days (Scheme 3, left). Switching to the sterically less encumbering Cp ligand precursor **NaCp** we found similar behavior for the lutetium complex **1-Lu**, while for the lanthanum complex **1-La** a full conversion to the corresponding cyclopentadienide complex **3-La** was observed after heating the reaction mixture for 24 h at 95 °C (Scheme 3, middle). The clean formation of **3-La** was evident by two features in its NMR spectra: (i) a low-field shift of the phosphorus resonance in the $^{31}P\{^1H\}$ NMR spectrum from δ 9.2 ppm for **1-La** to δ 11.0 ppm for **3-La** and (ii) the appearance of a new singlet in the ^1H NMR spectrum at δ 6.48 ppm corresponding to the cyclopentadienide protons. We have been able to grow X-ray quality crystals of **3-La** from a concentrated toluene solution at −40 °C overnight. The complex crystallizes in the monoclinic space group $P2_1/c$ with one molecule of the desired complex in the asymmetric unit (Figure 4). The lanthanum−cyclopentadienide (centroid) distance was found to be 2.555(1) Å which is comparable to the La−Cp$_{cent}$ distance reported for La(Cp)$_3$.[125] However, coordination of the Cp ligand has a major influence on the coordination environment around the lanthanum atom. For instance, the twisting of the two PN ligands is counteracted by the Cp ligand which results in a decrease of the angle between the two PN tolyl planes from 44.4(1)° in **1-La** to only 10.5(1)° in **3-La**. Concurrent with the

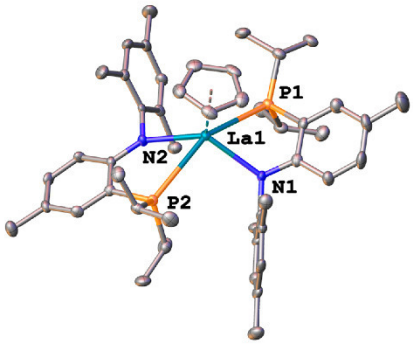

Figure 4. ORTEP plot of **3-La**. Thermal ellipsoids are shown at a probability level of 30%. Hydrogen atoms are omitted for clarity.

diminishing twisting angle between the two PN ligands the τ_5 value decreases from 0.874 in **1-La** to 0.355 in **3-La**. Therefore, the coordination polyhedron can now be seen as a distorted square pyramid instead of a distorted trigonal bipyramid. Due to the steric demand of the PN ligand, this change in conformation also has a noticeable impact on the lanthanum−heteroatom bond lengths: The average lanthanum−nitrogen bond lengths increase from 2.369(3) Å in **1-La** to 2.460(3) Å in **3-La**, and the lanthanum−phosphorus bond lengths La1−P1 and La1−P2 differ more strongly in **3-La** (3.098(1) Å and 3.216(1) Å) than in **1-La** (3.163(1) Å and 3.197(1) Å, respectively). We believe that this rather strong distortion of the coordination environment is not possible in **1-Lu** and to a certain degree limited in **1-La** if sterically more encumbering Cp ligands are used, resulting in the observed inertness described above. It is noteworthy at this point that switching to the iodide precursors **2-La** and **2-Lu** does not have any impact on this reaction behavior.

Since we found that the introduction of multidentate, π-coordinating ligands is sterically unfavored, we investigated other, monodentate ligands to access new heteroleptic complexes (Scheme 3, right). As a first choice, we have settled for the use of the potassium salt of mesitole (**KOMes**). To our satisfaction, the reaction between **1-La** as well as **1-Lu** and **KOMes** in toluene proceeded smoothly at room temperature, resulting in the quantitative formation of the new mesitolate complexes **4-La** and **4-Lu**, respectively. The formation of the

https://dx.doi.org/10.1021/acs.inorgchem.9b03071
Inorg. Chem. 2020, 59, 2719−2732

Inorganic Chemistry pubs.acs.org/IC Article

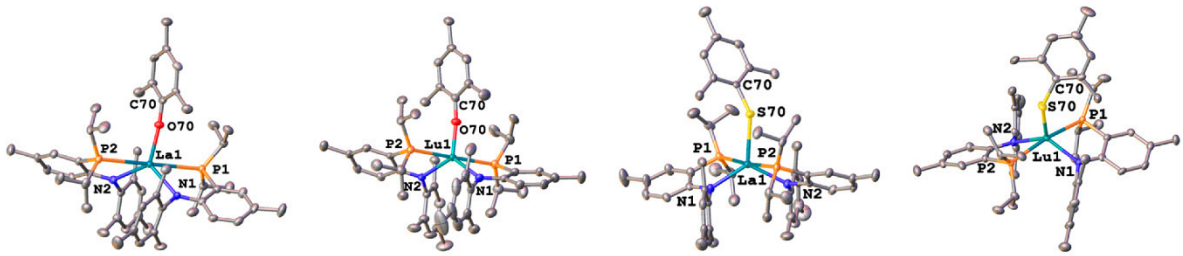

Figure 5. ORTEP plots of the chalcogenide complexes **4-La/Lu** and **5-La/Lu** (from left to right). Thermal ellipsoids are shown at a probability level of 30%. Hydrogen atoms and solvent molecules have been omitted for clarity.

new complexes was evident from several features in their NMR spectra, being (i) the appearance of a new set of mesityl resonances in the ^{1}H and ^{13}C{^{1}H} NMR spectra, (ii) the shift of the characteristic aryl proton of the PN ligand from δ 5.65 and δ 5.85 ppm for **1-La** and **1-Lu** to δ 5.76 and δ 5.99 ppm for **4-La** and **4-Lu**, and (iii) the high-field shift of the phosphorus resonances in the ^{31}P{^{1}H} NMR spectra from δ 9.2 and δ 5.0 ppm for **1-La** and **1-Lu** to δ 8.6 and δ 2.9 ppm for **4-La** and **4-Lu**. Additionally, either due to the lower symmetry of the complexes in solution or due to rotational barriers resulting from a greater steric demand of the mesitolate ligand, the methyl protons of the *iso*propyl groups on the PN ligands now split into four broad singlets and thereby also clearly indicating the successful formation of the mesitolate complexes **4-La** and **4-Lu**. Unambiguous proof of the formation of the new complexes was given by a X-ray diffraction study on high quality crystals of **4-La** and **4-Lu** which were obtained by slow evaporation of a concentrated diethyl ether solution of the respective complex (Figure 5, left). While complex **4-La** was found to crystallize in the monoclinic space group $P2_1/c$ without any residual solvent molecules in the crystal lattice, **4-Lu** crystallized in the triclinic space group $P\bar{1}$ with one molecule of diethyl ether in the lattice. Noteworthy, in contrast to the Cp complex **3-La**, the lanthanum–PN ligand distances remain largely unaffected by the coordination of the mesitolate ligand. However, the twisting angle between the two PN ligands is strongly affected by the sterically more encumbering mesitolate ligand changing from 44.4(1) and 37.4(1)° in **1-La** and **1-Lu** to 58.2(1) and 47.3(1)° in **4-La** and **4-Lu**, respectively. Simultaneously, the τ_5 values change from 0.874 and 0.765 for **1-La** and **1-Lu** to 0.841 and 0.953 for **4-La** and **4-Lu**. The metal–oxygen bond lengths were found to be 2.225(3) Å for La1–O70 and 2.028(3) Å for Lu1–O70 with nearly linear Ln1–O70–C70 angles being 173.8(3) and 171.7(3)° in **4-La** and **4-Lu**.

With this first success in introducing mesitolate as a third ligand at lanthanum(III) and lutetium(III), the next logical step for us was to continue our salt metathesis study with a heavier chalcogenide analog such as potassium thiomesitolate (**KSMes**). Gratifyingly, the reaction between **1-La** and **KSMes** proceeded as smoothly as previously observed for the mesitolate ligand resulting in the formation of the desired complex **5-La** in quantitative yields. However, performing the reaction with **1-Lu** and equimolar amounts as well as 1.5 equiv of **KSMes** at room temperature, we only have been able to reisolate the starting materials. Heating the reaction mixture to 50 °C only resulted in small conversions and decomposition of the starting materials. Therefore, we decided to switch to the iodide complex **2-Lu** as precursor complex, since the precipitation of potassium iodide is thermodynamically much more favored compared to that of potassium chloride. Additionally, we decided to use an excess (1.5 equiv) of **KSMes** to further push the equilibrium toward the desired reaction products. With these adjustments the reaction was found to proceed cleanly under full conversion to complex **5-Lu** at room temperature overnight. The product could be isolated after removal of toluene in vacuo and recrystallization from *n*-hexane in a yield of 44%. Formation of the desired complexes **5-La** and **5-Lu** was evident by several features in their NMR spectra: (i) the appearance of a new set of mesityl resonances in the ^{1}H and ^{13}C{^{1}H} NMR spectra, (ii) the shift of the characteristic aryl proton of the PN ligand from δ 5.65 and δ 5.84 ppm for **1-La** and **2-Lu** to δ 5.68 and δ 5.90 ppm for **5-La** and **5-Lu**, and (iii) the shift of the phosphorus resonances in the ^{31}P{^{1}H} NMR spectra from δ 9.2 and δ 6.6 ppm for **1-La** and **2-Lu** to δ 10.0 and δ 4.8 ppm for **5-La** and **5-Lu**. Unambiguous proof of the formation of the desired complexes was delivered by X-ray diffraction analysis (Figure 5, right). Complex **5-La** forms X-ray quality crystals by slow evaporation of a concentrated diethyl ether solution at room temperature and crystallizes in the triclinic space group $P\bar{1}$. X-ray quality crystals of **5-Lu** have been obtained by storing a *n*-hexane solution with minimal amounts of toluene at room temperature with the complex crystallizing in the monoclinic space group $P2_1/c$. It is noteworthy at this point, that **5-Lu** is the first structurally characterized lutetium thiolate complex reported so far. Both complexes crystallize with one formula unit in the asymmetric unit and without any additional solvent molecules in the lattice. Similar to the complexes **4-La** and **4-Lu**, the metal–PN ligand distances remain mostly unaffected by the ligand exchange reaction from halide to thiomesitolate. However, the twisting angle of the PN ligands changes again significantly to 54.7(1) and 33.9(1)° in **5-La** and **5-Lu**, respectively. This also results in a change of the τ_5 values to 0.918 and 0.708 which describe the coordination environments as distorted trigonal bipyramidal comparable to previous compounds (vide supra). The metal–sulfur distances were found to be 2.718(2) Å in **5-La** and 2.544(2) Å in **5-Lu**, which in the case of lanthanum is comparable to previously reported thiolate complexes.[126−129] The angles around the sulfur atoms are more acute compared to the oxygen analogs **4-La** and **4-Lu**, displaying a Ln1–S70–C70 angle of 145.8(1) and 137.8(2)° for **5-La** and **5-Lu**, respectively.

Switching from chalcogenide donors to pnictide donors, we have performed the reaction between the chloride complexes **1-La** as well as **1-Lu** and the lithium salt of mesitylamine **LiNHMes** in toluene, respectively. It is noteworthy at this point that we found the use of the lithium salt to be superior

https://dx.doi.org/10.1021/acs.inorgchem.9b03071
Inorg. Chem. 2020, 59, 2719−2732

Inorganic Chemistry pubs.acs.org/IC Article

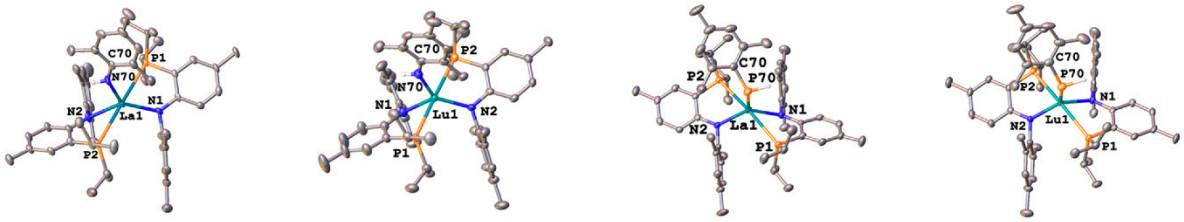

Figure 6. ORTEP plots of the pnictide complexes **6-La/Lu** and **7-La/Lu** (from left to right). Thermal ellipsoids are shown at a probability level of 30%. Hydrogen atoms and solvent molecules have been omitted for clarity.

over the use of the potassium salt **KNHMes**, as the use of **KNHMes** resulted in the formation of unexpected side products which cannot be easily removed. Formation of the desired complexes **6-La** and **6-Lu** was again evident by several features in their NMR spectra: (i) the appearance of a new set of mesityl resonances in the ^{1}H and ^{13}C{^{1}H} NMR spectra, (ii) the appearance of a new singlet in the ^{1}H NMR spectrum at δ 5.60 and δ 5.32 ppm for **6-La** and **6-Lu**, corresponding to the NH group of the mesitylamide ligand, (iii) the shift of the characteristic aryl proton of the PN ligand from δ 5.65 and δ 5.85 ppm for **1-La** and **1-Lu** to δ 5.81 and δ 6.01 ppm for **6-La** and **6-Lu**, and (iv) the shift of the phosphorus resonances in their ^{31}P{^{1}H} NMR spectra from δ 9.2 and δ 5.0 ppm for **1-La** and **1-Lu** to δ 9.5 and δ 1.8 ppm for **6-La** and **6-Lu**. The identities of the singlets at δ 5.60 and δ 5.32 ppm in the ^{1}H NMR spectra were furthermore supported by the observation of a cross peak in the ^{1}H−^{15}N HMBC NMR spectra of these complexes at 5.60/195.1 ppm for **6-La** and 5.32/172.1 ppm for **6-Lu**, respectively (compare Figure S76 and S82). These cross peaks also showed a doublet structure resulting from the strong coupling of the NH protons with the corresponding nitrogen atoms ($^{1}J_{NH}$ = 56 Hz for **6-La** and $^{1}J_{NH}$ = 49 Hz for **6-Lu**). Additionally, the presence of the NH group was supported by the presence of characteristic NH absorption bands in the IR spectra of the complexes at ν 3309 cm^{-1} and ν 3311 cm^{-1} for **6-La** and **6-Lu**, respectively. Formation of the desired complexes **6-La** and **6-Lu** was finally proven by X-ray crystallography (Figure 6, left). Crystals suitable for X-ray diffraction studies have been obtained by slow evaporation of a concentrated solution of diethyl ether for **6-La** and by gas diffusion of *n*-hexane into a concentrated solution of **6-Lu** in diethyl ether, both at room temperature. Both complexes crystallize isostructurally in the triclinic space group $P\bar{1}$ with two formula units and two molecules of diethyl ether in the asymmetric unit. The diethyl ether molecules in **6-Lu** were found to be strongly disordered, therefore they have been removed using the SQUEEZE operation.[130] Similar to the mesitolate and thiomesitolate complexes **4-La**, **4-Lu**, **5-La**, and **5-Lu**, the lanthanide−PN ligand distances remain mostly unaffected by the exchange of the halide vs mesitylamide, whereas the twisting of the PN ligands is strongly influenced and changing to 46.8(1)° in **6-La** and 45.9(1)° in **6-Lu**. In contrast, the lanthanide atoms are now coordinated in an almost ideal trigonal bipyramidal fashion, with the complexes displaying τ_5 values of 0.96 and 0.981 for **6-La** and **6-Lu**. The lanthanide−nitrogen distances Ln1−N70 were found to be 2.338(5) and 2.166(4) Å in **6-La** and **6-Lu** and the nitrogen atoms where found to be strongly depyramidalized, displaying a Ln1−N70−C70 angle of 149.2(4) and 146.4(3)° in **6-La** and **6-Lu**, respectively.

In the last consequence, completing our survey of chalcogenide and pnictide ligands, we aimed for the synthesis of the corresponding primary phosphido complexes **7-La** and **7-Lu**. While the reaction to **7-La** was found to proceed in a straightforward manner by mixing **1-La** with **KPHMes** in toluene and stirring overnight at room temperature, during the preparation of **7-Lu** we have observed similar issues when starting from **1-Lu** as already reported for the thiolate complex **5-Lu** (vide supra). Gratifyingly, switching to the iodide precursor **2-Lu** the reaction with **KPHMes** in toluene at room temperature proceeded under full and smooth conversion to the desired phosphido complex **7-Lu**. While secondary phosphido complexes have been reported earlier,[131−151] **7-La** and **7-Lu** are, to the best of our knowledge, the first primary phosphido complexes of lanthanum and lutetium so far, while the overall number of structurally characterized lanthanide complexes with primary phosphido ligands spans only four complexes to date.[152−155] Successful formation of the complexes and the presence of a PH bond was confirmed by several spectroscopic features: (i) the appearance of a new doublet in the ^{1}H NMR spectra at δ 3.42 ppm ($^{1}J_{PH}$ = 198.9 Hz) for **7-La** and at δ 3.43 ppm ($^{1}J_{PH}$ = 209.5 Hz) for **7-Lu**, corresponding to the introduced PH group, (ii) the presence of a doublet in the ^{31}P NMR spectra at δ −36.4 ppm ($^{1}J_{PH}$ = 198.9 Hz) for **7-La** and at δ −63.8 ppm ($^{1}J_{PH}$ = 209.5 Hz) for **7-Lu**, corresponding to the introduced PH group, and (iii) the appearance of a distinctive new absorption band in the IR spectra at ν 2294 and ν 2306 cm^{-1} for **7-La** and **7-Lu**, respectively.[156−162] Interestingly, in the case of **7-Lu** an additional coupling between the chemically inequivalent groups of phosphorus atoms (PN ligands vs phosphido ligand) was observed ($^{2}J_{PP}$ = 32.3 Hz) (see Figure S93 and S94 and the Experimental Section in the Supporting Information), further indicating the more compact arrangement of the ligands around lutetium compared to lanthanum (vide supra). Unambiguous proof for the formation of the new phosphido complexes was given by X-ray diffraction analysis (Figure 6, right). X-ray quality crystals were obtained by slow evaporation of a *n*-hexane solution at room temperature for **7-La** and by storing an oversaturated toluene solution (obtained during workup, see Experimental Section) at room temperature for several days in the case of **7-Lu**. While **7-La** crystallizes without any additional solvent molecules in the lattice, **7-Lu** was found to crystallize as its toluene solvate. The complexes crystallize in the monoclinic space groups $P2_1/n$ and $P2_1/c$ for **7-La** and **7-Lu**, respectively. In accordance with our previous observations for the mesitolate, thiomesitolate and mesitylamide complexes **4-Ln**, **5-Ln** and **6-Ln**, the influence of the phosphido ligand on the bond metrics of the PN ligand remain small. However, the twisting of the PN

https://dx.doi.org/10.1021/acs.inorgchem.9b03071
Inorg. Chem. 2020, 59, 2719−2732

Inorganic Chemistry pubs.acs.org/IC Article

Scheme 4. Synthetic Route to Mono Anilidophosphine Complexes 8-La/Ce Following a Protonolysis Reaction between HPN and Ln(HMDS)$_3$

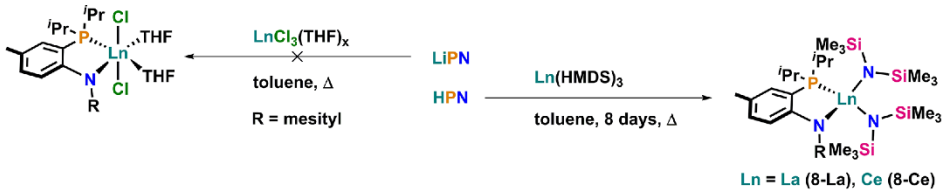

ligands is again strongly influenced with a twisting angle of 38.8(1)° in **7-La** and 33.6(1)° in **7-Lu** (compared to 44.4(1)° in **1-La** and 37.4(1)° in **1-Lu**) which results in a distorted trigonal bipyramidal coordination environment around the lanthanide atoms, displaying τ_5 values of 0.821 and 0.705 for **7-La** and **7-Lu**. The lanthanide−phosphide bond lengths Ln1−P70 were found to be 3.053(1) and 2.735(1) Å for **7-La** and **7-Lu**, respectively and are only about 0.08 Å (**7-La**) and 0.15 Å (**7-Lu**) shorter than the distances to the tertiary phosphine donors of the PN ligand. One striking feature in the structure of **7-La**, which is worth pointing out, is the relatively short distance between the phosphide phosphorus atom P70 and one of the ortho CH_3 carbon atoms of the mesityl group in the PN ligand, with only 3.874(1) Å in **7-La** combined with the pyramidalization at P70 ($\Sigma\angle$ = 309°) and the orientation of the P atom lone pair toward this carbon atom. A similar constellation has been observed in the past for bis-NHC thorium phosphido complexes which have been shown to be active in hydrophosphination catalysis with a C−H bond activation as a crucial step in the catalytic cycle.[156] Additionally, the authors reported a relatively rare, but indicative, $^{31}P-^{13}C$ through space coupling which we were not able to observe for **7-La**. In our case, substantial line broadening in our $^{13}C\{^1H\}$ NMR spectra due to rotational barriers prevented us to observe a possible $^{31}P-^{13}C$ through space coupling. To clarify the situation, we also measured a $^{31}P-^{1}H$ HMBC spectrum for **7-La** (see Figure S90). However, also in this spectrum we have not been able to observe any hints toward an interaction between the mesityl ortho CH_3 group and the phosphido ligand. Nevertheless, such couplings are rare and the structural relation between the literature known thorium phosphido and our complexes might point to a potential application of these complexes in hydrophosphination catalysis.

Lanthanide(III) Complexes Featuring One PN Ligand. After having accomplished the synthesis and characterization of various lanthanide(III) complexes featuring two PN ligands and having positively demonstrated that these are valuable precursors for further (salt metathesis) reactions, we were also interested, if it would be possible to obtain complexes that bear a single PN ligand. Complexes of the general formula **Ln(PN)X$_2$** (with X = halide or amide) would be interesting precursor molecules giving rise to a plethora of possible new reactions and catalytic applications of these species. In our first attempt, we have sought out for a simple salt metathesis protocol as this worked well for complexes of the general formula **Ln(PN)$_2$X** (vide supra). However, using the same conditions as for the syntheses of **1-Ln**, i. e. refluxing **LaCl$_3$(THF)$_x$** in toluene in the presence of 1 equiv of **LiPN**, we have not been able to obtain any useful products (Scheme 4, left). Instead, an inseparable mixture of compounds was obtained, of which we were only able to identify **1-La** as a minor side product. A change to more coordinating solvents such as THF or 1,2-dimethoxyethane (DME) did not lead to an improved selectivity and we have not been able to isolate analytically pure complexes by adapting this method. As an alternative to salt metathesis reactions we envisaged that protonolysis reactions might be more successful. Schelter and co-workers have recently reported on the synthesis of cerium(III) complexes featuring pincer type PNP ligands using a protonolysis reaction between **H(PNP)** and **Ce(HMDS)$_3$** in toluene at 100 °C for 1 week.[109] Using similar conditions for the bidentate PN ligand system, we also found that the desired complexes **8-La** and **8-Ce** can be obtained after long reaction times of 1 week at 120 °C in toluene (Scheme 4, right). It is noteworthy, that the prolonged heating is absolutely necessary as the reaction proceeds very slowly and takes a long time to be complete. The pure products can then be obtained by recrystallization of the bulk material from a concentrated *n*-pentane or *n*-hexane solution in the presence of residual toluene from the reaction (0.3 mmol in 3 mL *n*-hexane for **8-La**; 0.3 mmol in 3 mL *n*-pentane for **8-Ce**) at −40 °C, respectively. Formation of the desired complexes **8-La** and **8-Ce** is clear from several indicators: (i) the disappearance of the characteristic ^{31}P resonance of **HPN** at δ −17.4 ppm with the concomitant observation of a new resonance at δ 10.2 ppm for **8-La** and at δ 383.3 ppm for **8-Ce**, (ii) the observation of a singlet at δ 0.29 and δ −5.85 ppm in the ^1H NMR spectra of **8-La** and **8-Ce**, corresponding to a total of 36 HMDS protons, respectively, and (iii) a significant shift of the characteristic proton resonance of the tolyl unit in the PN ligand from δ 6.28 ppm in **HPN** to δ 5.84 ppm for **8-La** and to δ 18.7 ppm for **8-Ce**. The purification method described above also yielded X-ray quality crystals of both complexes **8-La** and **8-Ce** (Figure 7). Both complexes crystallize isostructurally in the monoclinic space group $P2_1/n$ with one complex molecule in the asymmetric unit. The lanthanide atoms are four-coordinate in a distorted tetrahedral fashion (τ_4' = 0.688 and 0.67 for **8-La** and **8-Ce**, respectively). The Ln−P distances were found to be slightly longer than in the bis-PN ligated complexes **1-La** and **1-Ce**, displaying Ln1−P1 distances of 3.243(1) and 3.187(1) Å in **8-La** and **8-Ce**. Thereby, the Ce−P distances are slightly longer than in previously reported Ce(III) phosphine complexes,[163,164] but are in the same range as the recently reported complexes by Schelter et al.[109] A similar elongation is also observed for the Ln1−N1 bonds from 2.373(3) Å in **1-La** to 2.436(3) Å in **8-La** and from 2.333(3) Å in **1-Ce** to 2.408(4) Å in **8-Ce**. The distances of the lanthanide atom to the silylamide nitrogen atoms in **8-La** and **8-Ce** are in the range of previously reported **Ln(HMDS)$_x$** complexes.[109,165−169] For further crystallographic information see the Supporting Information, Tables S1−S5.

https://dx.doi.org/10.1021/acs.inorgchem.9b03071
Inorg. Chem. 2020, 59, 2719−2732

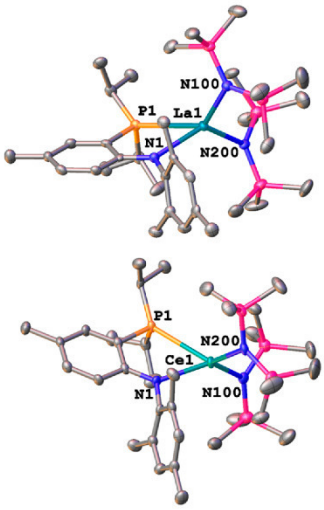

Figure 7. ORTEP plots of the complexes **8-La** (top) and **8-Ce** (bottom). Thermal ellipsoids are shown at a probability level of 30%. Hydrogen atoms have been omitted for clarity.

^{31}P NMR Spectroscopic Investigations of 1-Ce and 8-Ce. ^{31}P NMR spectroscopy can often be used to obtain further insights into the solution behavior of paramagnetic lanthanide complexes. Therefore, we employed ^{31}P NMR spectroscopy to elucidate the electronic and steric properties of our new cerium(III) complexes in solution. The paramagnetic nature of the cerium atom in **1-Ce** and **8-Ce** caused an immense low-field shift of the ^{31}P NMR resonance to δ 426.7 ppm in **1-Ce** and to δ 383.3 ppm in **8-Ce** compared to parent **HPN** (δ −17.4 ppm) or the corresponding diamagnetic lanthanum complexes **1-La** (δ 9.2 ppm) or **8-La** (δ 10.2 ppm). All these values were obtained in noncoordinating benzene (C_6D_6) solutions. To further probe the solution behavior and possibly accessible coordination sites in the complexes, we have also measured ^{31}P NMR spectra in coordinating solvents such as THF-d_8. While for the cerium complex holding two PN ligands **1-Ce**, the switch to a coordinating solvent had only a minor impact on the chemical shift of the phosphorus resonance (δ 426.7 ppm in C_6D_6 to δ 423.2 ppm in THF-d_8, see also Figure S29 and S30), for the mono-PN system **8-Ce** a more pronounced dependency was observed. The ^{31}P NMR spectrum of **8-Ce** in THF-d_8 shows two resonances at δ 386.1 and δ 365.5 ppm compared to only one resonance in C_6D_6 at δ 383.3 ppm (compare Figures S107 and S108). The second resonance at δ 365.5 ppm most likely results from coordination of THF to the cerium atom; however the THF coordinated complex seems to be in equilibrium with **8-Ce**. The reduced steric profile of complex **8-Ce** in comparison to **1-Ce** could serve as a plausible explanation for the different behavior of the two cerium complexes. A second explanation of the two ^{31}P NMR shifts for **8-Ce** in THF-d_8 could also be that the initial complex forms a mono- as well as a bis-THF adduct with the general formulas $\mathbf{Ce(PN)(HMDS)_2(THF)}_n$ (n = 1, 2). Unfortunately, we have not been able to study this behavior in more detail, since we have observed that **8-Ce** is unstable in THF-d_8 with protonolysis of the complex occurring already after 1 h at room temperature. The intolerance of some of our PN complexes toward coordinating solvents has already been mentioned in the paragraph concerning the synthesis of the complexes featuring two PN ligands (vide supra). Furthermore, Schelter and co-workers have recently shown,[109] that there is a positive linear correlation between the ^{31}P chemical shift and the Ce−P distance in the molecular structures in their cerium PNP complexes. Fitting our new data into this correlation it becomes obvious that, although there is a deterioration of the fit, a good approximation of the Ce−P distance is also possible for other P(^{i}Pr)$_2$ containing ligands (see Supporting Information, Figure S131).

Electrochemical Investigations of 1-Ce and 8-Ce. It has previously been reported that the PNP ligand framework inherently stabilizes the cerium(III) ion and no cerium(III/IV) redox couple could be observed.[109] Inspired by this observation, we became interested if a bidentate PN ligand would offer the possibility of isolating a cerium(IV) complex or also inherently stabilize the cerium(III) oxidation state. Therefore, we recorded the cyclic voltammograms (CVs) of both complexes **1-Ce** and **8-Ce** and compared the results to the CVs of the corresponding lanthanum complexes **1-La** and **8-La**, containing the redox innocent lanthanum(III) ions (Figure 8). For the systems with one anilidophosphine ligand, **8-La** and **8-Ce**, we observed only one single irreversible oxidation with a peak potential at +0.39 V vs Fc/[Fc]$^+$ in each case. This clearly indicates that the oxidation is ligand centered, as has also been observed in the examples by Schelter et al. Moving on to the systems containing two anilidophosphine ligands, **1-La** and **1-Ce**, both CVs were

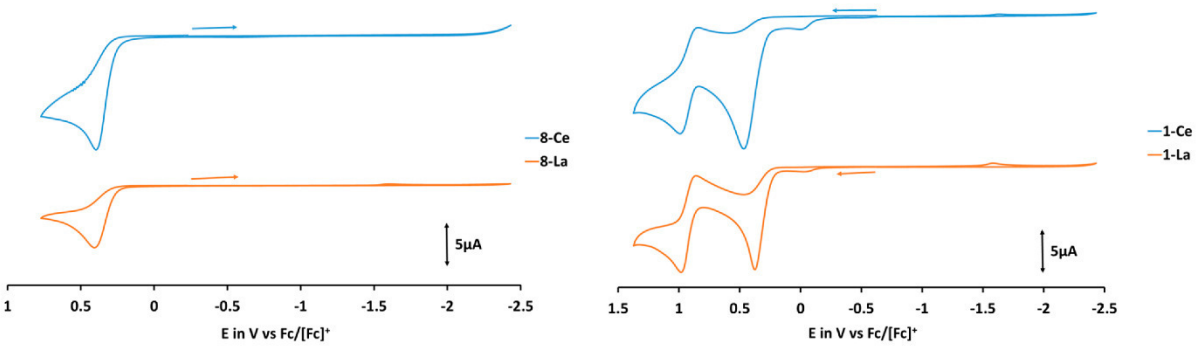

Figure 8. Cyclic voltammograms of **8-Ce**/**8-La** (left) and **1-Ce**/**1-La** (right) measured in 0.1 M [NBu_4][PF_6] in dichloromethane at room temperature. Scan rate: 100 mV·s^{-1}.

https://dx.doi.org/10.1021/acs.inorgchem.9b03071
Inorg. Chem. 2020, 59, 2719−2732

found to be identical as well, showing an irreversible oxidation at a peak potential of +0.39 V vs $Fc/[Fc]^+$ for **1-La** and of +0.46 V vs $Fc/[Fc]^+$ for **1-Ce** as well as a quasi-reversible oxidation wave centered at +0.91 V vs $Fc/[Fc]^+$ for both **1-La** and **1-Ce**. The close proximity of the first oxidation process of **1-La** and **1-Ce** to the one observed for the mono-PN ligated systems **8-La** and **8-Ce** further substantiates the notion of a ligand centered oxidation. The fact that the second oxidation occurs at the same potential for both **1-La** and **1-Ce** leads us to the assumption that also the second oxidation is ligand centered instead of metal centered. Since all CVs show identical processes, but no unequivocally assignable Ce(III/IV) redox couples, we believe that the chances of isolating a cerium(IV) complex using anilidophosphine ligands are rather small.

■ CONCLUSION

In summary, we have presented the synthesis and reactivity of a series of new lanthanide(III) complexes featuring either one or two anilidophosphine (PN) ligands. This ligand class seems to be applicable over the full range of the lanthanide series. In our comprehensive study, we have been able to show that the chloride and iodide complexes **1-Ln** and **2-Ln** (**Ln** = **La**, **Lu**) with two PN ligands are valuable starting materials leading to further functionalized metal complexes. We could further demonstrate that the functionalization strongly depends on the steric demand of the introduced ligands, indicating an extensive steric shielding of the central ions by the two PN ligands, which also gives a perspective for the isolation of complexes with lanthanide−ligand double bonds in the future. The steric shielding has furthermore been proven by the NMR experiments carried out for **1-Ce** in coordinating and noncoordinating solvents, in which cases almost identical ^{31}P chemical shifts were observed. We have been able to isolate a series of aryl chalcogenide and aryl pnictide functionalized metal complexes including the isolation and structural characterization of rare thiolato and primary phosphido complexes of lanthanum and lutetium. Furthermore, we have investigated the influence of the PN ligand on the cerium(III/IV) redox couple in **1-Ce** and **8-Ce** and found that, in agreement with a previous report by Schelter et al., phosphorus containing ligands lead to an inherent stabilization of the +III oxidation state. In the future, we will focus on exploring new reactivities with these systems including the reactivity toward even heavier chalcogenide/pnictide ligands, the reactivity of the lanthanide−phosphide bond, and the ability of stabilizing lanthanide complexes featuring lanthanide−ligand multiple bonds.

■ ASSOCIATED CONTENT

Supporting Information

The Supporting Information is available free of charge at https://pubs.acs.org/doi/10.1021/acs.inorgchem.9b03071.

Detailed experimental section, all NMR data, IR data, and crystallographic details, the molecular structures of the halide complexes, as well as the correlation between the ^{31}P NMR shifts, and the atomic Ce−P distances in all cerium complexes described (PDF)

Accession Codes

CCDC 1942368−1942379, 1942581, 1943224, 1946545, 1950170−1950171, 1954491, and 1957703−1957704 contain the supplementary crystallographic data for this paper. These data can be obtained free of charge via www.ccdc.cam.ac.uk/data_request/cif, or by emailing data_request@ccdc.cam.ac.uk, or by contacting The Cambridge Crystallographic Data Centre, 12 Union Road, Cambridge CB2 1EZ, UK; fax: +44 1223 336033.

■ AUTHOR INFORMATION

Corresponding Author

Stephan Hohloch − *Leopold-Franzens-University Innsbruck, Innsbruck, Austria;* orcid.org/0000-0002-5353-0801; Email: Stephan.Hohloch@uibk.ac.at

Other Authors

Fabian A. Watt − *Paderborn University, Paderborn, Germany*

Athul Krishna − *Paderborn University, Paderborn, Germany*

Grigoriy Golovanov − *Paderborn University, Paderborn, Germany*

Holger Ott − *Bruker AXS GmbH, Karlsruhe, Germany*

Roland Schoch − *Paderborn University, Paderborn, Germany*

Christoph Wölper − *University of Essen-Duisburg, Essen, Germany*

Adam G. Neuba − *Paderborn University, Paderborn, Germany*

Complete contact information is available at: https://pubs.acs.org/10.1021/acs.inorgchem.9b03071

Author Contributions

The project was designed by S.H. Experimental work was carried out by F.A.W., A.K., G.G., and S.H. NMR and IR spectra were recorded by F.A.W., A.K., and SH. CVs were measured by A.G.N. and plotted by S.H. X-ray structure analyses were performed by R.S., H.O., C.W., and S.H. The manuscript was written by S.H. and F.A.W. and proof read by all authors.

Notes

The authors declare no competing financial interest.

■ ACKNOWLEDGMENTS

We are grateful to the Daimler and Benz Foundation, to the Fonds der Chemischen Industrie, to the Young Academy of the North Rhine-Westphalian Academy of Sciences, Humanities and the Arts, and to the University of Paderborn for funding of this work. Prof. Dr. Matthias Bauer, Prof. Dr. Jan Paradies, and Prof. Dr. Thomas Kühne are acknowledged for helpful discussions. Jan Locher and Nicole Dickmann are kindly acknowledged for experimental help making multigrams of **LiPN**. Our special thanks goes also to Dr. Hans Egold from the NMR facility of the University of Paderborn. We are grateful to the vice rectorate for reseach of the University of Innsbruck for generous funding of this work.

■ REFERENCES

(1) Liddle, S. T. International Year of the Periodic Table: Lanthanide and Actinide Chemistry. *Angew. Chem., Int. Ed.* **2019**, *58*, 5140−5141.

(2) Kagan, H. B. Introduction: Frontiers in Lanthanide Chemistry. *Chem. Rev.* **2002**, *102*, 1805−1806.

https://dx.doi.org/10.1021/acs.inorgchem.9b03071
Inorg. Chem. 2020, 59, 2719−2732

(3) Piro, N. A.; Robinson, J. R.; Walsh, P. J.; Schelter, E. J. The electrochemical behavior of cerium(III/IV) complexes: Thermodynamics, kinetics and applications in synthesis. *Coord. Chem. Rev.* **2014**, *260*, 21−36.
(4) Bünzli, J.-C. G. Benefiting from the unique properties of lanthanide ions. *Acc. Chem. Res.* **2006**, *39*, 53−61.
(5) Bünzli, J.-C. G. Lanthanide luminescence for biomedical analyses and imaging. *Chem. Rev.* **2010**, *110*, 2729−2755.
(6) Jiang, J.; Ng, D. K. P. A decade journey in the chemistry of sandwich-type tetrapyrrolato-rare Earth complexes. *Acc. Chem. Res.* **2009**, *42*, 79−88.
(7) Rinehart, J. D.; Long, J. R. Exploiting single-ion anisotropy in the design of f-element single-molecule magnets. *Chem. Sci.* **2011**, *2*, 2078.
(8) Jahn, B.; Pol, A.; Lumpe, H.; Barends, T. R. M.; Dietl, A.; Hogendoorn, C.; Op den Camp, H. J. M.; Daumann, L. J. Similar but Not the Same: First Kinetic and Structural Analyses of a Methanol Dehydrogenase Containing a Europium Ion in the Active Site. *ChemBioChem* **2018**, *19*, 1147−1153.
(9) Lumpe, H.; Pol, A.; Op den Camp, H. J. M.; Daumann, L. J. Impact of the lanthanide contraction on the activity of a lanthanide-dependent methanol dehydrogenase - a kinetic and DFT study. *Dalton Trans.* **2018**, *47*, 10463−10472.
(10) McSkimming, A.; Cheisson, T.; Carroll, P. J.; Schelter, E. J. Functional Synthetic Model for the Lanthanide-Dependent Quinoid Alcohol Dehydrogenase Active Site. *J. Am. Chem. Soc.* **2018**, *140*, 1223−1226.
(11) Bao, G.; Wong, K.-L.; Jin, D.; Tanner, P. A. A stoichiometric terbium-europium dyad molecular thermometer: energy transfer properties. *Light: Sci. Appl.* **2018**, *7*, 96.
(12) Palumbo, C. T.; Zivkovic, I.; Scopelliti, R.; Mazzanti, M. Molecular Complex of Tb in the + 4 Oxidation State. *J. Am. Chem. Soc.* **2019**, *141*, 9827−9831.
(13) Rice, N. T.; Popov, I. A.; Russo, D. R.; Bacsa, J.; Batista, E. R.; Yang, P.; Telser, J.; La Pierre, H. S. Design, Isolation, and Spectroscopic Analysis of a Tetravalent Terbium Complex. *J. Am. Chem. Soc.* **2019**, *141*, 13222−13233.
(14) Trifonov, A. A.; Basalov, I. V.; Kissel, A. A. Use of organolanthanides in the catalytic intermolecular hydrophosphination and hydroamination of multiple C-C bonds. *Dalton Trans.* **2016**, *45*, 19172−19193.
(15) Weiss, C. J.; Marks, T. J. Organo-f-element catalysts for efficient and highly selective hydroalkoxylation and hydrothiolation. *Dalton Trans.* **2010**, *39*, 6576−6588.
(16) Edelmann, F. T. Lanthanide amidinates and guanidinates in catalysis and materials science: a continuing success story. *Chem. Soc. Rev.* **2012**, *41*, 7657−7672.
(17) Barger, C. J.; Motta, A.; Weidner, V. L.; Lohr, T. L.; Marks, T. J. La[N(SiMe 3) 2] 3 -Catalyzed Ester Reductions with Pinacolborane: Scope and Mechanism of Ester Cleavage. *ACS Catal.* **2019**, *9*, 9015−9024.
(18) Yin, H.; Carroll, P. J.; Manor, B. C.; Anna, J. M.; Schelter, E. J. Cerium Photosensitizers: Structure-Function Relationships and Applications in Photocatalytic Aryl Coupling Reactions. *J. Am. Chem. Soc.* **2016**, *138*, 5984−5993.
(19) Qiao, Y.; Yang, Q.; Schelter, E. J. Photoinduced Miyaura Borylation by a Rare-Earth-Metal Photoreductant: The Hexachlorocerate(III) Anion. *Angew. Chem., Int. Ed.* **2018**, *57*, 10999−11003.
(20) Qiao, Y.; Schelter, E. J. Lanthanide Photocatalysis. *Acc. Chem. Res.* **2018**, *51*, 2926−2936.
(21) Qiao, Y.; Cheisson, T.; Manor, B. C.; Carroll, P. J.; Schelter, E. J. A strategy to improve the performance of cerium(iii) photocatalysts. *Chem. Commun.* **2019**, *55*, 4067−4070.
(22) Pellissier, H. Recent developments in enantioselective lanthanide-catalyzed transformations. *Coord. Chem. Rev.* **2017**, *336*, 96−151.
(23) Birmingham, J. M.; Wilkinson, G. The Cyclopentadienides of Scandium, Yttrium and Some Rare Earth Elements. *J. Am. Chem. Soc.* **1956**, *78*, 42−44.
(24) Wilkinson, G.; Birmingham, J. M. CYCLOPENTADIENYL COMPOUNDS OF Sc, Y, La, Ce AND SOME LANTHANIDE ELEMENTS. *J. Am. Chem. Soc.* **1954**, *76*, 6210.
(25) Pugh, T.; Kerridge, A.; Layfield, R. A. Yttrium complexes of arsine, arsenide, and arsinidene ligands. *Angew. Chem., Int. Ed.* **2015**, *54*, 4255−4258.
(26) Day, B. M.; Guo, F.-S.; Giblin, S. R.; Sekiguchi, A.; Mansikkamäki, A.; Layfield, R. A. Rare-Earth Cyclobutadienyl Sandwich Complexes: Synthesis, Structure and Dynamic Magnetic Properties. *Chem. - Eur. J.* **2018**, *24*, 16779−16782.
(27) Day, B. M.; Guo, F.-S.; Layfield, R. A. Cyclopentadienyl Ligands in Lanthanide Single-Molecule Magnets: One Ring To Rule Them All? *Acc. Chem. Res.* **2018**, *51*, 1880−1889.
(28) Demir, S.; Boshart, M. D.; Corbey, J. F.; Woen, D. H.; Gonzalez, M. I.; Ziller, J. W.; Meihaus, K. R.; Long, J. R.; Evans, W. J. Slow Magnetic Relaxation in a Dysprosium Ammonia Metallocene Complex. *Inorg. Chem.* **2017**, *56*, 15049−15056.
(29) Demir, S.; Gonzalez, M. I.; Darago, L. E.; Evans, W. J.; Long, J. R. Giant coercivity and high magnetic blocking temperatures for N23- radical-bridged dilanthanide complexes upon ligand dissociation. *Nat. Commun.* **2017**, *8*, 2144.
(30) Demir, S.; Jeon, I.-R.; Long, J. R.; Harris, T. D. Radical ligand-containing single-molecule magnets. *Coord. Chem. Rev.* **2015**, *289*−*290*, 149−176.
(31) Demir, S.; Meihaus, K. R.; Long, J. R. Slow magnetic relaxation in a neodymium metallocene tetraphenylborate complex. *J. Organomet. Chem.* **2018**, *857*, 164−169.
(32) Demir, S.; Nippe, M.; Gonzalez, M. I.; Long, J. R. Exchange coupling and magnetic blocking in dilanthanide complexes bridged by the multi-electron redox-active ligand 2,3,5,6-tetra(2-pyridyl)pyrazine. *Chem. Sci.* **2014**, *5*, 4701−4711.
(33) Demir, S.; Zadrozny, J. M.; Nippe, M.; Long, J. R. Exchange coupling and magnetic blocking in bipyrimidyl radical-bridged dilanthanide complexes. *J. Am. Chem. Soc.* **2012**, *134*, 18546−18549.
(34) Goodwin, C. A. P.; Ortu, F.; Reta, D.; Chilton, N. F.; Mills, D. P. Molecular magnetic hysteresis at 60 K in dysprosocenium. *Nature* **2017**, *548*, 439−442.
(35) Goodwin, C. A. P.; Reta, D.; Ortu, F.; Chilton, N. F.; Mills, D. P. Synthesis and Electronic Structures of Heavy Lanthanide Metallocenium Cations. *J. Am. Chem. Soc.* **2017**, *139*, 18714−18724.
(36) Goodwin, C. A. P.; Reta, D.; Ortu, F.; Liu, J.; Chilton, N. F.; Mills, D. P. Terbocenium: completing a heavy lanthanide metallocenium cation family with an alternative anion abstraction strategy. *Chem. Commun.* **2018**, *54*, 9182−9185.
(37) Gould, C. A.; Darago, L. E.; Gonzalez, M. I.; Demir, S.; Long, J. R. A Trinuclear Radical-Bridged Lanthanide Single-Molecule Magnet. *Angew. Chem., Int. Ed.* **2017**, *56*, 10103−10107.
(38) Gould, C. A.; McClain, K. R.; Yu, J. M.; Groshens, T. J.; Furche, F.; Harvey, B. G.; Long, J. R. Synthesis and Magnetism of Neutral, Linear Metallocene Complexes of Terbium(II) and Dysprosium(II). *J. Am. Chem. Soc.* **2019**, *141*, 12967−12973.
(39) Guo, F.-S.; Chen, Y.-C.; Tong, M.-L.; Mansikkamäki, A.; Layfield, R. A. Uranocenium: Synthesis, Structure, and Chemical Bonding. *Angew. Chem., Int. Ed.* **2019**, *58*, 10163−10167.
(40) Guo, F.-S.; Day, B. M.; Chen, Y.-C.; Tong, M.-L.; Mansikkamäki, A.; Layfield, R. A. A Dysprosium Metallocene Single-Molecule Magnet Functioning at the Axial Limit. *Angew. Chem., Int. Ed.* **2017**, *56*, 11445−11449.
(41) Guo, F.-S.; Day, B. M.; Chen, Y.-C.; Tong, M.-L.; Mansikkamäki, A.; Layfield, R. A. Magnetic hysteresis up to 80 K in a dysprosium metallocene single-molecule magnet. *Science* **2018**, *362*, 1400−1403.
(42) Guo, F.-S.; Layfield, R. A. Strong direct exchange coupling and single-molecule magnetism in indigo-bridged lanthanide dimers. *Chem. Commun.* **2017**, *53*, 3130−3133.
(43) Liu, J.; Reta, D.; Cleghorn, J. A.; Yeoh, Y. X.; Ortu, F.; Goodwin, C. A. P.; Chilton, N. F.; Mills, D. P. Light Lanthanide Metallocenium Cations Exhibiting Weak Equatorial Anion Interactions. *Chem. - Eur. J.* **2019**, *25*, 7749−7758.

https://dx.doi.org/10.1021/acs.inorgchem.9b03071
Inorg. Chem. 2020, 59, 2719−2732

(44) Randall McClain, K.; Gould, C. A.; Chakarawet, K.; Teat, S. J.; Groshens, T. J.; Long, J. R.; Harvey, B. G. High-temperature magnetic blocking and magneto-structural correlations in a series of dysprosium(iii) metallocenium single-molecule magnets. *Chem. Sci.* **2018**, *9*, 8492−8503.
(45) Ortu, F.; Reta, D.; Ding, Y.-S.; Goodwin, C. A. P.; Gregson, M. P.; McInnes, E. J. L.; Winpenny, R. E. P.; Zheng, Y.-Z.; Liddle, S. T.; Mills, D. P.; Chilton, N. F. Studies of hysteresis and quantum tunnelling of the magnetisation in dysprosium(iii) single molecule magnets. *Dalton Trans.* **2019**, *48*, 8541−8545.
(46) Kilpatrick, A. F. R.; Guo, F.-S.; Day, B. M.; Mansikkamäki, A.; Layfield, R. A.; Cloke, F. G. N. Single-molecule magnet properties of a monometallic dysprosium pentalene complex. *Chem. Commun.* **2018**, *54*, 7085−7088.
(47) Ward, A. L.; Buckley, H. L.; Lukens, W. W.; Arnold, J. Synthesis and characterization of thorium(IV) and uranium(IV) corrole complexes. *J. Am. Chem. Soc.* **2013**, *135*, 13965−13971.
(48) Stradiotto, M.; Lundgren, R. *Ligand design in metal chemistry: Reactivity and catalysis*; Wiley: Chichester, West Sussex, U.K., 2016.
(49) Lu, G.; Yan, S.; Shi, M.; Yu, W.; Li, J.; Zhu, W.; Ou, Z.; Kadish, K. M. A new class of rare earth tetrapyrrole sandwich complexes containing corrole and phthalocyanine macrocycles: synthesis, physicochemical characterization and X-ray analysis. *Chem. Commun.* **2015**, *51*, 2411−2413.
(50) Buckley, H. L.; Anstey, M. R.; Gryko, D. T.; Arnold, J. Lanthanide corroles: a new class of macrocyclic lanthanide complexes. *Chem. Commun.* **2013**, *49*, 3104−3106.
(51) Boreen, M. A.; Parker, B. F.; Hohloch, S.; Skeel, B. A.; Arnold, J. f-Block complexes of a m-terphenyl dithiocarboxylate ligand. *Dalton Trans.* **2018**, *47*, 96−104.
(52) Armstrong, K. C.; Hohloch, S.; Lohrey, T. D.; Zarkesh, R. A.; Arnold, J.; Anstey, M. R. Control of clustering behavior in anionic cerium(iii) corrole complexes: from oligomers to monomers. *Dalton Trans.* **2016**, *45*, 18653−18660.
(53) Alexander, V. Design and Synthesis of Macrocyclic Ligands and Their Complexes of Lanthanides and Actinides. *Chem. Rev.* **1995**, *95*, 273−342.
(54) van der Vlugt, J. I.; Reek, J. N. H. Neutral tridentate PNP ligands and their hybrid analogues: versatile non-innocent scaffolds for homogeneous catalysis. *Angew. Chem., Int. Ed.* **2009**, *48*, 8832−8846.
(55) Benito-Garagorri, D.; Wiedermann, J.; Pollak, M.; Mereiter, K.; Kirchner, K. Iron(II) Complexes Bearing Tridentate PNP Pincer-Type Ligands as Catalysts for the Selective Formation of 3-Hydroxyacrylates from Aromatic Aldehydes and Ethyldiazoacetate. *Organometallics* **2007**, *26*, 217−222.
(56) Arce, P.; Vera, C.; Escudero, D.; Guerrero, J.; Lappin, A.; Oliver, A.; Jara, D. H.; Ferraudi, G.; Lemus, L. Structural diversity in Cu(i) complexes of the PNP ligand: from pincer to binuclear coordination modes and their effects upon the electrochemical and photophysical properties. *Dalton Trans.* **2017**, *46*, 13432−13445.
(57) Zhu, Y.; Fan, L.; Chen, C.-H.; Finnell, S. R.; Foxman, B. M.; Ozerov, O. V. C−H Oxidative Addition to a (PNP)Ir Center and Ligand-Induced Reversal of Benzyl/Aryl Selectivity. *Organometallics* **2007**, *26*, 6701−6703.
(58) Mossin, S.; Tran, B. L.; Adhikari, D.; Pink, M.; Heinemann, F. W.; Sutter, J.; Szilagyi, R. K.; Meyer, K.; Mindiola, D. J. A mononuclear Fe(III) single molecule magnet with a 3/2↔5/2 spin crossover. *J. Am. Chem. Soc.* **2012**, *134*, 13651−13661.
(59) Hounjet, L. J.; Adhikari, D.; Pink, M.; Carroll, P. J.; Mindiola, D. J. Synthesis of an Iron(II) Ethyl Complex Accompanied by Formation of an Unusual Dinitrogen-Ligated Iron(I) Hydride. *Z. Anorg. Allg. Chem.* **2015**, *641*, 45−48.
(60) Gatard, S.; Guo, C.; Foxman, B. M.; Ozerov, O. V. Thioether, Dinitrogen, and Olefin Complexes of (PNP)Rh: Kinetics and Thermodynamics of Exchange and Oxidative Addition Reactions. *Organometallics* **2007**, *26*, 6066−6075.
(61) Ozerov, O. V. Rigid PNP pincer ligands and their transition metal complexes. *The chemistry of pincer compounds* **2007**, 287−309.
(62) *The chemistry of pincer compounds*; Morales-Morales, D.; Jensen, C. M., Eds.; Elsevier: Amsterdam and Oxford, U.K., 2007.
(63) Bailey, B. C.; Huffman, J. C.; Mindiola, D. J.; Weng, W.; Ozerov, O. V. Remarkably Stable Titanium Complexes Containing Terminal Alkylidene, Phosphinidene, and Imide Functionalities. *Organometallics* **2005**, *24*, 1390−1393.
(64) Fafard, C. M.; Adhikari, D.; Foxman, B. M.; Mindiola, D. J.; Ozerov, O. V. Addition of ammonia, water, and dihydrogen across a single Pd-Pd bond. *J. Am. Chem. Soc.* **2007**, *129*, 10318−10319.
(65) Kurogi, T.; Carroll, P. J.; Mindiola, D. J. A Terminally Bound Niobium Methylidyne. *J. Am. Chem. Soc.* **2016**, *138*, 4306−4309.
(66) Kurogi, T.; Pinter, B.; Mindiola, D. J. Methylidyne Transfer Reactions with Niobium. *Organometallics* **2018**, *37*, 3385−3388.
(67) Kilgore, U. J.; Yang, X.; Tomaszewski, J.; Huffman, J. C.; Mindiola, D. J. Activation of atmospheric nitrogen and azobenzene N = N bond cleavage by a transient Nb(III) complex. *Inorg. Chem.* **2006**, *45*, 10712−10721.
(68) DeMott, J. C.; Basuli, F.; Kilgore, U. J.; Foxman, B. M.; Huffman, J. C.; Ozerov, O. V.; Mindiola, D. J. Silver(I) and thallium(I) complexes of a PNP ligand and their utility as PNP transfer reagents. *Inorg. Chem.* **2007**, *46*, 6271−6276.
(69) Kilgore, U. J.; Tomaszewski, J.; Fan, H.; Huffman, J. C.; Mindiola, D. J. Niobium Bis-alkylidene Complexes Prepared by a Multi-Electron Redox Process. *Organometallics* **2007**, *26*, 6132−6138.
(70) Kurogi, T.; Carroll, P. J.; Mindiola, D. J. A radical coupled pathway to a stable and terminally bound titanium methylidene. *Chem. Commun.* **2017**, *53*, 3412−3414.
(71) Lagaditis, P. O.; Schluschaß, B.; Demeshko, S.; Würtele, C.; Schneider, S. Square-Planar Cobalt(III) Pincer Complex. *Inorg. Chem.* **2016**, *55*, 4529−4536.
(72) Askevold, B.; Khusniyarov, M. M.; Kroener, W.; Gieb, K.; Müller, P.; Herdtweck, E.; Heinemann, F. W.; Diefenbach, M.; Holthausen, M. C.; Vieru, V.; Chibotaru, L. F.; Schneider, S. Square-planar ruthenium(II) complexes: control of spin state by pincer ligand functionalization. *Chem. - Eur. J.* **2015**, *21*, 579−589.
(73) Alig, L.; Fritz, M.; Schneider, S. First-Row Transition Metal (De)Hydrogenation Catalysis Based On Functional Pincer Ligands. *Chem. Rev.* **2019**, *119*, 2681−2751.
(74) DeMott, J. C.; Guo, C.; Foxman, B. M.; Yandulov, D. V.; Ozerov, O. V. Five-coordinate aluminum complexes of a PNP ligand. *Mendeleev Commun.* **2007**, *17*, 63−65.
(75) Henning, J.; Schubert, H.; Eichele, K.; Winter, F.; Pöttgen, R.; Mayer, H. A.; Wesemann, L. Synthesis and characterization of N-2-P(i-Pr)2−4-methylphenyl2- (PNP) pincer tin(IV) and tin(II) complexes. *Inorg. Chem.* **2012**, *51*, 5787−5794.
(76) Herbert, D. E.; Miller, A. D.; Ozerov, O. V. Phosphorus(III) cations supported by a PNP pincer ligand and sub-stoichiometric generation of P4 from thermolysis of a nickel insertion product. *Chem. - Eur. J.* **2012**, *18*, 7696−7704.
(77) Calimano, E.; Tilley, T. D. Synthesis and structure of PNP-supported iridium silyl and silylene complexes: catalytic hydrosilation of alkenes. *J. Am. Chem. Soc.* **2009**, *131*, 11161−11173.
(78) Brammell, C. M.; Pelton, E. J.; Chen, C.-H.; Yakovenko, A. A.; Weng, W.; Foxman, B. M.; Ozerov, O. V. Hafnium alkyl complexes of the anionic PNP pincer ligand and possible alkylidene formation. *J. Organomet. Chem.* **2011**, *696*, 4132−4137.
(79) Pell, C. J.; Zhu, Y.; Huacuja, R.; Herbert, D. E.; Hughes, R. P.; Ozerov, O. V. Fluorocarbene, fluoroolefin, and fluorocarbyne complexes of Rh. *Chem. Sci.* **2017**, *8*, 3178−3186.
(80) Scheibel, M. G.; Askevold, B.; Heinemann, F. W.; Reijerse, E. J.; de Bruin, B.; Schneider, S. Closed-shell and open-shell square-planar iridium nitrido complexes. *Nat. Chem.* **2012**, *4*, 552−558.
(81) Solowey, D. P.; Kurogi, T.; Manor, B. C.; Carroll, P. J.; Mindiola, D. J. Metallo-Wittig chemistry of an alkylidene to form a terminal titanium oxo complex. *Dalton Trans.* **2016**, *45*, 15894−15901.
(82) Weng, W.; Yang, L.; Foxman, B. M.; Ozerov, O. V. Chelate-Enforced Phosphine Coordination Enables α-Abstraction to Give Zirconium Alkylidenes. *Organometallics* **2004**, *23*, 4700−4705.

https://dx.doi.org/10.1021/acs.inorgchem.9b03071
Inorg. Chem. 2020, 59, 2719−2732

(83) Schendzielorz, F. S.; Finger, M.; Volkmann, C.; Würtele, C.; Schneider, S. A Terminal Osmium(IV) Nitride: Ammonia Formation and Ambiphilic Reactivity. *Angew. Chem., Int. Ed.* **2016**, *55*, 11417−11420.
(84) Abbenseth, J.; Diefenbach, M.; Hinz, A.; Alig, L.; Würtele, C.; Goicoechea, J. M.; Holthausen, M. C.; Schneider, S. Oxidative Coupling of Terminal Rhenium Pnictide Complexes. *Angew. Chem., Int. Ed.* **2019**, *58*, 10966−10970.
(85) Delony, D.; Kinauer, M.; Diefenbach, M.; Demeshko, S.; Würtele, C.; Holthausen, M. C.; Schneider, S. A Terminal Iridium Oxo Complex with a Triplet Ground State. *Angew. Chem., Int. Ed.* **2019**, *58*, 10971−10974.
(86) Abbenseth, J.; Delony, D.; Neben, M. C.; Würtele, C.; de Bruin, B.; Schneider, S. Interconversion of Phosphinyl Radical and Phosphinidene Complexes by Proton Coupled Electron Transfer. *Angew. Chem., Int. Ed.* **2019**, *58*, 6338−6341.
(87) Abbenseth, J.; Bete, S. C.; Finger, M.; Volkmann, C.; Würtele, C.; Schneider, S. Four- and Five-Coordinate Osmium(IV) Nitrides and Imides: Circumventing the "Nitrido Wall. *Organometallics* **2018**, *37*, 802−811.
(88) O, W. W. N.; Kang, X.; Luo, Y.; Hou, Z. PNP-Ligated Heterometallic Rare-Earth/Ruthenium Hydride Complexes Bearing Phosphinophenyl and Phosphinomethyl Bridging Ligands. *Organometallics* **2014**, *33*, 1030−1043.
(89) Herbert, D. E.; Ozerov, O. V. Binuclear Palladium Complexes Supported by Bridged Pincer Ligands. *Organometallics* **2011**, *30*, 6641−6654.
(90) Fafard, C. M.; Chen, C.-H.; Foxman, B. M.; Ozerov, O. V. Covalent palladium-zinc bonds and their reactivity. *Chem. Commun.* **2007**, 4465−4467.
(91) Pell, C. J.; Shih, W.-C.; Gatard, S.; Ozerov, O. V. Formation of (PNP)Rh complexes containing covalent rhodium-zinc bonds in studies of potential Rh-catalysed Negishi coupling. *Chem. Commun.* **2017**, *53*, 6456−6459.
(92) Walensky, J. R.; Fafard, C. M.; Guo, C.; Brammell, C. M.; Foxman, B. M.; Hall, M. B.; Ozerov, O. V. Understanding Pd-Pd bond length variation in (PNP)Pd-Pd(PNP) dimers. *Inorg. Chem.* **2013**, *52*, 2317−2322.
(93) Arashiba, K.; Miyake, Y.; Nishibayashi, Y. A molybdenum complex bearing PNP-type pincer ligands leads to the catalytic reduction of dinitrogen into ammonia. *Nat. Chem.* **2011**, *3*, 120−125.
(94) Feller, M.; Ben-Ari, E.; Diskin-Posner, Y.; Carmieli, R.; Weiner, L.; Milstein, D. O2 activation by metal-ligand cooperation with Ir(I) PNP pincer complexes. *J. Am. Chem. Soc.* **2015**, *137*, 4634−4637.
(95) Schwartsburd, L.; Iron, M. A.; Konstantinovski, L.; Diskin-Posner, Y.; Leitus, G.; Shimon, L. J. W.; Milstein, D. Synthesis and Reactivity of an Iridium(I) Acetonyl PNP Complex. Experimental and Computational Study of Metal−Ligand Cooperation in H−H and C−H Bond Activation via Reversible Ligand Dearomatization. *Organometallics* **2010**, *29*, 3817−3827.
(96) Verat, A. Y.; Fan, H.; Pink, M.; Chen, Y.-S.; Caulton, K. G. Spin state, structure, and reactivity of terminal oxo and dioxygen complexes of the (PNP)Rh moiety. *Chem. - Eur. J.* **2008**, *14*, 7680−7686.
(97) Wang, B.; Luo, G.; Nishiura, M.; Hu, S.; Shima, T.; Luo, Y.; Hou, Z. Dinitrogen Activation by Dihydrogen and a PNP-Ligated Titanium Complex. *J. Am. Chem. Soc.* **2017**, *139*, 1818−1821.
(98) Sekiguchi, Y.; Meng, F.; Tanaka, H.; Eizawa, A.; Arashiba, K.; Nakajima, K.; Yoshizawa, K.; Nishibayashi, Y. Synthesis and reactivity of titanium- and zirconium-dinitrogen complexes bearing anionic pyrrole-based PNP-type pincer ligands. *Dalton Trans* **2018**, *47*, 11322−11326.
(99) Rebreyend, C.; Gloaguen, Y.; Lutz, M.; van der Vlugt, J. I.; Siewert, I.; Schneider, S.; de Bruin, B. Electrocatalytic Azide Oxidation Mediated by a Rh(PNP) Pincer Complex. *Chem. - Eur. J.* **2017**, *23*, 17438−17443.
(100) Lindley, B. M.; van Alten, R. S.; Finger, M.; Schendzielorz, F.; Würtele, C.; Miller, A. J. M.; Siewert, I.; Schneider, S. Mechanism of Chemical and Electrochemical N2 Splitting by a Rhenium Pincer Complex. *J. Am. Chem. Soc.* **2018**, *140*, 7922−7935.
(101) Schendzielorz, F.; Finger, M.; Abbenseth, J.; Würtele, C.; Krewald, V.; Schneider, S. Metal-Ligand Cooperative Synthesis of Benzonitrile by Electrochemical Reduction and Photolytic Splitting of Dinitrogen. *Angew. Chem., Int. Ed.* **2019**, *58*, 830−834.
(102) Schneck, F.; Schendzielorz, F.; Hatami, N.; Finger, M.; Würtele, C.; Schneider, S. Photochemically Driven Reverse Water-Gas Shift at Ambient Conditions mediated by a Nickel Pincer Complex. *Angew. Chem., Int. Ed.* **2018**, *57*, 14482−14487.
(103) Silantyev, G. A.; Förster, M.; Schluschaß, B.; Abbenseth, J.; Würtele, C.; Volkmann, C.; Holthausen, M. C.; Schneider, S. Dinitrogen Splitting Coupled to Protonation. *Angew. Chem., Int. Ed.* **2017**, *56*, 5872−5876.
(104) Huacuja, R.; Graham, D. J.; Fafard, C. M.; Chen, C.-H.; Foxman, B. M.; Herbert, D. E.; Alliger, G.; Thomas, C. M.; Ozerov, O. V. Reactivity of a Pd(I)-Pd(I) dimer with O2: monohapto Pd superoxide and dipalladium peroxide in equilibrium. *J. Am. Chem. Soc.* **2011**, *133*, 3820−3823.
(105) Masuda, J. D.; Jantunen, K. C.; Ozerov, O. V.; Noonan, K. J. T.; Gates, D. P.; Scott, B. L.; Kiplinger, J. L. A lanthanide phosphinidene complex: synthesis, structure, and phospha-Wittig reactivity. *J. Am. Chem. Soc.* **2008**, *130*, 2408−2409.
(106) Scott, J.; Basuli, F.; Fout, A. R.; Huffman, J. C.; Mindiola, D. J. Evidence for the existence of a terminal imidoscandium compound: intermolecular C-H activation and complexation reactions with the transient Sc = NAr species. *Angew. Chem., Int. Ed.* **2008**, *47*, 8502−8505.
(107) Wicker, B. F.; Fan, H.; Hickey, A. K.; Crestani, M. G.; Scott, J.; Pink, M.; Mindiola, D. J. Evidence for the existence of terminal scandium imidos: mechanistic studies involving imido-scandium bond formation and C-H activation reactions. *J. Am. Chem. Soc.* **2012**, *134*, 20081−20096.
(108) Wicker, B. F.; Scott, J.; Andino, J. G.; Gao, X.; Park, H.; Pink, M.; Mindiola, D. J. Phosphinidene complexes of scandium: powerful PAr group-transfer vehicles to organic and inorganic substrates. *J. Am. Chem. Soc.* **2010**, *132*, 3691−3693.
(109) Zabula, A. V.; Qiao, Y.; Kosanovich, A. J.; Cheisson, T.; Manor, B. C.; Carroll, P. J.; Ozerov, O. V.; Schelter, E. J. Structure, Electronics and Reactivity of Ce(PNP) Complexes. *Chem. - Eur. J.* **2017**, *23*, 17923−17934.
(110) Levine, D. S.; Tilley, T. D.; Andersen, R. A. C−H Bond Activations by Monoanionic, PNP-Supported Scandium Dialkyl Complexes. *Organometallics* **2015**, *34*, 4647−4655.
(111) Levine, D. S.; Tilley, T. D.; Andersen, R. A. Evidence for the Existence of Group 3 Terminal Methylidene Complexes. *Organometallics* **2017**, *36*, 80−88.
(112) Wang, L.; Cui, D.; Hou, Z.; Li, W.; Li, Y. Highly Cis-1,4-Selective Living Polymerization of 1,3-Conjugated Dienes and Copolymerization with ε-Caprolactone by Bis(phosphino)carbazolide Rare-Earth-Metal Complexes. *Organometallics* **2011**, *30*, 760−767.
(113) Cantat, T.; Scott, B. L.; Morris, D. E.; Kiplinger, J. L. What a difference a 5f element makes: trivalent and tetravalent uranium halide complexes supported by one and two bis2-(diisopropylphosphino)-4-methylphenylamido (PNP) ligands. *Inorg. Chem.* **2009**, *48*, 2114−2127.
(114) Liu, B.; Cui, D.; Ma, J.; Chen, X.; Jing, X. Synthesis and reactivity of rare earth metal alkyl complexes stabilized by anilido phosphinimine and amino phosphine ligands. *Chem. - Eur. J.* **2007**, *13*, 834−845.
(115) Liu, B.; Liu, X.; Cui, D.; Liu, L. Reactivity of Rare-Earth Metal Complexes Stabilized by an Anilido-Phosphinimine Ligand. *Organometallics* **2009**, *28*, 1453−1460.
(116) Cheng, J.; Shima, T.; Hou, Z. Rare-earth polyhydride complexes bearing bis(phosphinophenyl)amido pincer ligands. *Angew. Chem., Int. Ed.* **2011**, *50*, 1857−1860.
(117) Li, S.; Miao, W.; Tang, T.; Cui, D.; Chen, X.; Jing, X. Rare earth metal bis(alkyl) complexes bearing amino phosphine ligands: Synthesis and catalytic activity toward ethylene polymerization. *J. Organomet. Chem.* **2007**, *692*, 4943−4952.

https://dx.doi.org/10.1021/acs.inorgchem.9b03071
Inorg. Chem. 2020, 59, 2719−2732

Protonolysis of the Yb−C 10 H 8 Bond by PhPH 2. *Organometallics* **2016**, *35*, 2401−2409.
(153) Rabe, G. W.; Guzei, I. A.; Rheingold, A. L. Synthesis and X-ray Crystal Structure Determination of the First Lanthanide Complexes Containing Primary Phosphide Ligands: Ln[P(H)Mes*] 2 (thf) 4 (Ln = Yb, Eu). *Inorg. Chem.* **1997**, *36*, 4914−4915.
(154) Hou, Z.; Zhang, Y.; Tezuka, H.; Xie, P.; Tardif, O.; Koizumi, T.-a.; Yamazaki, H.; Wakatsuki, Y. C 5 Me 5 /ER-Ligated Samarium(II) Complexes with the Neutral "C 5 Me 5 M" Ligand (ER = OAr, SAr, NRR′, or PHAr; M = K or Na): A Unique Catalytic System for Polymerization and Block-Copolymerization of Styrene and Ethylene. *J. Am. Chem. Soc.* **2000**, *122*, 10533−10543.
(155) Pugh, T.; Tuna, F.; Ungur, L.; Collison, D.; McInnes, E. J. L.; Chibotaru, L. F.; Layfield, R. A. Influencing the properties of dysprosium single-molecule magnets with phosphorus donor ligands. *Nat. Commun.* **2015**, *6*, 7492.
(156) Garner, M. E.; Parker, B. F.; Hohloch, S.; Bergman, R. G.; Arnold, J. Thorium Metallacycle Facilitates Catalytic Alkyne Hydrophosphination. *J. Am. Chem. Soc.* **2017**, *139*, 12935−12938.
(157) Garner, M. E.; Arnold, J. Reductive Elimination of Diphosphine from a Thorium−NHC−Bis(phosphido) Complex. *Organometallics* **2017**, *36*, 4511−4514.
(158) Behrle, A. C.; Castro, L.; Maron, L.; Walensky, J. R. Formation of a Bridging Phosphinidene Thorium Complex. *J. Am. Chem. Soc.* **2015**, *137*, 14846−14849.
(159) Behrle, A. C.; Walensky, J. R. Insertion of (t)BuNC into thorium-phosphorus and thorium-arsenic bonds: phosphaazaallene and arsaazaallene moieties in f element chemistry. *Dalton Trans.* **2016**, *45*, 10042−10049.
(160) Rungthanaphatsophon, P.; Duignan, T. J.; Myers, A. J.; Vilanova, S. P.; Barnes, C. L.; Autschbach, J.; Batista, E. R.; Yang, P.; Walensky, J. R. Influence of Substituents on the Electronic Structure of Mono- and Bis(phosphido) Thorium(IV) Complexes. *Inorg. Chem.* **2018**, *57*, 7270−7278.
(161) Vilanova, S. P.; Alayoglu, P.; Heidarian, M.; Huang, P.; Walensky, J. R. Metal-Ligand Multiple Bonding in Thorium Phosphorus and Thorium Arsenic Complexes. *Chem. - Eur. J.* **2017**, *23*, 16748−16752.
(162) Vilanova, S. P.; Tarlton, M. L.; Barnes, C. L.; Walensky, J. R. Double insertion of benzophenone into thorium-phosphorus bonds. *J. Organomet. Chem.* **2018**, *857*, 159−163.
(163) Brennan, J. G.; Stults, S. D.; Andersen, R. A.; Zalkin, A. Crystal structures of (MeC5H4)3 ML [M = uranium or cerium; L = quinuclidine or P(OCH2)3CEt]. Evidence for uranium to phosphorus.pi.-back-bonding. *Organometallics* **1988**, *7*, 1329−1334.
(164) Arliguie, T.; Doux, M.; Mézailles, N.; Thuéry, P.; Le Floch, P.; Ephritikhine, M. Lanthanide and uranium complexes with an SPS-based pincer ligand. *Inorg. Chem.* **2006**, *45*, 9907−9913.
(165) Chilton, N. F.; Goodwin, C. A. P.; Mills, D. P.; Winpenny, R. E. P. The first near-linear bis(amide) f-block complex: a blueprint for a high temperature single molecule magnet. *Chem. Commun.* **2015**, *51*, 101−103.
(166) Goodwin, C. A. P.; Chilton, N. F.; Natrajan, L. S.; Boulon, M.-E.; Ziller, J. W.; Evans, W. J.; Mills, D. P. Investigation into the Effects of a Trigonal-Planar Ligand Field on the Electronic Properties of Lanthanide(II) Tris(silylamide) Complexes (Ln = Sm, Eu, Tm, Yb). *Inorg. Chem.* **2017**, *56*, 5959−5970.
(167) Goodwin, C. A. P.; Chilton, N. F.; Vettese, G. F.; Moreno Pineda, E.; Crowe, I. F.; Ziller, J. W.; Winpenny, R. E. P.; Evans, W. J.; Mills, D. P. Physicochemical Properties of Near-Linear Lanthanide-(II) Bis(silylamide) Complexes (Ln = Sm, Eu, Tm, Yb). *Inorg. Chem.* **2016**, *55*, 10057−10067.
(168) Goodwin, C. A. P.; Mills, D. P. Silylamides: towards a half-century of stabilising remarkable f-element chemistry. *Organometallic Chemistry: A Specialist Periodical Report* **2017**, *41*, 123−156.
(169) Nicholas, H.; Vonci, M.; Goodwin, C. A. P.; Loo, S. W.; Murphy, S.; Cassim, D.; Winpenny, R. E. P.; McInnes, E. J. L.; Chilton, N. F.; Mills, D. P. Electronic Structures of Bent Lanthanide-(III) Complexes with Two N-Donor Ligands. *Chem. Sci.* **2019**, *10*, 10493−10502.

https://dx.doi.org/10.1021/acs.inorgchem.9b03071
Inorg. Chem. 2020, 59, 2719−2732

1.3 References

(1) Fryzuk, M. D. The 1992 Alcan Award Lecture Excursions around the periodic table: ligand design in inorganic chemistry. *Can. J. Chem.* **1992**, *70*, 2839–2845.
(2) Benito-Garagorri, D.; Kirchner, K. Modularly Designed Transition Metal PNP and PCP Pincer Complexes based on Aminophosphines: Synthesis and Catalytic Applications. *Acc. Chem. Res.* **2008**, *41*, 201–213.
(3) van der Vlugt, J. I.; Reek, J. N. H. Neutral Tridentate PNP Ligands and Their Hybrid Analogues: Versatile Non-Innocent Scaffolds for Homogeneous Catalysis. *Angew. Chem. Int. Ed.* **2009**, *48*, 8832–8846.
(4) Milstein, D. Discovery of Environmentally Benign Catalytic Reactions of Alcohols Catalyzed by Pyridine-Based Pincer Ru Complexes, Based on Metal–Ligand Cooperation. *Top. Catal.* **2010**, *53*, 915–923.
(5) Grotjahn, D. B. Bifunctional catalysts and related complexes: structures and properties. *Dalton Trans.* **2008**, 6497–6508.
(6) Mills, D. P.; Liddle, S. T. Ligand Design in Modern Lanthanide Chemistry. In *Ligand Design in Metal Chemistry*; Stradiotto, M., Lundgren, R. J., Eds.; John Wiley & Sons, Ltd: Chichester, UK, 2016; 330–363.
(7) Liang, L.-C. Metal complexes of chelating diarylamido phosphine ligands. *Coord. Chem. Rev.* **2006**, *250*, 1152–1177.
(8) Schneider, S.; Meiners, J.; Askevold, B. Cooperative Aliphatic PNP Amido Pincer Ligands - Versatile Building Blocks for Coordination Chemistry and Catalysis. *Eur. J. Inorg. Chem.* **2012**, *2012*, 412–429.
(9) Du Mont, W.-W.; Gimeno, R. G.; Lungu, D.; Bîrzoi, R. M.; Daniliuc, C. G.; Goers, C.; Riecke, A.; Bartsch, R. Nitrogen-bridged bidentate phosphaalkene ligands. *Pure Appl. Chem.* **2013**, *85*, 633–647.
(10) Yang, Y.; Liu, Z.; Liu, B.; Duchateau, R. Selective Ethylene Tri-/Tetramerization by in Situ-Formed Chromium Catalysts Stabilized by N,P-Based Ancillary Ligand Systems. *ACS Catal.* **2013**, *3*, 2353–2361.
(11) Wetzel, C.; Kunz, P. C.; Thiel, I.; Spingler, B. Gold(I) Catalysts with Bifunctional P, N Ligands. *Inorg. Chem.* **2011**, *50*, 7863–7870.
(12) Tribó, R.-M.; Ros, J.; Pons, J.; Yáñez, R.; Álvarez-Larena, A.; Piniella, J.-F. New stable cyclopentadienyl iron(II) complexes containing 3,5-dimethylpyrazolyl phosphine: X-ray structure of $[FeCp(CO)_2PPh_2(Me_2Pz)]BF_4$. *J. Organomet. Chem.* **2003**, *676*, 38–42.
(13) Tran, B. L.; Pink, M.; Mindiola, D. J. Catalytic Hydrosilylation of the Carbonyl Functionality via a Transient Nickel Hydride Complex. *Organometallics* **2009**, *28*, 2234–2243.
(14) Liang, L.-C.; Huang, M.-H.; Hung, C.-H. Aluminum Complexes Incorporating Bidentate Amido Phosphine Ligands. *Inorg. Chem.* **2004**, *43*, 2166–2174.
(15) Kisala, J.; Ruman, T. Pincer Complexes Based on Phosphinoaminopyridines: Synthesis, Structural Characterization and Catalytic Applications. *Curr. Org. Chem.* **2011**, *15*, 3486–3502.
(16) Giri, R.; Thapa, S. Copper-Catalyzed Cross-Couplings of Organometallic Reagents with and without Assistance from PN Ligands. *Synlett* **2015**, *26*, 709–715.
(17) Fryzuk, M. D.; Giesbrecht, G. R.; Olovsson, G.; Rettig, S. J. Synthesis and Characterization of Four- and Five-Coordinate Organoaluminum Complexes Incorporating the Amido Diphosphine Ligand System $N(SiMe_2CH_2PPr^i_2)_2$. *Organometallics* **1996**, *15*, 4832–4841.
(18) Baur, J.; Jacobsen, H.; Burger, P.; Artus, G.; Berke, H.; Dahlenburg, L. The Chemistry of New Nitrosyltungsten Complexes with Pyridyl-Functionalized Phosphane Ligands. *Eur. J. Inorg. Chem.* **2000**, *2000*, 1411–1422.
(19) Cohen, J. D.; Fryzuk, M. D.; Loehr, T. M.; Mylvaganam, M.; Rettig, S. J. Synthesis and Structure of a Zirconium Dinitrogen Complex with a Side-On Bridging N_2 Unit. *Inorg. Chem.* **1998**, *37*, 112–119.
(20) Todisco, S.; Gallo, V.; Mastrorilli, P.; Latronico, M.; Re, N.; Creati, F.; Braunstein, P. Pt–Mo and Pt–W Mixed-Metal Clusters with Chelating or Bridging Diphosphine Short-Bite Ligands $(Ph_2P)_2NH$

and $(Ph_2P)_2N(CH_2)_9CH_3$: A Combined Synthetic and Theoretical Study. *Inorg. Chem.* **2012**, *51*, 11549–11561.
(21) Bowes, E. G.; Beattie, D. D.; Love, J. A. Role of Phosphine Sterics in Strained Aminophosphine Chelate Formation. *Inorg. Chem.* **2019**, *58*, 2925–2929.
(22) Salvarese, N.; Refosco, F.; Seraglia, R.; Roverso, M.; Dolmella, A.; Bolzati, C. Synthesis and characterization of rhenium(III) complexes with $(Ph_2PCH_2CH_2)_2NR$ diphosphinoamine ligands. *Dalton Trans.* **2017**, *46*, 9180–9191.
(23) Junge, K.; Wendt, B.; Cingolani, A.; Spannenberg, A.; Wei, Z.; Jiao, H.; Beller, M. Cobalt Pincer Complexes for Catalytic Reduction of Carboxylic Acid Esters. *Chem. Eur. J.* **2018**, *24*, 1046–1052.
(24) van Oort, A. B.; Budzelaar, P. H.M.; Frijns, J. H.G.; Orpen, A. G. Mono- and bi-nuclear molybdenum complexes of 2,6-bis(diphenylphosphino)-N-methylaniline. *J. Organomet. Chem.* **1990**, *396*, 33–47.
(25) Liang, L.-C.; Lee, W.-Y.; Yin, C.-C. Nickel(II) Complexes Containing Bidentate Diarylamido Phosphine Ligands. *Organometallics* **2004**, *23*, 3538–3547.
(26) Klein, H.-F.; Beck, R.; Hetche, O. Dynamic Properties of Methyl(trimethylphosphane)nickel Complexes Containing (2-Diphenylphosphanyl)phenylamido Ligands. *Eur. J. Inorg. Chem.* **2003**, *2003*, 232–239.
(27) Klein, H.-F.; Beck, R.; Flörke, U.; Haupt, H.-J. Fluxional and Rigid (Trimethylphosphane)cobalt Complexes Containing Chelating (2-Diphenylphosphanyl)anilido Ligands. *Eur. J. Inorg. Chem.* **2003**, *2003*, 240–248.
(28) Liang, L.-C.; Lin, J.-M.; Hung, C.-H. Nickel(II) Complexes of Bis(2-diphenylphosphinophenyl)amide. *Organometallics* **2003**, *22*, 3007–3009.
(29) Fryzuk, M. D.; Johnson, S. A.; Rettig, S. J. New Mode of Coordination for the Dinitrogen Ligand: A Dinuclear Tantalum Complex with a Bridging N_2 Unit That Is Both Side-On and End-On. *J. Am. Chem. Soc.* **1998**, *120*, 11024–11025.
(30) Wang, L.; Cui, D.; Hou, Z.; Li, W.; Li, Y. Highly Cis-1,4-Selective Living Polymerization of 1,3-Conjugated Dienes and Copolymerization with ε-Caprolactone by Bis(phosphino)carbazolide Rare-Earth-Metal Complexes. *Organometallics* **2011**, *30*, 760–767.
(31) Levine, D. S.; Tilley, T. D.; Andersen, R. A. Evidence for the Existence of Group 3 Terminal Methylidene Complexes. *Organometallics* **2017**, *36*, 80–88.
(32) Levine, D. S.; Tilley, T. D.; Andersen, R. A. C–H Bond Activations by Monoanionic, PNP-Supported Scandium Dialkyl Complexes. *Organometallics* **2015**, *34*, 4647–4655.
(33) Kurogi, T.; Kamitani, M.; Manor, B. C.; Carroll, P. J.; Mindiola, D. J. Reactivity Studies of a Zirconium Methylidene Complex: Group Transfer and Methylenation Reactions. *Organometallics* **2017**, *36*, 74–79.
(34) Izod, K.; Liddle, S. T.; McFarlane, W.; Clegg, W. Synthesis and Reactions of Sterically Encumbered, Heteroleptic Lanthanum Phosphides. Structural Characterization of $[\{(Me_3Si)_2CH\}$-$(C_6H_4$-2-$CH_2NMe_2)P]_2La(OR)$ and $[\{(Me_3Si)_2CH\}$-$(C_6H_4$-2-$CH_2NMe_2)P]La(THF)[P(C_6H_4$-2-$CH_2NMe_2)$-$\{CH(SiMe_3)(SiMe_2CH_2)\}]$ [R = *i*-Pr, *t*-Bu]. *Organometallics* **2004**, *23*, 2734–2743.
(35) Fryzuk, M. D.; Giesbrecht, G. R.; Johnson, S. A.; Kickham, J. E.; Love, J. B. Chelating amides of lithium. Synthesis, structure and coordination chemistry. *Polyhedron* **1998**, *17*, 947–952.
(36) Fryzuk, M. D.; Love, J. B.; Rettig, S. J.; Young, V. G. Transformation of Coordinated Dinitrogen by Reaction with Dihydrogen and Primary Silanes. *Science* **1997**, *275*, 1445–1447.
(37) Müller, C.; Pidko, E. A.; Lutz, M.; Spek, A. L.; Vogt, D. Diphosphinine Derivatives of Terpyridine: A New Class of Neutral π-Accepting PNP-Pincer Ligands. *Chem. Eur. J.* **2008**, *14*, 8803–8807.
(38) Fan, L.; Foxman, B. M.; Ozerov, O. V. N−H Cleavage as a Route to Palladium Complexes of a New PNP Pincer Ligand. *Organometallics* **2004**, *23*, 326–328.
(39) Falconer, R. L.; Nichol, G. S.; Cowley, M. J. Flexible Coordination of N,P-Donor Ligands in Aluminum Dimethyl and Dihydride Complexes. *Inorg. Chem.* **2019**, *58*, 11439–11448.
(40) Scott, J.; Fan, H.; Wicker, B. F.; Fout, A. R.; Baik, M.-H.; Mindiola, D. J. Lewis Acid Stabilized Methylidene and Oxoscandium Complexes. *J. Am. Chem. Soc.* **2008**, *130*, 14438–14439.

(41) Bailey, B. C.; Basuli, F.; Huffman, J. C.; Mindiola, D. J. Terminal Titanium(IV) (Trimethylsilyl)imides Prepared by Oxidatively Induced Trimethylsilyl Abstraction. *Organometallics* **2006**, *25*, 2725–2728.
(42) Carroll, M. E.; Pinter, B.; Carroll, P. J.; Mindiola, D. J. Mononuclear and Terminally Bound Titanium Nitrides. *J. Am. Chem. Soc.* **2015**, *137*, 8884–8887.
(43) Grant, L. N.; Ahn, S.; Manor, B. C.; Baik, M.-H.; Mindiola, D. J. Structural elucidation of a mononuclear titanium methylidene. *Chem. Commun.* **2017**, *53*, 3415–3417.
(44) Grant, L. N.; Pinter, B.; Gu, J.; Mindiola, D. J. Molecular Zirconium Nitride Super Base from a Mononuclear Parent Imide. *J. Am. Chem. Soc.* **2018**, *140*, 17399–17403.
(45) Grant, L. N.; Pinter, B.; Kurogi, T.; Carroll, M. E.; Wu, G.; Manor, B. C.; Carroll, P. J.; Mindiola, D. J. Molecular titanium nitrides: nucleophiles unleashed. *Chem. Sci.* **2017**, *8*, 1209–1224.
(46) Kurogi, T.; Won, J.; Park, B.; Trofymchuk, O. S.; Carroll, P. J.; Baik, M.-H.; Mindiola, D. J. Room temperature olefination of methane with titanium–carbon multiple bonds. *Chem. Sci.* **2018**, *9*, 3376–3385.
(47) Kurogi, T.; Pinter, B.; Mindiola, D. J. Methylidyne Transfer Reactions with Niobium. *Organometallics* **2018**, *37*, 3385–3388.
(48) Chien, P.-S.; Liang, L.-C. Zirconium and Hafnium Complexes Containing Bidentate Diarylamido-Phosphine Ligands. *Inorg. Chem.* **2005**, *44*, 5147–5151.
(49) Weng, W.; Yang, L.; Foxman, B. M.; Ozerov, O. V. Chelate-Enforced Phosphine Coordination Enables α-Abstraction to Give Zirconium Alkylidenes. *Organometallics* **2004**, *23*, 4700–4705.
(50) Mullane, K. C.; Ryu, H.; Cheisson, T.; Grant, L. N.; Park, J. Y.; Manor, B. C.; Carroll, P. J.; Baik, M.-H.; Mindiola, D. J.; Schelter, E. J. C–H Bond Addition across a Transient Uranium–Nitrido Moiety and Formation of a Parent Uranium Imido Complex. *J. Am. Chem. Soc.* **2018**, *140*, 11335–11340.
(51) Fryzuk, M. D.; Haddad, T. S.; Berg, D. J. COMPLEXES OF GROUPS 3, 4, THE LANTHANIDES AND THE ACTINIDES CONTAINING NEUTRAL PHOSPHORUS DONOR LIGANDS. *Coord. Chem. Rev.* **1990**, *99*, 137–212.
(52) Fryzuk, M. D.; Haddad, T. S.; Rettig, S. J. Phosphine Complexes of Yttrium, Lanthanum, and Lutetium. Synthesis, Thermolysis, and Fluxional Behavior of the Hydrocarbyl Derivatives $MR'[N(SiMe_2CH_2PMe_2)_2]_2$. X-ray Crystal Structure of $Y[N(SiMe_2CHPMe_2)(SiMe_2CH_2PMe_2)][N(SiMe_2CH_2PMe_2)_2]$. *Organometallics* **1991**, *10*, 2026–2036.
(53) Fryzuk, M. D.; Jafarpour, L.; Kerton, F. M.; Love, J. B.; Patrick, B. O.; Rettig, S. J. Carbon−Carbon Bond Formation Using Yttrium(III) and the Lanthanide Elements. *Organometallics* **2001**, *20*, 1387–1396.
(54) Fryzuk, M. D.; Yu, P.; Patrick, B. O. Synthesis, structure, and reactivity of diamidophosphine complexes of yttrium and the lanthanides. *Can. J. Chem.* **2001**, *79*, 1194–1200.
(55) Fryzuk, M. D.; Jafarpour, L.; Kerton, F. M.; Love, J. B.; Rettig, S. J. Dinuclear π Complexes of Yttrium and Lutetium with Sandwiched Naphthalene and Anthracene Ligands: Evidence for Rapid Intramolecular Inter-Ring Rearrangements. *Angew. Chem. Int. Ed.* **2000**, *39*, 767–770.
(56) Shannon, R. D. Revised effective ionic radii and systematic studies of interatomic distances in halides and chalcogenides. *Acta Cryst A* **1976**, *32*, 751–767.
(57) Roesky, P. W.; Gamer, M. T.; Puchner, M.; Greiner, A. Homoleptic Lanthanide Complexes of Chelating Bis(phosphanyl)amides: Synthesis, Structure, and Ring-Opening Polymerization of Lactones. *Chem. Eur. J.* **2002**, *8*, 5265–5271.
(58) Roesky, P. W.; Gamer, M. T.; Marinos, N. Yttrium and Lanthanide Diphosphanylamides: Syntheses and Structures of Complexes with one $\{(Ph_2P)_2N\}^-$ ligand in the Coordination Sphere. *Chem. Eur. J.* **2004**, *10*, 3537–3542.
(59) Roesky, P. W. Syntheses and Structures of Strontium, Barium, and Europium Bis(diphosphanylamido) Complexes. *Inorg. Chem.* **2006**, *45*, 798–802.
(60) Panda, T. K.; Gamer, M. T.; Roesky, P. W. Yttrium and Lanthanide Complexes Having a Chiral Phosphanylamide in the Coordination Sphere. *Inorg. Chem.* **2006**, *45*, 910–916.

(61) Gamer, M. T.; Roesky, P. W. Ytterbium and Samarium Bis(diphosphanylamides): Syntheses and Structures of Lanthanide Complexes Having Two $\{(Ph_2P)_2N\}^-$ Ligands in the Coordination Sphere. *Inorg. Chem.* **2004**, *43*, 4903–4906.
(62) Wetzel, T. G.; Dehnen, S.; Roesky, P. W. Homoleptic Lanthanide Complexes of Chelating Phosphanamides—An Experimental and Theoretical Study. *Angew. Chem. Int. Ed.* **1999**, *38*, 1086–1088.
(63) Zabula, A. V.; Qiao, Y.; Kosanovich, A. J.; Cheisson, T.; Manor, B. C.; Carroll, P. J.; Ozerov, O. V.; Schelter, E. J. Structure, Electronics and Reactivity of Ce(PNP) Complexes. *Chem. Eur. J.* **2017**, *23*, 17923–17934.
(64) Masuda, J. D.; Jantunen, K. C.; Ozerov, O. V.; Noonan, K. J. T.; Gates, D. P.; Scott, B. L.; Kiplinger, J. L. A Lanthanide Phosphinidene Complex: Synthesis, Structure, and Phospha-Wittig Reactivity. *J. Am. Chem. Soc.* **2008**, *130*, 2408–2409.
(65) Cantat, T.; Scott, B. L.; Morris, D. E.; Kiplinger, J. L. What a Difference a 5f Element Makes: Trivalent and Tetravalent Uranium Halide Complexes Supported by One and Two Bis[2-(diisopropylphosphino)-4-methylphenyl]amido (PNP) Ligands. *Inorg. Chem.* **2009**, *48*, 2114–2127.
(66) Cantat, T.; Graves, C. R.; Scott, B. L.; Kiplinger, J. L. Challenging the Metallocene Dominance in Actinide Chemistry with a Soft PNP Pincer Ligand: New Uranium Structures and Reactivity Patterns. *Angew. Chem. Int. Ed.* **2009**, *48*, 3681–3684.
(67) Lisowski, J.; Sessler, J. L.; Mody, T. D. ^{13}C and ^{31}P NMR Study of Paramagnetic Lanthanide(III) Texaphyrins. *Inorg. Chem.* **1995**, *34*, 4336–4342.
(68) Copping, R.; Gaunt, A. J.; May, I.; Sarsfield, M. J.; Collison, D.; Helliwell, M.; Denniss, I. S.; Apperley, D. C. Trivalent lanthanide lacunary phosphomolybdate complexes: a structural and spectroscopic study across the series $[Ln(PMo_{11}O_{39})_2]^{11-}$. *Dalton Trans.* **2005**, 1256–1262.
(69) Li, S.; Miao, W.; Tang, T.; Cui, D.; Chen, X.; Jing, X. Rare earth metal bis(alkyl) complexes bearing amino phosphine ligands: Synthesis and catalytic activity toward ethylene polymerization. *J. Organomet. Chem.* **2007**, *692*, 4943–4952.
(70) Dahlenburg, L.; Herbst, K. Rhodium and Iridium Complexes with 2-(Diphenylphosphanyl)phenylamido Ligands. *Chem. Ber.* **1997**, *130*, 1693–1698.
(71) MacLachlan, E. A.; Fryzuk, M. D. A New Arene-Bridged Diamidophosphine Ligand and Its Coordination Chemistry with Zirconium(IV). *Organometallics* **2005**, *24*, 1112–1118.

Chapter 2:

Isocyanate Insertion into a La–P Phosphide Bond: A Versatile Route to Phosphaureate-Bridged Heterobimetallic Lanthanide–Coinage-Metal Complexes

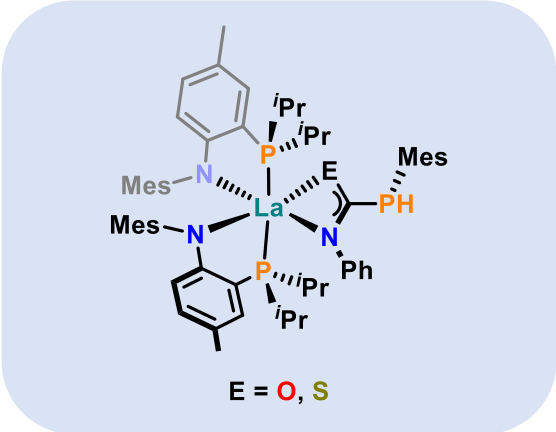

2.1 Introduction: Insertion Chemistry of M–P Bonds

From a synthetic chemist's point of view the Ln^{3+} ions have traditionally been mainly appreciated for their high Lewis acidity.[1–7] However, since the seminal work by Marks and colleagues from the late 1980s and early 1990s[8,9] the lanthanides have also been recognized for the facile insertion of unsaturated organic substrates such as olefins, alkynes, carbodiimides, nitriles or iso(thio)cyanates into Ln–E bonds (E = H, NR_2, PR_2, OR, SR or SeR). The propensity of the insertion products to undergo σ-bond metathesis results in a high efficiency of lanthanide(III)-mediated hydrofunctionalizations,[10–13] *i.e.*, the catalytic addition of E–H groups to unsaturated organic substrates.[10]

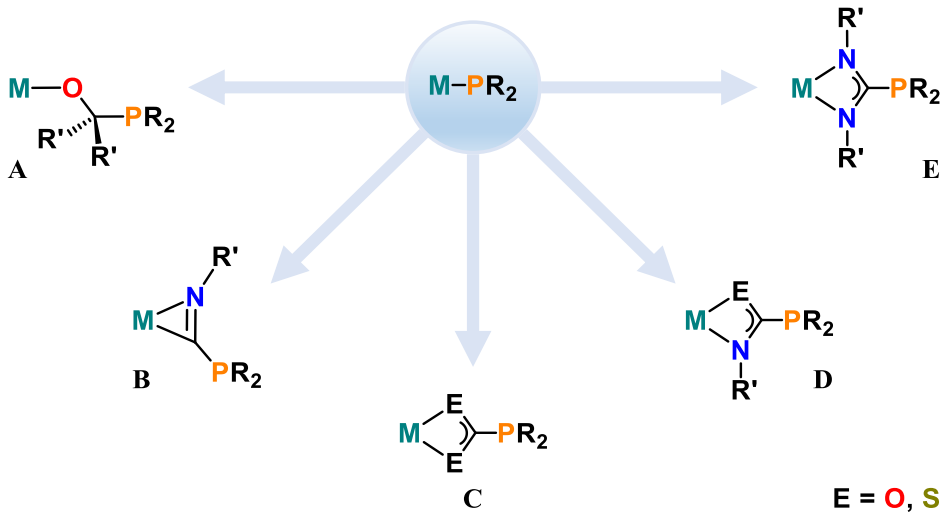

Scheme 2.1. Selection of structural motifs obtained by insertion of organic substrates with polar double bonds into M–P bonds (M = group 3, 4 or f-block metal ion; R, R' = alkyl, aryl).[14–19] Simplified representations; no supporting ligands shown.

Besides their importance for catalysis, such insertion reactions present a versatile, atom efficient way to obtain rare types of phosphorus-containing ligands[20–22] in the first coordination sphere of group 3, 4 and f-block metal ions, including those of the lanthanide(III) series (Scheme 2.1). While organic substrates with a polar double bond and one heteroatom (nitrogen or oxygen) such as, *e.g.*, benzophenone insert into a M–P bond without increasing the coordination number at the metal ion (case **A**),[17] isocyanides, carbon dioxide/disulfide, iso(thio)cyanates or carbodiimides generally lead to κ^2-bonded ligands and therefore an increase in the coordination number by one (cases **B** – **E**).[14–16,18,19] The thermodynamic driving force is provided by the formation of more stable M–O or M–N bonds compared to the M–P bond.[23] This applies similarly to labile M–S and M–Se bonds.[24]

The following sections describe examples of insertion reactions at early transition-metal and f-element phosphido complexes and how this reactivity may lead to new heterobimetallic lanthanide – coinage-metal systems. Since the number of reported insertion reactions at lanthanide phosphido complexes alone is still relatively small, relevant known insertion products of both early transition-metal and actinide (Ac) phosphido complexes will be included in the selection of examples presented hereinafter.

2.1.1 Insertion Products of Early Transition-Metal and f-Element Phosphido Complexes

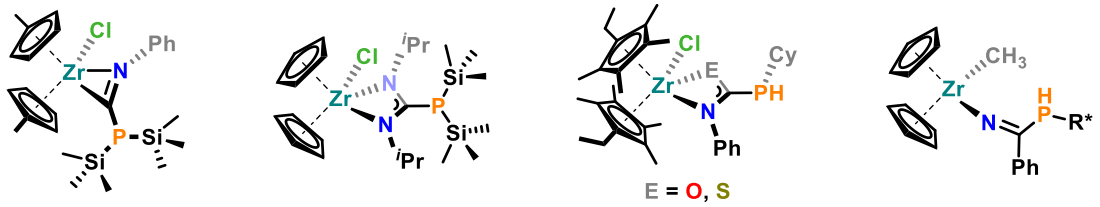

Figure 2.1. Selection of insertion products of zirconium(IV) phosphido complexes by the groups of Hey-Hawkins and Stephan (R* = C_6H_2-2,4,6-^{t}Bu).[20,21,25]

The usefulness of insertion reactions at labile (early transition) metal – phosphide bonds for the straight-forward access to rare and otherwise synthetically challenging phosphorus-containing structural motifs was worked out for zirconium by the groups of Hey-Hawkins[20,21,26] and Stephan[22,25,27] in the 1990s. Their comprehensive spectroscopic and structural studies covered, *i.a.*, phosphaguanidinates,[21] phospha(thio)ureates[20] and phosphaamidinates[22,27] bound to zirconium(IV) (Figure 2.1). The synthetic protocols are typically straight-forward: The insertions into the Zr–P bond take place almost instantaneously in solution or within minutes for suspensions at room temperature and generally give high yields (>70%) after crystallization from concentrated aliphatic or aromatic solvents, respectively.[20,21,25] The reactions of primary phosphido ligands proceed as cleanly as the ones of secondary phosphides with retention of the proton at phosphorus (Figure 2.1, right). Due to the pronounced high-field shifts of the ^{31}P resonances of the products, the reactions can be easily monitored by ^{31}P NMR spectroscopy: The ^{31}P resonances of the phospha(thio)ureate complexes [(η^5-C_5EtMe_4)$_2$ZrCl{EC(NPh)(PHCy)}] (E = O, S; Figure 2.1, third from left), for instance, lie at δ = –50.8 ppm (for E = O) and δ = –16.1 ppm (for E = S) compared to δ = 71.7 ppm for starting complex [(η^5-C_5EtMe_4)$_2$ZrCl(PHCy)].[20] Additionally, the respective $^1J_{PH}$ coupling constant of around 225 Hz is indicative of the retained *PH* group.[28] In the cases of the phospha(thio)ureate examples X-ray structure analyses revealed essentially trigonal-planar geometries at the central (thio)ureate quartenary carbon atoms and delocalization of π-electrons along the [E=C=N]-fragments, as might be expected for the κ^2 (carboxylate-like) binding mode. In contrast, the mean carbon – phosphorus distance of ≈1.86 Å as well as the pyramidalization at phosphorus indicate no substantial conjugation between the [E=C=N]-fragments and the PHCy substituent, which therefore resembles a "classical" phosphanyl group.[20]

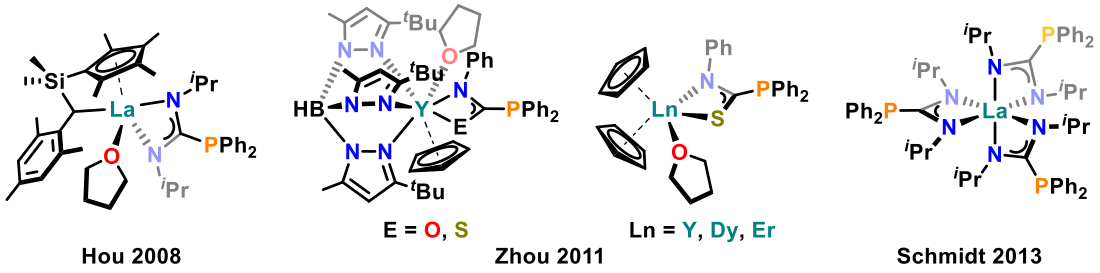

Figure 2.2. Structurally confirmed insertion products of lanthanide(III) and yttrium(III) phosphido complexes.[14–16]

Until now insertion reactions of lanthanide(III) phosphido complexes have been mainly investigated in the context of catalytic hydrophosphin(yl)ation reactions.[11,14–16,29–31] However, only a few structurally authenticated insertion products exist in the literature. These are namely phosphaguanidinates and phospha(thio)ureates of lanthanum, erbium and dysprosium as well as the rare earth metal yttrium (Figure 2.2), which were reported by the groups of Hou,[16] Zhou,[14] and Schmidt[15] from 2008 to 2013.

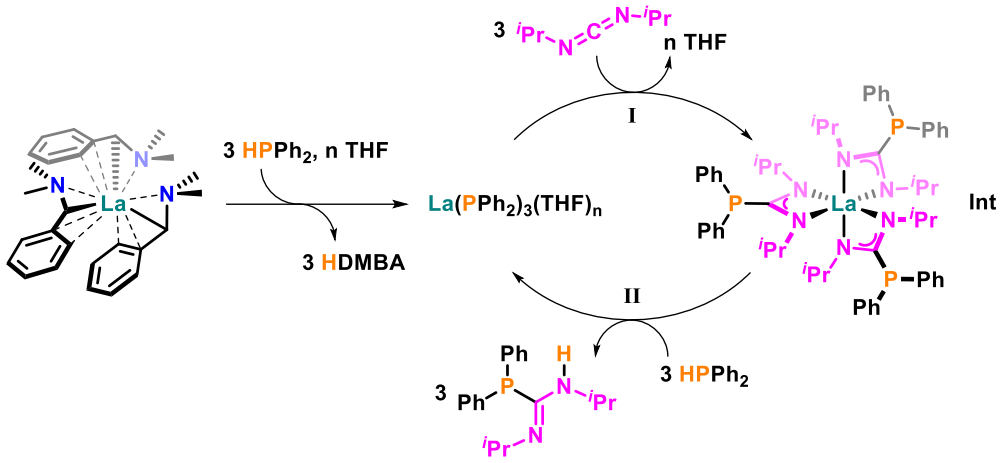

Scheme 2.2. Catalytic cycle for the hydrophosphination of *N*,*N*'-diisopropylcarbodiimide with diphenylphosphine and [La(α-DMBA)$_3$]-precatalyst at room temperature, as proposed by Behrle and Schmidt.[15] The inserted fragments are highlighted in pink.

An exemplary catalytic cycle for a room temperature lanthanide(III)-catalyzed hydrophosphination of *N*,*N*'-diisopropylcarbodiimide with diphenylphosphine from 2013 is given in Scheme 2.2. Behrle and Schmidt used 5 mol-% of the precatalyst [La(α-DMBA)$_3$][32] (α-DMBA$^-$ = α-deprotonated dimethylbenzylamine) and initiated the catalytic process by protonolysis with diphenylphosphine in THF (left).[15] The resulting active species [La(PPh$_2$)$_3$(THF)$_n$] can insert three equivalents of carbodiimide (step I), which the authors confirmed by isolating and structurally characterizing the corresponding insertion product (Int, right). Protonolysis with three equivalents of diphenylphosphine expels the phosphaguanidine products and regenerates [La(PPh$_2$)$_3$(THF)$_n$] (step II). Note that 5 mol-% of isolated tris(phosphaguanidinate) complex also showed a high catalytic activity, thereby strongly suggesting its occurrence in the catalytic cycle. Apart from carbodiimides, a wide range of alkyl and aryl iso(thio)cyanates could be hydrophosphinated employing the same precatalyst, presumably *via* the tris(phospha(thio)ureate) complexes.[15] However, as becomes clear from the selection of lanthanide(III) insertion products shown in both Figure 2.2 and Scheme 2.2, the use of diphenylphosphine has dominated the field, which left no further possibility for functionalization after insertion (see also the following discussion of thorium(IV) phosphido complexes and Section 2.1.2 for further explanations).

During the last few years compounds bearing Ac–P phosphide bonds (Ac = Th, U) have gained increasing attention because of their diverse insertion chemistry with small molecules such as carbon monoxide (CO) or carbon dioxide (CO$_2$) and organic substrates with polar double bonds.[17,18,33–35] In contrast to uranium, the strongly preferred oxidation state of thorium is +IV, so that any redox changes

associated the Th^{4+} ion itself can be ruled out under the mild, non-reductive conditions of the insertion reactions.[36–38] Similar to zirconium(IV), the redox stability, high Lewis acidity and oxophilicity of thorium(IV) should make its phosphido complexes behave in many respects much like similar lanthanide(III) compounds, in which the highly Lewis acidic, oxophilic Ln^{3+} ions do not engage in redox chemistry as well (with the exception of the $Ce^{3+/4+}$, $Sm^{2+/3+}$, $Eu^{2+/3+}$ and $Yb^{2+/3+}$ redox pairs).[39] Only the number of anionic ligands, which can be accommodated by the metal ion, is higher for Th^{4+} than for Ln^{3+} ions. As a consequence, stable (bis)phosphido complexes are more common for thorium(IV)[17,33,34,36,40,41] than for the lanthanides.[42,43] Apart from this difference, the insertion reactivity of thorium(IV) and lanthanide(III) phosphido complexes should be comparable to some extent.

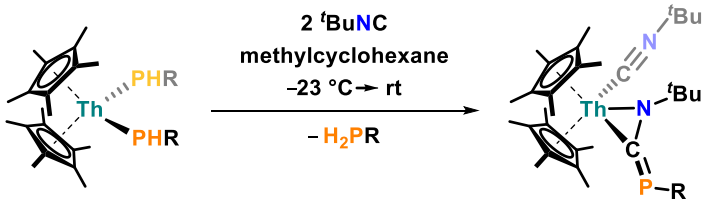

Scheme 2.3. Thorium(IV) phosphaazaallene complexes synthesized by Behrle and Walensky (R = 2,4,6-trimethylphenyl or 2,4,6-triisopropylphenyl).[33]

Important insights into the potential follow-up chemistry of f-element insertion products have been gained from thorium(IV) complexes featuring primary phosphido ligands with *PH* groups. For instance, Behrle and Walenksy found that the complexes $[(Cp^*)_2Th(PHR)_2]$ ($Cp^{*-} = C_5Me_5^-$; R = 2,4,6-trimethylphenyl or 2,4,6-triisopropylphenyl) react with two equivalents of *tert*-butyl isocyanide, respectively, to give rare η^2-(*N*,*C*)-phosphaazaallene structural motifs (Scheme 2.3).[33] Against the chemical intuition that insertion of *tert*-butyl isocyanide would take place at both phosphido ligands in a symmetrical fashion, insertion into one Th–P bound and deprotonation of the new P-functionalized ligand by the second phosphido ligand had occurred instead, with the second isocyanide ligand being coordinated to the Th^{4+} ion. This unusual transformation indicates that the proton bound to phosphorus can be removed relatively easily after insertion.

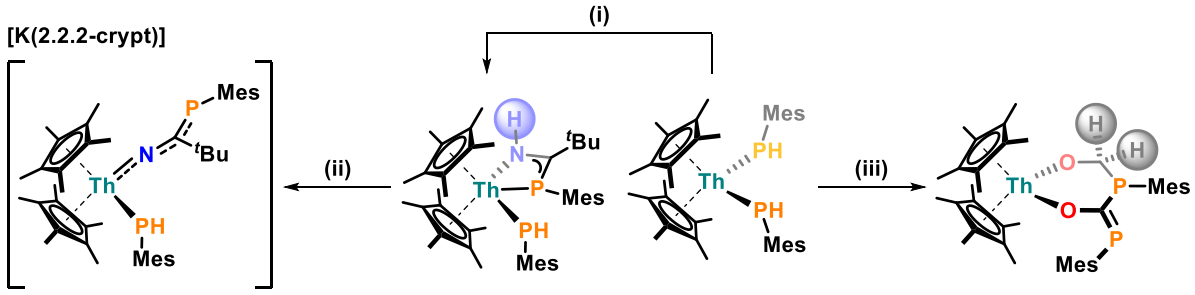

Scheme 2.4. Additional insertion reactions and follow-up chemistry reported for the complex $[(Cp^*)_2Th(PHMes)_2]$ by Walensky and co-workers in 2018.[34] The new positions of the protons which were transferred from the former phosphido ligands are highlighted by spheres. Conditions: (i) *tert*-butyl nitrile (excess), toluene, –40 °C → rt, 2 h, – remaining excess of *tert*-butyl nitrile; (ii) $KN(SiMe_3)_2$ (1.09 equiv), 2.2.2-cryptand (1.15 equiv), toluene, –25 °C → rt, 1 h, – $HN(SiMe_3)_2$, – excess 0.09 $KN(SiMe_3)_2$, – excess 0.15 2.2.2-cryptand; (iii) CO (1 atm), C_6D_6, –196 °C → rt, 10 min, – remaining excess of CO.

A similar example, in which *tert*-butyl nitrile inserts into one of the Th–P bonds of $[(Cp^*)_2Th(PHMes)_2]$, was reported by the group of Walensky in 2018 (Scheme 2.4).[34] In contrast to the reaction with *tert*-butyl isocyanide, the second mesitylphosphido ligand remained bound to thorium(IV), even with an excess of nitrile. However, it was found again that the P*H* proton of the reacted phosphido ligand was removed from the phosphorus atom and in this particular case transferred to the nitrogen atom of the new κ^2-(*N*,*P*)-bonded phosphaamidinate ligand (Scheme 2.4, middle). More significantly, deprotonation of the *NH* group with potassium hexamethyldisilazide and 2.2.2-cryptand led to a rare dianionic, κ^1-(*N*)-bonded aza-1-phosphaazaallyl moiety (Scheme 2.4, left). In the same contribution, the authors showed that the P*H* protons of both primary phosphido ligands can be transferred to the carbon atom of an inserted CO molecule (Scheme 2.4, right), further pointing out the high utility of *PH* groups in the follow-up chemistry of insertion products derived from f-element primary phosphido complexes.

2.1.2 Heterometallic Lanthanide–Coinage-Metal Complexes

During the last 20 years increasing efforts have been made to design and modify lanthanide-based systems, which exhibit intriguing physical properties for potential applications in chemical sensoring, medicine and information technologies.[44–49] Middle and late transition-metals have gained a lot of attention in this development,[50] since they are known to influence the magnetic and photophysical behavior of lanthanide(III) complexes (Figure 2.3).[51–54] While the effects of introducing 3d-metals into lanthanide(III)-based systems were studied in the context of magnetic behavior (red boxes),[55–72] mainly 4d- and 5d-metals were used as antennae for photosensitization of lanthanide(III) ions (yellow boxes).[53,73–90] Contrasting the large number of examples with iron,[59–66] nickel,[67–70] ruthenium,[53,73,76–79,81,82] platinum,[84–86,89] zinc[70–72,83,91] and cadmium,[75,80,83,88] which currently still dominate the field of heterometallic lanthanide–transition-metal systems, there are only a few cases, in which the coinage-metals copper,[52,55,56,58] silver[89] and gold[87,89,90] have been employed.

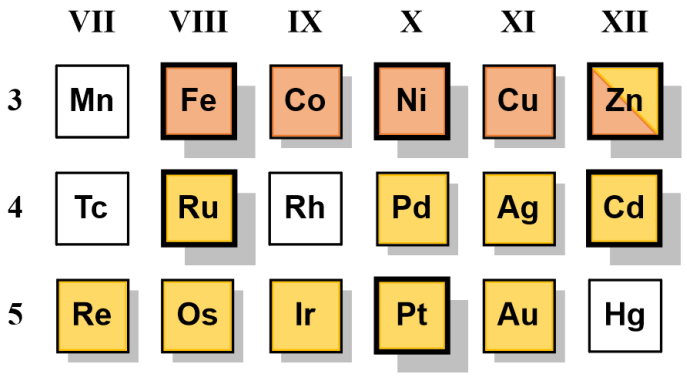

Figure 2.3. Middle and late transition-metals (groups VII – XII; rows 3 – 5), which have been used to influence the magnetic[55–72] (red) or photophysical[53,73–90] (yellow) properties of lanthanide(III) complexes. The thickness of the boxes serves as a rough relative measure of the number of reported examples for each element, respectively.

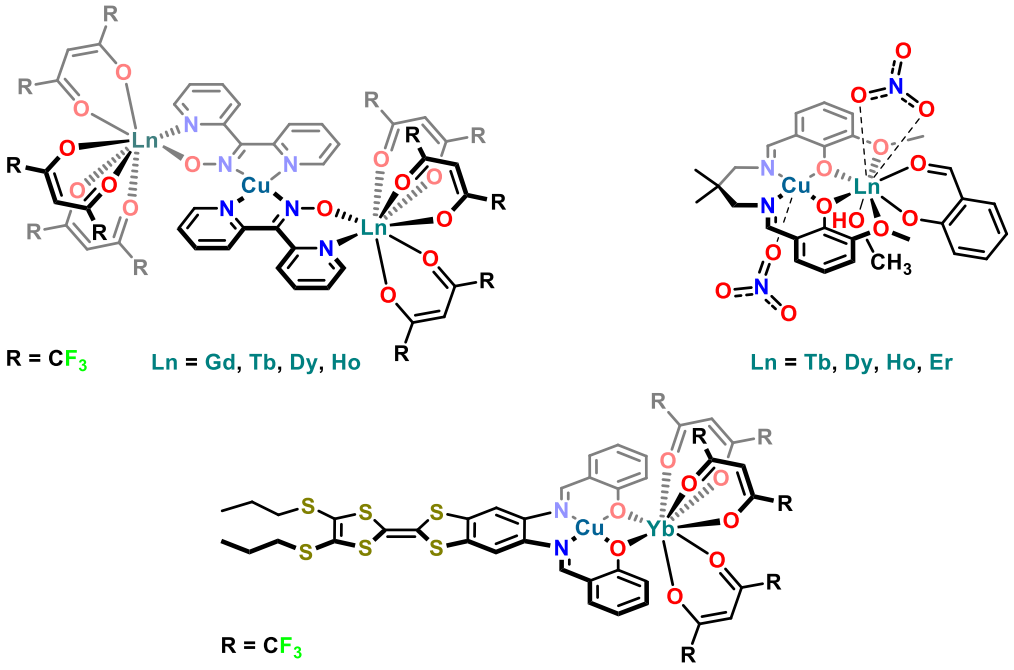

Figure 2.4. Selection of lanthanide(III)–copper(II) heterobimetallic and -trimetallic complexes.[52,55,56]

In the case of copper, so far the d^9-configurated Cu^{2+} ion was combined with Ln^{3+} ions in heterobimetallic or –trimetallic systems (Figure 2.4).[52,55,56] Therefore, the analyses of the physical properties of these complexes were focused on the magnetic interactions between the paramagnetic Cu^{2+} and Ln^{3+} ions. Ligand scaffolds with O and N donor atoms based on di-2-pyridyl-ketoxime[56] (top left) or *N*,*N*'-linked bis(salicylideneimine)[52,55] (top right and bottom) were selected for the bridging of the metal ions. Hexafluoroacetylacetonate (top left and bottom) and nitrate (top right) were used to complete the coordination spheres of the Ln^{3+} ions. Intriguingly, no lanthanide(III)–copper(I) systems have been reported to date.

Similar to the Ln–Cu systems, examples of lanthanide(III)–gold(I) heterobimetallic complexes are rare in the literature. A series of gold(I) phosphine acetylide bridged lanthanide(III) compounds were reported in 2008 and 2010 (Figure 2.5).[87,90] The Ln^{3+} ions were coordinated to 2,2'-bipyridine (top) or 2,2',2''-terpyridine ligands (bottom) tethered to gold (I) acetylide or phenyl acetylide, respectively. Two of these dinuclear arrangements were further connected by bis(phosphines) to give heteropolynuclear Ln_2Au_2 or Ln_4Au_4 (not shown) arrays, and – in the case of the 1,1'-bis(diphenylphosphino)ferrocene (dppf) bridging unit – iron(II) was integrated as well (top). Due to the rearrangements induced by the coordination of the sterically demanding lanthanide(III) complex fragments, in most of the Ln_2Au_2 complexes, the former aurophilic interactions[92] between the two Au^+ ions were not preserved (except for Ln = Er, which led to the Er_4Au_4 array).[87] Although the distances between the Ln^{3+} and Au^+ ions in these dyads lie in the range of approximately 8 to 9 Å (*e.g.*, 8.25 to 8.77 Å for Er^{3+}),[87] the gold(I) acetylide chromophores were shown to act as good energy donors for the sensitization of lanthanide(III)-centered emissions in the visible and near-infrared (NIR) part of the spectrum.[87,90] However, a major drawback of this series of Ln–Au systems is that larger amounts of gold(I) acetylides represent

potentially explosive materials, which has to be considered as a safety issue in the development of such arrays, even though acetylides with larger organic substituents are probably less prone to undergo sudden decomposition.

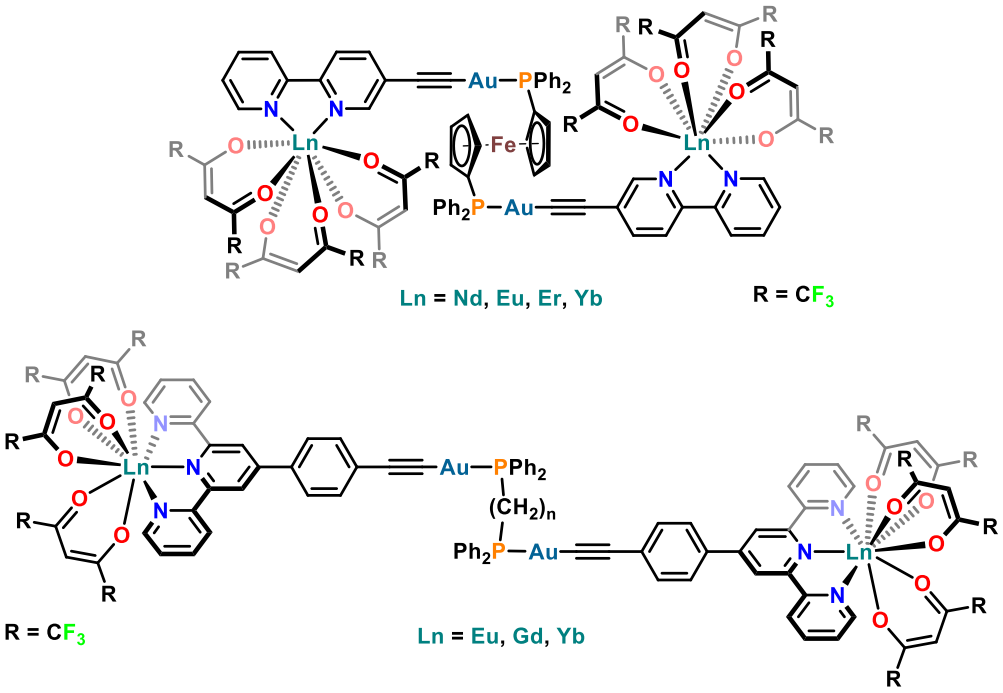

Figure 2.5. Selection of lanthanide(III)–gold(I) heterotetrametallic complexes (n = 2–5).[87,90]

A noteworthy example, in which gold(I) and also silver(I) – paired with either palladium(II) or platinum(II) – act as room temperature photosensitizers for the prominent red luminescence of europium(III), was reported only recently by Chorazy and co-workers.[89] The layered two-dimensional coordination polymers have the formal composition $\{[Eu^{III}(4,4'\text{-bpdo})(H_2O)_2][M^{II}(CN)_4]\}\cdot[M^{I}(CN)_2]\cdot H_2O$ (with $M^{II} = Pd^{II}$ or Pt^{II}; $M^{I} = Ag^{I}$ or Au^{I}; and 4,4'-bpdo = 4,4'-bipyridine-*N*,*N*'-dioxide) and benefit from intermetallic d–f cyanide bridges. However, the authors stated that the variation of the metal–metal distances, which is of importance for the tailoring of the emission properties, remains a challenge with these kind of systems, considering the different possible outcomes for related self-assembled supramolecular architectures.[89]

Despite the recent groundbreaking achievements with two-coordinate copper(I) and gold(I) carbene complexes in the fields of photochemistry,[93–96] such coinage-metal carbene units have not been combined with Ln^{3+} ions in heterobimetallic systems yet. This is not surprising, since the synthetic methodologies described above for the compounds drawn in Figures 2.4 and 2.5 do not give access to this particular type of lanthanide–coinage-metal complexes with carbene supporting ligand. However, in regard of the rich insertion chemistry of early transition-metal and f-element phosphido complexes (see Section 2.1.1), an innovative approach can be devised, which combines both oxygen and nitrogen with phosphorus in one bridging ligand obtained by insertion and takes advantage of the preferred binding of oxygen and nitrogen to lanthanides(III) as well as of phosphorus to copper(I) and gold(I).

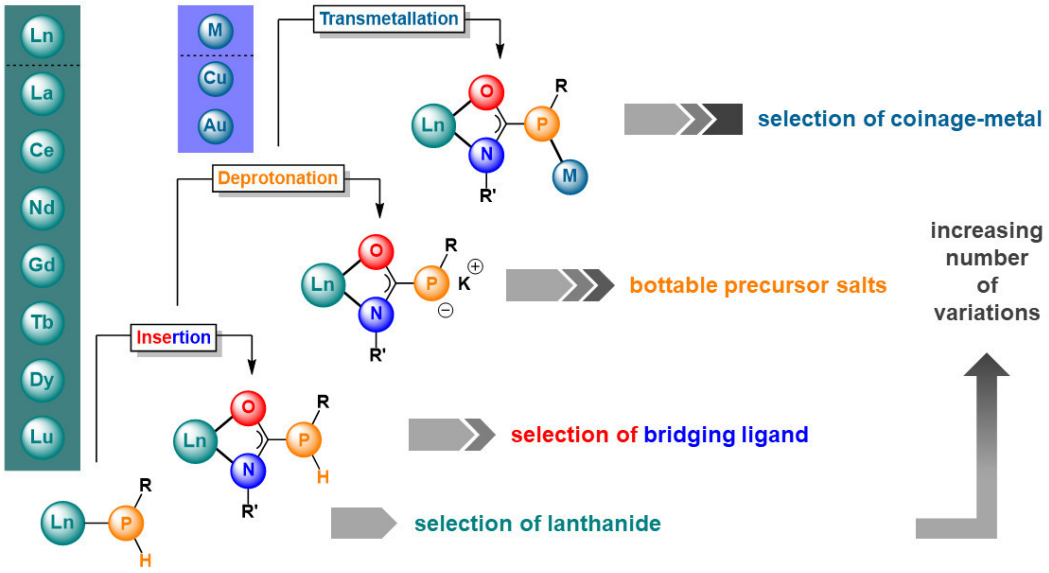

Scheme 2.5. Strategy developed for the synthesis of a library of heterobimetallic lanthanide-coinage-metal systems utilizing Ln–P primary phosphide groups (structures from bottom left to top right; R, R' = alkyl, aryl). Example with phosphaureate (bridging) ligand; simplified representations (no supporting ligands or charges at Ln and M shown). Selection of Ln^{3+} ions (from Chapter 1) and suitable coinage-metals in the +I oxidation state (M = Cu, Au) are listed in the turquoise and blue boxes in the top left corner, respectively. The grey arrow bars from bottom left to top right next to the structures illustrate the modular, bottom-up approach, which results in an increasing number of possible changes with each step (arrow in the bottom right corner).

The synthetic strategy is summarized in Scheme 2.5 and consists of consecutive insertion, deprotonation and transmetallation steps. As was already discussed in the context of insertion products derived from thorium(IV) primary phosphido complexes,[33,34] the *PH* group offers the possibility for further reactivity after insertion of an organic substrate (in this case an isocyanate) into the Ln–P bond: The P*H* proton in the new (phosphaureate) ligand should be acidic enough to be removed by conventional, strong bases such as potassium hexamethyldisilazide and consequently give a (phosphaureate) bridging unit. A great overall advantage of this synthetic strategy is that each step allows the selection of different Ln^{3+} ions, organic substrates for insertion or coinage-metal ions (M^+). The modularity of this bottom-up approach should therefore offer a lot of flexibility, if, *e.g.*, deprotonation and transmetallation of a particular insertion product to a defined heterobimetallic system turns out to be synthetically unfeasible. The intermediate isolation of the deprotonated insertion products is optional, but should ideally yield bottable precursor salts, which could in turn also be tested in transmetallation reactions with other late transition-metal ions favoring anionic P donors.[97–101] The desired carbene supporting ligands at the coinage-metals should be easily introduced with suitable coinage-metal precursor complexes as well.

A proof-of-principle for this route to new heterobimetallic lanthanide–coinage metal complexes is demonstrated in the following published manuscript.

2.2 Results and Discussion

Publication: Isocyanate Insertion into a La–P Phosphide Bond: A Versatile Route to Phosphaureate-Bridged Heterobimetallic Lanthanide–Coinage-Metal Complexes

Fabian A. Watt,[a] Nicole Dickmann,[a] Roland Schoch,[a] and Stephan Hohloch*[b]

* Corresponding author

[a] Paderborn University, Warburger Straße 100, 33098 Paderborn, Germany

[b] University of Innsbruck, Innrain 80-82, 6020 Innsbruck, Austria

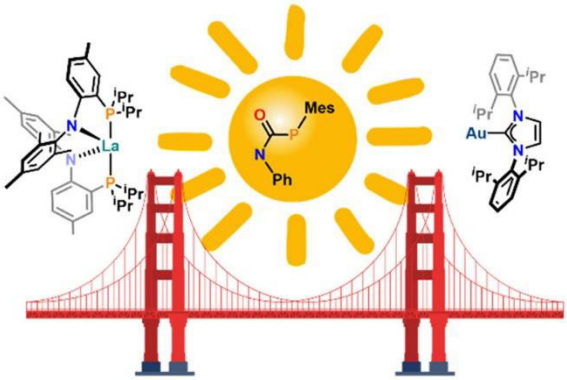

This article was published as follows:

Watt, F. A.; Dickmann, N.; Schoch, R.; Hohloch, S. *Inorg. Chem.* **2020**, *59*, 13621–13631.

DOI: 10.1021/acs.inorgchem.0c01971

https://doi.org/10.1021/acs.inorgchem.0c01971

Synopsis: A new route to heterobimetallic lanthanide–coinage-metal complexes is disclosed by capitalizing on the insertion of phenylisocyanate into a La–P primary phosphide bond and subsequent deprotonation and salt metathesis with a selection of coinage-metal carbene precursors.

Author Contributions: The project was designed by S. Hohloch and F. A. Watt. Experimental work was carried out by F. A. Watt and N. Dickmann. NMR and IR spectra were recorded by F. A. Watt and N. Dickmann. X-ray structure analyses were performed by R. Schoch and S. Hohloch. The manuscript was written by F. A. Watt and S. Hohloch and proof read by all authors.

Dr. Hans Egold from the NMR facility of Paderborn University and Athul Krishna are kindly acknowledged for helpful discussions. Christiane Gloger and Maria Busse are kindly acknowledged for conducting elemental analyses.

Inorganic Chemistry

pubs.acs.org/IC Article

Isocyanate Insertion into a La–P Phosphide Bond: A Versatile Route to Phosphaureate-Bridged Heterobimetallic Lanthanide–Coinage-Metal Complexes

Fabian A. Watt, Nicole Dickmann, Roland Schoch, and Stephan Hohloch*

Cite This: *Inorg. Chem.* 2020, 59, 13621–13631 Read Online

ACCESS | Metrics & More | Article Recommendations | Supporting Information

ABSTRACT: A new route to heterobimetallic lanthanide–coinage-metal complexes is disclosed. The selective insertion of organic substrates such as phenyl iso(thio)cyanate into the La–P bond of the primary phosphido complex **(PN)$_2$La(PHMes)** (**1**) (with PN$^-$ = (*N*-(2-(diisopropylphosphanyl)-4-methylphenyl)-2,4,6-trimethylanilide) yields the phospha(thio)ureate complexes **(PN)$_2$La(OC(NPh)(PHMes))** (**2**) and **(PN)$_2$La(SC(NPh)(PHMes))** (**3**) with retention of the P*H* protons. Subsequent deprotonation of the phosphaureate complex **2** with potassium hexamethyldisilazide (KHMDS, K[N(SiMe$_3$)$_2$]) leads to the polymeric complex **[K{(PN)$_2$La(OC(NPh)(PMes))}]$_n$** (**4**). Complex **4** was found to be an excellent precursor for salt metathesis reactions with copper(I) and gold(I) chlorides supported by an N-heterocyclic carbene (NHC, **5** and **6**) or a cyclic alkyl amino carbene (CAAC, **7** and **8**). This resulted in the unprecedented formation of heterobimetallic lanthanum–coinage-metal complexes, containing the first example of a $\mu,\kappa^2(O,N):\kappa^1(P)$-phosphaureate bridging ligand. For an alternative route to complex **8** a direct protonolysis protocol between a new basic gold(I) precursor, namely **(^{Me}CAAC)Au(HMDS)**, and **2** was also investigated. The complexes have been characterized by multinuclear NMR spectroscopy, IR spectroscopy, and X-ray crystallography (except for **8**).

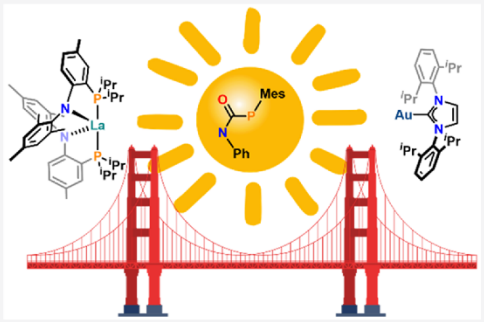

INTRODUCTION

The chemistry of the lanthanides (Ln) has advanced to be a very important field of research in modern inorganic chemistry.[1,2] As lanthanides are well-known for their magnetic and luminescent properties, the applications of lanthanide-containing molecules range from molecular magnetism[3−11] and (bio)analytical sensors[12−14] to optical communication[15] and modern catalysis.[16−31] In recent years, new strategies to systematically analyze and design lanthanide complexes with the desired chemical, magnetic, or photophysical properties have emerged.[4,6,32−35] In this context, transition metals such as iron(0/II/III),[36−43] nickel(II),[44−47] and zinc(II)[45,48,49] have been used to influence the magnetic behavior of lanthanide compounds, whereas e.g. iridium(III),[50] rhenium(I),[51] platinum(II),[51−54] palladium(II),[54] zinc(II),[48,55] gold(I),[54,56,57] and silver(I)[54] have been introduced for efficient sensitizing of lanthanide luminescence[58−60] in heterobimetallic or -trimetallic systems. Despite these significant advances, straightforward and rational designs of heterobimetallic lanthanide–coinage-metal complexes in particular have not been much developed as yet.

Early-transition-metal and f-element phosphido complexes are known to show a rich insertion chemistry which is very useful for the construction of exotic and rare types of phosphorus-containing ligands directly at the metal ion. A considerable number of examples have been reported by the groups of Hey-Hawkins and Stephan in the 1990s and include, for instance, phosphaguanidinates,[63] phospha(thio)ureates[64] and phosphaamidinates[65,66] at zirconium(IV). In recent years, more examples of analogous lanthanide and actinide (Ac) complexes have accumulated.[28,31,61,62,67−73] From a thermodynamic point of view, the favorable exchange of rather weak M–P bonds for more ionic M–N or M–O bonds provides the main driving force in these processes.[23] The insertion of carbodiimides, iso(thio)cyanates, and nitriles as well as alkynes and olefins into Ln–P (or Ac–P) bonds is also considered a crucial elementary step in lanthanide (or actinide)-catalyzed hydrophosphin(yl)ation reactions.[26−31,62,74] The complexes which are intermediately formed in these catalytic cycles can often be isolated and characterized in separate stoichiometric experiments (Figure 1).[28,31,61,62]

To date, in the case of lanthanide complexes diphenylphosphanyl-substituted insertion products have been investigated

Received: July 3, 2020
Published: September 4, 2020

https://dx.doi.org/10.1021/acs.inorgchem.0c01971
Inorg. Chem. 2020, 59, 13621−13631

Inorganic Chemistry pubs.acs.org/IC Article

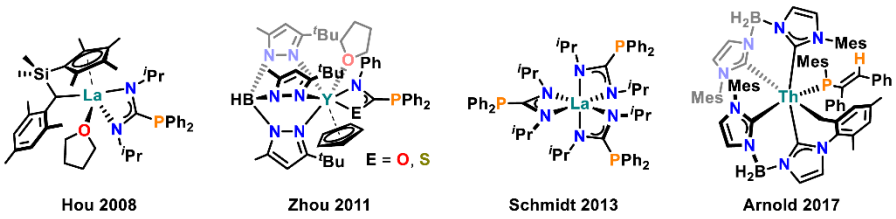

Figure 1. Selection of isolated insertion products of lanthanide and actinide phosphido complexes.[28,31,61,62]

almost exclusively, leaving no possibility for further functionalization of the newly formed coordinated ligand. Still, there is one example in the literature of functionalizing related guanidinate ligands at the pnictogen (N) atom in the first coordination sphere of lanthanide ions (Scheme 1).[75] This

Scheme 1. Functionalization of a Guanidinate Ligand in the First Coordination Sphere of Lanthanide Ions (R = Me, ^{t}Bu[75])

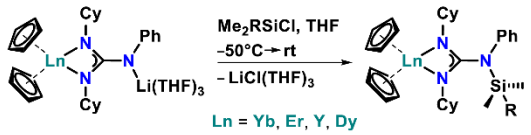

report by Zhou and co-workers from 2010 showed that heterobimetallic lanthanide–lithium complexes, obtained by deprotonation of coordinated guanidinate with *n*-butyllithium, can be selectively silylated. However, the authors did not further investigate transmetalation reactions to obtain other, more interesting heterobimetallic systems.

In 2018, Walensky and co-workers presented the addition of *tert*-butylnitrile across one of the Th–P bonds of a thorium(IV) bis(mesitylphosphido) complex with concurrent proton transfer from phosphorus to nitrogen (Scheme 2).[68] Intriguingly, the newly formed phosphaamidinate ligand could be selectively deprotonated by a strong base such as KHMDS in the presence of 2,2,2-cryptand, resulting in a rare example of an end-on-coordinated dianionic aza-1-phosphaallyl ligand.

Recently, our group has reported the synthesis of primary phosphido complexes **(PN)$_2$Ln(PHMes)** (Ln = La, Lu) supported by a bidentate, monoanionic anilidophosphine ligand (*N*-(2-(diisopropylphosphanyl)-4-methylphenyl)-2,4,6-trimethylanilide, abbreviated PN$^-$).[76] Intrigued by the examples of Walensky[68] and Zhou,[75] we were interested if our complex **(PN)$_2$La(PHMes)** (**1**) is prone to undergo a similar insertion chemistry with heterocumulenes. This type of reactivity has already been reported for group IV and actinide primary phosphido complexes[64,71] but is virtually nonexistent for lanthanides. We envisioned that retention of the P*H* proton after insertion might be a valuable tool to obtain further reactivity: i.e., deprotonation and subsequent metalation with late-transition-metal complexes. In the following, we will describe the successful application of this strategy to obtain new types of heterobimetallic lanthanum–copper(I) and lanthanum–gold(I) complexes.

RESULTS AND DISCUSSION

On consideration of the NMR spectroscopic advantages of diamagnetic lanthanum(III) compounds and the straightforward multigram-scale synthesis of the respective chloride precursor complex,[76] the primary phosphido complex **1** was chosen as the starting point for the evaluation of our targeted synthesis route. The first step of the reaction sequence, namely the insertion of either phenyl isocyanate or phenyl isothiocyanate into the La–P phosphide bond in **1** (Scheme 3), was found to proceed quickly at room temperature. This was indicated by an immediate color change from deep yellow to pale yellow during the addition of 1 equiv of phenyl iso(thio)cyanate.

The reactions could be easily monitored by ^{31}P NMR spectroscopy, showing that within minutes full and clean conversion to a new complex had occurred in both cases. Removal of toluene *in vacuo* followed by trituration and washing with *n*-hexane or *n*-pentane gave an analytically pure product as an off-white (**2**) or pale yellow (**3**) powder in good isolated yields (>80%), respectively. Like the phosphido complex **1**, the ^{31}P NMR spectra of the new complexes **2** and **3** in C_6D_6 show one singlet resonance for two chemically equivalent PN ligands as well as a doublet resonance for the PHMes moiety in a ratio of 2:1. A pronounced high-field shift of the *P*HMes doublet resonance from δ −36.4 ppm (**1**) to δ −90.1 and −56.4 ppm for **2** and **3**, respectively, indicated the successful insertion of phenyl iso(thio)cyanate. Similar ^{31}P shifts upon insertion of various iso(thio)cyanates into Zr–PHR (R = Cy, 2,4,6-^{i}Pr$_3$C$_6$H$_2$) bonds have been reported earlier.[64] Additionally, the large doublet splittings of 242.8 and 242.4 Hz magnitudes for **2** and **3**, respectively, lie in the typical range of $^1J_{PH}$ coupling constants.[64,69,76−78] These couplings disappear in the ^{31}P{^{1}H} NMR spectra to give singlet

Scheme 2. Insertion of *tert*-Butylnitrile into a Th–P Bond of a Thorium(IV) Bis(mesitylphosphido) Complex, Followed by Deprotonation of the Phosphaamidinate Ligand[68]

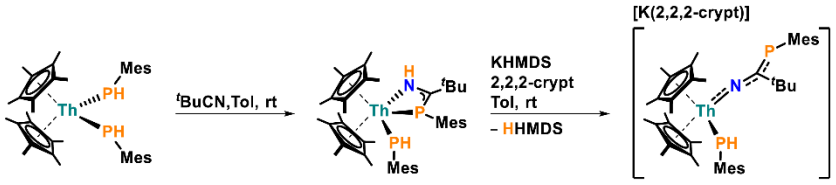

https://dx.doi.org/10.1021/acs.inorgchem.0c01971
Inorg. Chem. 2020, 59, 13621−13631

Inorganic Chemistry pubs.acs.org/IC Article

Scheme 3. Insertion of Phenyl Isocyanate or Phenyl Isothiocyanate into the La−P Phosphide Bond of 1, Yielding Phospha(thio)ureate Complex 2 or 3

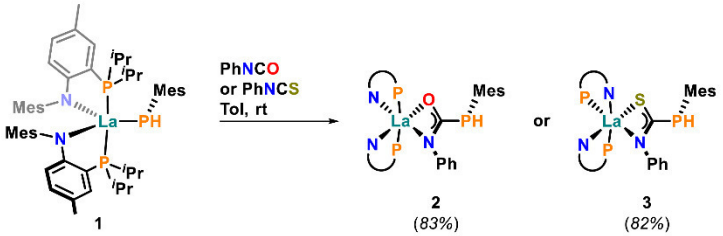

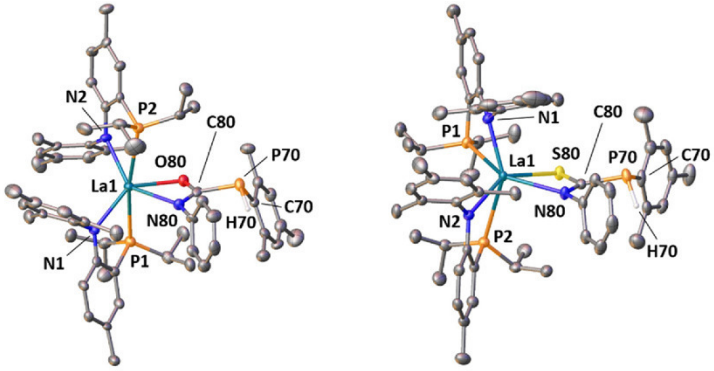

Figure 2. Thermal ellipsoid plots of **2** (left) and **3** (right). Thermal ellipsoids are shown at a probability level of 30%. Hydrogen atoms (except for H70) and solvent molecules have been omitted for clarity.

resonances, unambiguously confirming the retention of the P*H* proton. Likewise, the PN ligand resonances of **2** and **3** are also shifted to high fields (δ 6.3 ppm (**2**) and 6.9 ppm (**3**) compared to δ 11.0 ppm for **1**). This is in agreement with an increase in the coordination number at lanthanum(III) by +1 and a diminished degree of donation from the $^{i}Pr_2$-phosphanyl groups to the lanthanum atom after insertion. In the corresponding ^{1}H NMR spectra, the presence of a new set of aromatic resonances due to the introduced phenyl substituent as well as significant low-field shifts of the P*H* resonance from δ 3.42 ppm for **1** to δ 5.11 and 5.32 ppm for **2** and **3**, respectively, can be considered as additional indicators of successful phospha(thio)ureate formation. Finally, the expected connectivity was further confirmed by $^{13}C\{^{1}H\}$ NMR spectroscopy, with new resonances at low fields of δ 186.5 ppm (**2**) and 208.0 ppm (**3**) for the PhNCX quaternary carbon atom of the inserted iso(thio)cyanate fragment (X = O, S). The observed doublet splitting of 35 Hz magnitude in the case of **2** results from $^{1}J_{CP}$ coupling to the adjacent *P*HMes phosphorus atom and compares very well to reported literature values.[64]

Unambiguous structural proof for the formation of insertion products **2** and **3** was obtained by X-ray diffraction studies (Figure 2). X-ray-quality crystals were obtained by either storing a concentrated solution of **2** in a mixture of *n*-hexane and a minimal amount of toluene obtained during workup or gas diffusion of *n*-hexane into a C_6D_6 solution of **3**, at room temperature, respectively. Complex **2** crystallizes in the monoclinic space group $P2_1/n$ with half a molecule of *n*-hexane in the asymmetric unit, while complex **3** was found to crystallize in the triclinic space group $P\bar{1}$ without solvent molecules in the lattice.

In both cases, the lanthanum atom is six-coordinate in a strongly distorted octahedral, almost trigonal prismatic fashion[28] by two PN ligands as well as the nitrogen and chalcogenide atoms of the newly formed phospha(thio)ureate ligand. Complex **2** exhibits a *trans* arrangement of the $^{i}Pr_2$-phosphanyl groups (P1−La1−P2 angle of 170.40(4)°), with the inserted PhNCO fragment being roughly perpendicular to it (P1/2−La1−O80 and P1/2−La1−N80 angles between 80.08(1) and 95.40(1)°, respectively). Interestingly, in the case of **3** the phosphanyl groups are *cis* to each other (P1−La−P2 angle of 82.80(6)°), indicating a high flexibility of the PN ligands for rearrangement around the lanthanum atom. While the La1−N80 distances to the phospha(thio)ureate ligand of 2.616(5) and 2.646(3) Å in **2** and **3**, respectively, are slightly larger in comparison to the average La1−N1/N2 distances of around 2.41 and 2.45 Å, both La1−N80 and La1−O80/S80 distances (2.448(4) and 2.972(2) Å, respectively) are only somewhat larger (0.05−0.2 Å) than those in related lanthanide phosphido insertion products.[28,31,61] We attribute these minor differences to slightly different ionic radii as well as the high steric demand of the two PN supporting ligands.[76] The N80−La1−O80/S80 angles of 52.2(1) and 55.57(6)° are only slightly more acute than reported angles in related Zr(IV) phospha(thio)ureate complexes.[64] The new C80−P70 bond in **2**/**3** has a length of 1.856(6) Å/1.865(3) Å, and the XCNP core (X = O, S) of the phospha(thio)ureate ligand is found to be essentially planar with sums of angles around C80 of ~359.7 and ~359.1°, respectively. In summary, all these structural parameters lie in the expected range for phospha-(thio)ureates in the coordination sphere of highly electro-positive metal ions.[61,64] Additional information on the

https://dx.doi.org/10.1021/acs.inorgchem.0c01971
Inorg. Chem. 2020, 59, 13621−13631

Scheme 4. Deprotonation of Complexes 2 and 3 with KHMDS

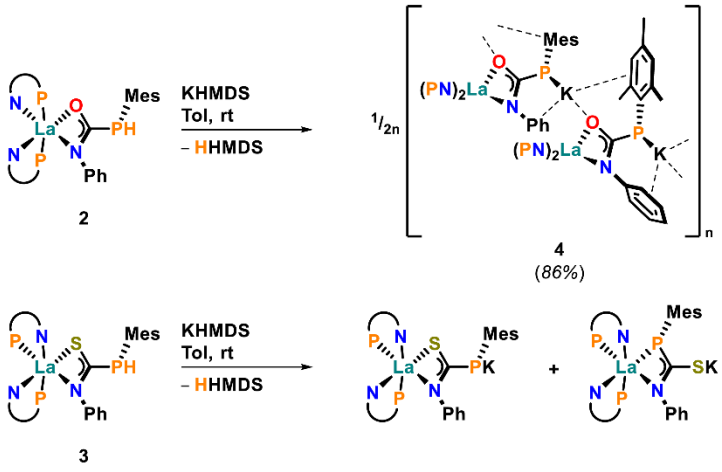

Scheme 5. Salt Metatheses of 4 with a Selection of Carbene Coinage-Metal Chlorides to Yield Complexes 5−8

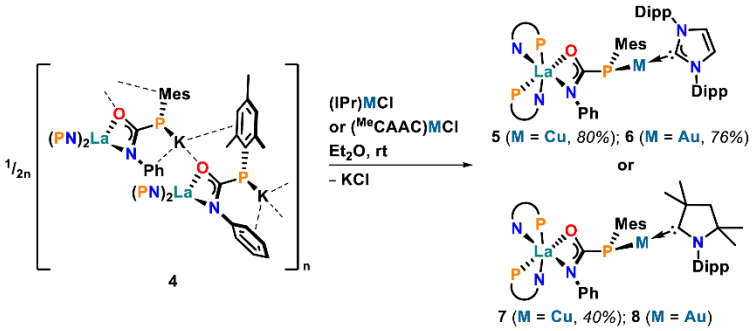

crystallographic data of **2** and **3** can be found in Tables S1 and S2 in the Supporting Information.

After having accomplished the construction of phospha-(thio)ureate ligands in the coordination sphere of PN-supported lanthanum(III), we investigated the possibility of deprotonating the *PH* group in **2** and **3**. For this purpose, complex **2** was treated with 1 equiv of KHMDS in toluene[79] at room temperature (Scheme 4, top). The initially yellow solution turned into a thick yellow suspension overnight. Clearly, this indicated the formation of a discrete salt or coordination polymer, since all other lanthanum complexes up to this point were readily soluble in toluene or benzene and the related potassium salt of the PN ligand (**KPN**) is also known to crystallize from concentrated aromatic solvents (i.e., C_6D_6).[76] This notion was substantiated by the fact that the isolated material of the new compound **4** could only be dissolved in a coordinating solvent such as tetrahydrofuran (THF). After filtering, washing with *n*-pentane, and drying of the precipitate *in vacuo*, the obtained bright yellow solid (86% isolated yield) was analyzed by means of ^{31}P and ^{1}H NMR spectroscopy in THF-d_8. In the ^{31}P NMR spectrum of **4**, the singlet resonance for the PN ligands can be found in the typical range at δ 1.9 ppm. For the phosphaureate ligand, a singlet instead of a doublet resonance is observed at δ −38.9 ppm in the ^{31}P NMR spectrum, proving successful deprotonation of the *PH* group. In addition, successful deprotonation was further indicated by the absence of the P*H* resonance in the ^{1}H NMR spectrum of **4**. Despite all our attempts, we have not been able to obtain X-ray-quality crystals suitable for a full structural elucidation. However, slow diffusion of *n*-hexane into a concentrated THF-d_8 solution of **4** yielded crystals of sufficient quality to unambiguously determine the connectivity of compound **4** in the solid state. As anticipated, the potassium salt **4** forms a one-dimensional polymeric chain in the solid state. Therein, the potassium ions are coordinated by the phosphorus atoms of the phosphaureate ligands as well as the oxygen atoms of neighboring complex molecules. Additional intra- and intermolecular interactions with arene substituents complete the coordination spheres of the potassium ions (see Figure S78 in the Supporting Information and the illustration in Scheme 4). A similar one-dimensional polymeric chain structure has been previously reported for the potassium salt **KPN**.[76]

Similarly, the reaction of **3** with KHMDS resulted in the deprotonation of the *PH* group (Scheme 4, bottom). However, even though the ^{1}H NMR spectrum of the product indicated that a quite defined material was obtained after workup, the ^{31}P NMR spectrum showed two surprisingly low field shifted singlet resonances at δ 60.8 and 10.2 ppm in addition to the typical PN ligand resonance at δ 3.3 ppm (see Figures S34 and S36 in the Supporting Information). Conducting a variable-temperature (VT) NMR spectroscopic investigation (Figures S38 and S39), we observed splitting of the initial three ^{31}P resonances at 303 K into a set of eight resonances at 243 K

https://dx.doi.org/10.1021/acs.inorgchem.0c01971
Inorg. Chem. 2020, 59, 13621−13631

(Figure S39). In addition, we noticed that the relative intensities of the ^{31}P resonances grouped at around δ 60.8 and 10.2 ppm changed from 0.83:0.17 at 303 K to roughly 0.94:0.06 at 243 K, with the sum of the PN ligand resonance intensities set to a constant relative integral of 2 (Figures S36 and S37). When the elemental analysis data were taken into account, which corroborated the formation of the desired potassium salt of **3**, the NMR spectroscopic results might suggest an equilibrium between at least two different isomers in solution. We therefore carefully hypothesize that the phosphathioureate is not only $\kappa^2(S,N)$-bound to lanthanum(III), as would be expected, but can also rearrange to the $\kappa^2(P,N)$-bound form (see Scheme 4 and Figure S36 for illustrations), since e.g. the electronegativities of the neighboring elements phosphorus and sulfur are very similar. The rather complex dynamic processes involved prevented us from isolating or crystallizing the isomers in question, and we are currently further pursuing their identification and the proper assignment of their spectroscopic features.

These findings caused us to concentrate our efforts on the defined polymeric complex **4** and its salt metathesis reactions to build heterobimetallic complexes (Scheme 5). For this we chose 1,3-bis(2,6-diisopropyphenyl)imidazol-2-ylidene (IPr)- or 1-(2,6-diisopropylphenyl)-3,3,5,5-tetramethylpyrrolidin-2-ylidene (^{Me}CAAC)-supported copper(I) and gold(I) chloride, since we assumed that these coinage-metal ions would be a good match for the rather "soft" phosphaureate P donor atom.

The use of different carbenes should also serve to demonstrate the possibility of a modular design: e.g., for fine-tuning of the electronic properties of the desired heterobimetallic systems. In addition, with regard to possible future photophysical applications, we considered the selected carbene ligands to be perfectly suited for (i) efficient steric shielding to minimize conformational flexibility as well as intermolecular interactions and (ii) a future comparison of photophysical properties with those of already reported luminescent coinage-metal carbene complexes.[80−91]

For the preparation of the heterobimetallic complexes **5** and **6** with an IPr supporting ligand at the coinage-metal ion a suspension of compound **4** and 1 equiv of either **(IPr)CuCl**[92] or **(IPr)AuCl**[93] were stirred in diethyl ether at room temperature (Scheme 5). After 10−15 min the solution of the suspension turned yellow, while the originally suspended yellow solid (starting material **4**) was replaced by a fine, colorless precipitate, indicating the formation of potassium chloride. Already at this point, reaction monitoring using ^{31}P NMR spectroscopy confirmed the full conversion to a new compound in each case. Centrifugation, filtration, and removal of the solvent *in vacuo* gave a solid which was washed with *n*-hexane or *n*-pentane and dried *in vacuo* to yield the pure product as light yellow powders in good isolated yields (80% for **5** and 76% for **6**). When the diethyl ether filtrate was allowed to rest at room temperature, reasonable amounts of crystalline material of both **5** and **6** could be obtained (*vide infra*). For the corresponding ^{Me}CAAC-supported systems **7** and **8**, with **(^{Me}CAAC)CuCl**[81] or **(^{Me}CAAC)AuCl**[94] as the starting materials (for the preparation, see the Supporting Information), similar synthesis and workup protocols were applicable. However, due to the higher solubility and the poor crystallization behavior, substantially lower yields were achieved in the case of the copper complex **7** (40%). Additionally, for complex **8** the reaction does not proceed as cleanly as for the previous examples and the impurities formed have solubilities similar to that of the anticipated complex **8**, rendering its isolation elusive as yet. Alternatively, a one-pot synthesis of heterobimetallic complexes by consecutive addition of KHMDS and **(IPr)MCl** (M = Cu, Au) to compound **2** in diethyl ether at room temperature was also found to be feasible. ^{31}P NMR spectroscopy confirmed the formation of the desired complexes **5** and **6** (see Figures S47 and S55), showing that the potassium salt **4** does not necessarily have to be isolated and at the same time emphasizing the potential of this simple reaction protocol.

Since we found salt metathesis not to be an ideal route for the isolation of complex **8**, we opted for a different approach for preparing **8**: namely, a direct protonolysis of a basic gold(I) precursor by complex **2** (Scheme 6). For this purpose, the new

Scheme 6. Alternative Route to Access Heterobimetallic Complex 8 by Reaction of 2 with (^{Me}CAAC)Au(HMDS)

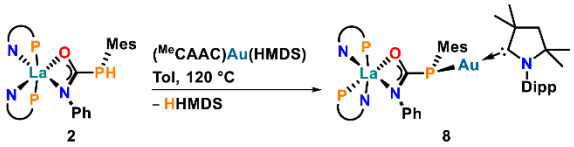

gold(I) precursor complex **(^{Me}CAAC)Au(HMDS)** containing the strongly basic bis(trimethylsilyl)amido ligand was synthesized by substitution of trimethylphosphine with ^{Me}CAAC in (Me$_3$P)Au(HMDS)[95] (for experimental, spectroscopic, and crystallographic details see the Experimental Section, Figures S1−S8, S70, and S77, and Tables S1 and S2 in the Supporting Information). Initially, no reaction between **2** and **(^{Me}CAAC)Au(HMDS)** in toluene was observed when the reaction mixture was stirred at room temperature for 24 h and only traces of **8** were formed at higher temperatures of 80 °C, according to ^{31}P{^{1}H} NMR spectroscopy. However, the full consumption of starting material **2** was finally achieved through refluxing at 120 °C for 2 weeks, albeit with the formation of significant amounts of the protonated ligand **HPN**, presumably due to decomposition during the prolonged heating (see Figure S68). We attribute the slow reaction rate to the low reactivity of **(^{Me}CAAC)Au(HMDS)**, since e.g. electrophilic alkylation with benzyl bromide was not possible under conditions reported for the related literature-known complex (IPr)Au(N^{t}Pr$_2$)[96] (see Figure S69). Even though the isolation of **8** was again hampered by similarly soluble impurities, the experiment still shows that in principle such heterobimetallic complexes can be also obtained by the reaction of **2** with transition-metal amide precursors.

The new heterobimetallic complexes were analyzed by means of multinuclear NMR spectroscopy in C$_6$D$_6$. Although we were unable to obtain pure material of complex **8**, the respective distinctive NMR resonances can be confidently assigned, especially in the ^{13}C{^{1}H} and ^{31}P NMR spectra (see the Experimental Section and Figures S65−S67 in the Supporting Information). Despite the complexity of the target compounds **5**−**8**, their ^{1}H NMR spectra were found to contain astonishingly sharp and well separated resonances, especially in the aromatic region (see Figures S40, S48, S56, and S65 in the Supporting Information), pointing to a high conformational rigidity of the heterobimetallic systems in solution. In addition, the fact that only one set of resonances of the complexes **5**−**8** is present in each ^{1}H NMR spectrum suggests the selective formation of one particular isomer, respectively. Apart from the

https://dx.doi.org/10.1021/acs.inorgchem.0c01971
Inorg. Chem. 2020, 59, 13621−13631

Inorganic Chemistry pubs.acs.org/IC Article

Table 1. Selected $^{13}C\{^1H\}$ and ^{31}P NMR Data of Heterobimetallic Complexes 5−8 in C_6D_6 at 303 K, with Chemical Shifts δ in ppm

	$^{13}C\{^1H\}$ NMR		^{31}P NMR	
complex	$C_{carbene}$	$C_{phosphaureate}$	PN^-	$P_{phosphaureate}$
5	182.9 (d, $^2J_{CP}$ = 44 Hz)	201.5 (br s)	3.7 (s)	−65.0 (s)
6	197.4 (d, $^2J_{CP}$ = 66 Hz)	201.6 (br s)	4.0 (s)	−42.0 (s)
7	251.4 (d, $^2J_{CP}$ = 42 Hz)	201.3 (d, $^1J_{CP}$ = 46 Hz)	3.7 (s)	−63.7 (s)
8	258.4 (d, $^2J_{CP}$ = 62 Hz)	202.2 (d, $^1J_{CP}$ = 48 Hz)	3.8 (s)	−38.2 (s)

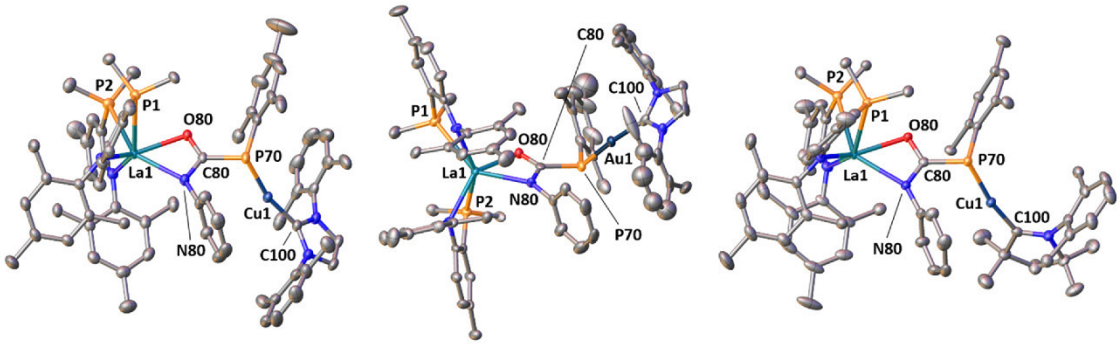

Figure 3. Thermal ellipsoid plots of **5**−**7** (from left to right). Thermal ellipsoids are shown at a probability level of 30%. Hydrogen atoms have been omitted and ^{i}Pr groups truncated for clarity.

appearance of a new set of carbene ligand resonances in the ^1H NMR spectra, the $^{13}C\{^1H\}$ NMR data obtained for **5**−**8** most clearly show the successful coordination of the different coinage-metal carbene fragments to the phosphaureate ligand (Table 1, left).

For the IPr systems **5** and **6** chemical shifts between δ 180 and 200 ppm for the $C_{carbene}$ resonance were recorded, while for the ^{Me}CAAC analogs **7** and **8** these resonances lay at lower fields of δ 250−260 ppm, as is typical of CAACs in comparison to NHCs.[97] Due to the higher electronegativity of gold(I),[98] the $C_{carbene}$ resonances of the gold(I) systems **6** and **8** are shifted to lower fields compared to the respective copper(I) analogues **5** and **7**. More importantly, all $C_{carbene}$ resonances show a doublet splitting due to characteristic $^2J_{CP}$ coupling to the $P_{phosphaureate}$ atom, thereby confirming coordination of the phosphaureate ligand via the P donor atom. The $^2J_{CP}$ coupling constants for the gold(I) complexes **6** and **8** of 60−70 Hz are considerably larger than for the copper(I) compounds **5** and **7** (40−45 Hz), possibly indicating a stronger binding of the gold(I) carbene fragment to phosphorus. Overall, the determined $^2J_{CP}$ values are smaller than those for the reference complexes $[(IPr)Au(P^tBu_3)][BF_4]$[99] ($^2J_{CP}$ = 112 Hz) and $[(IPr)Cu(P^tBu_3)][BF_4]$[100] ($^2J_{CP}$ = 61 Hz), which is in line with an inferior electron-donating ability of the bridging phosphaureate ligand in **5**−**8** in comparison to tertiary phosphines. Interestingly, the shift of the $C_{phosphaureate}$ resonance (δ ∼201−202 ppm) is essentially unaffected by the choice of coinage-metal ion or carbene supporting ligand, although it is noteworthy that only for the ^{Me}CAAC systems **7** and **8** doublet splittings of $^1J_{CP}$ = 46 and 48 Hz can be determined, respectively.

A ^{31}P NMR spectroscopic study of complexes **5**−**8** revealed that binding of copper(I) or gold(I) carbene to the phosphaureate ligand can also be easily followed by the shift of the $P_{phosphaureate}$ resonance (Table 1, right). In comparison to copper(I) complexes **5** and **7** (δ −63 to −65 ppm) resonances at lower fields of δ −38 to −42 ppm were recorded in the case of gold(I) complexes **6** and **8**, as would be expected for more electronegative gold(I). The type of carbene influences the ^{31}P shift of the phosphaureate bridging ligand in terms of slightly low field shifted resonances for the ^{Me}CAAC systems **7** and **8**, presumably due to the superior π-acceptor properties of CAACs versus NHCs.[81,87,101] The PN ligand resonances behave nearly the same for the whole series **5**−**8** and are shifted only slightly to higher fields by about 2 ppm in comparison to complex **2**.

For the three heterobimetallic complexes **5**−**7** structural proof was finally obtained by X-ray crystallography (Figure 3). Suitable single crystals for diffraction analysis of **5** and **6** were obtained by storing concentrated diethyl ether solutions of the corresponding complexes at room temperature (*vide supra*). In the case of **7**, slow evaporation of a concentrated toluene solution at room temperature yielded single crystals of suitable quality. Unfortunately, we have not been able to obtain X-ray-quality crystals for complex **8** by any methods investigated as yet.

All three compounds **5**−**7** crystallize in the monoclinic space group $P2_1/c$ with one molecule in the asymmetric unit and no solvent molecules in the lattice. In each case the unprecedented $\mu,\kappa^2(O,N):\kappa^1(P)$ binding mode of the phosphaureate bridging ligand, which was already inferred from the NMR spectroscopic features, can be confirmed. Interestingly, the coordination of the coinage-metal carbene fragments to the phosphaureate ligand induced an isomerization in the coordination sphere of La1: i.e., the relative arrangement of the ^{i}Pr$_2$-phosphanyl groups of the PN supporting ligands changed from *trans* in **2** (and **4**) to *cis* in **5**−**7**, exhibiting P1−La1−P2 angles between 84.79(4) and 88.09(2)°. Apart from the La1−N80 distances, which are about 0.1 Å shorter, all other bond metrics of the phosphaureate bridging ligand in **5**−**7** are found to be essentially the same as in compound **2** (see Table S2 in the Supporting Information). For the coinage-

https://dx.doi.org/10.1021/acs.inorgchem.0c01971
Inorg. Chem. 2020, 59, 13621−13631

metal carbene fragments bound to P70 merely subtle structural differences can be asserted, which most likely result from packing effects. The P70−Cu1 bond lengths in **5** and **7** (both 2.2043(7) Å) and the P70−Au1 distance in **6** (2.314(2) Å) fall into the range of the reference complexes [(IPr)M(P^tBu_3)][BF_4] (M = Cu, Au).[99,100] The same applies for the Cu1/Au1−C100 distances,[99,100] whereas the P70−Cu1/Au1−C100 angles between 164.57(7) and 169.57(8)° in **5**−**7** clearly deviate from linearity, most likely due to steric repulsion between the carbene ligand and the phosphaureate phenyl as well as mesityl group. The C80−P70−Cu1/Au1 angle in **7** (114.16(9)°) is somewhat larger than in **5** (111.03(7)°) or **6** (110.1(2)°), which might reflect a better ability of the unsymmetrical Cu(^{Me}CAAC) fragment to bend in one (sterically preferred) direction. For more details on the crystallographic data of **5**−**7** see Tables S1 and S2 in the Supporting Information.

In this context, one interesting stereochemical property of this first set of examples of a phosphaureate bridging ligand is worth mentioning. Since the phosphaureate ligand is locked in position by its $\kappa^2(O,N)$ binding mode to lanthanum, the coinage-metal carbene fragment bound to P70 can lie either in the hemisphere above or beneath the O80−N80−P70 plane, when one looks along the La1−C80−P70 trajectory shown in Figure 4. This is expressed by positive N80−C80−P70−Cu1

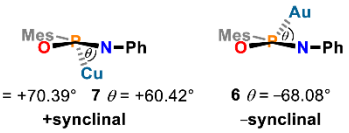

Figure 4. Views along the La1−C80−P70 trajectory in **5** and **7** (left) or **6** (right), respectively. The representations of **5**−**7** are simplified for clarity (i.e., no La(PN)$_2$ fragment or carbene ligand shown), and N80−C80−P70−Cu1/Au1 dihedral angles θ are given.

dihedral angles θ of +70.39 and +60.42° in **5** and **7**, respectively, in comparison to a negative N80−C80−P70−Au1 dihedral angle θ of −68.08° in the case of **6**. Even though already at this point it appears that there are different preferences for copper(I) (+synclinal) and gold(I) (−synclinal), a larger number of comparable examples is required to delineate conclusive parameters on how the stereochemical outcome in these heterobimetallic complexes is governed.

CONCLUSION

In conclusion, we have presented an attractive, straightforward route for the synthesis of a series of unprecedented heterobimetallic lanthanum−copper(I) and lanthanum−gold(I) complexes. Capitalizing on the insertion reactivity of the La−P primary phosphide bond in **1** toward phenyl iso(thio)cyanate, we were able to isolate **2** and **3** as rare examples of phospha(thio)ureate complexes of lanthanum(III). The retention of the P*H* proton was key to further functionalization: i.e., deprotonation and subsequent salt metathesis in the case of **2** to yield polymeric potassium salt **4** and furnish the new heterobimetallic complexes **5**−**8**, containing the first example of a phosphaureate bridging ligand with an unprecedented $\kappa^2(O,N):\kappa^1(P)$ binding mode. Additionally, compound **8** can be obtained by protonolysis of (**^{Me}CAAC**)**Au(HMDS)** with complex **2**. For **5** and **6**, we found that the two-step reaction sequence with intermediary isolation of **4** can be replaced by a one-pot reaction protocol, further emphasizing the simplicity with which such heterobimetallic systems can be constructed. All target compounds were analyzed in detail by NMR spectroscopic techniques and by X-ray diffraction analysis (except for complex **8**). Despite the high complexity of **5**−**8**, NMR spectroscopic investigations pointed to a high conformational rigidity of each compound in solution. X-ray diffraction studies of **5**−**7** revealed two stereochemically distinguishable coordination possibilities at $P_{phosphaureate}$ for the coinage-metal ion. In the future, our modular approach, as exemplified in this work by insertion of different organic substrates into the La−P primary phosphide bond as well as a variation of carbene supporting ligand and coinage-metal ion, should give access to a wide range of carefully designed heterobimetallic lanthanide(III)−coinage-metal complexes with intriguing properties for photochemistry and catalysis.

ASSOCIATED CONTENT

Supporting Information

The Supporting Information is available free of charge at https://pubs.acs.org/doi/10.1021/acs.inorgchem.0c01971.

Experimental section, all NMR and IR spectroscopy data, crystallographic details on the complexes (**^{Me}CAAC)Au(HMDS)**, **2**, **3**, and **5**−**7**, the molecular structure of (**^{Me}CAAC)Au(HMDS)**, and the connectivity found in polymeric **4** (PDF)

Accession Codes

CCDC 2012278−2012283 contain the supplementary crystallographic data for this paper. These data can be obtained free of charge via www.ccdc.cam.ac.uk/data_request/cif, or by emailing data_request@ccdc.cam.ac.uk, or by contacting The Cambridge Crystallographic Data Centre, 12 Union Road, Cambridge CB2 1EZ, UK; fax: +44 1223 336033.

AUTHOR INFORMATION

Corresponding Author

Stephan Hohloch − *University of Innsbruck, Faculty of Chemistry and Pharmacy, Institute of General, Inorganic and Theoretical Chemistry, 6020 Innsbruck, Austria;* orcid.org/0000-0002-5353-0801; Email: Stephan.Hohloch@uibk.ac.at

Authors

Fabian A. Watt − *Paderborn University, Faculty of Science, Department of Chemistry, 33098 Paderborn, Germany;* orcid.org/0000-0002-2213-0864

Nicole Dickmann − *Paderborn University, Faculty of Science, Department of Chemistry, 33098 Paderborn, Germany*

Roland Schoch − *Paderborn University, Faculty of Science, Department of Chemistry, 33098 Paderborn, Germany;* orcid.org/0000-0003-2061-7289

Complete contact information is available at: https://pubs.acs.org/10.1021/acs.inorgchem.0c01971

Author Contributions

The project was designed by S.H. and F.A.W. Experimental work was carried out by F.A.W. and N.D. NMR and IR spectra were recorded by F.A.W. and N.D. X-ray structure analyses were performed by R.S. and S.H. The manuscript was written by F.A.W. and S.H. and proofread by all authors. All authors have given approval to the final version of the manuscript.

https://dx.doi.org/10.1021/acs.inorgchem.0c01971
Inorg. Chem. 2020, 59, 13621−13631

Notes

The authors declare no competing financial interest.

■ ACKNOWLEDGMENTS

We are grateful to the Daimler and Benz Foundation, the Fonds der Chemischen Industrie, the Young Academy of the North-Rhine-Westphalian Academy of Sciences, Humanities and the Arts, Paderborn University, and the University of Innsbruck for financial support. Additionally, we thank Prof. Dr. Matthias Bauer for continuous support and fruitful discussions. Dr. Hans Egold from the NMR facility of the Paderborn University is kindly acknowledged for helpful discussions. Christiane Gloger and Maria Busse are kindly acknowledged for conducting elemental analyses.

■ REFERENCES

(1) Liddle, S. T. International Year of the Periodic Table: Lanthanide and Actinide Chemistry. *Angew. Chem., Int. Ed.* **2019**, *58*, 5140−5141.
(2) Martinez-Gomez, N. C.; Vu, H. N.; Skovran, E. Lanthanide Chemistry: From Coordination in Chemical Complexes Shaping Our Technology to Coordination in Enzymes Shaping Bacterial Metabolism. *Inorg. Chem.* **2016**, *55*, 10083−10089.
(3) Day, B. M.; Guo, F.-S.; Layfield, R. A. Cyclopentadienyl Ligands in Lanthanide Single-Molecule Magnets: One Ring To Rule Them All? *Acc. Chem. Res.* **2018**, *51*, 1880−1889.
(4) Guo, F.-S.; Day, B. M.; Chen, Y.-C.; Tong, M.-L.; Mansikkamäki, A.; Layfield, R. A. Magnetic hysteresis up to 80 K in a dysprosium metallocene single-molecule magnet. *Science* **2018**, *362*, 1400−1403.
(5) Goodwin, C. A. P.; Ortu, F.; Reta, D.; Chilton, N. F.; Mills, D. P. Molecular magnetic hysteresis at 60 K in dysprosocenium. *Nature* **2017**, *548*, 439−442.
(6) Randall McClain, K.; Gould, C. A.; Chakarawet, K.; Teat, S. J.; Groshens, T. J.; Long, J. R.; Harvey, B. G. High-temperature magnetic blocking and magneto-structural correlations in a series of dysprosium(iii) metallocenium single-molecule magnets. *Chem. Sci.* **2018**, *9*, 8492−8503.
(7) Guo, F.-S.; Day, B. M.; Chen, Y.-C.; Tong, M.-L.; Mansikkamäki, A.; Layfield, R. A. A Dysprosium Metallocene Single-Molecule Magnet Functioning at the Axial Limit. *Angew. Chem., Int. Ed.* **2017**, *56*, 11445−11449.
(8) Gould, C. A.; McClain, K. R.; Yu, J. M.; Groshens, T. J.; Furche, F.; Harvey, B. G.; Long, J. R. Synthesis and Magnetism of Neutral, Linear Metallocene Complexes of Terbium(II) and Dysprosium(II). *J. Am. Chem. Soc.* **2019**, *141*, 12967−12973.
(9) Gould, C. A.; Darago, L. E.; Gonzalez, M. I.; Demir, S.; Long, J. R. A Trinuclear Radical-Bridged Lanthanide Single-Molecule Magnet. *Angew. Chem., Int. Ed.* **2017**, *56*, 10103−10107.
(10) Demir, S.; Zadrozny, J. M.; Nippe, M.; Long, J. R. Exchange coupling and magnetic blocking in bipyrimidyl radical-bridged dilanthanide complexes. *J. Am. Chem. Soc.* **2012**, *134*, 18546−18549.
(11) Demir, S.; Gonzalez, M. I.; Darago, L. E.; Evans, W. J.; Long, J. R. Giant coercivity and high magnetic blocking temperatures for N_2^{3-} radical-bridged dilanthanide complexes upon ligand dissociation. *Nat. Commun.* **2017**, *8*, 2144.
(12) Bünzli, J.-C. G. Lanthanide luminescence for biomedical analyses and imaging. *Chem. Rev.* **2010**, *110*, 2729−2755.
(13) Mohamadi, A.; Miller, L. W. Brightly Luminescent and Kinetically Inert Lanthanide Bioprobes Based on Linear and Preorganized Chelators. *Bioconjugate Chem.* **2016**, *27*, 2540−2548.
(14) Oukhatar, F.; Eliseeva, S. V.; Bonnet, C. S.; Placidi, M.; Logothetis, N. K.; Petoud, S.; Angelovski, G.; Tóth, É. Toward MRI and Optical Detection of Zwitterionic Neurotransmitters: Near-Infrared Luminescent and Magnetic Properties of Macrocyclic Lanthanide(III) Complexes Appended with a Crown Ether and a Benzophenone Chromophore. *Inorg. Chem.* **2019**, *58*, 13619−13630.
(15) Wu, S.-Y.; Guo, X.-Q.; Zhou, L.-P.; Sun, Q.-F. Fine-Tuned Visible and Near-Infrared Luminescence on Self-Assembled Lanthanide-Organic Tetrahedral Cages with Triazole-Based Chelates. *Inorg. Chem.* **2019**, *58*, 7091−7098.
(16) Barger, C. J.; Motta, A.; Weidner, V. L.; Lohr, T. L.; Marks, T. J. La[N(SiMe$_3$)$_2$]$_3$-Catalyzed Ester Reductions with Pinacolborane: Scope and Mechanism of Ester Cleavage. *ACS Catal.* **2019**, *9*, 9015−9024.
(17) Basiouny, M. M. I.; Dollard, D. A.; Schmidt, J. A. R. Regioselective Single and Double Hydrophosphination and Hydrophosphinylation of Unactivated Alkynes. *ACS Catal.* **2019**, *9*, 7143−7153.
(18) Chen, W.; Song, H.; Li, J.; Cui, C. Catalytic Selective Dihydrosilylation of Internal Alkynes Enabled by Rare-Earth Ate Complex. *Angew. Chem., Int. Ed.* **2020**, *59*, 2365−2369.
(19) Gurina, G. A.; Kissel, A. A.; Lyubov, D. M.; Luconi, L.; Rossin, A.; Tuci, G.; Cherkasov, A. V.; Lyssenko, K. A.; Shavyrin, A. S.; Ob'edkov, A. M.; Giambastiani, G.; Trifonov, A. A. Bis(alkyl) scandium and yttrium complexes coordinated by an amidopyridinate ligand: synthesis, characterization and catalytic performance in isoprene polymerization, hydroelementation and carbon dioxide hydrosilylation. *Dalton Trans.* **2020**, *49*, 638−650.
(20) Kazeminejad, N.; Munzel, D.; Gamer, M. T.; Roesky, P. W. Bis(amidinate) ligands in early lanthanide chemistry − synthesis, structures, and hydroamination catalysis. *Chem. Commun.* **2017**, *53*, 1060−1063.
(21) Qiao, Y.; Schelter, E. J. Lanthanide Photocatalysis. *Acc. Chem. Res.* **2018**, *51*, 2926−2936.
(22) Qiao, Y.; Yang, Q.; Schelter, E. J. Photoinduced Miyaura Borylation by a Rare-Earth-Metal Photoreductant: The Hexachlorocerate(III) Anion. *Angew. Chem., Int. Ed.* **2018**, *57*, 10999−11003.
(23) Edelmann, F. T. Lanthanide amidinates and guanidinates in catalysis and materials science: a continuing success story. *Chem. Soc. Rev.* **2012**, *41*, 7657−7672.
(24) Gu, X.; Zhang, L.; Zhu, X.; Wang, S.; Zhou, S.; Wei, Y.; Zhang, G.; Mu, X.; Huang, Z.; Hong, D.; Zhang, F. Synthesis of Bis(NHC)-Based CNC-Pincer Rare-Earth-Metal Amido Complexes and Their Application for the Hydrophosphination of Heterocumulenes. *Organometallics* **2015**, *34*, 4553−4559.
(25) Kissel, A. A.; Mahrova, T. V.; Lyubov, D. M.; Cherkasov, A. V.; Fukin, G. K.; Trifonov, A. A.; Del Rosal, I.; Maron, L. Metallacyclic yttrium alkyl and hydrido complexes: synthesis, structures and catalytic activity in intermolecular olefin hydrophosphination and hydroamination. *Dalton Trans.* **2015**, *44*, 12137−12148.
(26) Basalov, I. V.; Yurova, O. S.; Cherkasov, A. V.; Fukin, G. K.; Trifonov, A. A. Amido Ln(II) Complexes Coordinated by Bi- and Tridentate Amidinate Ligands: Nonconventional Coordination Modes of Amidinate Ligands and Catalytic Activity in Intermolecular Hydrophosphination of Styrenes and Tolane. *Inorg. Chem.* **2016**, *55*, 1236−1244.
(27) Basiouny, M. M. I.; Schmidt, J. A. R. Lanthanum-Catalyzed Double Hydrophosphinylation of Nitriles. *Organometallics* **2017**, *36*, 721−729.
(28) Behrle, A. C.; Schmidt, J. A. R. Insertion Reactions and Catalytic Hydrophosphination of Heterocumulenes using α-Metalated *N*,*N*-Dimethylbenzylamine Rare-Earth-Metal Complexes. *Organometallics* **2013**, *32*, 1141−1149.
(29) Rina, Y. A.; Schmidt, J. A. R. Lanthanum-Catalyzed Regioselective Anti-Markovnikov Hydrophosphinylation of Styrenes. *Organometallics* **2019**, *38*, 4261−4270.
(30) Trifonov, A. A.; Basalov, I. V.; Kissel, A. A. Use of organolanthanides in the catalytic intermolecular hydrophosphination and hydroamination of multiple C−C bonds. *Dalton Trans.* **2016**, *45*, 19172−19193.
(31) Zhang, W.-X.; Nishiura, M.; Mashiko, T.; Hou, Z. Half-sandwich *o*-*N*,*N*-dimethylaminobenzyl complexes over the full size range of group 3 and lanthanide metals. synthesis, structural

https://dx.doi.org/10.1021/acs.inorgchem.0c01971
Inorg. Chem. 2020, 59, 13621−13631

characterization, and catalysis of phosphine P−H bond addition to carbodiimides. *Chem. - Eur. J.* **2008**, *14*, 2167−2179.
(32) Yin, H.; Carroll, P. J.; Manor, B. C.; Anna, J. M.; Schelter, E. J. Cerium Photosensitizers: Structure-Function Relationships and Applications in Photocatalytic Aryl Coupling Reactions. *J. Am. Chem. Soc.* **2016**, *138*, 5984−5993.
(33) Qiao, Y.; Cheisson, T.; Manor, B. C.; Carroll, P. J.; Schelter, E. J. A strategy to improve the performance of cerium(iii) photocatalysts. *Chem. Commun.* **2019**, *55*, 4067−4070.
(34) Manzur, J.; Poblete, C.; Morales, J.; de Santana, R. C.; Queiroz Maia, L. J.; Vega, A.; Fuentealba, P.; Spodine, E. Enhancement of Terbium(III)-Centered Luminescence by Tuning the Triplet Energy Level of Substituted Pyridylamino-4-R-Phenoxo Tripodal Ligands. *Inorg. Chem.* **2020**, *59*, 5447−5455.
(35) Rinehart, J. D.; Long, J. R. Exploiting single-ion anisotropy in the design of f-element single-molecule magnets. *Chem. Sci.* **2011**, *2*, 2078.
(36) Bag, P.; Goura, J.; Mereacre, V.; Novitchi, G.; Powell, A. K.; Chandrasekhar, V. Synthesis, magnetism and Mössbauer studies of tetranuclear heterometallic $\{Fe^{III}_2Ln_2\}$(Ln = Gd, Dy, Tb) complexes: evidence of slow relaxation of magnetization in the terbium analogue. *Dalton Trans.* **2014**, *43*, 16366−16376.
(37) Burns, C. P.; Yang, X.; Wofford, J. D.; Bhuvanesh, N. S.; Hall, M. B.; Nippe, M. Structure and Magnetization Dynamics of Dy−Fe and Dy−Ru Bonded Complexes. *Angew. Chem., Int. Ed.* **2018**, *57*, 8144−8148.
(38) Rigamonti, L.; Nava, A.; Boulon, M.-E.; Luzon, J.; Sessoli, R.; Cornia, A. Experimental and Theoretical Studies on the Magnetic Anisotropy in Lanthanide(III)-Centered Fe_3Ln Propellers. *Chem. - Eur. J.* **2015**, *21*, 12171−12180.
(39) Singh, N.; Das Gupta, S.; Butcher, R. J.; Christou, G. Synthesis and magnetochemistry of heterometallic triangular $Fe^{III}_2Ln^{III}$ (Ln = La, Gd, Tb, Dy, and Ho) and $Fe^{III}_2Y^{III}$ complexes. *Dalton Trans.* **2017**, *46*, 7897−7903.
(40) Wang, H.-S.; Long, Q.-Q.; Hu, Z.-B.; Yue, L.; Yang, F.-J.; Yin, C.-L.; Pan, Z.-Q.; Zhang, Y.-Q.; Song, Y. Synthesis, crystal structures and magnetic properties of a series of chair-like heterometallic $[Fe_4Ln_2]$ (Ln = Gd^{III}, Dy^{III}, Ho^{III}, and Er^{III}) complexes with mixed organic ligands. *Dalton Trans.* **2019**, *48*, 13472−13482.
(41) Stoian, S. A.; Paraschiv, C.; Kiritsakas, N.; Lloret, F.; Münck, E.; Bominaar, E. L.; Andruh, M. Mössbauer, electron paramagnetic resonance, and magnetic susceptibility studies on members of a new family of cyano-bridged 3d-4f complexes. Demonstration of anisotropic exchange in a Fe−Gd complex. *Inorg. Chem.* **2010**, *49*, 3387−3401.
(42) Qiu, J.-Z.; Wang, L.-F.; Chen, Y.-C.; Zhang, Z.-M.; Li, Q.-W.; Tong, M.-L. Magnetocaloric Properties of Heterometallic 3d−Gd Complexes Based on the $[Gd(oda)_3]^{3-}$ Metalloligand. *Chem. - Eur. J.* **2016**, *22*, 802−808.
(43) Burns, C. P.; Yang, X.; Sung, S.; Wofford, J. D.; Bhuvanesh, N. S.; Hall, M. B.; Nippe, M. Towards understanding of lanthanide-transition metal bonding: investigations of the first Ce−Fe bonded complex. *Chem. Commun.* **2018**, *54*, 10893−10896.
(44) Ahmed, N.; Das, C.; Vaidya, S.; Langley, S. K.; Murray, K. S.; Shanmugam, M. Nickel(II)−lanthanide(III) magnetic exchange coupling influencing single-molecule magnetic features in $\{Ni_2Ln_2\}$ complexes. *Chem. - Eur. J.* **2014**, *20*, 14235−14239.
(45) Ahmed, N.; Das, C.; Vaidya, S.; Srivastava, A. K.; Langley, S. K.; Murray, K. S.; Shanmugam, M. Probing the magnetic and magneto-thermal properties of M(II)−Ln(III) complexes (where M(II) = Ni or Zn; Ln(III) = La or Pr or Gd). *Dalton Trans.* **2014**, *43*, 17375−17384.
(46) Upadhyay, A.; Das, C.; Langley, S. K.; Murray, K. S.; Srivastava, A. K.; Shanmugam, M. Heteronuclear Ni(ii)−Ln(iii) (Ln = La, Pr, Tb, Dy) complexes: synthesis and single-molecule magnet behaviour. *Dalton Trans.* **2016**, *45*, 3616−3626.
(47) Vieru, V.; Pasatoiu, T. D.; Ungur, L.; Suturina, E.; Madalan, A. M.; Duhayon, C.; Sutter, J.-P.; Andruh, M.; Chibotaru, L. F. Synthesis, Crystal Structures, Magnetic Properties, and Theoretical Investigation of a New Series of Ni^{II}−Ln^{III}−W^{V} Heterotrimetallics: Understanding the SMM Behavior of Mixed Polynuclear Complexes. *Inorg. Chem.* **2016**, *55*, 12158−12171.
(48) Long, J.; Rouquette, J.; Thibaud, J.-M.; Ferreira, R. A. S.; Carlos, L. D.; Donnadieu, B.; Vieru, V.; Chibotaru, L. F.; Konczewicz, L.; Haines, J.; Guari, Y.; Larionova, J. A high-temperature molecular ferroelectric Zn/Dy complex exhibiting single-ion-magnet behavior and lanthanide luminescence. *Angew. Chem., Int. Ed.* **2015**, *54*, 2236−2240.
(49) Upadhyay, A.; Singh, S. K.; Das, C.; Mondol, R.; Langley, S. K.; Murray, K. S.; Rajaraman, G.; Shanmugam, M. Enhancing the effective energy barrier of a Dy(III) SMM using a bridged diamagnetic Zn(II) ion. *Chem. Commun.* **2014**, *50*, 8838−8841.
(50) Chen, F.-F.; Bian, Z.-Q.; Liu, Z.-W.; Nie, D.-B.; Chen, Z.-Q.; Huang, C.-H. Highly efficient sensitized red emission from europium (III) in Ir−Eu bimetallic complexes by ^{3}MLCT energy transfer. *Inorg. Chem.* **2008**, *47*, 2507−2513.
(51) Shavaleev, N. M.; Accorsi, G.; Virgili, D.; Bell, Z. R.; Lazarides, T.; Calogero, G.; Armaroli, N.; Ward, M. D. Syntheses and crystal structures of dinuclear complexes containing d-block and f-block luminophores. Sensitization of NIR luminescence from Yb(III), Nd(III), and Er(III) centers by energy transfer from Re(I)- and Pt(II)-bipyrimidine metal centers. *Inorg. Chem.* **2005**, *44*, 61−72.
(52) Shavaleev, N. M.; Moorcraft, L. P.; Pope, S. J. A.; Bell, Z. R.; Faulkner, S.; Ward, M. D. Sensitised near-infrared emission from lanthanides using a covalently-attached Pt(II) fragment as an antenna group. *Chem. Commun.* **2003**, 1134−1135.
(53) Shavaleev, N. M.; Moorcraft, L. P.; Pope, S. J. A.; Bell, Z. R.; Faulkner, S.; Ward, M. D. Sensitized near-infrared emission from complexes of Yb^{III}, Nd^{III} and Er^{III} by energy-transfer from covalently attached Pt^{II}-based antenna units. *Chem. - Eur. J.* **2003**, *9*, 5283−5291.
(54) Zakrzewski, J. J.; Sieklucka, B.; Chorazy, S. Europium(III) Photoluminescence Governed by d^8-d^{10} Heterometallophilic Interactions in Trimetallic Cyanido-Bridged Coordination Frameworks. *Inorg. Chem.* **2020**, *59*, 1393−1404.
(55) Wen, H.-R.; Hu, J.-J.; Yang, K.; Zhang, J.-L.; Liu, S.-J.; Liao, J.-S.; Liu, C.-M. Family of Chiral Zn^{II}−Ln^{III} (Ln = Dy and Tb) Heterometallic Complexes Derived from the Amine-Phenol Ligand Showing Multifunctional Properties. *Inorg. Chem.* **2020**, *59*, 2811−2824.
(56) Li, X.-L.; Zhang, K.-J.; Li, J.-J.; Cheng, X.-X.; Chen, Z.-N. Dual Luminescent Dinuclear Gold(I) Complexes of Terpyridyl-Functionalized Alkyne Ligands and Their Efficient Sensitization of Eu^{III} and Yb^{III} Luminescence. *Eur. J. Inorg. Chem.* **2010**, *2010*, 3449−3457.
(57) Xu, H.-B.; Zhang, L.-Y.; Ni, J.; Chao, H.-Y.; Chen, Z.-N. Conformation changes and luminescent properties of Au−Ln (Ln = Nd, Eu, Er, Yb) arrays with 5-ethynyl-2,2′-bipyridine. *Inorg. Chem.* **2008**, *47*, 10744−10752.
(58) Klink, S. I.; Keizer, H.; van Veggel, F. C. J. M. Transition Metal Complexes as Photosensitizers for Near-Infrared Lanthanide Luminescence. *Angew. Chem., Int. Ed.* **2000**, *39*, 4319−4321.
(59) Chen, F.-F.; Chen, Z.-Q.; Bian, Z.-Q.; Huang, C.-H. Sensitized luminescence from lanthanides in d−f bimetallic complexes. *Coord. Chem. Rev.* **2010**, *254*, 991−1010.
(60) Sakamoto, M.; Manseki, K.; Okawa, H. d−f Heteronuclear complexes: synthesis, structures and physicochemical aspects. *Coord. Coord. Chem. Rev.* **2001**, *219*−*221*, 379−414.
(61) Yi, W.; Zhang, J.; Hong, L.; Chen, Z.; Zhou, X. Insertion of Isocyanate and Isothiocyanate into the Ln−P σ-Bond of Organolanthanide Phosphides. *Organometallics* **2011**, *30*, 5809−5814.
(62) Garner, M. E.; Parker, B. F.; Hohloch, S.; Bergman, R. G.; Arnold, J. Thorium Metallacycle Facilitates Catalytic Alkyne Hydrophosphination. *J. Am. Chem. Soc.* **2017**, *139*, 12935−12938.
(63) Lindenberg, F.; Sieler, J.; Hey-Hawkins, E. FORMATION OF NOVEL P- AND As-FUNCTIONALIZED LIGANDS BY INSERTION REACTIONS INTO THE Zr−E BOND OF $(\eta^5$-$C_5H_4R)_2ZrCl\{E(SiMe_3)_2\}$ (R = Me, E = P, As; R = H, E = P). *Polyhedron* **1996**, *15*, 1459−1471.

https://dx.doi.org/10.1021/acs.inorgchem.0c01971
Inorg. Chem. 2020, 59, 13621−13631

(64) Segerer, U.; Sieler, J.; Hey-Hawkins, E. Formation of Novel P-Functionalized Ligands by Insertion Reactions of RNCX (R = Ph, X = O, S; R = Pr^i, X = O) into the Zr−P Bond of [Cp°$_2$ZrCl(PHCy)] (Cp° = η^5-C_5EtMe_4, Cy = Cyclohexyl) and [Cp$^x_2$ZrCl{PH(TRIP)}] (Cp^x = η^5 -C_5MeH_4, TRIP = 2,4,6-Pr$^i_3C_6H_2$). *Organometallics* **2000**, *19*, 2445−2449.

(65) Hou, Z.; Stephan, D. W. Generation and Reactivity of the First Mononuclear Early Metal Phosphinidene Complex, Cp*$_2$Zr = P($C_6H_2Me_3$-2,4,6). *J. Am. Chem. Soc.* **1992**, *114*, 10088−10089.

(66) Hou, Z.; Breen, T. L.; Stephan, D. W. Formation and Reactivity of the Early Metal Phosphides and Phosphinidenes Cp*$_2$Zr = PR, Cp*$_2$Zr(PR)$_2$, and Cp*$_2$Zr(PR)$_3$. *Organometallics* **1993**, *12*, 3158−3167.

(67) Vilanova, S. P.; Tarlton, M. L.; Barnes, C. L.; Walensky, J. R. Double insertion of benzophenone into thorium−phosphorus bonds. *J. Organomet. Chem.* **2018**, *857*, 159−163.

(68) Vilanova, S. P.; Del Rosal, I.; Tarlton, M. L.; Maron, L.; Walensky, J. R. Functionalization of Carbon Monoxide and *tert*-Butyl Nitrile by Intramolecular Proton Transfer in a Bis(Phosphido) Thorium Complex. *Angew. Chem., Int. Ed.* **2018**, *57*, 16748−16753.

(69) Behrle, A. C.; Walensky, J. R. Insertion of ^{t}BuNC into thorium−phosphorus and thorium−arsenic bonds: phosphaazaallene and arsaazaallene moieties in f element chemistry. *Dalton Trans.* **2016**, *45*, 10042−10049.

(70) Zhang, C.; Wang, Y.; Hou, G.; Ding, W.; Zi, G.; Walter, M. D. Experimental and computational studies on a three-membered diphosphido thorium metallaheterocycle [η^5-1,3-$(Me_3C)_2C_5H_3$]$_2$Th-[η^2-P$_2$(2,4,6-^{i}Pr$_3C_6H_2$)$_2$]. *Dalton Trans.* **2019**, *48*, 6921−6930.

(71) Tarlton, M. L.; Del Rosal, I.; Vilanova, S. P.; Kelley, S. P.; Maron, L.; Walensky, J. R. Comparative Insertion Reactivity of CO, CO_2, ^{t}BuCN, and ^{t}BuNC into Thorium− and Uranium−Phosphorus Bonds. *Organometallics* **2020**, *39*, 2152−2161.

(72) Rungthanaphatsophon, P.; Fajen, O. J.; Kelley, S. P.; Walensky, J. R. Thorium(IV) and Uranium(IV) Phosphaazaallenes. *Inorganics* **2019**, *7*, 105.

(73) Ward, R. J.; Rungthanaphatsophon, P.; Rosal, I. d.; Kelley, S. P.; Maron, L.; Walensky, J. R. Divergent uranium- versus phosphorus-based reduction of Me_3SiN_3 with steric modification of phosphido ligands. *Chem. Sci.* **2020**, *11*, 5830−5835.

(74) Weiss, C. J.; Marks, T. J. Organo-f-element catalysts for efficient and highly selective hydroalkoxylation and hydrothiolation. *Dalton Trans.* **2010**, *39*, 6576−6588.

(75) Zheng, P.; Hong, J.; Liu, R.; Zhang, Z.; Pang, Z.; Weng, L.; Zhou, X. Synthesis and Reactivities of Guanidinate Dianion Complexes of Heterobimetallic Lanthanide−Lithium Cp$_2$ Ln-[$(CyN)_2$CNPh]Li$(THF)_3$. *Organometallics* **2010**, *29*, 1284−1289.

(76) Watt, F. A.; Krishna, A.; Golovanov, G.; Ott, H.; Schoch, R.; Wölper, C.; Neuba, A. G.; Hohloch, S. Monoanionic Anilidophosphine Ligand in Lanthanide Chemistry: Scope, Reactivity, and Electrochemistry. *Inorg. Chem.* **2020**, *59*, 2719−2732.

(77) Garner, M. E.; Arnold, J. Reductive Elimination of Diphosphine from a Thorium−NHC−Bis(phosphido) Complex. *Organometallics* **2017**, *36*, 4511−4514.

(78) Kühl, O. *Phosphorus-31 NMR Spectroscopy*; Springer Berlin Heidelberg: Berlin, Heidelberg, 2009.

(79) Vilanova, S. P.; Alayoglu, P.; Heidarian, M.; Huang, P.; Walensky, J. R. Metal−Ligand Multiple Bonding in Thorium Phosphorus and Thorium Arsenic Complexes. *Chem. - Eur. J.* **2017**, *23*, 16748−16752.

(80) Romanov, A. S.; Becker, C. R.; James, C. E.; Di, D.; Credgington, D.; Linnolahti, M.; Bochmann, M. Copper and Gold Cyclic (Alkyl)(amino)carbene Complexes with Sub-Microsecond Photoemissions: Structure and Substituent Effects on Redox and Luminescent Properties. *Chem. - Eur. J.* **2017**, *23*, 4625−4637.

(81) Gernert, M.; Müller, U.; Haehnel, M.; Pflaum, J.; Steffen, A. A Cyclic Alkyl(amino)carbene as Two-Atom π-Chromophore Leading to the First Phosphorescent Linear CuI Complexes. *Chem. - Eur. J.* **2017**, *23*, 2206−2216.

(82) Di, D.; Romanov, A. S.; Yang, L.; Richter, J. M.; Rivett, J. P. H.; Jones, S.; Thomas, T. H.; Abdi Jalebi, M.; Friend, R. H.; Linnolahti, M.; Bochmann, M.; Credgington, D. High-performance light-emitting diodes based on carbene-metal-amides. *Science* **2017**, *356*, 159−163.

(83) Romanov, A. S.; Di, D.; Yang, L.; Fernandez-Cestau, J.; Becker, C. R.; James, C. E.; Zhu, B.; Linnolahti, M.; Credgington, D.; Bochmann, M. Highly photoluminescent copper carbene complexes based on prompt rather than delayed fluorescence. *Chem. Commun.* **2016**, *52*, 6379−6382.

(84) Shi, S.; Jung, M. C.; Coburn, C.; Tadle, A.; Sylvinson, M. R. D.; Djurovich, P. I.; Forrest, S. R.; Thompson, M. E. Highly Efficient Photo- and Electroluminescence from Two-Coordinate Cu(I) Complexes Featuring Nonconventional N-Heterocyclic Carbenes. *J. Am. Chem. Soc.* **2019**, *141*, 3576−3588.

(85) Hamze, R.; Peltier, J. L.; Sylvinson, D.; Jung, M.; Cardenas, J.; Haiges, R.; Soleilhavoup, M.; Jazzar, R.; Djurovich, P. I.; Bertrand, G.; Thompson, M. E. Eliminating nonradiative decay in Cu(I) emitters: 99% quantum efficiency and microsecond lifetime. *Science* **2019**, *363*, 601−606.

(86) Li, J.; Wang, L.; Zhao, Z.; Li, X.; Yu, X.; Huo, P.; Jin, Q.; Liu, Z.; Bian, Z.; Huang, C. Two-Coordinate Copper(I)/NHC Complexes: Dual Emission Properties and Ultralong Room-Temperature Phosphorescence. *Angew. Chem., Int. Ed.* **2020**, *59*, 8210−8217.

(87) Jazzar, R.; Soleilhavoup, M.; Bertrand, G. Cyclic (Alkyl)- and (Aryl)-(amino)carbene Coinage Metal Complexes and Their Applications. *Chem. Rev.* **2020**, *120*, 4141−4168.

(88) Bertrand, B.; Romanov, A. S.; Brooks, M.; Davis, J.; Schmidt, C.; Ott, I.; O'Connell, M.; Bochmann, M. Synthesis, structure and cytotoxicity of cyclic (alkyl)(amino) carbene and acyclic carbene complexes of group 11 metals. *Dalton Trans.* **2017**, *46*, 15875−15887.

(89) Frey, G. D.; Dewhurst, R. D.; Kousar, S.; Donnadieu, B.; Bertrand, G. Cyclic (Alkyl)(amino)carbene Gold(I) complexes: A Synthetic and Structural Investigation. *J. Organomet. Chem.* **2008**, *693*, 1674−1682.

(90) Romanov, A. S.; Bochmann, M. Gold(I) and Gold(III) Complexes of Cyclic (Alkyl)(amino)carbenes. *Organometallics* **2015**, *34*, 2439−2454.

(91) Romanov, A. S.; Bochmann, M. Synthesis, structures and photoluminescence properties of silver complexes of cyclic (alkyl)-(amino)carbenes. *J. Organomet. Chem.* **2017**, *847*, 114−120.

(92) Jurkauskas, V.; Sadighi, J. P.; Buchwald, S. L. Conjugate reduction of α,β-unsaturated carbonyl compounds catalyzed by a copper carbene complex. *Org. Lett.* **2003**, *5*, 2417−2420.

(93) de Frémont, P.; Scott, N. M.; Stevens, E. D.; Nolan, S. P. Synthesis and Structural Characterization of N-Heterocyclic Carbene Gold(I) Complexes. *Organometallics* **2005**, *24*, 2411−2418.

(94) Braunschweig, H.; Ewing, W. C.; Kramer, T.; Mattock, J. D.; Vargas, A.; Werner, C. Organometallic Probe for the Electronics of Base-Stabilized Group 11 Metal Cations. *Chem. - Eur. J.* **2015**, *21*, 12347−12356.

(95) Griffiths, M. B. E.; Koponen, S. E.; Mandia, D. J.; McLeod, J. F.; Coyle, J. P.; Sims, J. J.; Giorgi, J. B.; Sirianni, E. R.; Yap, G. P. A.; Barry, S. T. Surfactant Directed Growth of Gold Metal Nanoplates by Chemical Vapor Deposition. *Chem. Mater.* **2015**, *27*, 6116−6124.

(96) Johnson, M. W.; Shevick, S. L.; Toste, F. D.; Bergman, R. G. Preparation and reactivity of terminal gold(i) amides and phosphides. *Chem. Sci.* **2013**, *4*, 1023−1027.

(97) Lavallo, V.; Canac, Y.; Präsang, C.; Donnadieu, B.; Bertrand, G. Stable cyclic (alkyl)(amino)carbenes as rigid or flexible, bulky, electron-rich ligands for transition-metal catalysts: a quaternary carbon atom makes the difference. *Angew. Chem., Int. Ed.* **2005**, *44*, 5705−5709.

(98) Neogrády, P.; Kellö, V.; Urban, M.; Sadlej, A. J. Ionization Potentials and Electron Affinities of Cu, Ag, and Au: Electron Correlation and Relativistic Effects. *Int. J. Quantum Chem.* **1997**, *63*, 557−565.

(99) Gaillard, S.; Nun, P.; Slawin, A. M. Z.; Nolan, S. P. Expeditious Synthesis of [Au(NHC)(L)]$^+$ (NHC = N-Heterocyclic Carbene; L =

https://dx.doi.org/10.1021/acs.inorgchem.0c01971
Inorg. Chem. 2020, 59, 13621−13631

Phosphine or NHC) Complexes. *Organometallics* **2010**, *29*, 5402−5408.
(100) Lazreg, F.; Slawin, A. M. Z.; Cazin, C. S. J. Heteroleptic Bis(N-heterocyclic carbene)Copper(I) Complexes: Highly Efficient Systems for the [3 + 2] Cycloaddition of Azides and Alkynes. *Organometallics* **2012**, *31*, 7969−7975.
(101) Soleilhavoup, M.; Bertrand, G. Cyclic (alkyl)(amino)carbenes (CAACs): Stable Carbenes on the Rise. *Acc. Chem. Res.* **2015**, *48*, 256−266.

https://dx.doi.org/10.1021/acs.inorgchem.0c01971
Inorg. Chem. 2020, 59, 13621−13631

2.3 References

(1) Vougioukas, A. E.; Kagan, H. B. LANTHANIDES AS LEWIS-ACID CATALYSTS IN ALDOL ADDITION, CYANOHYDRIN-FORMING AND OXIRANE RING OPENING REACTIONS. *Tetrahedron Lett.* **1987**, *28*, 5513–5516.
(2) Collin, J.; Giuseppone, N.; van de Weghe, P. Lanthanide iodides, a new family of efficient Lewis acid catalysts. *Coord. Chem. Rev.* **1998**, *178-180*, 117–144.
(3) Ma, Y.; Wang, L.; Shao, J.; Tian, H. Recent Developments of Lewis Acids Catalysis: Lanthanide Catalysts with Long Perfluoro-Chain in Organic Chemistry. *Curr. Org. Chem.* **2007**, *11*, 559–576.
(4) Kobayashi, S.; Sugiura, M.; Kitagawa, H.; Lam, W. W.-L. Rare-Earth Metal Triflates in Organic Synthesis. *Chem. Rev.* **2002**, *102*, 2227–2302.
(5) Tripodi, G. L.; Correra, T. C.; Angolini, C. F. F.; Ferreira, B. R. V.; Maître, P.; Eberlin, M. N.; Roithová, J. The Intermediates in Lewis Acid Catalysis with Lanthanide Triflates. *Eur. J. Org. Chem.* **2019**, 3560–3566.
(6) Bayer, U.; Anwander, R. Carbonyl group and carbon dioxide activation by rare-earth-metal complexes. *Dalton Trans.* **2020**, *49*, 17472–17493.
(7) Ramirez, B. L.; Lu, C. C. Rare-Earth Supported Nickel Catalysts for Alkyne Semihydrogenation: Chemo- and Regioselectivity Impacted by the Lewis Acidity and Size of the Support. *J. Am. Chem. Soc.* **2020**, *142*, 5396–5407.
(8) Gagné, M. R.; Marks, T. J. Organolanthanide-Catalyzed Hydroamination. Facile, Regiospecific Cyclization of Unprotected Amino Olefins. *J. Am. Chem. Soc.* **1989**, *111*, 4108–4109.
(9) Gagné, M. R.; Stern, C. L.; Marks, T. J. Organolanthanide-Catalyzed Hydroamination. A Kinetic, Mechanistic, and Diastereoselectivity Study of the Cyclization of N-Unprotected Amino Olefins. *J. Am. Chem. Soc.* **1992**, *114*, 275–294.
(10) Hong, S.; Marks, T. J. Organolanthanide-Catalyzed Hydroamination. *Acc. Chem. Res.* **2004**, *37*, 673–686.
(11) Trifonov, A. A.; Basalov, I. V.; Kissel, A. A. Use of organolanthanides in the catalytic intermolecular hydrophosphination and hydroamination of multiple C–C bonds. *Dalton Trans.* **2016**, *45*, 19172–19193.
(12) Weiss, C. J.; Marks, T. J. Organo-f-element catalysts for efficient and highly selective hydroalkoxylation and hydrothiolation. *Dalton Trans.* **2010**, *39*, 6576–6588.
(13) Kazeminejad, N.; Munzel, D.; Gamer, M. T.; Roesky, P. W. Bis(amidinate) ligands in early lanthanide chemistry – synthesis, structures, and hydroamination catalysis. *Chem. Commun.* **2017**, *53*, 1060–1063.
(14) Yi, W.; Zhang, J.; Hong, L.; Chen, Z.; Zhou, X. Insertion of Isocyanate and Isothiocyanate into the Ln–P σ-Bond of Organolanthanide Phosphides. *Organometallics* **2011**, *30*, 5809–5814.
(15) Behrle, A. C.; Schmidt, J. A. R. Insertion Reactions and Catalytic Hydrophosphination of Heterocumulenes using α-Metalated *N*,*N*-Dimethylbenzylamine Rare-Earth-Metal Complexes. *Organometallics* **2013**, *32*, 1141–1149.
(16) Zhang, W.-X.; Nishiura, M.; Mashiko, T.; Hou, Z. Half-Sandwich *o*-*N*,*N*-Dimethylaminobenzyl Complexes over the Full Size Range of Group 3 and Lanthanide Metals. Synthesis, Structural Characterization, and Catalysis of Phosphine P–H Bond Addition to Carbodiimides. *Chem. Eur. J.* **2008**, *14*, 2167–2179.
(17) Vilanova, S. P.; Tarlton, M. L.; Barnes, C. L.; Walensky, J. R. Double insertion of benzophenone into thorium-phosphorus bonds. *J. Organomet. Chem.* **2018**, *857*, 159–163.
(18) Tarlton, M. L.; Del Rosal, I.; Vilanova, S. P.; Kelley, S. P.; Maron, L.; Walensky, J. R. Comparative Insertion Reactivity of CO, CO_2, ^{t}BuCN, and ^{t}BuNC into Thorium– and Uranium–Phosphorus Bonds. *Organometallics* **2020**, *39*, 2152–2161.
(19) Hey, E.; Lappert, M. F.; Atwood, J. L.; Bott, S. G. Bis(trimethylsilyl)phosphinodithioformates, the Phosphorus Analogues of Dithiocarbamates; *X*-ray Structures of $[Zr(cp)_2(Cl)(\eta^2\text{-}S_2CPR_2)]$ and its

Thermolysis Product [{Zr(cp)$_2$(μ-S)}$_2$] (cp = η-C$_5$H$_5$, R = SiMe$_3$). *J. Chem. Soc., Chem. Commun.* **1987**, 421–422.
(20) Segerer, U.; Sieler, J.; Hey-Hawkins, E. Formation of Novel P-Functionalized Ligands by Insertion Reactions of RNCX (R = Ph, X = O, S; R = Pr^i , X = O) into the Zr–P Bond of [Cp°$_2$ZrCl(PHCy)] (Cp° = η^5-C$_5$EtMe$_4$, Cy = Cyclohexyl) and [Cp‘$_2$ZrCl{PH(TRIP)}] (Cp‘ = η^5-C$_5$MeH$_4$, TRIP = 2,4,6-Pr$^i_3$C$_6$H$_2$). *Organometallics* **2000**, *19*, 2445–2449.
(21) Lindenberg, F.; Sieler, J.; Hey-Hawkins, E. FORMATION OF NOVEL P- and As-FUNCTIONALIZED LIGANDS BY INSERTION REACTIONS INTO THE Zr–E BOND OF (*η*^{5}-C$_5$H$_4$R)$_2$ZrCl{E(SiMe$_3$)$_2$} (R = Me, E = P, As; R = H, E = P). *Polyhedron* **1996**, *15*, 1459–1471.
(22) Hou, Z.; Breen, T. L.; Stephan, D. W. Formation and Reactivity of the Early Metal Phosphides and Phosphinidenes Cp*$_2$Zr=PR, Cp*$_2$Zr(PR)$_2$, and Cp*$_2$Zr(PR)$_3$. *Organometallics* **1993**, *12*, 3158–3167.
(23) Edelmann, F. T. Lanthanide amidinates and guanidinates in catalysis and materials science: a continuing success story. *Chem. Soc. Rev.* **2012**, *41*, 7657–7672.
(24) Evans, W. J.; Miller, K. A.; Ziller, J. W. Synthesis of (O$_2$CEPh)$^{1-}$ Ligands (E = S, Se) by CO$_2$ Insertion into Lanthanide Chalcogen Bonds and Their Utility in Forming Crystallographically Characterizable Organoaluminum Complexes Me$_2$Al(μ-O$_2$CEPh)$_2$. *Inorg. Chem.* **2006**, *45*, 424–429.
(25) Breen, T. L.; Stephan, D. W. Reactivity Studies of Methylzirconocene Phosphide Complexes. *Organometallics* **1996**, *15*, 4509–4514.
(26) Hey-Hawkins, E.; Lindenberg, F. Regiospezifische Insertion von Phenylacetylen in die Zr–P-Bindung von Cp$_2$Zr{P(SiMe$_3$)$_2$}(Cl) und Folgereaktionen des Insertionsprodukts (*Z*)-Cp$_2$Zr{C(Ph) = C(H)P(SiMe$_3$)$_2$}(Cl). *Chem. Ber.* **1992**, *125*, 1815–1819.
(27) Hou, Z.; Stephan, D. W. Generation and Reactivity of the First Mononuclear Early Metal Phosphinidene Complex, Cp*$_2$Zr=P(C$_6$H$_2$Me$_3$-2,4,6). *J. Am. Chem. Soc.* **1992**, *114*, 10088–10089.
(28) Kühl, O. *Phosphoros-31 NMR Spectroscopy: A Concise Introduction for the Synthetic Organic and Organometallic Chemist*; Springer: Berlin, Heidelberg, Germany, 2008.
(29) Basiouny, M. M. I.; Dollard, D. A.; Schmidt, J. A. R. Regioselective Single and Double Hydrophosphination and Hydrophosphinylation of Unactivated Alkynes. *ACS Catal.* **2019**, *9*, 7143–7153.
(30) Basiouny, M. M. I.; Schmidt, J. A. R. Lanthanum-Catalyzed Double Hydrophosphinylation of Nitriles. *Organometallics* **2017**, *36*, 721–729.
(31) Rina, Y. A.; Schmidt, J. A. R. Lanthanum-Catalyzed Regioselective Anti-Markovnikov Hydrophosphinylation of Styrenes. *Organometallics* **2019**, *38*, 4261–4270.
(32) Behrle, A. C.; Schmidt, J. A. R. Synthesis and Reactivity of Homoleptic α-Metalated *N*,*N*-Dimethylbenzylamine Rare-Earth-Metal Complexes. *Organometallics* **2011**, *30*, 3915–3918.
(33) Behrle, A. C.; Walensky, J. R. Insertion of ^{t}BuNC into thorium–phosphorus and thorium–arsenic bonds: phosphaazaallene and arsaazaallene moieties in f element chemistry. *Dalton Trans.* **2016**, *45*, 10042–10049.
(34) Vilanova, S. P.; Del Rosal, I.; Tarlton, M. L.; Maron, L.; Walensky, J. R. Functionalization of Carbon Monoxide and *tert*-Butyl Nitrile by Intramolecular Proton Transfer in a Bis(Phosphido) Thorium Complex. *Angew. Chem. Int. Ed.* **2018**, *57*, 16748–16753.
(35) Zhang, C.; Wang, Y.; Hou, G.; Ding, W.; Zi, G.; Walter, M. D. Experimental and computational studies on a three-membered diphosphido thorium metallaheterocycle [η^5-1,3-(Me$_3$C)$_2$C$_5$H$_3$]$_2$Th[η^2-P$_2$(2,4,6-^{i}Pr$_3$C$_6$H$_2$)$_2$]. *Dalton Trans.* **2019**, *48*, 6921–6930.
(36) Garner, M. E.; Arnold, J. Reductive Elimination of Diphosphine from a Thorium–NHC–Bis(phosphido) Complex. *Organometallics* **2017**, *36*, 4511–4514.
(37) Konings, R. J. M.; Morss, L. R.; Fuger, J. *The Chemistry of the Actinide and Transactinide Elements*, 4th Ed.; Springer: Dordrecht, The Netherlands, 2010.
(38) Langeslay, R. R.; Fieser, M. E.; Ziller, J. W.; Furche, F.; Evans, W. J. Synthesis, structure, and reactivity of crystalline molecular complexes of the {[C$_5$H$_3$(SiMe$_3$)$_2$]$_3$Th}$^{1-}$ anion containing thorium in the formal +2 oxidation state. *Chem. Sci.* **2015**, *6*, 517–521.
(39) Cotton, S. *Lanthanide and Actinide Chemistry*; John Wiley & Sons, Ltd.: Chichester, UK, 2006.

(40) Rungthanaphatsophon, P.; Duignan, T. J.; Myers, A. J.; Vilanova, S. P.; Barnes, C. L.; Autschbach, J.; Batista, E. R.; Yang, P.; Walensky, J. R. Influence of Substituents on the Electronic Structure of Mono- and Bis(phosphido) Thorium(IV) Complexes. *Inorg. Chem.* **2018**, *57*, 7270–7278.
(41) Garner, M. E.; Parker, B. F.; Hohloch, S.; Bergman, R. G.; Arnold, J. Thorium Metallacycle Facilitates Catalytic Alkyne Hydrophosphination. *J. Am. Chem. Soc.* **2017**, *139*, 12935–12938.
(42) Rabe, G. W.; Guzei, I. A.; Rheingold, A. L. Synthesis and X-ray Crystal Structure Determination of the First Lanthanide Complexes Containing Primary Phosphide Ligands: $Ln[P(H)Mes^*]_2(thf)_4$ (Ln = Yb, Eu). *Inorg. Chem.* **1997**, *36*, 4914–4915.
(43) Clegg, W.; Izod, K.; Liddle, S. T. Synthesis and crystal structure of a homoleptic, alkali metal-free lanthanide(II) phosphide complex. *J. Organomet. Chem.* **2000**, *613*, 128–131.
(44) Martinez-Gomez, N. C.; Vu, H. N.; Skovran, E. Lanthanide Chemistry: From Coordination in Chemical Complexes Shaping Our Technology to Coordination in Enzymes Shaping Bacterial Metabolism. *Inorg. Chem.* **2016**, *55*, 10083–10089.
(45) Day, B. M.; Guo, F.-S.; Layfield, R. A. Cyclopentadienyl Ligands in Lanthanide Single-Molecule Magnets: One Ring To Rule Them All? *Acc. Chem. Res.* **2018**, *51*, 1880–1889.
(46) Bünzli, J.-C. G. Lanthanide Luminescence for Biomedical Analyses and Imaging. *Chem. Rev.* **2010**, *110*, 2729–2755.
(47) Iman, K.; Shahid, M. Life sensors: current advances in oxygen sensing by lanthanide complexes. *New J. Chem.* **2019**, *43*, 1094–1116.
(48) Aulsebrook, M. L.; Graham, B.; Grace, M. R.; Tuck, K. L. Lanthanide complexes for luminescence-based sensing of low molecular weight analytes. *Coord. Chem. Rev.* **2018**, *375*, 191–220.
(49) Cable, M. L.; Kirby, J. P.; Gray, H. B.; Ponce, A. Enhancement of Anion Binding in Lanthanide Optical Sensors. *Acc. Chem. Res.* **2013**, *46*, 2576–2584.
(50) Plecnik, C. E.; Liu, S.; Shore, S. G. Lanthanide–Transition-Metal Complexes: From Ion Pairs to Extended Arrays. *Acc. Chem. Res.* **2003**, *36*, 499–508.
(51) Chen, F.-F.; Chen, Z.-Q.; Bian, Z.-Q.; Huang, C.-H. Sensitized luminescence from lanthanides in d–f bimetallic complexes. *Coord. Chem. Rev.* **2010**, *254*, 991–1010.
(52) Cosquer, G.; Pointillart, F.; Le Guennic, B.; Le Gal, Y.; Golhen, S.; Cador, O.; Ouahab, L. 3d4f Heterobimetallic Dinuclear and Tetranuclear Complexes Involving Tetrathiafulvalene as Ligands: X-ray Structures and Magnetic and Photophysical Investigations. *Inorg. Chem.* **2012**, *51*, 8488–8501.
(53) Klink, S. I.; Keizer, H.; van Veggel, F. C. J. M. Transition Metal Complexes as Photosensitizers for Near-Infrared Lanthanide Luminescence. *Angew. Chem. Int. Ed.* **2000**, *39*, 4319–4321.
(54) Øwre, A.; Vinum, M.; Kern, M.; van Slageren, J.; Bendix, J.; Perfetti, M. Chiral, Heterometallic Lanthanide–Transition Metal Complexes by Design. *Inorganics* **2018**, *6*, 72.
(55) Kajiwara, T.; Nakano, M.; Takahashi, K.; Takaishi, S.; Yamashita, M. Structural Design of Easy-Axis Magnetic Anisotropy and Determination of Anisotropic Parameters of Ln(III)–Cu(II) Single-Molecule Magnets. *Chem. Eur. J.* **2011**, *17*, 196–205.
(56) Atsushi, O.; Ryo, W.; Masaru, N.; Takashi, S.; Shunsuke, Y.; Hiroyuki, N.; Takayuki, I. Ferromagnetic Gd–Cu, Tb–Cu, and Ho–Cu Couplings in Isomorphous $[Ln_2Cu]$ Complexes. *Chem. Lett.* **2010**, *39*, 1331–1332.
(57) Ungur, L.; Thewissen, M.; Costes, J.-P.; Wernsdorfer, W.; Chibotaru, L. F. Interplay of Strongly Anisotropic Metal Ions in Magnetic Blocking of Complexes. *Inorg. Chem.* **2013**, *52*, 6328–6337.
(58) Zhu, M.; Li, C.; Wang, X.; Li, L.; Sutter, J.-P. Thermal Magnetic Hysteresis in a Copper–Gadolinium–Radical Chain Compound. *Inorg. Chem.* **2016**, *55*, 2676–2678.
(59) Bag, P.; Goura, J.; Mereacre, V.; Novitchi, G.; Powell, A. K.; Chandrasekhar, V. Synthesis, magnetism and Mössbauer studies of tetranuclear heterometallic $\{Fe^{III}_2Ln_2\}$(Ln = Gd, Dy, Tb) complexes: evidence of slow relaxation of magnetization in the terbium analogue. *Dalton Trans.* **2014**, *43*, 16366–16376.
(60) Burns, C. P.; Yang, X.; Wofford, J. D.; Bhuvanesh, N. S.; Hall, M. B.; Nippe, M. Structure and Magnetization Dynamics of Dy–Fe and Dy–Ru Bonded Complexes. *Angew. Chem. Int. Ed.* **2018**, *57*, 8144–8148.

(61) Rigamonti, L.; Nava, A.; Boulon, M.-E.; Luzon, J.; Sessoli, R.; Cornia, A. Experimental and Theoretical Studies on the Magnetic Anisotropy in Lanthanide(III)-Centered Fe_3Ln Propellers. *Chem. Eur. J.* **2015**, *21*, 12171–12180.
(62) Singh, N.; Das Gupta, S.; Butcher, R. J.; Christou, G. Synthesis and magnetochemistry of heterometallic triangular $Fe^{III}_2Ln^{III}$ (Ln = La, Gd, Tb, Dy, and Ho) and $Fe^{III}_2Y^{III}$ complexes. *Dalton Trans.* **2017**, *46*, 7897–7903.
(63) Wang, H.-S.; Long, Q.-Q.; Hu, Z.-B.; Yue, L.; Yang, F.-J.; Yin, C.-L.; Pan, Z.-Q.; Zhang, Y.-Q.; Song, Y. Synthesis, crystal structures and magnetic properties of a series of chair-like heterometallic $[Fe_4Ln_2]$ (Ln = Gd^{III}, Dy^{III}, Ho^{III}, and Er^{III}) complexes with mixed organic ligands. *Dalton Trans.* **2019**, *48*, 13472–13482.
(64) Stoian, S. A.; Paraschiv, C.; Kiritsakas, N.; Lloret, F.; Münck, E.; Bominaar, E. L.; Andruh, M. Mössbauer, Electron Paramagnetic Resonance, and Magnetic Susceptibility Studies on Members of a New Family of Cyano-Bridged 3d-4f Complexes. Demonstration of Anisotropic Exchange in a Fe-Gd Complex. *Inorg. Chem.* **2010**, *49*, 3387–3401.
(65) Qiu, J.-Z.; Wang, L.-F.; Chen, Y.-C.; Zhang, Z.-M.; Li, Q.-W.; Tong, M.-L. Magnetocaloric Properties of Heterometallic 3d–Gd Complexes Based on the $[Gd(oda)_3]^{3-}$ Metalloligand. *Chem. Eur. J.* **2016**, *22*, 802–808.
(66) Burns, C. P.; Yang, X.; Sung, S.; Wofford, J. D.; Bhuvanesh, N. S.; Hall, M. B.; Nippe, M. Towards understanding of lanthanide–transition metal bonding: investigations of the first Ce–Fe bonded complex. *Chem. Commun.* **2018**, *54*, 10893–10896.
(67) Ahmed, N.; Das, C.; Vaidya, S.; Langley, S. K.; Murray, K. S.; Shanmugam, M. Nickel(II)–Lanthanide(III) Magnetic Exchange Coupling Influencing Single-Molecule Magnetic Features in $\{Ni_2Ln_2\}$ Complexes. *Chem. Eur. J.* **2014**, *20*, 14235–14239.
(68) Upadhyay, A.; Das, C.; Langley, S. K.; Murray, K. S.; Srivastava, A. K.; Shanmugam, M. Heteronuclear Ni(II)–Ln(III) (Ln = La, Pr, Tb, Dy) complexes: synthesis and single-molecule magnet behaviour. *Dalton Trans.* **2016**, *45*, 3616–3626.
(69) Vieru, V.; Pasatoiu, T. D.; Ungur, L.; Suturina, E.; Madalan, A. M.; Duhayon, C.; Sutter, J.-P.; Andruh, M.; Chibotaru, L. F. Synthesis, Crystal Structures, Magnetic Properties, and Theoretical Investigation of a New Series of Ni^{II}–Ln^{III}–W^{V} Heterotrimetallics: Understanding the SMM Behavior of Mixed Polynuclear Complexes. *Inorg. Chem.* **2016**, *55*, 12158–12171.
(70) Ahmed, N.; Das, C.; Vaidya, S.; Srivastava, A. K.; Langley, S. K.; Murray, K. S.; Shanmugam, M. Probing the magnetic and magnetothermal properties of M(II)–Ln(III) complexes (where M(II) = Ni or Zn; Ln(III) = La or Pr or Gd). *Dalton Trans.* **2014**, *43*, 17375–17384.
(71) Long, J.; Rouquette, J.; Thibaud, J.-M.; Ferreira, R. A. S.; Carlos, L. D.; Donnadieu, B.; Vieru, V.; Chibotaru, L. F.; Konczewicz, L.; Haines, J.*; et al.* A High-Temperature Molecular Ferroelectric Zn/Dy Complex Exhibiting Single-Ion-Magnet Behavior and Lanthanide Luminescence. *Angew. Chem. Int. Ed.* **2015**, *54*, 2236–2240.
(72) Upadhyay, A.; Singh, S. K.; Das, C.; Mondol, R.; Langley, S. K.; Murray, K. S.; Rajaraman, G.; Shanmugam, M. Enhancing the effective energy barrier of a Dy(III) SMM using a bridged diamagnetic Zn(II) ion. *Chem. Commun.* **2014**, *50*, 8838–8841.
(73) Boulay, A.; Deraeve, C.; Vander Elst, L.; Leygue, N.; Maury, O.; Laurent, S.; Muller, R. N.; Mestre-Voegtlé, B.; Picard, C. Terpyridine-Based Heteroditopic Ligand for $Ru^{II}Ln_3^{III}$ Metallostar Architectures (Ln = Gd, Eu, Nd, Yb) with MRI/Optical or Dual-Optical Responses. *Inorg. Chem.* **2015**, *54*, 1414–1425.
(74) Chen, F.-F.; Bian, Z.-Q.; Liu, Z.-W.; Nie, D.-B.; Chen, Z.-Q.; Huang, C.-H. Highly Efficient Sensitized Red Emission from Europium (III) in Ir–Eu Bimetallic Complexes by ^{3}MLCT Energy Transfer. *Inorg. Chem.* **2008**, *47*, 2507–2513.
(75) Chi, Y.-X.; Niu, S.-Y.; Jin, J.; Wang, R.; Li, Y. Syntheses, structures and photophysical properties of tetranuclear Cd–Ln coordination complexes. *Dalton Trans.* **2009**, 7653–7659.
(76) Crowston, B. J.; Shipp, J. D.; Chekulaev, D.; McKenzie, L. K.; Jones, C.; Weinstein, J. A.; Meijer, A. J. H.; Bryant, H. E.; Natrajan, L.; Woodward, A.*;* Ward, M. D. Heteronuclear d–d and d–f Ru(II)/M complexes [M = Gd(III), Yb(III), Nd(III), Zn(II) or Mn(II)] of ligands combining phenanthroline and

aminocarboxylate binding sites: combined relaxivity, cell imaging and photophysical studies. *Dalton Trans.* **2019**, *48*, 6132–6152.
(77) Lazarides, T.; Sykes, D.; Faulkner, S.; Barbieri, A.; Ward, M. D. On the Mechanism of d–f Energy Transfer in Ru^{II}/Ln^{III} and Os^{II}/Ln^{III} Dyads: Dexter-Type Energy Transfer Over a Distance of 20 Å. *Chem. Eur. J.* **2008**, *14*, 9389–9399.
(78) Lazarides, T.; Tart, N. M.; Sykes, D.; Faulkner, S.; Barbieri, A.; Ward, M. D. $[Ru(bipy)_3]^{2+}$ and $[Os(bipy)_3]^{2+}$ chromophores as sensitisers for near-infrared luminescence from Yb(III) and Nd(III) in d/f dyads: contributions from Förster, Dexter, and redox-based energy-transfer mechanisms. *Dalton Trans.* **2009**, 3971–3979.
(79) Moore, E. G.; Benaglia, M.; Bergamini, G.; Ceroni, P. Synthesis, Stability and Sensitised Lanthanide Luminescence of Heterobimetallic d/f Terpyridine Complexes. *Eur. J. Inorg. Chem.* **2015**, 414–420.
(80) Liu, C.; Yang, W.; Zhang, Y.; Jiang, J. Quintuple-Decker Heteroleptic Phthalocyanine Heterometallic Samarium–Cadmium Complexes. Synthesis, Crystal Structure, Electrochemical Behavior, and Spectroscopic Investigation. *Inorg. Chem.* **2020**, *59*, 17591–17599.
(81) Lazarides, T.; Adams, H.; Sykes, D.; Faulkner, S.; Calogero, G.; Ward, M. D. Heteronuclear bipyrimidine-bridged Ru–Ln and Os–Ln dyads: low-energy ^{3}MLCT states as energy-donors to Yb(III) and Nd(III). *Dalton Trans.* **2008**, 691–698.
(82) Norel, L.; Di Piazza, E.; Feng, M.; Vacher, A.; He, X.; Roisnel, T.; Maury, O.; Rigaut, S. Lanthanide Sensitization with Ruthenium Carbon-Rich Complexes and Redox Commutation of Near-IR Luminescence. *Organometallics* **2014**, *33*, 4824–4835.
(83) Samanta, S. K.; Abtab, S. M. T.; Sardar, P. S.; Sanyal, S.; Chaudhury, M.; Ghosh, S. Role of Triplet States of Two Different Ligands in the Sensitized Emission of Ln^{III} (Eu^{III} , Tb^{III}) in d–f Hybrid Tetranuclear Heterometal ($Zn^{II}_2Ln^{III}_2$, $Cd^{II}_2Ln^{III}_2$) Complexes. *Eur. J. Inorg. Chem.* **2014**, 3101–3113.
(84) Shavaleev, N. M.; Accorsi, G.; Virgili, D.; Bell, Z. R.; Lazarides, T.; Calogero, G.; Armaroli, N.; Ward, M. D. Syntheses and Crystal Structures of Dinuclear Complexes Containing d-Block and f-Block Luminophores. Sensitization of NIR Luminescence from Yb(III), Nd(III), and Er(III) Centers by Energy Transfer from Re(I)– and Pt(II)–Bipyrimidine Metal Centers. *Inorg. Chem.* **2005**, *44*, 61–72.
(85) Shavaleev, N. M.; Moorcraft, L. P.; Pope, S. J. A.; Bell, Z. R.; Faulkner, S.; Ward, M. D. Sensitised near-infrared emission from lanthanides using a covalently-attached Pt(II) fragment as an antenna group. *Chem. Commun.* **2003**, 1134–1135.
(86) Shavaleev, N. M.; Moorcraft, L. P.; Pope, S. J. A.; Bell, Z. R.; Faulkner, S.; Ward, M. D. Sensitized Near-Infrared Emission from Complexes of Yb^{III}, Nd^{III} and Er^{III} by Energy-Transfer from Covalently Attached Pt^{II}-Based Antenna Units. *Chem. Eur. J.* **2003**, *9*, 5283–5291.
(87) Xu, H.-B.; Zhang, L.-Y.; Ni, J.; Chao, H.-Y.; Chen, Z.-N. Conformation Changes and Luminescent Properties of Au-Ln (Ln = Nd, Eu, Er, Yb) Arrays with 5-Ethynyl-2,2'-Bipyridine. *Inorg. Chem.* **2008**, *47*, 10744–10752.
(88) Yang, X.; Schipper, D.; Jones, R. A.; Lytwak, L. A.; Holliday, B. J.; Huang, S. Anion-Dependent Self-Assembly of Near-Infrared Luminescent 24- and 32-Metal Cd–Ln Complexes with Drum-like Architectures. *J. Am. Chem. Soc.* **2013**, *135*, 8468–8471.
(89) Zakrzewski, J. J.; Sieklucka, B.; Chorazy, S. Europium(III) Photoluminescence Governed by d^8–d^{10} Heterometallophilic Interactions in Trimetallic Cyanido-Bridged Coordination Frameworks. *Inorg. Chem.* **2020**, *59*, 1393–1404.
(90) Li, X.-L.; Zhang, K.-J.; Li, J.-J.; Cheng, X.-X.; Chen, Z.-N. Dual Luminescent Dinuclear Gold(I) Complexes of Terpyridyl-Functionalized Alkyne Ligands and Their Efficient Sensitization of Eu^{III} and Yb^{III} Luminescence. *Eur. J. Inorg. Chem.* **2010**, *2010*, 3449–3457.
(91) Wen, H.-R.; Hu, J.-J.; Yang, K.; Zhang, J.-L.; Liu, S.-J.; Liao, J.-S.; Liu, C.-M. Family of Chiral Zn^{II}–Ln^{III} (Ln = Dy and Tb) Heterometallic Complexes Derived from the Amine–Phenol Ligand Showing Multifunctional Properties. *Inorg. Chem.* **2020**, *59*, 2811–2824.
(92) Mirzadeh, N.; Privér, S. H.; Blake, A. J.; Schmidbaur, H.; Bhargava, S. K. Innovative Molecular Design Strategies in Materials Science Following the Aurophilicity Concept. *Chem. Rev.* **2020**, *120*, 7551–7591.

(93) Conaghan, P. J.; Matthews, C. S. B.; Chotard, F.; Jones, S. T. E.; Greenham, N. C.; Bochmann, M.; Credgington, D.; Romanov, A. S. Highly efficient blue organic light-emitting diodes based on carbene-metal-amides. *Nat. Commun.* **2020**, *11*, 1758.
(94) Gernert, M.; Balles-Wolf, L.; Kerner, F.; Müller, U.; Schmiedel, A.; Holzapfel, M.; Marian, C. M.; Pflaum, J.; Lambert, C.; Steffen, A. Cyclic (Amino)(aryl)carbenes Enter the Field of Chromophore Ligands: Expanded π System Leads to Unusually Deep Red Emitting Cu^{I} Compounds. *J. Am. Chem. Soc.* **2020**, *142*, 8897–8909.
(95) Hamze, R.; Peltier, J. L.; Sylvinson, D.; Jung, M.; Cardenas, J.; Haiges, R.; Soleilhavoup, M.; Jazzar, R.; Djurovich, P. I.; Bertrand, G.*; et al.* Eliminating nonradiative decay in Cu(I) emitters: >99% quantum efficiency and microsecond lifetime. *Science* **2019**, *363*, 601–606.
(96) Di, D.; Romanov, A. S.; Le Yang; Richter, J. M.; Rivett, J. P. H.; Jones, S.; Thomas, T. H.; Abdi Jalebi, M.; Friend, R. H.; Linnolahti, M.*; et al.* High-performance light-emitting diodes based on carbene-metal-amides. *Science* **2017**, *356*, 159–163.
(97) Geer, A. M.; Serrano, Á. L.; Bruin, B. de; Ciriano, M. A.; Tejel, C. Terminal Phosphanido Rhodium Complexes Mediating Catalytic P–P and P–C Bond Formation. *Angew. Chem. Int. Ed.* **2015**, *54*, 472–475.
(98) Creutz, S. E.; Krummenacher, I.; Clough, C. R.; Cummins, C. C. A trigonal and hindered tertiary phosphine ligand rendered anionic by a niobate anchor: Formation of zwitterionic M(I) (M = Cu, Ag, Au, Rh) complexes. *Chem. Sci.* **2011**, *2*, 2166.
(99) Serrano, Á. L.; Casado, M. A.; Ciriano, M. A.; Bruin, B. de; López, J. A.; Tejel, C. Nucleophilicity and P–C Bond Formation Reactions of a Terminal Phosphanido Iridium Complex. *Inorg. Chem.* **2016**, *55*, 828–839.
(100) Takeuchi, K.; Kim, K.-W.; Kim, Y.-J.; Fukaya, N.; Sato, K.; Choi, J.-C. Synthesis and Structure of Multinuclear Pd(II) Complexes Bridged by Phosphide or Azide Ligands. *ACS Omega* **2020**, *5*, 29706–29713.
(101) Hierlmeier, G.; Coburger, P.; van Leest, N. P.; Bruin, B. de; Wolf, R. Aggregation and Degradation of White Phosphorus Mediated by N-Heterocyclic Carbene Nickel(0) Complexes. *Angew. Chem. Int. Ed.* **2020**, *59*, 14148–14153.

Chapter 3:

A Transient Lanthanum Phosphinidene Complex

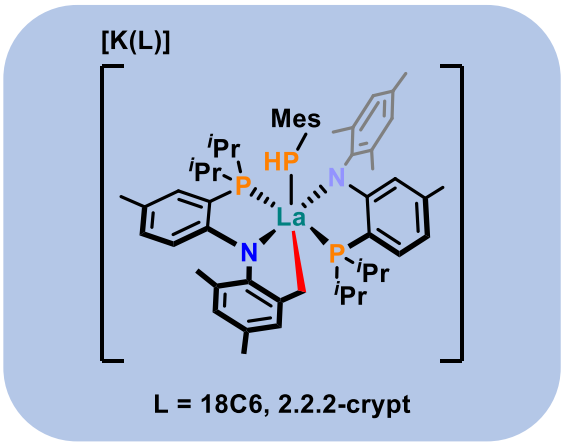

3.1 Introduction: Lanthanide Complexes with Double-Bonded Ligands

The isolation and characterization of complexes featuring double bonds between lanthanide ion and main group element (*e.g.*, C, Si, N, P, O or S) based ligands of the general form Ln=X (X = alkylidene, silylene, imido, phosphinidene, oxo or sulfido) remains a considerable challenge for synthetic chemists to date.[1] The difficulties in synthesizing such systems, especially those with a terminal Ln=X group, arise mainly from the limited number of additional anionic supporting ligands which can be accommodated by $Ln^{3+/4+}$ ions, their large ionic radii and the predominantly ionic character of the Ln=X unit which drives the thermodynamically favored cluster formation with other $Ln^{3+/4+}$ ions (Scheme 3.1).[2–5]

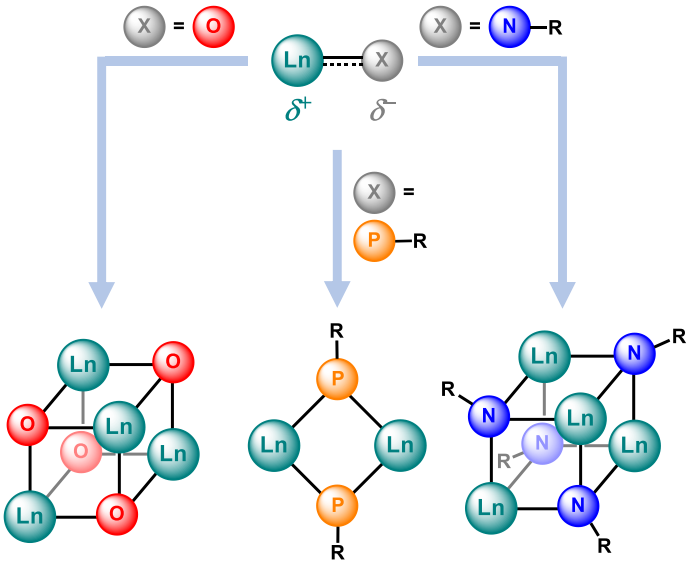

Scheme 3.1. Dimerization (middle) or cluster formation (left and right) of Ln=X groups (R = alkyl, aryl).[2–5] Exemplary and simplified representations; no supporting ligands at Ln shown.

The strong ionic character of the Ln=X unit can be rationalized in terms of a mismatch of the relative energies between HOMO and LUMO of ligand and $Ln^{3+/4+}$ ion.[6] Thus, compounds with a terminal Ln=X group are expected to exhibit a very high reactivity, which is crucial for synthetically useful (catalytic) transformations of organic substrates such as metathesis and group transfer reactions as well as metallacycle formations and C–H bond activation chemistry.[7–11] However, in order to access the desired Ln=X motif and prevent di- or oligomerization, adduct formation or intramolecular reactions causing the loss of double bond character, strategies such as steric protection by the (supporting) ligands or electronic stabilization by, *e.g.*, electron-withdrawing substituents on the ligand X have to be applied.

After the first reports of lanthanide complexes with bridging imido ligands in 2002,[12,13] the last decade has seen an unprecedented emergence of lanthanide oxo and imido chemistry,[14] with a particular emphasis on gaining a deeper understanding of the electronic structure of the (terminal) Ln=X double bond and its behavior in chemical transformations.[15–20] The goal to address such fundamental questions in lanthanide chemistry[21] has indeed led to a number of remarkable compounds.

In this context, cerium(IV) oxo and imido complexes have proven to be more accessible than the corresponding lanthanide(III) compounds, since the higher oxidation state of cerium(IV) results in a higher degree of covalent bonding in the Ln=X unit[22] and allows a higher number of anionic supporting ligands for stabilization. The introduction of (terminal) oxo and imido groups was more successful than that of phosphinidenes. In the following these findings are described in more detail.

3.1.1 Lanthanide Oxo Complexes

The isolation of a terminal Ln=X group was first achieved in 2014 by Leung and co-workers who targeted a cerium(IV) oxo complex stabilized by the bulky Kläui tripodal ligand $[Co(Cp)\{P(O)(OEt_2)\}_3]^-$ (L_{OEt}^-).[17] Interestingly, the authors found that, beside one molecule of water, an additional hydrogen bonded acetamide ligand in the second coordination sphere contributed significantly to the stability of the obtained complex $[(L_{OEt})_2(H_2O)Ce{=}O]\cdot H_2NC(O)CH_3$ (Figure 3.1). The experimentally determined short Ce–O distance of only 1.857(3) Å along with DFT calculations support the notion of a Ce=O double bond through σ- and π-bonding interactions, although the NBO analysis suggests a strong ionic character of the Ce=O fragment. The resulting high nucleophilicity of the oxygen atom was demonstrated in its reactivity towards small molecules such as carbon monoxide and carbon dioxide as well as Brønsted and Lewis acids.[20]

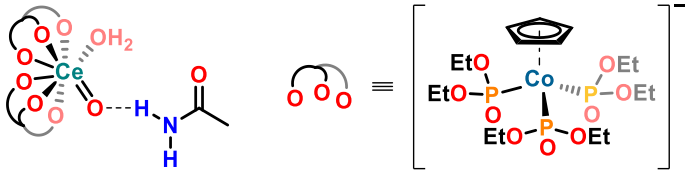

Figure 3.1. First example of a terminal Ln=X double bond in the cerium(IV) oxo complex $[(L_{OEt})_2(H_2O)Ce{=}O]\cdot H_2NC(O)CH_3$ reported by Leung *et al.* in 2014.[17]

An elegant route to alkali metal capped cerium(IV) oxo complexes was identified in 2016 by Hayton and colleagues who observed an inner sphere oxidation of $[N\{C_2H_4N(Si^tBuMe_2)\}_3]^{3-}$ ($TREN^{3-}$) supported cerium(III) by coordinated nitrate in the presence of 12-crown-4 (12-c-4) ligated lithium to yield [Li(12-c-4)][(TREN)Ce=O] (Scheme 3.2).[16] The lithium capped cerium(IV) oxo complex, for which a short Ce–O distance of 1.902(2) Å was determined crystallographically, could be cleanly silylated with chlorodimethyl-*tert*-butylsilane at the oxygen atom. The authors noted, that this can also take place without external silylating reagent by cannibalization of the TREN ligand framework, pointing out the importance of supporting ligand design.

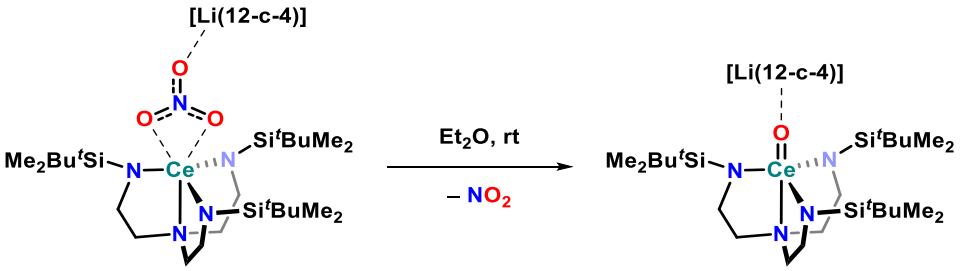

Scheme 3.2. Formation of a lithium capped cerium(IV) oxo complex after an inner sphere redox reaction between cerium(III) and nitrate, as reported by Hayton *et al.* in 2016.[16]

In 2017, the group of Schelter described an aza-Wittig reaction between a rubidium capped cerium(IV) imido complex (*vide infra*) and benzophenone leading to a cluster of four cerium(IV) oxo complexes capped by rubidium counterions (Scheme 3.3).[18] Remarkably, due to the clustering this compound is thermally stable as well as air and moisture tolerant.

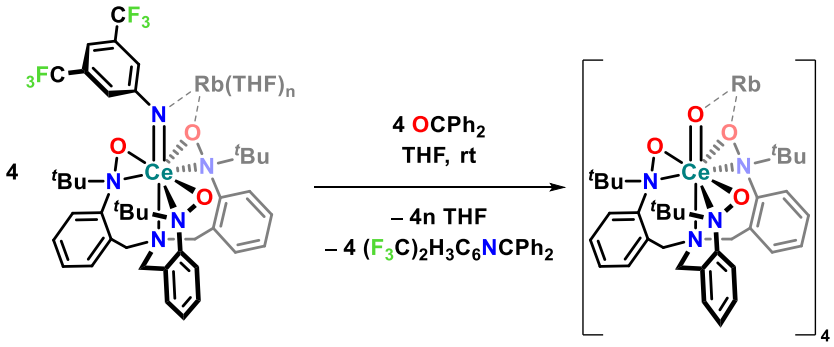

Scheme 3.3. Aza-Wittig reaction between a rubidium capped cerium(IV) imido complex and benzophenone leading to a cluster of cerium(IV) oxo complexes, as described by Schelter *et al.* in 2017.[18]

3.1.2 Lanthanide Imido Complexes

After reports of terminal imido groups at the related rare earth metal scandium(III) and reactivity studies on such compounds in the early 2010s,[23–30] the first lanthanide complex featuring a terminal imido ligand was presented in 2015 by the group of Anwander.[3]

Through the use of the sterically demanding tridentate, monoanionic hydrotris(pyrazolyl)borato ligand $[HB(1\text{-pyrazolyl-3-}^{t}\text{Bu-5-Me})_3]^-$ ($Tp^{tBu,Me-}$) the authors were able to first isolate neutral mono(methyl) arylamido complexes of yttrium(III) and lutetium(III), which upon addition of Lewis base 4-dimethylaminopyridine (DMAP) eliminated methane with concurrent formation of an end-on bound arylimido ligand, respectively (Scheme 3.4). Notably, in the case of the slightly smaller lutetium(III) ion only the 3,5-bis(trifluoromethyl)phenyl substituent furnished the targeted terminal Lu=N moiety, most likely due to the higher Brønsted acidity and better accessibility of the NH group in the amido precursor complex.

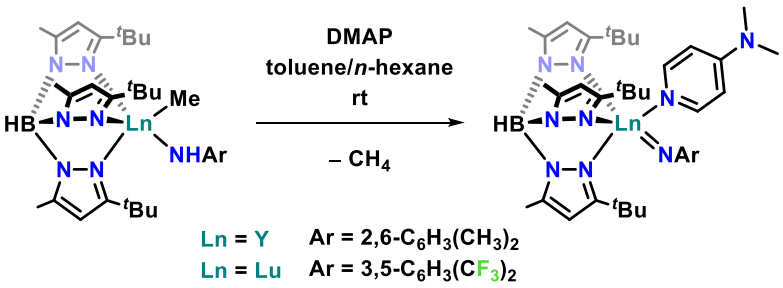

Scheme 3.4. Formation of the first terminal lanthanide(III) imido complex (Ln = Lu) by Lewis base induced methane elimination, as reported by the group of Anwander in 2015.[3] For reasons of simplicity yttrium is also abbreviated as "lanthanide" (Ln = Y).

Expanding the types of supporting ligands for lanthanide imido complexes, Schelter and co-workers reported on the synthesis of a (terminal) cerium(IV) imido complex in 2016 (Scheme 3.5).[15] The synthetic strategy combined the selection of tetravalent cerium(IV) as a better electrostatic match for the dianionic imido ligand with the use of the sterically demanding tripodal, trianionic hydroxylaminato ligand framework $[\{(2\text{-}^t\text{BuNO})C_6H_4CH_2\}_3N]^{3-}$ ($TriNOx^{3-}$)[31,32] which, the authors reasoned, should not only favor a 1:1 cerium(IV) imido complex, but also stabilize it electronically.

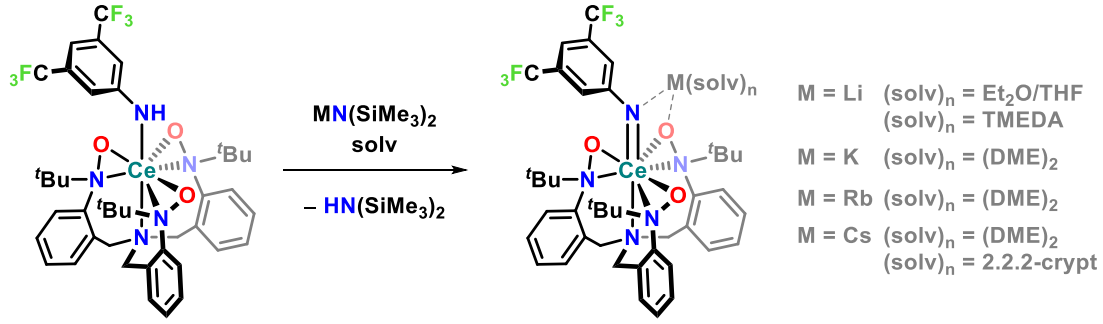

Scheme 3.5. Preparation of the first cerium(IV) imido complex capped by different solvated alkali metal counterions, as published by Schelter and co-workers in 2016.[15,18] In the case of $[Cs(2.2.2\text{-crypt})]^+$ counterion the Ce=N group can be classified as terminal.

The desired cerium(IV) imido group could be obtained in the form of the anionic (ate) complex $[(TriNOx)Ce{=}N(3,5\text{-}C_6H_3(CF_3)_2]^-$ by deprotonation of the cerium(IV) arylamido precursor with various alkali metal hexamethyldisilazide bases.[15,18] In each case the imido group of the ate complex was found to be capped by the solvated alkali metal counter ion, with the exception of $[Cs(2.2.2\text{-crypt})]^+$ which resulted in a rare example of an uncapped terminal Ce=N double bond. The $Ce–N_{imido}$ bond lengths of 2.077(3)–2.129(3) Å, depending on the counterion, were found to be significantly shorter than the $Ce–N_{amido}$ bond length of 2.379(3) Å in the starting complex, clearly indicating a double bond character in the ate complex. The analogous thorium(IV) complex was also synthesized by the group of Schelter to discern general trends concerning the covalency in the 4f- and 5f-element imido groups and the degree of contribution of the metal ion to the bonding interactions.[19] Theoretical calculations showed that the

covalency is higher in the respective cerium(IV) complex and that a higher degree of contribution of the metal ion to the M=N bonding interactions is present in this complex.

Reactivity studies on the cerium(IV) imido complex (Scheme 3.6) revealed a range of possible functionalizations, *i.e.*, silylation at the N_{imido} atom with chlorotrimethylsilane, activation of hexamethyldisiloxane with concomitant ligand exchange or imido group transfer to benzophenone in an aza-Wittig reaction, resulting in the formation of a cerium(IV) oxo complex (*vide supra*).[15,18] In addition, insertion of heteroallenes like carbon dioxide or organic isocyanates into the Ce=N bond was observed.[33] Notably, the formation of a stable carbamate complex after carbon dioxide insertion is in contrast to other d- and f-element imido complexes which generally undergo isocyanate extrusion to form thermodynamically favored oxo complexes or yield dicarbamates by insertion of a second molecule of carbon dioxide.[26,29,34,35]

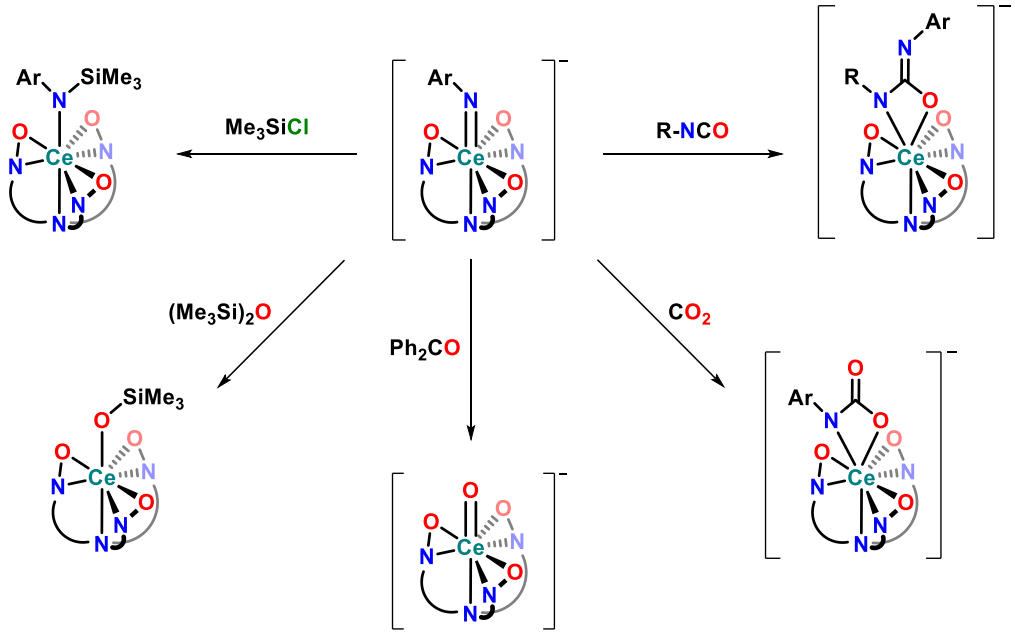

Scheme 3.6. Reactivity of the cerium(IV) imido ate complex by Schelter *et al.* towards chlorotrimethylsilane, hexamethyldisiloxane, benzophenone, carbon dioxide and organic isocyanates.[15,18,33] Simplified representation of the $TriNOx^{3-}$ ligand framework and reaction equations not balanced for reasons of clarity; Ar = 3,5-$C_6H_3(CF_3)_2$; R = Adamantyl or 3,5-$C_6H_3(CF_3)_2$.

3.1.3 Lanthanide Phosphinidene Complexes

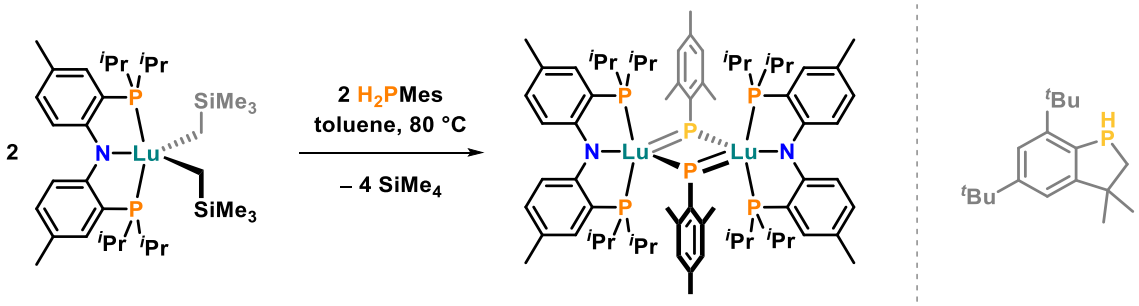

Scheme 3.7. Synthesis of a PNP ligand supported dinuclear lutetium(III) complex with two bridging phosphinidene ligands by Kiplinger and co-workers in 2008 (left) and identified C–H-activation product when employing supermesitylphosphine (Mes*PH_2; Mes* = 2,4,6-tri(*tert*-butyl)phenyl) instead of mesitylphosphine under the same reaction conditions (right).[5]

In comparison to imido and oxo complexes, no reports of terminal phosphinidene complexes of the lanthanide series exist to date. For the related rare earth metal scandium[36] and the actinides (particularly uranium and thorium)[37–41] a small number of terminal phosphinidene complexes, which in the case of uranium are known since 1996,[41] could be uncovered during the last decade. Besides two phosphinidene bridged metal clusters of dysprosium(III) and lutetium(III),[42,43] only four cases of dinuclear lanthanide compounds with bridging phosphinidene ligands are known so far, namely a lutetium(III) phosphinidene complex by Kiplinger and co-workers from 2008[5] and a series of neodymium(III) phosphinidene complexes by Chen *et al.*, reported in 2008 and 2010.[44,45]

In the approach of Kiplinger and co-workers a rigid, symmetrical bis-(2-diisopropylphosphanyl-4-methylphenyl)amido (PNP) supporting ligand was employed together with two alkyl ligands at lutetium(III) functioning as internal bases during the reaction with mesitylphosphine (Scheme 3.7, left).[5] Notably, the deprotonation required temperatures of 80 °C over 12 h for full conversion. The $^{31}P\{^1H\}$ NMR spectrum of the diamagnetic, cherry red lutetium(III) product complex exhibits a strongly low-field shifted resonance at δ = 186.8 ppm as it is typical for f-element phosphinidene units.[39] However, the diagnostic quintet splitting of this resonance together with a triplet splitting of the PNP ligand resonance at δ = 18.1 ppm ($^2J_{PP}$ = 14.6 Hz) indicate a dimeric structure in solution. Indeed, X-ray structure determination revealed a slightly asymmetric Lu_2P_2 core unit with Lu–P bond lengths of ≈2.60 Å and ≈2.65–2.67 Å which is consistent with the formulation as a dimer of a terminal phosphinidene complex [(PNP)Lu=PMes]. Additionally, the authors could show that this compound readily engages in phospha-Wittig reactions. Such kind of reactivity is considered a typical feature of nucleophilic phosphinidene complexes.[8] Attempts to stabilize a terminal phosphinidene complex by addition of Lewis bases such as DMAP failed, and the use of more sterically demanding supermesitylphosphine (Mes*PH_2; Mes* = 2,4,6-tri(*tert*-butyl)phenyl) resulted in the C–H-activation of one of the *ortho*-^{t}Bu groups to give a phosphaindole under the same reaction conditions (Scheme 3.7, right). The authors concluded that a higher steric demand of supporting ligand as well as the substituent

on the phosphinidene unit would be necessary to prevent dimerization or C–H-activation and achieve the isolation of a terminal lanthanide phosphinidene complex.

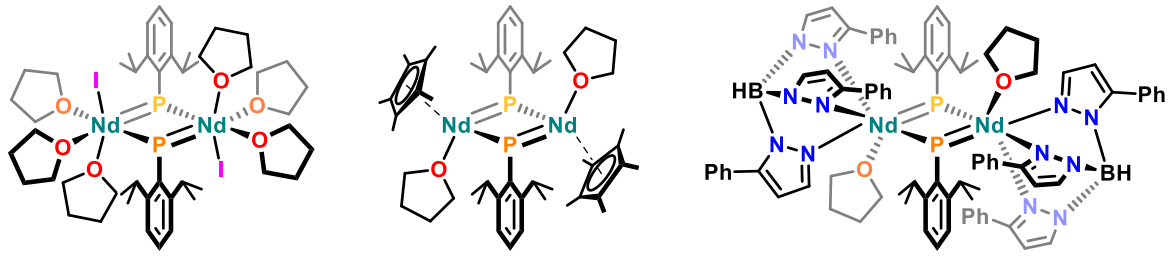

Figure 3.2. A dinuclear neodymium(III) halide complex with bridging phosphinidene ligands by the group of Chen from 2008[44] (left) and derived phosphinidene complexes obtained by subsequent salt metatheses, as published in 2010[45] (middle and right).

An alternative entry into (early) lanthanide phosphinidene chemistry was established by Chen and co-workers. The reaction of $NdI_3(THF)_{3.5}$ with the potassium phosphide K[P(SiMe$_3$)(Dipp)] resulted in the replacement of two iodide ligands and the formation of a dinuclear phosphinidene bridged neodymium(III) complex after salt metathesis and silyl group exchange (Figure 3.2, left).[44] Although the paramagnetic nature of neodymium(III) prevented a NMR spectroscopic study, similar to Kiplinger's report,[5] X-ray structure determination showed the Nd_2P_2 core unit to be asymmetric with Nd–P bond lengths of ≈2.73 Å and ≈2.78 Å. Interestingly, the [PAr] plane was found to be nearly perpendicular to the Nd_2P_2 plane (angle of ≈81.3°), whereas in Kiplinger's case the [PAr] plane is close to planar with the Lu_2P_2 plane (angles of ≈5.8 and ≈7.1°).[5] The presence of another iodide ligand in Chen's complex allowed for the investigation of further salt metathesis reactions with KCp* (Cp*$^-$ = $C_5Me_5^-$) and KTp^{Ph} (Tp^{Ph-} = [HB(1-pyrazolyl-3-Ph)$_3$]$^-$), the result of which was the isolation of two additional phosphinidene bridged dinuclear complexes of neodymium(III) (Figure 3.2, middle and right).[45] The high steric demand of the hydrotris(pyrazolyl)borato supporting ligand caused notable structural changes in the respective product, *i.e.*, a convergence of the different Nd–P bond lengths (≈2.78 Å and ≈2.79 Å) and a significant decrease of the angle between [PAr] and Nd_2P_2 plane (≈50.2°). However, the supporting ligand could not enforce a terminal Nd=P group, but underwent a formal 1,2-borotropic shift of one of the pyrazolyl substituents instead, resulting in a 5-phenylpyrazole unit.

The results of Kiplinger and Chen underline the challenges in finding a well-tailored supporting ligand system suitable for the isolation of the first lanthanide complex with a terminal Ln=P functional group. In the following section a discussion of the potential use of the PN ligand system (see Chapter 1) for this purpose is presented, the relevant findings of which have been summarized in a published manuscript.

3.2 Results and Discussion

Publication: A transient lanthanum phosphinidene complex

Fabian A. Watt,[a] Karl N. McCabe,[b] Roland Schoch,[a] Laurent Maron*[b] and Stephan Hohloch*[c]

* Corresponding authors

[a] Paderborn University, Warburger Straße 100, 33098 Paderborn, Germany

[b] Université de Toulouse, 135 Avenue de Rangueil, 31077 Toulouse, France

[c] University of Innsbruck, Innrain 80-82, 6020 Innsbruck, Austria

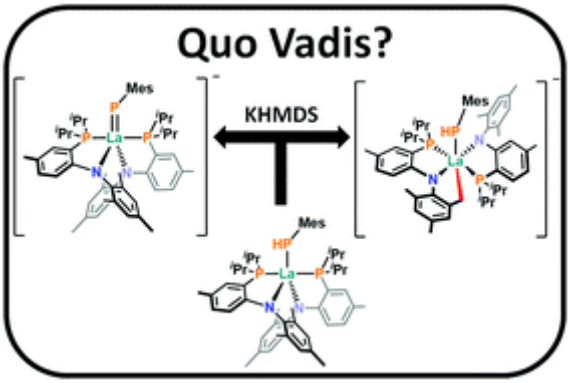

This article was published as follows:

Watt, F. A.; McCabe, K. N.; Schoch, R.; Maron, L.; Hohloch, S. *Chem. Commun.* **2020**, *56*, 15410–15413.

DOI: 10.1039/d0cc06670b

https://doi.org/10.1039/D0CC06670B

Synopsis: Deprotonation of the terminal phosphido complex $(PN)_2La(PHMes)$ results in the C–H-activation of one of the PN ligands *via* a transient phosphinidene complex.

Author Contributions: The project was designed by S. Hohloch, L. Maron and F. A. Watt. Experimental work was carried out by F. A. Watt. NMR and IR data were recorded by F. A. Watt. Theoretical calculations were performed by K. N. McCabe. X-ray structure analyses were performed by R. Schoch and S. Hohloch. The manuscript was written by F. A. Watt and S. Hohloch and proofread by all authors. All authors have given approval to the final version of the manuscript.

Dr. Hans Egold from the NMR facility of Paderborn University and Athul Krishna are kindly acknowledged for helpful discussions. Christiane Gloger and Maria Busse are kindly acknowledged for conducting elemental analyses.

Volume 56
Number 98
21 December 2020
Pages 15351–15474

ChemComm

Chemical Communications
rsc.li/chemcomm

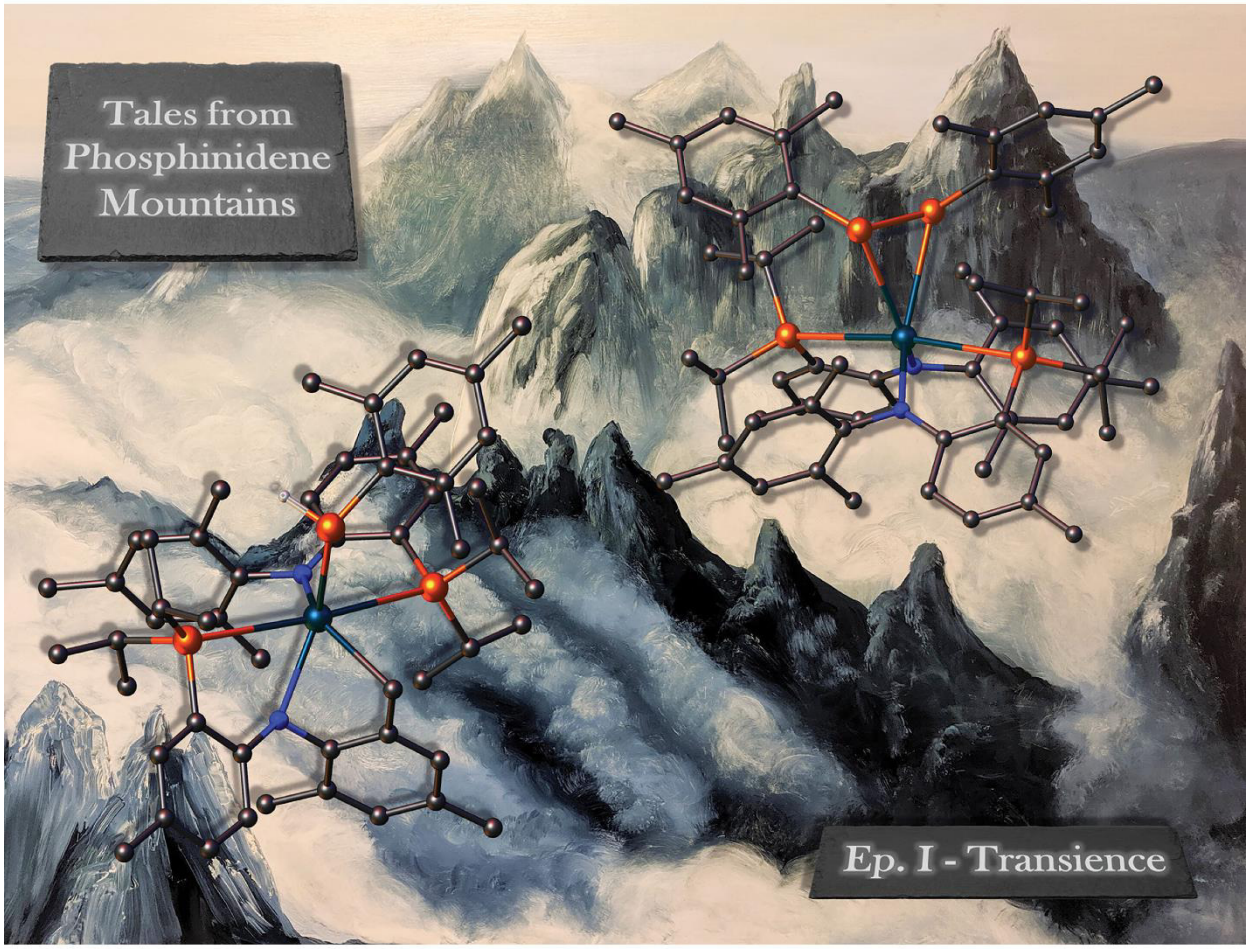

ISSN 1359-7345

ROYAL SOCIETY OF CHEMISTRY

COMMUNICATION
Laurent Maron, Stephan Hohloch *et al.*
A transient lanthanum phosphinidene complex

ChemComm

ROYAL SOCIETY OF CHEMISTRY

COMMUNICATION

View Article Online
View Journal | View Issue

Cite this: *Chem. Commun.*, 2020, 56, 15410

Received 6th October 2020,
Accepted 6th November 2020

DOI: 10.1039/d0cc06670b

rsc.li/chemcomm

A transient lanthanum phosphinidene complex†

Fabian A. Watt, [a] Karl N. McCabe,[b] Roland Schoch, [a] Laurent Maron *[b] and Stephan Hohloch *[c]

Deprotonation of the terminal phosphido complex $(PN)_2La(PHMes)$ (1) results in the C–H-activation of one of the PN ligands, formally retaining the PHMes group. The reaction mechanism and the possible involvement of the transient phosphinidene complex 2 are investigated by theoretical and chemical means including a deuteration experiment employing $(PN)_2La(PDMes)$ (1-*d*). Furthermore, the thermal stability of product [K(2.2.2-cryptand)][$(PN)(PN_{cyclo})$La(PHMes)] (3b) is examined, giving the diphosphido complex [K(2.2.2-cryptand)][$(PN)_2La(P_2Mes_2)$)] (6).

Transition metal complexes with double-bonded ligands are known to be valuable synthons and catalysts.[1] Due to their capability of activating small molecules,[2,3] to perform C–H-activation[4] and undergo group transfer reactions,[5,6] a lot of effort has been expended on developing such systems. However, the chemistry of f-elements with double-bonded ligands is still a considerable challenge for synthetic chemists.[7] Due to the strong charge polarisation and low covalency, resulting from the energy mismatch and low spatial overlap between the frontier orbitals of lanthanide and ligand,[8] these species tend to be very reactive and hard to handle.

Nevertheless, the last decade has seen the isolation of Ce^{IV}=O groups,[9,10] (alkali metal capped) Ce^{IV}=N(Aryl) bonds (Fig. 1, **A**)[9,11] and nucleophilic Ce^{IV} carbene complexes,[12] to name only a few examples which underline the growing interest in f-elements with double-bonded ligands. However, even though a variety of double-bonded ligands has been explored employing cerium(IV),[13] the isolation of terminal phosphinidene complexes of the "classical" trivalent lanthanides remains elusive as yet. Besides a small number of (multi-metallic) Sc^{III} phosphinidene complexes[2,6,14] and two Sc^{III} phosphinophosphinidene complexes,[15] to date, only four examples of phosphinidene bridged dinuclear lanthanide(III) complexes have been reported by Kiplinger (Fig. 1, **C**)[16] and Chen (Fig. 1, **D**).[17]

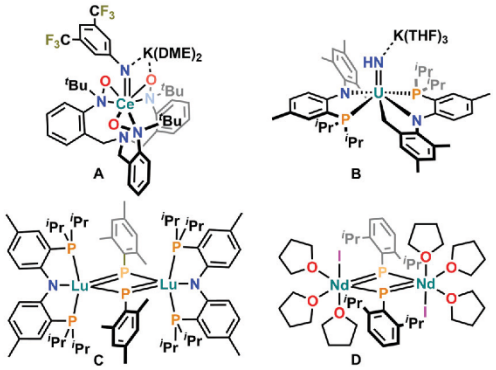

Fig. 1 Selection of f-element complexes with double-bonded ligands.

Recently, our group started to study a series of lanthanide complexes using the bidentate *N*-(2-(diisopropyl-phosphanyl)-4-methylphenyl)-2,4,6-trimethylanilide ligand, short PN, which included the isolation[18] and insertion reactivity[19] of the terminal phosphido complex $(PN)_2La(PHMes)$ (**1**). Notably, the same PN ligand was found to stabilise a rare example of a potassium capped uranium(IV) imido complex (Fig. 1, **B**) by the groups of Schelter and Mindiola,[20] which most likely forms *via* 1,2-CH addition across the U^{IV}≡N triple bond of a transient uranium(IV) nitrido complex. Inspired by these results, we became interested, if the bidentate PN ligand would also allow the isolation of the first terminal lanthanum phosphinidene complex with a La^{III}=P double bond (Scheme 1, target compound **2**).

Deprotonation of the phosphido complex **1** with potassium hexamethyldisilazide (KHMDS, $KN(SiMe_3)_2$) or benzyl potassium (KBn) in 1,2-dimethoxyethane (DME) at room temperature in the presence of 18-crown-6 (18C6) or 2.2.2-cryptand

[a] *Paderborn University, Warburger Straße 100, 33098 Paderborn, Germany*
[b] *Université de Toulouse, 135 Avenue de Rangueil, 31077 Toulouse, France*
[c] *University of Innsbruck, Innrain 80-82, 6020 Innsbruck, Austria.*
E-mail: Stephan.Hohloch@uibk.ac.at

† Electronic supplementary information (ESI) available. CCDC 2020112–2020114 and 2021044. For ESI and crystallographic data in CIF or other electronic format see DOI: 10.1039/d0cc06670b

View Article Online

Communication ChemComm

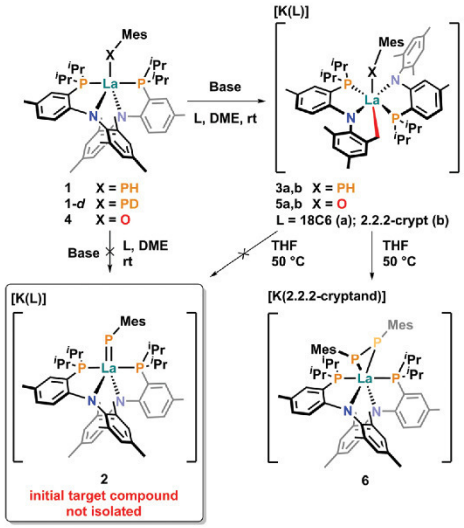

Scheme 1 Attempts to isolate terminal phosphinidene complex **2**, starting from **1**, leading to anionic alkyl complexes **3a,b** (a: L = 18C6, b: L = 2.2.2-cryptand; base: KHMDS or KBn), the thermal decomposition of **3b** leading to **6** and the deprotonation of **4** to give **5a,b**.

led to the formation of the orange-coloured complexes **3a** and **3b** (Scheme 1, top), respectively. The new complexes can be obtained in crude yields of ≈53% (**3a**) and ≈92% (**3b**), either by crystallisation from DME/diethyl ether at −40 °C to give orange-coloured blocks (**3a**) or by trituration of a toluene extract with *n*-hexane to give an orange-coloured powder (**3b**). Note that we only give crude yields, since one inseparable side product is being formed in the reactions (Fig. S3, ESI†). Nevertheless, both complexes can be obtained in purities of at least 85% under these conditions. Notably, complex **3a** can be obtained in purities of ≈94% by a switch to cyclohexene as solvent (*vide infra*). Complex **3b** was found to be much more difficult to (re)crystallise in useful quantities and decomposes easily, wherefore we have not been able to fully characterise this complex.

The ^{31}P NMR spectra (THF-d_8) of both **3a** and **3b** show no signal above 100 ppm, which would be indicative of a phosphinidene complex.[16] Instead, a doublet of doublets which is shifted to δ = −87.4 ppm ($^1J_{PH}$ = 181.6 Hz, $^2J_{PP}$ = 22.6 Hz) for **3a** and δ = −86.9 ppm ($^1J_{PH}$ = 180.8 Hz, $^2J_{PP}$ =21.6 Hz) for **3b** (compared to δ = −36.4 ppm (d, $^1J_{PH}$ = 198.9 Hz) for **1**) is observed,[18] clearly showing the presence of a PH group in the complexes **3a,b**. The resonances of the PN ligands between δ = 2.5 and 4.0 ppm are split into a complicated multiplet structure. A more detailed analysis in the $^{31}P\{^1H\}$ NMR spectrum of **3a** reveals that the phosphorous atoms of two chemically inequivalent PN ligands couple to each other across the lanthanum(III) ion ($^2J_{PP}$ = 36.8 Hz). One of the PN ligands shows an additional coupling to the mesitylphosphido ligand ($^2J_{PP}$ = 22.6 Hz). Furthermore, the ^{1}H NMR spectra of **3a,b** exhibit two distinct sets of PN ligand resonances, indicating that the deprotonation must have happened at one of the PN ligands. The presence of two new doublets of doublets at δ = 1.07 ppm and δ = 2.78 ppm corresponding to one proton each and a coupling constant of $^2J_{HH}$ = 4.8 Hz is consistent with an anionic mesityl-CH_2 group showing geminal coupling.[21] The notion of diastereotopic methylene protons is also confirmed by the ^{1}H–^{13}C HSQC NMR spectrum of **3a**, which contains two cross peaks at δ = 1.07/65.4 and 2.78/65.4 ppm. Given the spectroscopic signatures of the minor impurity (*e.g.*, see Fig. S15 in the ESI†), we assume it to be a hitherto unidentifiable C–H-activated product.

Orange-coloured, X-ray quality crystals of **3a,b** could be obtained either during work-up as described above (**3a**) or by gas diffusion of *n*-hexane into a solution of **3b** in THF at room temperature (Fig. 2). The La1–P70 distances are found to be 3.049(1) Å and 3.025(1) Å for **3a** and **3b** and are in the same range as in complex **1**,[18] thereby unambiguously confirming the La–P single bond character. The presence of the PH proton (found in the Fourier Map) also proves that the PHMes group is retained. However, as expected one of the PN ligands is deprotonated, displaying a lanthanum – methylene distance La1–C25 of 2.634(3) Å (**3a**) and 2.617(2) Å (**3b**).

Schelter and Mindiola and co-workers recently reported a similar C–H-activated uranium complex (Fig. 1, **B**), using the same PN ligand in the attempt to isolate a terminal uranium nitrido complex.[20] Theoretical investigations revealed that **B** most likely formed *via* the 1,2-addition of the mesityl C–H bond across a transient uranium(IV) nitrido group. We assumed that a similar process, *via* a transient phosphinidene, could also be viable in our case. To evaluate the possibility of transient terminal phosphinidene **2** during the deprotonation of **1**, we calculated the enthalpy profiles of two pathways which would

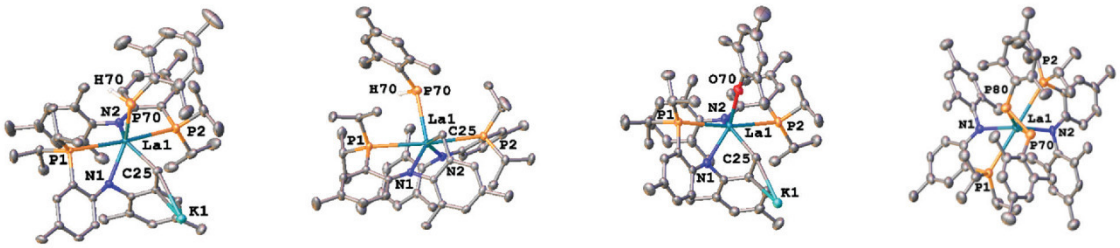

Fig. 2 Thermal ellipsoid plots of the complexes **3a**, **3b**, **5a** and **6** (from left to right). Hydrogen atoms, sequestration agents (including K1 in the cases of **3b** and **6**) and solvent molecules have been omitted for clarity. Thermal ellipsoids are shown at a probability level of 50%.

View Article Online
ChemComm Communication

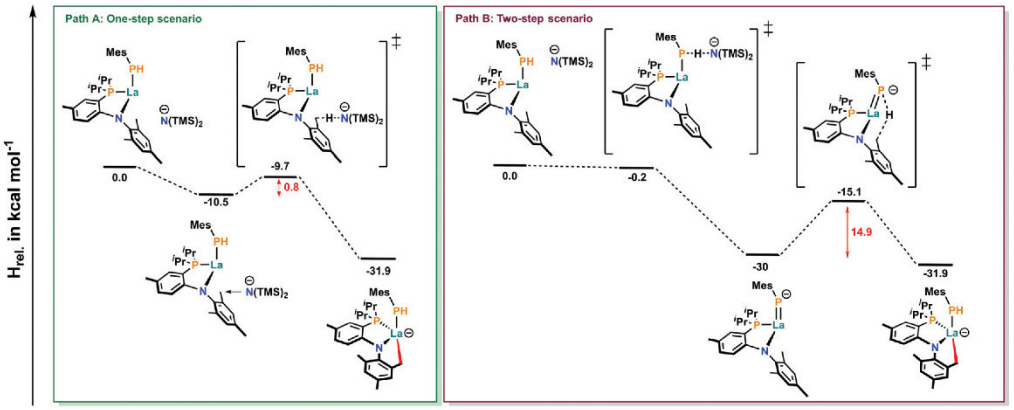

Fig. 3 Enthalpy profiles of the potential C–H-activation pathways in the reaction of **1** with $N(TMS)_2$: direct deprotonation of the mesityl-CH_3 group of a PN ligand (path A, left) or 1,2-CH addition *via* a transient phosphinidene (path B, right). Product $HN(TMS)_2$ and one PN supporting ligand are omitted for clarity. Theoretical calculations were performed with B3PW91 functional and RECP for La (gas phase).

both lead to **3a,b**: (I) a one-step reaction with direct deprotonation of the mesityl-CH_3 group of the PN ligand by KHMDS (Fig. 3, path A) or (II) a two-step reaction proceeding *via* transient phosphinidene complex **2** followed by the 1,2-addition of the C–H bond (Fig. 3, path B). The calculations show that in both cases the deprotonation step itself is exothermic by −31.9 kcal mol^{-1} (path A) and −30 kcal mol^{-1} (path B) with essentially no activation barrier. However, in the case of path B the following 1,2-CH addition across the La=P double bond of **2** has to overcome a barrier of 14.9 kcal mol^{-1} to form complex **3**.

To differentiate between the two competing reaction pathways experimentally, we subjected the deuterated complex **1-*d*** to the same conditions used for the deprotonation of complex **1** leading to **3a** (Fig. S64, ESI†). While we started from 86% deuterium enrichment, we obtained 78% hydrogen on the phosphorous atom after the reaction (Scheme 2). In addition, $DN(SiMe_3)_2$ was detected in the ^{2}H NMR spectrum of the reaction (Fig. S65, ESI†). Notably, when the reaction was carried out in cyclohexene, full conversion of the PD group to the PH group was observed after 10 min and no subsequent isotope scrambling could be detected even after 3 d (Fig. S67 and S24, ESI†). These observations provide clear evidence for the formation of a transient lanthanum phosphinidene complex **2** as the dominant reaction pathway to **3a**. Attempts to trap the reactive intermediate in cyclohexene led to ≈94% pure **3a** (*vide supra*), pointing to a very fast intramolecular reaction of **2** to form **3a**. While these experiments do not fully exclude a transient dimerisation of **2** or its association with $[K(18C6)]^+$ prior to the formation of **3a**, the occurrence of a transient terminal phosphinidene complex prior to the formation of **3b** can be considered to be very likely, based on literature reports employing 2.2.2.-cryptand[9,10] and the similarity of our deprotonations with 18C6 and 2.2.2.-cryptand.

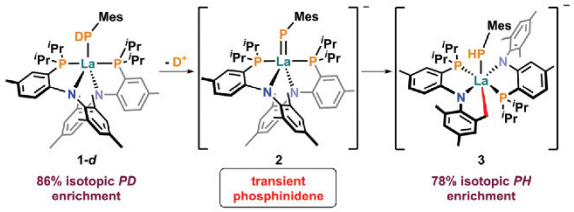

Scheme 2 NMR scale reaction between deuterated complex **1-*d*** and KHMDS/18C6 in DME showing the isotopic enrichment (D/H) prior and after the addition of base (counter ions and reaction by-products are omitted).

Although the deuteration experiment demonstrated the formation of **3a,b** to proceed mainly *via* a phosphinidene intermediate, we were interested if the direct deprotonation pathway is also facile. Deprotonation of the mesitolate complex **4** (Scheme 1, top) resulted in the clean formation of yellow complexes **5a** (74%) and **5b** (89%). X-ray quality crystals of complex **5a** unambiguously prove the depicted structure of **5a** as an anionic alkyl complex (Fig. 2 and Fig. S73, ESI†). The facile direct deprotonation to give **5a,b** underlines that the intermediate phosphinidene formation in the cases of **3a,b** must be highly competitive, which could also be the cause for the formation of the undesired side products.

Next, we examined the thermal stability of the complexes **3a,b**. Acknowledging the approach of Kiplinger and co-workers to obtain phosphinidene complex **C**,[16] we envisioned that due to the small energy gap of 1.9 kcal mol^{-1} between **2** and the obtained products **3a,b**, heating the alkyl complexes **3a** or **3b** might facilitate intramolecular deprotonation of the PH group to give the desired phosphinidene complex **2** (Scheme 1, bottom). While for **3a** heating led to intractable mixtures, for **3b** we observed a moderately clean NMR scale reaction in THF-d_8 at 50 °C (Fig. S68, ESI†), from which we obtained small quantities of X-ray quality crystals of the diphosphido complex **6** with $[P_2Mes_2]^{2-}$ ligand. Strikingly, the $^{31}P\{^1H\}$ NMR spectrum of the raw product contains only one singlet resonance for the PN ligands at δ = 9.3 ppm, suggestive of a symmetrical structure of the main product complex. In addition, P–P bond formation is evident by a new broad resonance at δ = 30.5 ppm,

corresponding to the diphosphido ligand. The P70–P80 bond length in **6** is found to be 2.168(5) Å (Fig. 2), which is in the range of reported diphosphido ligands.[22,23] The protonation of the mesityl-CH_2 group indicates that it is possible to reverse the cyclometallation and generate complex **2** *in situ*. This is in line with literature reports, in which, *e.g.* Stephan[24] and Walter[22] and co-workers have shown that such P–P coupled species most likely form *via* (transient) phosphinidene complexes.

In summary, our results provide strong evidence for a transient (terminal) phosphinidene complex of a "classical" trivalent lanthanide ion. Future work will be directed to isolate such a species in a crystalline form, as well as to study the reactivity of such transient and isolated species in more detail.

We are grateful to the Daimler and Benz Foundation, the Fonds der Chemischen Industrie, the Paderborn University, and the University of Innsbruck for financial support. LM is a senior member of the Institut Universitaire de France. CalMip is acknowledged for a generous grant of computing time. We are grateful to the vice rectorate for research of the University of Innsbruck for generous funding of this work.

Conflicts of interest

There are no conflicts to declare.

Notes and references

1 (*a*) M. Stradiotto and R. J. Lundgren, *Ligand Design in Metal Chemistry*, John Wiley & Sons, Ltd, Chichester, UK, 2016; (*b*) C. C. Cummins, *Angew. Chem., Int. Ed.*, 2006, **45**, 862–870.
2 Y. Lv, C. E. Kefalidis, J. Zhou, L. Maron, X. Leng and Y. Chen, *J. Am. Chem. Soc.*, 2013, **135**, 14784–14796.
3 (*a*) K. Arashiba, E. Kinoshita, S. Kuriyama, A. Eizawa, K. Nakajima, H. Tanaka, K. Yoshizawa and Y. Nishibayashi, *J. Am. Chem. Soc.*, 2015, **137**, 5666–5669; (*b*) Y.-C. Tsai, F. H. Stephens, K. Meyer, A. Mendiratta, M. D. Gheorghiu and C. C. Cummins, *Organometallics*, 2003, **22**, 2902–2913.
4 (*a*) J. Scott, F. Basuli, A. R. Fout, J. C. Huffman and D. J. Mindiola, *Angew. Chem., Int. Ed.*, 2008, **47**, 8502–8505; (*b*) J. Chu, X. Han, C. E. Kefalidis, J. Zhou, L. Maron, X. Leng and Y. Chen, *J. Am. Chem. Soc.*, 2014, **136**, 10894–10897.
5 (*a*) B. F. Wicker, H. Fan, A. K. Hickey, M. G. Crestani, J. Scott, M. Pink and D. J. Mindiola, *J. Am. Chem. Soc.*, 2012, **134**, 20081–20096; (*b*) B. M. Kriegel, R. G. Bergman and J. Arnold, *J. Am. Chem. Soc.*, 2016, **138**, 52–55; (*c*) T. D. Lohrey, R. G. Bergman and J. Arnold, *Inorg. Chem.*, 2016, **55**, 11993–12000.
6 B. F. Wicker, J. Scott, J. G. Andino, X. Gao, H. Park, M. Pink and D. J. Mindiola, *J. Am. Chem. Soc.*, 2010, **132**, 3691–3693.
7 (*a*) D. Schädle and R. Anwander, *Chem. Soc. Rev.*, 2019, **48**, 5752–5805; (*b*) D. Schädle, M. Meermann-Zimmermann, C. Schädle, C. Maichle-Mössmer and R. Anwander, *Eur. J. Inorg. Chem.*, 2015, 1334–1339; (*c*) G. R. Giesbrecht and J. C. Gordon, *Dalton Trans.*, 2004, 2387–2393; (*d*) C. Zhang, G. Hou, G. Zi, W. Ding and M. D. Walter, *J. Am. Chem. Soc.*, 2018, **140**, 14511–14525; (*e*) E. Lu, J. Chu, Y. Chen, M. V. Borzov and G. Li, *Chem. Commun.*, 2011, **47**, 743–745; (*f*) E. Lu, Y. Li and Y. Chen, *Chem. Commun.*, 2010, **46**, 4469–4471; (*g*) T. Chu, W. E. Piers, J. L. Dutton and M. Parvez, *Organometallics*, 2013, **32**, 1159–1165; (*h*) M. A. Boreen, G. Rao, D. G. Villarreal, F. A. Watt, R. D. Britt, S. Hohloch and J. Arnold, *Chem. Commun.*, 2020, **56**, 4535–4538; (*i*) M. E. Garner, S. Hohloch, L. Maron and J. Arnold, *Organometallics*, 2016, **35**, 2915–2922.
8 O. T. Summerscales and J. C. Gordon, *RSC Adv.*, 2013, **3**, 6682.
9 L. A. Solola, A. V. Zabula, W. L. Dorfner, B. C. Manor, P. J. Carroll and E. J. Schelter, *J. Am. Chem. Soc.*, 2017, **139**, 2435–2442.
10 (*a*) Y.-M. So, G.-C. Wang, Y. Li, H. H.-Y. Sung, I. D. Williams, Z. Lin and W.-H. Leung, *Angew. Chem., Int. Ed.*, 2014, **53**, 1626–1629; (*b*) P. L. Damon, G. Wu, N. Kaltsoyannis and T. W. Hayton, *J. Am. Chem. Soc.*, 2016, **138**, 12743–12746; (*c*) M. P. Coles, P. B. Hitchcock, A. V. Khvostov, M. F. Lappert, Z. Li and A. V. Protchenko, *Dalton Trans.*, 2010, **39**, 6780–6788; (*d*) M. K. Assefa, G. Wu and T. W. Hayton, *Chem. Sci.*, 2017, **8**, 7873–7878.
11 (*a*) T. Cheisson, K. D. Kersey, N. Mahieu, A. McSkimming, M. R. Gau, P. J. Carroll and E. J. Schelter, *J. Am. Chem. Soc.*, 2019, **141**, 9185–9190; (*b*) L. A. Solola, A. V. Zabula, W. L. Dorfner, B. C. Manor, P. J. Carroll and E. J. Schelter, *J. Am. Chem. Soc.*, 2016, **138**, 6928–6931; (*c*) T. Cheisson, L. A. Solola, M. R. Gau, P. J. Carroll and E. J. Schelter, *Organometallics*, 2018, **37**, 4332–4335; (*d*) E. N. Lapsheva, T. Cheisson, C. Álvarez Lamsfus, P. J. Carroll, M. R. Gau, L. Maron and E. J. Schelter, *Chem. Commun.*, 2020, **56**, 4781–4784.
12 (*a*) M. Gregson, E. Lu, J. McMaster, W. Lewis, A. J. Blake and S. T. Liddle, *Angew. Chem., Int. Ed.*, 2013, **52**, 13016–13019; (*b*) M. Gregson, E. Lu, F. Tuna, E. J. L. McInnes, C. Hennig, A. C. Scheinost, J. McMaster, W. Lewis, A. J. Blake, A. Kerridge and S. T. Liddle, *Chem. Sci.*, 2016, **7**, 3286–3297.
13 Y.-M. So and W.-H. Leung, *Coord. Chem. Rev.*, 2017, **340**, 172–197.
14 K. Wang, G. Luo, J. Hong, X. Zhou, L. Weng, Y. Luo and L. Zhang, *Angew. Chem., Int. Ed.*, 2014, **53**, 1053–1056.
15 B. Feng, L. Xiang, K. N. McCabe, L. Maron, X. Leng and Y. Chen, *Nat. Commun.*, 2020, **11**, 2916.
16 J. D. Masuda, K. C. Jantunen, O. V. Ozerov, K. J. T. Noonan, D. P. Gates, B. L. Scott and J. L. Kiplinger, *J. Am. Chem. Soc.*, 2008, **130**, 2408–2409.
17 (*a*) P. Cui, Y. Chen, X. Xu and J. Sun, *Chem. Commun.*, 2008, 5547–5549; (*b*) P. Cui, Y. Chen and M. V. Borzov, *Dalton Trans.*, 2010, **39**, 6886–6890.
18 F. A. Watt, A. Krishna, G. Golovanov, H. Ott, R. Schoch, C. Wölper, A. G. Neuba and S. Hohloch, *Inorg. Chem.*, 2020, **59**, 2719–2732.
19 F. A. Watt, N. Dickmann, R. Schoch and S. Hohloch, *Inorg. Chem.*, 2020, **59**, 13621–13631.
20 K. C. Mullane, H. Ryu, T. Cheisson, L. N. Grant, J. Y. Park, B. C. Manor, P. J. Carroll, M.-H. Baik, D. J. Mindiola and E. J. Schelter, *J. Am. Chem. Soc.*, 2018, **140**, 11335–11340.
21 M. E. Garner, B. F. Parker, S. Hohloch, R. G. Bergman and J. Arnold, *J. Am. Chem. Soc.*, 2017, **139**, 12935–12938.
22 C. Zhang, Y. Wang, G. Hou, W. Ding, G. Zi and M. D. Walter, *Dalton Trans.*, 2019, **48**, 6921–6930.
23 (*a*) E. Hey-Hawkins and K. Fromm, *Polyhedron*, 1995, **14**, 2825–2834; (*b*) J. Ho, T. L. Breen, A. Ozarowski and D. W. Stephan, *Inorg. Chem.*, 1994, **33**, 865–870; (*c*) S. Kurz and E. Hey-Hawkins, *J. Organomet. Chem.*, 1993, **462**, 203–207; (*d*) S. Kurz, H. Oesen, J. Sieler and E. Hey-Hawkins, *Phosphorus, Sulfur Silicon Relat. Elem.*, 1996, **117**, 189–196.
24 Z. Hou, T. L. Breen and D. W. Stephan, *Organometallics*, 1993, **12**, 3158–3167.

3.3 References

(1) Giesbrecht, G. R.; Gordon, J. C. Lanthanide alkylidene and imido complexes. *Dalton Trans.* **2004**, 2387–2393.
(2) Shima, T.; Hou, Z. Hydrogenation of Carbon Monoxide by Tetranuclear Rare Earth Metal Polyhydrido Complexes. Selective Formation of Ethylene and Isolation of Well-Defined Polyoxo Rare Earth Metal Clusters. *J. Am. Chem. Soc.* **2006**, *128*, 8124–8125.
(3) Schädle, D.; Meermann-Zimmermann, M.; Schädle, C.; Maichle-Mössmer, C.; Anwander, R. Rare-Earth Metal Complexes with Terminal Imido Ligands. *Eur. J. Inorg. Chem.* **2015**, 1334–1339.
(4) Cui, D.; Nishiura, M.; Hou, Z. Lanthanide-Imido Complexes and Their Reactions with Benzonitrile. *Angew. Chem. Int. Ed.* **2005**, *44*, 959–962.
(5) Masuda, J. D.; Jantunen, K. C.; Ozerov, O. V.; Noonan, K. J. T.; Gates, D. P.; Scott, B. L.; Kiplinger, J. L. A Lanthanide Phosphinidene Complex: Synthesis, Structure, and Phospha-Wittig Reactivity. *J. Am. Chem. Soc.* **2008**, *130*, 2408–2409.
(6) Summerscales, O. T.; Gordon, J. C. Complexes containing multiple bonding interactions between lanthanoid elements and main-group fragments. *RSC Adv.* **2013**, *3*, 6682.
(7) Gade, L. H.; Mountford, P. New transition metal imido chemistry with diamido-donor ligands. *Coord. Chem. Rev.* **2001**, *216-217*, 65–97.
(8) Aktaş, H.; Slootweg, J. C.; Lammertsma, K. Nucleophilic Phosphinidene Complexes: Access and Applicability. *Angew. Chem. Int. Ed.* **2010**, *49*, 2102–2113.
(9) Odom, A. L. Conversions between metal–ligand multiple bond (MLMB) types: carbonyl olefination and other applications. *Dalton Trans.* **2011**, *40*, 2689–2695.
(10) Scott, J.; Mindiola, D. J. A tribute to Frederick Nye Tebbe. Lewis acid stabilized alkylidyne, alkylidene, and imides of 3d early transition metals. *Dalton Trans.* **2009**, 8463–8472.
(11) Waterman, R.; Hayes, P. G.; Tilley, T. D. Synthetic Development and Chemical Reactivity of Transition-Metal Silylene Complexes. *Acc. Chem. Res.* **2007**, *40*, 712–719.
(12) Chan, H.-S.; Li, H.-W.; Xie, Z. Synthesis and structural characterization of imido–lanthanide complexes with a metal–nitrogen multiple bond. *Chem. Commun.* **2002**, 652–653.
(13) Gordon, J. C.; Giesbrecht, G. R.; Clark, D. L.; Hay, P. J.; Keogh, D. W.; Poli, R.; Scott, B. L.; Watkin, J. G. The First Example of a μ_2-Imido Functionality Bound to a Lanthanide Metal Center: X-ray Crystal Structure and DFT Study of $[(\mu\text{-ArN})Sm(\mu\text{-NHAr})(\mu\text{-Me})AlMe_2]_2$ (Ar = 2,6-^{i}Pr$_2$C$_6$H$_3$). *Organometallics* **2002**, *21*, 4726–4734.
(14) Schädle, D.; Anwander, R. Rare-earth metal and actinide organoimide chemistry. *Chem. Soc. Rev.* **2019**, *48*, 5752–5805.
(15) Solola, L. A.; Zabula, A. V.; Dorfner, W. L.; Manor, B. C.; Carroll, P. J.; Schelter, E. J. An Alkali Metal-Capped Cerium(IV) Imido Complex. *J. Am. Chem. Soc.* **2016**, *138*, 6928–6931.
(16) Damon, P. L.; Wu, G.; Kaltsoyannis, N.; Hayton, T. W. Formation of a Ce(IV) Oxo Complex via Inner Sphere Nitrate Reduction. *J. Am. Chem. Soc.* **2016**, *138*, 12743–12746.
(17) So, Y.-M.; Wang, G.-C.; Li, Y.; Sung, H. H.-Y.; Williams, I. D.; Lin, Z.; Leung, W.-H. A Tetravalent Cerium Complex Containing a Ce=O Bond. *Angew. Chem. Int. Ed.* **2014**, *53*, 1626–1629.
(18) Solola, L. A.; Zabula, A. V.; Dorfner, W. L.; Manor, B. C.; Carroll, P. J.; Schelter, E. J. Cerium(IV) Imido Complexes: Structural, Computational, and Reactivity Studies. *J. Am. Chem. Soc.* **2017**, *139*, 2435–2442.
(19) Cheisson, T.; Kersey, K. D.; Mahieu, N.; McSkimming, A.; Gau, M. R.; Carroll, P. J.; Schelter, E. J. Multiple Bonding in Lanthanides and Actinides: Direct Comparison of Covalency in Thorium(IV)- and Cerium(IV)-Imido Complexes. *J. Am. Chem. Soc.* **2019**, *141*, 9185–9190.
(20) So, Y.-M.; Li, Y.; Au-Yeung, K.-C.; Wang, G.-C.; Wong, K.-L.; Sung, H. H. Y.; Arnold, P. L.; Williams, I. D.; Lin, Z.; Leung, W.-H. Probing the Reactivity of the Ce=O Multiple Bond in a Cerium(IV) Oxo Complex. *Inorg. Chem.* **2016**, *55*, 10003–10012.
(21) Evans, W. J. The Importance of Questioning Scientific Assumptions: Some Lessons from f Element Chemistry. *Inorg. Chem.* **2007**, *46*, 3435–3449.
(22) Clark, D. L.; Gordon, J. C.; Hay, P. J.; Poli, R. Existence and Stability of Lanthanide−Main Group Element Multiple Bonds. New Paradigms in the Bonding of the 4f Elements. A DFT Study of Cp_2CeZ ($Z = F^+$, O, NH, CH^-, CH_2) and the Ligand Adduct $Cp_2Ce(CH_2)(NH_3)$. *Organometallics* **2005**, *24*, 5747–5758.

(23) Scott, J.; Basuli, F.; Fout, A. R.; Huffman, J. C.; Mindiola, D. J. Evidence for the Existence of a Terminal Imidoscandium Compound: Intermolecular C–H Activation and Complexation Reactions with the Transient Sc=NAr species. *Angew. Chem. Int. Ed.* **2008**, *47*, 8502–8505.
(24) Lu, E.; Li, Y.; Chen, Y. A scandium terminal imido complex: synthesis, structure and DFT studies. *Chem. Commun.* **2010**, *46*, 4469–4471.
(25) Lu, E.; Chu, J.; Chen, Y.; Borzov, M. V.; Li, G. Scandium terminal imido complex induced C–H bond selenation and formation of an Sc–Se bond. *Chem. Commun.* **2011**, *47*, 743–745.
(26) Chu, J.; Lu, E.; Liu, Z.; Chen, Y.; Leng, X.; Song, H. Reactivity of a Scandium Terminal Imido Complex Towards Unsaturated Substrates. *Angew. Chem. Int. Ed.* **2011**, *50*, 7677–7680.
(27) Chu, T.; Piers, W. E.; Dutton, J. L.; Parvez, M. Synthesis and Reactivity of a Terminal Scandium Imido Complex. *Organometallics* **2013**, *32*, 1159–1165.
(28) Rong, W.; Cheng, J.; Mou, Z.; Xie, H.; Cui, D. Facile Preparation of a Scandium Terminal Imido Complex Supported by a Phosphazene Ligand. *Organometallics* **2013**, *32*, 5523–5529.
(29) Lu, E.; Chu, J.; Chen, Y. Scandium Terminal Imido Chemistry. *Acc. Chem. Res.* **2018**, *51*, 557–566.
(30) Chu, J.; Han, X.; Kefalidis, C. E.; Zhou, J.; Maron, L.; Leng, X.; Chen, Y. Lewis Acid Triggered Reactivity of a Lewis Base Stabilized Scandium-Terminal Imido Complex: C–H Bond Activation, Cycloaddition, and Dehydrofluorination. *J. Am. Chem. Soc.* **2014**, *136*, 10894–10897.
(31) Bogart, J. A.; Lippincott, C. A.; Carroll, P. J.; Schelter, E. J. An Operationally Simple Method for Separating the Rare-Earth Elements Neodymium and Dysprosium. *Angew. Chem. Int. Ed.* **2015**, *54*, 8222–8225.
(32) Bogart, J. A.; Lippincott, C. A.; Carroll, P. J.; Booth, C. H.; Schelter, E. J. Controlled Redox Chemistry at Cerium within a Tripodal Nitroxide Ligand Framework. *Chem. Eur. J.* **2015**, *21*, 17850–17859.
(33) Lapsheva, E. N.; Cheisson, T.; Álvarez Lamsfus, C.; Carroll, P. J.; Gau, M. R.; Maron, L.; Schelter, E. J. Reactivity of Ce(IV) imido compounds with heteroallenes. *Chem. Commun.* **2020**, *56*, 4781–4784.
(34) Bart, S. C.; Anthon, C.; Heinemann, F. W.; Bill, E.; Edelstein, N. M.; Meyer, K. Carbon Dioxide Activation with Sterically Pressured Mid- and High-Valent Uranium Complexes. *J. Am. Chem. Soc.* **2008**, *130*, 12536–12546.
(35) Guiducci, A. E.; Cowley, A. R.; Skinner, M. E. G.; Mountford, P. Novel double substrate insertion versus isocyanate extrusion in reactions of imidotitanium complexes with CO_2: critical dependence on imido N-substituents. *J. Chem. Soc., Dalton Trans.* **2001**, 1392–1394.
(36) Feng, B.; Xiang, L.; McCabe, K. N.; Maron, L.; Leng, X.; Chen, Y. Synthesis and versatile reactivity of scandium phosphinophosphinidene complexes. *Nat Commun* **2020**, *11*, 2916.
(37) Vilanova, S. P.; Alayoglu, P.; Heidarian, M.; Huang, P.; Walensky, J. R. Metal-Ligand Multiple Bonding in Thorium Phosphorus and Thorium Arsenic Complexes. *Chem. Eur. J.* **2017**, *23*, 16748–16752.
(38) Wildman, E. P.; Balázs, G.; Wooles, A. J.; Scheer, M.; Liddle, S. T. Thorium–phosphorus triamidoamine complexes containing Th–P single- and multiple-bond interactions. *Nat Commun* **2016**, *7*, 12884.
(39) Zhang, C.; Hou, G.; Zi, G.; Ding, W.; Walter, M. D. A Base-Free Terminal Actinide Phosphinidene Metallocene: Synthesis, Structure, Reactivity, and Computational Studies. *J. Am. Chem. Soc.* **2018**, *140*, 14511–14525.
(40) Gardner, B. M.; Balázs, G.; Scheer, M.; Tuna, F.; McInnes, E. J. L.; McMaster, J.; Lewis, W.; Blake, A. J.; Liddle, S. T. Triamidoamine–Uranium(IV)-Stabilized Terminal Parent Phosphide and Phosphinidene Complexes. *Angew. Chem. Int. Ed.* **2014**, *53*, 4484–4488.
(41) Arney, D. S. J.; Schnabel, R. C.; Scott, B. C.; Burns, C. J. Preparation of Actinide Phosphinidene Complexes: Steric Control of Reactivity. *J. Am. Chem. Soc.* **1996**, *118*, 6780–6781.
(42) Wang, K.; Luo, G.; Hong, J.; Zhou, X.; Weng, L.; Luo, Y.; Zhang, L. Homometallic Rare-Earth Metal Phosphinidene Clusters: Synthesis and Reactivity. *Angew. Chem. Int. Ed.* **2014**, *53*, 1053–1056.
(43) Pugh, T.; Tuna, F.; Ungur, L.; Collison, D.; McInnes, E. J. L.; Chibotaru, L. F.; Layfield, R. A. Influencing the properties of dysprosium single-molecule magnets with phosphorus donor ligands. *Nat Commun* **2015**, *6*, 7492.
(44) Cui, P.; Chen, Y.; Xu, X.; Sun, J. An unprecedented lanthanide phosphinidene halide: synthesis, structure and reactivity. *Chem. Commun.* **2008**, 5547–5549.

(45) Cui, P.; Chen, Y.; Borzov, M. V. Neodymium(III) phosphinidene complexes supported by pentamethylcyclopentadienyl and hydrotris(pyrazolyl)borate ligands. *Dalton Trans.* **2010**, *39*, 6886–6890.

Chapter 4:

η^3-Coordination and Functionalization of the 2-Phosphaethynthiolate Anion at Lanthanum(III)

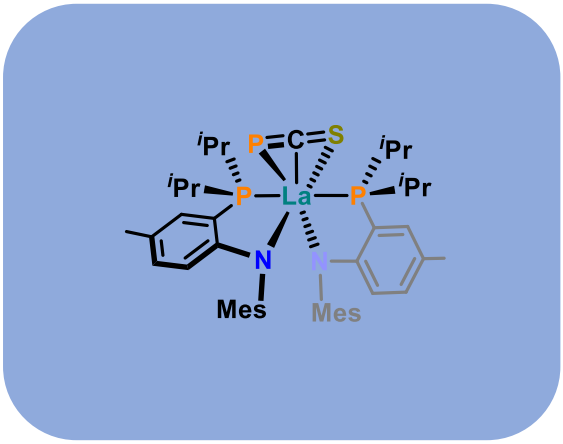

4.1 Introduction: Historical Background of Cyanate-Type Anions

The cyanate anion ([OCN]$^-$) and its heavier homologues have played a significant role in the development of modern chemistry (Figure 4.1). Liebig and Gay-Lussac's result from 1824[1,2] that silver fulminate (AgCNO) has the same elemental composition as silver cyanate (AgOCN) is still seen as a great feat of the first precise analytical methods developed in the late 18th and early 19th centuries[3,4] and marks the discovery of (constitutional) isomerism.[5,6] Wöhler's subsequent conversion of ammonium cyanate into urea in 1828[7] extended the isomerism concept and overthrew the dogma that chemicals produced by plants and animals could not be obtained by synthetic means.[8] His insight might even be seen as the original inspiration for studies on possible prebiotic chemistry scenarios on earth, which were initiated in the early 1950s[9,10] by the famous electric discharge experiment of Miller and Urey and which are pursued to this day using many different approaches.[11–17] Intriguingly, since 1979[18] modern astrophysical observations point to the occurrence of [OCN]$^-$ in icy objects of our solar system and the interstellar medium,[19–23] giving it a potential role as a precursor of more complex organic molecules formed by abiotic processes.[24]

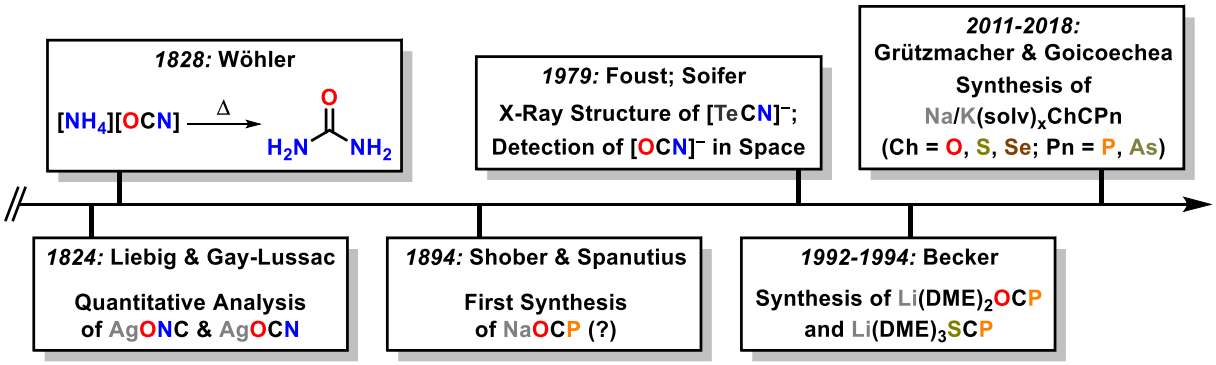

Figure 4.1. Timeline with selected discoveries and achievements in the history of triatomic, cyanate-type anions [ChCPn]$^-$ (Pn = N, P, As; Ch = O, S, Se).[1,2,7,18,25–32] For simplicity only the principal investigators are listed. The dates refer to the year of publication.

For the chemists of the 19th and 20th centuries the heavier thiocyanate ([SCN]$^-$) was another important representative of the family of cyanate-type ions with the general formula [ChCPn]$^-$ (Ch = chalcogenide; Pn = pnictide). It was already described in 1799 by Buchholz and named "rhodanide" in 1820 by Berzelius, because of its deep red iron(III) complex.[33] In coordination chemistry thiocyanate in particular is considered as the archetypical example of an ambidentate ligand:[34–36] It can bind to a metal ion with either sulfur or nitrogen and helped the descriptive (but not always correct)[37] "Hard and Soft Acids and Bases" (HSAB) concept[38,39] of Pearson to become popular in university textbooks on inorganic chemistry from the 1960s onwards.[40,41] Selenocyanate ([SeCN]$^-$) was the first air-sensitive cyanate-type anion.[42] Due to its sensitivity and the strong odor of selenium compounds, complexes of [SeCN]$^-$ were not thoroughly investigated before the 1960s.[43–45] The successful synthesis and linear structure of the even more reactive tellurocyanate ([TeCN]$^-$)[46] were confirmed crystallographically only in 1979.[26]

Although the related, air-sensitive 2-phosphaethynolate anion ([OCP]⁻) was probably synthesized as early as 1894,[25] the first heavier homologues containing phosphorus were structurally authenticated only in the early 1990s,[27,28] when Becker and co-workers reported the syntheses of $Li(DME)_2OCP$ and $Li(DME)_3SCP$. Multi-gram scale preparations of more stable sodium and potassium salts of [OCP]⁻ by the groups of Grützmacher and Goicoechea between 2011 and 2014[29,30,47] has recently led to a remarkable resurgence of its chemistry, giving access to a wide range of exotic P-containing molecules.[25,48] This triggered a renewed interest in heavier analogues of cyanate and led to the preparation of 2-arsaethynolate ([OCAs]⁻) in 2016[49] and first reactivity studies of this anion.[49–51] A general synthetic protocol for the sodium or potassium salts of [SCP]⁻ and [SeCP]⁻ as well as [SCAs]⁻ and [SeCAs]⁻ was developed between 2016 and 2018.[31,32] However, the chemistry of these four anions remains to be explored.

In the following sections the electronic structure and coordination behavior of the cyanate-type [ChCPn]⁻ anions (with focus on Ch = O, S and Pn = N, P) are discussed. In addition, selected complexes of [OCP]⁻ and [SCP]⁻ as well as relevant rearrangement reactions of the [OCP]⁻ anion are highlighted to give a background for the own results obtained with the [SCP]⁻ anion (see Section 4.2).

4.1.1 Electronic Structure and Coordination Behavior of Selected [ChCPn]⁻ Ligands (Ch = O, S; Pn = N, P)

Although commonly called "heterocumulene anions", there are in fact two predominant resonance structures for the family of linear [ChCPn]⁻ ligands (Figure 4.2, top left; **A** and **B**). According to natural resonance theory (NRT) analysis, the relative contributions of these resonance structures vary depending on the nature of the chalcogen (Ch) and pnictogen (Pn) atoms (Figure 4.2, bottom left).[52,53]

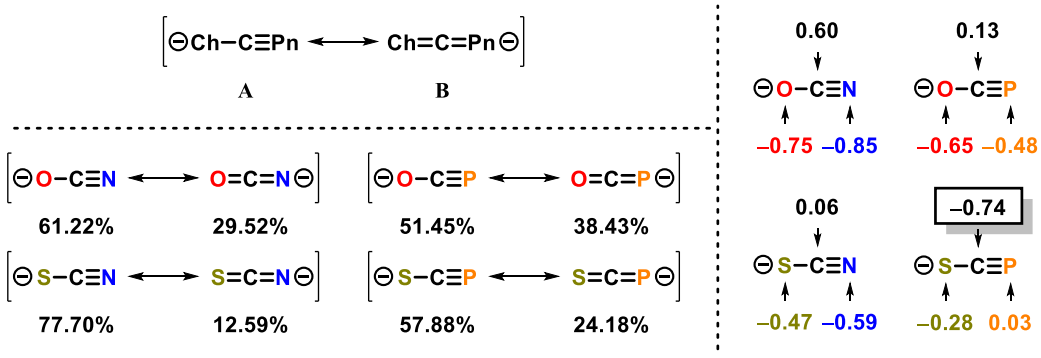

Figure 4.2. The two predominant resonance structures for the family of [ChCPn]⁻ anions (top left) and calculated weights for [OCN]⁻, [SCN]⁻, [OCP]⁻ and [SCP]⁻ according to NRT analyses (bottom left). Annotated NBO atomic charges (right).[32,52]

For instance, in case of the "classical" anions cyanate and thiocyanate resonance structure **A** has a pronounced weight in the electronic description (61.22% and 77.70%, respectively).[53] Exchange of nitrogen by the heavier homologue phosphorus results in an increased weight of heterocumulene-type

resonance structure **B** in $[OCP]^-$ and $[SCP]^-$, although X-ray diffraction data (Table 4.1, left)[28,30] and NRT analysis[52] still point to a C≡P triple bond[32] and therefore a dominance of resonance structure **A** (51.45% and 57.88%, respectively). This is in line with the calculated Wiberg bond indices (WBI) of the C–Pn unit being larger than 2 for all of the four $[ChCPn]^-$ anions with Ch = O or S and Pn = N or P (Table 4.1, right).[32]

Table 4.1. Experimentally determined bond metric data[30,32,54,55] (left) and calculated WBI[32] (right) for a selection of $[ChCPn]^-$ anions (Ch = O or S and Pn = N or P). Counter-cations for the bond metric data: Na^+ (for $[OCN]^-$),[55] $[Na(2.2.1\text{-crypt})]^+$ (for $[SCN]^-$),[54] $[K(18\text{-crown-6})]^+$ (for $[OCP]^-$)[30] and $[Na(18\text{-crown-6})(THF)_2]^+$ (for $[SCP]^-$).[32]

Anion	*Ch–C in Å*	*C–Pn in Å*	*Ch–C–Pn in °*	*WBI (Ch–C)*	*WBI (C–Pn)*
$[OCN]^-$	1.211(2)	1.211(2)	180	1.5203	2.4250
$[SCN]^-$	1.655(5)	1.053(6)	176.2(4)	1.3839	2.6267
$[OCP]^-$	1.212(4)	1.579(3)	178.9(3)	1.6673	2.2031
$[SCP]^-$	1.613(4)	1.579(4)	179.3(3)	1.5210	2.3798

A closer look at the bond metrics[30,32,54,55] summarized in Table 4.1 shows that differences in the electronic structure cannot be accurately described or inferred by only using these data: The O–C and S–C bond lengths of ≈1.21 Å and ≈1.61 to 1.65 Å are comparable within the selected set of anions and the C–P bond length (1.579 Å) is identical for $[OCP]^-$ and $[SCP]^-$. Only thiocyanate shows a mentionable difference in C–N bond length (≈1.05 Å) compared to cyanate (≈1.21 Å) and a slightly larger deviation of ≈3.8° from the 180° angle compared to the other three anions.

Further information on the electronic structure of $[OCP]^-$ and $[SCP]^-$ could be gained indirectly by a combination of negative ion photoelectron spectroscopy (NIPES), photoelectron imaging spectroscopy and theoretical calculations.[52] Electron photodetachment of the respective anions revealed the electron affinities (EA) of the radicals $[OCP]^{\cdot}$ and $[SCP]^{\cdot}$: It was found that EA($[OCP]^{\cdot}$) is smaller than EA($[SCP]^{\cdot}$), which is at first glance counterintuitive when considering general electronegativity (EN) trends (EN(O) > EN(S)) and the results obtained for the lighter homologues, that EA($[OCN]^{\cdot}$) is greater than EA($[SCN]^{\cdot}$). However, the higher EA of $[SCP]^{\cdot}$ is consistent with a larger contribution of the more electronegative chalcogen atom to the HOMO of $[SCP]^-$ than to the HOMO of $[OCP]^-$.[52] Apart from the different contributions to the HOMO, the 2-phosphaethynthiolate anion also exhibits a drastically different distribution of its negative charge density along the $[S–C≡P]^-$ unit compared to (thio)cyanate and 2-phosphaethynolate (Figure 4.2, right): According to the calculated natural bond orbital (NBO) atomic charges the highest negative charge density in (thio)cyanate and $[OCP]^-$ is located either on the terminal pnictogen ($[OCN]^-$ and $[SCN]^-$) or chalcogen atom ($[OCP]^-$), whereas in the case of $[SCP]^-$ the negative charge density resides mostly at the central carbon atom (highlighted box).[32] Each of the four cyanate-type anions has a characteristic range of IR stretching frequencies as well as ^{13}C and ^{31}P chemical shifts (selected examples of precursor salts are listed in Table 4.2), which is very useful for NMR spectroscopic reaction monitoring and the characterization of isolated complexes of these anions.[30,32,56–62]

Table 4.2. Characteristic (experimental) IR stretching frequencies[29,32,55] and NMR[30,32] spectroscopic data for a selection of $[ChCPn]^-$ anions (Ch = O or S and Pn = N or P). Counter-cations for IR stretching frequencies (measured in the solid state): Na^+ (for $[OCN]^-$),[55] K^+ (for $[SCN]^-$),[46] $[Na(DME)_2]^+$ (for $[OCP]^-$)[29] and $[Na(18\text{-crown-6})]^+$ (for $[SCP]^-$).[32] Counter-cations and solvents for NMR spectroscopic data: K^+ and D_2O (for $[OCN]^-$ and $[SCN]^-$),[60] $[K(18\text{-crown-6})]^+$ and THF-d_8 (for $[OCP]^-$),[30] $[Na(18\text{-crown-6})]^+$ and pyridine-d_5 (for $[SCP]^-$).[32]

Anion	$\nu_{C\equiv Pn}$ *in* cm^{-1}	$\delta(^{13}C)$ *in ppm*	$\delta(^{31}P)$ *in ppm*	$^1J_{CP}$ *in Hz*
$[OCN]^-$	2232	129.7 (s)	-	-
$[SCN]^-$	2048	134.0 (s)	-	-
$[OCP]^-$	1780	170.3 (d)	–396.8 (s)	62
$[SCP]^-$	1374	193.6 (d)	–120.9 (s)	19.3

For instance, the $\nu_{C\equiv N}$ stretching frequencies of cyanate and thiocyanate are easily identified at ≈2200 cm^{-1} or ≈2000 cm^{-1} and can give information about the binding mode of (thio)cyanate.[43] Due to the heavier phosphorus atom, the homologues' $\nu_{C\equiv P}$ stretching frequencies are shifted noticeably to smaller wavenumbers of ≈1800 cm^{-1} for $[OCP]^-$ or ≈1400 cm^{-1} for $[SCP]^-$. While in the case of 2-phosphaethynolate this is still well separated from the fingerprint region of most organic ligands (500–1500 cm^{-1}),[62] it should be more difficult to unequivocally assign the 2-phosphaethynthiolate ligand's C≡P absorption band. Another helpful indicator of the $[ChCPn]^-$ ligands' successful coordination to a metal ion is the ^{13}C NMR signal of the central carbon atom: In the case of sodium cyanate and potassium thiocyanate a singlet can be found at $\delta \approx 130$ ppm, whereas for [M(18-crown-6)][ChCP] (M = Na, K; Ch = O, S) doublets at $\delta \approx 170$ ppm and $\delta \approx 190$ ppm are recorded. The doublet splittings arise from ^1J coupling with the phosphorus atom and amount to ≈60 Hz for $[OCP]^-$ and ≈20 Hz for $[SCP]^-$. The ^{13}C resonances can experience shifts of up to ≈20 ppm upon coordination of the different ligands to a metal ion.[60] However, the ^{31}P singlet resonances of both $[OCP]^-$ and $[SCP]^-$, which are found at $\delta \approx -370$ ppm and $\delta \approx -120$ ppm for the precursor salts, are even more sensitive to electronic changes. Depending on the metal ion and binding mode, these resonances can experience shifts of up to several 100 ppm to lower fields in the case of $[OCP]^-$[31,63–67] or up to ≈70 ppm to higher fields in the case of $[SCP]^-$.[31]

The selected cyanate-type anions exhibit a variety of coordination modes in metal complexes, depending on such factors as the nature of the chalcogen and pnictogen atoms, the nature and oxidation state of the metal and the steric demand of the supporting ligands. Besides the typical end-on linear or bent coordination to one metal atom *via* the chalcogen or nitrogen atom, (thio)cyanate can show a bridging $\mu,\kappa^2(N)$-, $\mu,\kappa^2(Ch)$- or $\mu,\kappa^1(Ch):\kappa^1(N)$-coordination mode (Figure 4.3, left; Ch = O, S).[43,59,64,68–74] The 2-phosphaethynolate can bind in an analogous $\kappa^1(O)$-, $\kappa^1(P)$-, $\mu,\kappa^2(O)$- *or* $\mu,\kappa^1(O):\kappa^1(P)$-fashion (Figure 4.3, middle)[29,30,63–67,75–78] – with the difference that the M–P–C angle in complexes with P-bound $[OCP]^-$ is around 90° and thus much more strongly bent than the typical M–N–C angle (between ≈143° and ≈180°) found in cyanate complexes.[31,73,75] This is attributed to the predominant heteroallene character of the P-coordinated $[O{=}C{=}P]^-$ unit and the coordination through one of the p-orbitals at the phosphorus atom.

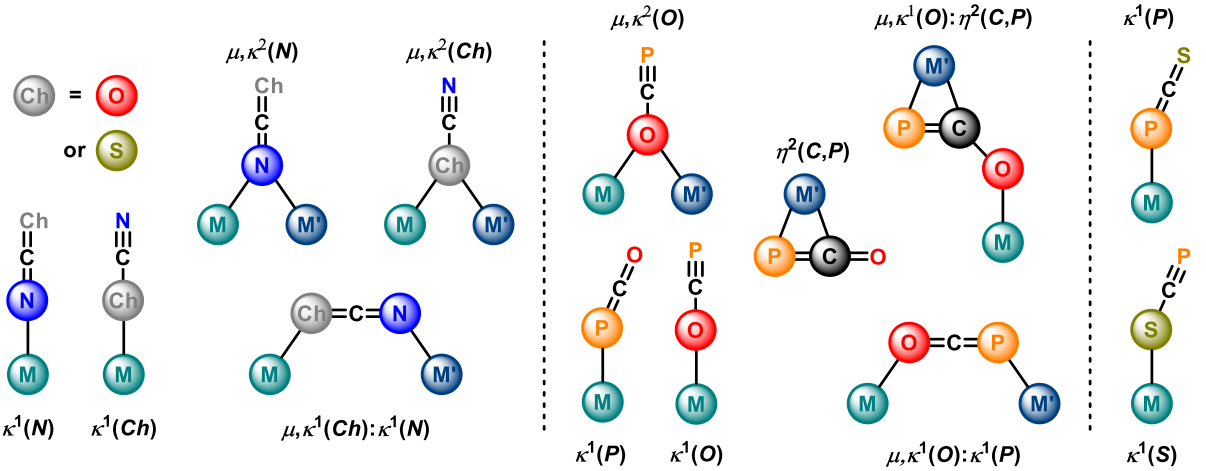

Figure 4.3. Selection of structurally authenticated coordination modes of $[ChCPn]^-$ anions with Ch = O, S and Pn = N, P in metal (M, M') complexes.[29–31,43,59,63–65,68–78] Simplified representations; no exact M/M'–Ch/Pn–C angles, formal charges or supporting ligands at M and M' shown. The coordinating atoms are highlighted as spheres. Coordination modes of constitutional isomers of $[ChCPn]^-$ have been excluded for clarity.

The $[OCP]^-$ ligand can also exhibit a more diverse coordination behavior (see also Section 4.1.2): Although no end-on $\mu,\kappa^2(P)$-binding has been reported yet, the η^2-coordination of carbon and phosphorus in a mononuclear copper(I) complex[65] and the bridging $\mu,\kappa^1(O):\eta^2(C,P)$-mode in a heterobimetallic thorium(IV)–nickel(0) complex[64] represent novel and exotic binding motifs of cyanate-type anions. Especially the participation of the central carbon atom of a cyanate-type anion in a side-on binding to a metal ion has been so far unique to the $[OCP]^-$ ligand. In addition to the examples shown in Figure 4.3, a phosphaethynolato-borane gave access to bridging $\mu,\kappa^1(C):\kappa^1(P)$-, $\mu,\kappa^1(C):\kappa^2(P)$- or even μ, $\kappa^1(O):\kappa^1(C):\kappa^1(P)$-binding modes.[79] In contrast, the coordination behavior of 2-phosphaethynthiolate is clearly under-investigated, with only bent, end-on $\kappa^1(S)$- and $\kappa^1(P)$-coordinated versions[31] (Figure 4.3, right) being known prior to the results presented in this work (see Section 4.2).

4.1.2 Selected Metal Complexes of 2-Phosphaethynolate and 2-Phosphaethynthiolate

The first structural comparison between a cyanate and its corresponding 2-phosphaethynolate complex was published in 2012 by the groups of Grützmacher and Peruzzini.[73] They investigated the rhenium(I) complexes $[(triphos)(CO)_2Rh(PnCO)]$ (triphos = $MeC(CH_2PPh_2)_3$; Pn = N, P), which were obtained by salt metathesis between the corresponding rhenium(I) triflate complex and KOCN or NaOCP. X-ray diffraction studies showed that the most striking difference between the pnictogen-bound anions lies in the approximately linear (Rh–N–C angle of 166.2°) *vs.* strongly bent (Rh–P–C angle of 92.6°) end-on coordination of $[OCN]^-$ *vs.* $[OCP]^-$ (Figure 4.4). Therefore, the authors argued that the cyanate ligand can be better described by resonance structure **A**, and that 2-phosphaethynolate has a more pronounced heteroallene-type character of resonance structure **B** (see Figure 4.2). This is in line with the NBO

analysis and the calculated IR spectrum of the $[OCP]^-$ complex, which indicate a weakening of the C≡P bond upon coordination to rhenium(I).

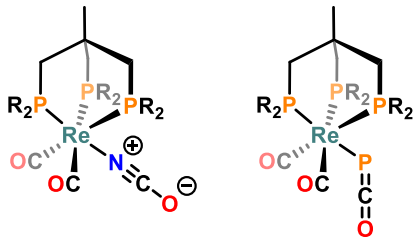

Figure 4.4. Structural comparison between the rhenium(I) complexes [(triphos)$(CO)_2$Re(NCO)] and [(triphos)$(CO)_2$Re(PCO)] with pnictogen-bound cyanate or 2-phosphaethynolate ligand (R= Ph).[73]

A series of thorium(IV) and uranium(IV) complexes featuring a cyanate, thiocyanate or 2-phosphaethynolate ligand were synthesized and structurally compared by the Arnold group in 2015 (Scheme 4.1, left and middle).[64] Although $\kappa^1(P)$-binding of $[OCP]^-$ to Lewis acids had been far more often encountered prior to this report, it was reasoned that the oxophilic actinides should favor $\kappa^1(O)$-binding. X-ray structure analyses revealed that the $[OCP]^-$ ligand indeed favors a linear, end-on coordination to both actinides *via* the oxygen atom, contrasting the coordination behavior of $[OCN]^-$ and $[SCN]^-$, which bind end-on *via* the nitrogen atom. The $\kappa^1(O)$-coordination mode of $[OCP]^-$ is retained in solution as judged by the NMR and IR spectroscopic data, which support a description of the $[OCP]^-$ ligand by the phosphaalkyne-limiting resonance structure (Figure 4.2, **A**).

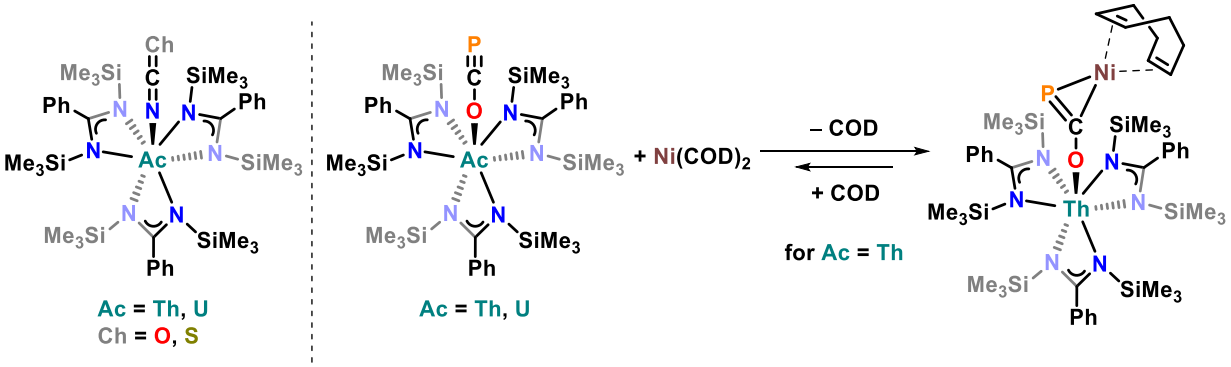

Scheme 4.1. Series of actinide(IV) complexes with different cyanate-type anions (left: $[OCN]^-$ and $[SCN]^-$; middle: $[OCP]^-$) presented by the Arnold group in 2015.[64] Unusal bridging $\mu,\kappa^1(O):\eta^2(C,P)$-mode of the $[OCP]^-$ ligand in a heterobimetallic thorium–nickel complex (right). COD = cycloocta-1,5-diene.

The authors also investigated the reactivity of the diamagnetic thorium(IV) phosphaethynolato complex and found that "soft" metal atoms such as nickel(0) can bind in a reversible fashion to the CP unit of the $[OCP]^-$ ligand (Scheme 4.1, right). Binding of the Ni(COD) fragment can be inferred from a strong darkening of the reaction solution and a drastic deshielding of the phosphorus atom ($\delta(^{31}P)$ = –7.7 ppm *vs.* –334 ppm for the starting complex), which points to $\eta^2(C,P)$-coordination. In addition, a pronounced tilt at the $[OCP]^-$ carbon atom (P–C–O angle of 148.1(3)° *vs.* 179.7(4)° in the starting complex) and an elongation of the C–P bond length from 1.561(4) Å to 1.660(4) Å is induced, as was elucidated by X-ray diffraction analysis. Significantly, the bridging $\mu,\kappa^1(O):\eta^2(C,P)$-binding mode in this

heterobimetallic system represented the first example featuring a participation of a [ChCPn]⁻ ligand's central carbon atom in the binding to a metal atom.

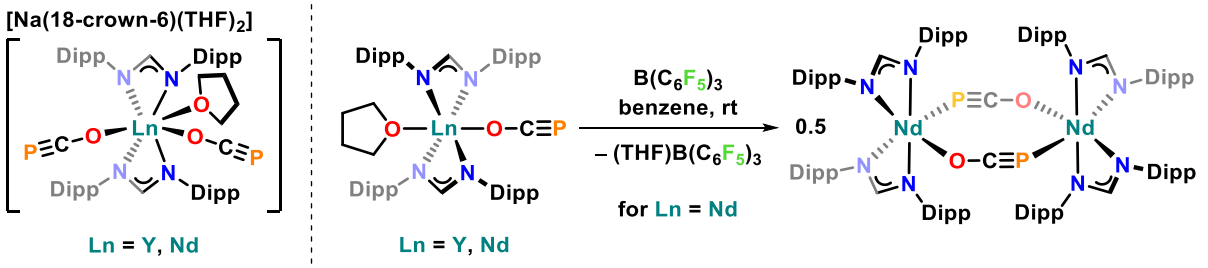

Scheme 4.2. Selected examples of the first series of lanthanide complexes (only Ln = Y, Dy shown) featuring a heavier cyanate-analogue ([OCP]⁻), as reported by Goicoechea and co-workers in 2018.[63] Note that Y is also denoted as Ln for simplicity.

The first lanthanide complexes of a heavier cyanate-analogue were again obtained with [OCP]⁻ and presented in 2018 by the group of Goicoechea.[63] Similar to the Arnold group's report,[64] it was reasoned that the oxophilic lanthanides should favor $\kappa^1(O)$-binding. This was demonstrated representatively with neodymium(III) and samarium(II) as well as the related rare earth yttrium(III), supported by amidinate ligands (Scheme 4.2). The series of complexes had either terminally bound (left and middle) or bridging (right) [OCP]⁻ ligands. Notably, ate complexes with two [OCP]⁻ ligands (both binding *via* the oxygen atom) could be isolated as well (left). Moreover, the neodymium(III) mono(phosphaethynolato) complex (middle) could be dimerized after removal of the ligated THF molecule by tris(pentafluorophenyl)borane and subsequent bridging of two Nd^{3+} ions in a $\mu,\kappa^1(O):\kappa^1(P)$-fashion (right).

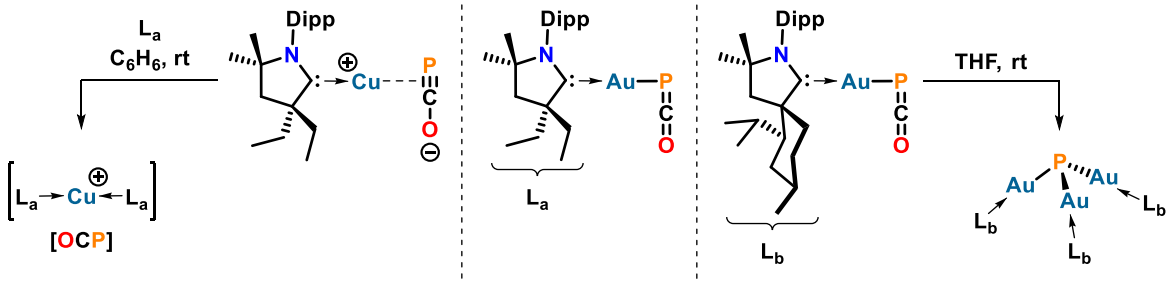

Scheme 4.3. Coordination modes of [OCP]⁻ at CAAC-supported coinage-metal ions (left: Cu^+; middle and right: Au^+) and resulting reactivities (left and right), as reported by the groups of Bertrand and Grützmacher in 2016.[65] L_a = 1-(2,6-diisopropylphenyl)-3,3-diethyl-5,5-dimethyl-pyrrolidin-2-ylidene (^{Et}CAAC); L_b = 1-(2,6-diisopropylphenyl)-3-menthyl-5,5-dimethyl-pyrrolidin-2-ylidene (^{Menth}CAAC). Reaction equation on the right not balanced for better clarity.

An intriguing series of CAAC-supported copper(I) and gold(I) complexes of 2-phosphaethynolate was presented by Bertrand, Grützmacher and co-workers in 2016 (Scheme 4.3).[65] According to X-ray diffraction studies of the systems with ^{Et}CAAC ligand, the [OCP]⁻ anion was found to bind in a strongly bent fashion to the coinage-metal ion in both cases, with M–P–C angles of 79.15(5)° (for M = Cu) and 86.2(1)° (for M = Au). However, while gold(I) is only coordinated by the terminal phosphorus atom (middle), copper(I) is bound to both the terminal phosphorus as well as the central carbon atom (left).

Moreover, NBO analysis of the ^{Et}CAAC systems indicate that the side-on $\eta^2(C,P)$-coordinated $[OCP]^-$ ligand is less strongly bound to copper(I) than the end-on η^1-coordinated version in the gold(I) complex. This results in a difference in reactivity: The copper(I) complex slowly decomposes in solution to a mixture of unidentifiable products, whereas the gold(I) system takes a cleaner decarbonylation route to form a trinuclear gold(I) parent phosphide complex as the main product, which could be crystallized using ^{Menth}CAAC instead of ^{Et}CAAC (Scheme 4.3, right). The authors could also benefit from the more weakly η^2-bound $[OCP]^-$ ligand in the copper(I) complex by demonstrating its smooth displacement with a second equivalent of ^{Et}CAAC, giving an interaction-free 2-phosphaethynolate (left).

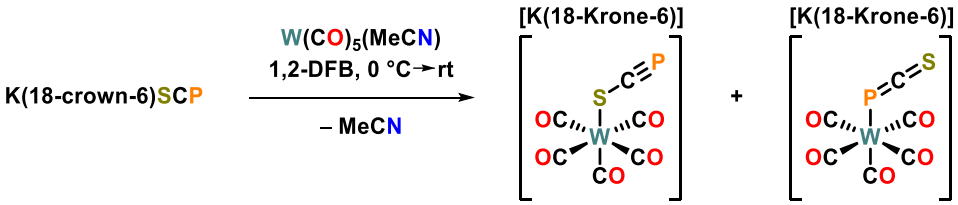

Scheme 4.4. Mixture of S- and P-coordinated 2-phosphaethynthiolate at tungsten(0), as described by the group of Goicoechea in 2016.[31] Reaction equation not balanced for simplicity. 1,2-DFB = 1,2-difluorobenzene.

In contrast to the increasing number of metal complexes of $[OCP]^-$, defined coordination compounds of the 2-phosphaethynthiolate have remained elusive so far. Prior to the results presented in this dissertation, only one publication by the Goicoechea group from 2016[31] reported the coordination of $[SCP]^-$ to a metal atom (or ion) other than lithium, sodium or potassium. The authors described the displacement of the acetonitrile ligand in $[W(CO)_5(MeCN)]$ by $[SCP]^-$, employing the quite polar, but still relatively non-coordinating arene solvent 1,2-difluorobenzene (Scheme 4.4). However, the reaction was found to proceed only sluggishly and ^{31}P NMR spectroscopy after several days indicates the presence of two products in a 1:1 ratio, apart from significant amounts of starting material K(18-crown-6)SCP ($\delta(^{31}P) \approx 120$ ppm (s)). The characteristic shifts of the products' ^{31}P singlet resonances at $\delta = -92.9$ ppm and $\delta = -192.6$ ppm as well as the tungsten satellites in the latter case ($^1J_{WP} = 46.0$ Hz) allows the assignment as S- and P-bound isomers of ate-complex $[W(CO)_5(SCP)]^-$, respectively. The rather small $^1J_{WP}$ coupling constant points to a binding of $[SCP]^-$ through the p-orbital of the phosphorus atom and therefore an approximate 90° W–P–C angle in solution. Even though X-ray diffraction studies showed an end-on, bent coordination mode of the $[SCP]^-$ ligand, the data allowed no definite assignment as S- or P-bound version. Apart from the fact that the conversion to $[W(CO)_5(SCP)]^-$ is rather slow and no defined compound can be obtained from the reaction mixture, it is noteworthy that these complexes are prone to decompose in solution within four days. This further impedes any selective follow-up reactions or even the isolation of a material with a defined composition. The results of the Goicoechea group therefore strongly suggest that neutral metal atoms such as tungsten(0) are not the best match for the 2-phosphaethynthiolate anion and that the strikingly different distribution of electronegative charge density along the $[S–C{\equiv}P]^-$ unit compared to (thio)cyanate and $[OCP]^-$ (see Section 4.1.1) very likely precludes a straight-forward and stable binding *via* the sulfur or the phosphorus atom.

4.1.3 OCP to OPC Rearrangement of 2-Phosphaethynolate

In the last decade the 2-phosphaethynolate anion has not only given access to a wide range of novel and rare P-containing molecules,[25] but also caused a renewed interest in the fundamental constitutional isomerization of ChCPn to ChPnC units. For cyanate ($[OCN]^-$) or cyanic acid (HOCN) the rearrangement to fulminate ($[ONC]^-$) or fulminic acid (ONCH) is thermodynamically strongly disfavored[80–83] and has not been observed experimentally yet. In contrast, the reversed isomerization of coordinated fulminate to cyanate[57,84] and that of organic nitrile oxides (ONCR) to the respective isocyanates (OCNR)[85] have been reported. However, since 2016 the analogous OCP to OPC rearrangement has appeared a few times in the literature.[86–88]

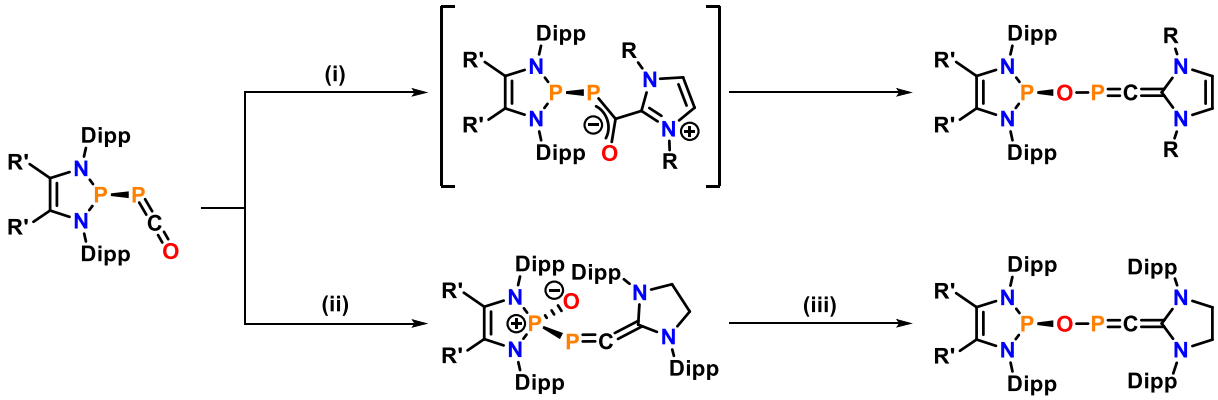

Scheme 4.5. Reactions of selected phosphanyl phosphaketenes (left, R' = H or Me) with different NHCs to give rearranged heterocumulene π-systems, as published by the groups of Bertrand, Su and Grützmacher in 2016.[86] Conditions: (i) IPr (R = Dipp; 1.0 equiv) or IMes (R = Mes; 1.0 equiv), THF, rt; (ii) SIPr (1.0 equiv), THF, rt; (iii) toluene, 80 °C.

The groups of Bertrand, Su and Grützmacher investigated the NHC-induced rearrangements of phosphanyl phosphaketenes, which were derived from sodium 2-phosphaethynolate and *P*-chloro-1,2,3-diazaphospholes (Scheme 4.5, left).[86] The phosphanyl phosphaketenes feature a long P–P bond (≈2.44 Å) and are therefore best described as very close ion pairs of $[OCP]^-$ and the respective 1,2,3-diazaphospholenium cations.[89] The authors found that NHCs with an unsaturated backbone (IPr or IMes) first add to the central carbon atom of the OCP unit (step (i), top middle), which X-ray diffraction studies showed to cause a bending of the O–C–P angle (from roughly 179° to 130° for R = Dipp and R' = H). Although the P–P bond in the zwitter-ionic products is at first retained, the new compounds further rearrange in solution: C–O bond cleavage and insertion of the oxygen atom into the P–P bond give a heavy fulminate-type OPC arrangement flanked by the 1,2,3-diazaphosphole unit on the side of the oxygen atom and the formal NHC unit on the side of the carbon atom, respectively (top right). When SIPr with a saturated backbone was used, different zwitter-ionic products could be obtained, in which the oxygen atom was transferred to the phosphorus atom of the 1,2,3-diazaphosphole substituent, respectively (step (ii), bottom middle). These new compounds were found to be much more stable towards insertion of the oxygen atom into the P–P bond and required heating at 80 °C in toluene for this "phosphorotropic tautomerism"[90] to occur (step (iii), bottom right). In fact, theoretical calculations

confirmed that the transfer of the oxygen atom from the bent OCP fragment to the phosphole proceeds the insertion into the P–P bond in the overall OCP to OPC rearrangement. While the P–C and C–C_{NHC} bond lengths in the heavy fulminate-type products (of, *e.g.*, 1.581(3) Å and 1.360(4) Å for R' = H and R = Mes) indicate a double bond character in both cases and therefore a heteroallene structure, the P–C–C_{NHC} angles from 169° to 148° deviate from linearity, depending on the nature of the NHC. The O–P–C angle is strongly bent and averages around 112° for this set of examples.

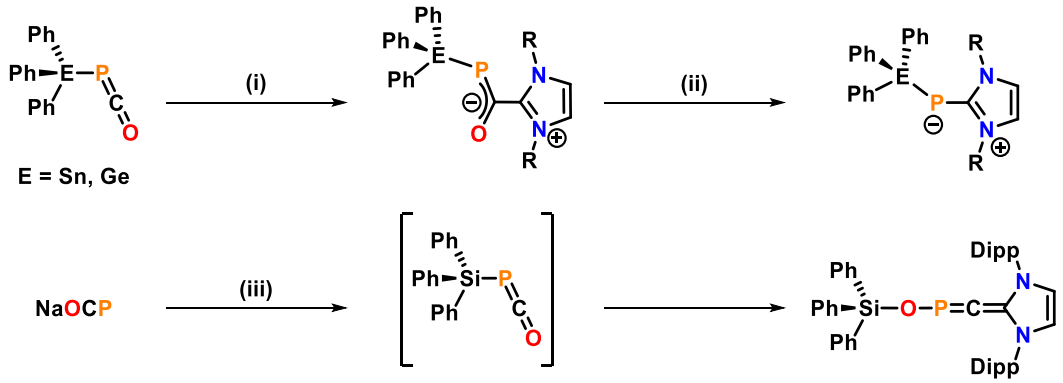

Scheme 4.6. Reactions of different heavy tetrel-substituted phosphaketenes with NHCs by Grützmacher and co-workers from 2016.[87] Conditions: (i) IPr (R = Dipp; 1.0 equiv) or IMes (R = Mes; 1.0 equiv), toluene, rt; (ii) toluene, 90 °C, – CO; (iii) chlorotriphenylsilane (1.0 equiv), IPr (1.0 equiv), toluene/THF (3:1), rt, – NaCl.

The family of formally NHC-substituted phospha-fulminate derivatives were extended by Grützmacher and co-workers to heavy tetrel-functionalized compounds.[87] Similar to the 1,2,3-diazaphosphole-substituted systems (see Scheme 4.5, left), the phosphaketenes $Ph_3E(PCO)$ (with E = Sn, Ge) react with either IPr or IMes to give zwitterionic adducts with bent PCO units (Scheme 4.6, step (i), top left). Notably, heating toluene solutions of the phosphaketene-NHC adducts to 90 °C for prolonged times leads to the loss of carbon monoxide, resulting in zwitter-ionic imidazolium-phosphanide adducts (step (ii), top right). In contrast, when the triphenylsilyl group is employed a rearrangement of the OCP to the OPC unit under mild conditions takes place, with the silicon atom finally being bound to the oxygen atom (step (iii), bottom). The heavy fulminate-type product shows a characteristic low-field shifted singlet resonance at $\delta(^{31}P)$ = 170.3 ppm and a doublet resonance at $\delta(^{13}C)$ = 194.8 ppm ($^{1}J_{CP}$ = 3.0 Hz).

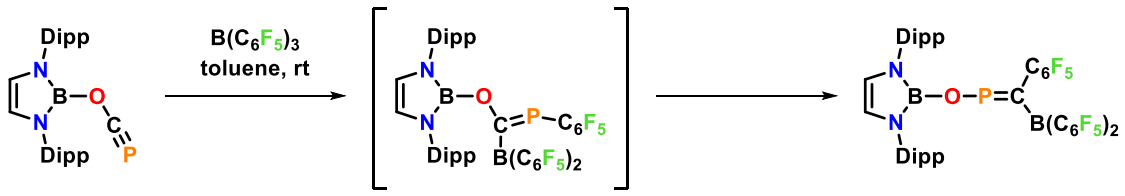

Scheme 4.7. Reaction of a boryl-phosphaethynolate with tris(pentafluorophenyl)borane to a rearranged OPC moiety by the Goicoechea group from 2020.[88]

Recently, Goicoechea and co-workers also isolated a rearranged product with an OPC unit from carboboration of an *O*-borylated phosphaethynolate (Scheme 4.7), thereby identifying other reagents than NHCs, which can be employed to induce such an isomerization.

Overall, the examples of the last two sections clearly show that on the one hand heavy cyanate-type anions such as $[OCP]^-$ can indeed participate in unusual coordination chemistry and undergo very interesting rearrangements, but that on the other hand a defined coordination of the $[SCP]^-$ ligand and an analogous SCP to SPC rearrangement still had to be achieved prior to the own results presented in this dissertation. The following published manuscript describes the strategy and the unexpected findings concerning the first stable coordination and selective functionalization of the 2-phosphaethynthiolate anion.

4.2 Results and Discussion

Publication: η^3-Coordination and Functionalization of the 2-Phosphaethynthiolate Anion at Lanthanum(III)

Fabian A. Watt,[b] Lukas Burkhardt,[b] Roland Schoch,[b] Stefan Mitzinger,[c] Matthias Bauer,[b] Florian Weigend,*[d] Jose M. Goicoechea,*[c] Frank Tambornino,*[d] and Stephan Hohloch*[a]

* Corresponding authors

[a] University of Innsbruck, Innrain 80-82, 6020 Innsbruck, Austria

[b] Paderborn University, Warburger Straße 100, 33098 Paderborn, Germany

[c] University of Oxford, 12 Mansfield Road, OX1 3TA Oxford, United Kingdom

[d] Philipps-Universität Marburg, Hans-Meerwein Straße 4, 35043 Marburg, Germany

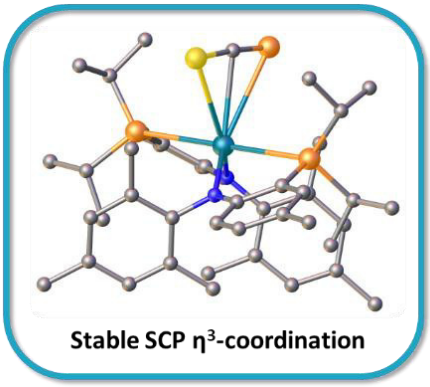

This article was published as follows:

Watt, F. A.; Burkhardt, L.; Schoch, R.; Mitzinger, S.; Bauer, M.; Weigend, F.; Goicoechea, J. M.; Tambornino, F.; Hohloch, S. *Angew. Chem. Int. Ed.* **2021**, *60*, 9534–9539.

DOI: 10.1002/anie.202100559

https://doi.org/10.1002/anie.202100559

Synopsis: The first stable coordination of the 2-phosphaethynthiolate ([SCP]$^-$) anion at a Lewis-acidic lanthanum(III) ion and its subsequent rearrangement to form a substituted heavy "fulminate-like" anion, induced by CAACs, is reported.

Author Contributions: The project was designed by F. Tambornino and S. Hohloch. Experimental work was performed by F. A. Watt, S. Hohloch, S. Mitzinger and F. Tambornino. X-Ray diffraction analysis was performed by S. Hohloch and R. Schoch. Theoretical calculations were performed by L. Burkhardt and F. Weigend. The manuscript was written by F. A. Watt, M. Bauer, J. M. Goicoechea, F. Weigend, F. Tambornino, and S. Hohloch. All authors have given approval to the final version of the manuscript. Dr. Hans Egold from the NMR facility of Paderborn University and Athul Krishna are kindly acknowledged for helpful discussions. Christiane Gloger and Maria Busse are kindly acknowledged for conducting elemental analyses.

GDCh **Research Articles** Angewandte International Edition Chemie

Check for updates

How to cite: *Angew. Chem. Int. Ed.* **2021**, *60*, 9534–9539
International Edition: doi.org/10.1002/anie.202100559
German Edition: doi.org/10.1002/ange.202100559

Lanthanide Complexes

η^3-Coordination and Functionalization of the 2-Phosphaethynthiolate Anion at Lanthanum(III)**

Fabian A. Watt, Lukas Burkhardt, Roland Schoch, Stefan Mitzinger, Matthias Bauer, Florian Weigend, Jose M. Goicoechea,* Frank Tambornino,* and Stephan Hohloch**

In memory of Gerd Becker

Abstract: *We present the η^3-coordination of the 2-phosphaethynthiolate anion in the complex $(PN)_2La(SCP)$ (**2**) [PN = N-(2-(diisopropylphosphanyl)-4-methylphenyl)-2,4,6-trimethylanilide)]. Structural comparison with dinuclear thiocyanate-bridged $(PN)_2La(\mu\text{-}1,3\text{-}SCN)_2La(PN)_2$ (**3**) and azide-bridged $(PN)_2La(\mu\text{-}1,3\text{-}N_3)_2La(PN)_2$ (**4**) complexes indicates that the $[SCP]^-$ coordination mode is mainly governed by electronic, rather than steric factors. Quantum mechanical investigations reveal large contributions of the antibonding π^*-orbital of the $[SCP]^-$ ligand to the LUMO of complex **2**, rendering it the ideal precursor for the first functionalization of the $[SCP]^-$ anion. Complex **2** was therefore reacted with CAACs which induced a selective rearrangement of the $[SCP]^-$ ligand to form the first CAAC stabilized group 15–group 16 fulminate-type complexes $(PN)_2La\{SPC(^RCAAC)\}$ (**5a,b**, R = Ad, Me). A detailed reaction mechanism for the SCP-to-SPC isomerization is proposed based on DFT calculations.*

Introduction

The (coordination) chemistry of the 2-phosphaethynolate ($[OCP]^-$) anion continues to be a vibrant, highly topical research field in the chemical sciences[1] and has already led to the isolation of a plethora of novel or rare phosphorus-containing heterocycles,[2] the first stable singlet phosphinidene,[3] as well as many (functional) coordination compounds covering the whole periodic table[1,4]—from main group elements[5,6] and transition metals[7] to the lanthanides[8] and actinides.[9] In contrast, the chemistry of the heavier analogues, for example, the 2-phosphaethynthiolate ($[SCP]^-$) anion, has been much less developed so far, although both the $[OCP]^-$[10] and the $[SCP]^-$ anion[11] were first reported in the 1990s by Becker and co-workers as their lithium salts. This can partly be attributed to the notorious instability of $Li(DME)_3SCP$ (similar to $Li(DME)_2OCP$).[1] However, even after establishing high-yielding routes to long-term stable (room temperature and moderately air tolerant) sodium or potassium salts of both $[SCP]^-$ and $[OCP]^-$,[12,13] the chemistry of the former remains largely dormant. To date, apart from electrochemical and spectroscopic investigations,[14] only one $[SCP]^-$ coordination compound in the form of $[K(18\text{-crown-}6)][W(CO)_5(SCP)]$ has been reported.[12] This first example demonstrated the potential difficulties to be encountered in $[SCP]^-$ coordination chemistry: Due to the unusually high negative charge density on the central carbon atom of the $[SCP]^-$ anion (natural bond orbital (NBO) atomic charges correspond to −0.28 for S, −0.74 for C and 0.03 for P),[13] only a mixture of S- and P-bound isomers could be obtained, which decomposed at room temperature within four days.

We have recently begun to investigate the chemistry of anilidophosphine-supported lanthanum(III) complexes of the general formula $(PN)_2LaX$ with X = Cl (**1-Cl**) and I (**1-I**),[15] and have shown them to be versatile precursors for the synthesis of pentacoordinate lanthanum(III) primary phosphido and sulfido complexes $(PN)_2La(EMes)$ (E = PH, S). Due to the insertion reactivity of the La–P phosphide bond, the former allowed us to construct phosphaureate and phosphathioureate ligands, which can be used to build

[*] Prof. Dr. S. Hohloch
Institute for General, Inorganic and Theoretical Chemistry
University of Innsbruck
Innrain 80–82, 6020 Innsbruck (Austria)
E-mail: Stephan.Hohloch@uibk.ac.at
M. Sc. F. A. Watt, Dr. L. Burkhardt, Dr. R. Schoch, Prof. Dr. M. Bauer
Department of Chemistry and Center for Sustainable Systems Design (CSSD)
Paderborn University
Warburger Strasse 100, 33098 Paderborn (Germany)
Dr. S. Mitzinger, Prof. Dr. J. M. Goicoechea
Department of Chemistry, University of Oxford
Chemistry Research Laboratory
12 Mansfield Road, Oxford, OX1 3TA (UK)
E-mail: jose.goicoechea@chem.ox.ac.uk
Prof. Dr. F. Weigend, Dr. F. Tambornino
Fachbereich Chemie und Wissenschaftliches Zentrum für Materialwissenschaften (WZMW)
Philipps-Universität Marburg
Hans-Meerwein-Strasse 4, 35032 Marburg (Germany)
E-mail: florian.weigend@chemie.uni-marburg.de
Frank.Tambornino@chemie.uni-marburg.de

[**] A previous version of this manuscript has been deposited on a preprint server (https://doi.org/10.26434/chemrxiv.13567400).
Supporting information and the ORCID identification number(s) for the author(s) of this article can be found under: https://doi.org/10.1002/anie.202100559.

heterobimetallic systems.[16] Furthermore, the same phosphido complex led us to study a transient (terminal) phosphinidene complex.[17] Acknowledging that the use of a neutral metal atom such as tungsten(0) did not favor a defined coordination of the $[SCP]^-$ anion and considering the high utility of our anilidophosphine-supported lanthanum(III) framework to obtain relatively stable, yet still potentially reactive La–P and La–S bonds, we envisioned that the use of a Lewis-acidic metal ion such as lanthanum(III) might alter the charge distribution of the $[SCP]^-$ anion sufficiently to give access to a defined S- or P-bound version and to study its chemistry in more detail.

Results and Discussion

Starting from either **1-Cl** or **1-I**, salt metathesis with an excess of $Na(diox)_{2.3}SCP$ (1.4 equiv) in toluene was found to take place at room temperature and to result in the formation of a single new product **2** overnight (Scheme 1). This was

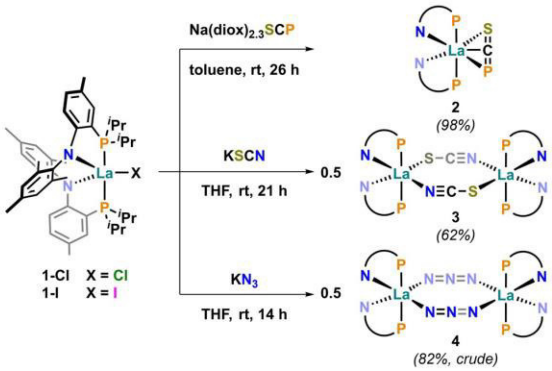

Scheme 1. Syntheses of complexes **2**–**4**, starting from **1-X**.

evident by the darkening of the initially pale yellow suspension and the $^{31}P\{^1H\}$ NMR spectrum, showing a new singlet at $\delta = -44.9$ ppm which was assigned to the $[SCP]^-$ phosphorus atom. After filtration, removal of toluene in vacuo and trituration with *n*-pentane, **2** was obtained as an amber solid in 98% isolated yield. In the $^{13}C\{^1H\}$ NMR spectrum (C_6D_6) of the isolated material a doublet at $\delta = 191.8$ ppm ($^1J_{CP} = 20.6$ Hz), corresponding to the $[SCP]^-$ carbon atom,[13] suggested a defined coordination. Additionally, sharp signals indicated little to no rearrangement on the NMR timescale. Notably, **2** is well soluble and stable for weeks in aromatic (benzene, toluene) and for days in etheric (diethyl ether, tetrahydrofuran) solvents at room temperature, in stark contrast to the previously reported $[K(18\text{-crown-6})][W(CO)_5(SCP)]$.[12] It is also slightly soluble and very stable in aliphatic solvents (*n*-pentane, *n*-hexane), and decomposes only very slowly (over days of refluxing at 45 °C) in dichloromethane to reform the halide complex **1-Cl** (Figure S10) and intractable, insoluble precipitates. Having uncovered a clean reaction for the $[SCP]^-$ anion, we sought to assess the influence of the charge distribution of the (hetero-)cumulene anion on its binding mode at lanthanum(III). Due to the different distribution of negative charge density in the thiocyanate anion ($[SCN]^-$; NBO atomic charges correspond to −0.47 for S, 0.06 for C and −0.59 for N),[13] complex **3** was selected as a reference compound. To also study a trinuclear anion with a more evenly distributed charge density, we synthesized the azide complex **4**. Complexes **3** and **4** were both obtained by salt metathesis from **1-I** and KSCN (1.2 equiv) or KN_3 (1.5 equiv) in THF at room temperature overnight and isolated in 62% yield (for **3**) and 82% crude yield (for **4**).[18] Besides a minor shift of the PN ligand singlet resonance in the $^{31}P\{^1H\}$ NMR spectrum (C_6D_6) from $\delta = 9.9$ ppm for **1-I** to $\delta = 10.1$ ppm for **3** and a new broad singlet resonance at $\delta = 142.6$ ppm in the $^{13}C\{^1H\}$ NMR spectrum, a dominant absorption band in the IR spectrum at $\nu = 2008$ cm^{-1} indicated the coordination of thiocyanate.[19] Similarly, the coordination of the azide anion in complex **4** was inferred from a shift of the PN ligand resonance in the $^{31}P\{^1H\}$ NMR spectrum (C_6D_6) to $\delta = 5.1$ ppm and a strong IR absorption band at $\nu = 2113$ cm^{-1}.[20]

X-ray quality crystals of complex **2** could be grown by slow evaporation of a concentrated toluene solution at room temperature (Figure 1). To our great surprise, we found that the $[SCP]^-$ anion is neither solely S- nor P-coordinated, but instead is bound in a side-on η^3-fashion. Although this was unexpected, considering the fact that most of the negative charge density is located on the central carbon atom of a linear $[S\text{-}C{\equiv}P]^-$ unit,[13] the participation of all three atoms in the coordination to a strongly Lewis-acidic metal ion such as lanthanum(III) can be reasonably rationalized. In fact, significant coordination of the central carbon atom to lanthanum(III) is evident by comparing the La1–S1, La1–C1, and La1–P5 distances which lie at 3.036(2), 2.837(7), and 3.343(2) Å, respectively. These values also show that the $[SCP]^-$ anion is slightly tilted with respect to the lanthanum(III) ion in the solid state. The bond lengths within the $[SCP]^-$ anion are 1.607(7) and 1.568(7) Å for S1–C1 and C1–P5, respectively, resembling the values which are reported for the

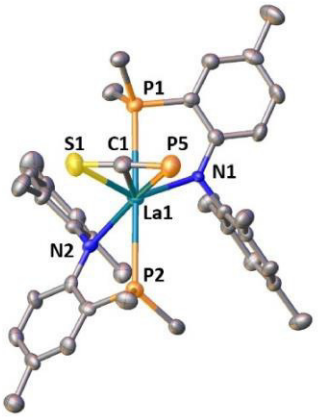

Figure 1. Thermal ellipsoid plot of complex **2**. Thermal ellipsoids are shown at a probability level of 50%. Hydrogen atoms have been omitted and ^{i}Pr groups truncated for clarity.[35]

free $[SCP]^-$ anion (S–C 1.613(4) Å and C–P 1.579(4) Å).[12,13] The S1–C1–P5 angle of 175.4(5)° in complex **2** is slightly more acute compared to 179.3(3)° in the free anion. X-ray quality crystals of reference compounds **3** and **4** were obtained either by gas diffusion of *n*-hexane into a C_6D_6 solution of **3** at room temperature overnight or by storing a concentrated toluene extract of **4** at room temperature for 24 h. In contrast to the $[SCP]^-$ anion, in both reference complexes, the thiocyanate and the azide anions do not engage in side-on coordination, but instead show a 1,3-bridging coordination mode in the solid state (see Figure S49). In this context, the dinuclear structures of **3** and **4** strongly suggest that the unique binding mode of the $[SCP]^-$ anion in **2** is not enforced by potentially unfavorable steric interactions, but rather results from the distinctive electronic structure of 2-phosphaethynthiolate.[13]

To gain further insights into the reasons for the stability of the unexpected side-on η^3-coordination mode of the $[SCP]^-$ ligand, we investigated complex **2** by means of density functional theory[21] with functionals PBE[22] and PBE0[23] together with def2-SV(P) bases;[24] for details concerning the calculations see the Supporting Information (Section 5). The total interaction energy between $[SCP]^-$ and the cationic moiety amounts to 523 kJ mol^{-1}, calculated as energy difference without structure relaxation for the fragments. The interaction is mainly ionic, as is evident from the indicators for covalent bonds being very small. For the sum of the contacts S–La, C–La and P–La, the Mulliken overlap population[25] is 0.01, and the shared electron number[26] is 0.12. An increase of the La–E–C angles (E = P or S) from the optimum structure results in a rise of energy (by approx. 20 kJ mol^{-1} for 15–20°) to a maximum at 65 kJ mol^{-1} and 75 kJ mol^{-1} for a linearly S-bound and P-bound isomer of complex **2**, respectively (Figure 2, Tables S3 and S4). The overall distance of the $[SCP]^-$ anion to the cation is larger for these configurations, and thus the favorable ionic interaction is smaller. For clarity we note that for none of the structures shown in Figure 2 significant covalent interactions between $[SCP]^-$ anion and the cation are observed. More strikingly however, for the η^3-coordination mode of $[SCP]^-$ ligand the LUMO of **2** corresponds to the antibonding $[SCP]^-$ π^*-orbital (Figure 3, top) with a significant admixture of the matching

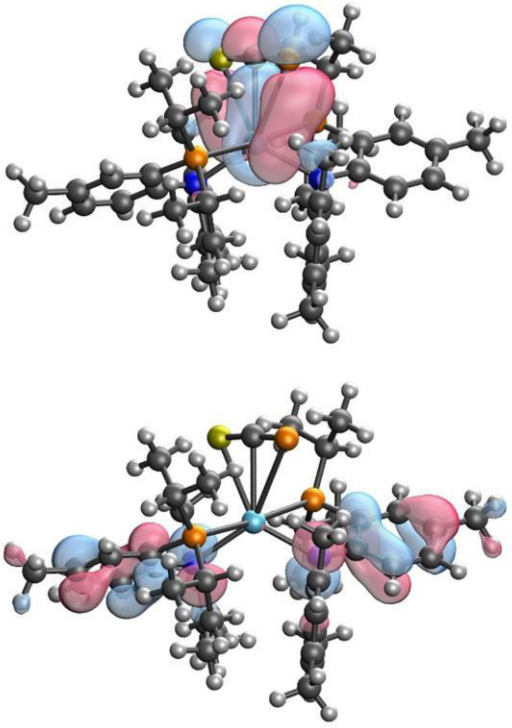

Figure 3. Frontier orbitals (HOMO, bottom; and LUMO, top) of complex **2**. Note that the LUMO of complex **2** reflects the bonding interaction of a π^*-orbital of the $[SCP]^-$ ligand with the matching d-orbital of the lanthanum(III) center.

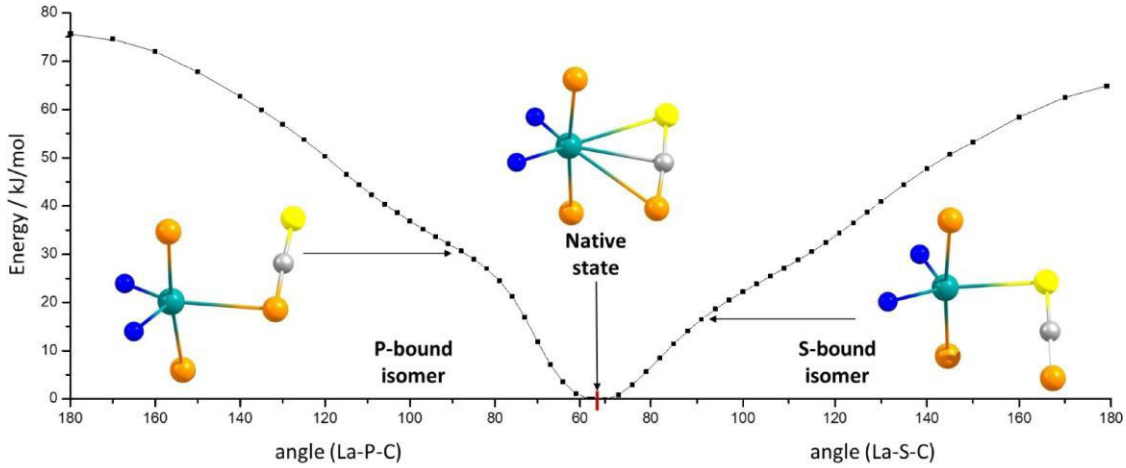

Figure 2. Relative energies of differently bound $[SCP]^-$ coordination isomers (P- vs. S-bound) compared to the side-on η^3-coordinated $[SCP]^-$ anion, depending on the La–E–C (E = P or S) bond angles. The PN supporting ligands have been truncated for clarity.

La(d) orbital (Mulliken contribution ca. 35 %). This should render complex **2** an ideal candidate to study the reactivity of the $[SCP]^-$ anion towards nucleophiles.

Since cyclic alkyl amino carbenes (CAACs) are generally known for their ability to stabilize highly reactive, exotic structural motifs of main group elements,[27] we decided to focus our efforts on this class of carbenes to achieve a potential functionalization of the $[SCP]^-$ ligand. Indeed, when the sterically encumbering 1-(2,6-diisopropylphenyl)-3-adamantyl-5,5-dimethyl-pyrrolidin-2-ylidene (^{Ad}CAAC) was employed, a highly selective reaction with **2** in aromatic (benzene, toluene) and aliphatic (*n*-pentane, *n*-hexane) solvents was observed at room temperature (Scheme 2).

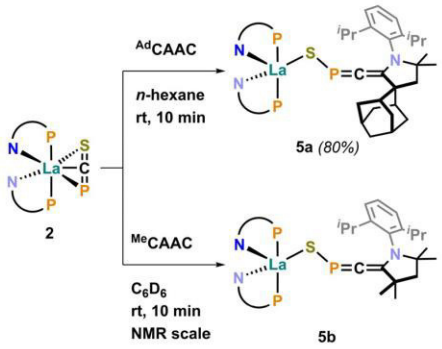

Scheme 2. Reactivity of complex **2** towards CAACs, yielding the "fulminate-type" complexes **5a** and **5b**.

Independent of the chosen solvent, the initially yellow reaction mixture immediately turned dark red upon addition of the CAAC (1 equiv), but returned to pale yellow within seconds. The $^{31}P\{^1H\}$ NMR spectrum showed that the singlet of the former $[SCP]^-$ ligand shifted from $\delta = -44.9$ ppm for **2** to $\delta = 139.4$ ppm for **5a**, indicating a major change of the electronic situation around the phosphorus atom. Product **5a** could be isolated in 80 % yield by crystallization (see below). Its $^{13}C\{^1H\}$ NMR spectrum (C_6D_6) showed a resonance at $\delta =$ 237.3 ppm (vs. $\delta = 191.8$ ppm for **2**). A doublet splitting of this resonance with a larger coupling constant ($^1J_{CP} = 34.9$ Hz for **5a** vs. $^1J_{CP} = 20.6$ Hz for **2**) suggested that the phosphorus atom of the newly formed ligand in **5a** remained bound to the carbon atom, apparently with a stronger electronic interaction than in **2**. Importantly, no typical $C_{carbene}$ resonance above $\delta = 200$ ppm could be detected for **5a**. Instead, ^1H–^{13}C HMBC NMR spectroscopic studies of the new compound revealed the former $C_{carbene}$ of the CAAC moiety to resonate at $\delta = 152.2$ ppm ($^2J_{CP} = 6.1$ Hz), indicating a nucleophilic attack of the CAAC at the central carbon atom of the $[SCP]^-$ ligand. This reactivity does not seem to depend on the steric profile of the CAAC, since the less sterically encumbering CAAC 1-(2,6-diisopropylphenyl)-3,3,5,5-tetramethyl-pyrrolidin-2-ylidene (^{Me}CAAC, Scheme 2, complex **5b**) gave comparable results (for details see Figures S34–S44 in the Supporting Information).

Due to the high solubility of **5b** even in non-polar solvents such as hexamethyldisiloxane (HMDSO), this product could not be crystallized under any conditions tested (see experimental section in the Supporting Information). On the contrary, X-ray quality crystals of **5a** could be grown from a concentrated *n*-hexane solution (see above) over three days at room temperature (Figure 4). Strikingly, the connectivity as

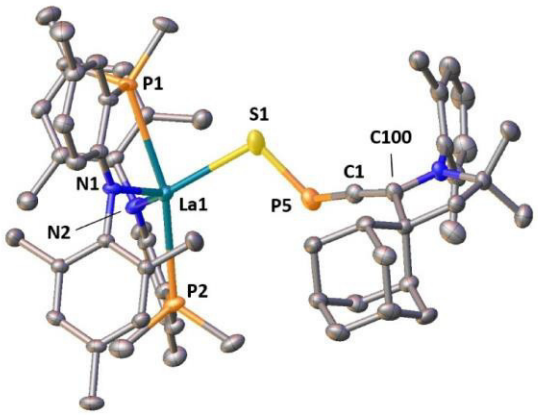

Figure 4. Thermal ellipsoid plot of complex **5a**. Thermal ellipsoids are shown at a probability level of 50 %. Hydrogen atoms have been omitted and ^{i}Pr groups truncated for clarity.[35]

found in the former $[SCP]^-$ ligand has changed to a formally CAAC-stabilized "fulminate-like" $[CPS]^-$ anion, with the sulfur atom binding κ^1 to lanthanum(III). A closer examination of the bond metrics within the $[^{Ad}CAAC{-}CPS]^-$ ligand of **5a** suggests a $C_{CAAC}{=}C{=}P{-}S^-$ heteroallene structure (C100–C1 1.36(2) Å; C1–P5 1.63(2) Å). While the $C_{CAAC}{=}C{=}P$ unit is almost linear (C100–C1–P5 173.8(1)°), the angle around the phosphorus atom is strongly bent (C1–P5–S1 111.1(5)°). The La1–S1 distance was found to be 2.950(2) Å and is slightly longer compared to the reported lanthanum–sulfur single bond in $(PN)_2La(SMes)$ (2.718(1) Å),[15] indicating a reduced negative charge on the sulfur atom and a potential partial conjugation of the $C_{CAAC}{=}C{=}P$ unit with the P–S bond. This would be in line with the P5–S1 bond length of 2.081(3) Å, which lies in between the values for a S=P double (ca. 1.95 Å)[28] and S–P single bond (ca. 2.12 Å).[29] A phosphaalkene thioether has recently been reported by Jones and Kollmann,[30] showing a S–P bond length (2.095(1) Å) comparable to the one determined in **5a**. Additionally, the solid state structure of **5a** reveals a close contact between the C*P*S phosphorus atom and one of the Dipp-CH_3 substituents of the formal ^{Ad}CAAC unit (P···C distance of approx. 3.682 Å). The retention of this close contact in solution can be inferred from a strong cross correlation peak between the corresponding Dipp-CH_3 protons and the C*P*S phosphorus atom at $\delta = 1.36$/139.3 ppm in the ^1H–^{31}P HMBC NMR spectrum of **5a** (Figure S33). Furthermore, in the $^{13}C\{^1H\}$ NMR spectrum a doublet splitting of the corresponding methyl resonance at $\delta =$ 27.0 ppm ($^{TS}J_{CP} = 9.8$ Hz) gives further evidence for a through-space interaction. Similar interactions have been previously shown to be harbingers of intriguing reactivity.[31] Finally, in contrast to the IR spectrum of **2**, complex **5a** shows

a distinct strong absorption band at $\nu = 1674\ cm^{-1}$, which serves as another useful indicator for the C=C=P–S$^-$ structural motif.

For a better understanding of the SCP to CPS rearrangement, the reaction pathway from **2** and ^{Ad}CAAC to **5a** was calculated and optimized as specified in detail in the Supporting Information. The results are shown in Figure 5,

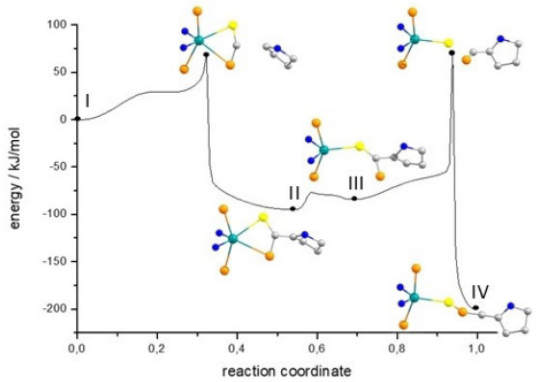

Figure 5. Optimized reaction pathway for the formation of **5a** out of **2** and ^{Ad}CAAC. Stationary points (black circles) are fully optimized; imaginary frequencies: TS1: 166i cm^{-1}, TS2: 244i cm^{-1}. The pathways between the stationary points are optimized by a nudged-elastic-band-type procedure. The PN ligands and the ^{Ad}CAAC fragment have been truncated for clarity.

with the stationary points (black circles) being fully optimized. Structures II–IV are local minima (no imaginary frequencies); for the two transition structures, which are ca. 50 kJ mol^{-1} higher in energy than the initial structure I, the imaginary frequencies amount to 166i cm^{-1} and 244i cm^{-1}. Finally, the pathways between the stationary points were optimized by a nudged-elastic-band-type procedure proposed by Plessow.[32] The initial step is the nucleophilic attack of the CAAC at the central carbon atom of the [SCP]$^-$ unit, leading to structure II, a thio-carboxphosphide (a heavy analogue of a carboxamide). A barrier of ca. 70 kJ mol^{-1} needs to be overcome to reach this intermediate structure, which is lower in energy by ca. 100 kJ mol^{-1} compared to structure I. Proceeding along the reaction coordinate, the next step is the dissociation of the phosphorus atom from the lanthanum(III) center, leading to structure III, which is higher in energy by ca. 20 kJ mol^{-1} than structure II and can be reached without a significant barrier. For the ultimate "flip" of the CP unit to the CPS arrangement in the fulminate anion (structure IV) another transition state must be passed, which is as high in energy as the first one. We note in passing that for this transition structure the covalent interactions between S and P or C are very weak, with shared electron numbers[26] of ca. 0.1 between S and the other two atoms; the two units are held together rather by ionic interactions between the negatively charged S and the positively charged P atom, as worked out in detail in the Supporting Information (Figure S52). The formation of a thermodynamically favored P–S bond might be one of the driving forces of this unusual rearrangement reaction with an overall energy gain of ca. 200 kJ mol^{-1}. The experimental observation that upon addition of the CAAC the reaction mixture initially turns dark red, before brightening up to a yellow color within the first 30 seconds of the reaction, is in line with the calculated electronic excitation spectra (Figure S51). The lowest-energy excitations for the product (structure IV) are at 2.8 eV, for the starting material (structure I) at 2.6 eV, but at only 2.2 eV for the "thio-carboxphosphide-type" intermediate structure II. Moreover, the character of the excitation for structure II is of a very different form compared to that of the other structures, see Figure S51. Similar carbene-induced rearrangements of the [OCP]$^-$ anion to "fulminate-like" structural motifs have been described by Grützmacher[33,34] and Goicoechea[6] and co-workers for systems based on phosphorus,[33] silicon,[34] and boron.[6] With the synthesis of complexes **5a** and **5b** we could extend this type of isomerization chemistry to a f-block metal-based system, yielding the first heavier group 15–group 16 analogue of a substituted "fulminate-like" anion.

Conclusion

We have presented the first stable coordination of the [SCP]$^-$ anion to a lanthanum(III) ion. Strikingly, the [SCP]$^-$ anion in complex **2** neither adopts a S- nor a P-bound end-on coordination mode as is typically encountered for other (hetero-)cumulene ligands such as, for example, thiocyanate or azide (complexes **3** and **4**). Instead, η^3-coordination was found, which had been an unknown coordination behavior for such (heavy) [*ChCPn*]$^-$ (*Ch* = Chalcogen, *Pn* = Pnictogen) anions up to this point and which is likely governed by the electronic structure of the [SCP]$^-$ anion. Despite the interactions between the lanthanum(III) complex fragment and the [SCP]$^-$ ligand being mostly ionic, theoretical studies revealed the LUMO of complex **2** to correspond mainly to a linear combination of the antibonding π^*-orbital of the [SCP]$^-$ ligand and the geometrically compatible lanthanum(III) d-orbital. Complex **2** therefore showed a high reactivity towards strongly nucleophilic CAACs, which resulted in the rearrangement and concomitant functionalization of the [SCP]$^-$ unit to give formally CAAC-stabilized heavy fulminate-type anions in the products **5a,b**. Future work will be dedicated to expanding our studies towards other heavy [*ChCPn*]$^-$ anions, to investigating different modes of reactivity of the side-on coordinate [SCP]$^-$ anion and to exploring the synthetic utility of the new fulminate-type anions (in, for example, cycloadditions) for disclosing new avenues of f- and heavy main group element chemistry.

Acknowledgements

We are grateful to the Daimler and Benz Foundation, the Fonds der Chemischen Industrie, the Young Academy of the North-Rhine-Westphalian Academy of Sciences, Humanities and the Arts, Paderborn University, the University of Innsbruck, and the University of Marburg for financial support. FT, SM, LB, and MB thank the DFG (TA 1357/1-1, MI

2561/1-1, and BA 4467/6-1) for financial support. Dr. Klaus Hübler from University of Stuttgart is kindly acknowledged for helpful discussions about the reactivity of the $[SCP]^-$ anion. Finally, SH would like to thank Prof. Dr. G. Becker whose lectures and never-ending passion for chemistry and (chemical) history inspired him to pursue a career in academia.

Keywords: cyanates · f-elements · lanthanides · main-group chemistry · phosphines

[1] J. M. Goicoechea, H. Grützmacher, *Angew. Chem. Int. Ed.* **2018**, *57*, 16968; *Angew. Chem.* **2018**, *130*, 17214.
[2] a) R. Suter, Z. Benkő, M. Bispinghoff, H. Grützmacher, *Angew. Chem. Int. Ed.* **2017**, *56*, 11226; *Angew. Chem.* **2017**, *129*, 11378; b) G. Becker, G. Heckmann, K. Huebler, W. Schwarz, *Z. Anorg. Allg. Chem.* **1995**, *621*, 34; c) D. W. N. Wilson, A. Hinz, J. M. Goicoechea, *Angew. Chem. Int. Ed.* **2018**, *57*, 2188; *Angew. Chem.* **2018**, *130*, 2210; d) T. Krachko, A. W. Ehlers, M. Nieger, M. Lutz, J. C. Slootweg, *Angew. Chem. Int. Ed.* **2018**, *57*, 1683; *Angew. Chem.* **2018**, *130*, 1699; e) M. M. Hansmann, D. A. Ruiz, L. L. Liu, R. Jazzar, G. Bertrand, *Chem. Sci.* **2017**, *8*, 3720; f) D. Heift, Z. Benkő, H. Grützmacher, *Angew. Chem. Int. Ed.* **2014**, *53*, 6757; *Angew. Chem.* **2014**, *126*, 6875.
[3] L. Liu, D. A. Ruiz, D. Munz, G. Bertrand, *Chem* **2016**, *1*, 147.
[4] L. N. Grant, D. J. Mindiola, *Chem. Eur. J.* **2019**, *25*, 16171.
[5] a) S. Bestgen, M. Mehta, T. C. Johnstone, P. W. Roesky, J. M. Goicoechea, *Chem. Eur. J.* **2020**, *26*, 9024; b) D. W. N. Wilson, J. Feld, J. M. Goicoechea, *Angew. Chem. Int. Ed.* **2020**, *59*, 20914; *Angew. Chem.* **2020**, *132*, 21100; c) D. W. N. Wilson, M. P. Franco, W. K. Myers, J. E. McGrady, J. M. Goicoechea, *Chem. Sci.* **2020**, *11*, 862; d) A. M. Tondreau, Z. Benkő, J. R. Harmer, H. Grützmacher, *Chem. Sci.* **2014**, *5*, 1545.
[6] D. W. N. Wilson, M. Mehta, M. P. Franco, J. E. McGrady, J. M. Goicoechea, *Chem. Eur. J.* **2020**, *26*, 13462.
[7] a) L. Liu, D. A. Ruiz, F. Dahcheh, G. Bertrand, R. Suter, A. M. Tondreau, H. Grützmacher, *Chem. Sci.* **2016**, *7*, 2335; b) J. M. Kieser, R. J. Gilliard, A. L. Rheingold, H. Grützmacher, J. D. Protasiewicz, *Chem. Commun.* **2017**, *53*, 5110; c) J. Abbenseth, M. Diefenbach, A. Hinz, L. Alig, C. Würtele, J. M. Goicoechea, M. C. Holthausen, S. Schneider, *Angew. Chem. Int. Ed.* **2019**, *58*, 10966; *Angew. Chem.* **2019**, *131*, 11082.
[8] S. Bestgen, Q. Chen, N. H. Rees, J. M. Goicoechea, *Dalton Trans.* **2018**, *47*, 13016.
[9] a) C. Camp, N. Settineri, J. Lefèvre, A. R. Jupp, J. M. Goicoechea, L. Maron, J. Arnold, *Chem. Sci.* **2015**, *6*, 6379; b) C. J. Hoerger, F. W. Heinemann, E. Louyriac, L. Maron, H. Grützmacher, K. Meyer, *Organometallics* **2017**, *36*, 4351; c) S. T. Liddle, J. Du, G. Balazs, A. J. Wooles, M. Scheer, *Angew. Chem. Int. Ed.* **2021**, *60*, 1197; *Angew. Chem.* **2021**, *133*, 1217; d) R. Magnall, G. Balázs, E. Lu, F. Tuna, A. J. Wooles, M. Scheer, S. T. Liddle, *Angew. Chem. Int. Ed.* **2019**, *58*, 10215; *Angew. Chem.* **2019**, *131*, 10321.
[10] G. Becker, W. Schwarz, N. Seidler, M. Westerhausen, *Z. Anorg. Allg. Chem.* **1992**, *612*, 72.
[11] G. Becker, K. Huebler, *Z. Anorg. Allg. Chem.* **1994**, *620*, 405.
[12] A. R. Jupp, M. B. Geeson, J. E. McGrady, J. M. Goicoechea, *Eur. J. Inorg. Chem.* **2016**, 639.
[13] F. Tambornino, A. Hinz, R. Köppe, J. M. Goicoechea, *Angew. Chem. Int. Ed.* **2018**, *57*, 8230; *Angew. Chem.* **2018**, *130*, 8362.
[14] a) Q. Yuan, F. Tambornino, A. Hinz, W. T. Borden, J. M. Goicoechea, B. Chen, X.-B. Wang, *Angew. Chem. Int. Ed.* **2019**, *58*, 15062; *Angew. Chem.* **2019**, *131*, 15206; b) G.-L. Hou, B. Chen, W. J. Transue, Z. Yang, H. Grützmacher, M. Driess, C. C. Cummins, W. T. Borden, X.-B. Wang, *J. Am. Chem. Soc.* **2017**, *139*, 8922.
[15] F. A. Watt, A. Krishna, G. Golovanov, H. Ott, R. Schoch, C. Wölper, A. G. Neuba, S. Hohloch, *Inorg. Chem.* **2020**, *59*, 2719.
[16] F. A. Watt, N. Dickmann, R. Schoch, S. Hohloch, *Inorg. Chem.* **2020**, *59*, 13621.
[17] F. A. Watt, K. N. McCabe, R. Schoch, L. Maron, S. Hohloch, *Chem. Commun.* **2020**, *56*, 15410.
[18] Please note that we only give crude yields for complex **4** as it easily decomposes upon drying to form intractable mixtures.
[19] R. E. Wilson, T. J. Carter, M. Autillo, S. Stegman, *Chem. Commun.* **2020**, *56*, 2622.
[20] a) M. A. Boreen, G. Rao, D. G. Villarreal, F. A. Watt, R. D. Britt, S. Hohloch, J. Arnold, *Chem. Commun.* **2020**, *56*, 4535; b) T. A. Bazhenova, V. S. Mironov, I. A. Yakushev, R. D. Svetogorov, O. V. Maximova, Y. V. Manakin, A. B. Kornev, A. N. Vasiliev, E. B. Yagubskii, *Inorg. Chem.* **2020**, *59*, 563; c) X.-L. Li, J. Wu, L. Zhao, W. Shi, P. Cheng, J. Tang, *Chem. Commun.* **2017**, *53*, 3026.
[21] TURBOMOLE V7.5 2020, a development of University of Karlsruhe and Forschungszentrum Karlsruhe GmbH, 1989–2007, TURBOMOLE GmbH, since 2007, available from http://www.turbomole.com.
[22] J. P. Perdew, K. Burke, M. Ernzerhof, *Phys. Rev. Lett.* **1996**, *77*, 3865.
[23] J. P. Perdew, M. Ernzerhof, K. Burke, *J. Chem. Phys.* **1996**, *105*, 9982.
[24] F. Weigend, R. Ahlrichs, *Phys. Chem. Chem. Phys.* **2005**, *7*, 3297.
[25] R. S. Mulliken, *J. Chem. Phys.* **1955**, *23*, 1833.
[26] R. Heinzmann, R. Ahlrichs, *Theor. Chim. Acta* **1976**, *42*, 33.
[27] a) M. Melaimi, R. Jazzar, M. Soleilhavoup, G. Bertrand, *Angew. Chem. Int. Ed.* **2017**, *56*, 10046; *Angew. Chem.* **2017**, *129*, 10180; b) M. Soleilhavoup, G. Bertrand, *Acc. Chem. Res.* **2015**, *48*, 256.
[28] S. R. Daly, J. R. Klaehn, K. S. Boland, S. A. Kozimor, M. M. MacInnes, D. R. Peterman, B. L. Scott, *Dalton Trans.* **2012**, *41*, 2163.
[29] N. Burford, B. W. Royan, P. S. White, *Acta Crystallogr. Sect. C* **1990**, *46*, 274.
[30] P. G. Jones, R. Bîrzoi, W.-W. Du Mont, S. Kollmann, CCDC 1055259: *Experimental Crystal Structure Determination*, Cambridge Crystallographic Data Centre, **2015**.
[31] M. E. Garner, B. F. Parker, S. Hohloch, R. G. Bergman, J. Arnold, *J. Am. Chem. Soc.* **2017**, *139*, 12935.
[32] P. Plessow, *J. Chem. Theory Comput.* **2013**, *9*, 1305.
[33] Z. Li, X. Chen, Z. Benkő, L. Liu, D. A. Ruiz, J. L. Peltier, G. Bertrand, C.-Y. Su, H. Grützmacher, *Angew. Chem. Int. Ed.* **2016**, *55*, 6018; *Angew. Chem.* **2016**, *128*, 6122.
[34] Z. Li, X. Chen, Y. Li, C.-Y. Su, H. Grützmacher, *Chem. Commun.* **2016**, *52*, 11343.
[35] Deposition Numbers 2039082 (**2**) and 2039085 (**5a**) contain the supplementary crystallographic data for this paper. These data are provided free of charge by the joint Cambridge Crystallographic Data Centre and Fachinformationszentrum Karlsruhe Access Structures service www.ccdc.cam.ac.uk/structures.

Manuscript received: January 13, 2021
Accepted manuscript online: February 10, 2021
Version of record online: March 11, 2021

4.3 References

(1) Liebig, J.; Gay-Lussac, J. L. Analyse du Fulminate d'Argent. *Ann. Chim. Phys.* **1824**, *25*, 285–311.
(2) Beck, W. The First Chemical Achievements and Publications by Justus von Liebig (1803−1873) on Metal Fulminates and Some Further Developments in Metal Fulminates and Related Areas of Chemistry. *Eur. J. Inorg. Chem.* **2003**, 4275–4288.
(3) Siegfried, R. The Chemical Revolution in the History of Chemistry. *Osiris* **1988**, *4*, 34–50.
(4) Szabadváry, F. Joseph Louis Gay-Lussac (1778–1850) and analytical chemistry. *Talanta* **1978**, *25*, 611–617.
(5) Esteban, S. Liebig–Wöhler Controversy and the Concept of Isomerism. *J. Chem. Educ.* **2008**, *85*, 1201.
(6) Wurzenberger, M. H. H.; Gruhne, M. S.; Lommel, M.; Braun, V.; Szimhardt, N.; Stierstorfer, J. Taming the Dragon: Complexation of Silver Fulminate with Nitrogen-Rich Azole Ligands. *Inorg. Chem.* **2020**, *59*, 17875–17879.
(7) Wöhler, F. Ueber künstliche Bildung des Harnstoffs. *Ann. Phys. Chem.* **1828**, *88*, 253–256.
(8) Warren, W. H. CONTEMPORARY RECEPTION OF WÖHLER'S DISCOVERY OF THE SYNTHESIS OF UREA. *J. Chem. Educ.* **1928**, *5*, 1539–1552.
(9) MILLER, S. L. A Production of Amino Acids Under Possible Primitive Earth Conditions. *Science* **1953**, *117*, 528–529.
(10) Urey, H. C. ON THE EARLY CHEMICAL HISTORY OF THE EARTH AND THE ORIGIN OF LIFE. *Proc. Natl. Acad. Sci. U. S. A.* **1952**, *38*, 351–363.
(11) Ferus, M.; Pietrucci, F.; Saitta, A. M.; Knížek, A.; Kubelík, P.; Ivanek, O.; Shestivska, V.; Civiš, S. Formation of nucleobases in a Miller–Urey reducing atmosphere. *Proc. Natl. Acad. Sci. U. S. A.* **2017**, *114*, 4306–4311.
(12) Richert, C. Prebiotic chemistry and human intervention. *Nat. Commun.* **2018**, *9*, 5177.
(13) Krishnamurthy, R. Giving Rise to Life: Transition from Prebiotic Chemistry to Protobiology. *Acc. Chem. Res.* **2017**, *50*, 455–459.
(14) Krishnamurthy, R. Life's Biological Chemistry: A Destiny or Destination Starting from Prebiotic Chemistry? *Chem. Eur. J.* **2018**, *24*, 16708–16715.
(15) Muchowska, K. B.; Moran, J. Peptide synthesis at the origin of life. *Science* **2020**, *370*, 767–768.
(16) Muchowska, K. B.; Chevallot-Beroux, E.; Moran, J. Recreating ancient metabolic pathways before enzymes. *Bioorg. Med. Chem.* **2019**, *27*, 2292–2297.
(17) Muchowska, K. B.; Varma, S. J.; Moran, J. Nonenzymatic Metabolic Reactions and Life's Origins. *Chem. Rev.* **2020**, *120*, 7708–7744.
(18) Hudson, R. L.; Moore, M. H.; Gerakines, P. A. THE FORMATION OF CYANATE ION (OCN^-) IN INTERSTELLAR ICE ANALOGS. *Astrophys. J.* **2001**, *550*, 1140–1150.
(19) Blanksby, S. J.; McAnoy, A. M.; Dua, S.; Bowie, J. H. Cumulenic and heterocumulenic anions: potential interstellar species? *Mon. Not. R. Astron. Soc.* **2001**, *328*, 89–100.
(20) Hudson, R. L.; Moore, M. H. Reactions of nitriles in ices relevant to Titan, comets, and the interstellar medium: formation of cyanate ion, ketenimines, and isonitriles. *Icarus* **2004**, *172*, 466–478.
(21) Martinez, R.; Bordalo, V.; da Silveira, E. F.; Boechat-Roberty, H. M. Production of NH_4^+ and OCN^- ions by the interaction of heavy-ion cosmic rays with CO–NH_3 interstellar ice. *Mon. Not. R. Astron. Soc.* **2014**, *444*, 3317–3327.
(22) Moreno, M. A.; Maté, B.; Rodríguez-Lazcano, Y.; Gálvez, O.; Gómez, P. C.; Herrero, V. J.; Escribano, R. The Structure and Spectroscopy of Cyanate and Bicarbonate Ions. Astrophysical Implications. *J. Phys. Chem. A* **2013**, *117*, 9564–9573.
(23) Park, J.-Y.; Woon, D. E. COMPUTATIONAL CONFIRMATION OF THE CARRIER FOR THE "XCN" INTERSTELLAR ICE BAND: OCN– CHARGE TRANSFER COMPLEXES. *Astrophys. J.* **2004**, *601*, L63–L66.
(24) Ritson, D.; Sutherland, J. D. Prebiotic synthesis of simple sugars by photoredox systems chemistry. *Nat. Chem.* **2012**, *4*, 895–899.

(25) Goicoechea, J. M.; Grützmacher, H. The Chemistry of the 2-Phosphaethynolate Anion. *Angew. Chem. Int. Ed.* **2018**, *57*, 16968–16994.
(26) Foust, A. S. Tellurocyanate: X-Ray Crystal Structure of the Bis(triphenylphosphoranylidene)ammonium Salt. *J. Chem. Soc., Chem. Commun.* **1979**, 414.
(27) Becker, G.; Schwarz, W.; Seidler, N.; Westerhausen, M. Acyl- und Alkylidenphosphane. XXXIII Lithoxy-methylidenphosphan · DME und -methylidinphosphan · 2 DME – Synthese und Struktur. *Z. Anorg. Allg. Chem.* **1992**, *612*, 72–82.
(28) Becker, G.; Hübler, K. Alkylidinphosphane und -arsane. I $[P{\equiv}C{-}S]^{-}[Li(dme)_3]^{+}$ – Synthese und Struktur. *Z. Anorg. Allg. Chem.* **1994**, *620*, 405–417.
(29) Puschmann, F. F.; Stein, D.; Heift, D.; Hendriksen, C.; Gal, Z. A.; Grützmacher, H.-F.; Grützmacher, H. Phosphination of Carbon Monoxide: A Simple Synthesis of Sodium Phosphaethynolate (NaOCP). *Angew. Chem. Int. Ed.* **2011**, *50*, 8420–8423.
(30) Jupp, A. R.; Goicoechea, J. M. The 2-Phosphaethynolate Anion: A Convenient Synthesis and [2+2] Cycloaddition Chemistry. *Angew. Chem. Int. Ed.* **2013**, *52*, 10064–10067.
(31) Jupp, A. R.; Geeson, M. B.; McGrady, J. E.; Goicoechea, J. M. Ambient-Temperature Synthesis of 2-Phosphathioethynolate, PCS^{-}, and the Ligand Properties of ECX^{-} (E = N, P; X = O, S). *Eur. J. Inorg. Chem.* **2016**, 639–648.
(32) Tambornino, F.; Hinz, A.; Köppe, R.; Goicoechea, J. M. A General Synthesis of Phosphorus- and Arsenic-Containing Analogues of the Thio- and Seleno-cyanate Anions. *Angew. Chem. Int. Ed.* **2018**, *57*, 8230–8234.
(33) Arlt, S.; Harloff, J.; Schulz, A.; Stoffers, A.; Villinger, A. Heavy Neutral and Anionic Pnictogen Thiocyanates. *Inorg. Chem.* **2019**, *58*, 5305–5313.
(34) Burmeister, J. L. LINKAGE ISOMERISM IN METAL COMPLEXES. *Coord. Chem. Rev.* **1968**, *3*, 225–245.
(35) Burmeister, J. AMBIDENTATE LIGANDS, THE SCHIZOPHRENICS OF COORDINATION CHEMISTY. *Coord. Chem. Rev.* **1990**, *105*, 77–133.
(36) Hsieh, C.-H.; Brothers, S. M.; Reibenspies, J. H.; Hall, M. B.; Popescu, C. V.; Darensbourg, M. Y. Ambidentate Thiocyanate and Cyanate Ligands in Dinitrosyl Iron Complexes. *Inorg. Chem.* **2013**, *52*, 2119–2124.
(37) Mayr, H.; Breugst, M.; Ofial, A. R. Farewell to the HSAB Treatment of Ambident Reactivity. *Angew. Chem. Int. Ed.* **2011**, *50*, 6470–6505.
(38) Pearson, R. G. Hard and Soft Acids and Bases. *J. Am. Chem. Soc.* **1963**, *85*, 3533–3539.
(39) Pearson, R. G. Acids and Bases. *Science* **1966**, *151*, 172–177.
(40) Huheey, J. E.; Keiter, E. A.; Keiter, R. L.; Medhi, O. K. *Inorganic Chemistry: Principles of Structure and Reactivity*, 4th ed.; Pearson: New Delhi, 2013.
(41) House, J. E. *INORGANIC CHEMISTRY*, 3rd ed.; Elsevier Academic Press: London, 2020.
(42) Heredia, A. Potassium Selenocyanate. *Synlett* **2014**, *25*, 748–749.
(43) Norbury, A. H. Coordination Chemistry of the Cyanate, Thiocyanate, and Selenocyanate Ions. *Adv. Inorg. Chem. Radiochem.* **1975**, *17*, 231–386.
(44) Greenwood, N. N.; Earnshaw, A. *Chemistry of the Elements*, 2nd ed.; Elsevier-Butterworth-Heinemann: Amsterdam, 2010.
(45) Burmeister, J. L.; Williams, L. E. Coordination Complexes of the Selenocyanate Ion. *Inorg. Chem.* **1966**, *5*, 1113–1117.
(46) Greenwood, N. N.; Little, R.; Sprague, M. J. The Tellurocyanate Ion, $TeCN^{-}$. *J. Chem. Soc.* **1964**, 1292–1295.
(47) Heift, D.; Benkő, Z.; Grützmacher, H. Coulomb repulsion versus cycloaddition: formation of anionic four-membered rings from sodium phosphaethynolate, Na(OCP). *Dalton Trans.* **2014**, *43*, 831–840.
(48) Grant, L. N.; Mindiola, D. J. The Rise of Phosphaethynolate Chemistry in Early Transition Metals, Actinides, and Rare-Earth Complexes. *Chem. Eur. J.* **2019**, *25*, 16171–16178.
(49) Hinz, A.; Goicoechea, J. M. The 2-Arsaethynolate Anion: Synthesis and Reactivity Towards Heteroallenes. *Angew. Chem. Int. Ed.* **2016**, *55*, 8536–8541.

(50) Hoerger, C. J.; Heinemann, F. W.; Louyriac, E.; Rigo, M.; Maron, L.; Grützmacher, H.; Driess, M.; Meyer, K. Cyaarside (CAs^-) and 1,3-Diarsaallendiide ($AsCAs^{2-}$) Ligands Coordinated to Uranium and Generated via Activation of the Arsaethynolate Ligand ($OCAs^-$). *Angew. Chem. Int. Ed.* **2019**, *58*, 1679–1683.
(51) Magnall, R.; Balázs, G.; Lu, E.; Kern, M.; van Slageren, J.; Tuna, F.; Wooles, A. J.; Scheer, M.; Liddle, S. T. Photolytic and Reductive Activations of 2-Arsaethynolate in a Uranium-Triamidoamine Complex: Decarbonylative Arsenic-Group Transfer Reactions and Trapping of a Highly Bent and Reduced Form. *Chem. Eur. J.* **2019**, *25*, 14246–14252.
(52) Hou, G.-L.; Chen, B.; Transue, W. J.; Yang, Z.; Grützmacher, H.; Driess, M.; Cummins, C. C.; Borden, W. T.; Wang, X.-B. Spectroscopic Characterization, Computational Investigation, and Comparisons of ECX^- (E = As, P, and N; X = S and O) Anions. *J. Am. Chem. Soc.* **2017**, *139*, 8922–8930.
(53) Yuan, Q.; Tambornino, F.; Hinz, A.; Borden, W. T.; Goicoechea, J. M.; Chen, B.; Wang, X.-B. Photoelectron Spectroscopy and Theoretical Studies of $PCSe^-$, $AsCS^-$, $AsCSe^-$, and $NCSe^-$: Insights into the Electronic Structures of the Whole Family of ECX^- Anions (E = N, P, As; X = O, S, Se). *Angew. Chem. Int. Ed.* **2019**, *58*, 15062–15068.
(54) Mathieu, F.; Metz, B.; Moras, D.; Weiss, R. Cavities in Macrobicyclic Ligands and Complexation Selectivity. Crystal Structures of Two Cryptates, $|Na^+ \subset 221|{\bullet}SCN^-$ and $|K^+ \subset 221|{\bullet}SCN^-$. *J. Am. Chem. Soc.* **1978**, *100*, 4412–4416.
(55) Reckeweg, O.; Schulz, A.; Leonard, B.; DiSalvo, F. J. Single-Crystal X-Ray Diffraction Study of Na[OCN] at 170 K and its Vibrational Spectra. *Z. Naturforsch.* **2010**, *65b*, 528–532.
(56) Bailey, R. A.; Michelsen, T. W.; Mills, W. N. Observations on the i.r. intensity criterion for the bonding mode in thiocyanate complexes. *J. Inorg. Nucl. Chem.* **1971**, *33*, 3206–3210.
(57) Beck, F.; Fehlhammer, W. P. PENTACARBONYLFULMINATOWOLFRAMAT, $NET_4[W(CNO)(CO)_5]$, UND ISOMERISIERUNG FULMINAT–ISOCYANAT AM METALL. *J. Organomet. Chem.* **1985**, *279*, C22–C24.
(58) Davidson, G. Vibrational Spectra of Some Co-ordinated Ligands. *Spectroscp. Prop. Inorg. Organomet. Compd.* **2006**, *38*, 284–347.
(59) Dodds, C. A.; Kennedy, A. R.; Thompson, R. Taming Copper(I) Cyanate and Selenocyanate with N-Heterocyclic Carbenes. *Eur. J. Inorg. Chem.* **2019**, 3581–3587.
(60) Kargol, J. A.; Crecely, R. W.; Burmeister, J. L. Carbon-13 Nuclear Magnetic Resonance Study of Coordinated Thiocyanate, Selenocyanate, and Cyanate. *Inorg. Chem.* **1979**, *18*, 2532–2535.
(61) Hübler, K.; Schwerdtfeger, P. Theoretical Studies of NMR Chemical Shifts and Vibrational Frequencies in λ^3-Phosphaalkynes P≡C−R. *Inorg. Chem.* **1999**, *38*, 157–164.
(62) Nakamoto, K. *Infrared and Raman Spectra of Inorganic and Coordination Compounds: Part B: Applications in Coordination, Organometallic, and Bioinorganic Chemistry*, 6th ed.; Wiley: Hoboken, N.J, 2009.
(63) Bestgen, S.; Chen, Q.; Rees, N. H.; Goicoechea, J. M. Synthesis and reactivity of rare-earth metal phosphaethynolates. *Dalton Trans.* **2018**, *47*, 13016–13024.
(64) Camp, C.; Settineri, N.; Lefèvre, J.; Jupp, A. R.; Goicoechea, J. M.; Maron, L.; Arnold, J. Uranium and thorium complexes of the phosphaethynolate ion. *Chem. Sci.* **2015**, *6*, 6379–6384.
(65) Liu, L.; Ruiz, D. A.; Dahcheh, F.; Bertrand, G.; Suter, R.; Tondreau, A. M.; Grützmacher, H. Isolation of Au-, Co-η^1PCO and Cu-η^2PCO complexes, conversion of an Ir-η^1PCO complex into a dimetalladiphosphene, and an interaction-free PCO anion. *Chem. Sci.* **2016**, *7*, 2335–2341.
(66) Grant, L. N.; Pinter, B.; Manor, B. C.; Grützmacher, H.; Mindiola, D. J. A Scandium-Stabilized Diisophosphaethynolate Ligand: $[OCPPCO]^{4-}$. *Angew. Chem. Int. Ed.* **2018**, *57*, 1049–1052.
(67) Magnall, R.; Balázs, G.; Lu, E.; Tuna, F.; Wooles, A. J.; Scheer, M.; Liddle, S. T. Trapping of a Highly Bent and Reduced Form of 2-Phosphaethynolate in a Mixed-Valence Diuranium-Triamidoamine Complex. *Angew. Chem. Int. Ed.* **2019**, *58*, 10215–10219.
(68) Goher, M. A. S.; Mautner, F. A. The first copper(I) complex containing a cyanato ligand. Synthesis and structural characterization of $[Cu(pyz)(\mu\text{-}NCO)]_n$ (pyz = pyrazine). *J. Chem. Soc., Dalton Trans.* **1999**, 1923–1924.

(69) Biswas, B.; Raghavaiah, P.; Aliaga-Alcalde, N.; Chen, J.-D.; Ghosh, R. Syntheses, crystal structures and properties of a new family of isostructural and isomorphous compounds of type [M(L)(NCS)$_3$] [M = La, Gd, Tb and Dy; L = a neutral hexadentate Schiff base]. *Polyhedron* **2010**, *29*, 2716–2721.
(70) Jeremies, A.; Gruschinski, S.; Schmorl, S.; Severin, T.; Kersting, B. Selective coordination of cyanate and thiocyanate in the end-on mode: synthesis, structures and properties of [Ni$^{II}_2$L($\mu_{1,1}$-NCO)]$^+$ and [Ni$^{II}_2$L($\mu_{1,1}$-NCS)]$^+$ (L^{2-} = macrocyclic N_6S_2 ligand). *New J. Chem.* **2018**, *42*, 7630–7639.
(71) Liu, J.; Meyers, E. A.; Cowan, J. A.; Shore, S. G. The cyanate ion as a bridging ligand between lanthanide and transition metals. Formation of one-dimensional extended arrays {(DMF)$_6$Ln$_2$Ni(NCO)$_8$}$_\infty$ (Ln = Sm, Eu) and monomeric complexes (DMF)$_8$Ln$_2$Ni(NCO)$_8$ (Ln = Sm, Eu) with three bridging cyanate ligands. *Chem. Commun.* **1998**, 2043–2044.
(72) Siai, A.; Hämmerle, L.; Ströbele, M.; Enseling, D.; Jüstel, T.; Meyer, H.-J. Structure, polymorphism and luminescence of cyanate iodides MI(OCN) (M = Ba, Eu, and Sr). *Dalton Trans.* **2020**, *49*, 14133–14139.
(73) Alidori, S.; Heift, D.; Santiso-Quinones, G.; Benkő, Z.; Grützmacher, H.; Caporali, M.; Gonsalvi, L.; Rossin, A.; Peruzzini, M. Synthesis and Characterization of Terminal [Re(XCO)(CO)$_2$(triphos)] (X = N, P): Isocyanate versus Phosphaethynolate Complexes. *Chem. Eur. J.* **2012**, *18*, 14805–14811.
(74) Boreen, M. A.; McCabe, K. N.; Lohrey, T. D.; Watt, F. A.; Maron, L.; Hohloch, S.; Arnold, J. Uranium Metallocene Azides, Isocyanates, and Their Borane-Capped Lewis Adducts. *Inorg. Chem.* **2020**, *59*, 8580–8588.
(75) Grant, L. N.; Krzystek, J.; Pinter, B.; Telser, J.; Grützmacher, H.; Mindiola, D. J. Finding a soft spot for vanadium: a P-bound OCP ligand. *Chem. Commun.* **2019**, *55*, 5966–5969.
(76) Xiong, Y.; Yao, S.; Szilvási, T.; Ballestero-Martínez, E.; Grützmacher, H.; Driess, M. Unexpected Photodegradation of a Phosphaketenyl-Substituted Germyliumylidene Borate Complex. *Angew. Chem. Int. Ed.* **2017**, *56*, 4333–4336.
(77) Gilliard, R. J.; Heift, D.; Benkő, Z.; Keiser, J. M.; Rheingold, A. L.; Grützmacher, H.; Protasiewicz, J. D. An isolable magnesium diphosphaethynolate complex. *Dalton Trans.* **2018**, *47*, 666–669.
(78) Westerhausen, M.; Schneiderbauer, S.; Piotrowski, H.; Suter, M.; Nöth, H. Synthesis of alkaline earth metal bis(2-phosphaethynolates). *J. Organomet. Chem.* **2002**, *643-644*, 189–193.
(79) Wilson, D. W. N.; Goicoechea, J. M. Synthesis of metallophosphaalkenes by reaction of organometallic nucleophiles with a phosphaethynolato-borane. *Chem. Commun.* **2019**, *55*, 6842–6845.
(80) Pak, Y.; Woods, R. C.; Peterson, K. A. Coupled cluster spectroscopic properties and isomerization pathway for the cyanate/fulminate isomer pair, NCO$^-$/CNO$^-$. *J. Chem. Phys.* **1997**, *106*, 5123–5132.
(81) Poppinger, D.; Radom, L.; Pople, J. A. A Theoretical Study of the CHNO Isomers. *J. Am. Chem. Soc.* **1977**, *99*, 7806–7816.
(82) Shapley, W. A.; Bacskay, G. B. A Gaussian-2 Quantum Chemical Study of CHNO: Isomerization and Molecular Dissociation Reactions. *J. Phys. Chem. A* **1999**, *103*, 6624–6631.
(83) Vega-Vega, Á.; Largo, A.; Redondo, P.; Barrientos, C. Structure and Spectroscopic Properties of [Mg,C,N,O] Isomers: Plausible Astronomical Molecules. *ACS Earth Space Chem.* **2017**, *1*, 158–167.
(84) Li, W.-K.; Baker, J.; Radom, L. Rearrangement of the Fulminate Anion (CNO$^-$) to the Cyanate Anion (OCN$^-$): Possible Intermediacy of the Oxazirinyl Anion. *Aust. J. Chem.* **1986**, *39*, 913–921.
(85) Trickes, G.; Meier, H. Catalyzed Rearrangement of Nitrile Oxides to Isocyanates. *Angew. Chem. Int. Ed.* **1977**, *16*, 555.
(86) Li, Z.; Chen, X.; Benkő, Z.; Liu, L.; Ruiz, D. A.; Peltier, J. L.; Bertrand, G.; Su, C.-Y.; Grützmacher, H. N-Heterocyclic Carbenes as Promotors for the Rearrangement of Phosphaketenes to Phosphaheteroallenes: A Case Study for OCP to OPC Constitutional Isomerism. *Angew. Chem. Int. Ed.* **2016**, *55*, 6018–6022.
(87) Li, Z.; Chen, X.; Li, Y.; Su, C.-Y.; Grützmacher, H. N-Heterocyclic carbene phosphaketene adducts as precursors to carbene–phosphinidene adducts and a rearranged π-system. *Chem. Commun.* **2016**, *52*, 11343–11346.

(88) Wilson, D. W. N.; Mehta, M.; Franco, M. P.; McGrady, J. E.; Goicoechea, J. M. Linkage Isomerism Leading to Contrasting Carboboration Chemistry: Access to Three Constitutional Isomers of a Borylated Phosphaalkene. *Chem. Eur. J.* **2020**, *26*, 13462–13467.
(89) Li, Z.; Chen, X.; Bergeler, M.; Reiher, M.; Su, C.-Y.; Grützmacher, H. A stable phosphanyl phosphaketene and its reactivity. *Dalton Trans.* **2015**, *44*, 6431–6438.
(90) Donath, M.; Hennersdorf, F.; Weigand, J. J. Recent highlights in mixed-coordinate oligophosphorus chemistry. *Chem. Soc. Rev.* **2016**, *45*, 1145–1172.

Summary & Outlook

In summary, the results obtained during the doctoral research study and presented in this dissertation emphasize the potential of anilidophosphines in lanthanide coordination chemistry (Figure 5.1).

Chapter 1 introduced the straight-forward synthetic routes to lanthanide(III) bis(anilidophosphine) chloride or iodide complexes, covering the early (La^{3+}, Ce^{3+}, Nd^{3+}), middle (Gd^{3+}, Tb^{3+}, Dy^{3+}) and late (Lu^{3+}) lanthanides. The halide complexes were shown to be valuable precursors for the synthesis of a series of pentacoordinate lanthanide(III) mesitylchalcogenide as well as –pnictide complexes, which contained rare examples of a thiolato and a primary phosphido ligand at lanthanum(III) or lutetium(III).

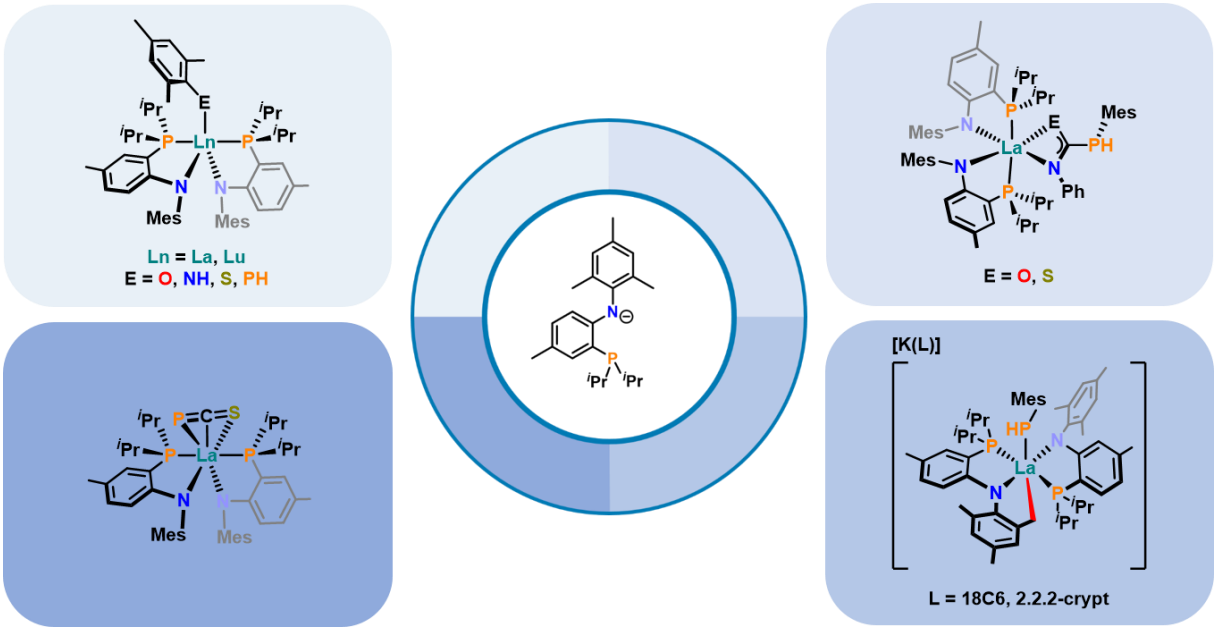

Figure 5.1. Overview of the main achievements of the doctoral research study by using an anilidophosphine ligand (middle) in lanthanide coordination chemistry: Synthesis of (rare) pentacoordinate lanthanide(III) mesitylchalcogenide and –pnictide complexes (top left; see Chapter 1), construction of phospha(thio)ureate bridging ligands by insertion chemistry (top right; see Chapter 2), experimental evidence for a transient (terminal) lanthanum(III) phosphinidene complex (bottom right; see Chapter 3), and unique η^3-coordination and functionalization of the $[SCP]^-$ anion at lanthanum(III) (bottom left; see Chapter 4).

The insertion reactivity of the La–P bond in the mesitylphosphido complex was further investigated in **Chapter 2** and led to the isolation of rare lanthanum(III)-bound phospha(thio)ureate ligands with a *PH* group. Using this functional group, a versatile route for the construction of novel types of phosphaureate-bridged heterobimetallic lanthanide–coinage-metal systems was devised and successfully demonstrated.

In **Chapter 3** the attempted synthesis of the first terminal lanthanide(III) phosphinidene complex by deprotonation of the lanthanum(III) mesitylphosphido complex was described. Although the observed C–H-activation to the final product prevented the isolation of a phosphinidene, a detailed mechanistic study including theoretical calculations and a deuteration experiment gave strong evidence for the occurrence of a terminal La=P double bond during the reaction.

Finally, in **Chapter 4** the first stable coordination of the 2-phosphaethynthiolate anion was achieved with the bis(anilidophosphine) lanthanum(III) framework. A combined experimental and theoretical study enabled a rationalization of the unexpected and unique η^3-coordination mode. In addition, the first selective functionalization of this heterocumulene anion with CAACs gave access to previously unknown, heavy fulminate-type anions with a $^{-}$[S–P=C=C_{CAAC}] structural motif.

To conclude, the anilidophosphine-supported lanthanide(III) complexes of this work have been proven to be versatile precursors for the isolation of rare and exotic structural motifs featuring the heavy main group elements phosphorus and sulfur. Given the results obtained in this work, the following directions for expanding the fundamental research on anilidophosphine-supported lanthanide(III) complexes can be regarded as worthwile.

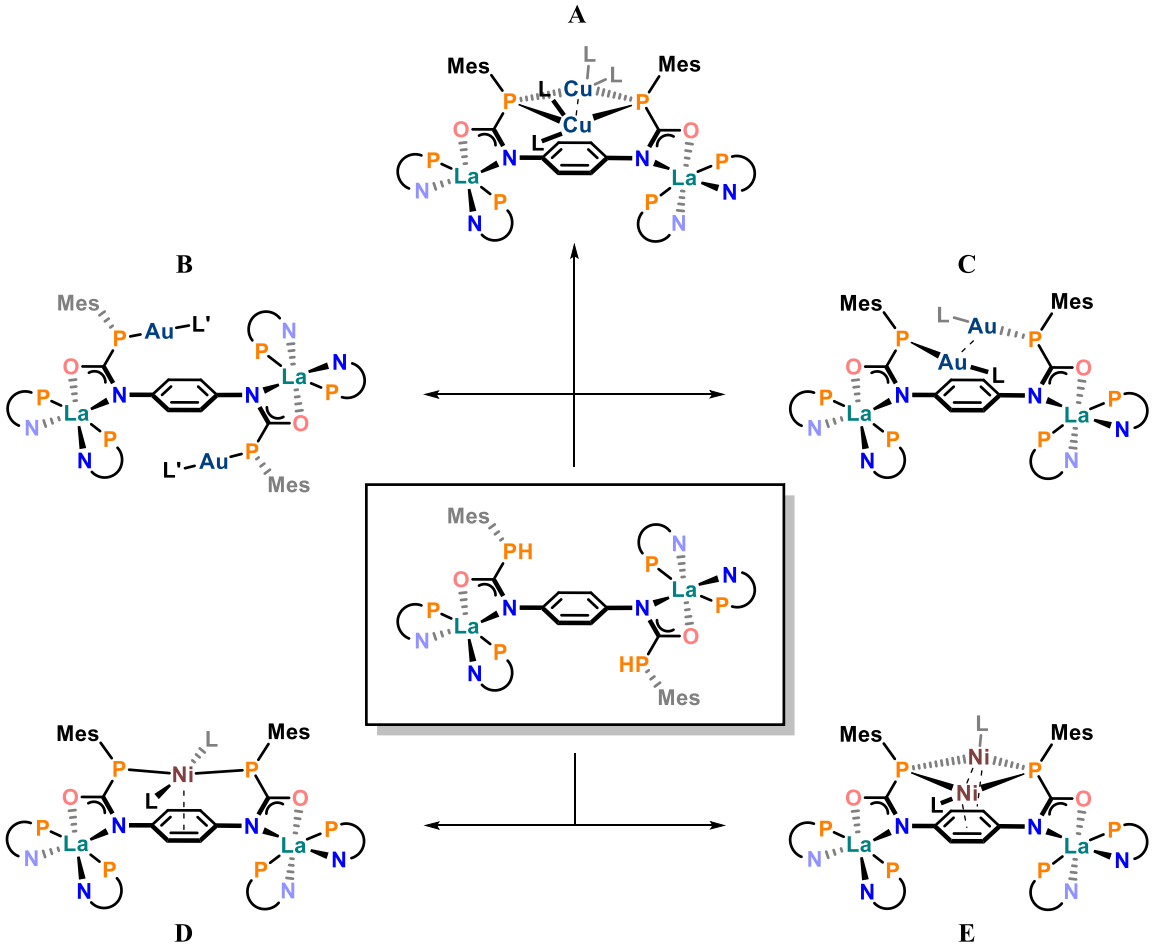

Scheme 5.1. Conceived bimetallic lanthanum(III) complex (highlighted structure in the middle) from the double insertion of 1,4-phenylene diisocyanate into the La–P bonds of two equivalents of $(PN)_2La(PHMes)$ and its potential for accessing new types of heterotrimetallic or –tetrametallic lanthanum–transition-metal systems (structures **A** – **E**). No reagents or conditions shown for clarity; L = phosphine ligand (*e.g.*, PMe_3), L' = carbene ligand (*e.g.*, IPr, IMes).

Capitalizing on the disclosed route to heterobimetallic phosphaureate-bridged lanthanide–coinage-metal complexes in Chapter 2, analogous systems with other Ln^{3+} ions (Ce^{3+}, Nd^{3+}, Gd^{3+}, Tb^{3+} or Dy^{3+}), which exhibit more favorable photophysical properties for luminescence in the visible or near infrared part of

the electromagnetic spectrum, should be accessible in a straight-forward manner. A subsequent comprehensive photophysical study with these Ln^{3+} ions would be the first for lanthanide–coinage metal carbene systems. In the light of the current interest in luminescent coinage-metal carbene complexes with high quantum yields and the preliminary results for the reference complexes with La^{3+}, which suggest strong fluorescence in the UV region (see Appendix, Figure A50), such a study seems very promising. Furthermore, variation of the bridging ligand will be an obvious follow-up project to pursue. For instance, the reaction of 1,4-phenylene diisocyanate with two equivalents of $(PN)_2La(PHMes)$ will very likely yield the double insertion product highlighted in Scheme 5.1. Deprotonation followed by transmetallation with suitable transition-metal halides should allow the synthesis of intriguing heterotrimetallic or –tetrametallic systems. In case of the coinage-metal systems, the steric profile of the supporting ligand (*e.g.*, PMe_3 *vs.* IPr) will likely affect the arrangement of the coinage-metal ions (structures **A** and **C** *vs.* **B**). The introduction of other transition-metal ions such as Ni^{2+} or Ni^+, which are also good matches for the "soft" phosphaureate P-donor atoms and known to coordinate to phenylene units,[1] could be feasible as well (structures **D** and **E**).

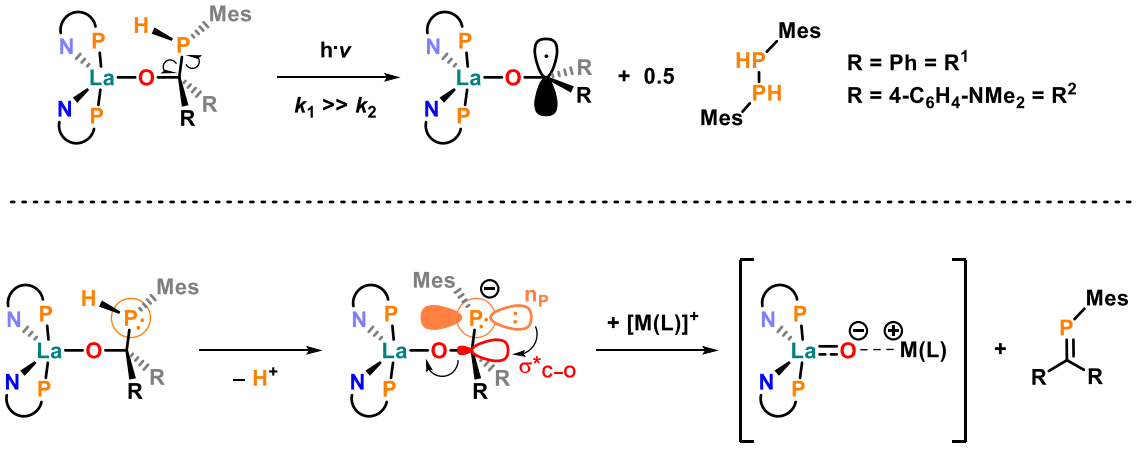

Scheme 5.2. Proposed homolytic C–P bond cleavage to account for the experimentally observed light-induced formation of 1,2-dimesityldiphosphine from $(PN)_2La\{OCR_2(PHMes)\}$ (top; conditions: C_6D_6, rt, visible light or UV lamp (254 nm, 4 W); rate constants k_1 for R = R^1 and k_2 for R = R^2). Potential alternative follow-up chemistry through deprotonation of the *PH* group and negative hyperconjugation of a phosphorus lone pair with the σ^*_{C-O} orbital (bottom; simplified equations, base and conditions not specified). R = Ph or 4-C_6H_4-NMe_2; M = alkali metal; L = crown ether or cryptand.

Following up on the insertion chemistry presented in Chapter 2, preliminary experiments concerning the insertion of benzophenone derivatives into the La–P bond of $(PN)_2La(PHMes)$ point to an intriguing photochemically induced redox chemistry of the phosphahemiketal-like products (see Appendix, Figure A36). While the phenyl-substituted system is sensitive to visible or UV light and gives a strongly violet-colored solution under slow release of 1,2-dimesityldiphosphine, the corresponding 4-dimethylamino-phenyl version does not react in significant rates under the same conditions. The P–P bond coupling under retention of the *PH* groups as well as the dark violet color reminiscent of the ketyl radical suggest a homolytic C–P bond cleavage process under concomitant formation of a lanthanum(III) ketyl complex (Scheme 5.2, top). Although ligand-centered redox reactions have been reported by the

Arnold group for thorium(IV) phosphido and bipyridine complexes,[2] using light as an external stimulus for a P–C bond cleavage would be a new reactivity pattern for f-element complexes of this kind. Judging from the rather slow reaction rates obtained so far, more complete conversions to the final products by the use of an UV reactor and a crystallographic as well as an EPR spectroscopic characterization of the lanthanum(III) product complex can be seen as the next logical steps. Theoretical calculations will be key to understand the mechanism and the influence of the aryl-substituent on the C–P bond dissociation enthalpy. Furthermore, it seems worth inquiring whether the benzophenone insertion products show negative hyperconjugation of the phosphorus lone pair with the σ^*_{C-O} orbital, which could be taken advantage of for the synthesis of the first (terminal or alkali metal-capped) lanthanide(III) oxo complex (Scheme 5.2, bottom). In this case deprotonation of the *PH* group might cause a P=C double bond formation and at the same time the cleavage of the C–O single bond, which would yield a phosphaalkene and the $[La{=}O]^-$ moiety (stabilized by interactions with $[M(L)]^+$) as thermodynamically favorable products. If successful, this reaction would not only yield a lanthanide(III) oxo complex, but would also mimic the reactivity of a phosphinidene complex.

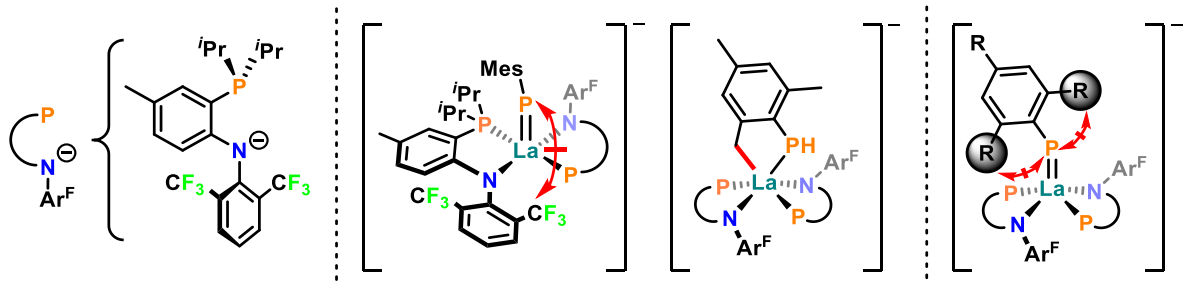

Figure 5.2. Optimization of the anilidophosphine supporting ligand for the isolation of a terminal lanthanum(III) phosphinidene complex (left), possible outcomes of the deprotonation of (PN-Ar^F)$_2$La(PHMes) with the new supporting ligand (middle) and further adjustments of the substituents at the phosphido/phosphinidene ligand (right; R = 2,4,6-$C_6H_2(^tBu)_3$ or 2,4,6-$C_6H_2(C_6H_5)_3$). The red double arrows with the perpendicular bar in the middle indicate blocked activation pathways (middle left; right).

Concerning the isolation of a [La=P] unit, the results of Chapter 3 clearly suggest an exchange of the methyl substituents *ortho* to the nitrogen atom of the anilidophosphine supporting ligand. In this context, trifluoromethyl groups are good candidates (Figure 5.2, left), since they are far less prone to be activated by nucleophiles (such as phosphinidenes) and similar in size to methyl groups (middle left). The latter factor is particularly important to avoid too much additional steric strain in the system and thus guarantee the integrity of the bis(anilidophosphine) lanthanum(III) framework. Still, further adjustments of the phosphido ligand may have to be made, in case a C–H activation at the methyl groups in *ortho* position to the phosphorus atom becomes more favorable (middle right). In this case a change from mesityl to supermesityl (2,4,6-$C_6H_2(^tBu)_3$) or 2,4,6-triphenylphenyl might still be sterically tolerated by the system and sufficient to block potential C–H activation pathways (right). The synthesis of a primary phosphido complex would also solve the problem of an undesired C–H activation at the phosphido ligand upon deprotonation and will probably lead to intriguing results.

The first stable coordination of 2-phosphaethynthiolate from Chapter 4 opens up new possibilities for heavy main group element lanthanide chemistry with $[ChCPn]^-$ ions. Based on the NBO atomic charges in $[SeCP]^-$, $[SCAs]^-$ and $[SeCAs]^-$,[3] which are comparable to those found in $[SCP]^-$, these three heterocumulene anions should all favor the same side-on η^3-coordination to a Lewis-acidic lanthanum(III) ion (Scheme 5.3, top left). It will be of great fundamental interest to see whether carbene-induced rearrangement reactions can occur for these anions as well and if the heavy fulminate-type reaction products are stable enough to be isolated and further investigated.

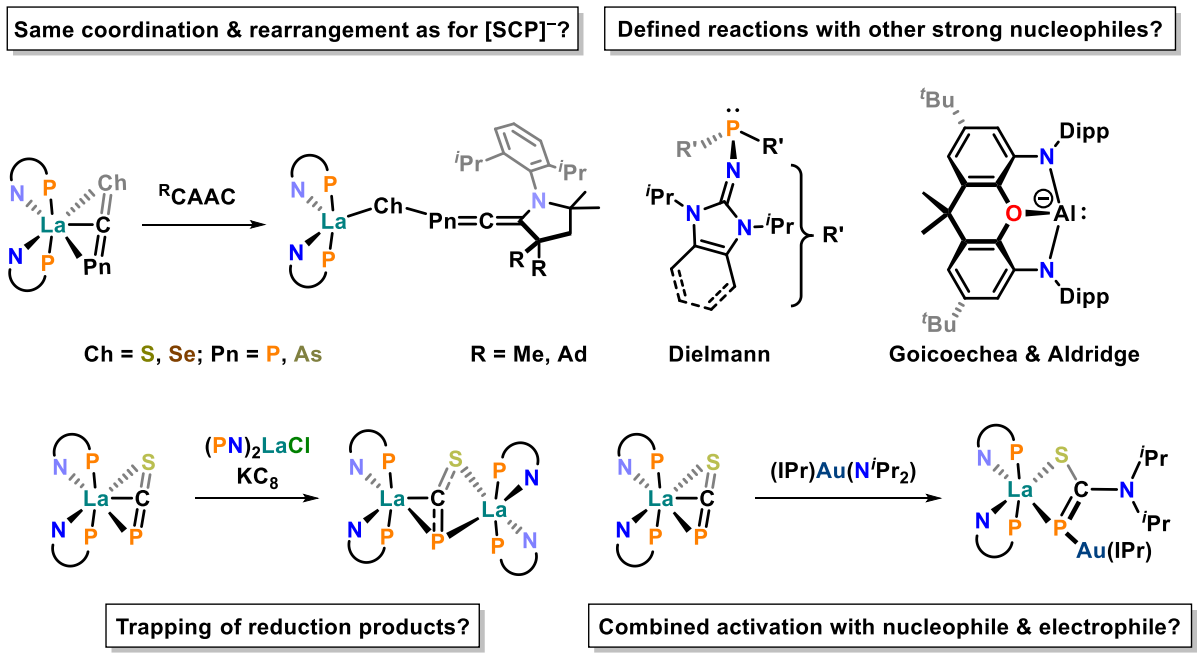

Scheme 5.3. Questions arising with regard to the coordination chemistry of other $[ChCPn]^-$ anions at the $[(PN)_2La]^+$ framework (top left) and possible scenarios for other types of follow-up chemistry of $(PN)_2La(SCP)$ (top right and bottom). $[K(2.2.2\text{-crypt})]^+$ counter-ion of the aluminyl anion (top right) is not shown for clarity. The reaction equation at the bottom left corner is not balanced for simplicity and only the chloride starting complex is shown. At the bottom right corner only one possible product with the $[Au(IPr)]^+$ fragment being bound to the phosphorus atom is shown.

Besides these comparative studies, alternative modes of reactivity can be explored for the already available $[SCP]^-$ complex, especially with other strong nucleophiles or under reducing conditions: For instance, reactions with aluminyl anions[4,5] or very electron rich, neutral imidazolin-2-ylidenamino-substituted phosphines (IAPs)[6,7] in corporation with the Goicoechea & Aldridge groups or the Dielmann group will almost certainly lead to some intriguing follow-up chemistry of $(PN)_2La(SCP)$ (top right). A reduction of a mixture of $(PN)_2La(SCP)$ and $(PN)_2LaX$ (X = Cl, I) with potassium graphite could potentially yield a dinuclear complex with a reduced, bridging $[SCP]^{2-}$ unit (bottom left), in analogy to Liddle and co-workers' $[OCP]^{2-}$ and $[OCAs]^{2-}$ bridged, dinuclear complexes of uranium.[8,9] In addition, the reaction with easily prepared nucleophilic gold(I) carbene complex $(IPr)Au(N^iPr_2)$[10] is a promising candidate to study: The gold(I) carbene fragment is well suited to bind to either phosphorus or sulfur and can assist in stabilizing the product after nucleophilic attack of the amide ligand at the central carbon atom of the $[SCP]^-$ anion (bottom right). It would also lead to another novel class of intriguing

heterobimetallic lanthanide–coinage-metal complexes. In case the functionalization works well for this test system, the accessibility of the coordinated $[SCP]^-$ ligand for frustrated Lewis pairs (FLPs) will deserve an investigation, since they also combine a nucleophilic part necessary for the interaction with the LUMO of $(PN)_2La(SCP)$ and an electrophilic part for trapping and stabilizing the product of the nucleophilic addition. Furthermore, the cycloaddition chemistry of the η^3-bound $[SCP]^-$ with unsaturated functional groups presents an attractive area of research, especially because of the potential incorporation of this exotic ligand into organic substrates. Under a judicious choice of reagents and conditions, even catalytic reactions involving the 2-phosphaethynthiolate ligand may be devised in the future. Finally, photochemical studies should not be neglected in order to uncover the full scope of the $(PN)_2La(SCP)$ complex.

References

(1) Koch, F.; Schubert, H.; Sirsch, P.; Berkefeld, A. Binuclear complexes of Ni(I) from 4-terphenyldithiophenol. *Dalton Trans.* **2015**, *44*, 13315–13324.
(2) Garner, M. E.; Arnold, J. Reductive Elimination of Diphosphine from a Thorium–NHC–Bis(phosphido) Complex. *Organometallics* **2017**, *36*, 4511–4514.
(3) Tambornino, F.; Hinz, A.; Köppe, R.; Goicoechea, J. M. A General Synthesis of Phosphorus- and Arsenic-Containing Analogues of the Thio- and Seleno-cyanate Anions. *Angew. Chem. Int. Ed.* **2018**, *57*, 8230–8234.
(4) Hicks, J.; Vasko, P.; Goicoechea, J. M.; Aldridge, S. Synthesis, structure and reaction chemistry of a nucleophilic aluminyl anion. *Nature* **2018**, *557*, 92–95.
(5) Hicks, J.; Vasko, P.; Goicoechea, J. M.; Aldridge, S. The Aluminyl Anion: A New Generation of Aluminium Nucleophile. *Angew. Chem. Int. Ed.* **2021**, *60*, 1702–1713.
(6) Wünsche, M. A.; Mehlmann, P.; Witteler, T.; Buß, F.; Rathmann, P.; Dielmann, F. Imidazolin-2-ylidenaminophosphines as Highly Electron-Rich Ligands for Transition-Metal Catalysts. *Angew. Chem. Int. Ed.* **2015**, *54*, 11857–11860.
(7) Buß, F.; Mehlmann, P.; Mück-Lichtenfeld, C.; Bergander, K.; Dielmann, F. Reversible Carbon Dioxide Binding by Simple Lewis Base Adducts with Electron-Rich Phosphines. *J. Am. Chem. Soc.* **2016**, *138*, 1840–1843.
(8) Magnall, R.; Balázs, G.; Lu, E.; Kern, M.; van Slageren, J.; Tuna, F.; Wooles, A. J.; Scheer, M.; Liddle, S. T. Photolytic and Reductive Activations of 2-Arsaethynolate in a Uranium-Triamidoamine Complex: Decarbonylative Arsenic-Group Transfer Reactions and Trapping of a Highly Bent and Reduced Form. *Chem. Eur. J.* **2019**, *25*, 14246–14252.
(9) Magnall, R.; Balázs, G.; Lu, E.; Tuna, F.; Wooles, A. J.; Scheer, M.; Liddle, S. T. Trapping of a Highly Bent and Reduced Form of 2-Phosphaethynolate in a Mixed-Valence Diuranium-Triamidoamine Complex. *Angew. Chem. Int. Ed.* **2019**, *58*, 10215–10219.
(10) Johnson, M. W.; Shevick, S. L.; Toste, F. D.; Bergman, R. G. Preparation and reactivity of terminal gold(I) amides and phosphides. *Chem. Sci.* **2013**, *4*, 1023–1027.

Supporting Information
for
Chapter 1

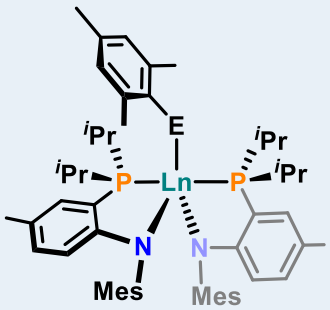

Ln = La, Lu
E = O, NH, S, PH

Supporting Information

A Monoanionic Anilidophosphine Ligand in Lanthanide Chemistry: Scope, Reactivity and Electrochemistry

Fabian A. Watt,[a] Athul Krishna,[a] Grigoriy Golovanov,[a] Holger Ott,[b] Roland Schoch,[a] Christoph Wölper,[c] Adam G. Neuba,[a] and Stephan Hohloch[a,d]*

[a] Paderborn University, Faculty of Science, Department of Chemistry, Warburger Straße 100, 33098 Paderborn, Germany.
[b] Bruker AXS GmbH, Training Center, Östliche Rheinbrückenstraße 49, 76187 Karlsruhe, Germany.
[c] University of Essen-Duisburg, Faculty of Chemistry, Universitätsstraße 5-7, 45141 Essen, Germany.
[d] Leopold-Franzens-University Innsbruck, Faculty of Chemistry and Pharmacy, Institute of General, Inorganic and Theoretical Chemistry, Innrain 80-82, 6020 Innsbruck.

Table of contents

1. Experimental section

General Remarks. If not otherwise mentioned, all transformations were carried out under inert conditions using the Schlenk technique or an argon filled glovebox. Solvents were dried by a MBraun SPS system and stored over activated molecular sieves (3 Å) for at least 24 h. The deuterated solvents C_6D_6 and THF-d_8 were dried by storage over activated molecular sieves (3 Å) for at least 24 h. IR spectra were recorded at room temperature under inert conditions using a Bruker Vertex 70 with ATR equipment. If not otherwise stated, the NMR spectra were collected at 298 K on a Bruker AV-500 or an Ascent 700 spectrometer using a J-Young NMR tube. All chemical shifts (δ) are reported in ppm. ^{1}H and ^{13}C chemical shifts were calibrated to residual solvent peaks. ^{15}N chemical shifts were calibrated to liquid ammonia (NH_3). ^{29}Si chemical shifts were calibrated to tetramethylsilane ($Si(CH_3)_4$, TMS). ^{31}P chemical shifts were calibrated to phosphoric acid (H_3PO_4, 85% in water). Elemental analyses were performed using an Elementar vario microcube instrument at the University of Paderborn. Cyclic and square-wave voltammograms at room temperature were performed with the PAR101 potentiostat from Metrohm in DCM/0.1 M $[NBu_4]PF_6$ (analyte conc. = 0.001 mol l^{-1}) with the following three electrode arrangement: Pt working electrode (1 mm diameter), Ag wire reference electrode and Pt wire counter electrode. Ferrocene was added as internal standard after the measurements and all potentials are referenced relative to the $Fc/[Fc]^+$ couple. All measurements were carried out under argon atmosphere, with absolute and degassed solvents. Magnetic moments have been obtained using the Evans method at room temperature. For details and literature please see section 6 in the SI below. Lanthanide chlorides were activated by refluxing in THF at 80 °C for 2 d. After concentrating the suspensions under reduced pressure, respectively, *n*-pentane was added, the solid **$LnCl_3(THF)_x$** isolated by filtration and left for drying in the glovebox atmosphere. The amount x of THF present in the samples was determined by elemental analysis. **HPN**,[1] **LiPN**,[1] **LiNHMes**,[2] **KPHMes**,[3,4] **KOMes**,[5] **KSMes**,[6] **KCp***,[7] **NaCp**[8] and **Ce(HMDS)$_3$**[9,10] were synthesized following literature known procedures. **KHMDS**, **Me$_3$SiI** and **La(HMDS)$_3$** were used as received.

Synthetic Procedures.

*Preparation of **KPN**.* A solution of **HPN** (1 eq., 16.46 mmol, 5.62 g,) in *n*-hexane (200 mL) was added to solid **KHMDS** (0.95 eq., 15.64 mmol, 3.12 g) at room temperature. The resulting yellow suspension was stirred at room temperature for 14 h. All volatile components were removed *in vacuo*. The yellow powder was resuspended in 100 mL *n*-hexane and the suspension filtered. The pale yellow solid was further washed with 2 x 100 mL *n*-hexane as well as 100 mL *n*-pentane and then dried *in vacuo*. Single crystals suitable for X-ray structure determination were obtained by storing a C_6D_6 solution of **KPN** (40 mg in 0.6 mL) at room temperature for 2 h. Yield: 5.47 g (14.4 mmol, 88%); ^{1}H NMR (C_6D_6, 298 K, 700 MHz, in ppm): δ = 6.98 (s, C*H*$_{Ar}$, 2 H), 6.87 (m, C*H*$_{Ar}$, 1 H), 6.69 (dd, $^{3}J_{HH}$ = 8.3 Hz, $^{4}J_{HH}$ = 1.8 Hz, C*H*$_{Ar}$, 1 H), 5.86 (m, C*H*$_{Ar}$, 1 H), 2.35 (s, C*H*$_{3Ar}$, 3 H), 2.23 (s, C*H*$_{3Ar}$, 3 H), 2.13 (s, C*H*$_{3Ar}$, 6 H), 2.04 (dsept, $^{2}J_{HP}$ = 3.2 Hz, $^{3}J_{HH}$ = 6.9 Hz, C*H*$_{iPr}$, 2 H), 1.13 (d, $^{3}J_{HH}$ = 6.9 Hz, C*H*$_{3iPr}$, 3 H), 1.11 (d, $^{3}J_{HH}$ = 6.9 Hz, C*H*$_{3iPr}$, 3 H), 1.06 (d, $^{3}J_{HH}$ = 6.9 Hz, C*H*$_{3iPr}$, 3 H), 1.05 (d, $^{3}J_{HH}$ = 6.9 Hz, C*H*$_{3iPr}$, 3 H); ^{31}P{^{1}H} NMR (C_6D_6, 298 K 283 MHz, in ppm): δ = –6.1 (s, *P*N^{-}, 1 P).

*General procedure for the preparation of **Ln(PN)$_2$Cl** (**1-Ln**) complexes.* A solution of **LiPN** (2 eq.) in toluene was added to solid **$LnCl_3(THF)_x$** (1 eq.) at room temperature. The resulting pale yellow suspension was stirred at 110 °C for 17 h. The reaction mixture was then allowed to cool down to room temperature and filtered through a medium porosity frit. The filtrate was evaporated to dryness *in vacuo* and the remaining solid resuspended in *n*-hexane. The solid was filtered off, washed with *n*-hexane and dried *in vacuo* to yield the analytically pure product.

Preparation of ***La(PN)$_2$Cl (1-La)****.* Following the general procedure, **LiPN** (2 eq., 37.12 mmol, 12.89 g) and **LaCl$_3$(THF)$_{1.2}$** (1 eq., 18.56 mmol, 6.16 g) were refluxed in toluene (180 mL). For the resuspension 100 mL of *n*-hexane were applied and the solid was washed with 2 x 30 mL of *n*-hexane after filtration. Single crystals suitable for X-ray structure determination were obtained by slow evaporation of a concentrated solution of **1-La** in diethyl ether in an atmosphere of *n*-hexane at room temperature. Yield: 12.45 g (14.48 mmol, 78%); ^{1}H NMR (C_6D_6, 298 K, 700 MHz, in ppm): δ = 6.89 (m, C*H*$_{Ar}$, 2 H), 6.86 (br. s, C*H*$_{Ar}$, 4 H), 6.82 (dd, $^3J_{HH}$ = 8.4 Hz, $^4J_{HH}$ = 1.9 Hz, C*H*$_{Ar}$, 2 H), 5.65 (m, C*H*$_{Ar}$, 2 H), 2.28 (br. s, C*H*$_{3Ar}$, 12 H), 2.16 (s, C*H*$_{3Ar}$, 6 H), 2.12 (s, C*H*$_{3Ar}$, 6 H), 1.87 (br. s, C*H*$_{iPr}$, 4 H), 1.21 (br. s, C*H*$_{3iPr}$, 12 H), 0.93 (br. s, C*H*$_{3iPr}$, 12 H); ^{13}C{^{1}H} NMR (C_6D_6, 298 K, 176 MHz, in ppm): δ = 160.3 (*pseudo*-t, J_{CP} = 11.4 Hz, C_{qAr}), 138.3 (br. s, C_{qAr}), 137.5 (s, C_{qAr}), 135.4 (s, C_{qAr}), 133.9 (s, *C*H$_{Ar}$), 133.4 (s, *C*H$_{Ar}$), 131.8 (s, *C*H$_{Ar}$), 123.3 (s, C_{qAr}), 114.3 (d, J_{CP} = 6.7 Hz, C_{qAr}), 114.2 (d, J_{CP} = 6.7 Hz, C_{qAr}), 112.7 (*pseudo*-t, J_{CP} = 3.8 Hz, *C*H$_{Ar}$), 22.8 (br. s, *C*H$_{iPr}$), 21.0 (s, *C*H$_{3Ar}$), 20.6 (s, *C*H$_{3Ar}$), 19.6 (*pseudo*-t, J_{CP} = 5.3 Hz, *C*H$_{3iPr}$), 19.2 (s, *C*H$_{3Ar}$), 17.6 (br. s, *C*H$_{3iPr}$); ^{31}P{^{1}H} NMR (C_6D_6, 298 K, 283 MHz, in ppm): δ = 9.2 (s, *P*N$^-$, 2 P); elemental analysis (in %): $C_{44}H_{62}N_2P_2ClLa$: calcd.: C 61.79, H 7.31, N 3.28; found: C 61.43, H 6.96, N 3.31.

Preparation of ***Ce(PN)$_2$Cl (1-Ce)****.* Following the general procedure, **LiPN** (2 eq., 0.8 mmol, 278 mg) and **CeCl$_3$(THF)** (1 eq., 0.4 mmol, 127 mg) were refluxed in toluene (10 mL). After work-up, a yellow powder was obtained. Single crystals suitable for X-ray determination were obtained by slow evaporation of a diethyl ether solution of **1-Ce** at room temperature. Yield: 208 mg (0.243 mmol, 61%); ^{1}H NMR (C_6D_6, 298 K, 700 MHz, in ppm): δ = 24.3 (s, 3 H), 22.6 (s, 2 H), 18.4 (s, 3 H), 10.3 (s, 9 H), –3.7 (s, 9 H), –5.0 (s, 4 H), –9.9 (s, 12 H), –10.9 (s, 12 H) (Due to the paramagnetic nature of the Ce(III) ion we have not been able to observe all protons in the ^{1}H NMR spectrum of the complex.); ^{31}P{^{1}H} NMR (C_6D_6, 298 K, 283 MHz, in ppm): δ = 426.7 (br. s, *P*N$^-$, 2 P); ^{31}P{^{1}H} NMR (THF-d$_8$, 298 K, 283 MHz, in ppm): δ = 423.2 (br. s, *P*N$^-$, 2 P); Evans Method: μ_{eff} = 2.23 μ_B (C_6D_6); elemental analysis (in %): $C_{44}H_{62}N_2P_2ClCe \cdot C_7H_8$: calcd.: C 64.57, H 7.44, N 2.95; found: C 64.32, H 7.33, N 3.40.

Preparation of ***Nd(PN)$_2$Cl (1-Nd)****.* Following the general procedure, **LiPN** (2 eq., 1 mmol, 347 mg) and **NdCl$_3$(THF)** (1 eq., 0.5 mmol, 161 mg) were refluxed in toluene (10 mL). After work-up, the complex directly crystallizes out of the concentrated toluene solution as green crystals. Single crystals suitable for X-ray determination were obtained by slow evaporation of a diethyl ether solution of **1-Nd** at room temperature. Yield: 250 mg (0.29 mmol, 58%); Evans Method: μ_{eff} = 3.38 μ_B; elemental analysis (in %): $C_{44}H_{62}N_2P_2ClNd$: calcd.: C 61.41, H 7.26, N 3.26; found: C 60.61, H 7.02, N 3.13.

Preparation of ***Gd(PN)2Cl (1-Gd)****.* Following the general procedure, **LiPN** (2 eq., 1 mmol, 347 mg) and **GdCl$_3$(THF)$_2$** (1 eq., 0.5 mmol, 204 mg) were refluxed in toluene (10 mL). After work-up, the complex directly crystallizes out of the concentrated toluene solution as yellow crystals which are suitable for X-ray structure determination. Yield: 277 mg (0.317 mmol, 63%); Evans Method: μ_{eff} = 8.24 μ_B; elemental analysis (in %): $C_{44}H_{62}N_2P_2ClGd$: calcd.: C 60.49, H 7.15, N 3.21; found: C 59.97, H 6.84, N 3.15.

Preparation of ***Tb(PN)$_2$Cl (1-Tb)****.* Following the general procedure, **LiPN** (2 eq., 1 mmol, 347 mg) and **TbCl$_3$(THF)$_3$** (1 eq., 0.5 mmol, 241 mg) were refluxed in toluene (10 mL). After work-up, the complex directly crystallizes out of the concentrated toluene solution as yellow crystals which are suitable for X-ray structure determination. Yield: 255 mg (0.291 mmol, 58%); Evans Method: μ_{eff} = 9.37 μ_B; elemental analysis (in %): $C_{44}H_{62}N_2P_2ClTb$: calcd.: C 60.38, H 7.14, N 3.20; found: C 60.69, H 7.15, N 3.13.

Preparation of ***Dy(PN)$_2$Cl (1-Dy)****.* Following the general procedure, **LiPN** (2 eq., 1 mmol, 347 mg) and **DyCl$_3$(THF)$_3$** (1 eq., 0.5 mmol, 241 mg) were refluxed in toluene (10 mL). After work-up, a yellow powder was obtained. Single crystals suitable for X-ray determination were obtained by slow evaporation of a diethyl ether solution of **1-Dy** at room temperature. Yield: 273 mg (0.31 mmol, 62%);

Evans Method: μ_{eff} = 10.02 μ_B; elemental analysis (in %): $C_{44}H_{62}N_2P_2ClDy$: calcd.: C 60.13, H 7.11, N 3.19; found: C 60.48, H 6.80, N 3.32.

Preparation of ***Lu(PN)₂Cl (1-Lu)***. Following the general procedure, **LiPN** (2 eq., 1.52 mmol, 530 mg) and **$LuCl_3(THF)_{2.75}$** (1 eq., 0.760 mmol, 360 mg) were refluxed in toluene (50 mL). The product was found to be analytically pure after evaporation of the solvent, wherefore no further washing with *n*-hexane was necessary. (Note: The product is slightly soluble in *n*-hexane and excessive washing can result in diminishing the yields.) The product was obtained as a beige powder. Single crystals suitable for X-ray structure determination were obtained by slow evaporation of solvent from a concentrated *n*-pentane solution of **1-Lu** at room temperature. Yield: 482 mg (0.54 mmol, 71%); ^{1}H NMR (C_6D_6, 282 K, 700 MHz, in ppm): δ = 6.85 (br. s, C*H*$_{Ar}$, 4 H), 6.83 (dd, $^3J_{HH}$ = 8.7 Hz, $^4J_{HH}$ = 1.7 Hz, C*H*$_{Ar}$, 2 H), 6.80 (m, C*H*$_{Ar}$, 2 H), 5.85 (m, C*H*$_{Ar}$, 2 H), 2.64 (br. s, C*H*$_{3Ar}$, 6 H), 2.28 (br. s, C*H*$_{3Ar}$, 6 H), 2.20 (br. s, C*H*$_{iPr}$, 2 H), 2.16 (s, C*H*$_{3Ar}$, 6 H), 2.14 (s, C*H*$_{3Ar}$, 6 H), 1.46 (br. s, C*H*$_{3iPr}$, 6 H), 1.18 (br. s, C*H*$_{3iPr}$, 6 H), 0.82 (br. s, C*H*$_{3iPr}$, 6 H), 0.76 (br. s, C*H*$_{3iPr}$, 6 H), 0.51 (br. s, C*H*$_{iPr}$, 2 H); ^{13}C{^{1}H} NMR (C_6D_6, 282 K, 176 MHz, in ppm): δ = 161.2 (*pseudo*-t, J_{CP} = 9.8 Hz, C_{qAr}), 142.9 (s, C_{qAr}), 138.5 (br. s, C_{qAr}), 137.3 (br. s, C_{qAr}), 134.1 (s, C_{qAr}), 133.8 (s, *C*H$_{Ar}$), 133.1 (s, *C*H$_{Ar}$), 130.6 (br. s, *C*H$_{Ar}$), 123.7 (s, C_{qAr}), 113.5 (*pseudo*-t, J_{CP} = 3.2 Hz, *C*H$_{Ar}$), 111.5 (d, J_{CP} = 9.7 Hz, C_{qAr}), 111.4 (d, J_{CP} = 10.3 Hz, C_{qAr}), 21.7 (br. s, *C*H$_{iPr}$), 21.6 (br. s, *C*H$_{iPr}$), 21.5 (s, *C*H$_{3iPr}$), 20.9 (s, *C*H$_{3Ar}$), 20.6 (br. s, *C*H$_{3Ar}$), 20.5 (s, *C*H$_{3Ar}$), 19.9 (br. s, *C*H$_{3Ar}$), 18.8 (br. s, *C*H$_{3iPr}$), 18.0 (br. s, *C*H$_{3iPr}$), 15.3 (br. s, *C*H$_{3iPr}$); ^{31}P{^{1}H} NMR (C_6D_6, 282 K, 283 MHz, in ppm): δ = 5.0 (s, *P*N$^-$, 2 P); elemental analysis (in %): $C_{44}H_{62}N_2P_2ClLu$: calcd.: C 59.29, H 7.01, N 3.14; found: C 58.96, H 6.71, N 3.35.

Preparation of ***La(PN)₂I (2-La)***. To a solution of **1-La** (1 eq., 1 mmol, 855 mg) in toluene (25 mL) was added **Me_3SiI** (5 eq., 5 mmol, 1 g) at room temperature. The resulting reaction mixture was stirred at room temperature for 18 h. The slightly turbid solution was filtered and all volatile components of the filtrate removed *in vacuo* to yield analytically pure product as an off-white solid. Yield: 858 mg (0.91 mmol, 91%); ^{1}H NMR (C_6D_6, 298 K, 700 MHz, in ppm): δ = 6.86 (m, C*H*$_{Ar}$, 2 H), 6.84 (s, C*H*$_{Ar}$, 4 H), 6.81 (dd, $^3J_{HH}$ = 8.5 Hz, $^4J_{HH}$ = 1.8 Hz, C*H*$_{Ar}$, 2 H), 5.60 (m, C*H*$_{Ar}$, 2 H), 2.31 (br. s, C*H*$_{3Ar}$, 12 H), 2.16 (s, C*H*$_{3Ar}$, 6 H), 2.10 (s, C*H*$_{3Ar}$, 6 H), 1.85 (br. s, C*H*$_{iPr}$, 4 H), 1.22 (br. s, C*H*$_{3iPr}$, 12 H), 0.93 (br. s, C*H*$_{3iPr}$, 12 H); ^{13}C{^{1}H} NMR (C_6D_6, 298 K, 176 MHz, in ppm): δ = 160.1 (*pseudo*-t, J_{CP} = 11.6 Hz, C_{qAr}), 138.6 (br. s, C_{qAr}), 136.9 (s, C_{qAr}), 135.7 (s, C_{qAr}), 133.9 (s, *C*H$_{Ar}$), 133.3 (s, *C*H$_{Ar}$), 131.9 (s, *C*H$_{Ar}$), 123.8 (s, C_{qAr}), 114.4 (*pseudo*-t, J_{CP} = 7.3 Hz, C_{qAr}), 112.8 (*pseudo*-t, J_{CP} = 3.7 Hz, *C*H$_{Ar}$), 22.6 (br. s, *C*H$_{iPr}$), 20.9 (s, *C*H$_{3Ar}$), 20.6 (s, *C*H$_{3Ar}$), 19.9 (s, *C*H$_{3Ar}$), 19.8 (br. s, *C*H$_{3iPr}$), 17.8 (br. s, *C*H$_{3iPr}$); ^{31}P{^{1}H} NMR (C_6D_6, 298 K, 283 MHz, in ppm): δ = 9.9 (s, *P*N$^-$, 2 P); elemental analysis (in %): $C_{44}H_{62}N_2P_2ILa$: calcd.: C 55.82, H 6.60, N 2.96; found: C 56.28, H 6.52, N 3.13.

Preparation of ***Lu(PN)₂I (2-Lu)***. To a solution of **1-Lu** (1 eq., 0.5 mmol, 446 mg) in toluene (20 mL) was added **Me_3SiI** (7 eq., 3.5 mmol, 700 mg) at room temperature. The resulting reaction mixture was stirred at 60 °C for 3 d. The slightly turbid solution was cooled down to room temperature and filtered. Removal of all volatile components *in vacuo* yielded analytically pure product as an off-white solid. Yield: 492 mg (0.5 mmol, quant.); ^{1}H NMR (C_6D_6, 283 K, 700 MHz, in ppm): δ = 6.84 (m, C*H*$_{Ar}$, 2 H), 6.83 (s, C*H*$_{Ar}$, 4 H), 6.78 (m, C*H*$_{Ar}$, 2 H), 5.84 (m, C*H*$_{Ar}$, 2 H), 2.76 (br. s, C*H*$_{3Ar}$, 6 H), 2.28 (br. s, C*H*$_{iPr}$, 2 H), 2.24 (br. s, C*H*$_{3Ar}$, 6 H), 2.15 (s, C*H*$_{3Ar}$, 6 H), 2.14 (s, C*H*$_{3Ar}$, 6 H), 1.56 (br. s, C*H*$_{3iPr}$, 6 H), 1.25 (br. s, C*H*$_{3iPr}$, 6 H), 0.83 (br. s, C*H*$_{3iPr}$, 6 H), 0.71 (br. s, C*H*$_{3iPr}$, 6 H), 0.40 (br. s, C*H*$_{iPr}$, 2 H); ^{13}C{^{1}H} NMR (C_6D_6, 283 K, 176 MHz, in ppm): δ = 160.9 (*pseudo*-t, J_{CP} = 9.7 Hz, C_{qAr}), 142.8 (s, C_{qAr}), 138.5 (br. s, C_{qAr}), 137.8 (br. s, C_{qAr}), 134.3 (s, C_{qAr}), 133.8 (s, *C*H$_{Ar}$), 133.4 (s, *C*H$_{Ar}$), 130.7 (br. s, *C*H$_{Ar}$), 124.2 (s, *C*H$_{Ar}$), 113.8 (*pseudo*-t, J_{CP} = 4.0 Hz, *C*H$_{Ar}$), 111.6 (d, J_{CP} = 9.4 Hz, *C*H$_{Ar}$), 111.5 (d, J_{CP} = 9.7 Hz, *C*H$_{Ar}$), 22.0 (br. s, *C*H$_{3iPr}$), 21.9 (br. s, *C*H$_{Ar}$), 21.6 (br. s, *C*H$_{iPr}$), 20.8 (s, *C*H$_{3Ar}$), 20.5 (s, *C*H$_{3Ar}$), 20.2 (br. s, *C*H$_{3Ar}$), 19.6 (br. s, *C*H$_{3iPr}$), 17.8 (br. s, *C*H$_{3iPr}$), 15.3 (br. s, *C*H$_{3iPr}$); ^{31}P{^{1}H} NMR (C_6D_6, 300 K, 283 MHz, in ppm): δ = 6.6 (s, *P*N$^-$, 2 P); elemental analysis (in %): $C_{44}H_{62}N_2P_2ILu$: calcd.: C 53.77, H 6.36, N 2.85; found: C 54.32, H 6.68, N 3.11.

Preparation of ***La(PN)$_2$(Cp) (3-La)***. A solution of **1-La** (1 eq., 0.2 mmol, 170 mg) in toluene (10 mL) was added to a suspension of **NaCp** (1.3 eq., 0.26 mmol, 23 mg) in toluene (5 mL) and the reaction mixture was heated at 95 °C overnight. The reaction mixture was then cooled to room temperature and filtered. The toluene solution was concentrated to about 1 mL and placed in the freezer (–40 °C) overnight, which caused the formation of large yellow crystals. The crystals were isolated and washed with small amounts of *n*-pentane to give **3-La** as yellow blocks which could also be used for X-ray structure determination. Yield: 80 mg (0.093 mmol, 47%); ^{1}H NMR (C_6D_6, 298 K, 700 MHz, in ppm): δ = 6.95 (m, C*H*$_{Ar}$, 2 H), 6.85 (s, C*H*$_{Ar}$, 4 H), 6.82 (m, C*H*$_{Ar}$, 2 H), 6.48 (s, Cp*H*, 5 H), 5.80 (m, C*H*$_{Ar}$,2 H), 2.21 (m, C*H*$_{3Ar}$, 24 H), 1.26 (hept, $^3J_{HH}$ = 7.2 Hz, C*H*$_{iPr}$, 4 H), 1.13 (s, broad, C*H*$_{3iPr}$, 24 H); ^{13}C{^{1}H} NMR (C_6D_6, 298 K, 176 MHz, in ppm): 160.0 (*pseudo*-t, J_{CP} = 10.3 Hz, C_{qAr}), 152.9 (C_{qAr}), 142.5 (C_{qAr}), 137.5 (C_{qAr}), 133.2 (C_{qAr}), 132.9 (*C*H$_{Ar}$), 132.7 (*C*H$_{Ar}$), 130.9 (*C*H$_{Ar}$), 122.4 (C_{qAr}), 114.3 (*C*H$_{Cp}$), 113.7 (*C*H$_{Ar}$), 113.5 (C_{qAr}), 21.0 (*C*H$_{3Ar}$), 20.7 (*C*H$_{3Ar}$), 20.3 (C_{Alk}), 18.5 (C_{Alk}); ^{31}P{^{1}H} NMR (C_6D_6, 298 K, 283 MHz, in ppm): δ = 11.0 (s, *P*N$^-$, 2 P) elemental analysis (in %): $C_{49}H_{67}N_2P_2La$: calcd.: C 65.51, H 7.63, N 3.17; found: C 65.21, H 7.51, N 3.40.

Preparation of ***La(PN)$_2$(OMes) (4-La)***. A solution of **1-La** (1 eq., 0.2 mmol, 170 mg) in toluene (10 mL) was added to solid **KOMes** (1.2 eq., 0.24 mmol, 42 mg) at room temperature. The resulting suspension was stirred at room temperature for 2 d and then centrifuged and filtered. All volatile components of the filtrate were removed *in vacuo* and the remaining oil triturated with *n*-pentane (3 x 2 mL). After removal of all volatiles *in vacuo*, the desired compound was obtained as an off-white solid. Single crystals suitable for X-ray structure determination were obtained by evaporation of a saturated diethyl ether solution of **4-La** at room temperature overnight. Yield: 190 mg (0.199 mmol, 99%); ^{1}H NMR (C_6D_6, 298 K, 700 MHz, in ppm): δ = 6.94 (br. s, C*H*$_{Ar}$, 2 H), 6.89 (br. s, C*H*$_{Ar}$, 2 H), 6.87 (br. s, C*H*$_{Ar}$, 2 H), 6.84 (br. s, C*H*$_{Ar}$, 2 H), 6.80 (br. d, $^3J_{HH}$ = 8.6 Hz, C*H*$_{Ar}$, 2 H), 5.76 (m, C*H*$_{Ar}$, 2 H), 2.59 (br. s, C*H*$_{3Ar}$, 6 H), 2.27 (br. s, C*H*$_{3Ar}$, 6 H), 2.21 (br. s, C*H*$_{3Ar}$, 3 H), 2.18 (br. s, C*H*$_{3Ar}$, 6 H), 2.13 (br. s, C*H*$_{3Ar}$, 6 H), 2.07 (br. s, C*H*$_{iPr}$, 2 H), 2.01 (br. s, C*H*$_{3Ar}$, 6 H), 1.80 (br. s, C*H*$_{iPr}$, 2 H), 1.06 (br. s, C*H*$_{3iPr}$, 6 H), 0.98 (br. s, C*H*$_{3iPr}$, 6 H), 0.88 (br. s, C*H*$_{3iPr}$, 6 H), 0.53 (br. s, C*H*$_{3iPr}$, 6 H); ^{13}C{^{1}H} NMR (C_6D_6, 298 K, 176 MHz, in ppm): δ = 162.1 (s, C_{qAr}), 160.7 (*pseudo*-t, J_{CP} = 11.5 Hz, C_{qAr}), 140.1 (br. s, C_{qAr}), 139.8 (s, C_{qAr}), 134.6 (s, C_{qAr}), 134.3 (br. s, C_{qAr}), 133.8 (s, *C*H$_{Ar}$), 133.5 (s, *C*H$_{Ar}$), 132.0 (s, *C*H$_{Ar}$), 130.6 (s, *C*H$_{Ar}$), 129.2 (s, *C*H$_{Ar}$), 125.5 (s, C_{qAr}), 125.4 (s, C_{qAr}), 122.7 (s, C_{qAr}), 113.4 (*pseudo*-t, J_{CP} = 5.2 Hz, C_{qAr}), 112.8 (s, *C*H$_{Ar}$), 25.9 (br. s, *C*H$_{iPr}$), 22.1 (br. s, *C*H$_{iPr}$), 21.1 (s, *C*H$_{3Ar}$), 20.9 (s, *C*H$_{3Ar}$), 20.6 (s, *C*H$_{3Ar}$), 20.3 (br. s, *C*H$_{3Ar}$), 20.1 (br. s, *C*H$_{3Ar}$), 19.9 (s, *C*H$_{3Ar}$), 19.8 (br. s, *C*H$_{3iPr}$), 19.3 (br. s, *C*H$_{3iPr}$), 18.4 (br. s, *C*H$_{3iPr}$), 16.4 (br. s, *C*H$_{3iPr}$); ^{31}P{^{1}H} NMR (C_6D_6, 298 K, 283 Mhz, in ppm): δ = 8.6 (s, *P*N$^-$, 2 P); elemental analysis (in %): $C_{53}H_{73}N_2OP_2La$: calcd.: C 66.66, H 7.70, N 2.93; found: C 66.77, H 7.73, N 3.19.

Preparation of ***Lu(PN)$_2$(OMes) (4-Lu)***. A solution of **1-Lu** (1 eq., 0.1 mmol, 89 mg) in toluene (4 mL) was added to solid **KOMes** (1.2 eq., 0.12 mmol, 21 mg) at room temperature and the resulting suspension stirred at 100 °C for 14 h. The reaction mixture was cooled down to room temperature and filtered. All volatile components of the filtrate were removed *in vacuo* to give a slightly yellow oil. After trituration with *n*-hexane (1 mL) and further drying *in vacuo*, the analytically pure product was obtained as a slightly yellow solid. Single crystals suitable for X-ray structure determination were obtained by evaporation of a saturated diethyl ether solution of **4-Lu** at room temperature overnight. Yield: 99 mg (0.1 mmol, quant.); ^{1}H NMR (C_6D_6, 298 K, 700 MHz, in ppm): δ = 6.94 (s, C*H*$_{Ar}$, 2 H), 6.89 (s, C*H*$_{Ar}$, 2 H), 6.83 (m, C*H*$_{Ar}$, 3 H), 6.81 (m, C*H*$_{Ar}$, 3 H), 5.99 (m, C*H*$_{Ar}$, 2 H), 2.65 (s, C*H*$_{3Ar}$, 6 H), 2.28 (s, C*H*$_{3Ar}$, 6 H), 2.24 (s, C*H*$_{3Ar}$, 6 H), 2.21 (s, C*H*$_{3Ar}$, 6 H), 2.17 (s, C*H*$_{3Ar}$, 3 H), 2.15 (m, C*H*$_{iPr}$, 2 H), 2.11 (s, C*H*$_{3Ar}$, 6 H), 1.27 (m, C*H*$_{iPr}$, 2 H), 1.03 (m, C*H*$_{3iPr}$, 6 H), 0.98 (m, C*H*$_{3iPr}$, 6 H), 0.79 (m, C*H*$_{3iPr}$, 6 H), 0.61 (m, C*H*$_{3iPr}$, 6 H); ^{13}C{^{1}H} NMR (C_6D_6, 298 K 176 MHz, in ppm): δ = 161.5 (*pseudo*-t, J_{CP} = 9.4 Hz, C_{qAr}), 160.2 (s, C_{qAr}), 144.9 (s, C_{qAr}), 138.0 (s, C_{qAr}), 136.4 (s, C_{qAr}), 133.8 (s, *C*H$_{Ar}$), 133.7 (s, C_{qAr}), 133.4 (s, *C*H$_{Ar}$), 131.3 (s, *C*H$_{Ar}$), 130.1 (s, *C*H$_{Ar}$), 129.4 (s, *C*H$_{Ar}$), 126.4 (s, C_{qAr}), 126.2 (s, C_{qAr}), 123.3 (s, C_{qAr}), 114.0 (*pseudo*-t, J_{CP} = 3.3 Hz, *C*H$_{Ar}$),

110.2 (d, J_{CP} = 8.1 Hz, C_{qAr}), 110.1 (d, J_{CP} = 8.1 Hz, C_{qAr}), 24.9 (*pseudo*-t, J_{CP} = 4.2 Hz, CH_{iPr}), 22.5 (s, CH_{3Ar}), 22.3 (*pseudo*-t, J_{CP} = 7.0 Hz, CH_{iPr}), 20.9 (s, CH_{3Ar}), 20.8 (s, CH_{3Ar}), 20.8 (s, CH_{3Ar}), 20.6 (s, CH_{3Ar}), 20.5 (*pseudo*-t, J_{CP} = 3.1 Hz, CH_{3iPr}), 19.6 (s, CH_{3Ar}), 18.7 (*pseudo*-t, J_{CP} = 5.8 Hz, CH_{iPr}), 18.4 (*pseudo*-t, J_{CP} = 3.8 Hz, CH_{3iPr}), 15.9 (*pseudo*-t, J_{CP} = 3.1 Hz, CH_{3iPr}); $^{31}P\{^1H\}$ NMR (C_6D_6, 298 K, 283 MHz, in ppm): δ = 2.9 (s, PN^-, 2 P); elemental analysis (in %) $C_{53}H_{73}N_2OP_2Lu$: calcd.: C 64.23, H 7.42, N 2.83; found: C 64.03, H 7.39, N 2.95.

Preparation of ***La(PN)$_2$(SMes) (5-La)****.* A solution of **1-La** (1 eq., 0.2 mmol, 171 mg) in toluene (6 mL) was added to solid **KSMes** (1.2 eq., 0.24 mmol, 46 mg) at room temperature. The resulting pale yellow suspension was stirred at room temperature for 3.5 d and then centrifuged and filtered. All volatile components of the filtrate were removed *in vacuo* and the remaining oil triturated with *n*-pentane (3 x 2 mL). After removal of all volatiles *in vacuo*, the desired compound was obtained as a pale yellow solid. Single crystals suitable for X-ray structure determination were obtained by evaporation of a saturated diethyl ether solution of **5-La** at room temperature overnight. Yield: 193 mg (0.199 mmol, 99%); ^1H NMR (C_6D_6, 298 K, 700 MHz, in ppm): δ = 6.90 (br. s, CH_{Ar}, 2 H), 6.89 (br. s, CH_{Ar}, 4 H), 6.86 (m, CH_{Ar}, 2 H), 6.81 (dd, J = 8.5 Hz, J = 1.5 Hz, CH_{Ar}, 2 H), 5.68 (m, CH_{Ar}, 2 H), 2.58 (s, CH_{3Ar}, 6 H), 2.35 (br. s, CH_{3Ar}, 12 H), 2.21 (s, CH_{3Ar}, 3 H), 2.15 (s, CH_{3Ar}, 6 H), 2.14 (s, CH_{3Ar}, 6 H), 1.90 (br. s, CH_{iPr}, 4 H), 1.0 (br. s, CH_{3iPr}, 12 H), 0.9 (br. s, CH_{3iPr}, 12 H); $^{13}C\{^1H\}$ NMR (C_6D_6, 298 K, 176 MHz, in ppm): δ = 160.3 (*pseudo*-t, J_{CP} = 11.4 Hz, C_{qAr}), 145.0 (s, C_{qAr}), 138.4 (s, C_{qAr}), 138.3 (s, C_{qAr}), 135.2 (s, C_{qAr}), 133.9 (s, CH_{Ar}), 133.3 (s, CH_{Ar}), 131.7 (br. s, CH_{Ar}), 131.6 (s, C_{qAr}), 123.4 (s, C_{qAr}), 114.2 (d, J_{CP} = 6.5 Hz, C_{qAr}), 114.1 (d, J_{CP} = 6.5 Hz, C_{qAr}), 112.9 (*pseudo*-t, J_{CP} = 3.8 Hz, CH_{Ar}), 24.9 (s, CH_{3Ar}), 23.2 (br. s, CH_{iPr}), 21.0 (s, CH_{3Ar}), 21.0 (s, CH_{3Ar}), 20.6 (s, CH_{3Ar}), 20.0 (br. s, CH_{3iPr}), 19.7 (br. s, CH_{3iPr}), 18.2 (br. s, CH_{3iPr}), 17.5 (br. s, CH_{iPr}); $^{31}P\{^1H\}$ NMR (C_6D_6, 298 K, 283 MHz, in ppm): δ = 10.0 (s, PN^-); elemental analysis (in %): $C_{53}H_{73}N_2P_2SLa$: calcd.: C 65.55, H 7.58, N 2.88, S 3.30; found: C 66.22, H 7.23, N 3.02, S 3.02.

Preparation of ***Lu(PN)$_2$(SMes) (5-Lu)****.* A solution of **2-Lu** (1 eq., 0.2 mmol, 197 mg) in toluene (4 mL) was added to solid **KSMes** (1.5 eq., 0.3 mmol, 57 mg) and the resulting reaction mixture stirred for 15 h at room temperature. The yellow suspension was centrifuged, the solution filtered and concentrated under reduced pressure to give a yellow oil. Subsequently, *n*-hexane (1 mL) was added and the resulting turbid solution stored for 3 d at room temperature for crystallization. The solution was removed from the crystalline material, the solid washed with minimal amounts of –40 °C cold *n*-hexane and dried *in vacuo* to give the first batch of the analytically pure product (62 mg) as an off-white solid. Concentrating the *n*-hexane washing solution resulted in the precipitation of a second batch of product (27 mg after drying *in vacuo*) of the same purity. Single crystals of **5-Lu** suitable for X-ray structure determination were obtained during work-up as described above. Yield: 89 mg (0.88 mmol, 44%); ^1H NMR (C_6D_6, 298 K, 700 MHz, in ppm): δ = 6.90 (br. s, CH_{Ar}, 4 H), 6.83 (s, CH_{Ar}, 2 H), 6.82 (m, CH_{Ar}, 2 H), 6.80 (m, CH_{Ar}, 2 H), 5.90 (m, CH_{Ar}, 2 H), 2.85 (br. s, CH_{3Ar}, 6 H), 2.56 (s, CH_{3Ar}, 6 H), 2.25 (br. s, CH_{3Ar}, 6 H), 2.19 (s, CH_{3Ar}, 6 H), 2.17 (s, CH_{3Ar}, 3 H), 2.11 (s, CH_{3Ar}, 6 H), 1.24 (br. s, CH_{iPr}, 2 H), 1.18 (br. s, CH_{3iPr}, 12 H), 0.80 (br. s, CH_{3iPr}, 6 H), 0.76 (br. s, CH_{3iPr}, 6 H), 0.67 (br. s, CH_{iPr}, 2 H); $^{13}C\{^1H\}$ NMR (C_6D_6, 298 K, 176 MHz, in ppm): δ = 161.2 (*pseudo*-t, J_{CP} = 9.5 Hz, C_{qAr}), 144.2 (s, C_{qAr}), 141.8 (s, C_{qAr}), 139.4 (s, C_{qAr}), 138.4 (br. s, C_{qAr}), 137.5 (br. s, C_{qAr}), 134.0 (s, C_{qAr}), 133.8 (s, CH_{Ar}), 133.4 (s, CH_{Ar}), 132.4 (s, C_{qAr}), 130.9 (br. s, CH_{Ar}), 130.4 (br. s, CH_{Ar}), 128.5 (s, CH_{Ar}), 123.7 (s, C_{qAr}), 114.0 (*pseudo*-t, J_{CP} = 3.6 Hz, CH_{Ar}), 111.1 (d, J_{CP} = 8.9 Hz, C_{qAr}), 111.0 (d, J_{CP} = 9.5 Hz, C_{qAr}), 25.2 (s, CH_{3Ar}), 23.0 (br. s, CH_{iPr}), 22.4 (br. s, CH_{3Ar}), 21.9 (br. s, CH_{3iPr}), 20.9 (s, CH_{3Ar}), 20.8 (s, CH_{3Ar}), 20.5 (s, CH_{3Ar}), 20.5 (br. s, CH_{iPr}), 18.8 (br. s, CH_{3iPr}), 18.2 (br. s, CH_{3iPr}), 15.9 (br. s, CH_{3iPr}); $^{31}P\{^1H\}$ NMR (C_6D_6, 298 K, 283 MHz, in ppm): δ = 4.8 (s, PN^-, 2 P); elemental analysis (in %): $C_{53}H_{73}N_2P_2SLu$: calcd.: C 63.21, H 7.31, N 2.78, S 3.18; found: C 63.29, H 7.24, N 3.05, S 2.87.

Preparation of ***La(PN)$_2$(NHMes) (6-La)****.* A solution of **1-La** (1 eq., 0.3 mmol, 257 mg) in toluene (10 mL) was added to solid **LiNHMes** (1 eq., 0.3 mmol, 42 mg) at room temperature. The resulting pale yellow

suspension was stirred at 100 °C for 18 h. The suspension was then allowed to cool down to room temperature, centrifuged and the pale yellow solution decanted and filtered. All volatile components of the filtrate were removed *in vacuo* upon which a crystalline material covered by a brown oil was obtained. This raw product was washed with *n*-hexane (3 x 3 mL) and dried *in vacuo* to yield the desired compound as a pale yellow solid (70 mg). The *n*-hexane solution was concentrated to a volume of 1-2 mL under reduced pressure and a second batch of crystalline material isolated and washed with 1 mL cold (–40 °C) *n*-pentane (209 mg after drying *in vacuo*). Single crystals suitable for X-ray structure determination were obtained by evaporation of a diethyl ether solution of **6-La** at room temperature overnight. Yield: 279 mg (0.292 mmol, 97%); ^{1}H NMR (C_6D_6, 298 K, 700 MHz, in ppm): δ = 6.92 (br. s, CH_{Ar}, 2 H), 6.89 (br. s, CH_{Ar}, 2 H), 6.86 (m, CH_{Ar}, 2 H), 6.84–6.81 (m, CH_{Ar}, 2 H), 6.83 (s, CH_{Ar}, 2 H), 5.81 (m, CH_{Ar}, 2 H), 5.60 (br. s, N*H*, 1 H), 2.52 (br. s, CH_{3Ar}, 6 H), 2.26 (br. s, CH_{3Ar}, 3 H), 2.25 (br. s, CH_{3Ar}, 6 H), 2.18 (br. s, CH_{3Ar}, 6 H), 2.14 (br. s, CH_{3Ar}, 6 H), 2.09 (br. s, C$H_{i\mathrm{Pr}}$, 2 H), 2.01 (br. s, CH_{3Ar}, 6 H), 1.76 (m, C$H_{i\mathrm{Pr}}$, 2 H), 1.04 (m, C$H_{3i\mathrm{Pr}}$, 6 H), 0.93 (m, C$H_{3i\mathrm{Pr}}$, 6 H), 0.84 (m, C$H_{3i\mathrm{Pr}}$, 6 H), 0.57 (m, C$H_{3i\mathrm{Pr}}$, 6 H); ^{13}C{^{1}H} NMR (C_6D_6, 298 K, 176 MHz, in ppm): δ = 160.9 (*pseudo*-t, J_{CP} = 11.6 Hz, C_{qAr}), 154.3 (s, C_{qAr}), 139.9 (s, C_{qAr}), 139.7 (s, C_{qAr}), 135.8 (s, C_{qAr}), 134.5 (s, C_{qAr}), 134.0 (s, CH_{Ar}), 133.4 (s, CH_{Ar}), 131.8 (s, CH_{Ar}), 130.7 (s, CH_{Ar}), 129.1 (s, CH_{Ar}), 122.9 (s, C_{qAr}), 122.8 (br. s, C_{qAr}), 121.6 (s, C_{qAr}), 113.5 (br. s, C_{qAr}), 113.2 (s, CH_{Ar}), 26.5 (br. s, C$H_{i\mathrm{Pr}}$), 22.4 (br. s, C$H_{i\mathrm{Pr}}$), 22.3 (s, CH_{3Ar}), 21.0 (s, CH_{3Ar}), 20.9 (s, CH_{3Ar}), 20.6 (s, CH_{3Ar}), 20.5 (m, CH_{3Ar}), 20.1 (br. s, C$H_{3i\mathrm{Pr}}$), 19.7 (br. s, CH_{3Ar}), 19.2 (m, C$H_{3i\mathrm{Pr}}$), 18.7 (br. s, C$H_{3i\mathrm{Pr}}$), 16.8 (br. s, C$H_{3i\mathrm{Pr}}$); ^{31}P{^{1}H} NMR (C_6D_6, 298 K, 283 MHz, in ppm): δ = 9.5 (s, PN^{-}, 2 P); elemental analysis (in %): $C_{53}H_{74}N_3P_2La$: calcd.: C 66.72, H 7.82, N 4.40; found: C 65.57, H 7.54, N 4.39.

Preparation of ***Lu(PN)$_2$(NHMes) (6-Lu)****.* A solution of **1-Lu** (1 eq., 0.2 mmol, 178 mg) in toluene (5 mL) was added to solid **LiNHMes** (1.2 eq., 0.24 mmol, 34 mg) at room temperature and the resulting suspension stirred at 100 °C for 2 d. The reaction mixture was cooled down to room temperature and centrifuged. The solution was decanted, filtered and the solvent removed *in vacuo*. The slightly yellow solid was washed with *n*-hexane (3 x 3 mL) and dried *in vacuo*. Recrystallization by gas diffusion of *n*-hexane into a concentrated diethyl ether solution (1 mL) at room temperature afforded analytically pure product. Single crystals of **6-Lu** suitable for X-ray structure determination were also obtained in this way. Yield: 64 mg (0.73 mmol, 36%); ^{1}H NMR (C_6D_6, 298 K, 700 MHz, in ppm): δ = 6.93 (s, CH_{Ar}, 2 H), 6.89 (s, CH_{Ar}, 2 H), 6.85–6.80 (m, CH_{Ar}, 6 H), 6.01 (m, CH_{Ar}, 2 H), 5.32 (s, N*H*, 1 H), 2.61 (s, CH_{3Ar}, 6 H), 2.27 (s, CH_{3Ar}, 6 H), 2.24 (s, CH_{3Ar}, 3 H), 2.21 (s, CH_{3Ar}, 6 H), 2.21 (s, CH_{3Ar}, 6 H), 2.18 (m, C$H_{i\mathrm{Pr}}$, 2 H), 2.11 (s, CH_{3Ar}, 6 H), 1.48 (m, C$H_{i\mathrm{Pr}}$, 2 H), 1.06 (m, C$H_{3i\mathrm{Pr}}$, 6 H), 0.89 (m, C$H_{3i\mathrm{Pr}}$, 6 H), 0.80 (m, C$H_{3i\mathrm{Pr}}$, 6 H), 0.53 (m, C$H_{3i\mathrm{Pr}}$, 6 H); ^{13}C{^{1}H} NMR (C_6D_6, 298 K, 176 MHz, in ppm): δ = 161.5 (*pseudo*-t, J_{CP} = 10.1 Hz, C_{qAr}), 153.1 (s, C_{qAr}), 144.8 (s, C_{qAr}), 137.9 (s, C_{qAr}), 136.7 (s, C_{qAr}), 133.8 (s, CH_{Ar}), 133.7 (s, CH_{Ar}), 131.3 (s, CH_{Ar}), 130.2 (s, CH_{Ar}), 129.2 (s, CH_{Ar}), 123.5 (s, C_{qAr}), 123.4 (s, C_{qAr}), 122.5 (s, C_{qAr}), 114.4 (*pseudo*-t, J_{CP} = 3.6 Hz, CH_{Ar}), 110.5 (d, J_{CP} = 7.6 Hz, C_{qAr}), 110.4 (d, J_{CP} = 7.6 Hz, C_{qAr}), 25.6 (*pseudo*-t, J_{CP} = 3.9 Hz, C$H_{i\mathrm{Pr}}$), 22.7 (*pseudo*-t, J_{CP} = 6.8 Hz, C$H_{i\mathrm{Pr}}$), 21.8 (s, CH_{3Ar}), 21.7 (s, CH_{3Ar}), 21.2 (s, CH_{3Ar}), 20.9 (s, CH_{3Ar}), 20.8 (s, CH_{3Ar}), 20.6 (s, CH_{3Ar}), 20.2 (*pseudo*-t, J_{CP} = 3.2 Hz, C$H_{3i\mathrm{Pr}}$), 18.8 (*pseudo*-t, J_{CP} = 5.5 Hz, C$H_{3i\mathrm{Pr}}$), 18.2 (s, C$H_{3i\mathrm{Pr}}$), 16.4 (s, C$H_{3i\mathrm{Pr}}$); ^{31}P{^{1}H} NMR (C_6D_6, 298 K, 283 MHz, in ppm): δ = 1.8 (s, PN^{-}, 2 P); elemental analysis (in %): $C_{53}H_{74}N_3P_2Lu$: calcd.: C 64.29, H 7.53, N 4.24; found: C 63.49, H 7.44, N 4.20.

Preparation of ***La(PN)$_2$(PHMes) (7-La)****.* A solution of **1-La** (1 eq., 1 mmol, 855 mg) in toluene (10 mL) was added to solid **KPHMes** (1.2 eq., 1.2 mmol, 228 mg) at room temperature. The resulting deep yellow suspension was stirred at room temperature for 4 h and then filtered. All volatile components of the deep orange filtrate were removed *in vacuo* to yield the desired compound as a yellow solid. (Note: If necessary, the product can be washed with minimal amounts of –40 °C cold *n*-hexane or *n*-pentane to remove traces of **HPN**, although this results in diminishing the yield to about 80%.) Single crystals suitable for X-ray structure determination were obtained by evaporation of a concentrated *n*-hexane solution of **7-La** at room temperature overnight. Yield: 931 mg (0.959 mmol, 96%); ^{1}H NMR

(C_6D_6, 298 K, 700 MHz, in ppm): δ = 6.89 (br. s, CH_{Ar}, 4 H), 6.86 (br. s, CH_{Ar}, 2 H), 6.84 (br. s, CH_{Ar}, 2 H), 6.82 (d, $^3J_{HH}$ = 8.7 Hz, CH_{Ar}, 2 H), 5.69 (m, CH_{Ar}, 2 H), 3.42 (d, $^1J_{PH}$ = 198.9 Hz, P*H*Mes, 1 H), 2.45 (br. s, CH_{3Ar}, 6 H), 2.36 (br. s, CH_{3Ar}, 12 H), 2.26 (s, CH_{3Ar}, 3 H), 2.14 (br. s, CH_{3Ar}, 12 H), 1.81 (br. s, C$H_{i\text{Pr}}$, 4 H), 1.05 (br. s, C$H_{3i\text{Pr}}$, 12 H), 0.91 (br. s, C$H_{3i\text{Pr}}$, 12 H); $^{13}C\{^1H\}$ NMR (C_6D_6, 298 K, 176 MHz, in ppm): δ = 160.2 (*pseudo*-t, J_{CP} = 11.4 Hz, C_{qAr}), 144.3 (d, J_{CP} = 22.3 Hz, C_{qAr}), 138.5 (s, C_{qAr}), 136.2 (d, J_{CP} = 8.6 Hz, C_{qAr}), 135.2 (s, C_{qAr}), 133.9 (s, *C*H$_{Ar}$), 133.4 (s, *C*H$_{Ar}$), 131.7 (br. s, *C*H$_{Ar}$), 130.7 (s, C_{qAr}), 123.5 (s, C_{qAr}), 113.9 (d, J_{CP} = 6.5 Hz, C_{qAr}), 113.8 (d, J_{CP} = 6.3 Hz, C_{qAr}), 112.8 (*pseudo*-t, J_{CP} = 3.8 Hz, *C*H$_{Ar}$), 25.3 (d, J_{CP} = 11.7 Hz, *C*H$_{3Ar}$), 22.8 (br. s, *C*H$_{i\text{Pr}}$), 21.1 (s, *C*H$_{3Ar}$), 21.0 (s, *C*H$_{3Ar}$), 20.6 (s, *C*H$_{3Ar}$), 20.1 (br. s, *C*H$_{3Ar}$), 19.9 (br. s, *C*H$_{3i\text{Pr}}$), 17.6 (br. s, *C*H$_{3i\text{Pr}}$); $^{31}P\{^1H\}$ NMR (C_6D_6, 298 K, 283 MHz, in ppm): δ = 11.0 (s, *P*N$^-$, 2 P), –36.4 (s, *P*HMes, 1 P); $^{31}P\{\}$ NMR (C_6D_6, 298 K, 283 MHz, in ppm): δ = 11.0 (br. s, *P*N$^-$, 2 P), –36.4 (d, $^1J_{PH}$ = 198.9 Hz, *P*HMes, 1 P); elemental analysis (in %): $C_{53}H_{74}LaN_2P_2$: calcd.: C 65.56, H 7.68, N 2.89; found: C 64.79, H 7.61, N 3.36.

Preparation of ***Lu(PN)$_2$(PHMes) (7-Lu)****.* A solution of **2-Lu** (1 eq., 0.1 mmol, 98 mg) in toluene (2 mL) was added to a suspension of **KPHMes** (1.2 eq., 0.12 mmol, 23 mg) in toluene (2 mL) at room temperature. Within seconds the resulting reaction mixture took on a deep yellow color. After stirring for 36 h at room temperature, the suspension was centrifuged and the solution was filtered. All volatile components of the filtrate were removed under reduced pressure, the oily residue triturated with *n*-hexane (2 x 1 mL) and further dried *in vacuo*. The yellow solid was washed with –40 °C cold *n*-hexane (2 x 1 mL) and then thoroughly dried *in vacuo* to give analytically pure product. Single crystals of **7-Lu** suitable for X-ray structure determination were obtained by storing the above mentioned oily residue at room temperature for 3 d before further work-up. Yield: 52 mg (0.052 mmol, 52%); ^1H NMR (C_6D_6, 298 K, 700 MHz, in ppm): δ = 6.89 (br. s, CH_{Ar}, 4 H), 6.83 (dd, $^3J_{HH}$ = 8.7 Hz, $^4J_{HH}$ = 2.0 Hz, CH_{Ar}, 2 H), 6.80 (m, CH_{Ar}, 2 H), 6.79 (s, CH_{Ar}, 2 H), 5.89 (m, CH_{Ar}, 2 H), 3.43 (d, $^1J_{PH}$ = 209.5 Hz, P*H*Mes, 1 H), 2.85 (br. s, CH_{3Ar}, 6 H), 2.43 (s, CH_{3Ar}, 6 H), 2.26–2.14 (br. s, CH_{3Ar}, 6 H), 2.23 (s, CH_{3Ar}, 3 H), 2.18 (s, CH_{3Ar}, 6 H), 2.11 (s, CH_{3Ar}, 6 H), 1.19 (br. s, C$H_{3i\text{Pr}}$, 12 H), 0.83 (br. s, C$H_{3i\text{Pr}}$, 6 H), 0.76 (br. s, C$H_{3i\text{Pr}}$ & C$H_{i\text{Pr}}$, 8 H), 0.54 (br. s, C$H_{i\text{Pr}}$, 2 H); $^{13}C\{^1H\}$ NMR (C_6D_6, 298 K, 176 MHz, in ppm): δ = 161.0 (*pseudo*-t, J_{CP} = 9.5 Hz, C_{qAr}), 144.3 (s, C_{qAr}), 141.8 (d, J_{CP} = 20.7 Hz, C_{qAr}), 138.0 (br. s, C_{qAr}), 137.2 (d, J_{CP} = 9.3 Hz, C_{qAr}), 134.0 (s, C_{qAr}), 133.9 (s, *C*H$_{Ar}$), 133.5 (s, *C*H$_{Ar}$), 131.3 (s, C_{qAr}), 130.9 (br. s, C_{qAr}), 130.5 (br. s, C_{qAr}), 123.9 (s, C_{qAr}), 114.0 (*pseudo*-t, J_{CP} = 4.0 Hz, *C*H$_{Ar}$), 111.4 (d, J_{CP} = 9.3 Hz, C_{qAr}), 111.3 (d, J_{CP} = 8.5 Hz, C_{qAr}), 25.6 (s, *C*H$_{3Ar}$), 25.5 (s, *C*H$_{3Ar}$), 22.6 (br. s, *C*H$_{i\text{Pr}}$), 22.3 (br. s, *C*H$_{i\text{Pr}}$), 22.0 (br. s, *C*H$_{3i\text{Pr}}$), 20.9 (s, *C*H$_{3Ar}$), 20.8 (s, *C*H$_{3Ar}$), 20.5 (s, *C*H$_{3Ar}$), 18.9 (s, *C*H$_{3i\text{Pr}}$), 18.0 (s, *C*H$_{3i\text{Pr}}$), 15.8 (s, *C*H$_{3i\text{Pr}}$) (Due to extensive line broadening caused by rotational barriers, we have not been able to observe all *ortho* methyl groups of the mesityl substituents at around 2 ppm.); $^{31}P\{^1H\}$ NMR (C_6D_6, 298 K, 283 MHz, in ppm): δ = 5.1 (d, $^2J_{PP}$ = 32.3 Hz, *P*N$^-$, 2 P), –63.8 (t, $^2J_{PP}$ = 32.3 Hz, *P*HMes, 1 P); $^{31}P\{\}$ NMR (C_6D_6, 298 K, 283 MHz, in ppm): δ = 5.1 (br. s, *P*N$^-$, 2 P), –63.8 (dt, $^1J_{PH}$ = 209.5 Hz, $^2J_{PP}$ = 32.3 Hz, *P*HMes, 1 P); elemental analysis (in %): $C_{53}H_{74}LuN_2P_3$: calcd.: C 63.21, H 7.41, N 2.78; found: C 62.33, H 7.42, N 3.04.

Preparation of ***La(PN)(HMDS)$_2$ (8-La)****.* **La(HMDS)$_3$** (1 eq., 0.3 mmol, 186 mg) and **HPN** (1 eq., 0.3 mmol, 102 mg) were dissolved in toluene (7 mL) and the resulting reaction mixture stirred at 120 °C for 8 d. The reaction mixture was then cooled to room temperature and filtered. After removal of the volatiles *in vacuo*, the obtained raw product was washed with –40 °C cold *n*-hexane (2 x 2 mL) and dried *in vacuo* to give analytically pure product as an off-white solid. Single crystals of **8-La** suitable for X-ray structure determination were obtained by concentrating a *n*-hexane solution to about 3 mL and storing it at –40 °C overnight. Yield: 121 mg (0.151 mmol, 50%); ^1H NMR (C_6D_6, 298 K, 700 MHz, in ppm): δ = 6.98 (s, CH_{Ar}, 2 H), 6.86 (dd, $^3J_{HP}$ = 5.9 Hz, $^4J_{HH}$ = 1.8 Hz, CH_{Ar}, 1 H), 6.84 (dd, $^3J_{HH}$ = 8.3 Hz, $^4J_{HH}$ = 1.8 Hz, CH_{Ar}, 1 H), 5.84 (dd, $^3J_{HH}$ = 8.3 Hz, $^4J_{HP}$ = 5.3 Hz, CH_{Ar}, 1 H), 2.34 (s, CH_{3Ar}, 6 H), 2.21 (sept. (overlap with two s), $^3J_{HH}$ = 7.0 Hz, C$H_{i\text{Pr}}$, 2 H), 2.21 (s, CH_{3Ar}, 3 H), 2.20 (s, CH_{3Ar}, 3 H), 1.24 (d, $^3J_{HH}$ = 7.0 Hz, C$H_{3i\text{Pr}}$, 3 H), 1.22 (d, $^3J_{HH}$ = 7.0 Hz, C$H_{3i\text{Pr}}$, 3 H), 1.13 (d, $^3J_{HH}$ = 7.1 Hz, C$H_{3i\text{Pr}}$, 3 H), 1.11 (d, $^3J_{HH}$ = 7.1 Hz, C$H_{3i\text{Pr}}$, 3 H), 0.29 (s,

Si(CH_3)$_3$, 36 H); $^{13}C\{^1H\}$ NMR (C_6D_6, 298 K, 176 MHz, in ppm): δ = 160.6 (d, J_{CP} = 22.8 Hz, C_{qAr}), 138.8 (d, J_{CP} = 2.0 Hz, C_{qAr}), 138.7 (s, C_{qAr}), 135.2 (s, C_{qAr}), 133.5 (s, CH_{Ar}), 133.4 (d, J_{CP} = 2.8 Hz, CH_{Ar}), 131.5 (s, CH_{Ar}), 122.7 (d, J_{CP} = 2.7 Hz, C_{qAr}), 114.1 (d, J_{CP} = 7.3 Hz, CH_{Ar}), 113.9 (s, C_{qAr}), 24.5 (d, $^2J_{CP}$ = 5.2 Hz, CH_{iPr}), 21.0 (s, CH_{3Ar}), 20.7 (s, CH_{3Ar}), 20.5 (s, CH_{3Ar}), 20.1 (s, CH_{3iPr}), 20.1 (s, CH_{3iPr}), 19.6 (s, CH_{3iPr}), 19.5 (s, CH_{3iPr}), 4.9 (s, Si(CH_3)$_3$); $^{29}Si\{^1H\}$ NMR (C_6D_6, 298 K, 139 MHz, in ppm): δ = –13.5 (s, Si(CH_3)$_3$, 2 Si); $^{31}P\{^1H\}$ NMR (C_6D_6, 298 K, 283 MHz, in ppm): δ = 10.2 (s, PN^-, 1 P); elemental analysis (in %): $C_{34}H_{67}LaN_3PSi_4$: calcd.: C 51.04, H 8.44, N 5.25; found: C 51.20, H 8.33, N 5.25.

Preparation of ***Ce(PN)(HMDS)$_2$*** *(**8-Ce**).* **Ce(HMDS)$_3$** (1 eq., 0.29 mmol, 181 mg) and **HPN** (1 eq., 0.29 mmol, 99 mg) were dissolved in toluene (15 mL) and the resulting reaction mixture stirred at 120 °C for 8 d. The reaction mixture was then cooled to room temperature and filtered. After removal of the volatiles *in vacuo*, the obtained raw product was washed with –40 °C cold *n*-pentane (2 x 2 mL) and dried *in vacuo* to give analytically pure product as an off-white solid. Single crystals of **8-Ce** suitable for X-ray structure determination were obtained by concentrating a *n*-pentane solution to about 3 mL and storing it at –40 °C overnight. Yield: 151 mg (0.188 mmol, 54%); ^1H NMR (C_6D_6, 298 K, 700 MHz, in ppm): δ = 18.70 (s, 1 H), 14.14 (s, 1 H), 14.08 (s, 1 H), 6.42 (s, 3 H), 3.56 (br. s, 2 H), 2.16 (br. s, 6 H), 0.61 (s, 2 H), –0.20 (br. s, 6 H), –1.85 (s, 3 H), –3.04 (br.s , 3 H), –5.85 (br. s, 36 H) (Due to the paramagnetic nature of the Ce(III) ion, we have not been able to observe all protons in the ^1H NMR spectrum of the complex.); $^{31}P\{^1H\}$ NMR (C_6D_6, 298 K, 283 MHz, in ppm): δ = 383.3 (br. s, PN^-, 1 P); $^{31}P\{^1H\}$ NMR (THF-d_8, 298 K, 283 MHz, in ppm): 386.1 (br. s, PN^-, 1 P), 365.5 (br. s, PN^-, 1 P); Evans Method: μ_{eff} = 2.59 μ_B (C_6D_6); elemental analysis (in %): $C_{34}H_{67}CeN_3PSi_4$: calcd.: C 50.96, H 8.43, N 5.24; found: C 51.28, H 7.99, N 5.10.

X-ray crystallography. Single crsystals for X-ray diffraction experiments were measured at the analytical facility of the University of Paderborn, the University of Duisburg-Essen, and the Bruker Training Center in Karlsruhe. All crystals were kept at 130(2) or 100(2) K throughout data collection. Data was collected using either the Smart or the APEXIII software package. Data refinement and reduction were performed with Bruker Saint (V8.34A). All structures were solved with SHELXT and refined using the OLEX 2 software package.[11,12] Strongly disordered solvent molecules were removed using the SQUEEZE operation.[13] All non-hydrogen atoms were refined anisotropically, and hydrogen atoms were included at the geometrically calculated positions and refined using a riding model. All structures have been submitted to the CCDC and can be obtained under the numbers presented in the SI Tables S1, S2 and S3. For further crystallographic details regarding crystal measurements, please check Tables S1 to S5 in the Supporting Information.

2. NMR spectra

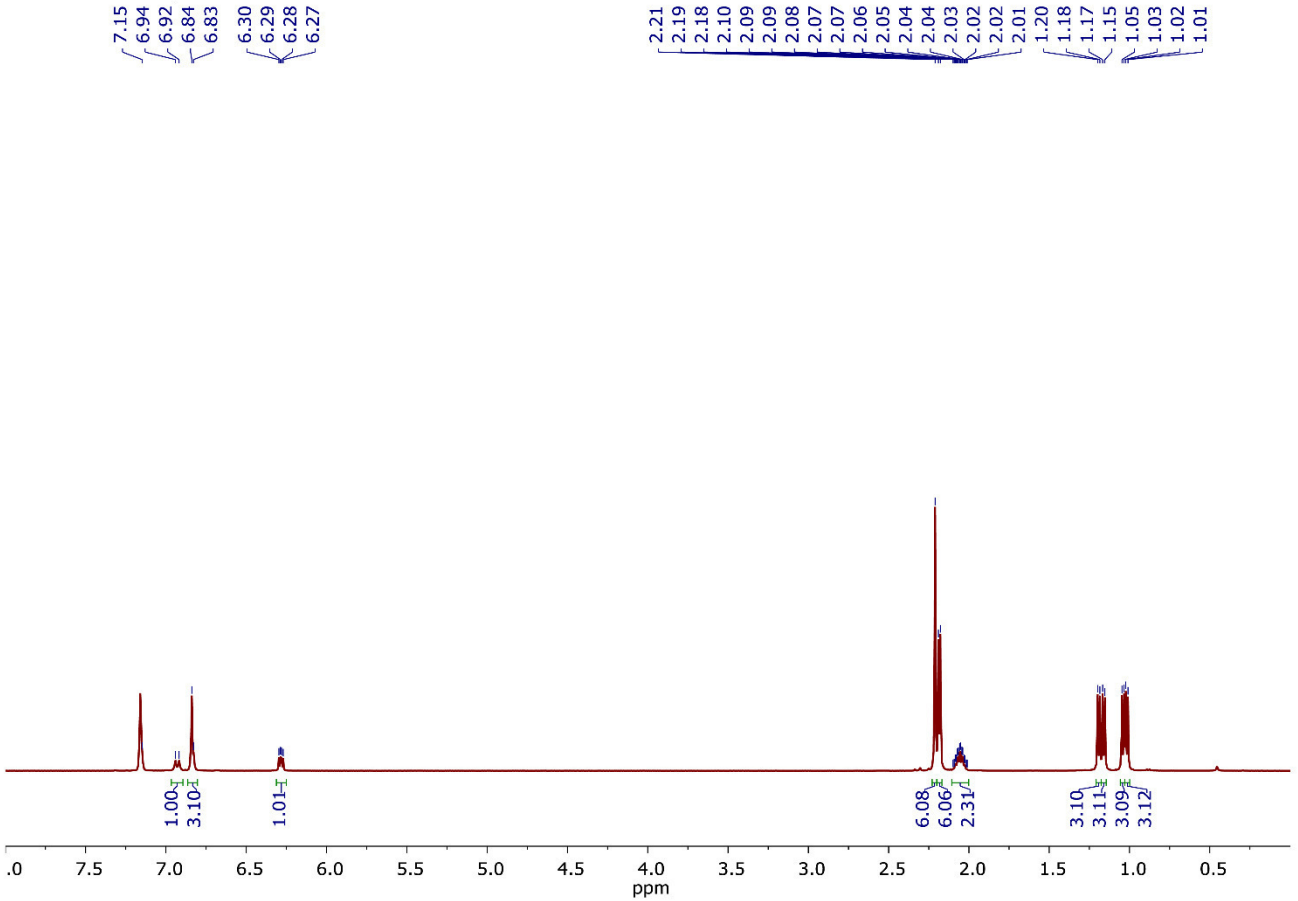

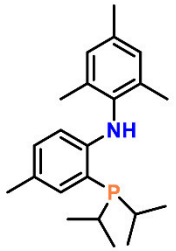

Figure S1: *^{1}H NMR spectrum of **HPN** in C_6D_6 (298 K).*

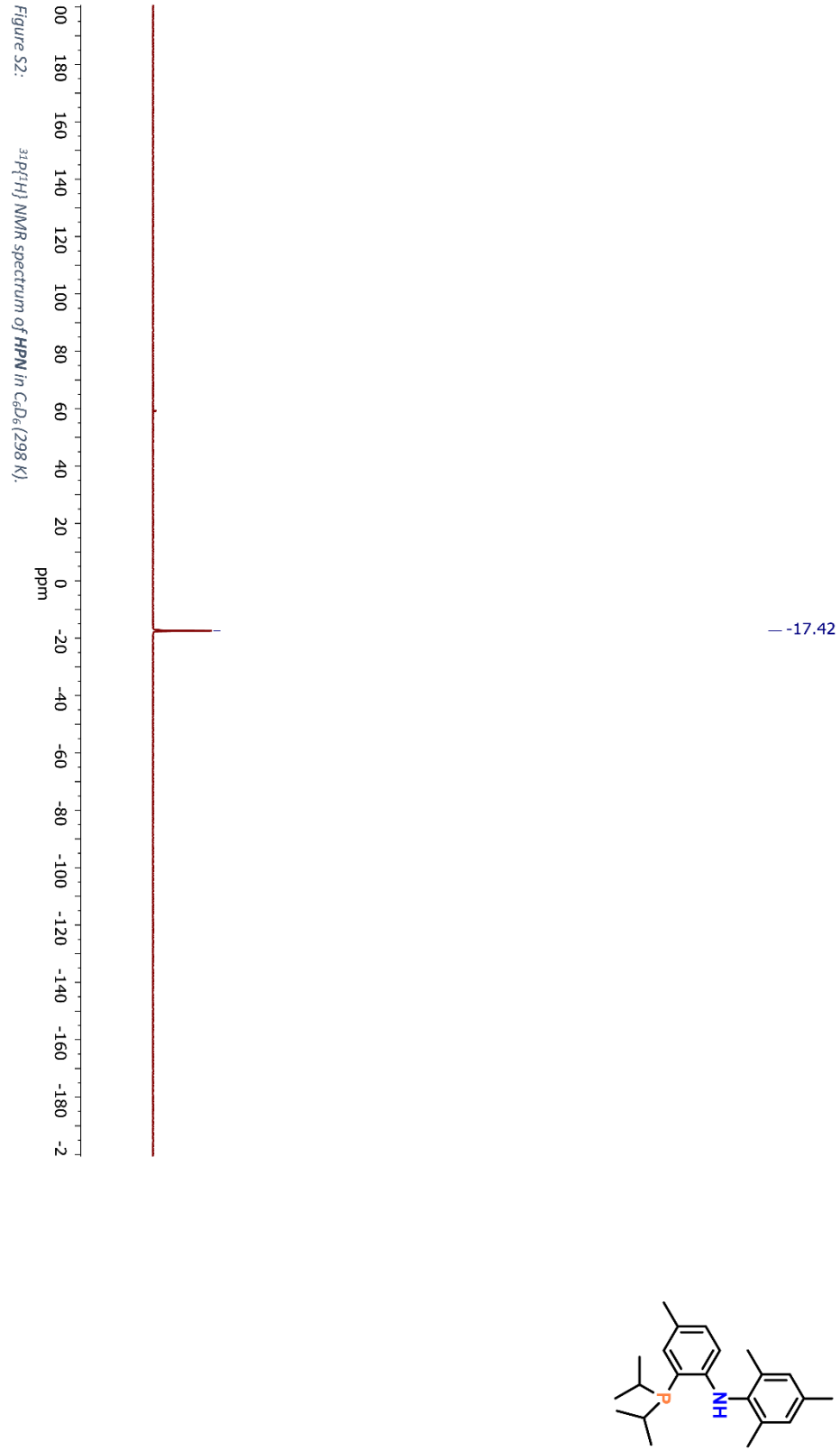

Figure S2: $^{31}P\{^1H\}$ *NMR spectrum of* ***HPN*** *in* C_6D_6 *(298 K).*

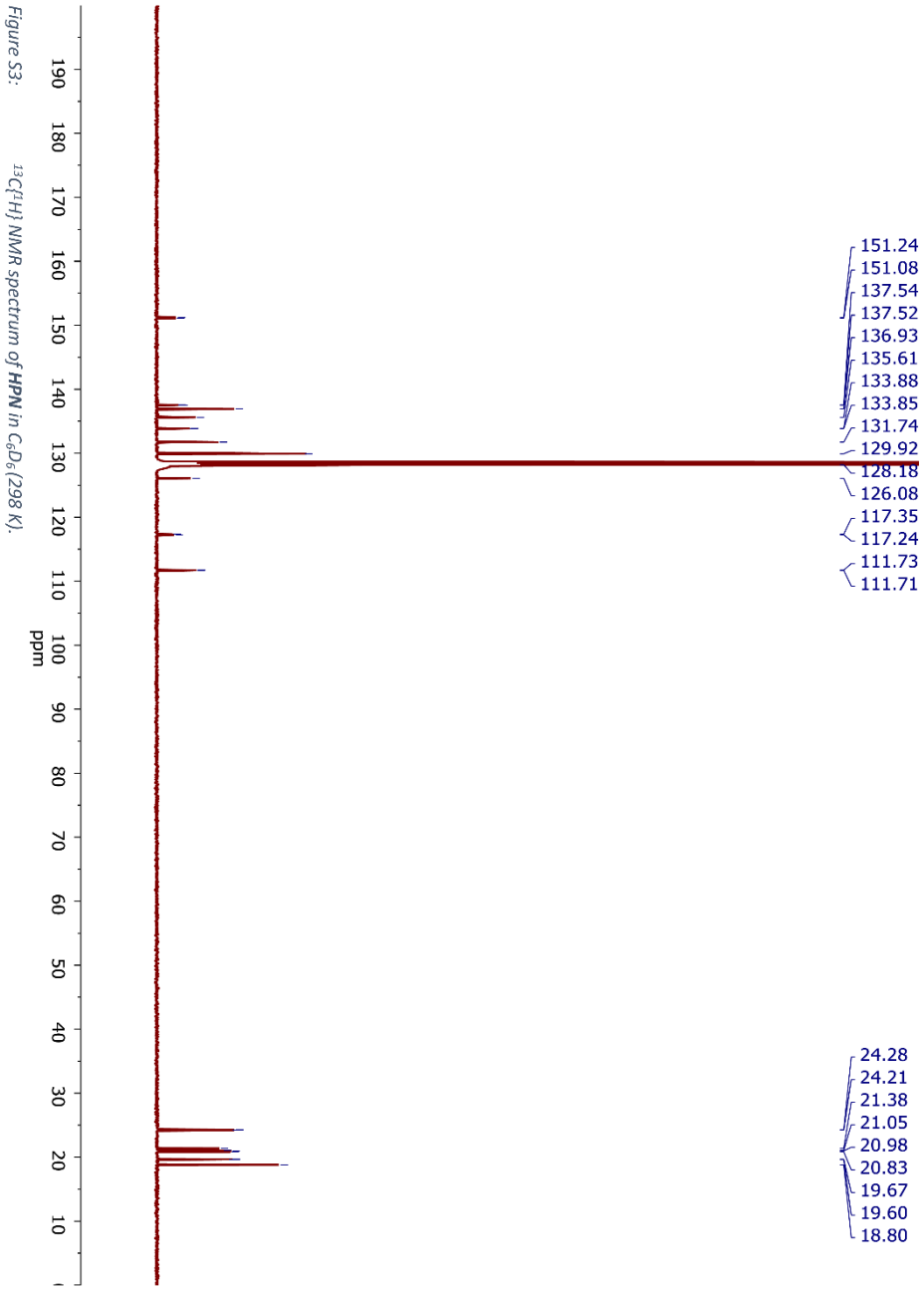

*Figure S3: $^{13}C\{^1H\}$ NMR spectrum of **HPN** in C_6D_6 (298 K).*

S12

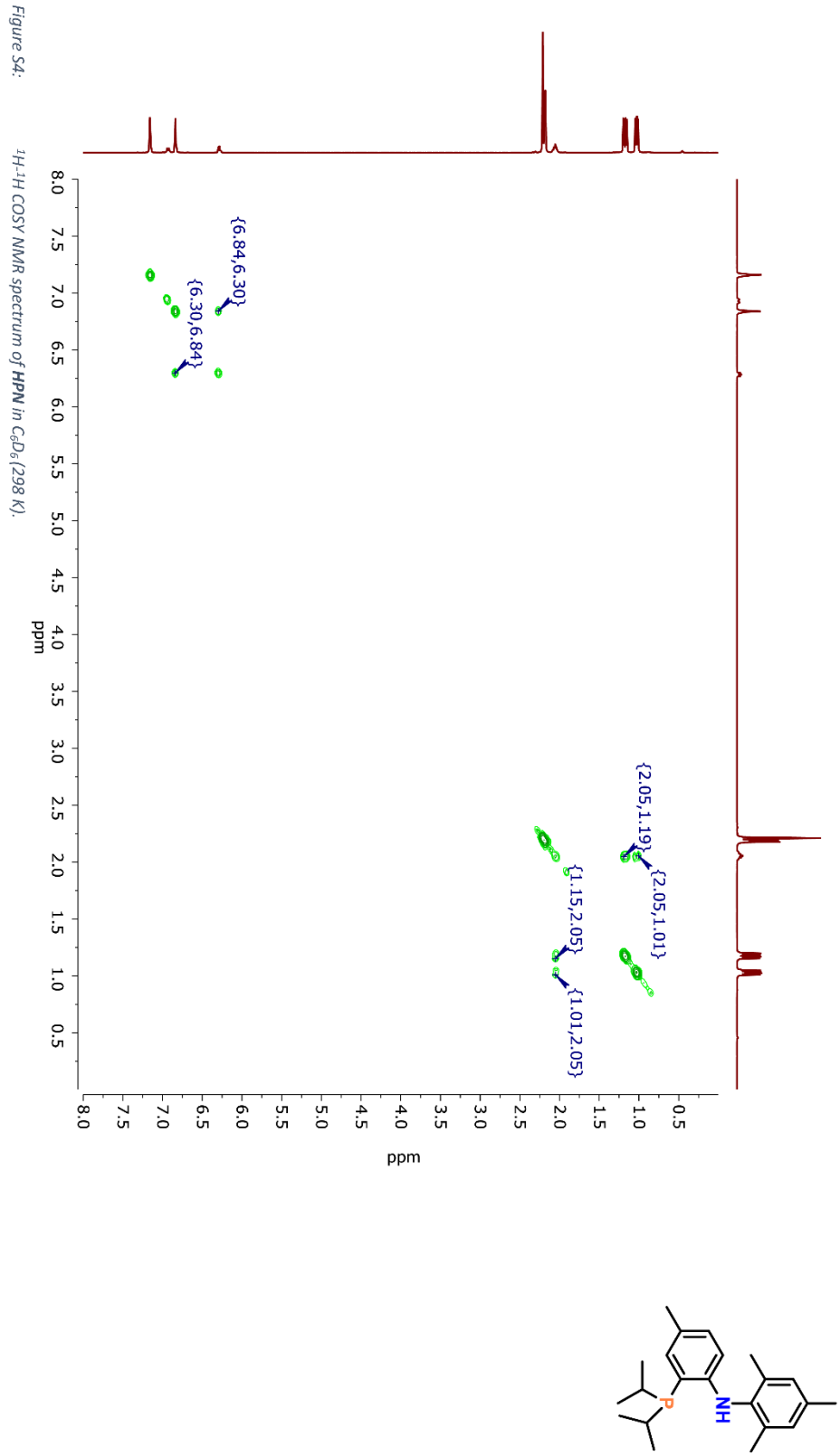

*Figure S4: ^{1}H-^{1}H COSY NMR spectrum of **HPN** in C_6D_6 (298 K).*

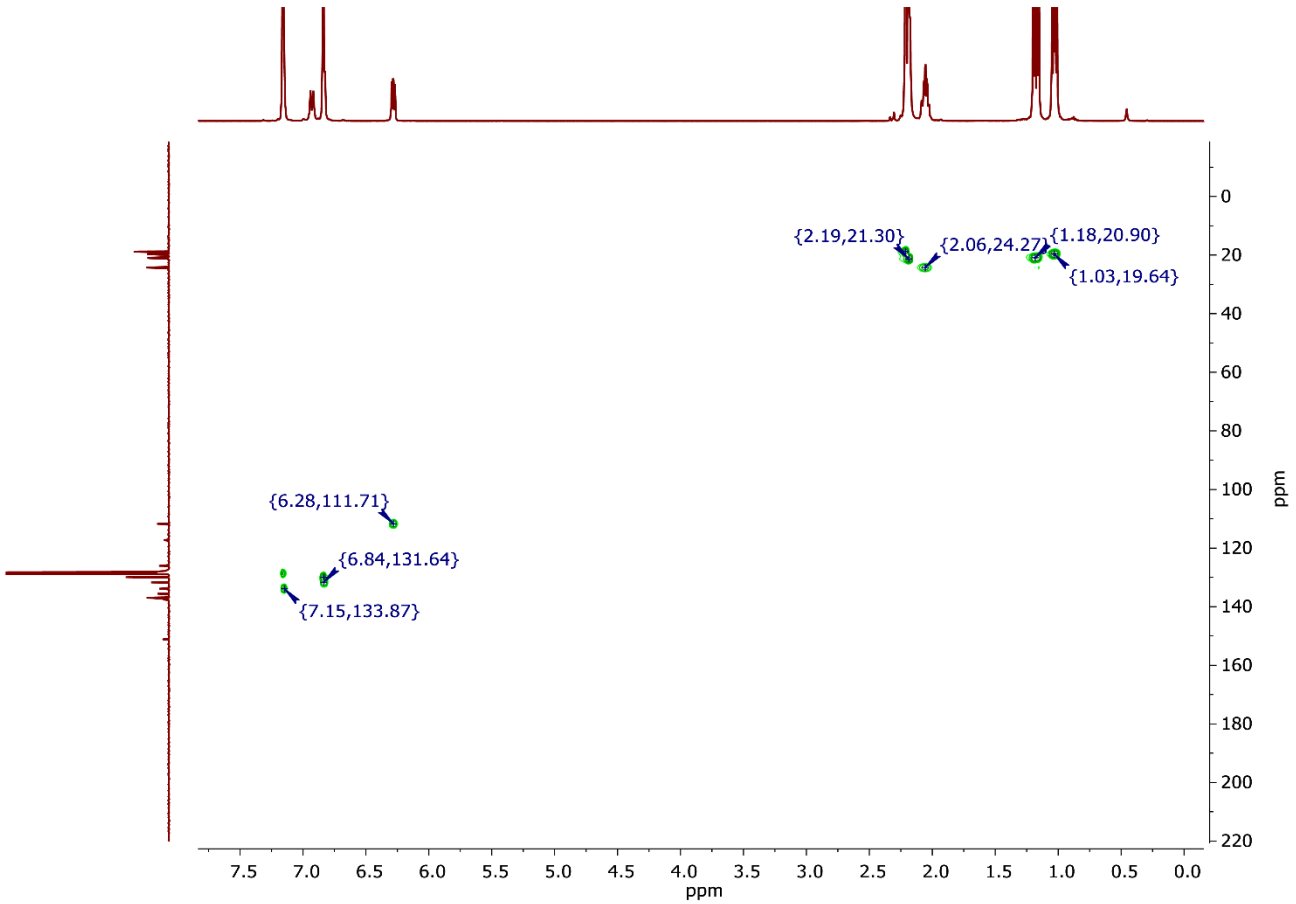

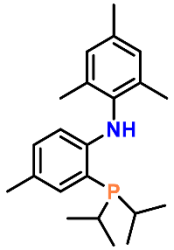

Figure S5: *^{1}H-^{13}C HSQC NMR spectrum of **HPN** in C_6D_6 (298 K).*

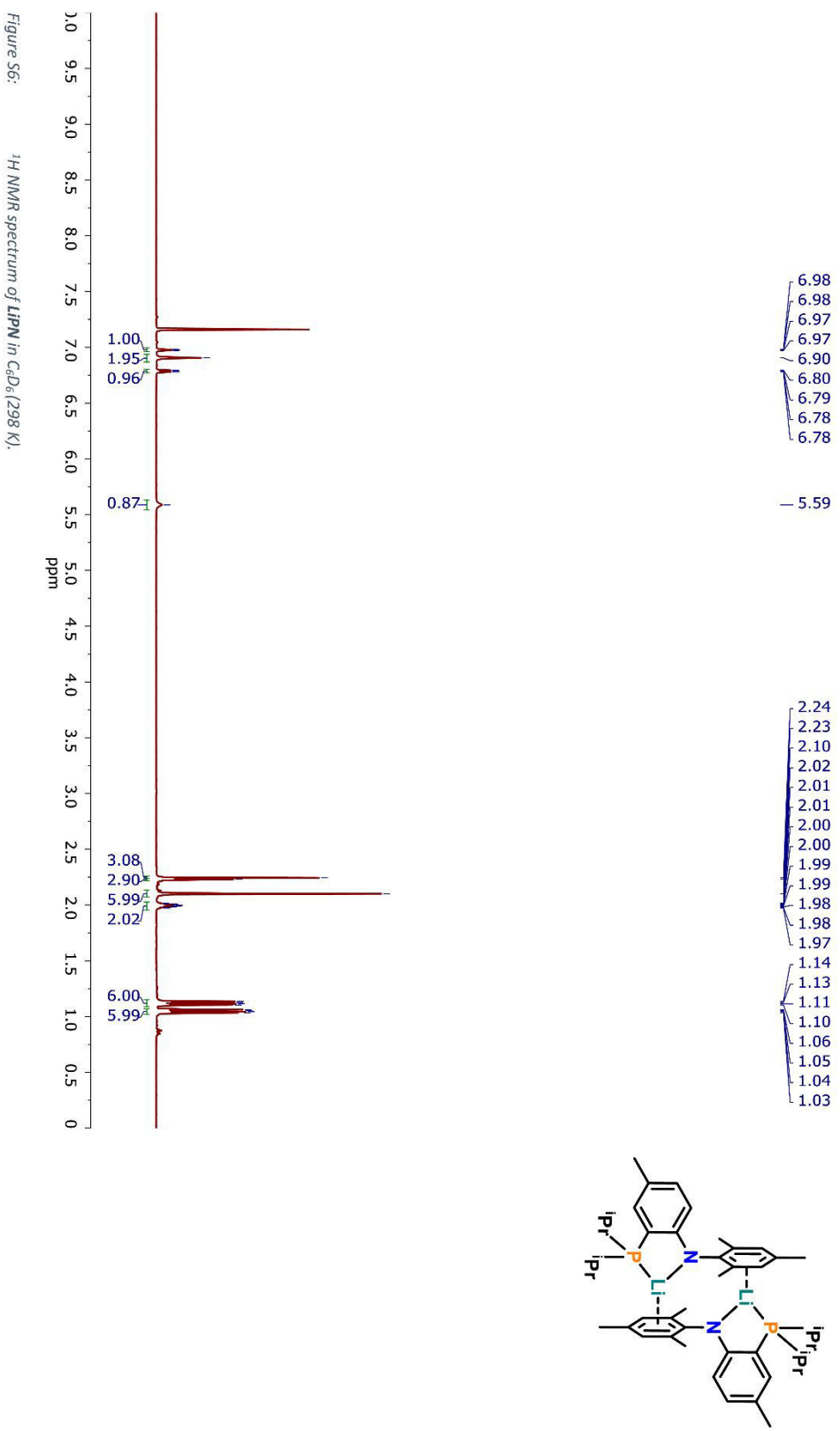

*Figure S6: ^{1}H NMR spectrum of **LiPN** in C_6D_6 (298 K).*

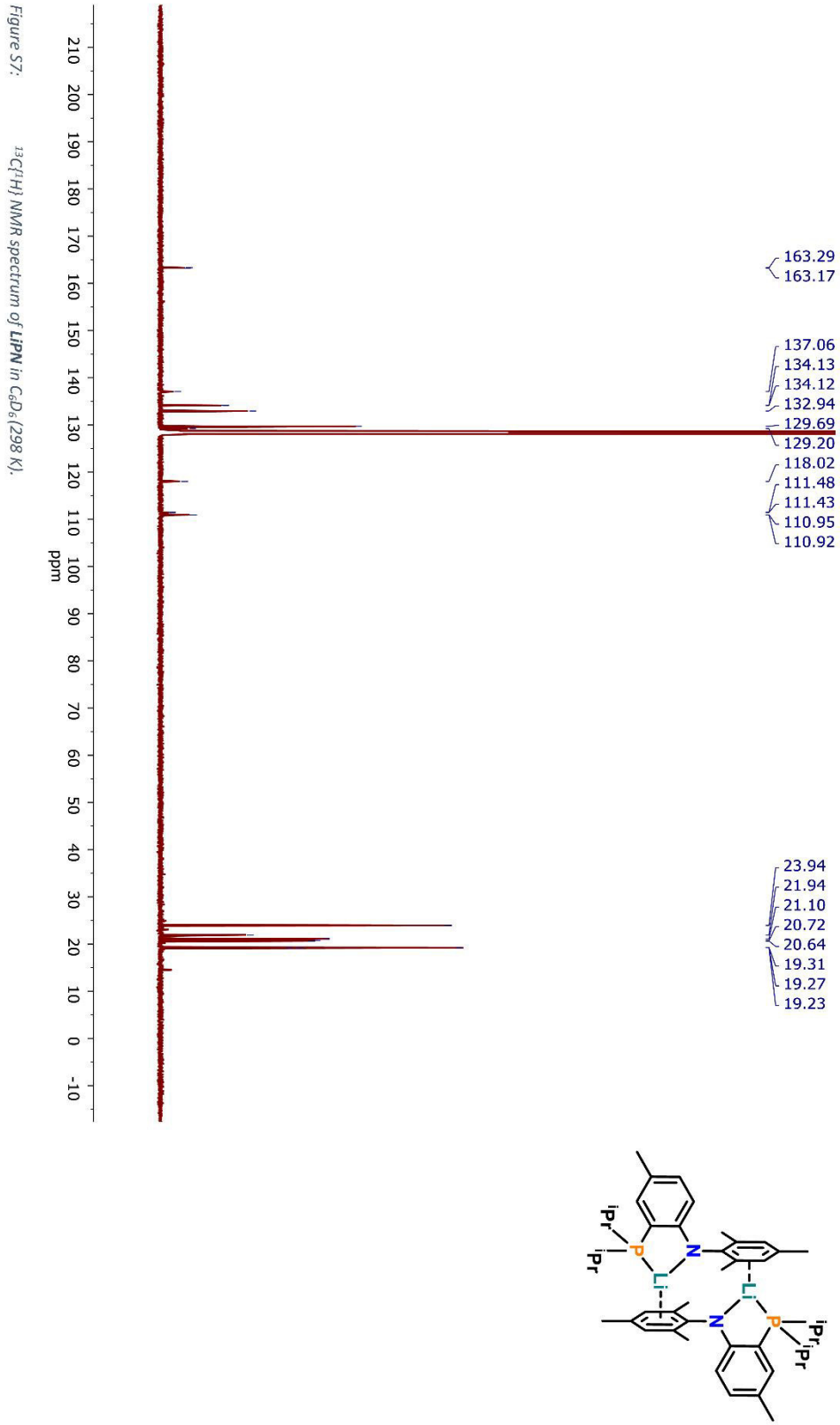

Figure S7: $^{13}C\{^1H\}$ *NMR spectrum of* ***LiPN*** *in* C_6D_6 *(298 K).*

*Figure S8: $^{31}P\{^{1}H\}$ NMR spectrum of **LiPN** in C_6D_6 (298 K).*

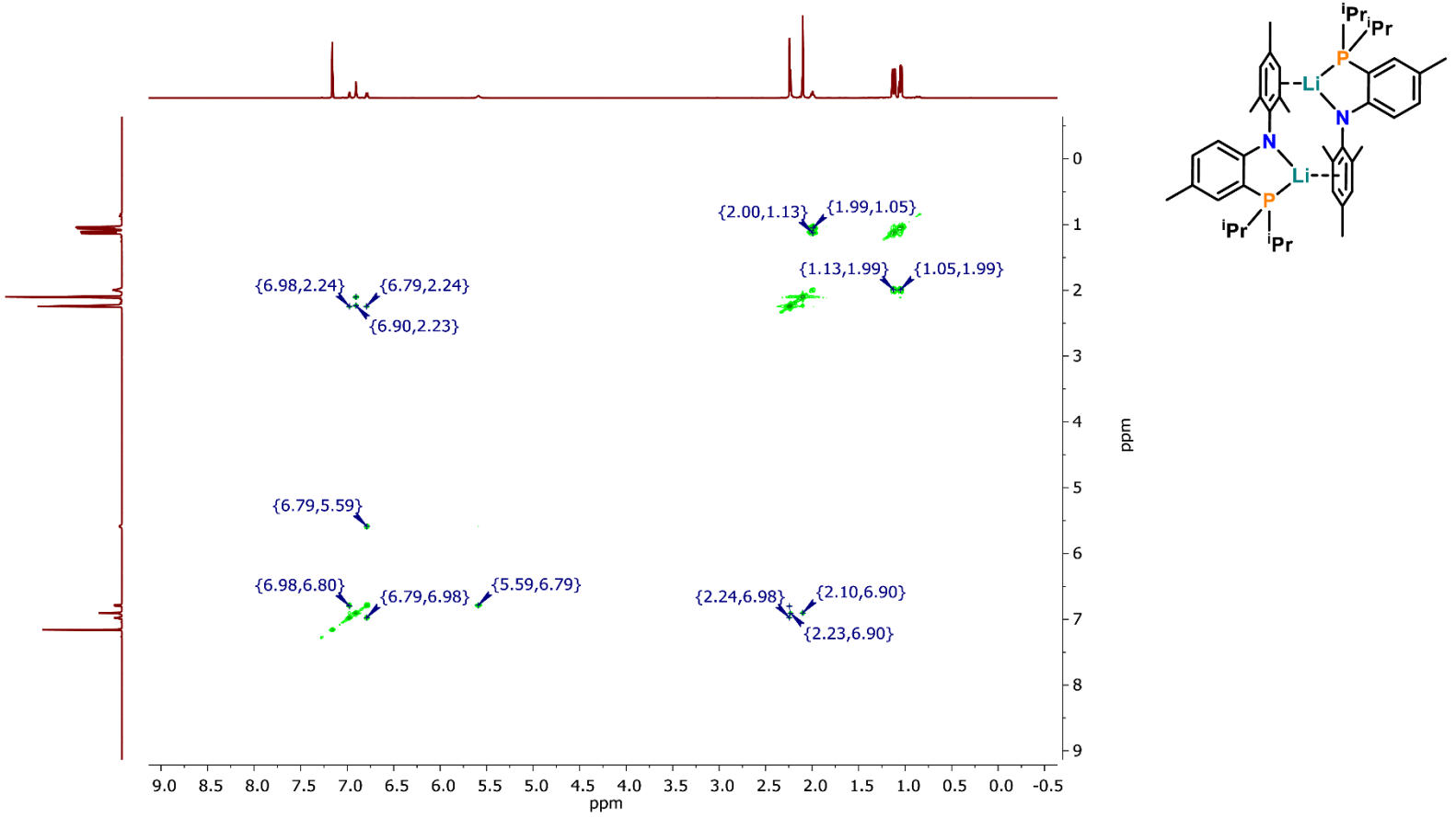

Figure S9: *^{1}H-^{1}H COSY NMR spectrum of **LiPN** in C_6D_6 (298 K).*

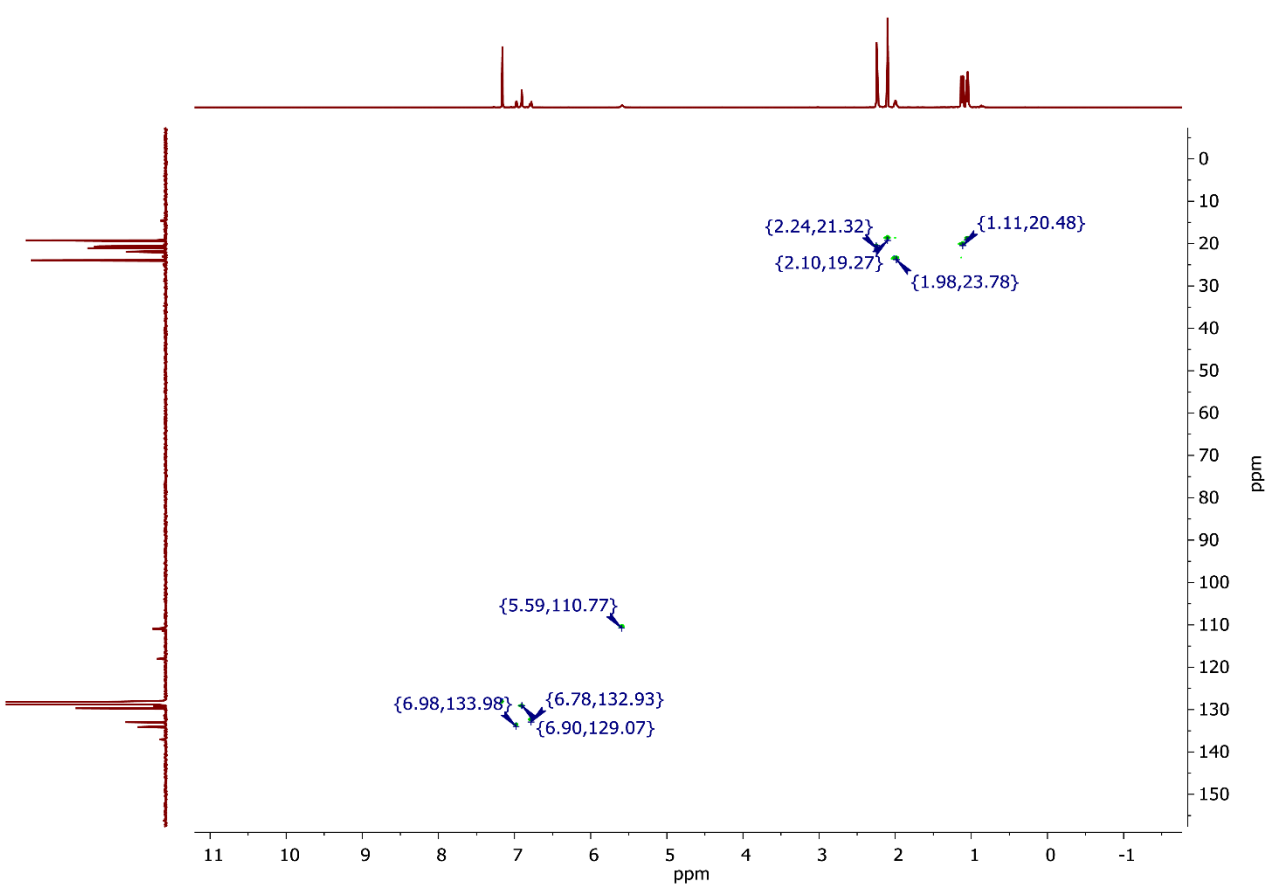

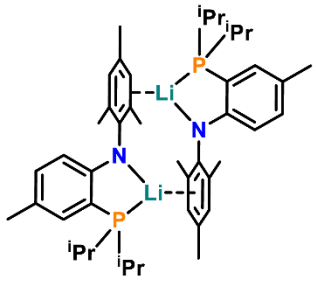

Figure S10: *^{1}H-^{13}C HSQC NMR spectrum of **LiPN** in C_6D_6 (298 K).*

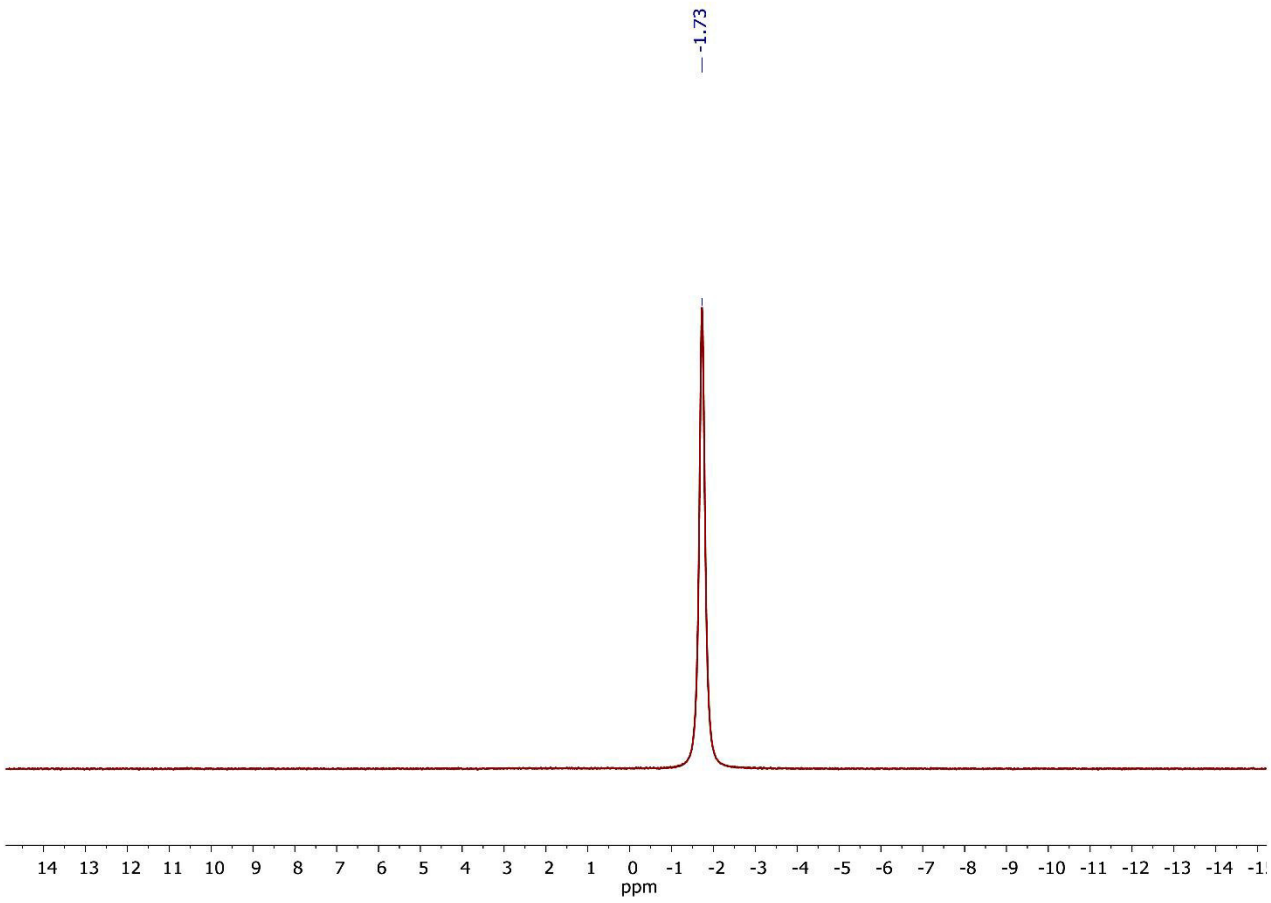

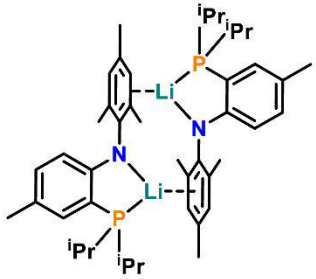

Figure S11: *^{7}Li NMR spectrum of **LiPN** in C_6D_6 (298 K).*

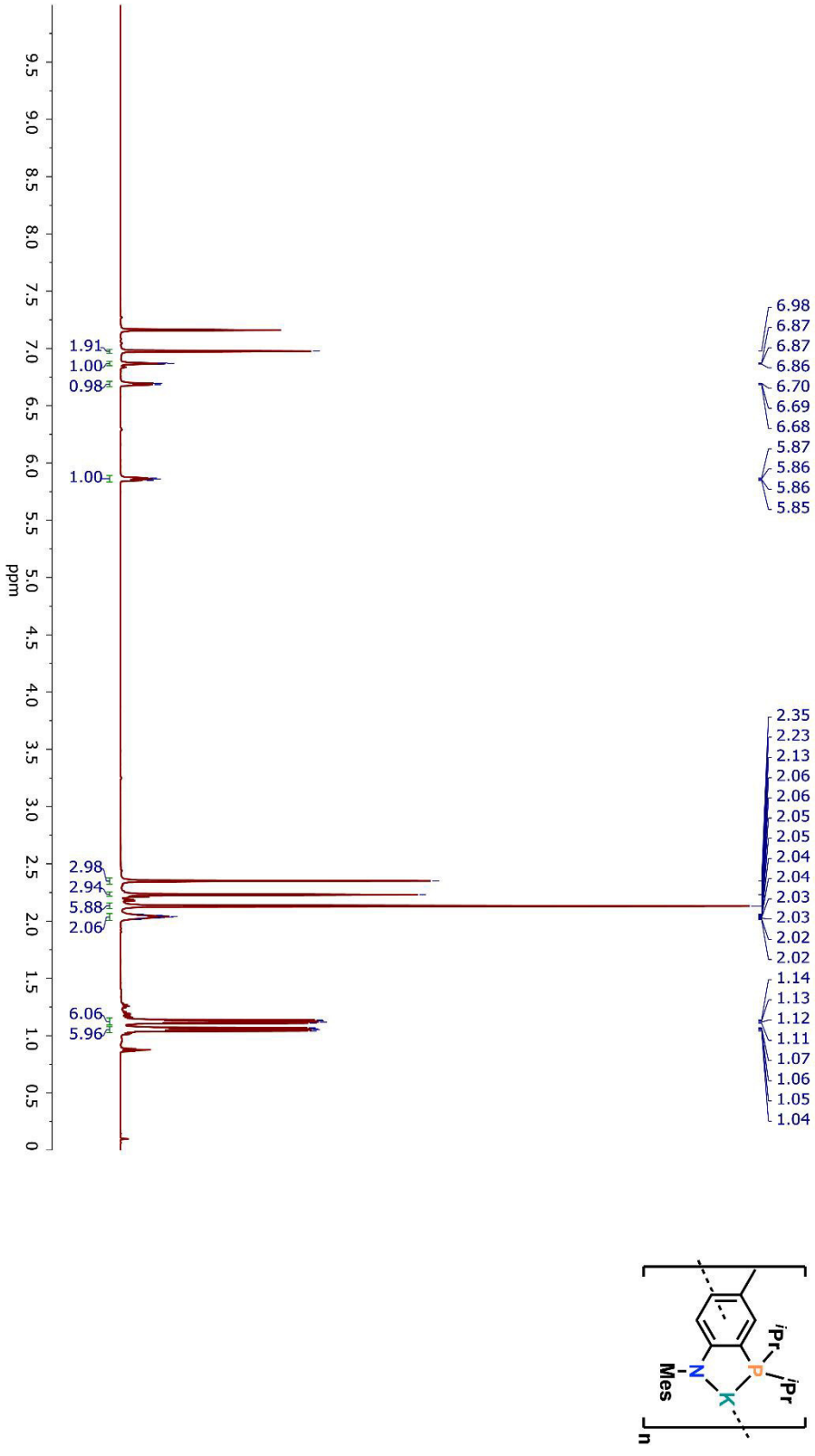

*Figure S12: ^1H NMR spectrum of **KPN** in C_6D_6 (298 K).*

Figure S13: $^{31}P\{^{1}H\}$ *NMR spectrum of* ***KPN*** *in* C_6D_6 *(298 K).*

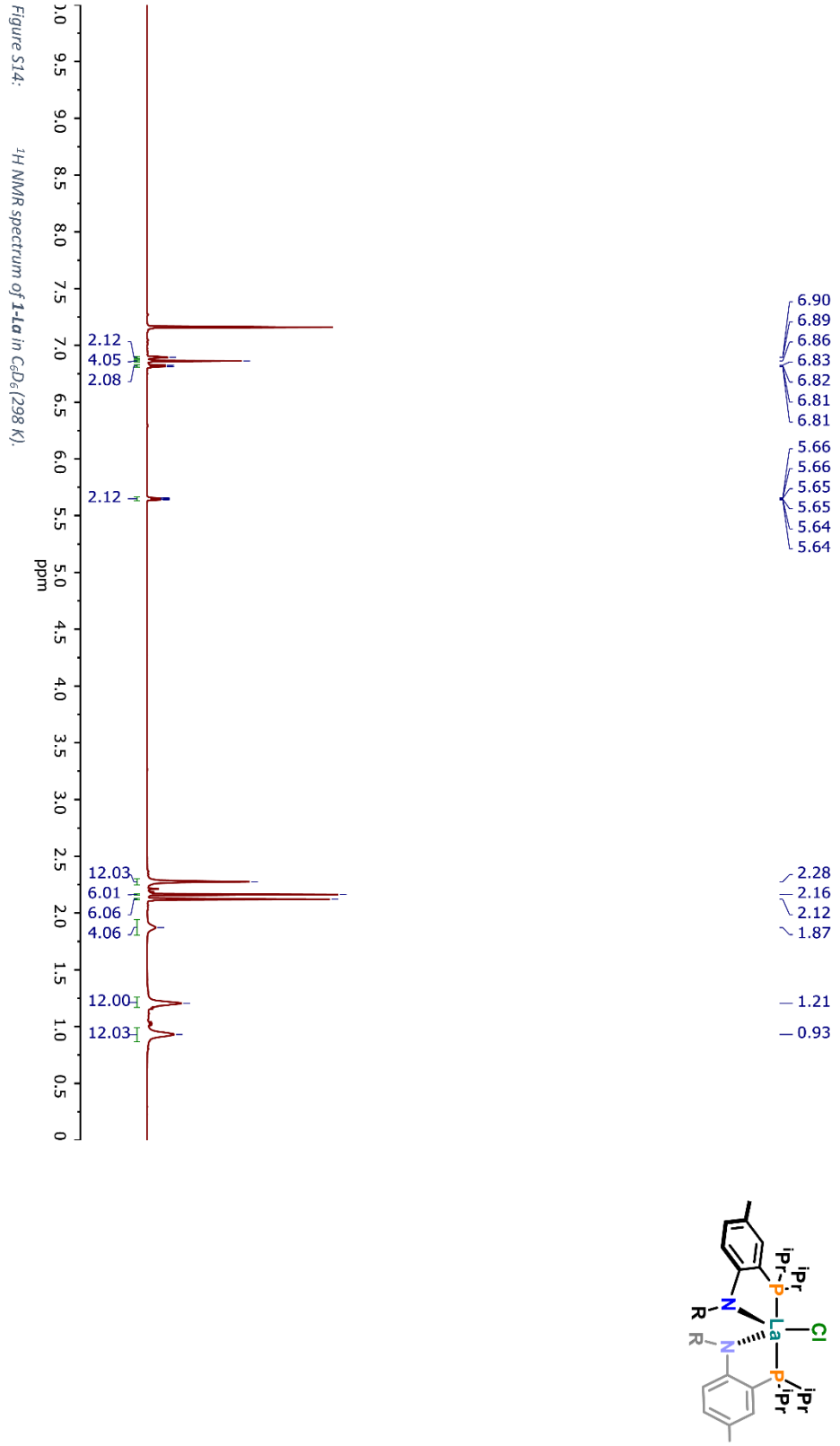

*Figure S14. ^{1}H NMR spectrum of **1-La** in C_6D_6 (298 K).*

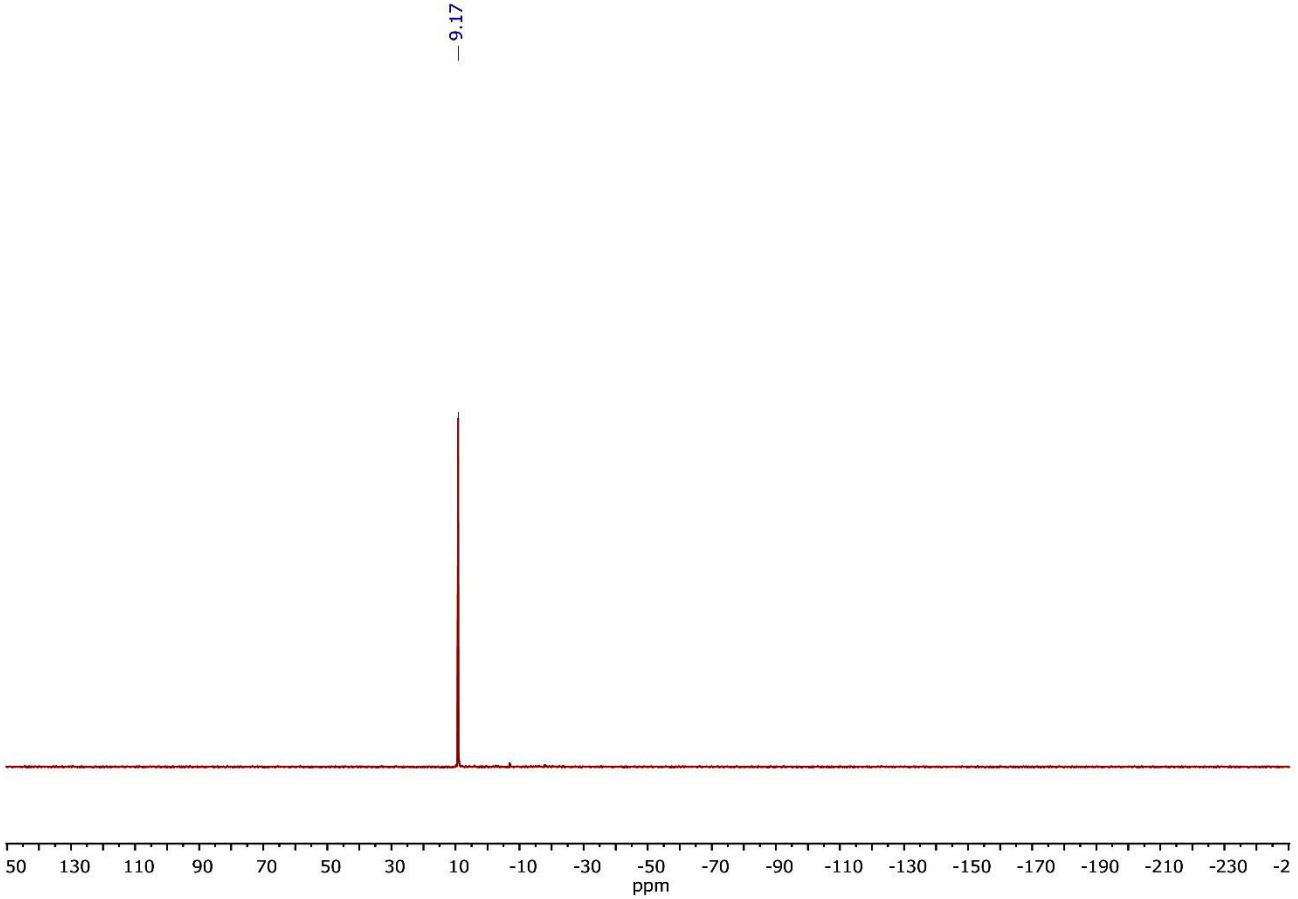

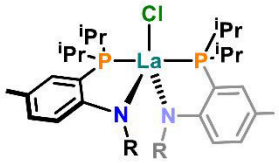

Figure S15: *$^{31}P\{^{1}H\}$ NMR spectrum of **1-La** in C_6D_6 (298 K).*

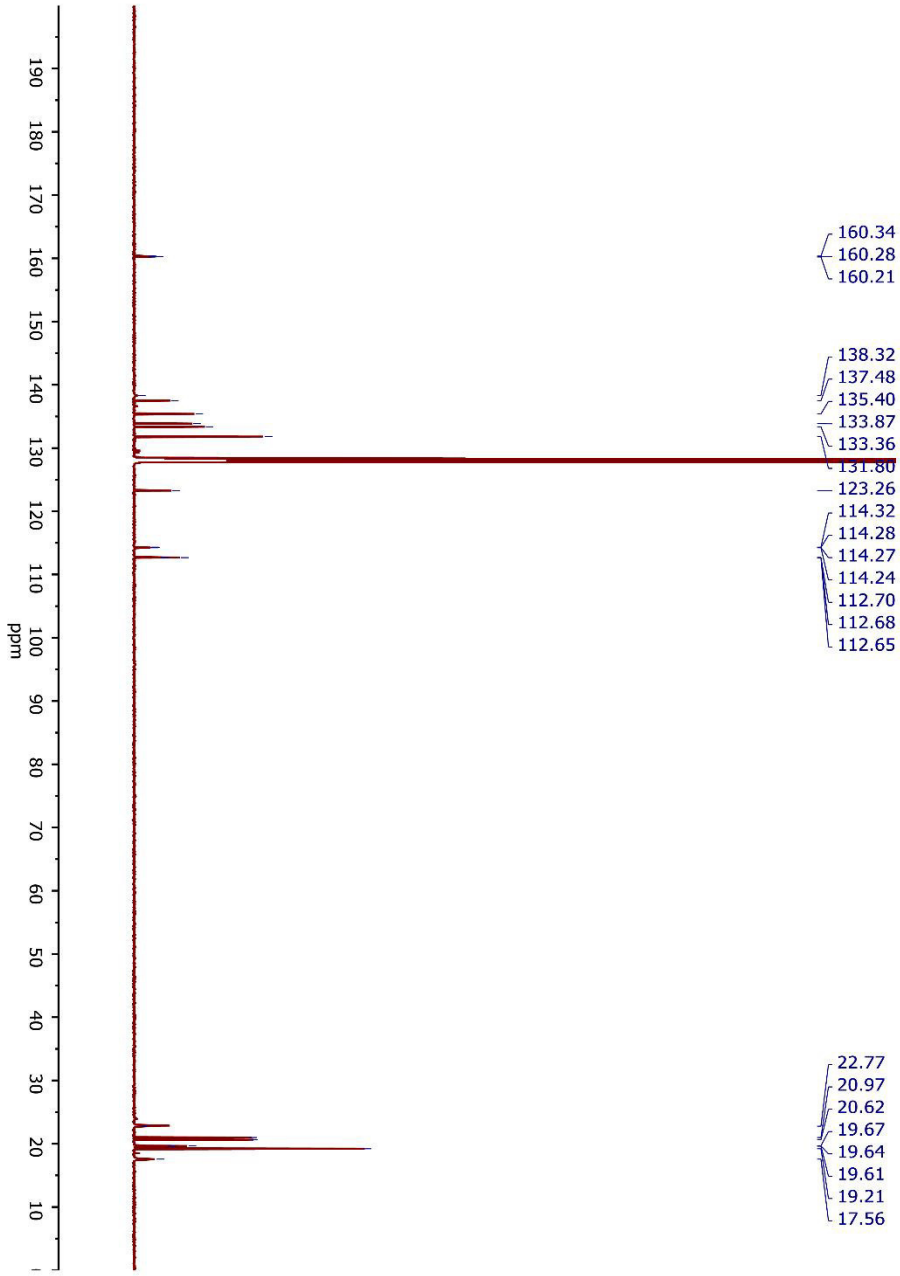

Figure S16: $^{13}C\{^{1}H\}$ *NMR spectrum of* **1-La** *in* C_6D_6 *(298 K).*

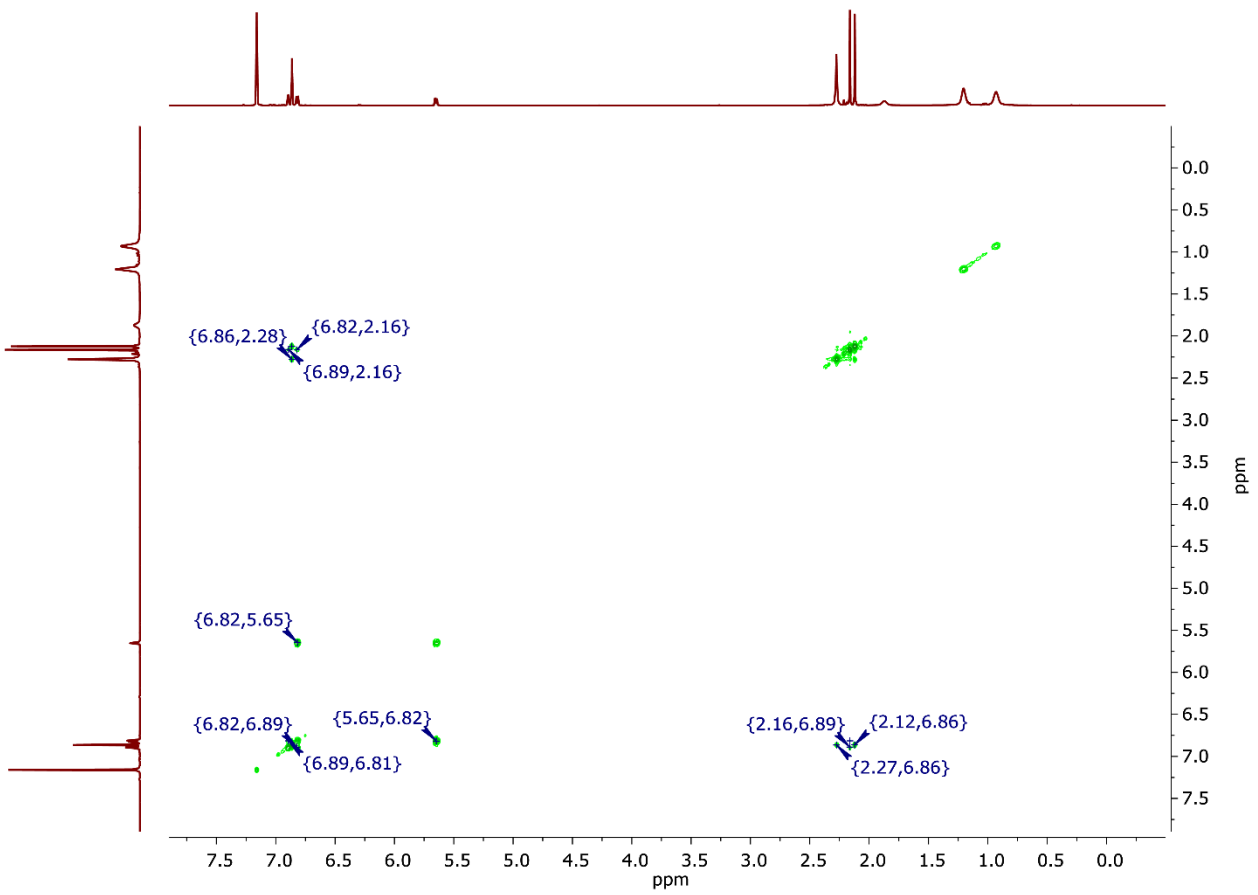

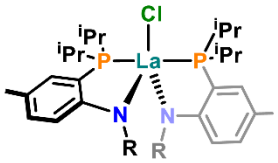

Figure S17: *^{1}H-^{1}H COSY NMR spectrum of **1-La** in C_6D_6 (298 K).*

Figure S18: ^{1}H-^{13}C *HSQC NMR spectrum of* ***1-La*** *in* C_6D_6 *(298 K).*

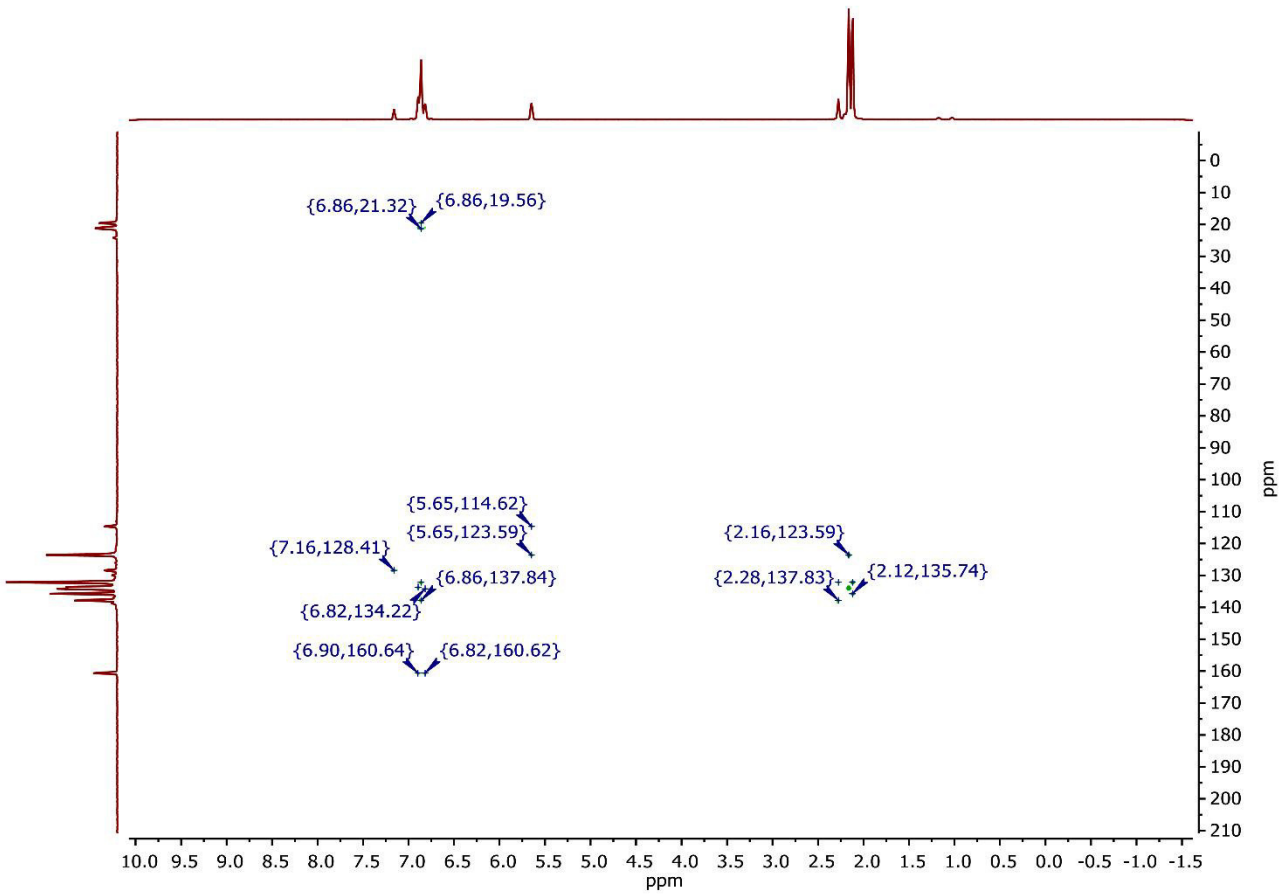

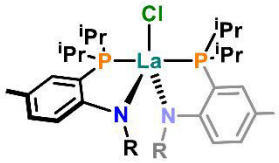

Figure S19: *^{1}H-^{13}C HMBC NMR spectrum of **1-La** in C_6D_6 (298 K).*

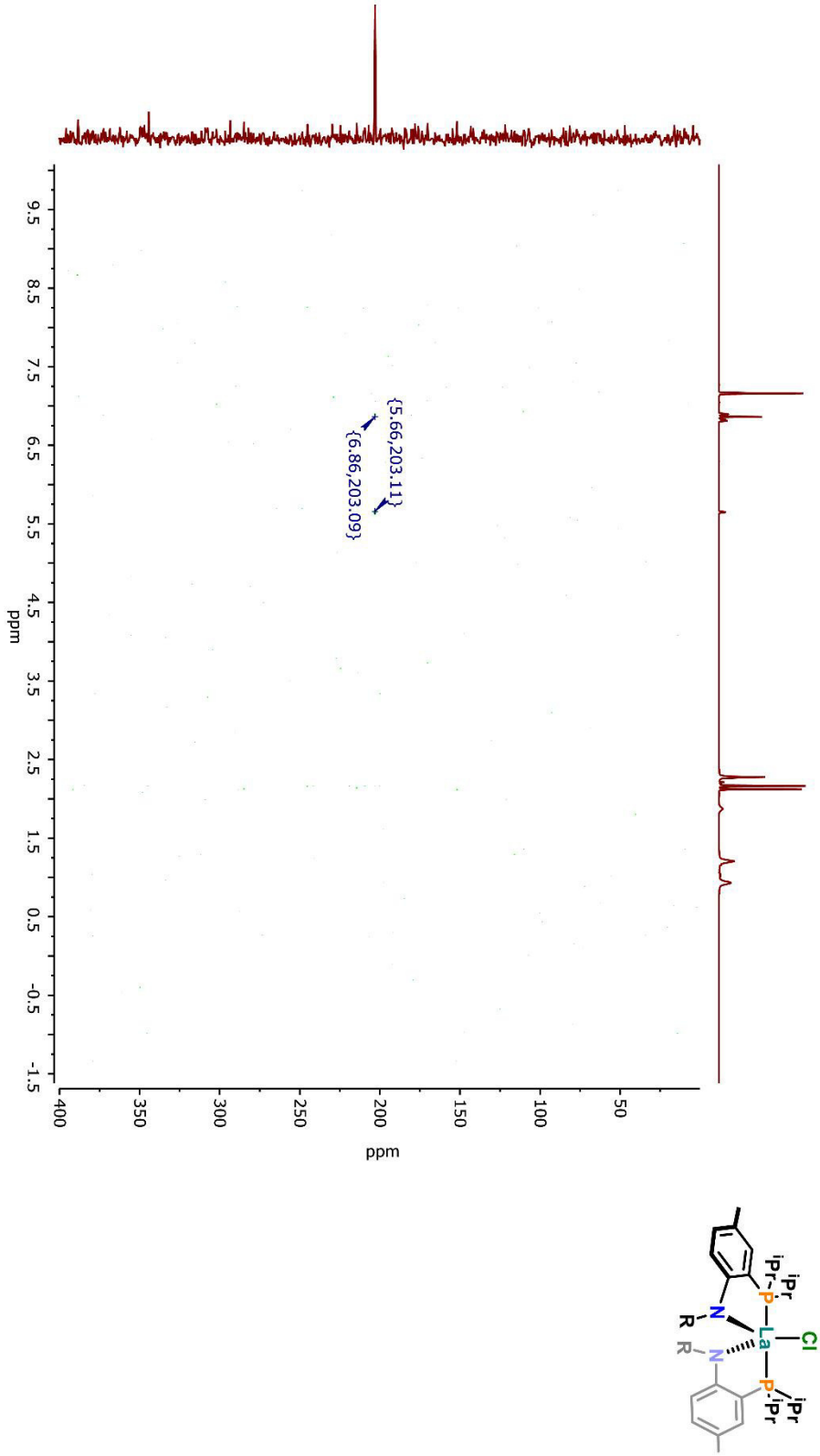

Figure S20: ^{1}H-^{15}N *HMBC NMR spectrum of* ***1-La*** *in* C_6D_6 *(298 K).*

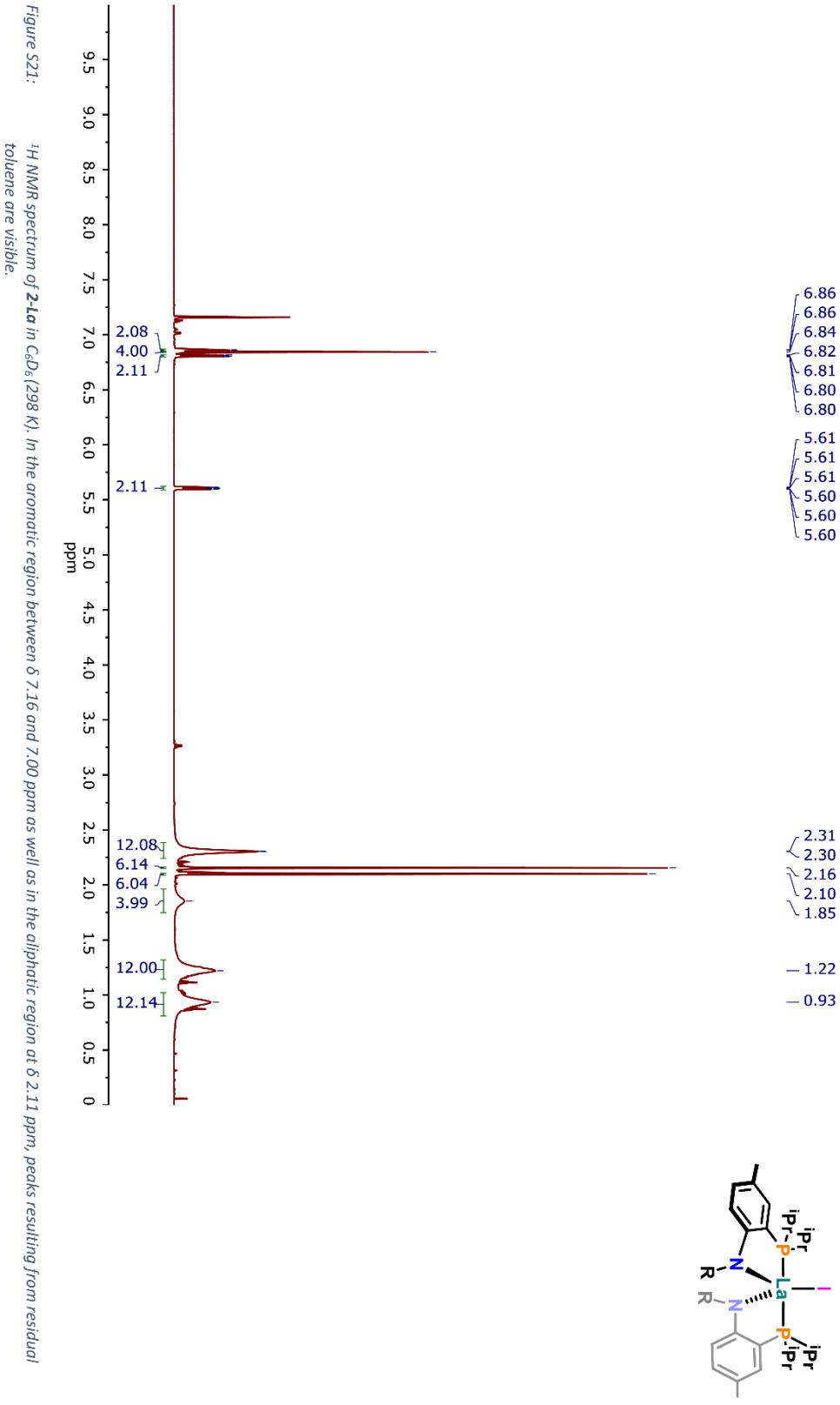

*Figure S21: ^1H NMR spectrum of **2-Lα** in C_6D_6 (298 K). In the aromatic region between δ 7.16 and 7.00 ppm as well as in the aliphatic region at δ 2.11 ppm, peaks resulting from residual toluene are visible.*

Figure S22: $^{31}P\{^{1}H\}$ *NMR spectrum of* **2-La** *in* C_6D_6 *(298 K).*

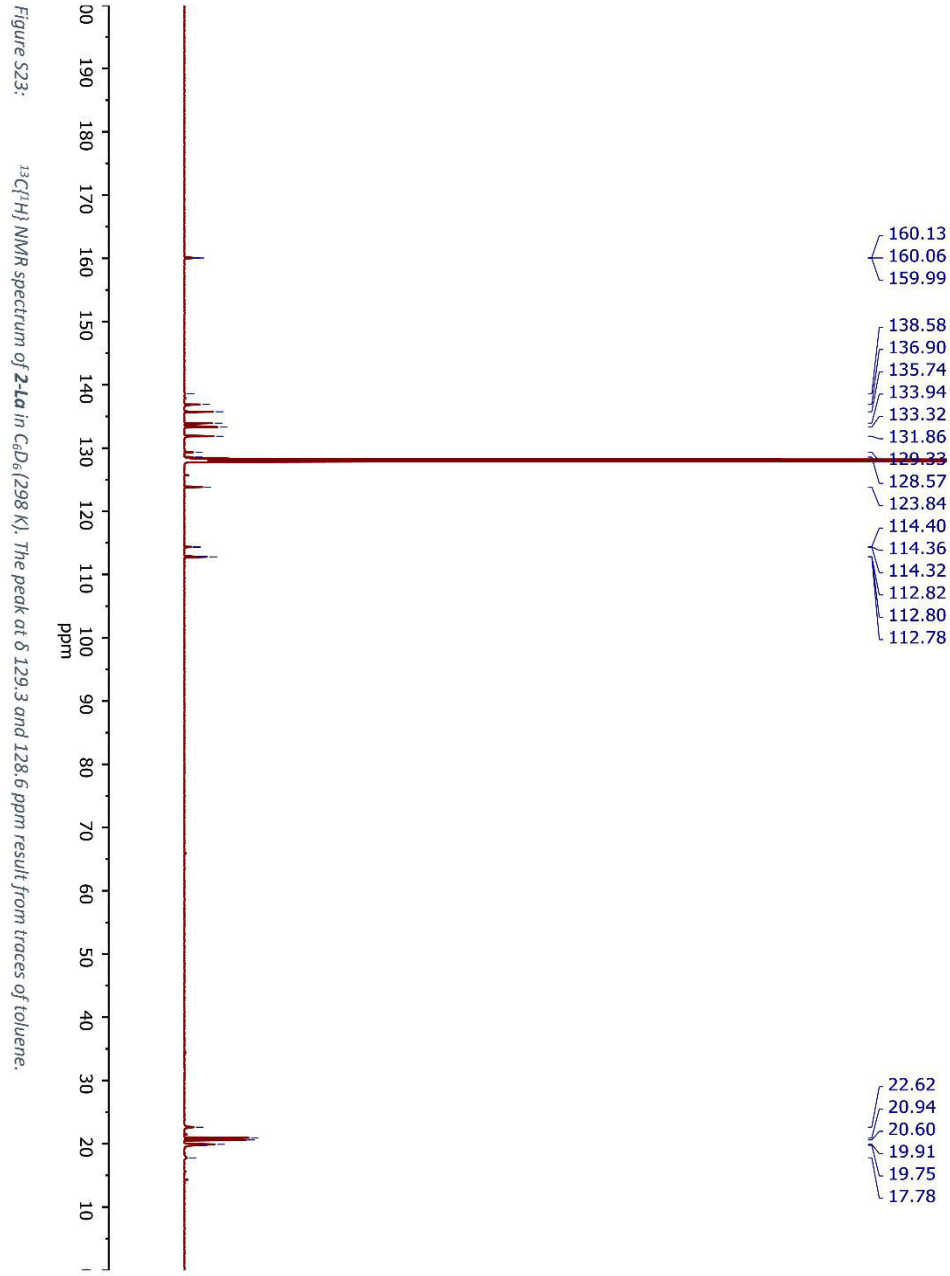

*Figure S23: $^{13}C\{^1H\}$ NMR spectrum of **2-La** in C_6D_6 (298 K). The peak at δ 129.3 and 128.6 ppm result from traces of toluene.*

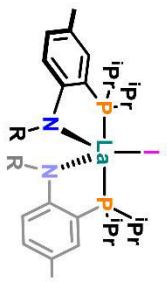

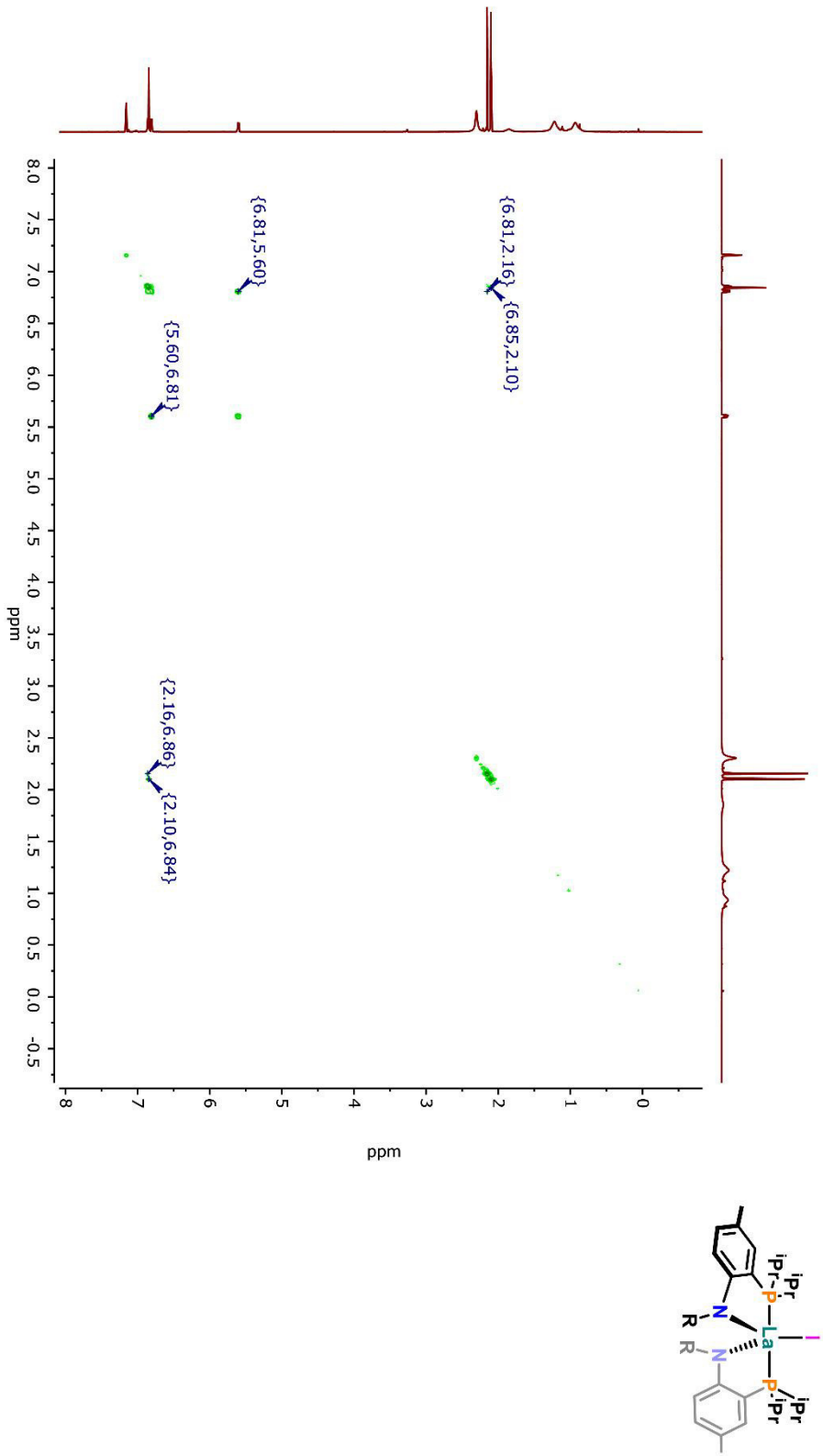

Figure S24: ^{1}H-^{1}H COSY NMR spectrum of **2-La** in C_6D_6 (298 K).

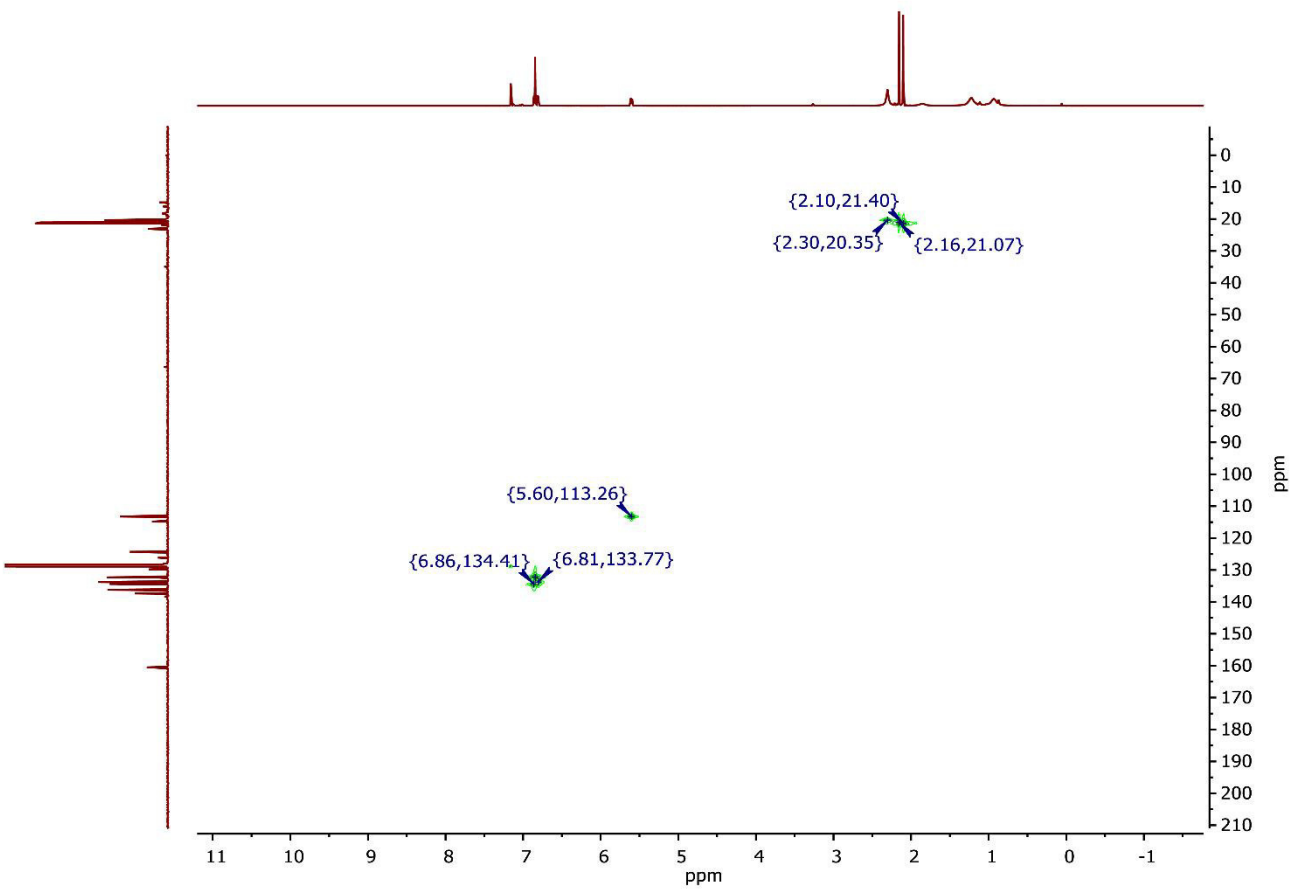

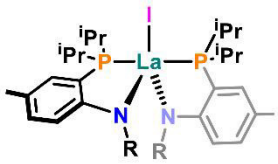

Figure S25: *^{1}H-^{13}C HSQC NMR spectrum of **2-La** in C_6D_6 (298 K).*

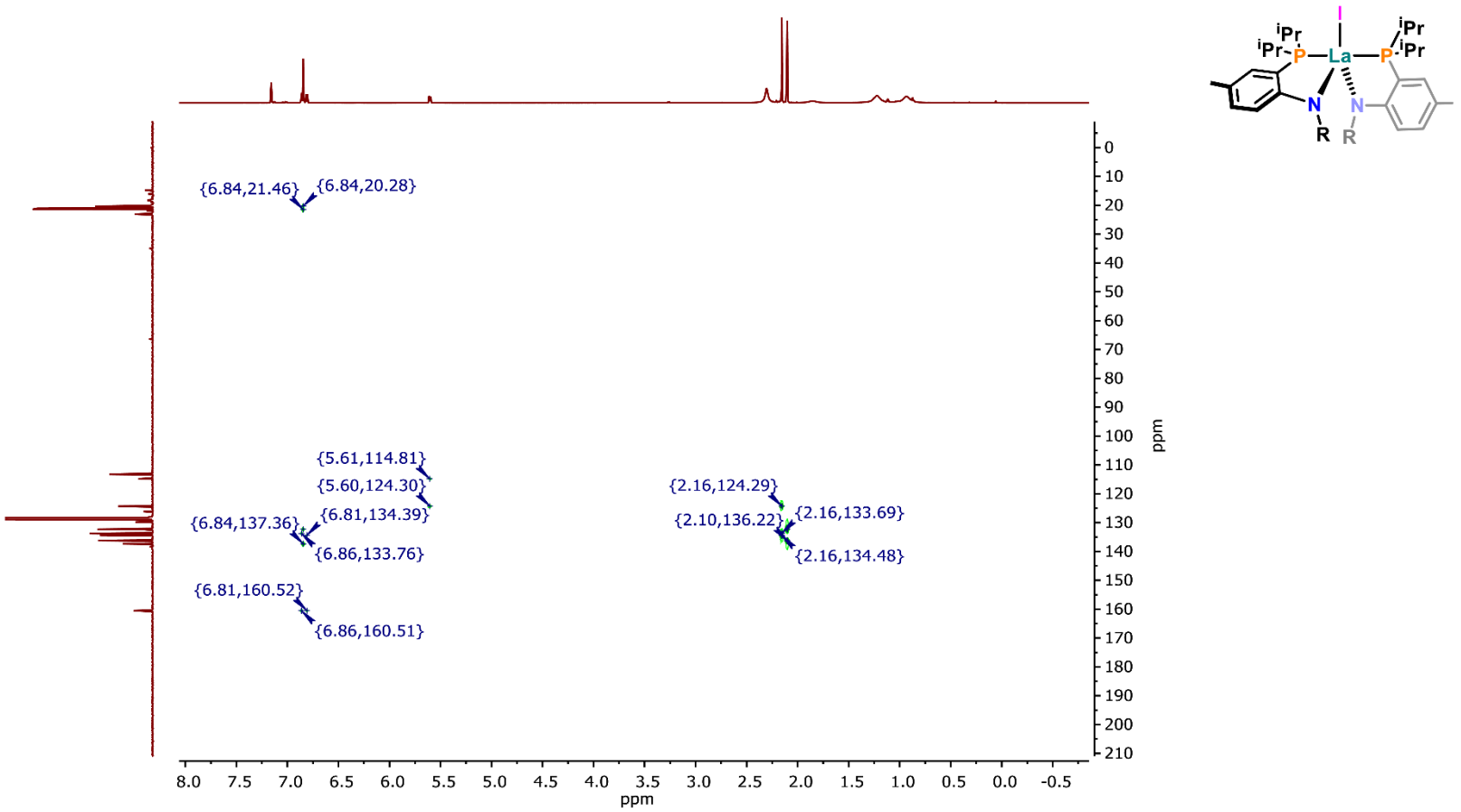

Figure S26: *^{1}H-^{13}C HMBC NMR spectrum of **2-La** in C_6D_6 (298 K).*

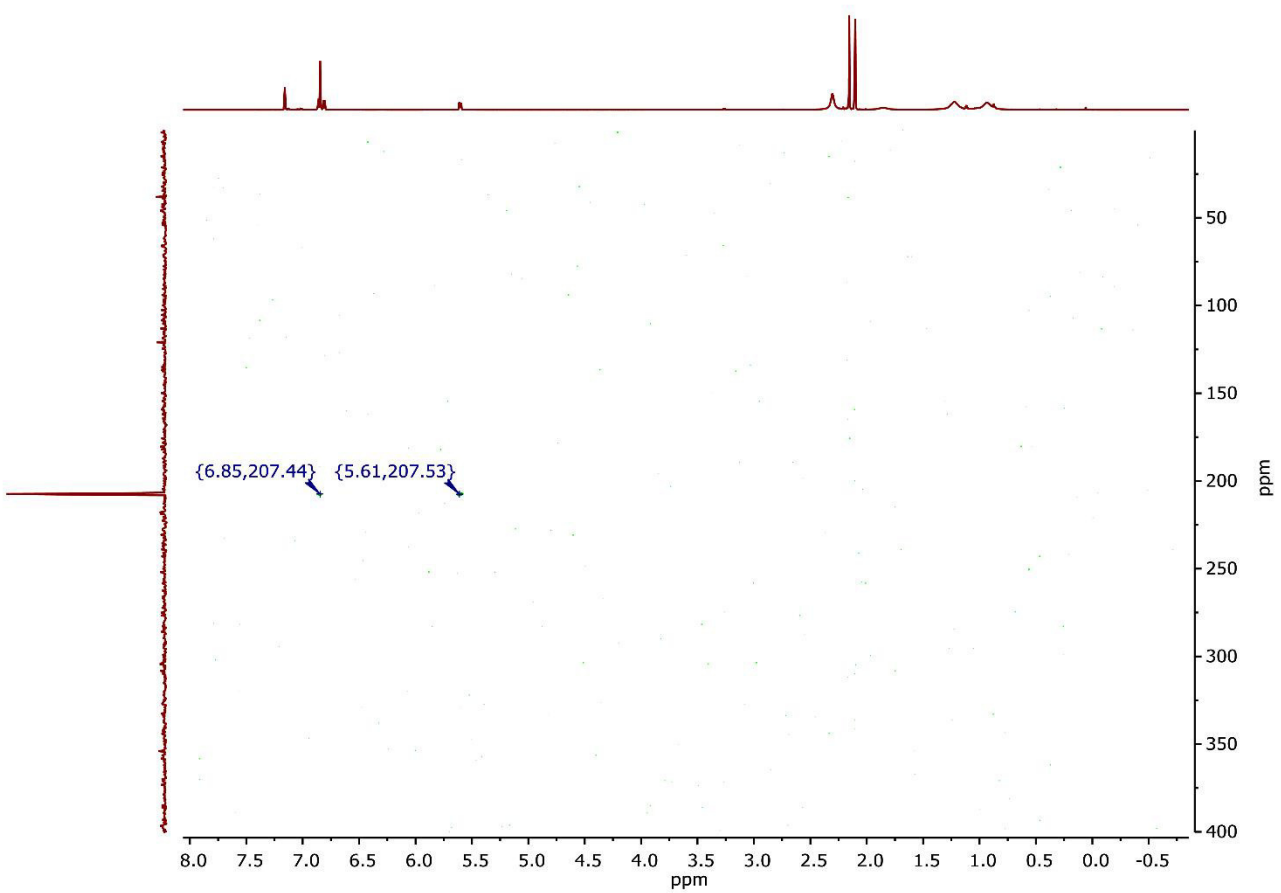

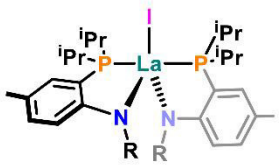

Figure S27: *^{1}H-^{15}N HMBC NMR spectrum of **2-La** in C_6D_6 (298 K).*

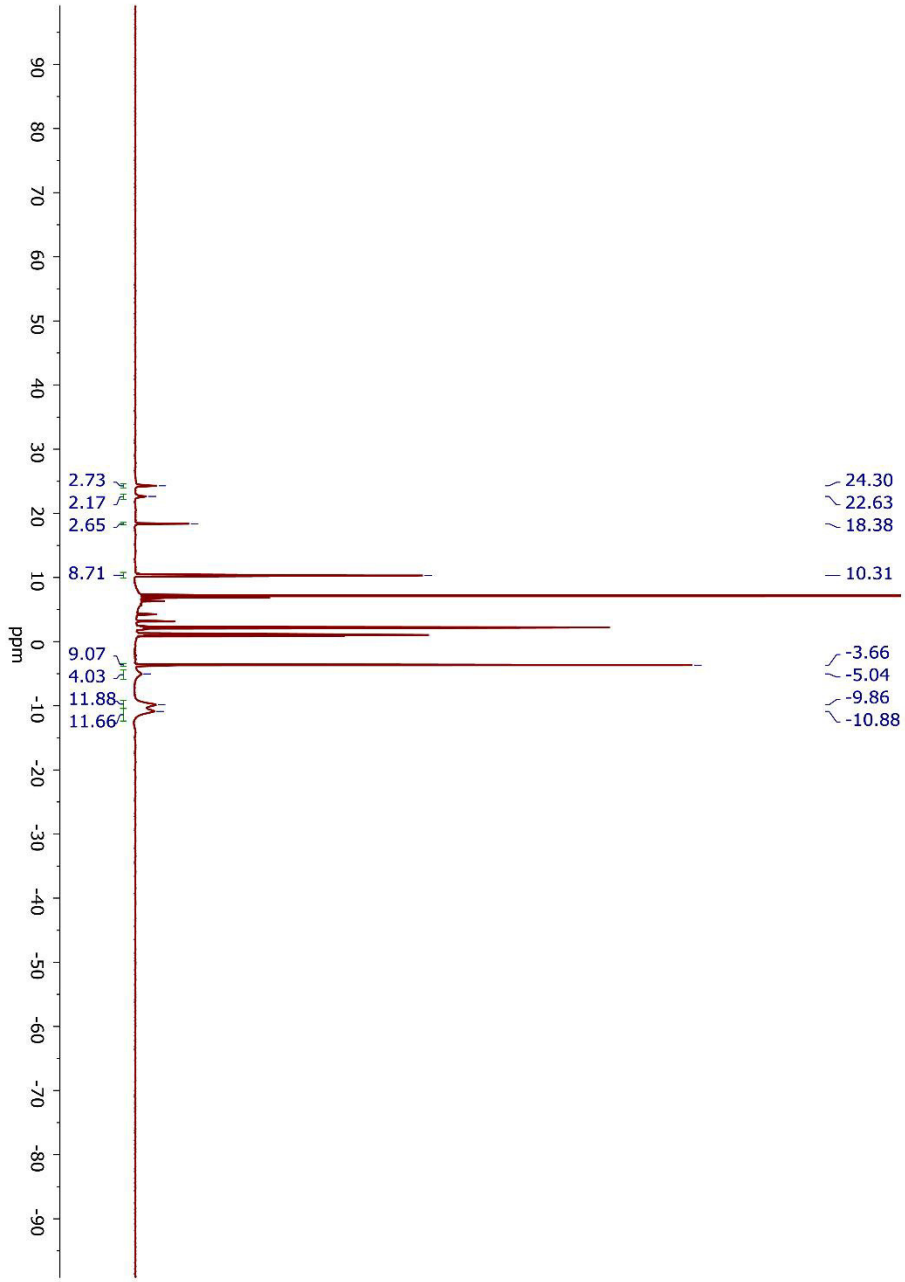

*Figure S28: ^{1}H NMR spectrum of **1-Ce** in C_6D_6 (298 K).*

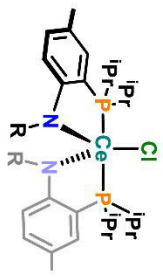

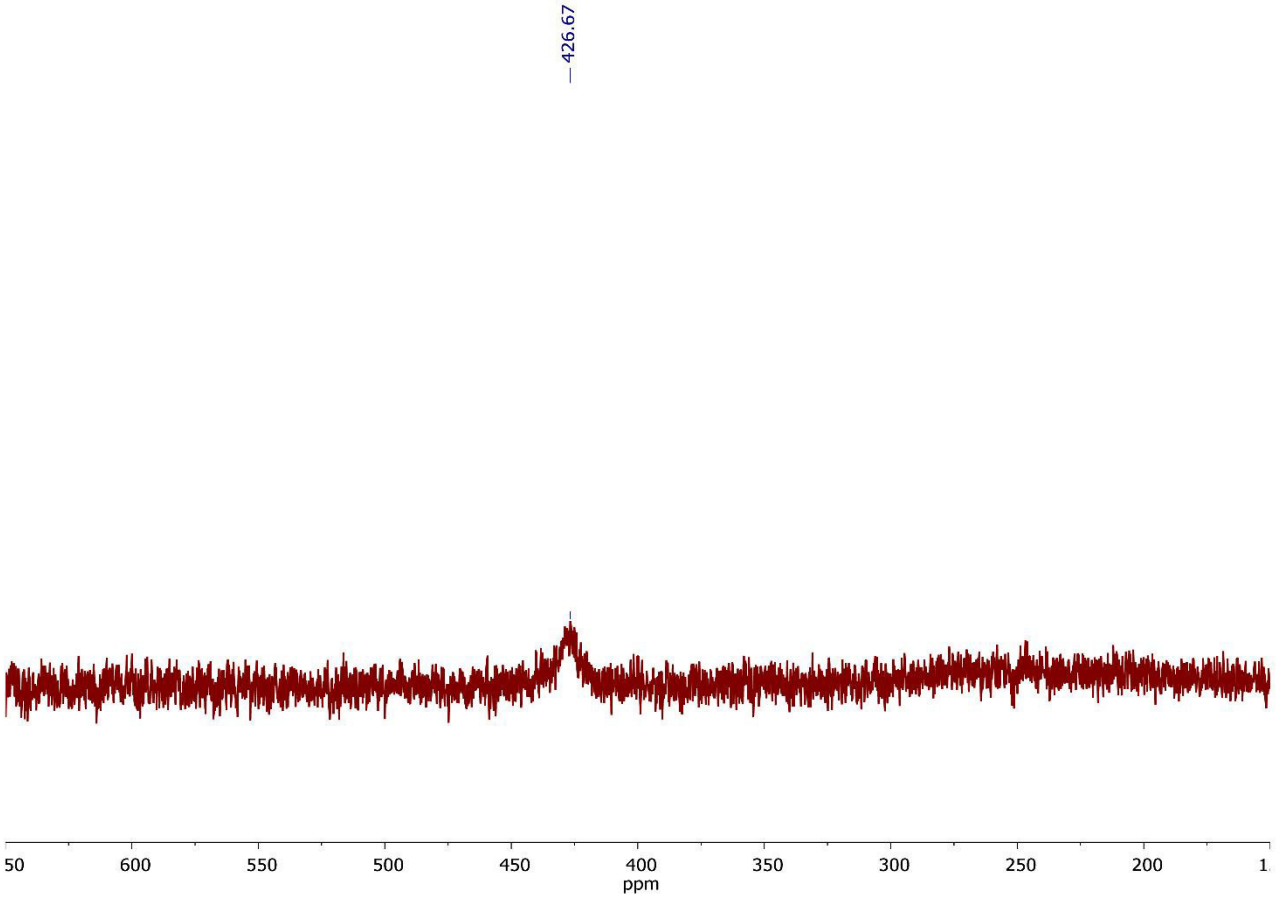

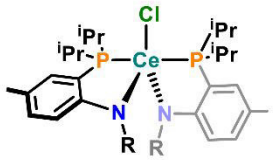

Figure S29: *$^{31}P\{^{1}H\}$ NMR spectrum of **1-Ce** in C_6D_6 (298 K).*

Figure S30: $^{31}P\{^1H\}$ *NMR of* ***1-Ce*** *in THF-d_8 (298 K).*

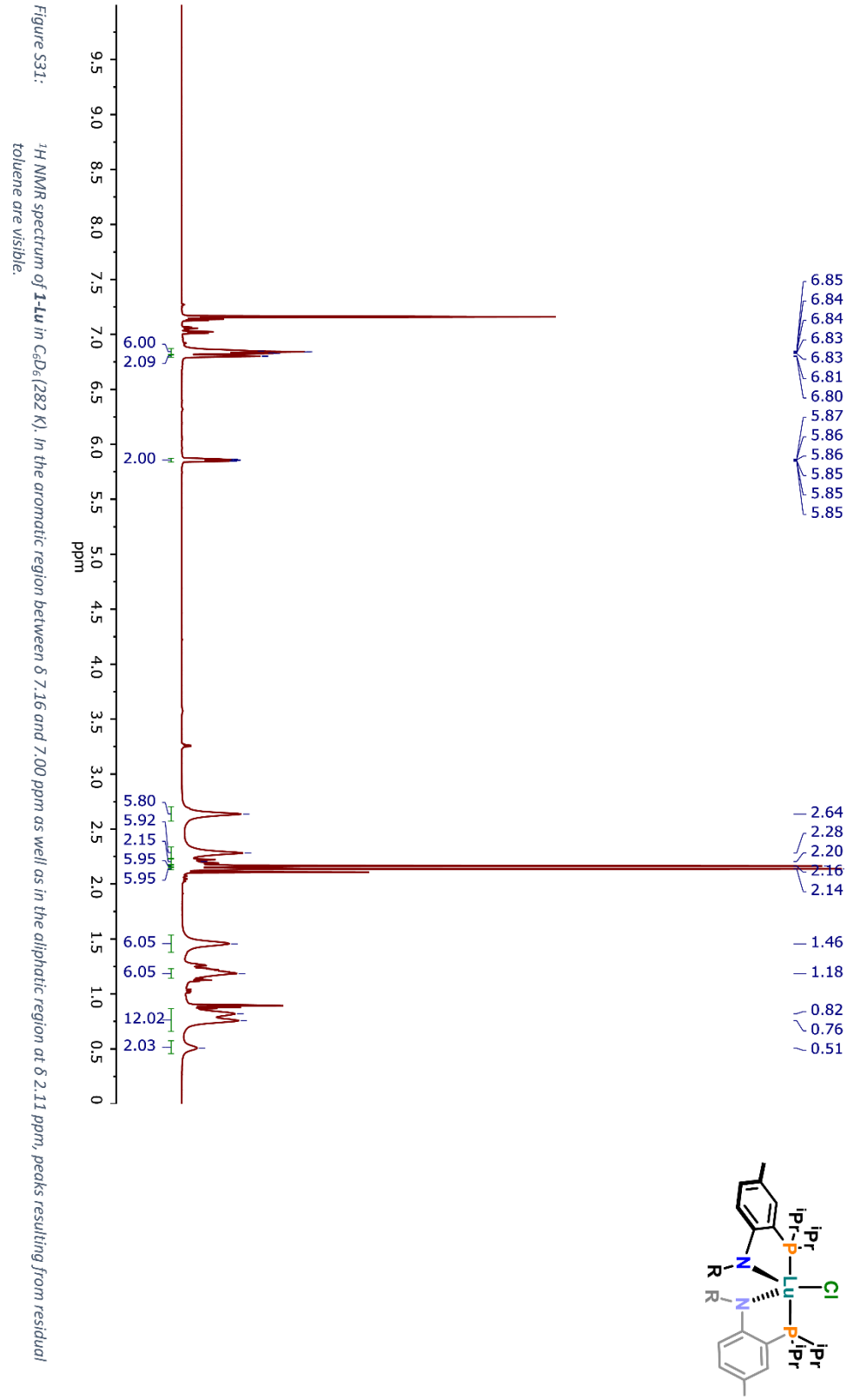

*Figure S31: ^1H NMR spectrum of **1-Lu** in C_6D_6 (282 K). In the aromatic region between δ 7.16 and 7.00 ppm as well as in the aliphatic region at δ 2.11 ppm, peaks resulting from residual toluene are visible.*

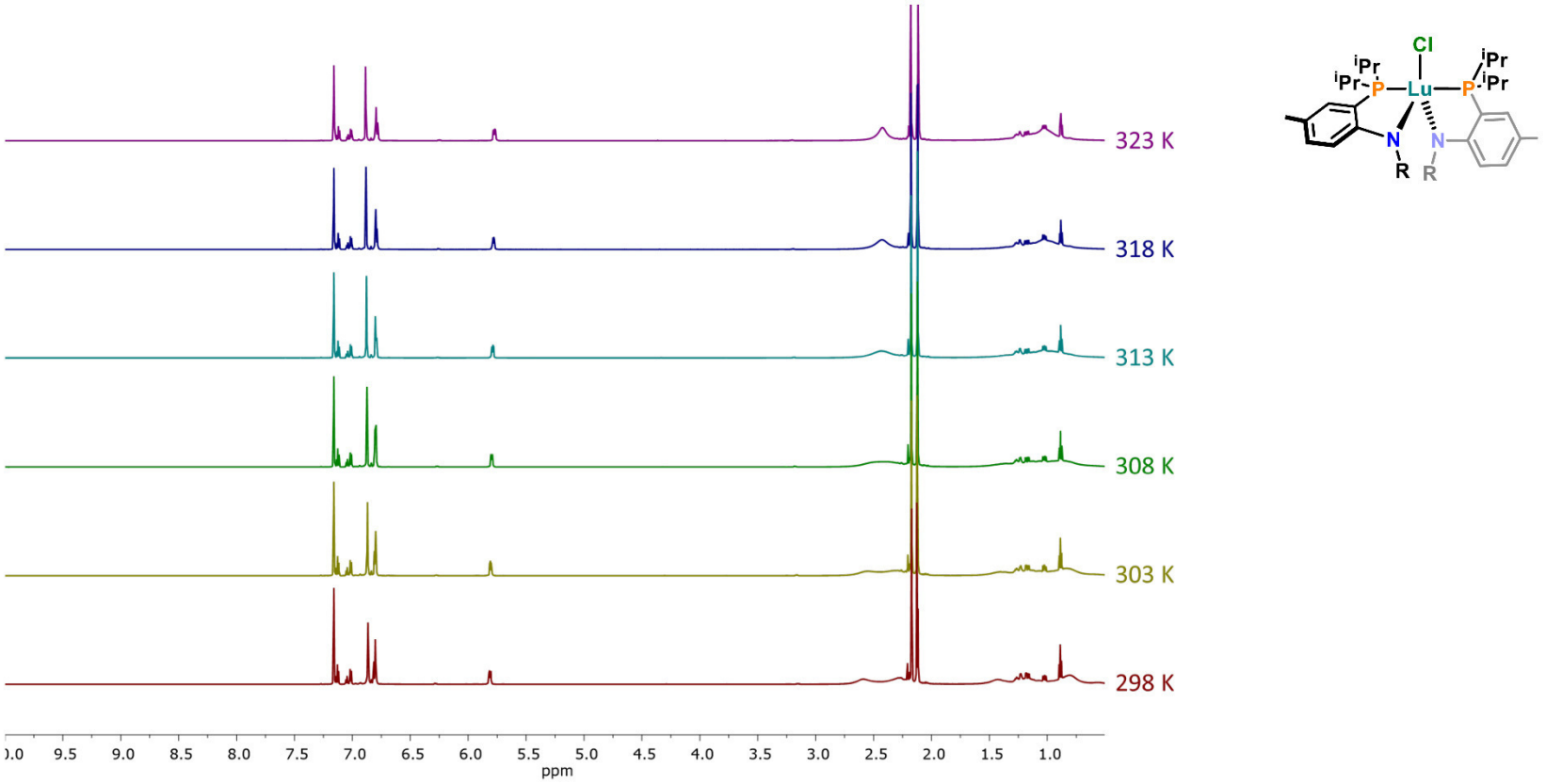

Figure S32: *^{1}H VT NMR spectra of **1-Lu** from 298 K to 323 K in C_6D_6. In the aromatic region between δ 7.16 and 7.00 ppm as well as in the aliphatic region at δ 2.11 ppm, peaks resulting from residual toluene are visible.*

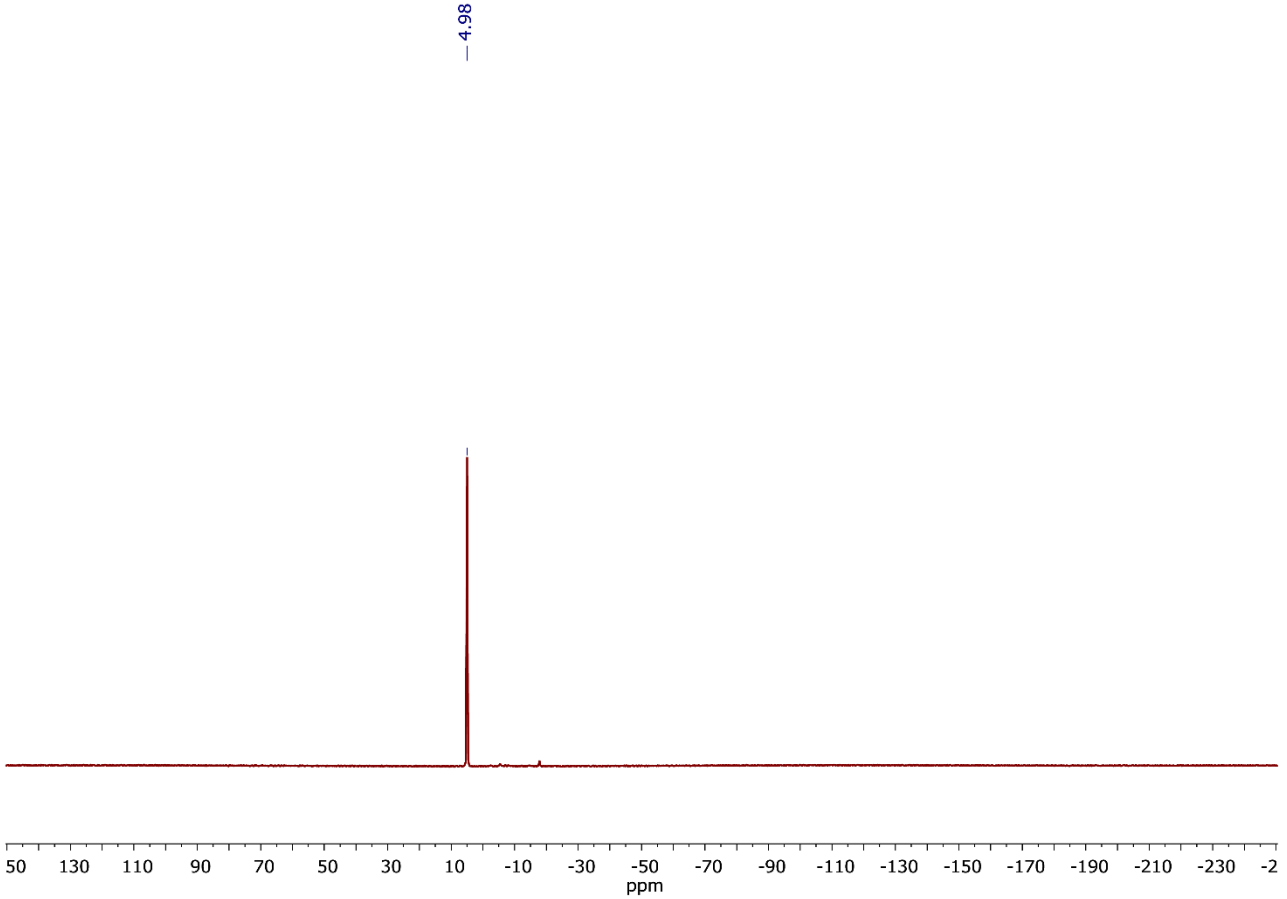

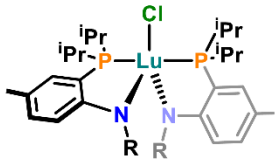

Figure S33: *$^{31}P\{^{1}H\}$ NMR spectrum of **1-Lu** in C_6D_6 (282 K).*

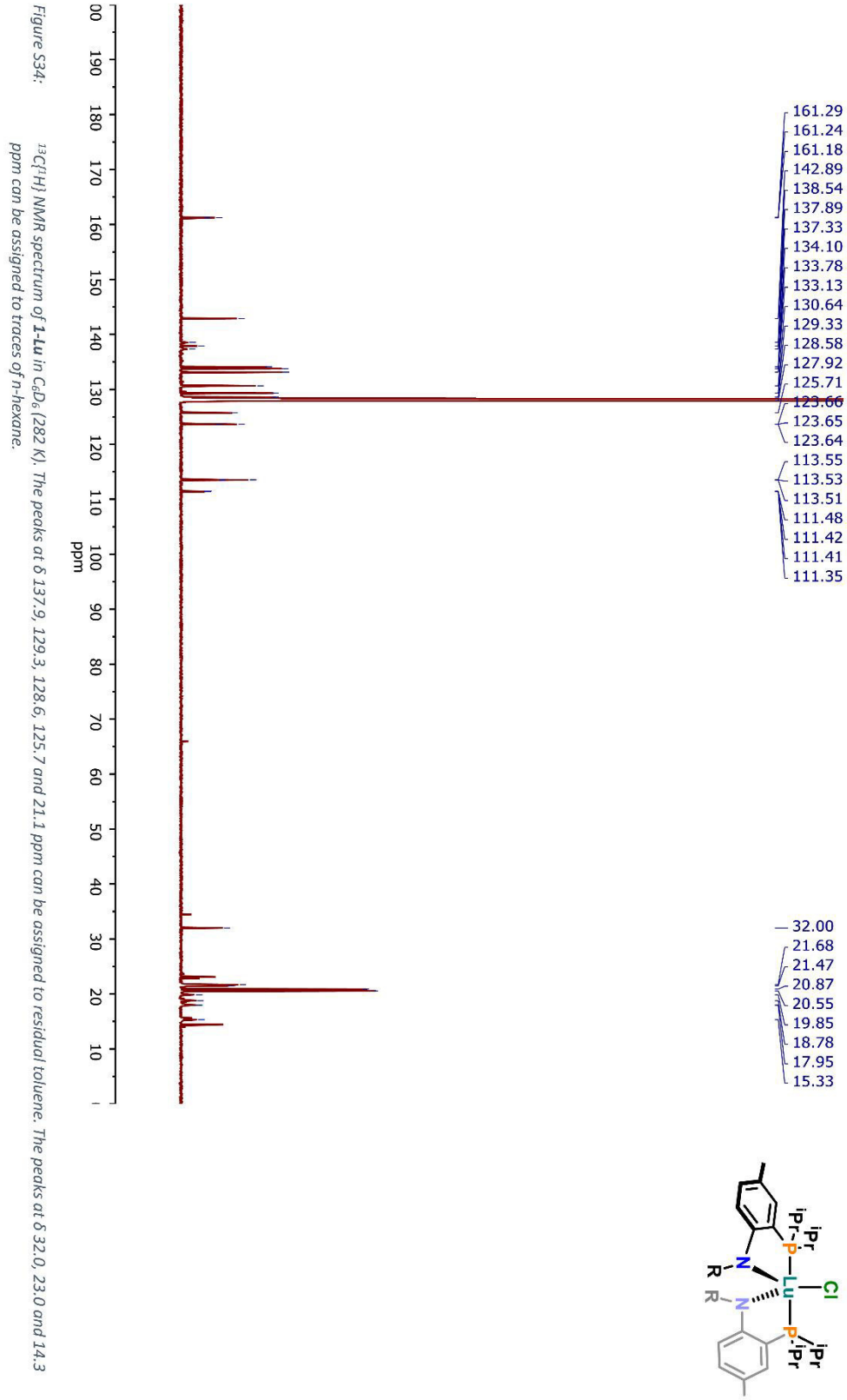

*Figure S34: $^{13}C\{^1H\}$ NMR spectrum of **1-Lu** in C_6D_6 (282 K). The peaks at δ 137.9, 129.3, 128.6, 125.7 and 21.1 ppm can be assigned to residual toluene. The peaks at δ 32.0, 23.0 and 14.3 ppm can be assigned to traces of n-hexane.*

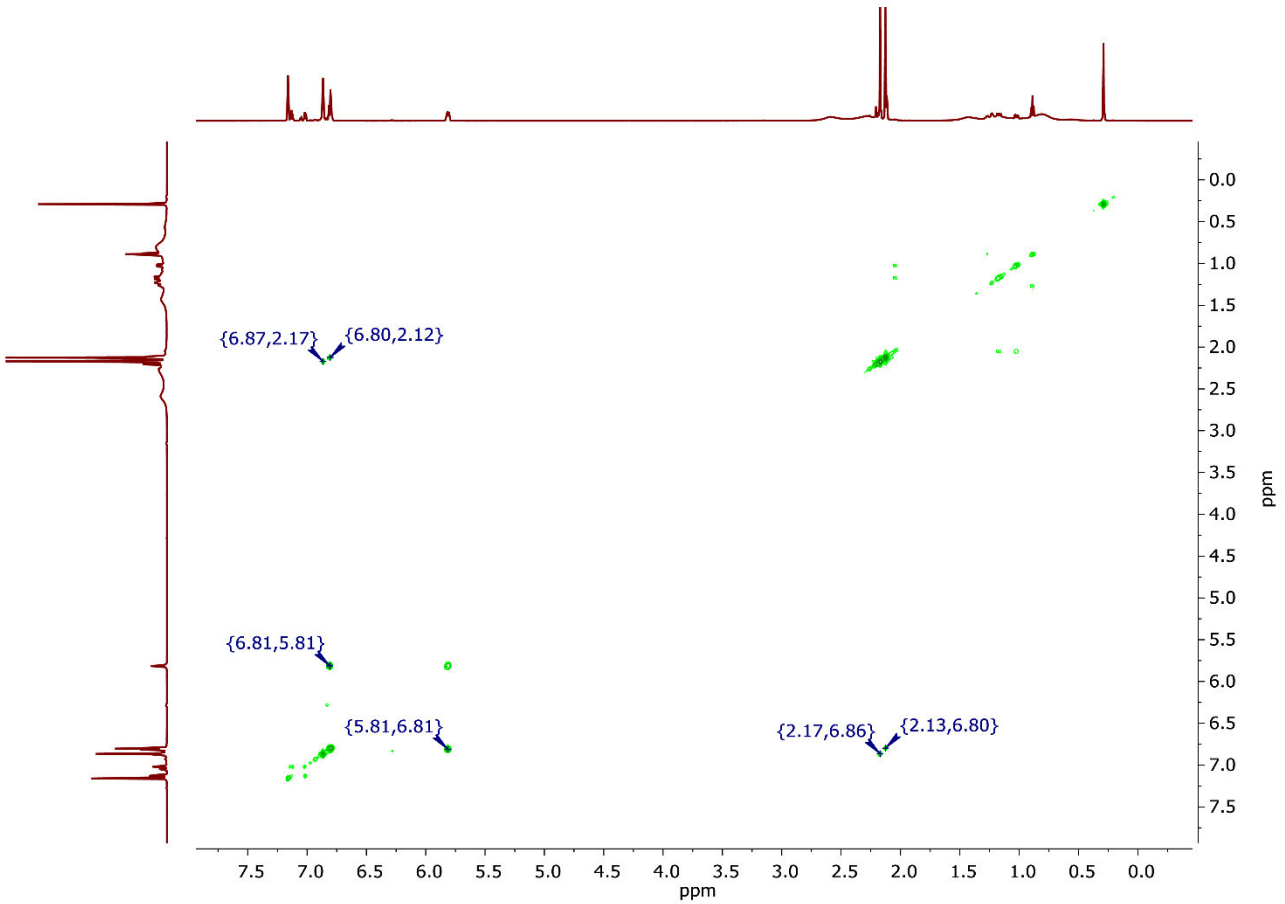

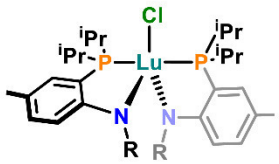

Figure S35: *^{1}H-^{1}H COSY NMR spectrum of **1-Lu** in C_6D_6 (282 K). Small impurities of **HPN** are visible in the aliphatic region.*

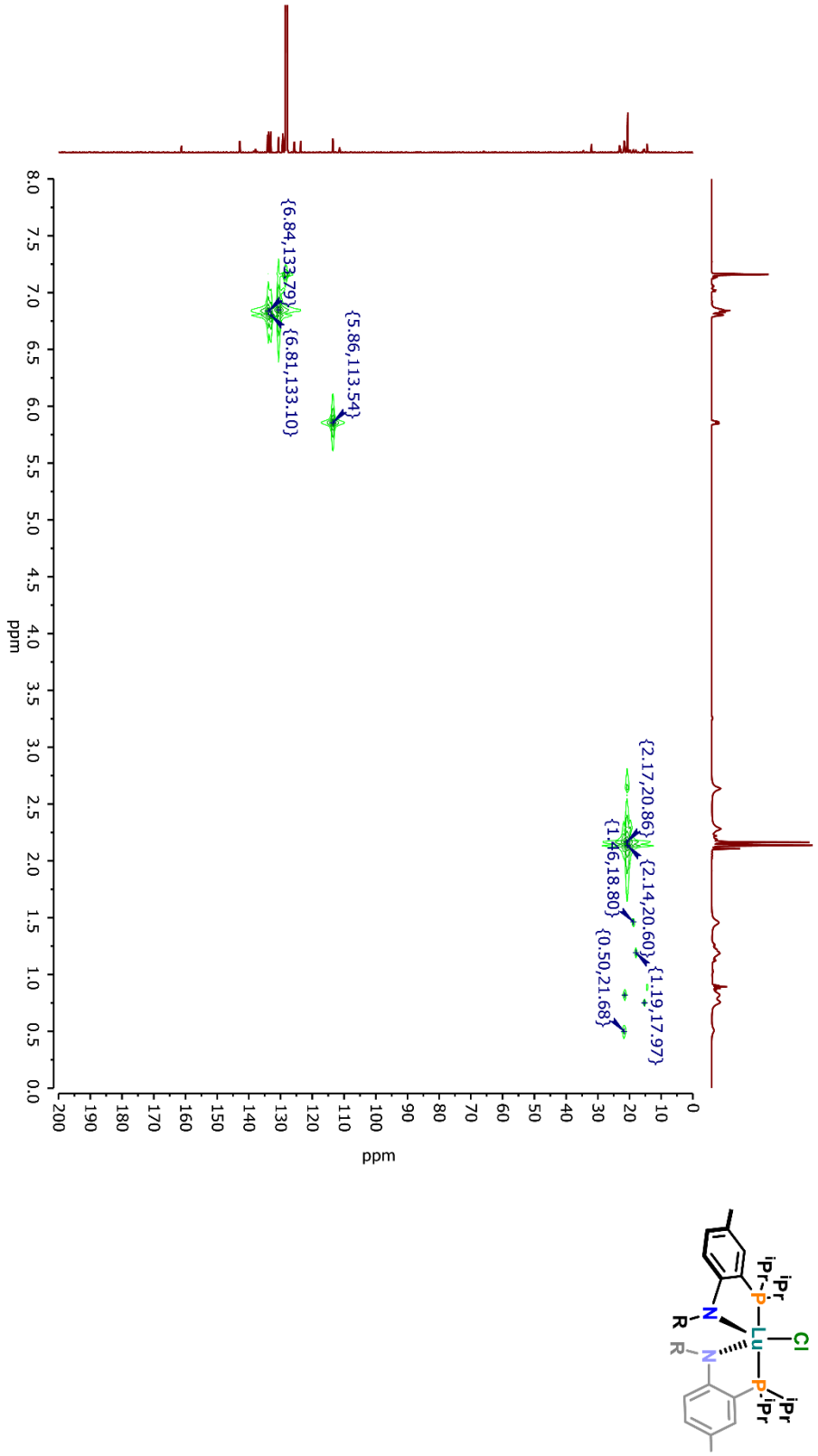

Figure S36: *^{1}H-^{13}C HSQC NMR spectrum of **1-Lu** in C_6D_6 (282 K).*

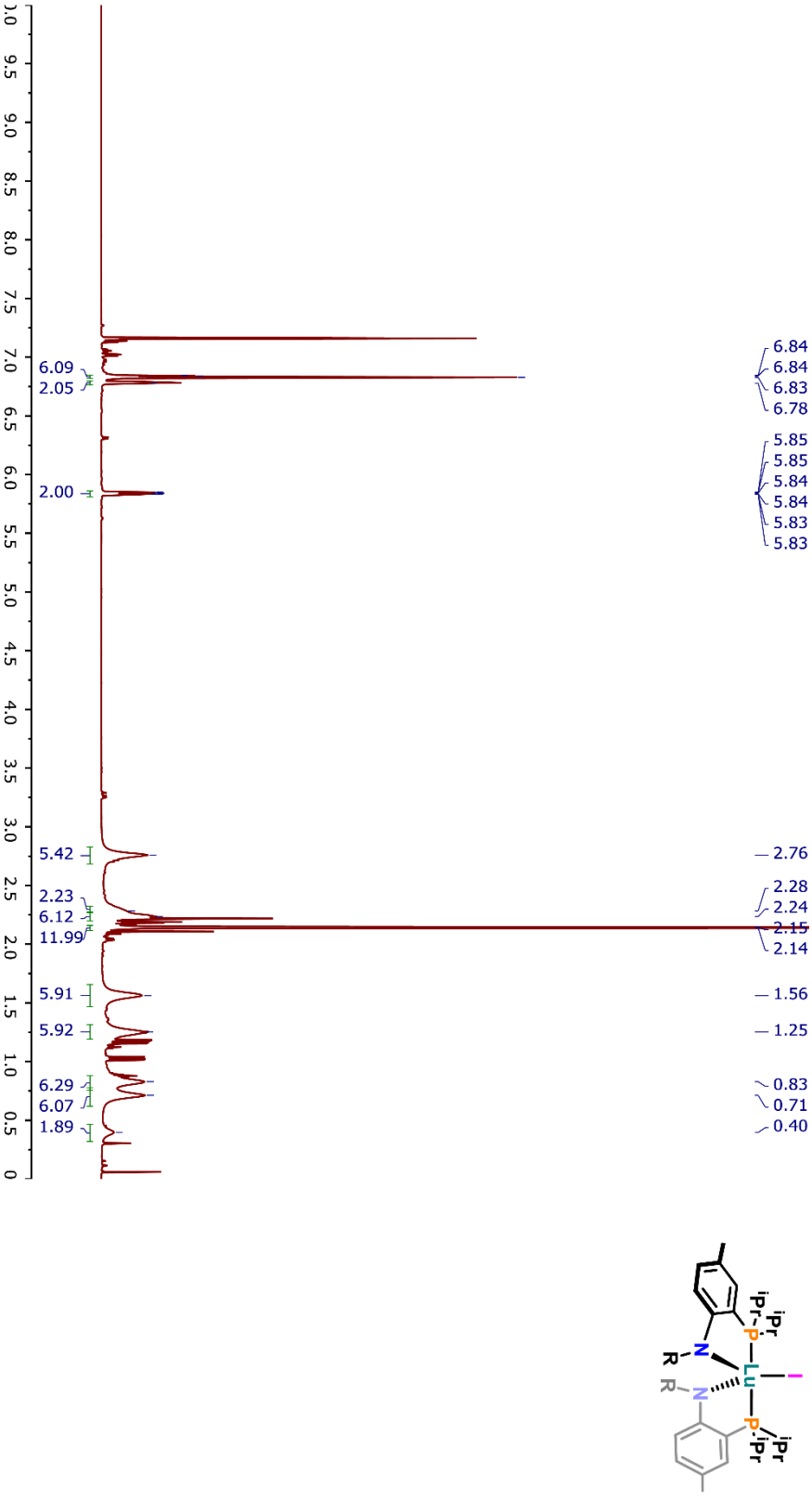

*Figure S37: ^1H NMR spectrum of **2-Lu** in C_6D_6 (283 K). In the aromatic region between δ 7.16 and 7.00 ppm as well as in the aliphatic region at δ 2.11 ppm, peaks resulting from residual toluene are visible.*

Figure S38: $^{31}P\{^{1}H\}$ *NMR spectrum of* **2-Lu** *in* C_6D_6 *(300 K).*

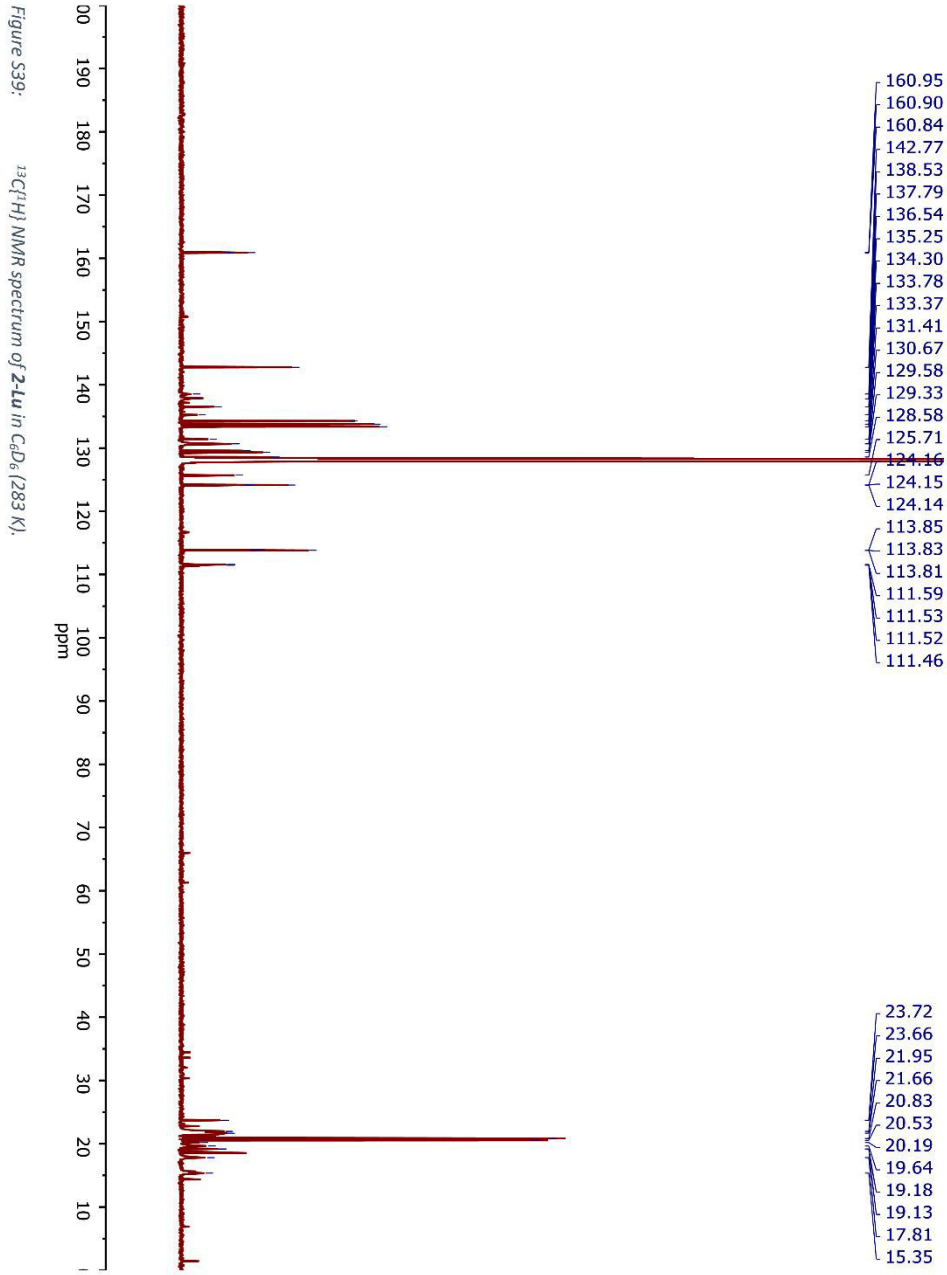

Figure S39: $^{13}C\{^1H\}$ *NMR spectrum of* ***2-Lu*** *in* C_6D_6 *(283 K).*

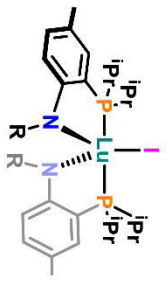

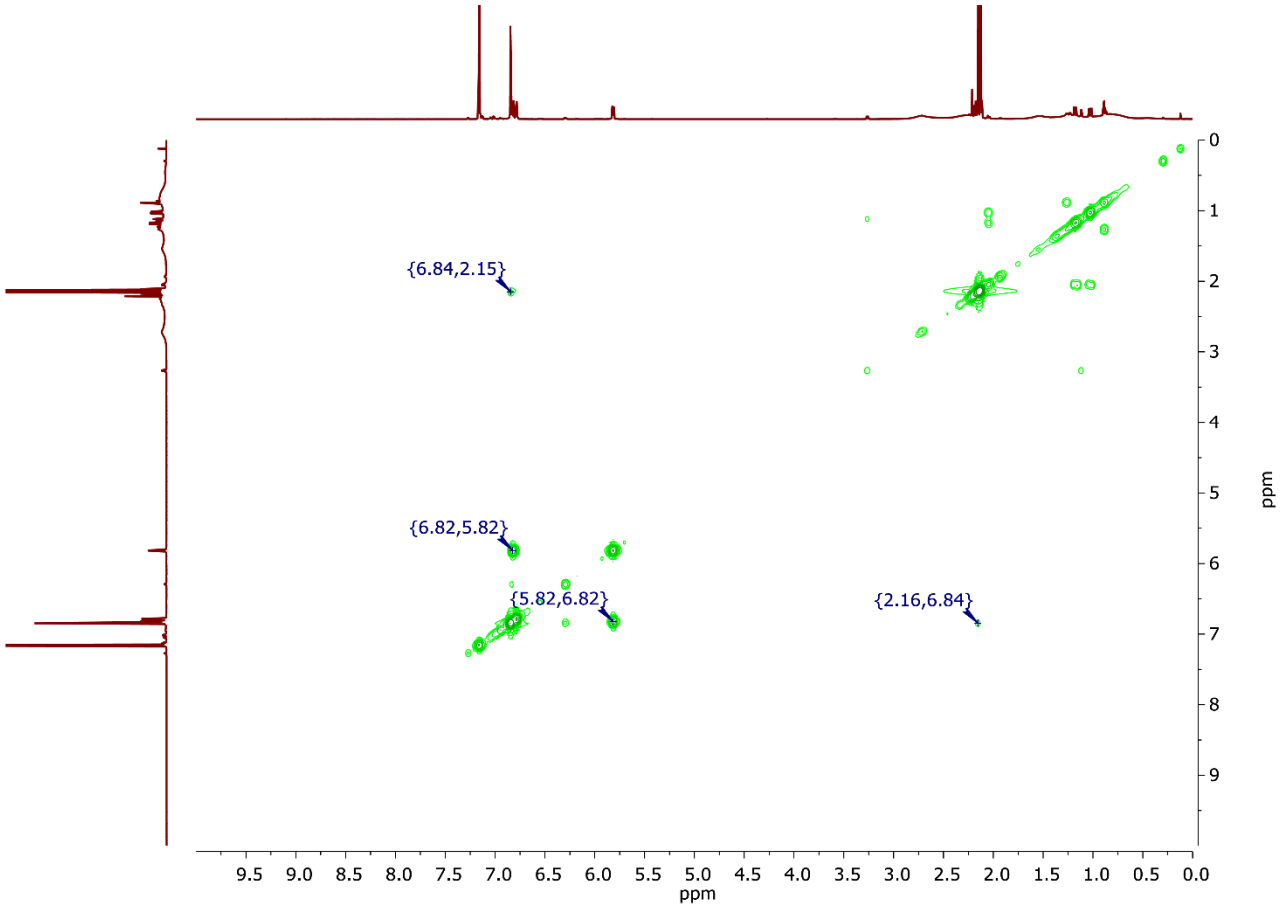

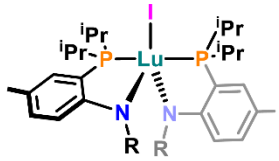

Figure S40: *^{1}H-^{1}H COSY NMR spectrum of **2-Lu** in C_6D_6 (283 K). Small impurities of **HPN** are present in the aliphatic region.*

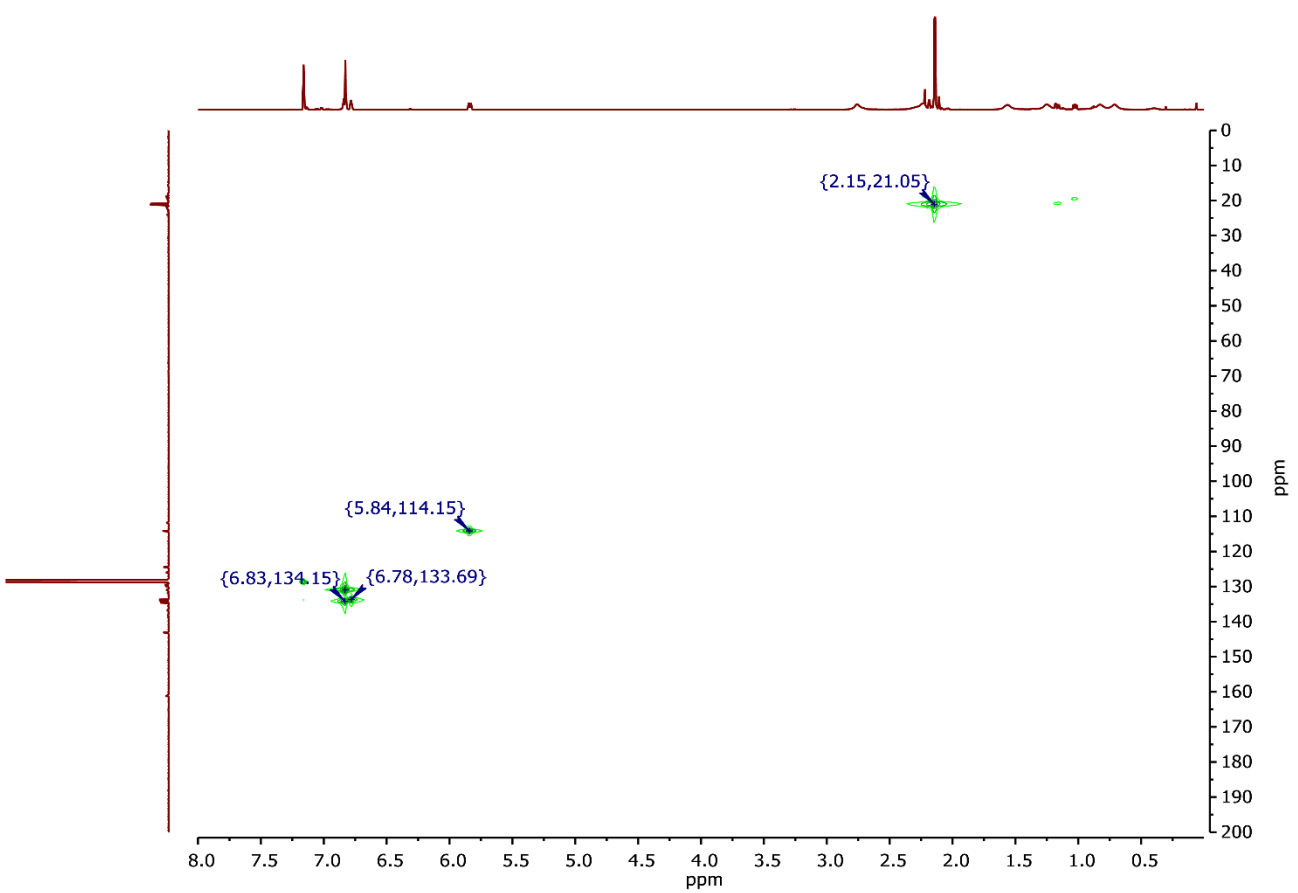

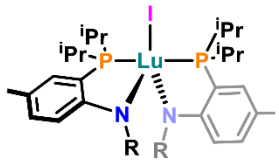

Figure S41: *^{1}H-^{13}C HSQC NMR spectrum of **2-Lu** in C_6D_6 (283 K).*

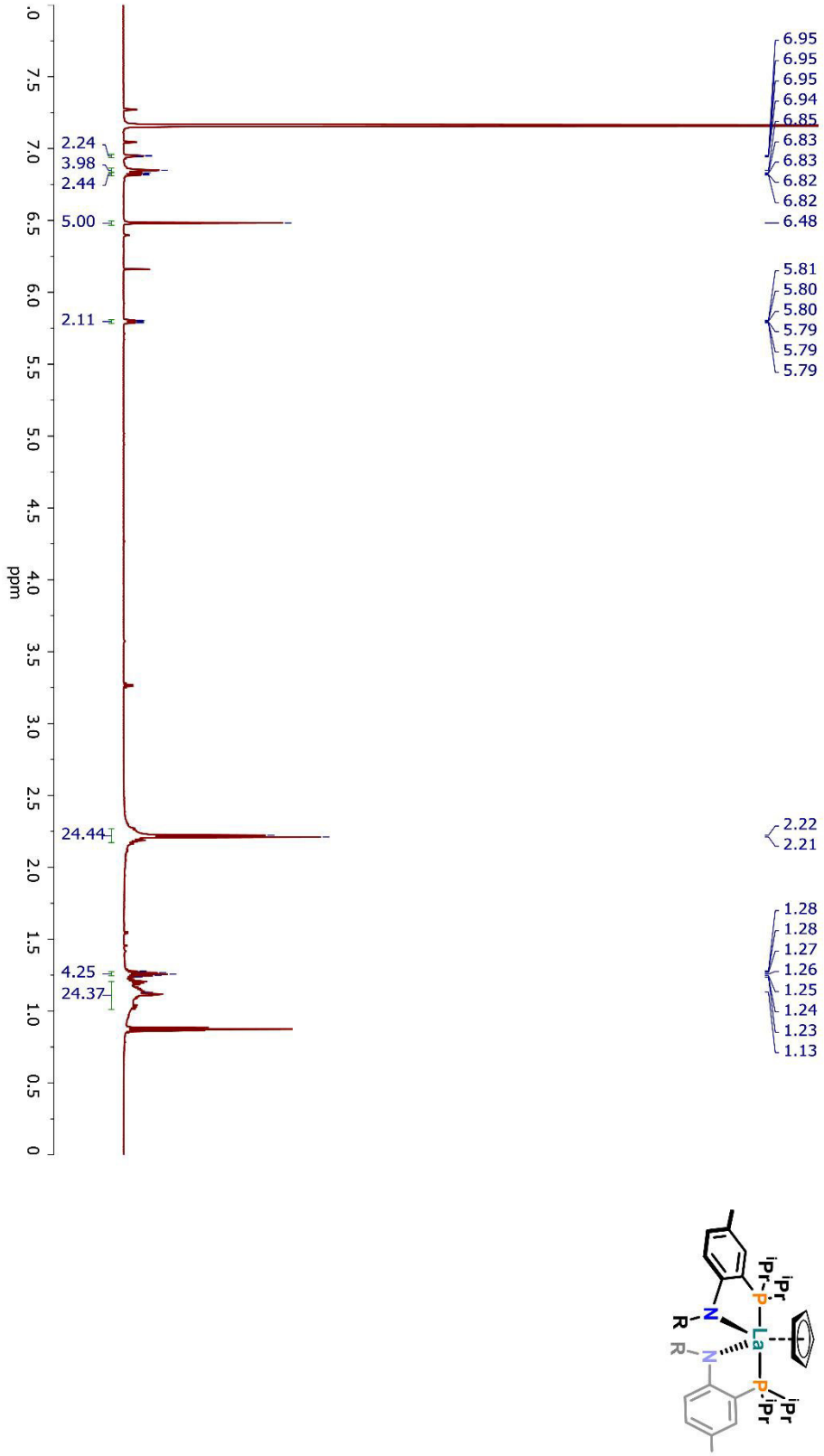

Figure S42: ^{1}H *NMR spectrum of* ***3-La*** *in* C_6D_6 *(298 K).*

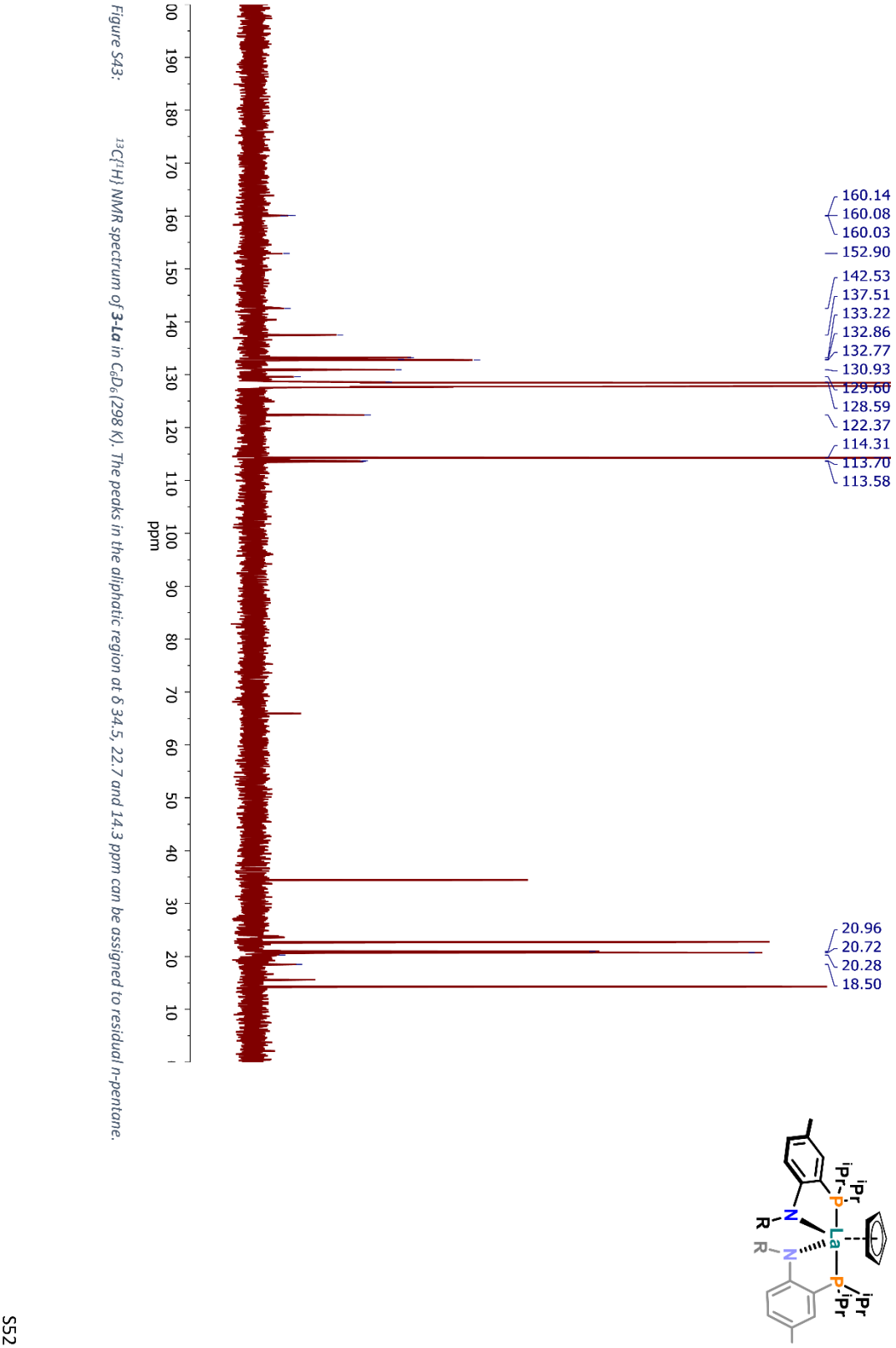

Figure S43: $^{13}C\{^1H\}$ *NMR spectrum of* **3-La** *in* C_6D_6 *(298 K). The peaks in the aliphatic region at δ 34.5, 22.7 and 14.3 ppm can be assigned to residual n-pentane.*

S52

Figure S44: $^{31}P\{^1H\}$ *NMR spectrum of* ***3-La*** *in* C_6D_6 *(298 K).*

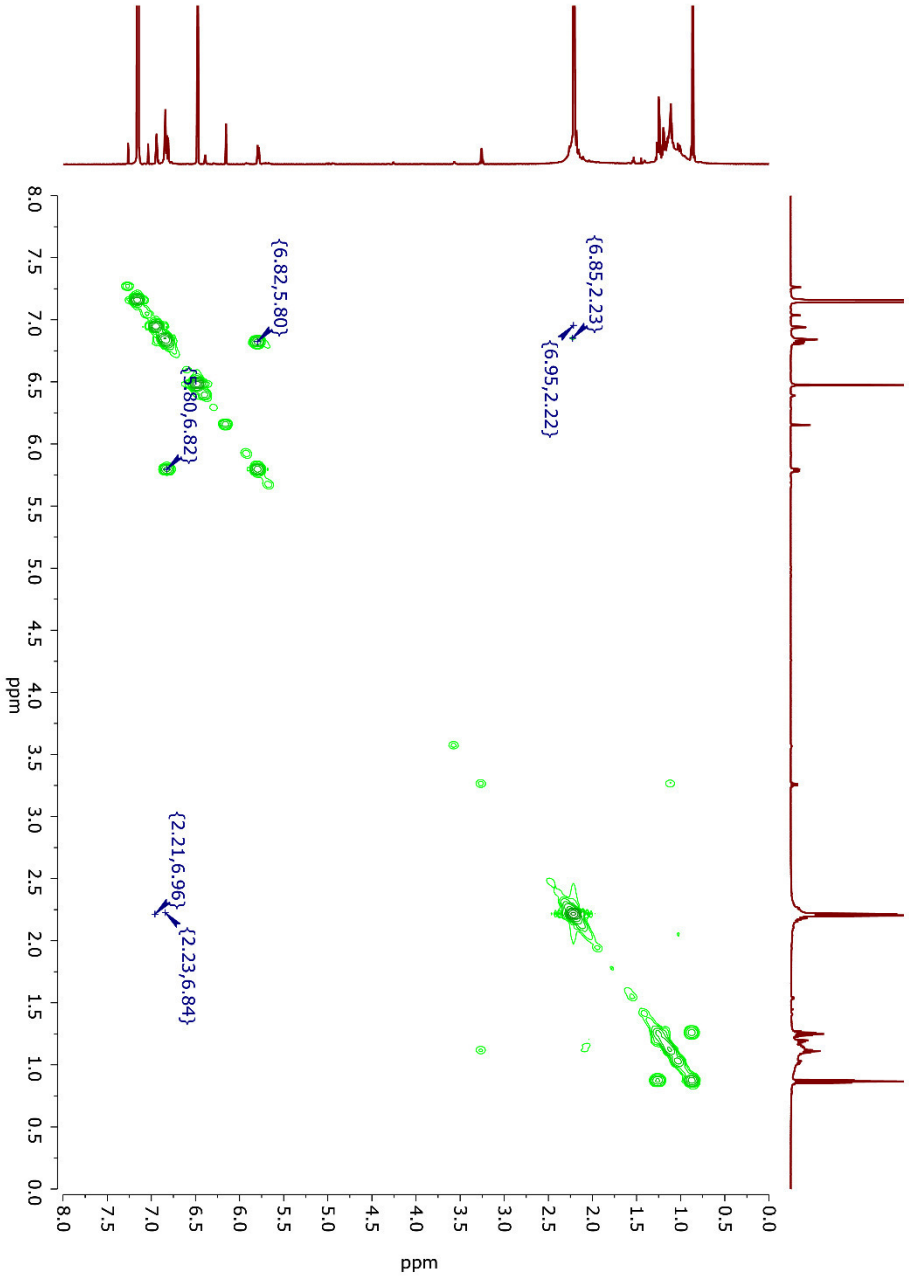

Figure S45: ^{1}H-^{1}H *COSY NMR spectrum of* ***3-La*** *in* C_6D_6 *(298 K).*

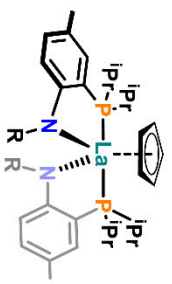

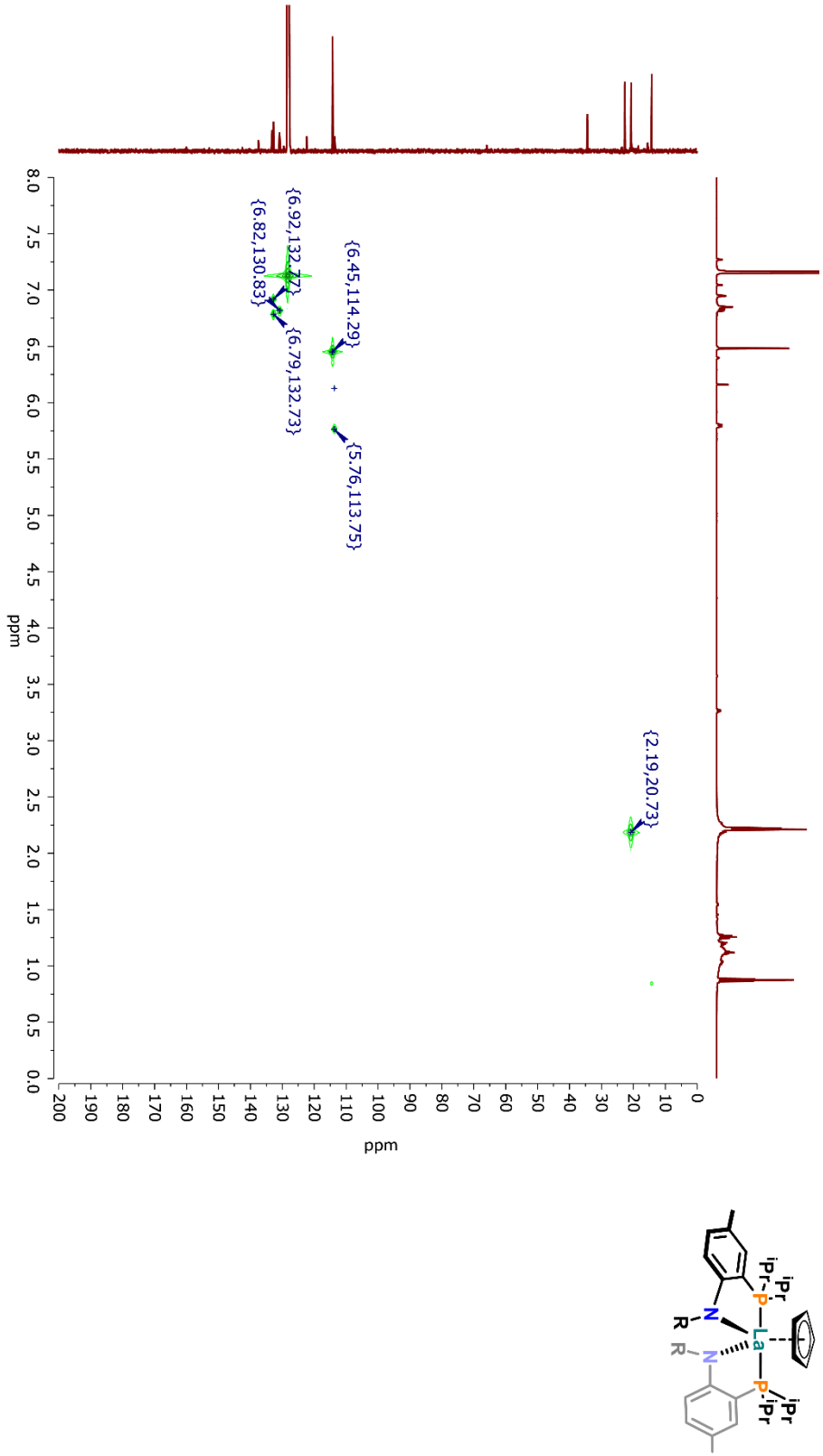

Figure S46: ^{1}H-^{13}C HSQC NMR spectrum of **3-La** in C_6D_6 (298 K).

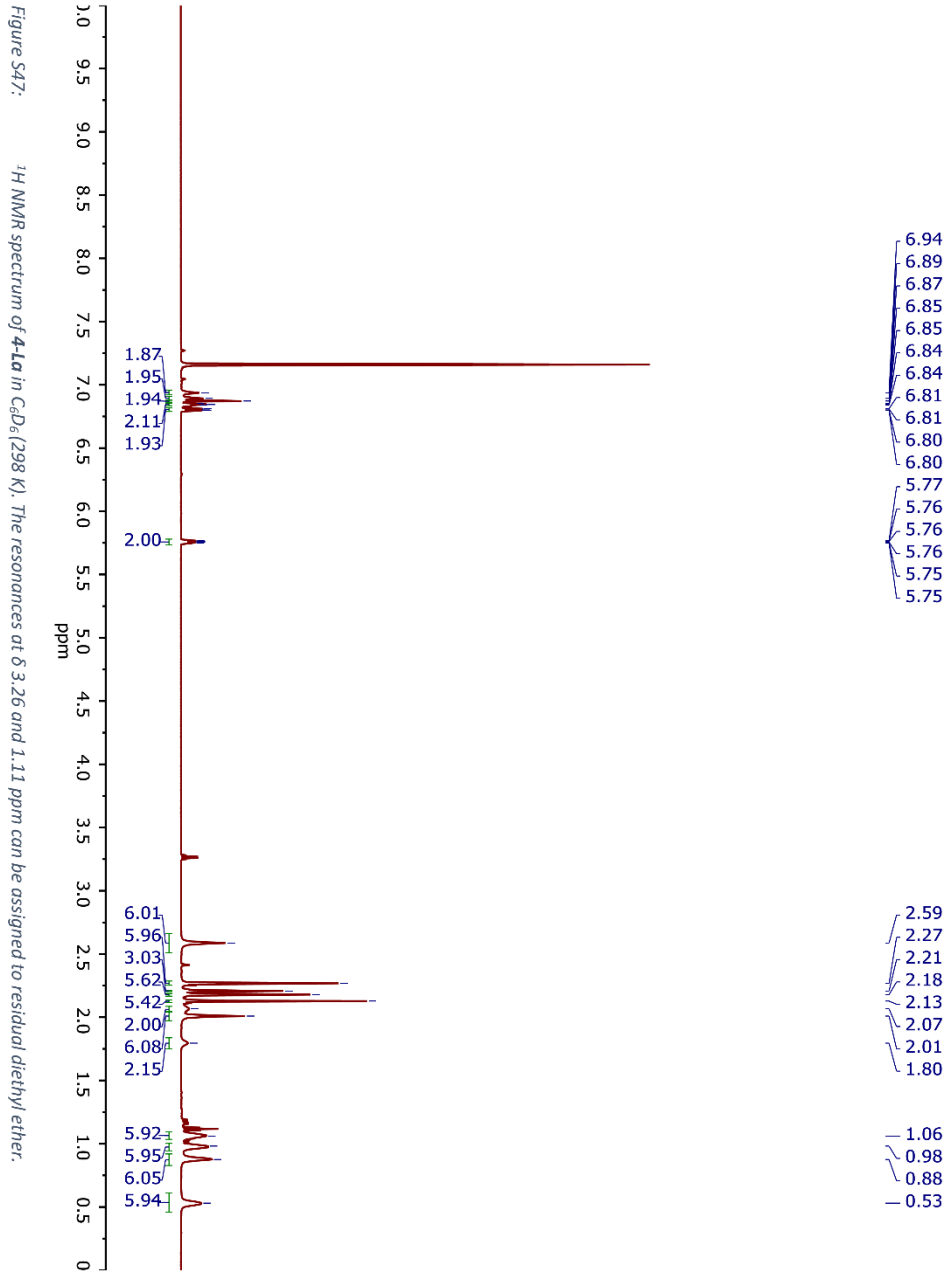

*Figure S47: ^1H NMR spectrum of **4-La** in C_6D_6 (298 K). The resonances at δ 3.26 and 1.11 ppm can be assigned to residual diethyl ether.*

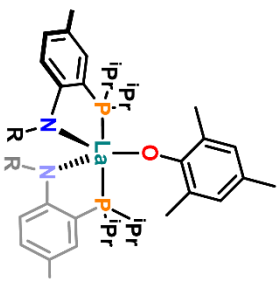

Figure S48: $^{31}P\{^{1}H\}$ *NMR spectrum of* ***4-La*** *in* C_6D_6 *(298 K).*

S57

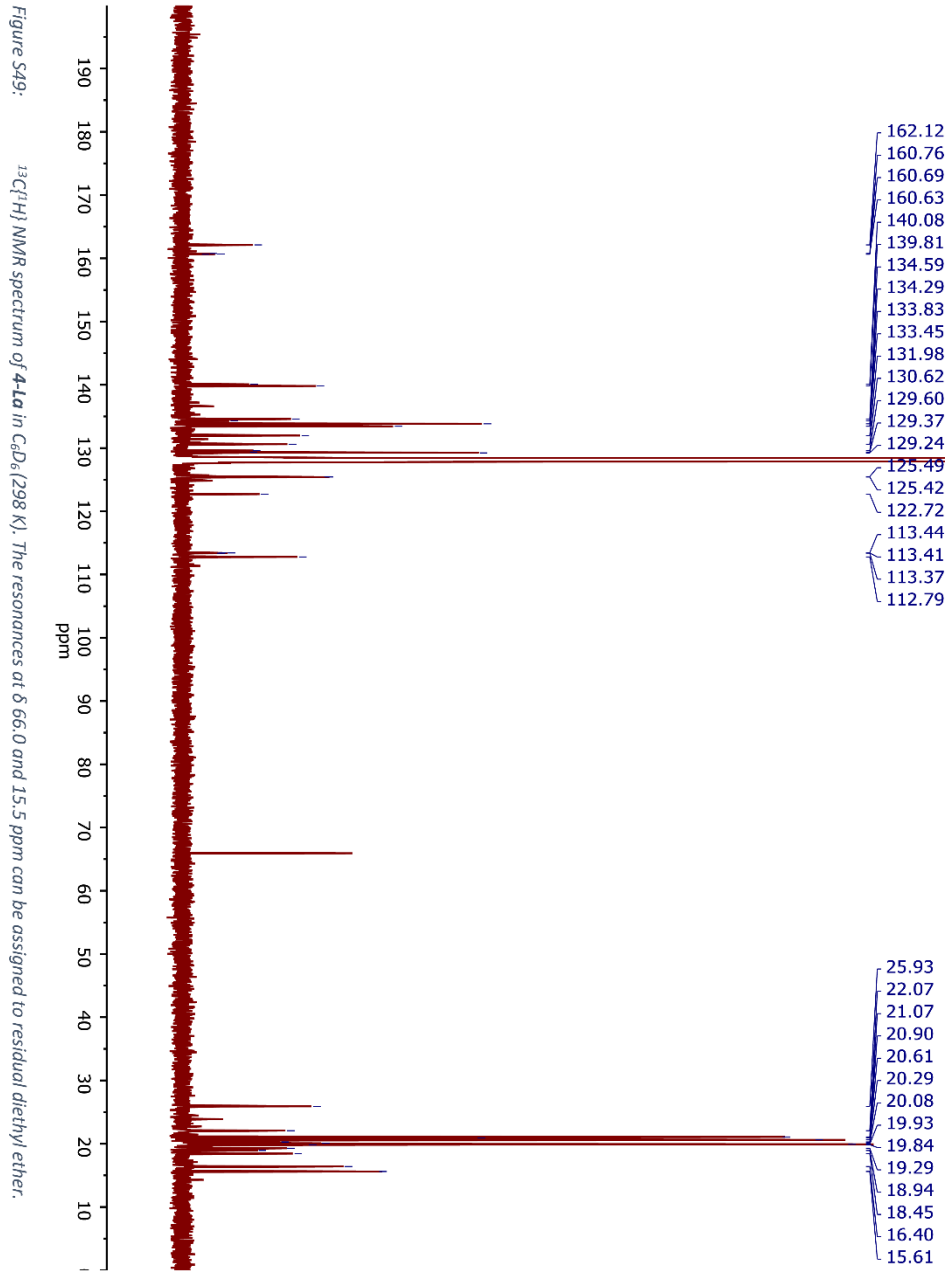

Figure S49: $^{13}C\{^1H\}$ *NMR spectrum of* ***4-La*** *in* C_6D_6 *(298 K). The resonances at δ 66.0 and 15.5 ppm can be assigned to residual diethyl ether.*

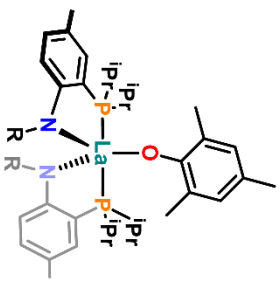

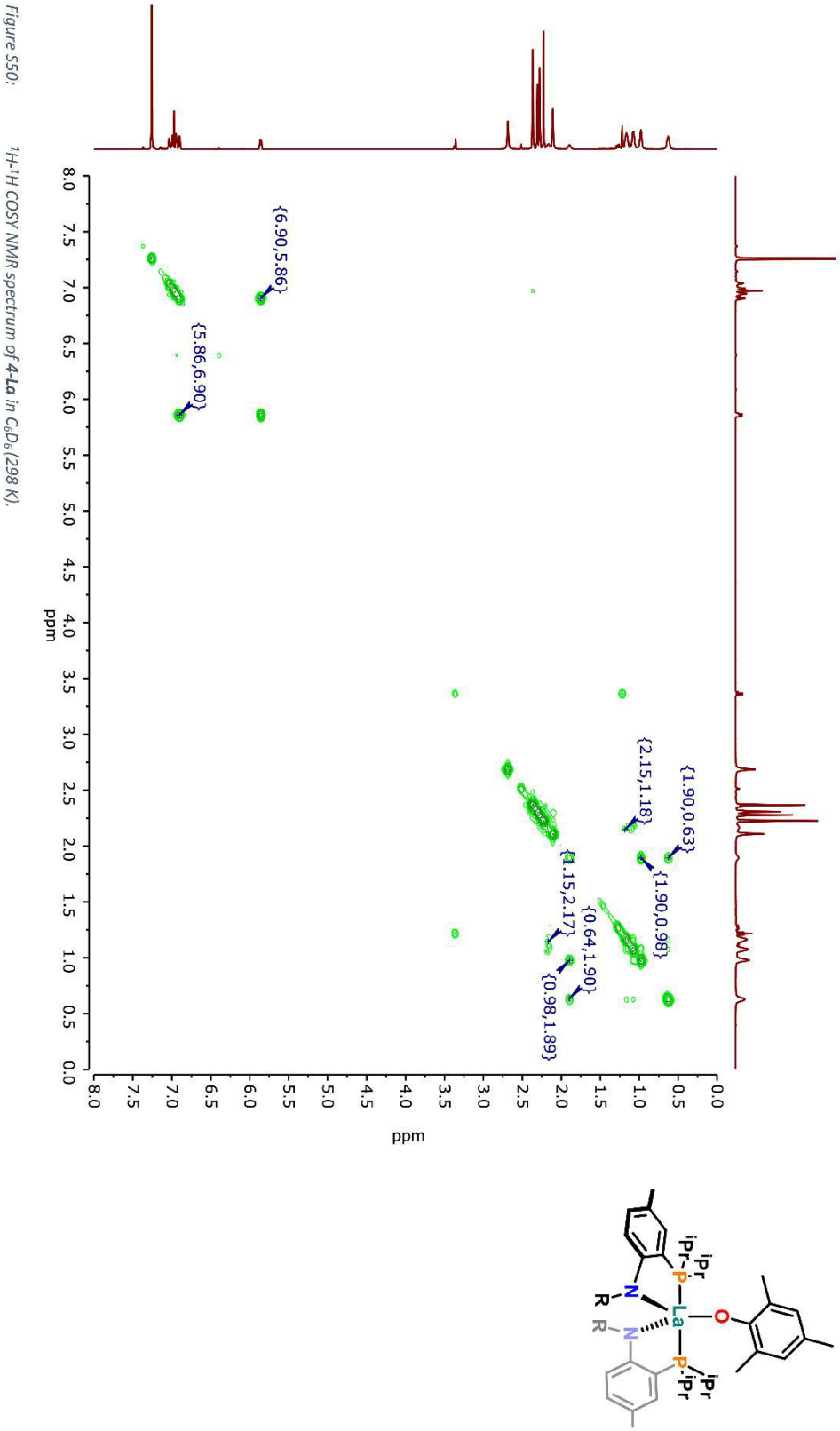

Figure S50: ^{1}H-^{1}H *COSY NMR spectrum of* ***4-La*** *in* C_6D_6 *(298 K).*

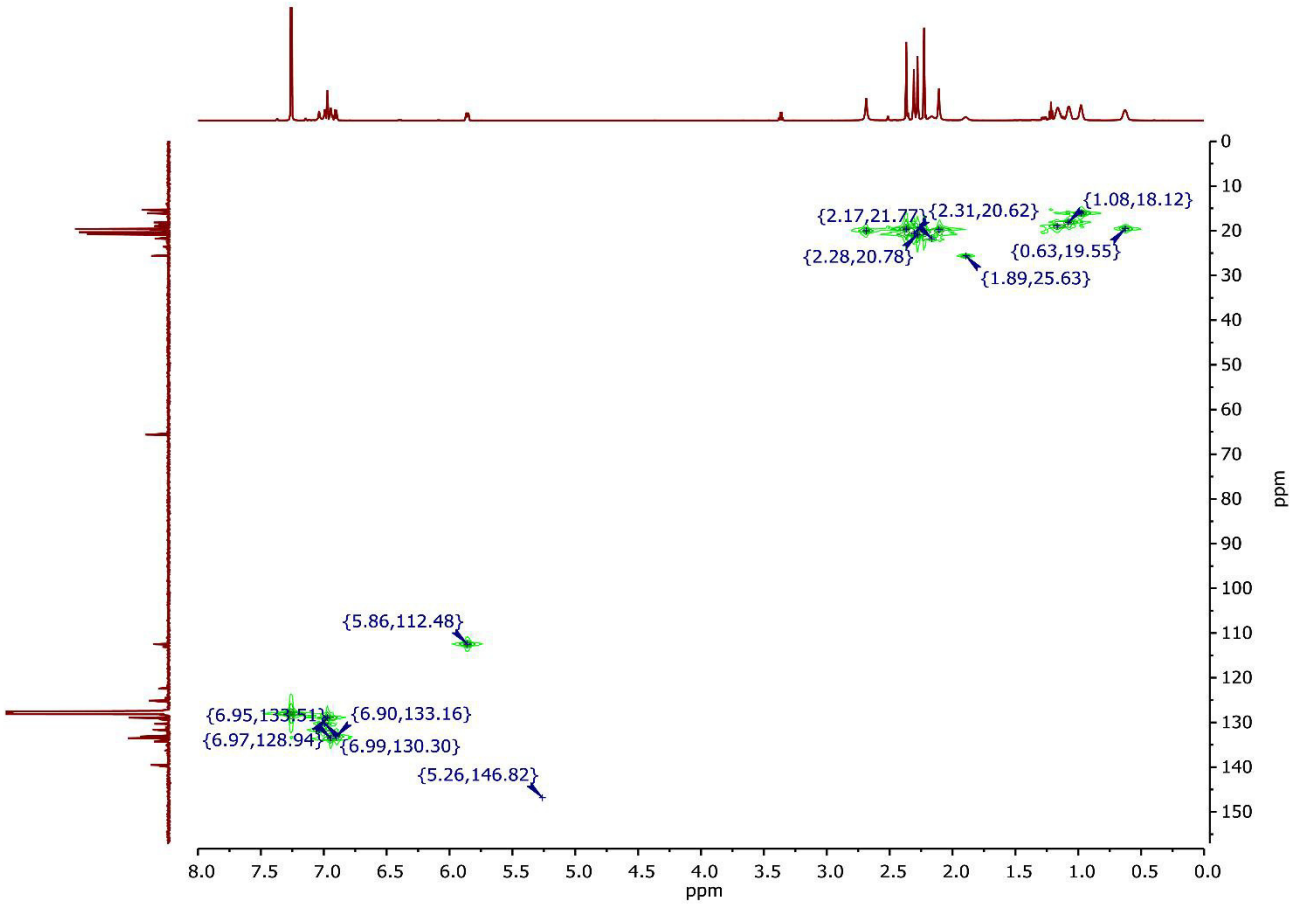

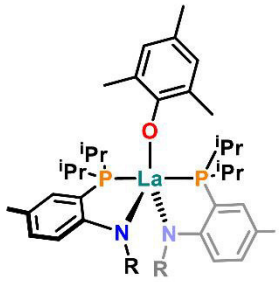

Figure S51: *^{1}H-^{13}C HSQC NMR spectrum of **4-La** in C_6D_6 (298 K).*

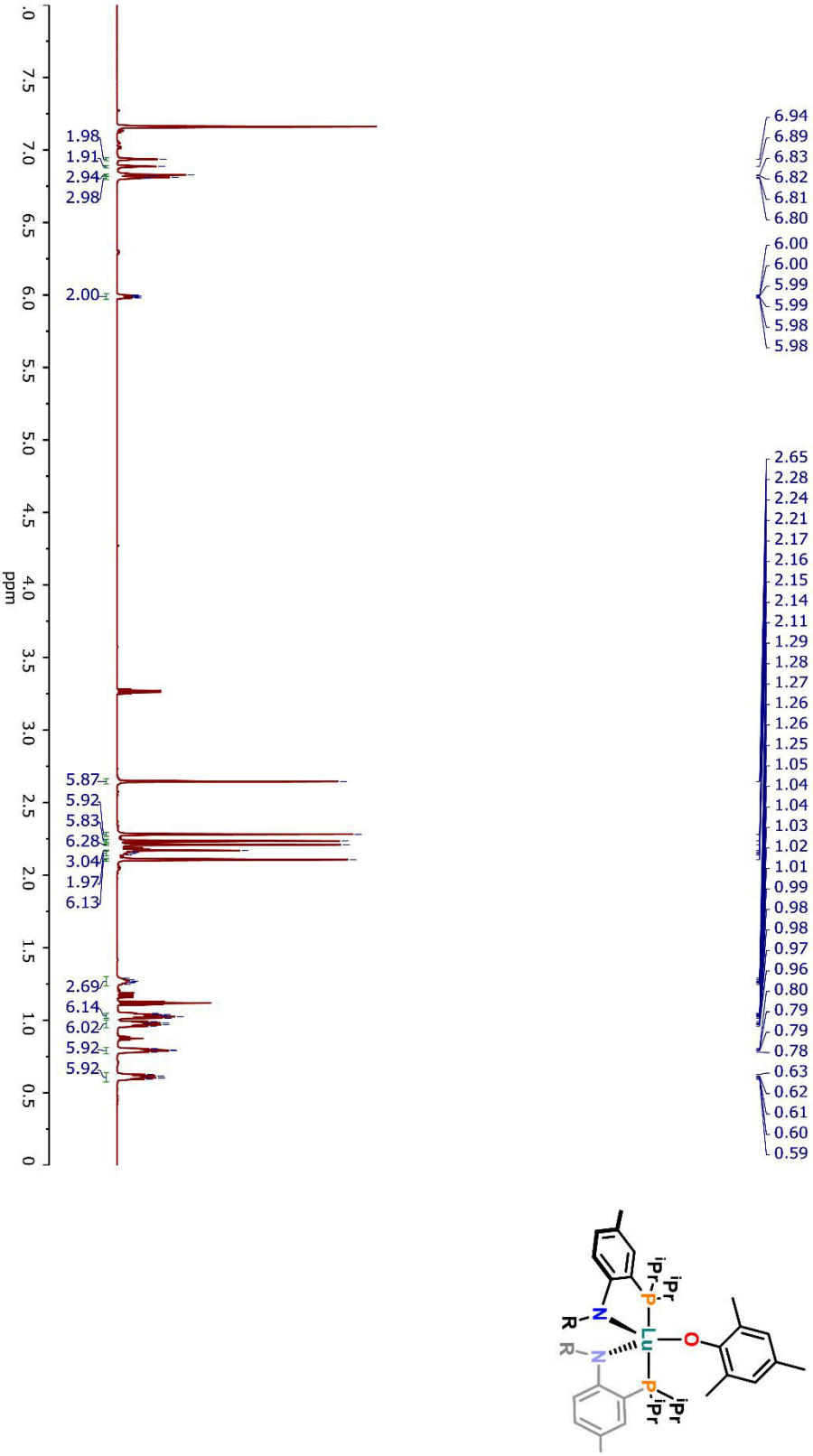

*Figure S52: ^{1}H NMR spectrum of **4-Lu** in C_6D_6 (298 K). The resonances at δ 3.26 and 1.11 ppm can be assigned to residual diethyl ether. Small impurities of **HPN** (e. g. δ 1.17 ppm) as well as n-hexane (δ 0.87 ppm) are also visible.*

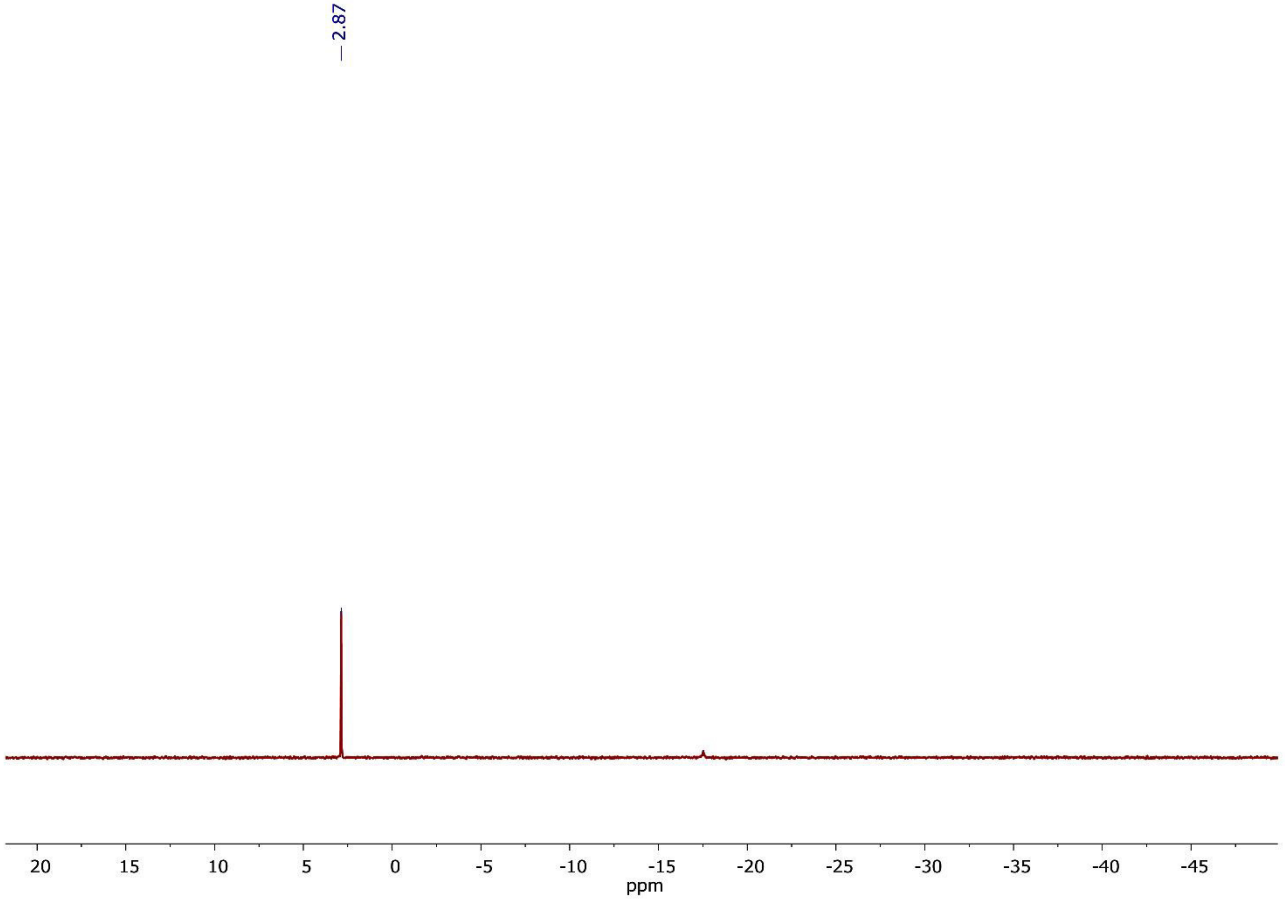

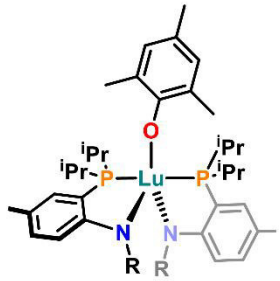

Figure S53: *$^{31}P\{^{1}H\}$ NMR spectrum of **4-Lu** in C_6D_6 (298 K).*

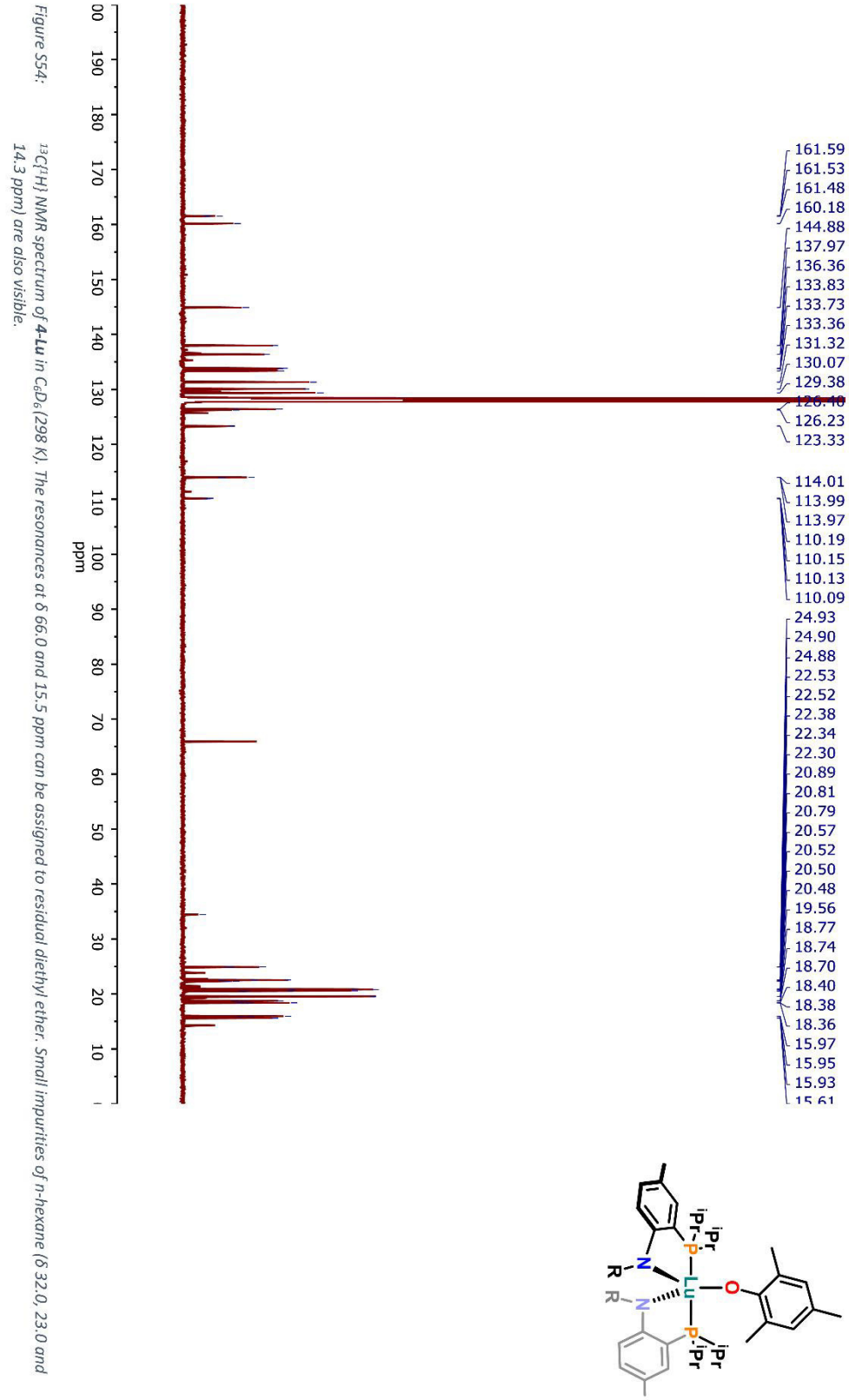

*Figure S54: $^{13}C\{^1H\}$ NMR spectrum of **4-Lu** in C_6D_6 (298 K). The resonances at δ 66.0 and 15.5 ppm can be assigned to residual diethyl ether. Small impurities of n-hexane (δ 32.0, 23.0 and 14.3 ppm) are also visible.*

S63

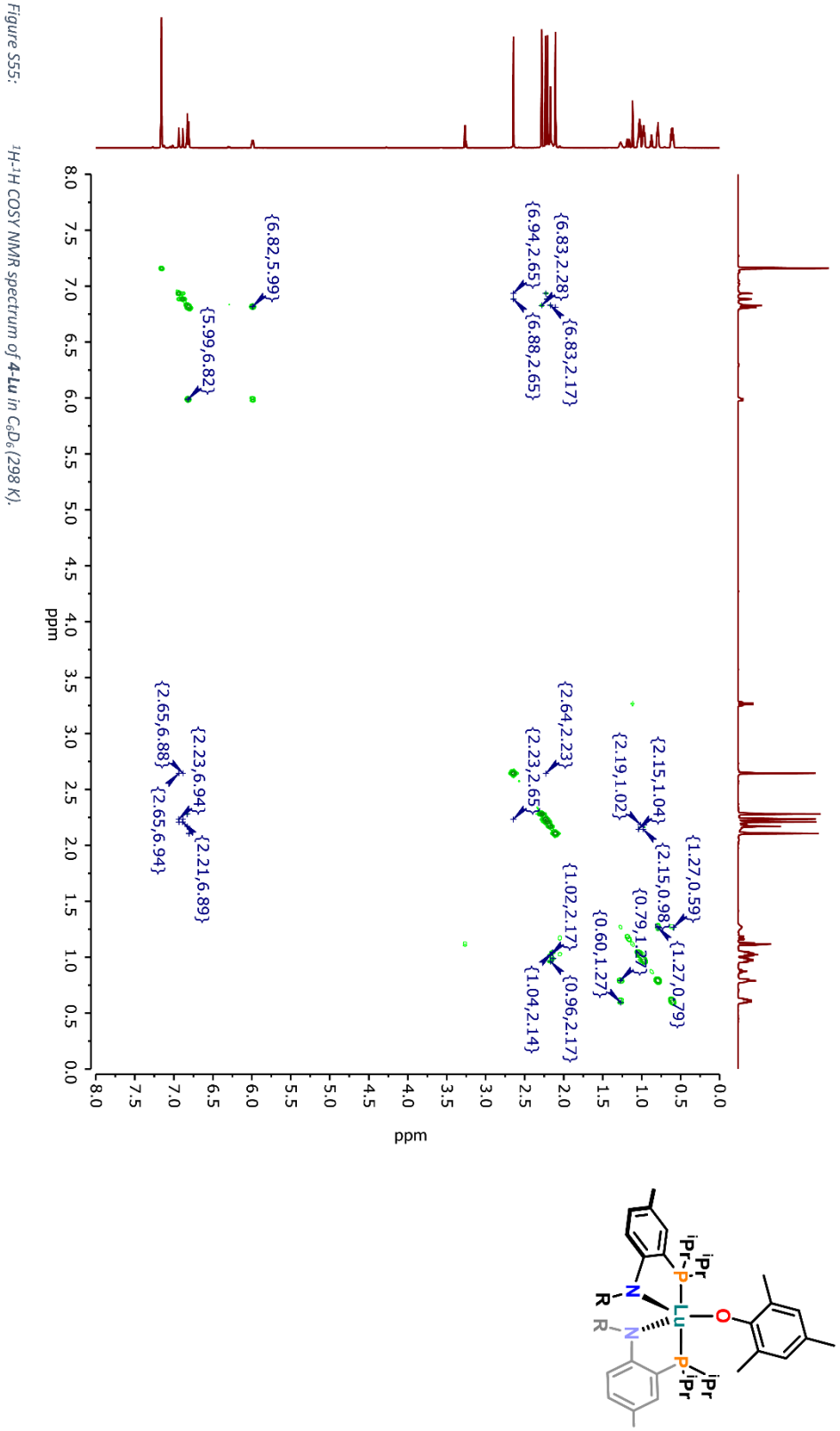

Figure S55: *^{1}H-^{1}H COSY NMR spectrum of **4-Lu** in C_6D_6 (298 K).*

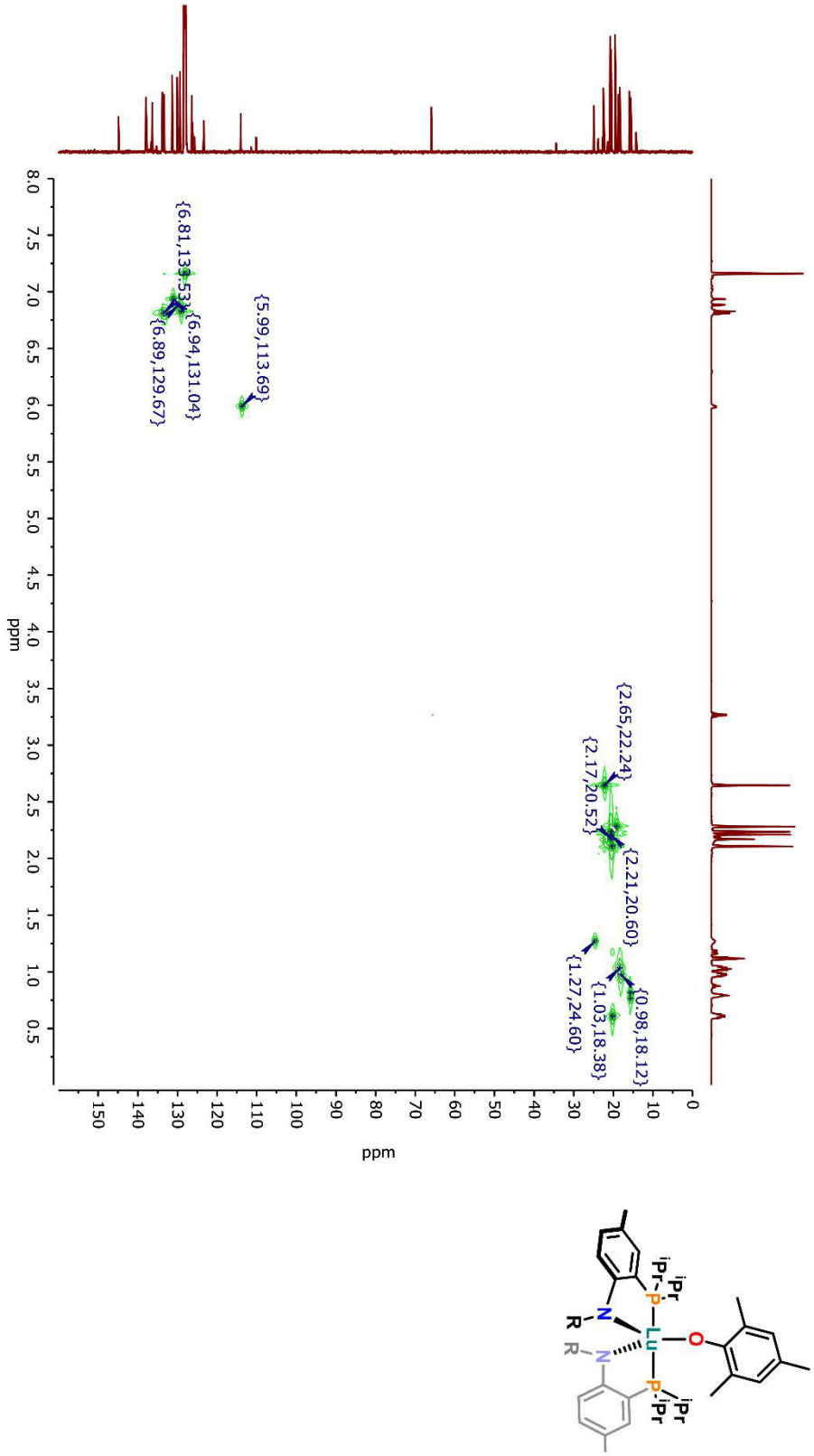

Figure S56: ^{1}H-^{13}C *HSQC NMR spectrum of* ***4-Lu*** *in* C_6D_6 *(298 K).*

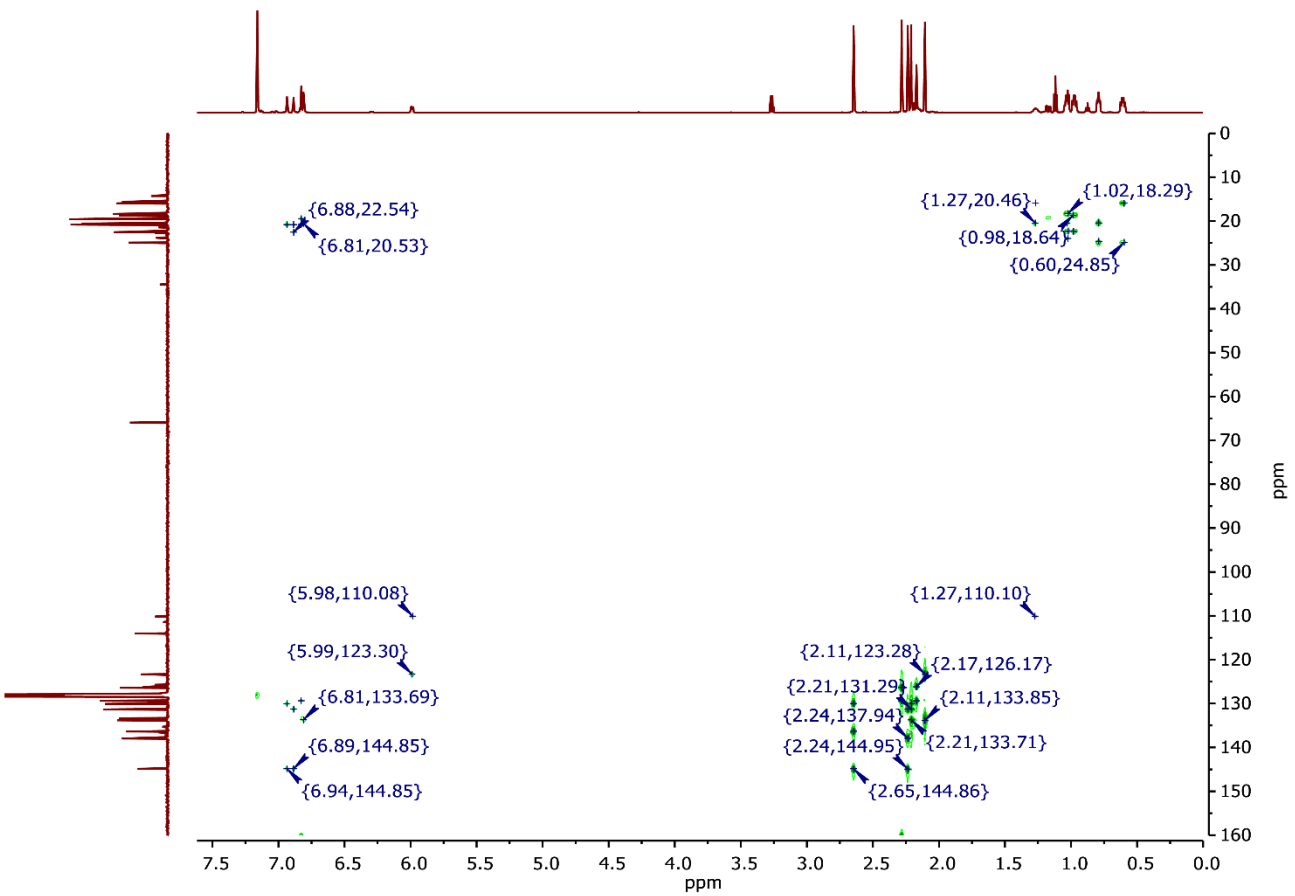

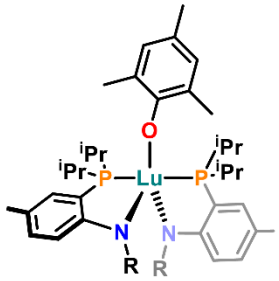

Figure S57: *^{1}H-^{13}C HMBC NMR spectrum of **4-Lu** in C_6D_6 (298 K).*

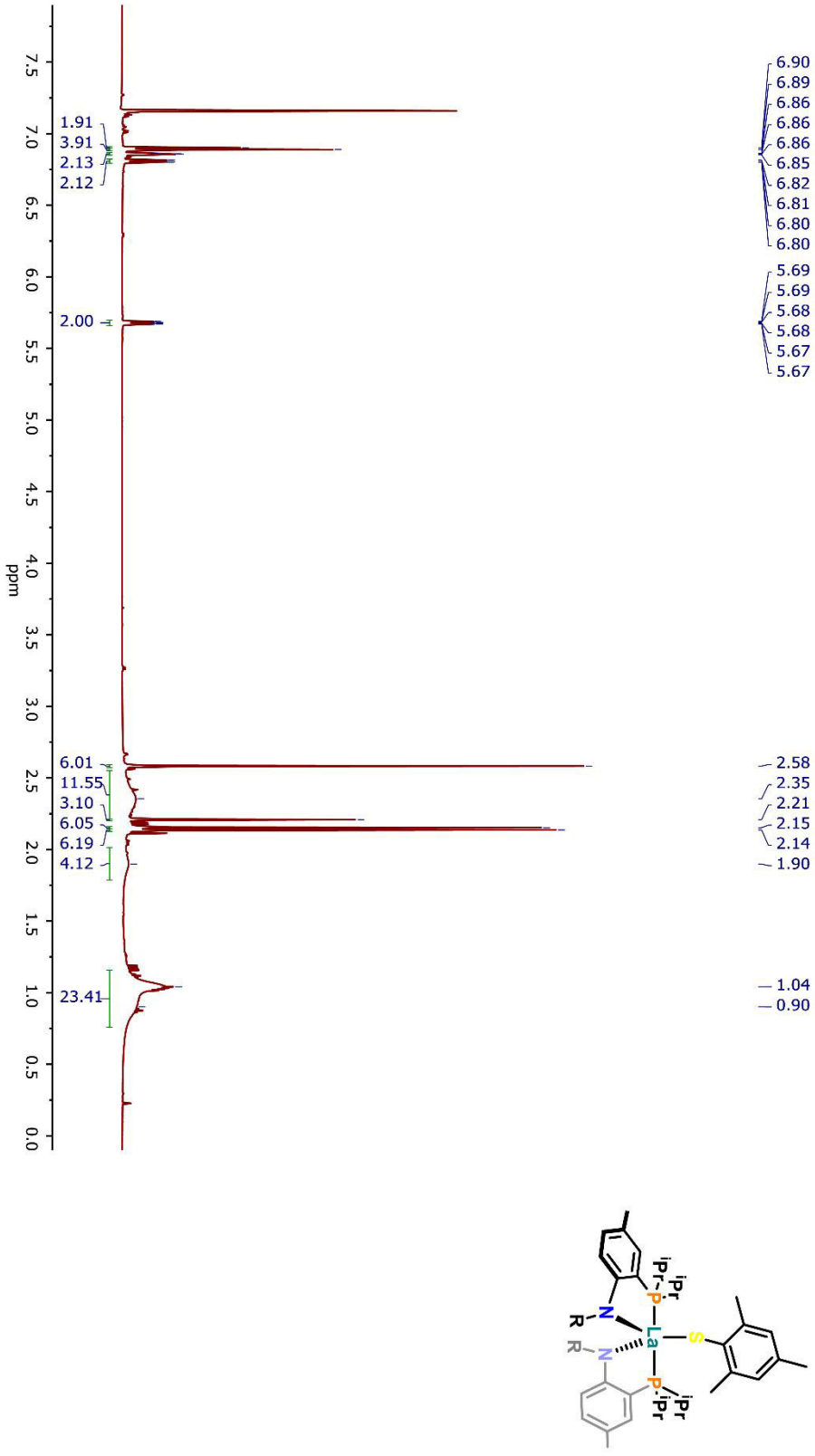

*Figure S58: ^{1}H NMR spectrum of **5-La** in C_6D_6 (298 K).*

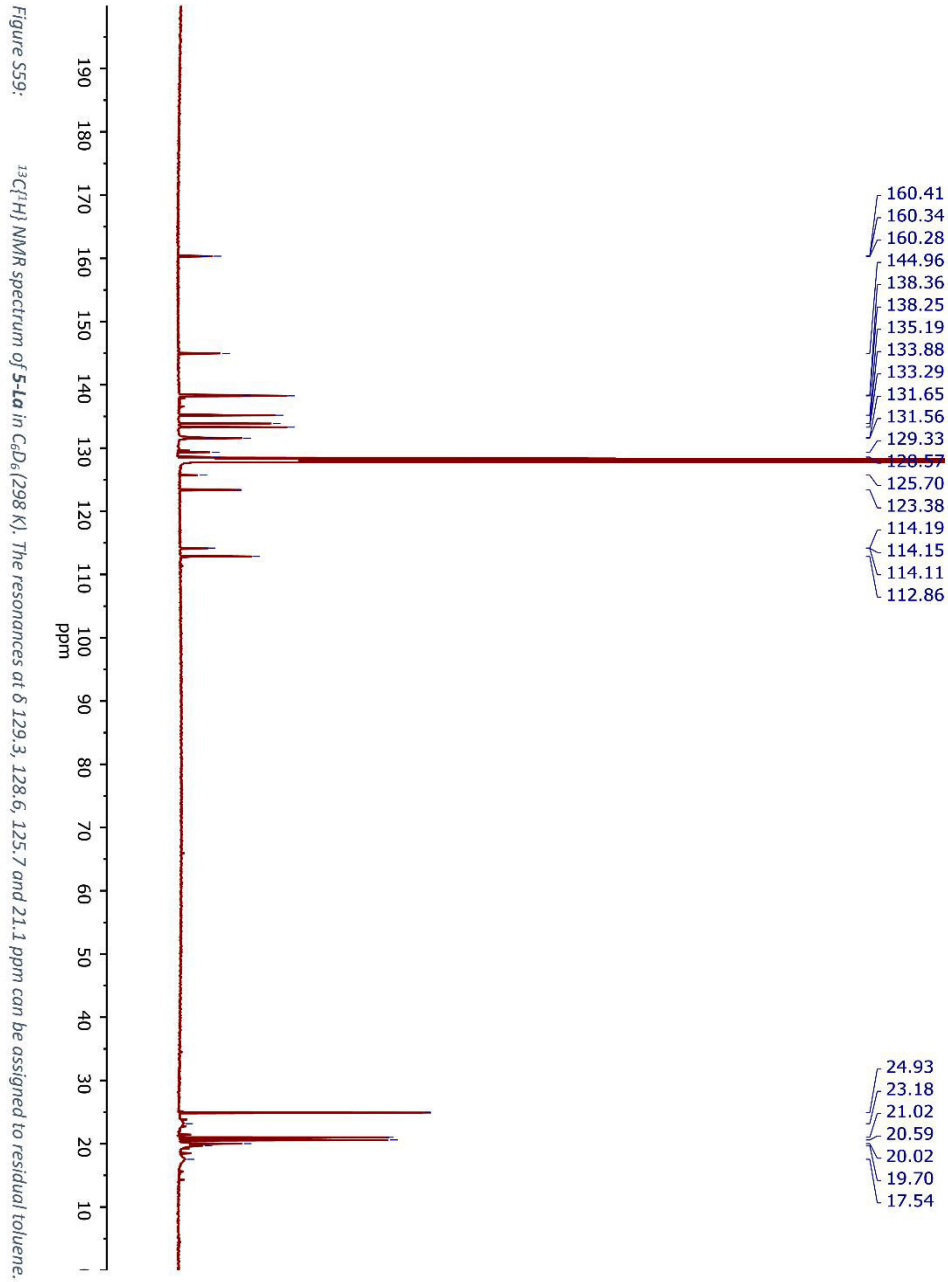

Figure S59: $^{13}C\{^1H\}$ *NMR spectrum of* **5-La** *in* C_6D_6 *(298 K). The resonances at δ 129.3, 128.6, 125.7 and 21.1 ppm can be assigned to residual toluene.*

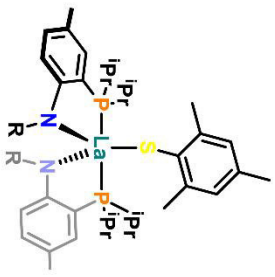

Figure S60: $^{31}P\{^{1}H\}$ *NMR spectrum of* **5-La** *in* C_6D_6 *(298 K).*

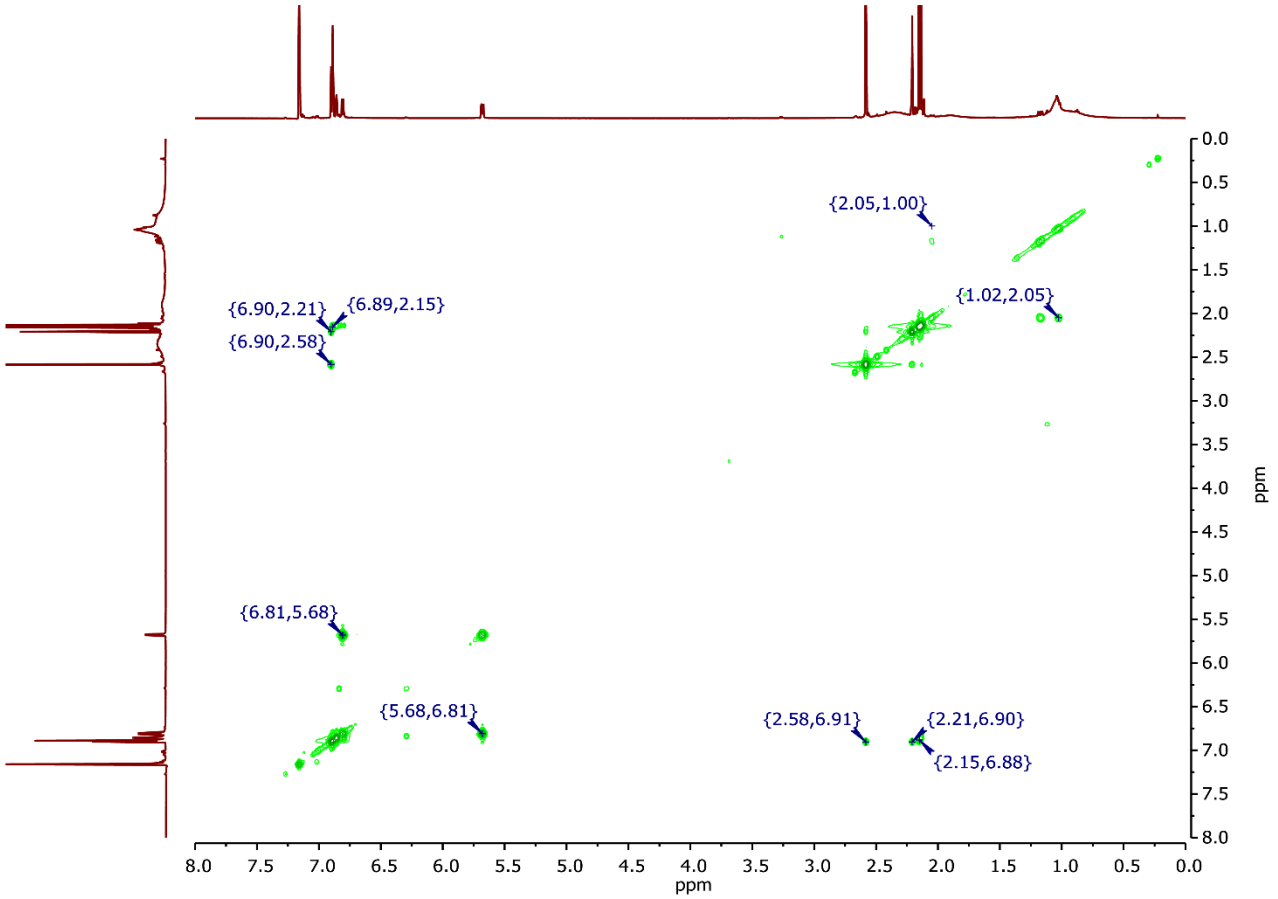

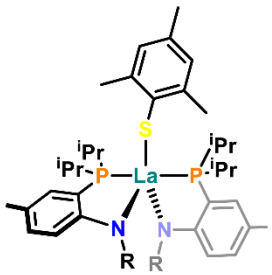

Figure S61: *^{1}H-^{1}H COSY NMR spectrum of **5-La** in C_6D_6 (298 K).*

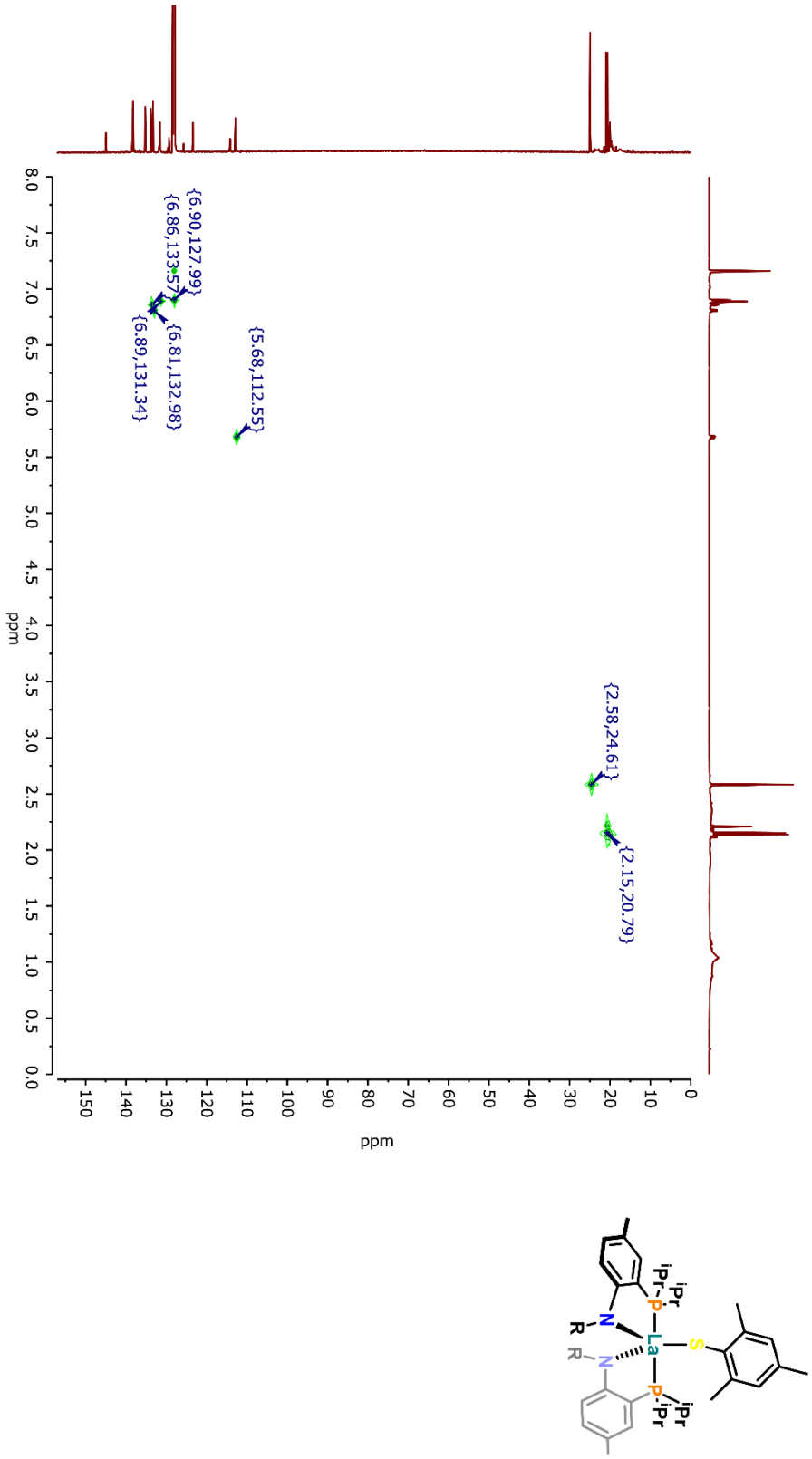

Figure S62: ^{1}H-^{13}C HSQC NMR spectrum of **5-La** in C_6D_6 (298 K).

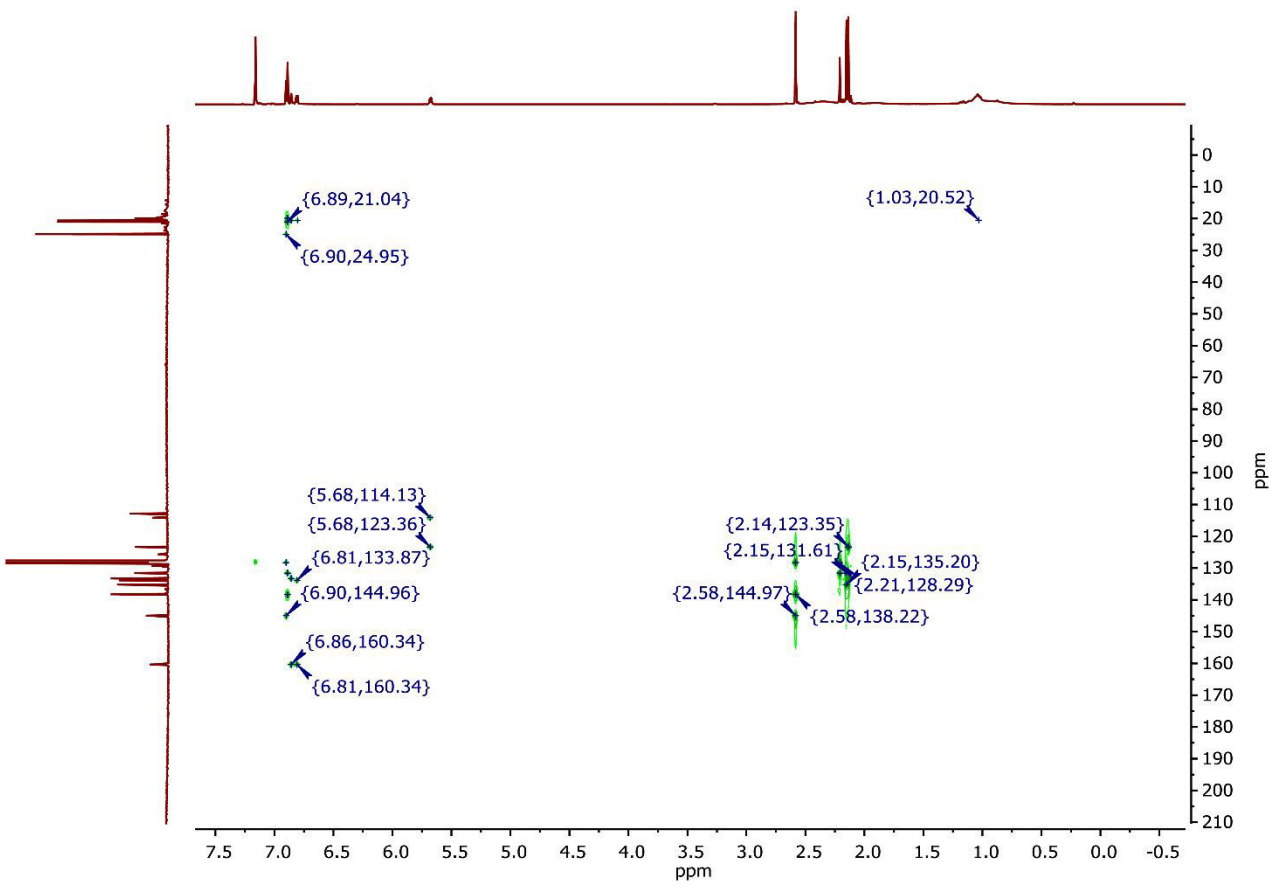

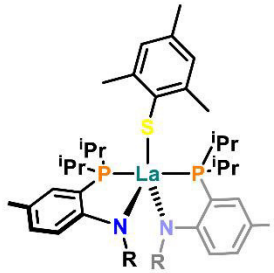

Figure S63: *^{1}H-^{13}C HMBC NMR spectrum of **5-La** in C_6D_6 (298 K).*

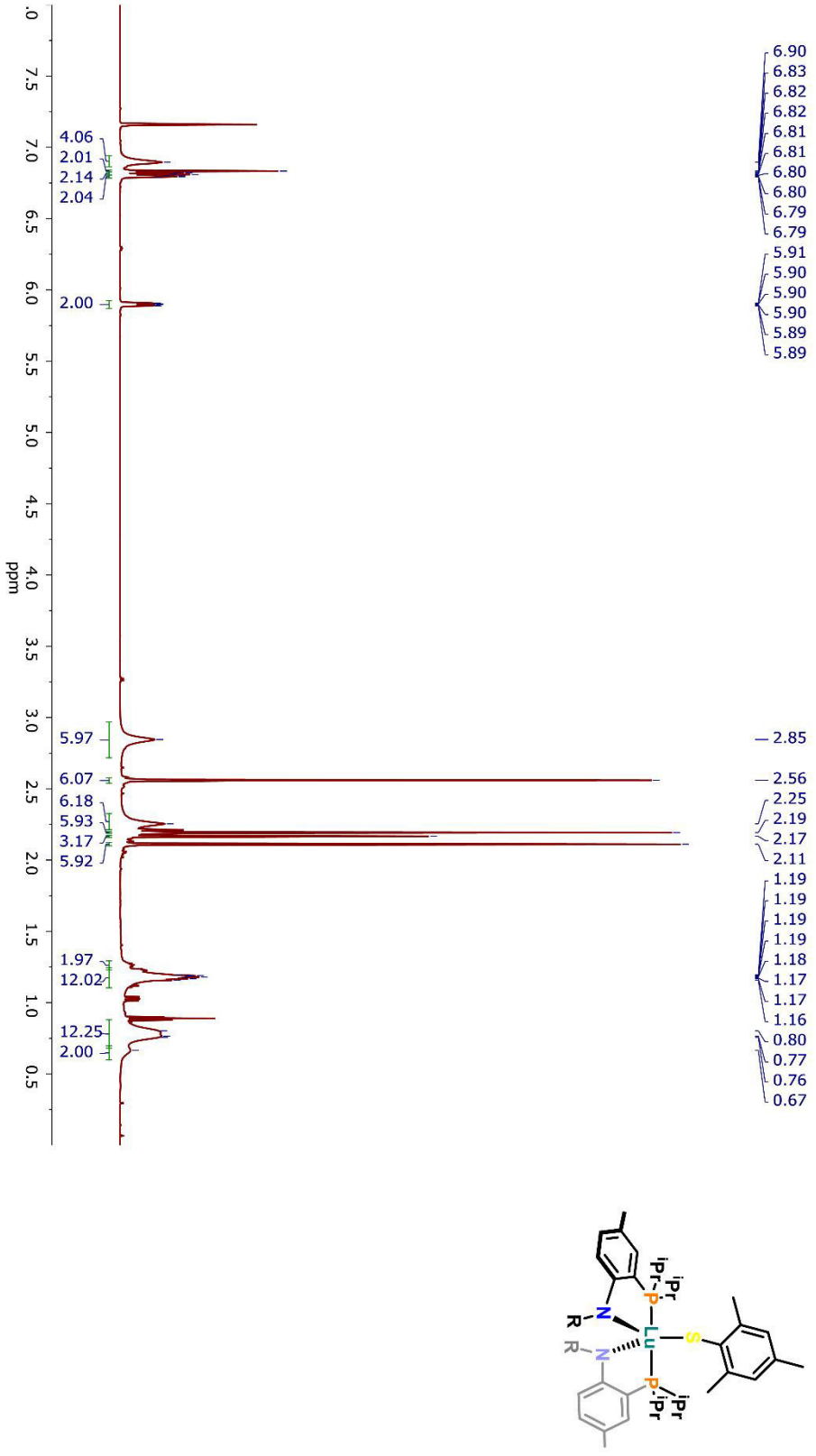

*Figure S64: ^{1}H NMR spectrum of **5-Lu** in C_6D_6 (298 K).*

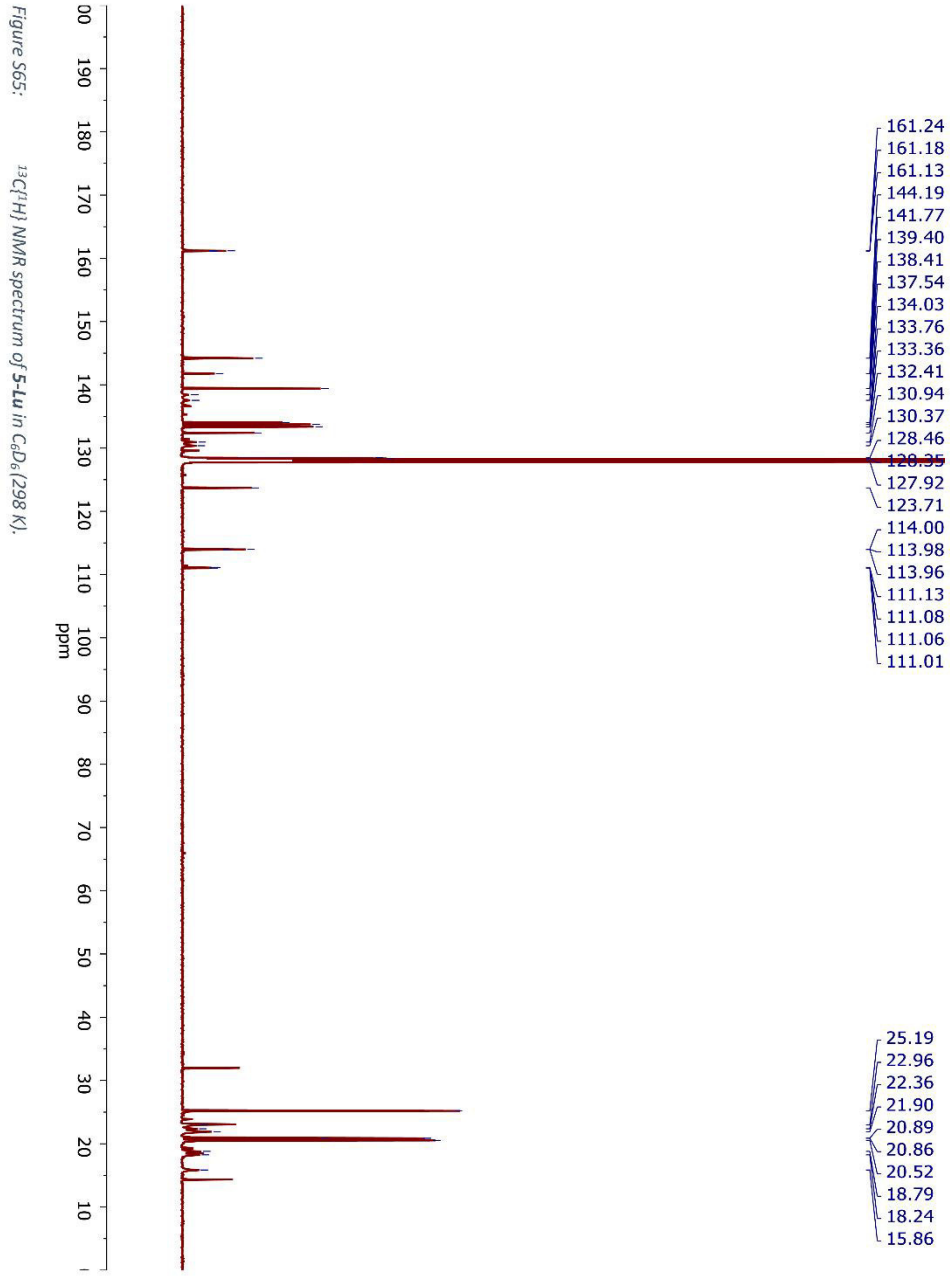

Figure S65: $^{13}C\{^1H\}$ *NMR spectrum of* **5-Lu** *in* C_6D_6 *(298 K).*

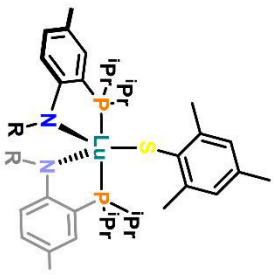

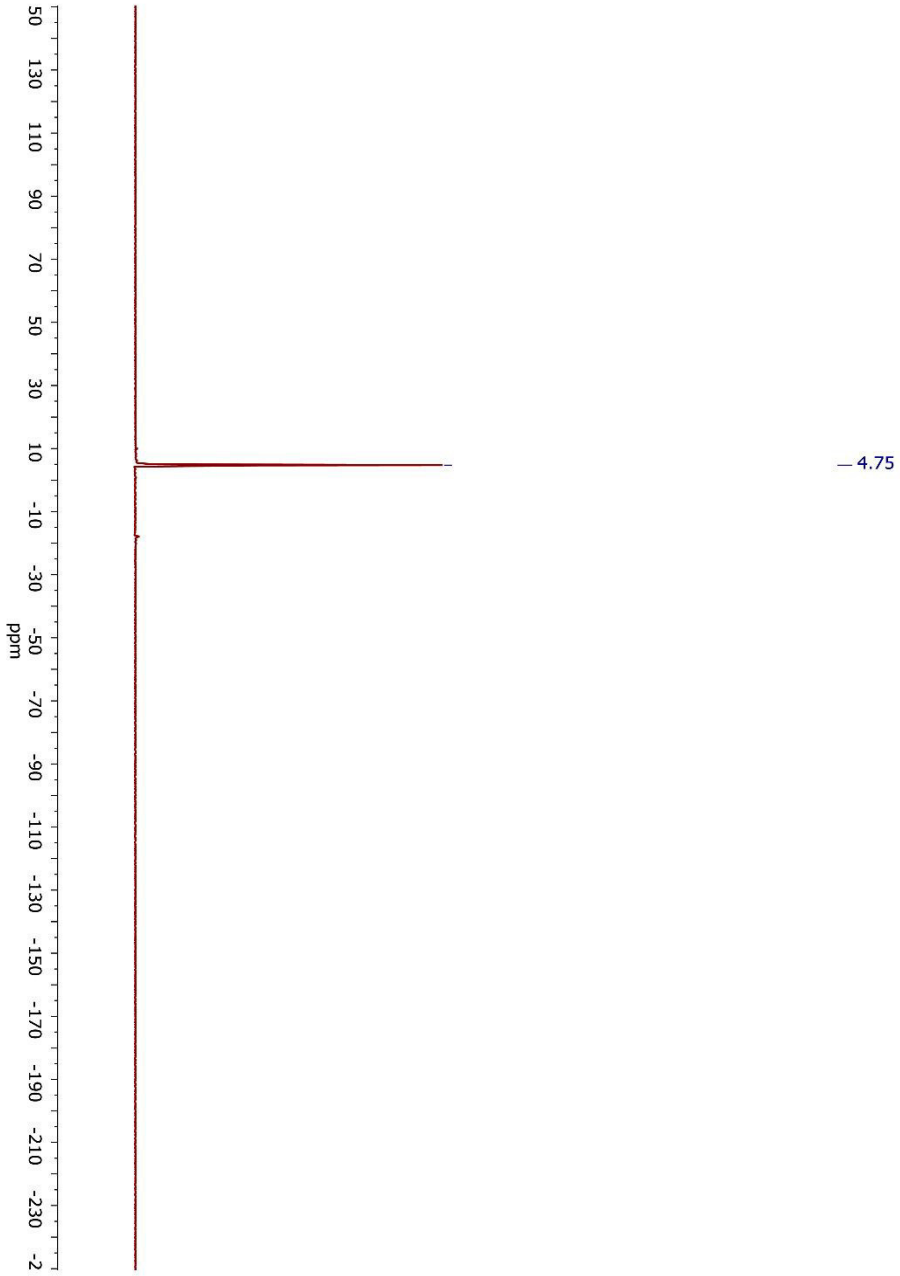

Figure S66: $^{31}P\{^{1}H\}$ *NMR spectrum of* **5-Lu** *in* C_6D_6 *(298 K).*

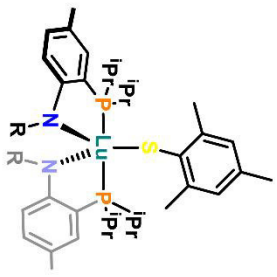

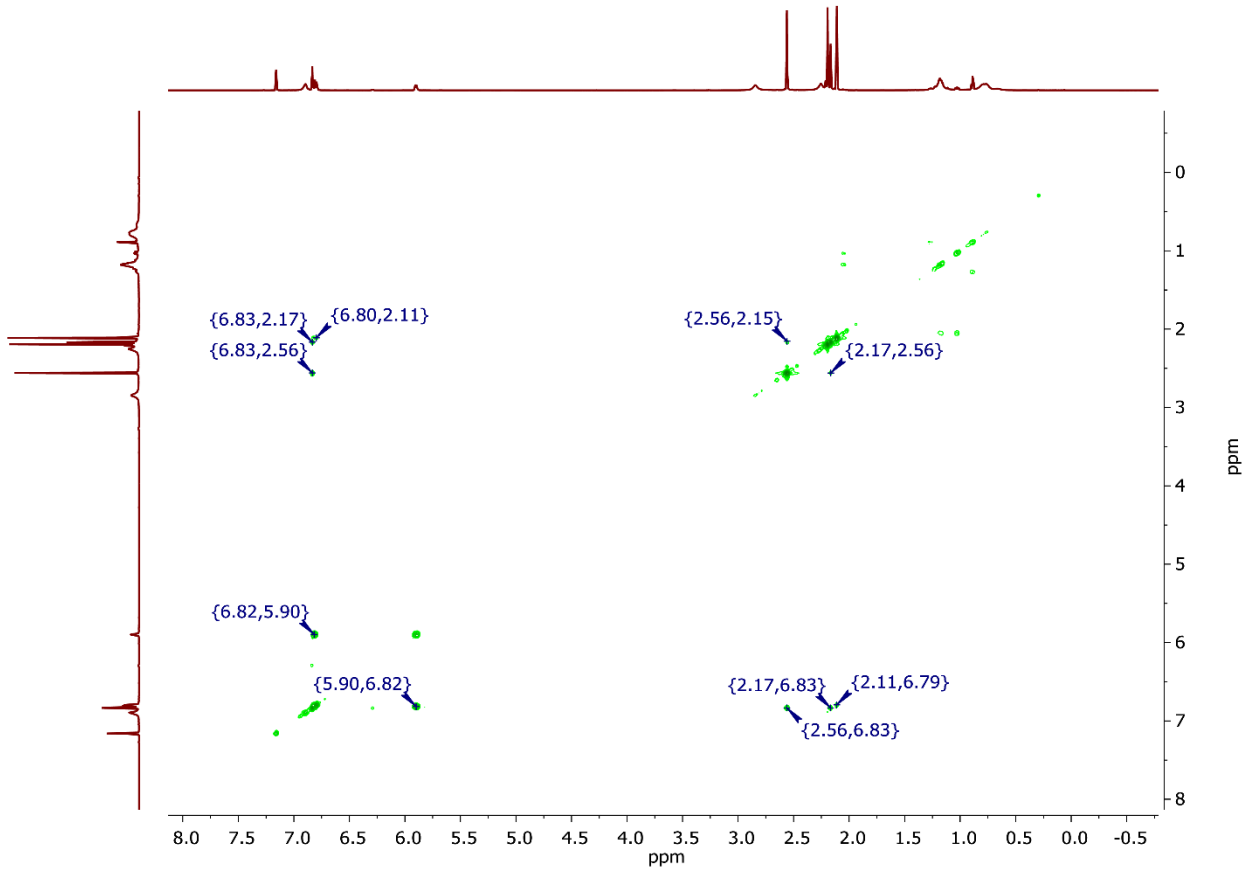

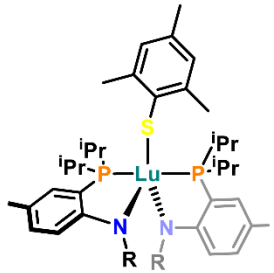

Figure S67: *^{1}H-^{1}H COSY NMR spectrum of **5-Lu** in C_6D_6 (298 K).*

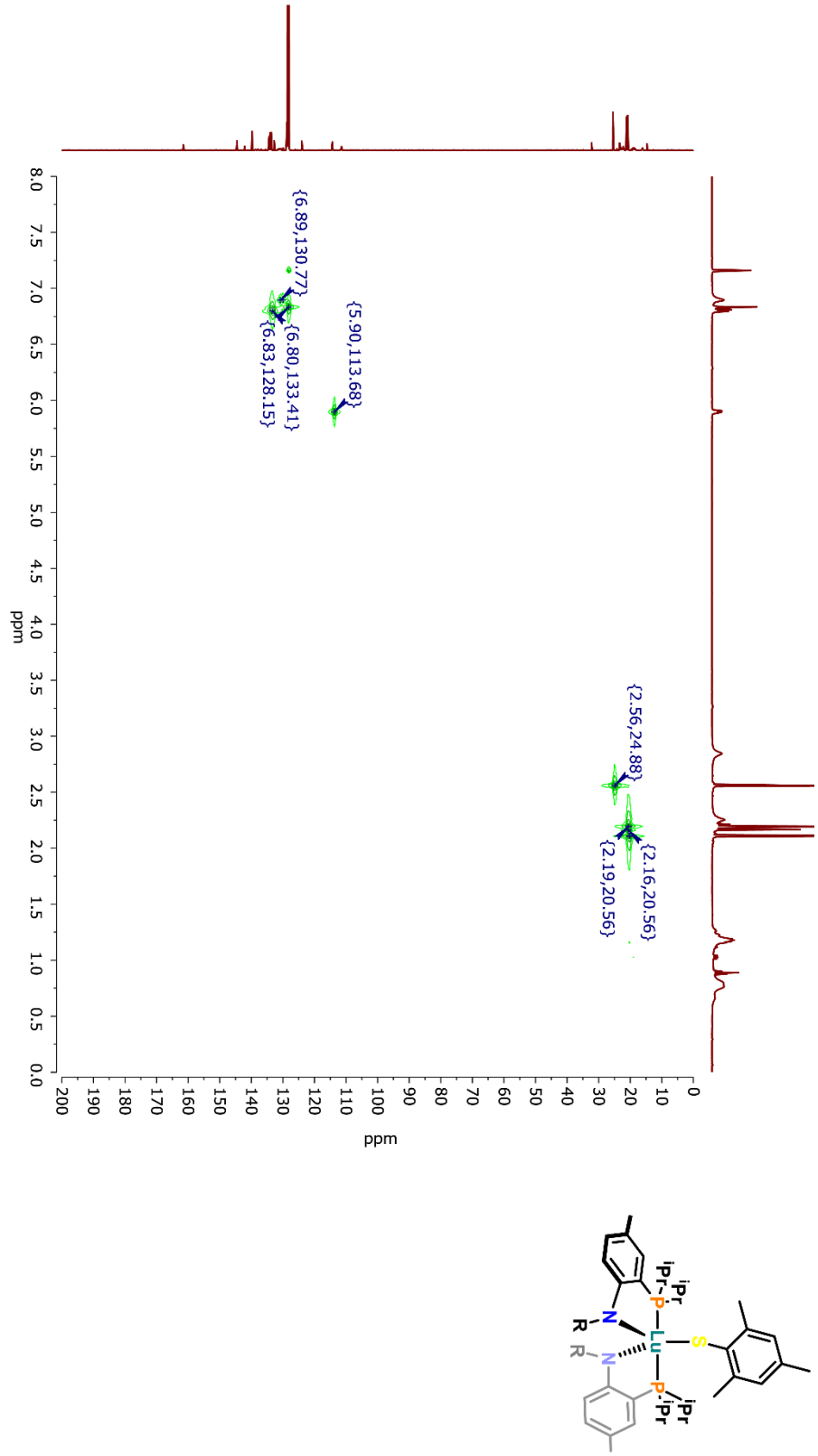

Figure S68: ^{1}H-^{13}C HSQC NMR spectrum of **5-Lu** in C_6D_6 (298 K).

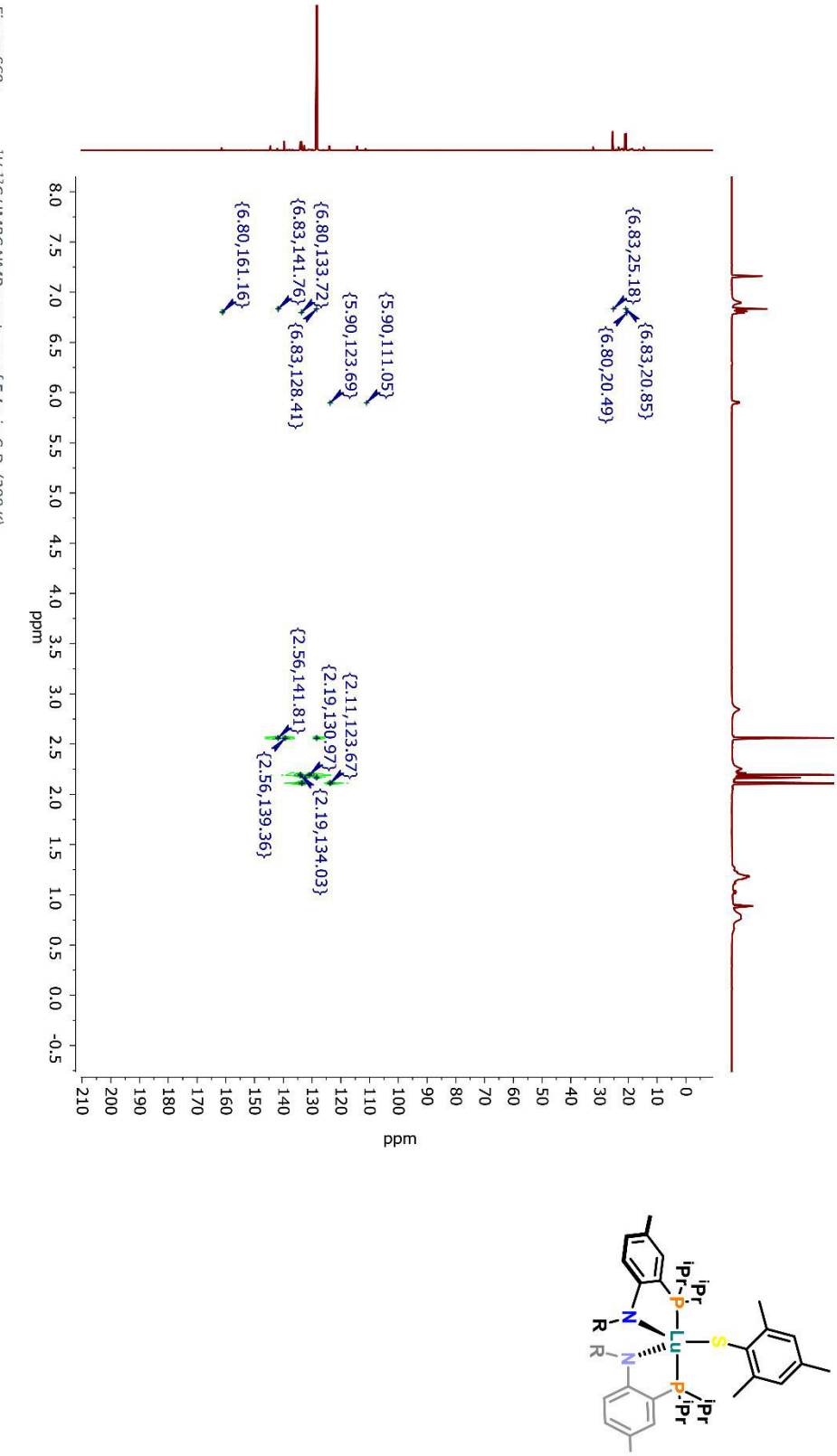

Figure S69: *^{1}H-^{13}C HMBC NMR spectrum of **5-Lu** in C_6D_6 (298 K).*

S78

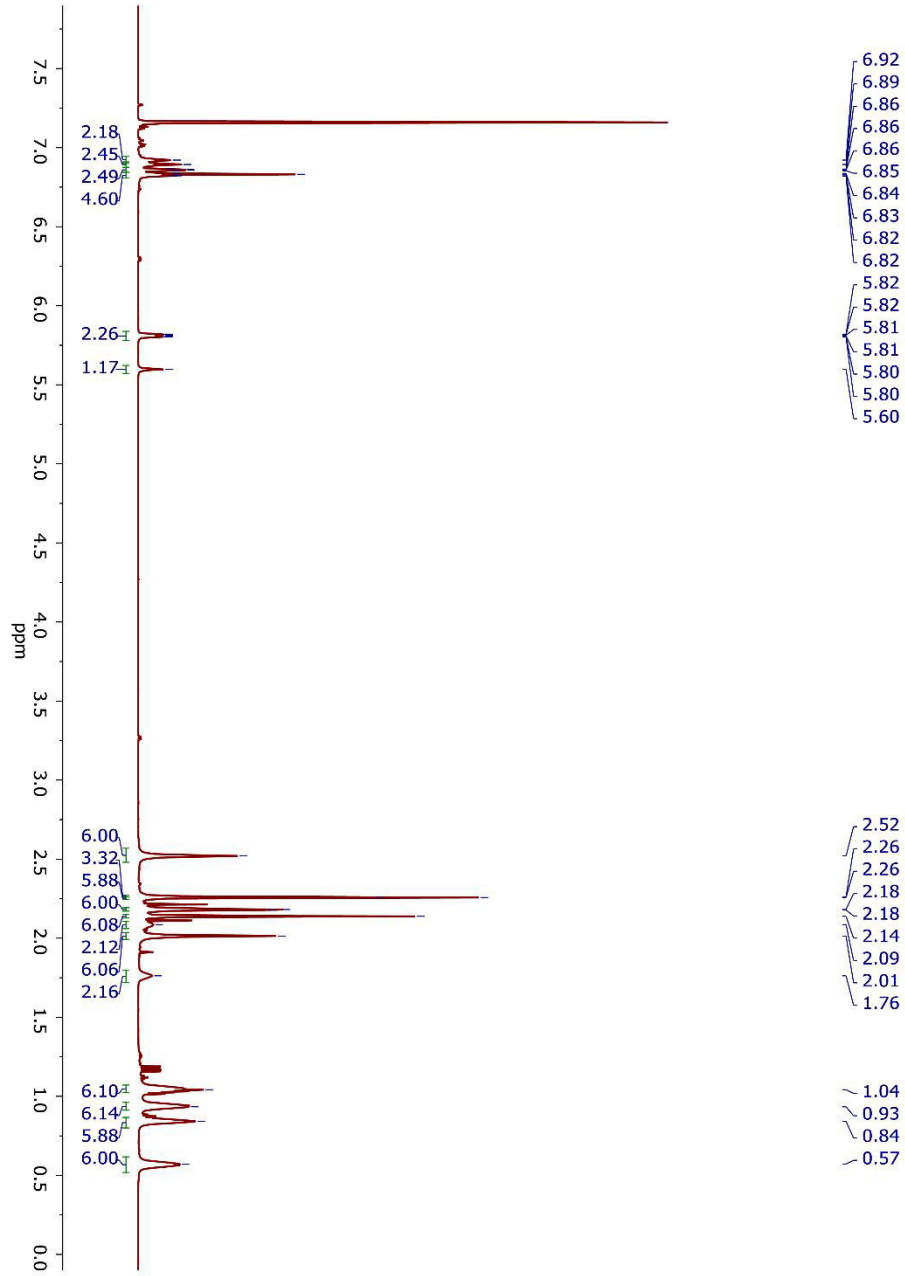

*Figure S70: ^{1}H NMR spectrum of **6-La** in C_6D_6 (298 K).*

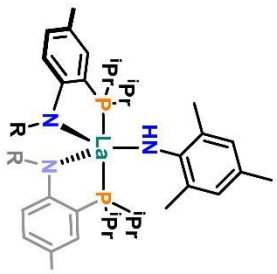

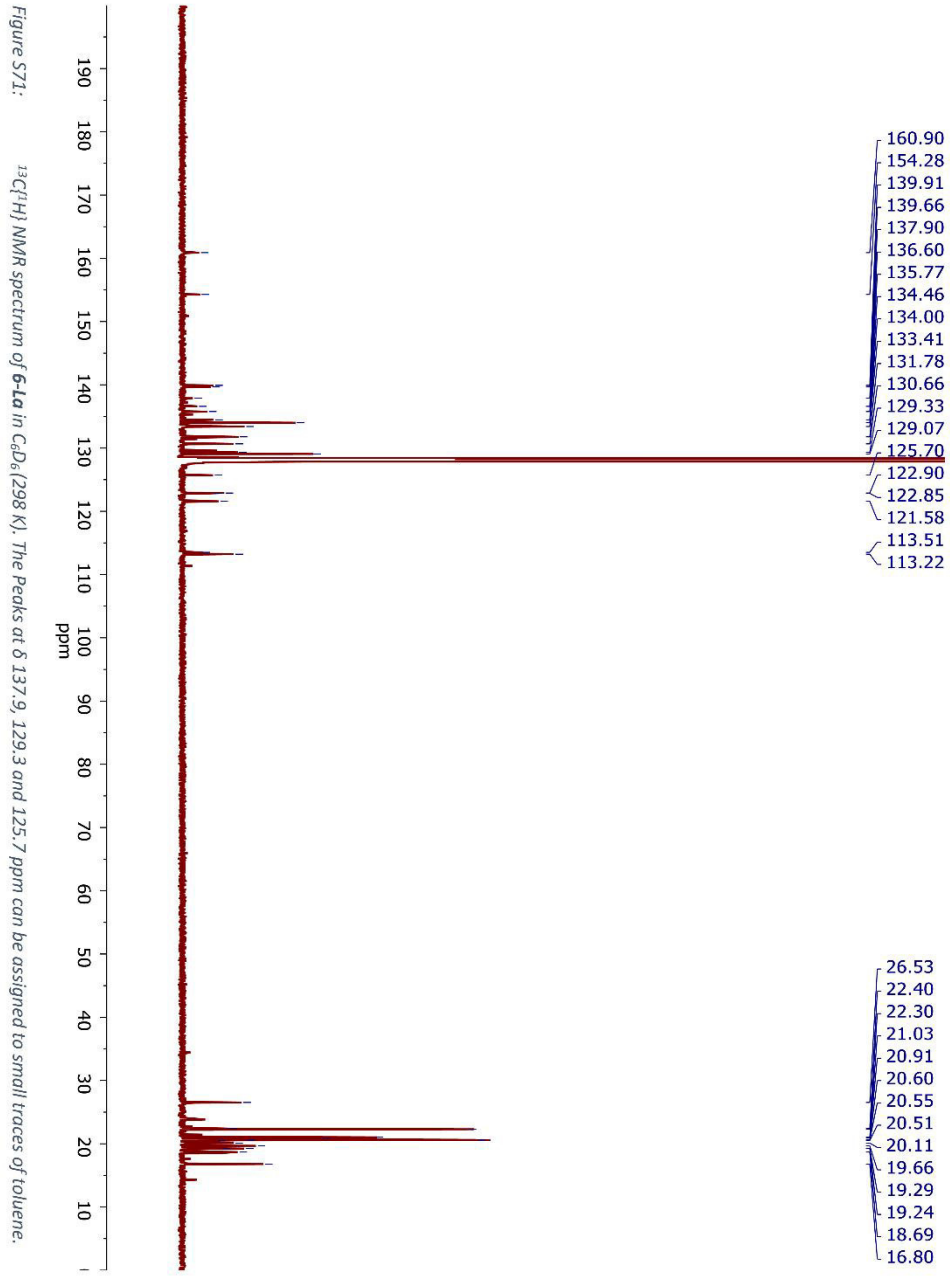

Figure S71: $^{13}C\{^1H\}$ *NMR spectrum of* **6-La** *in* C_6D_6 *(298 K). The Peaks at δ 137.9, 129.3 and 125.7 ppm can be assigned to small traces of toluene.*

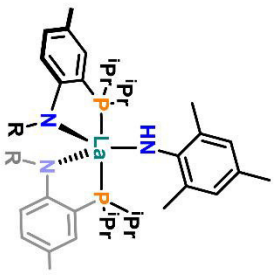

Figure S72: $^{31}P\{^{1}H\}$ *NMR spectrum of* ***6-La*** *in* C_6D_6 *(298 K).*

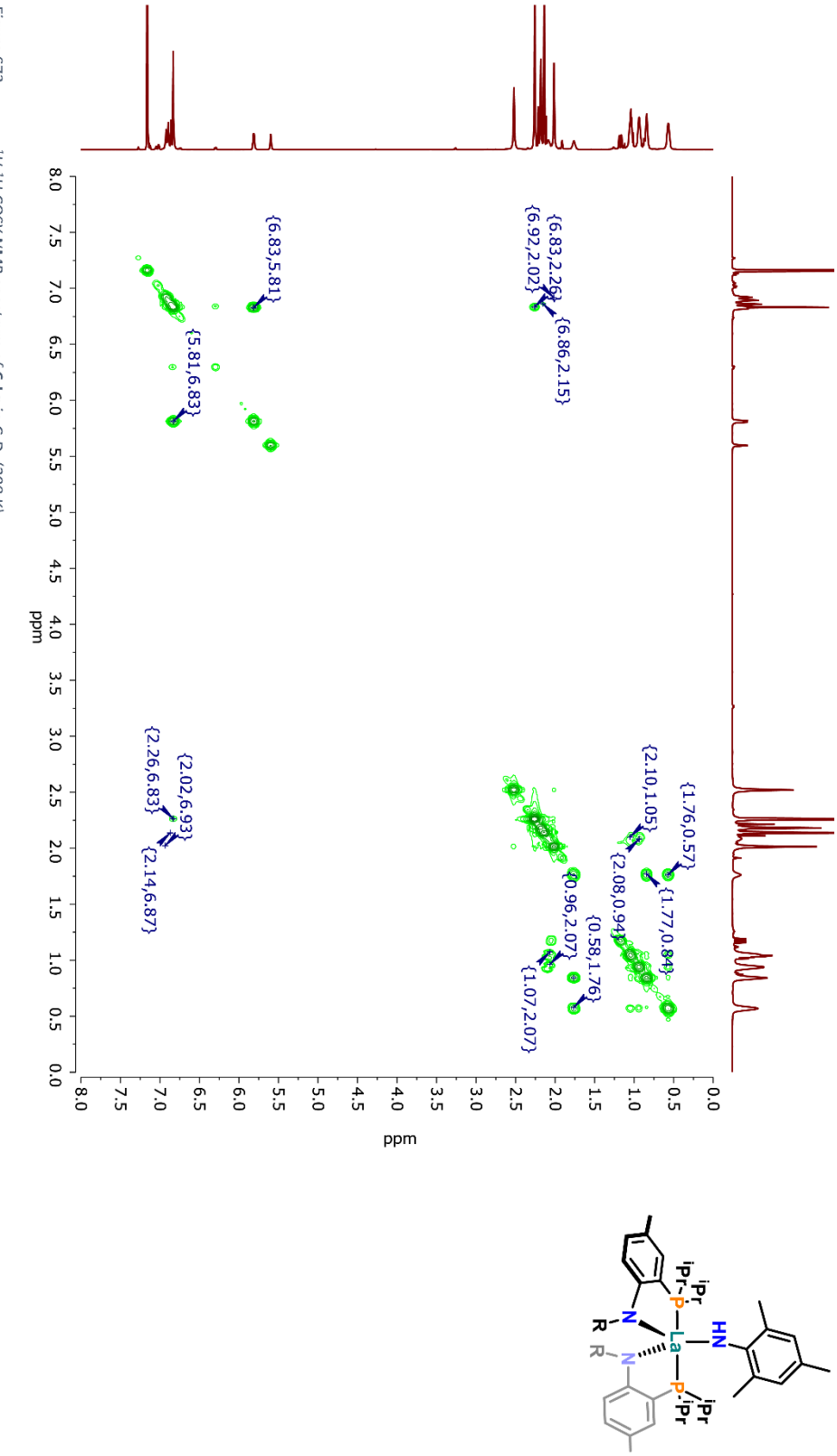

*Figure S73: ^{1}H-^{1}H COSY NMR spectrum of **6-La** in C_6D_6 (298 K).*

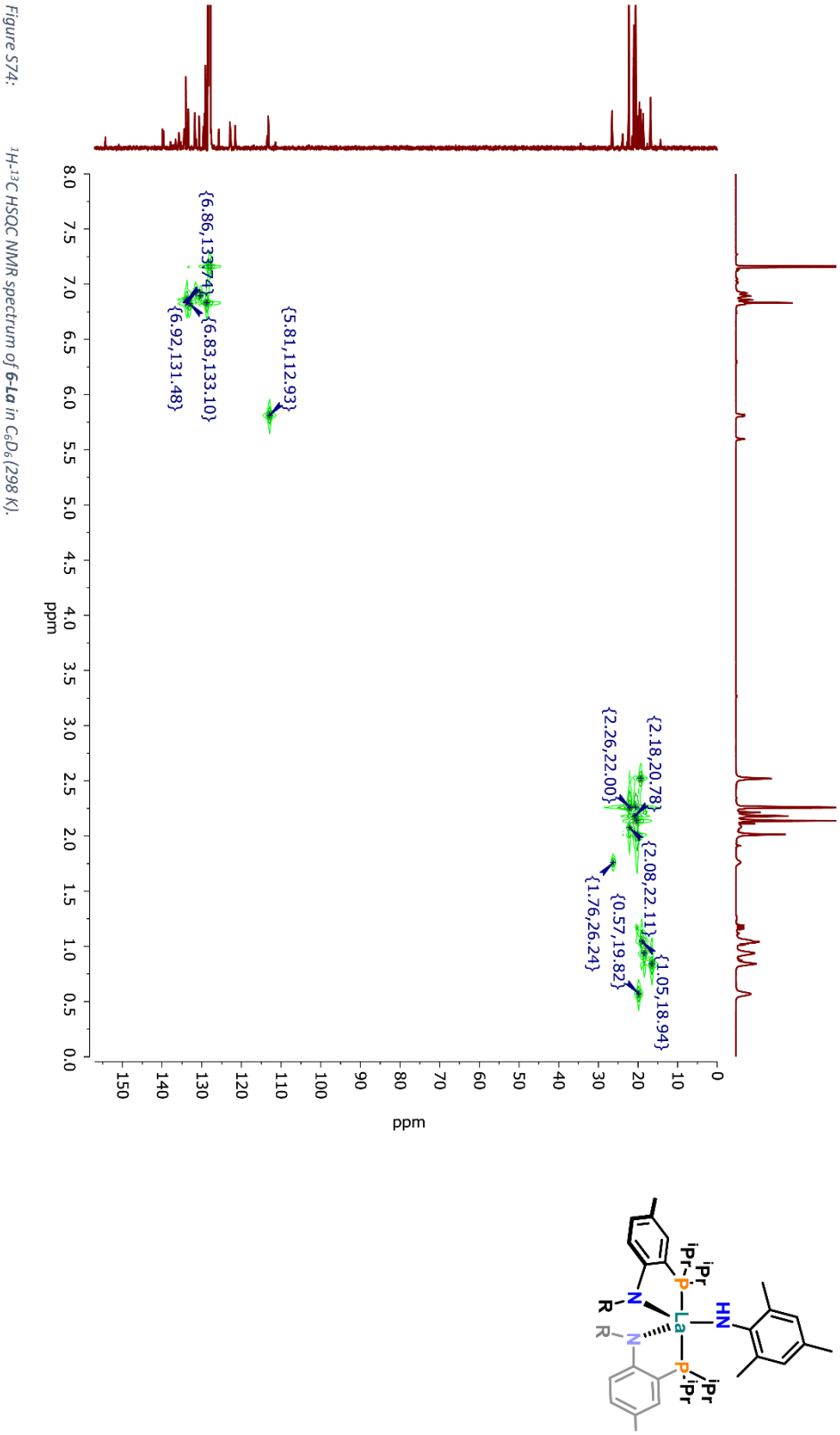

Figure S74: ^{1}H-^{13}C *HSQC NMR spectrum of* **6-La** *in* C_6D_6 *(298 K).*

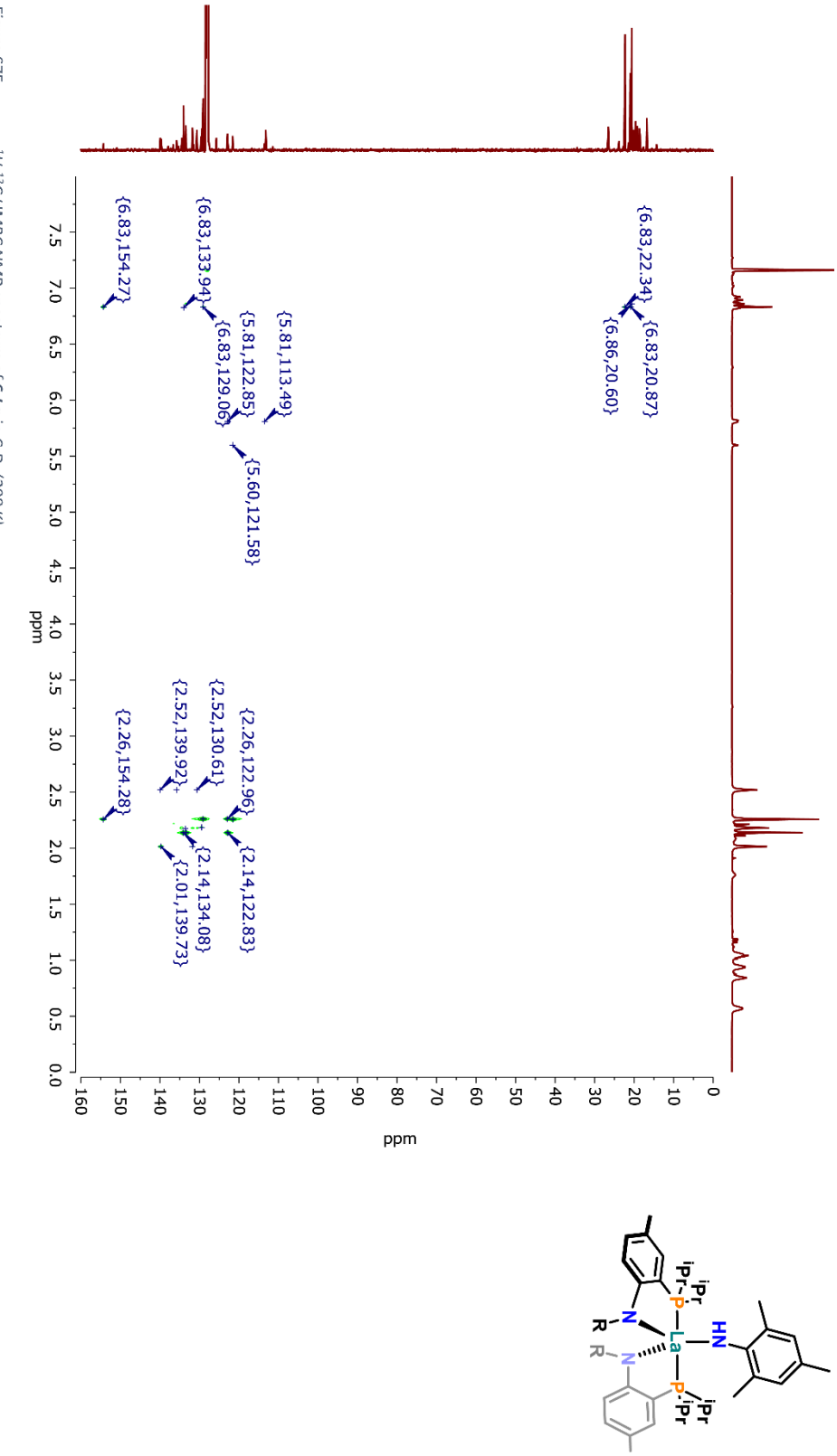

Figure S75: ^{1}H-^{13}C *HMBC NMR spectrum of* ***6-La*** *in* C_6D_6 *(298 K).*

Figure S76: ^{1}H-^{15}N *HMBC NMR spectrum of* **6-La** *in* C_6D_6 *(298 K).*

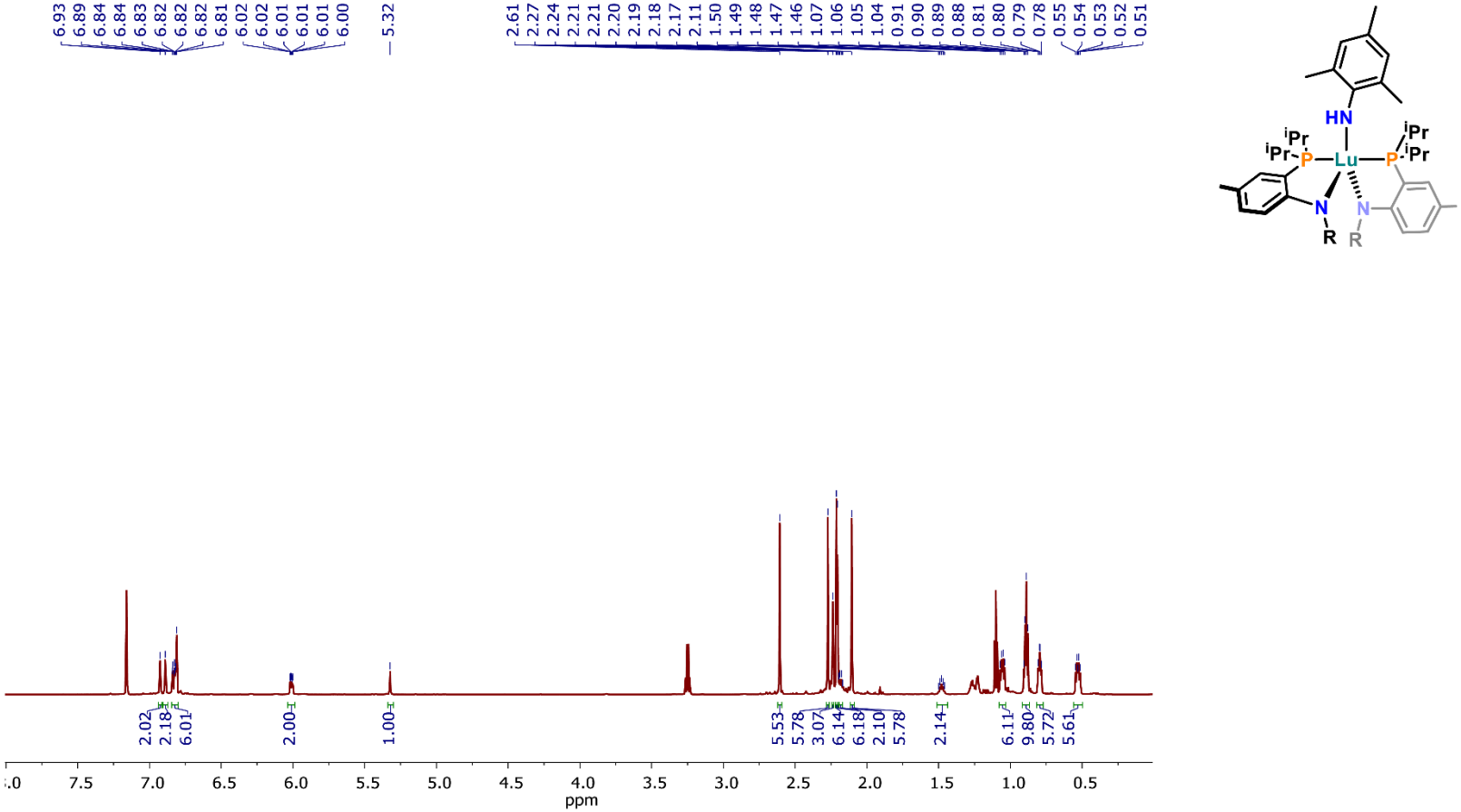

Figure S77: *^{1}H NMR spectrum of **6-Lu** in C_6D_6 (298 K). The peaks at δ 3.26 and 1.11 ppm can be assigned to residual diethyl ether. Impurities of n-hexane are visible in the aliphatic region (δ 1.24 and 0.89 ppm, the additional peak at 0.89 ppm causes the integral to be larger than 6).*

Figure S78: $^{13}C\{^1H\}$ *NMR spectrum of* ***6-Lu*** *in* C_6D_6 *(298 K). The resonances at δ 65.9 and 15.6 ppm can be assigned to residual diethyl ether; the ones at δ 32.0, 23.1 and 14.3 ppm to residual n-hexane.*

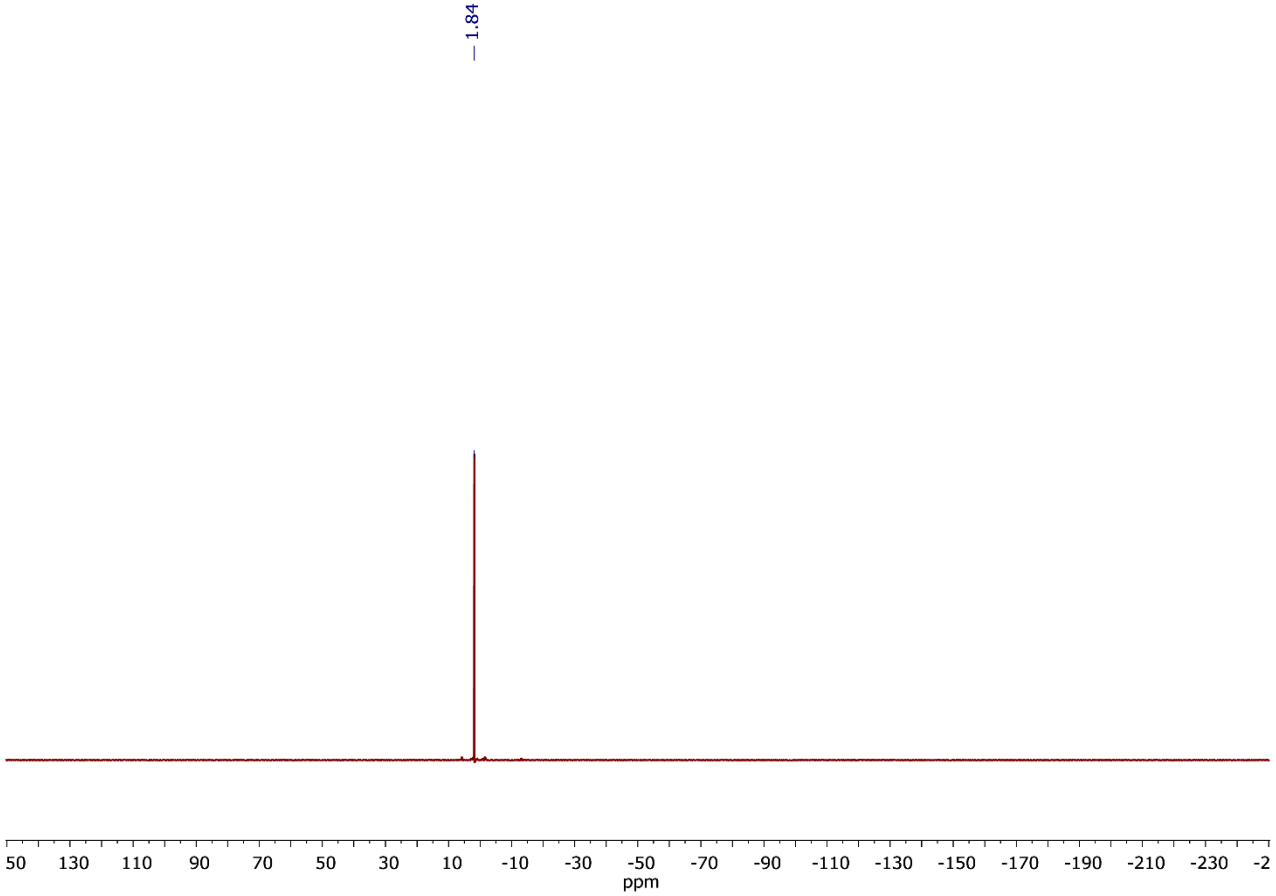

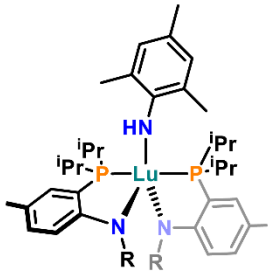

Figure S79: *$^{31}P\{^{1}H\}$ NMR spectrum of **6-Lu** in C_6D_6 (298 K).*

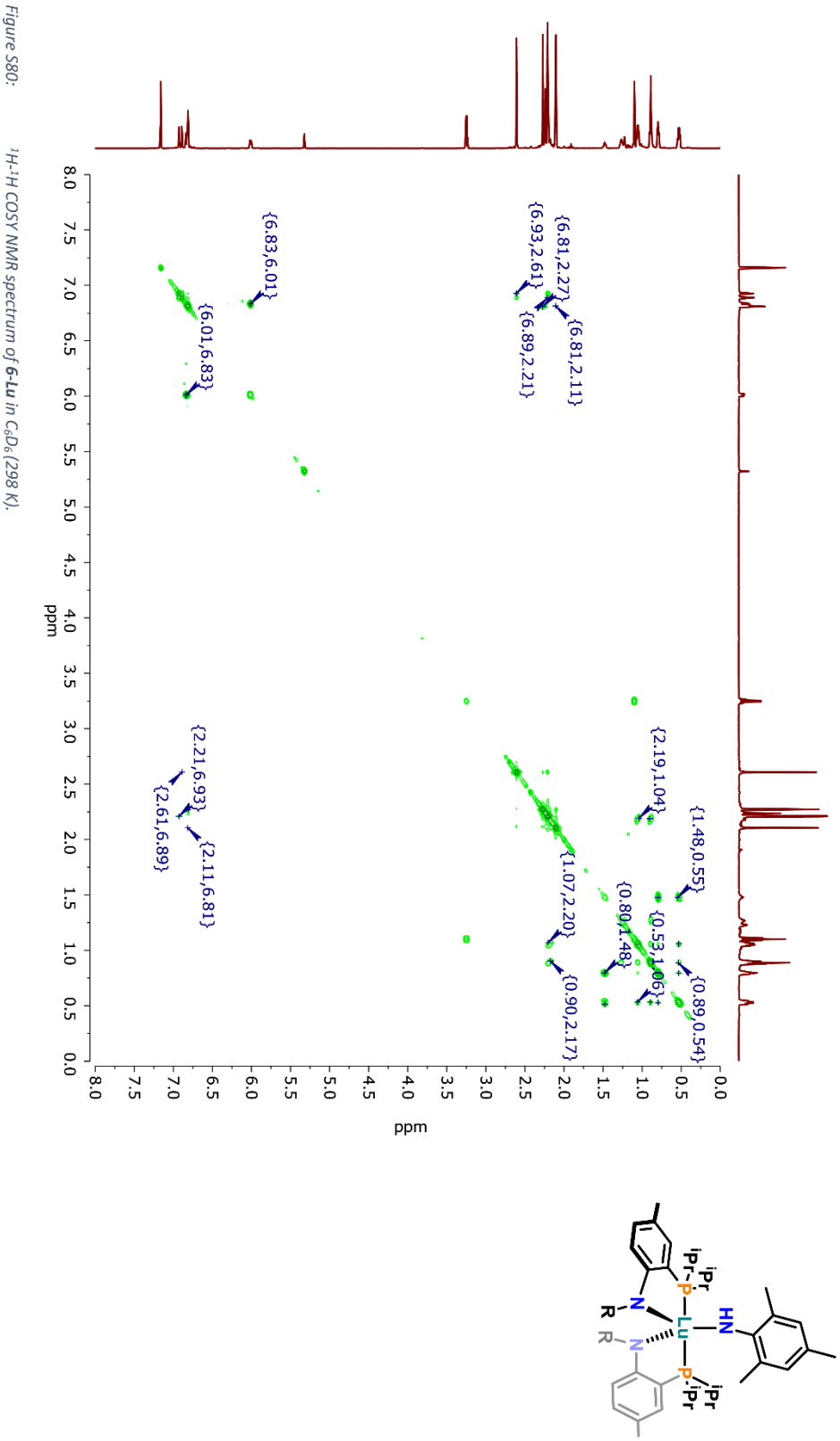

Figure S80: ^{1}H-^{1}H COSY NMR spectrum of **6-Lu** in C_6D_6 (298 K).

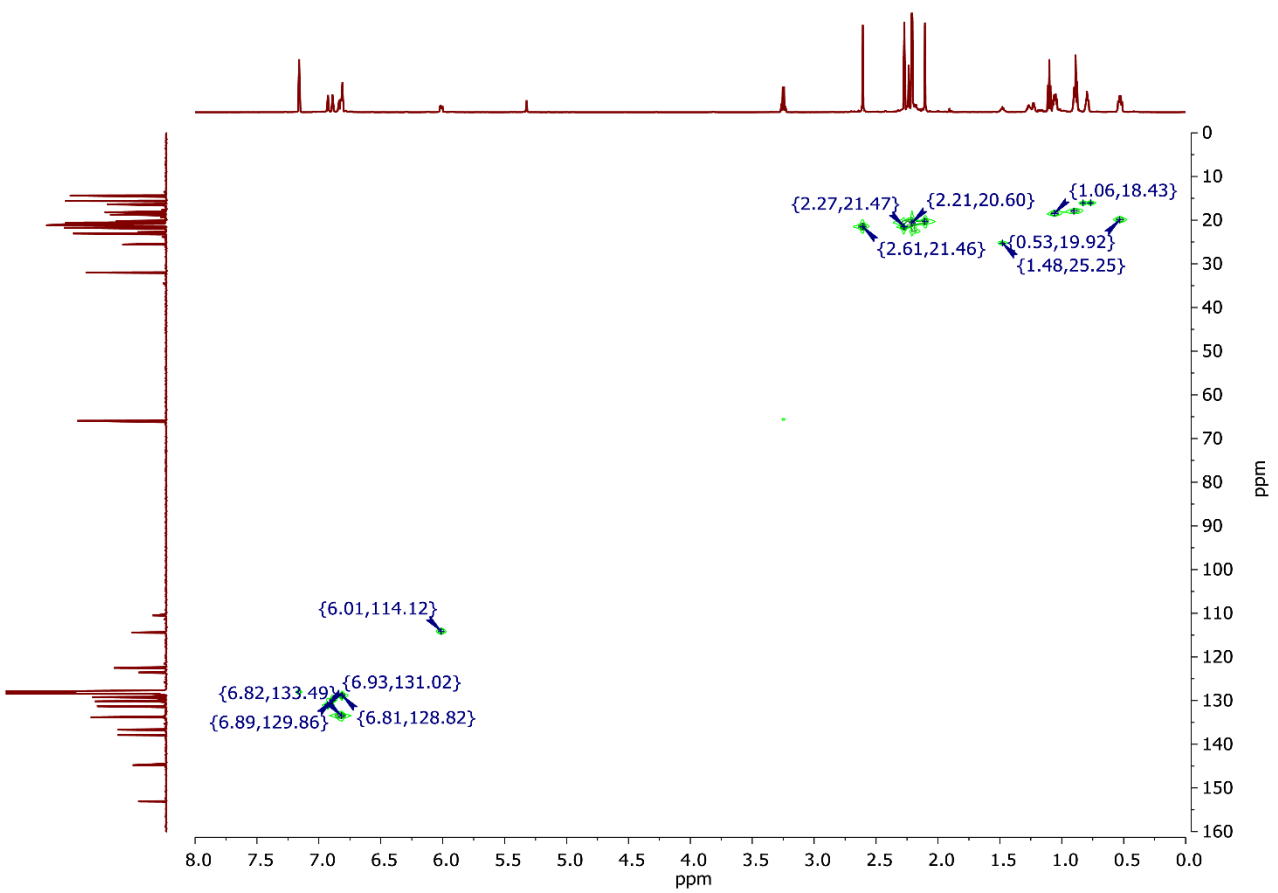

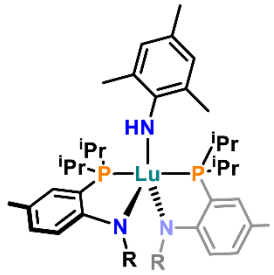

Figure S81: *^{1}H-^{13}C HSQC NMR spectrum of **6-Lu** in C_6D_6 (298 K).*

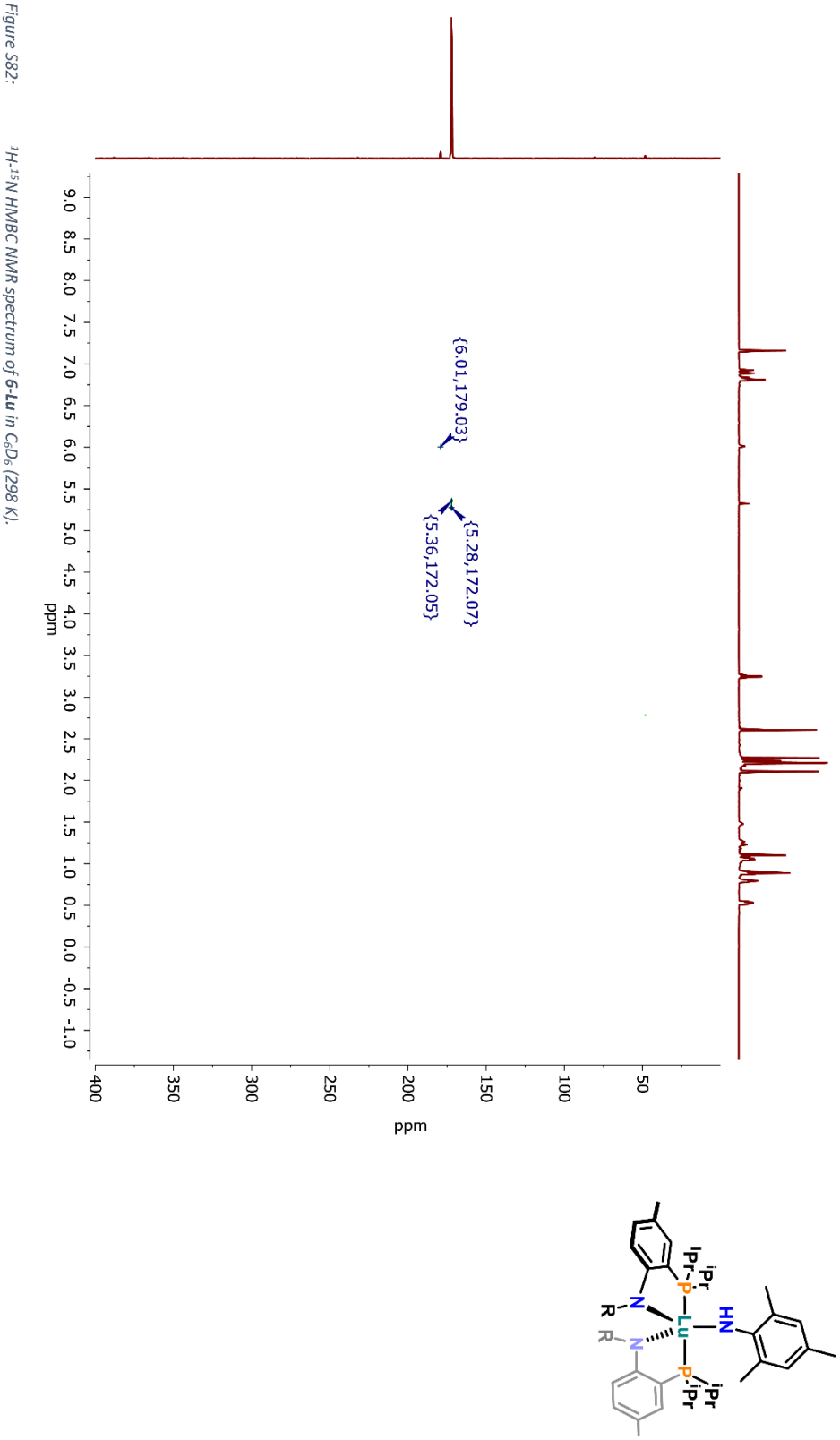

Figure S82: *^{1}H-^{15}N HMBC NMR spectrum of **6-Lu** in C_6D_6 (298 K).*

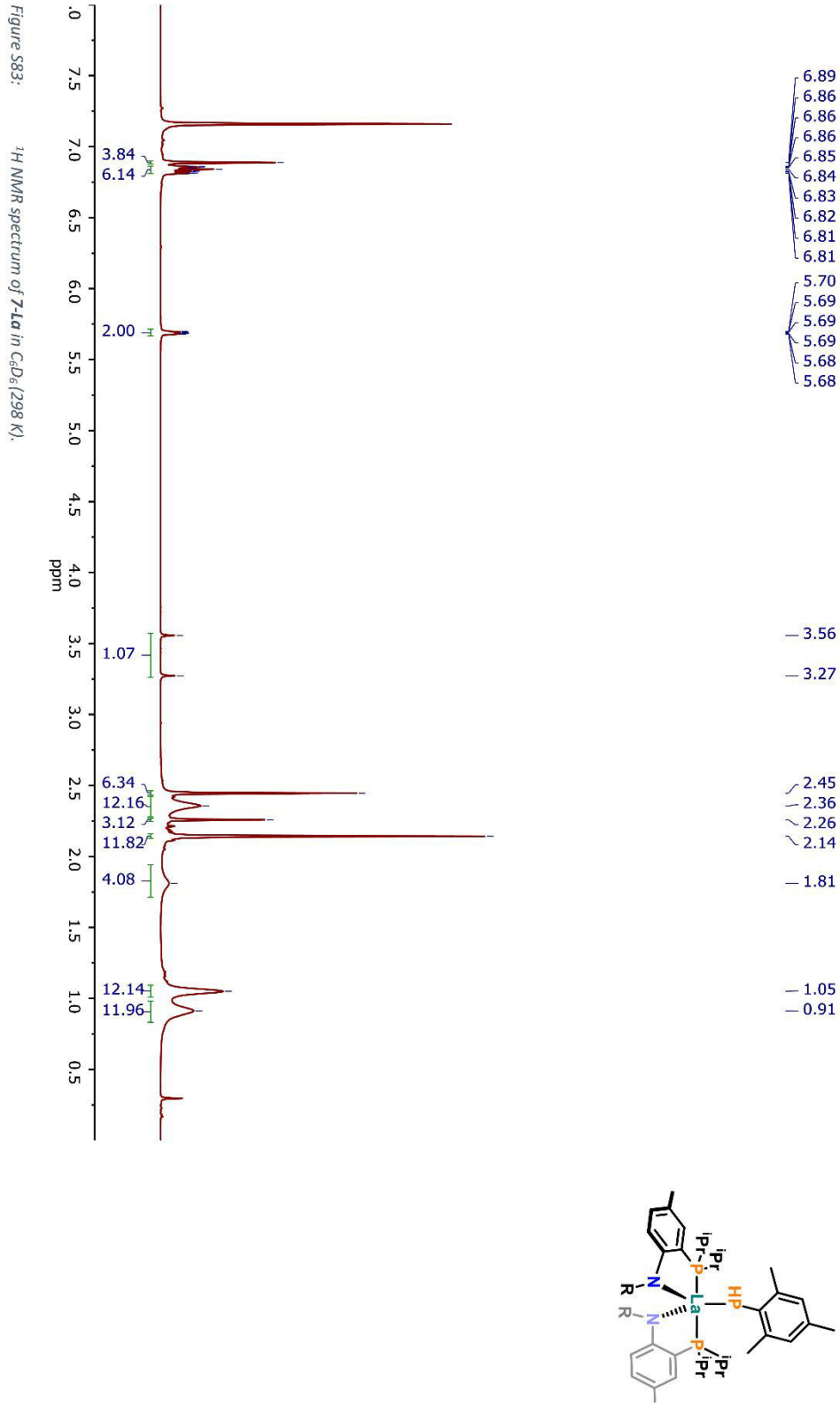

*Figure S83: ^{1}H NMR spectrum of **7-La** in C_6D_6 (298 K).*

S92

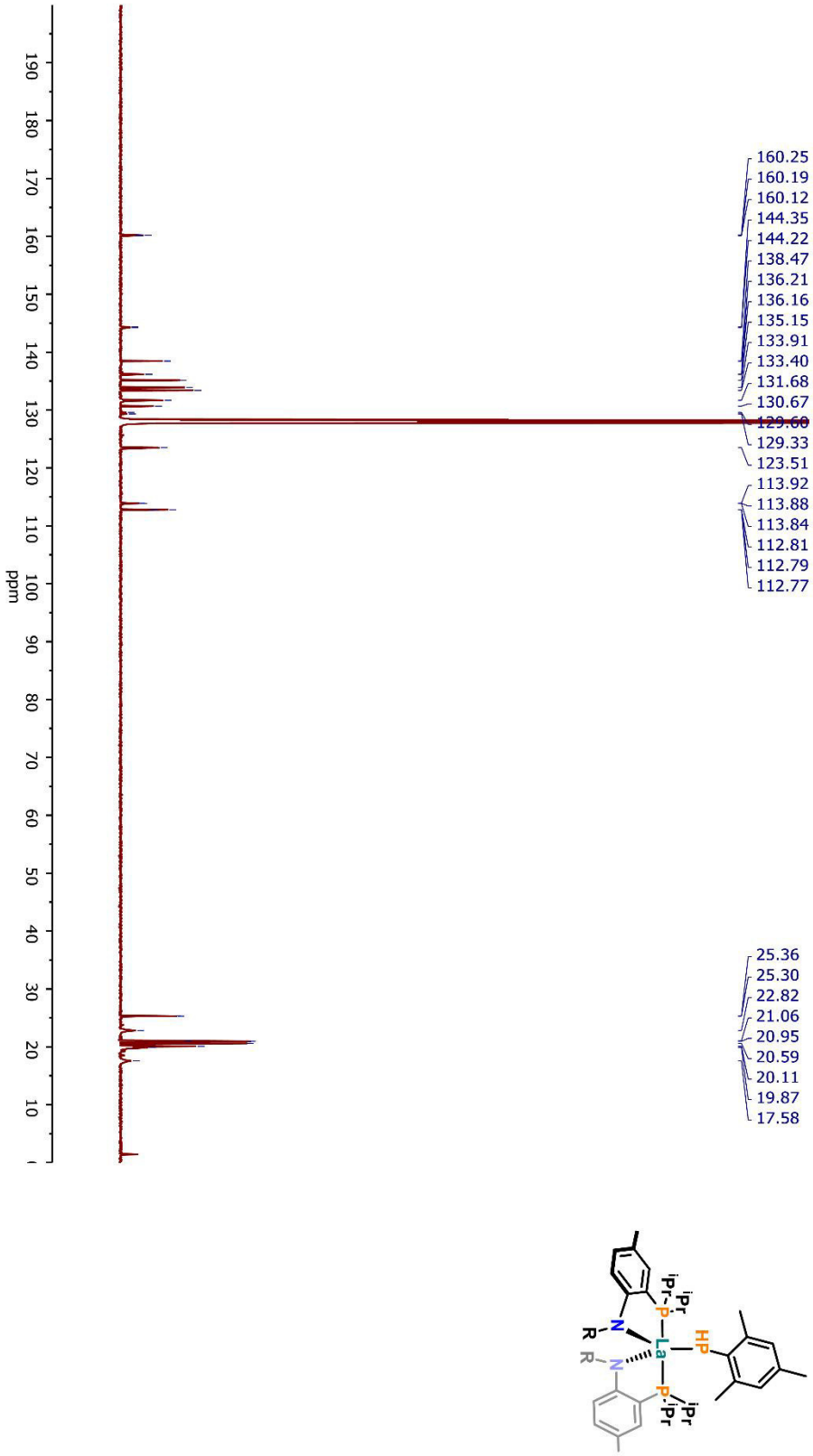

Figure S84: $^{13}C\{^{1}H\}$ *NMR spectrum of* ***7-La*** *in* C_6D_6 *(298 K).*

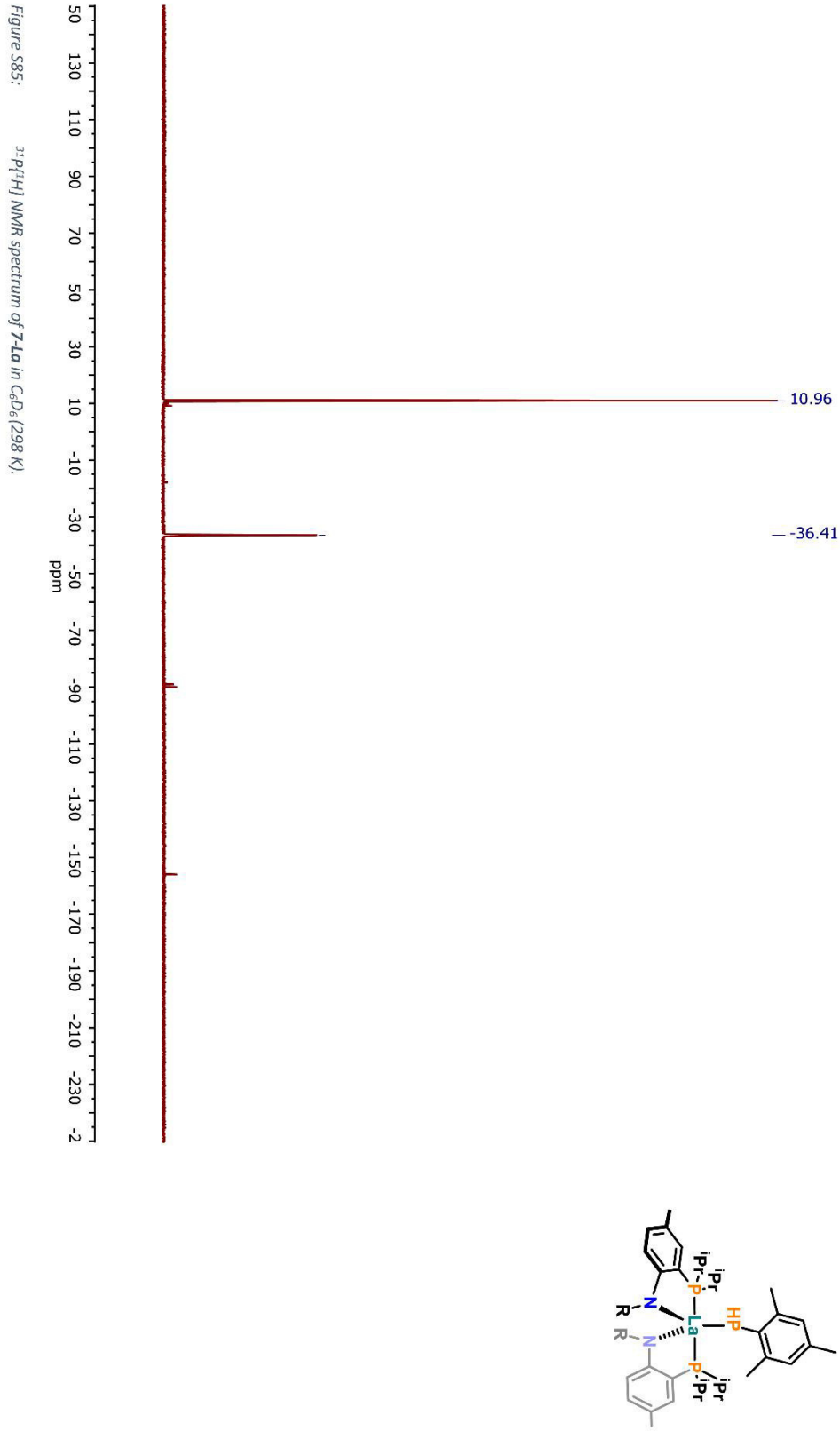

Figure S85: $^{31}P\{^1H\}$ *NMR spectrum of* ***7-La*** *in* C_6D_6 *(298 K).*

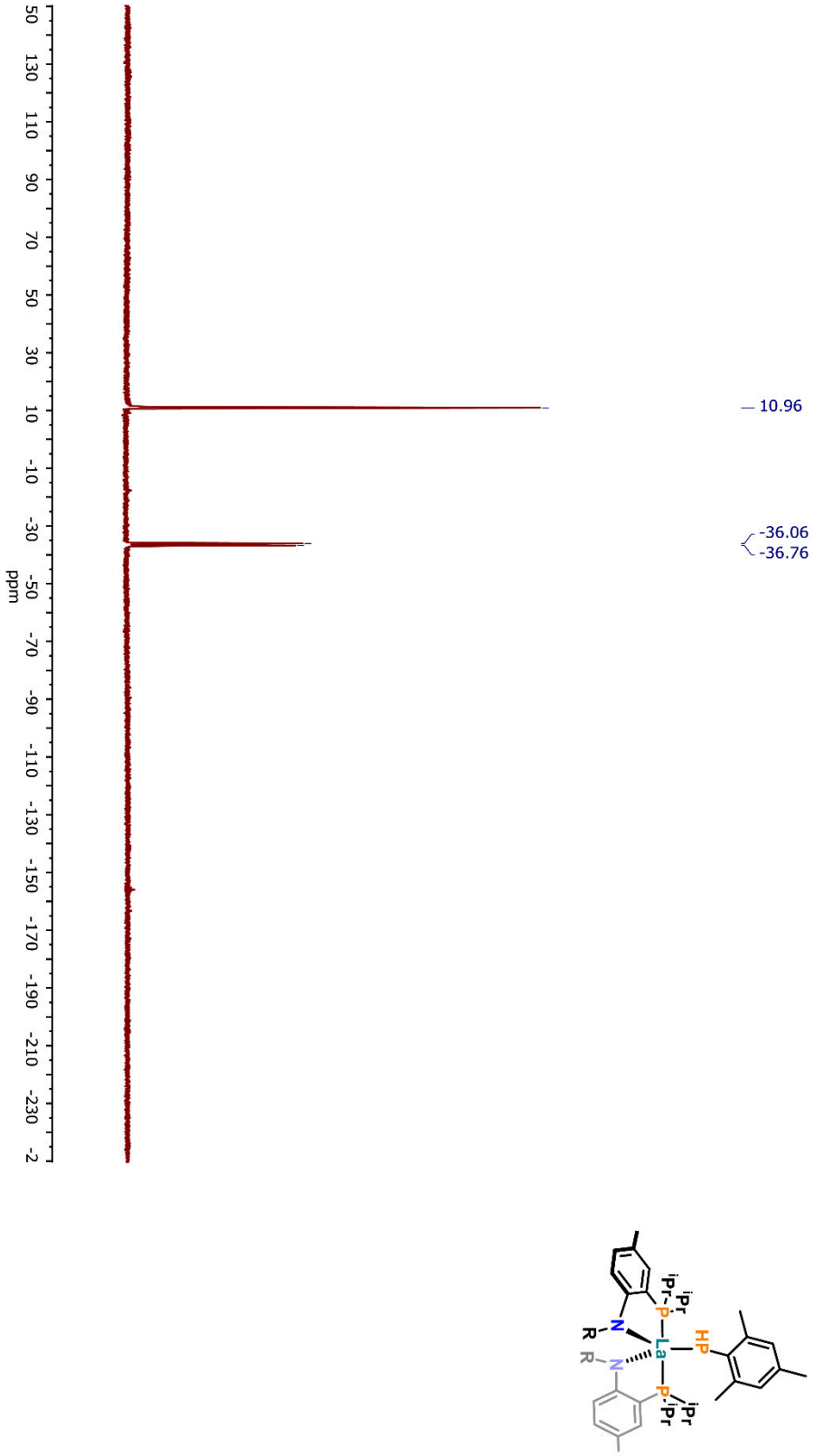

Figure S86: *^{31}P NMR spectrum of* ***7-La*** *in C_6D_6 (298 K).*

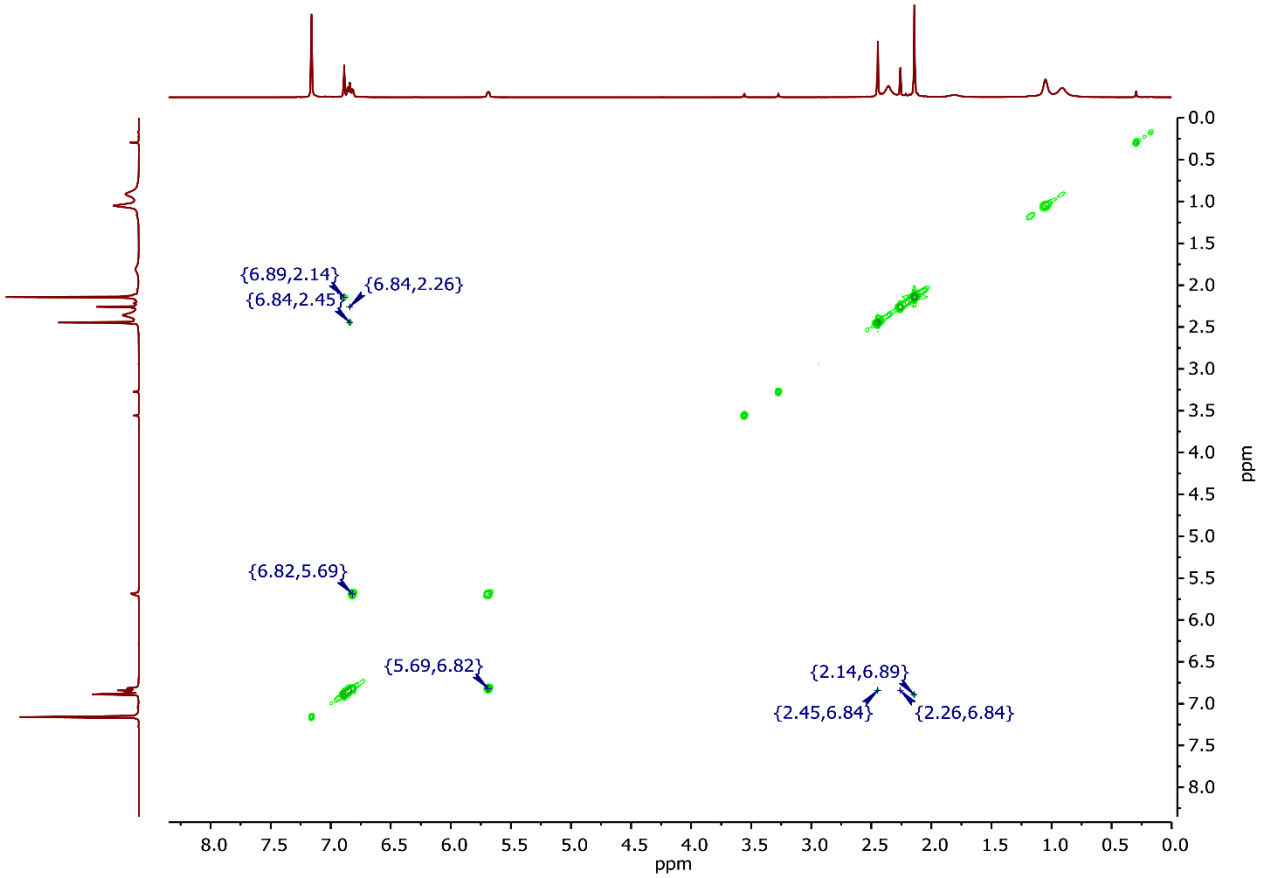

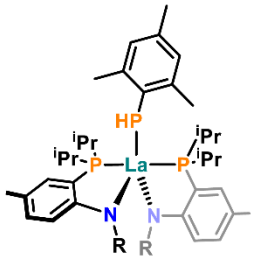

Figure S87: *^{1}H-^{1}H COSY NMR spectrum of **7-La** in C_6D_6 (298 K).*

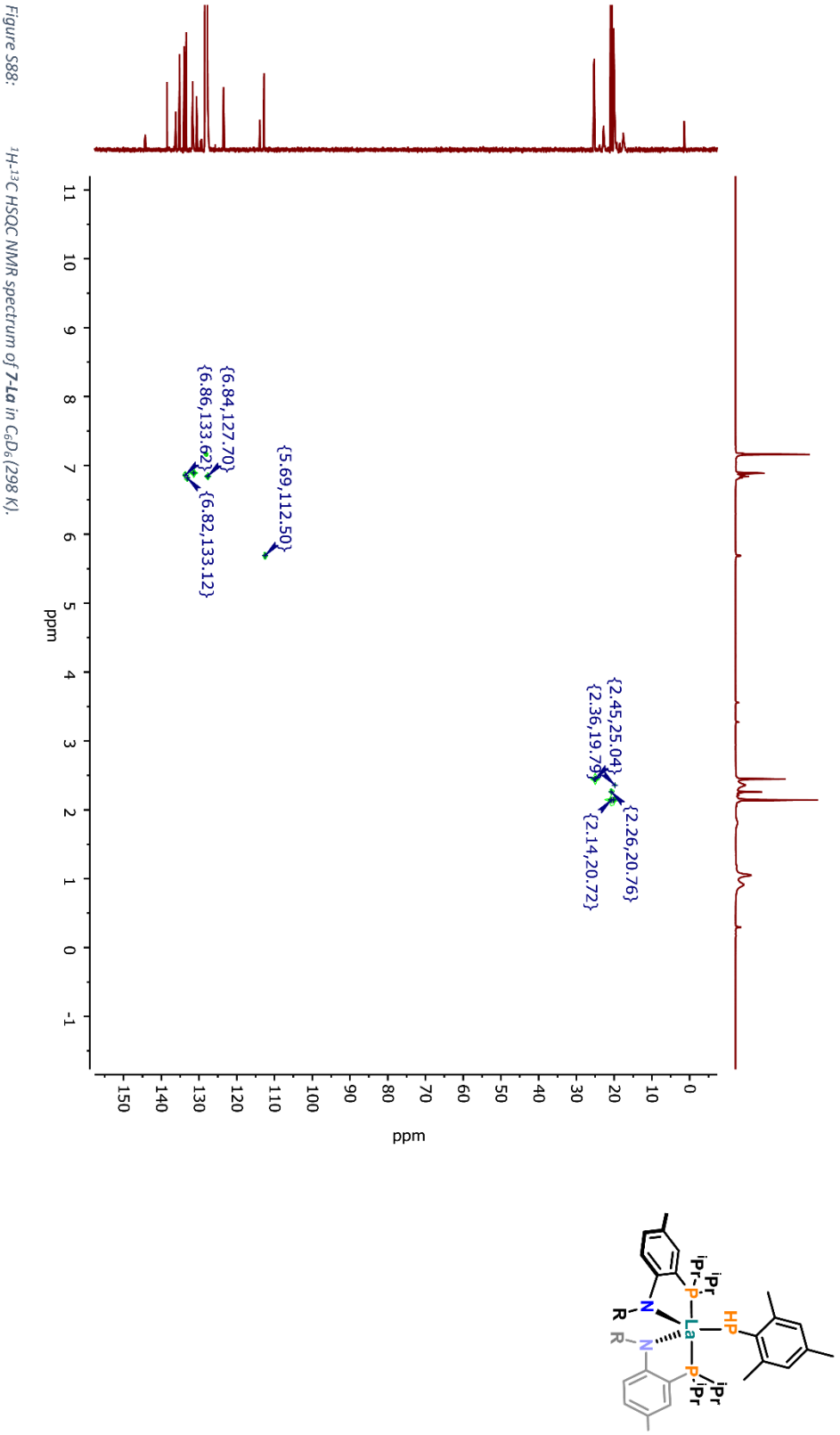

Figure S88: ^{1}H-^{13}C *HSQC NMR spectrum of* ***7-La*** *in* C_6D_6 *(298 K).*

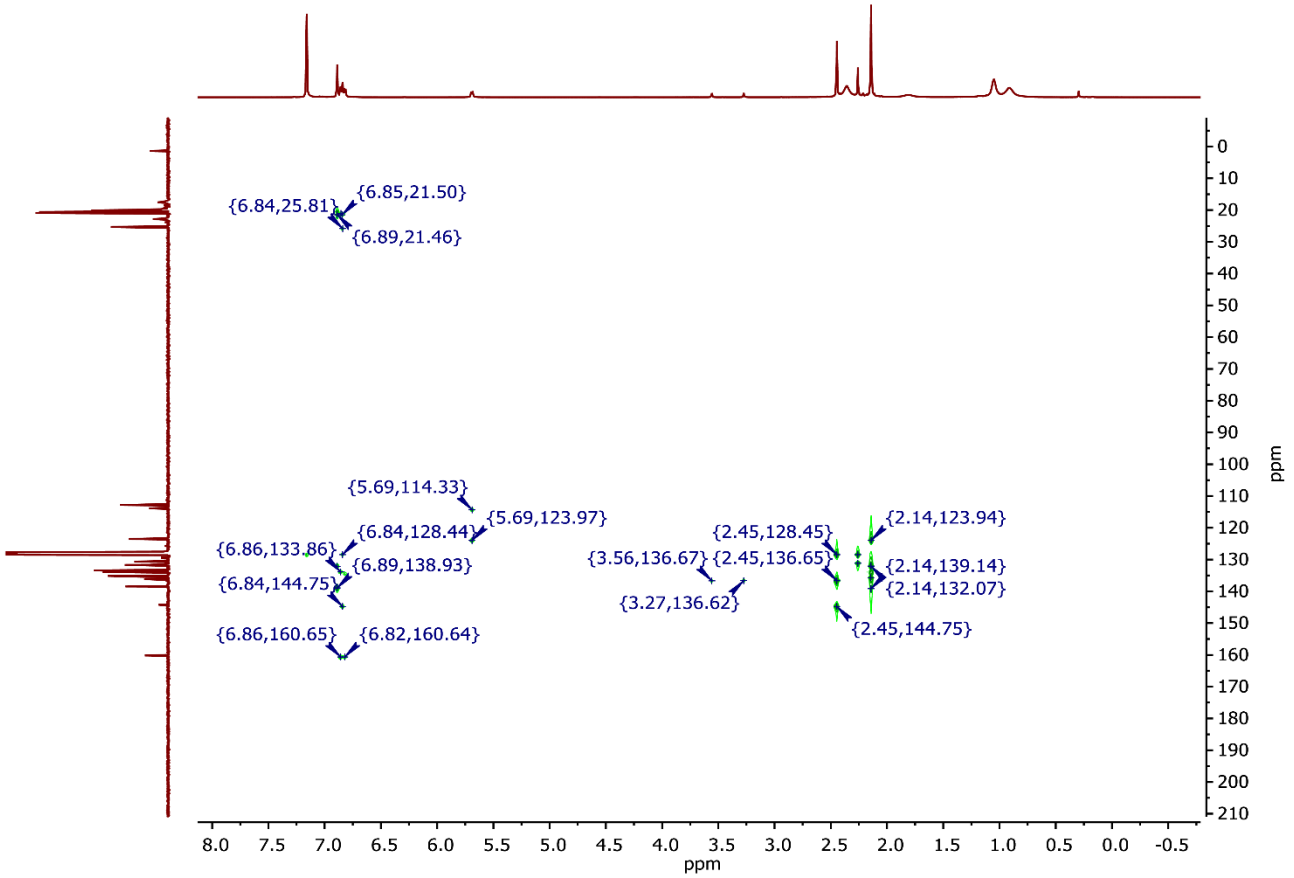

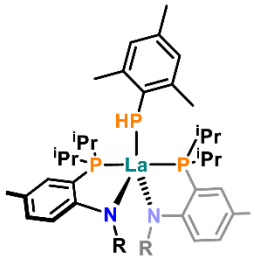

Figure S89: *^{1}H-^{13}C HMBC NMR spectrum of **7-La** in C_6D_6 (298 K).*

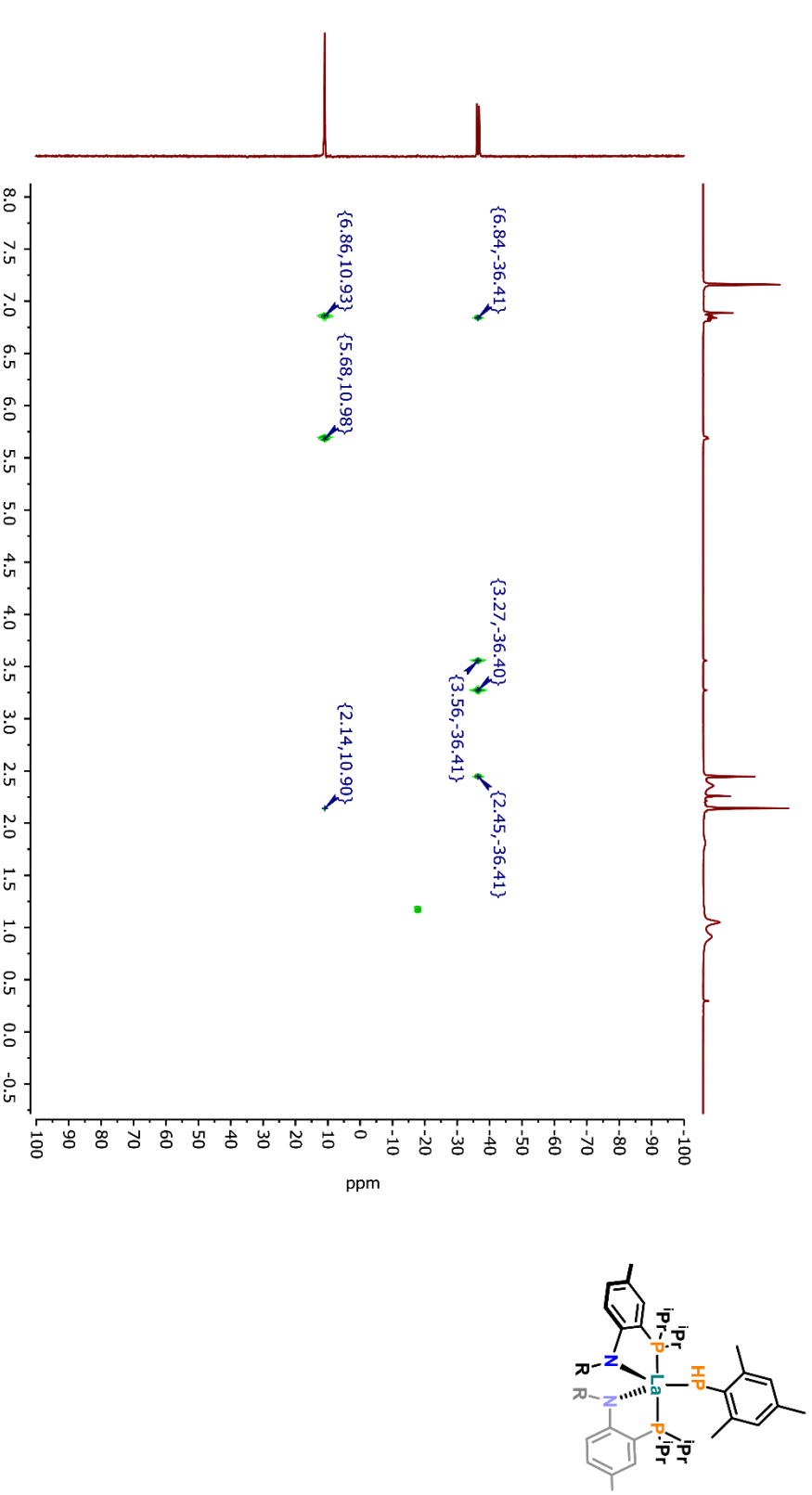

Figure S90: ^{1}H-^{31}P *HMBC NMR spectrum of* ***7-La*** *in* C_6D_6 *(298 K). The cross peak at δ –17 ppm belongs to a small impurity of* ***HPN****.*

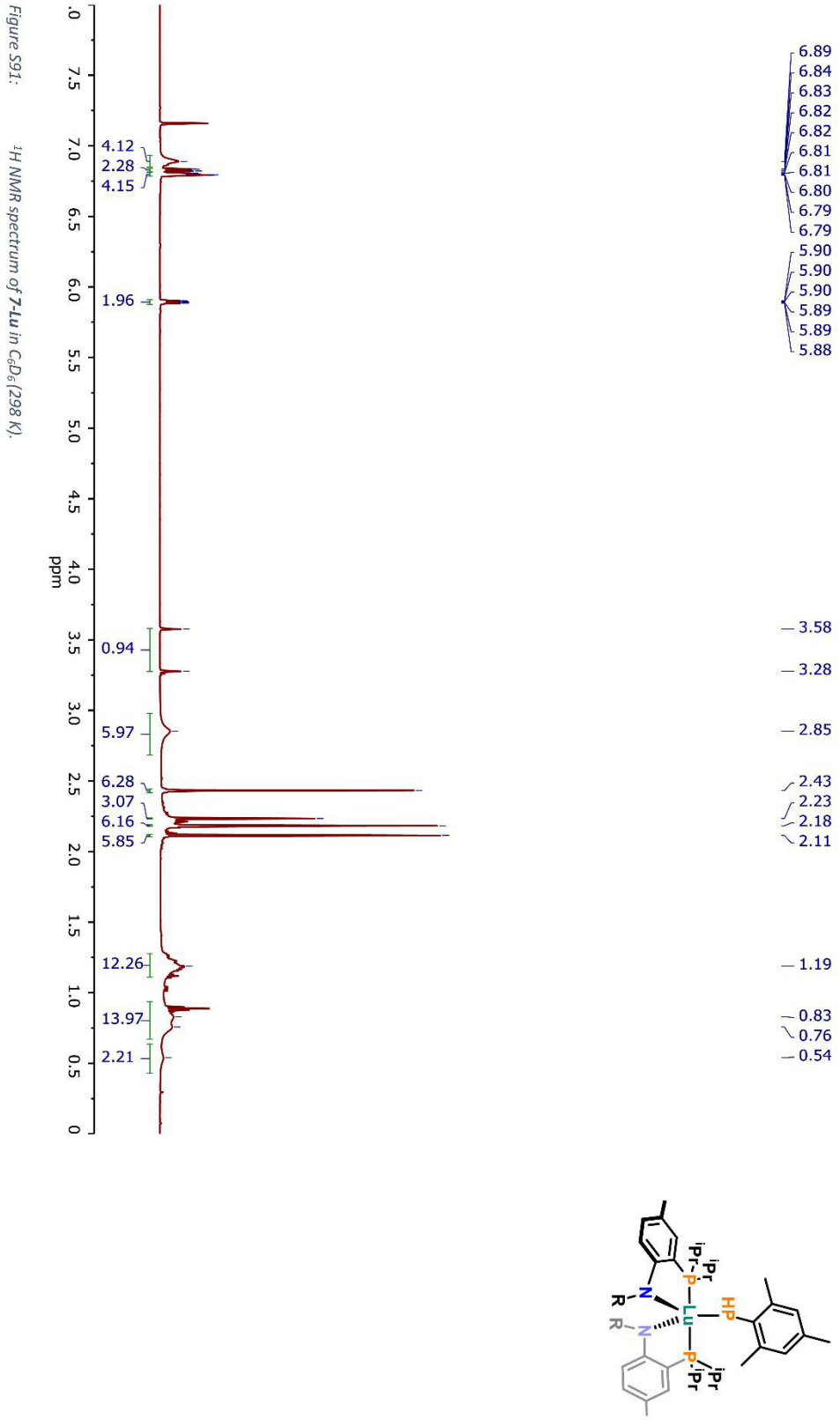

*Figure S91: ^{1}H NMR spectrum of **7-Lu** in C_6D_6 (298 K).*

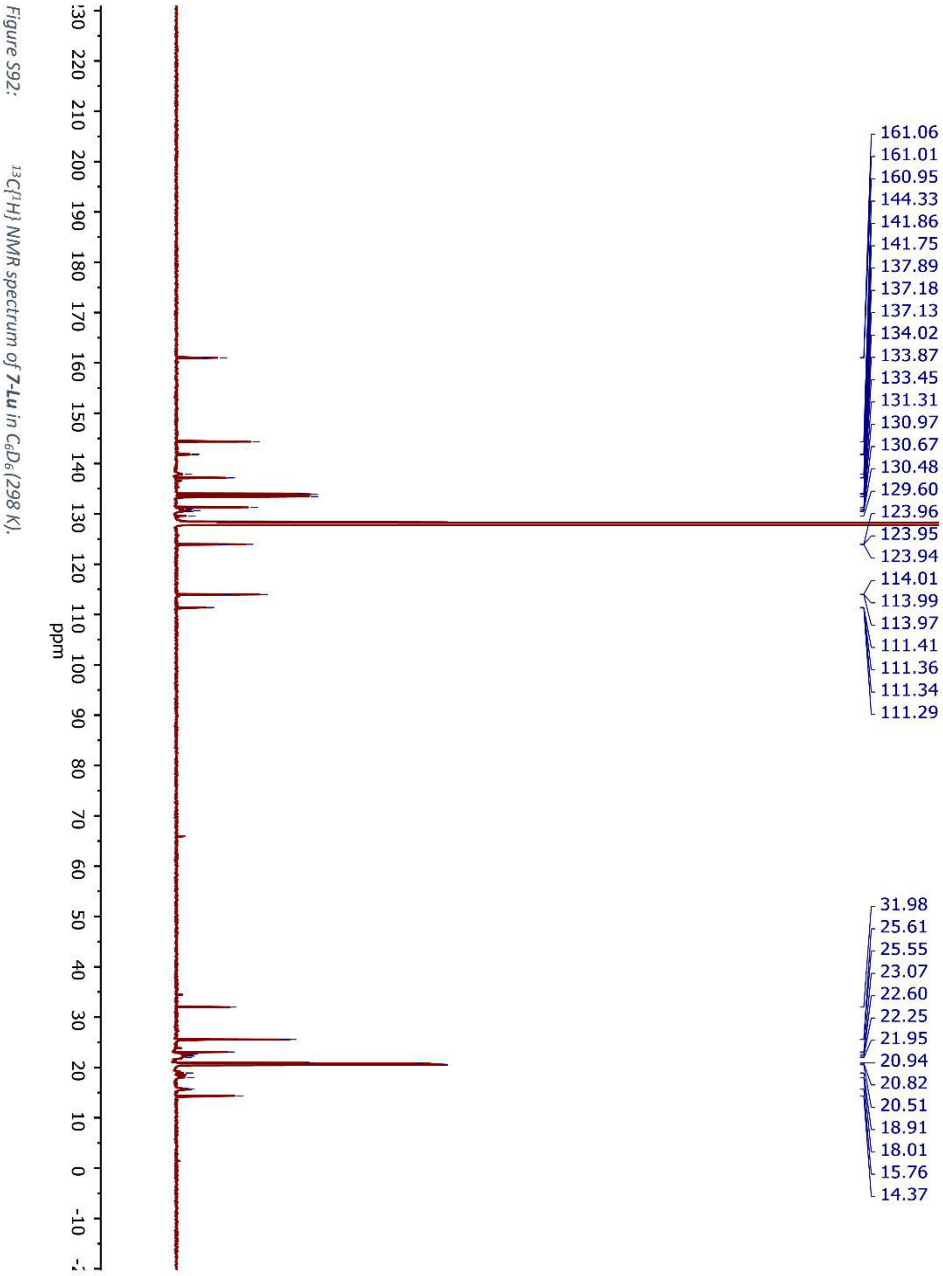

Figure S92: $^{13}C\{^{1}H\}$ NMR spectrum of **7-Lu** in C_6D_6 (298 K).

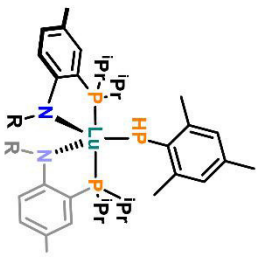

S101

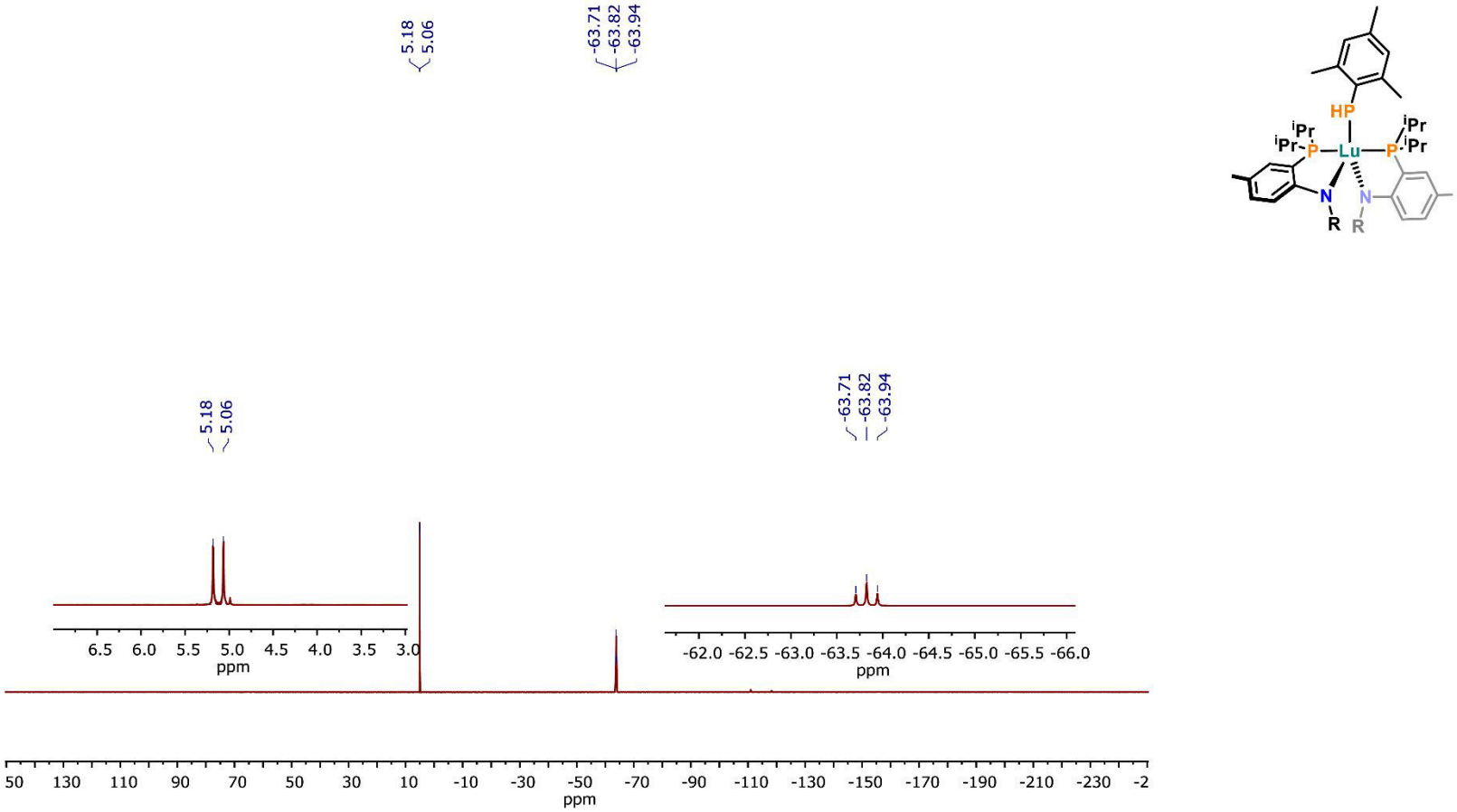

Figure S93: *$^{31}P\{^{1}H\}$ NMR spectrum of **7-Lu** in C_6D_6 (298 K). The inserts show the resonance multiplicities which indicate a $^{2}J_{PP}$ coupling between the PN ligands and the phosphido ligand.*

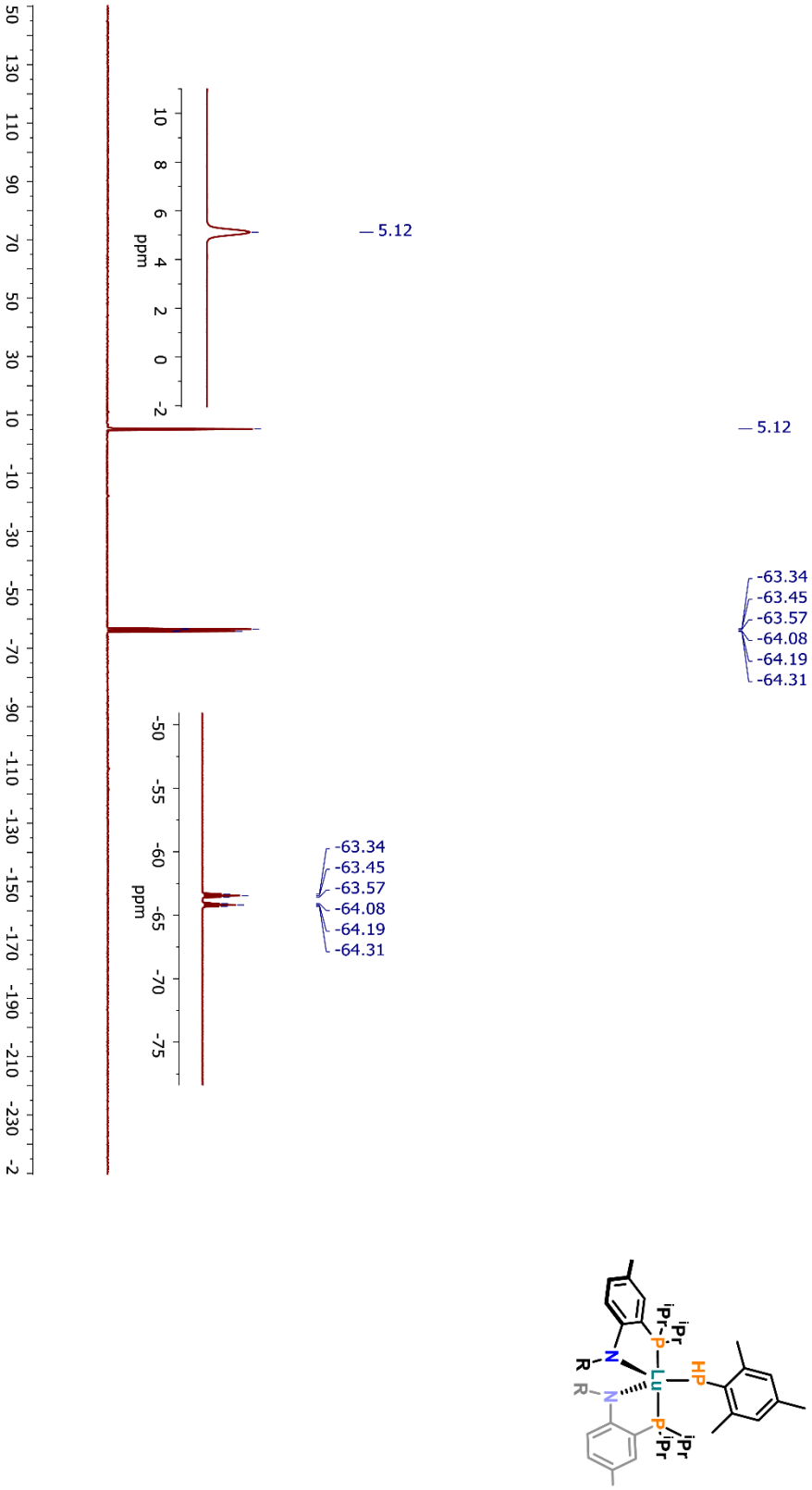

*Figure S94: ^{31}P NMR spectrum of **7-Lu** in C_6D_6 (298 K). The inserts show the resonance multiplicities which indicate a $^2J_{PP}$ coupling between the PN ligands and the phosphido ligand.*

S103

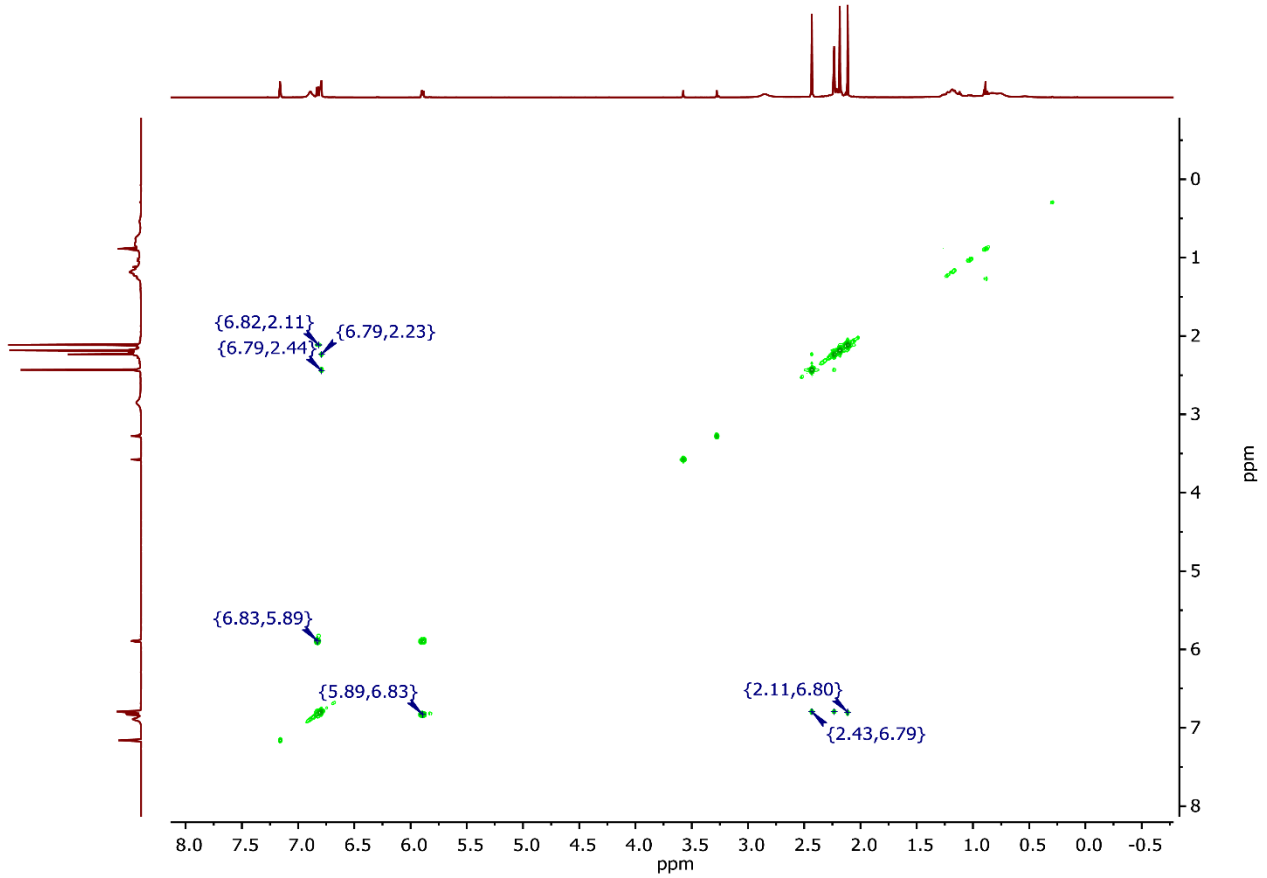

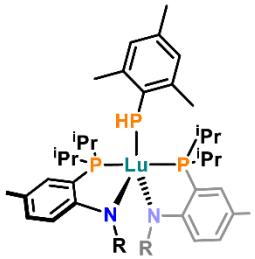

Figure S95: *^{1}H-^{1}H COSY NMR spectrum of **7-Lu** in C_6D_6 (298 K).*

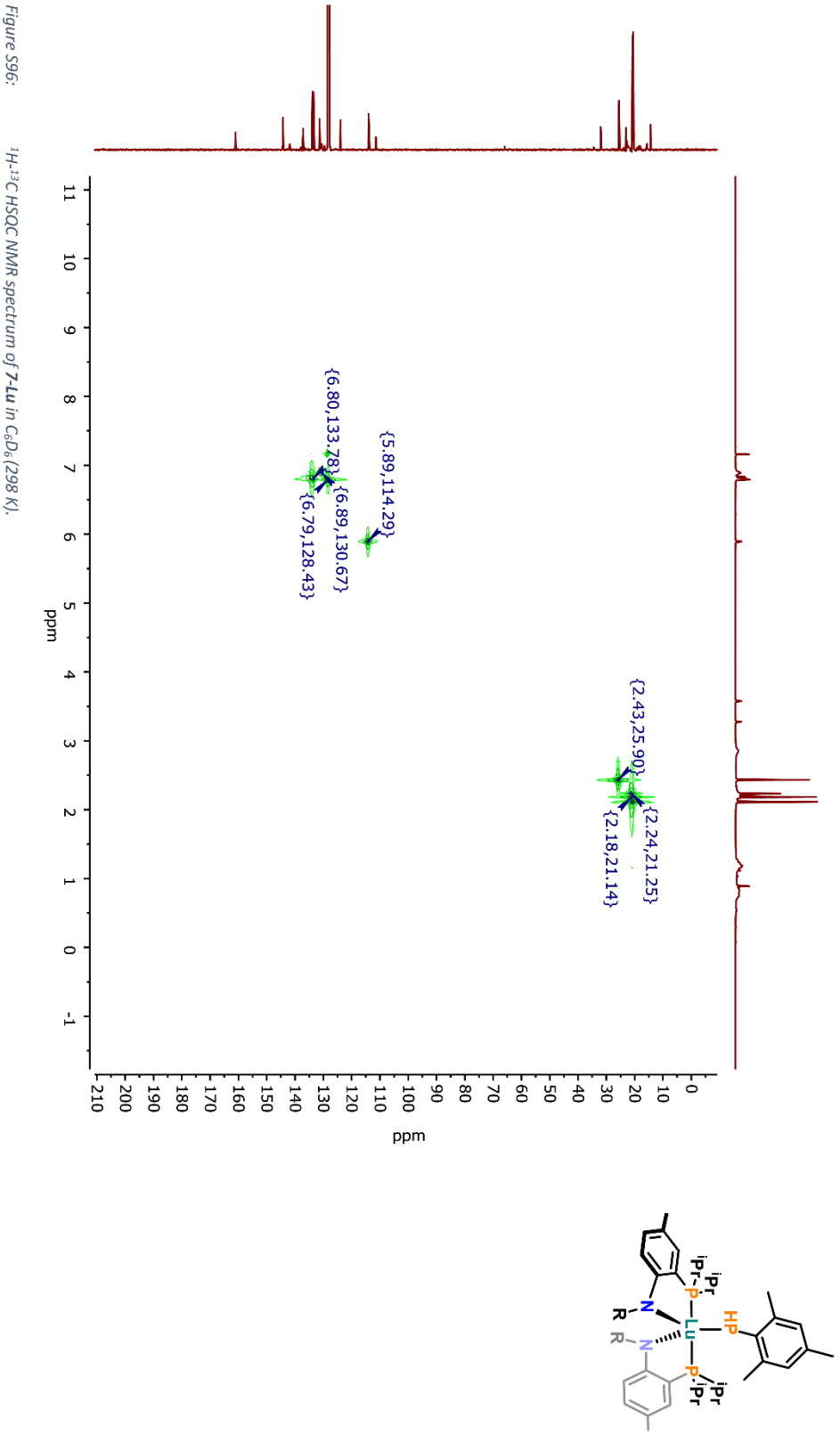

Figure S96: *^{1}H-^{13}C HSQC NMR spectrum of **7-Lu** in C_6D_6 (298 K).*

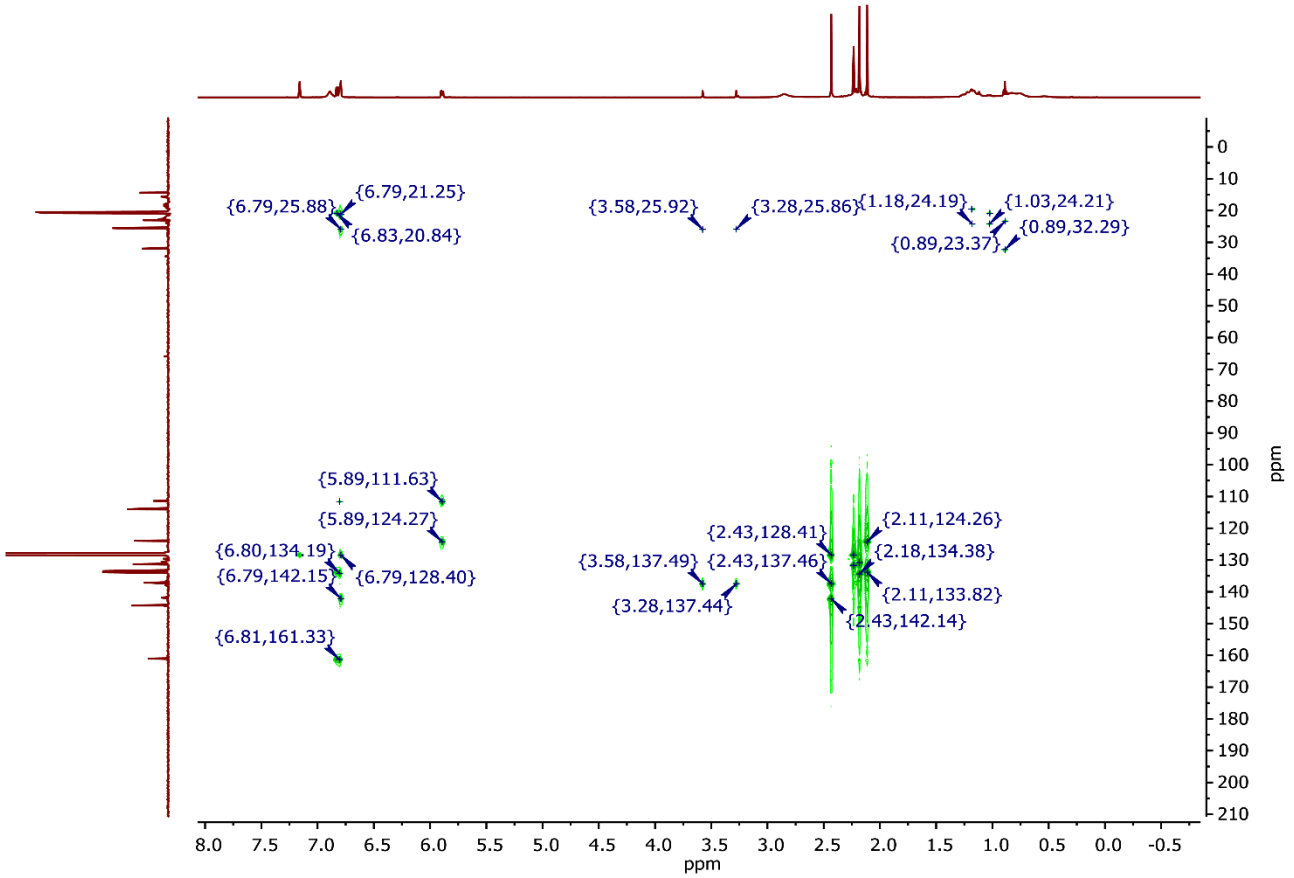

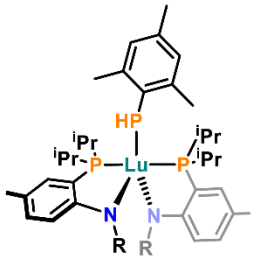

Figure S97: *^{1}H-^{13}C HMBC NMR spectrum of **7-Lu** in C_6D_6 (298 K).*

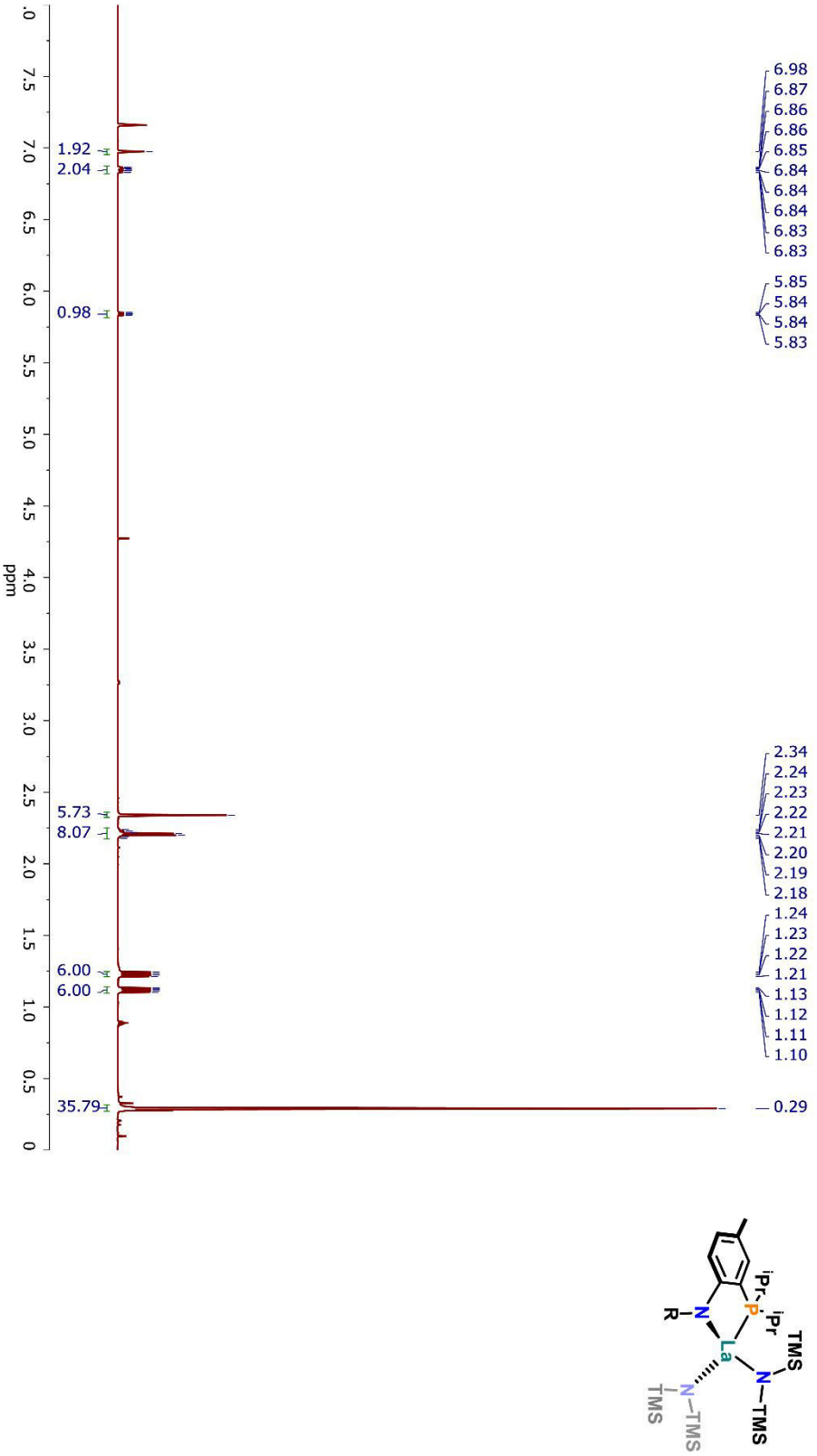

*Figure S98: ^{1}H NMR spectrum of **8-La** in C_6D_6 (298 K). Traces of HMDS are visible at δ 4.27 and 0.28 ppm.*

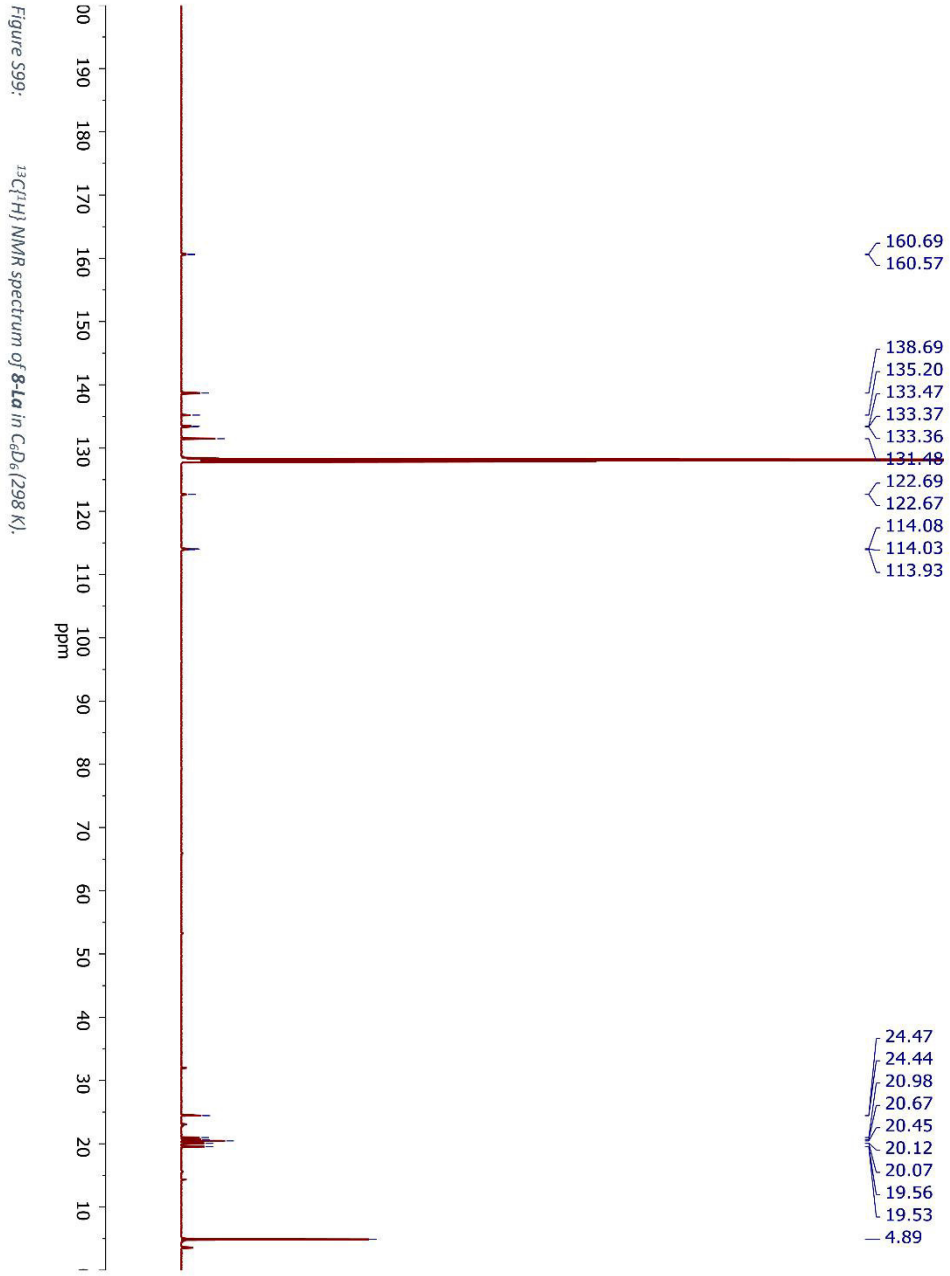

Figure S99: $^{13}C\{^1H\}$ *NMR spectrum of* ***8-La*** *in* C_6D_6 *(298 K).*

S108

Figure S100: $^{31}P\{^{1}H\}$ *NMR spectrum of* ***8-La*** *in* C_6D_6 *(298 K).*

S109

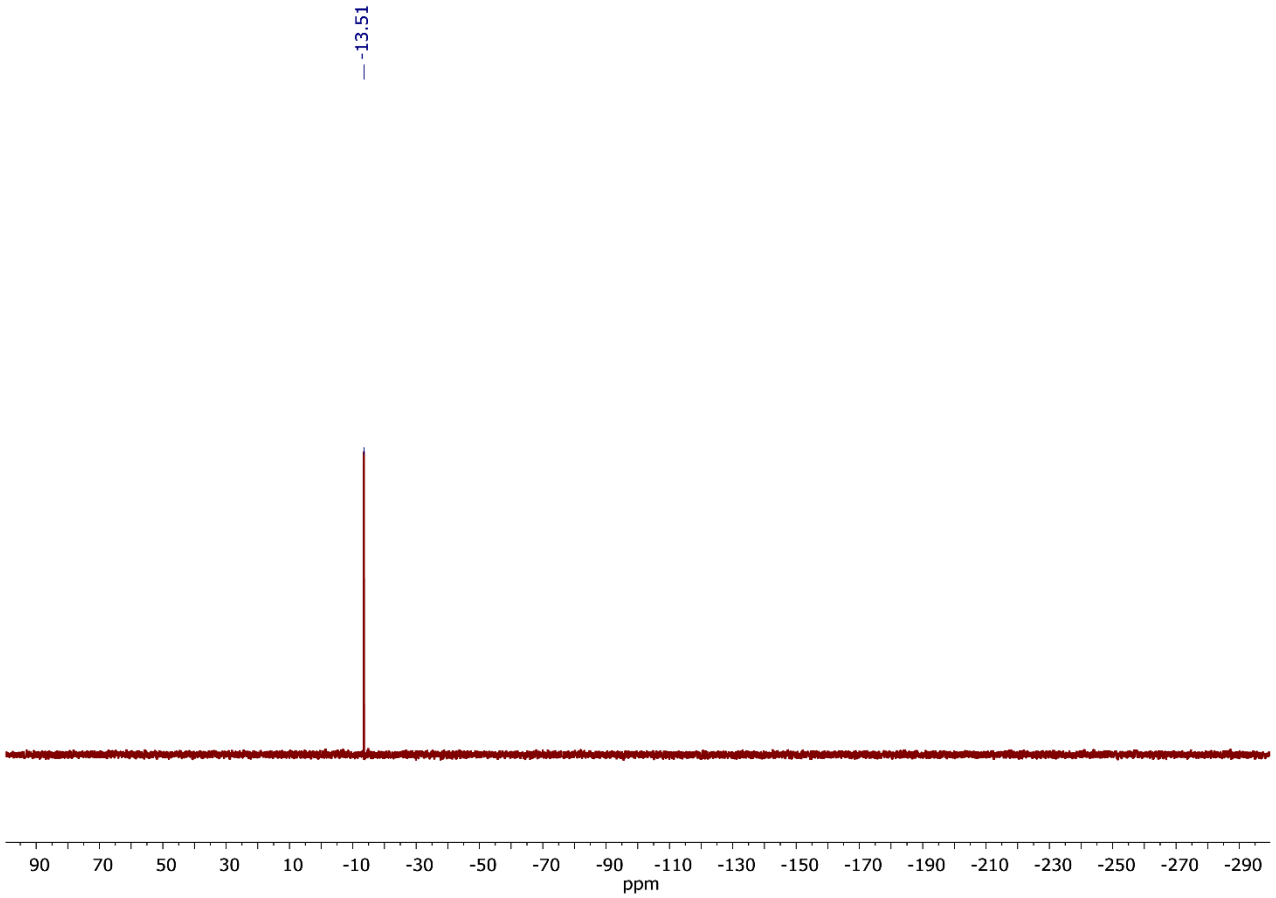

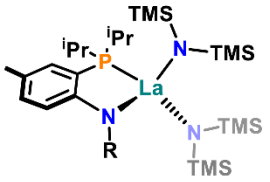

Figure S101: *$^{29}Si\{^{1}H\}$ NMR spectrum of **8-La** in C_6D_6 (298 K).*

Figure S102: ^{1}H-^{1}H *COSY NMR spectrum of* **8-La** *in* C_6D_6 *(298 K).*

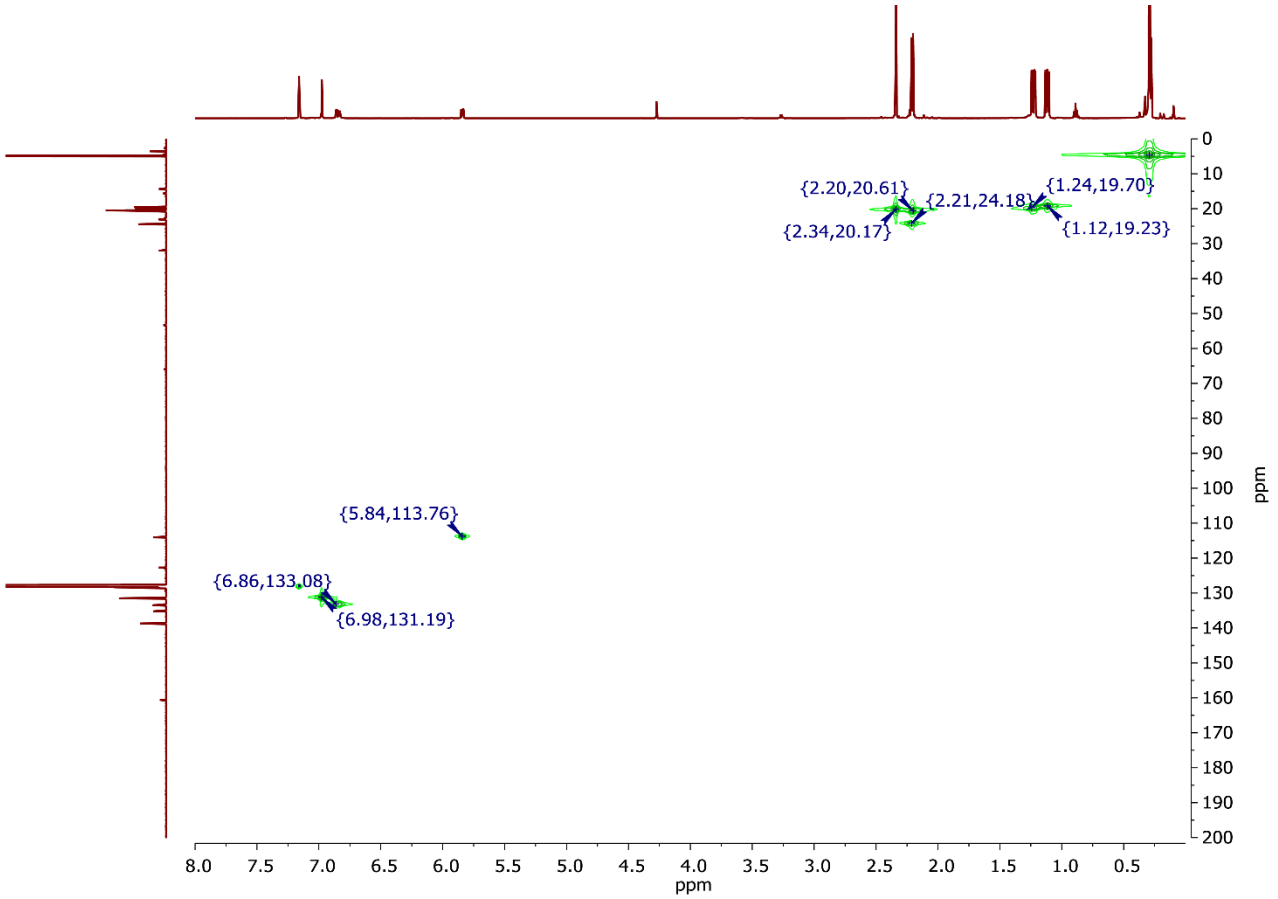

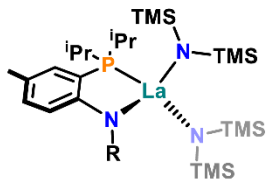

Figure S103: *^{1}H-^{13}C HSQC NMR spectrum of **8-La** in C_6D_6 (298 K).*

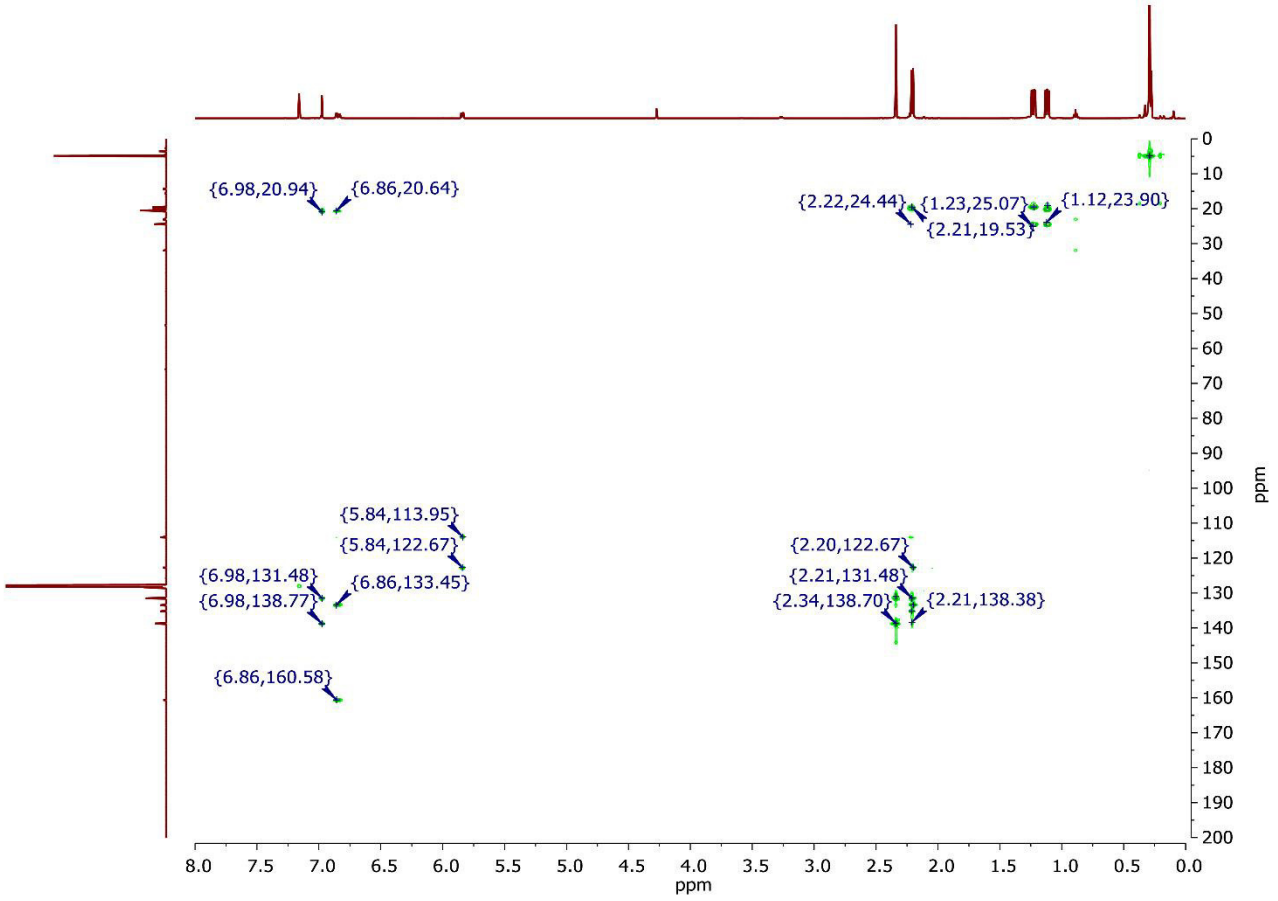

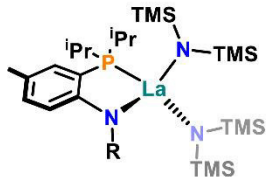

Figure S104: *^{1}H-^{13}C HMBC NMR spectrum of **8-La** in C_6D_6 (298 K).*

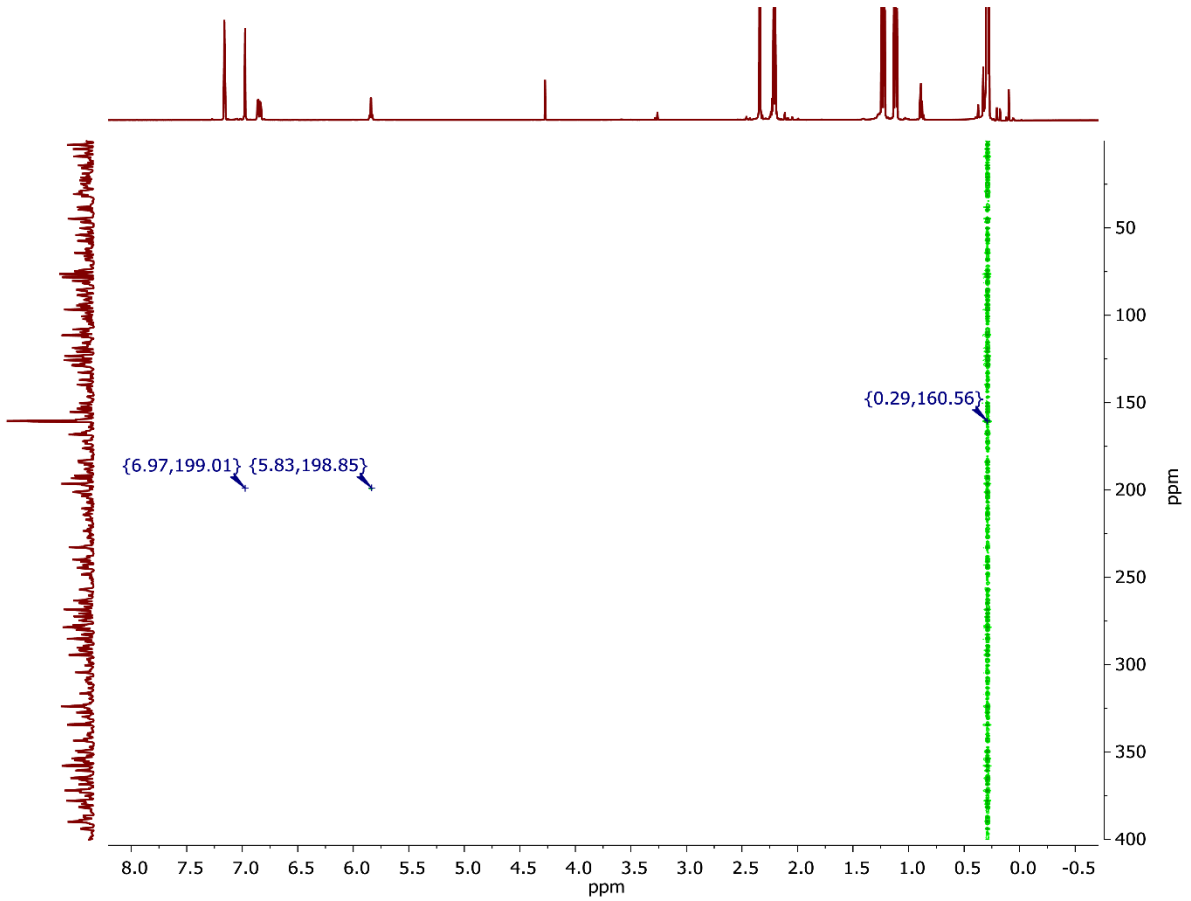

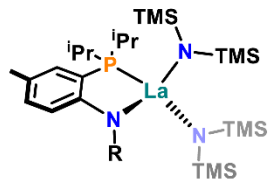

Figure S105: *^{1}H-^{15}N HMBC NMR spectrum of **8-La** in C_6D_6 (298 K).*

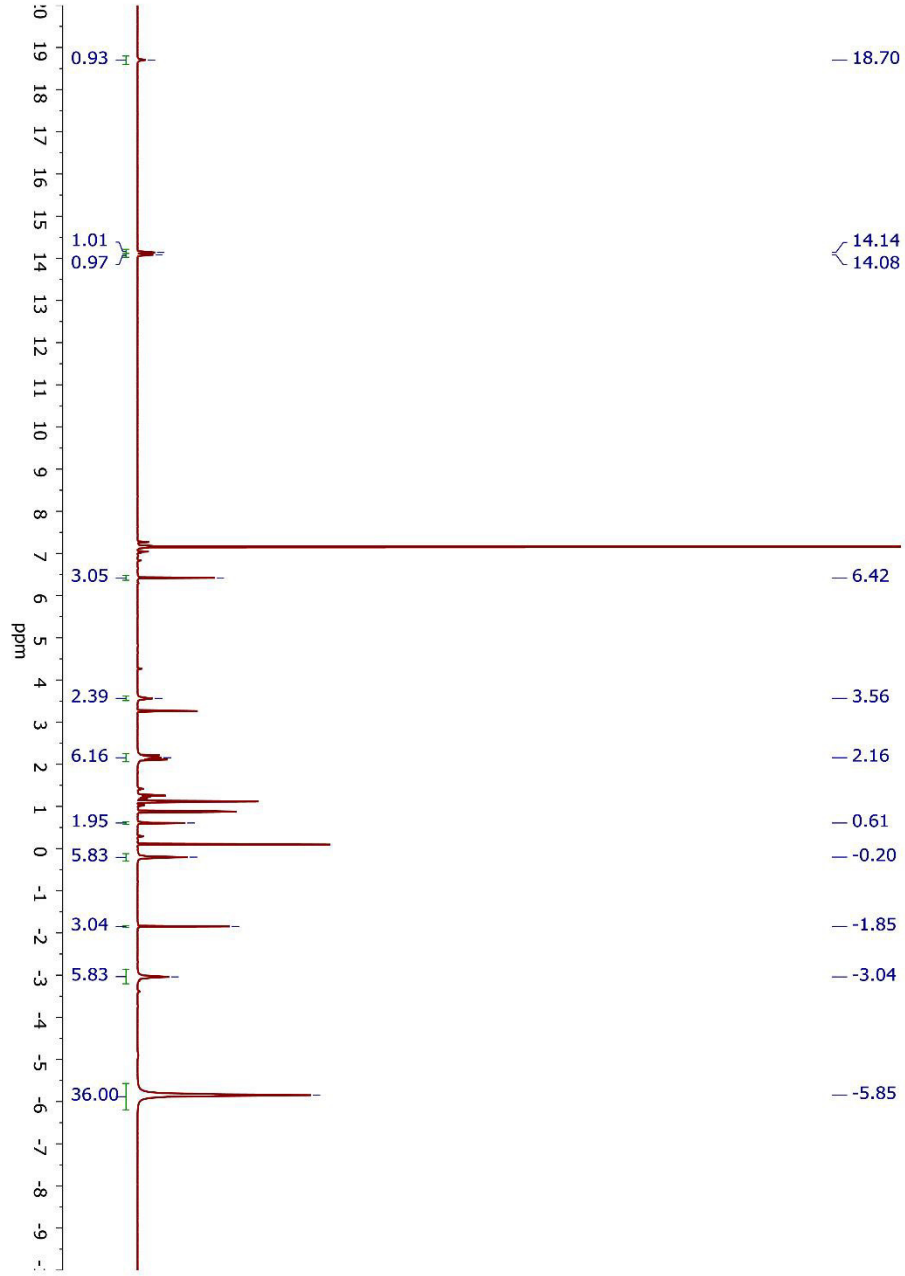

Figure S106: ^{1}H NMR spectrum of **8-Ce** in C_6D_6 (298 K).

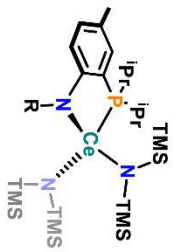

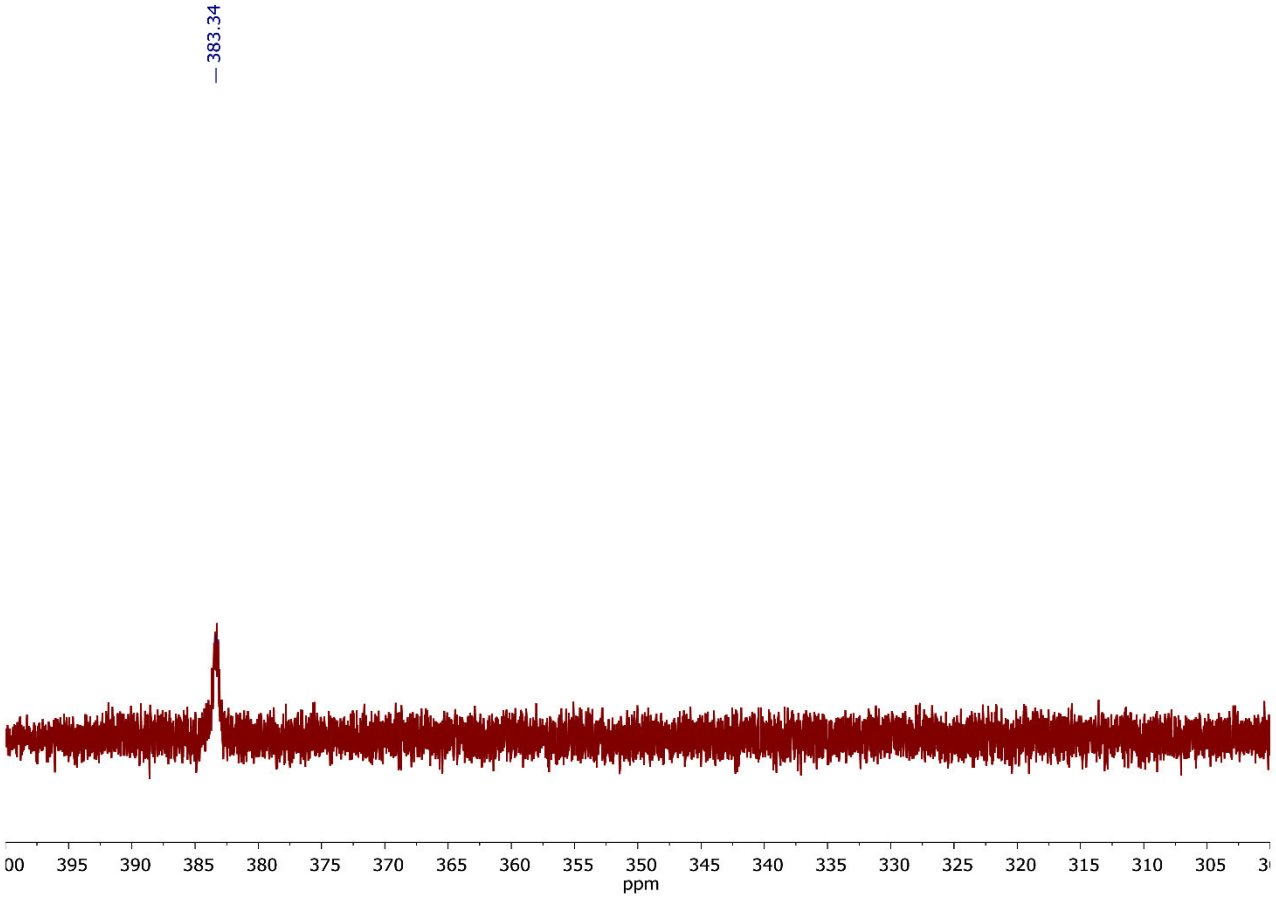

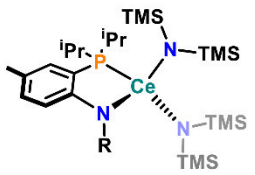

Figure S107: $^{31}P\{^{1}H\}$ *NMR spectrum of* ***8-Ce*** *in* C_6D_6 *(298 K).*

Figure S108: $^{31}P\{^{1}H\}$ *NMR spectrum of* ***8-Ce*** *in THF-d_8 (298 K).*

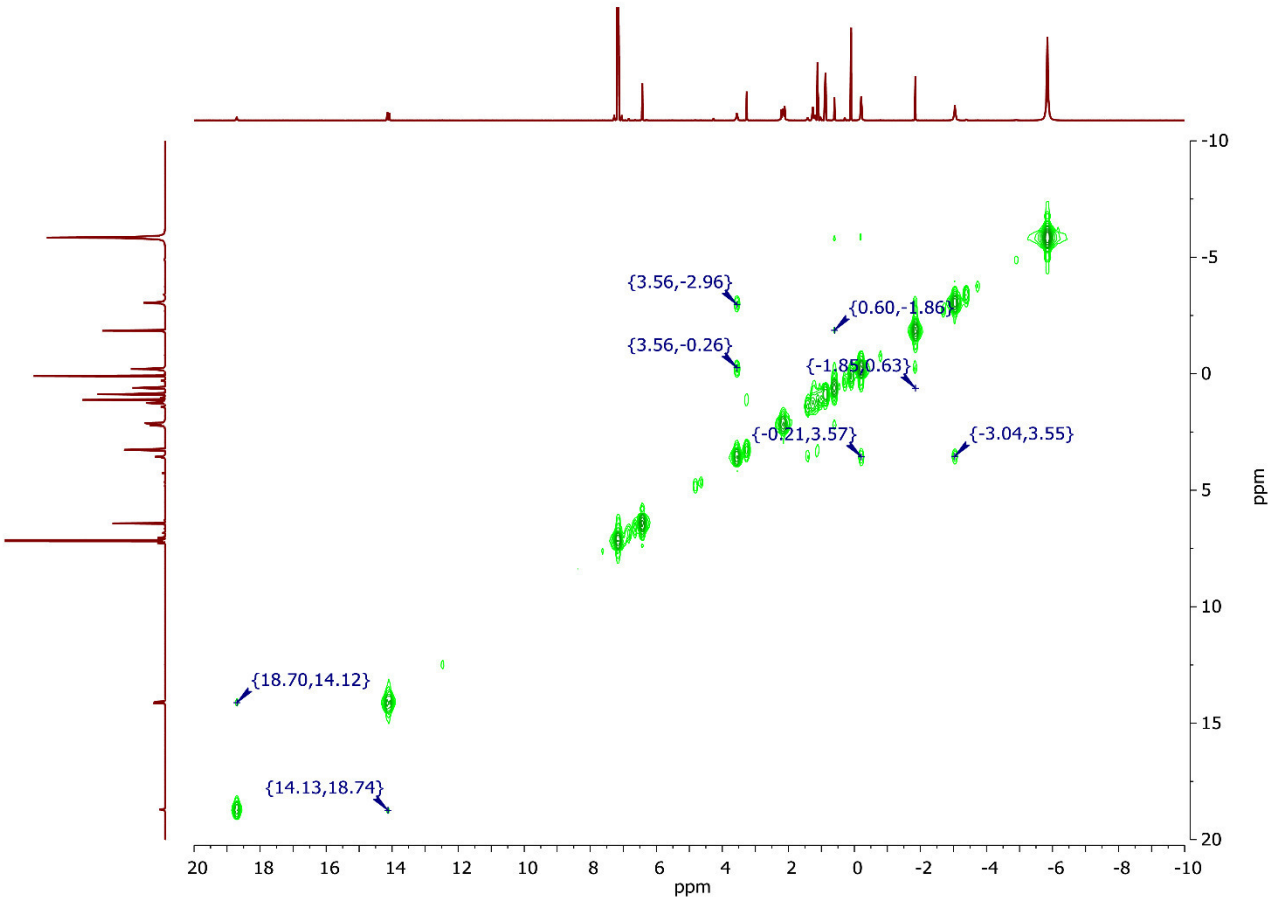

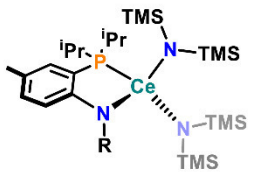

Figure S109: *^1H-^1H COSY NMR spectrum of **8-Ce** in C_6D_6 (298 K).*

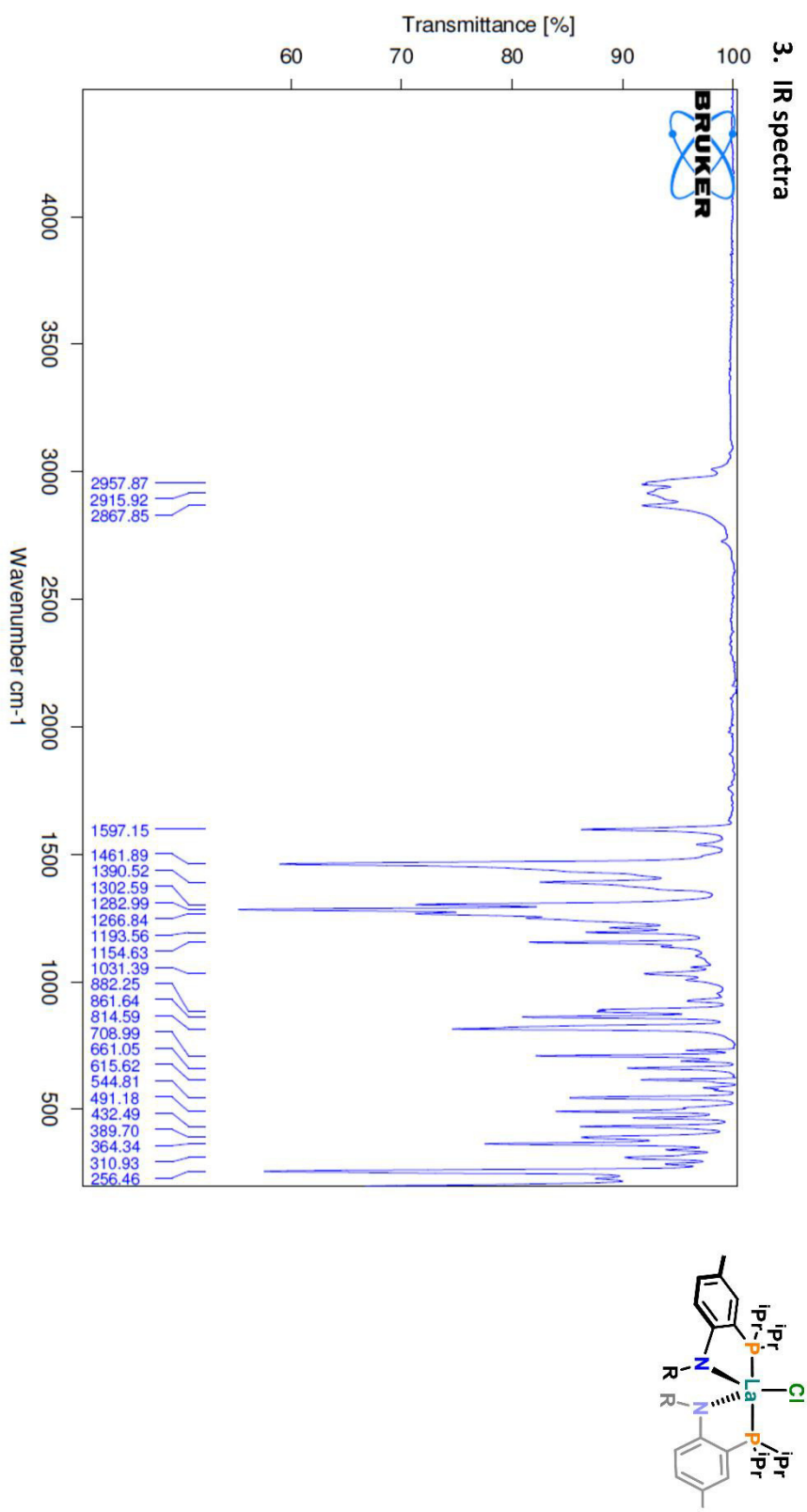

Figure S110: IR spectrum (ATR) of ***1-La****.*

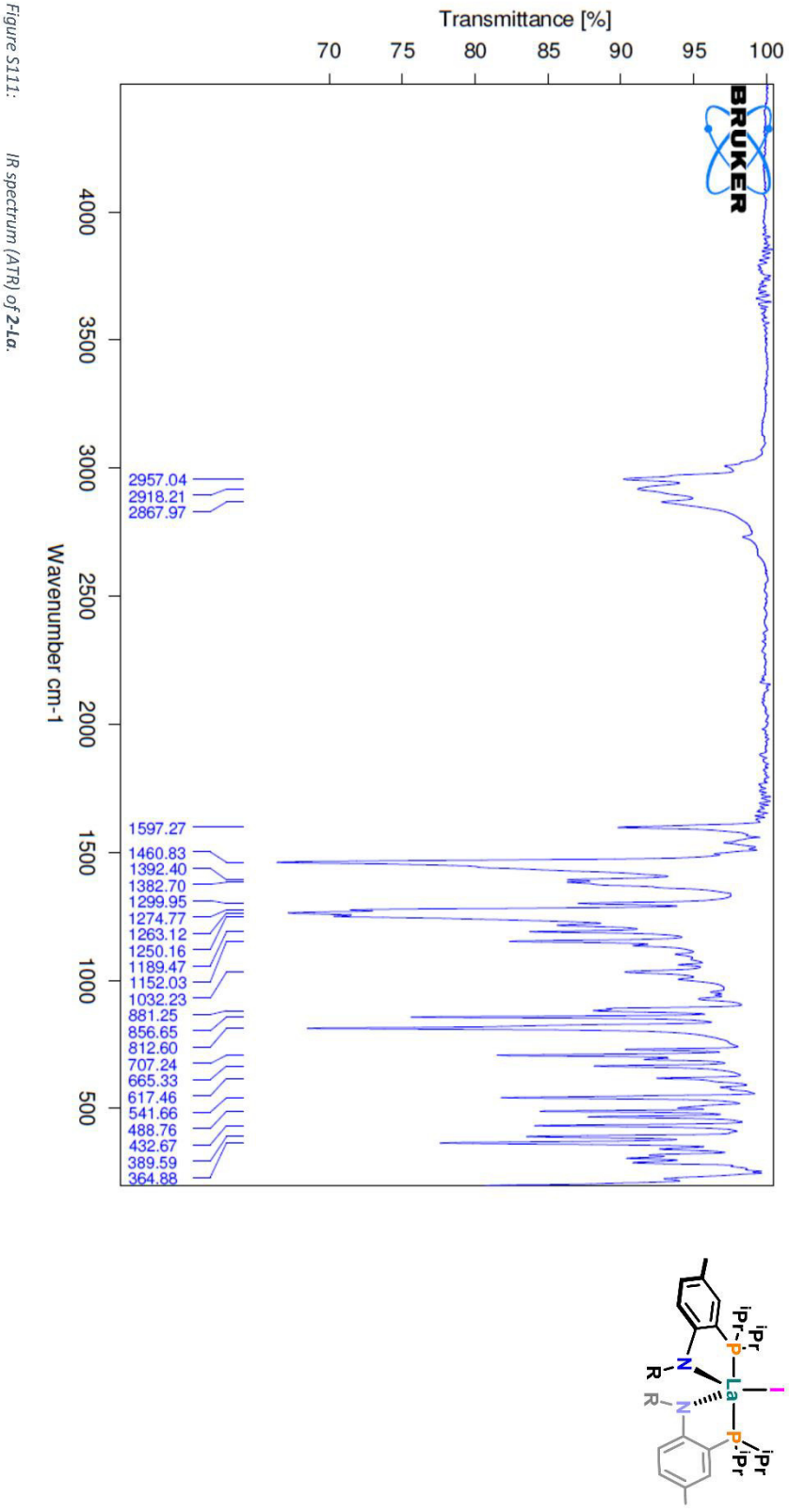

Figure S111: IR spectrum (ATR) of ***2-La****.*

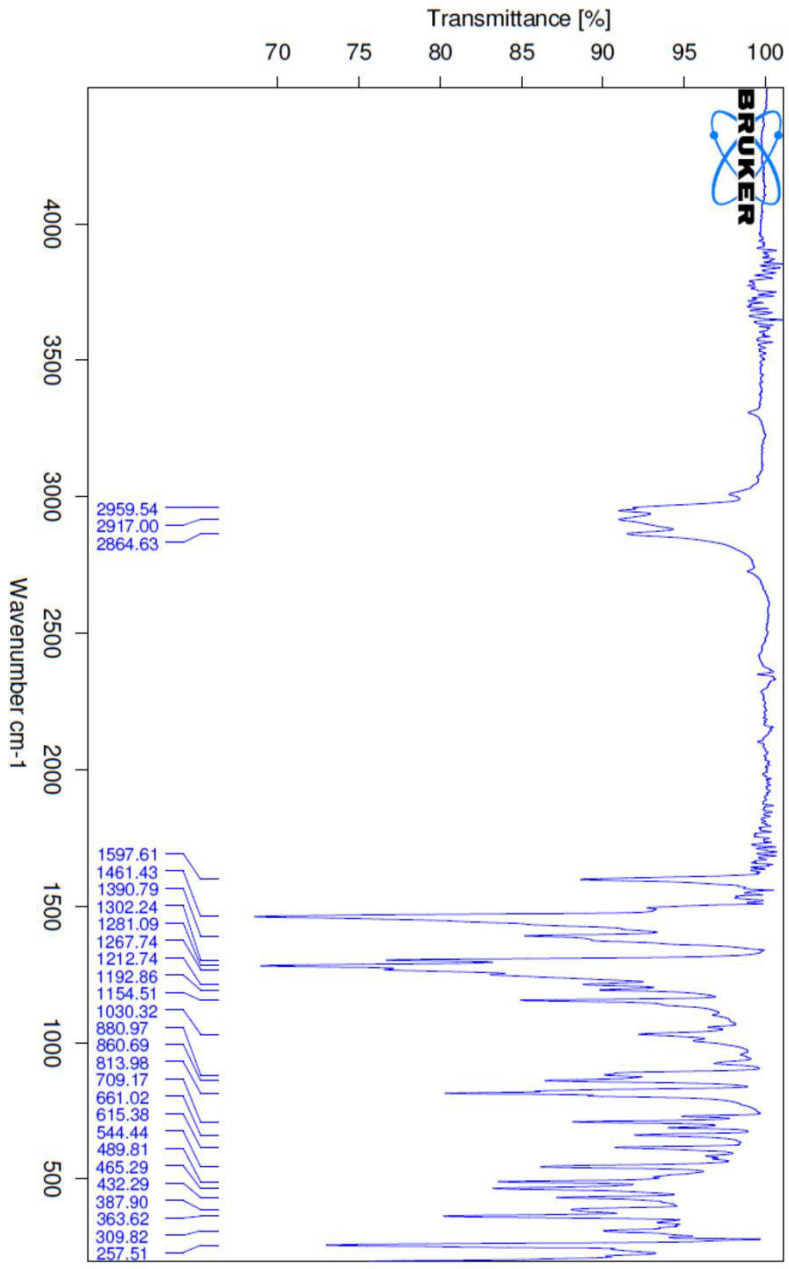

Figure S112: IR spectrum (ATR) of ***1-Ce****.*

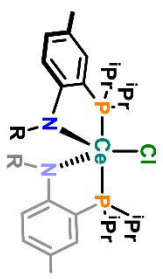

S121

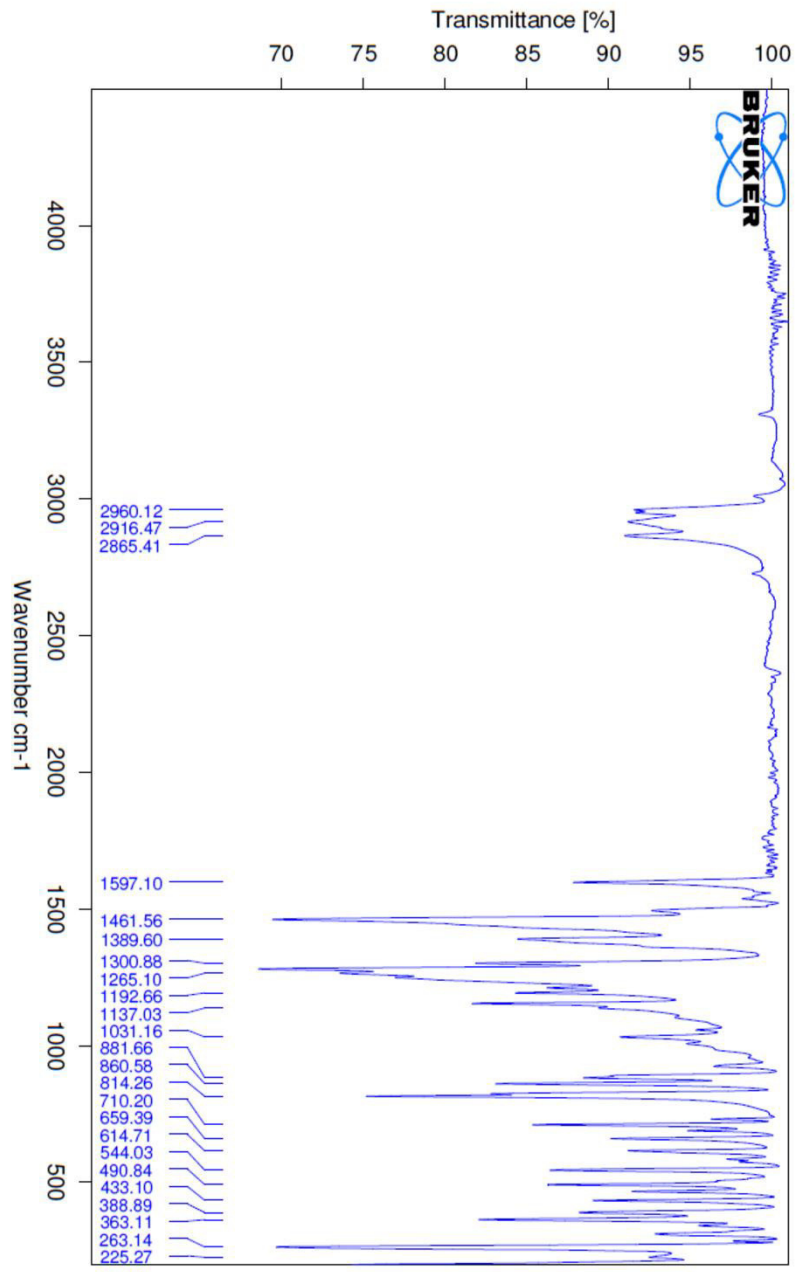

Figure S113: IR spectrum (ATR) of ***1-Nd****.*

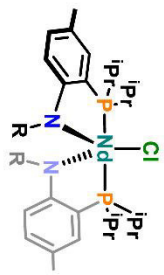

S122

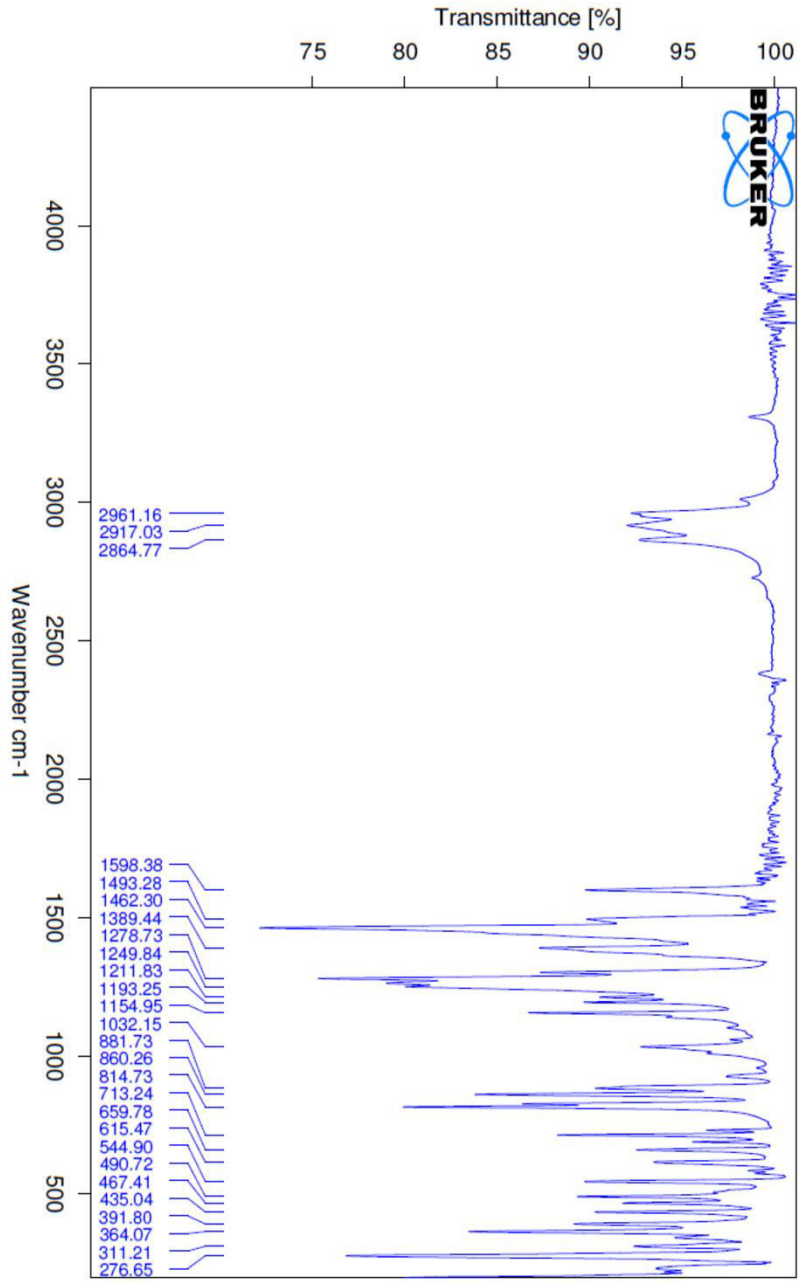

Figure S114: IR spectrum (ATR) of **1-Gd**.

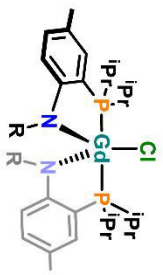

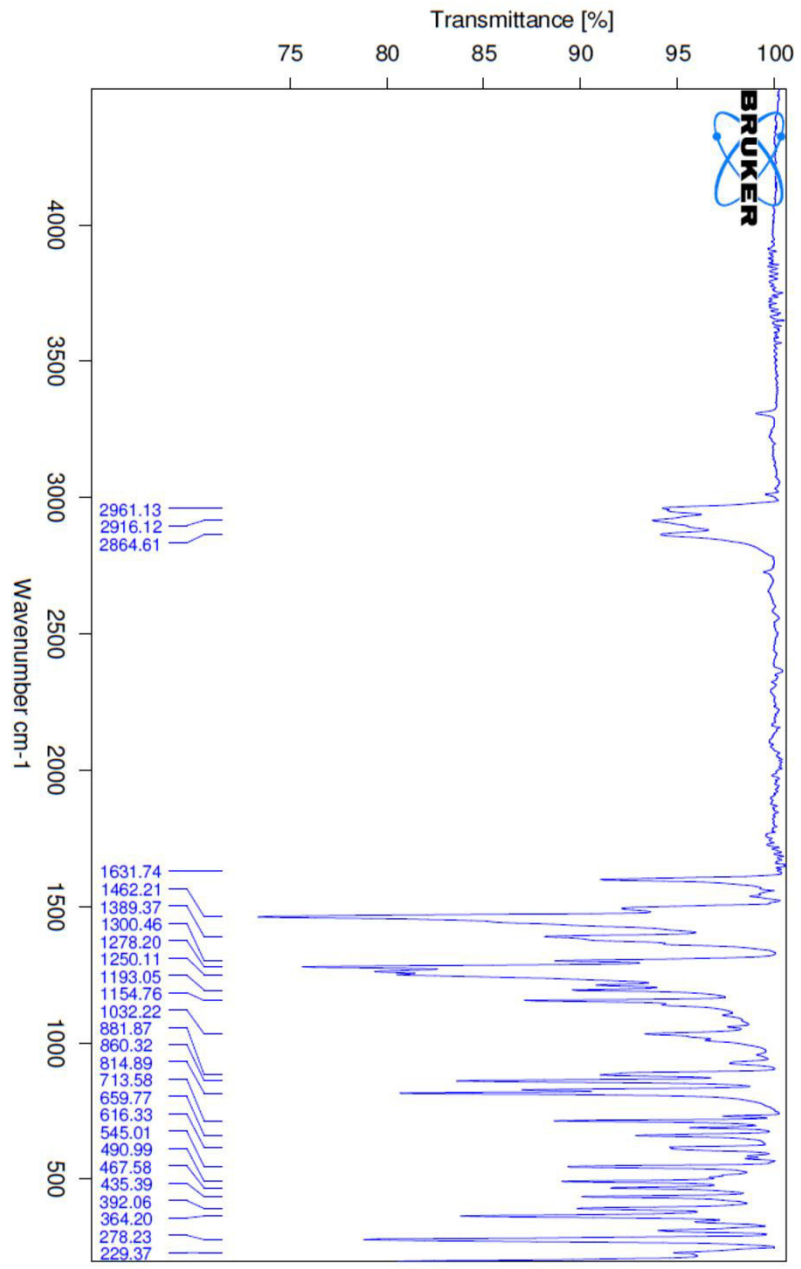

Figure S115: IR spectrum (ATR) of **1-Tb**.

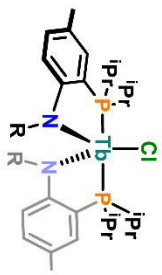

S124

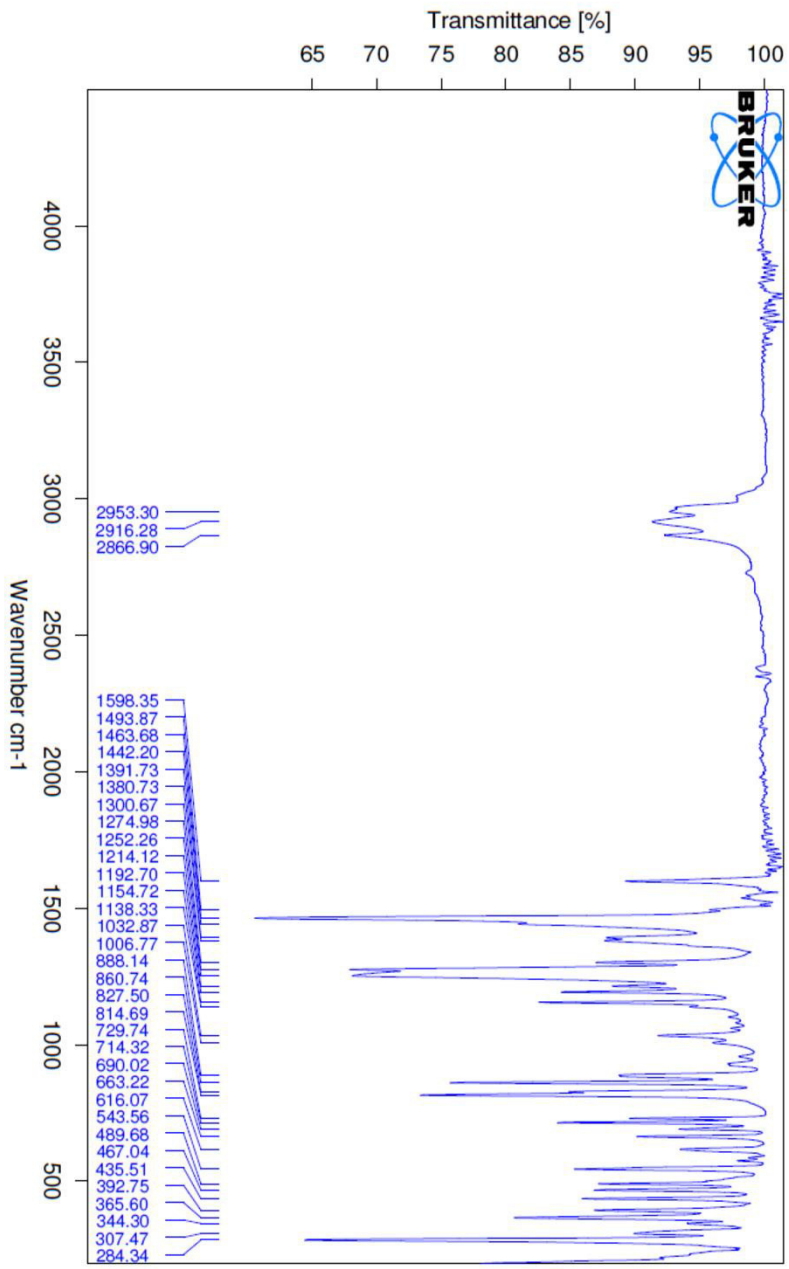

Figure S116: IR spectrum (ATR) of ***1-Dy****.*

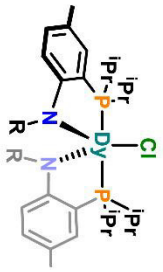

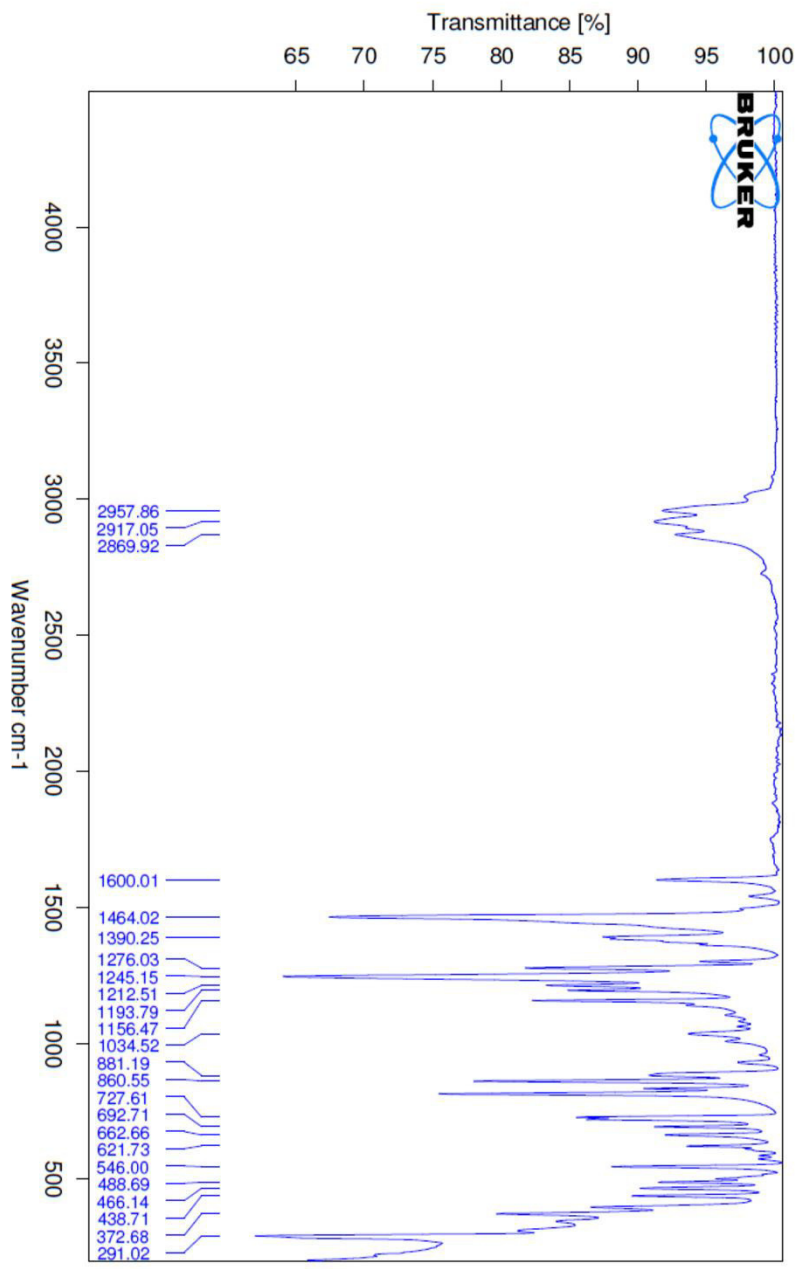

Figure S117: IR spectrum (ATR) of **1-Lu**.

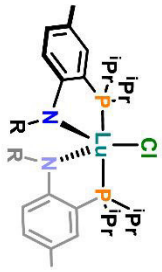

S126

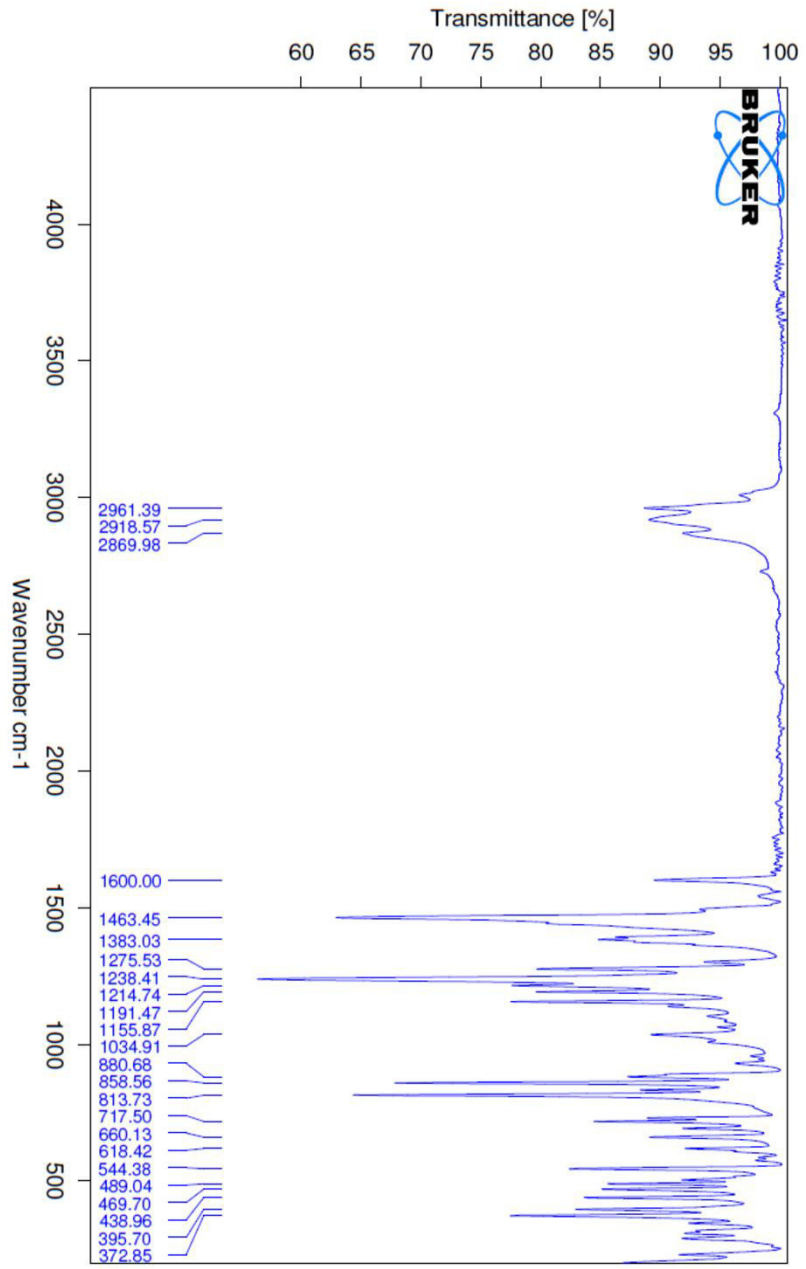

Figure S118: IR spectrum (ATR) of ***2-Lu****.*

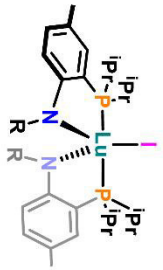

S127

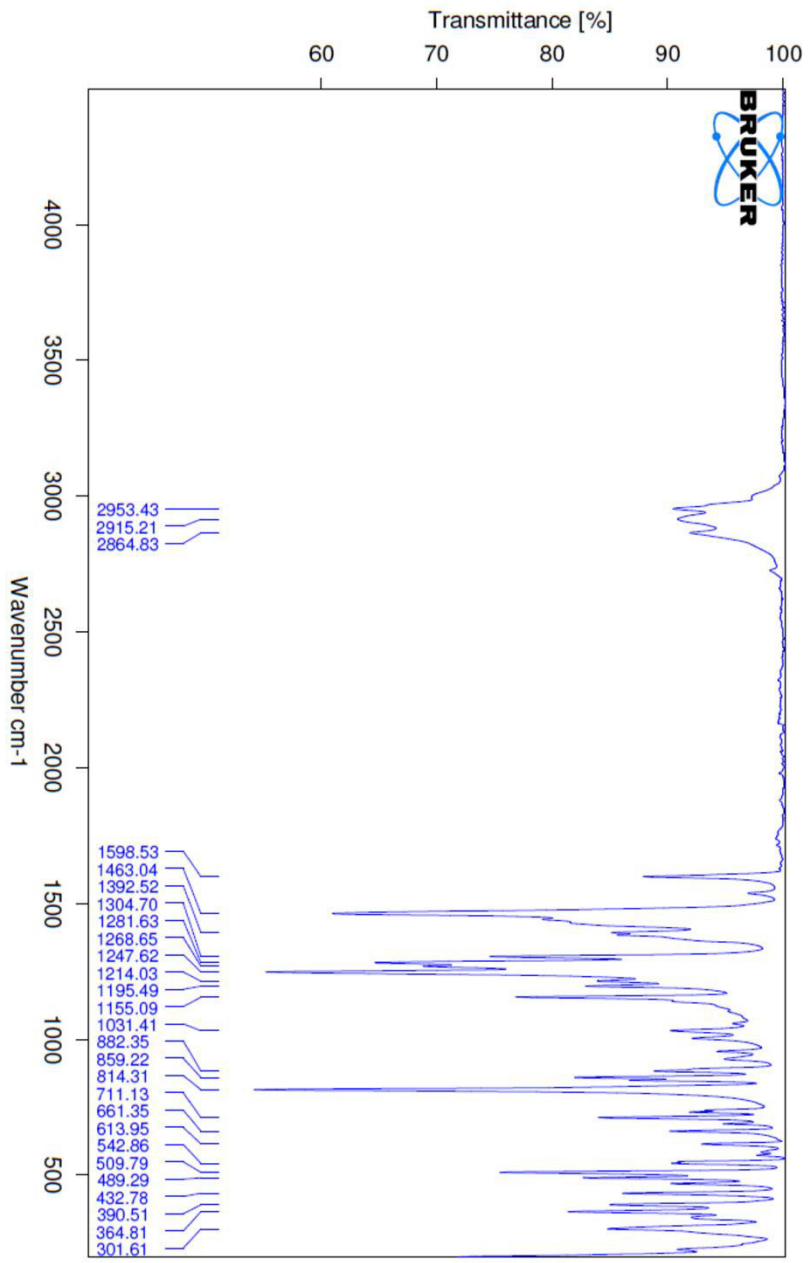

Figure S119: IR spectrum (ATR) of ***4-La****.*

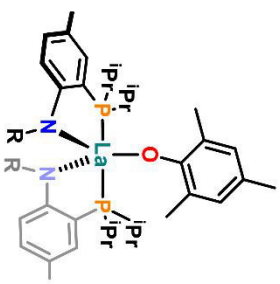

S128

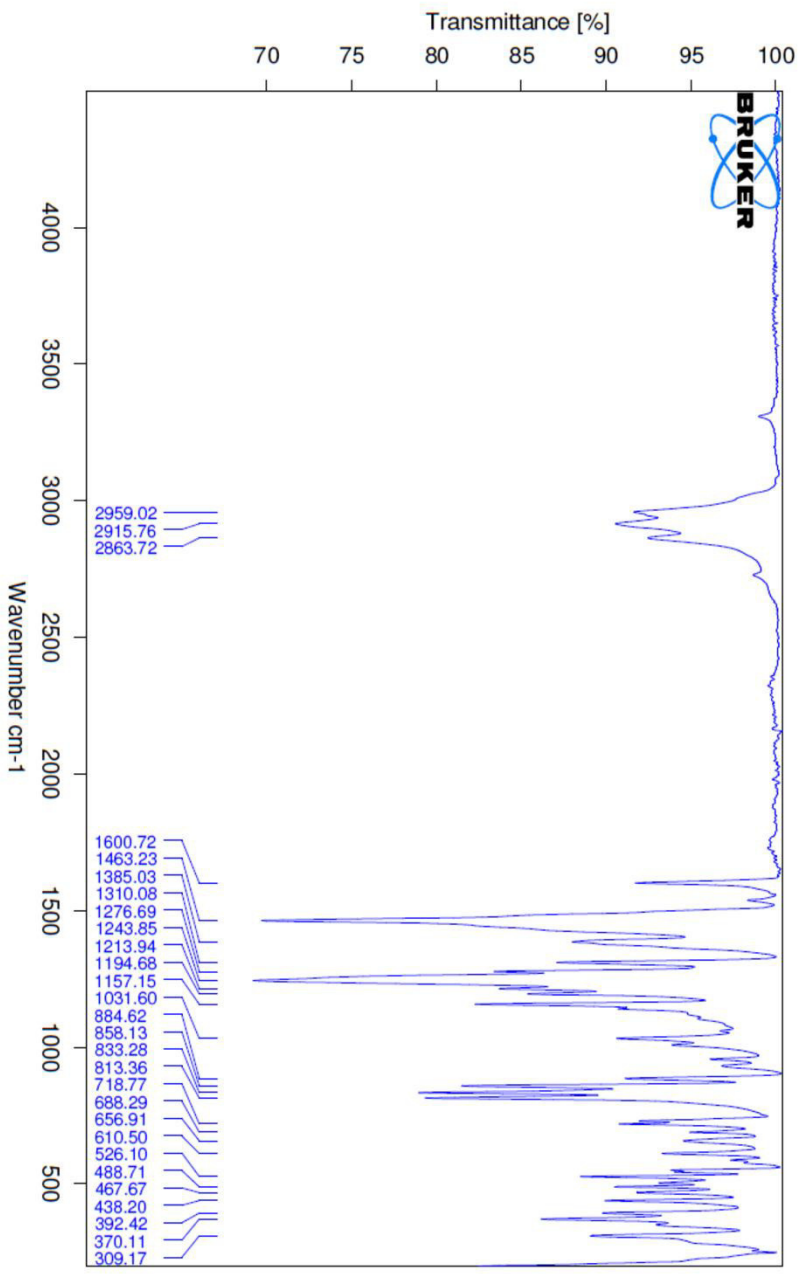

Figure S120: IR spectrum (ATR) of ***4-Lu****.*

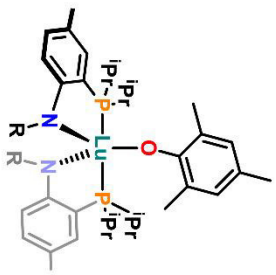

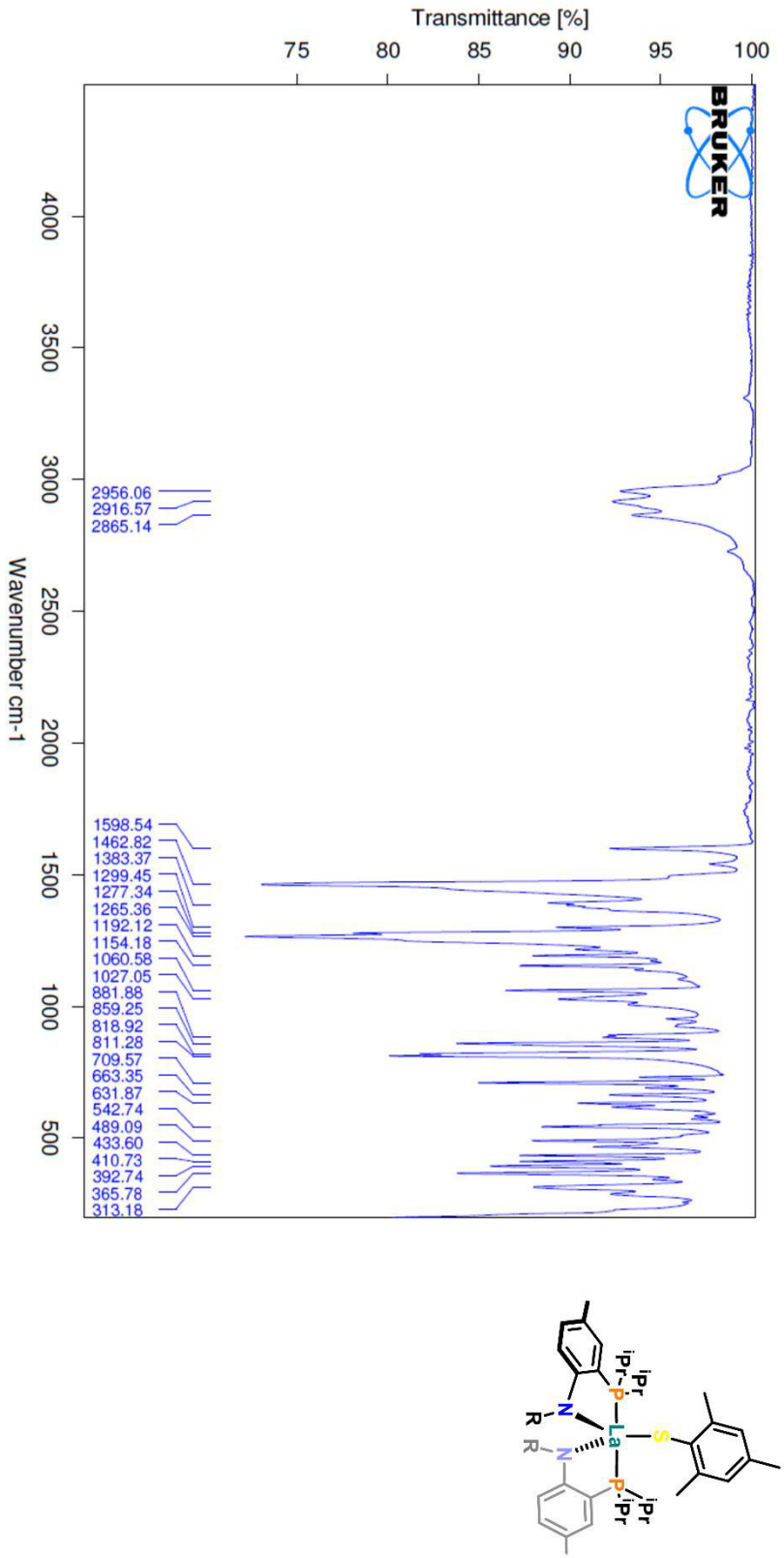

Figure S121: IR spectrum (ATR) of ***5-La****.*

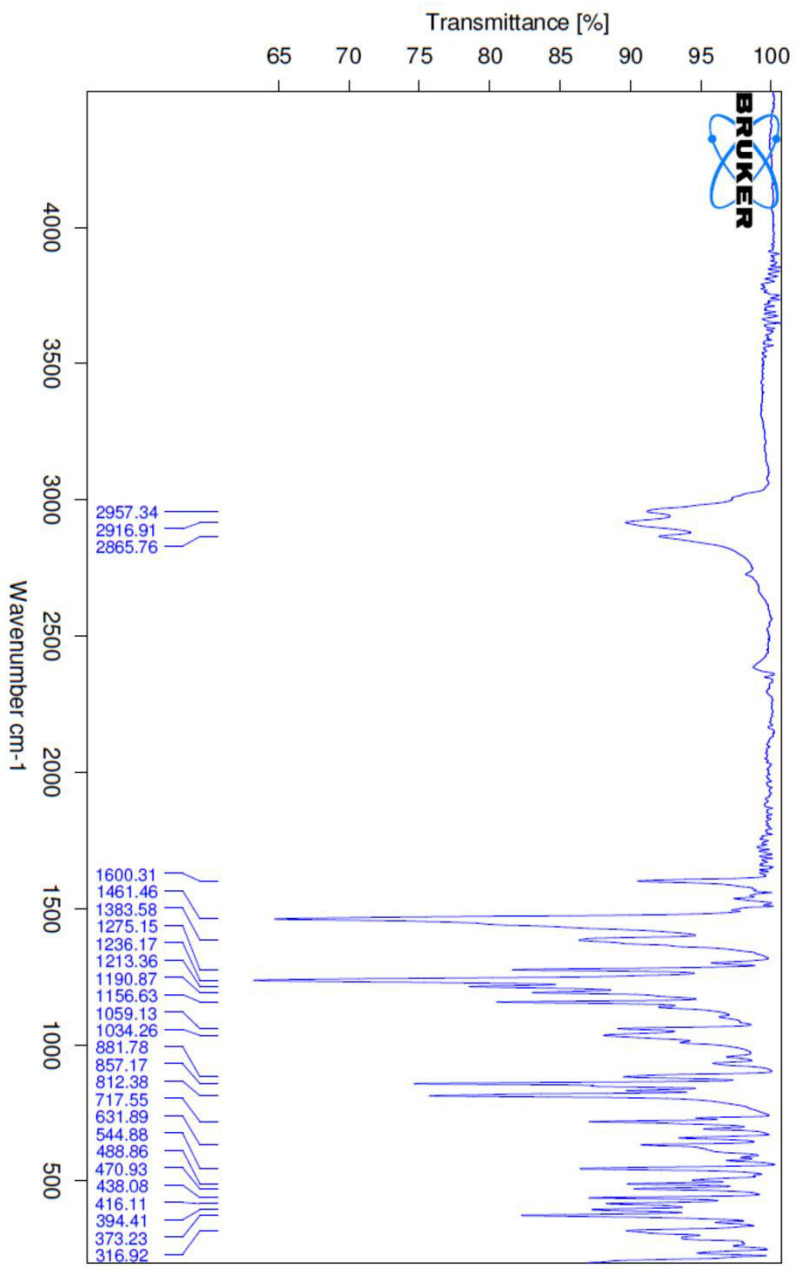

Figure S122: IR spectrum (ATR) of ***5-Lu****.*

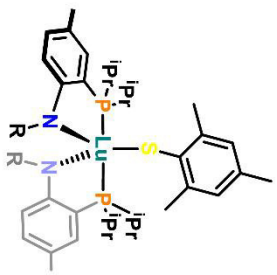

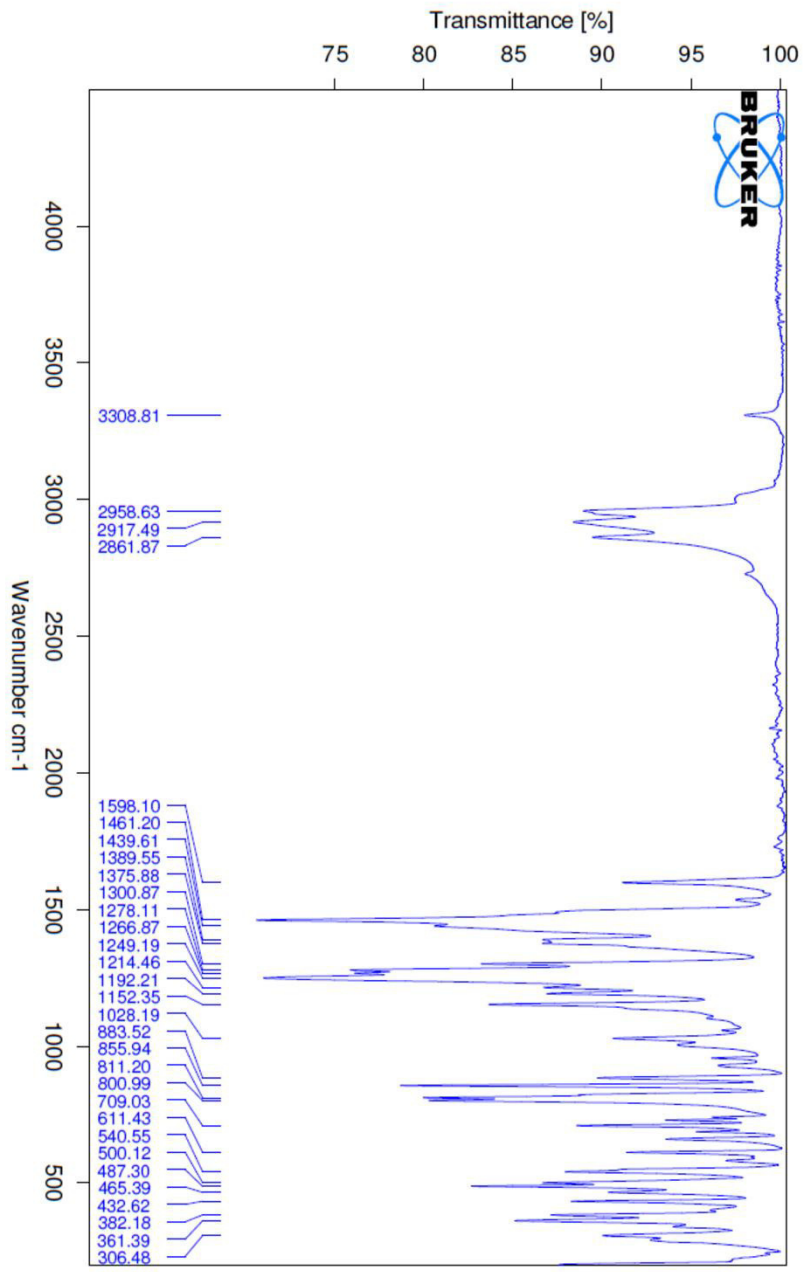

Figure S123: IR spectrum (ATR) of **6-La**.

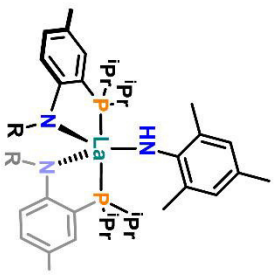

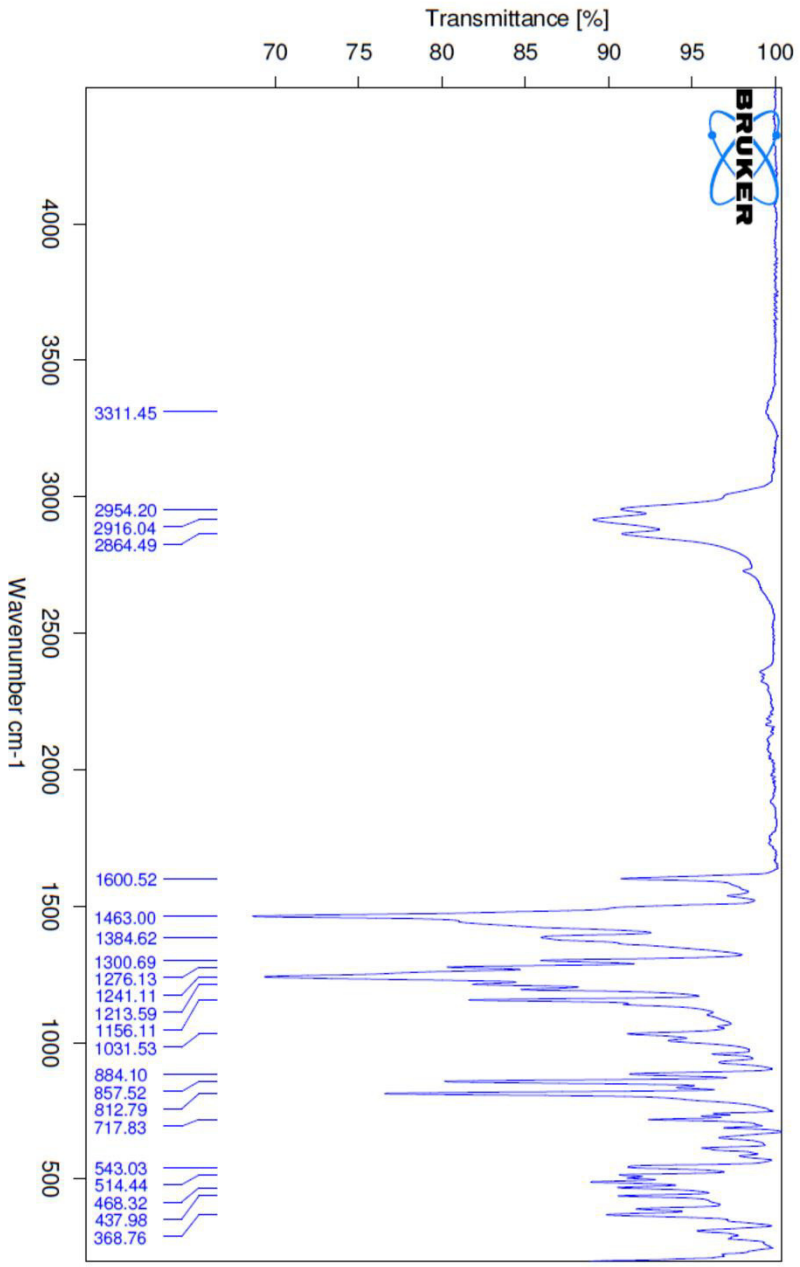

Figure S124: IR spectrum (ATR) of ***6-Lu****.*

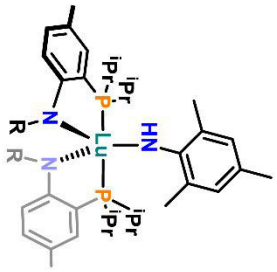

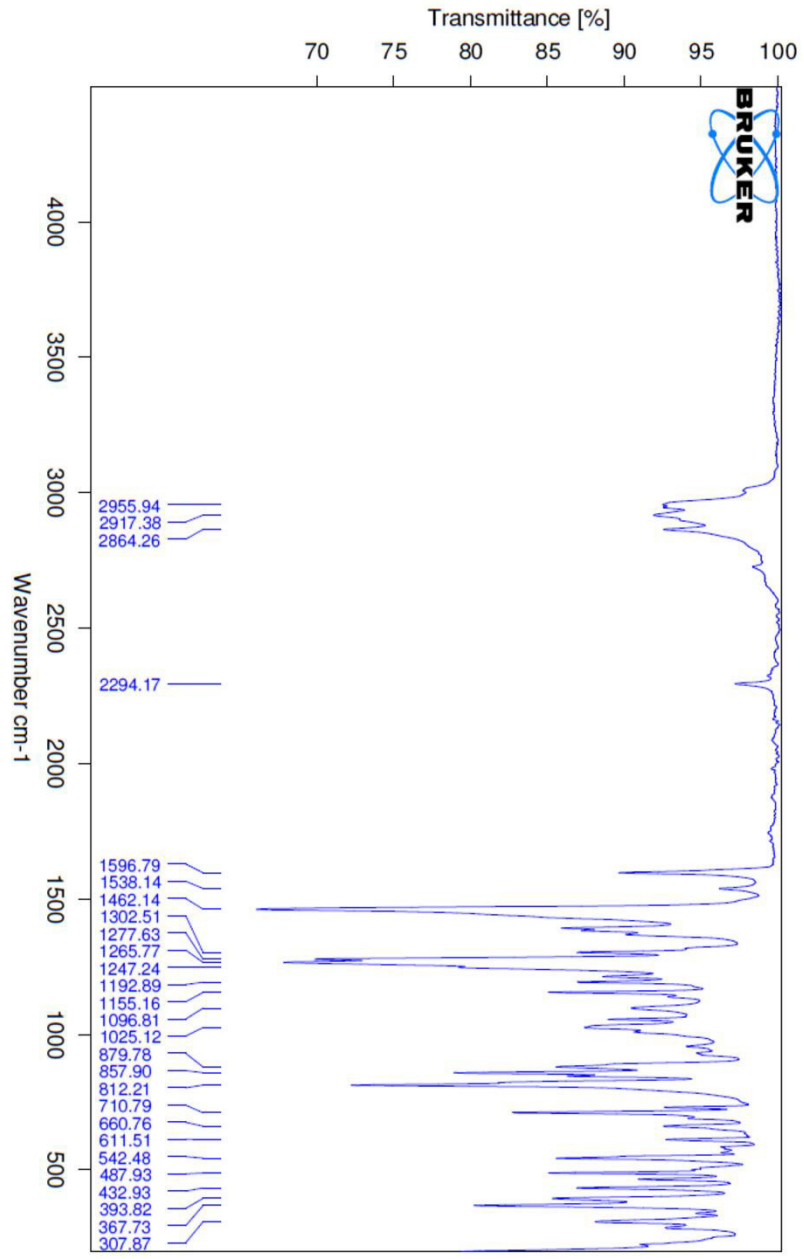

Figure S125: IR spectrum (ATR) of **7-La**.

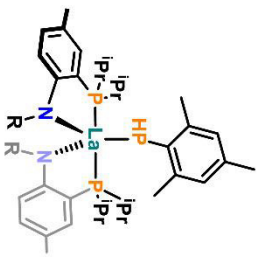

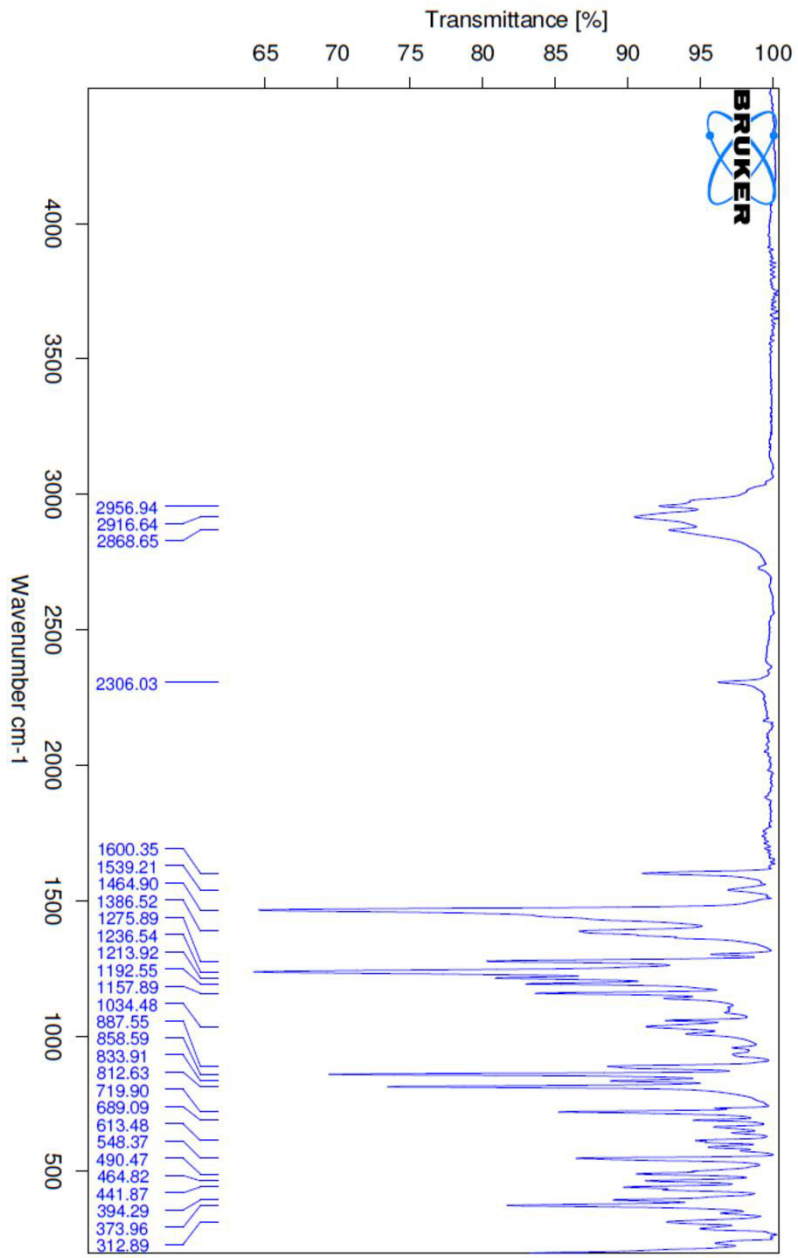

Figure S126: IR spectrum (ATR) of ***7-Lu****.*

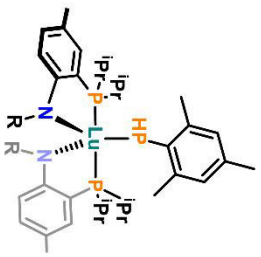

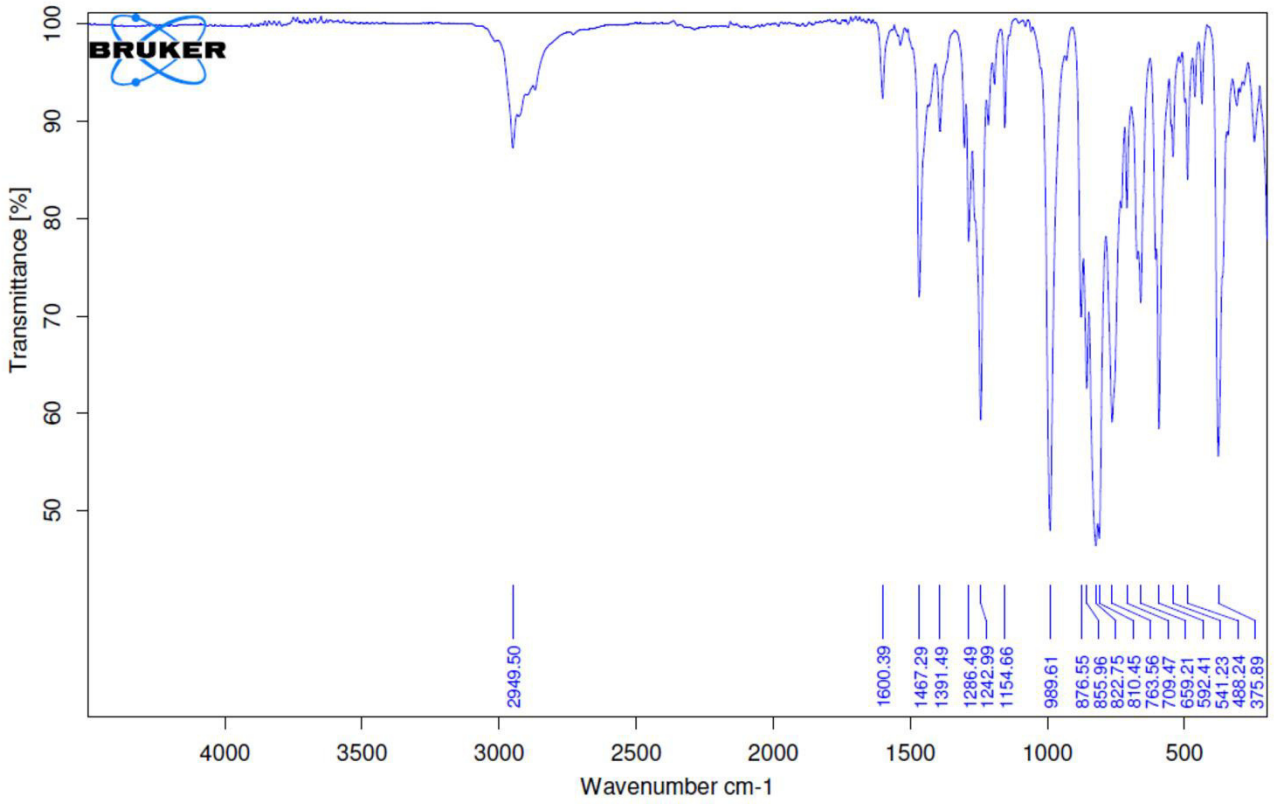

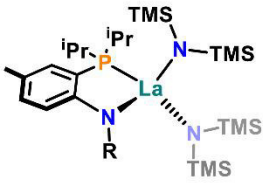

*Figure S127: IR spectrum (ATR) of **8-La**.*

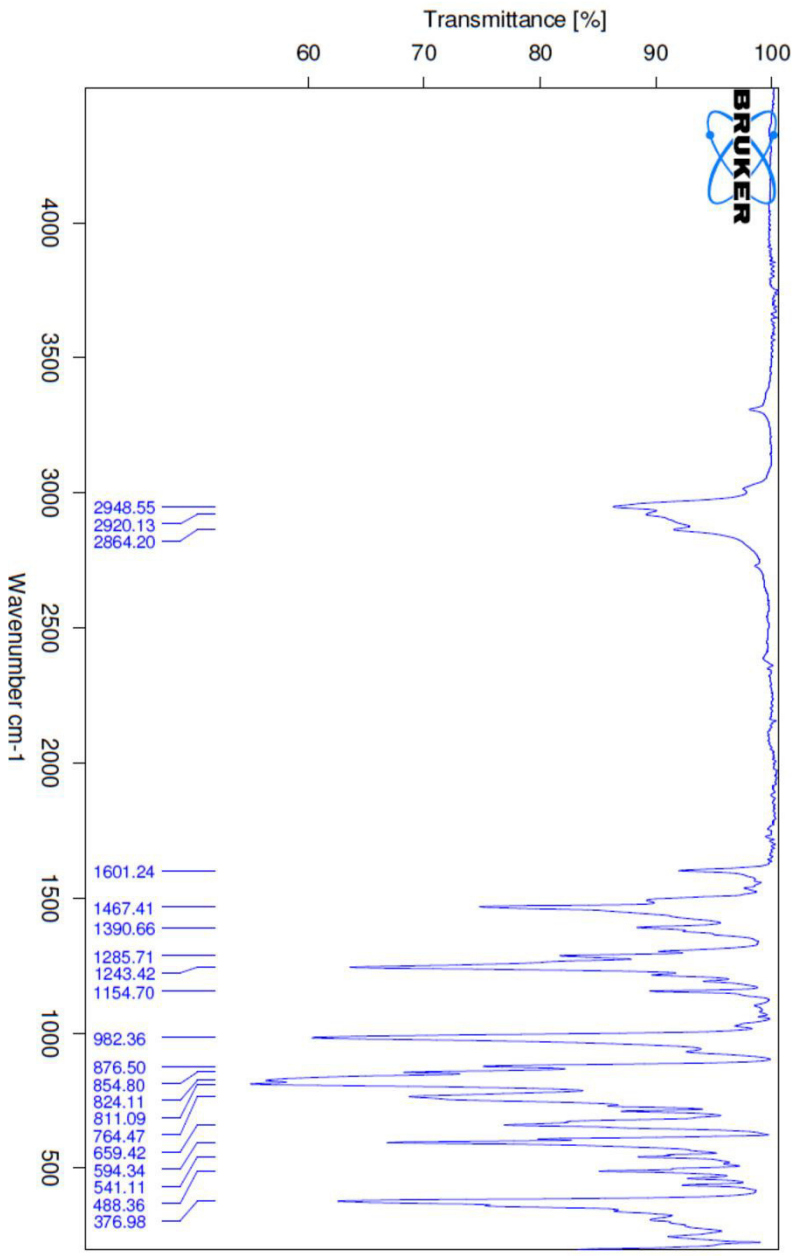

Figure S128: IR spectrum (ATR) of ***8-Ce****.*

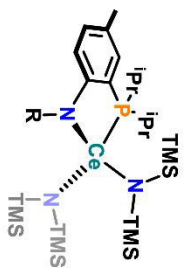

4. Molecular structures of LiPN, KPN, 1-Ce, 1-Nd, 1-Gd, 1-Dy, 1-Tb, 1-Lu

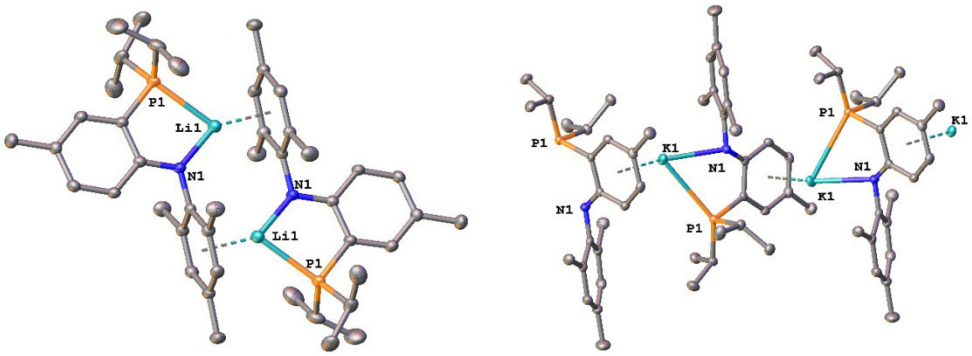

Figure S129: *ORTEP plots of [**LiPN**]$_2$ (left) and [**KPN**]$_n$ (right). Thermal ellipsoids are shown at a probability level of 30%. Hydrogen atoms and solvent molecules are omitted for clarity.*

X-ray quality crystals of **KPN** were obtained by leaving a moderately concentrated NMR sample of **KPN** in C_6D_6 (40 mg in 0.6 mL) at room temperature for 2 h (Figure S129, right). The potassium salt of the ligand crystallizes in the monoclinic space group $P2_1/c$ as an indefinite one-dimensional polymer chain with half a molecule of benzene per **KPN** unit. Thereby, each potassium cation is coordinated by the phosphorus and nitrogen atoms of the PN ligand as well as by the tolyl ring of the neighboring PN unit in an η^6 fashion. The bond distances of the potassium atom K1 to the hetero atoms P1 and N1 are 3.281(1) Å and 2.654(2) Å, while the distance to the centroid of the tolyl ring of the next ligand is only 2.788(1) Å, indicating a strong interaction between the arene ring and the potassium ion. In addition to this potassium arene interaction, we have also found close contacts between the potassium ion and the methyl and the methine hydrogen atoms of one of the *iso*propyl substituents (2.845(2) Å and 2.869(2) Å, respectively), indicating potential agostic interactions in the solid state. The potassium ions are slightly shifted out of the PN arene plane resulting in a zig-zag arrangement of the potassium ions in the polymer chain. In contrast, the isolation of X-ray quality crystals for **LiPN** was found to be much harder and crystals could only be obtained by storing a very concentrated solution of **LiPN** in toluene (300 mg in 1 mL) at –40 °C for two weeks (Figure S129, left). The lithium salt of the ligand crystallizes in the monoclinic space group $P2_1/n$ as a dimer (**[LiPN]$_2$**) with one **LiPN** unit forming the asymmetric unit. Each lithium atom is coordinated by the nitrogen and the phosphorus atom of one PN ligand, as well as by the mesityl substituent of the second PN ligand in an η^6 fashion. The bond distances of the lithium atom Li1 to the hetero atoms P1 and N1 are 2.513(2) Å and 1.940(3) Å, while the distance to the centroid of the mesityl ligand was found to be 2.113(1) Å.

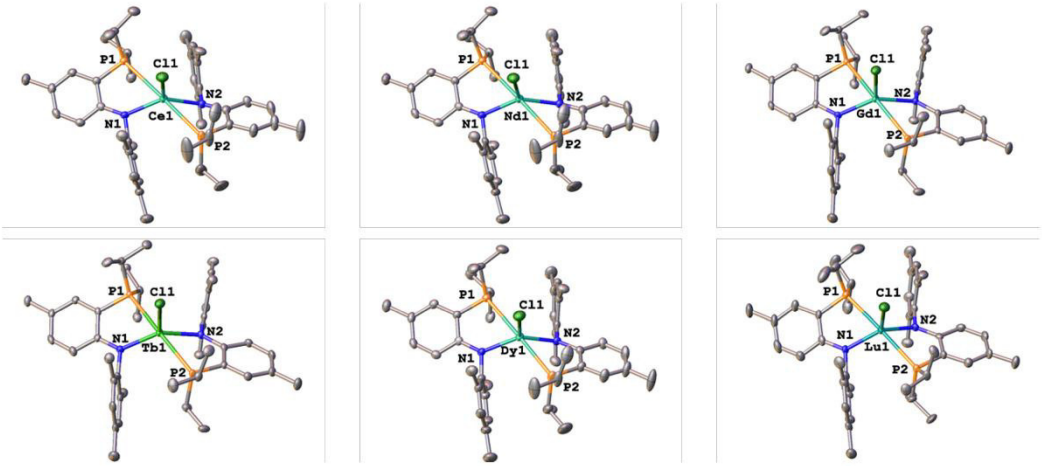

*Figure S130: ORTEP plots of **1-Ce**, **1-Nd**, **1-Gd** (top, left to right) and **1-Tb**, **1-Dy**, **1-Lu** (bottom, left to right). Thermal ellipsoids are shown at a probability level of 30%. Hydrogen atoms and solvent molecules have been omitted for clarity.*

5. Crystallographic details

*Table S1: Crystallographic details of **LiPN**, **KPN** and the chloride complexes **1-Ln**.*

	LiPN	**KPN**	**1-La**	**1-Ce**	**1-Nd**	**1-Gd**	**1-Tb**	**1-Dy**	**1-Lu***
Chemical formula	$C_{22}H_{31}N_1P_1Li_1$	$C_{22}H_{31}N_1P_1K_1$ 0.5 (C_6H_6)	$C_{44}H_{62}N_2P_2Cl_1La_1$	$C_{44}H_{62}N_2P_2Cl_1Ce_1$	$C_{44}H_{62}N_2P_2Cl_1Nd_1$	$C_{44}H_{62}N_2P_2Cl_1Gd_1$ 2 (C_7H_8)	$C_{44}H_{62}N_2P_2Cl_1Tb_1$ 2 (C_7H_8)	$C_{44}H_{62}N_2P_2Cl_1Dy_1$	$C_{44}H_{62}N_2P_2Cl_1La_1$
M_r	347.39	418.60	855.25	856.46	860.58	1057.86	1059.53	878.84	891.31
Crystal system	Monoclinic	Monoclinic	Monoclinic	Monoclinic	Monoclinic	Monoclinic	Monoclinic	Monoclinic	Triclinic
Space group	$P2_1/n$	$P2_1/c$	$P2_1/c$	$P2_1/c$	$P2_1/c$	$P2_1/n$	$P2_1/n$	$P2_1/c$	$P\bar{1}$
a (Å)	9.281(1)	8.7122(3)	13.819(1)	13.775(1)	13.7741(6)	12.894(1)	12.893(1)	13.654(2)	12.885(1)
b (Å)	13.091(2)	11.6493(4)	19.113(2)	19.148(2)	19.1967(8)	31.564(2)	31.524(2)	19.491(3)	15.788(1)
c (Å)	17.095(3)	23.6105(9)	17.797(2)	17.703(2)	17.6643(8)	14.574(1)	14.563(1)	17.553(3)	25.622(2)
α (°)	90	90	90	90	90	90	90	90	99.574(2)
β (°)	98.126(8)	96.647(1)	109.605(2)	109.603(2)	109.738(2)	113.207(1)	113.389(1)	109.906(3)	103.096(2)
γ (°)	90	90	90	90	90	90	90	90	90.902(2)
V (Å^3)	2056.1(5)	2380.2(2)	4428.0(7)	4398.5(7)	4396.3(3)	5451.8(7)	5433.0(7)	4392(1)	4998.3(7)
Z	4	4	4	4	4	4	4	4	4
Densitiy (g cm^{-3})	1.122	1.168	1.283	1.293	1.300	1.289	1.295	1.329	1.184
F(000)	752	900	1776	1780	1788	2204	2208	1812	1832
Radiation Type	MoKα	MoKα	MoKα	MoKα	MoKα	MoKα	MoKα	MoKα	MoKα
μ (mm^{-1})	0.137	0.301	1.128	1.199	1.345	1.361	1.447	1.865	2.119
Crystal size	0.28x0.15x0.11	0.18x0.15x0.10	0.25x0.21x0.20	0.25x0.24x0.21	0.25x0.18x0.08	0.42x0.37x0.36	0.35x0.31x0.29	0.35x0.32x0.03	0.32x0.30x0.28
Meas. Refl.	70989	27085	37118	39545	82566	41840	60985	35795	40486
Indep. Refl.	6265	4365	8192	8454	8978	12629	10070	8344	17612
Obsvd. [$I > 2\sigma(I)$]	4795	3685	6165	6416	7787	9876	8494	6307	13594
R_{int}	0.0479	0.0614	0.0737	0.0782	0.0244	0.0539	0.0582	0.0765	0.0495
R [$F^2 > 2\sigma(F^2)$]	0.0455	0.0355	0.0403	0.0371	0.0236	0.0380	0.0321	0.0356	0.0435
wR(F^2)	0.1378	0.0822	0.0972	0.0846	0.0546	0.0828	0.0749	0.0800	0.1111
S	1.058	1.040	1.013	1.028	1.070	1.017	1.069	1.008	1.026
$\Delta\rho_{max}$	0.472	0.302	1.093	0.092	0.603	1.000	0.728	0.858	3.010
$\Delta\rho_{min}$	-0.290	-0.240	-0.796	-0.386	-0.406	-0.398	-0.341	-0.616	-0.638
CCDC	1942375	1942377	1942368	1942378	1954491	1950170	1950171	1942581	1942379

*The SQUEEZE operation has been applied due to a partially occupied, strongly disordered *n*-pentane molecule.

*Table S2: Crystallographic details of the functionalized complexes **3-Ln–7-Ln**.*

	3-La	**4-La**	**4-Lu**	**5-La**	**5-Lu**	**6-La**	**6-Lu***	**7-La**	**7-Lu**
Chemical formula	$C_{49}H_{67}N_2P_2La_1$	$C_{53}H_{73}N_2O_1P_2La_1$	$C_{53}H_{73}N_2O_1P_2Lu_1$ $C_4H_{10}O_1$	$C_{53}H_{73}N_2P_2S_1La_1$	$C_{53}H_{73}N_2P_2S_1Lu_1$	$C_{53}H_{74}N_3P_2La_1$ $C_4H_{10}O_1$	$C_{53}H_{74}N_3P_2Lu_1$	$C_{53}H_{74}N_2P_3La_1$	$C_{53}H_{74}N_2P_3Lu_1$ C_7H_8
M_r	884.89	954.98	1065.16	971.04	1007.10	1028.12	990.06	970.96	1099.15
Crystal system	Monoclinic	Monoclinic	Triclinic	Triclinic	Monoclinic	Triclinic	Triclinic	Monoclinic	Monoclinic
Space group	$P2_1/c$	$P2_1/c$	$P\bar{1}$	$P\bar{1}$	$P2_1/c$	$P\bar{1}$	$P\bar{1}$	$P2_1/n$	$P2_1/c$
a (Å)	16.881(1)	15.148(3)	11.632(2)	13.433(3)	14.933(3)	11.808(2)	11.581(1)	15.009(3)	14.624(1)
b (Å)	22.018(2)	18.943(4)	19.291(3)	13.708(4)	13.053(3)	19.584(3)	19.741(1)	11.980(3)	19.238(1)
c (Å)	13.038(1)	18.997(4)	25.412(4)	15.265(4)	25.433(5)	24.210(4)	24.651(2)	28.729(6)	21.223(1)
α (°)	90	90	85.328(3)	89.241(5)	90	86.292(2)	87.354(1)	90	90
β (°)	108.186(1)	113.439(4)	80.975(3)	67.705(4)	95.842(5)	83.534(2)	82.377(1)	96.361(4)	106.804(1)
γ (°)	90	90	89.009(3)	82.502(5)	90	88.592(2)	88.118(1)	90	90
V (Å^3)	4603.6(6)	5001.1(2)	5613(1)	2576.6(1)	4932(2)	5550.3(2)	5577.8(6)	5134(2)	5717.0(5)
Z	4	4	4	2	4	4	4	4	4
Densitiy (g cm^{-3})	1.277	1.268	1.260	1.252	1.356	1.230	1.179	1.256	1.277
F(000)	1848	2000	2224	1016	2088	2168	2056	2032	2288
Radiation Type	MoKα	MoKα	MoKα	MoKα	MoKα	MoKα	MoKα	MoKα	MoKα
μ (mm^{-1})	1.031	0.956	1.855	0.966	2.145	0.866	1.860	0.960	1.848
Crystal size	0.35x0.34x0.29	0.25 x0.24x0.09	0.38x0.35x0.31	0.35x0.30x0.28	0.12x0.12x0.11	0.35x0.33x0.31	0.44x0.42x0.37	0.15x0.12x0.04	0.55x0.48x0.45
Meas. Refl.	33292	24425	65881	29323	23176	60217	65143	47168	63680
Indep. Refl.	8107	9239	22070	9531	8916	20507	21351	9537	10530
Obsvd. [$I > 2\sigma(I)$]	5797	6548	17295	7409	6430	13337	16188	6619	8587
R_{int}	0.1194	0.0758	0.0503	0.0708	0.0696	0.0877	0.0504	0.0979	0.0656
R [$F^2 > 2\sigma(F^2)$]	0.0404	0.0470	0.0349	0.0407	0.0447	0.0603	0.0360	0.0492	0.0288
wR(F^2)	0.0968	0.0797	0.0905	0.0610	0.0984	0.1836	0.0978	0.1178	0.0671
S	1.014	1.008	1.033	0.989	0.988	1.014	1.034	1.015	1.050
$\Delta\rho_{max}$	0.965	0.577	1.058	0.836	1.879	2.138	1.190	0.798	0.941
$\Delta\rho_{min}$	–0.655	–1.165	–0.457	–0.913	–0.671	–0.971	–0.393	–2.404	–0.633
CCDC	1942376	1942370	1942371	1942369	1942374	1942373	1943224	1957704	1957703

*The SQUEEZE operation has been applied due to partially occupied, strongly disordered diethyl ether molecules.

*Table S3: Crystallographic details of the functionalized complexes **8-Ln**.*

	8-La	**8-Ce**
Chemical formula	$C_{34}H_{67}N_3P_2Si_4La_1$	$C_{34}H_{67}N_3P_2Si_4Ce_1$
M_r	800.14	801.35
Crystal system	Monoclinic	Monoclinic
Space group	$P2_1/n$	$P2_1/n$
a (Å)	15.306(2)	15.270(2)
b (Å)	17.624(2)	17.722(2)
c (Å)	15.654(2)	15.595(2)
α (°)	90	90
β (°)	99.013(2)	98.822(3)
γ (°)	90	90
V (Å^3)	4170.5(9)	4169(1)
Z	4	4
Densitiy (g cm^{-3})	1.274	1.277
F(000)	1680	1684
Radiation Type	MoKα	MoKα
μ (mm^{-1})	1.203	1.270
Crystal size	0.15x0.15x0.15	0.25x0.24x0.19
Meas. Refl.	18550	23265
Indep. Refl.	7568	7936
Obsvd. [$I > 2\sigma(I)$]	5608	5782
R_{int}	0.0589	0.0873
R [$F^2 > 2\sigma(F^2)$]	0.0431	0.0501
wR(F^2)	0.0941	0.1256
S	0.985	0.998
$\Delta\rho_{max}$	1.164	2.136
$\Delta\rho_{min}$	−0.636	−1.435
CCDC	1942372	1946545

Table S4: Selected bond lengths and angles.

	LiPN	KPN	1-La	1-Ce	1-Nd	1-Gd	1-Tb	1-Dy	1-Lu	3-La	4-La	4-Lu
M1 – N1	1.940(3)	2.654(2)	2.373(3)	2.333(3)	2.307(2)	2.296(2)	2.274(3)	2.249(3)	2.213(4)	2.499(4)	2.399(4)	2.224(3)
M1 – N2	-	-	2.364(3)	2.348(3)	2.319(2)	2.297(2)	2.282(3)	2.251(3)	2.237(4)	2.420(4)	2.422(4)	2.233(3)
M1 – P1	2.513(2)	3.281(1)	3.163(1)	3.157(1)	3.112(1)	2.965(1)	2.946(1)	2.990(1)	2.866(1)	3.098(1)	3.158(2)	2.901(1)
M1 – P2	-	-	3.197(1)	3.133(1)	3.097(1)	2.967(1)	2.950(1)	2.973(1)	2.862(1)	3.216(1)	3.165(1)	2.903(1)
M1 – X70/C11/N100/N200/Cp_{cent}	-	-	2.691(1)	2.668(1)	2.631(1)	2.561(8)	2.545(1)	2.524(1)	2.467(1)	2.555(1)	2.225(3)	2.028(3)
M1 – Mes/Tol_{cent}	2.113(1)	2.788(1)	-	-	-	-	-	-	-	-	-	-
C10 – N1	1.370(1)	1.355(2)	1.390(5)	1.391(4)	1.388(3)	1.401(4)	1.398(4)	1.381(5)	1.405(7)	1.387(6)	1.381(5)	1.399(5)
C11 – P1	1.811(1)	1.831(2)	1.809(4)	1.818(4)	1.823(2)	1.810(3)	1.813(3)	1.818(4)	1.802(6)	1.816(5)	1.821(5)	1.817(4)
C10 – C11	1.429(2)	1.441(2)	1.415(6)	1.410(5)	1.416(3)	1.407(4)	1.405(4)	1.418(5)	1.404(8)	1.419(6)	1.421(6)	1.416(5)
M1 – X70 – C70	-	-	-	-	-	-	-	-	-	-	173.8(3)	171.7(3)
N1 – M1 – N2	-	-	125.8(1)	128.3(1)	128.1(1)	127.8(1)	129.8(1)	131.5(1)	126.6(2)	132.5(1)	114.0(1)	118.3(1)
P2 – M1 –P2	-	-	178.2(1)	177.7(1)	177.7(1)	171.6(1)	172.9(2)	178.6(1)	172.5(1)	153.8(1)	177.2(1)	178.5(3)
N1 – M1 – P1	83.52(9)	56.76(3)	62.0(1)	63.0(1)	64.4(1)	67.1(1)	67.4(1)	67.6(1)	70.5(1)	64.6(1)	62.9(1)	70.3(1)
N2 – M1 – P2	-	-	62.3(1)	62.3(1)	63.5(1)	68.5(1)	68.7(1)	67.1(1)	71.4(1)	61.0(1)	62.9(1)	71.6(1)
(PN) *vs.* (PN)	-	-	44.4(1)	43.7(1)	42.7(1)	37.3(1)	37.1(1)	38.3(1)	37.4(1)	10.5(1)	58.2(1)	47.3(1)
τ_5	-	-	0.874	0.823	0.826	0.730	0.718	0.785	0.765	0.355	0.841	0.953

Table S5: Selected bond lengths and angles.

	5-La	5-Lu	6-La	6-Lu	7-La	7-Lu	8-La	8-Ce
M1 – N1	2.388(3)	2.245(4)	2.427(5)	2.217(3)	2.397(4)	2.229(2)	2.436(3)	2.408(4)
M1 – N2	2.372(3)	2.236(4)	2.396(5)	2.254(3)	2.388(4)	2.216(3)	-	-
M1 – P1	3.151(1)	2.878(2)	3.154(2)	2.912(1)	3.133(1)	2.884(1)	3.243(1)	3.187(1)
M1 – P2	3.149(1)	2.864(2)	3.139(2)	2.905(1)	3.137(1)	2.895(1)	-	-
M1 – X70/C11/N100/N200/Cp_{cent}	2.718(1)	2.544(2)	2.338(5)	2.166(4)	3.053(1)	2.735(1)	2.376(3) / 2.388(3)	2.356(4) / 2.355(4)
M1 – Mes/Tol_{cent}	-	-	-	-	-	-	-	-
C10 – N1	1.389(4)	1.411(6)	1.399(7)	1.389(5)	1.382(5)	1.399(4)	1.386(5)	1.378(6)
C11 – P1	1.805(4)	1.811(6)	1.821(6)	1.821(4)	1.805(5)	1.810(3)	1.812(4)	1.815(5)
C10 – C11	1.415(5)	1.418(7)	1.418(8)	1.419(6)	1.423(6)	1.419(4)	1.421(6)	1.426(6)
M1 – X70 – C70	145.8(1)	137.8(2)	149.2(4)	146.4(3)	116.8(1)	130.7(1)	-	-
N1 – M1 – N2	120.2(1)	126.7(2)	120.8(2)	119.3(1)	119.7(1)	125.4(1)	-	-
P1 – M1 –P2	175.3(1)	169.2(4)	178.4(1)	178.2(1)	169.0(1)	167.7(1)	-	-
N1 – M1 – P1	63.2(1)	71.5(1)	63.9(1)	71.1(1)	62.8(1)	71.2(1)	62.71(8)	63.96(9)
N2 – M1 – P2	62.9(1)	70.8(1)	63.9(1)	71.2(1)	63.5(1)	70.3(1)	-	-
(PN) *vs.* (PN)	54.7(1)	33.9(1)	46.8(1)	45.9(1)	38.8(1)	33.6(1)	-	-
								-
τ_5 / τ_4'	0.918	0.708	0.960	0.981	0.821	0.705	0.688	0.670

6. Paramagnetic susceptibility measurements of 1-Ln (with Ln = Ce, Nd, Gd, Tb, Dy) and 8-Ce

Table S6: Paramagnetic susceptibility data obtained by the Evans method[14] in C_6D_6 (298 K).

	1-Ce	1-Nd	1-Gd	1-Tb	1-Dy	8-Ce
experimental μ_{eff} in μ_B	2.23	3.38	8.24	9.37	10.02	2.59
literature μ_{eff} in μ_B	1.79–2.46 (exp.)[15, 16]; 2.54 (theor.)[16]	2.98–3.95 (exp.)[15, 17]; 3.62 (theor.)[17]	7.70–8.86 (exp.)[15, 16]; 7.94 (theor.)[16]	8.90–10.70 (exp.)[15, 18]; 9.72 (theor.)[19]	9.90–11.81 (exp.)[15]; 10.63 (theor.)[19]	1.79–2.46 (exp.)[15, 16]; 2.54 (theor.)[16]

7. ^{31}P NMR correlations of 1-Ce and 8-Ce

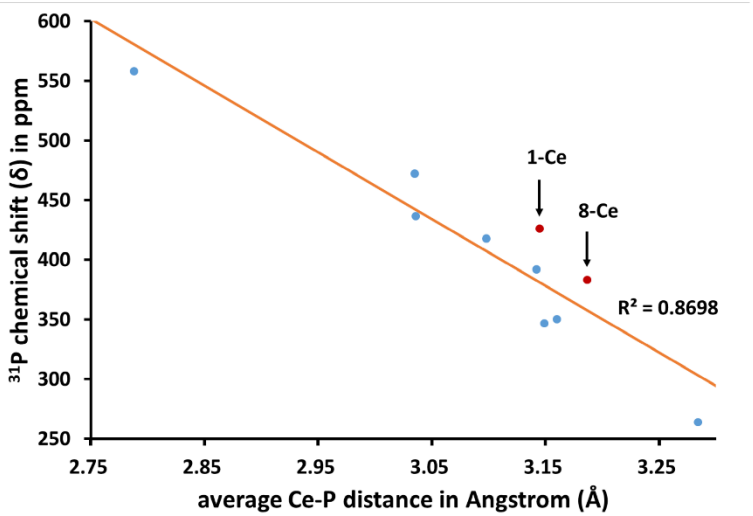

*Figure S131: Linear correlation between the ^{31}P NMR shifts measured at 25 °C in C_6D_6 and Ce–P distances for the new complexes **1-Ce** and **8-Ce** (red dots) in comparison with previously reported PNP Ce complexes by Schelter et al.[20] (blue dots).*

8. Literature

[1] Tran, B. L.; Pink, M.; Mindiola, D. J. Catalytic Hydrosilylation of the Carbonyl Functionality via a Transient Nickel Hydride Complex. *Organometallics* **2009**, *28*, 2234–2243.

[2] Li, J.; Li, Y.; Purushothaman, I.; De, S.; Li, B.; Zhu, H.; Parameswaran, P.; Ye, Q.; Liu, W. Fine Tuning of the Substituents on the N-Geminal Phosphorus/Silicon-Based Lewis Pairs for the Synthesis of Z -Type Silyliminophosphoranylalkenes. *Organometallics* **2015**, *34*, 4209–4217.

[3] Garner, M. E.; Parker, B. F.; Hohloch, S.; Bergman, R. G.; Arnold, J. Thorium Metallacycle Facilitates Catalytic Alkyne Hydrophosphination. J. Am. Chem. Soc. **2017**, 139, 12935–12938.

[4] Garner, M. E.; Arnold, J. Reductive Elimination of Diphosphine from a Thorium–NHC–Bis(phosphido) Complex. *Organometallics* **2017**, *36*, 4511–4514.

[5] Dahl, E. W.; Szymczak, N. K. Hydrogen Bonds Dictate the Coordination Geometry of Copper: Characterization of a Square-Planar Copper(I) Complex. *Angew. Chem. Int. Ed.* **2016**, *55*, 3101–3105.

[6] Mede, R.; Lorett-Velásquez, V. P.; Klein, M.; Görls, H.; Schmitt, M.; Gessner, G.; Heinemann, S. H.; Popp, J.; Westerhausen, M. Carbon monoxide release properties and molecular structures of phenylthiolatomanganese(I) carbonyl complexes of the type (OC)4Mn(μ-S-aryl)2. *Dalton Trans.* **2015**, 44, 3020–3033

[7] Monreal, M. J.; Thomson, R. K.; Cantat, T.; Travia, N. E.; Scott, B. L.; Kiplinger, J. L. UI 4 (1,4-dioxane) 2 , [UCl 4 (1,4-dioxane)] 2 , and UI 3 (1,4-dioxane) 1.5 : Stable and Versatile Starting Materials for Low- and High-Valent Uranium Chemistry. *Organometallics* **2011**, *30*, 2031–2038.

[8] Panda, T. K.; Gamer, M. T.; Roesky, P. W. An Improved Synthesis of Sodium and Potassium Cyclopentadienide. *Organometallics* **2003**, *22*, 877–878.

[9] Windorff, C. J.; Dumas, M. T.; Ziller, J. W.; Gaunt, A. J.; Kozimor, S. A.; Evans, W. J. Small-Scale Metal-Based Syntheses of Lanthanide Iodide, Amide, and Cyclopentadienyl Complexes as Analogues for Transuranic Reactions. *Inorg. Chem.* **2017**, *56*, 11981–11989.

[10] Hitchcock, P. B.; Hulkes, A. G.; Lappert, M. F.; Li, Z. Cerium(III) dialkyl dithiocarbamates from $Ce[N(SiMe3)_2]_3$ and tetraalkylthiuram disulfides, and $Ce(kappa2\text{-}S_2CNEt_2)_4$ from the Ce(III) precursor; Tb(III) and Nd(III) analogues. *Dalton Trans.* **2004**, 129–136.

[11] Sheldrick, G. M. Crystal structure refinement with SHELXL. *Acta cryst. C* **2015**, 71, 3–8.

[12] Dolomanov, O. V.; Bourhis, L. J.; Gildea, R. J.; Howard, J. A. K.; Puschmann, H. OLEX2 : a complete structure solution, refinement and analysis program. *J Appl Crystallogr* **2009**, *42*, 339–341.

[13] van der Sluis, P.; Spek, A. L. BYPASS: an effective method for the refinement of crystal structures containing disordered solvent regions. *Acta Crystallogr A* **1990**, *46*, 194–201.

[14] Evans, D. F. The Determination of the Paramagnetic Susceptibility of Substances in Solution by Nuclear Magnetic Resonance. *J. Chem. Soc.* **1959**, 2003–2005.

[15] Evans, W. J.; Hozbor, M. A. Paramagnetism in Organolanthanide Complexes. *J. Organomet. Chem.* **1987**, *326*, 299–306.

[16] Rosenstengel, K.; Schulz, A.; Niehaus, O.; Janka, O.; Pöttgen, R.; Villinger, A. Binary Polyazides of Cerium and Gadolinium. *Eur. J. Inorg. Chem.* **2018**, 778–790.

[17] Galley, S. S.; Pattenaude, S. A.; Higgins, R. F.; Tatebe, C. J.; Stanley, D. A.; Fanwick, P. E.; Zeller, M.; Schelter, E. J.; Bart, S. C. A reduction series of neodymium supported by pyridine(diimine) ligands. *Dalton Trans.* **2019**, *48*, 8021–8025.

[18] Goodwin, C. A. P.; Reta, D.; Ortu, F.; Liu, J.; Chilton, N. F.; Mills, D. P. Terbocenium: completing a heavy lanthanide metallocenium cation family with an alternative anion abstraction strategy. *Chem. Commun.* **2018**, *54*, 9182–9185.

[19] Cotton, S. Lanthanide and Actinide Chemistry, *Wiley & Sons*, **2006**, Chapter 5, p. 65.

[20] Zabula, A. V.; Qiao, Y.; Kosanovich, A. J.; Cheisson, T.; Manor, B. C.; Carroll, P. J.; Ozerov, O. V.; Schelter, E. J. Structure, Electronics and Reactivity of Ce(PNP) Complexes. *Chem. Eur. J.* **2017**, *23*, 17923–17934.

Supporting Information
for
Chapter 2

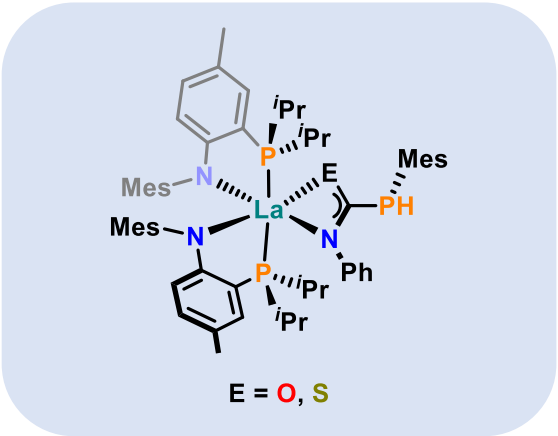

Supporting Information

Isocyanate Insertion into a La–P Phosphide Bond: A Versatile Route to Phosphaureate Bridged Heterobimetallic Lanthanide – Coinage Metal Complexes

Fabian A. Watt,[a] Nicole Dickmann,[a] Roland Schoch,[a] and Stephan Hohloch[b]*

[a] Paderborn University, Faculty of Science, Department of Chemistry, Warburger Str. 100, 33098 Paderborn, Germany.
[b] University of Innsbruck, Faculty of Chemistry and Pharmacy, Institute of General, Inorganic and Theoretical Chemistry, Innrain 80-82, 6020 Innsbruck, Austria.

Table of Contents

1. Experimental Section

General Remarks. If not otherwise mentioned, all transformations were carried out under inert conditions using the Schlenk technique or an argon filled glovebox. Solvents were dried by a MBraun SPS system, degassed and stored over activated molecular sieves (3 Å) for at least 24 h prior to use. The deuterated solvents C_6D_6, $CDCl_3$ and THF-d_8 were dried by storage over activated molecular sieves (3 Å) for at least 24 h. IR spectra were recorded at room temperature under inert conditions using a Bruker Vertex 70 with ATR equipment. If not otherwise stated, the NMR spectra were collected at 303 K on a Bruker AV-500 or an Ascent 700 spectrometer using a J-Young NMR tube. All chemical shifts (δ) are reported in ppm and coupling constants are given in Hz. ^{1}H and ^{13}C chemical shifts were calibrated to residual solvent peaks. ^{15}N chemical shifts (obtained by ^{1}H–^{15}N HMBC NMR spectroscopy) were calibrated externally to liquid ammonia (NH_3). ^{29}Si chemical shifts were calibrated externally to tetramethylsilane ($Si(CH_3)_4$, TMS). ^{31}P chemical shifts were calibrated externally to phosphoric acid (H_3PO_4, 85% in water). Elemental analyses were performed using an Elementar vario microcube instrument at the Paderborn University. Starting materials **1**,[1] (tht)AuCl,[2] (Me_3P)Au(HMDS),[3] **(IPr)AuCl**,[4] ^{Me}CAAC[5] and **(^{Me}CAAC)CuCl**[6] were synthesized following literature known procedures. Phenylisocyanate, phenylisothiocyanate and benzyl bromide were stored over activated molecular sieves (3 Å) for 24 h prior to use. KHMDS and **(IPr)CuCl** were used as received.

Synthetic Procedures

Preparation of (^{Me}CAAC)Au(HMDS).

(Me_3P)Au(HMDS) (87 mg, 200 µmol, 1 eq.) and ^{Me}CAAC (57 mg, 200 µmol, 1 eq.) were dissolved separately in toluene (2 mL each) and the solutions cooled to –40 °C. The solution of ^{Me}CAAC was slowly added dropwise to the solution of (Me_3P)Au(HMDS) under stirring at –40 °C. The resulting clear, colorless reaction mixture was stirred for 30 min while warming up to ambient temperature. Most of the volatile components were removed *in vacuo*, giving a colorless, oily residue. Addition of –40 °C cold *n*-hexane (1 mL) caused the formation of a colorless, microcrystalline solid which was separated, washed again with –40 °C cold *n*-hexane (1 mL) and dried *in vacuo* to give the desired product. Single crystals of **(^{Me}CAAC)Au(HMDS)** suitable for X-ray structure determination were obtained by storing the concentrated *n*-hexane extract (with residual toluene, obtained during work-up) at –40°C overnight. Yield: 74 mg (115 µmol, 58%); ^{1}H NMR (C_6D_6, 303 K, 700 MHz, in ppm): δ = 7.17 (t, $^{3}J_{HH}$ = 7.7 Hz, C$H_{Ar,Dipp}$, 1 H), 7.02 (d, $^{3}J_{HH}$ = 7.7 Hz, C$H_{Ar,Dipp}$, 2 H), 2.66 (sept, $^{3}J_{HH}$ = 6.8 Hz, C$H_{iPr,Dipp}$, 2 H), 1.54 (d, $^{3}J_{HH}$ = 6.8 Hz, C$H_{3iPr,Dipp}$, 6 H), 1.42 (s, CH_{2CAAC}, 2 H), 1.32 (s, CH_{3CAAC}, 6 H), 1.09 (d, $^{3}J_{HH}$ = 6.8 Hz, C$H_{3iPr,Dipp}$, 6 H), 0.81 (s, CH_{3CAAC}, 6 H), 0.34 (s, Si(CH_3)$_3$, 18 H); ^{13}C{^{1}H} NMR (C_6D_6, 303 K, 176 MHz, in ppm): δ = 242.2 (s, $C_{carbene}$), 145.3 (s, $C_{qAr,Dipp}$), 135.2 (s, $C_{qAr,Dipp}$), 129.8 (s, C$H_{Ar,Dipp}$), 125.3 (s, C$H_{Ar,Dipp}$), 79.0 (s, C_{qCAAC}), 54.3 (s, C_{qCAAC}), 50.0 (s, CH_{2CAAC}), 29.3 (s, C$H_{iPr,Dipp}$), 29.2 (s, CH_{3CAAC}), 28.6 (s, CH_{3CAAC}), 27.1 (s, C$H_{3iPr,Dipp}$), 23.2 (s, C$H_{3iPr,Dipp}$), 6.6 (s, Si(CH_3)$_3$); ^{29}Si{^{1}H} NMR (C_6D_6, 303 K, 139 MHz, in ppm): δ = –5.6 (s, *Si*(CH_3)$_3$, 2 Si); elemental analysis (in %): $C_{26}H_{49}AuN_2Si_2$: calcd.: C 48.58, H 7.68, N 4.36; found: C 49.24, H 7.45, N 4.59. (We were not able to obtain better elemental analysis results for carbon.).

Preparation of (^{Me}CAAC)AuCl.

A procedure similar to the one reported by Romanov *et al.* for (^{Et}CAAC)AuCl was adapted.[6] To a –78 °C cold suspension of (tht)AuCl (122 mg, 381 µmol, 1 eq.) in THF (10 mL) was added dropwise solution of ^{Me}CAAC (109 mg, 381 µmol, 1 eq.) in THF (5 mL) under stirring. The resulting reaction mixture was stirred for 16 h, while warming up to room temperature. This yielded a grey-brown suspension. All volatile components were removed *in vacuo* and the remaining solid washed with *n*-hexane (2 x 3 mL). The grey solid was then extracted into dichloromethane (4 mL) and filtered through a glass fibre filter, leaving a black solid on the filter and a brown-red solution. The solvent was removed from the filtrate, leaving a rose-colored solid which ^{1}H and ^{13}C{^{1}H} NMR spectroscopy showed to be a mixture of **(^{Me}CAAC)AuCl** (δ(^{13}C) = 235.9 ppm (s, $C_{carbene}$)), [(^{Me}CAAC)$_2$Au]Cl (δ(^{13}C) = 250.9 ppm (s, $C_{carbene}$)) and

[H^{Me}CAAC]Cl. [(^{Me}CAAC)$_2$Au]Cl could be removed by extraction of **(^{Me}CAAC)AuCl** into THF (2 x 3 mL). After filtration and removal of solvent *in vacuo* from the THF filtrate, crude **(^{Me}CAAC)AuCl** was obtained with [H^{Me}CAAC]Cl as the only impurity (see Figures S9 and S10). Yield: 165 mg (84%, crude); ^{1}H NMR ($CDCl_3$, 303 K, 700 MHz, in ppm): δ = 7.41 (t, $^3J_{HH}$ = 7.8 Hz, C*H*$_{Ar,Dipp}$, 1 H), 7.24 (d, $^3J_{HH}$ = 7.8 Hz, C*H*$_{Ar,Dipp}$, 2 H), 2.74 (sept, $^3J_{HH}$ = 6.7 Hz, C*H*$_{iPr,Dipp}$, 2 H), 2.13 (s, C*H*$_{2CAAC}$, 2 H), 1.51 (s, C*H*$_{3CAAC}$, 6 H), 1.40 (d, $^3J_{HH}$ = 6.7 Hz, C*H*$_{3iPr,Dipp}$, 6 H), 1.35 (s, C*H*$_{3CAAC}$, 6 H), 1.30 (d, $^3J_{HH}$ = 6.7 Hz, C*H*$_{3iPr,Dipp}$, 6 H); ^{13}C{^{1}H} NMR ($CDCl_3$, 303 K, 176 MHz, in ppm): δ = 235.9 (s, $C_{carbene}$), 145.1 (s, $C_{qAr,Dipp}$), 133.7 (s, $C_{qAr,Dipp}$), 130.1 (s, *C*H$_{Ar,Dipp}$), 125.1 (s, *C*H$_{Ar,Dipp}$), 80.9 (s, C_{qCAAC}), 54.1 (s, C_{qCAAC}), 49.6 (s, *C*H$_{2CAAC}$), 29.3 (s, *C*H$_{3CAAC}$), 29.2 (s, *C*H$_{3CAAC}$), 27.3 (s, *C*H$_{3iPr,Dipp}$), 22.9 (s, *C*H$_{3iPr,Dipp}$) (The resonance of *C*H$_{iPr,Dipp}$ could not be assigned confidently, since it its either obscured by the resonances at δ 29.3–29.2 ppm or not intense enough to be distinguished from the resonances of impurity [H^{Me}CAAC]Cl.).

Preparation of 2.

A solution of phenylisocyanate (60 mg, 500 µmol, 1 eq.) in toluene (2 mL) was added dropwise to a solution of **1** (485 mg, 500 µmol, 1 eq.) in toluene (8 mL) at room temperature. Upon addition, the color of the solution turned from dark to pale yellow and the resulting reaction mixture was stirred for 1 h. The solvent was removed *in vacuo* and *n*-hexane (4 mL) added to the residue. The resulting suspension was centrifuged, the off-white solid separated from the yellow solution, washed with *n*-hexane (2 x 4 mL) and *n*-pentane (1 mL). Drying *in vacuo* gave the product as an off-white solid. Single crystals of **2** suitable for X-ray structure determination were obtained by storing the concentrated (ca. 1 mL) *n*-hexane extract (with residual toluene, obtained during work-up) at room temperature overnight. Yield: 451 mg (414 µmol, 83%); ^{1}H NMR (C_6D_6, 303 K, 700 MHz, in ppm): δ = 7.06–7.08 (m, C*H*$_{Ar}$, 2 H), 7.05–7.02 (m, C*H*$_{Ar}$, 2 H), 6.94 (m, C*H*$_{Ar}$, 2 H), 6.89 (tt, $^3J_{HH}$ = 7.3 Hz, $^4J_{HH}$ = 1.2 Hz, C*H*$_{Ar}$, 1 H), 6.86 (br. s, C*H*$_{Ar}$, 2 H), 6.84 (br. s, C*H*$_{Ar}$, 2 H), 6.77 (dd, $^3J_{HH}$ = 8.5 Hz, $^4J_{HH}$ = 2.0 Hz, C*H*$_{Ar}$, 2 H), 6.72 (br. s, C*H*$_{Ar}$, 2 H), 5.68 (m, C*H*$_{Ar}$, 2 H), 5.11 (d, $^1J_{PH}$ = 242.8 Hz, P*H*Mes, 1 H), 2.38 (br. s, C*H*$_{3Ar}$, 6 H), 2.19 (s, C*H*$_{3Ar}$, 6 H), 2.18 (br. m, C*H*$_{iPr}$, 2 H), 2.16 (s, C*H*$_{3Ar}$, 6 H), 2.13–2.09 (2 br. s, C*H*$_{3Ar}$, 9 H), 2.06 (br. s, C*H*$_{3Ar}$, 6 H), 2.05–2.01 (br. m, C*H*$_{iPr}$, 2 H), 1.14–1.10 (br. m, C*H*$_{3iPr}$, 6 H), 1.08–1.01 (2 br. m, C*H*$_{3iPr}$, 12 H), 0.96–0.89 (br. m, C*H*$_{3iPr}$, 6 H); ^{13}C{^{1}H} NMR (C_6D_6, 303 K, 176 MHz, in ppm): δ = 186.5 (d, $^1J_{CP}$ = 34.5 Hz, O*C*(NPh)(PHMes)), 161.2 (m, C_{qAr}), 149.0 (s, C_{qAr}), 143.4 (br. s, C_{qAr}), 140.5 (s, C_{qAr}), 138.8 (br. s, C_{qAr}), 138.3 (s, C_{qAr}), 137.0 (br. s, C_{qAr}), 134.2 (s, C_{qAr}), 133.5 (s, *C*H$_{Ar}$,), 133.4 (s, *C*H$_{Ar}$), 131.3 (s, *C*H$_{Ar}$), 131.0 (s, *C*H$_{Ar}$), 129.0 (d, J_{CP} = 3.5 Hz, *C*H$_{Ar}$), 128.8 (s, *C*H$_{Ar}$), 126.4 (d, J_{CP} = 8.0 Hz, C_{qAr}), 125.3 (s, *C*H$_{Ar}$), 124.4 (s, *C*H$_{Ar}$), 122.3 (s, C_{qAr}), 113.6 (m, C_{qAr}), 113.3 (*pseudo*-t, J_{CP} = 3.8 Hz, *C*H$_{Ar}$), 24.2 (br. s, *C*H$_{iPr}$), 24.1 (s, *C*H$_{3Ar}$), 24.1 (s, *C*H$_{3Ar}$), 22.9 (br. s, *C*H$_{iPr}$), 21.1 (s, *C*H$_{3Ar}$), 20.7 (s, *C*H$_{3Ar}$), 20.0 (*pseudo*-t, J_{CP} = 5.0 Hz, *C*H$_{3iPr}$), 19.8 (s, *C*H$_{3Ar}$), 19.3 (br. s, *C*H$_{3Ar}$), 19.2 (br. s, *C*H$_{3iPr}$), 18.6 (br. s, *C*H$_{3iPr}$), 17.5 (br. s, *C*H$_{3iPr}$); ^{31}P{^{1}H} NMR (C_6D_6, 303 K, 283 MHz, in ppm): δ = 6.3 (s, *P*N$^-$, 2 P), –90.1 (s, *P*HMes, 1 P); ^{31}P NMR (C_6D_6, 303 K, 283 MHz, in ppm): δ = 6.3 (s, *P*N$^-$, 2 P), –90.1 (d, $^1J_{PH}$ = 242.8 Hz, *P*HMes, 1 P); elemental analysis (in %): $C_{60}H_{79}LaN_3OP_3$: calcd.: C 66.11, H 7.30, N 3.85; found: C 65.78, H 7.28, N 3.87.

Preparation of 3.

A solution of phenylthioisocyanate (27 mg, 200 µmol, 1 eq.) in toluene (2 mL) was added dropwise to a solution of **1** (194 mg, 200 µmol, 1 eq.) in toluene (2 mL) at room temperature. The resulting yellow solution was stirred for 1 h. The solvent was removed *in vacuo* and the residue triturated with *n*-hexane (2 x 1 mL). After washing with –40 °C cold *n*-pentane (2 x 3 mL) and drying *in vacuo* the product was obtained as a bright yellow solid. Single crystals of **3** suitable for X-ray structure determination were obtained by gas diffusion of *n*-hexane into a solution of **3** in C_6D_6 at room temperature for 5 d. Yield: 182 mg (165 µmol, 82%); ^{1}H NMR (C_6D_6, 303 K, 700 MHz, in ppm): δ = 6.97–6.93 (m, C*H*$_{Ar}$, 4 H), 6.90 (d, $^3J_{HH}$ = 7.6 Hz, C*H*$_{Ar}$, 2 H), 6.83 (tt, $^3J_{HH}$ = 7.3 Hz, $^4J_{HH}$ = 1.1 Hz, C*H*$_{Ar}$, 1 H), 6.82 (br. s, C*H*$_{Ar}$, 2 H), 6.79–6.75 (m, C*H*$_{Ar}$, 6 H), 5.63 (m, C*H*$_{Ar}$, 2 H), 5.32 (d, $^1J_{PH}$ = 242.4 Hz, P*H*Mes, 1 H), 2.54 (br. s, C*H*$_{Ar}$, 6 H), 2.30 (br. s, C*H*$_{iPr}$, 2 H), 2.25 (br. s, C*H*$_{iPr}$, 2 H), 2.21 (s, C*H*$_{3Ar}$, 6 H), 2.18 (s, C*H*$_{3Ar}$, 6 H), 2.07 (s, C*H*$_{3Ar}$, 3 H), 1.96 (br. s, C*H*$_{3Ar}$, 6 H), 1.78 (br. s, C*H*$_{3Ar}$, 6 H), 1.39–1.24 (br. s, C*H*$_{3iPr}$, 12 H), 1.22–1.13 (br. s, C*H*$_{3iPr}$, 12 H); ^{13}C{^{1}H} NMR (C_6D_6, 303 K, 176 MHz, in ppm): δ = 208.0 (br. s, S*C*(NPh)(PHMes)), 160.8 (d, J_{CP} = 24.0 Hz, C_{qAr}), 151.7 (d, J_{CP} = 6.2 Hz, C_{qAr}), 144.3 (br. s, C_{qAr}), 141.1 (br. s, C_{qAr}), 139.5 (s, C_{qAr}), 137.9

(br. s, C_{qAr}), 134.1 (s, C_{qAr}), 133.7 (s, CH_{Ar}), 133.4 (s, CH_{Ar}), 131.5 (br. s, CH_{Ar}), 131.2 (br. s, CH_{Ar}), 129.3 (d, J_{CP} = 4.2 Hz, CH_{Ar}), 129.0 (s, CH_{Ar}), 127.8 (d, J_{CP} = 4.4 Hz, C_{qAr}), 125.3 (s, CH_{Ar}), 123.4 (s, CH_{Ar}), 122.7 (s, C_{qAr}), 113.7 (m, C_{qAr}), 113.5 (m, CH_{Ar}), 24.4 (s, CH_{3Ar}), 24.3 (s, CH_{3Ar}), 24.1 (br. s, CH_{iPr}), 21.2 (s, CH_{3Ar}), 21.1 (s, CH_{3Ar}), 20.7 (s, CH_{3Ar}), 20.3 (br. s, CH_{3iPr}), 19.7 (br. s, CH_{3Ar}), 19.3 (br. s, CH_{3Ar}), 18.7 (br. s, CH_{iPr}); $^{31}P\{^{1}H\}$ NMR (C_6D_6, 303 K, 283 MHz, in ppm): δ = 6.9 (s, PN^{-}, 2 P), –56.4 (br. s, PHMes, 1 P); ^{31}P NMR (C_6D_6, 303 K, 283 MHz, in ppm): δ = 6.9 (s, PN^{-}, 2 P), –56.4 (br. d, $^{1}J_{PH}$ = 242.4 Hz, PHMes, 1 P); elemental analysis (in %): $C_{60}H_{79}LaN_3P_3S$: calcd.: C 65.15, H 7.20, N 3.80, S 2.90; found: C 65.47, H 7.23, N 3.88, S 2.96.

Preparation of 4.

A solution of KHMDS (240 mg, 1.21 mmol, 1 eq.) in toluene (10 mL) was added in small portions to a solution of **2** (1.32 g, 1.21 mmol, 1 eq.) in toluene (40 mL) at room temperature, upon which the originally colorless solution turned bright yellow. The reaction mixture was stirred for 15 h, during which a thick yellow suspension formed. The suspension was centrifuged, the solid separated and washed with *n*-pentane (3 x 5 mL). After drying *in vacuo* the product was isolated as a light yellow solid. Crystals of **4** which were used for X-ray structure determination were obtained by gas diffusion of *n*-hexane into THF-d_8 at room temperature overnight. Although this allowed the determination of the connectivity (see Figure S78), no accurate structural parameters could be determined, due to the poor quality of the crystals. All other crystallization methods tested did not yield crystals of higher quality. Yield: 1.17 g (1.04 mmol, 86%); ^{1}H NMR (THF-d_8, 303 K, 700 MHz, in ppm): δ = 7.14–7.10 (m, CH_{Ar}, 2 H), 6.99 (t, $^{3}J_{HH}$ = 7.5 Hz, CHAr, 2 H), 6.76 (br. s, CH_{Ar}, 2 H), 6.74 (br. s, CH_{Ar}, 4 H), 6.71 (t, $^{3}J_{HH}$ = 7.5 Hz, CH_{Ar}, 1 H), 6.58 (br. s, CH_{Ar}, 2 H), 6.46 (dd, ^{3}J = 8.5 Hz, ^{4}J = 1.8 Hz, CH_{Ar}, 2 H), 5.16 (m, CH_{Ar}, 2 H), 2.42 (s, CH_{3Ar}, 6 H), 2.25 (s, CH_{3Ar}, 6 H), 2.12 (s, CH_{3Ar}, 3 H), 2.09 (br. s, CH_{iPr}, 4 H), 2.05 (s, CH_{3Ar}, 6 H), 1.79 (br. s, CH_{3Ar}, 12 H), 1.06 (br. s, CH_{3iPr}, 12 H), 0.98 (br. s, CH_{3iPr}, 12 H); $^{13}C\{^{1}H\}$ NMR (THF-d_8, 303 K, 176 MHz, in ppm): δ = 208.4 (br. s, OC(NPh)(PKMes)), 162.5 (m, C_{qAr}), 155.9 (s, C_{qAr}), 143.7 (s, C_{qAr}), 141.9 (s, C_{qAr}), 141.7 (s, C_{qAr}), 137.9 (br. s, C_{qAr}), 133.8 (s, CH_{Ar}), 132.4 (s, CH_{Ar}), 132.2 (s, C_{qAr}), 130.9 (s, CH_{Ar}), 127.8 (br. s, CH_{Ar}), 127.5 (s, CH_{Ar}), 127.0 (s, CH_{Ar}), 120.1 (br. s, CH_{Ar}), 119.8 (s, C_{qAr}), 113.8 (br. s, C_{qAr}), 112.7 (s, CH_{Ar}), 25.5 (m, CH_{3Ar}), 23.9 (br. s, CH_{3iPr}), 21.1 (s, CH_{3Ar}), 21.0 (s, CH_{3Ar}), 20.4 (s, CH_{3Ar}), 20.0 (br. s, CH_{3iPr}), 19.5 (br. s, CH_{3Ar}), 17.8 (br. s, CH_{iPr}); ^{31}P NMR (THF-d_8, 303 K, 283 MHz, in ppm): δ = 1.9 (s, PN^{-}, 2 P), –38.9 (s, PKMes, 1 P); elemental analysis (in %): $C_{60}H_{78}KLaN_3OP_3$: calcd.: C 63.88, H 6.97, N 3.72; found: C 63.37, H 6.93, N 3.97 (Due to the high sensitivity of **4** towards moisture, a slight deviation in the value for carbon of 0.51% is recorded. We were not able to obtain better elemental analysis results for this compound.).

Deprotonation of 3.

A solution of KHMDS (26 mg, 130 µmol, 1 eq.) in toluene (2 mL) was added dropwise to a solution of **3** (144 mg, 130 µmol, 1 eq.) in toluene (4 mL) at room temperature, upon which the originally light yellow solution turned deep yellow. The reaction mixture was stirred for 17 h, after which all volatile components of the still clear solution were removed *in vacuo*. The residue was triturated and washed with *n*-hexane (3 x 2 mL) and dried *in vacuo* to give a deep yellow solid (133 mg, 89% of the theoretical yield of potassium salt of **3**) which subsequently was analyzed by (VT) NMR spectroscopy (see Figures S34 – S39). The results of this investigation indicated the presence of at least two isomers in solution (e.g. isomers A and B as shown in Figure S36), which interconvert into each other. This made a definite assignment of the crowded ^{1}H and ^{13}C resonances difficult (Figures S34 and S35). Therefore, only the better separated ^{31}P resonances were tentatively assigned (Figure S36). Repeated crystallization attempts under different conditions failed to produce suitable crystals for X-ray structure determination of either isomer in question. Elemental analyses of different batches were carried out repeatedly, and each time the elemental composition was found to fit well to the calculated composition of the potassium salt of **3**, with only minor deviation (< 0.5%) in the value for carbon. ^{31}P NMR (THF-d_8, 303 K, 283 MHz, in ppm): δ = 60.8 (s, PMes, isomer B), 10.2 (s, PMes, isomer A), 3.3 (s, PN^{-}, 2 P); elemental analysis (in %): $C_{60}H_{78}KLaN_3P_3S$: calcd.: C 62.98, H 6.87, N 3.67, S 2.80; found: C 62.56, H 6.97, N 3.64, S 2.99.

Preparation of 5.

To a mixture of **4** (113 mg, 100 µmol, 1 eq.) and **(IPr)CuCl** (49 mg, 100 µmol, 1 eq.) was added diethyl ether (4 mL) and the resulting suspension stirred for 1 h at room temperature. After removal of the colorless precipitate by centrifugation and filtration a light yellow solution was obtained. The solvent was removed *in vacuo* and the obtained solid recrystallized from *n*-pentane (1.5 mL) at –40 °C. After drying the microcrystalline material *in vacuo* the product was obtained as a light yellow solid. Single crystals of **5** suitable for X-ray structure determination were obtained by storing a concentrated solution of **5** in diethyl ether at room temperature. Yield: 123 mg (80 µmol, 80%); ^{1}H NMR (C_6D_6, 303 K, 700 MHz, in ppm): δ = 7.21 (t, $^{3}J_{HH}$ = 7.8 Hz, C$H_{Ar,Dipp}$, 2 H), 7.04 (m, CH_{Ar}, 2 H), 6.98 (m, CH_{Ar}, 2 H), 6.94 (d, $^{3}J_{HH}$ = 7.8 Hz, C$H_{Ar,Dipp}$, 4 H), 6.87 (s, CH_{Ar}, 4 H), 6.76 (s, CH_{Ar}, 2 H), 6.74 (dd, $^{3}J_{HH}$ = 8.5 Hz, $^{4}J_{HH}$ = 1.8 Hz, CH_{Ar}, 2 H), 6.46 (m, CH_{Ar}, 3 H), 6.13 (s, C(N(Dipp)CH)$_2$, 2 H), 5.73 (m, CH_{Ar}, 2 H), 2.46 (sept, $^{3}J_{HH}$ = 6.9 Hz, C$H_{iPr,Dipp}$, 4 H), 2.43–2.35 (br. s at 2.39 & s at 2.37, CH_{3Ar}, 9 H), 2.27 (br. s, CH_{3Ar}, 6 H), 2.23–2.15 (br. s, CH_{iPr}, 4 H), 2.14 (s, CH_{3Ar}, 6 H), 2.05 (br. s, CH_{3Ar}, 12 H), 1.25–1.06 (2 br. s, CH_{3iPr}, 24 H), 1.10 (d, $^{3}J_{HH}$ = 6.9 Hz, C$H_{3iPr,Dipp}$, 12 H), 0.96 (d, $^{3}J_{HH}$ = 6.9 Hz, C$H_{3iPr,Dipp}$, 12 H); ^{13}C{^{1}H} NMR (C_6D_6, 303 K, 176 MHz, in ppm): δ = 201.5 (br. s, O*C*(NPh)(PMes)), 182.9 (d, $^{2}J_{CP}$ = 43.7 Hz, *C*(N(Dipp)CH)$_2$), 162.0 (m, C_{qAr}), 151.2 (d, J_{CP} = 5.4 Hz, C_{qAr}), 145.2 (s, C_{qAr}), 144.9 (br. s, C_{qAr}), 142.4 (s, C_{qAr}), 137.9 (br. s, C_{qAr}), 135.4 (s, C_{qAr}), 135.3 (d, J_{CP} = 12.1 Hz, C_{qAr}), 134.1 (s, C_{qAr}), 133.6 (s, *C*H$_{Ar}$), 133.2 (s, *C*H$_{Ar}$), 132.9 (s, C_{qAr}), 131.0 (br. s, *C*H$_{Ar}$), 130.6 (s, *C*H$_{Ar}$), 127.7 (br. s, *C*H$_{Ar}$), 127.5 (s, *C*H$_{Ar}$), 125.0 (d, J_{CP} = 4.4 Hz, *C*H$_{Ar}$), 124.6 (s, *C*H$_{Ar}$), 123.0 (s, C(N(Dipp)*C*H)$_2$), 122.3 (s, *C*H$_{Ar}$), 121.0 (s, C_{qAr}), 113.5 (*pseudo*-t, J_{CP} = 6.3 Hz, C_{qAr}), 113.1 (m, *C*H$_{Ar}$), 28.9 (s, *C*H$_{iPr,Dipp}$), 26.4 (s, *C*H$_{3Ar}$), 26.3 (s, *C*H$_{3Ar}$), 24.4 (s, *C*H$_{3iPr,Dipp}$), 24.1 (s, *C*H$_{3iPr,Dipp}$), 23.6 (br. s, *C*H$_{3iPr}$), 21.5 (s, *C*H$_{3Ar}$), 21.2 (s, *C*H$_{3Ar}$), 20.7 (s, *C*H$_{3Ar}$), 19.9 (br. s, *C*H$_{3iPr}$), 19.5 (br. s, *C*H$_{3Ar}$), 18.0 (br. s, *C*H$_{iPr}$); ^{31}P NMR (C_6D_6, 303 K, 283 MHz, in ppm): δ = 3.7 (s, *P*N^{-}, 2 P), –65.0 (s, *P*(Cu(IPr))Mes, 1 P); elemental analysis (in %): $C_{87}H_{114}CuLaN_5OP_3$: calcd.: C 67.80, H 7.46, N 4.54; found: C 67.85, H 7.41, N 4.62.

Preparation of 6.

To a mixture of **4** (89 mg, 79 µmol, 1 eq.) and **(IPr)AuCl** (49 mg, 79 µmol, 1 eq.) was added diethyl ether (4 mL) and the resulting suspension stirred for 1 h at room temperature. After removal of the colorless precipitate by centrifugation and filtration a light yellow solution was obtained. The solvent was removed *in vacuo* and the obtained solid washed with –40 °C cold *n*-pentane (2 x 4 mL). After drying *in vacuo* the product was obtained as a light yellow to peach-colored solid. Single crystals of **6** suitable for X-ray structure determination were obtained by storing a concentrated solution of **6** in diethyl ether at room temperature. Yield: 100 mg (60 µmol, 76%); ^{1}H NMR (C_6D_6, 303 K, 700 MHz, in ppm): δ = 7.21 (t, $^{3}J_{HH}$ = 7.7 Hz, C$H_{Ar,Dipp}$, 2 H), 7.07 (br. d, $^{3}J_{HH}$ = 7.0 Hz, CH_{Ar}, 2 H), 6.98 (m, CH_{Ar}, 2 H), 6.93 (d, $^{3}J_{HH}$ = 7.7 Hz, C$H_{Ar,Dipp}$, 4 H), 6.87 (br. s, CH_{Ar}, 4 H), 6.76 (br. s, CH_{Ar}, 2 H), 6.73 (dd, $^{3}J_{HH}$ = 8.5 Hz, $^{4}J_{HH}$ = 1.7 Hz, CH_{Ar}, 2 H), 6.50–6.43 (m, CH_{Ar}, 3 H), 6.16 (s, C(N(Dipp)CH)$_2$, 2 H), 5.72 (m, CH_{Ar}, 2 H), 2.50–2.40 (br. s & m, CH_{3Ar} & CH_{iPr}, 10 H), 2.37 (s, CH_{3Ar}, 3 H), 2.28 (br. s, CH_{3Ar}, 6 H), 2.24–2.15 (br. s, CH_{iPr}, 4 H), 2.12 (s, CH_{3Ar}, 6 H), 2.11–1.90 (br. s, CH_{3Ar}, 12 H), 1.29–1.07 (2 br. s, CH_{3iPr}, 24 H), 1.16 (d, ^{3}J = 6.9 Hz, C$H_{3iPr,Dipp}$, 12 H), 0.98 (d, ^{3}J = 6.9 Hz, C$H_{3iPr,Dipp}$, 12 H); ^{13}C{^{1}H} NMR (C_6D_6, 303 K, 176 MHz, in ppm): δ = 201.6 (br. s, O*C*(NPh)(PMes)), 197.4 (d, $^{2}J_{CP}$ = 65.9 Hz, *C*(N(Dipp)CH)$_2$), 161.9 (m, C_{qAr}), 150.0 (d, J_{CP} = 5.6 Hz, C_{qAr}), 145.3 (s, C_{qAr}), 144.9 (br. s, C_{qAr}), 142.2 (s, C_{qAr}), 137.9 (br. s, C_{qAr}), 135.8 (d, J_{CP} = 12.9 Hz, C_{qAr}), 135.0 (s, C_{qAr}), 134.5 (s, C_{qAr}), 133.6 (s, *C*H$_{Ar}$), 133.2 (s, *C*H$_{Ar}$), 133.0 (s, C_{qAr}), 131.1 (br. s, *C*H$_{Ar}$), 130.6 (s, *C*H$_{Ar}$), 128.1 (signal underneath C_6D_6 peak, *C*H$_{Ar}$), 127.3 (s, *C*H$_{Ar}$), 125.8 (s, *C*H$_{Ar}$), 124.4 (s, *C*H$_{Ar}$), 122.9 (s, C(N(Dipp)*C*H)$_2$), 122.8 (s, *C*H$_{Ar}$), 121.1 (s, C_{qAr}), 113.4 (m, C_{qAr}), 113.1 (m, *C*H$_{Ar}$), 28.9 (s, *C*H$_{iPr,Dipp}$), 26.1 (s, *C*H$_{3Ar}$), 26.0 (s, *C*H$_{3Ar}$), 24.3 (s, *C*H$_{3iPr,Dipp}$), 24.1 (s, *C*H$_{3iPr,Dipp}$), 23.6 (br. s, *C*H$_{3iPr}$), 21.5 (s, *C*H$_{3Ar}$), 21.2 (s, *C*H$_{3Ar}$), 20.7 (s, *C*H$_{3Ar}$), 20.0 (br. s, *C*H$_{3iPr}$), 19.5 (br. s, *C*H$_{3Ar}$), 18.1 (br. s, *C*H$_{iPr}$); ^{31}P NMR (C_6D_6, 303 K, 283 MHz, in ppm): δ = 4.0 (br. s, *P*N^{-}, 2 P), –42.0 (s, *P*(Au(IPr))Mes, 1 P); elemental analysis (in %): $C_{87}H_{114}AuLaN_5OP_3$: calcd.: C 62.40, H 6.86, N 4.18; found: C 62.77, H 6.78, N 4.28.

Alternative One Pot Syntheses of 5 and 6.

To a mixture of **2** (113 mg, 100 µmol, 1 eq.) in diethyl ether (4 mL) was added solid KHMDS (20 mg, 100 µmol, 1 eq.), upon which the solution turned yellow. The reaction mixture was stirred for 30 min at room temperature, after which either **(IPr)CuCl** (49 mg, 100 µmol, 1 eq.) or **(IPr)AuCl** (62 mg, 100 µmol, 1 eq.) was added as a solid, respectively. After stirring for 1 h at room temperature, a sample of the respective reaction solution (0.6 mL) was transferred to a J Young NMR tube equipped with a sealed C_6D_6 capillary (for a lock signal) and a ^{31}P NMR spectrum was measured. In each case, full and smooth conversion to either complex **5** or **6** could be ascertained (see Figures S47and S55). Work-up procedures were applicable as described above.

Preparation of 7.

To a mixture of **4** (480 mg, 430 µmol, 1 eq.) and **(^{Me}CAAC)CuCl** (160 mg, 430 µmol, 1 eq.) was added diethyl ether (1 mL) and the resulting suspension stirred for 1 h at room temperature. The orange suspension was centrifuged and filtered. After all volatile components of the solution were removed *in vacuo* the light orange solid was dissolved in toluene (1 mL) and filtered. The filtrate was concentrated *in vacuo* to dryness and the remaining solid washed with *n*-hexane (2 x 1 mL). After drying *in vacuo* the product was obtained as a light peach-colored solid. Single crystals of **7** suitable for X-ray structure determination were obtained by slow evaporation of solvent from a concentrated toluene solution of **7** at room temperature. Yield: 240 mg (172 µmol, 40%); ^{1}H NMR (C_6D_6, 303 K, 700 MHz, in ppm): δ = 7.30 (d, $^3J_{HH}$ = 7.7 Hz, C*H*$_{Ar}$, 2 H), 7.06 (t, $^3J_{HH}$ = 7.8 Hz, C*H*$_{Ar}$, 1 H), 7.01 (m, C*H*$_{Ar}$, 2 H), 6.97 (t, $^3J_{HH}$ = 7.7 Hz, C*H*$_{Ar}$, 2 H), 6.91 (br.s, C*H*$_{Ar}$, 4 H), 6.84–6.82 (m, C*H*$_{Ar}$, 4 H), 6.79–6.74 (m, C*H*$_{Ar}$, 3 H), 5.74 (m, C*H*$_{Ar}$, 2 H), 2.53 (br. s, C*H*$_{3Ar}$, 6 H), 2.40 (sept, $^3J_{HH}$ = 6.8 Hz, C*H*$_{iPr,Dipp}$, 2 H), 2.30 (br. s, C*H*$_{3Ar}$, 9 H), 2.26–2.20 (br. s, C*H*$_{iPr}$, 4 H), 2.16 (s, C*H*$_{3Ar}$, 6 H), 2.14–2.07 (br. s, C*H*$_{3Ar}$, 12 H), 1.28 (s, C*H*$_{2CAAC}$, 2 H), 1.27–1.15 (2 br. s, C*H*$_{3iPr}$, 24 H), 1.10 (s, C*H*$_{3CAAC}$, 6 H), 0.96 (d, ^3J = 6.8 Hz, C*H*$_{3iPr,Dipp}$, 6 H), 0.78 (d, $^3J_{HH}$ = 6.8 Hz, C*H*$_{3iPr,Dipp}$, 6 H), 0.73 (s, C*H*$_{3CAAC}$, 6 H); ^{13}C{^{1}H} NMR (C_6D_6, 303 K, 176 MHz, in ppm): δ = 251.4 (d, $^2J_{CP}$ = 41.5 Hz, $C_{carbene}$), 201.3 (d, $^1J_{CP}$ = 46.3 Hz, O*C*(NPh)(PMes)), 162.1 (m, C_{qAr}), 151.9 (d, J_{CP} = 5.2 Hz, C_{qAr}), 145.2 (s, C_{qAr}), 144.5 (br. s, C_{qAr}), 142.5 (s, C_{qAr}), 137.7 (br. s, C_{qAr}), 136.6 (s, C_{qAr}), 135.6 (d, J_{CP} = 9.6 Hz, C_{qAr}), 134.6 (s, C_{qAr}), 134.4 (s, C_{qAr}), 133.7 (s, *C*H$_{Ar}$), 133.2 (s, *C*H$_{Ar}$), 132.9 (s, C_{qAr}), 131.1 (br. s, *C*H$_{Ar}$), 129.6 (s, *C*H$_{Ar}$), 128.2 (signal underneath C_6D_6 peak, *C*H$_{Ar}$), 127.7 (d, J_{CP} = 4.0 Hz, *C*H$_{Ar}$), 125.8 (d, J_{CP} = 3.5 Hz, *C*H$_{Ar}$), 124.8 (s, *C*H$_{Ar}$), 122.4 (s, *C*H$_{Ar}$), 121.0 (s, C_{qAr}), 113.6 (m, C_{qAr}), 113.1 (m, *C*H$_{Ar}$), 80.8 (s, C_{qCAAC}), 54.4 (s, C_{qCAAC}), 49.6 (s, *C*H$_{2CAAC}$), 29.1 (s, *C*H$_{iPr,Dipp}$), 28.8 (s, *C*H$_{3CAAC}$), 28.5 (s, *C*H$_{3CAAC}$), 26.9 (br. s, *C*H$_{3iPr,Dipp}$), 26.3 (s, *C*H$_{3Ar}$), 26.2 (s, *C*H$_{3Ar}$), 23.8 (br. s, *C*H$_{3iPr}$), 22.7 (s, *C*H$_{3iPr,Dipp}$), 21.5 (s, *C*H$_{3Ar}$), 21.3 (s, *C*H$_{3Ar}$), 20.7 (s, *C*H$_{3Ar}$), 20.1 (br. s, *C*H$_{3iPr}$), 19.6 (br. s, *C*H$_{3Ar}$), 18.0 (br. s, *C*H$_{iPr}$); ^{31}P NMR (C_6D_6, 303 K, 283 MHz, in ppm): δ = 3.7 (s, *P*N$^-$, 2 P), −63.7 (s, *P*(Cu(CAAC))Mes, 1 P); elemental analysis (in %): $C_{80}H_{109}CuLaN_4OP_3$: calcd.: C 66.81, H 7.64, N 3.90; found: C 66.70, H 7.50, N 3.68.

Preparation of 8.

<u>*Route A:*</u> To a mixture of **4** (72 mg, 64 µmol, 1 eq.) and **(^{Me}CAAC)AuCl** (33 mg, 64 µmol, 1 eq.) was added diethyl ether (1 mL) and the resulting suspension stirred for 1 h at room temperature. The orange suspension was centrifuged and filtered. After all volatile components of the solution were removed *in vacuo* the light orange solid was dissolved in toluene (0.5 mL) and filtered. The filtrate was dried *in vacuo* and the remaining solid washed with *n*-hexane (2 x 1 mL). After drying *in vacuo* a light peach-colored solid was obtained. Repeated recrystallization and washing attempts to purify this raw product failed and no yield could be determined. However, NMR spectroscopy clearly showed that **8** is the main product of the reaction, since the ^{1}H NMR data are comparable to those of **7** (compare Figures S56 and S65) and the distinctive ^{13}C and ^{31}P resonances can be confidently assigned to the PN, phosphaureate and carbene ligands, in analogy to complexes **5** – **7** (see Figures S66 and S67).

<u>*Route B:*</u> To a mixture of **2** (54 mg, 49 µmol, 1 eq.) and **(^{Me}CAAC)Au(HMDS)** (32 mg, 49 µmol, 1 eq.) was added toluene (5 mL) and the resulting light yellow solution heated to 120 °C for 13 d. The progress of

the reaction was checked regularly (every few days, see Figure 68) by $^{31}P\{^{1}H\}$ NMR spectroscopy of the reaction mixture to which a C_6D_6 capillary was added (for a lock signal). Although the desired complex **8** was found to be the main product, presumably due to decomposition during the prolonged heating, protonated ligand **HPN** had also formed in significant amounts. After cooling to room temperature, filtration and concentration of the filtrate to about 0.5 mL volume, only non-reacted **(MeCAAC)Au(HMDS)** could be crystallized from the mixture. Several attempts to remove **HPN** by washing with –40 °C cold *n*-hexane or hexamethyldisiloxane (HMDSO) failed, since complex **8** also readily dissolved in these solvents. Attempts to crystallize the desired product **8** from concentrated toluene, *n*-hexane or HMDSO solutions at room temperature or –40 °C also failed.

^{1}H NMR (C_6D_6, 303 K, 700 MHz, in ppm): δ = 7.33 (d, $^{3}J_{HH}$ = 7.8 Hz, CH_{Ar}, 2 H), 7.06 (t, $^{3}J_{HH}$ = 7.8 Hz, CH_{Ar}, 2 H), 7.04 (t, $^{3}J_{HH}$ = 7.8 Hz, CH_{Ar}, 1H), 7.02–7.00 (m, CH_{Ar}, 2 H), 6.94–6.91 (m, CH_{Ar}, 4 H), 6.84–6.81 (m, CH_{Ar}, 2 H), 6.80–6.78 (m, CH_{Ar}, 2 H), 6.77–6.74 (m, CH_{Ar}, 2 H), 5.75–5.72 (m, CH_{Ar}, 2 H), 2.56 (br. s, CH_{3Ar}, 6 H), 2.38 (sept, $^{3}J_{HH}$ = 6.8 Hz, C$H_{iPr,Dipp}$, 2 H), 2.32 (s, CH_{3Ar}, 6 H), 2.30 (s, CH_{3Ar}, 3 H), 2.26 (br. s, CH_{iPr}, 4 H), 2.15 (s, CH_{3Ar}, 6 H), 2.12–2.05 (br. s, CH_{3Ar}, 12 H), 1.33 (s, CH_{2CAAC}, 2 H), 1.25–1.18 (br. s, CH_{3iPr}, 24 H), 1.19 (s, CH_{3CAAC}, 6 H), 0.96 (d, $^{3}J_{HH}$ = 6.8 Hz, C$H_{3iPr,Dipp}$, 6 H), 0.90 (br. d, $^{3}J_{HH}$ = 6.8 Hz, C$H_{3iPr,Dipp}$, 6 H), 0.73 (s, CH_{3CAAC}, 6 H); $^{13}C\{^{1}H\}$ NMR (C_6D_6, 303 K, 176 MHz, in ppm, only distinctive resonances listed): δ = 258.4 (d, $^{2}J_{CP}$ = 62 Hz, $C_{carbene}$), 202.2 (d, $^{1}J_{CP}$ = 48 Hz); ^{31}P NMR (C_6D_6, 303 K, 283 MHz, in ppm): δ = 3.8 (s, *P*N^{-}, 2 P), –38.2 (s, *P*(Au(CAAC))Mes, 1 P).

X-ray Crystallography

Single crystals for X-ray diffraction experiments were measured at the analytical facility of the Paderborn University using a Bruker Smart AXS or a Bruker D8 Venture instrument. All crystals were kept at 130(2) K or 120(2) K throughout data collection. Data collection was performed using either the APEXIII or the Smart software package. Data refinement and reduction were performed with Bruker Saint (V8.34A). All structures were solved with SHELXT[7] and refined using the OLEX 2 software package.[8] All non-hydrogen atoms were refined anisotropically, and hydrogen atoms were included at the geometrically calculated positions and refined using a riding model. All structures have been submitted to the CCDC and can be obtained under the numbers presented in Table S1. For further crystallographic details regarding crystal measurements, please check Tables S1 and S2. The quality of the data obtained for **4** was very poor. Problems during the integration led to high R_{int} values and an incomplete dataset. Many atomic displacement parameters refine to negative values and R1 will not improve to less than about 25%. The model as such cannot be considered reliable. However, it matches well with other analytical means suggesting that at least the connectivity and overall conformation of the molecule are correctly described.

2. NMR Spectra

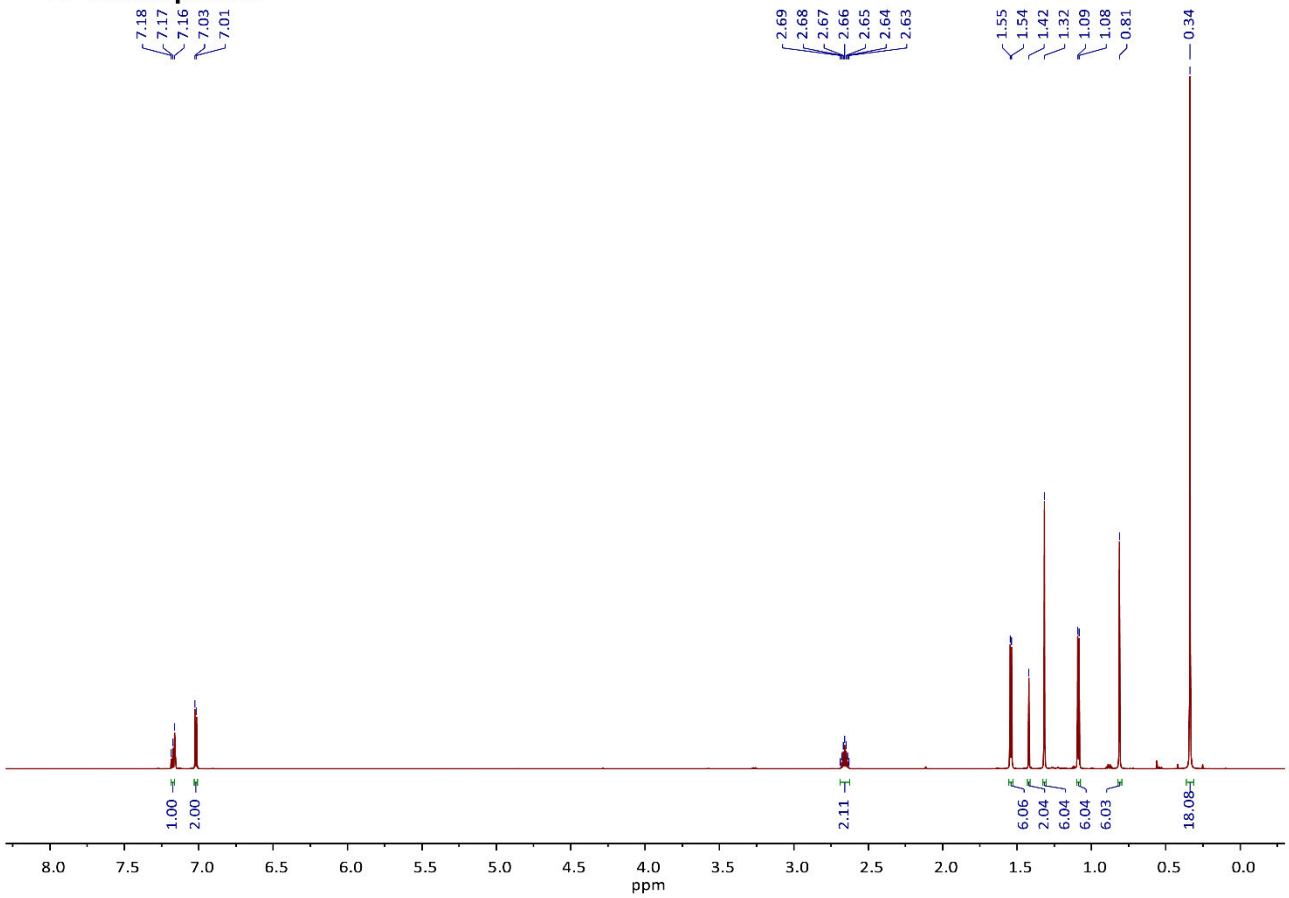

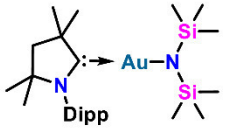

Figure S1: *^{1}H NMR spectrum of **(^{Me}CAAC)Au(HMDS)** in C_6D_6 (303 K).*

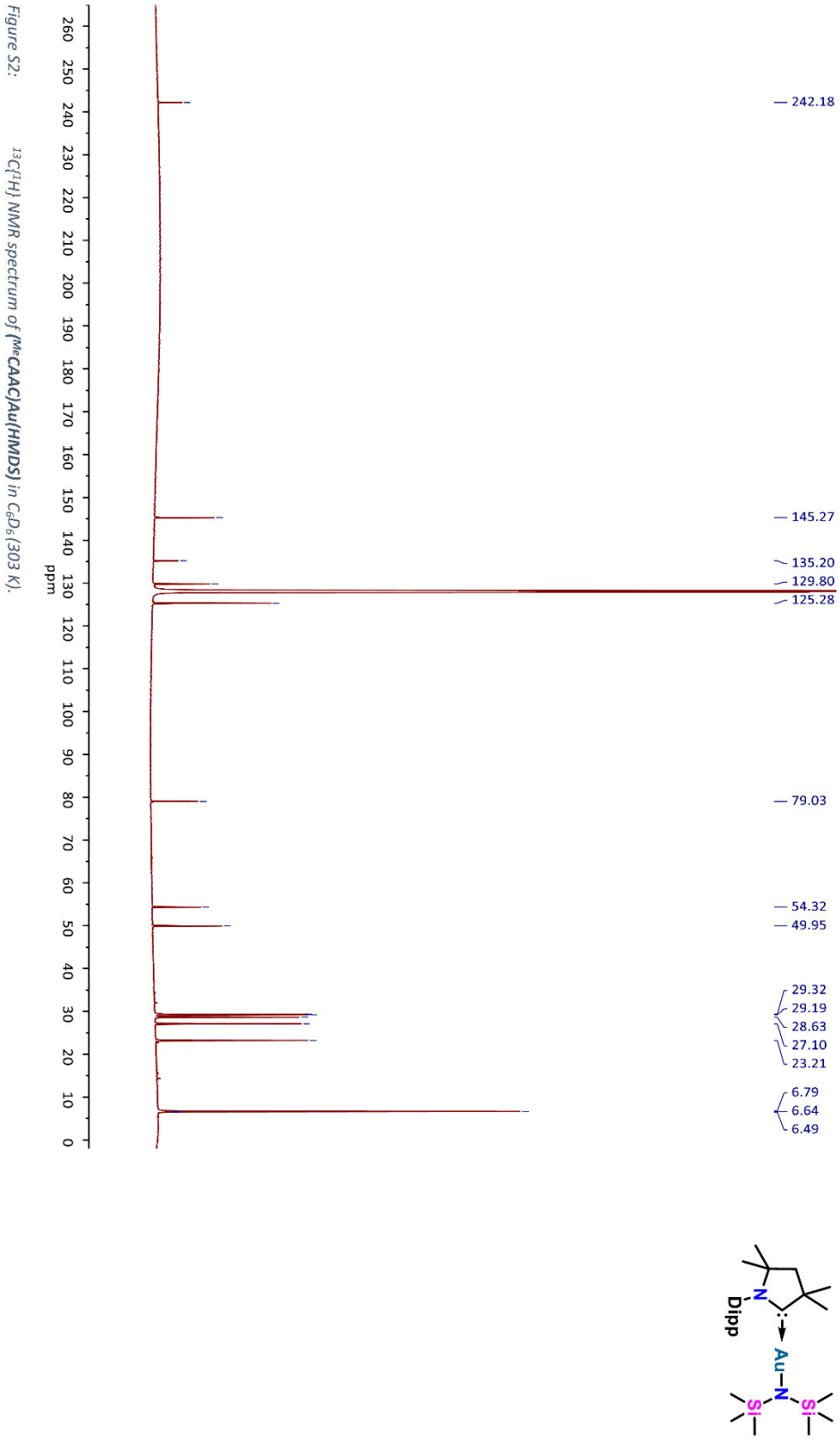

Figure S2: $^{13}C\{^1H\}$ *NMR spectrum of* ***[^{Me}CAAC]Au(HMDS)*** *in* C_6D_6 *(303 K).*

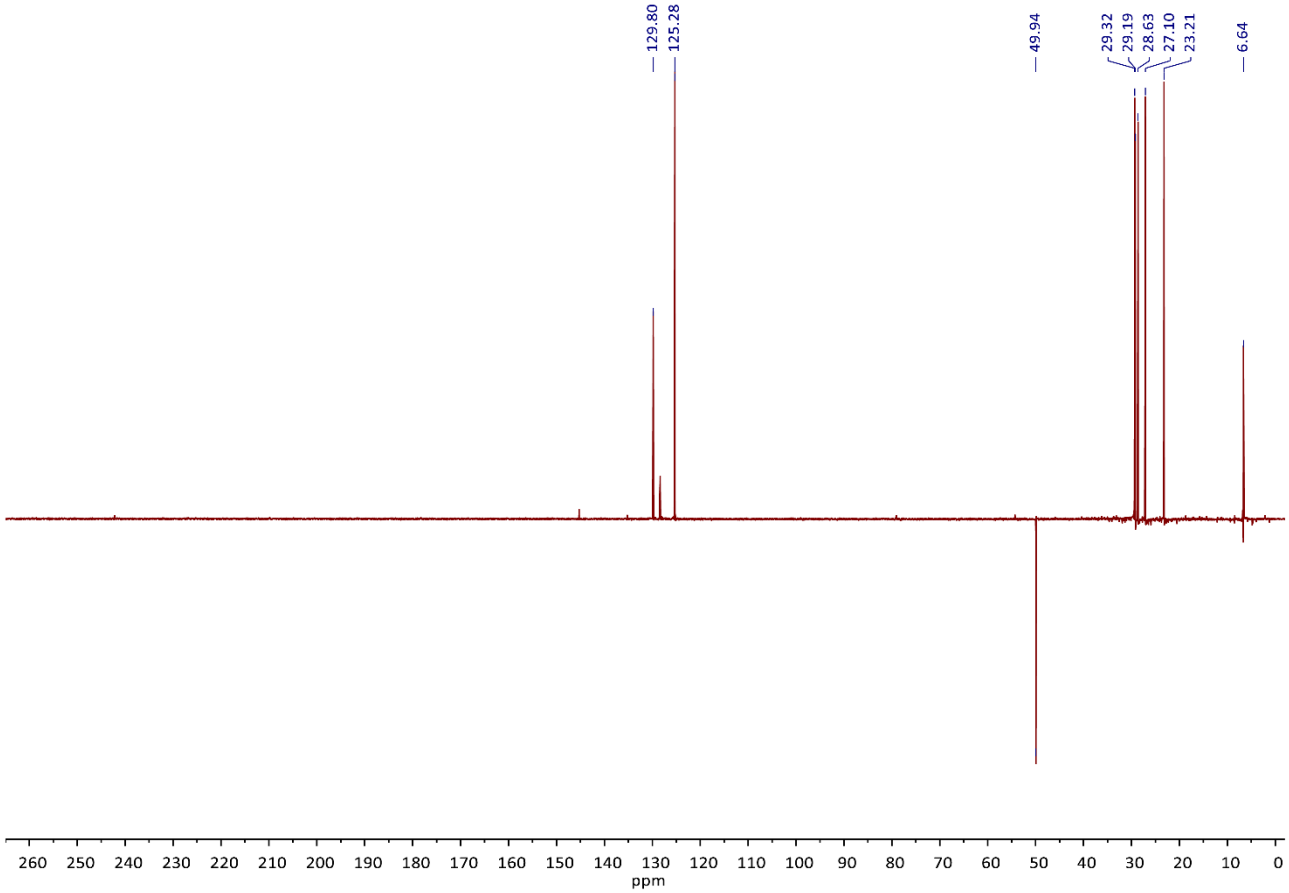

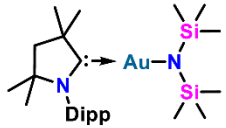

Figure S3: *$^{13}C\{^{1}H\}$ DEPT135 NMR spectrum of **(^{Me}CAAC)Au(HMDS)** in C_6D_6 (303 K). The negative spike at δ 6.6 ppm is an artefact of manual phase correction.*

Figure S4: $^{29}Si\{^1H\}$ *NMR spectrum of* $[^{Me}CAAC]Au(HMDS)$ *in* C_6D_6 *(303 K).*

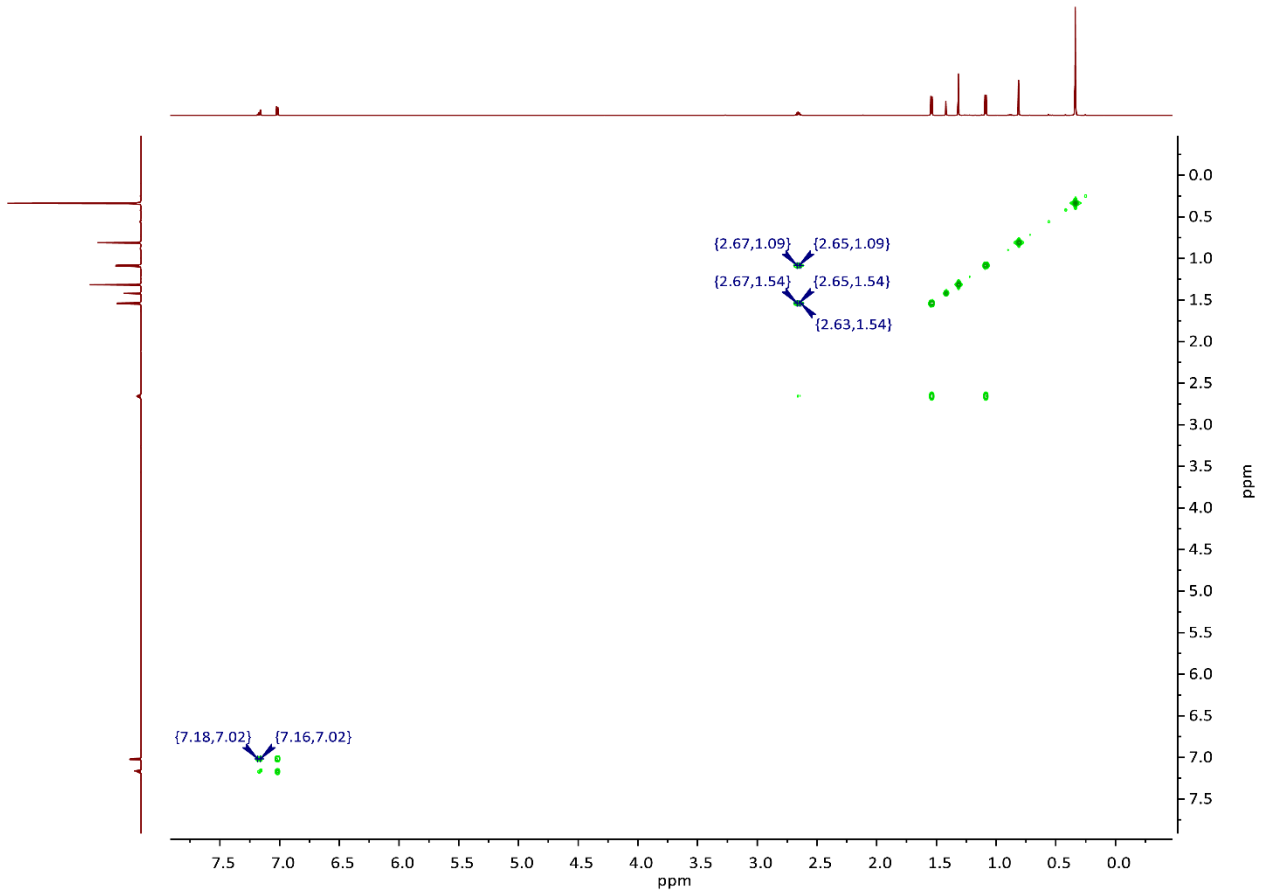

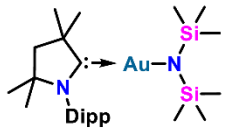

Figure S5: *^{1}H–^{1}H COSY NMR spectrum of **(^{Me}CAAC)Au(HMDS)** in C_6D_6 (303 K).*

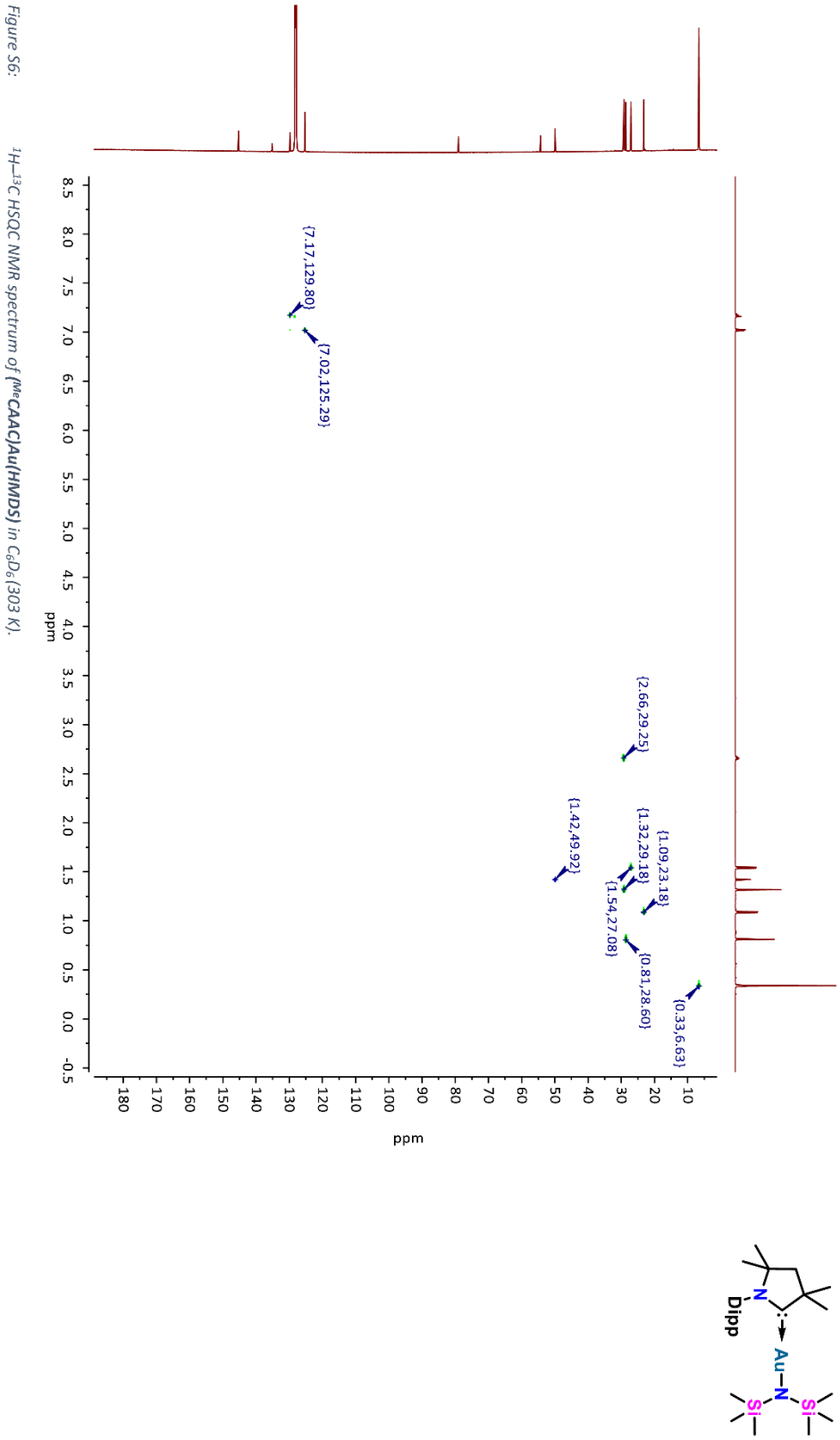

Figure S6: *^{1}H–^{13}C HSQC NMR spectrum of* ***[^{Me}CAAC]Au(HMDS)*** *in C_6D_6 (303 K).*

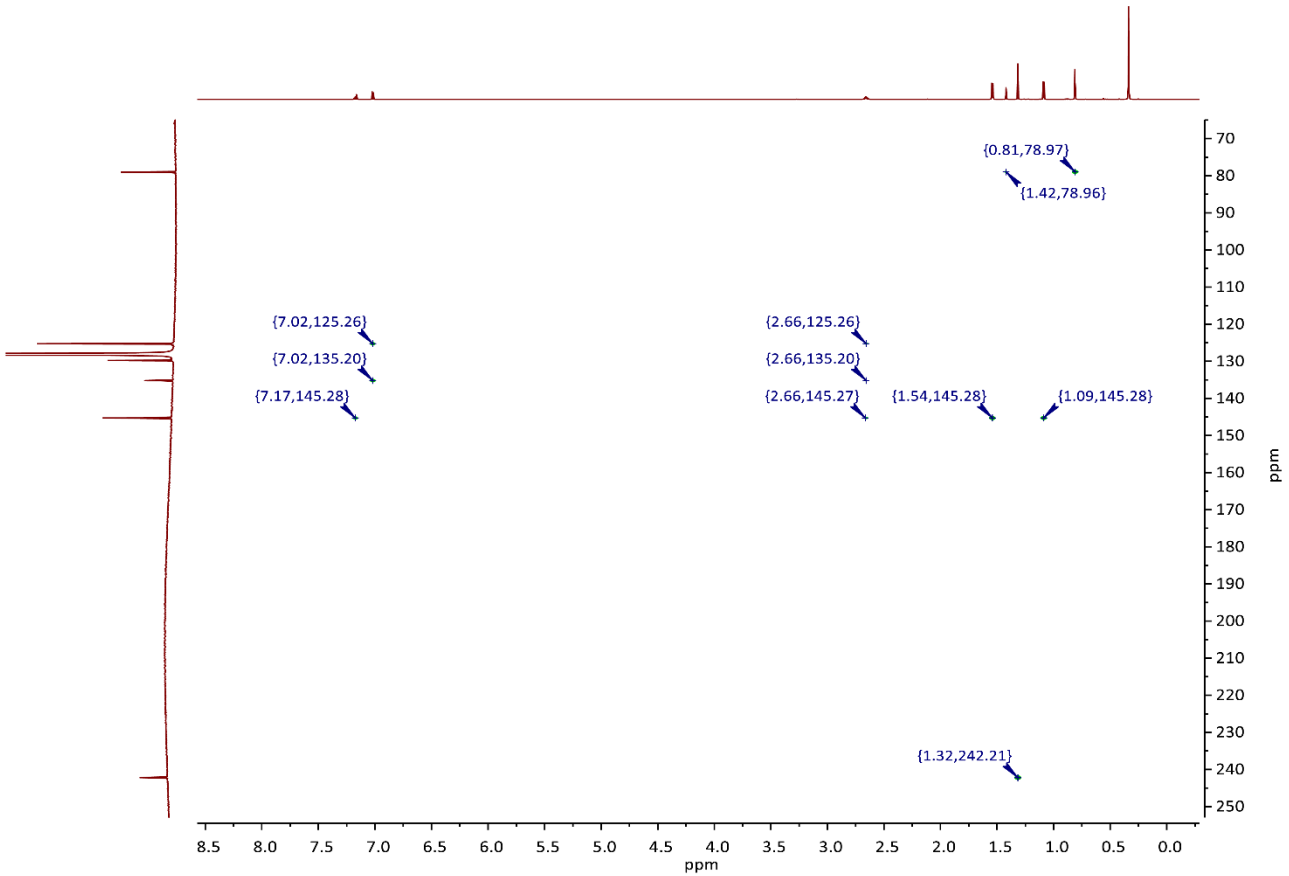

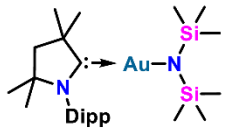

Figure S7: *^{1}H–^{13}C HMBC NMR spectrum of* ***(^{Me}CAAC)Au(HMDS)*** *in C_6D_6 (303 K).*

Figure S8: ^{1}H–^{15}N HMBC NMR spectrum of **[^{Me}CAAC]Au(HMDS)** in C_6D_6 (303 K).

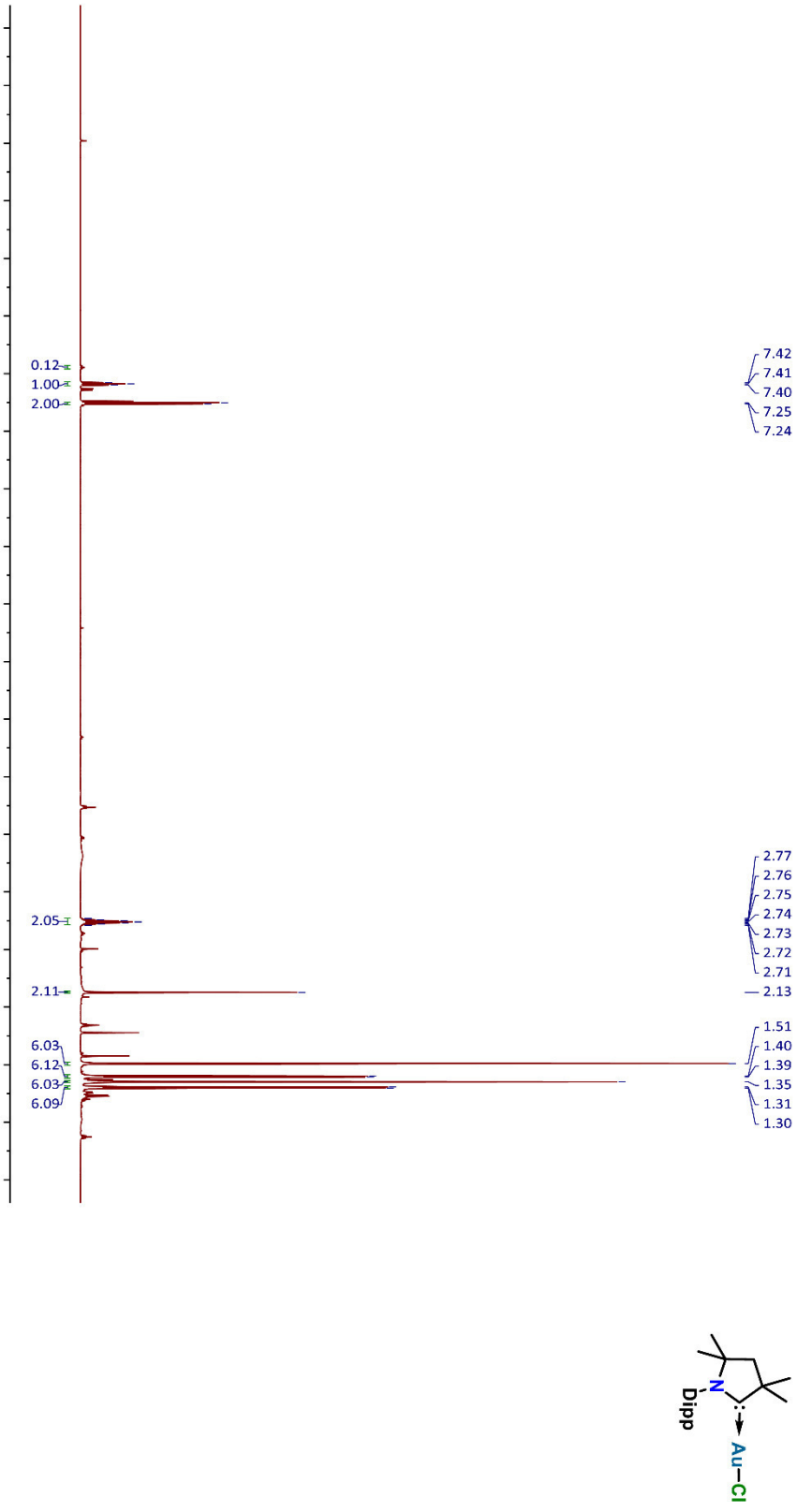

*Figure S9: ^{1}H NMR spectrum of crude **[^{Me}CAAC]AuCl** in $CDCl_3$ (303 K). The resonances at δ 9.52, 7.55, 7.36, 2.51, 1.78, 1.58, 1.37 and 1.23 ppm can be assigned to impurities of ≈10 mol% [H^{Me}CAAC]Cl. The resonances at δ 3.74 and 1.84 ppm result from residual THF.*

Figure S10: $^{13}C\{^1H\}$ NMR spectrum of crude ***[IMeCAAC]AuCl*** in $CDCl_3$ (303 K). Due to impurities of $[H^{Me}CAAC]Cl$, the less intense resonance of $CH_{iPr,Dipp}$ cannot be assigned confidently. The resonances at δ 67.8 and 25.6 ppm result from residual THF.

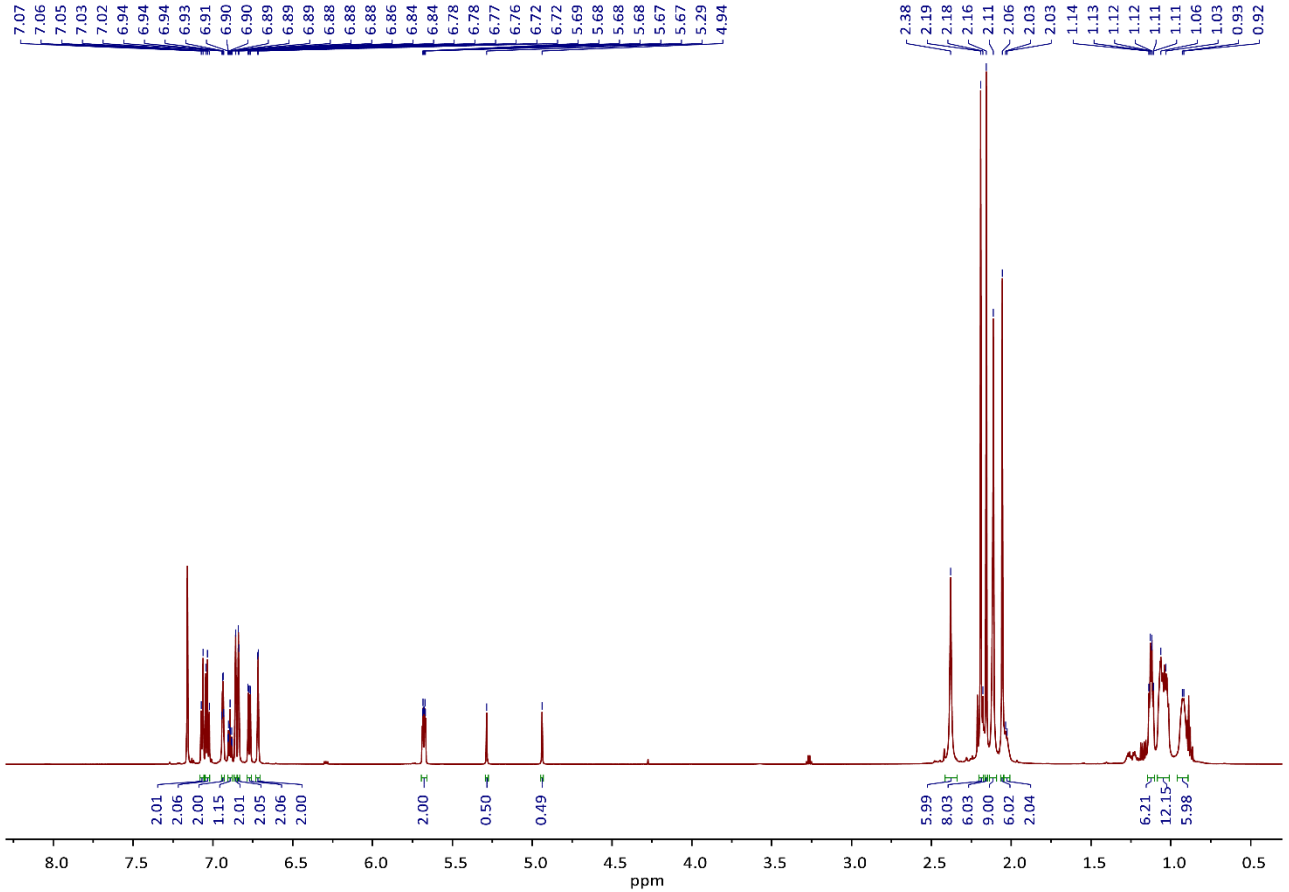

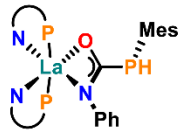

2

Figure S11: *^{1}H NMR spectrum of **2** in C_6D_6 (303 K). The resonances at δ 4.27 and 3.27 ppm result from small contaminations with dichloromethane and diethyl ether; the ones at δ 1.24, 1.23, 0.88 and 0.87 ppm belong to residual n-hexane and n-pentane.*

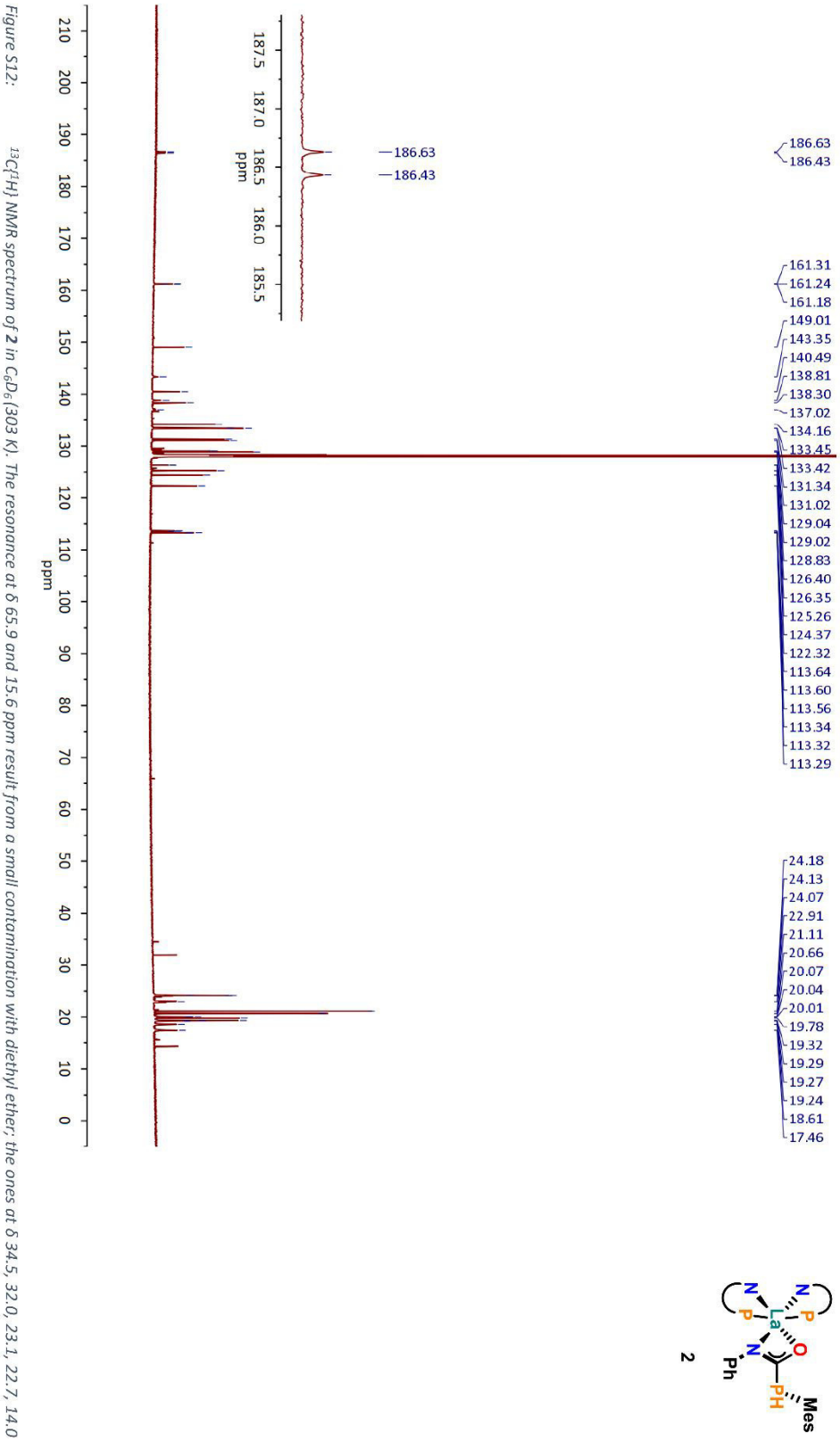

*Figure S12: $^{13}C\{^{1}H\}$ NMR spectrum of **2** in C_6D_6 (303 K). The resonance at δ 65.9 and 15.6 ppm result from a small contamination with diethyl ether, the ones at δ 34.5, 32.0, 23.1, 22.7, 14.0 and 14.3 ppm belong to residual n-hexane and n-pentane. The detail shows the characteristic doublet splitting of the $C_{phosphaureate}$ resonance caused by ^{1}J coupling to $P_{phosphaureate}$.*

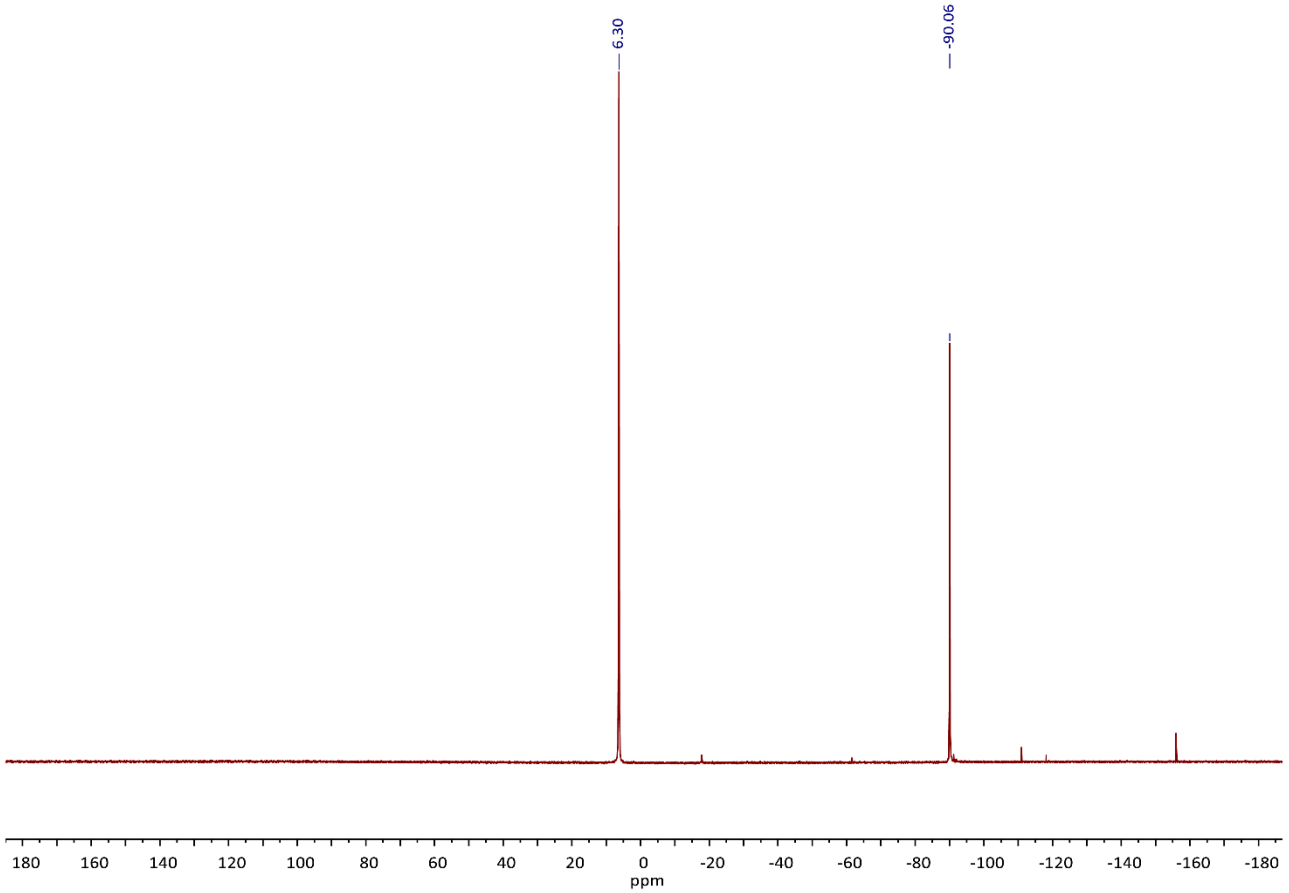

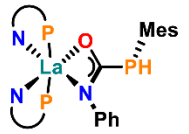

2

Figure S13: *$^{31}P\{^{1}H\}$ NMR spectrum of **2** in C_6D_6 (303 K). The resonances at δ –17.8 and –155.9 ppm can be assigned to traces of **HPN** and mesitylphosphine, respectively.*

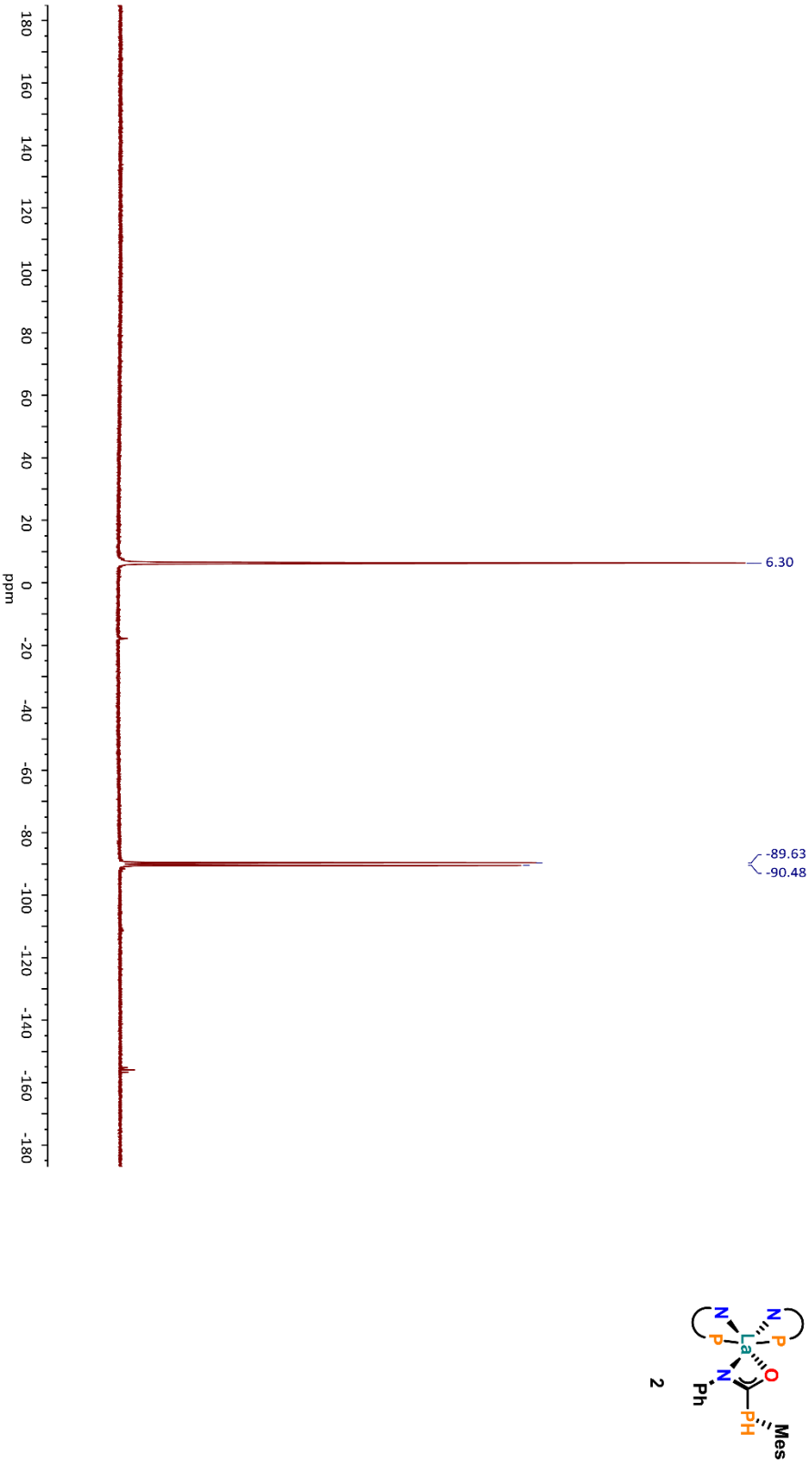

Figure S14: ^{31}P *NMR spectrum of* **2** *in* C_6D_6 *(303 K). The resonances at δ −17.8 and −155.9 ppm can be assigned to traces of* ***HPN*** *and mesitylphosphine, respectively.*

Figure S15: ^{1}H–^{1}H *COSY NMR spectrum of* **2** *in* C_6D_6 *(303 K).*

2

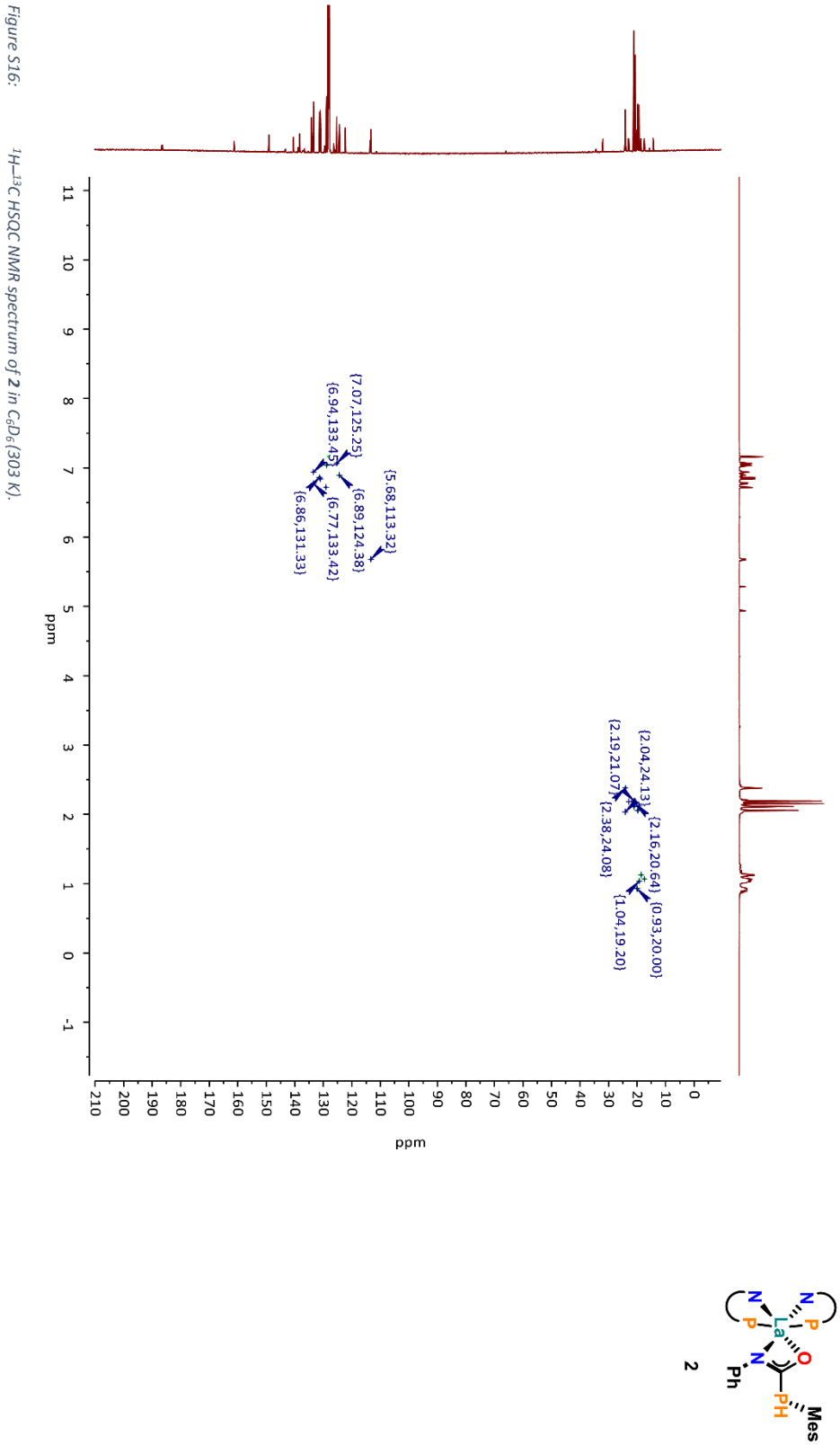

Figure S16: *^{1}H–^{13}C HSQC NMR spectrum of **2** in C_6D_6 (303 K).*

2

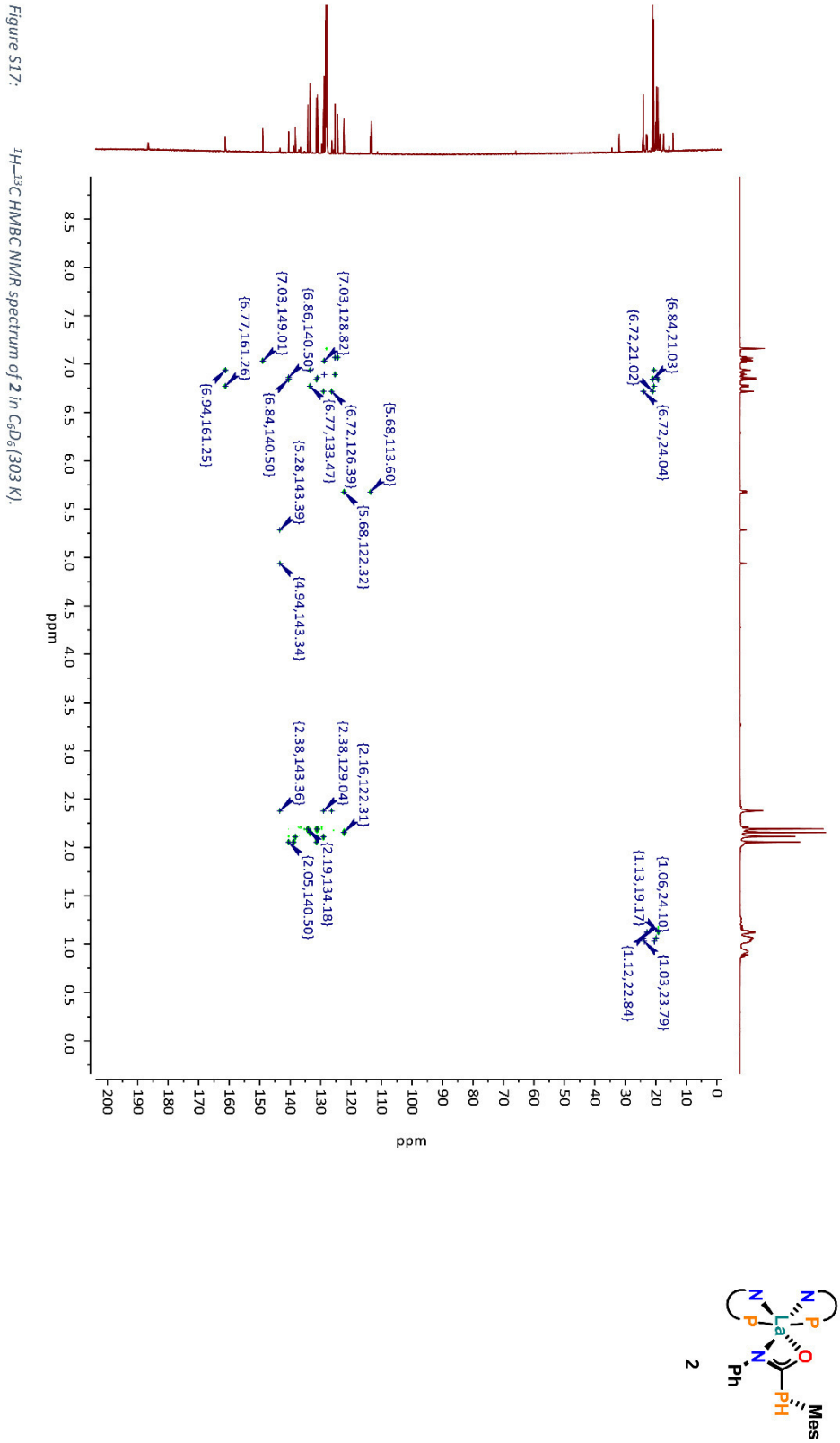

Figure S17: ^{1}H–^{13}C *HMBC NMR spectrum of* **2** *in* C_6D_6 *(303 K).*

2

Figure S18: ^{1}H–^{15}N *HMBC NMR spectrum of* **2** *in* C_6D_6 *(303 K).*

2

*Figure S19: ^{1}H NMR spectrum of **3** in C_6D_6 (303 K). The resonances at δ 3.27 and 1.12 ppm result from a small contamination with diethyl ether; the ones at δ 1.23 and 0.89 ppm belong to residual n-hexane.*

Figure S20: $^{13}C\{^1H\}$ NMR spectrum of **3** in C_6D_6 (303 K). The resonances at δ 65.9 and 15.6 ppm result from a small contamination with diethyl ether; the ones at δ 32.0, 23.0 and 14.4 ppm belong to residual n-hexane.

S27

Figure S21: $^{31}P\{^{1}H\}$ *NMR spectrum of* ***3*** *in* C_6D_6 *(303 K). The peak at δ –17.8 ppm can be assigned to traces of* ***HPN****.*

3

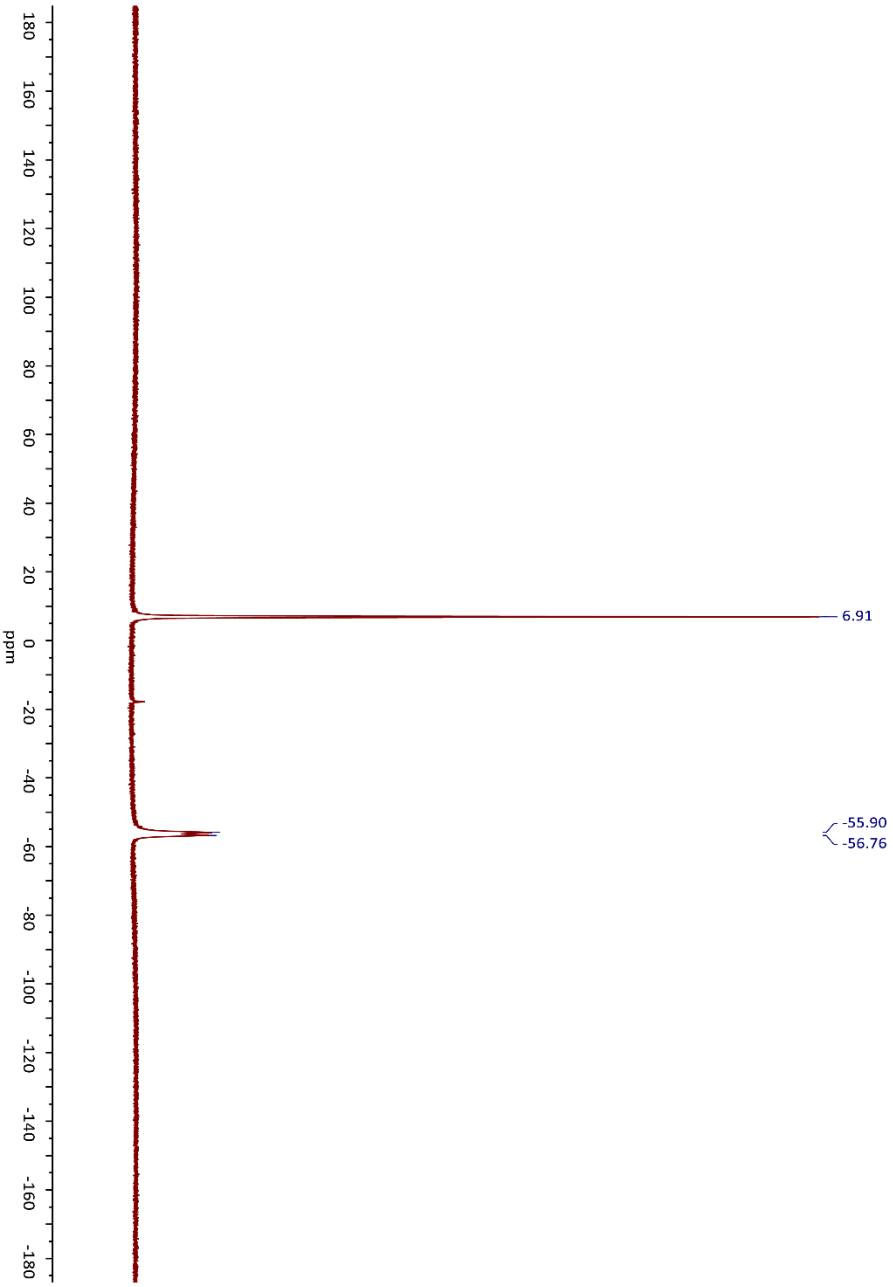

Figure S22: ^{31}P *NMR spectrum of* ***3*** *in* C_6D_6 *(303 K). The peak at δ –17.8 ppm can be assigned to traces of* ***HPN****.*

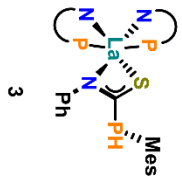

3

S29

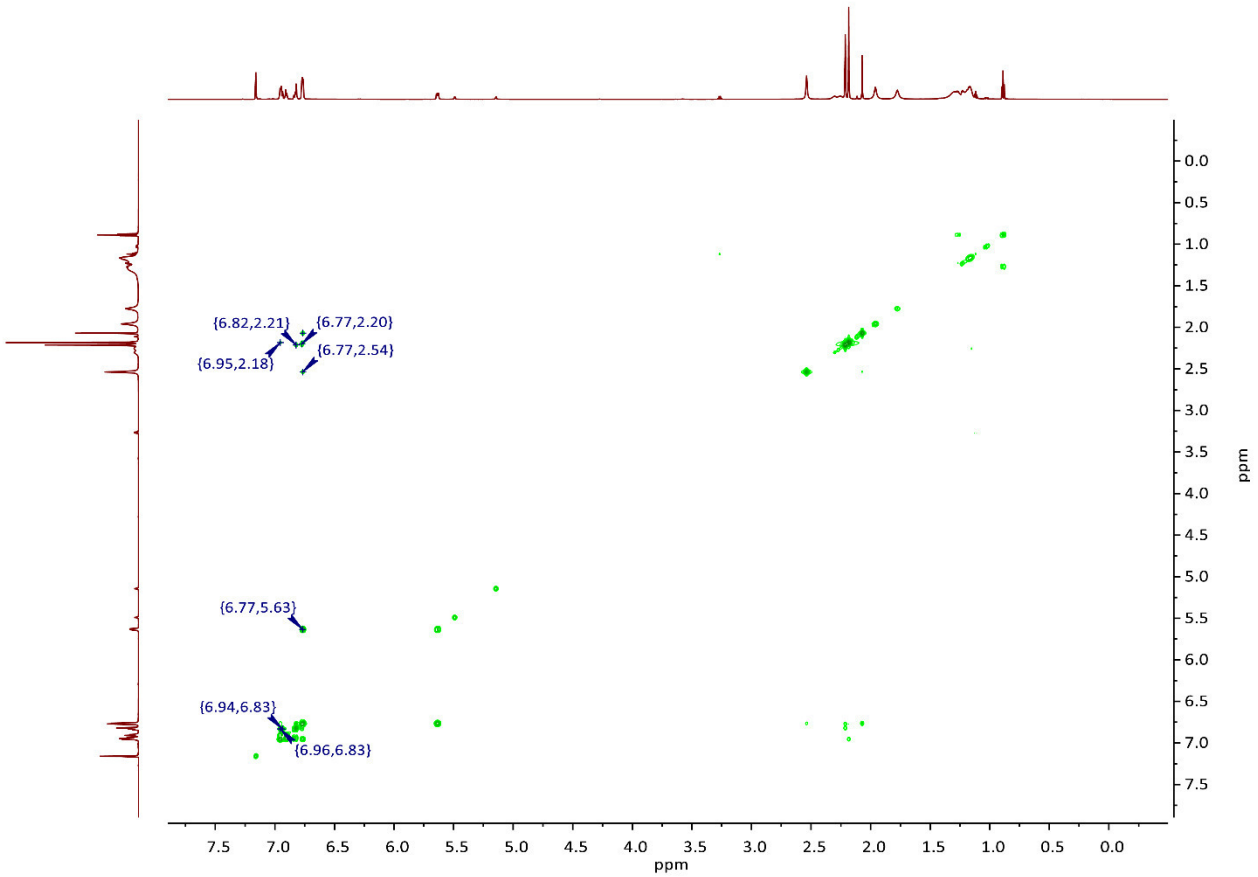

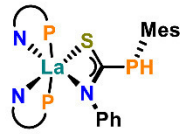

3

Figure S23: *^{1}H–^{1}H COSY NMR spectrum of **3** in C_6D_6 (303 K).*

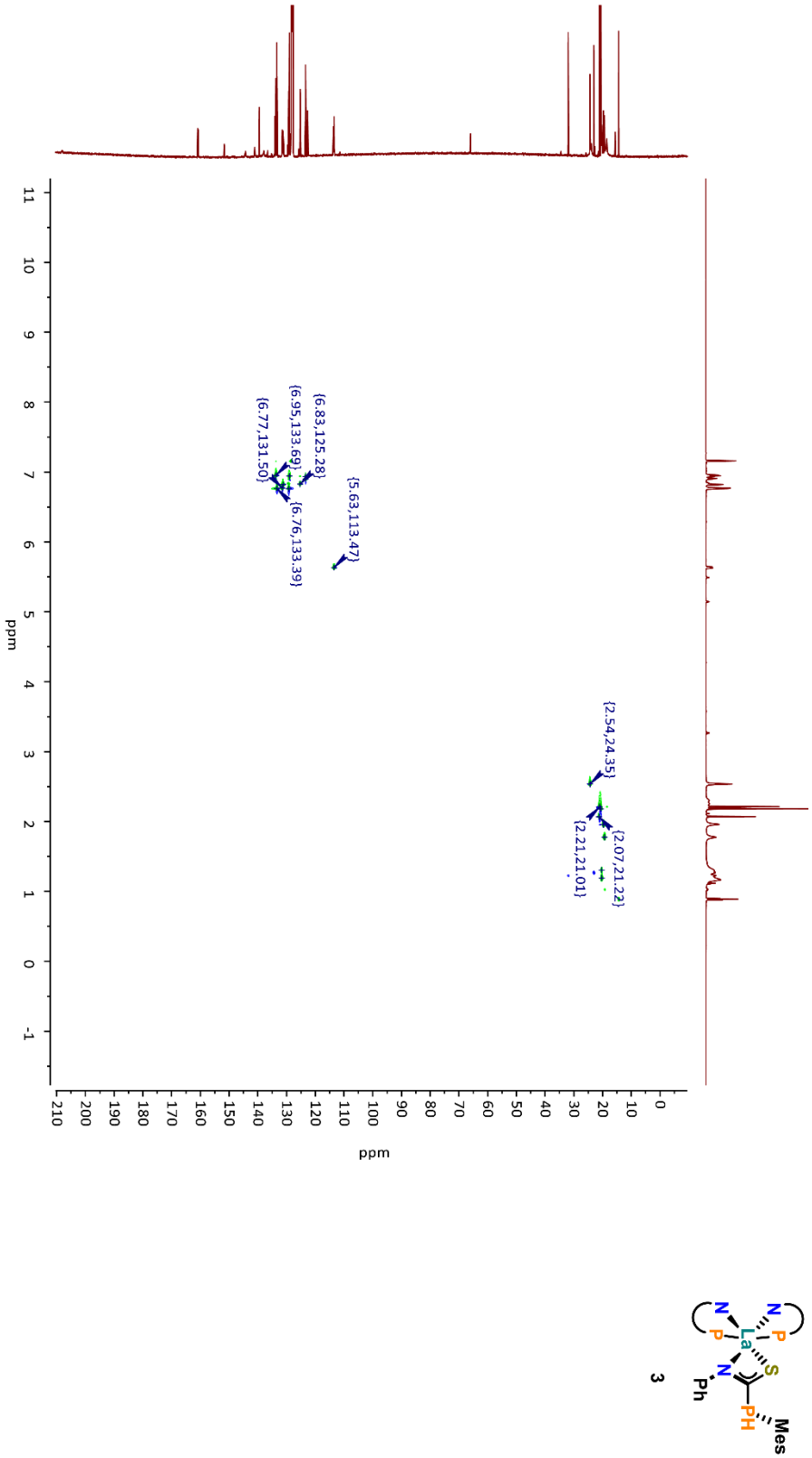

Figure S24. ^{1}H–^{13}C HSQC NMR spectrum of **3** in C_6D_6 (303 K).

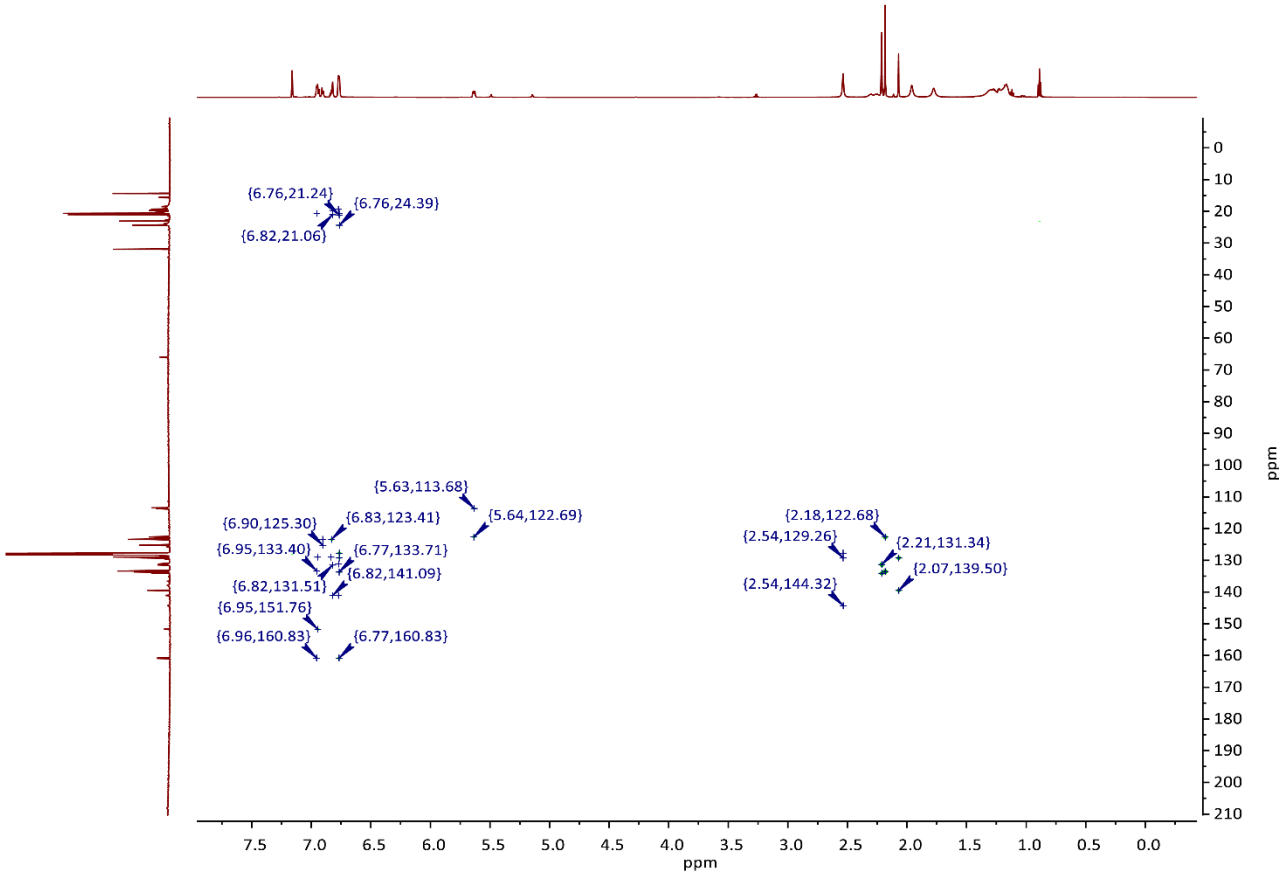

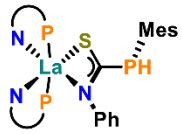

3

Figure S25: *^{1}H–^{13}C HMBC NMR spectrum of **3** in C_6D_6 (303 K).*

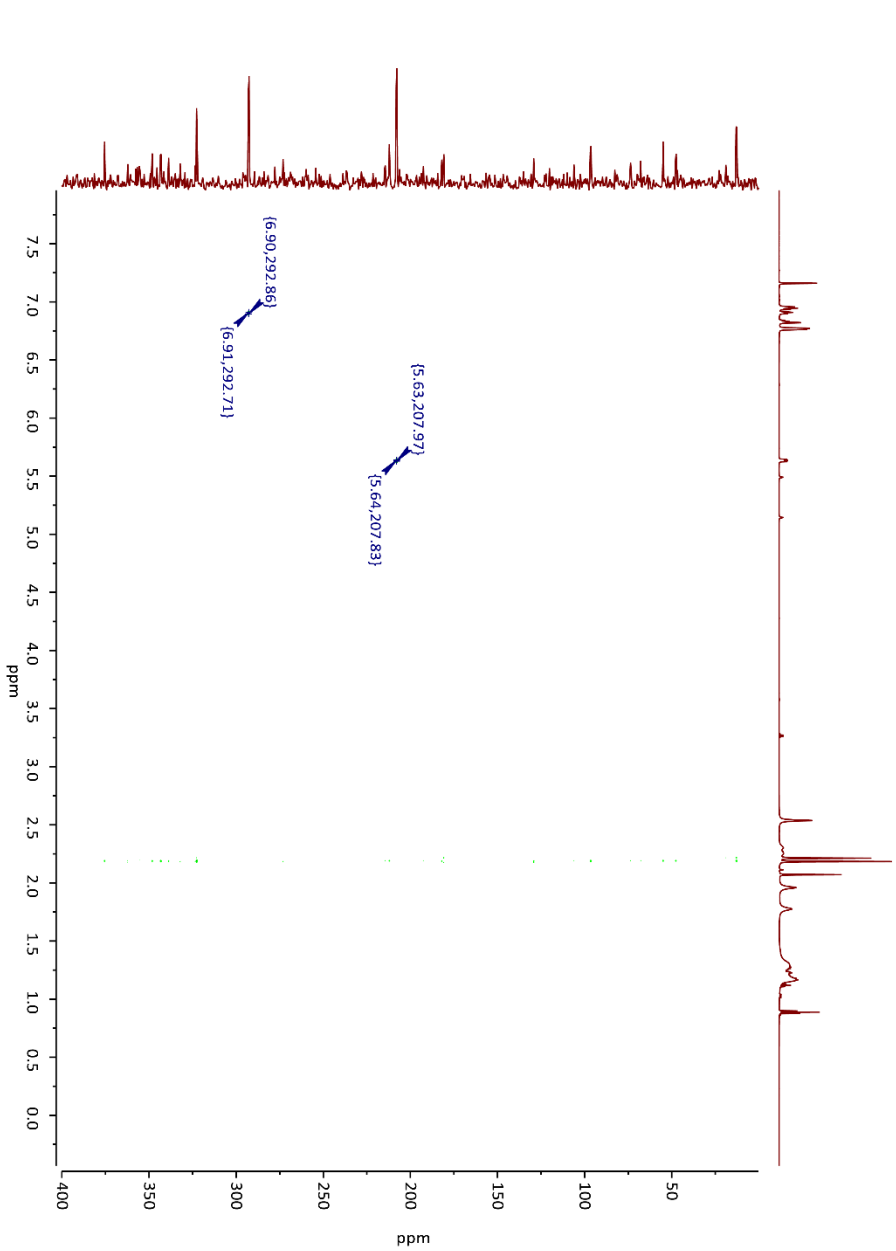

Figure S26: ^{1}H–^{15}N *HMBC NMR spectrum of* **3** *in* C_6D_6 *(303 K).*

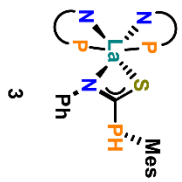

3

S33

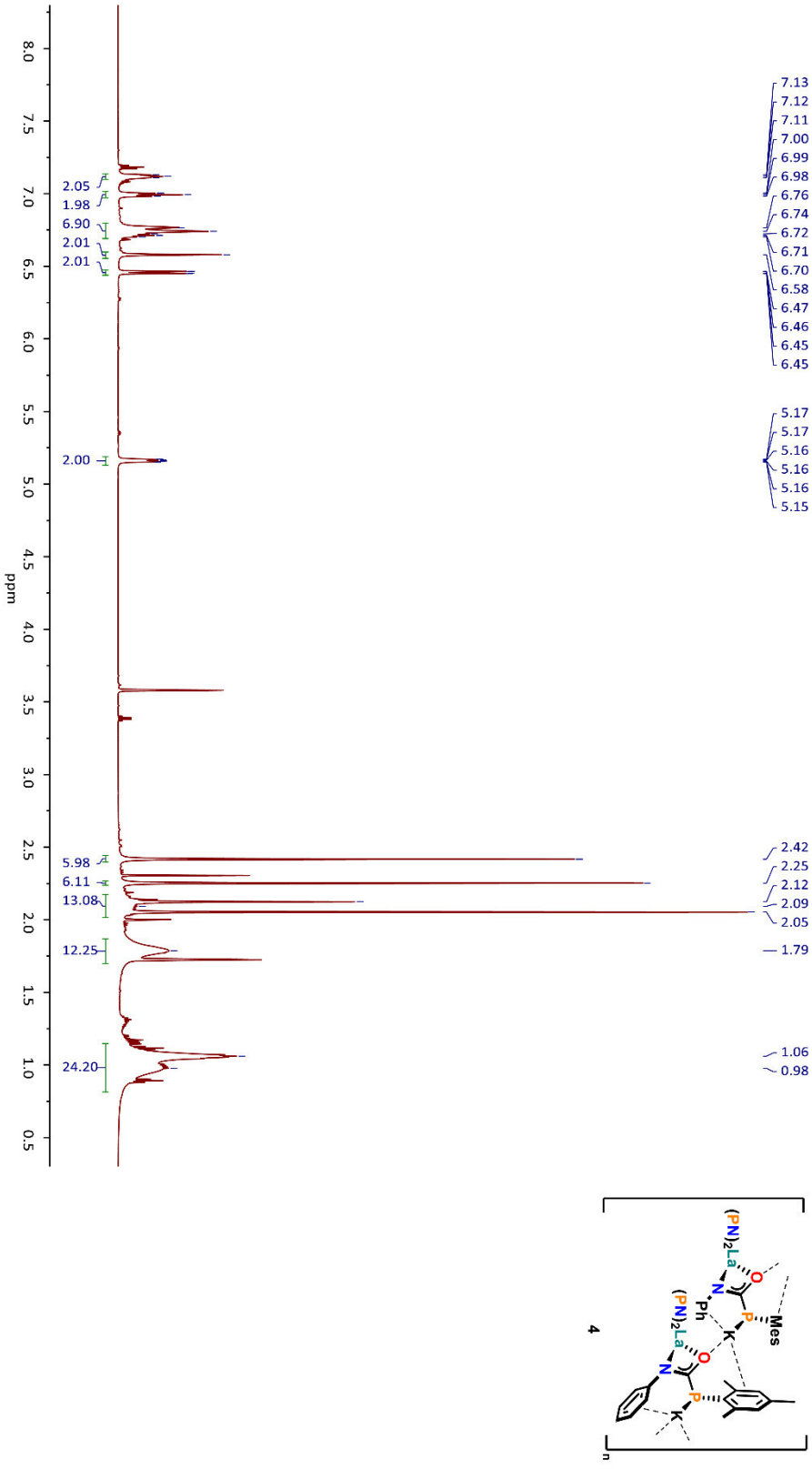

Figure S27: *^{1}H NMR spectrum of **4** in THF-d_8 (303 K). The resonances at δ 7.18, 7.08 and 2.31 ppm can be assigned to residual toluene, the ones at δ 1.29 and 0.29 ppm to residual n-pentane. The resonances at δ 3.39 and 1.12 ppm result from a small contamination with diethyl ether.*

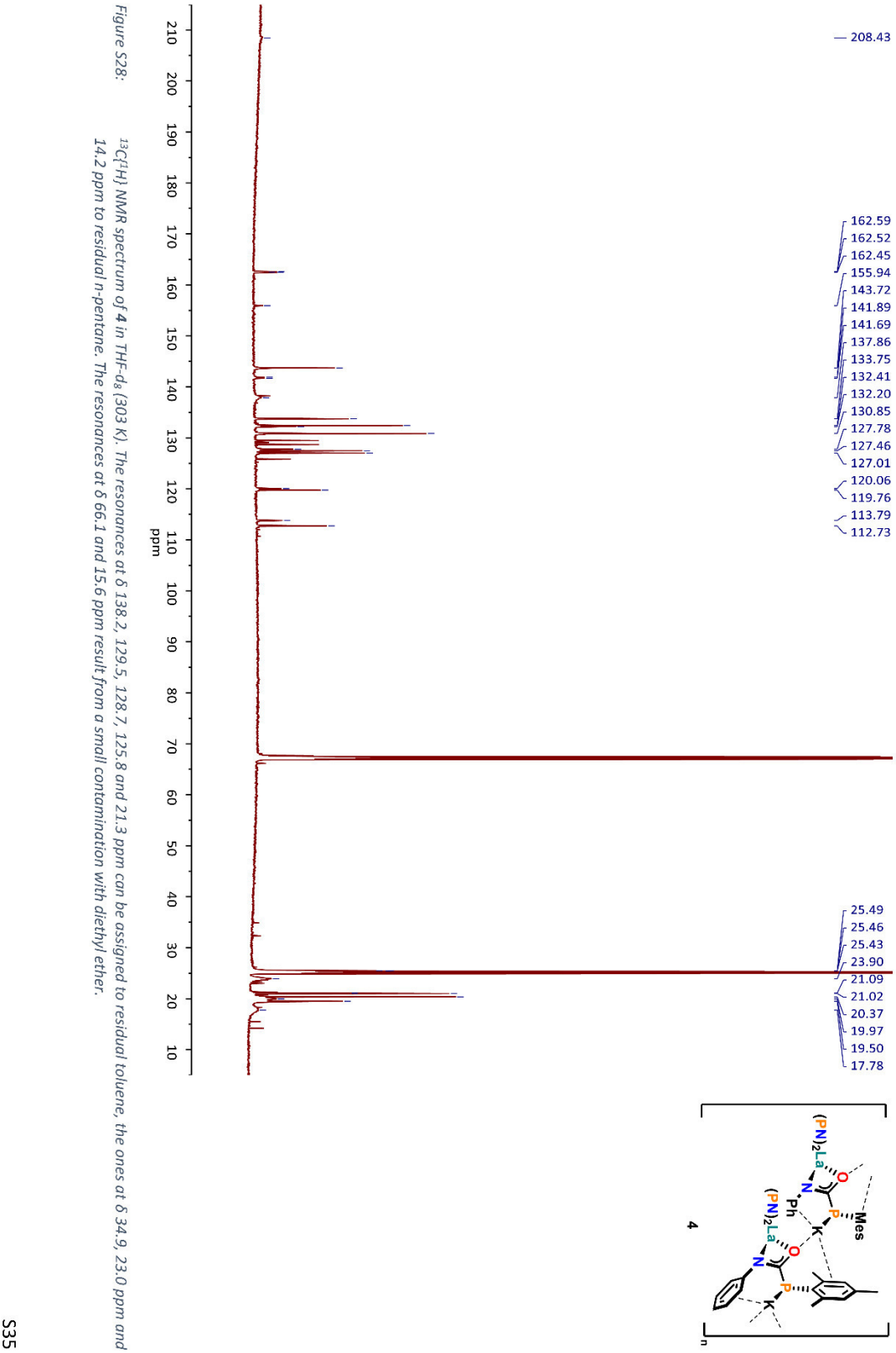

Figure S28: $^{13}C\{^1H\}$ *NMR spectrum of* **4** *in THF-d*$_8$ *(303 K). The resonances at δ 138.2, 129.5, 128.7, 125.8 and 21.3 ppm can be assigned to residual toluene, the ones at δ 34.9, 23.0 ppm and 14.2 ppm to residual n-pentane. The resonances at δ 66.1 and 15.6 ppm result from a small contamination with diethyl ether.*

S35

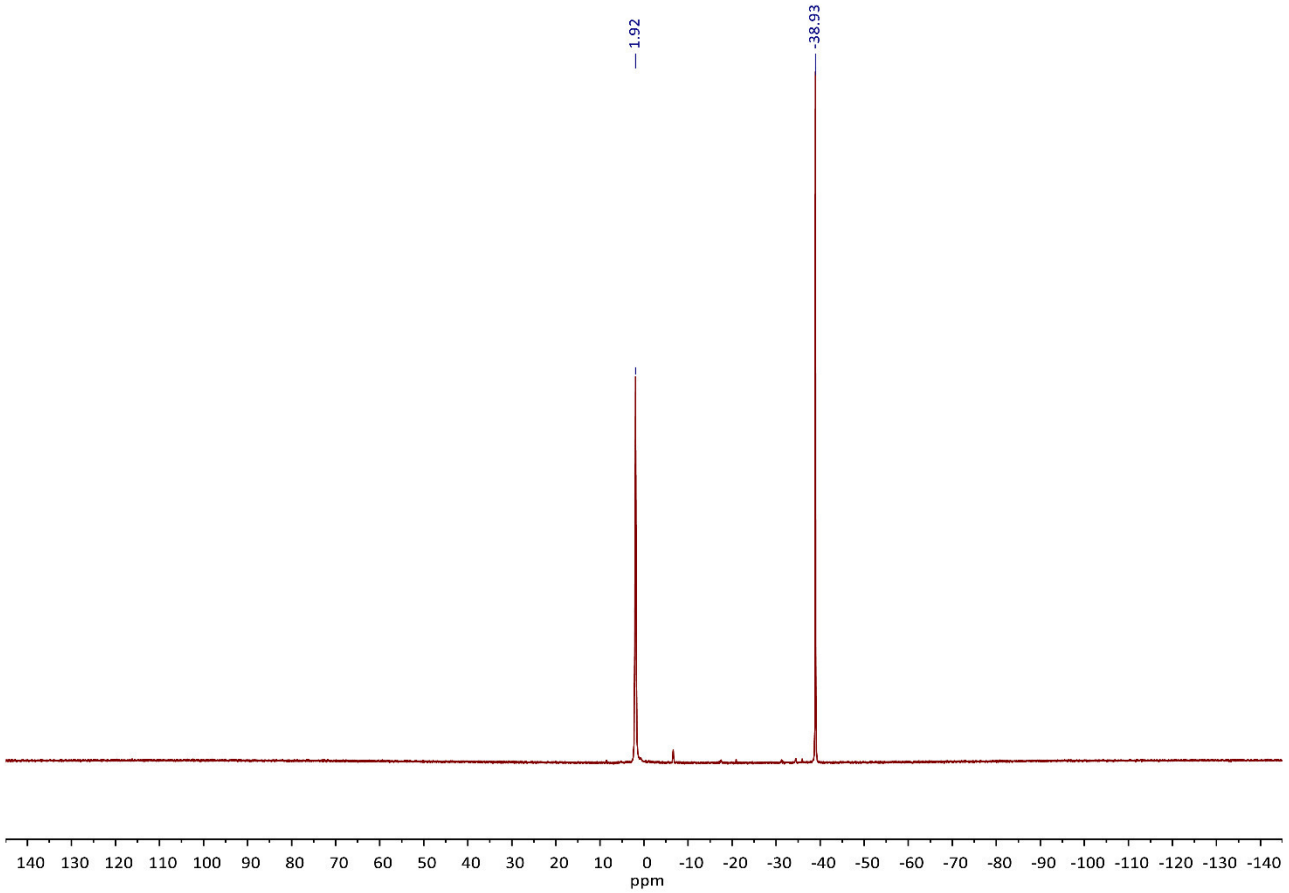

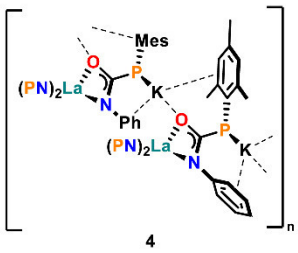

4

Figure S29: *^{31}P NMR spectrum of **4** in THF-d_8 (303 K). The resonance at δ –6.7 ppm belongs to traces of **KPN**.*

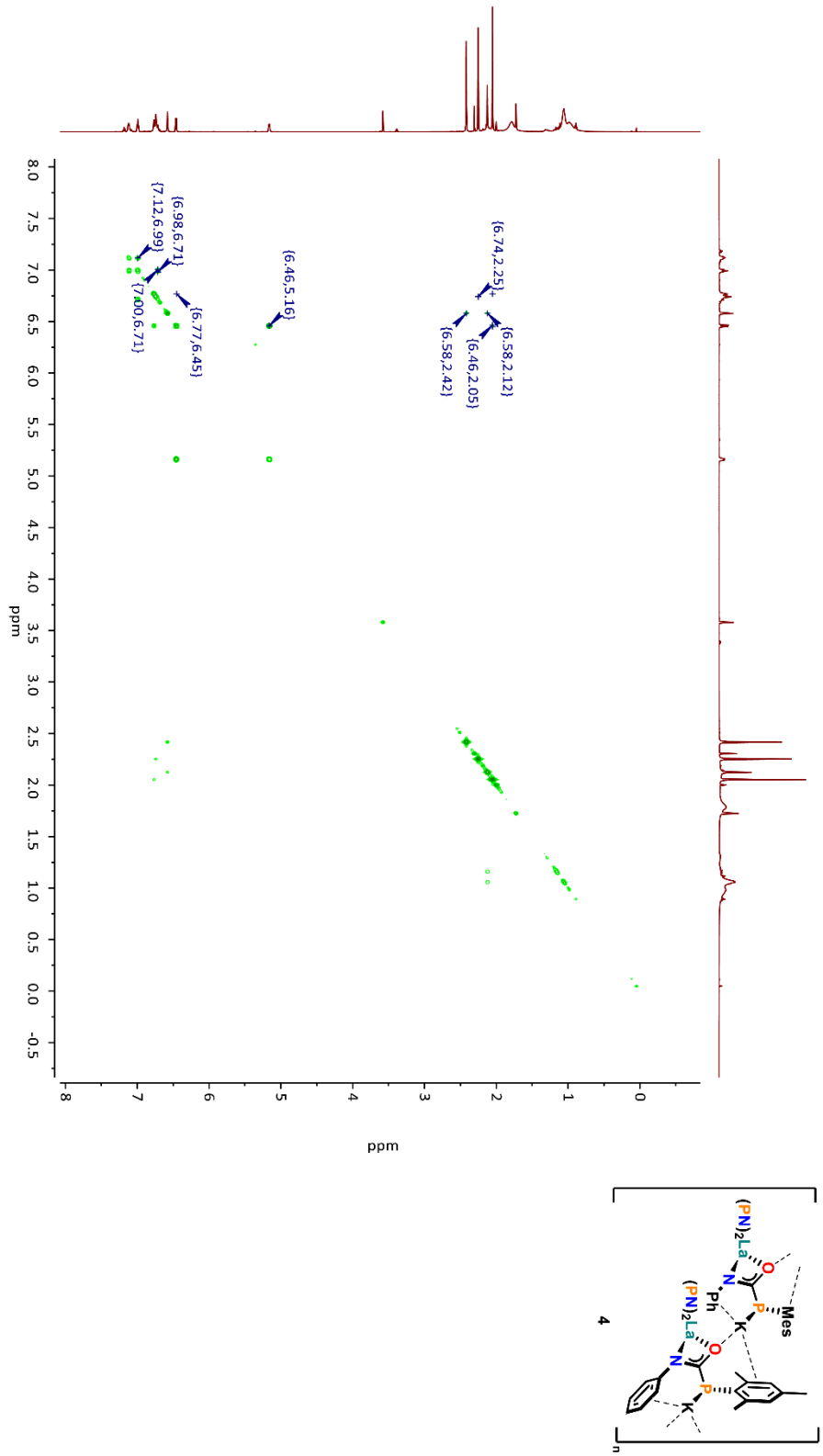

Figure S30: ^{1}H–^{1}H *COSY NMR spectrum of* **4** *in THF-d*$_8$ *(303 K).*

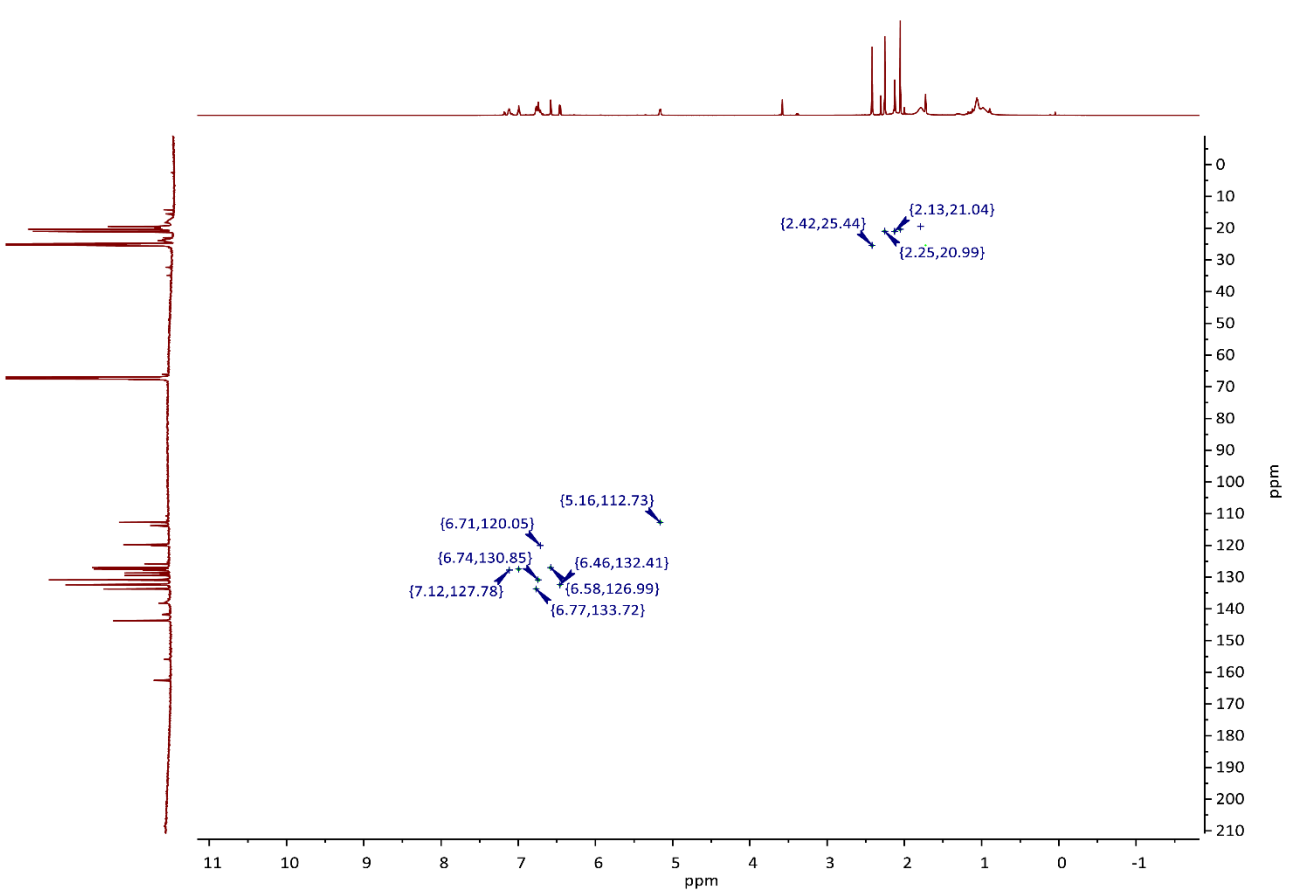

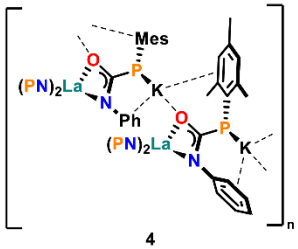

4

Figure S31: *^{1}H–^{13}C HSQC NMR spectrum of **4** in THF-d_8 (303 K).*

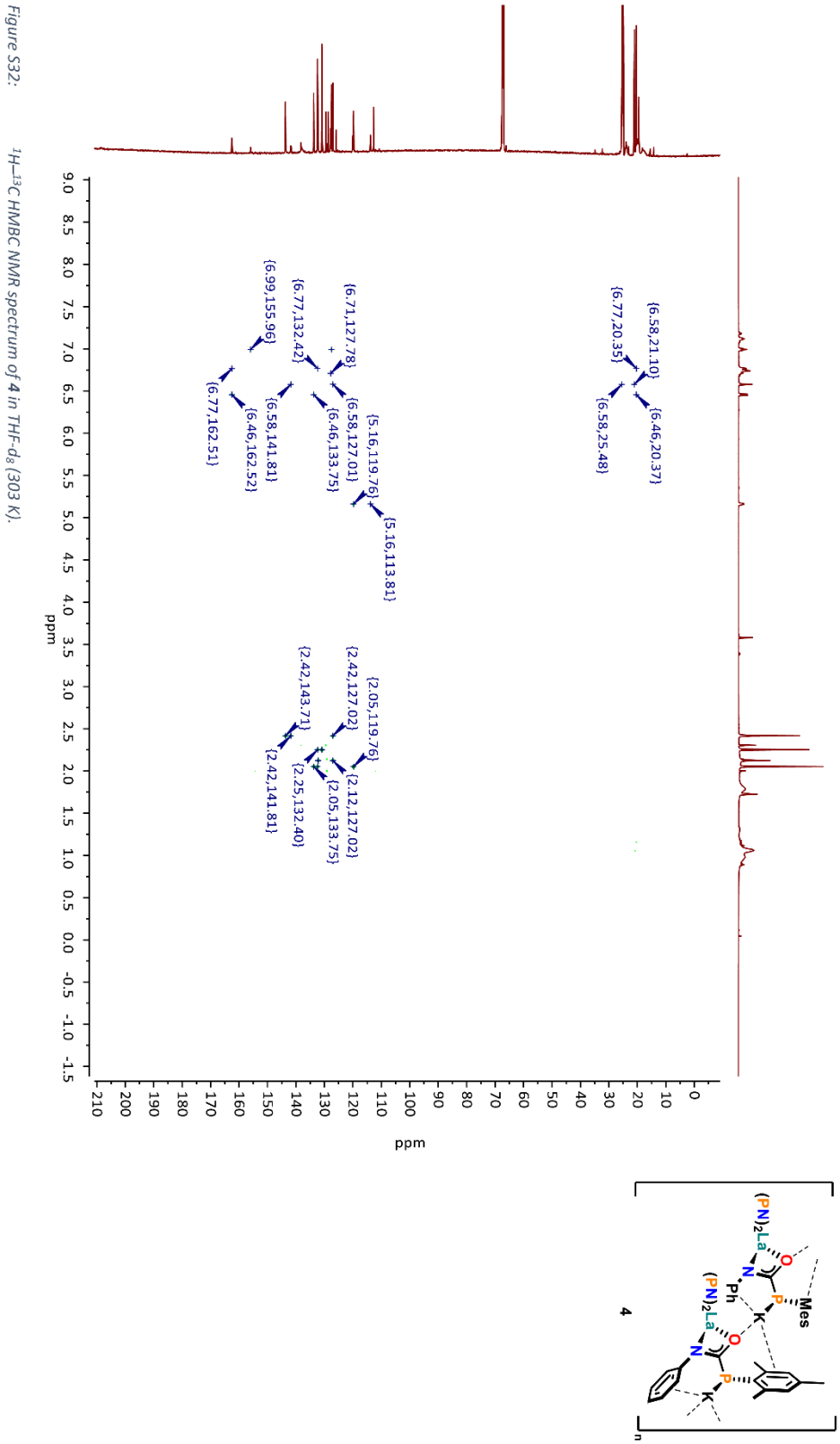

Figure S32: *^{1}H–^{13}C HMBC NMR spectrum of **4** in THF-d_8 (303 K).*

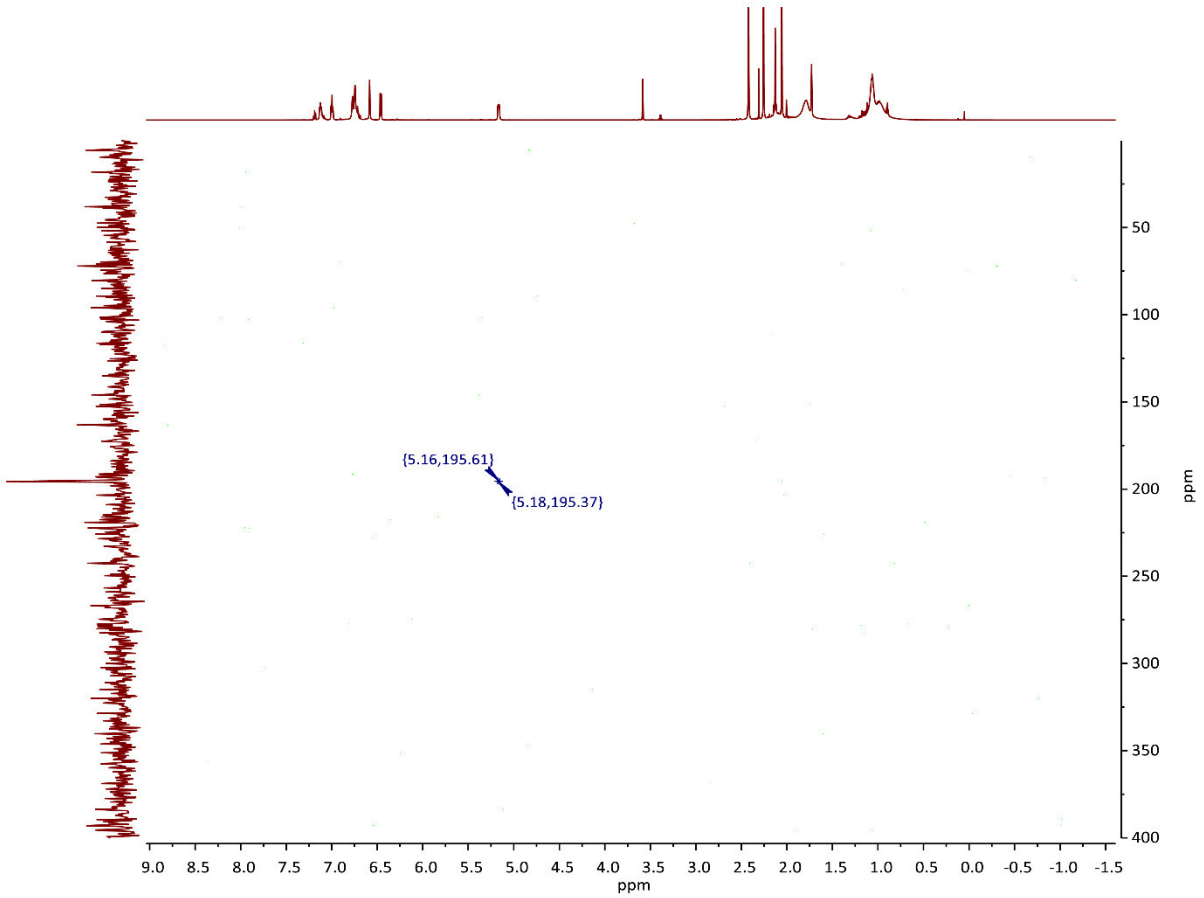

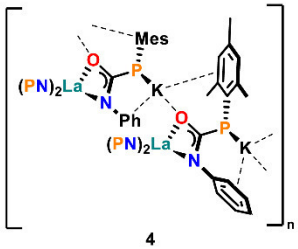

4

Figure S33: *^{1}H–^{15}N HMBC NMR spectrum of **4** in THF-d_8 (303 K).*

*Figure S34: ^1H NMR spectrum of the deprotonation product of **3** (using KHMDS) in THF-d_8 (303 K). Note the absence of a doublet resonance for the PH group, indicating successful deprotonation. Due to the crowding and overlapping of resonances from at least two isomers, no definite assignments and integration values are given.*

*Figure S35: $^{13}C\{^1H\}$ NMR spectrum of the deprotonation product of **3** (using KHMDS) in THF-d_8 (303 K). Due to the presence of at least two isomers, no definite assignments are given.*

S42

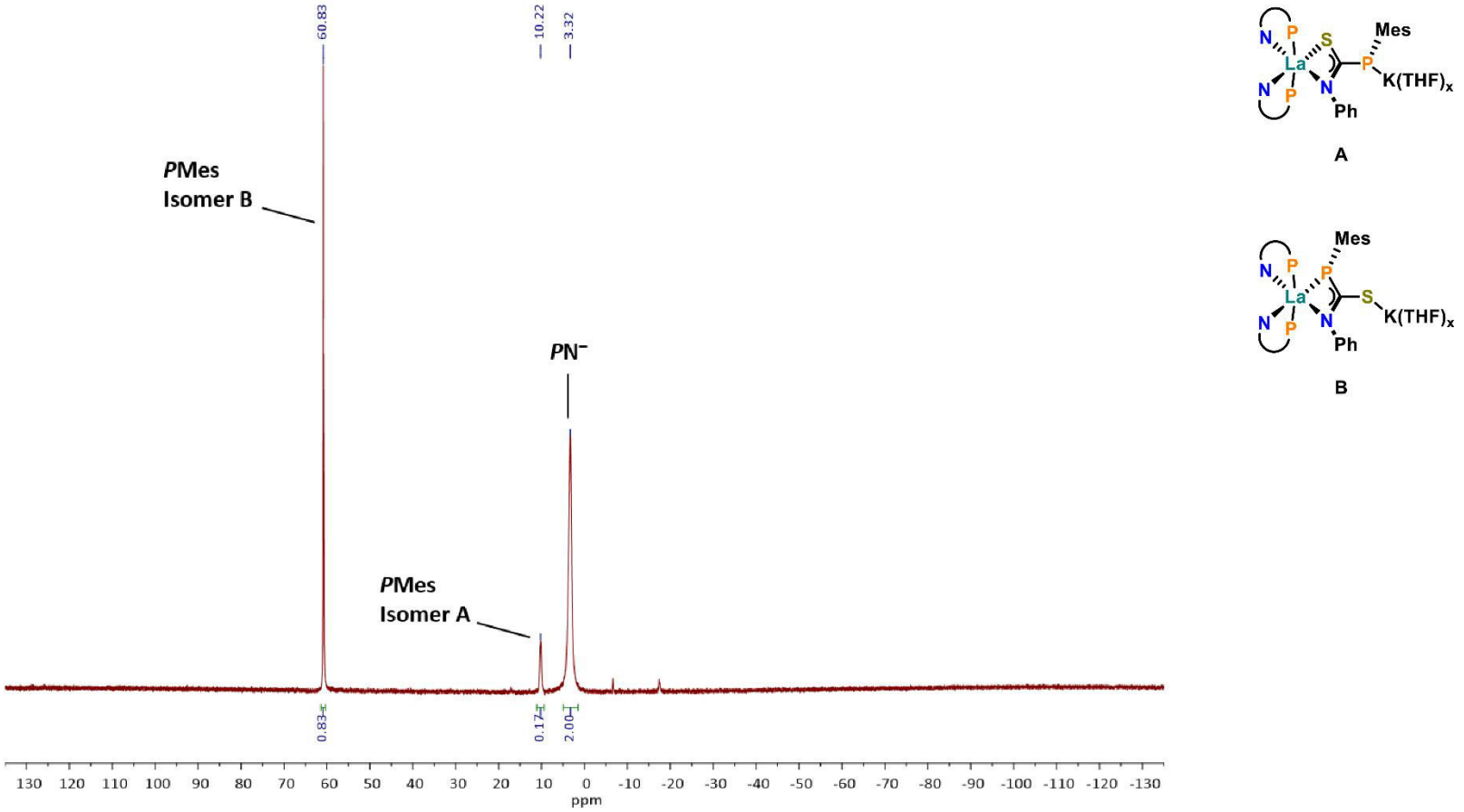

Figure S36: *^{31}P NMR spectrum of the deprotonation product of **3** (using KHMDS) in THF-d_8 (303 K). Note the absence of a doublet resonance for the PH group, indicating successful deprotonation. The peak at δ –17.5 ppm can be assigned to traces of **HPN**. The resonances at δ 60.8 ppm and δ 10.2 ppm are tentatively assigned to two different isomers of the structure **A** and **B**, respectively.*

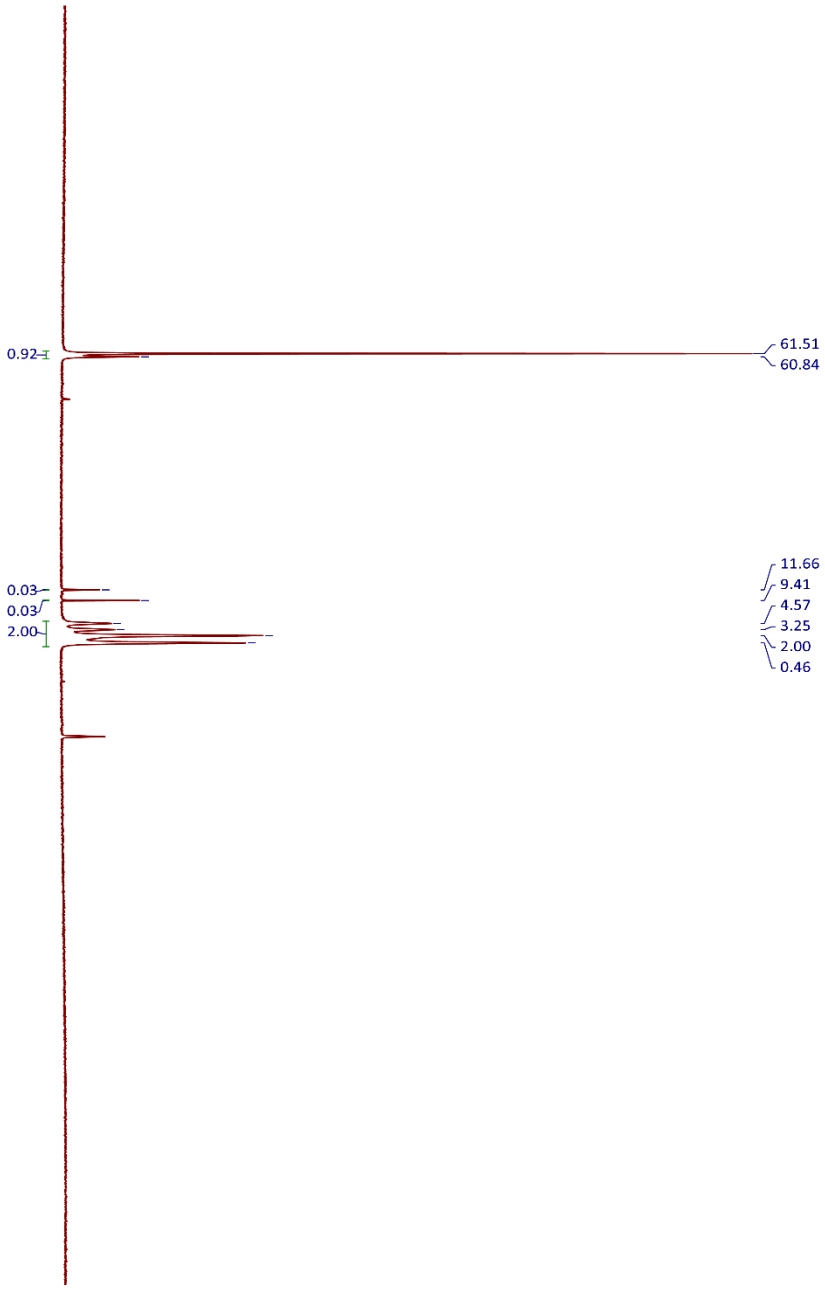

*Figure S37: ^{31}P NMR spectrum of the deprotonation product of **3** (using KHMDS) in THF-d_8 (243 K). The peak at δ –17.5 ppm can be assigned to traces of **HPN**.*

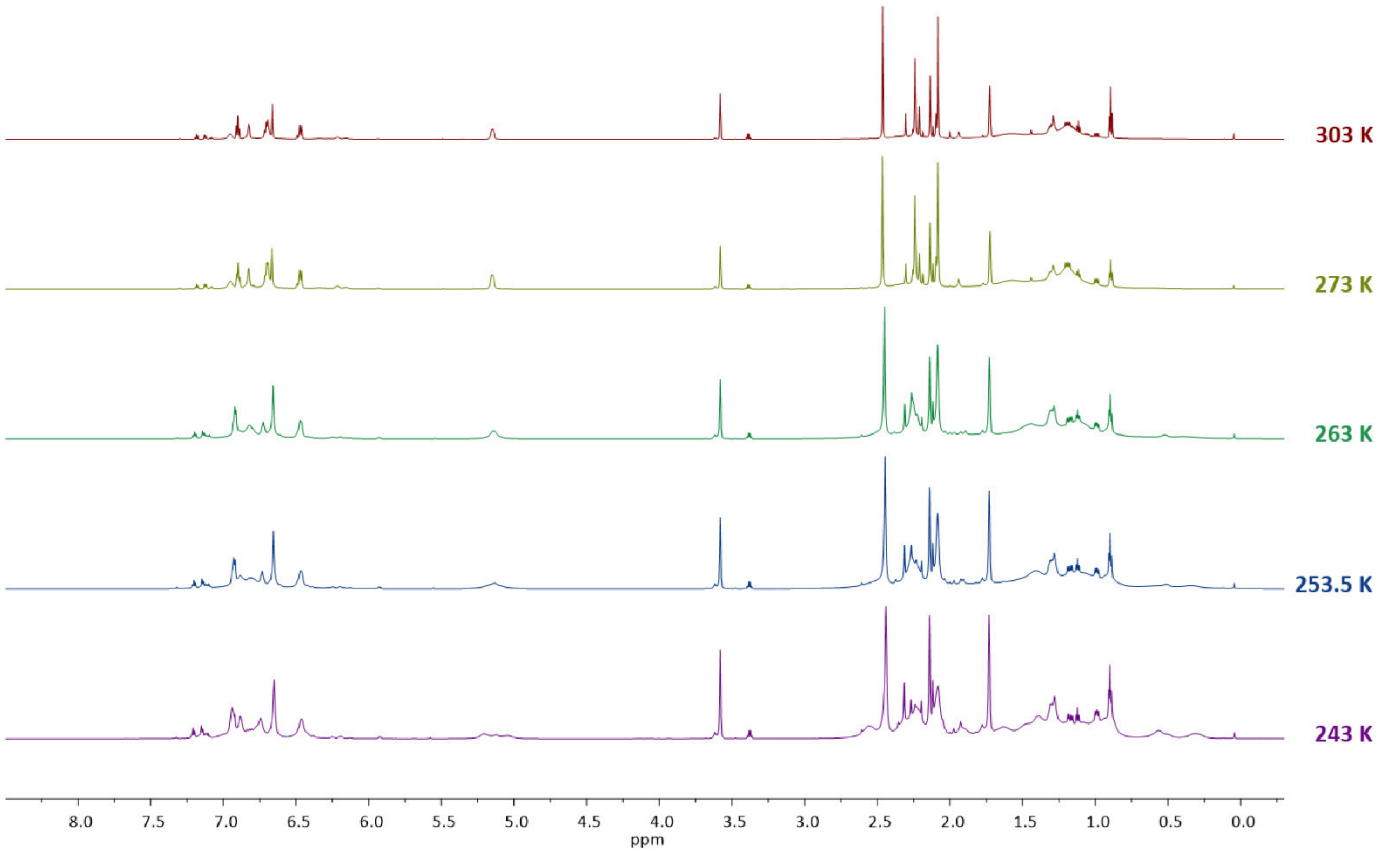

Figure S38: *Stacked ^{1}H VT NMR spectra of the deprotonation product of **3** (using KHMDS) in THF-d_8 from 243 K to 303 K. Note the broadening and splitting of some resonances (e.g. at δ 5.15 ppm) at 243 K, most likely due to less dynamics.*

Figure S39: Stacked ^{31}P VT NMR spectra of the deprotonation product of **3** *(using KHMDS) in THF-d_8 from 243 K to 303 K. The peak at δ –17.5 ppm can be assigned to traces of* **HPN**. *Note the splitting of the three resonances observed at 303 K into a total of eight resonances at 243 K, most likely due to less dynamics. Also note the change in relative intensities of the two groups of resonances at around δ 60.8 ppm and δ 10.2 ppm (with the grouped resonances at δ 3.3 ppm set to a constant integral value of 2, see also Figures S36 and S37), possibly indicating an equilibrium between at least two isomers (see Figure S36 for illustration).*

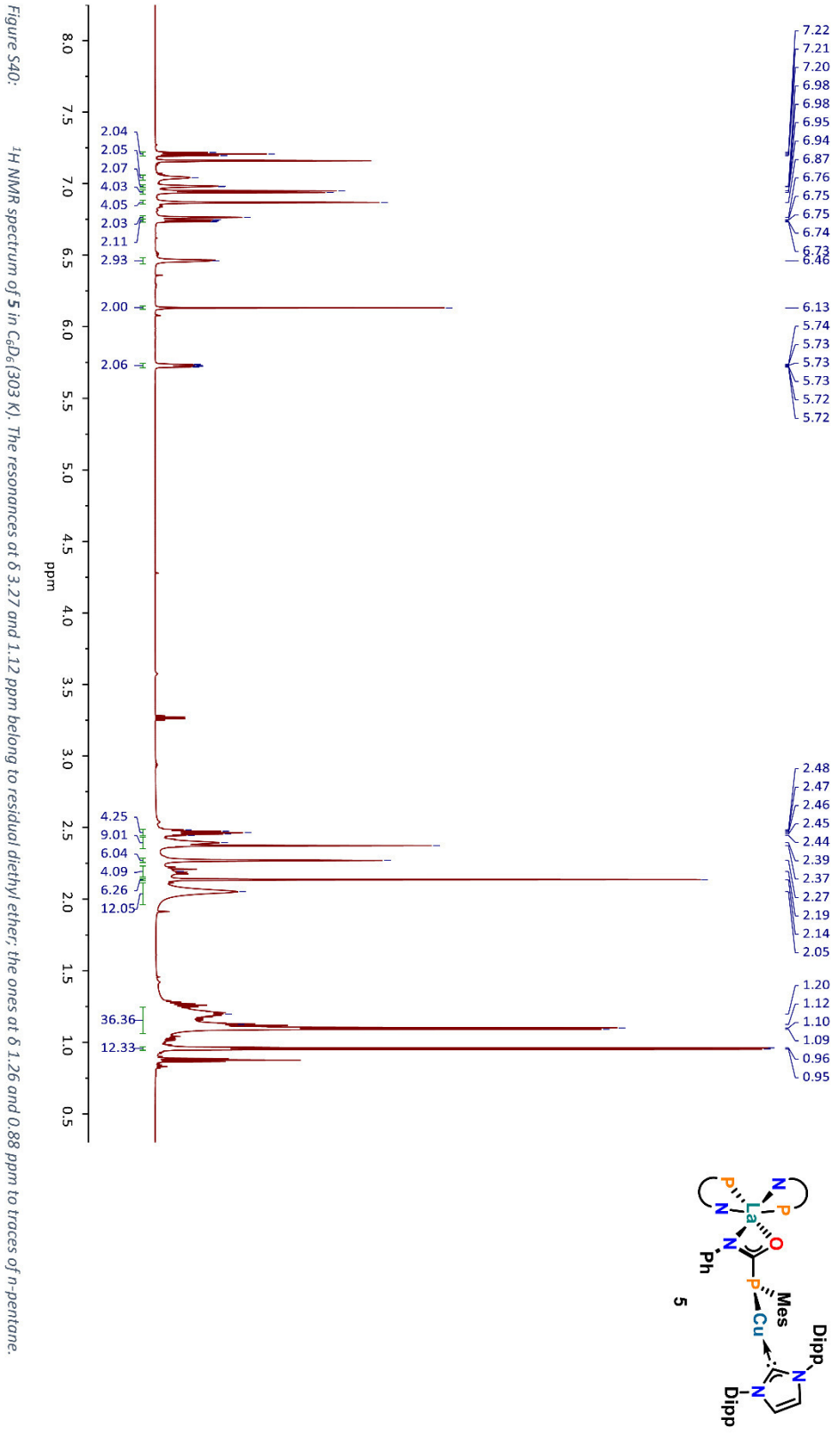

*Figure S40: ^{1}H NMR spectrum of **5** in C_6D_6 (303 K). The resonances at δ 3.27 and 1.12 ppm belong to residual diethyl ether; the ones at δ 1.26 and 0.88 ppm to traces of n-pentane.*

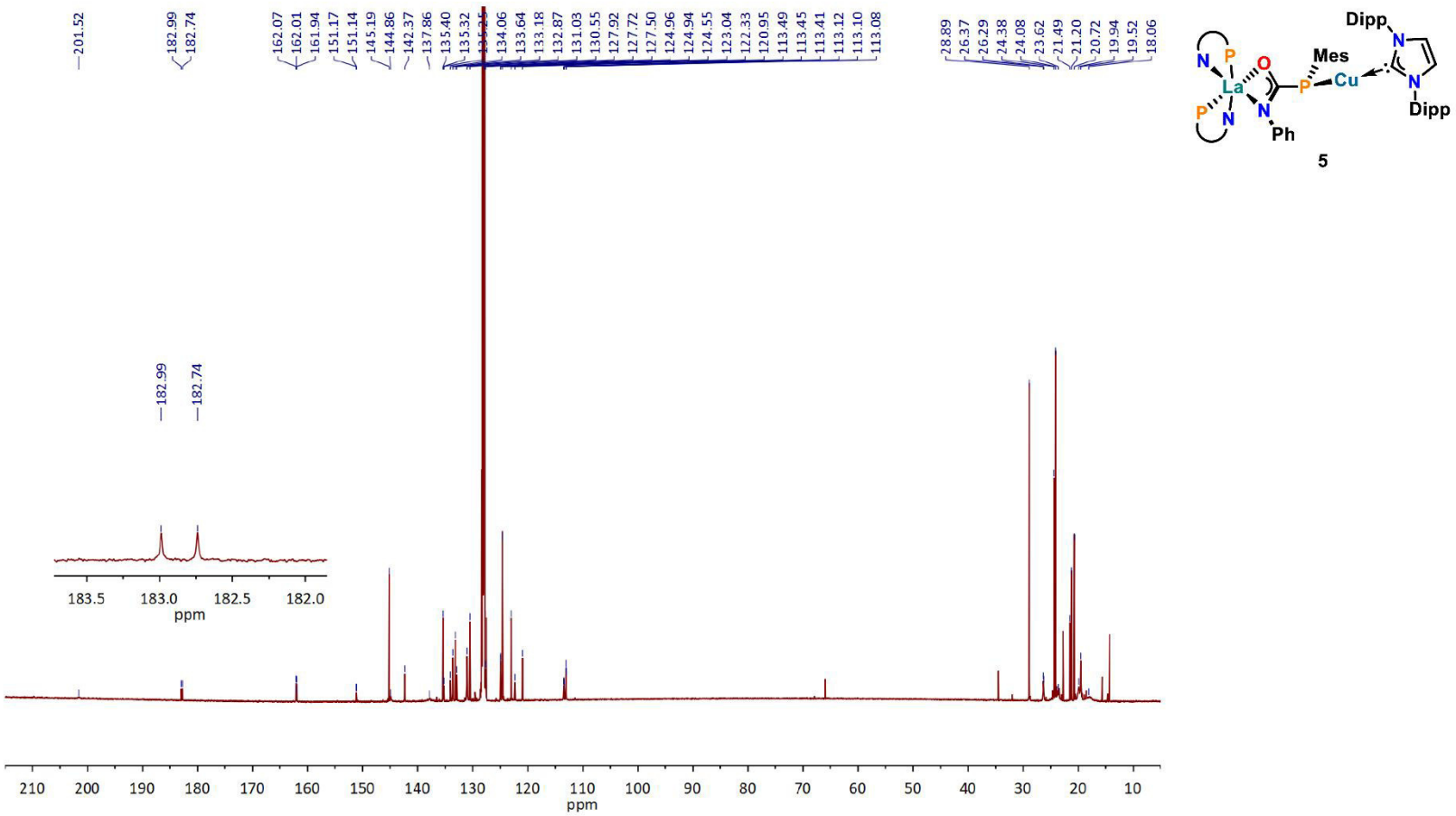

Figure S41: *$^{13}C\{^{1}H\}$ NMR spectrum of **5** in C_6D_6 (303 K). The resonances at δ 65.9 and 15.6 ppm belong to residual diethyl ether; the ones at δ 34.5, 22.7 and 14.3 ppm to traces of n-pentane. The detail shows the characteristic doublet splitting of the $C_{carbene}$ resonance caused by ^{2}J coupling to $P_{phosphaureate}$.*

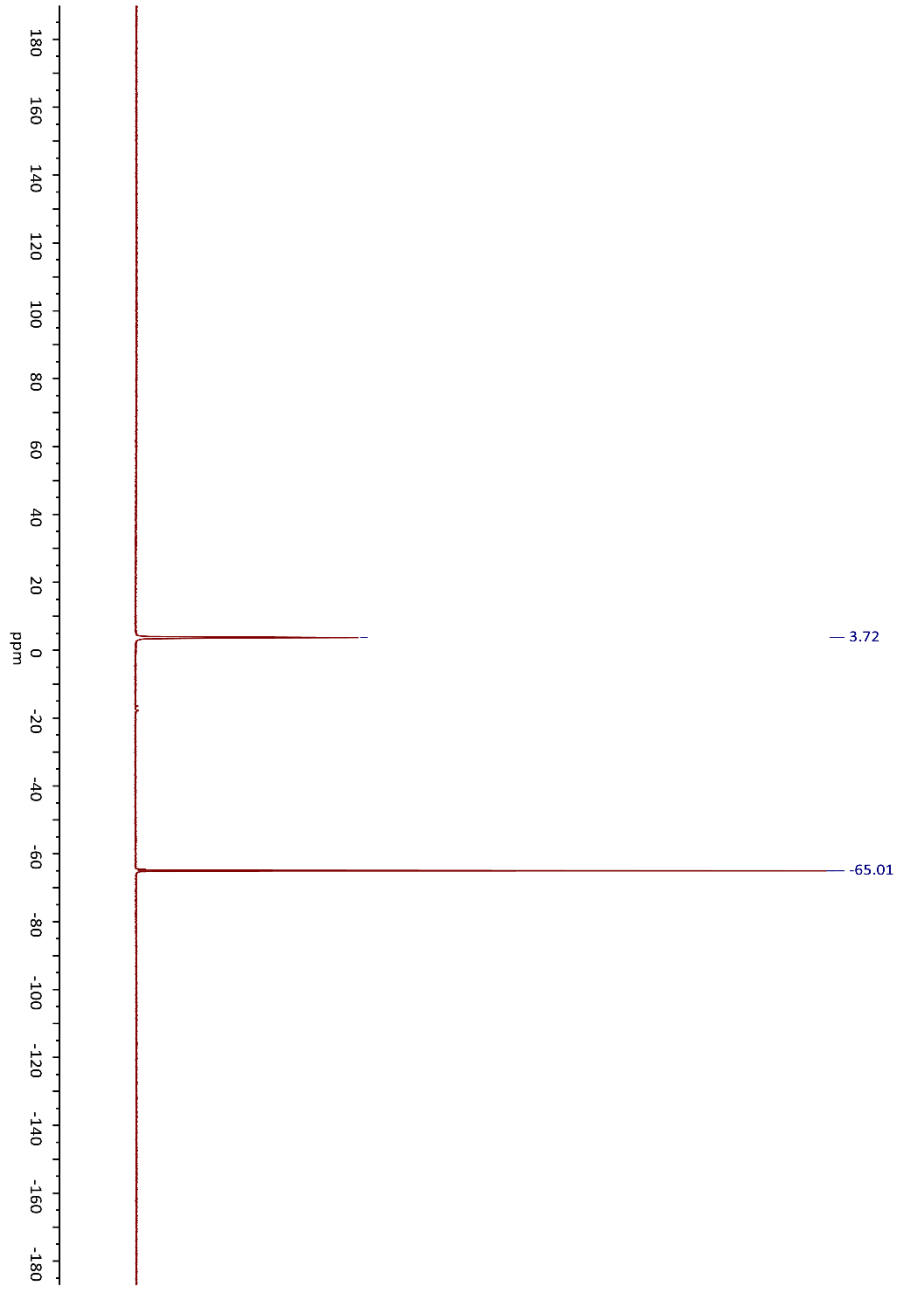

Figure S42: ^{31}P *NMR spectrum of* **5** *in* C_6D_6 *(303 K).*

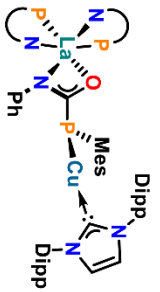

5

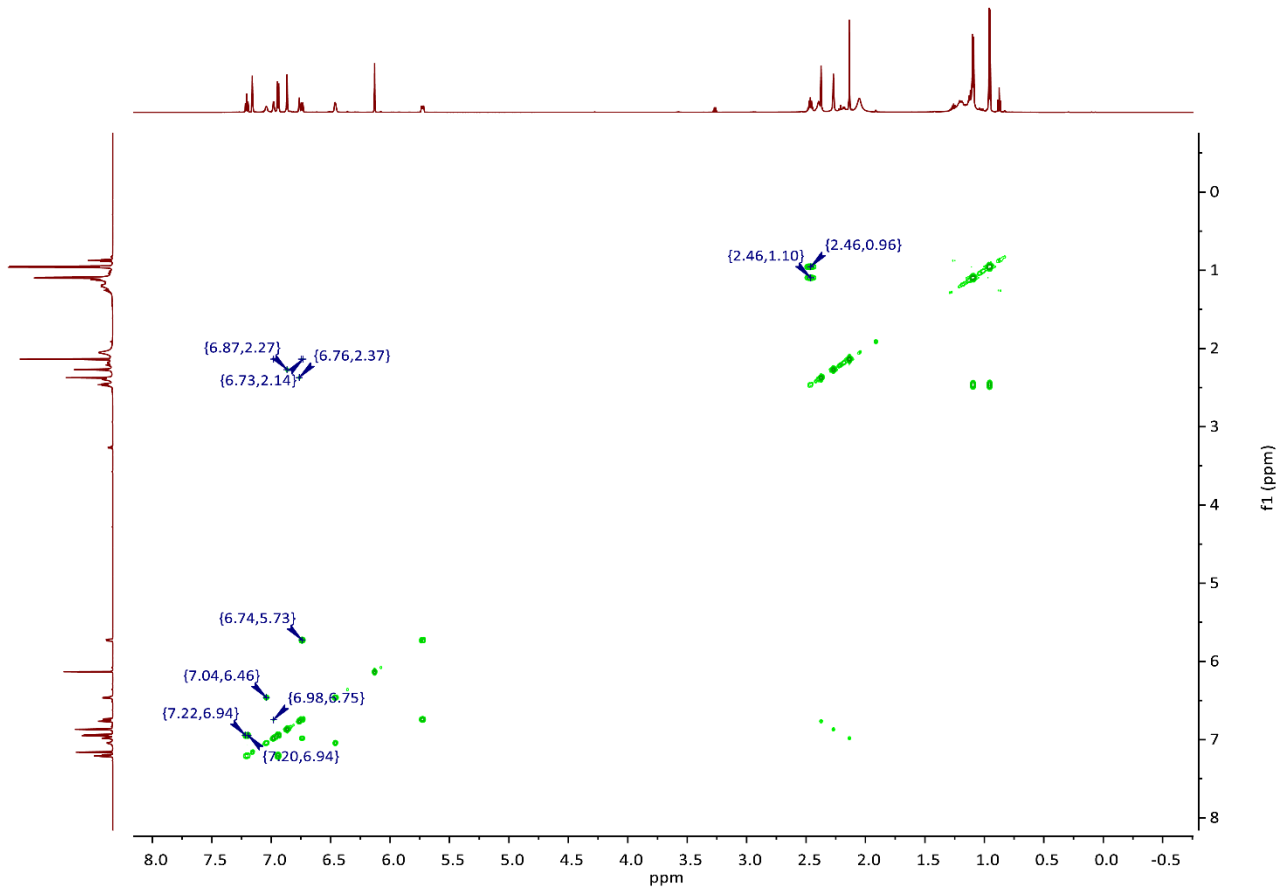

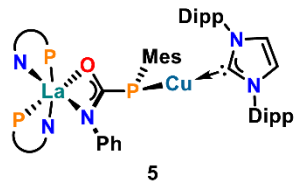

5

Figure S43: *^{1}H–^{1}H COSY NMR spectrum of **5** in C_6D_6 (303 K).*

Figure S44: ^{1}H–^{13}C *HSQC NMR spectrum of* **5** *in* C_6D_6 *(303 K).*

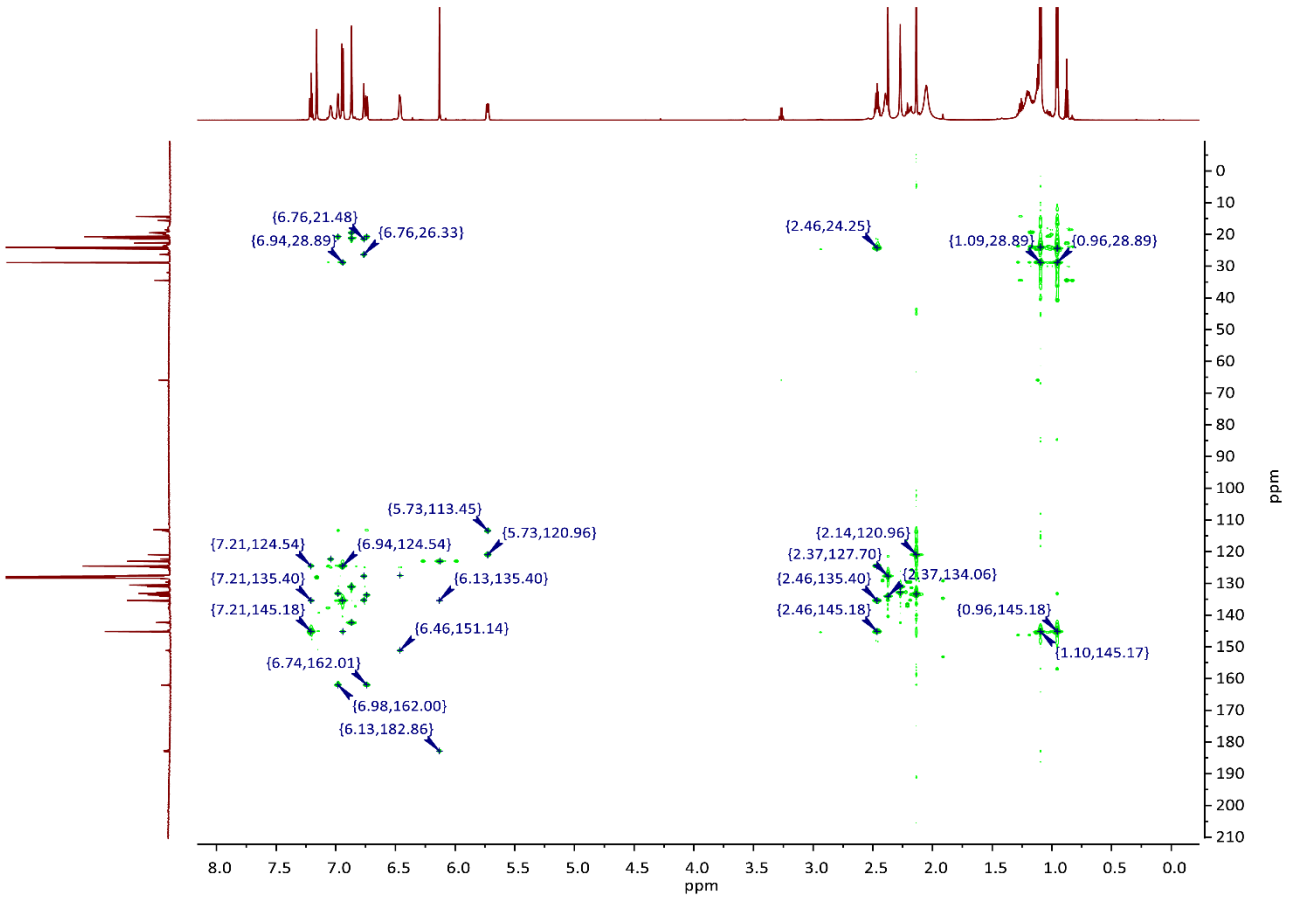

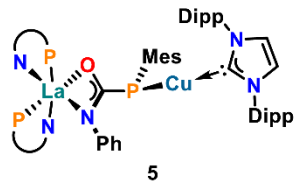

5

Figure S45: *^{1}H–^{13}C HMBC NMR spectrum of **5** in C_6D_6 (303 K).*

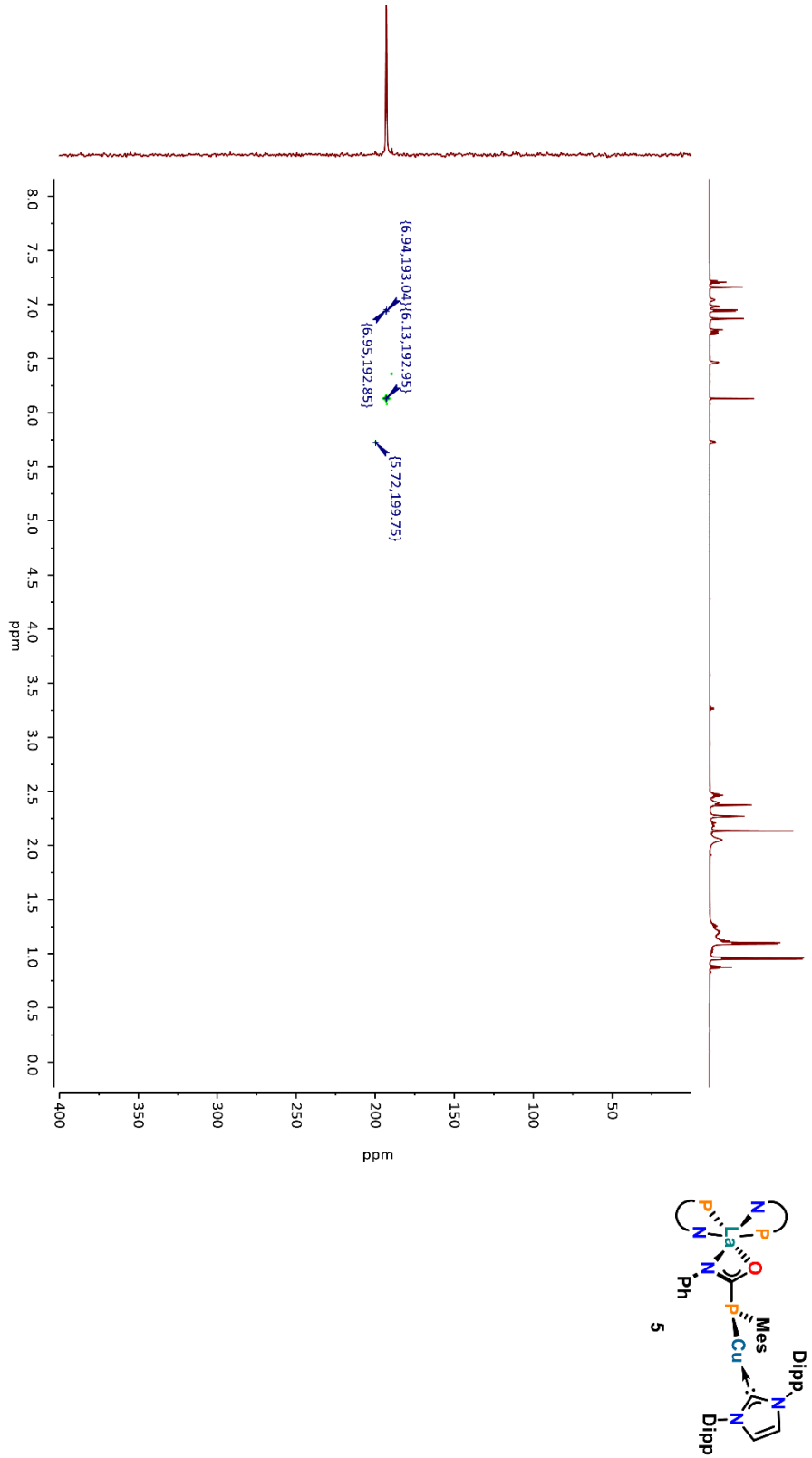

Figure S46: ^{1}H–^{15}N HMBC NMR spectrum of **5** in C_6D_6 (303 K).

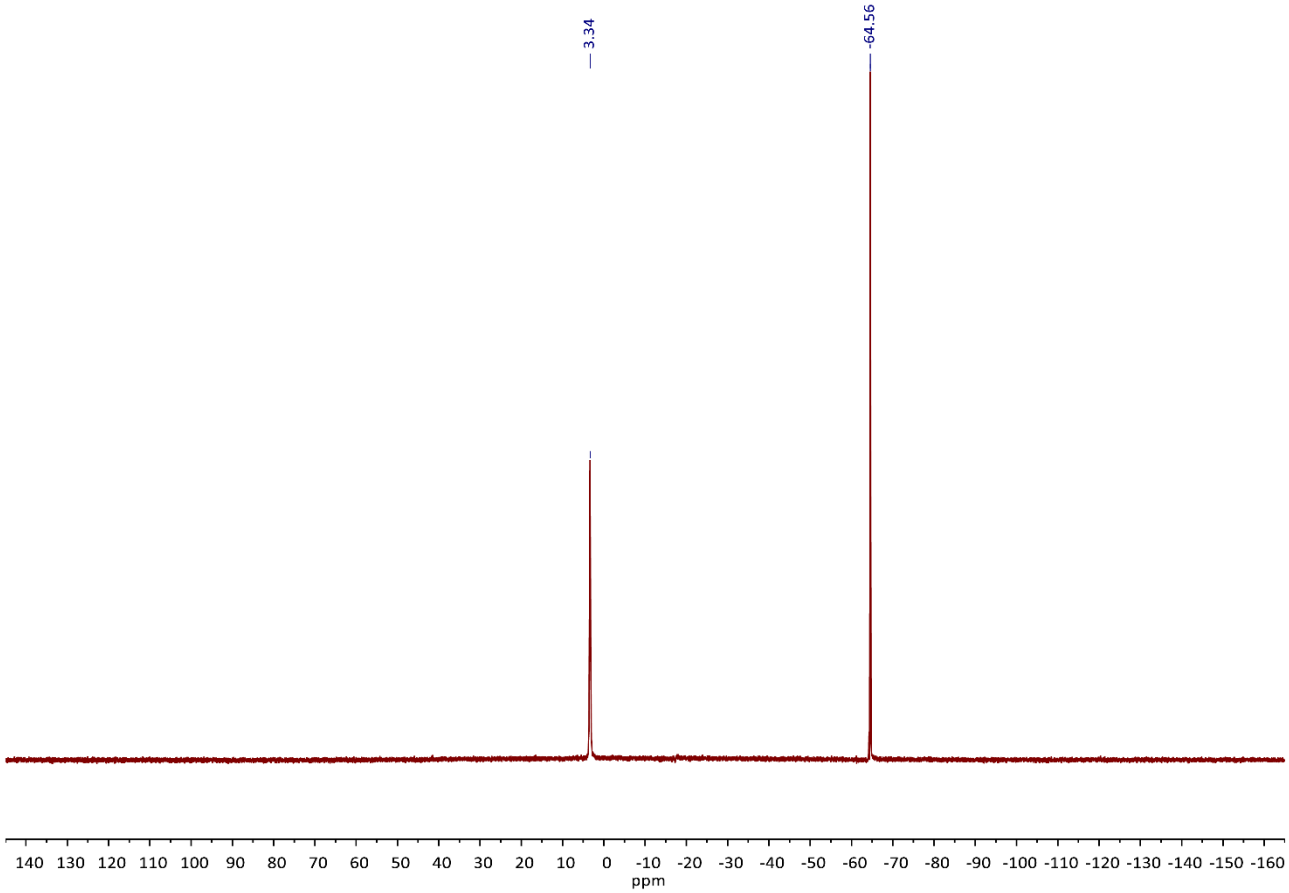

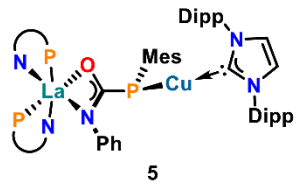

5

*Figure S47: Reaction control ^{31}P NMR spectrum after consecutive addition of KHMDS and **(IPr)CuCl** to **2** in diethyl ether (with C_6D_6 capillary, 303 K).*

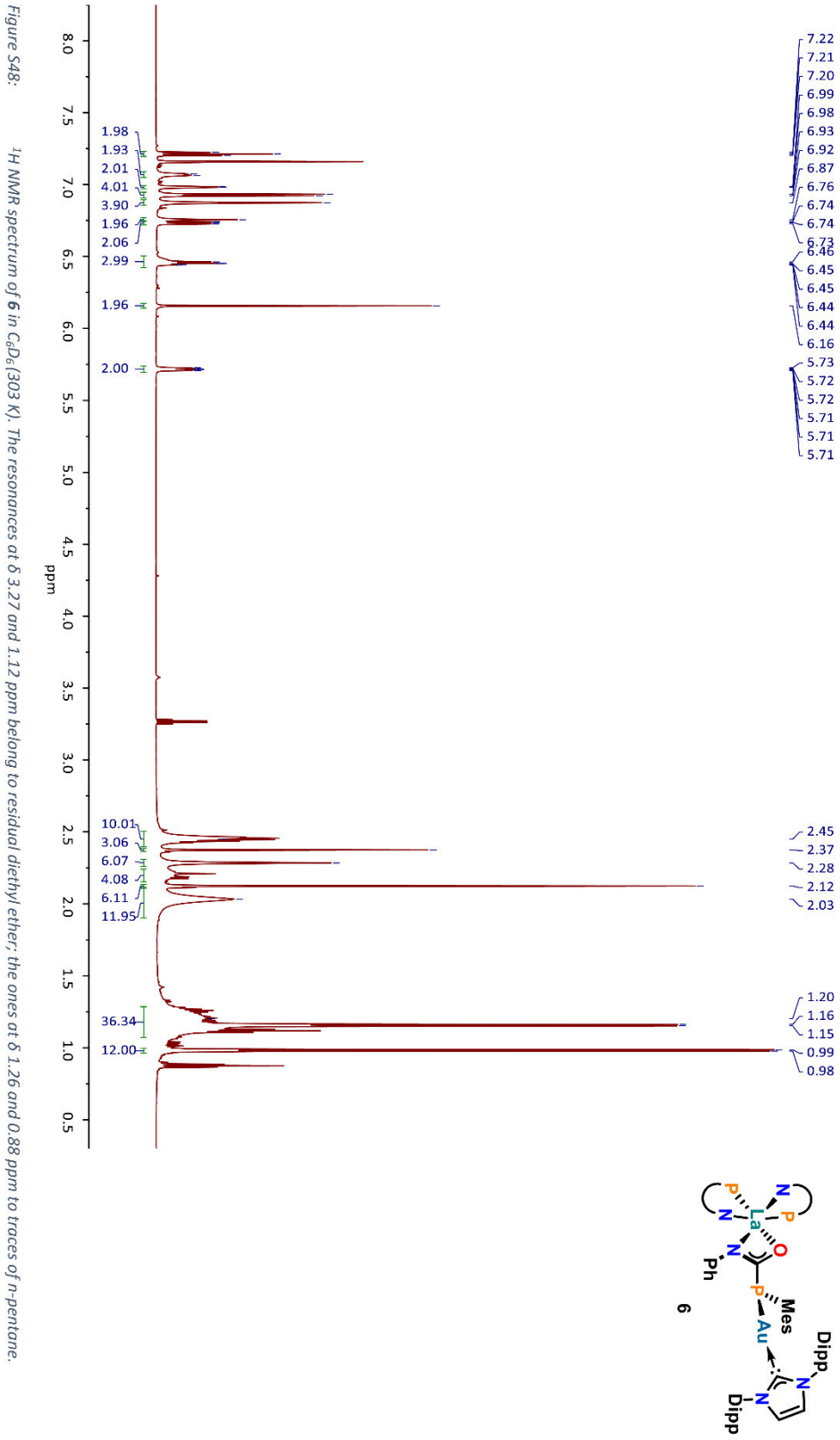

*Figure S48: ^1H NMR spectrum of **6** in C_6D_6 (303 K). The resonances at δ 3.27 and 1.12 ppm belong to residual diethyl ether; the ones at δ 1.26 and 0.88 ppm to traces of n-pentane.*

S55

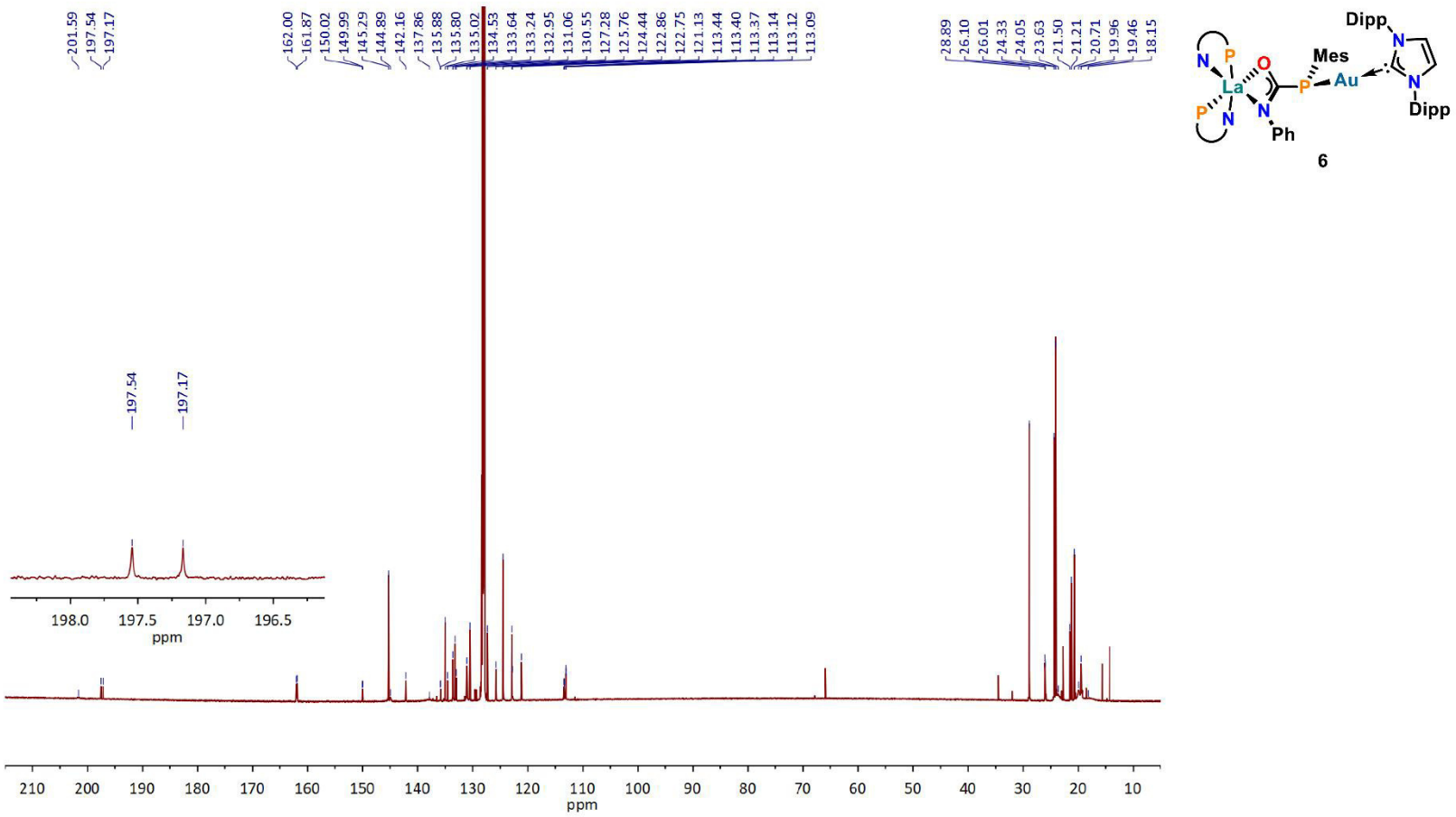

Figure S49: *$^{13}C\{^{1}H\}$ NMR spectrum of **6** in C_6D_6 (303 K). The resonances at δ 65.9 and 15.6 ppm belong to residual diethyl ether; the ones at δ 34.5, 22.7 and 14.3 ppm to traces of n-pentane. The detail shows the characteristic doublet splitting of the $C_{carbene}$ resonance caused by ^{2}J coupling to $P_{phosphaureate}$.*

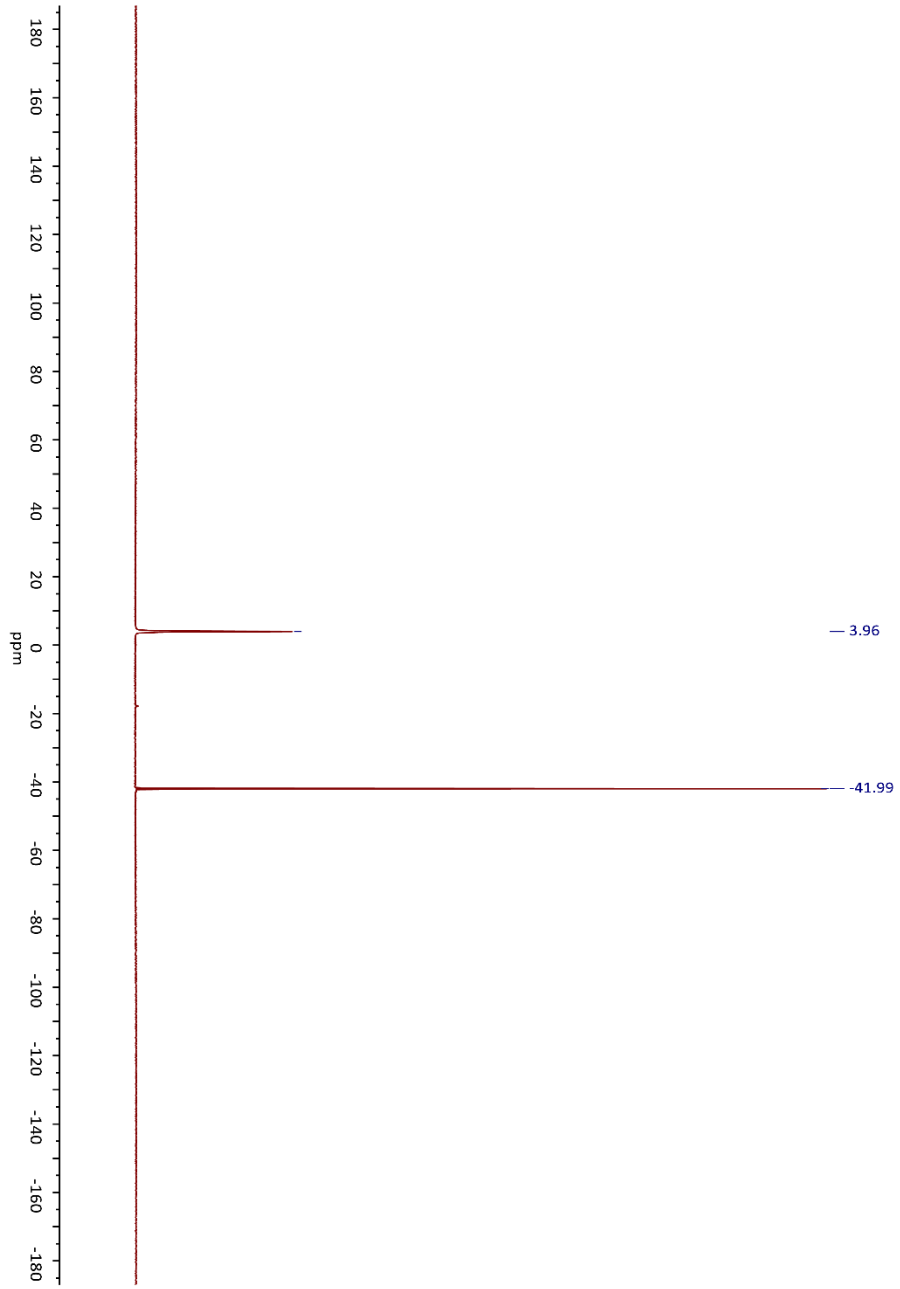

Figure S50: ^{31}P *NMR spectrum of* **6** *in* C_6D_6 *(303 K).*

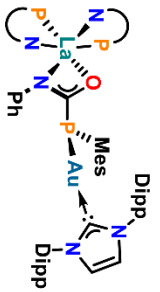

6

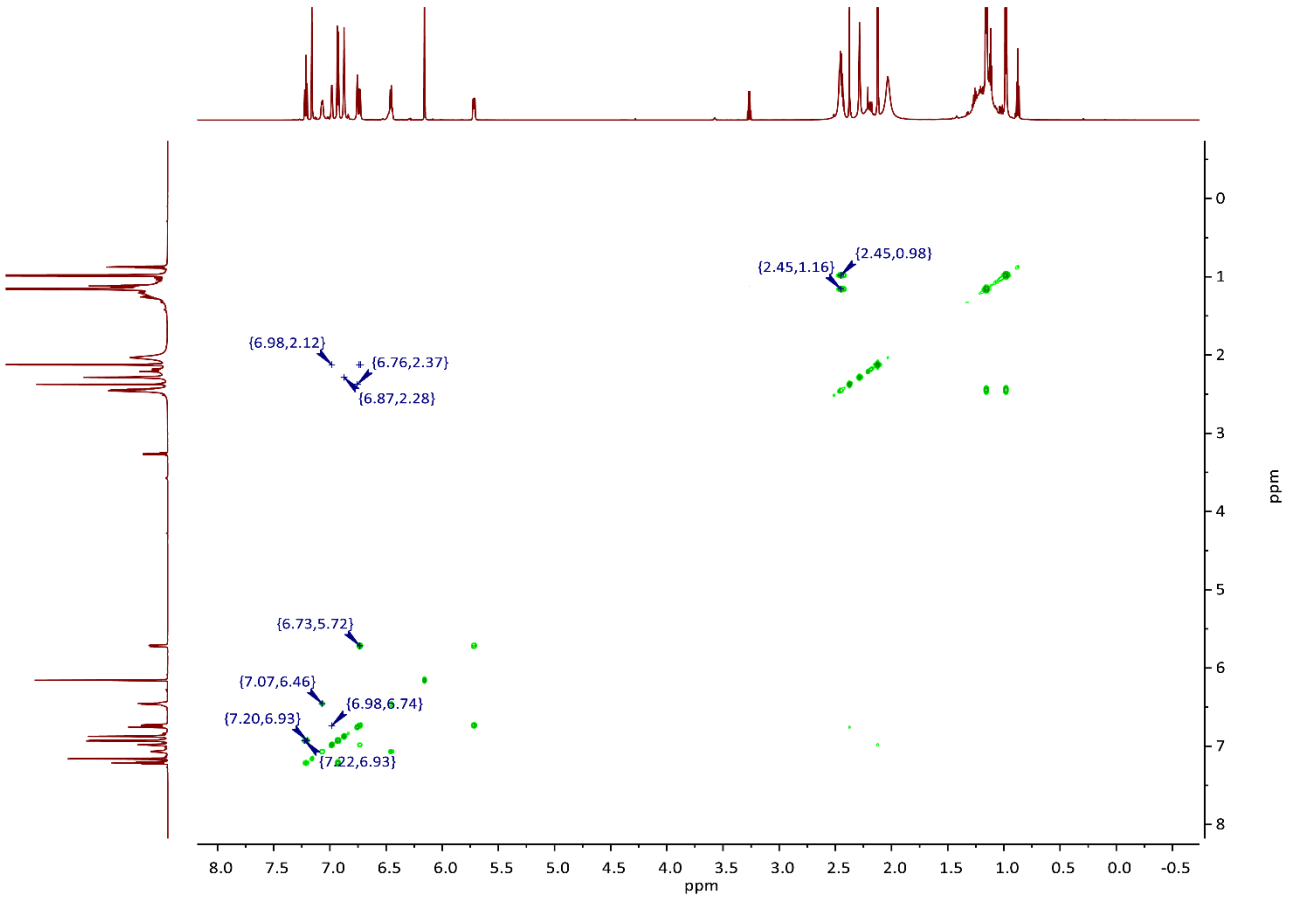

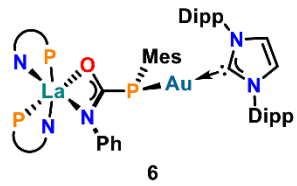

6

Figure S51: *^{1}H–^{1}H COSY NMR spectrum of **6** in C_6D_6 (303 K).*

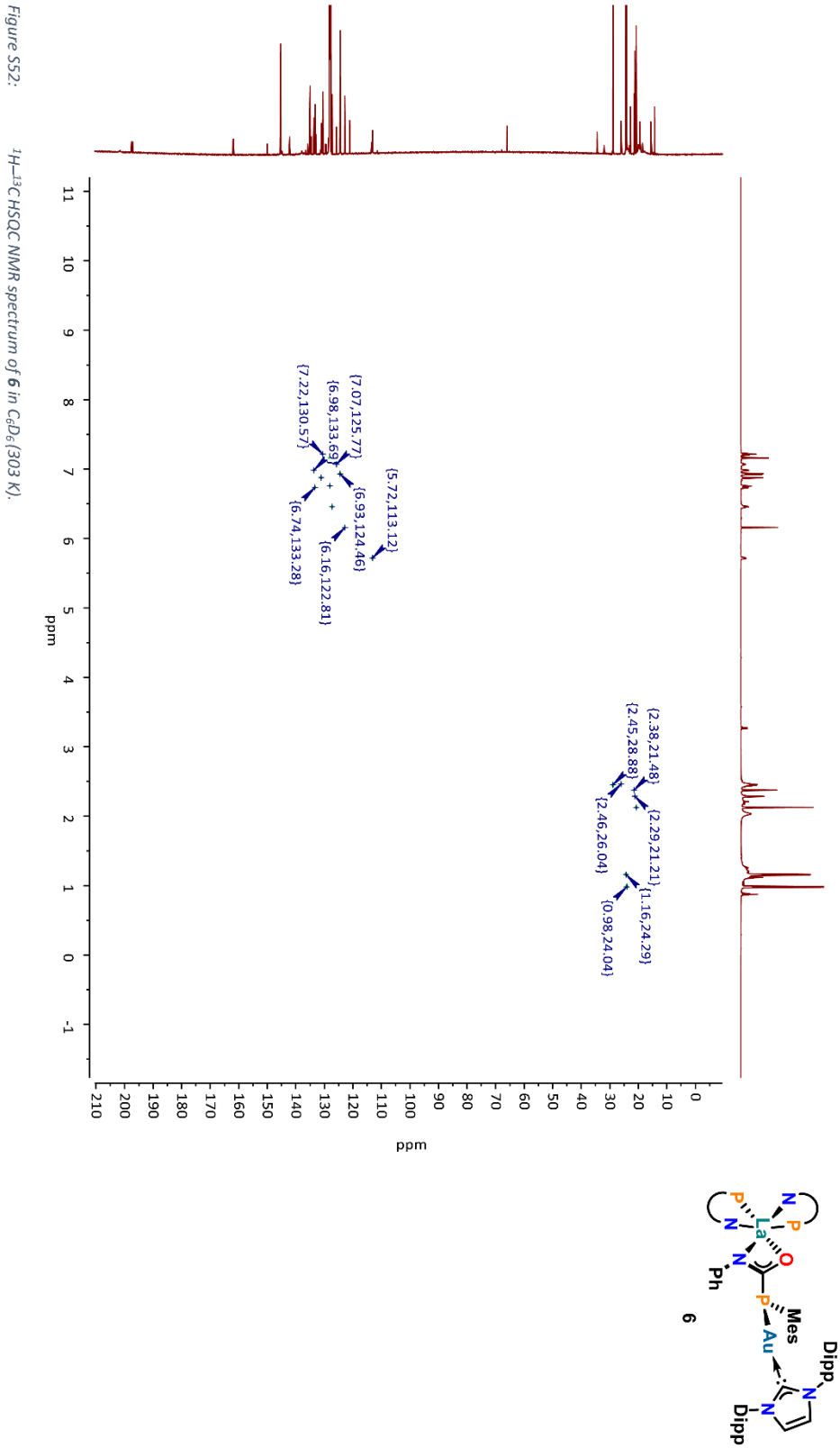

Figure S52: *^{1}H–^{13}C HSQC NMR spectrum of **6** in C_6D_6 (303 K).*

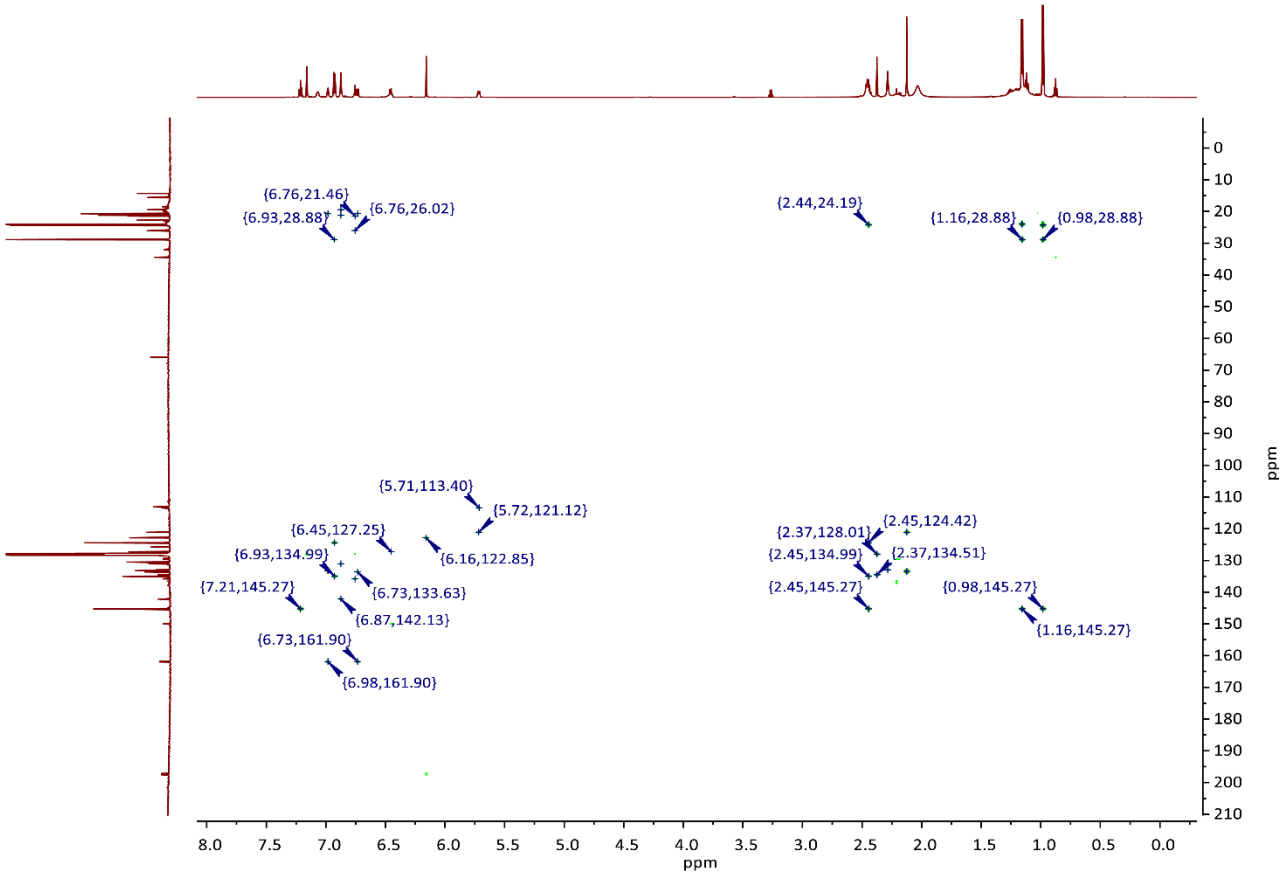

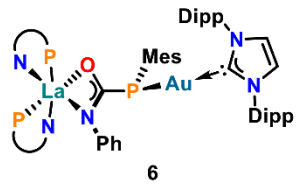

6

Figure S53: *^{1}H–^{13}C HMBC NMR spectrum of **6** in C_6D_6 (303 K).*

Figure S54: ^{1}H–^{15}N *HMBC NMR spectrum of* **6** *in* C_6D_6 *(303 K).*

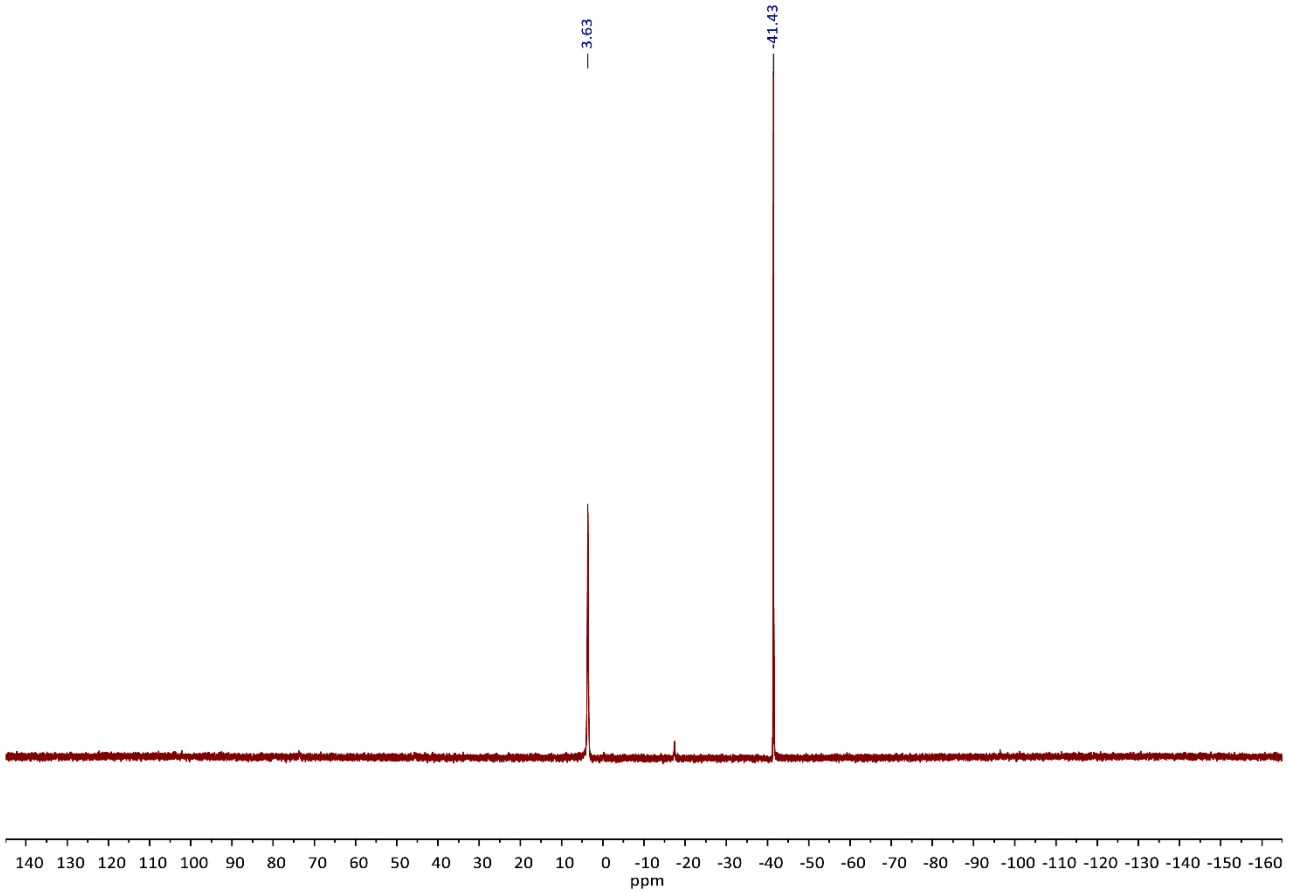

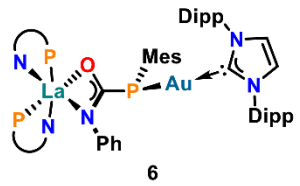

6

Figure S55: *Reaction control ^{31}P NMR spectrum after consecutive addition of KHMDS and **(IPr)AuCl** to **2** in diethyl ether (with C_6D_6 capillary, 303 K). The peak at δ –17.8 ppm can be assigned to traces of **HPN**.*

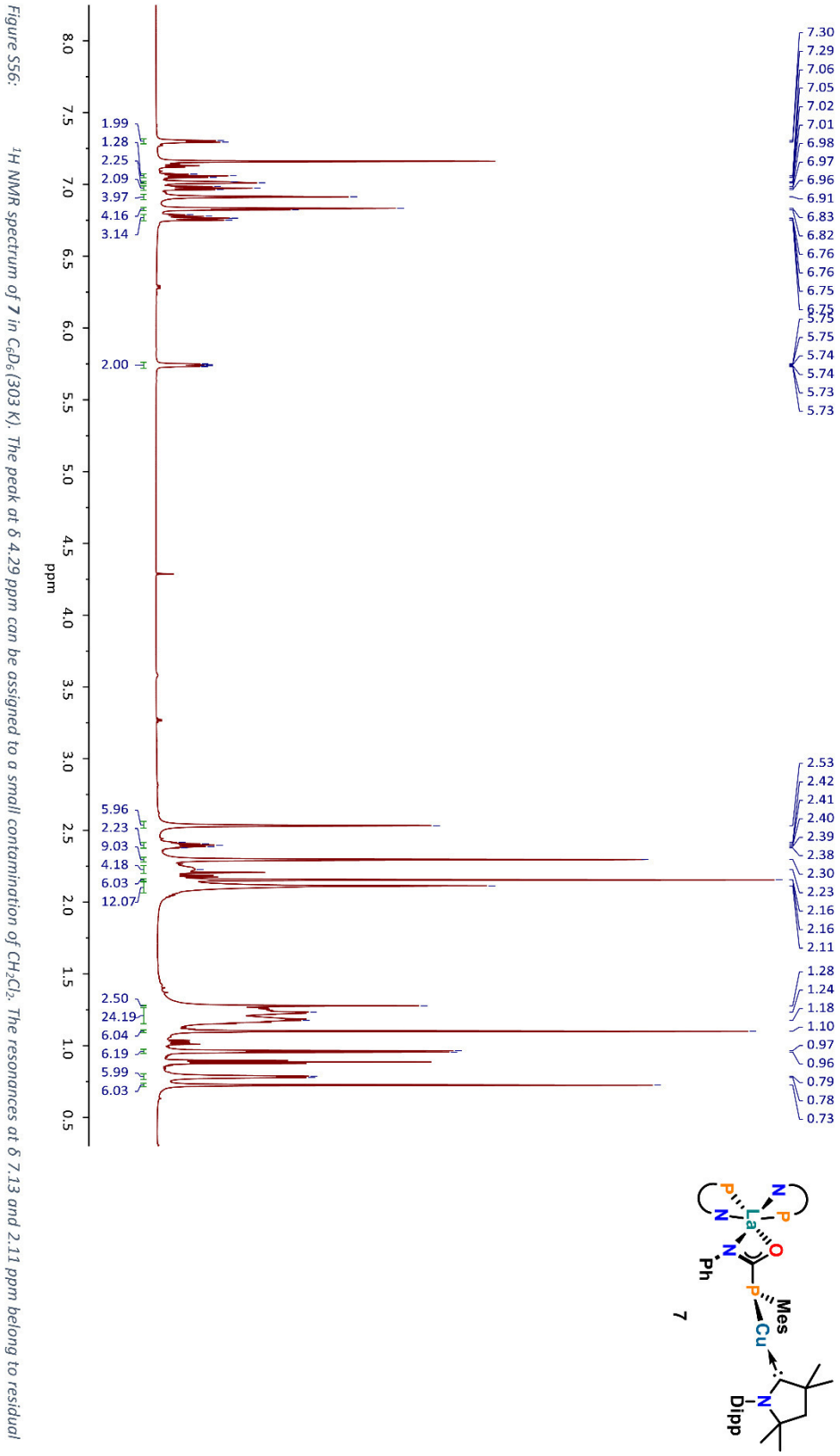

*Figure S56: ^1H NMR spectrum of **7** in C_6D_6 (303 K). The peak at δ 4.29 ppm can be assigned to a small contamination of CH_2Cl_2. The resonances at δ 7.13 and 2.11 ppm belong to residual toluene; the ones at δ 1.23 and 0.89 ppm to traces of n-hexane.*

S63

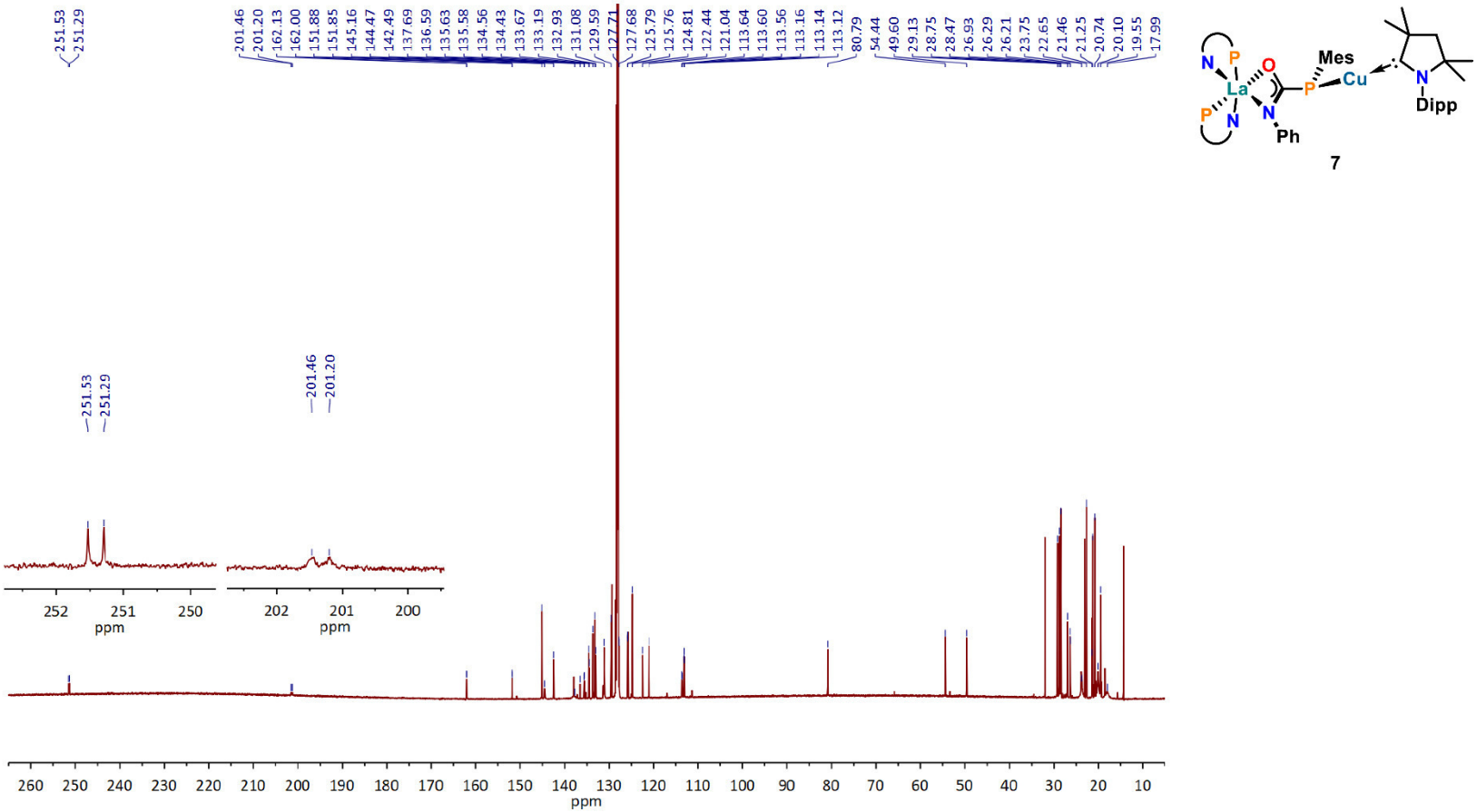

Figure S57: *$^{13}C\{^{1}H\}$ NMR spectrum of **7** in C_6D_6 (303 K). The peaks at δ 137.9, 129.3, 128.6, 125.7 and 21.4 ppm can be assigned to residual toluene. The resonances at δ 32.0, 23.1 and 14.4 ppm belong to traces of n-hexane. The two details show the characteristic doublet splitting of the $C_{carbene}$ and $C_{phosphaureate}$ resonances caused by ^{2}J or ^{1}J coupling to $P_{phosphaureate}$, respectively.*

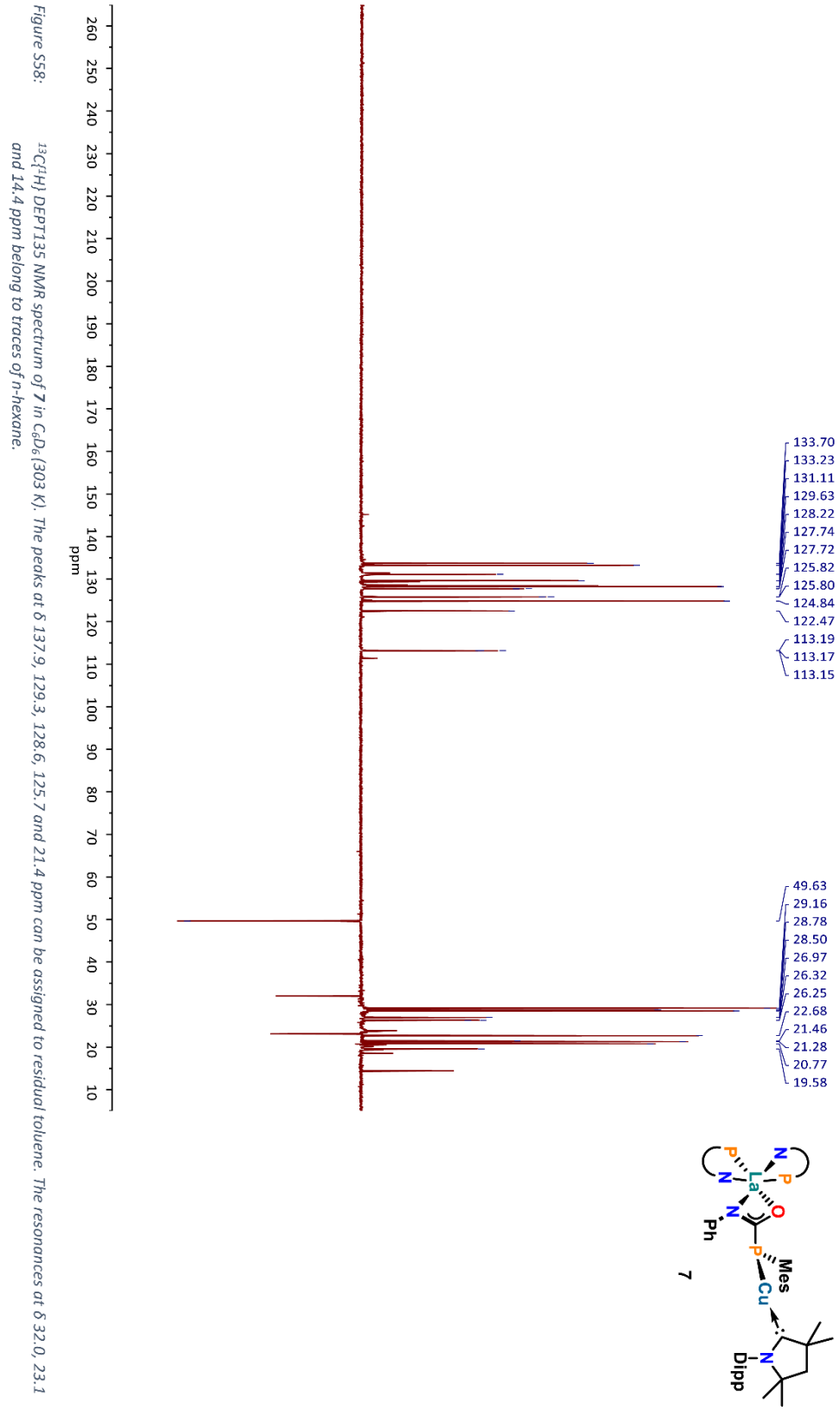

Figure S58: $^{13}C\{^1H\}$ *DEPT135 NMR spectrum of* **7** *in* C_6D_6 *(303 K). The peaks at δ 137.9, 129.3, 128.6, 125.7 and 21.4 ppm can be assigned to residual toluene. The resonances at δ 32.0, 23.1 and 14.4 ppm belong to traces of n-hexane.*

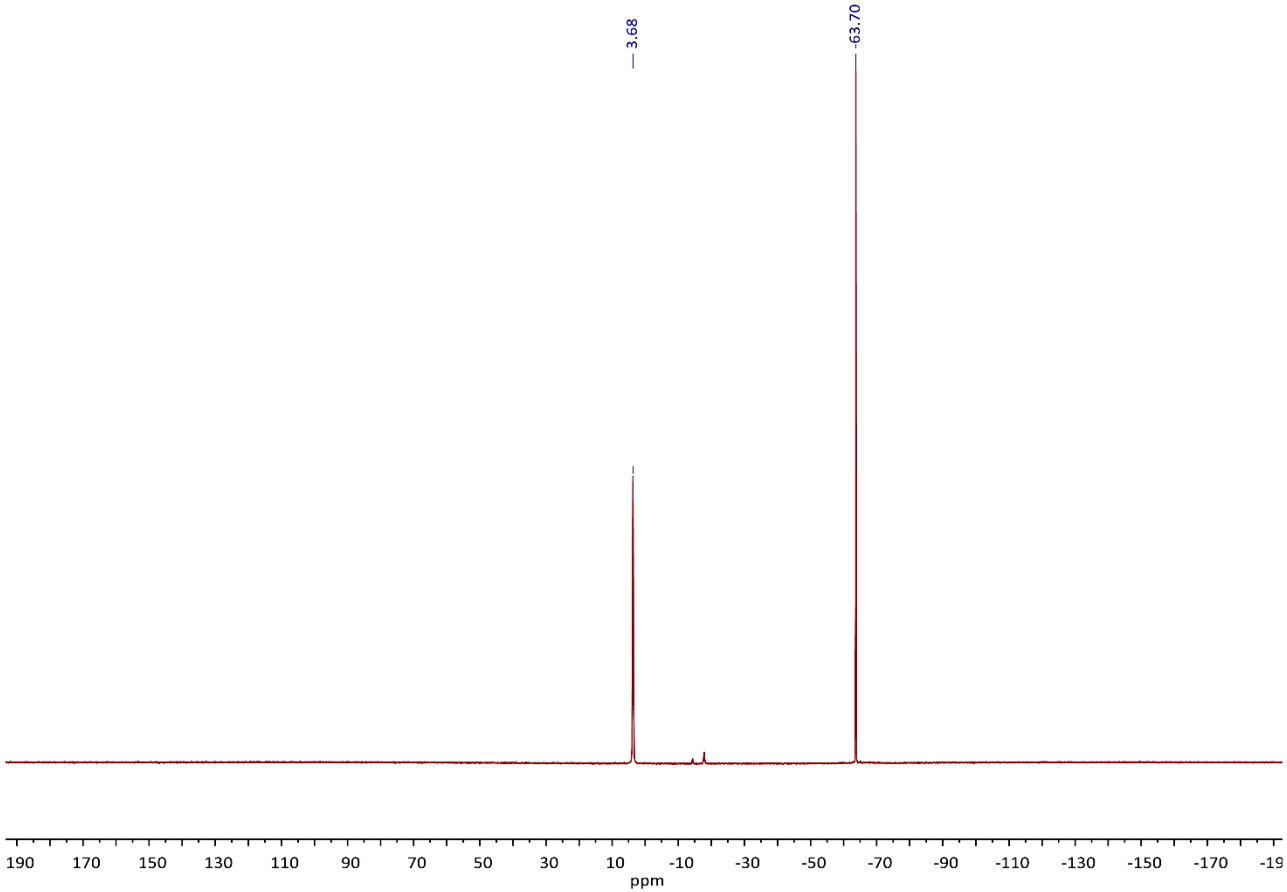

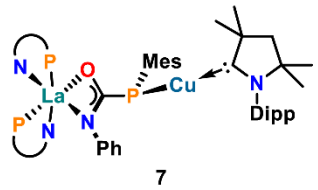

7

Figure S59: *^{31}P NMR spectrum of **7** in C_6D_6 (303 K). The peak at δ –17.8 ppm can be assigned to traces of **HPN**.*

Figure S60: ^{1}H–^{1}H *COSY NMR spectrum of* **7** *in* C_6D_6 *(303 K).*

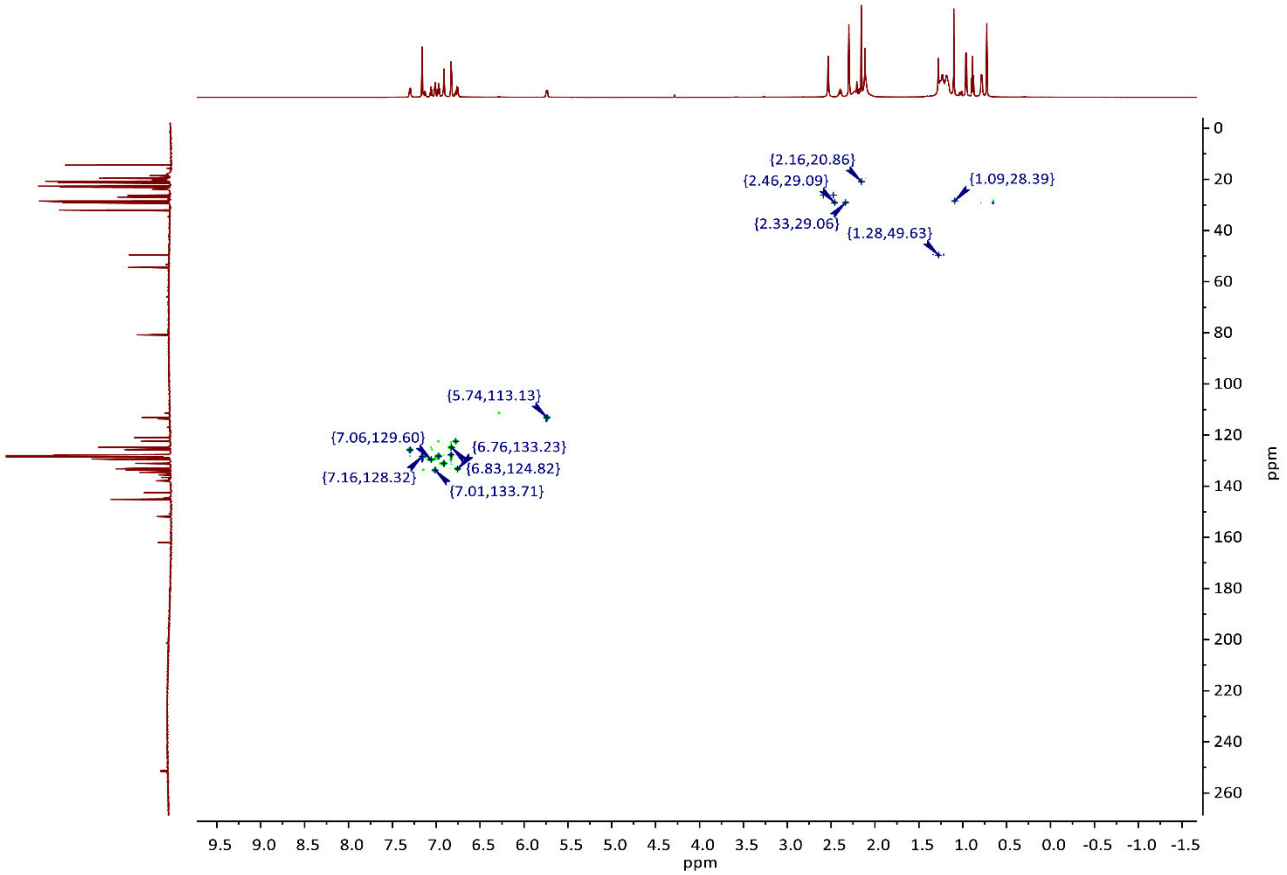

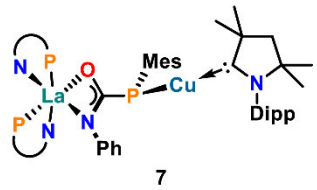

7

Figure S61: *^{1}H–^{13}C HSQC NMR spectrum of **7** in C_6D_6 (303 K).*

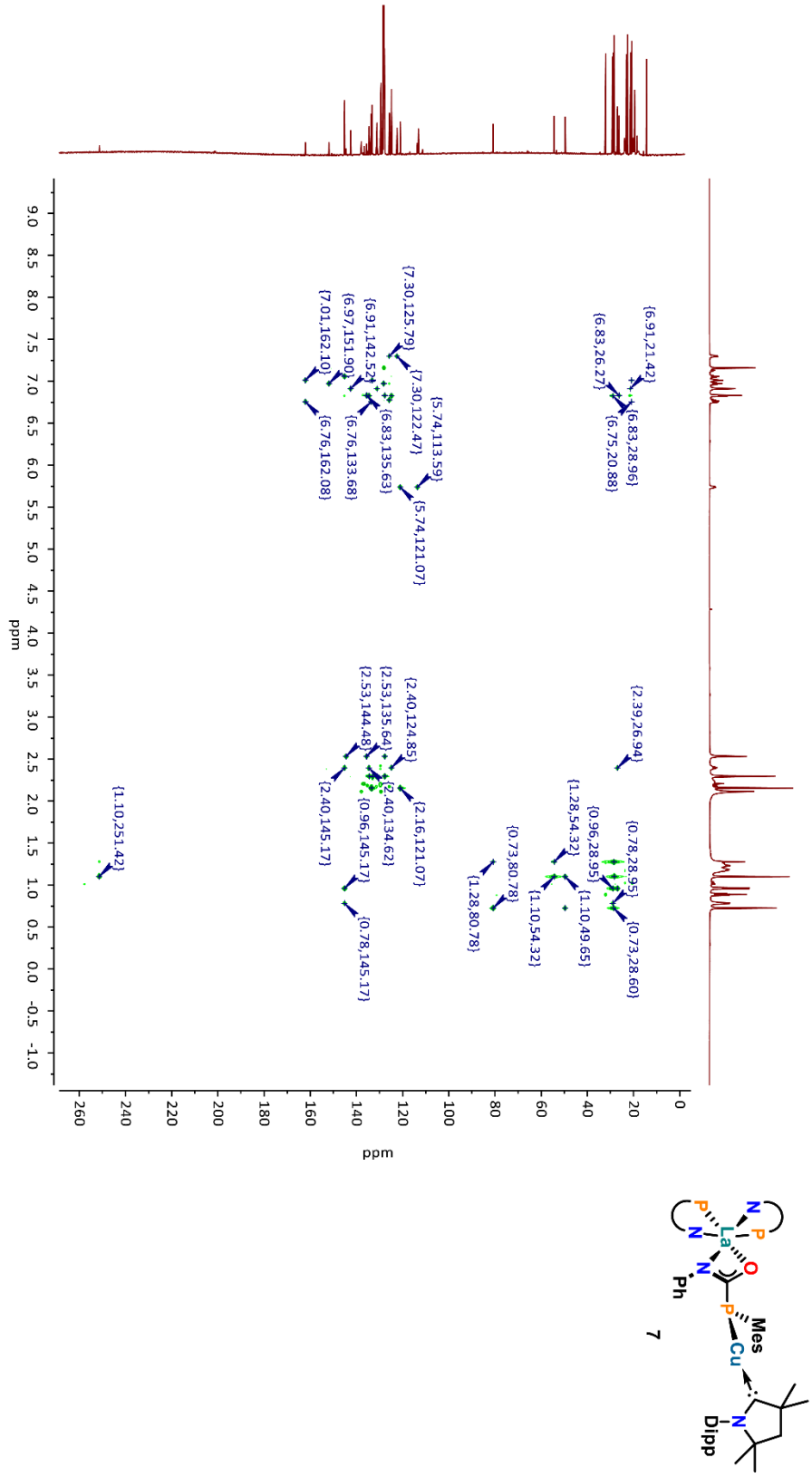

Figure S62: ^{1}H–^{13}C *HMBC NMR spectrum of* **7** *in* C_6D_6 *(303 K).*

7

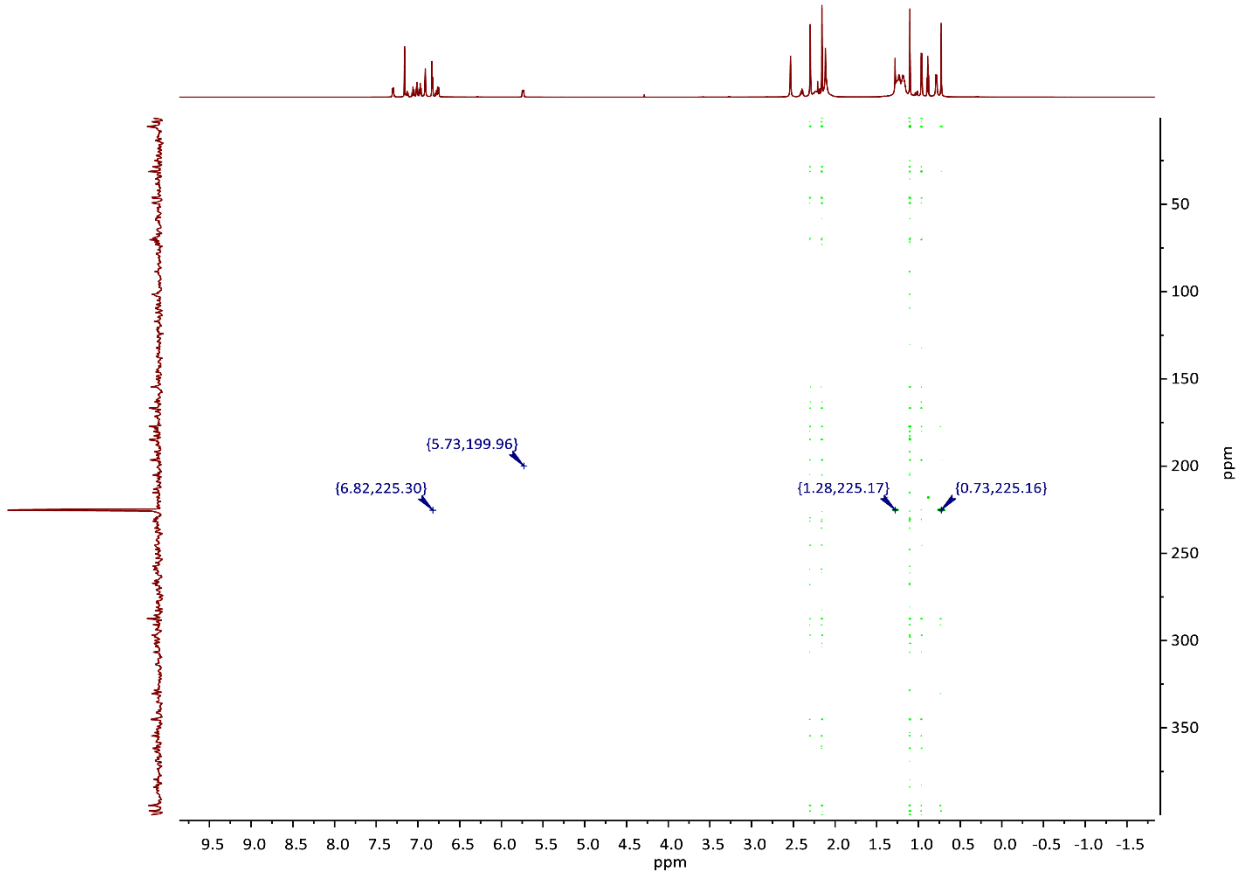

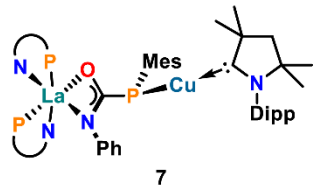

7

Figure S63: *^{1}H–^{15}N HMBC NMR spectrum of **7** in C_6D_6 (303 K).*

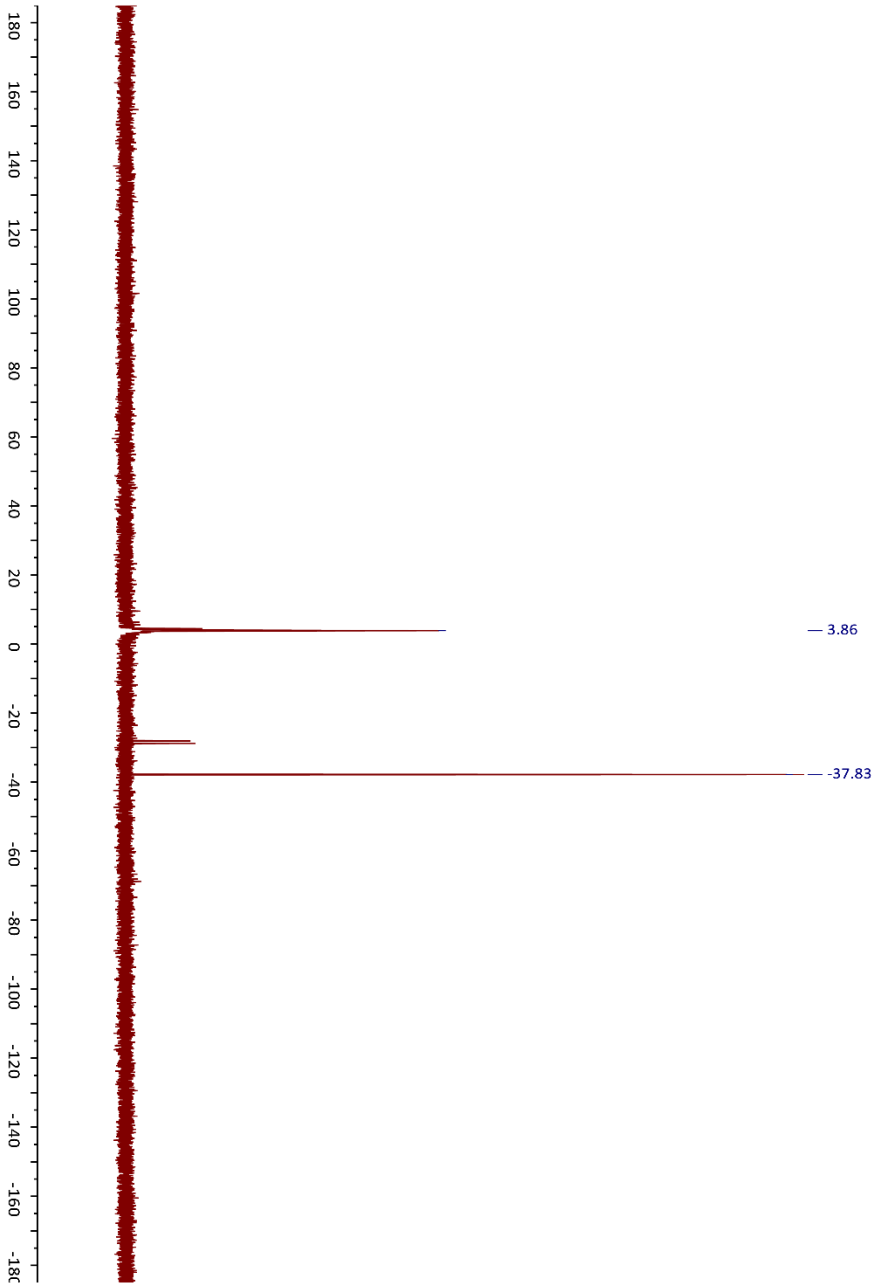

Figure S64: Reaction control ^{31}P NMR spectrum of ***4*** *and* ***[^{Me}CAAC]AuCl*** *in diethyl ether (route A, with C_6D_6 capillary, 303 K).*

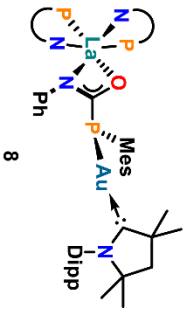

8

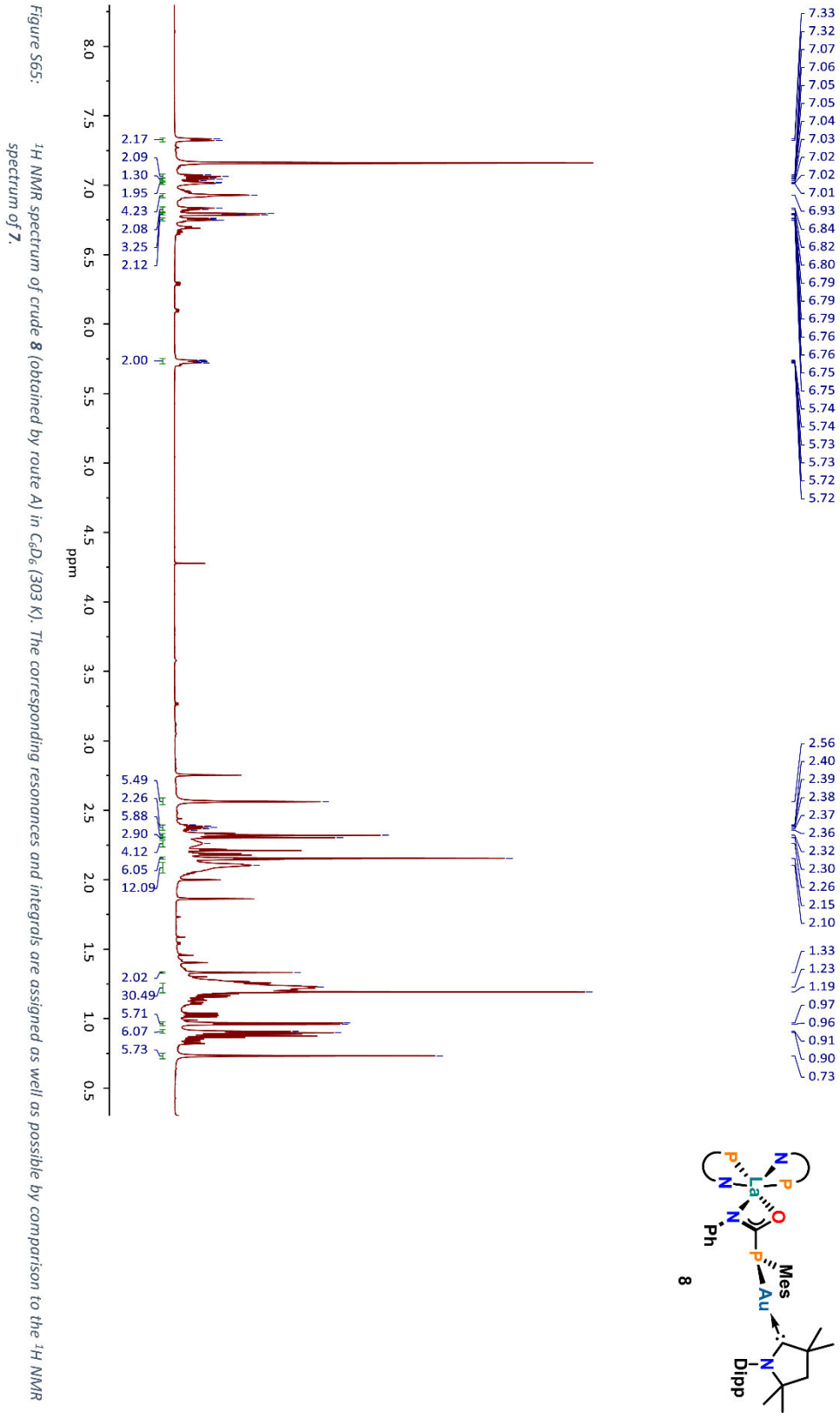

*Figure S65: ^{1}H NMR spectrum of crude **8** (obtained by route A) in C_6D_6 (303 K). The corresponding resonances and integrals are assigned as well as possible by comparison to the ^{1}H NMR spectrum of **7**.*

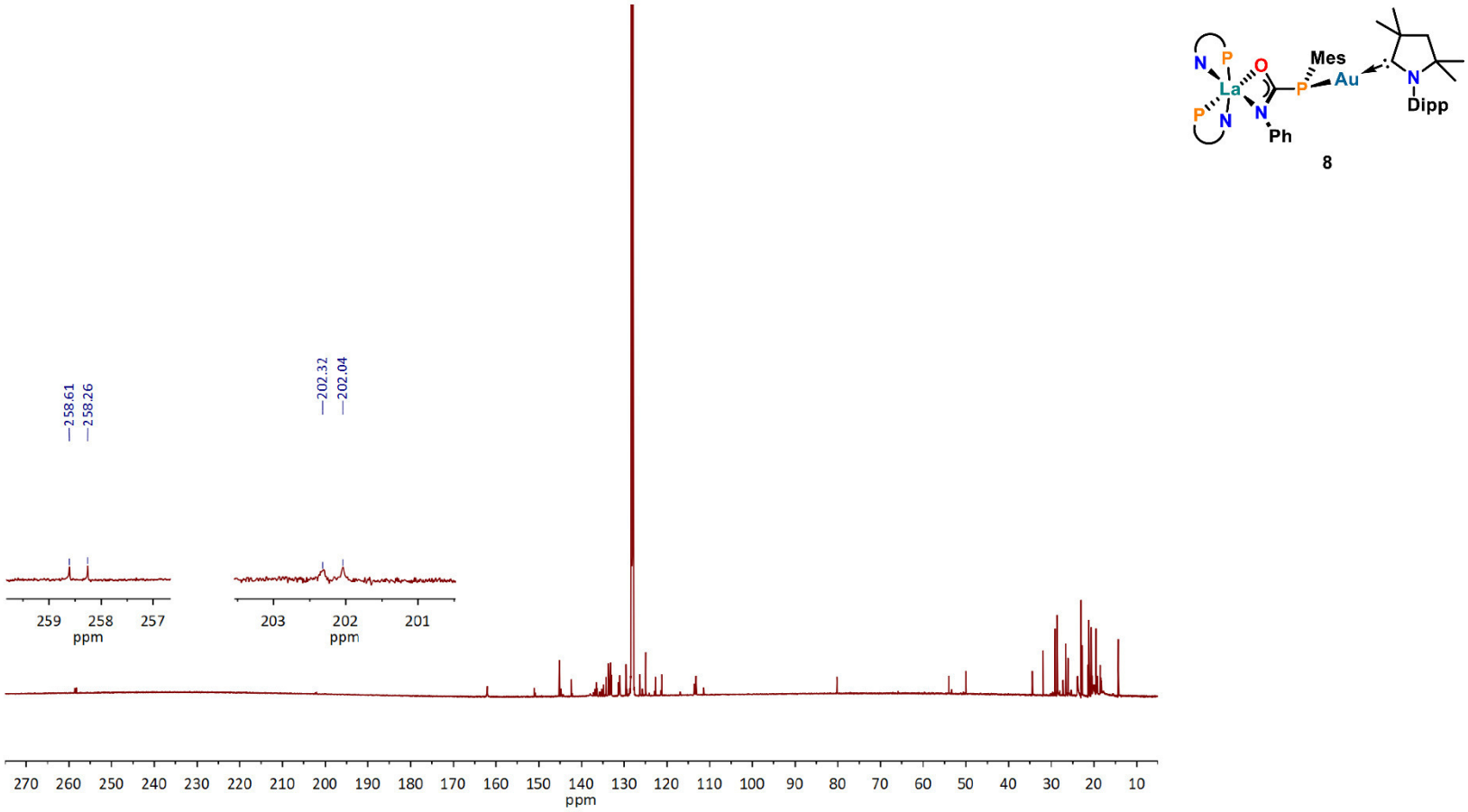

8

Figure S66: *$^{13}C\{^{1}H\}$ NMR spectrum of crude **8** (obtained by route A) in C_6D_6 (303 K). The two details show the characteristic doublet splitting of $C_{carbene}$ and $C_{phosphaureate}$ caused by ^{2}J and ^{1}J coupling to $P_{phosphaureate}$, respectively. Due to significant amounts of unidentified impurities in the sample, the other resonances are left unassigned.*

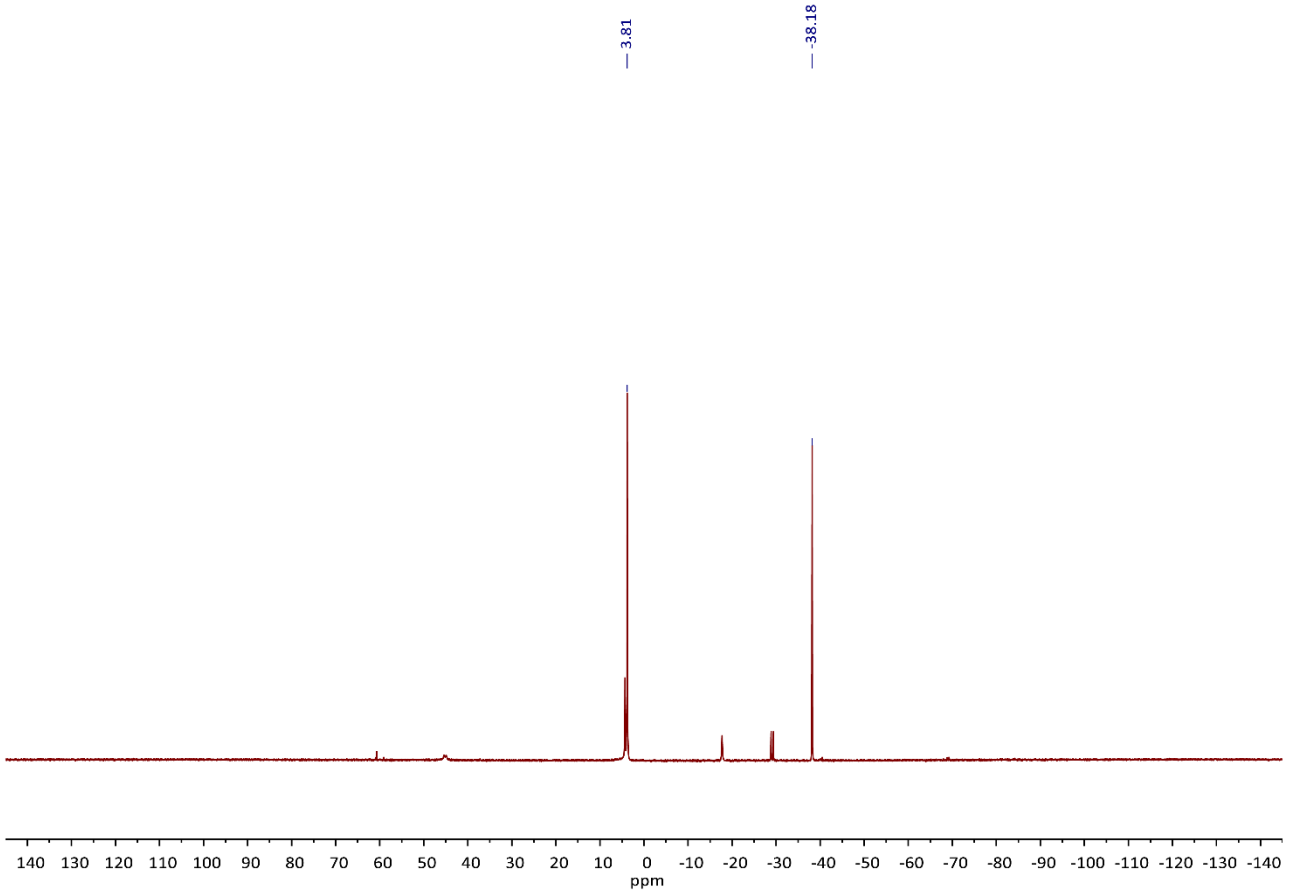

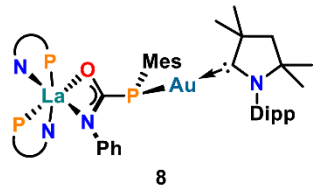

8

Figure S67: *^{31}P NMR spectrum of crude **8** (obtained by route A) in C_6D_6 (303 K). The resonance at δ –17.7 ppm can be assigned to **HPN**.*

*Figure S68: Stacked reaction control $^{31}P\{^1H\}$ NMR spectra of **2** and **(^{Me}CAAC)Au(HMDS)** in toluene (route B, with C_6D_6 capillary, 303 K). The resonances of unreacted starting material **2**, main product **8** as well as decomposition product **HPN** are labeled in the bottom and top spectrum, respectively. The reaction temperature and times are specified on the right.*

S75

Figure S69: Stacked ^{1}H NMR spectra of ***(MeCAAC)Au(HMDS)*** *(top) and material obtained from the test reaction of* ***(MeCAAC)Au(HMDS)*** *and benzyl bromide in THF at room temperature[9] (bottom) (both C_6D_6, 303 K). Note the essentially identical resonances for* ***(MeCAAC)Au(HMDS)****, indicating that no reaction had occurred after 1 h. The resonances at δ 7.03–6.92 and 3.96 ppm belong to unreacted benzyl bromide.*

3. IR Spectra

Figure S70: IR spectrum (ATR) of (IMeCAAC)Au(HMDS).

S77

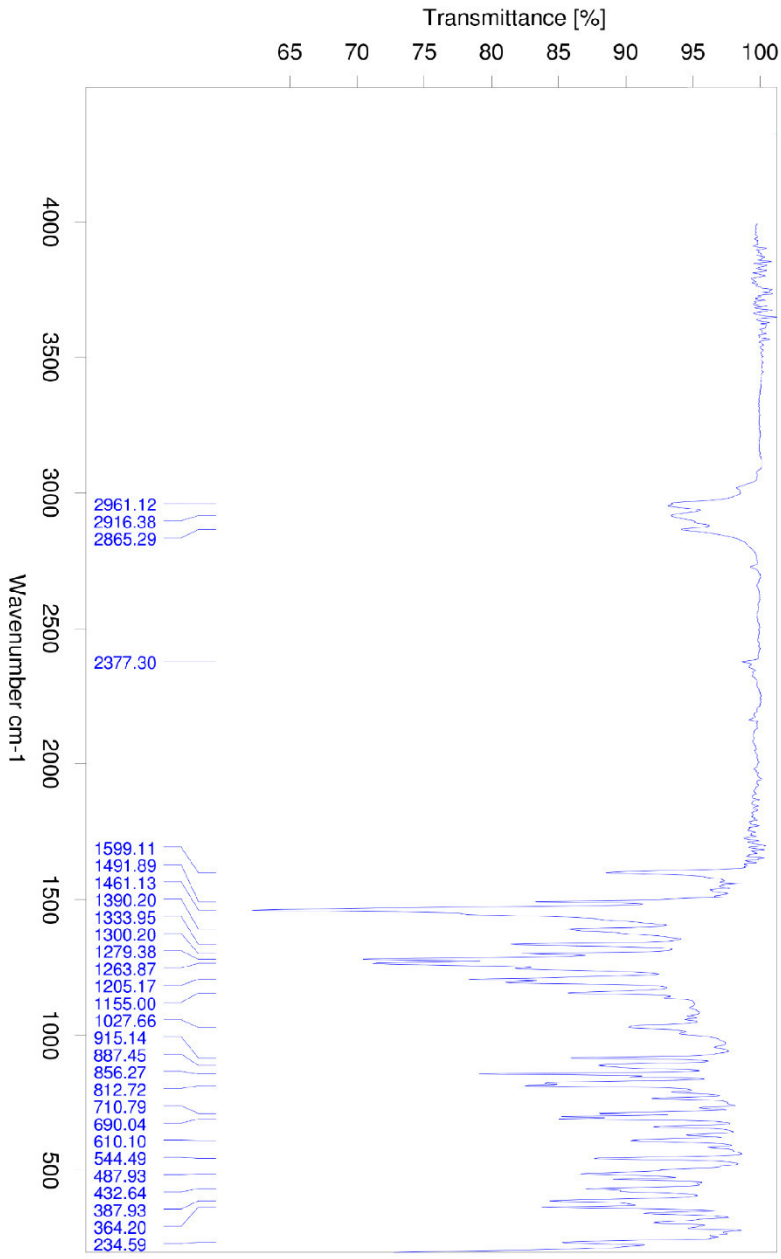

Figure S71: IR spectrum (ATR) of **2**.

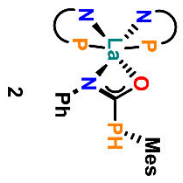

2

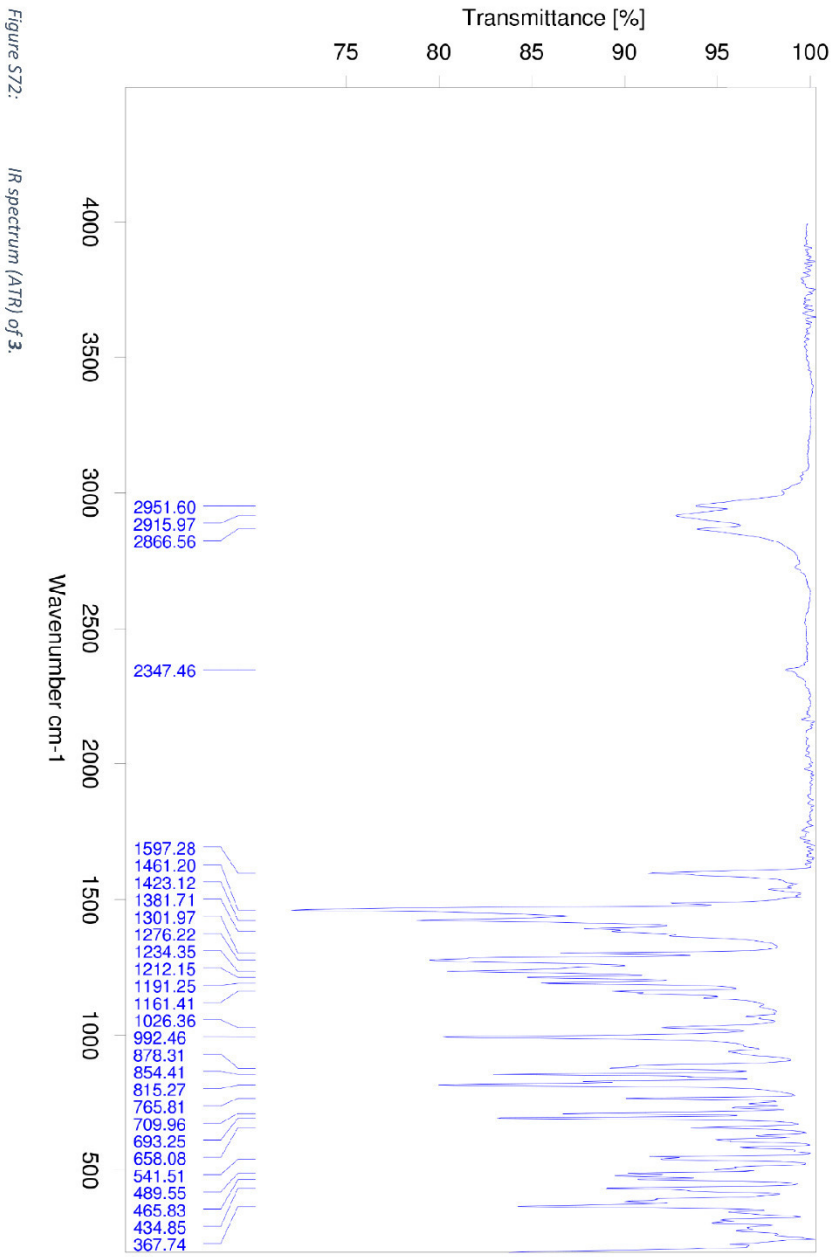

Figure S72: IR spectrum (ATR) of **3**.

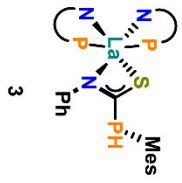

S79

Figure S73: IR spectrum (ATR) of ***4****.*

4

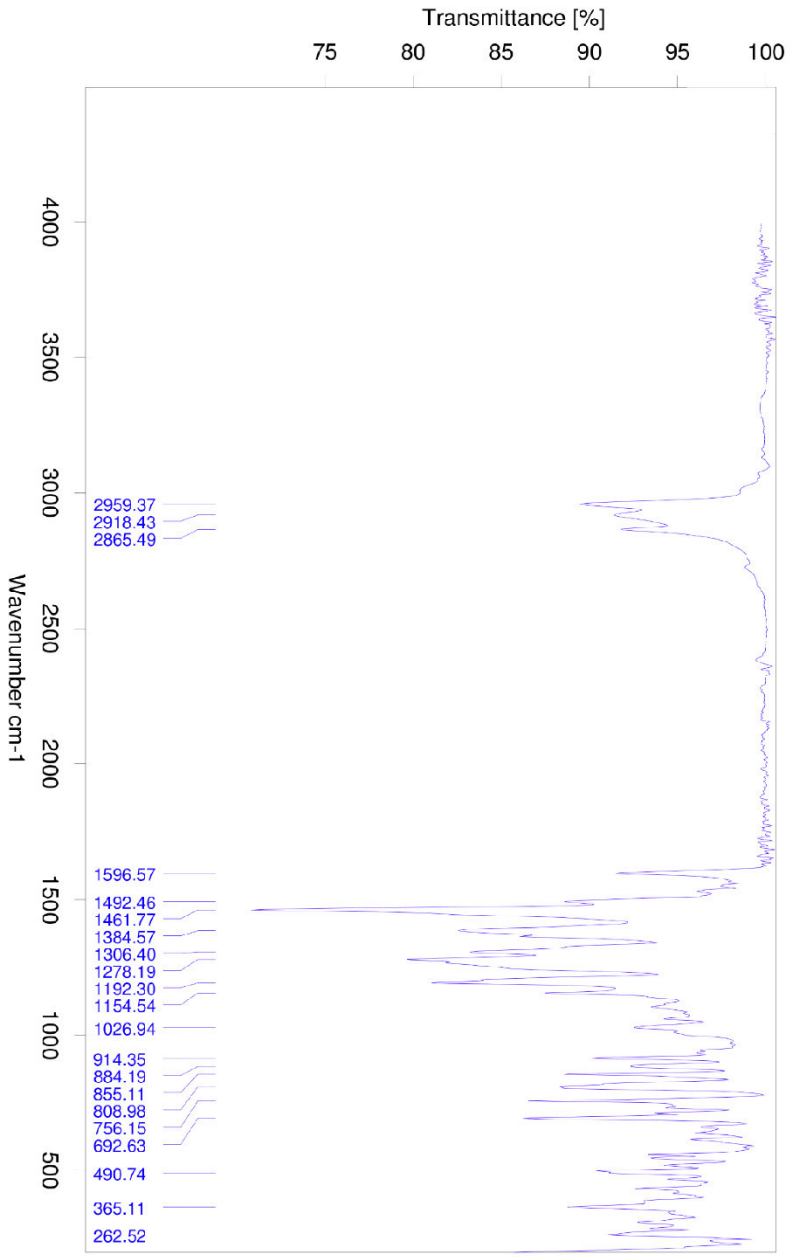

Figure S74: IR spectrum (ATR) of **5**.

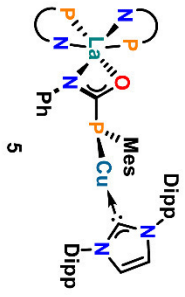

5

Figure S75: IR spectrum (ATR) of ***6****.*

6

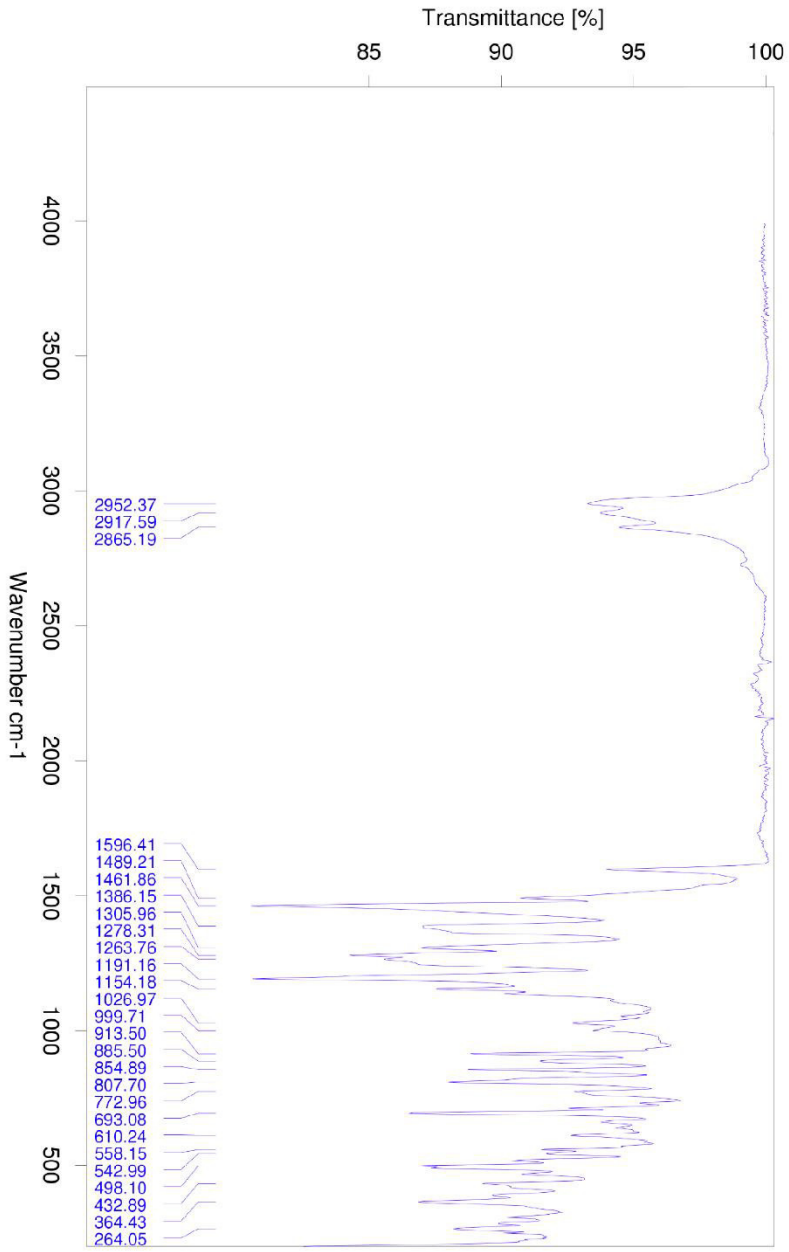

Figure S76: IR spectrum (ATR) of 7.

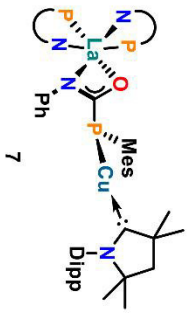

7

4. Crystallographic Details

Table S1: Crystallographic details on complexes (MeCAAC)Au(HMDS) and 2 – 7.

	(MeCAAC)Au(HMDS)	2	3	4*	5	6	7
Chemical formula	$C_{26}H_{49}AuN_2Si_2$	$C_{60}H_{79}N_3OP_3La \cdot 0.5\ (C_6H_{14})$	$C_{60}H_{79}N_3PSLa$	$C_{60}H_{78}N_3OP_3LaK$	$C_{87}H_{114}N_5OP_3CuLa$	$C_{87}H_{114}N_5OP_3AuLa$	$C_{80}H_{109}N_4OP_3CuLa$
M_r	642.82	1133.16	1106.14	1128.23	1541.19	1674.61	1438.07
Crystal system	Triclinic	Monoclinic	Triclinic	Tetragonal	Monoclinic	Monoclinic	Monoclinic
Space group	*P*–1	$P2_1/n$	*P*–1	$I4_1/a$	$P2_1/c$	$P2_1/c$	$P2_1/c$
a (Å)	9.8104(6)	12.079(5)	11.52(1)	36.1(1)	16.2817(5)	16.422(3)	19.2167(6)
b (Å)	12.0080(7)	25.64(1)	12.41(1)	36.1(1)	25.6054(8)	25.613(5)	19.9347(6)
c (Å)	13.3907(8)	20.369(9)	22.10(2)	25.0(1)	23.3037(8)	23.264(5)	22.4058(7)
α (°)	99.119(2)	90	87.48(2)	90	90	90	90
β (°)	91.326(2)	101.774(7)	83.32(2)	90	106.287(1)	106.600(4)	97.055(1)
γ (°)	108.076(2)	90	67.80(2)	90	90	90	90
V (Å^3)	1476.26(15)	6175(5)	2907(5)	32447(208)	9325.4(5)	9377(3)	8518.2(5)
Z	2	4	2	16	4	4	4
Densitiy (g cm^{-3})	1.446	1.219	1.264	0.918	1.098	1.186	1.121
F(000)	652	2380	1156	9296	3240	3440	3024
Radiation Type	MoKα	MoKα	MoKα	MoKα	MoKα	MoKα	MoKα
μ (mm^{-1})	5.079	0.810	0.892	0.666	0.773	2.104	0.841
Crystal size	0.24x0.22x0.16	0.08x0.07x0.05	0.25x0.24x0.18	0.08x0.06x0.02	0.15x0.13x0.11	0.20x0.15x0.03	0.09x0.08x0.01
Meas. Refl.	127820	45118	30652	18270	295761	63725	223608
Indep. Refl.	5425	11350	10743	6453	21397	17219	14990
Obsvd. [$I > 2\sigma(I)$]	5342	6992	9157	1918	17653	11534	12708
R_{int}	0.0260	0.1531	0.0460	-	0.0743	0.1003	0.0939
R [$F^2 > 2\sigma(F^2)$]	0.0376	0.0642	0.0343	-	0.0348	0.0491	0.0309
wR(F^2)	0.0547	0.1202	0.0446		0.0889	0.0863	0.0777
S	1.026	0.997	1.030		1.078	1.001	1.023
$\Delta\rho_{max}$	0.760	0.876	0.811	-	0.884	1.496	0.548
$\Delta\rho_{min}$	–0.906	–1.245	–0.523		–0.640	–0.887	–0.298
CCDC	2012282	2012280	2012278	-	2012283	2012279	2012281

* The model as such cannot be considered reliable. However, it matches well with other analytical means suggesting that at least the connectivity and overall conformation of the molecule are correctly described. The cell parameters are given for orientation.

Table S2: Selected bond lengths in Å and angles in ° of complexes (ᴹᵉCAAC)Au(HMDS), 2, 3 and 5 – 7.

	(ᴹᵉCAAC)Au(HMDS)	2	3	5	6	7
La1 – N1	-	2.416(5)	2.419(3)	2.465(2)	2.409(4)	2.477(2)
La1 – N2	-	2.397(5)	2.474(3)	2.420(2)	2.477(5)	2.423(2)
La1 – P1	-	3.145(2)	3.236(2)	3.1515(6)	3.201(2)	3.1564(7)
La1 – P2	-	3.171(2)	3.149(2)	3.2165(6)	3.155(2)	3.2077(7)
La1 – N80	-	2.616(5)	2.646(3)	2.510(2)	2.513(4)	2.538(2)
La1 – O80 / S80	-	2.448(4)	2.972(2)	2.418(2)	2.421(4)	2.419(2)
C80 – N80	-	1.309(8)	1.311(4)	1.336(3)	1.325(7)	1.335(3)
C80 – O80 / S80	-	1.303(7)	1.730(3)	1.297(3)	1.291(7)	1.300(3)
C80 – P70	-	1.856(6)	1.865(3)	1.830(2)	1.844(6)	1.822(3)
P70 – Cu1 / Au1	-	-	-	2.2043(7)	2.314(2)	2.2043(7)
Cu1 / Au1 – C100	1.970(3)	-	-	1.916(2)	2.043(6)	1.911(3)
Au1 – N1	2.027(2)	-	-	-	-	-
N1 – La1 – N2	-	117.8(2)	116.84(8)	117.49(6)	117.9(2)	116.23(7)
P1 – La1 –P2	-	170.4(4)	82.80(6)	84.96(2)	84.79(4)	88.09(2)
N80 – La1 – O80 / S80	-	52.2(1)	55.57(6)	53.75(6)	53.4(1)	53.36(6)
N80 – C80 – O80 / S80	-	117.5(5)	119.4(2)	115.7(2)	116.2(5)	115.6(2)
N80 – C80 – P70	-	126.5(5)	120.6(2)	120.7(2)	121.3(4)	123.5(2)
O80 / S80 – C80 – P70	-	115.7(5)	119.1(2)	123.5(2)	122.1(4)	120.7(2)
C80 – P70 – K1 / Cu1 / Au1	-	-	-	111.03(7)	110.1(2)	114.16(9)
P70 – Cu1 / Au1 – C100	-	-	-	164.57(7)	167.8(2)	168.57(8)
N1 – Au1 – C100	179.23(7)	-	-	-	-	-
N100 – C100 – C101	109.3(2)	-	-	-	-	-

*Figure S77: Thermal ellipsoid plot of (Me**CAAC**)Au(**HMDS**). Thermal ellipsoids are shown at a probability level of 30%. Hydrogen atoms have been omitted for clarity.*

*Figure S78: Section of the polymeric structure of **4** as obtained by X-ray diffraction analysis, showing the intra- and intermolecular interactions of the potassium ion with the P and O atoms as well as the phenyl and mesityl substituents of the phosphaureate ligands. Due the poor quality of the crystals, only the connectivity but no accurate structural parameters could be determined.*

5. Literature

(1) Watt, F. A.; Krishna, A.; Golovanov, G.; Ott, H.; Schoch, R.; Wölper, C.; Neuba, A. G.; Hohloch, S. Monoanionic Anilidophosphine Ligand in Lanthanide Chemistry: Scope, Reactivity, and Electrochemistry. *Inorg. Chem.* **2020**, *59*, 2719–2732.

(2) Zhu, H.; Shen, Y.; Wen, D.; Le, Z.-G.; Tu, T. Selective Synthesis of ortho-Substituted Diarylsulfones by Using NHC-Au Catalysts under Mild Conditions. *Organic letters* **2019**, *21*, 974–979.

(3) Griffiths, M. B. E.; Koponen, S. E.; Mandia, D. J.; McLeod, J. F.; Coyle, J. P.; Sims, J. J.; Giorgi, J. B.; Sirianni, E. R.; Yap, G. P. A.; Barry, S. T. Surfactant Directed Growth of Gold Metal Nanoplates by Chemical Vapor Deposition. *Chem. Mater.* **2015**, *27*, 6116–6124.

(4) Frémont, P. de; Scott, N. M.; Stevens, E. D.; Nolan, S. P. Synthesis and Structural Characterization of N -Heterocyclic Carbene Gold(I) Complexes. *Organometallics* **2005**, *24*, 2411–2418.

(5) Grünwald, A.; Goodner, S. J.; Munz, D. Isolating Free Carbenes, their Mixed Dimers and Organic Radicals. *Journal of visualized experiments : JoVE* [Online early access]. DOI: 10.3791/59389.

(6) Romanov, A. S.; Becker, C. R.; James, C. E.; Di, D.; Credgington, D.; Linnolahti, M.; Bochmann, M. Copper and Gold Cyclic (Alkyl)(amino)carbene Complexes with Sub-Microsecond Photoemissions: Structure and Substituent Effects on Redox and Luminescent Properties. *Chemistry (Weinheim an der Bergstrasse, Germany)* **2017**, *23*, 4625–4637.

(7) Sheldrick, G. M. Crystal structure refinement with SHELXL. *Acta crystallographica. Section C, Structural chemistry* **2015**, *71*, 3–8.

(8) Dolomanov, O. V.; Bourhis, L. J.; Gildea, R. J.; Howard, J. A. K.; Puschmann, H. OLEX2 : a complete structure solution, refinement and analysis program. *J Appl Crystallogr* **2009**, *42*, 339–341.

(9) Johnson, M. W.; Shevick, S. L.; Toste, F. D.; Bergman, R. G. Preparation and reactivity of terminal gold(i) amides and phosphides. *Chem. Sci.* **2013**, *4*, 1023–1027.

Supporting Information
for
Chapter 3

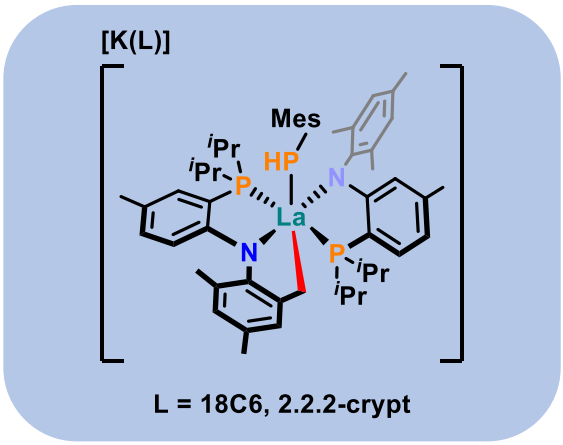

Supporting Information

A Transient Lanthanum Phosphinidene Complex

Fabian A. Watt,[a] Roland Schoch,[a] Karl N. McCabe,[b] Laurent Maron[b]* and Stephan Hohloch[c]*

Table of Contents

[a] *Paderborn University, Warburger Straße 100, 33098 Paderborn, Germany*
[b] *Université de Toulouse, 135 Avenue de Rangueil, 31077 Toulouse, France*
[c] *University of Innsbruck, Innrain 80-82, 6020 Innsbruck, Austria*
† Electronic Supplementary Information (ESI) available: [details of any supplementary information available should be included here]. See DOI: 10.1039/x0xx00000x

1. Experimental Section

General Remarks. If not otherwise mentioned, all transformations were carried out under inert conditions using an argon filled glovebox. All glassware (including glass-fibre filters) was stored in an oven at 150 °C for at least 12 h prior to use. Solvents were dried by a MBraun SPS system, degassed and stored over activated molecular sieves (3 Å) for at least 24 h prior to use. Cyclohexene and THF-d_8 were degassed by three freeze-pump-thaw cycles and then dried by storage over activated molecular sieves (3 Å) for at least 24 h. D_2O was degassed by sonication and sparging with argon prior to use. IR spectra were recorded at room temperature under inert conditions using a Bruker Vertex 70 with ATR equipment. If not otherwise stated, the NMR spectra were collected at 303 K on a Bruker AV-500 or an Ascent 700 spectrometer using a J-Young NMR tube. All chemical shifts (δ) are reported in ppm and coupling constants are given in Hz. ^{1}H and ^{13}C chemical shifts were calibrated to residual solvent peaks. ^{15}N chemical shifts (obtained by ^{1}H–^{15}N HMBC NMR spectroscopy) were calibrated externally to liquid ammonia (NH_3). ^{31}P chemical shifts were calibrated externally to phosphoric acid (H_3PO_4, 85% in water). Elemental analyses were performed using an Elementar vario microcube instrument at the Paderborn University. Starting materials KPHMes,[1a,b] $(PN)_2LaCl$,[1c] **1**,[1c] **4**[1c] and KBn[2] were synthesised following literature known procedures. 18-crown-6 (18C6) was recrystallised twice from hot acetonitrile, washed with diethyl ether and dried *in vacuo* prior to use. KHMDS and 2.2.2-cryptand were used as received.

Synthetic Procedures

Preparation of KPDMes.

A suspension of KPHMes (632 mg, 3.32 mmol, 1 eq.) in toluene (10 mL) was cooled to 0 °C and D_2O (0.1 mL, 5.54 mmol, 1.67 eq.) was added dropwise. After stirring for 15 min toluene and residual D_2O were carefully removed *in vacuo* at room temperature. The oily residue was extracted with *n*-hexane (2 x 3 mL), filtered and the solvent removed *in vacuo*. The mixture of H_2PMes (≈12%), HDPMes (≈47%) and D_2PMes (≈41%) was then reacted again with KHMDS (1 eq.) in toluene. The whole cycle was repeated two more times and KPDMes of >95% isotopic purity was finally isolated by filtration, washing with *n*-hexane (2 x 2 mL) and drying *in vacuo*. Yield: 200 mg (1.05 mmol, 32%).

Preparation of $(PN)_2La(PDMes)$ (1-d).

Toluene (6 mL) was added to $(PN)_2LaCl$ (171 mg, 200 µmol, 1 eq.) and KPDMes (46 mg, 240 µmol, 1.2 eq.) and the resulting yellow reaction mixture stirred for 3 d at room temperature. After centrifugation the solution was filtered and another portion of KPDMes (10 mg, 52 µmol, 0.26 eq.) was added. After stirring for another 24 h at room temperature the reaction mixture was again centrifuged, the solution filtered and all volatiles were removed *in vacuo*. The remaining solid was washed with –40 °C cold *n*-pentane (1 mL) and dried *in vacuo* to give the mono-deuterated complex **1-*d*** in ≈97% purity and ≈86–88% isotopic purity. Yield: 164 mg (169 µmol, 85%). ^{1}H NMR (C_6D_6, 303 K, 500 MHz, in ppm): δ = 0.85–0.98 (br. s, CH_{3iPr}, 12 H), 1.01–1.09 (br. s, CH_{3iPr}, 12 H), 1.72–1.91 (br. s, CH_{iPr}, 4 H), 2.14 (s, CH_{3Ar}, 6 H), 2.15 (s, CH_{3Ar}, 6 H), 2.25 (s, CH_{3Ar}, 3 H), 2.29–2.42 (br. s, CH_{3Ar}, 12 H), 2.44 (s, CH_{3Ar}, 6 H), 5.66–5.70 (m, CH_{Ar}, 2 H), 6.81 (dd, J = 8.4 Hz, J = 1.9 Hz, CH_{Ar}, 2 H), 6.83 (s, CH_{Ar}, 2 H), 6.84–6.87 (m, CH_{Ar}, 2 H), 6.89 (s, CH_{Ar}, 4 H); ^{31}P{^{1}H} NMR (C_6D_6, 303 K, 202 MHz, in ppm): δ = –38.2 (t, $^{1}J_{PD}$ = 28.6 Hz, *P*DMes, 1 P), 11.2 (s, P(^{i}Pr)$_2$, 2 P).

Preparation of [K(18C6)][(PN)(PN_{cyclo})La(PHMes)] (3a).

Route A: A solution of either KHMDS (20 mg, 100 µmol, 1 eq.) or KBn (13 mg, 100 µmol, 1 eq.) in DME (1 mL) was added dropwise to a mixture of **1** (97 mg, 100 µmol, 1 eq.) and 18-crown-6 (26 mg, 100 µmol, 1 eq.) in DME (3 mL) at room temperature, giving an orange-coloured solution. After 10 min the reaction mixture was filtered through a glass-fibre filter and most of the volatiles were removed *in vacuo* until an oily residue was obtained. Diethyl ether (3 mL) was added, which caused the dissolution

of the oil followed by the formation of orange-coloured crystalline blocks at –40 °C within 1 h. The crystals were isolated from the mother liquor, washed with diethyl ether (3 x 2 mL) and left to dry in the glovebox atmosphere, since prolonged drying *in vacuo* caused significant decomposition. Over a period of several hours to days, slow decomposition was also observed when storing a NMR sample of **3a** in, e.g., THF-d_8 at room temperature. NMR spectroscopic analysis of the obtained material in THF-d_8 revealed the presence of significant amounts (ca. 15%) of a second, as yet unidentified C–H-activated product, which could not be removed by repeated recrystallisation or washing. Attempts to optimise the reaction with THF, diethyl ether or toluene as alternative solvents, different rate of addition of base, stoichiometry of base or larger scaled batches as well as low temperature experiments at –40 °C did not yield better results and reaction monitoring of the DME reaction solution (with C_6D_6 capillary) by means of $^{31}P\{^1H\}$ NMR spectroscopy indicated that the formation of the unknown side product occurs already before work-up (see Fig. S3). Even though the NMR spectroscopic features of **3a** could still be assigned, due to the impurity no useful IR data or elemental analysis could be obtained. Single crystals of **3a** suitable for X-ray structure determination were obtained during work-up as described above. Yield: 67 mg (53 µmol, 53%, crude); ^1H NMR (THF-d_8, 303 K, 700 MHz, in ppm): δ = 0.26 (dd, J = 15.7 Hz, J = 6.9 Hz, CH_{3iPr}, 3 H), 0.64 (dd, J = 14.3 Hz, J = 6.9 Hz, CH_{3iPr}, 3 H), 0.76–0.81 (m, CH_{3iPr}, 6 H), 0.88–0.90 (m, CH_{3iPr}, 3 H), 1.02 (dd, J = 13.3 Hz, J = 7.0 Hz, CH_{3iPr}, 3 H), 1.07 (dd, $^2J_{HH}$ = 4.8 Hz, J = 3.1 Hz, C$H_{2Mes(PNcyclo)}$, 3 H), 1.15 (dd, J = 15.8 Hz, J = 6.9 Hz, CH_{3iPr}, 3 H), 1.25 (dd, J = 15.3 Hz, J = 6.8 Hz, CH_{3iPr}, 3 H), 1.41–1.44 (br. m, CH_{iPr}, 1 H), 1.73 (s, CH_{3Ar}, 3 H), 1.79–1.83 (m, CH_{iPr}, 1 H), 1.86 (s, CH_{3Ar}, 3 H), 1.99 (s, CH_{3Ar}, 3 H), 2.01 (s, CH_{3Ar}, 3 H), 2.08 (s, CH_{3Ar}, 3 H), 2.09 (s, CH_{3Ar}, 3 H), 2.10–2.17 (br. m, CH_{iPr}, 2 H), 2.19 (s, CH_{3Ar}, 6 H), 2.22 (s, CH_{3Ar}, 3 H), 2.48 (s, CH_{3Ar}, 3 H), 2.58 (d, $^1J_{PH}$ = 181.6 Hz, P*H*Mes, 1 H), 2.78 (dd, $^2J_{HH}$ = 4.8 Hz, J = 0.8 Hz, C$H_{2Mes(PNcyclo)}$, 1 H), 3.54 (s, C$H_{2(18C6)}$, 24 H), 5.09 (dd, J = 8.6 Hz, J = 4.9 Hz, CH_{Ar}, 1 H), 5.52 (dd, J = 8.5 Hz, J = 5.0 Hz, CH_{Ar}, 1 H), 6.07–6.09 (m, CH_{Ar}, 1 H), 6.36 (dd, J = 8.6 Hz, J = 1.9 Hz, CH_{Ar}, 1 H), 6.37–6.38 (m, CH_{Ar}, 1 H), 6.41–6.44 (m, CH_{Ar}, 3 H), 6.53 (dd, J = 5.0 Hz, J = 1.8 Hz, CH_{Ar}, 1 H), 6.63 (dd, J = 4.9 Hz, J = 1.9 Hz, CH_{Ar}, 1 H), 6.79–6.80 (m, CH_{Ar}, 1 H), 6.90–6.92 (m, CH_{Ar}, 1 H); $^{13}C\{^1H\}$ NMR (THF-d_8, 303 K, 176 MHz, in ppm): δ = 16.5 (d, J_{CP} = 5.4 Hz, *C*H$_{3iPr}$), 16.6 (d, J_{CP} = 3.8 Hz, *C*H$_{3iPr}$), 19.2 (m, *C*H$_{3iPr}$), 19.3 (m, *C*H$_{3iPr}$), 19.4 (m, *C*H$_{3iPr}$), 19.5 (s, *C*H$_{3Ar}$), 19.9 (m, *C*H$_{3iPr}$), 20.4 (m, *C*H$_{3iPr}$), 20.5 (s, *C*H$_{3Ar}$), 20.7 (s, *C*H$_{3Ar}$), 20.9 (s, *C*H$_{3Ar}$), 21.11 (s, *C*H$_{3Ar}$), 21.15 (s, *C*H$_{3Ar}$), 21.27 (s, *C*H$_{3Ar}$), 21.28 (m, *C*H$_{3iPr}$), 21.8 (s, *C*H$_{iPr}$), 22.1 (s, *C*H$_{3Ar}$), 22.6 (d, J_{CP} = 2.9 Hz, *C*H$_{iPr}$), 24.4 (d, J_{CP} = 2.5 Hz, *C*H$_{iPr}$), 25.9 (s, *C*H$_{iPr}$), 65.4 (s, *C*H$_{2Mes(PNcyclo)}$), 71.3 (s, *C*H$_{2(18C6)}$), 111.9 (d, J_{CP} = 7.1 Hz, *C*H$_{Ar}$), 112.7 (d, J_{CP} = 6.3 Hz, *C*H$_{Ar}$), 114.7 (d, J_{CP} = 8.7 Hz, C_{qAr}), 115.6 (d, J_{CP} = 10.7 Hz, C_{qAr}), 118.5 (s, C_{qAr}), 120.1 (s, *C*H$_{Ar}$), 125.0 (s, *C*H$_{Ar}$), 126.5 (s, C_{qAr}), 127.2 (s, *C*H$_{Ar}$), 130.5 (s, *C*H$_{Ar}$), 131.3 (s, *C*H$_{Ar}$), 131.7 (s, *C*H$_{Ar}$), 132.2 (s, *C*H$_{Ar}$), 132.3 (s, C_{qAr}), 133.2 (s, *C*H$_{Ar}$), 133.3 (s, C_{qAr}), 134.0 (s, *C*H$_{Ar}$), 136.7 (d, J_{CP} = 9.0 Hz, C_{qAr}), 137.3 (s, C_{qAr}), 138.8 (s, C_{qAr}), 139.1 (s, C_{qAr}), 143.8 (s, C_{qAr}), 146.4 (s, C_{qAr}), 150.8 (d, J_{CP} = 42.9 Hz, C_{qAr}), 162.0 (d, J_{CP} = 21.8 Hz, C_{qAr}), 163.4 (d, J_{CP} = 24.1 Hz, C_{qAr}); ^{31}P NMR (THF-d_8, 303 K, 283 MHz, in ppm): δ = –87.4 (dd, $^1J_{PH}$ = 181.6 Hz, $^2J_{PP}$ = 22.6 Hz, *P*HMes, 1 P), 2.6–3.8 (br. m, *P*(^{i}Pr)$_2$, 2 P); $^{31}P\{^1H\}$ NMR (THF-d_8, 303 K, 283 MHz, in ppm): δ = –87.4 (d, $^2J_{PP}$ = 22.6 Hz, *P*HMes, 1 P), 3.0 (dd, $^2J_{PP}$ = 36.8 Hz, $^2J_{PP}$ = 22.6 Hz, *P*(^{i}Pr)$_2$, 1 P), 3.4 (d, $^2J_{PP}$ = 36.8 Hz, *P*(^{i}Pr)$_2$, 1 P).

Route B: A solution of KHMDS (10 mg, 50 µmol, 1. eq.) in cyclohexene (1 mL) was added dropwise to a mixture of **1-*d*** (49 mg, 50 µmol, 1 eq.) and 18-crown-6 (13 mg, 50 µmol, 1 eq.) in cyclohexene (2 mL) at room temperature, giving an orange-coloured solution. The reaction solution was allowed to rest at room temperature for 3 d, during which orange-coloured crystals formed. The crystalline material was separated from the mother liquor, washed with *n*-pentane (4 x 2 mL) and left to dry in the glovebox atmosphere for 2 h, yielding **3a** of ≈94% purity (see Fig. S18–S24). The obtained material gave satisfying elemental analysis results and therefore was also used to collect an IR spectrum. Yield: 32 mg (25 µmol, 50%); elemental analysis (in %): $C_{65}H_{97}KLaN_2O_6P_3$: calcd.: C 61.31, H 7.68, N 2.20; found: C 61.56, H 7.41, N 2.11.

Preparation of [K(2.2.2-cryptand)][(PN)(PN$_{cyclo}$)La(PHMes)] (3b).

A solution of either KHMDS (20 mg, 100 µmol, 1 eq.) or KBn (13 mg, 100 µmol, 1 eq.) in DME (1 mL) was added dropwise to a mixture of **1** (97 mg, 100 µmol, 1 eq.) and 2.2.2-cryptand (38 mg, 100 µmol, 1 eq.) in DME (3 mL) at room temperature, giving an orange-coloured solution. After 10 min the reaction mixture was filtered through a glass-fibre filter and most of the volatiles were removed *in vacuo* until an oily residue was obtained. Since crystallisation from DME/diethyl ether was not feasible due to the formation of a layer of oil, the residue was extracted with toluene (2 mL). The extract was concentrated *in vacuo* and triturated with *n*-hexane (3 x 2 mL) to give a light orange-coloured solid which was washed with *n*-pentane (2 x 2 mL) and left to dry in the glovebox atmosphere. Recrystallisation of this raw product in useful quantities was not possible due to the poor crystallisation behaviour of **3b**, i.e., the formation of mainly oily precipitates from different solvent combinations of DME, THF or toluene with diethyl ether, *n*-hexane or *n*-pentane. Since **3b** was found to be very difficult to isolate as pure material and prone to decomposition, a full characterisation was not feasible. The ^{1}H NMR resonances are assigned as well as possible by comparison with the spectrum of **3a**. Single crystals of **3b** suitable for X-ray structure determination were obtained by gas phase diffusion of *n*-hexane into a THF solution of **3b** (ca. 15 mg in 300 µL) at room temperature overnight. Yield: 128 mg (92 µmol, 92%, crude); ^{1}H NMR (THF-d_8, 303 K, 500 MHz, in ppm): δ = 0.28 (dd, J = 15.2 Hz, J = 7.0 Hz, CH_{3iPr}, 3 H), 0.65 (dd, J = 13.8 Hz, J = 6.9 Hz, CH_{3iPr}, 3 H), 0.75–0.85 (m, CH_{3iPr}, 6 H), 0.95–1.06 (m, CH_{3iPr}, 6 H), 1.11–1.16 (dd, J = 15.2 Hz, J = 6.8 Hz, CH_{3iPr}, 3 H), 1.23–1.28 (dd, J = 13.8 Hz, J = 6.9 Hz, CH_{3iPr}, 3 H), 1.41–1.46 (br. m, CH_{iPr}, 1 H), 1.74 (s, CH_{3Ar}, 3 H), 1.79–1.84 (br. m, CH_{iPr}, 1 H), 1.86 (s, CH_{3Ar}, 3 H), 2.00 (s, CH_{3Ar}, 3 H), 2.01 (s, CH_{3Ar}, 3 H), 2.08 (s, CH_{3Ar}, 3 H), 2.09 (s, CH_{3Ar}, 3 H), 2.10–2.15 (br. m, CH_{iPr}, 2 H), 2.20 (s, CH_{3Ar}, 6 H), 2.22 (s, CH_{3Ar}, 3 H), 2.48–2.49 (m, C$H_{2(2.2.2\text{-cryptand})}$, 12 H; s, C$H_{3Ar}$), 2.59 (d, $^{1}J_{PH}$ = 180.8 Hz, P*H*Mes, 1 H), 2.78 (dd, $^{2}J_{HH}$ = 4.9 Hz, J = 0.7 Hz, C$H_{2Mes(PNcyclo)}$, 1 H), 3.46–3.48 (m, C$H_{2(2.2.2\text{-cryptand})}$, 12 H), 3.52 (s, C$H_{2(2.2.2\text{-cryptand})}$, 12 H), 5.09 (dd, J = 8.5 Hz, J = 4.9 Hz, CH_{Ar}, 1 H), 5.53 (dd, J = 8.5 Hz, J = 4.8 Hz, CH_{Ar}, 1 H), 6.07–6.09 (m, CH_{Ar}, 1 H), 6.35–6.39 (m, CH_{Ar}, 2 H), 6.42–6.45 (m, CH_{Ar}, 3 H), 6.54 (dd, J = 5.1 Hz, J = 2.0 Hz, CH_{Ar}, 1 H), 6.64 (dd, J = 4.9 Hz, J = 2.1 Hz, CH_{Ar}, 1 H), 6.79–6.81 (m, CH_{Ar}, 1 H), 6.90–6.92 (m, CH_{Ar}, 1 H) (One of the C$H_{2Mes(PNcyclo)}$ resonances is obscured by the CH_{3iPr} multiplet resonances and therefore cannot be assigned.); ^{31}P NMR (THF-d_8, 303 K, 283 MHz, in ppm): δ = –86.9 (dd, $^{1}J_{PH}$ = 180.8 Hz, $^{2}J_{PP}$ = 21.6 Hz, *P*HMes, 1 P), 2.7–4.0 (br. m, *P*(^{i}Pr)$_2$, 2 P); ^{31}P{^{1}H} NMR (THF-d_8, 303 K, 283 MHz, in ppm): δ = –86.9 (d, $^{2}J_{PP}$ = 21.6 Hz, *P*HMes, 1 P), 3.2 (dd, $^{2}J_{PP}$ = 36.7 Hz, $^{2}J_{PP}$ = 22.7 Hz, *P*(^{i}Pr)$_2$, 1 P), 3.6 (d, $^{2}J_{PP}$ = 36.7 Hz, *P*(^{i}Pr)$_2$, 1 P).

Preparation of [K(18C6)][(PN)(PN$_{cyclo}$)La(OMes)] (5a).

A solution of either KHMDS (25 mg, 126 µmol, 1.05 eq.) or KBn (17 mg, 126 µmol, 1.05 eq.) in DME (1 mL) was added dropwise to a mixture of **4** (115 mg, 120 µmol, 1 eq.) and 18-crown-6 (32 mg, 120 µmol, 1 eq.) in DME (3 mL) at room temperature, causing the dissolution of **4** and formation of a deep-yellow solution. After 10 min the reaction mixture was filtered through a glass-fibre filter and most of the volatiles were removed *in vacuo* until an oily residue was obtained. Diethyl ether (3 mL) was added, which caused the dissolution of the oil followed by the formation of yellow crystals in the form of radially growing aggregates of needles within 1 h. The crystalline material was isolated from the mother liquor, washed with diethyl ether (3 x 1 mL) and dried *in vacuo* to give analytically pure **5a** as a yellow microcrystalline powder. Single crystals of **5a** suitable for X-ray structure determination were obtained by gas phase diffusion of *n*-hexane into a concentrated benzene solution of **5a** (ca. 15 mg in 300 µL) at room temperature over a period of two days. Yield: 111 mg (88 µmol, 74%); ^{1}H NMR (THF-d_8, 303 K, 700 MHz, in ppm): δ = 0.43 (dd, J = 14.8 Hz, J = 6.9 Hz, CH_{3iPr}, 3 H), 0.68 (dd, J = 15.3 Hz, J = 6.9 Hz, CH_{3iPr}, 3 H), 0.72–0.79 (m, CH_{3iPr}, 6 H), 0.82 (*pseudo*-t, J = 7.3 Hz, CH_{3iPr}, 3 H), 0.93–0.99 (m, CH_{3iPr}, 6 H), 1.15 (dd, J = 15.1 Hz, J = 6.9 Hz, CH_{3iPr}, 3 H), 1.34 (dd, $^{2}J_{HH}$ = 5.0 Hz, J = 3.1 Hz, C$H_{2Mes(PNcyclo)}$, 1 H), 1.63 (s, CH_{3Ar}, 3 H), 1.65–1.70 (m, CH_{iPr}, 1 H), 1.74 (s, CH_{3Ar}, 3 H), 1.97 (s, CH_{3Ar}, 3 H), 1.99 (s, CH_{3Ar}, 3 H), 2.01–2.06 (br. m, CH_{iPr}, 2 H), 2.03 (s, CH_{3Ar}, 3 H), 2.05 (s, CH_{3Ar}, 3 H), 2.06 (s, CH_{3Ar}, 6 H), 2.09–2.12 (br. m, CH_{iPr}, 1 H), 2.13 (dd, $^{2}J_{HH}$ = 5.0 Hz, J = 1.6 Hz, C$H_{2Mes(PNcyclo)}$, 1 H), 2.20 (s, CH_{3Ar}, 3 H), 2.36 (s, CH_{3Ar}, 3 H), 3.57 (s, C$H_{2(18C6)}$, 24 H), 5.11 (dd, J = 8.6 Hz, J = 5.2 Hz, CH_{Ar}, 1 H), 5.53 (dd,

J = 8.3 Hz, *J* = 5.2 Hz, C*H*$_{Ar}$, 1 H), 5.94–5.96 (m, C*H*$_{Ar}$, 1 H), 6.33 (dd, *J* = 8.6 Hz, *J* = 1.9 Hz, C*H*$_{Ar}$, 1 H), 6.35–6.38 (m, C*H*$_{Ar}$, 2 H), 6.46 (s, C*H*$_{Ar}$, 2 H), 6.52 (dd, *J* = 5.2 Hz, *J* = 1.9 Hz, C*H*$_{Ar}$, 1 H), 6.66 (dd, *J* = 5.2 Hz, *J* = 2.1 Hz, C*H*$_{Ar}$, 1 H), 6.75–6.77 (m, C*H*$_{Ar}$, 1 H), 6.82–6.85 (m, C*H*$_{Ar}$, 1 H); ^{13}C{^{1}H} NMR (THF-d_8, 303 K, 176 MHz, in ppm): δ = 16.5 (d, J_{CP} = 4.5 Hz, *C*H$_{3iPr}$), 17.2 (d, J_{CP} = 2.1 Hz, *C*H$_{3iPr}$), 18.7 (d, J_{CP} = 11.7 Hz, *C*H$_{3iPr}$), 19.0 (d, J_{CP} = 10.9 Hz, *C*H$_{3iPr}$), 19.2 (d, J_{CP} = 16.7 Hz, *C*H$_{3iPr}$), 19.7 (d, J_{CP} = 16.2 Hz, *C*H$_{3iPr}$), 19.72 (s, *C*H$_{3Ar}$), 20.3 (s, *C*H$_{3Ar}$), 20.34 (s, *C*H$_{3Ar}$; d, J_{CP} = 9.3 Hz, *C*H$_{3iPr}$), 20.8 (s, *C*H$_{3Ar}$), 21.0 (s, *C*H$_{3Ar}$), 21.02 (d, J_{CP} = 11.1 Hz, *C*H$_{3iPr}$), 21.1 (d, J_{CP} = 3.8 Hz, *C*H$_{3Ar}$), 21.2 (s, *C*H$_{3Ar}$), 21.5 (s, C*H*$_{3Ar}$), 22.3 (s, *C*H$_{3Ar}$), 23.1 (s, *C*H$_{iPr}$), 25.9 (s, *C*H$_{iPr}$), 26.2 (d, J_{CP} = 4.3 Hz, *C*H$_{iPr}$), 61.2 (s, *C*H$_{2Mes(PNcyclo)}$), 71.3 (s, *C*H$_{2(18C6)}$), 111.7 (d, J_{CP} = 7.3 Hz, *C*H$_{Ar}$), 112.0 (d, J_{CP} = 6.3 Hz, *C*H$_{Ar}$), 114.9 (d, J_{CP} = 10.8 Hz, *C*$_{qAr}$), 115.2 (d, J_{CP} = 7.9 Hz, *C*$_{qAr}$), 116.2 (d, J_{CP} = 2.7 Hz, *C*$_{qAr}$), 117.6 (d, J_{CP} = 2.5 Hz, *C*$_{qAr}$), 118.7 (s, *C*H$_{Ar}$), 121.0 (s, *C*$_{qAr}$), 123.8 (s, *C*H$_{Ar}$), 126.3 (s, *C*$_{qAr}$), 128.7 (s, *C*H$_{Ar}$), 130.2 (s, *C*H$_{Ar}$), 130.9 (s, *C*H$_{Ar}$),131.8 (s, *C*$_{qAr}$), 131.82 (s, *C*H$_{Ar}$), 131.9 (s, *C*$_{qAr}$), 132.2 (s, *C*H$_{Ar}$), 133.3 (d, J_{CP} = 3.3 Hz, *C*H$_{Ar}$), 133.6 (d, J_{CP} = 2.8 Hz, *C*H$_{Ar}$), 136.1 (d, J_{CP} = 3.1 Hz, *C*$_{qAr}$), 136.5 (s, *C*$_{qAr}$), 137.3 (s, *C*$_{qAr}$), 139.1 (s, *C*$_{qAr}$), 146.7 (d, J_{CP} = 2.9 Hz, *C*$_{qAr}$), 147.0 (s, *C*$_{qAr}$), 162.6 (d, J_{CP} = 21.4 Hz, *C*$_{qAr}$), 163.9 (d, J_{CP} = 24.8 Hz, *C*$_{qAr}$),164.2 (s, *C*$_{qAr}$); ^{31}P{^{1}H} NMR (THF-d_8, 303 K, 283 MHz, in ppm): δ = –1.4 (d, $^{2}J_{PP}$ = 33.7 Hz, *P*(^{i}Pr)$_2$, 1 P), 1.1 (d, $^{2}J_{PP}$ = 33.7 Hz, *P*(^{i}Pr)$_2$, 1 P); elemental analysis (in %): $C_{65}H_{96}KLaN_2O_7P_2$: calcd.: C 62.09, H 7.70, N 2.23; found: C 61.67, H 7.66, N 2.38.

Preparation of [K(2.2.2-cryptand)][(PN)(PN$_{cyclo}$)La(OMes)] (5b).

A solution of either KHMDS (28 mg, 142 µmol, 1.15 eq.) or KBn (19 mg, 142 µmol, 1.15 eq.) in DME (1 mL) was added dropwise to a mixture of **4** (118 mg, 124 µmol, 1 eq.) and 2.2.2-cryptand (47 mg, 124 µmol, 1 eq.) in DME (3 mL) at room temperature, causing the dissolution of **4** and formation of a deep-yellow solution. After 20 min the reaction mixture was filtered through a glass-fibre filter and most of the volatiles were removed *in vacuo* until an oily residue was obtained. Diethyl ether (2 mL) was added, which caused the dissolution of the oil followed by the formation of yellow crystals in the form of radially growing aggregates of very thin needles after 2 d. The crystalline material was isolated from the mother liquor, washed with diethyl ether (2 x 2 mL) and dried *in vacuo* to give analytically pure **5b** as a yellow microcrystalline powder. Yield: 152 mg (111 µmol, 89%); ^{1}H NMR (THF-d_8, 303 K, 700 MHz, in ppm): δ = 0.44 (dd, *J* = 14.8 Hz, *J* = 7.0 Hz, C*H*$_{3iPr}$, 3 H), 0.68 (dd, *J* = 15.4 Hz, *J* = 7.0 Hz, C*H*$_{3iPr}$, 3 H), 0.72–0.80 (m, C*H*$_{3iPr}$, 6 H), 0.82 (*pseudo*-t, *J* = 7.3 Hz, C*H*$_{3iPr}$, 3 H), 0.95–0.99 (m, C*H*$_{3iPr}$, 6 H), 1.16 (dd, *J* = 15.1 Hz, *J* = 6.9 Hz, C*H*$_{3iPr}$, 3 H), 1.35 (dd, $^{2}J_{HH}$ = 5.0 Hz, *J* = 3.1 Hz, C*H*$_{2Mes(PNcyclo)}$, 1 H), 1.63 (s, C*H*$_{3Ar}$, 3 H), 1.65–1.71 (m, C*H*$_{iPr}$, 1 H), 1.75 (s, C*H*$_{3Ar}$, 3 H), 1.98 (s, C*H*$_{3Ar}$, 3 H), 1.99 (s, C*H*$_{3Ar}$, 3 H), 2.01–2.07 (br. m, C*H*$_{iPr}$, 2 H), 2.04 (s, C*H*$_{3Ar}$, 3 H), 2.06 (s, C*H*$_{3Ar}$, 3 H), 2.08 (s, C*H*$_{3Ar}$, 6 H), 2.11–2.13 (br. m, C*H*$_{iPr}$, 1 H), 2.14 (dd, $^{2}J_{HH}$ = 5.0 Hz, *J* = 1.6 Hz, C*H*$_{2Mes(PNcyclo)}$, 1 H), 2.20 (s, C*H*$_{3Ar}$, 3 H), 2.36 (s, C*H*$_{3Ar}$, 3 H), 2.51–2.54 (m, C*H*$_{2(2.2.2\text{-cryptand})}$, 12 H), 3.49–3.52 (m, C*H*$_{2(2.2.2\text{-cryptand})}$, 12 H), 3.55 (s, C*H*$_{2(2.2.2\text{-cryptand})}$, 12 H), 5.11 (dd, *J* = 8.6 Hz, *J* = 5.2 Hz, C*H*$_{Ar}$, 1 H), 5.55 (dd, *J* = 8.5 Hz, *J* = 5.2 Hz, C*H*$_{Ar}$, 1 H), 5.94–5.96 (m, C*H*$_{Ar}$, 1 H), 6.34 (dd, *J* = 8.6 Hz, *J* = 1.8 Hz, C*H*$_{Ar}$, 1 H), 6.36–6.40 (m, C*H*$_{Ar}$, 2 H), 6.46 (s, C*H*$_{Ar}$, 2 H), 6.52 (dd, *J* = 5.2 Hz, *J* = 1.8 Hz, C*H*$_{Ar}$, 1 H), 6.66 (dd, *J* = 5.2 Hz, *J* = 2.1 Hz, C*H*$_{Ar}$, 1 H), 6.75–6.78 (m, C*H*$_{Ar}$, 1 H), 6.83–6.85 (m, C*H*$_{Ar}$, 1 H); ^{13}C{^{1}H} NMR (THF-d_8, 303 K, 176 MHz, in ppm): δ = 16.5 (d, J_{CP} = 4.4 Hz, *C*H$_{3iPr}$), 17.2 (d, J_{CP} = 1.9 Hz, *C*H$_{3iPr}$), 18.7 (d, J_{CP} = 11.6 Hz, *C*H$_{3iPr}$), 19.0 (d, J_{CP} = 11.0 Hz, *C*H$_{3iPr}$), 19.2 (d, J_{CP} = 16.7 Hz, *C*H$_{3iPr}$), 19.7 (d, J_{CP} = 16.2 Hz, *C*H$_{3iPr}$), 19.8 (s, C*H*$_{3Ar}$), 20.3 (s, C*H*$_{3Ar}$), 20.4 (s, C*H*$_{3Ar}$; d, J_{CP} = 9.1 Hz, *C*H$_{3iPr}$), 20.8 (s, C*H*$_{3Ar}$), 21.0 (s, C*H*$_{3Ar}$), 21.03 (s, C*H*$_{3Ar}$), 21.04 (d, J_{CP} = 11.1 Hz, *C*H$_{3iPr}$), 21.1 (d, J_{CP} = 3.7 Hz, *C*H$_{3Ar}$), 21.2 (s, C*H*$_{3Ar}$), 21.5 (s, C*H*$_{3Ar}$), 22.2 (s, C*H*$_{3Ar}$), 23.1 (s, *C*H$_{iPr}$), 25.9 (s, *C*H$_{iPr}$), 26.2 (d, J_{CP} = 4.2 Hz, *C*H$_{iPr}$), 54.9 (s, *C*H$_{2(2.2.2\text{-cryptand})}$), 61.3 (s, *C*H$_{2Mes(PNcyclo)}$), 68.7 (s, *C*H$_{2(2.2.2\text{-cryptand})}$), 71.5 (s, *C*H$_{2(2.2.2\text{-cryptand})}$), 111.7 (d, J_{CP} = 7.1 Hz, *C*H$_{Ar}$), 112.0 (d, J_{CP} = 6.3 Hz, *C*H$_{Ar}$), 114.9 (d, J_{CP} = 11.0 Hz, *C*$_{qAr}$), 115.2 (d, J_{CP} = 7.9 Hz, *C*$_{qAr}$), 116.2 (d, J_{CP} = 2.6 Hz, *C*$_{qAr}$), 117.6 (d, J_{CP} = 2.3 Hz, *C*$_{qAr}$), 118.7 (s, *C*H$_{Ar}$), 121.0 (s, *C*$_{qAr}$), 123.8 (s, *C*H$_{Ar}$), 126.3 (s, *C*$_{qAr}$), 128.7 (s, *C*H$_{Ar}$), 130.2 (s, *C*H$_{Ar}$), 130.9 (s, *C*H$_{Ar}$), 131.8 (s, *C*$_{qAr}$), 131.9 (s, *C*H$_{Ar}$), 132.2 (s, *C*H$_{Ar}$), 133.3 (d, J_{CP} = 3.4 Hz, *C*H$_{Ar}$), 133.6 (d, J_{CP} = 2.7 Hz, *C*H$_{Ar}$), 136.2 (d, J_{CP} = 3.4 Hz, *C*$_{qAr}$), 136.5 (s, *C*$_{qAr}$), 137.3 (s, *C*$_{qAr}$), 139.1 (s, *C*$_{qAr}$), 146.7 (d, J_{CP} = 2.6 Hz, *C*$_{qAr}$), 147.0 (s, *C*$_{qAr}$), 162.6 (d, J_{CP} = 21.4 Hz, *C*$_{qAr}$), 163.9 (d, J_{CP} = 24.7 Hz, *C*$_{qAr}$), 164.2 (s, *C*$_{qAr}$); ^{31}P{^{1}H} NMR (THF-d_8, 303 K, 283 MHz, in ppm): δ = –1.4 (d, $^{2}J_{PP}$ = 33.3 Hz, *P*(^{i}Pr)$_2$, 1 P), 1.0 (d, $^{2}J_{PP}$ = 33.3 Hz, *P*(^{i}Pr)$_2$, 1 P); elemental analysis (in %): $C_{71}H_{108}KLaN_4O_7P_2$: calcd.: C 62.26, H 7.95, N 4.09; found: C 61.83, H 7.53, N 4.10.

Isotope labelling experiment: Reaction of 1-d with KHMDS in the presence of 18-crown-6.

A solution of KHMDS (5 mg, 25 µmol, 1. eq.) in DME (0.5 mL) was added dropwise to a mixture of **1-*d*** (24 mg, 25 µmol, 1 eq.) and 18-crown-6 (6.6 mg, 25 µmol, 1 eq.) in DME (0.5 mL) at room temperature, giving an orange-coloured solution. After 10 min an aliquot of ≈0.6 mL was transferred to a J-Young NMR tube equipped with a sealed C_6D_6 capillary and $^{31}P\{^1H\}$, ^{31}P and ^2H NMR spectra were measured to determine the deuteration level of the product and to check for $DN(SiMe_3)_2$ (Fig. S60–S65). Prior to the experiment the respective NMR data of the starting material **1-*d*** in DME with a sealed C_6D_6 capillary were collected as a reference.

Trapping experiment: Reaction of 1-d with KHMDS in the presence of 18-crown-6 in cyclohexene.

A solution of KHMDS (10 mg, 50 µmol, 1. eq.) in cyclohexene (1 mL) was added dropwise to a mixture of **1-*d*** (49 mg, 50 µmol, 1 eq.) and 18-crown-6 (13 mg, 50 µmol, 1 eq.) in cyclohexene (2 mL) at room temperature, giving an orange-coloured solution. After 10 min an aliquot of ≈0.6 mL was transferred to a J-Young NMR tube equipped with a sealed C_6D_6 capillary. $^{31}P\{^1H\}$ as well as ^{31}P NMR spectra were measured (Fig. S66 and S67) which indicated quite clean formation of **3a** (see also: Preparation of **3a**, Route B), but no trapping of transient phosphinidene complex **2** with cyclohexene in significant amounts. (Notably, >99% conversion of the *PD* group in **1-*d*** to the *PH* group in **3a** had occurred. After 3 d, no D/H scrambling between **3a** and DHMDS was observed and only **3a** containing >99% *PH* was crystallised from the reaction mixture (see Fig. S24).)

NMR scale conversion of 3b into [K(2.2.2-cryptand)][(PN)$_2$La(P$_2$Mes$_2$)] (6).

A solution of **3b** (25 mg, 18 µmol) in THF-d_8 (0.6 mL) was transferred to a J-Young NMR tube and heated at 50 °C for 3 d. The progress of the reaction was regularly controlled by means of $^{31}P\{^1H\}$ NMR spectroscopy (Fig. S68). After full consumption of starting material **3b**, gas diffusion of *n*-hexane into the reaction solution at room temperature overnight yielded only a layer of orange-coloured oil. Therefore, all volatiles were removed *in vacuo*, the residue extracted with diethyl ether (1 mL) and filtered through a glass-fibre filter. Concentrating the filtrate to ca. 0.2 mL and storing it at room temperature for 2 d yielded orange-coloured crystals of **6** suitable for X-ray structure determination. Despite the low X-ray quality of the crystals, the connectivity of **6** could be unambiguously determined. No yield could be determined. $^{31}P\{^1H\}$ NMR (THF-d_8, 303 K, 202 MHz, in ppm): δ = 9.3 (s, PN^-, 2 P), 30.5 (br. s, $P_2Mes_2^{2-}$, 2 P).

X-ray Crystallography

Single crystals for X-ray diffraction experiments were measured at the analytical facility of the Paderborn University using a Bruker Smart AXS or a Bruker D8 Venture instrument. All crystals were kept at 130(2) K or 120(2) K throughout data collection. Data collection was performed using either the APEXIII or the Smart software package. Data refinement and reduction were performed with Bruker Saint (V8.34A). All structures were solved with SHELXT[3,4] and refined using the OLEX 2 software package.[5] All non-hydrogen atoms were refined anisotropically, and hydrogen atoms were included at the geometrically calculated positions and refined using a riding model. All structures have been submitted to the CCDC and can be obtained under the numbers presented in Table S1. For further crystallographic details regarding crystal measurements, please check Tables S1 and S2.

2. NMR Spectra

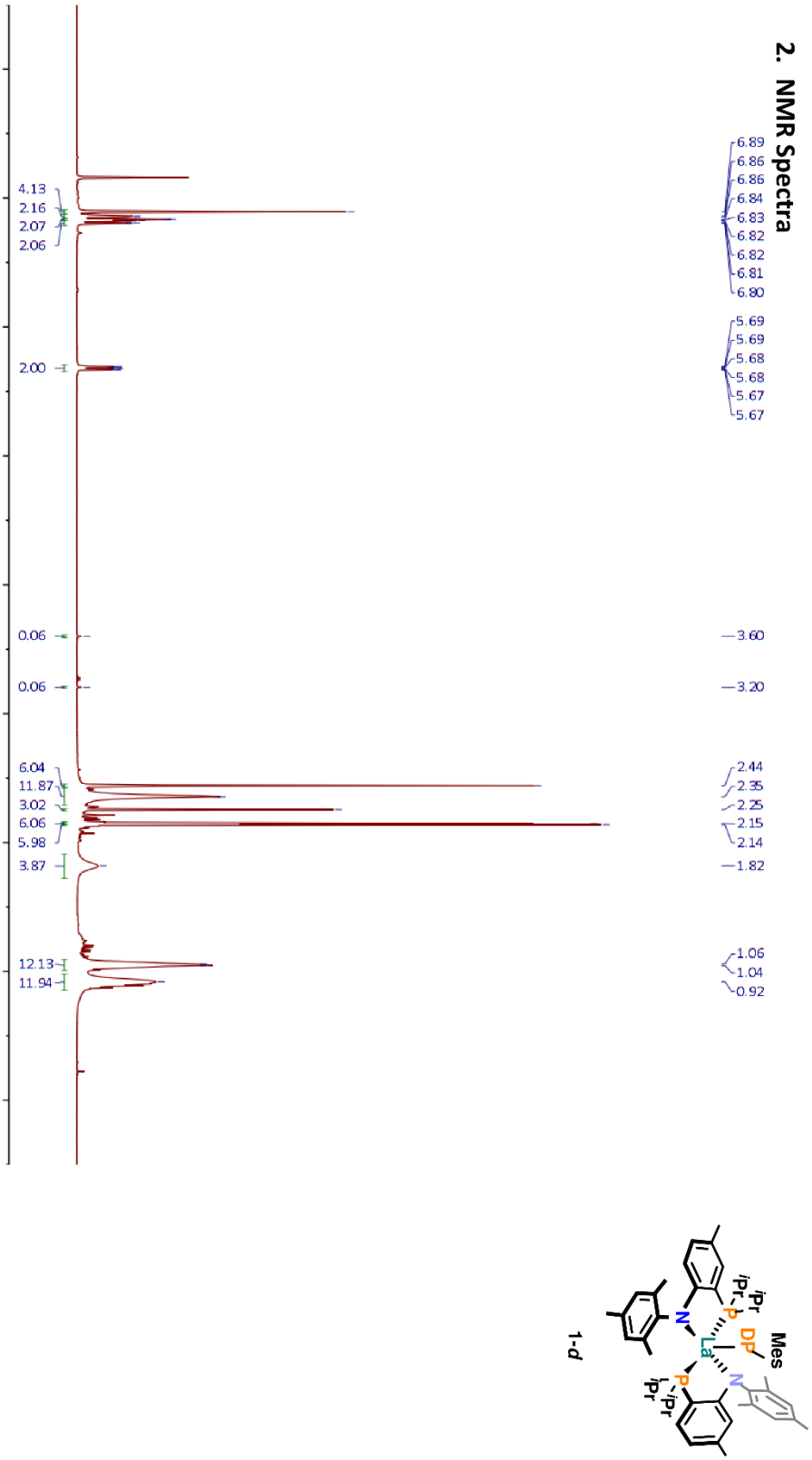

*Fig. S1: ^1H NMR spectrum of **1-d** (≈86–88% isotopic purity) in C_6D_6 (303 K). The integral values of the doublet at δ = 3.40 ppm ($^1J_{PH}$ = 198.5 Hz) of 0.06 each correspond to in total ≈12% remaining PH groups.*

1-d

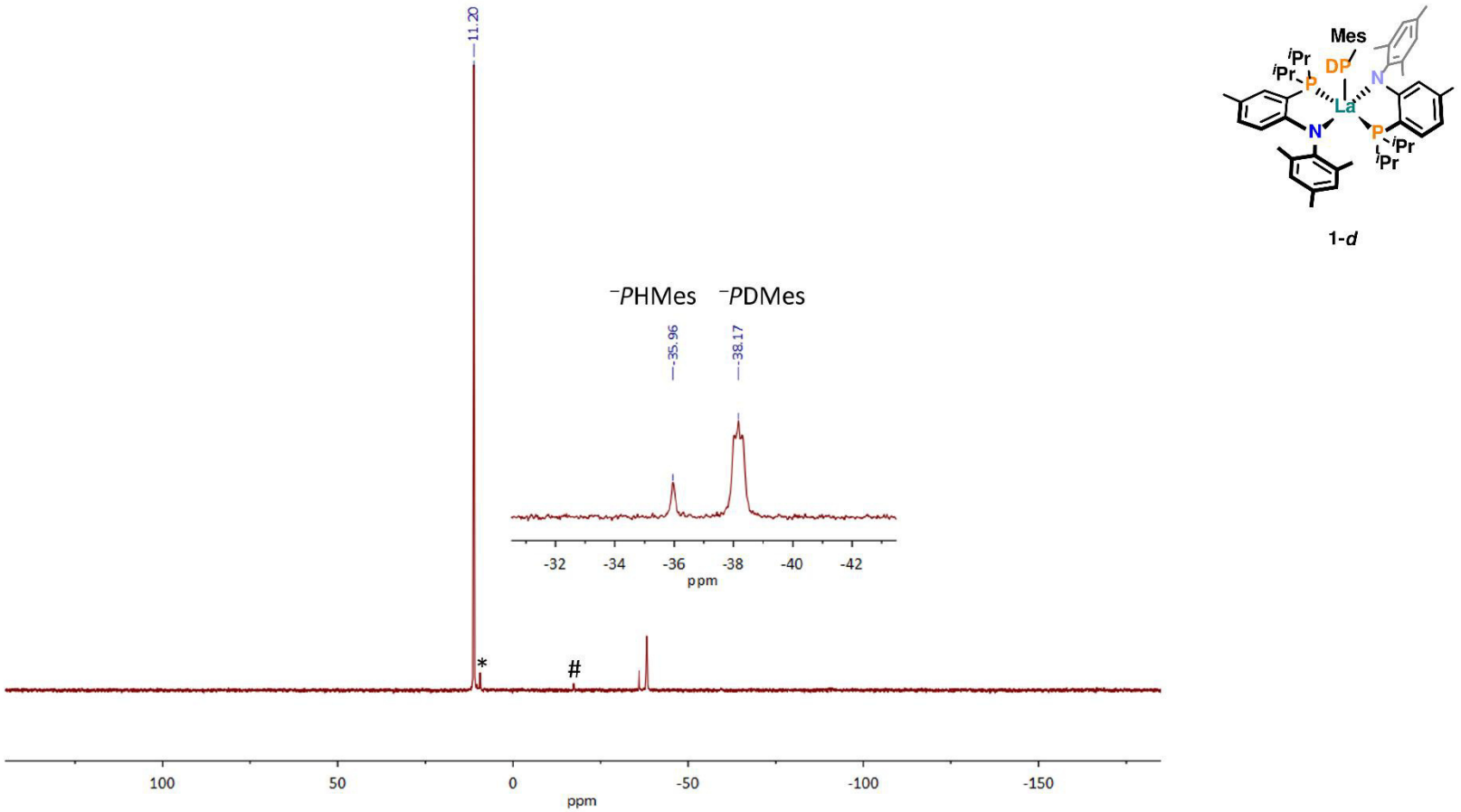

1-*d*

Fig. S2: *$^{31}P\{^{1}H\}$ NMR spectrum of **1-d** (≈86–88% isotopic purity) in C_6D_6 (303 K). The enlargement shows the resonances of the ⁻PDMes ligand as well as residual ⁻PHMes ligand (see caption of Fig. S1). Traces of starting complex $(PN)_2LaCl$ are marked by an asterisk (*). Traces of protonated ligand HPN are marked by #.*

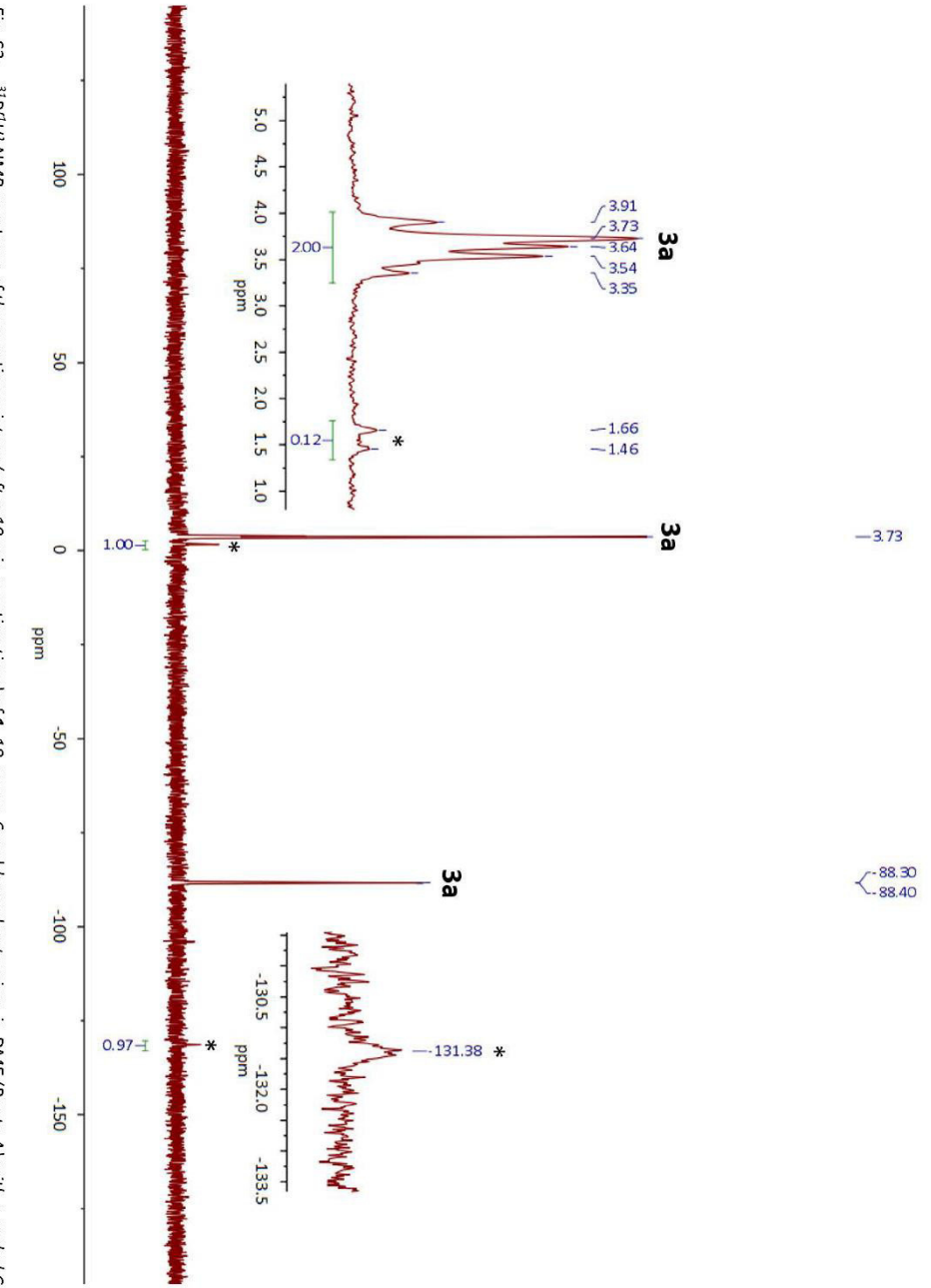

*Fig. S3: $^{31}P\{^1H\}$ NMR spectrum of the reaction mixture (after 10 min reaction time) of **1**, 18-crown-6 and benzyl potassium in DME (Route A) with a sealed C_6D_6 capillary (303 K). Besides the main product **3a**, significant amounts of an unknown C–H activated side product (δ = 1.6 ppm; ≈12%) form along with the appearance of a new resonance at δ = 131.4 ppm (see the two enlargements). The impurities seem to form in a defined ratio of ≈1:1 as indicated by the integral values given at the bottom.*

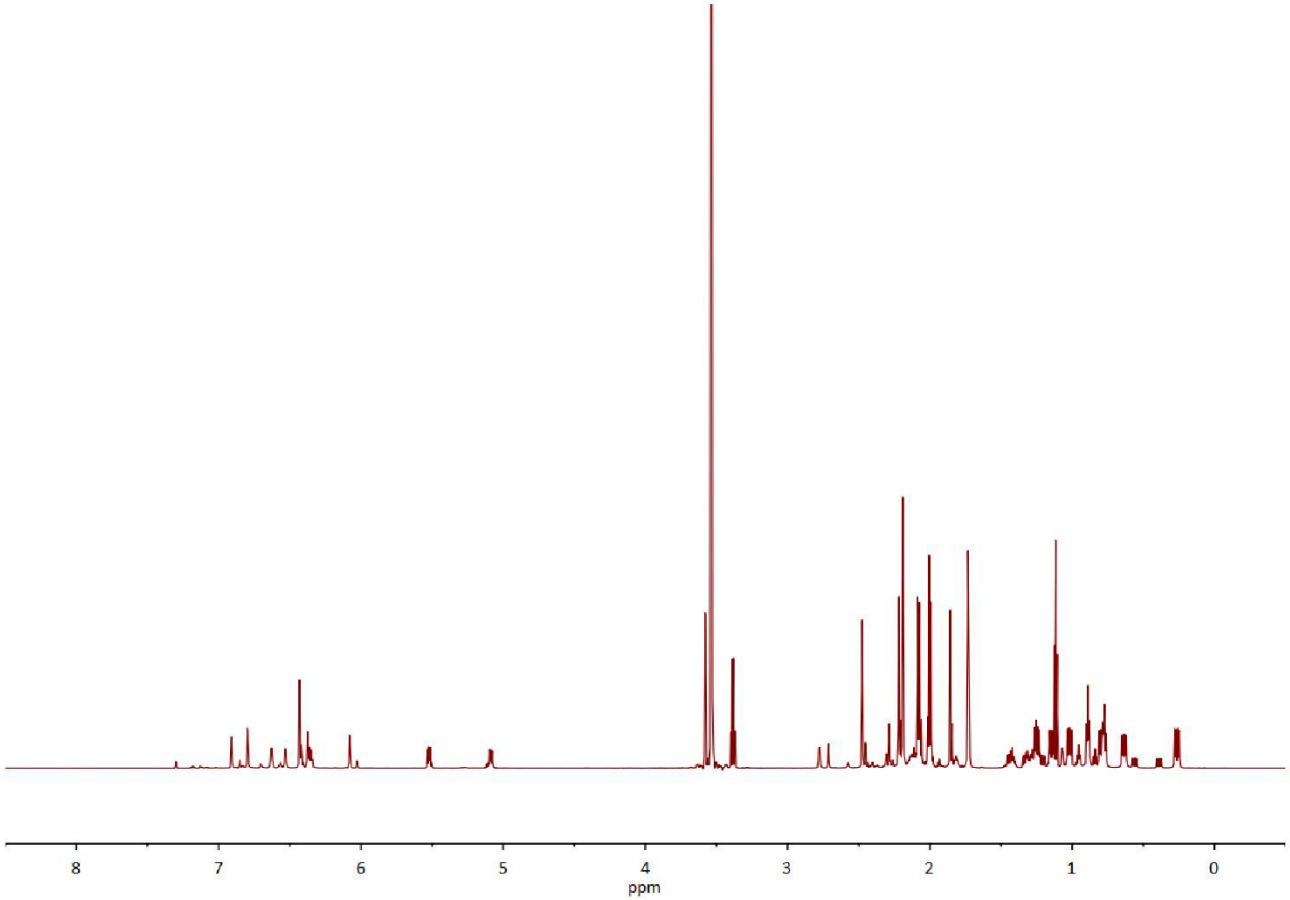

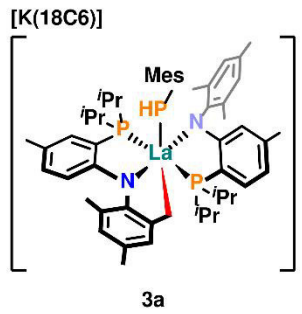

3a

Fig. S4: *^{1}H NMR spectrum of **3a** (≈85% purity, obtained by Route A) in THF-d_8 (303 K).*

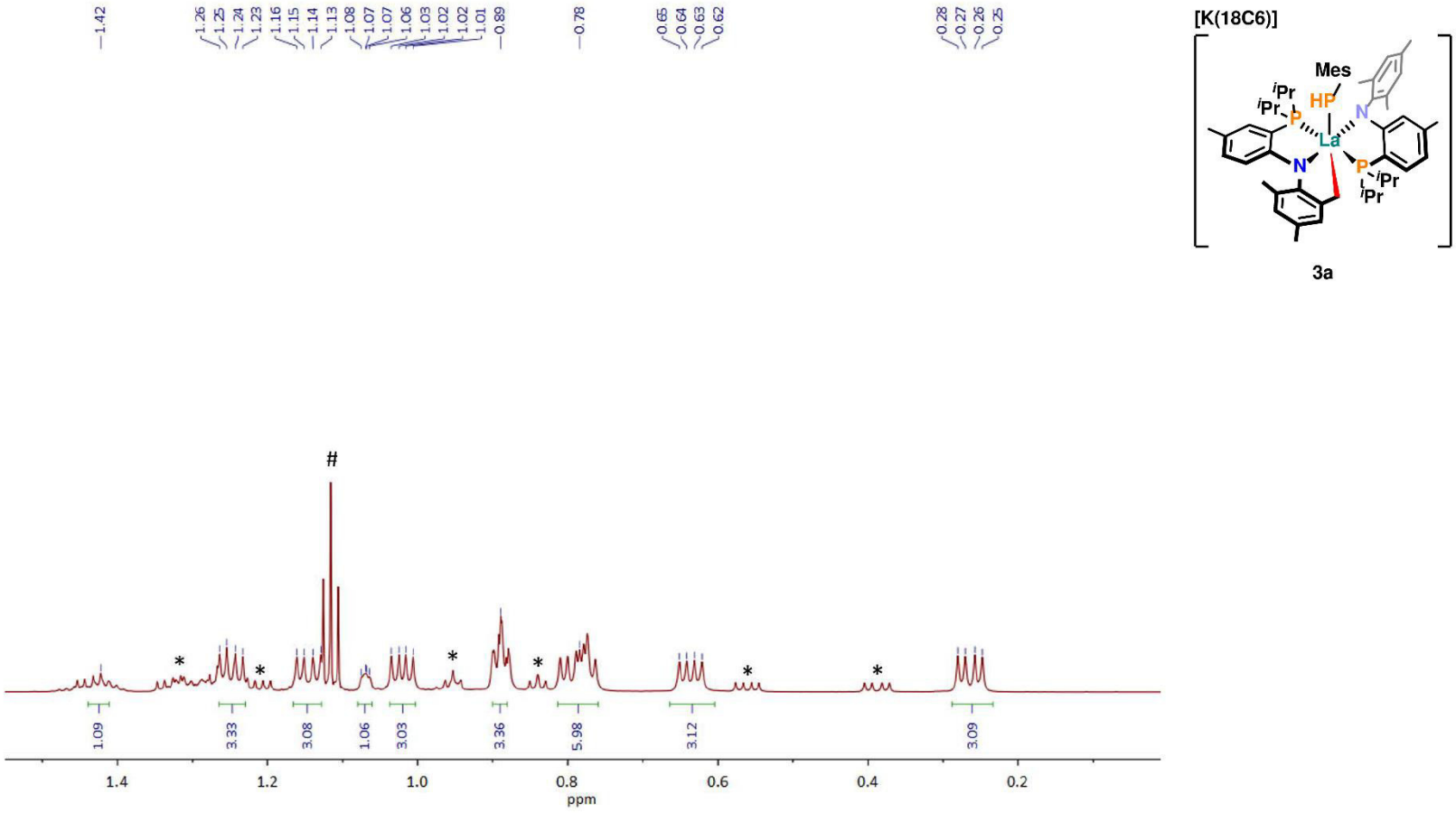

Fig. S5: *Section of the ^{1}H NMR spectrum (δ = 0.1 – 1.55 ppm) of **3a** (≈85% purity, obtained by Route A) in THF-d_8 (303 K). The resonances of an as yet unidentified C–H activated side product are marked by asterisks (*). Residual diethyl ether from work-up is marked by #.*

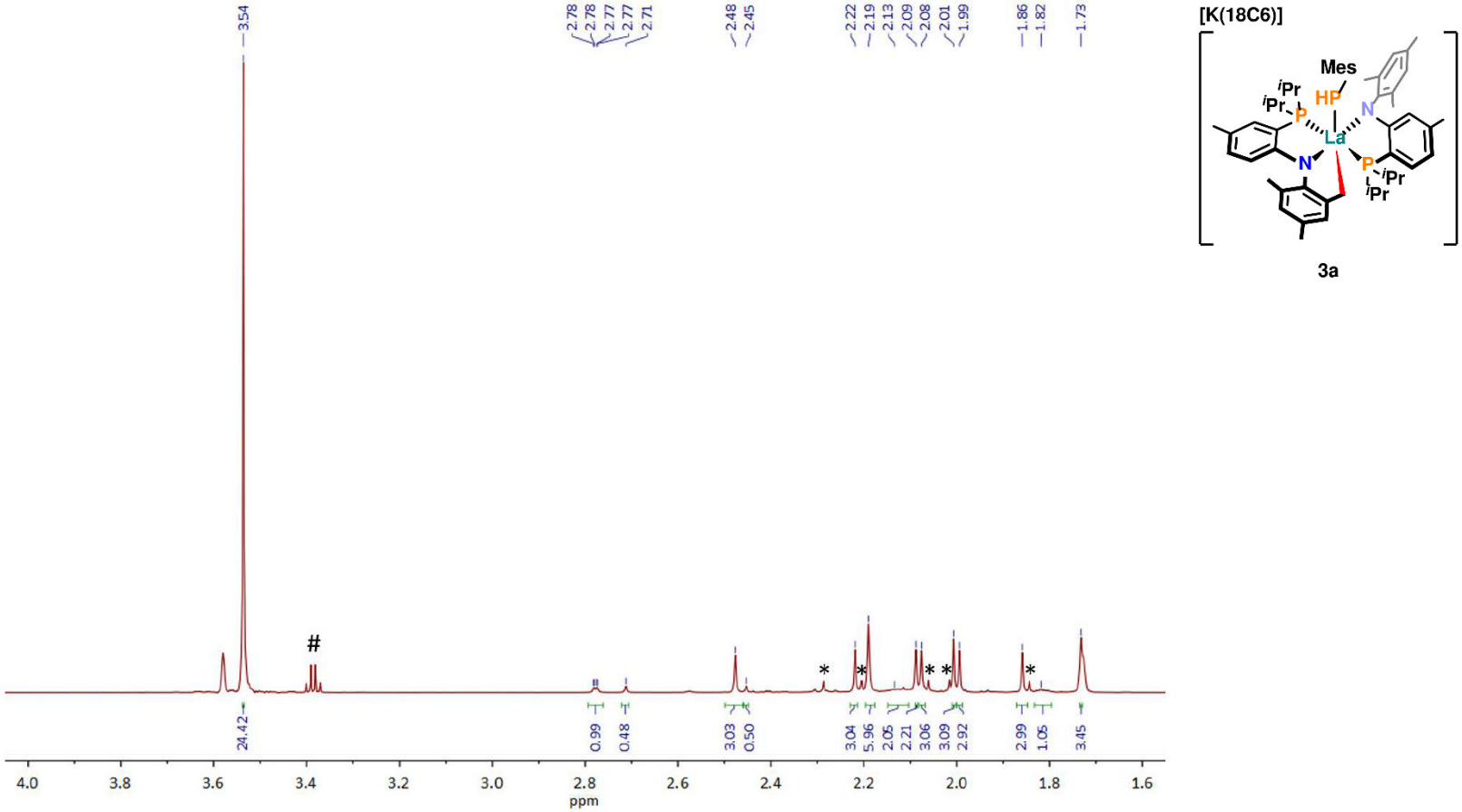

Fig. S6: *Section of the ^{1}H NMR spectrum (δ = 1.55 – 4.05 ppm) of **3a** (≈85% purity, obtained by Route A) in THF-d_8 (303 K). The resonances of an as yet unidentified C–H activated side product are marked by asterisks (*). Residual diethyl ether from work-up is marked by #.*

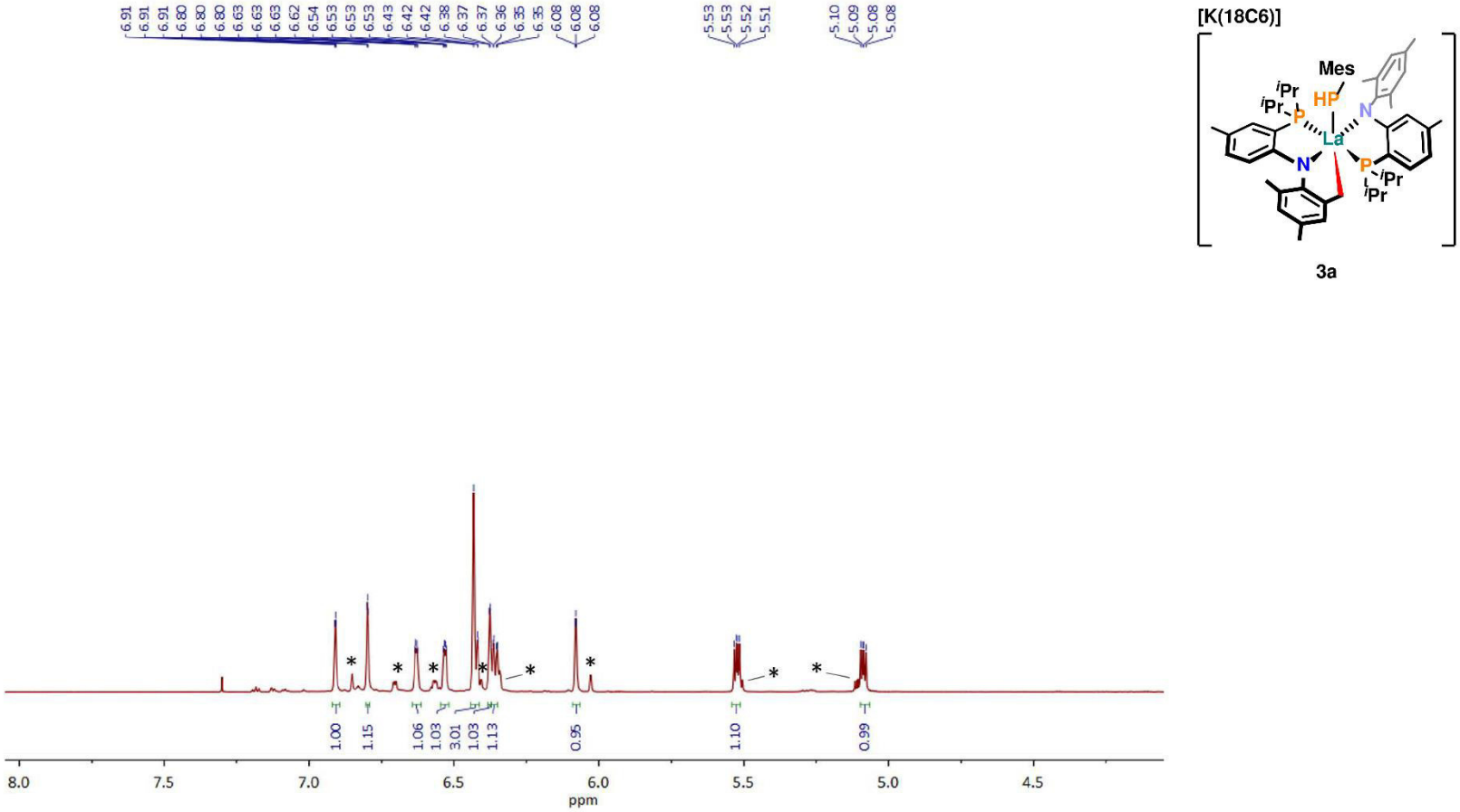

Fig. S7: *Section of the ^{1}H NMR spectrum (δ = 4.05 – 8.05 ppm) of **3a** (≈85% purity, obtained by Route A) in THF-d_8 (303 K). The resonances of an as yet unidentified C–H activated side product are marked by asterisks (*).*

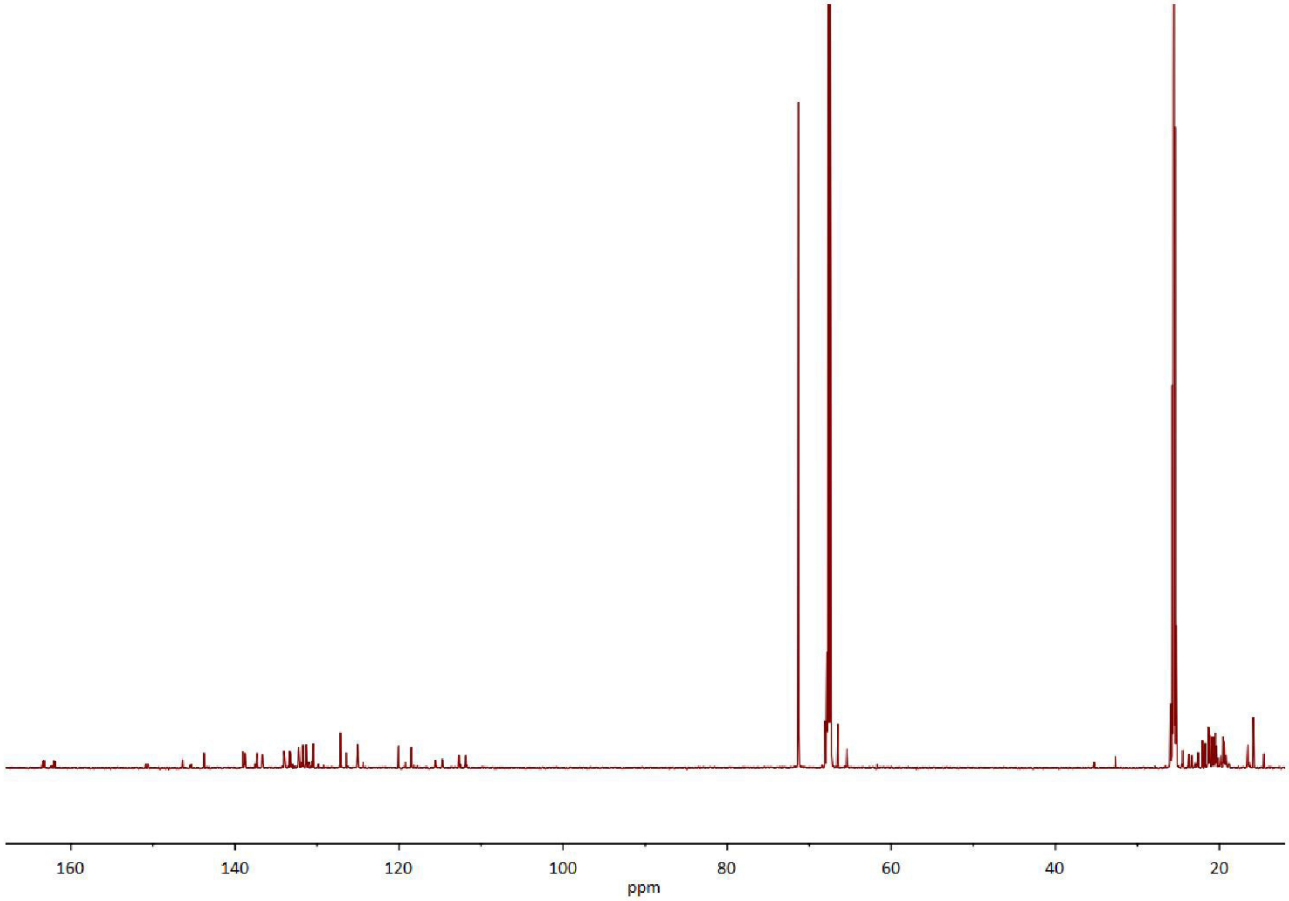

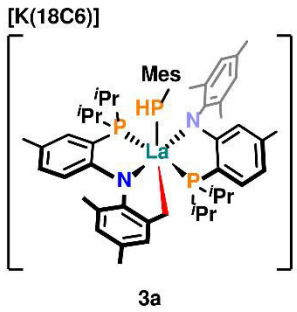

Fig. S8: *$^{13}C\{^{1}H\}$ NMR spectrum of **3a** (≈85% purity, obtained by Route A) in THF-d_8 (303 K).*

*Fig. S9: Section of the $^{13}C\{^{1}H\}$ NMR spectrum (δ = 15.5 – 26.5 ppm) of **3a** (≈85% purity, obtained by Route A) in THF-d_8 (303 K). The resonances of an as yet unidentified C–H activated side product are marked by asterisks (*). Residual diethyl ether from work-up is marked by #.*

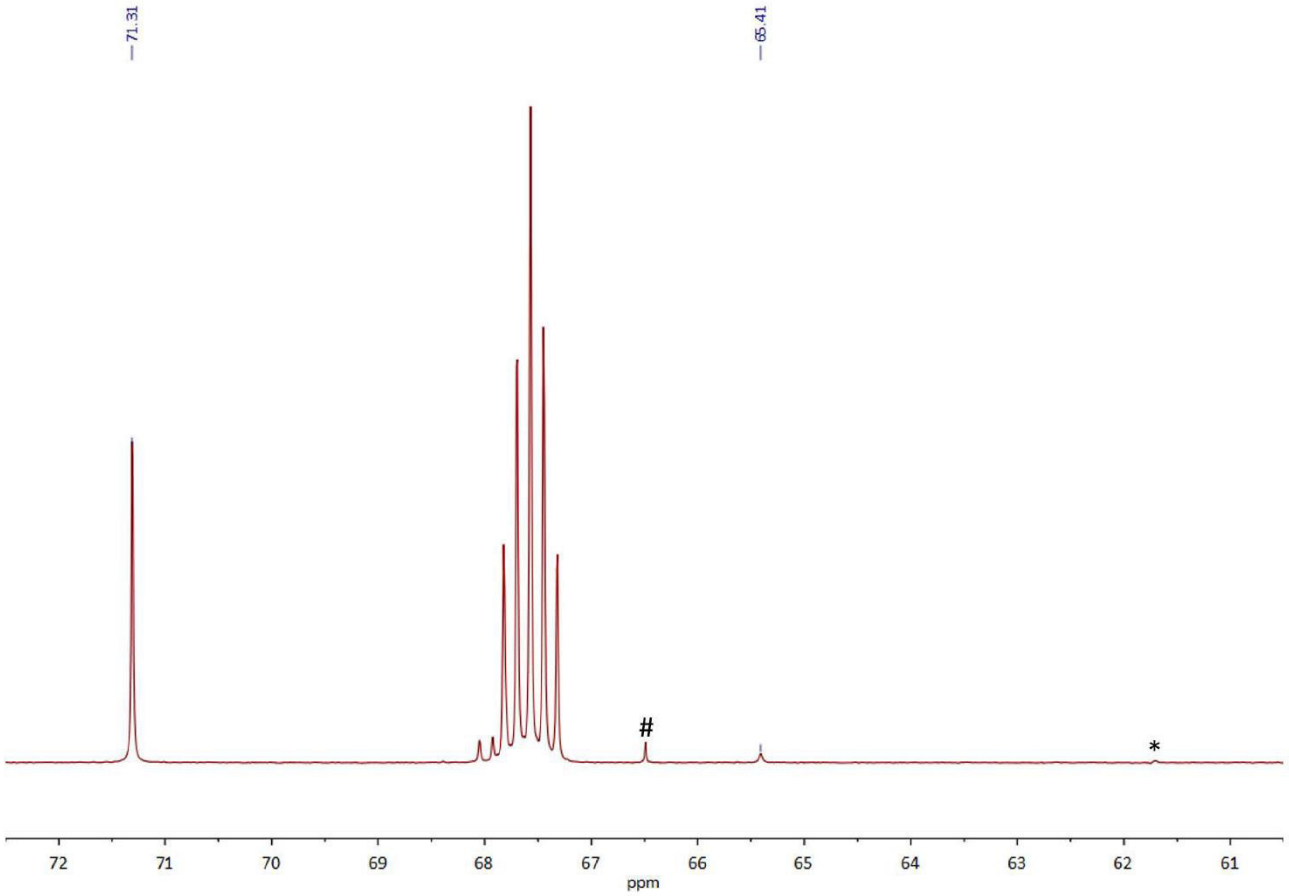

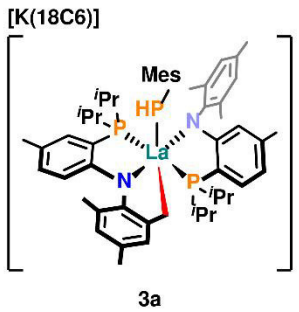

3a

Fig. S10: *Section of the $^{13}C\{^{1}H\}$ NMR spectrum (δ = 60.5 – 72.5 ppm) of **3a** (≈85% purity, obtained by Route A) in THF-d_8 (303 K). The resonance of an as yet unidentified C–H activated side product is marked by an asterisk (*). Residual diethyl ether from work-up is marked by #.*

*Fig. S11: Section of the $^{13}C\{^{1}H\}$ NMR spectrum (δ = 108.5 – 166.5 ppm) of **3a** (≈85% purity, obtained by Route A) in THF-d_8 (303 K). The resonances of an as yet unidentified C–H activated side product are marked by asterisks (*). Residual diethyl ether from work-up is marked by #.*

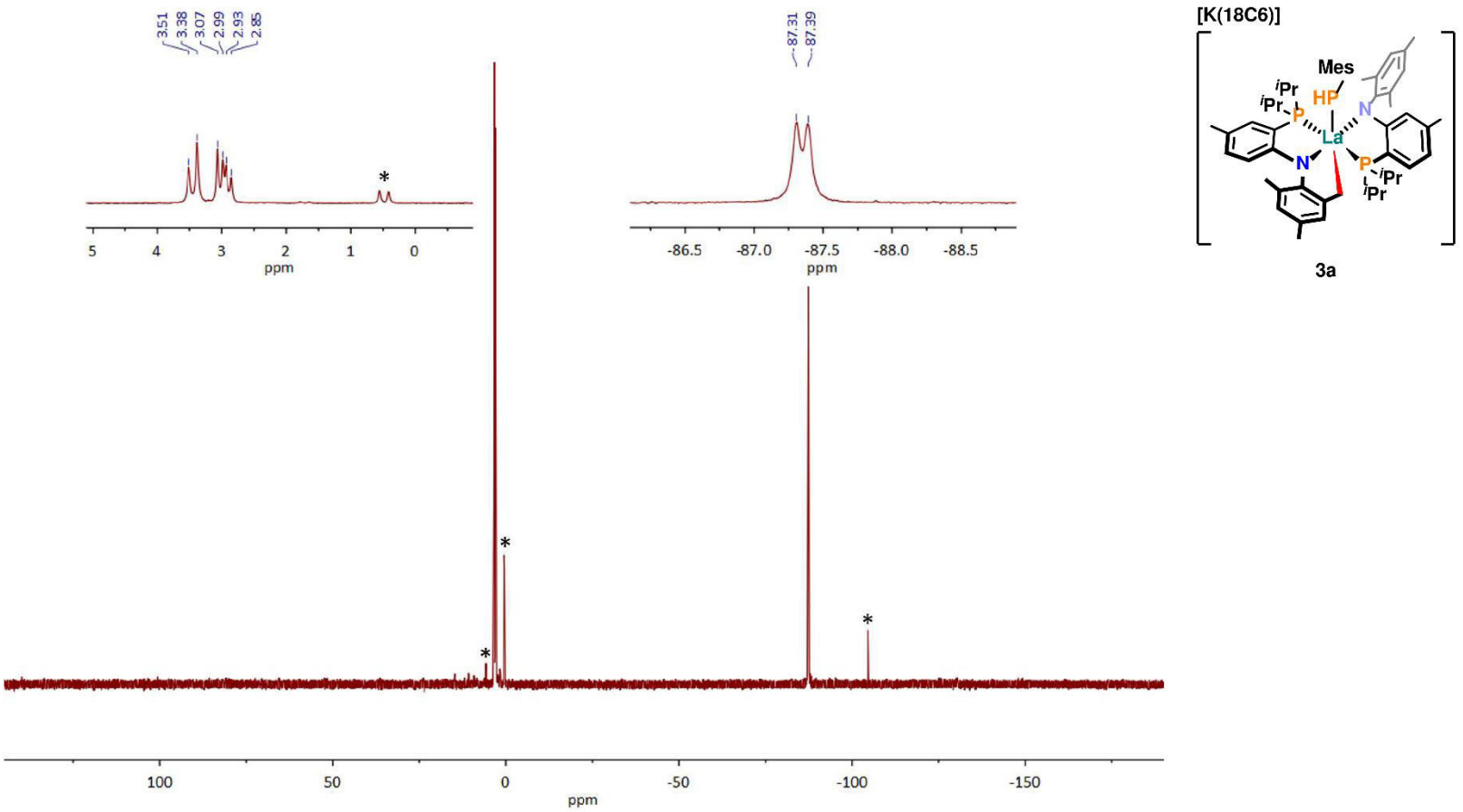

Fig. S12: *$^{31}P\{^{1}H\}$ NMR spectrum of **3a** (≈85% purity, obtained by Route A) in THF-d_8 (303 K). The two enlargements show the main product's multiplet at δ = 2.7 –3.7 ppm (left) and doublet at δ = –87.4 ppm (right). In the left enlargement one resonance of the as yet unidentified C–H activated side product is marked by an asterisk (*), the other one is obscured by the resonances of **3a** at δ = 2.7 –3.7 ppm. Other unknown impurities are also marked by asterisks (*).*

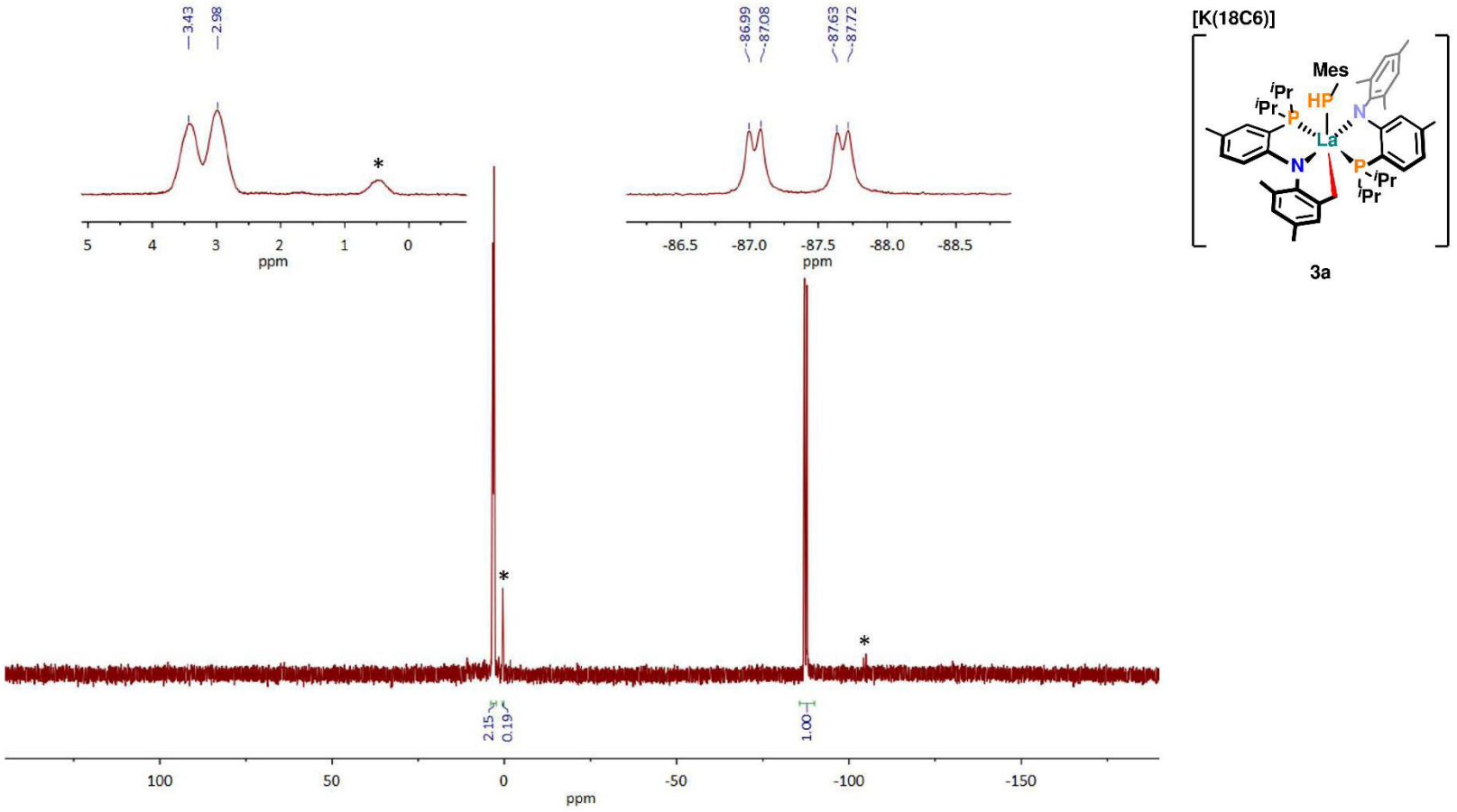

Fig. S13: *^{31}P NMR spectrum of **3a** (≈85% purity, obtained by Route A) in THF-d_8 (303 K). The two enlargements show the main product's broad multiplet at δ = 2.7 –3.7 ppm (left) and the doublet of doublets at δ = –87.4 ppm (right). In the left enlargement one resonance of the as yet unidentified C–H activated side product is marked by an asterisk (*), the other one is obscured by the resonances of **3a** at δ = 2.7 –3.7 ppm. Other unknown impurities are also marked by asterisks (*).*

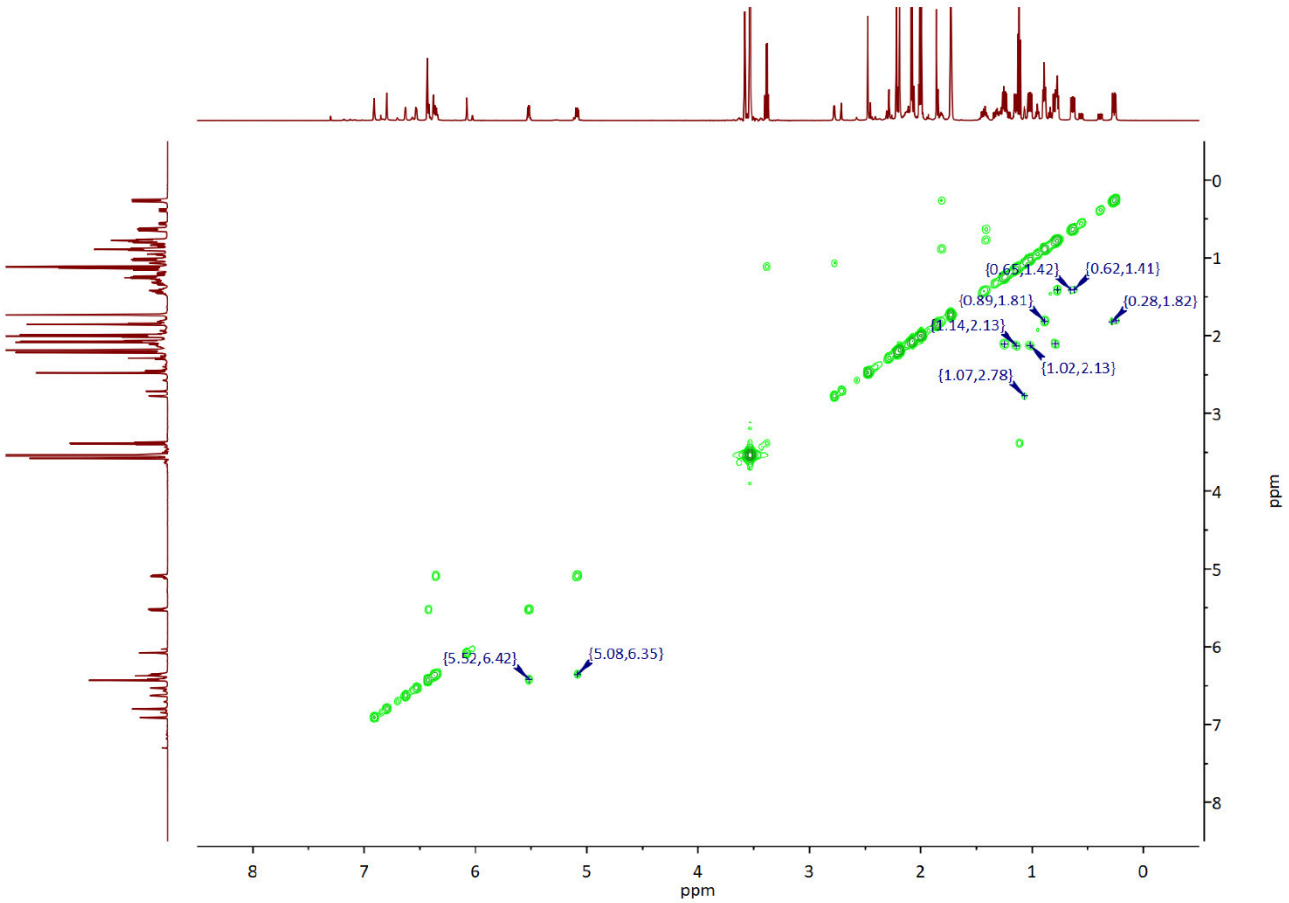

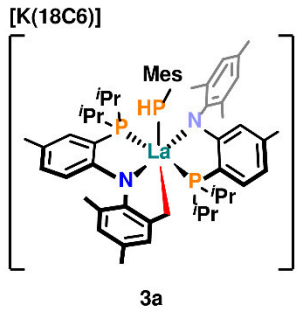

Fig. S14: *^{1}H–^{1}H COSY NMR spectrum of **3a** (≈85% purity, obtained by Route A) in THF-d_8 (303 K).*

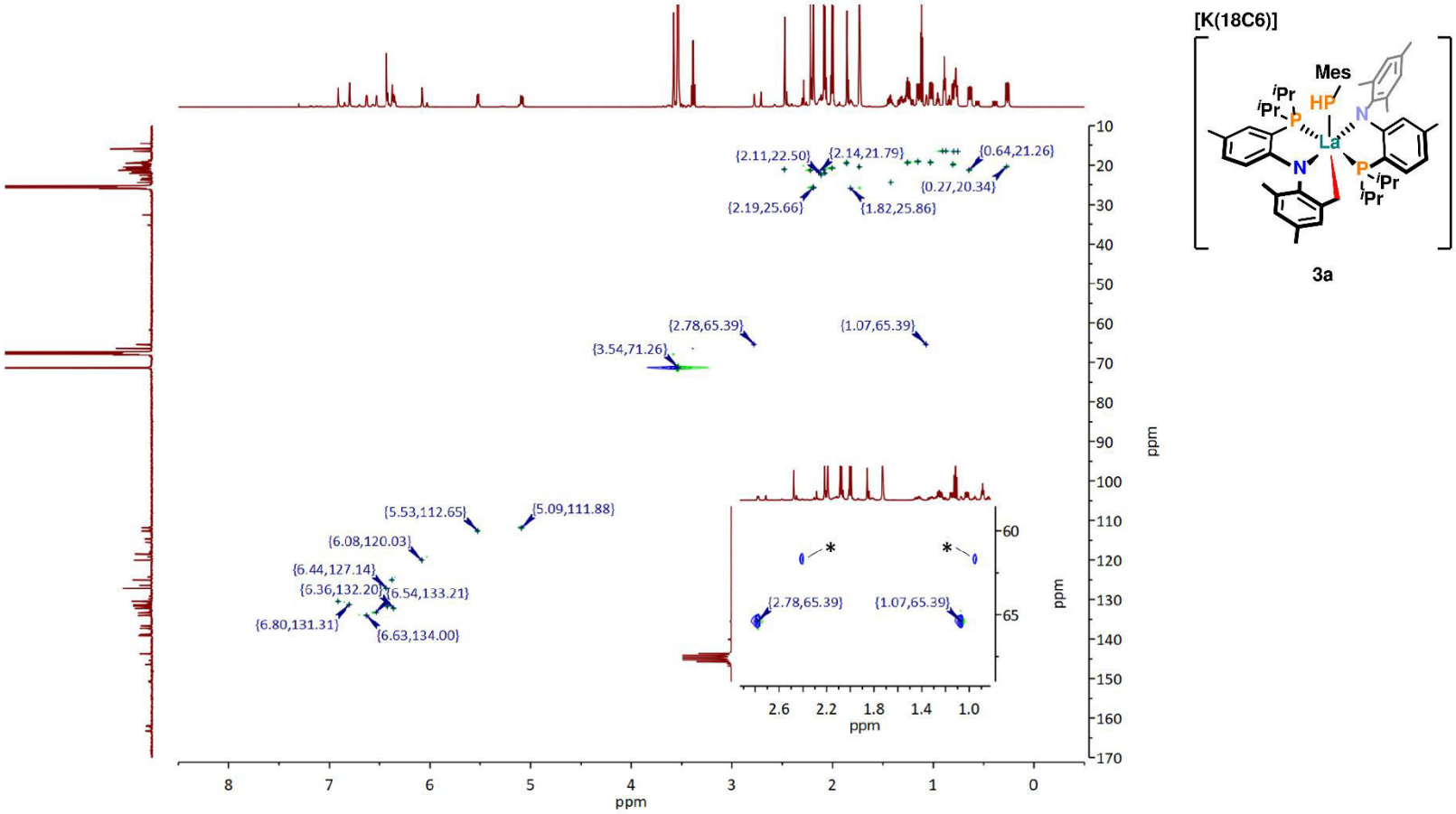

Fig. S15: *^{1}H–^{13}C HSQC NMR spectrum of **3a** (≈85% purity, obtained by Route A) in THF-d_8 (303 K). The enlargement shows the two cross peaks for the $CH_{2Mes(PNcyclo)}$ methylene protons of **3a**, the analogous cross peaks of the as yet unidentified C–H activated side product are marked by asterisks (*).*

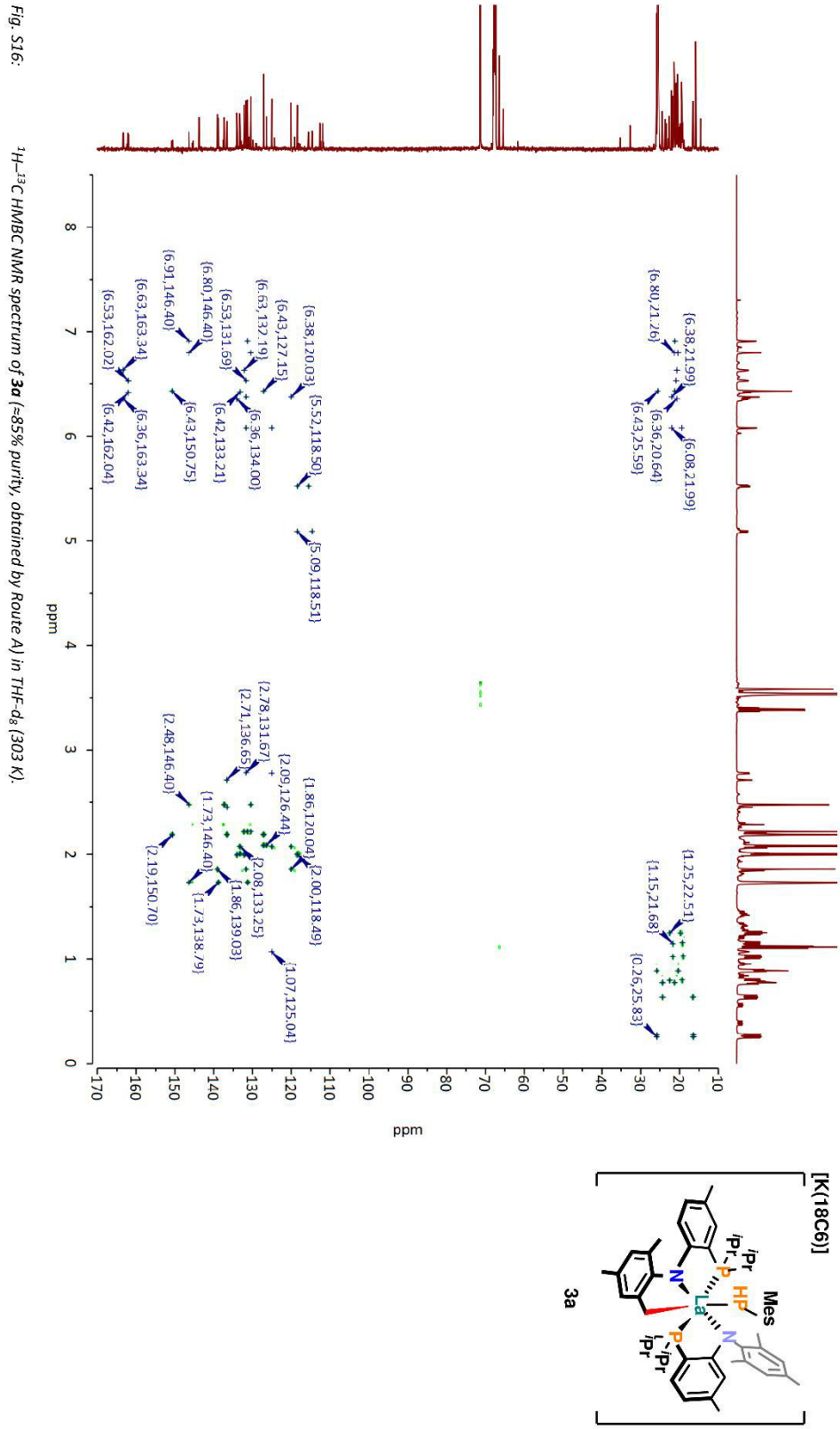

Fig. S16: *^{1}H–^{13}C HMBC NMR spectrum of **3a** (≈85% purity, obtained by Route A) in THF-d_8 (303 K).*

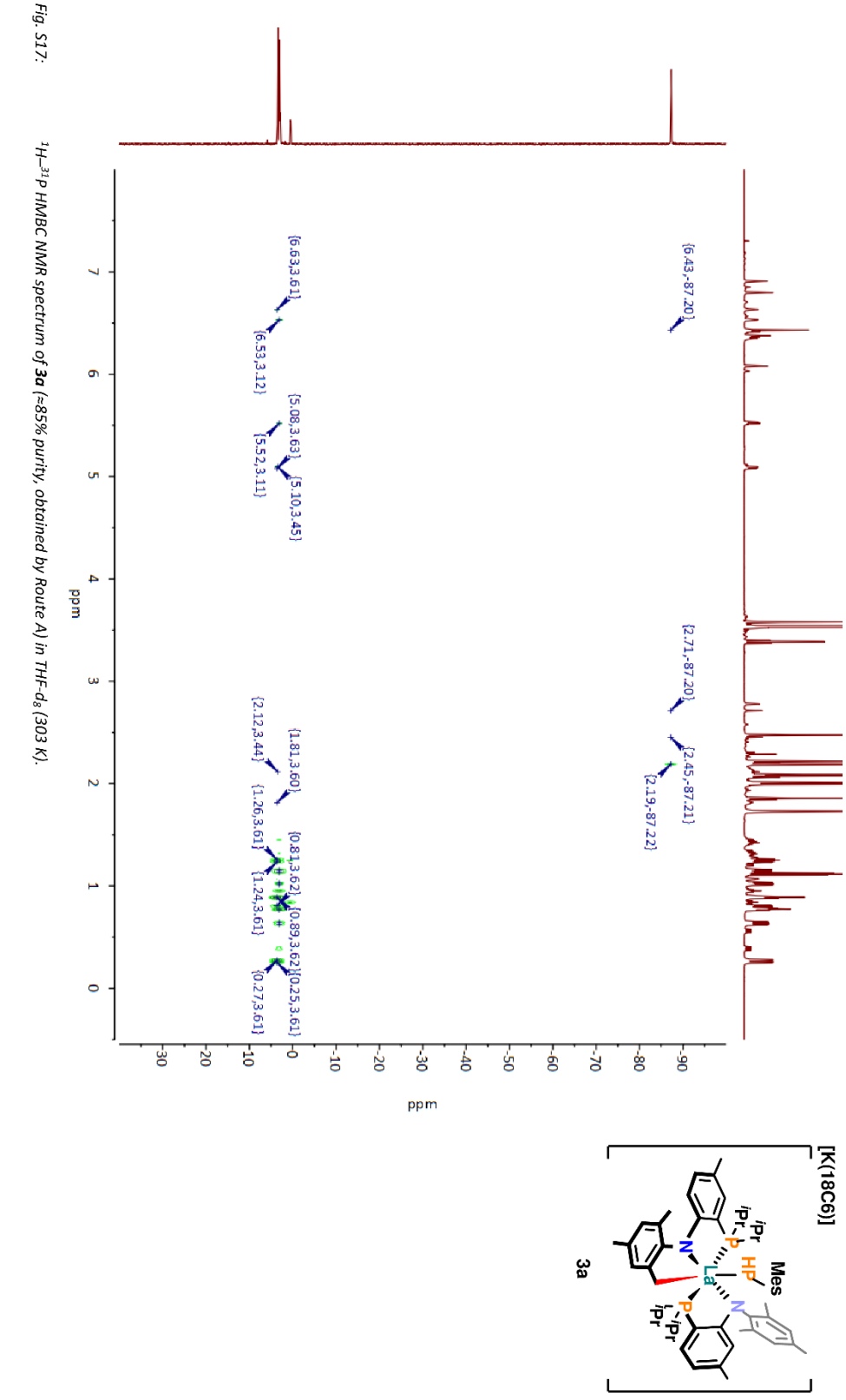

Fig. S17: ^{1}H–^{31}P *HMBC NMR spectrum of* **3a** *(≈85% purity, obtained by Route A) in THF-*d_8 *(303 K).*

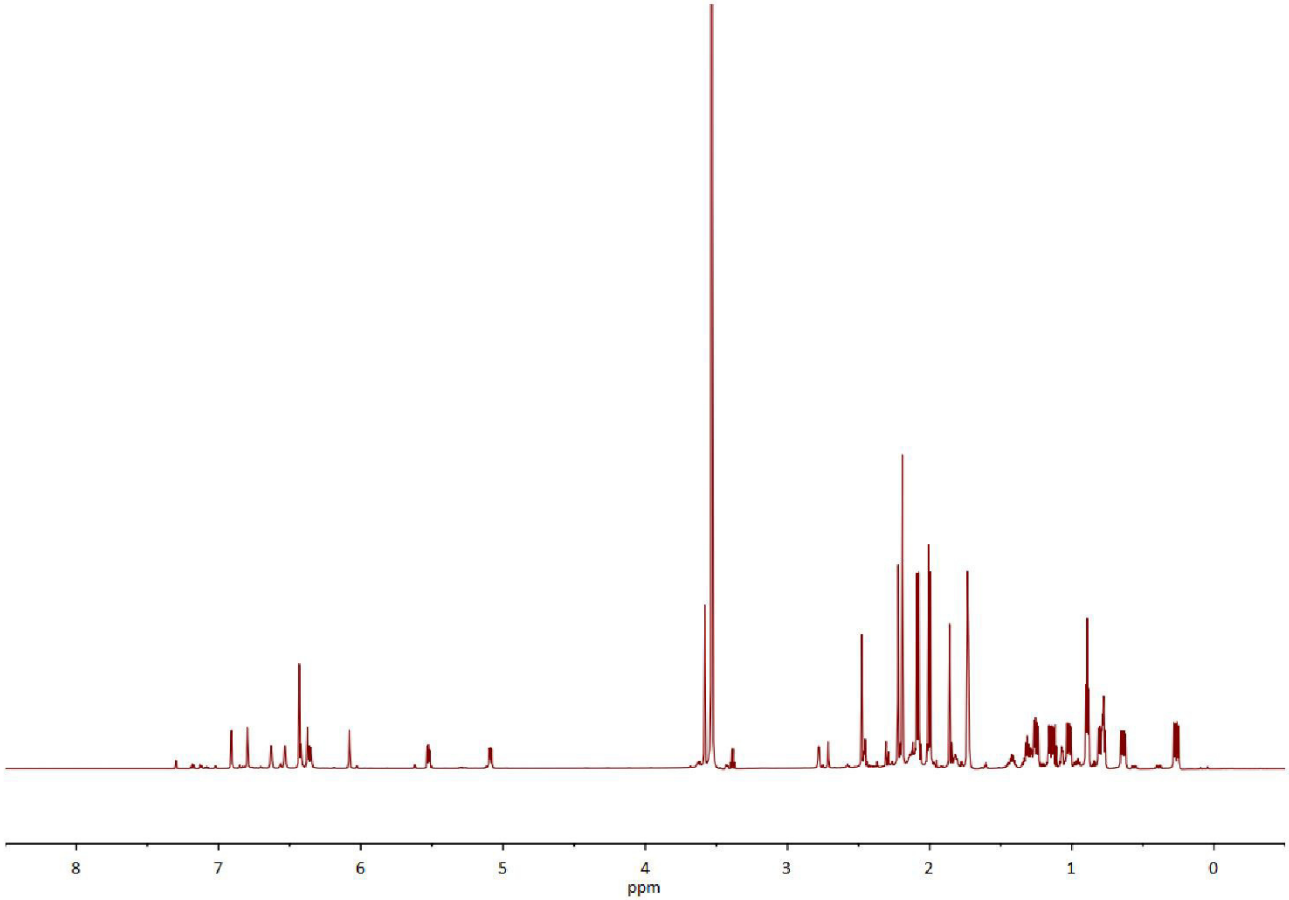

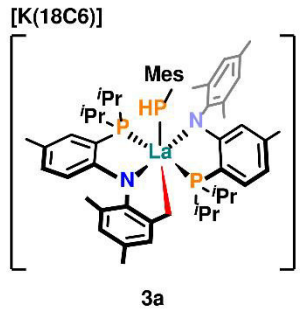

3a

Fig. S18: *^{1}H NMR spectrum of **3a** (≈94% purity, obtained by Route B) in THF-d_8 (303 K).*

*Fig. S19: Section of the ^{1}H NMR spectrum (δ = 0.1 – 1.55 ppm) of **3a** (≈94% purity, obtained by Route B) in THF-d_8 (303 K). The peak at δ = 0.89 ppm overlaps with a peak of n-pentane. Residual n-pentane from work-up is marked by #. Traces of diethyl ether are marked by °. Traces of unknown impurities are marked by asterisks (*).*

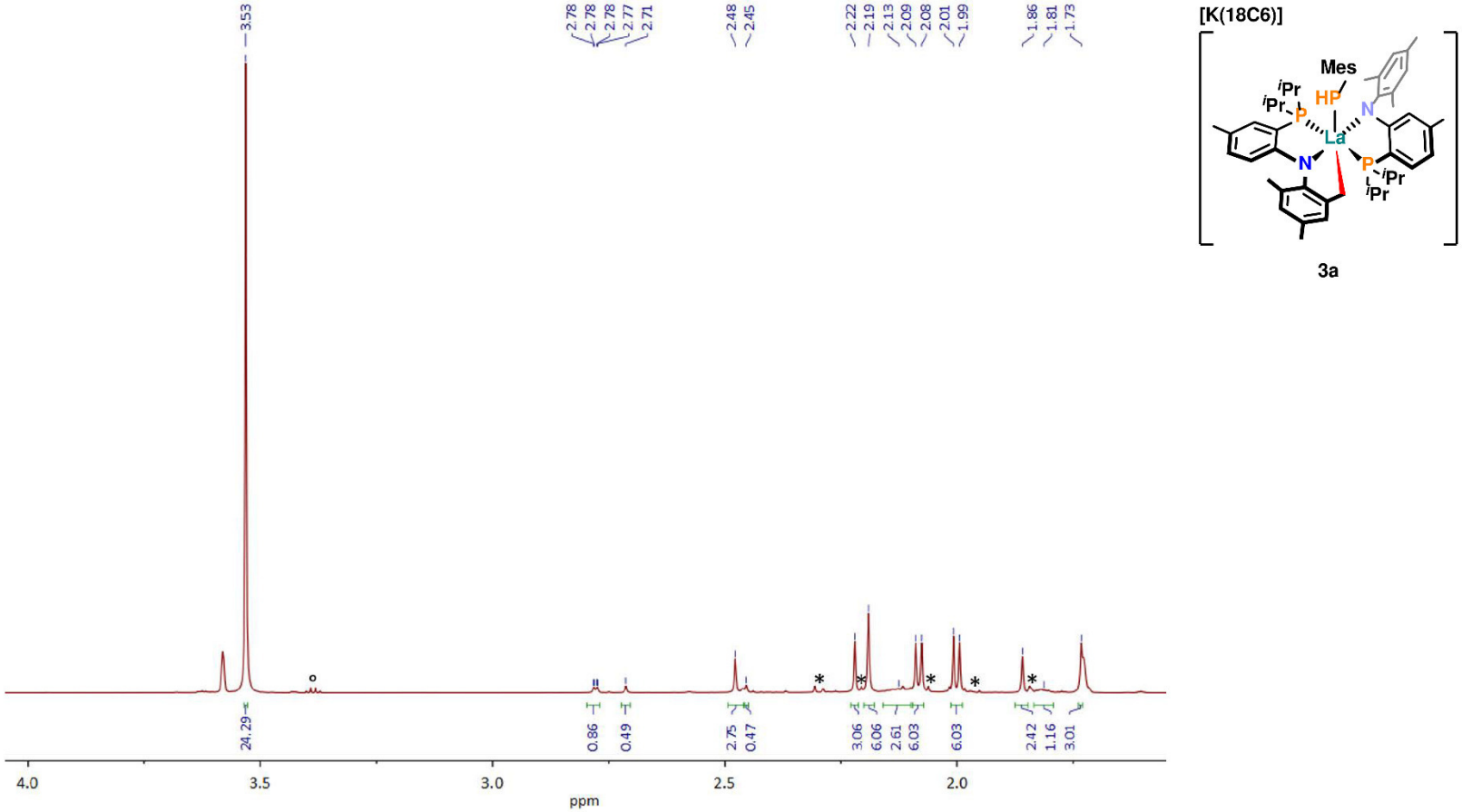

Fig. S20: *Section of the ^{1}H NMR spectrum (δ = 1.55 – 4.05 ppm) of **3a** (≈94% purity, obtained by Route B) in THF-d_8 (303 K). Traces of diethyl ether are marked by °. Traces of unknown impurities are marked by asterisks (*).*

*Fig. S21: Section of the ^{1}H NMR spectrum (δ = 4.05 – 8.05 ppm) of **3a** (≈94% purity, obtained by Route B) in THF-d_8 (303 K). Traces of toluene are marked by °. Traces of benzene are marked by `. Traces of unknown impurities are marked by asterisks (*).*

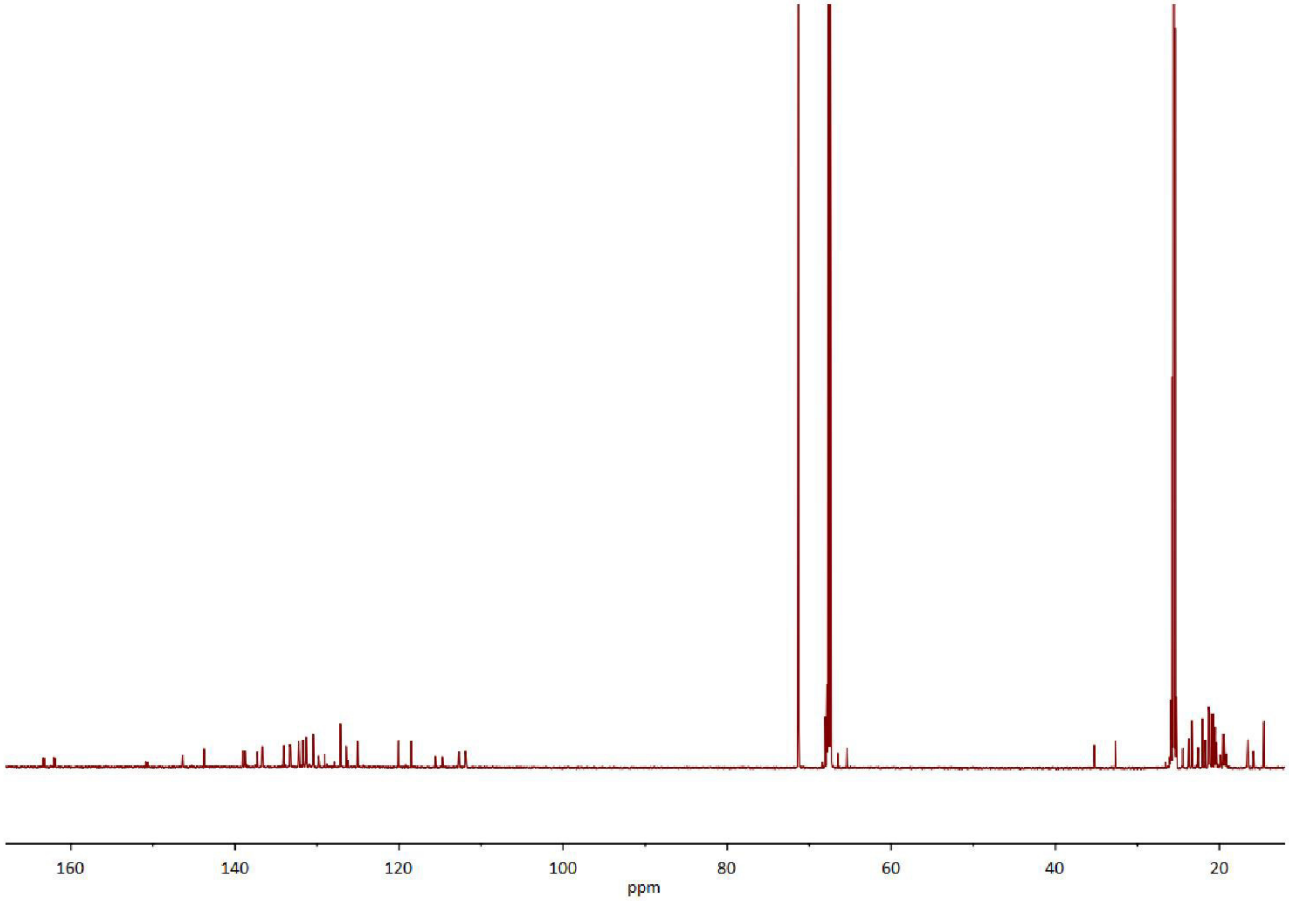

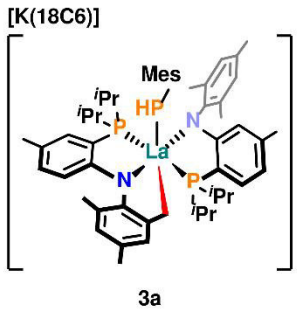

3a

Fig. S22: *$^{13}C\{^1H\}$ NMR spectrum of **3a** (≈94% purity, obtained by Route B) in THF-d_8 (303 K). For assignments please see the corresponding $^{13}C\{^1H\}$ NMR data of material obtained by Route A (Fig. S9–S11).*

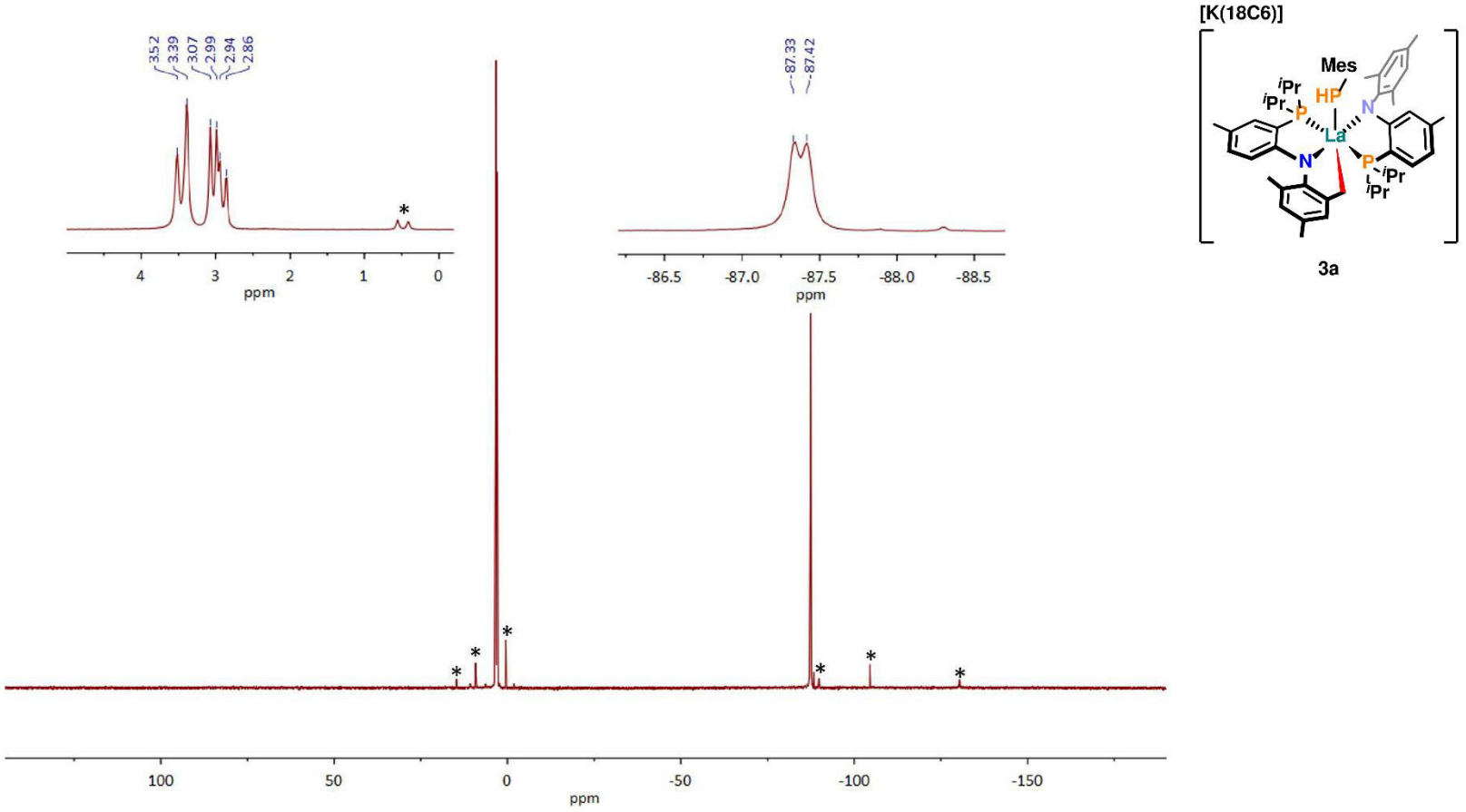

Fig. S23: *$^{31}P\{^{1}H\}$ NMR spectrum of **3a** (≈94% purity, obtained by Route B) in THF-d_8 (303 K). The two enlargements show the main product's multiplet at δ = 2.7 –3.7 ppm (left) and doublet at δ = –87.4 ppm (right). In the left enlargement one resonance of the as yet unidentified C–H activated side product is marked by an asterisk (*), the other one is obscured by the resonances of **3a** at δ = 2.7 –3.7 ppm. Other traces of unknown impurities are also marked by asterisks (*).*

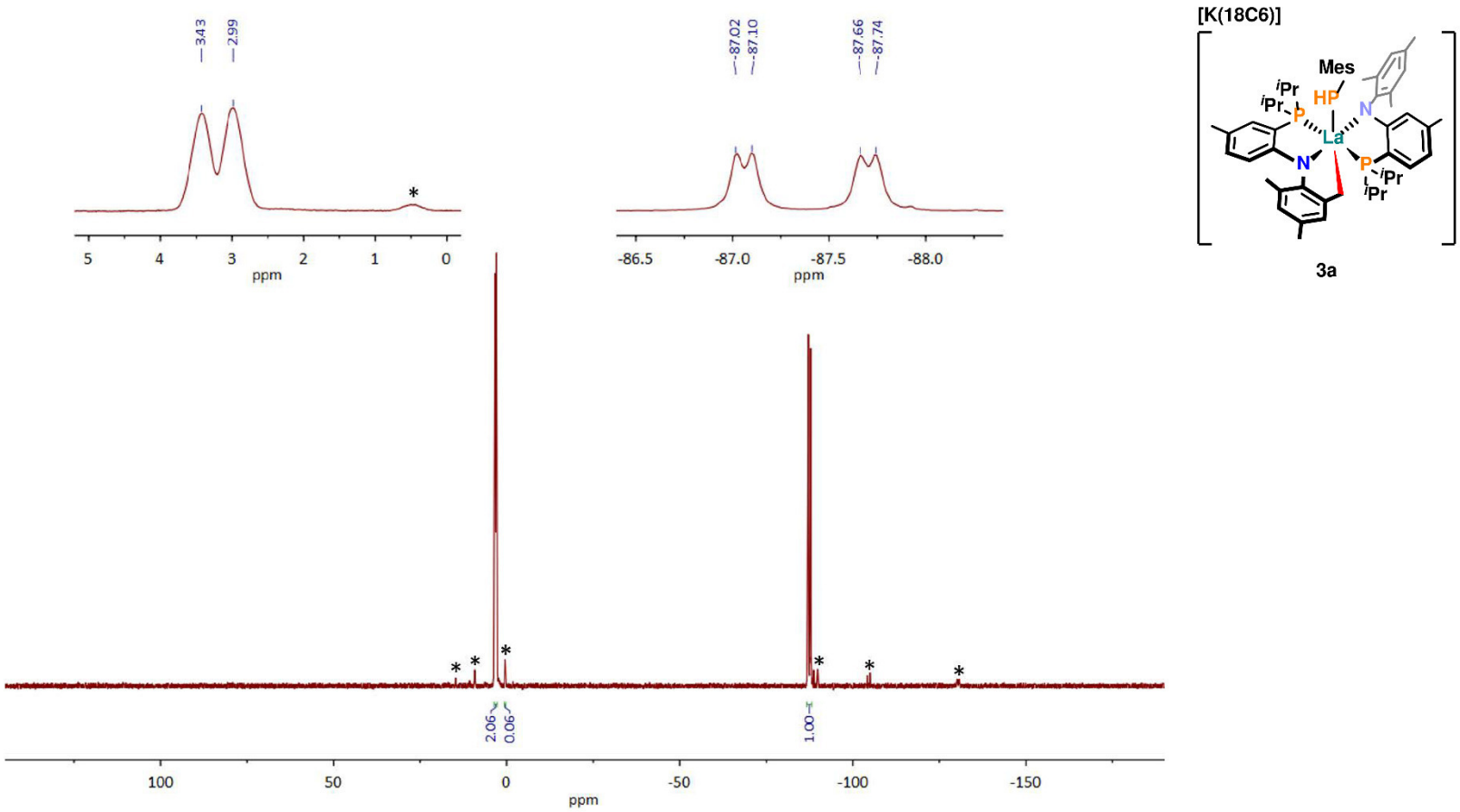

Fig. S24: *^{31}P NMR spectrum of **3a** (≈94% purity, obtained by Route B) in THF-d_8 (303 K). The two enlargements show the main product's broad multiplet at δ = 2.7 –3.7 ppm (left) and the doublet of doublets at δ = –87.4 ppm (right). In the left enlargement one resonance of the as yet unidentified C–H activated side product is marked by an asterisk (*), the other one is obscured by the resonances of **3a** at δ = 2.7 –3.7 ppm. Other traces of unknown impurities are also marked by asterisks (*).*

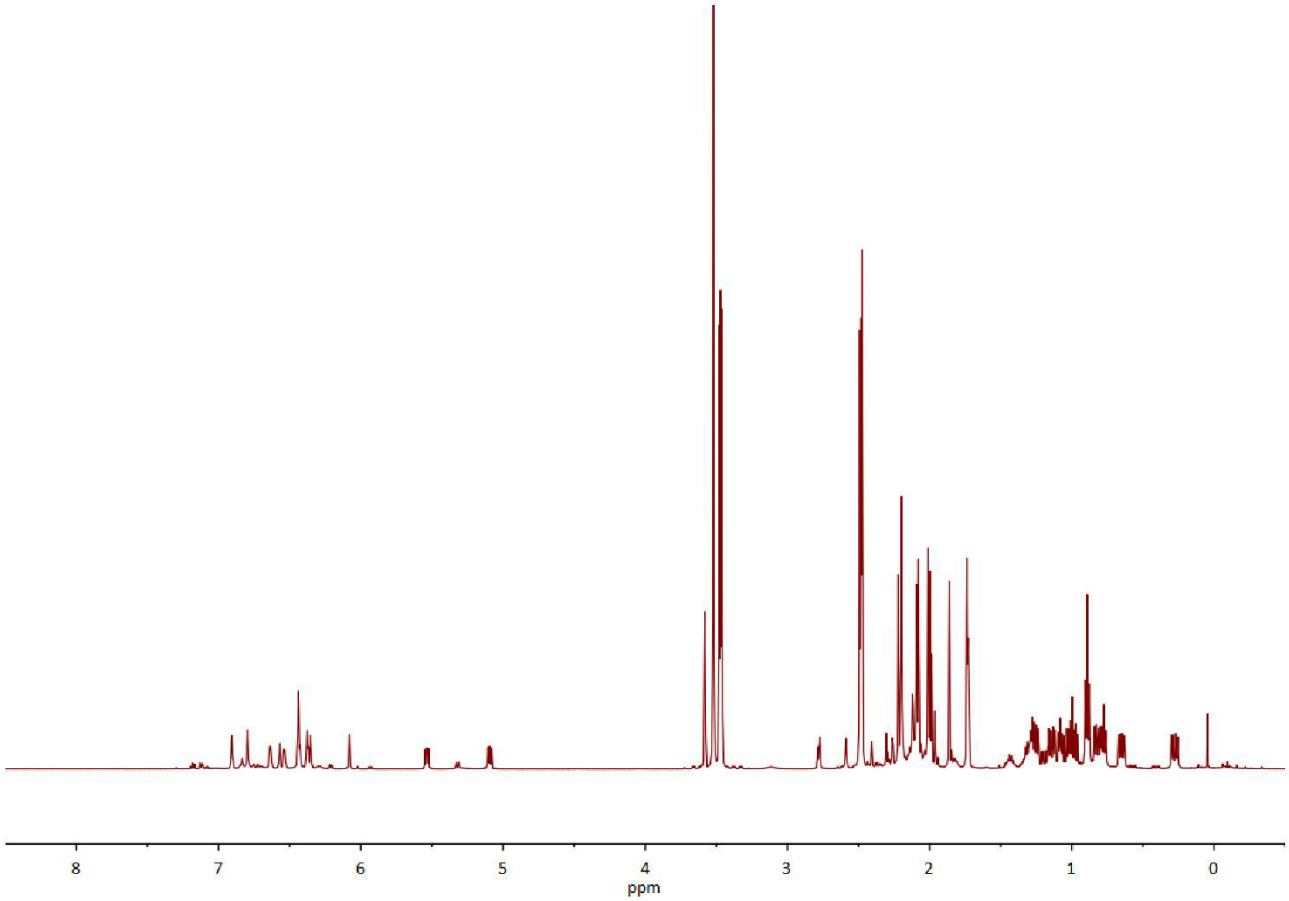

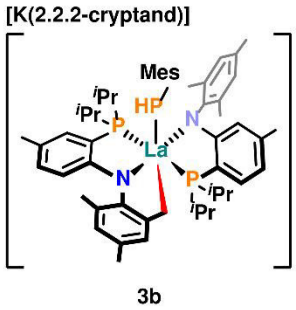

Fig. S25: *^{1}H NMR spectrum of **3b** (crude) in THF-d_8 (303 K).*

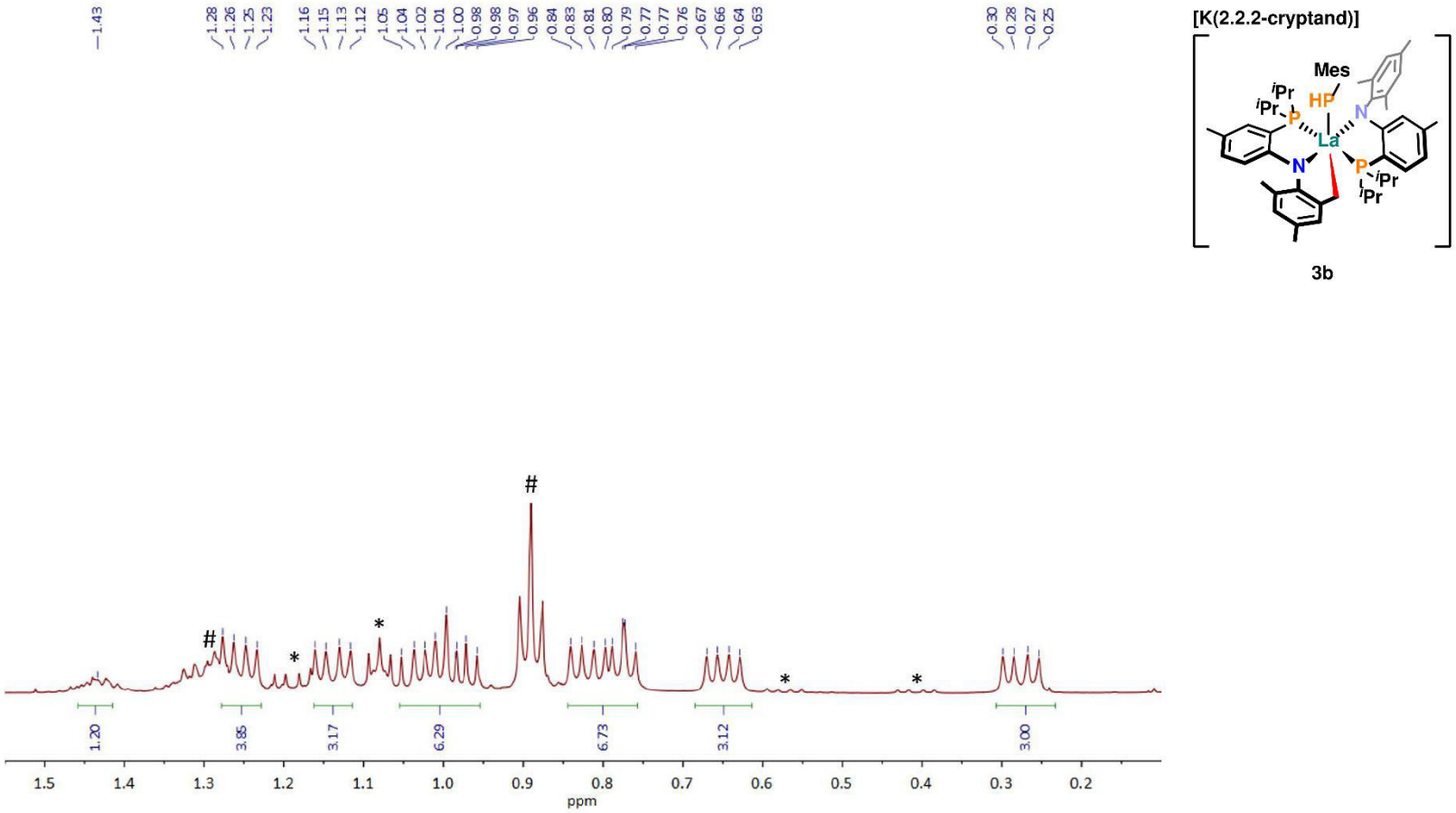

Fig. S26: *Section of the ^{1}H NMR spectrum (δ = 0.1 – 1.55 ppm) of **3b** (crude) in THF-d_8 (303 K). The integration values are only estimates, due to the presence of obscured resonances of unknown impurities underneath the main product's peaks. Well separated resonances of unknown impurities are marked by asterisks (*). Residual n-pentane from work-up is marked by #.*

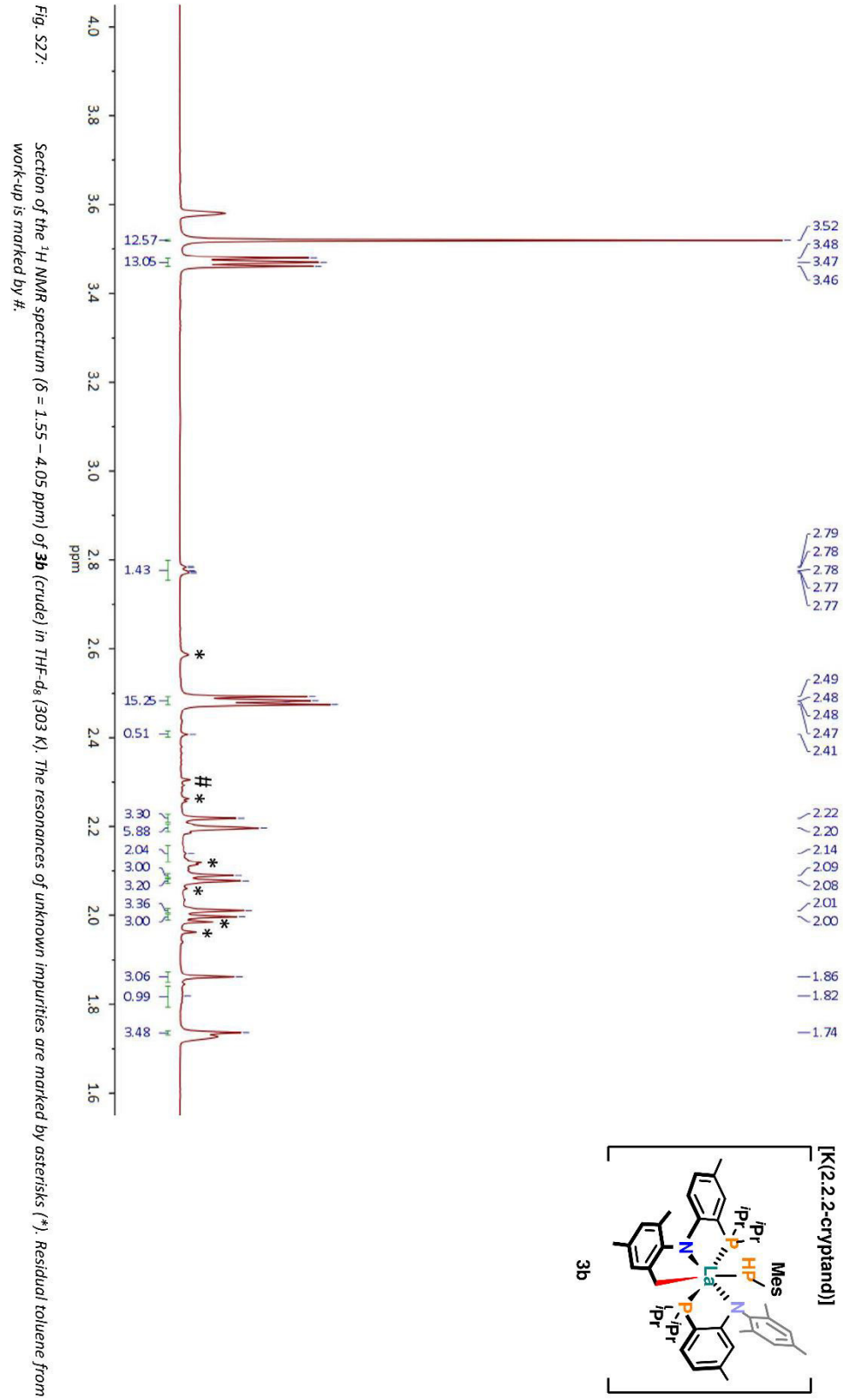

*Fig. S27: Section of the ^{1}H NMR spectrum (δ = 1.55 – 4.05 ppm) of **3b** (crude) in THF-d_8 (303 K). The resonances of unknown impurities are marked by asterisks (*). Residual toluene from work-up is marked by #.*

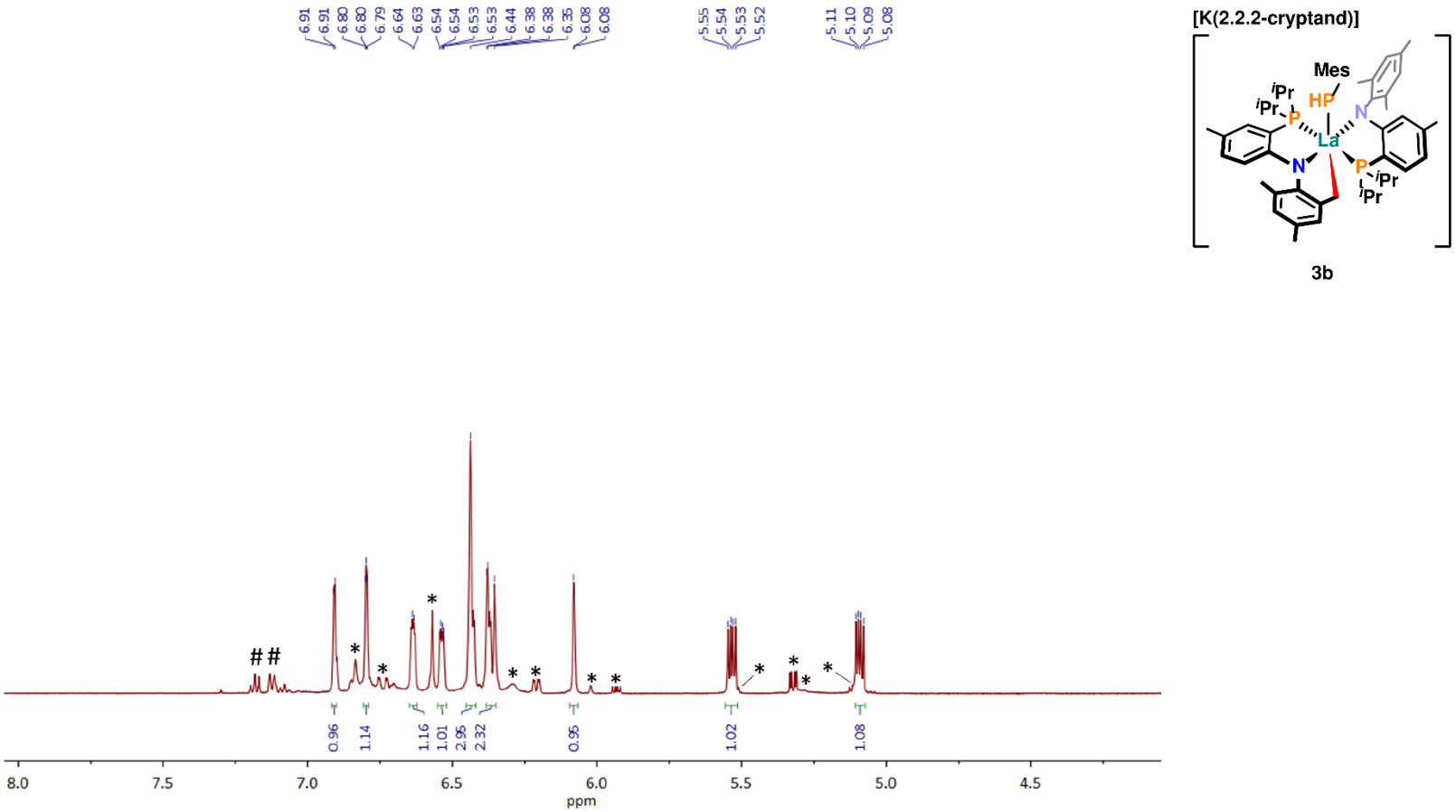

Fig. S28: *Section of the ^{1}H NMR spectrum (δ = 4.05 – 8.05 ppm) of **3b** (crude) in THF-d_8 (303 K). The resonances of unknown impurities are marked by asterisks (*). Residual toluene from work-up is marked by #.*

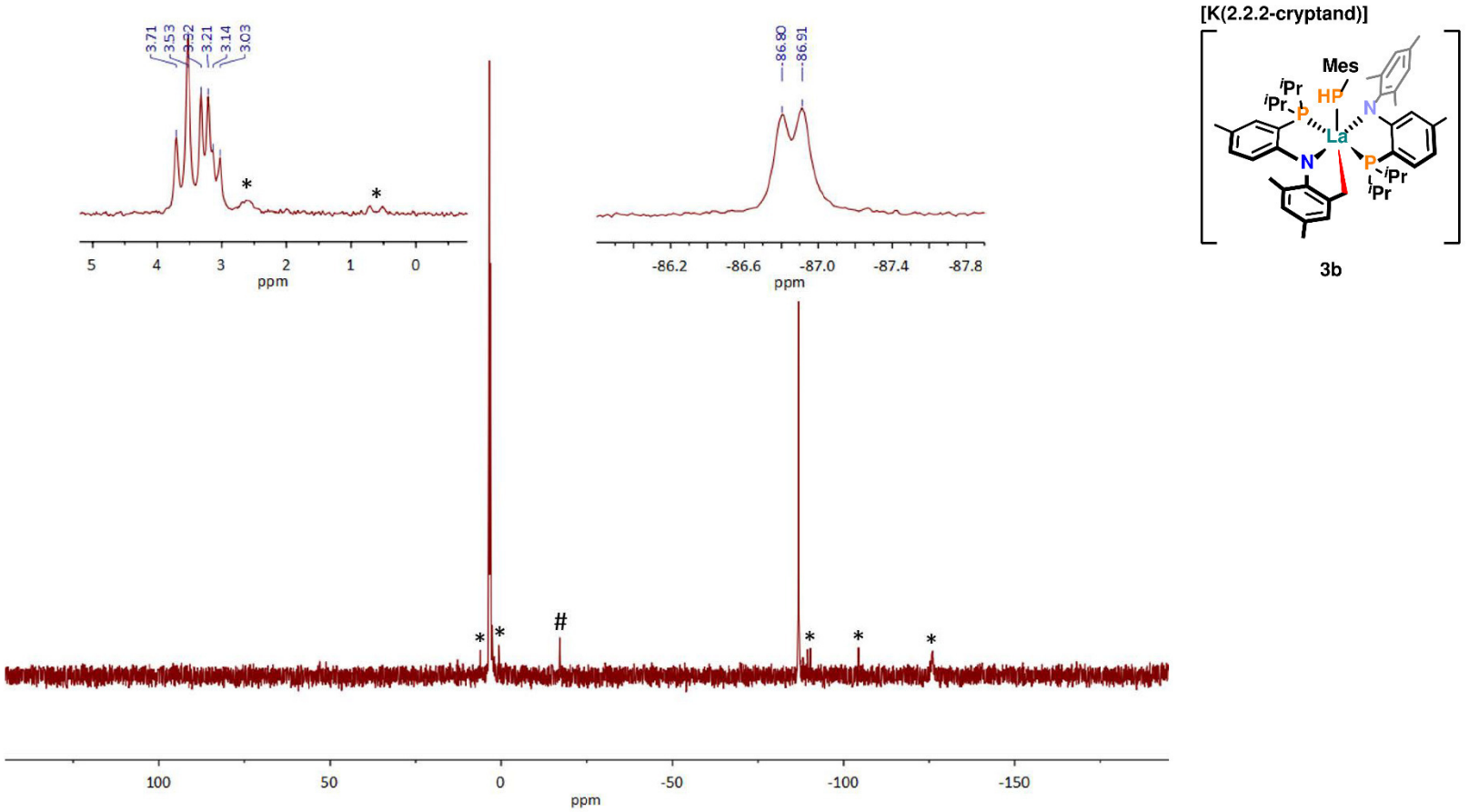

Fig. S29: *$^{31}P\{^{1}H\}$ NMR spectrum of **3b** (crude) in THF-d_8 (303 K). The two enlargements show the main product's multiplet at δ = 2.9 –3.9 ppm (left) and the doublet at δ = –86.9 ppm (right). The resonances of unknown impurities are marked by asterisks (*). Traces of protonated ligand HPN are marked by #.*

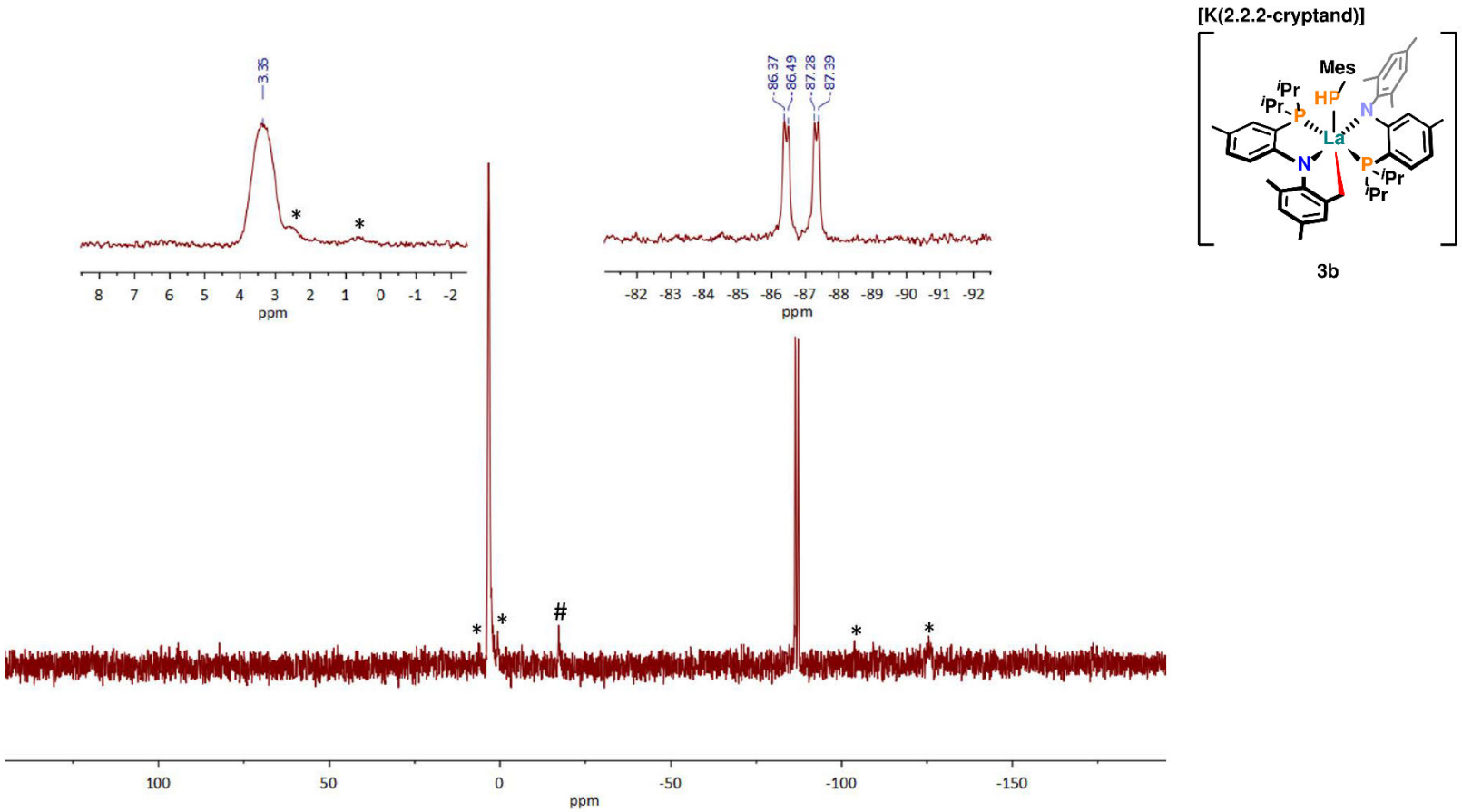

Fig. S30: *^{31}P NMR spectrum of **3b** (crude) in THF-d_8 (303 K). The two enlargements show the main product's broad multiplet at δ = 2.9 –3.9 ppm (left) and the doublet of doublets at δ = –86.9 ppm (right). The resonances of unknown impurities are marked by asterisks (*). Traces of protonated ligand HPN are marked by #.*

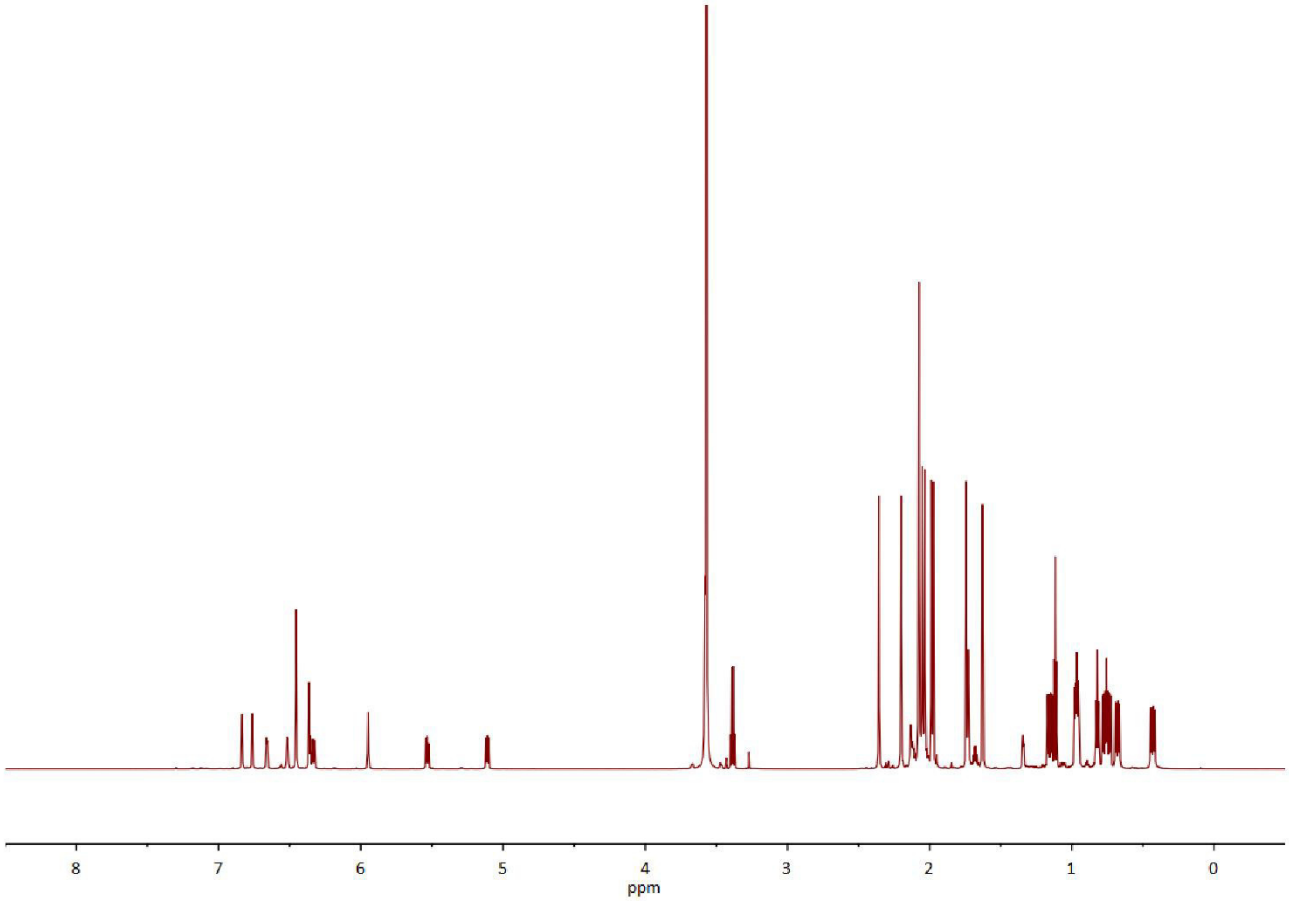

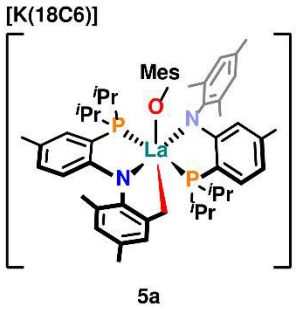

5a

Fig. S31: *^{1}H NMR spectrum of **5a** in THF-d_8 (303 K).*

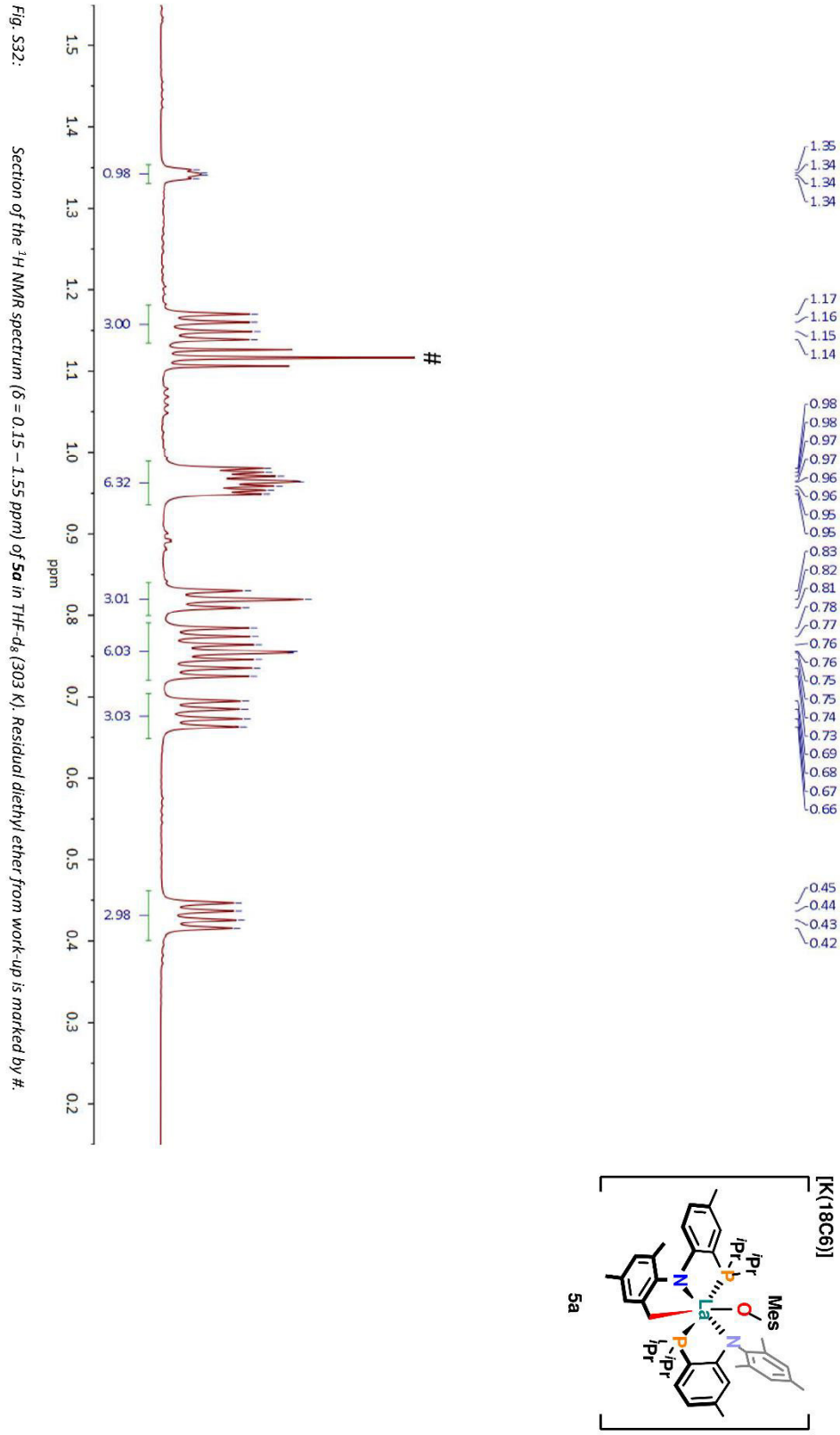

*Fig. S32: Section of the ^{1}H NMR spectrum (δ = 0.15 – 1.55 ppm) of **5a** in THF-d_8 (303 K). Residual diethyl ether from work-up is marked by #.*

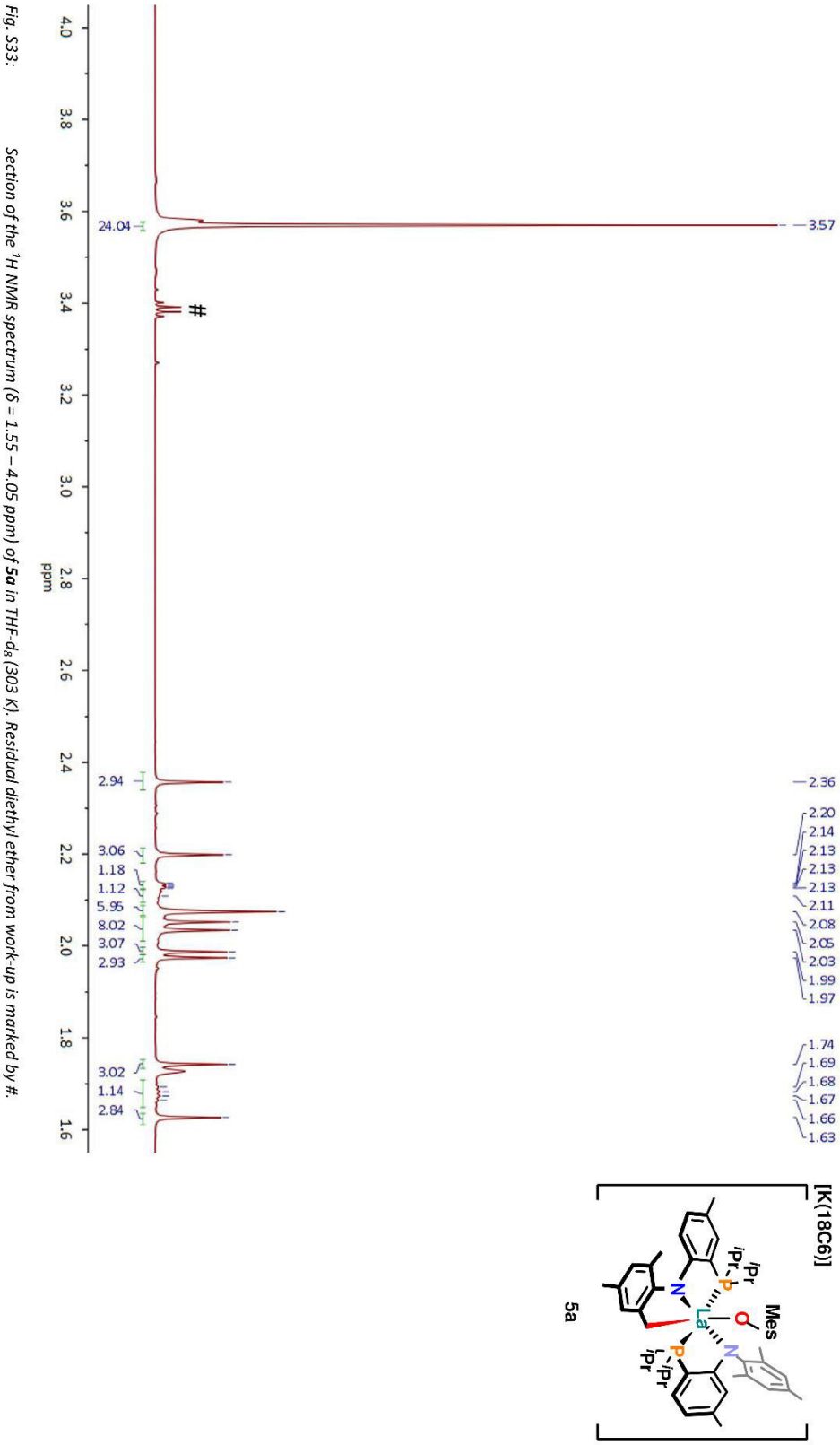

*Fig. S33: Section of the ^{1}H NMR spectrum (δ = 1.55 – 4.05 ppm) of **5a** in THF-d_8 (303 K). Residual diethyl ether from work-up is marked by #.*

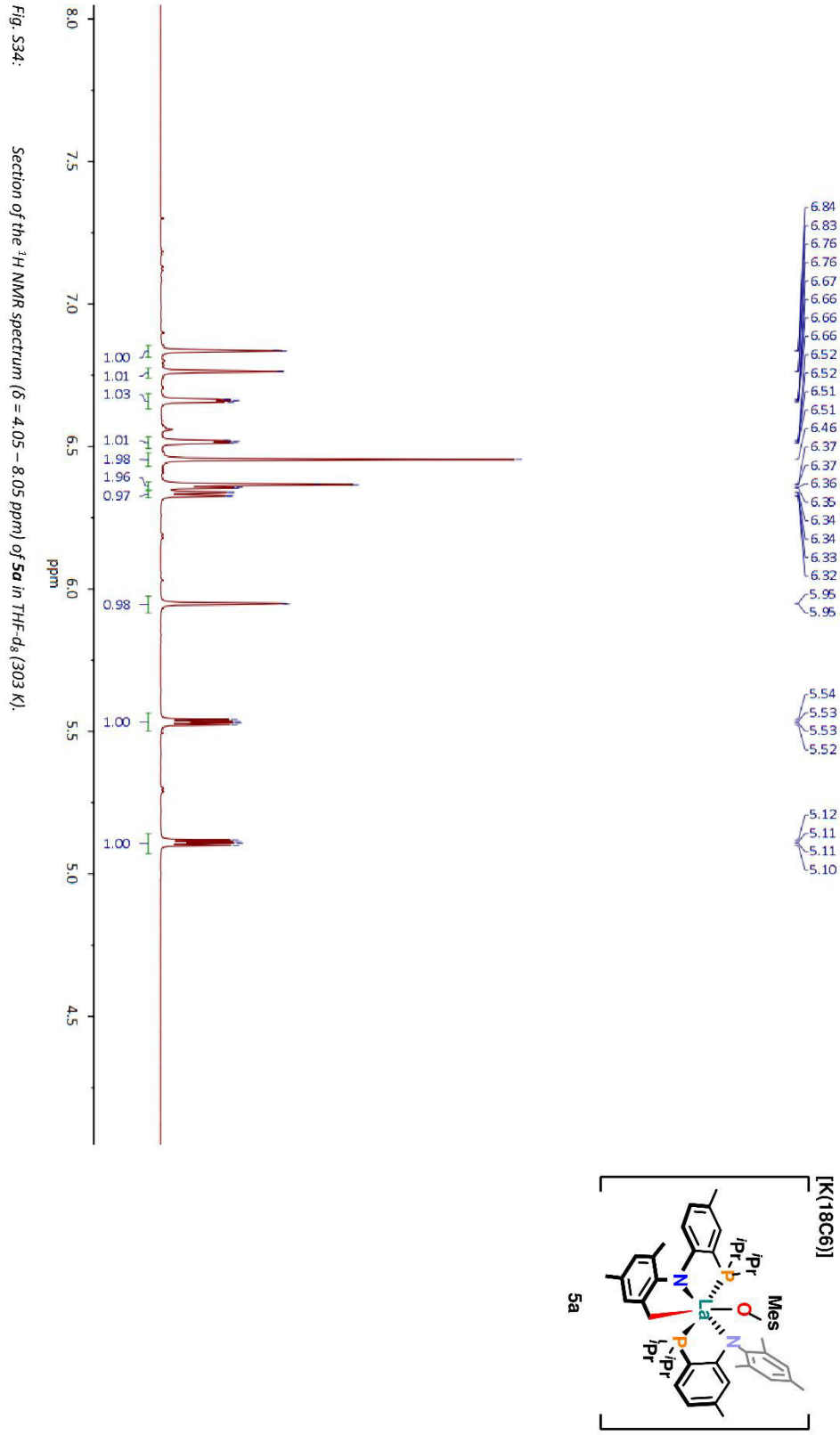

*Fig. S34: Section of the ^{1}H NMR spectrum (δ = 4.05 – 8.05 ppm) of **5a** in THF-d_8 (303 K).*

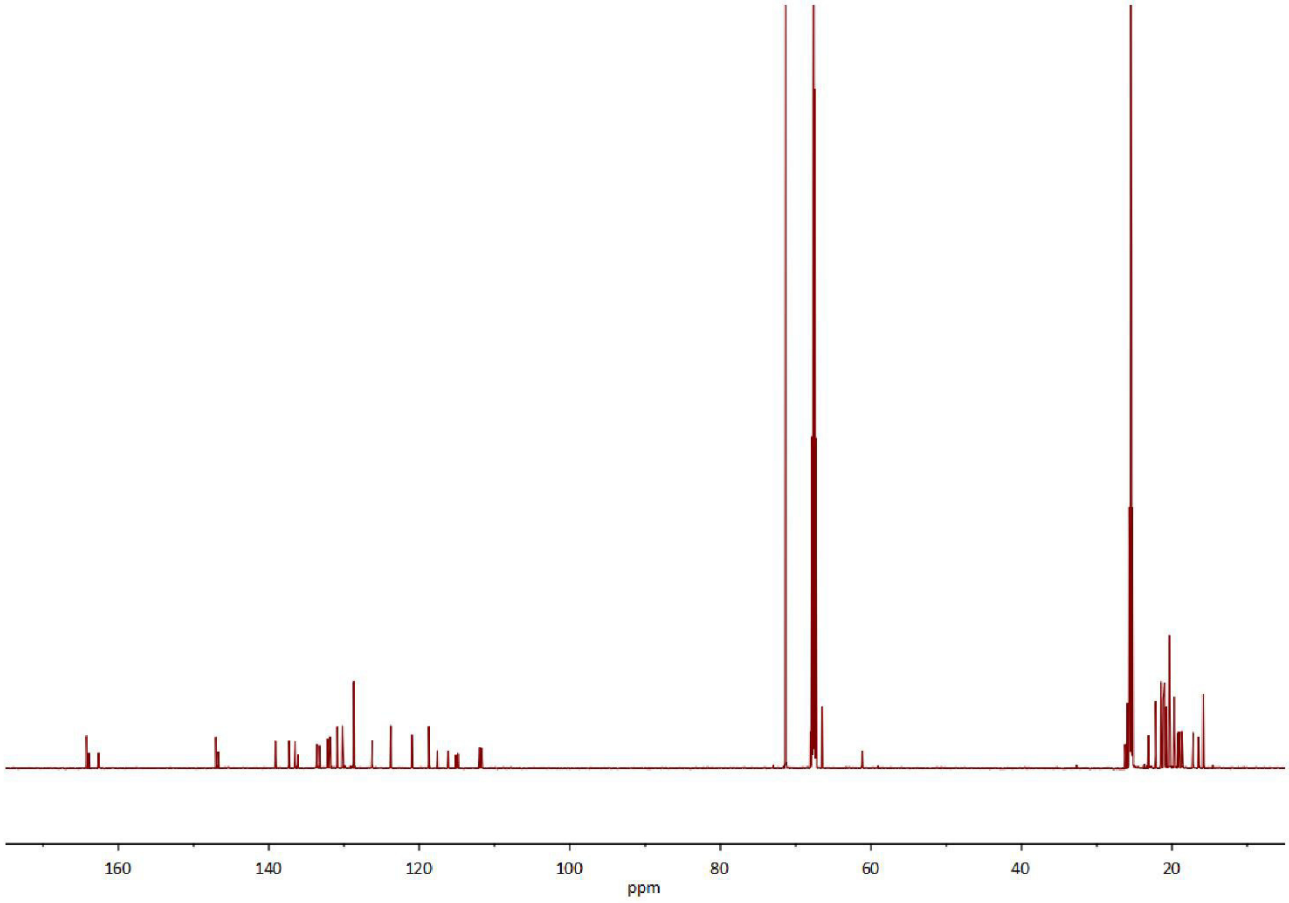

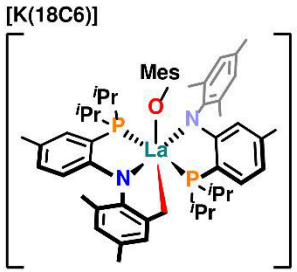

5a

Fig. S35: *$^{13}C\{^{1}H\}$ NMR spectrum of **5a** in THF-d_8 (303 K).*

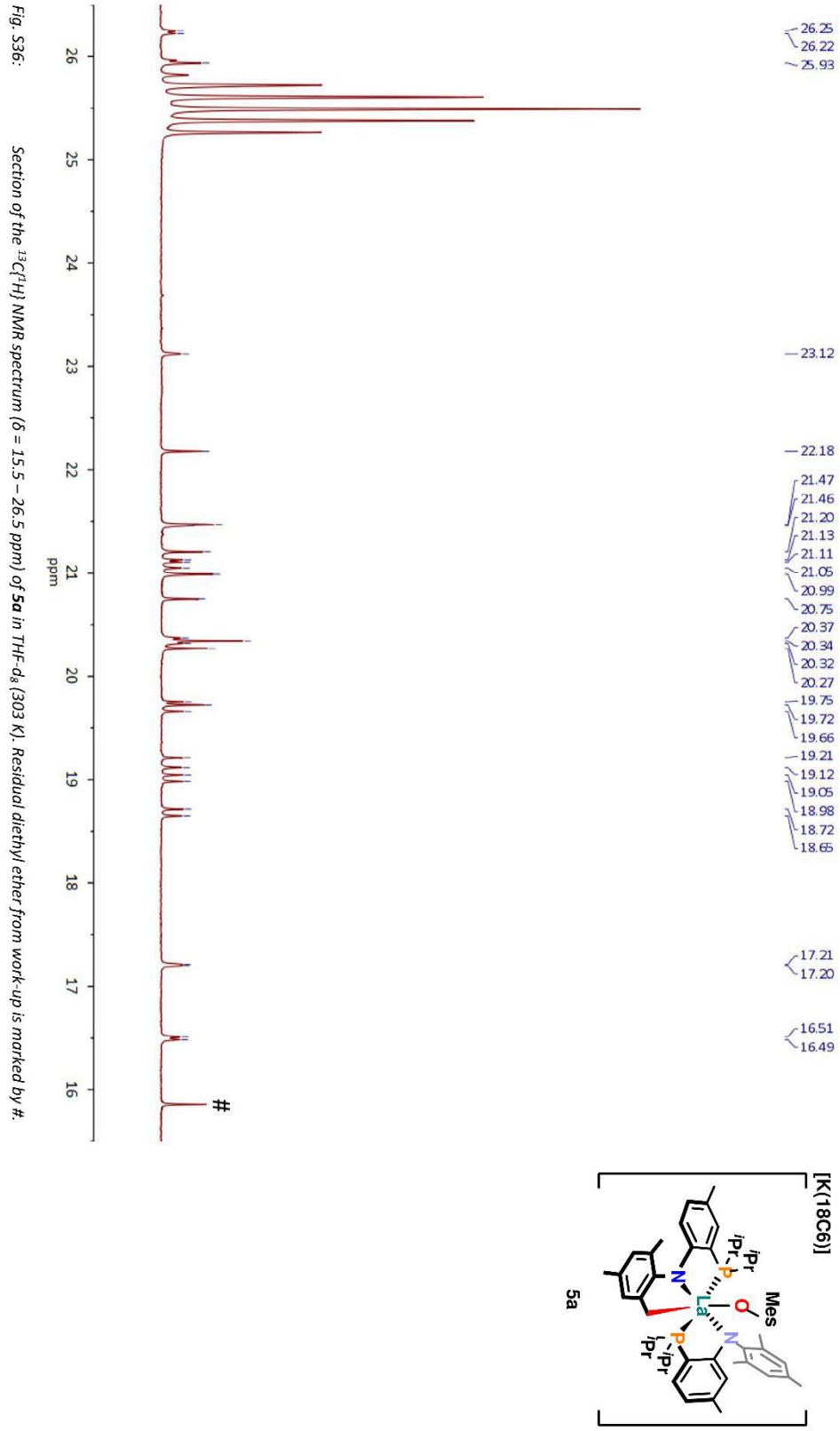

*Fig. S36: Section of the $^{13}C\{^{1}H\}$ NMR spectrum (δ = 15.5 – 26.5 ppm) of **5a** in THF-d_8 (303 K). Residual diethyl ether from work-up is marked by #.*

*Fig. S37: Section of the $^{13}C\{^{1}H\}$ NMR spectrum (δ = 60.5 – 72.5 ppm) of **5a** in THF-d_8 (303 K). Residual diethyl ether from work-up is marked by #.*

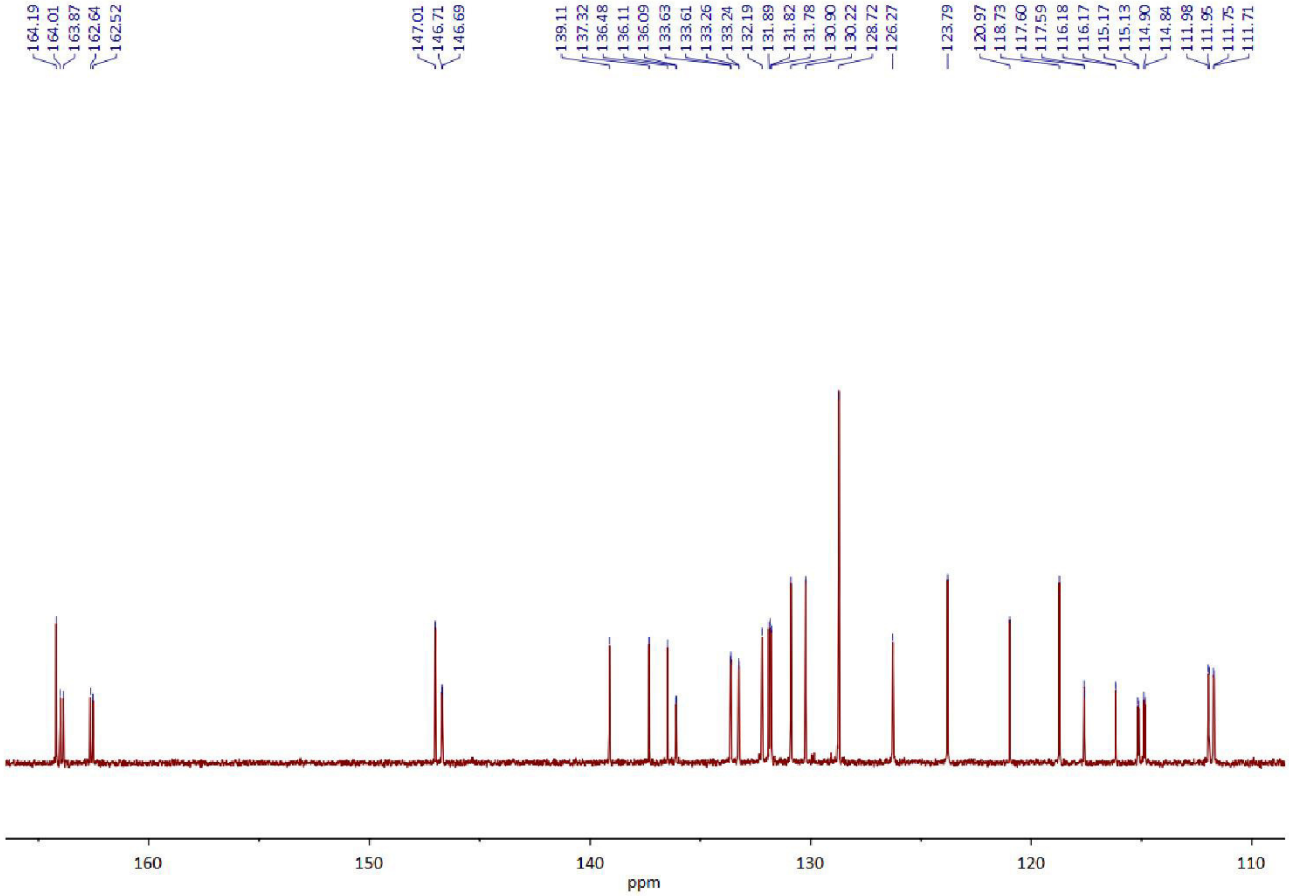

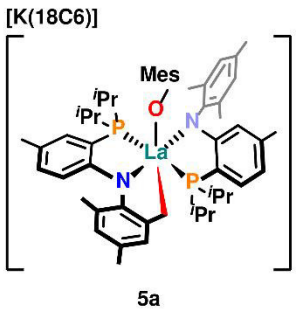

5a

Fig. S38: *Section of the $^{13}C\{^1H\}$ NMR spectrum (δ = 108.5 – 166.5 ppm) of **5a** in THF-d_8 (303 K).*

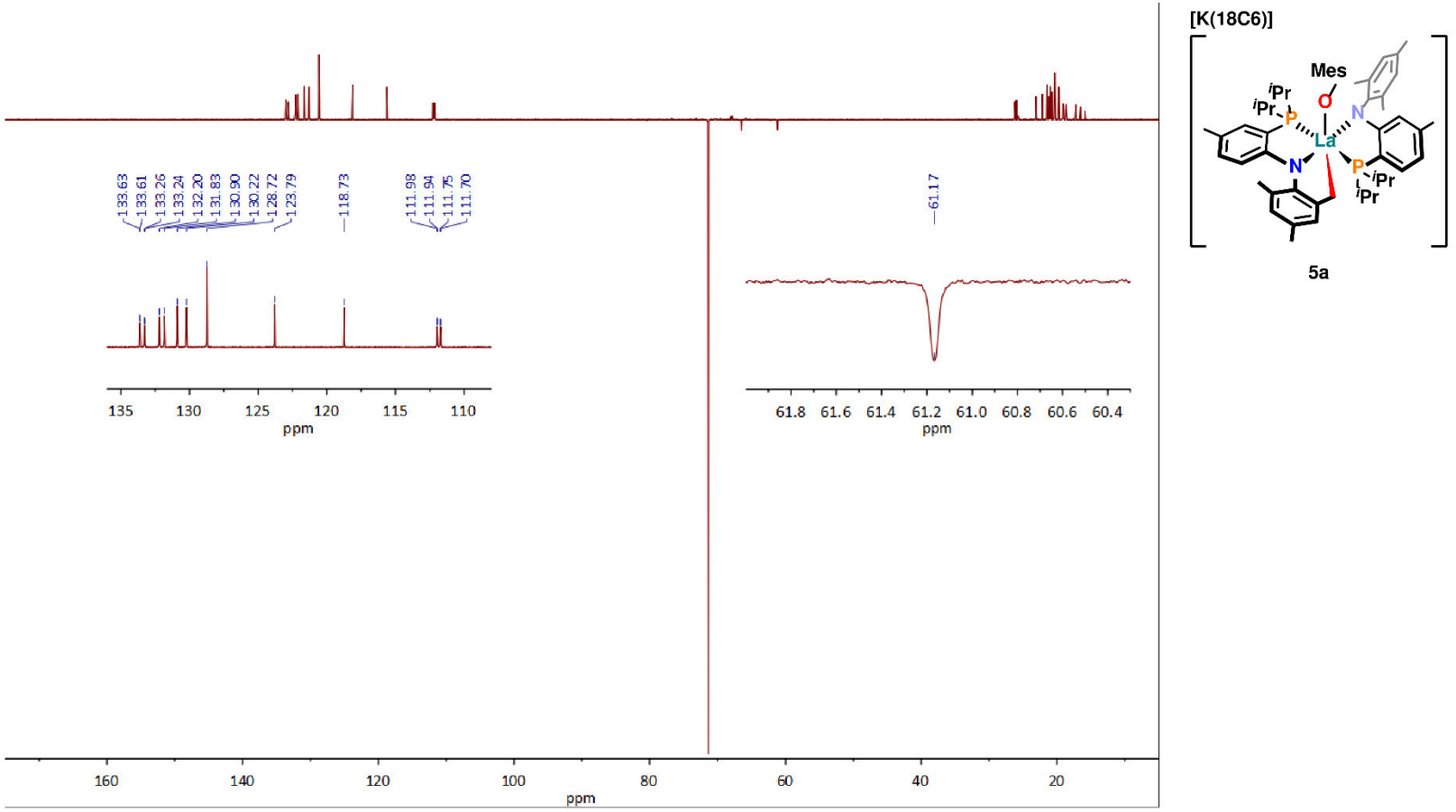

Fig. S39: *$^{13}C\{^1H\}$ DEPT135 NMR spectrum of **5a** in THF-d_8 (303 K). The two enlargements show the ^{13}C chemical shifts of the CH groups in the aromatic region (left) and a close-up of the peak for the $CH_{2Mes(PNcyclo)}$ methylene group at δ = 61.2 ppm (right) of **5a**.*

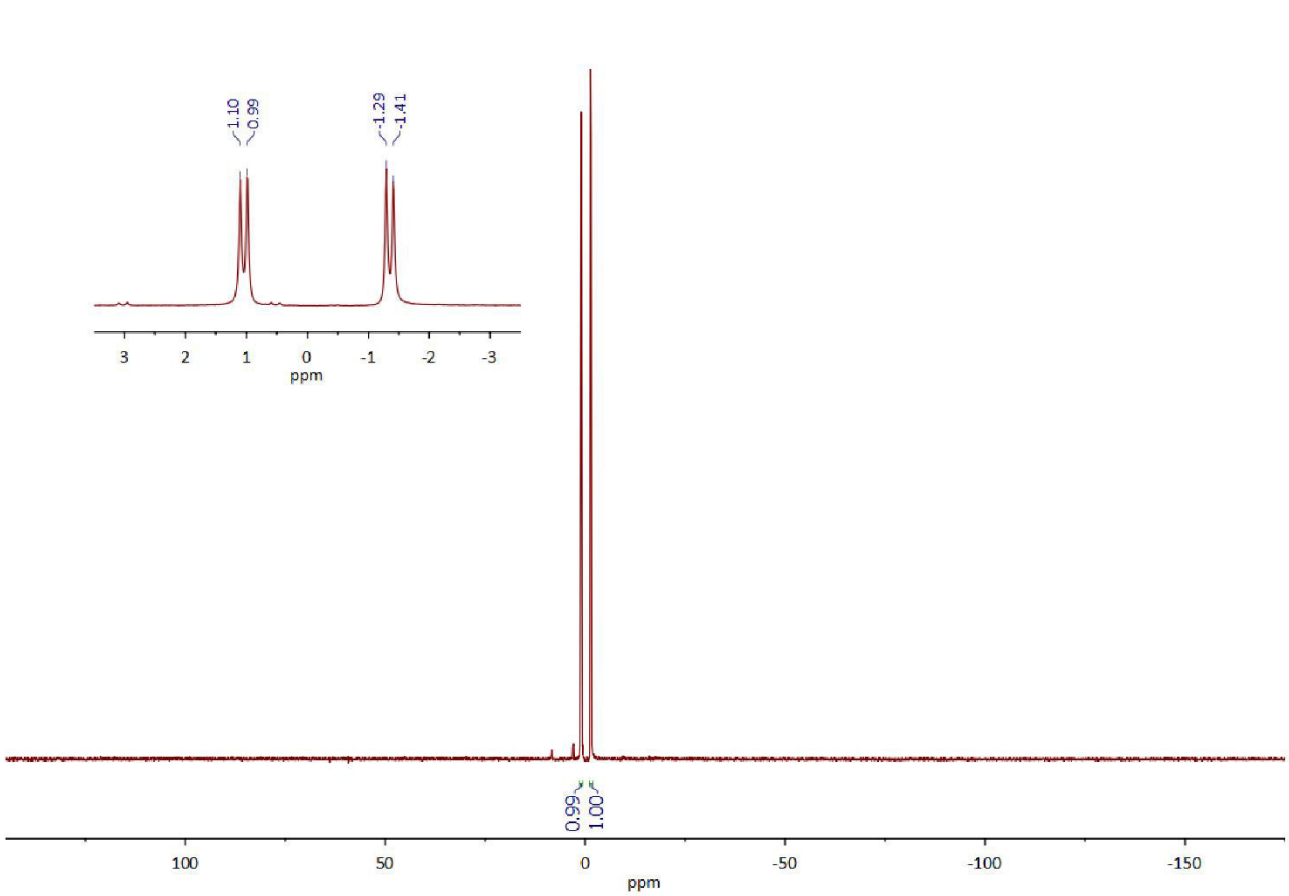

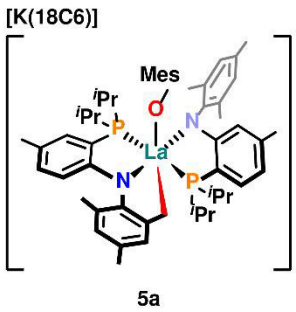

5a

Fig. S40: *$^{31}P\{^{1}H\}$ NMR spectrum of **5a** in THF-d_8 (303 K). The enlargement shows the doublet splitting of the resonances at δ = –1.4 and 1.1 ppm.*

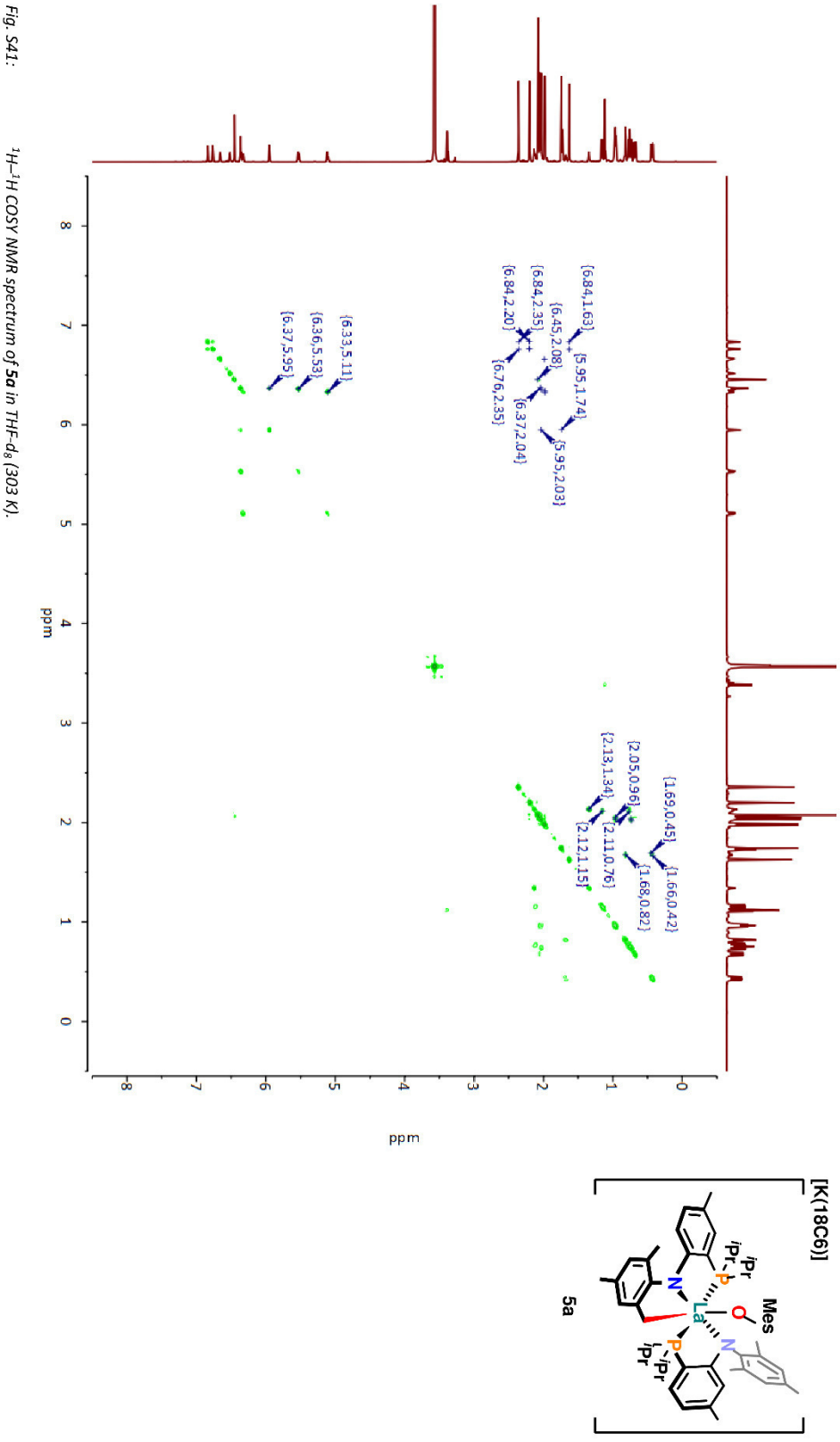

*Fig. S41: ^1H–^1H COSY NMR spectrum of **5a** in THF-d_8 (303 K).*

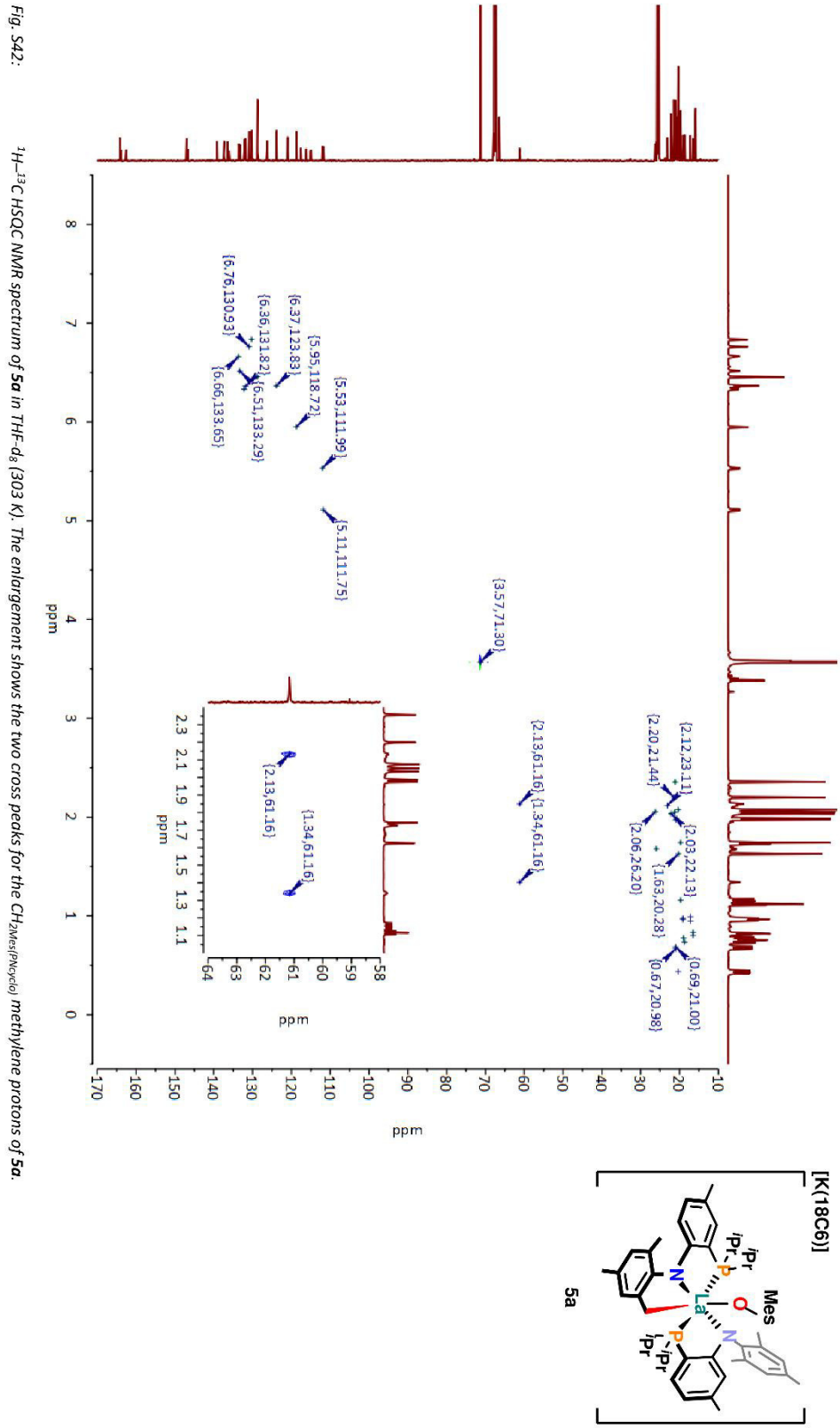

*Fig. S42: $^{1}H–^{13}C$ HSQC NMR spectrum of **5a** in THF-d_8 (303 K). The enlargement shows the two cross peaks for the $CH_{2Mes(PNcyclo)}$ methylene protons of **5a**.*

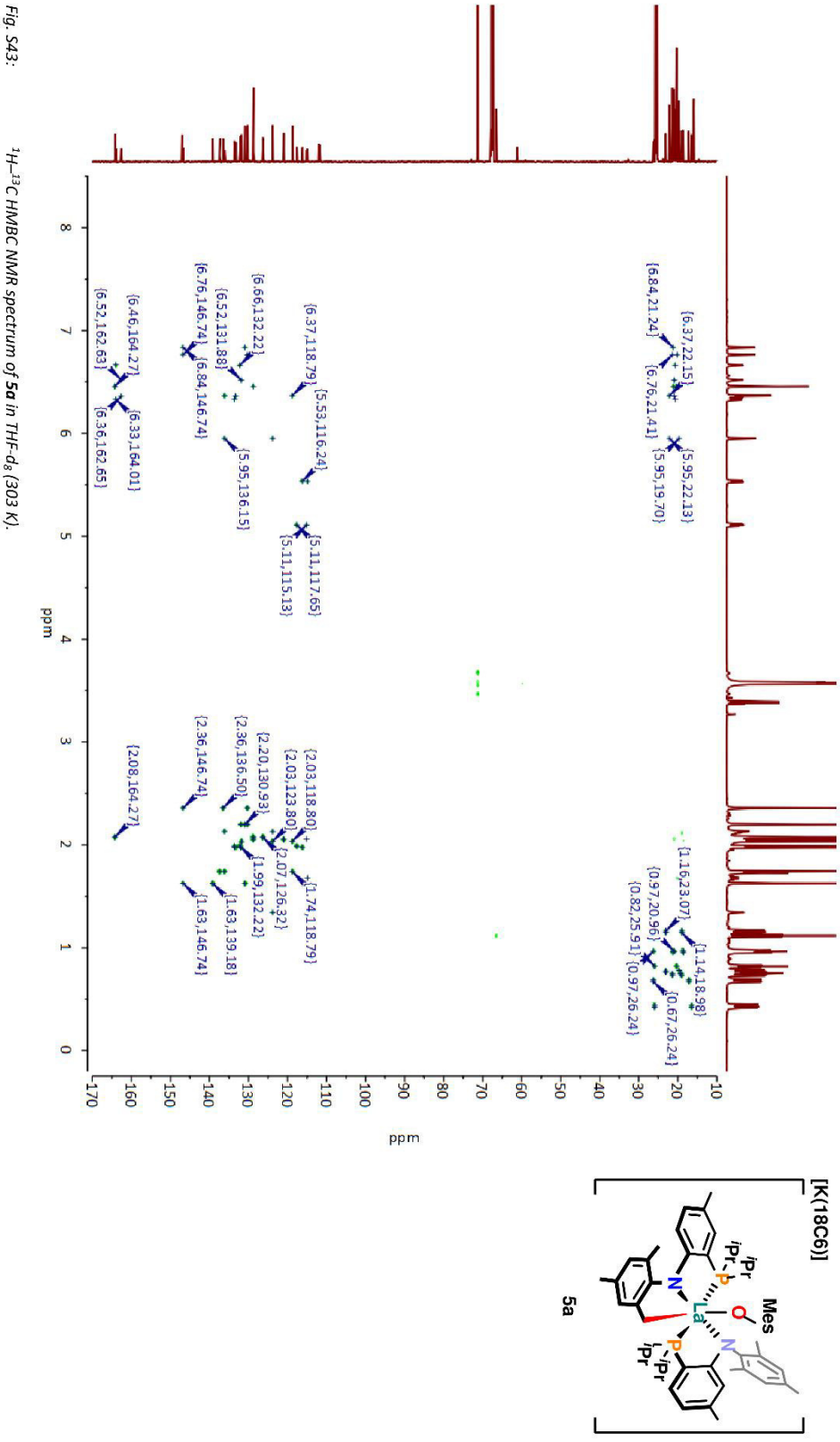

Fig. S43: ^{1}H–^{13}C *HMBC NMR spectrum of* **5a** *in THF-*d_8 *(303 K).*

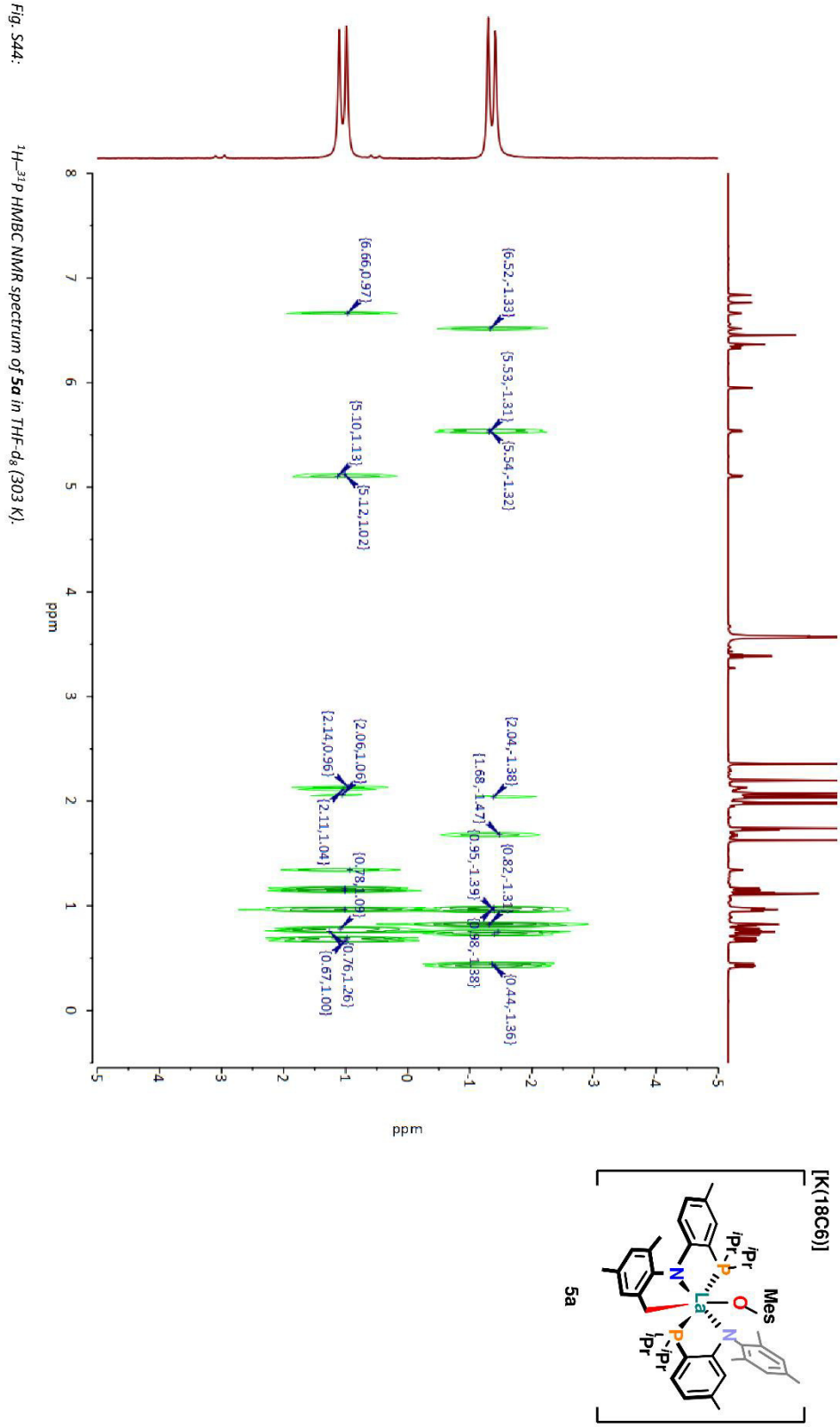

Fig. S44: ^{1}H–^{31}P *HMBC NMR spectrum of* **5a** *in THF-*d_8 *(303 K).*

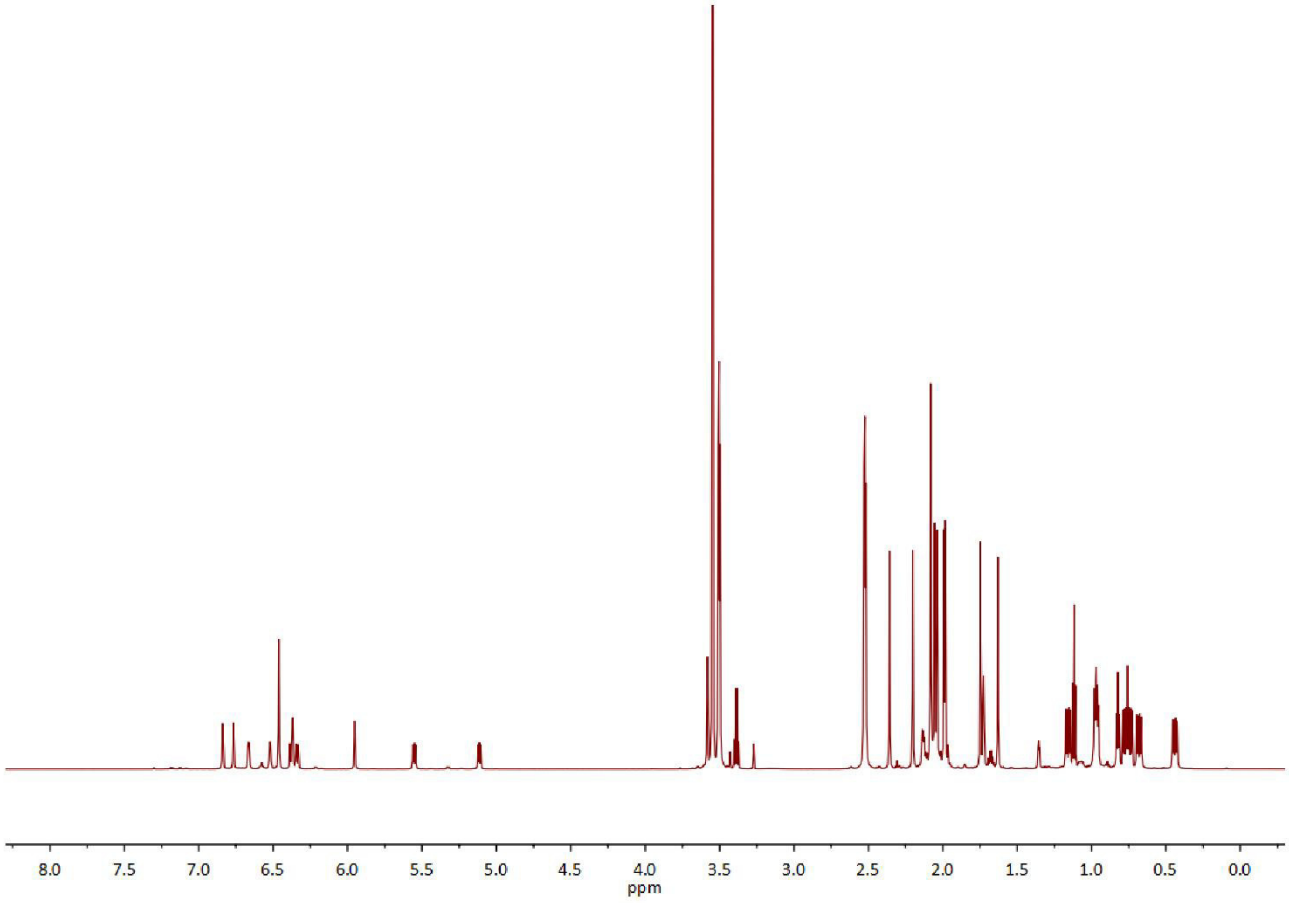

[K(2.2.2-cryptand)]

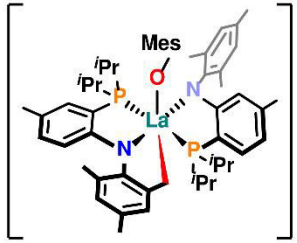

5b

Fig. S45: *^{1}H NMR spectrum of **5b** in THF-d_8 (303 K).*

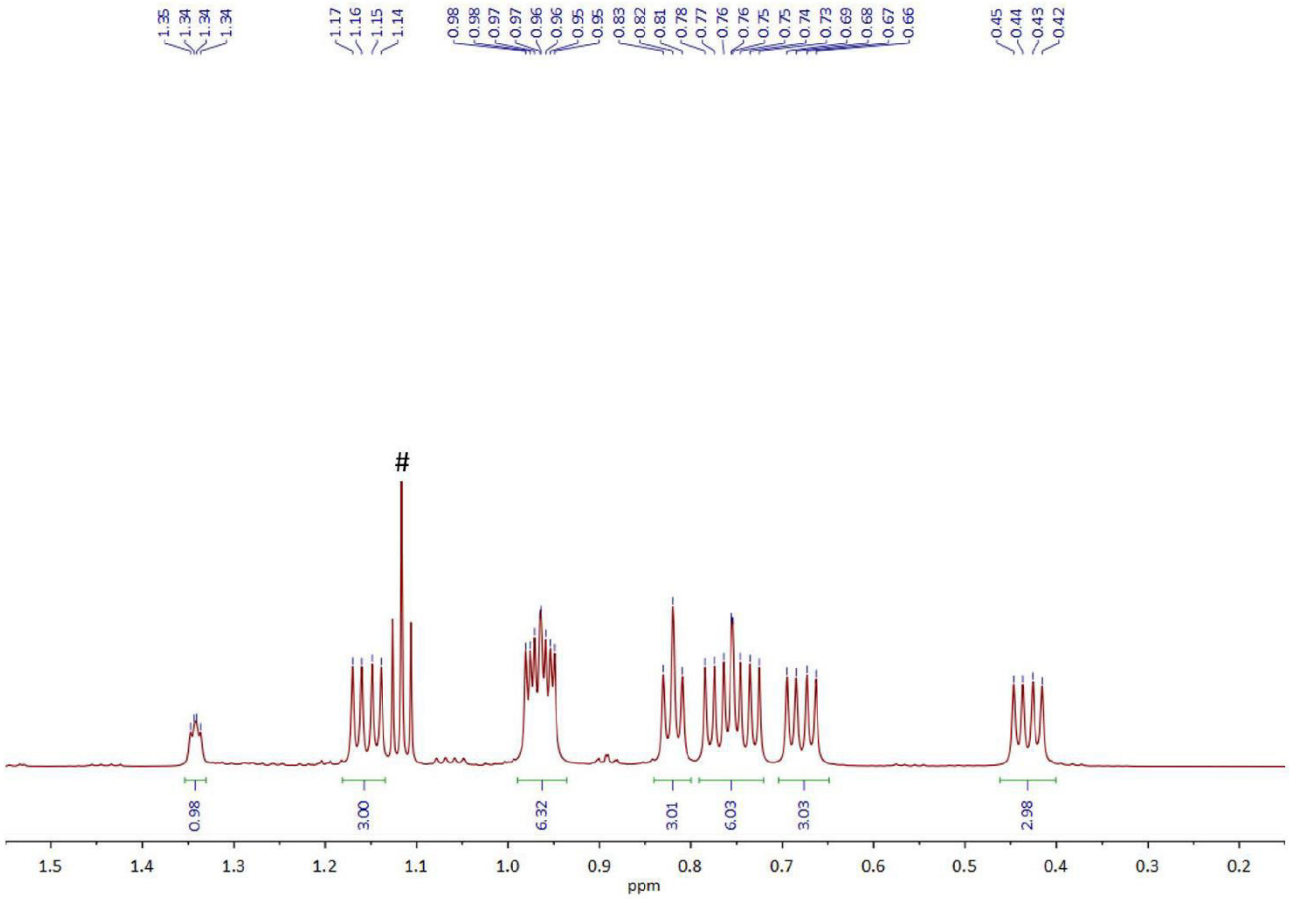

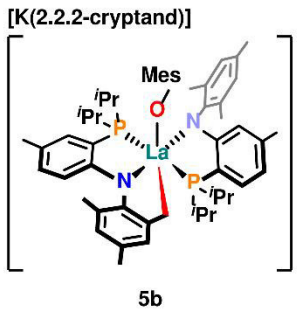

5b

*Fig. S46: Section of the ^{1}H NMR spectrum (δ = 0.15 – 1.55 ppm) of **5b** in THF-d_8 (303 K). Residual diethyl ether from work-up is marked by #.*

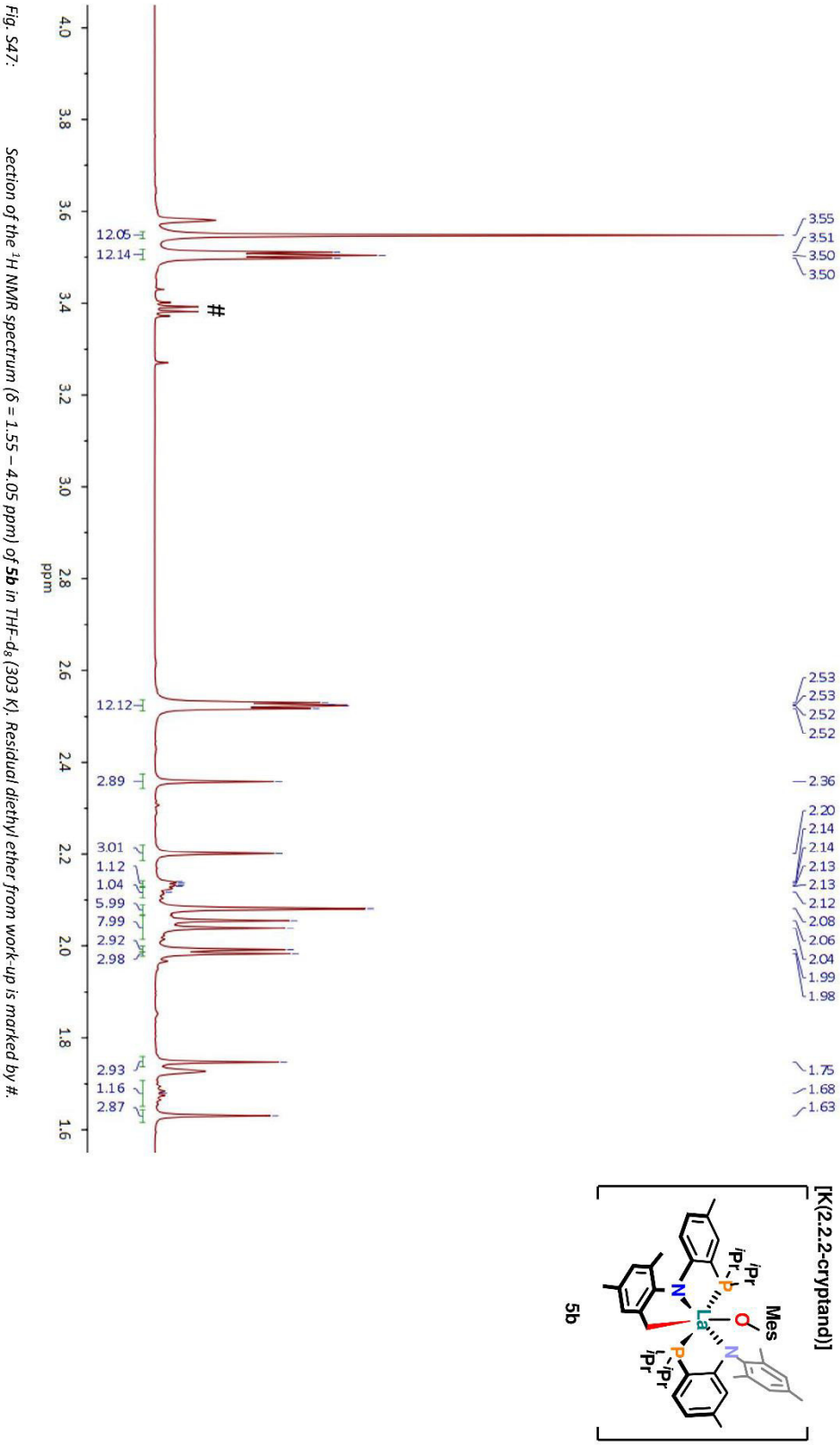

*Fig. S47: Section of the ^{1}H NMR spectrum (δ = 1.55 – 4.05 ppm) of **5b** in THF-d_8 (303 K). Residual diethyl ether from work-up is marked by #.*

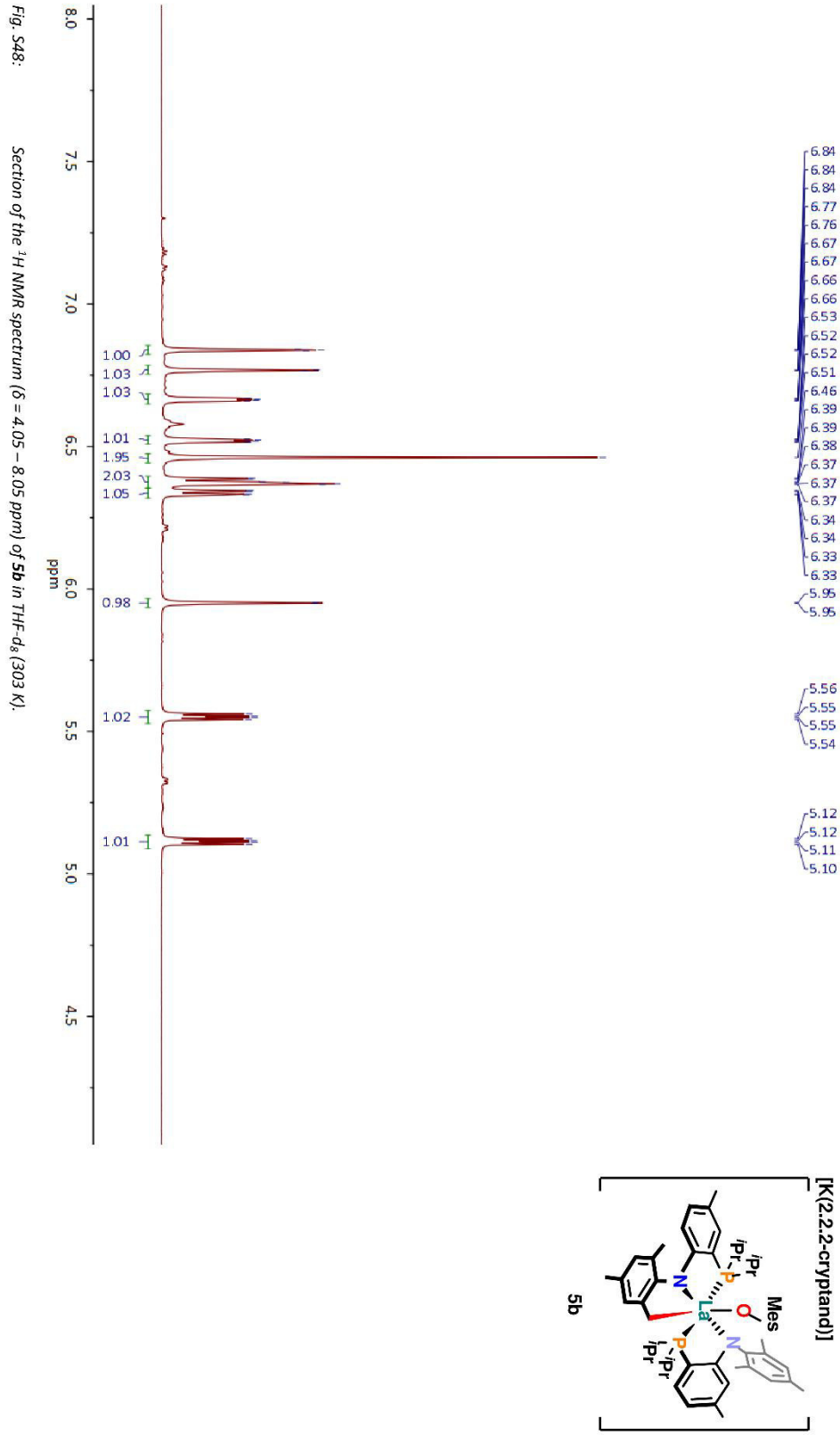

*Fig. S48: Section of the ^{1}H NMR spectrum (δ = 4.05 – 8.05 ppm) of **5b** in THF-d_8 (303 K).*

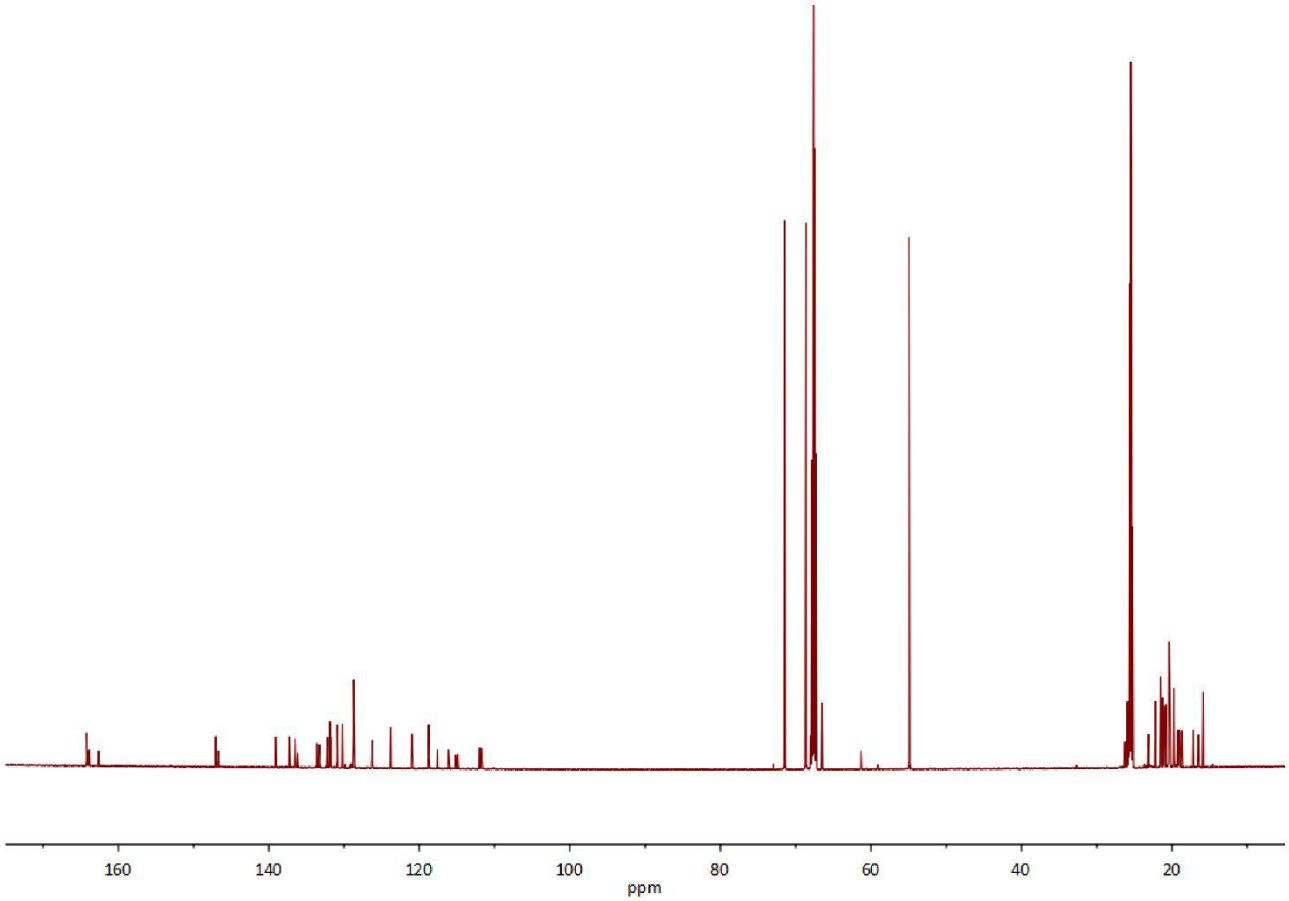

[K(2.2.2-cryptand)]

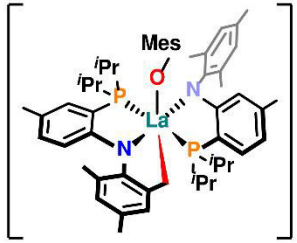

5b

Fig. S49: *$^{13}C\{^{1}H\}$ NMR spectrum of **5b** in THF-d_8 (303 K).*

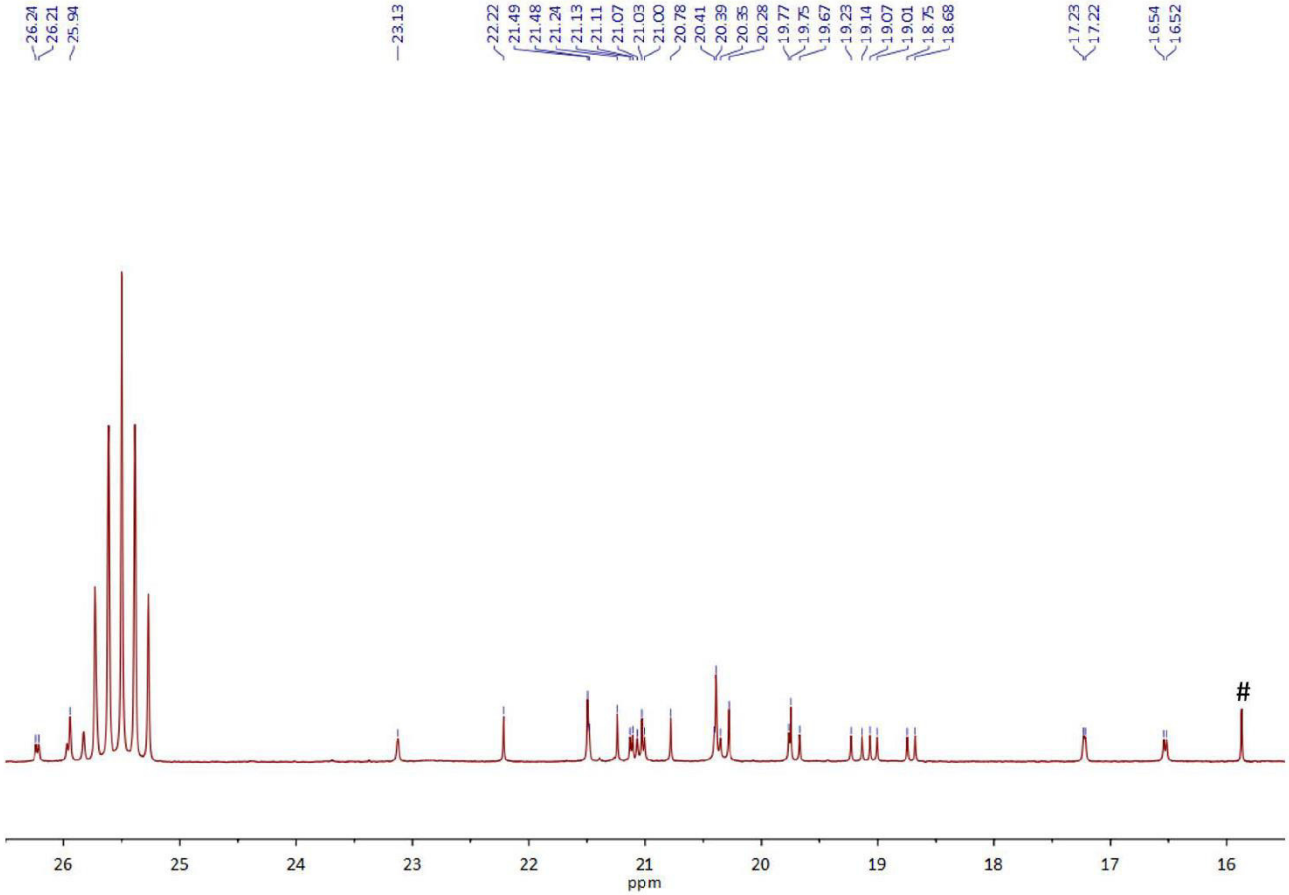

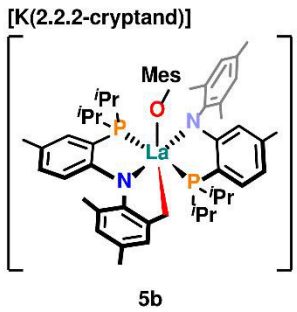

5b

*Fig. S50: Section of the $^{13}C\{^{1}H\}$ NMR spectrum (δ = 15.5 – 26.5 ppm) of **5b** in THF-d_8 (303 K). Residual diethyl ether from work-up is marked by #.*

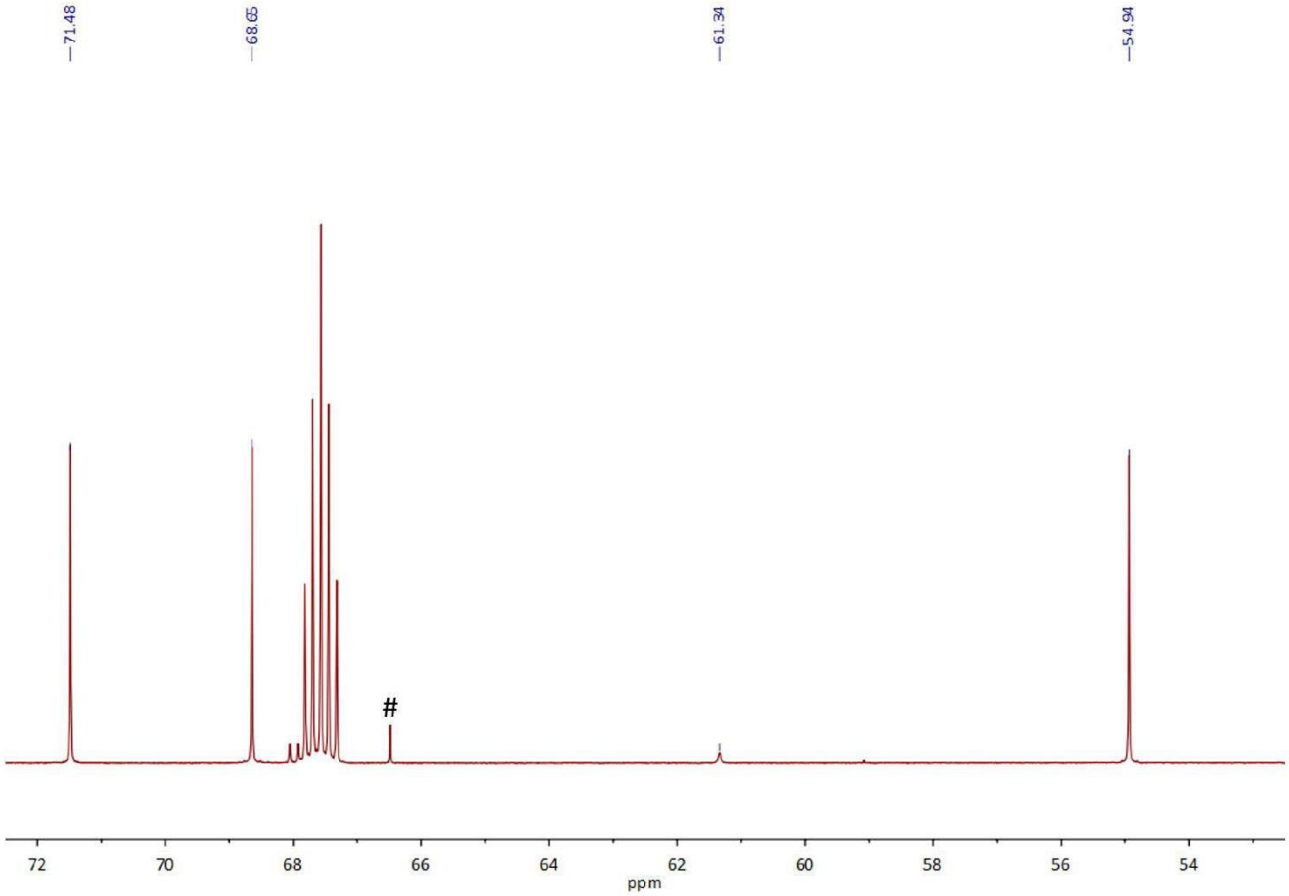

[K(2.2.2-cryptand)]

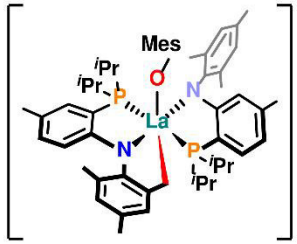

5b

Fig. S51: *Section of the $^{13}C\{^{1}H\}$ NMR spectrum (δ = 52.5 – 72.5 ppm) of **5b** in THF-d_8 (303 K). Residual diethyl ether from work-up is marked by #.*

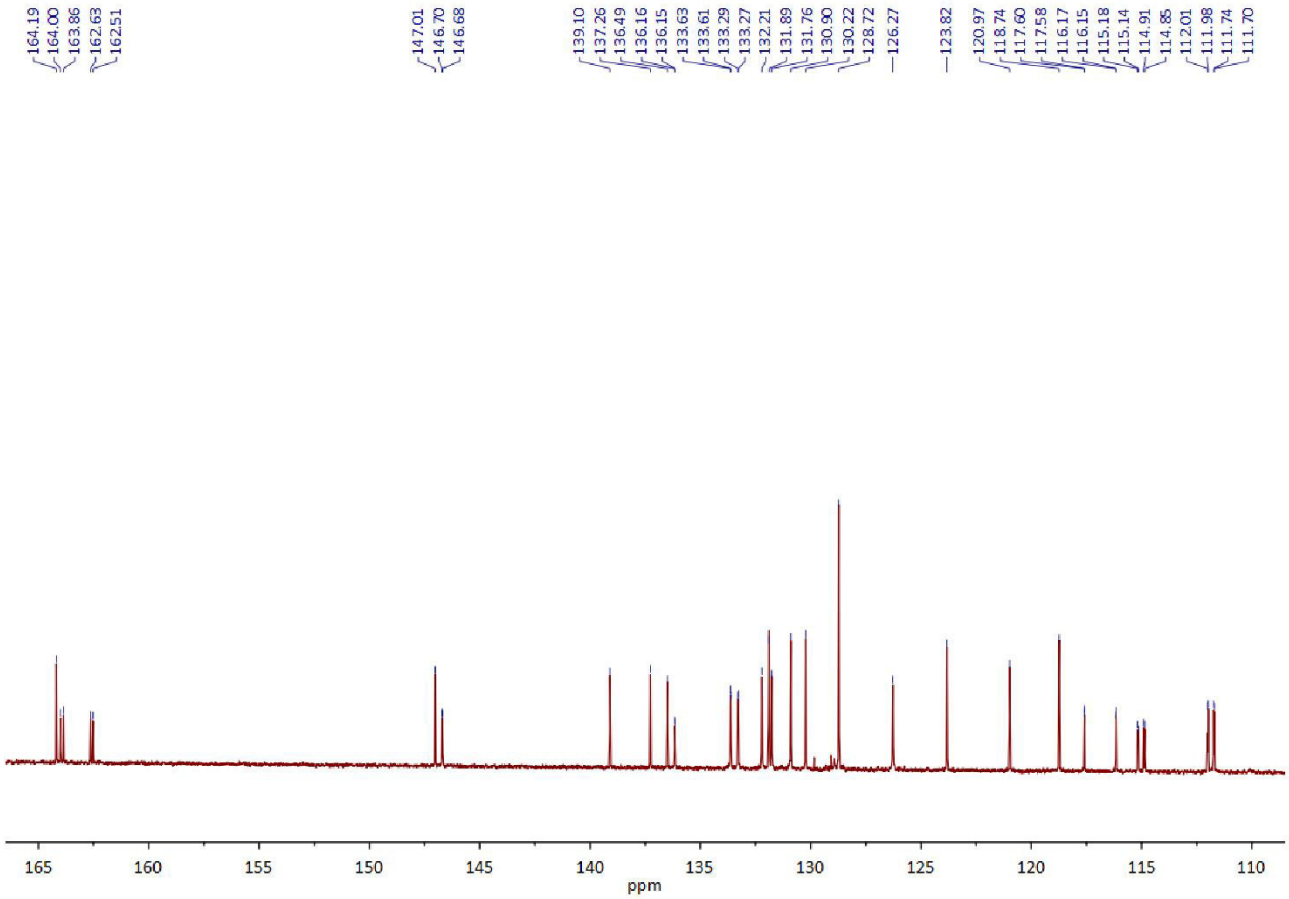

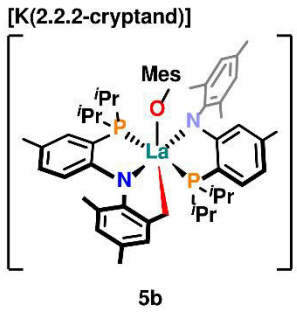

Fig. S52: *Section of the $^{13}C\{^{1}H\}$ NMR spectrum (δ = 108.5 – 166.5 ppm) of **5b** in THF-d_8 (303 K).*

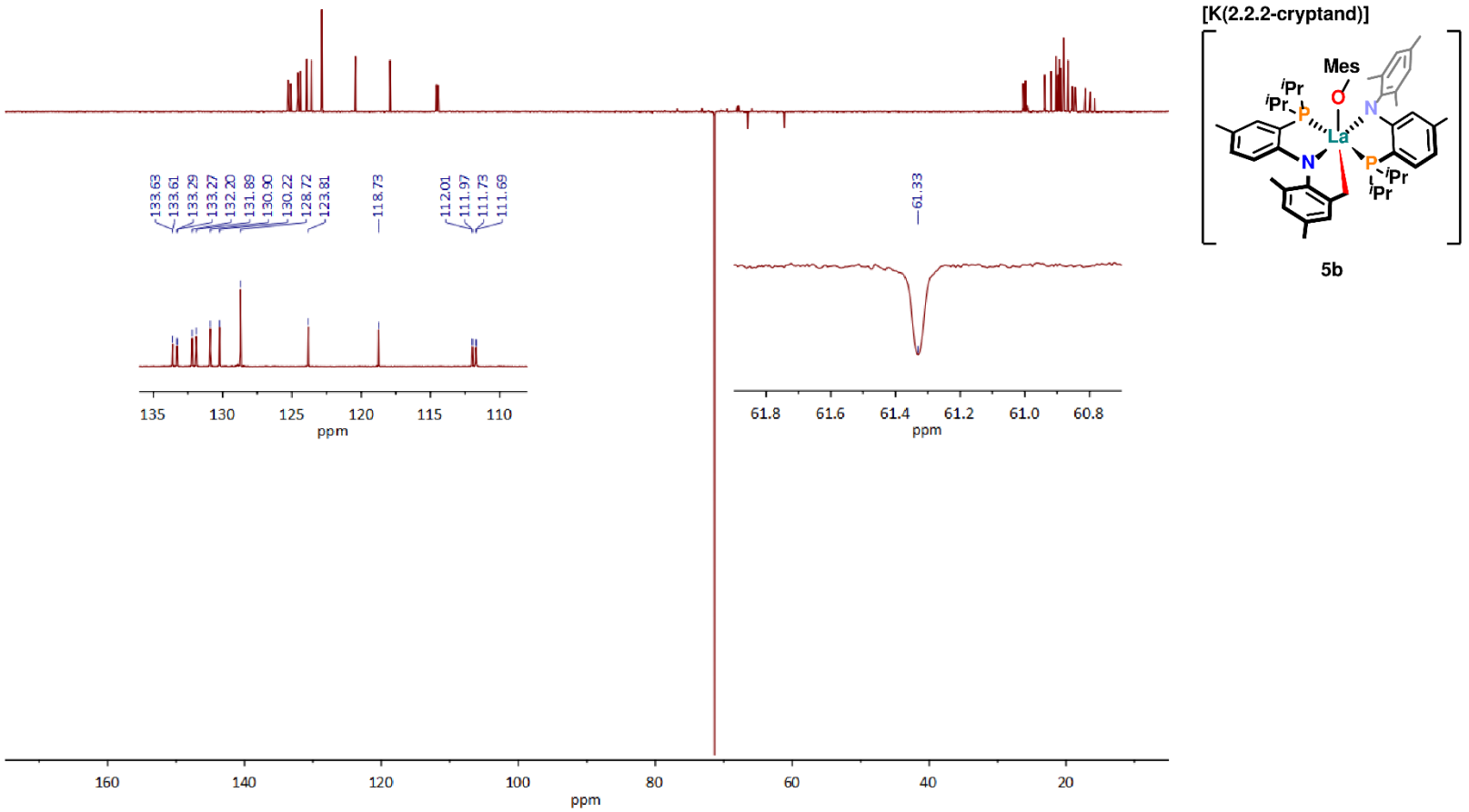

Fig. S53: *$^{13}C\{^{1}H\}$ DEPT135 NMR spectrum of **5b** in THF-d_8 (303 K). The two enlargements show the ^{13}C chemical shifts of the CH groups in the aromatic region (left) and a close-up of the peak for the $CH_{2Mes(PNcyclo)}$ methylene group at δ = 61.3 ppm (right) of **5b**.*

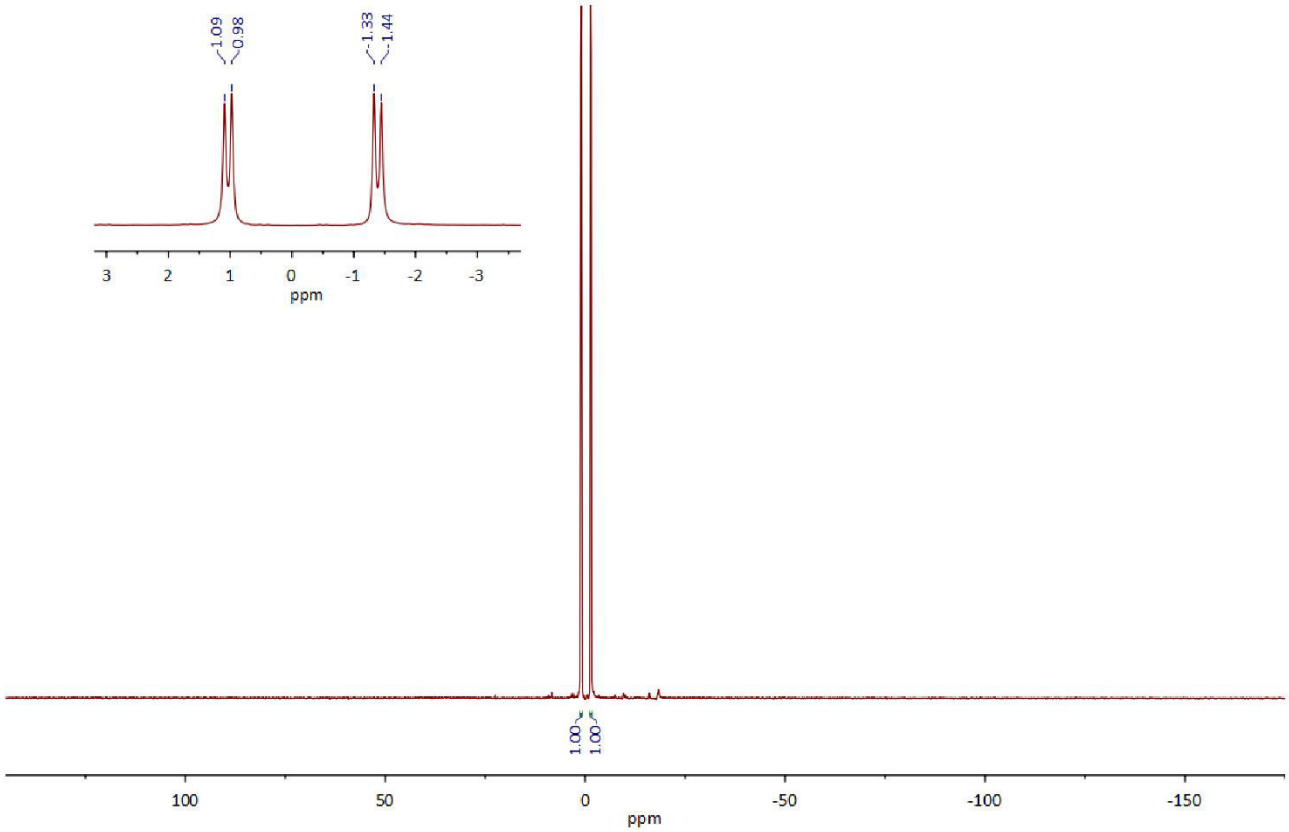

[K(2.2.2-cryptand)]

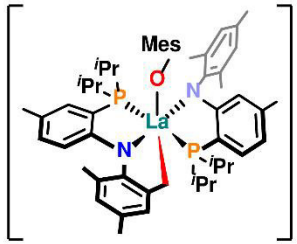

5b

Fig. S54: *$^{31}P\{^{1}H\}$ NMR spectrum of **5b** in THF-d_8 (303 K). The enlargement shows the doublet splitting of the resonances at δ = –1.4 and 1.0 ppm.*

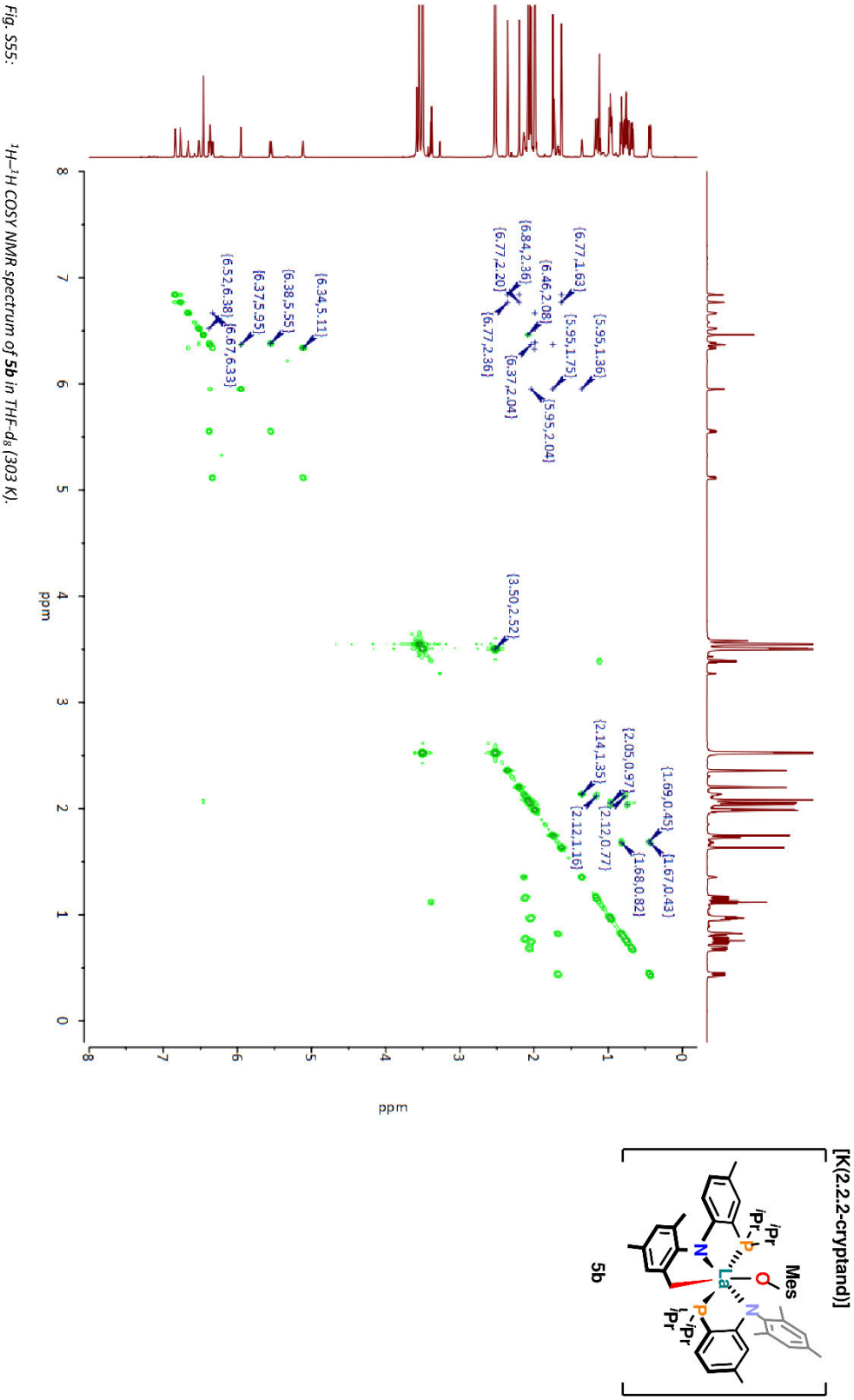

Fig. S55: *^1H–^1H COSY NMR spectrum of **5b** in THF-d_8 (303 K).*

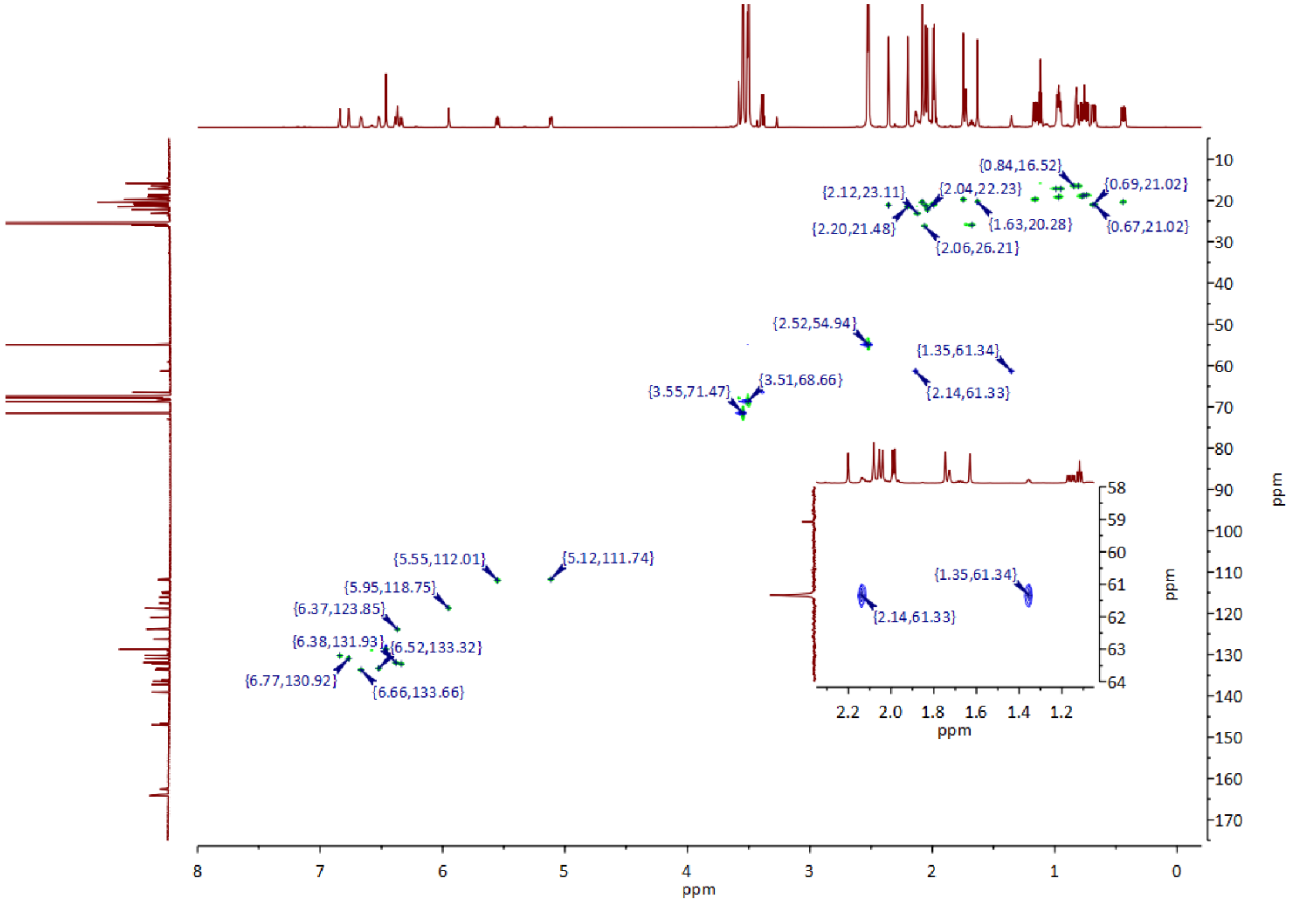

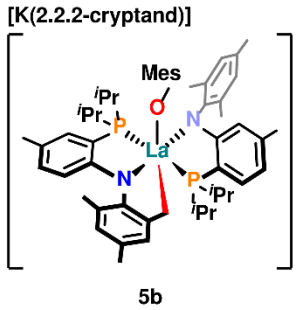

Fig. S56: *^{1}H–^{13}C HSQC NMR spectrum of **5b** in THF-d_8 (303 K). The enlargement shows the two cross peaks for the $CH_{2Mes(PNcyclo)}$ methylene protons of **5b**.*

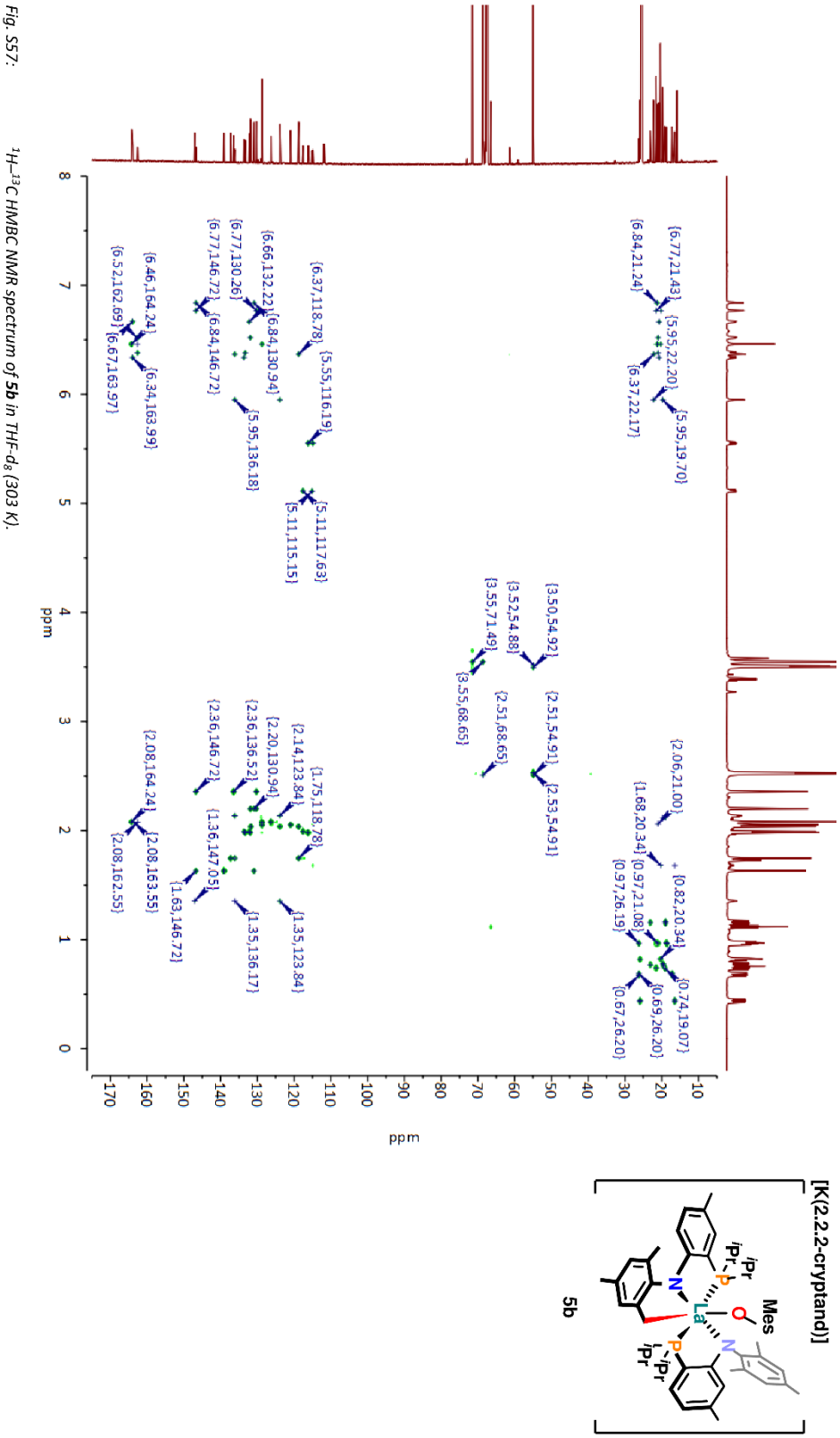

*Fig. S57: ^{1}H–^{13}C HMBC NMR spectrum of **5b** in THF-d_8 (303 K).*

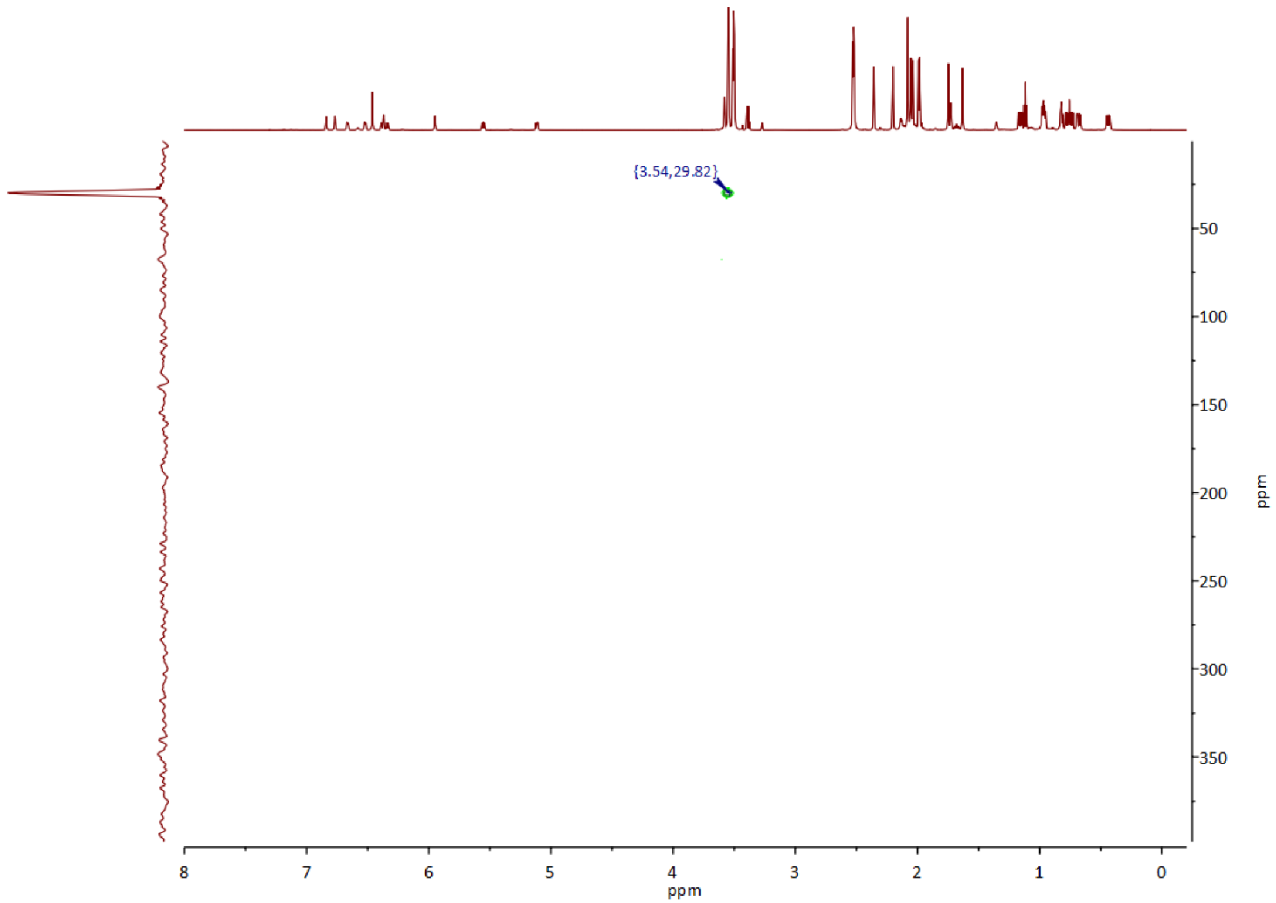

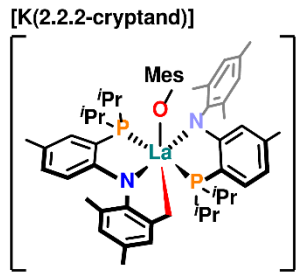

Fig. S58: *^{1}H–^{15}N HMBC NMR spectrum of **5b** in THF-d_8 (303 K).*

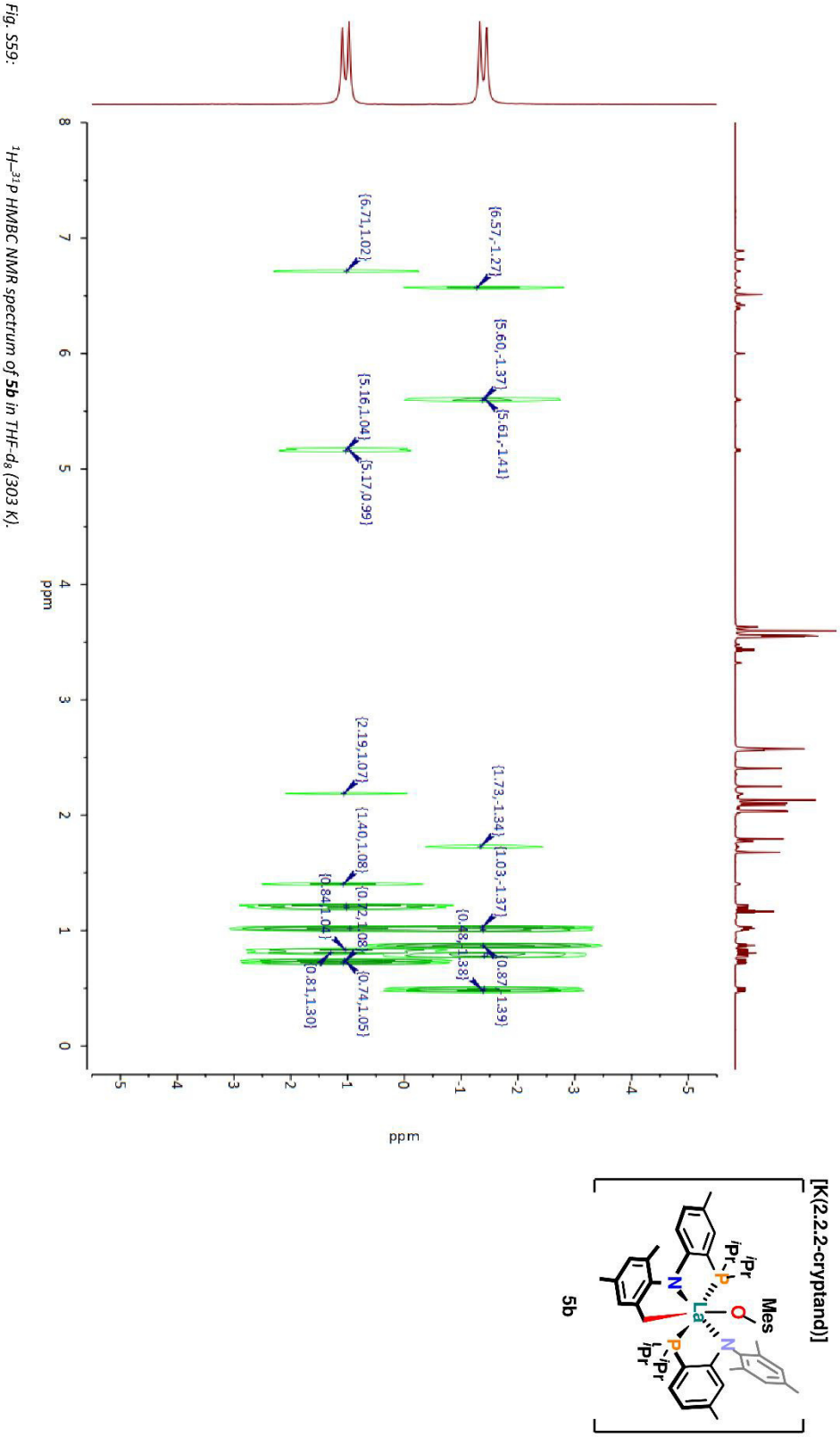

Fig. S59: *^{1}H–^{31}P HMBC NMR spectrum of **5b** in THF-d_8 (303 K).*

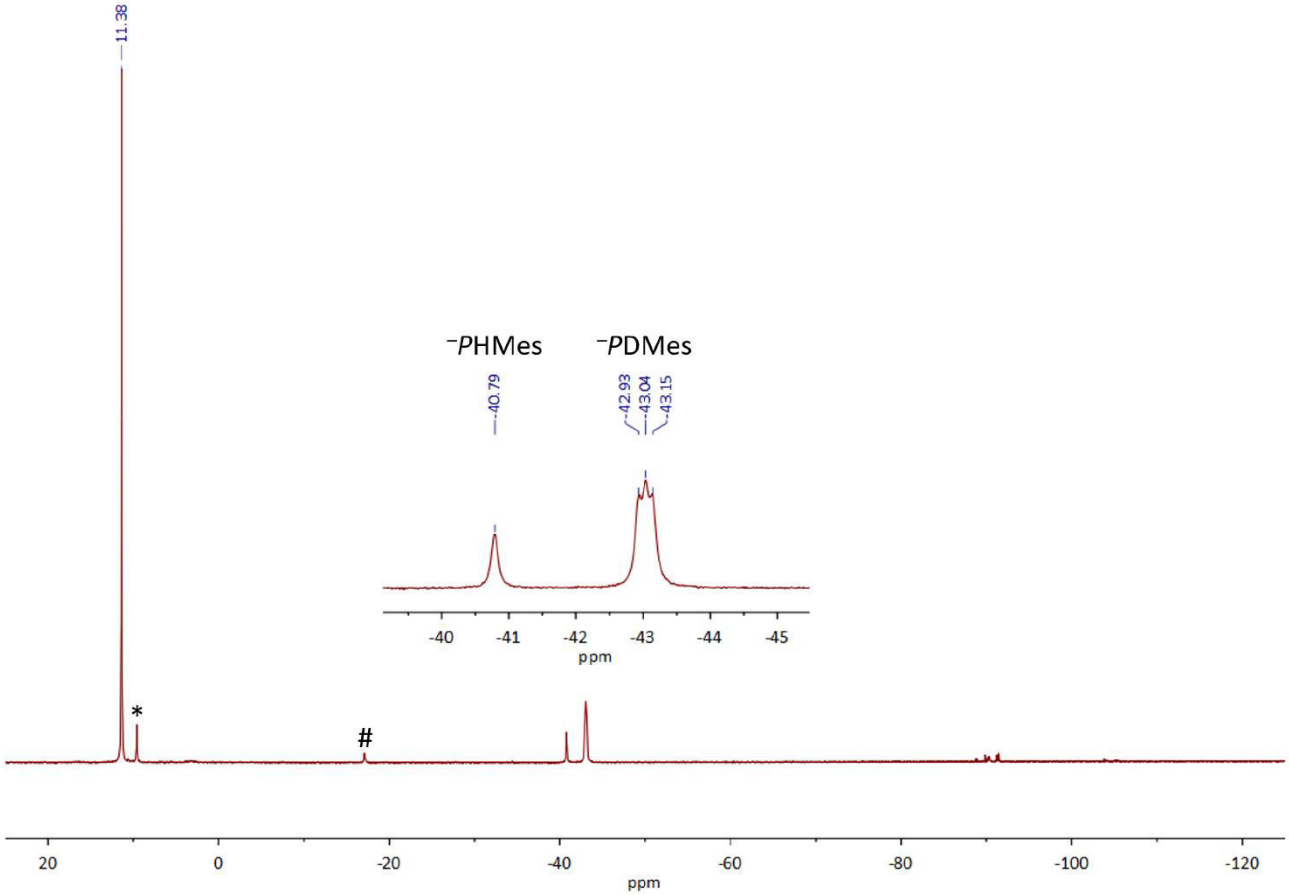

Fig. S60: *Reference for the isotope labelling experiment: $^{31}P\{^{1}H\}$ NMR spectrum of **1-d** (≈86% isotopic purity) in DME with a sealed C_6D_6 capillary (303 K). The enlargement shows the singlet resonance at δ = –40.8 ppm for the ⁻PHMes ligand and the triplet resonance at δ = –43.0 ppm for the ⁻PDMes ligand. Traces of precursor complex $(PN)_2LaCl$ are marked by an asterisk (*). Traces of protonated ligand HPN are denoted as #.*

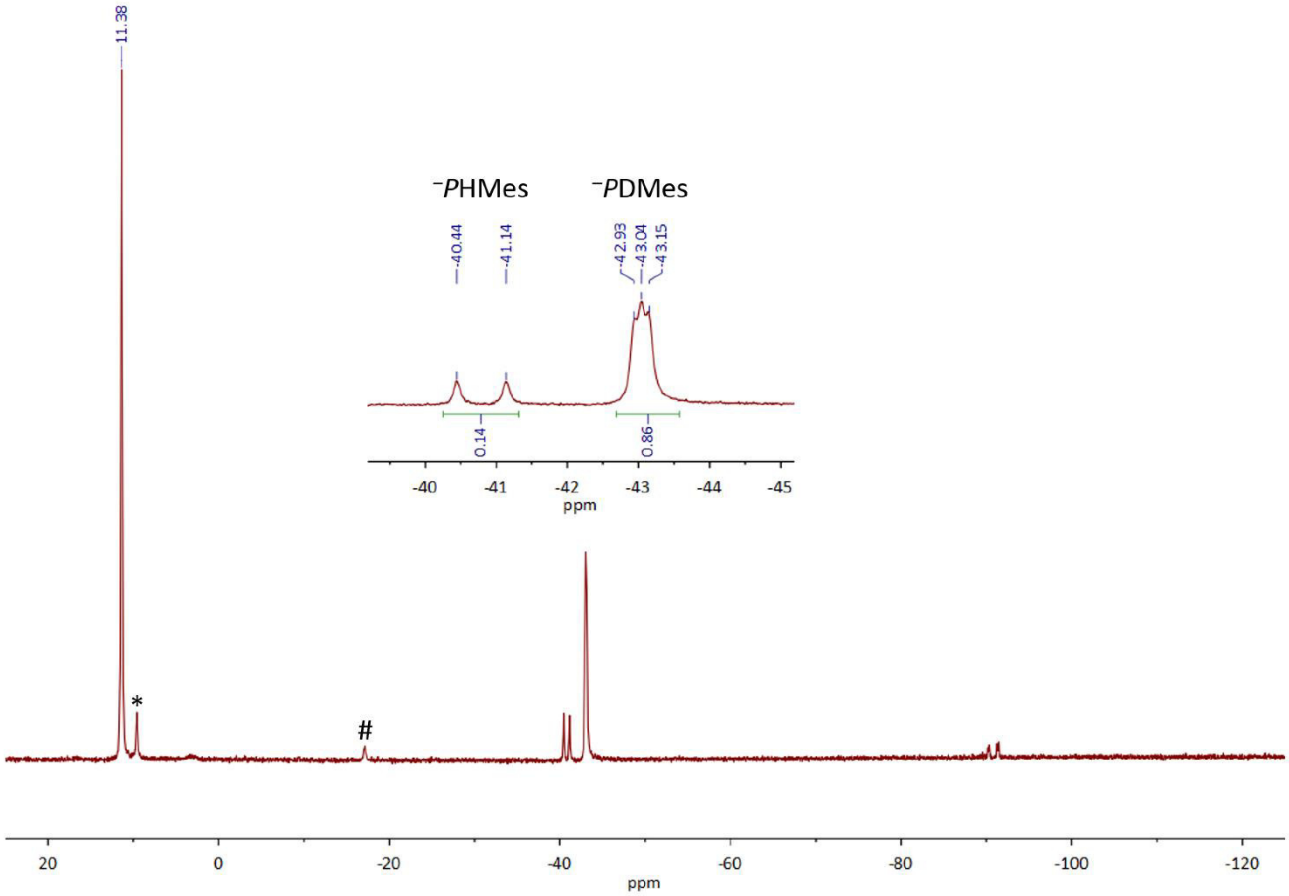

Fig. S61: *Reference for the isotope labelling experiment: ^{31}P NMR spectrum of **1-d** (≈86% isotopic purity) in DME with a sealed C_6D_6 capillary (303 K). The enlargement shows the doublet resonance at δ = –40.8 ppm for the ⁻PHMes ligand and the triplet resonance at δ = –43.0 ppm for the ⁻PDMes ligand. Traces of precursor complex $(PN)_2LaCl$ are marked by an asterisk (*). Traces of protonated ligand HPN are denoted as #.*

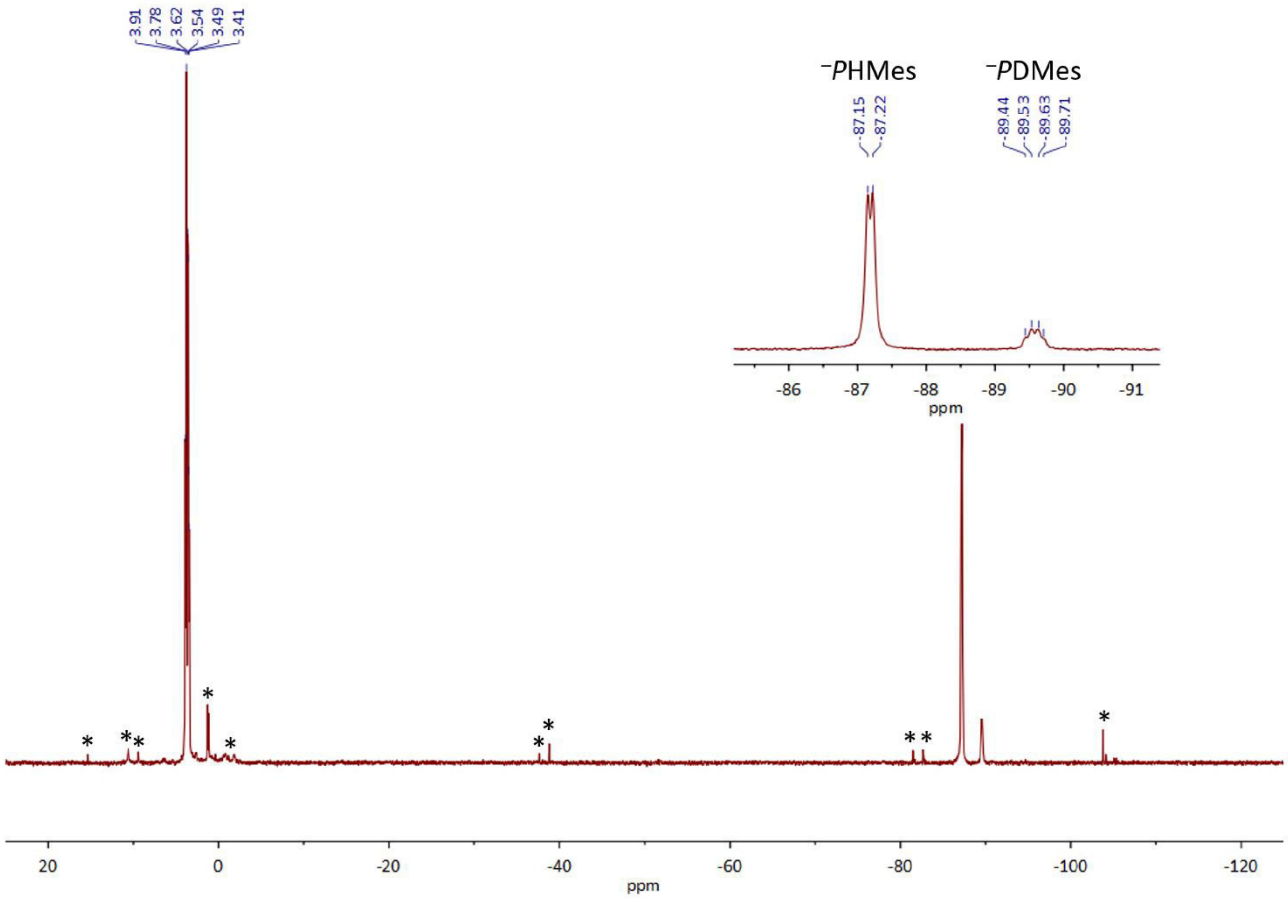

Fig. S62: *Isotope labelling experiment: $^{31}P\{^{1}H\}$ NMR spectrum of the reaction between **1-d** (≈86% isotopic purity) and KHMDS in the presence of 18-crown-6 in DME with a sealed C_6D_6 capillary (303 K). The enlargement shows the doublet resonance at δ = –87.2 ppm ($^{2}J_{PP}$ = 22.6 Hz) for the ⁻PHMes ligand and the multiplet resonance at δ = –89.6 ppm for the ⁻PDMes ligand. Traces of unknown impurities are marked by asterisks (*).*

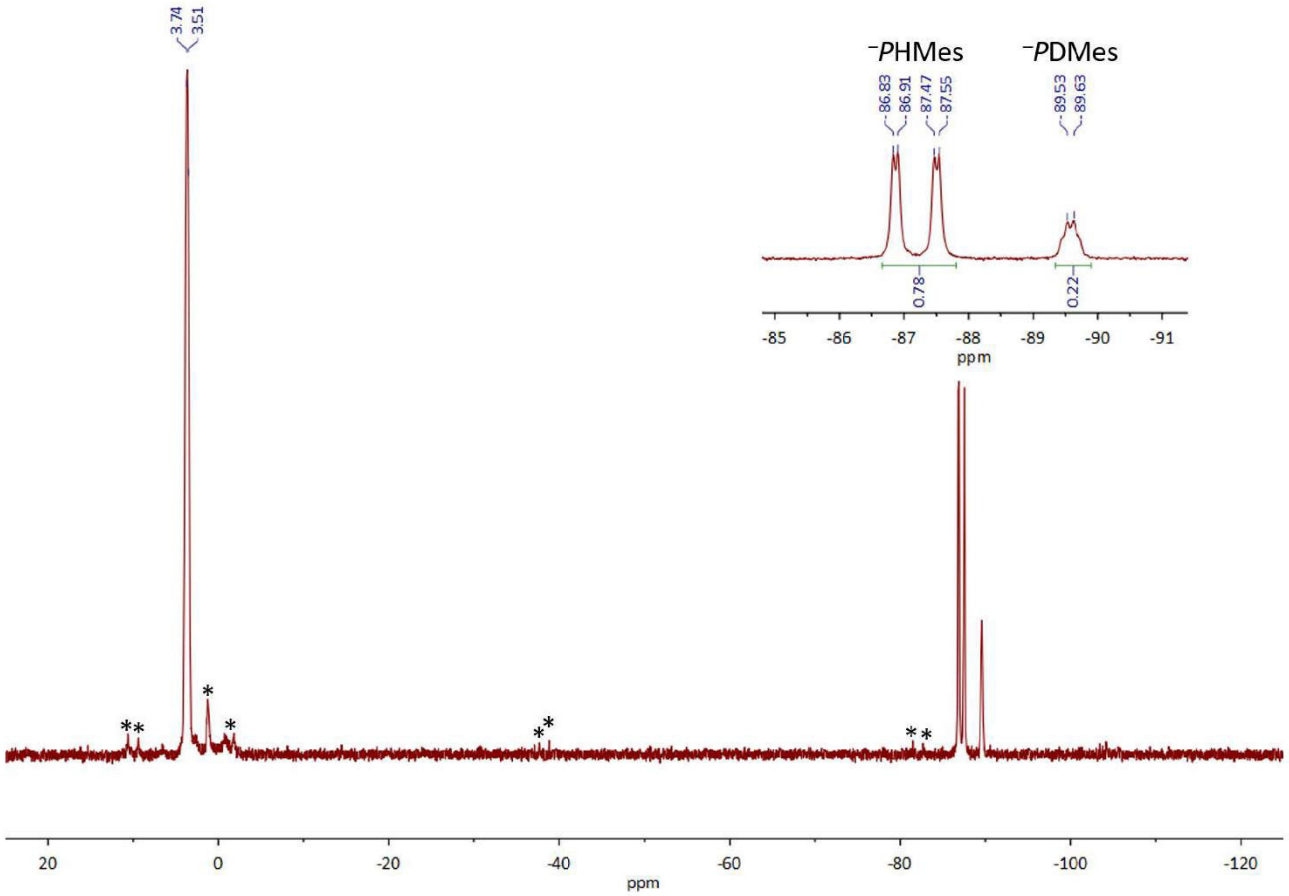

Fig. S63: *Isotope labelling experiment: ^{31}P NMR spectrum of the reaction between **1-d** (≈86% isotopic purity) and KHMDS in the presence of 18-crown-6 in DME with a sealed C_6D_6 capillary (303 K). The enlargement shows the doublet of doublets at δ = –87.2 ppm for the ⁻PHMes ligand and the multiplet resonance at δ = –89.6 ppm for the ⁻PDMes ligand. Note the drastic changes in the integral values for the PH and PD groups compared to the ones found for starting material **1-d** (see reference spectrum in Fig. 61). Traces of unknown impurities are marked by asterisks (*).*

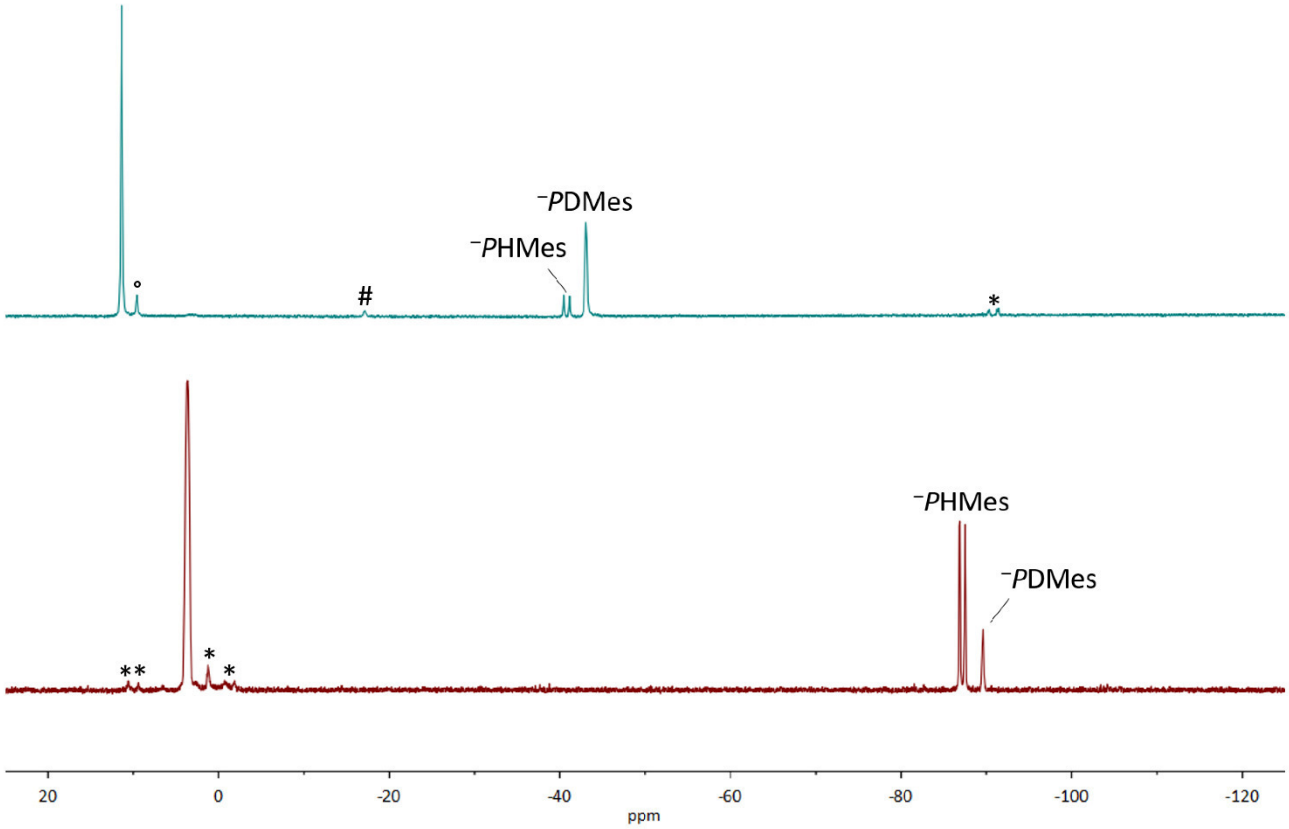

Fig. S64: *Isotope labelling experiment: Stacked ^{31}P NMR spectra of **1-d** (≈86% isotopic purity, top) and the reaction between **1-d** (≈86% isotopic purity) and KHMDS in the presence of 18-crown-6 (bottom) in DME with a sealed C_6D_6 capillary (303 K). The direct comparison clearly shows the inversion of the D/H isotopic ratio at phosphorous (for integral values see Fig. S61 and S63). Traces of precursor complex $(PN)_2LaCl$ are marked by ° and traces of protonated ligand HPN are labelled by # (top). Traces of unknown impurities are marked by asterisks (*).*

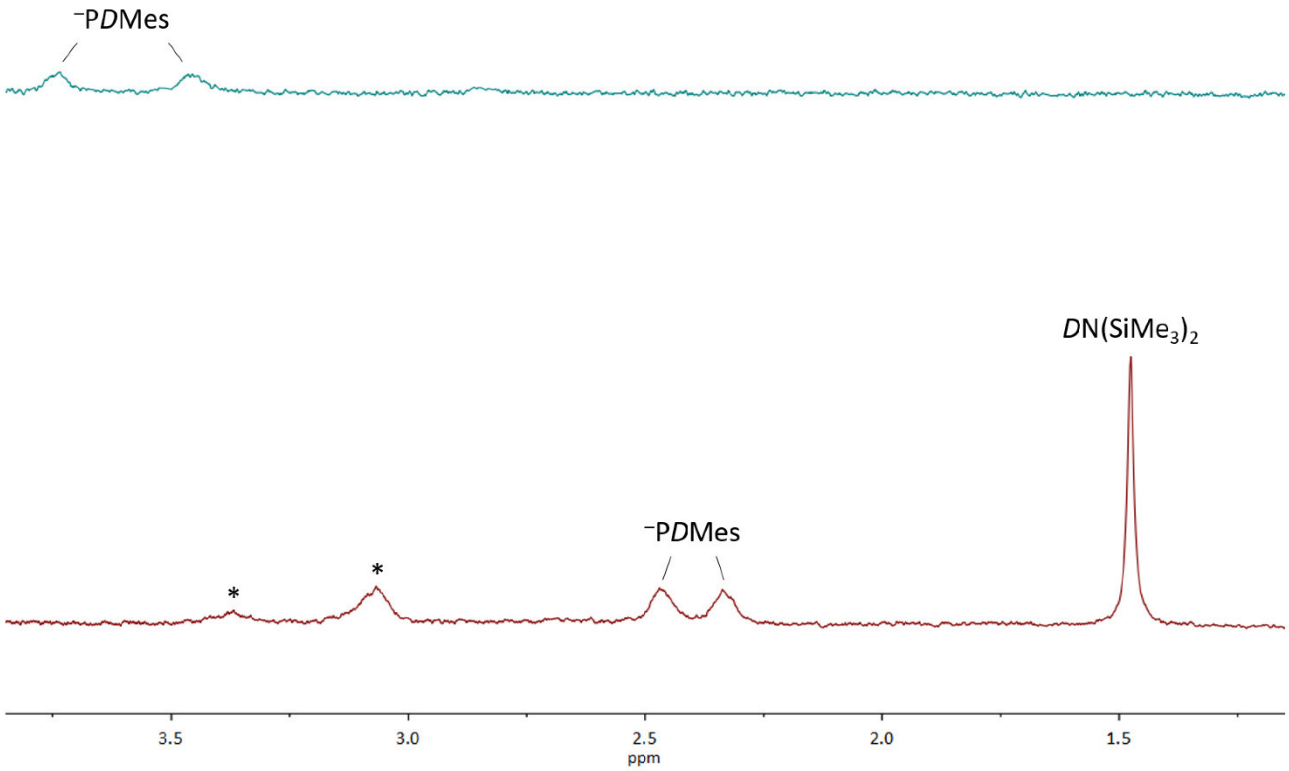

Fig. S65: *Isotope labelling experiment: Stacked details of the ^{2}H NMR spectra of* **1-d** *(≈86% isotopic purity, top) and the reaction between* ***1-d*** *(≈86% isotopic purity) and KHMDS in the presence of 18-crown-6 (bottom) in DME with a sealed C_6D_6 capillary (303 K). The new intense singlet resonance at δ = 1.48 ppm can be assigned to $DN(SiMe_3)_2$. Unknown deuterated compounds are marked by asterisks (*).*

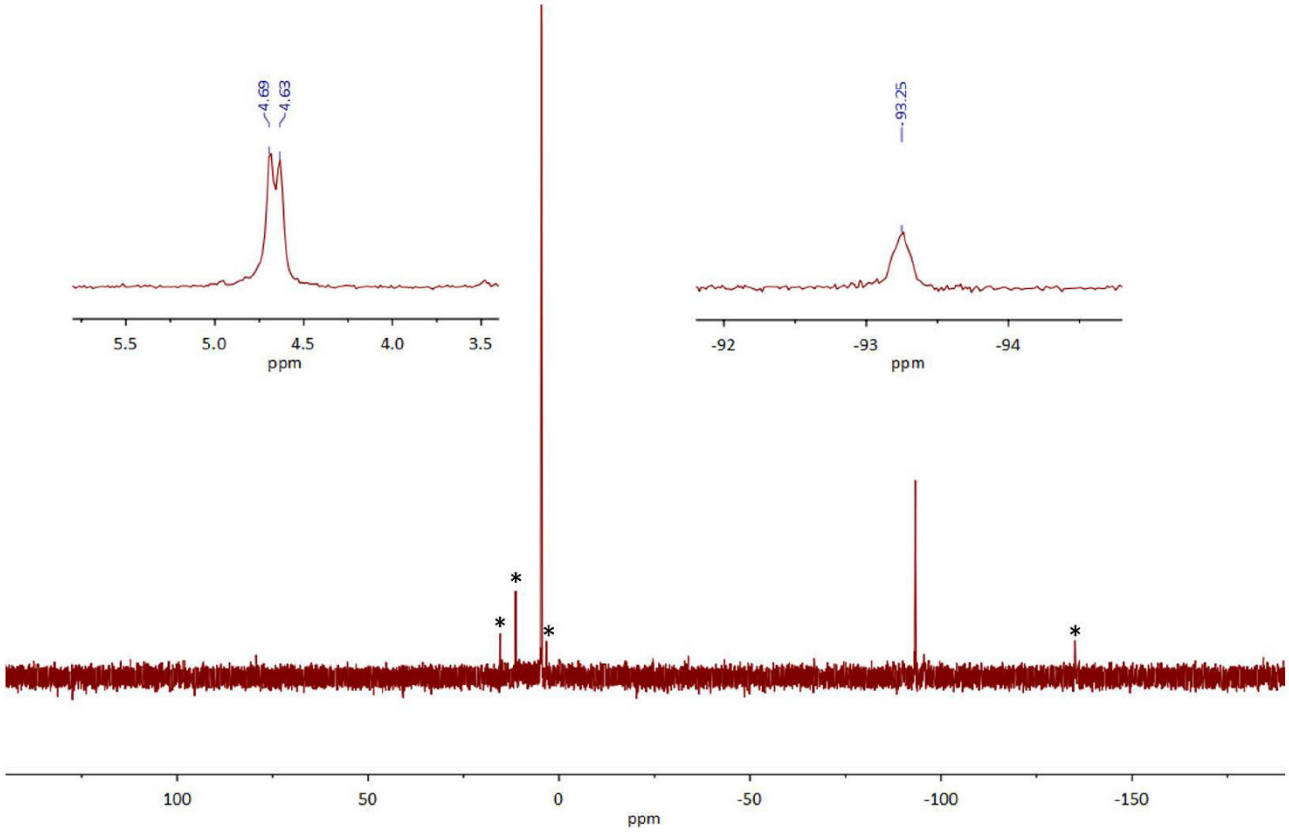

Fig. S66: *Trapping experiment: $^{31}P\{^{1}H\}$ NMR spectrum of the reaction between **1-d** and KHMDS in the presence of 18-crown-6 in cyclohexene with a sealed C_6D_6 capillary (303 K). The enlargements show the resonances of the main product **3a**. Traces of unknown impurities are marked by asterisks (*).*

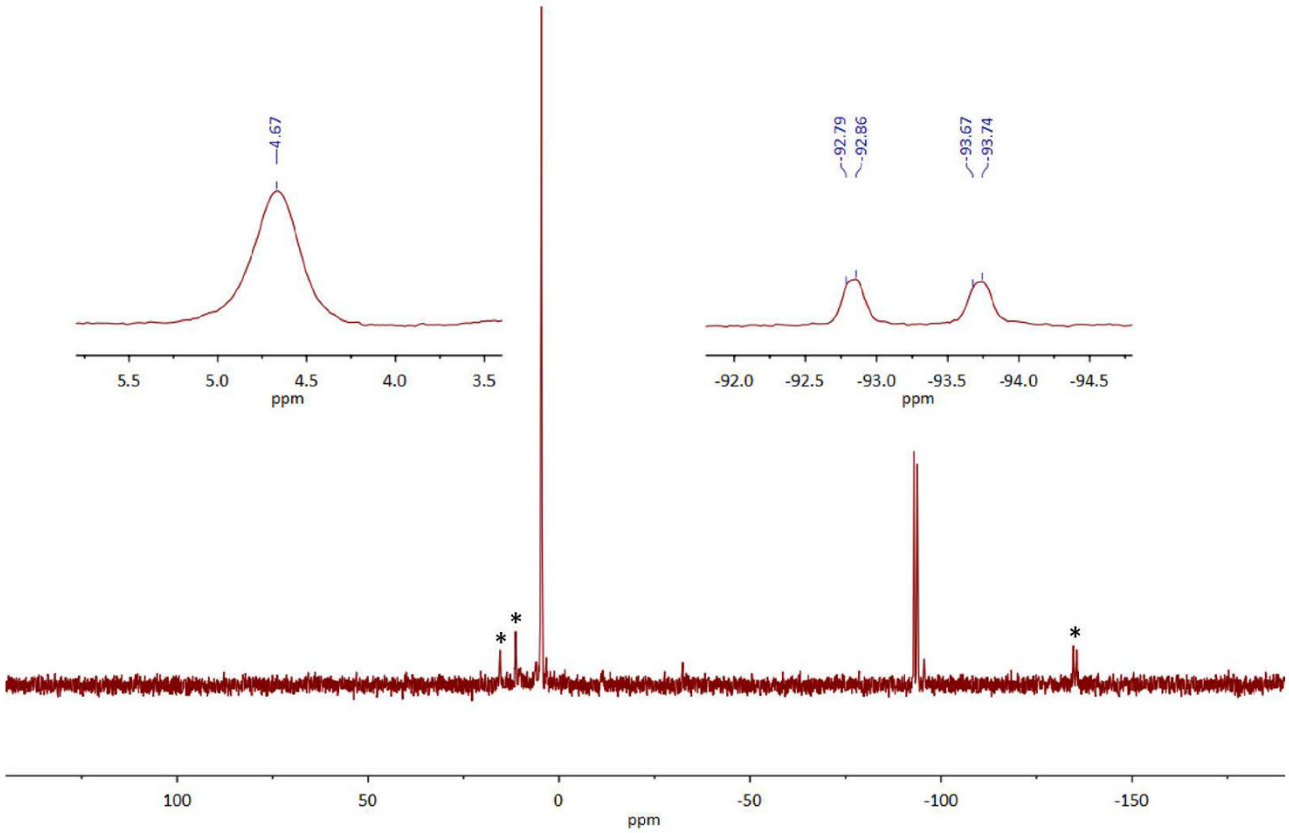

Fig. S67: *Trapping experiment: ^{31}P NMR spectrum of the reaction between **1-d** and KHMDS in the presence of 18-crown-6 in cyclohexene with a sealed C_6D_6 capillary (303 K). The enlargements show the resonances of the main product **3a**. Note also the >99% conversion of the PD groups into PH groups as is obvious by the doublet splitting in the right enlargement. Traces of unknown impurities are marked by asterisks (*).*

*Fig. S68: Stacked reaction control $^{31}P\{^1H\}$ NMR spectra of the conversion of **3b** to **6** (THF-d_8, 303 K). The resonances of freshly prepared starting material **3b** (reference) and main product **6** are labelled in the bottom and top spectrum, respectively. Unknown impurities in the starting material and after full conversion of **3b** are marked with asterisks (*). The temperature and reaction times are specified on the left.*

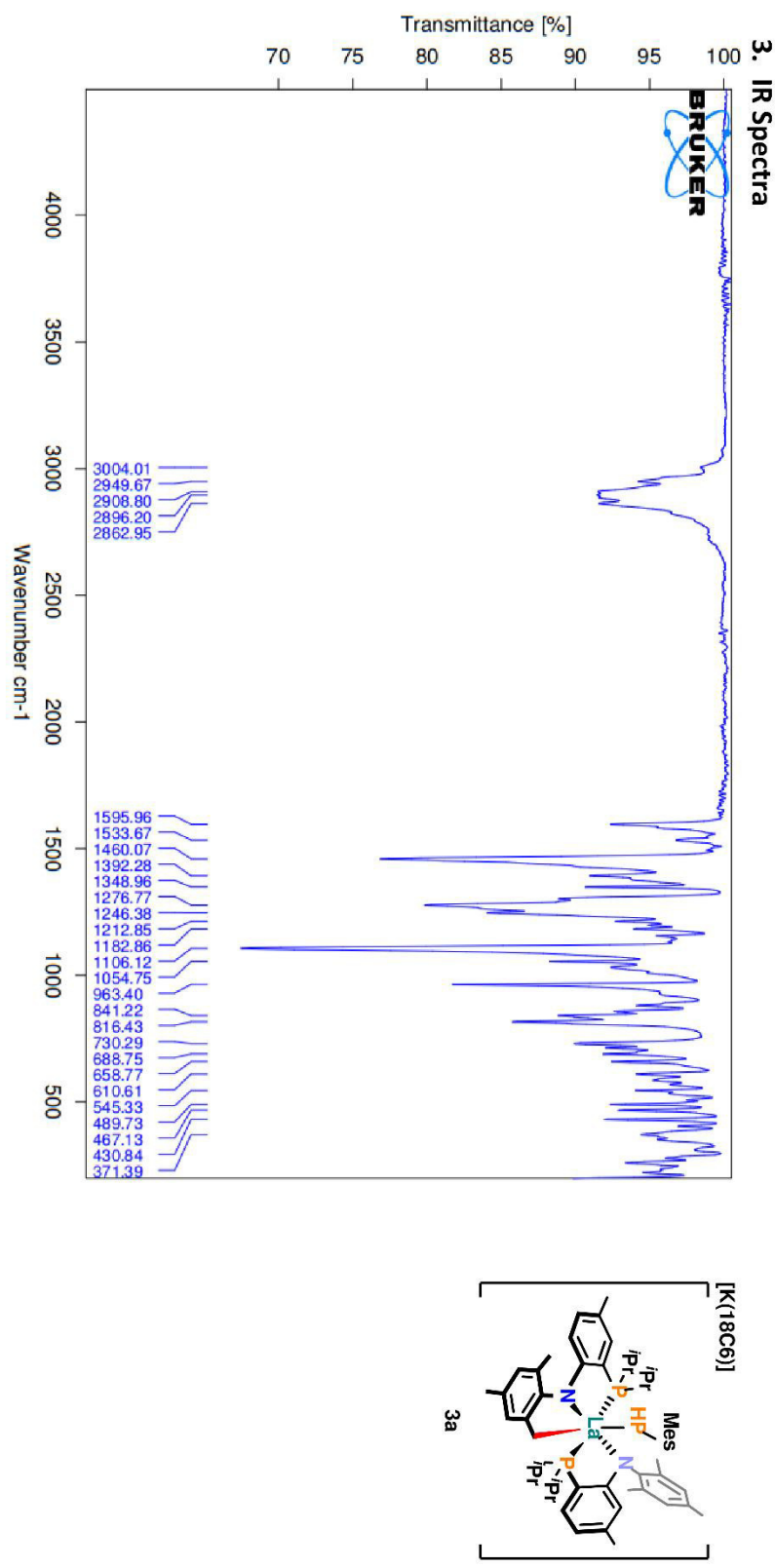

Fig. S69: IR spectrum (ATR) of ***3a****.*

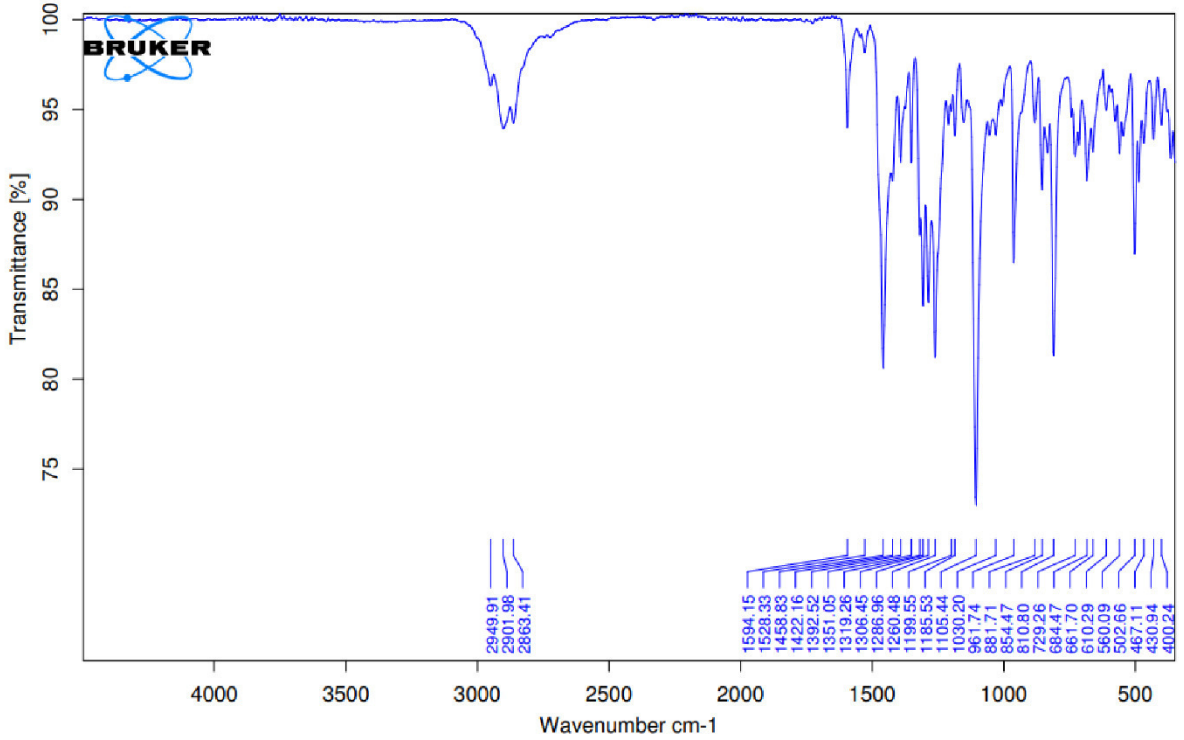

*Fig. S70: IR spectrum (ATR) of **5a**.*

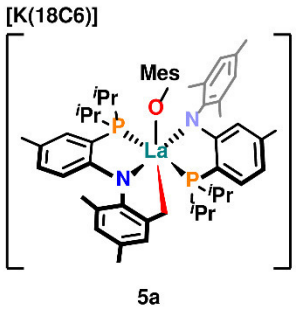

5a

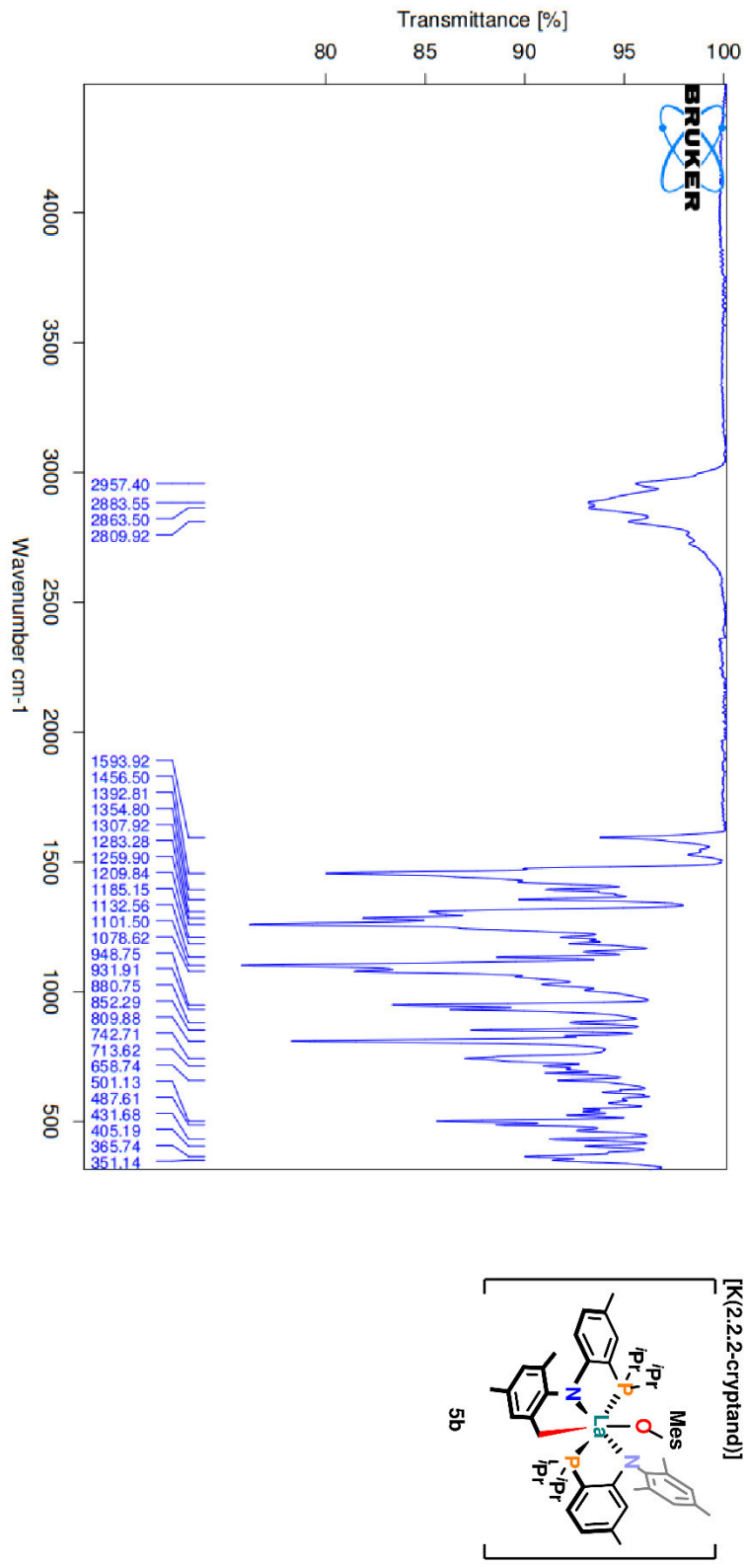

Fig. S71: IR spectrum (ATR) of ***5b****.*

4. Crystallographic Details

*Table S1: Crystallographic details on complexes **3a**, **3b**, **5a** and **6**.*

	3a	**3b**	**5a**	**6***#
Chemical formula	2 ($C_{65}H_{97}N_2O_6P_3KLa$) · ($C_4H_{10}O$)	$C_{71}H_{109}N_4O_6P_3KLa$	2 ($C_{65}H_{96}N_2O_7P_2KLa$)	$C_{80}H_{120}N_4O_6P_4KLa$
M_r	2620.84	1385.54	2514.76	1535.68
Crystal system	Triclinic	Triclinic	Triclinic	Triclinic
Space group	*P*–1	*P*–1	*P*–1	*P*–1
a (Å)	14.0506(8)	12.7500(8)	13.3178(9)	14.168(15)
b (Å)	14.3744(8)	15.9812(8)	25.286(2)	18.79(2)
c (Å)	18.1614(10)	21.2031(14)	25.521(2)	19.86(2)
α (°)	99.417(2)	105.285(2)	116.117(2)	105.16(3)
β (°)	90.617(2)	94.133(3)	98.326(2)	97.23(3)
γ (°)	91.294(2)	109.532(3)	99.911(2)	104.28(3)
V (Å^3)	3617.3(4)	3866.2(4)	7361.7(9)	4841(9)
Z	1	2	2	2
Densitiy (g cm^{-3})	1.203	1.190	1.134	1.053
F(000)	1382	1464	2648	1624
Radiation Type	MoKα	MoKα	MoKα	MoKα
μ (mm^{-1})	0.71073	0.71073	0.71073	0.593
Crystal size	0.22x0.18x0.17	0.35x0.32x0.28	0.26x0.22x0.04	0.02x0.01x0.005
Meas. Refl.	337081	266834	672658	53580
Indep. Refl.	14757	17757	32352	16395
Obsvd. [$I > 2\sigma(I)$]	13249	15847	24047	6842
R_{int}	0.0530	0.0709	0.0938	0.3354
R [$F^2 > 2\sigma(F^2)$]	0.0326	0.0303	0.0518	0.0981
wR(F^2)	0.0979	0.0861	0.1437	0.2883
S	1.124	1.097	1.088	0.959
$\Delta\rho_{max}$	1.842	0.545	4.627	1.839
$\Delta\rho_{min}$	–0.553	–0.704	–1.625	–2.263
CCDC	2020114	2020113	2021044	2020112

#Due to strong disorder of three diethyl ether molecules, the SQUEEZE technique had to be applied for this crystal.

*Despite numerous attempts, only low quality crystals could be obtained, which did not diffract very well. This results in the high R_{int} as well as the moderately good R1 and wR2 values. Nevertheless, the model as such can be considered as reliable in combination with the other analytical data obtained.

*Table S2: Selected bond lengths in Å and angles in ° of complexes **3a**, **3b**, **5a** and **6**.*

	3a	**3b**	**5a**	**6**
La1 – P1	3.285(1)	3.169(1)	3.240(1)	3.237(4)
La1 – P2	3.191(1)	3.175(1)	3.160(1)	3.241(4)
La1 – P70 / O70	3.049(1)	3.025(1)	2.283(3)	2.921(4)
La1 – P80	-	-	-	2.914(4)
La1 – N1	2.395(2)	2.433(2)	2.440(3)	2.454(9)
La1 – N2	2.473(2)	2.514(2)	2.498(3)	2.511(10)
La1 – C25	2.634(3)	2.617(2)	2.653(4)	-
P70 – P80	-	-	-	2.168(5)
N1 – La1 – N2	113.80(7)	122.31(6)	109.9(1)	124.3(3)
P1 – La1 – P2	172.25(2)	172.39(1)	171.46(3)	172.5(1)
N1 – La1 – P1	59.81(5)	61.87(4)	59.29(8)	62.6(2)
C70 – P70 / O70 – La1	129.20(1)	128.10(8)	166.3(3)	126.6(4)
C80 – P80 – La1	-	-	-	128.8(4)

Fig. S72: Molecular view of the polymeric chain structure of complex ***3a****. Hydrogen atoms and solvent molecules have been omitted for clarity. Thermal ellipsoids are shown at a probability level of 50%.*

Fig. S73: Molecular view of the polymeric chain structure of complex ***5a****. Hydrogen atoms have been omitted for clarity. Thermal ellipsoids are shown at a probability level of 50%.*

5. Computational Details

All DFT calculations were performed with Gaussian 09.[6] Geometries were fully optimized in gas phase without symmetry constraints, employing the B3PW91 functional.[7] Si and La atoms were treated with a Stuttgart effective core potential[8] augmented with a polarization function (ζ_d = 0.284 for Si and ζ_f = 1.000 for La).[9] For P, N, C and H atoms, Pople's double-ζ basis set 6-31G(d,p) was used.[10] Calculations of vibrational frequencies were systematically done in order to characterize the nature of stationary points. Analytical frequency calculations at 298.15 K and 1 atm were systematically done in order to characterize the nature of stationary points. IRC calculations were carried out in order to confirm the connectivity between reactant(s), transition state and product(s).

! H abstraction by HMDS on the adjacent methyl group - Adduct !

P	3.796169	-0.854550	-0.338321
La	0.607123	-0.517065	-0.757602
N	1.688266	1.108460	0.588847
C	0.675214	2.086104	0.814228
C	-0.412710	1.820170	1.680357
C	-0.512394	0.535984	2.468355
H	-1.208223	0.684438	3.302971
N	-3.124719	2.175856	4.530615
Si	-4.705274	1.525845	4.466468
C	-4.826495	-0.381864	4.798034
H	-4.192380	-0.938359	4.098919
C	-5.466898	1.758238	2.704360
C	-6.044627	2.274620	5.658009
Si	-2.319859	2.751371	5.929650
C	-2.957581	4.448895	6.622004
N	0.351518	-2.464602	0.552811
C	0.105721	-3.822311	0.643919
C	0.145621	-4.615400	-0.530981
C	-0.092259	-5.986590	-0.463700
C	-0.374688	-6.634229	0.740507
C	-0.401455	-5.847416	1.895601
C	-0.170670	-4.473083	1.878147

C	-1.388649	2.801990	1.905180
C	-1.316625	4.043448	1.272594
C	-0.240167	4.297183	0.413088
C	0.758608	3.352998	0.180181
C	0.479934	-3.951217	-1.830110
C	-0.667267	-8.111304	0.789683
C	-0.218402	-3.680713	3.156260
N	0.060942	-0.072415	-3.145508
C	1.158974	0.446563	-3.886391
C	2.190348	-0.395570	-4.362853
C	3.265424	0.151127	-5.073686
C	3.361152	1.514757	-5.341488
C	2.325680	2.335839	-4.887030
C	1.232204	1.833360	-4.181233
P	-2.484548	-0.458713	-1.405213
C	-3.526416	1.100462	-1.081302
C	-4.966827	1.061242	-1.585045
C	5.064059	-0.135337	-1.569757
C	4.664013	1.298937	-1.911531
C	3.911317	0.259888	1.128899
C	2.816883	1.138712	1.378490
C	2.949897	2.019193	2.483473
C	4.072022	2.006809	3.294381
C	5.140926	1.127131	3.069915
C	5.026495	0.268791	1.977149
C	4.621554	-2.458709	0.234287
C	3.860441	-3.068476	1.411213
C	2.124339	-1.886108	-4.167438
C	4.537382	2.088952	-6.086637
C	0.116752	2.755915	-3.781532
C	-2.369507	5.089389	1.531149

C	1.951406	3.702568	-0.667052
C	6.347476	1.108899	3.971271
C	6.528206	-0.199646	-1.138901
C	-2.331135	1.588556	7.486641
C	-0.446589	3.054872	5.574939
C	-1.091078	-0.330830	-3.872329
C	-1.085628	-0.369879	-5.293255
C	-2.214987	-0.680606	-6.032345
C	-3.438549	-0.978573	-5.420094
C	-3.466001	-0.918490	-4.027170
C	-2.349607	-0.589667	-3.246395
C	-4.657672	-1.345098	-6.224798
C	-3.665950	-1.851903	-0.911666
C	-3.148713	-3.219675	-1.351215
C	-3.902970	-1.810732	0.599470
C	-2.794503	2.326627	-1.618741
C	4.727359	-3.442767	-0.932245
H	0.410377	-2.080450	1.496864
H	-2.158733	2.605409	2.668618
H	-0.156139	-0.159936	-5.813109
H	-4.405332	-1.138314	-3.524794
H	-2.948623	-3.256504	-2.425970
H	-3.896473	-3.988436	-1.121000
H	-2.234991	-3.491622	-0.814963
H	5.635237	-2.203211	0.566674
H	-2.139783	-0.701579	-7.119075
H	-5.004672	0.986515	-2.676868
H	-5.475466	1.989231	-1.297942
H	-5.545598	0.237295	-1.158367
H	-3.532531	1.165588	0.013833
H	-0.050683	-6.566950	-1.385392

H	3.653418	1.354549	-2.324092
H	5.347957	1.712214	-2.662155
H	4.710528	1.937078	-1.023578
H	-0.159312	5.271224	-0.069248
H	4.929009	-0.751597	-2.468934
H	2.361819	3.403676	-5.098345
H	-0.612929	-6.321932	2.853634
H	1.098194	-2.252583	-4.248568
H	2.504337	-2.185612	-3.182838
H	2.739019	-2.402004	-4.911724
H	4.041012	-0.519078	-5.442495
H	-1.798342	2.431718	-1.180858
H	-3.354862	3.234149	-1.367061
H	-2.698690	2.280853	-2.708221
H	3.839701	-2.389505	2.268152
H	4.343327	-4.001176	1.727534
H	2.826950	-3.298671	1.135749
H	-4.616214	-1.657831	-1.424000
H	0.462761	0.224229	2.857078
H	-0.923053	-0.296274	1.875904
H	-0.277997	-3.212156	-2.129503
H	0.564456	-4.670139	-2.650502
H	1.439782	-3.422119	-1.752884
H	5.839694	-0.428109	1.785115
H	2.866553	3.722396	-0.063607
H	1.827355	4.687854	-1.126257
H	2.119891	2.971671	-1.463152
H	-2.963381	-1.956865	1.142190
H	-4.582752	-2.618384	0.895108
H	-4.346084	-0.870505	0.938647
H	-4.888561	-0.586063	-6.982349

H	-5.539064	-1.448854	-5.584329
H	-4.526122	-2.296584	-6.756246
H	4.111731	2.693478	4.138605
H	-0.816181	2.477177	-4.283515
H	0.351194	3.790972	-4.045735
H	-0.081251	2.713448	-2.707522
H	0.739204	-3.188566	3.376133
H	-0.453473	-4.324593	4.008042
H	-0.980306	-2.891250	3.123229
H	-0.333467	-8.556020	1.733602
H	-0.167022	-8.646200	-0.025018
H	-1.742076	-8.320258	0.699258
H	2.133753	2.698635	2.709194
H	4.221334	2.840027	-6.818790
H	5.091238	1.310603	-6.620491
H	5.241081	2.582743	-5.404496
H	6.700020	0.398753	-0.238720
H	7.164967	0.212958	-1.932124
H	6.872389	-1.220073	-0.944531
H	3.734699	-3.725695	-1.298172
H	5.227183	-4.363150	-0.606615
H	5.297125	-3.038111	-1.775274
H	-1.927177	6.085308	1.648164
H	-2.934539	4.847564	2.434975
H	-3.082595	5.149892	0.698538
H	7.076035	0.359882	3.644506
H	6.076928	0.873509	5.008162
H	6.859122	2.079550	3.988652
H	-2.376498	4.772439	7.495015
H	-2.882043	5.226299	5.853538
H	-4.009537	4.377356	6.918817

H	-1.765320	2.028032	8.317859
H	-3.354436	1.404817	7.833568
H	-1.884455	0.617830	7.244410
H	0.051763	3.495388	6.447029
H	0.062553	2.116163	5.331290
H	-0.317865	3.733863	4.725626
H	-5.855524	-0.749185	4.694796
H	-4.481300	-0.615016	5.811408
H	-6.436621	1.254727	2.610882
H	-5.607748	2.821389	2.481368
H	-4.792451	1.348641	1.944597
H	-7.021931	1.802017	5.498002
H	-5.766425	2.127666	6.707744
H	-6.153491	3.351775	5.490867

! H abstraction by HMDS on the adjacent methyl group - Transition State !

P	14.680505	5.437210	18.843804
La	11.461936	5.915087	18.250703
N	12.709899	7.615249	19.407263
C	11.708365	8.612813	19.430243
C	10.414176	8.275123	19.926732
C	10.126912	7.010570	20.644661
H	9.592755	7.266993	21.887698
N	9.071860	7.470363	23.117480
Si	7.356957	7.505122	23.360351
C	6.648260	6.066309	24.439259
H	6.919753	5.097062	24.007801
C	6.420678	7.342017	21.685315
C	6.667940	9.122577	24.165945
Si	10.244881	7.779746	24.364620

C	10.753735	9.635795	24.506034
N	11.098811	3.911137	19.509620
C	11.067202	2.535733	19.528749
C	11.401379	1.817247	18.351149
C	11.385369	0.424279	18.341913
C	11.042062	-0.322528	19.470985
C	10.717596	0.390617	20.629731
C	10.722027	1.782514	20.687954
C	9.391707	9.243648	19.813568
C	9.608161	10.506313	19.281700
C	10.895586	10.821755	18.819747
C	11.936607	9.900421	18.870412
C	11.775875	2.602421	17.134414
C	10.991942	-1.827922	19.435500
C	10.370275	2.491703	21.967071
N	11.129985	6.237667	15.748043
C	12.264724	6.814118	15.107090
C	13.323360	6.019672	14.605367
C	14.405285	6.628120	13.959951
C	14.490942	8.009156	13.793116
C	13.435927	8.783239	14.279390
C	12.328336	8.217031	14.914263
P	8.459384	5.602120	17.179022
C	7.210730	7.044081	17.298976
C	5.813808	6.783403	16.738432
C	16.045614	5.905308	17.593511
C	15.809773	7.344182	17.134408
C	14.842486	6.731761	20.151140
C	13.795466	7.694131	20.240404
C	13.936932	8.695185	21.237146
C	15.034861	8.734229	22.080502

C	16.063253	7.784540	22.003341
C	15.931425	6.795340	21.028207
C	15.372842	3.887349	19.683262
C	14.532047	3.526862	20.908475
C	13.288024	4.518954	14.707159
C	15.681044	8.645828	13.124550
C	11.182613	9.094842	15.330998
C	8.500011	11.524627	19.206240
C	13.288028	10.259979	18.317770
C	17.238870	7.819460	22.944230
C	17.486682	5.718347	18.064842
C	9.700917	7.274092	26.149398
C	11.856622	6.789926	24.037597
C	10.104719	5.867964	14.896538
C	10.255083	5.869169	13.479597
C	9.256627	5.438841	12.622183
C	8.022339	4.975806	13.094653
C	7.840132	5.011734	14.476421
C	8.818925	5.458339	15.374165
C	6.955544	4.465719	12.162199
C	7.369150	4.101266	17.563996
C	8.068981	2.784725	17.235603
C	6.938588	4.146411	19.031028
C	7.820818	8.290342	16.661639
C	15.441970	2.721995	18.693908
H	10.848504	4.261644	20.432943
H	8.416224	8.996827	20.223471
H	11.194106	6.210584	13.056899
H	6.885969	4.671581	14.873820
H	8.403681	2.749993	16.194849
H	7.377436	1.947884	17.394896

H	8.931882	2.617892	17.885913
H	16.391705	4.126940	20.012547
H	9.447548	5.456791	11.549399
H	5.849664	6.579704	15.663258
H	5.190840	7.675554	16.881242
H	5.302819	5.951790	17.232084
H	7.132941	7.212606	18.381010
H	11.648689	-0.092361	17.418698
H	14.804891	7.483436	16.728022
H	16.524806	7.612233	16.347595
H	15.942351	8.041584	17.967643
H	11.086587	11.808032	18.398257
H	15.861890	5.237467	16.741036
H	13.461232	9.863484	14.142396
H	10.450813	-0.160847	21.531666
H	12.273076	4.132676	14.590956
H	13.660280	4.173213	15.678189
H	13.923245	4.065114	13.939777
H	15.199997	5.994887	13.566756
H	8.789503	8.538295	17.100956
H	7.160239	9.152689	16.812167
H	7.952952	8.149038	15.583939
H	14.558686	4.319950	21.660419
H	14.911984	2.606120	21.368176
H	13.487789	3.358351	20.627881
H	6.477603	4.188071	16.931040
H	11.016300	6.413810	20.872603
H	9.311547	6.409634	20.220456
H	10.944337	3.224377	16.770668
H	12.084999	1.960849	16.304018
H	12.615504	3.277335	17.356442

H	16.706542	6.034209	20.964501
H	14.055718	10.274108	19.099955
H	13.264015	11.246222	17.844256
H	13.614687	9.526974	17.572968
H	7.811156	4.098164	19.690882
H	6.298343	3.287118	19.264930
H	6.377830	5.052673	19.278846
H	6.756262	5.171505	11.346355
H	6.011769	4.300473	12.691922
H	7.237797	3.512142	11.696212
H	15.085664	9.517162	22.835895
H	10.249417	8.761519	14.867129
H	11.362348	10.133001	15.036396
H	11.024907	9.081958	16.413682
H	11.196650	3.114668	22.335300
H	10.122786	1.777116	22.757202
H	9.507259	3.160159	21.847588
H	11.309768	-2.265041	20.389043
H	11.644275	-2.231134	18.653153
H	9.978894	-2.203781	19.234103
H	13.143975	9.428784	21.347992
H	15.390085	9.523614	12.537813
H	16.186395	7.943837	12.453501
H	16.421351	8.982240	13.861728
H	17.705341	6.361845	18.922828
H	18.178946	6.000149	17.260647
H	17.714703	4.684839	18.343521
H	14.439278	2.396367	18.400469
H	15.935828	1.860933	19.160967
H	16.001922	2.969924	17.785527
H	8.799689	12.475344	19.662674

H	7.602891	11.174616	19.724620
H	8.222423	11.741243	18.166778
H	17.963679	7.035581	22.701531
H	16.931553	7.669461	23.987172
H	17.767763	8.780179	22.903015
H	11.549293	9.778769	25.247148
H	11.110526	10.006770	23.539925
H	9.895305	10.249202	24.800302
H	10.504101	7.499366	26.861240
H	8.803581	7.809620	26.476422
H	9.491349	6.200798	26.201208
H	12.588365	6.968431	24.833701
H	11.639871	5.716858	24.006776
H	12.321017	7.072197	23.088759
H	5.554035	6.124277	24.492521
H	7.039983	6.097563	25.460629
H	5.352026	7.182177	21.866446
H	6.524693	8.241657	21.070292
H	6.799277	6.489780	21.113174
H	5.574576	9.089143	24.240120
H	7.069118	9.271092	25.174501
H	6.947118	9.994866	23.565838

! H abstraction by HMDS on the adjacent methyl group - Product !

P	3.483382	-0.856315	0.002756
La	0.252794	-0.340448	-0.649901
N	1.570457	1.389089	0.528621
C	0.583291	2.402950	0.587765
C	-0.724954	2.019862	1.026990
C	-0.967022	0.638415	1.435953

H	-2.156951	1.148348	4.048702
N	-2.474184	1.401245	4.982074
Si	-4.231250	1.368317	5.192167
C	-4.752860	0.153600	6.576320
H	-4.389639	-0.853523	6.350132
C	-5.003646	0.782945	3.547882
C	-4.934875	3.096999	5.628344
Si	-1.208660	2.143056	5.984679
C	-0.915434	3.979414	5.535175
N	-0.103356	-2.478176	0.424163
C	-0.085967	-3.846819	0.505893
C	0.295049	-4.613769	-0.631712
C	0.327051	-6.003885	-0.567936
C	-0.009563	-6.710018	0.591007
C	-0.380249	-5.953863	1.706165
C	-0.426488	-4.561123	1.692885
C	-1.743044	2.998279	0.965992
C	-1.509029	4.302460	0.537759
C	-0.214153	4.654050	0.139053
C	0.828008	3.722463	0.145875
C	0.669446	-3.885665	-1.885106
C	-0.002986	-8.216317	0.625724
C	-0.825491	-3.804838	2.930391
N	-0.153678	0.104759	-3.172903
C	0.986419	0.680549	-3.795828
C	2.025191	-0.116431	-4.333674
C	3.125987	0.493075	-4.945068
C	3.248872	1.878108	-5.043360
C	2.214876	2.655923	-4.518869
C	1.091517	2.089463	-3.912964
P	-2.746958	-0.581624	-1.711014

C	-3.994698	0.851608	-1.497206
C	-5.411648	0.604511	-2.012974
C	4.846530	-0.340936	-1.230774
C	4.565393	1.088788	-1.693839
C	3.634599	0.405343	1.345050
C	2.606480	1.396391	1.417531
C	2.729466	2.348549	2.469492
C	3.787032	2.323934	3.363225
C	4.798054	1.355078	3.291251
C	4.683923	0.409945	2.269834
C	4.197480	-2.419599	0.801656
C	3.337508	-2.842355	1.993540
C	1.947392	-1.618276	-4.292917
C	4.458090	2.515064	-5.677126
C	-0.023820	2.975507	-3.434215
C	-2.628180	5.311479	0.483034
C	2.195362	4.117261	-0.340234
C	5.939855	1.328877	4.273291
C	6.285203	-0.474415	-0.735797
C	-1.738727	2.044541	7.822125
C	0.410767	1.169410	5.746637
C	-1.189431	-0.219921	-4.019258
C	-1.075657	-0.146488	-5.439450
C	-2.095348	-0.539769	-6.289668
C	-3.316947	-1.029899	-5.809788
C	-3.465797	-1.058933	-4.422849
C	-2.464757	-0.655488	-3.531325
C	-4.402900	-1.505070	-6.738665
C	-3.820628	-2.094903	-1.332847
C	-3.104627	-3.389678	-1.710854
C	-4.196320	-2.085717	0.150793

C	-3.414751	2.121665	-2.116107
C	4.307474	-3.548184	-0.225839
H	-0.429661	-2.094300	1.311864
H	-2.740666	2.723998	1.307039
H	-0.149042	0.222447	-5.867221
H	-4.410725	-1.417212	-4.017605
H	-2.826369	-3.401868	-2.768697
H	-3.759382	-4.250190	-1.523272
H	-2.201009	-3.527712	-1.110835
H	5.205511	-2.177607	1.161459
H	-1.933117	-0.468813	-7.365325
H	-5.413397	0.437277	-3.094994
H	-6.034522	1.487684	-1.818804
H	-5.900303	-0.248362	-1.532561
H	-4.029161	0.985925	-0.407972
H	0.625867	-6.555711	-1.459938
H	3.559333	1.196421	-2.107102
H	5.278106	1.381223	-2.474419
H	4.667613	1.790133	-0.859469
H	-0.013188	5.668431	-0.203241
H	4.698143	-1.014816	-2.085560
H	2.272025	3.740924	-4.598068
H	-0.642578	-6.469748	2.630695
H	0.928273	-1.972729	-4.464068
H	2.268694	-2.009958	-3.321269
H	2.602414	-2.060952	-5.050249
H	3.906565	-0.140950	-5.364854
H	-2.437957	2.367673	-1.694489
H	-4.080891	2.972865	-1.927085
H	-3.308940	2.009507	-3.200230
H	3.321769	-2.071637	2.769050

H	3.732481	-3.765221	2.436833
H	2.306731	-3.034719	1.680046
H	-4.735231	-2.011824	-1.933249
H	-0.238585	0.262846	2.165879
H	-1.994543	0.432469	1.746590
H	-0.159876	-3.275471	-2.267873
H	0.974600	-4.570938	-2.682148
H	1.504299	-3.197034	-1.697466
H	5.445180	-0.365498	2.207039
H	2.928359	4.133508	0.475632
H	2.175504	5.110299	-0.800298
H	2.566666	3.397766	-1.077121
H	-3.294344	-2.121264	0.770575
H	-4.808057	-2.963054	0.395545
H	-4.765003	-1.194081	0.434618
H	-4.587441	-0.789873	-7.549957
H	-5.348213	-1.646253	-6.203976
H	-4.153125	-2.464679	-7.212102
H	3.823848	3.076611	4.150711
H	-0.975860	2.682753	-3.886889
H	0.174035	4.020877	-3.689844
H	-0.153937	2.920853	-2.348661
H	-0.035338	-3.119723	3.267666
H	-1.043033	-4.488805	3.756315
H	-1.722132	-3.190201	2.768218
H	0.135721	-8.592196	1.645679
H	0.803288	-8.630902	0.009281
H	-0.943020	-8.646448	0.251036
H	1.954748	3.103393	2.570591
H	4.188951	3.413382	-6.243418
H	4.962028	1.824340	-6.360997

H	5.193544	2.820046	-4.921381
H	6.458956	0.166658	0.134552
H	6.982011	-0.155330	-1.522296
H	6.549202	-1.501245	-0.463703
H	3.317297	-3.872851	-0.559687
H	4.798521	-4.420549	0.223343
H	4.889161	-3.260564	-1.108264
H	-2.278621	6.314347	0.752942
H	-3.441170	5.044121	1.165993
H	-3.058789	5.380780	-0.524700
H	6.618086	0.494291	4.066956
H	5.590615	1.216833	5.308238
H	6.536433	2.250281	4.238177
H	-0.085707	4.398901	6.115001
H	-0.674502	4.074365	4.472050
H	-1.809918	4.578782	5.732287
H	-0.975706	2.513761	8.452479
H	-2.685641	2.560733	8.008306
H	-1.846817	1.002484	8.137149
H	1.206939	1.579382	6.377238
H	0.267510	0.117647	6.012381
H	0.753353	1.216633	4.708614
H	-5.844377	0.115140	6.664708
H	-4.343507	0.449878	7.546534
H	-6.092562	0.709028	3.637601
H	-4.774467	1.481208	2.737464
H	-4.618652	-0.201603	3.265581
H	-6.022861	3.052087	5.749854
H	-4.509210	3.482498	6.560195
H	-4.705567	3.812443	4.832782

! Direct N - H abstraction by the HMDS anion - Adduct !

C	-1.259297	3.107817	1.564421
C	-0.052381	3.039862	0.827914
C	0.174243	4.001688	-0.189780
C	-0.789116	4.977983	-0.448434
C	-1.988657	5.046491	0.265382
C	-2.199522	4.100196	1.268306
N	0.884297	2.015938	1.077445
C	1.944255	2.310754	1.888763
C	3.020744	1.385871	2.086390
C	4.049359	1.685284	2.987499
C	4.122153	2.881487	3.702413
C	3.094764	3.807165	3.471645
C	2.049893	3.540720	2.604142
P	3.014242	-0.183737	1.109760
C	4.466066	0.022217	-0.108922
C	5.861072	0.153974	0.497586
C	5.235973	3.159399	4.677490
C	1.463490	3.986280	-0.962717
C	-3.022290	6.096608	-0.049635
C	-1.496530	2.159344	2.708587
La	-0.049926	-0.226830	0.151494
N	-0.512897	-1.769754	1.490548
C	-0.782035	-2.801234	2.334145
C	-0.695365	-4.170642	1.910648
C	-0.973201	-5.212547	2.792291
C	-1.343734	-4.997151	4.123021
C	-1.423474	-3.667206	4.546892
C	-1.160785	-2.590689	3.702717
C	-0.283476	-4.473435	0.500804

C	-1.673770	-6.141100	5.046166
C	-1.271547	-1.188298	4.222574
N	-0.435529	-0.555055	-2.405192
C	-1.529730	-0.968579	-3.116448
C	-1.432643	-1.496397	-4.437990
C	-2.530890	-1.980357	-5.126981
C	-3.815930	-1.982763	-4.566480
C	-3.932887	-1.444355	-3.284536
C	-2.850519	-0.926013	-2.562841
C	-5.001337	-2.549230	-5.302951
P	-3.075451	-0.169445	-0.891558
C	-4.362481	-1.272470	-0.051556
C	-4.712094	-0.689876	1.319433
C	0.787505	-0.442282	-3.095768
C	1.055974	0.663889	-3.945204
C	2.295176	0.768860	-4.577945
C	3.301568	-0.186626	-4.411880
C	3.027199	-1.272989	-3.582014
C	1.799888	-1.418021	-2.926785
C	-0.000019	1.706244	-4.181487
C	1.534898	-2.642754	-2.093130
C	4.638570	-0.035201	-5.089830
C	-4.044646	1.439325	-1.229685
C	-3.176020	2.364453	-2.080259
C	-5.436369	1.287225	-1.838602
C	3.643980	-1.487813	2.327751
C	3.788046	-2.832315	1.612125
C	2.687320	-1.598552	3.515138
C	4.156752	1.199824	-1.032508
C	-3.828924	-2.698572	0.078900
H	-3.115216	4.144912	1.857275

H	-0.451967	-1.539573	-4.903340
H	-4.918553	-1.434455	-2.823017
H	-3.617660	-3.137776	-0.900242
H	-4.569157	-3.332041	0.583738
H	-2.908131	-2.716825	0.670824
H	4.630651	-1.170327	2.689822
H	-2.383733	-2.383377	-6.129207
H	-5.381821	0.844569	-2.838435
H	-5.909549	2.273020	-1.941041
H	-6.101364	0.669649	-1.226723
H	-4.138238	1.885684	-0.230632
H	-0.895556	-6.237647	2.424804
H	3.205301	1.064384	-1.554553
H	4.938662	1.305767	-1.794588
H	4.108534	2.135062	-0.465161
H	-0.593414	5.710206	-1.231479
H	4.423689	-0.897841	-0.707335
H	2.477888	1.626483	-5.225190
H	-1.700874	-3.458654	5.582092
H	1.574458	-2.442905	-1.013086
H	2.284371	-3.416642	-2.287099
H	0.543572	-3.055156	-2.297766
H	3.782986	-2.047089	-3.451572
H	-2.213749	2.569700	-1.602638
H	-3.678947	3.327005	-2.235866
H	-2.987015	1.920939	-3.063316
H	2.619875	-0.654991	4.064040
H	3.037828	-2.372738	4.209283
H	1.681440	-1.874657	3.182017
H	-5.265543	-1.282695	-0.675987
H	-2.392369	2.442050	3.270264

H	-0.643986	2.151753	3.394608
H	-1.636808	1.119971	2.386744
H	-0.873722	-3.894264	-0.219004
H	-0.392875	-5.539718	0.272331
H	0.763642	-4.196443	0.320495
H	4.832817	0.946931	3.148015
H	2.319913	4.157155	-0.300587
H	1.467145	4.760523	-1.736099
H	1.631475	3.016755	-1.441638
H	-3.818797	-0.643650	1.951740
H	-5.443682	-1.329414	1.828516
H	-5.140107	0.316469	1.254210
H	-5.933242	-2.352479	-4.762519
H	-4.926095	-3.637465	-5.433045
H	-5.106698	-2.116748	-6.306319
H	3.107696	4.762407	3.996907
H	-0.852221	1.287457	-4.729838
H	0.398370	2.547074	-4.757582
H	-0.397625	2.086286	-3.236315
H	-0.384147	-0.598979	3.964729
H	-1.403879	-1.174616	5.310441
H	-2.124029	-0.659578	3.775284
H	-1.097531	-7.040087	4.796332
H	-2.736427	-6.423845	5.003253
H	-1.455413	-5.890066	6.091055
H	1.266355	4.281562	2.472381
H	5.152139	-0.997951	-5.179478
H	5.302246	0.636042	-4.529130
H	4.534211	0.384432	-6.096530
H	5.941742	1.061842	1.103510
H	6.611215	0.223806	-0.301488

H	6.132653	-0.701257	1.124587
H	2.816967	-3.169531	1.234217
H	4.151732	-3.596529	2.310116
H	4.489021	-2.790262	0.771385
H	-2.556759	7.054109	-0.308134
H	-3.690093	6.267129	0.800993
H	-3.649687	5.804039	-0.901686
H	4.876997	3.204397	5.714792
H	5.732377	4.116795	4.472449
H	6.002338	2.378299	4.634680

! Direct N - H abstraction by the HMDS anion - Transition State !

C	10.281666	8.719068	19.234771
C	11.478254	9.155243	18.593272
C	11.476578	10.339683	17.821239
C	10.299741	11.081307	17.699146
C	9.107196	10.664650	18.303278
C	9.116821	9.491018	19.054724
N	12.604114	8.312614	18.661559
C	13.611713	8.562327	19.541509
C	14.710725	7.654412	19.653846
C	15.729501	7.896148	20.580561
C	15.746099	9.010720	21.422395
C	14.671132	9.903894	21.302667
C	13.640667	9.695944	20.401801
P	14.677779	6.177248	18.540604
C	16.036226	6.561652	17.258932
C	17.452276	6.703216	17.813262
C	16.855428	9.238579	22.415714
C	12.746496	10.795274	17.156933

C	7.841158	11.465831	18.133293
C	10.310016	7.517541	20.124365
La	11.461050	6.270735	17.834937
N	10.975736	4.861598	19.425747
C	10.652286	3.822672	20.252025
C	10.435098	2.513823	19.700664
C	10.064600	1.443385	20.510381
C	9.913992	1.563619	21.894560
C	10.188097	2.816136	22.446689
C	10.552633	3.922750	21.679597
C	10.667716	2.285937	18.236624
C	9.470741	0.402697	22.745785
C	10.878856	5.212323	22.379826
N	11.202718	5.751954	15.284580
C	10.132714	5.233863	14.599112
C	10.276594	4.566300	13.346718
C	9.208259	3.986339	12.684545
C	7.906777	4.022878	13.202075
C	7.740520	4.706045	14.407479
C	8.791107	5.318290	15.101007
C	6.754710	3.351148	12.502230
P	8.496391	6.288145	16.647214
C	7.048127	5.418362	17.504339
C	6.598970	6.240744	18.714815
C	12.447362	5.748459	14.611757
C	12.810976	6.812464	13.747999
C	14.058929	6.805834	13.122141
C	14.980392	5.773052	13.308223
C	14.607687	4.720964	14.144863
C	13.367889	4.688615	14.791139
C	11.844238	7.929910	13.476659

C	12.994405	3.502107	15.635793
C	16.332147	5.804136	12.643550
C	7.674452	7.893949	16.031303
C	8.684444	8.693690	15.212648
C	6.362756	7.722846	15.268095
C	15.450069	4.803068	19.587862
C	15.685155	3.556490	18.732426
C	14.541789	4.495844	20.778675
C	15.632503	7.808013	16.469752
C	7.436170	4.002703	17.926058
H	8.206283	9.178018	19.563518
H	11.268936	4.498480	12.910988
H	6.738015	4.762510	14.827008
H	7.747771	3.397452	17.070258
H	6.580305	3.503696	18.398204
H	8.254895	4.017033	18.652763
H	16.419744	5.158453	19.959579
H	9.393414	3.479345	11.737370
H	6.514210	7.146458	14.349829
H	5.966099	8.705643	14.980415
H	5.590127	7.221874	15.860324
H	7.486877	8.444637	16.961714
H	9.898327	0.472137	20.041586
H	14.666629	7.678783	15.974380
H	16.376194	8.022618	15.692100
H	15.568581	8.681483	17.127119
H	10.311664	11.999789	17.113297
H	15.998685	5.703214	16.575566
H	14.315880	7.634598	12.463014
H	10.125079	2.940087	23.529280
H	12.994858	3.742599	16.706437

H	13.706095	2.682465	15.495952
H	11.991619	3.139975	15.392843
H	15.292995	3.886095	14.288943
H	9.587298	8.909092	15.790956
H	8.252715	9.654820	14.905659
H	8.970334	8.149945	14.307072
H	14.436224	5.366916	21.431054
H	14.959012	3.673298	21.373363
H	13.538940	4.204504	20.448458
H	6.216851	5.362455	16.789951
H	9.350142	7.425553	20.643749
H	11.091023	7.662962	20.879972
H	10.550428	6.297210	19.867709
H	10.155680	3.029314	17.616418
H	10.334717	1.288231	17.929876
H	11.735322	2.371640	17.995285
H	16.542556	7.177499	20.667853
H	13.497508	11.096837	17.897273
H	12.562924	11.643558	16.490094
H	13.197168	9.981406	16.579605
H	7.422475	6.362053	19.425949
H	5.782007	5.726534	19.236445
H	6.239081	7.236857	18.438399
H	5.796675	3.646414	12.943073
H	6.814622	2.255753	12.563729
H	6.718613	3.607321	11.435831
H	14.635533	10.784502	21.944361
H	10.934610	7.552261	12.996361
H	12.289367	8.684186	12.820320
H	11.526658	8.419230	14.401480
H	11.763883	5.683958	21.938419

H	11.070628	5.039137	23.444624
H	10.068424	5.947904	22.312158
H	9.826209	-0.552861	22.341931
H	8.375353	0.329615	22.815836
H	9.849139	0.489320	23.771062
H	12.811793	10.397481	20.356431
H	16.735669	4.795061	12.509475
H	17.061578	6.368220	13.239331
H	16.284273	6.280748	11.658451
H	17.516862	7.543893	18.511530
H	18.158471	6.898443	16.995111
H	17.795672	5.802363	18.332379
H	14.742322	3.178715	18.322908
H	16.121456	2.755288	19.342011
H	16.365029	3.742973	17.894367
H	8.047171	12.541806	18.112222
H	7.134846	11.274828	18.947843
H	7.328834	11.218436	17.193965
H	16.480090	9.300626	23.445719
H	17.401018	10.171857	22.220830
H	17.586143	8.423396	22.385083

! Direct N - H abstraction by the HMDS anion - Product !

C	-1.052995	3.031725	0.924821
C	0.282441	3.139204	0.418411
C	0.625780	4.182181	-0.469825
C	-0.347277	5.106826	-0.859789
C	-1.667337	5.012131	-0.401884
C	-1.998327	3.980039	0.471279
N	1.199276	2.121802	0.783192

C	2.188450	2.396414	1.683173
C	3.127981	1.387047	2.061750
C	4.133041	1.673196	2.991790
C	4.280908	2.923845	3.594915
C	3.350716	3.908492	3.231171
C	2.341460	3.662601	2.316456
P	2.909385	-0.280263	1.294031
C	4.349162	-0.376555	0.043375
C	5.753071	-0.411191	0.643617
C	5.378904	3.202059	4.587792
C	2.027564	4.287025	-1.005067
C	-2.708826	6.001190	-0.861288
C	-1.393591	1.926009	1.812950
La	-0.237899	0.169091	0.302546
N	-0.825526	-1.361887	2.085398
C	-0.931076	-2.588042	2.687830
C	-0.597860	-3.761868	1.953729
C	-0.692841	-5.017480	2.546479
C	-1.113874	-5.193454	3.868236
C	-1.434563	-4.039133	4.587901
C	-1.355390	-2.760638	4.039397
C	-0.130948	-3.604655	0.540316
C	-1.246692	-6.565084	4.477475
C	-1.708805	-1.556325	4.868581
N	-0.544416	-0.368741	-2.234135
C	-1.594266	-0.899205	-2.946215
C	-1.454613	-1.397034	-4.276063
C	-2.498001	-1.999483	-4.959094
C	-3.770713	-2.149617	-4.393141
C	-3.942543	-1.613922	-3.116008
C	-2.917429	-0.986109	-2.399796

C	-4.885648	-2.856184	-5.118098
P	-3.216073	-0.165752	-0.775480
C	-4.455960	-1.286838	0.111271
C	-4.839528	-0.649676	1.449316
C	0.670103	-0.204220	-2.951662
C	0.963339	1.040205	-3.564787
C	2.164712	1.211077	-4.255988
C	3.100181	0.182997	-4.387466
C	2.791990	-1.045032	-3.804452
C	1.604497	-1.258092	-3.095903
C	-0.038244	2.159533	-3.522852
C	1.319974	-2.626998	-2.539836
C	4.396594	0.400005	-5.123451
C	-4.283710	1.353537	-1.224180
C	-3.545147	2.196630	-2.261227
C	-5.713114	1.068761	-1.681901
C	3.461147	-1.462448	2.668867
C	3.509212	-2.902013	2.152659
C	2.526605	-1.340408	3.873156
C	4.214750	0.779978	-0.947167
C	-3.872160	-2.682674	0.319766
H	-3.013549	3.919580	0.862593
H	-0.488917	-1.310539	-4.764112
H	-4.925916	-1.692283	-2.655076
H	-3.597381	-3.151448	-0.629532
H	-4.606207	-3.328903	0.817686
H	-2.984118	-2.639207	0.956456
H	4.473224	-1.169733	2.976222
H	-2.314424	-2.371133	-5.967418
H	-5.722378	0.485401	-2.608648
H	-6.231133	2.014918	-1.887887

H	-6.303377	0.532022	-0.932883
H	-4.313086	1.918822	-0.283727
H	-0.427239	-5.891795	1.951024
H	3.234040	0.796717	-1.428682
H	4.972044	0.692049	-1.735471
H	4.360295	1.739249	-0.440085
H	-0.071177	5.906840	-1.545659
H	4.167391	-1.314901	-0.498278
H	2.365184	2.175964	-4.720447
H	-1.759181	-4.136229	5.624788
H	1.512389	-2.676826	-1.463438
H	1.959471	-3.376855	-3.016610
H	0.276728	-2.913479	-2.694830
H	3.490121	-1.874894	-3.911347
H	-2.550550	2.483621	-1.913532
H	-4.103874	3.118369	-2.466597
H	-3.441010	1.646767	-3.202376
H	2.535247	-0.327112	4.284420
H	2.836677	-2.033993	4.665115
H	1.498100	-1.588672	3.593383
H	-5.351716	-1.368179	-0.517296
H	-2.423205	1.953297	2.177324
H	-0.685378	1.818151	2.645207
H	-1.139573	-0.638609	2.733201
H	-0.893906	-3.136652	-0.096490
H	0.137719	-4.564363	0.087645
H	0.754050	-2.954430	0.497409
H	4.826670	0.884346	3.277565
H	2.742349	4.555755	-0.217486
H	2.090464	5.042708	-1.794573
H	2.360910	3.326889	-1.412005

H	-3.950289	-0.522025	2.075503
H	-5.543781	-1.293925	1.990664
H	-5.311062	0.331624	1.329772
H	-5.855029	-2.652822	-4.650451
H	-4.752826	-3.947143	-5.122425
H	-4.953585	-2.541029	-6.166722
H	3.413054	4.895862	3.689123
H	-1.007349	1.828045	-3.907382
H	0.301809	3.007589	-4.124964
H	-0.206062	2.524665	-2.504569
H	-0.870555	-0.850172	4.946857
H	-1.991637	-1.847668	5.884851
H	-2.550667	-0.993831	4.440757
H	-0.494923	-7.257140	4.080355
H	-2.229988	-7.016197	4.280211
H	-1.123157	-6.533758	5.566044
H	1.623649	4.443020	2.080305
H	4.836479	-0.548711	-5.447632
H	5.138529	0.904486	-4.490928
H	4.254291	1.026059	-6.011301
H	5.951092	0.496726	1.222574
H	6.501800	-0.458923	-0.158363
H	5.916940	-1.275640	1.294740
H	2.507692	-3.258978	1.894142
H	3.899103	-3.569779	2.931175
H	4.150764	-3.012187	1.271736
H	-2.296529	7.013963	-0.936841
H	-3.558710	6.035110	-0.171685
H	-3.103416	5.740205	-1.852183
H	4.988770	3.624458	5.522791
H	6.117473	3.917954	4.201145

H	5.920762	2.285728	4.845031

! Direct P-H abstraction - Adduct !

C	13.385569000	9.685506301	20.684915000
C	13.369793699	8.519131000	19.889961301
C	14.443746699	7.602215000	20.083750301
C	15.416513000	7.876110000	21.033325301
C	15.428717000	9.035964000	21.826818000
C	14.372364301	9.947945000	21.607852000
N	12.345907699	8.247916000	18.981887601
C	11.357106000	9.239894301	18.778198301
C	10.111700000	9.148188902	19.448876301
C	9.128470301	10.130683902	19.208523000
C	9.357072301	11.195943601	18.355187399
C	10.599908301	11.267109301	17.696485699
C	11.589979301	10.328794000	17.898510000
C	9.857648699	8.057678504	20.452529902
C	8.284171601	12.236677601	18.102715098
C	12.928610301	10.480582699	17.229527000
P	14.507207699	6.090696000	19.020406301
C	15.251014301	4.761938000	20.136798000
C	14.358862601	4.495811399	21.350905000
C	16.461173301	9.272248000	22.879244000
La	11.418525098	6.248563098	18.127460504
P	10.562168594	4.415977007	20.123549511
C	10.295758098	2.621137406	20.253395105
C	10.862894000	1.831527308	19.231600804
C	10.765839902	0.452913007	19.285628601
C	10.117794601	-0.197200196	20.326438699
C	9.514908699	0.587310902	21.321958699

C	9.563542098	1.981459902	21.321689601
C	11.550311301	2.512493909	18.086163406
C	10.070586203	-1.703391196	20.401752496
C	8.802946196	2.763348399	22.356601902
N	11.311937000	5.971579399	15.678677601
C	12.537666000	6.261047699	15.022602601
C	13.597083000	5.326578699	14.978873301
C	14.775508000	5.653076699	14.297887301
C	14.969058699	6.880534699	13.661591301
C	13.910590699	7.790388699	13.713910301
C	12.716169699	7.504763699	14.376693301
C	13.449839000	3.936902000	15.559224601
C	16.254149699	7.202158000	12.971442000
C	11.586807699	8.493825699	14.312925601
C	10.307145000	5.506936699	14.849838301
C	10.578893000	5.075489000	13.515398301
C	9.595477000	4.586202000	12.672313301
C	8.262810000	4.464266000	13.102736000
C	7.977104000	4.883354000	14.401020000
C	8.941504000	5.420012699	15.257624301
P	8.494466699	6.006847699	16.946480301
C	7.448302699	7.576545699	16.672026000
C	6.099403000	7.382812699	15.966052699
C	7.199631000	3.907402000	12.193084000
C	7.194460699	4.754478699	17.533358000
C	7.713376601	3.321402000	17.517154203
C	6.665225098	5.156198000	18.925530399
C	15.920754699	6.487363000	17.798379301
C	15.590386699	7.779158000	17.074278000
C	17.323237699	6.559790000	18.418168000
C	15.508767601	3.501555000	19.330681699

C	8.279068000	8.611944000	15.946993301
N	9.531133804	5.847295496	23.774291286
Si	8.038508504	6.526783496	24.131151091
C	6.808568601	6.405014699	22.620505294
Si	10.969752203	5.796234797	24.654562391
C	12.281049601	7.143753699	24.204439594
C	10.849440496	5.926658098	26.606109790
C	11.943297902	4.132673797	24.374251895
C	7.970519007	8.423818895	24.579863895
C	7.039645706	5.688849594	25.583396091
H	10.099697895	4.769587112	21.178643623
H	8.201833000	10.048163504	19.747484000
H	11.599262000	5.134044000	13.151086301
H	6.951023000	4.797387000	14.750760000
H	8.080846504	3.029074699	16.538503504
H	6.900203902	2.630943699	17.779792203
H	8.502736301	3.168227203	18.270806504
H	16.229738000	5.162099000	20.483792000
H	9.857999301	4.278244000	11.665507301
H	6.233887301	7.005040000	14.943311699
H	5.574541000	8.344564699	15.898714699
H	5.432284000	6.704061399	16.499516399
H	7.246981699	7.926055699	17.693315000
H	11.229499504	-0.151459790	18.476225601
H	14.618143699	7.740491699	16.579757000
H	16.343935699	7.976152000	16.302930000
H	15.597080399	8.629487000	17.763247000
H	10.791711601	12.104896000	17.028472399
H	15.881158699	5.660511000	17.077473301
H	14.009782699	8.751344699	13.210674301
H	8.972340399	0.103764000	22.140628797

H	13.690497098	3.923192301	16.639818601
H	14.113658902	3.240229000	15.061126504
H	12.405427601	3.581519399	15.457653699
H	15.570210000	4.891500000	14.247382301
H	9.203967699	8.871197699	16.489921601
H	7.709459000	9.542085000	15.832236301
H	8.569000000	8.271106000	14.948124301
H	14.257263000	5.377046399	21.981580000
H	14.788039203	3.694686699	21.961594000
H	13.361437601	4.206272496	21.057217000
H	6.356605301	4.813877098	16.820507399
H	9.059716000	8.327029406	21.145008902
H	10.721727000	7.816295504	21.068308601
H	9.496845399	7.110116504	20.015380203
H	10.842867301	3.136491007	17.496812804
H	12.005763504	1.806079210	17.401544706
H	12.340154399	3.186770511	18.466391007
H	16.229100699	7.149487000	21.206469000
H	13.720702301	10.656016399	17.988442699
H	12.935677301	11.344586399	16.553817699
H	13.212183000	9.594005399	16.676124000
H	7.475037797	5.150213301	19.664232699
H	5.903647098	4.456463699	19.252927399
H	6.213104797	6.162799699	18.921241098
H	6.217209000	3.924040000	12.675345000
H	7.407271000	2.867355000	11.910563000
H	7.100138301	4.480514000	11.260781000
H	14.337089301	10.850334301	22.206769699
H	10.717045000	8.084470699	13.776303301
H	11.898464699	9.421540699	13.824130601
H	11.220657699	8.756701399	15.313295601

H	7.922806797	3.215945601	21.889892902
H	9.350007196	3.632361895	22.813491406
H	8.466231993	2.094608496	23.160762399
H	10.345887504	-2.161945294	19.445275196
H	9.059042504	-2.063335797	20.678730895
H	10.747599504	-2.094715496	21.165290196
H	12.566174301	10.408623301	20.566921000
H	16.070661699	7.798239000	12.053085301
H	16.797481699	6.299803000	12.673584000
H	16.923956699	7.805998699	13.614259000
H	17.388912699	7.338015301	19.166447000
H	18.049806699	6.774586301	17.628859000
H	17.622135000	5.604210301	18.884514000
H	14.578680601	3.062778000	18.955159699
H	15.993049601	2.743723000	19.958123699
H	16.182058301	3.671489301	18.473362699
H	7.543026601	12.252924902	18.906799098
H	7.763484301	12.045505301	17.169724098
H	8.722404601	13.235618601	18.021816797
H	16.758276601	10.321630000	22.925806699
H	17.352553301	8.662188000	22.717587699
H	16.090099301	9.000816301	23.880667000
H	11.849473895	5.872002699	27.093997391
H	10.391891594	6.874690797	26.895080489
H	10.228201797	5.127195496	27.012863189
H	12.936182601	4.153435098	24.857312196
H	11.384812601	3.275846399	24.797075196
H	12.067694504	3.946181895	23.301269196
H	13.218986000	7.026185000	24.785549196
H	12.529686504	7.114390000	23.134312895
H	11.873206000	8.142875399	24.406739594

H	6.050020706	6.151924294	25.729892391
H	6.884612007	4.626465594	25.372392790
H	7.585004007	5.776521294	26.519284091
H	5.828894203	6.847930000	22.864484496
H	7.205358000	6.902027301	21.736124294
H	6.633611000	5.355051000	22.359185692
H	6.927861609	8.763985895	24.764169399
H	8.550197210	8.619074993	25.503006993
H	8.399376105	9.038427496	23.782158895

! Direct P-H abstraction - Transition State !

C	13.385569000	9.703576000	20.684915000
C	13.351724000	8.519131000	19.908031000
C	14.425677000	7.602215000	20.101820000
C	15.416513000	7.876110000	21.051395000
C	15.428717000	9.035964000	21.826818000
C	14.390434000	9.947945000	21.607852000
N	12.327838000	8.247916000	19.018027000
C	11.357106000	9.257964000	18.796268000
C	10.111700000	9.202398000	19.466946000
C	9.146540000	10.184893000	19.208523000
C	9.375142000	11.232083000	18.319048000
C	10.617978000	11.285179000	17.678416000
C	11.608049000	10.328794000	17.898510000
C	9.839579000	8.148027000	20.506739000
C	8.320311000	12.272817000	18.048506000
C	12.946680000	10.462513000	17.229527000
P	14.489138000	6.090696000	19.038476000
C	15.269084000	4.761938000	20.136798000
C	14.395002000	4.459672000	21.350905000

C	16.479243000	9.272248000	22.879244000
La	11.364316000	6.194354000	18.217809000
P	10.417611000	4.596674000	20.394595000
C	10.241549000	2.765695000	20.379883000
C	10.862894000	2.030294000	19.340019000
C	10.820049000	0.633610000	19.321768000
C	10.153934000	-0.088782000	20.308369000
C	9.496839000	0.641520000	21.303889000
C	9.509333000	2.035669000	21.357829000
C	11.568381000	2.747400000	18.230721000
C	10.142865000	-1.594973000	20.311404000
C	8.694528000	2.727209000	22.410811000
N	11.311937000	5.935440000	15.714817000
C	12.537666000	6.242978000	15.058742000
C	13.597083000	5.308509000	14.996943000
C	14.775508000	5.635007000	14.315957000
C	14.950989000	6.862465000	13.679661000
C	13.892521000	7.772319000	13.731980000
C	12.698100000	7.486694000	14.394763000
C	13.449839000	3.936902000	15.595364000
C	16.236080000	7.202158000	12.971442000
C	11.568738000	8.475756000	14.349065000
C	10.307145000	5.488867000	14.867908000
C	10.578893000	5.075489000	13.533468000
C	9.595477000	4.586202000	12.690383000
C	8.262810000	4.464266000	13.102736000
C	7.977104000	4.883354000	14.401020000
C	8.941504000	5.401943000	15.275694000
P	8.476397000	5.988778000	16.964550000
C	7.430233000	7.558476000	16.672026000
C	6.099403000	7.364743000	15.947983000

C	7.199631000	3.907402000	12.193084000
C	7.176391000	4.736409000	17.533358000
C	7.749516000	3.321402000	17.589433000
C	6.611016000	5.156198000	18.889391000
C	15.902685000	6.487363000	17.816449000
C	15.572317000	7.779158000	17.074278000
C	17.305168000	6.559790000	18.418168000
C	15.544907000	3.501555000	19.312612000
C	8.279068000	8.611944000	15.965063000
N	9.639552000	5.756947000	23.430967000
Si	8.128857000	6.436435000	23.896245000
C	6.844708000	6.386945000	22.457878000
Si	11.042031000	5.723956000	24.437726000
C	12.317189000	7.125684000	24.059882000
C	10.759092000	5.872449000	26.353134000
C	11.997507000	4.060395000	24.247764000
C	8.151216000	8.297331000	24.453376000
C	7.202273000	5.544292000	25.348490000
H	9.973210000	5.076772000	21.756874000
H	8.201833000	10.138512000	19.747484000
H	11.599262000	5.134044000	13.169156000
H	6.951023000	4.797387000	14.750760000
H	8.171195000	3.011005000	16.628852000
H	6.954413000	2.612874000	17.852071000
H	8.520806000	3.240506000	18.361155000
H	16.229738000	5.162099000	20.483792000
H	9.876069000	4.278244000	11.683577000
H	6.251957000	7.005040000	14.925242000
H	5.574541000	8.326495000	15.880645000
H	5.432284000	6.667922000	16.463377000
H	7.228912000	7.907986000	17.693315000

H	11.319848000	0.101516000	18.512365000
H	14.600074000	7.722422000	16.579757000
H	16.325866000	7.976152000	16.302930000
H	15.560941000	8.629487000	17.763247000
H	10.827851000	12.104896000	16.992333000
H	15.863089000	5.660511000	17.095543000
H	13.991713000	8.733275000	13.228744000
H	8.936201000	0.103764000	22.068350000
H	13.636288000	3.941262000	16.675958000
H	14.167868000	3.240229000	15.151475000
H	12.441567000	3.545380000	15.439584000
H	15.570210000	4.891500000	14.265452000
H	9.185898000	8.853128000	16.526061000
H	7.709459000	9.542085000	15.850306000
H	8.569000000	8.271106000	14.966194000
H	14.257263000	5.340907000	21.981580000
H	14.860318000	3.676617000	21.961594000
H	13.397577000	4.115924000	21.057217000
H	6.374675000	4.759668000	16.784368000
H	9.059716000	8.471587000	21.199218000
H	10.721727000	7.906644000	21.104448000
H	9.460706000	7.200465000	20.087659000
H	10.860937000	3.317188000	17.605231000
H	12.096112000	2.059055000	17.564172000
H	12.304015000	3.457816000	18.647088000
H	16.211031000	7.149487000	21.206469000
H	13.738772000	10.619877000	17.970373000
H	12.953747000	11.308447000	16.535748000
H	13.212183000	9.557866000	16.676124000
H	7.402759000	5.168283000	19.646163000
H	5.849438000	4.438394000	19.216788000

H	6.140826000	6.144730000	18.867032000
H	6.217209000	3.924040000	12.675345000
H	7.407271000	2.867355000	11.910563000
H	7.118208000	4.480514000	11.260781000
H	14.355159000	10.868404000	22.188700000
H	10.717045000	8.066401000	13.794373000
H	11.880395000	9.403471000	13.860270000
H	11.202588000	8.720562000	15.349435000
H	7.850528000	3.252085000	21.944102000
H	9.241589000	3.505874000	22.958049000
H	8.285535000	2.004260000	23.124623000
H	10.436236000	-1.999318000	19.336857000
H	9.149391000	-1.991057000	20.552243000
H	10.837948000	-2.004367000	21.056872000
H	12.584244000	10.426693000	20.566921000
H	16.052592000	7.798239000	12.071155000
H	16.779412000	6.299803000	12.673584000
H	16.905887000	7.787929000	13.614259000
H	17.370843000	7.356085000	19.166447000
H	18.031737000	6.792656000	17.628859000
H	17.622135000	5.622280000	18.884514000
H	14.614820000	3.062778000	18.937090000
H	16.029189000	2.743723000	19.940054000
H	16.200128000	3.689559000	18.455293000
H	7.579166000	12.307134000	18.852590000
H	7.781554000	12.063575000	17.115515000
H	8.758544000	13.271758000	17.949538000
H	16.794416000	10.321630000	22.907737000
H	17.370623000	8.662188000	22.699518000
H	16.108169000	9.018886000	23.880667000
H	11.722986000	5.853933000	26.877161000

H	10.247334000	6.802412000	26.624035000
H	10.155923000	5.036847000	26.723748000
H	12.972322000	4.099226000	24.748894000
H	11.420952000	3.239707000	24.688657000
H	12.158043000	3.819694000	23.192851000
H	13.218986000	7.026185000	24.677131000
H	12.620035000	7.114390000	23.007825000
H	11.873206000	8.106736000	24.262182000
H	6.212648000	5.989297000	25.513056000
H	7.065309000	4.481908000	25.119417000
H	7.765701000	5.613894000	26.284378000
H	5.901173000	6.847930000	22.774136000
H	7.205358000	6.920097000	21.573497000
H	6.633611000	5.355051000	22.160419000
H	7.144698000	8.637498000	24.728030000
H	8.803173000	8.438378000	25.322310000
H	8.525864000	8.948079000	23.655671000

! Direct P-H abstraction - Product !

C	13.385569000	9.719644828	20.684915000
C	13.335655172	8.519131000	19.924099828
C	14.409608172	7.602215000	20.117888828
C	15.416513000	7.876110000	21.067463828
C	15.428717000	9.035964000	21.826818000
C	14.406502828	9.947945000	21.607852000
N	12.311769172	8.247916000	19.050164656
C	11.357106000	9.274032828	18.812336828
C	10.111700000	9.250604484	19.483014828
C	9.162608828	10.233099484	19.208523000
C	9.391210828	11.264220656	18.286910344

C	10.634046828	11.301247828	17.662347172
C	11.624117828	10.328794000	17.898510000
C	9.823510172	8.228371140	20.554945484
C	8.352448656	12.304954656	18.000299516
C	12.962748828	10.446444172	17.229527000
P	14.473069172	6.090696000	19.054544828
C	15.285152828	4.761938000	20.136798000
C	14.427139656	4.427534344	21.350905000
C	16.495311828	9.272248000	22.879244000
La	11.316109516	6.146147516	18.298153140
P	10.289060376	4.757362280	20.635627420
C	10.193342516	2.894245624	20.492364796
C	10.862894000	2.207051108	19.436431968
C	10.868255484	0.794298280	19.353905656
C	10.186071656	0.007630968	20.292300172
C	9.480770172	0.689726484	21.287820172
C	9.461126516	2.083875484	21.389966656
C	11.584449828	2.956294764	18.359271624
C	10.207140312	-1.498560032	20.231059860
C	8.598115032	2.695071344	22.459017484
N	11.311937000	5.903302344	15.746954656
C	12.537666000	6.226909172	15.090879656
C	13.597083000	5.292440172	15.013011828
C	14.775508000	5.618938172	14.332025828
C	14.934920172	6.846396172	13.695729828
C	13.876452172	7.756250172	13.748048828
C	12.682031172	7.470625172	14.410831828
C	13.449839000	3.936902000	15.627501656
C	16.220011172	7.202158000	12.971442000
C	11.552669172	8.459687172	14.381202656
C	10.307145000	5.472798172	14.883976828

C	10.578893000	5.075489000	13.549536828
C	9.595477000	4.586202000	12.706451828
C	8.262810000	4.464266000	13.102736000
C	7.977104000	4.883354000	14.401020000
C	8.941504000	5.385874172	15.291762828
P	8.460328172	5.972709172	16.980618828
C	7.414164172	7.542407172	16.672026000
C	6.099403000	7.348674172	15.931914172
C	7.199631000	3.907402000	12.193084000
C	7.160322172	4.720340172	17.533358000
C	7.781653656	3.321402000	17.653708312
C	6.562809516	5.156198000	18.857253344
C	15.886616172	6.487363000	17.832517828
C	15.556248172	7.779158000	17.074278000
C	17.289099172	6.559790000	18.418168000
C	15.577044656	3.501555000	19.296543172
C	8.279068000	8.611944000	15.981131828
N	9.735964968	5.676602860	23.125659268
Si	8.209201140	6.356090860	23.687350236
C	6.876845656	6.370876172	22.313258548
Si	11.106306312	5.659680688	24.244900064
C	12.349326656	7.109615172	23.931331376
C	10.678747860	5.824242516	26.128170408
C	12.045713484	3.996119688	24.135282204
C	8.311904280	8.184849204	24.340894204
C	7.346892452	5.415741376	25.139595236
H	9.860728204	5.349942076	22.271076496
H	8.201833000	10.218856140	19.747484000
H	11.599262000	5.134044000	13.185224828
H	6.951023000	4.797387000	14.750760000
H	8.251539140	2.994936172	16.709196140

H	7.002619484	2.596805172	17.916346312
H	8.536874828	3.304781312	18.441499140
H	16.229738000	5.162099000	20.483792000
H	9.892137828	4.278244000	11.699645828
H	6.268025828	7.005040000	14.909173172
H	5.574541000	8.310426172	15.864576172
H	5.432284000	6.635784344	16.431239344
H	7.212843172	7.891917172	17.693315000
H	11.400192140	0.326479592	18.544502656
H	14.584005172	7.706353172	16.579757000
H	16.309797172	7.976152000	16.302930000
H	15.528803344	8.629487000	17.763247000
H	10.859988656	12.104896000	16.960195344
H	15.847020172	5.660511000	17.111611828
H	13.975644172	8.717206172	13.244812828
H	8.904063344	0.103764000	22.004074688
H	13.588081516	3.957330828	16.708095656
H	14.216074484	3.240229000	15.231819140
H	12.473704656	3.513242344	15.423515172
H	15.570210000	4.891500000	14.281520828
H	9.169829172	8.837059172	16.558198656
H	7.709459000	9.542085000	15.866374828
H	8.569000000	8.271106000	14.982262828
H	14.257263000	5.308769344	21.981580000
H	14.924593312	3.660548172	21.961594000
H	13.429714656	4.035579860	21.057217000
H	6.390743828	4.711461516	16.752230344
H	9.059716000	8.600137624	21.247424484
H	10.721727000	7.986988140	21.136585656
H	9.428568344	7.280809140	20.151934312
H	10.877005828	3.477876280	17.701643968

H	12.176456140	2.284018592	17.708791452
H	12.271877344	3.698848420	18.807776280
H	16.194962172	7.149487000	21.206469000
H	13.754840828	10.587739344	17.954304172
H	12.969815828	11.276309344	16.519679172
H	13.212183000	9.525728344	16.676124000
H	7.338483688	5.184351828	19.630094172
H	5.801231516	4.422325172	19.184650344
H	6.076550688	6.128661172	18.818825516
H	6.217209000	3.924040000	12.675345000
H	7.407271000	2.867355000	11.910563000
H	7.134276828	4.480514000	11.260781000
H	14.371227828	10.884472828	22.172631172
H	10.717045000	8.050332172	13.810441828
H	11.864326172	9.387402172	13.892407656
H	11.186519172	8.688424344	15.381572656
H	7.786252688	3.284222656	21.992308484
H	9.145176032	3.393392204	23.086599624
H	8.124846720	1.923915860	23.092485344
H	10.516580140	-1.854698548	19.240444032
H	9.229735140	-1.926781688	20.439761204
H	10.918292140	-1.924022860	20.960459032
H	12.600312828	10.442761828	20.566921000
H	16.036523172	7.798239000	12.087223828
H	16.763343172	6.299803000	12.673584000
H	16.889818172	7.771860172	13.614259000
H	17.354774172	7.372153828	19.166447000
H	18.015668172	6.808724828	17.628859000
H	17.622135000	5.638348828	18.884514000
H	14.646957656	3.062778000	18.921021172
H	16.061326656	2.743723000	19.923985172

H	16.216196828	3.705627828	18.439224172
H	7.611303656	12.355340484	18.804383516
H	7.797622828	12.079643828	17.067308516
H	8.790681656	13.303895656	17.885262688
H	16.826553656	10.321630000	22.891668172
H	17.386691828	8.662188000	22.683449172
H	16.124237828	9.034954828	23.880667000
H	11.610504204	5.837864172	26.684335064
H	10.118783376	6.738136688	26.383002580
H	10.091647688	4.956502860	26.466646752
H	13.004459656	4.051019516	24.652481032
H	11.453089656	3.207569344	24.592244032
H	12.238387140	3.707212204	23.096438032
H	13.218986000	7.026185000	24.580718032
H	12.700379140	7.114390000	22.895343204
H	11.873206000	8.074598344	24.133631376
H	6.357267452	5.844677548	25.320230064
H	7.225997280	4.353357376	24.894453408
H	7.926389280	5.469274548	26.075483236
H	5.965448312	6.847930000	22.693791860
H	7.205358000	6.936165828	21.428877548
H	6.633611000	5.355051000	21.983661892
H	7.337523936	8.525016204	24.695892344
H	9.028136592	8.277689720	25.161621720
H	8.638345796	8.867734860	23.543189204

! Internal C-H activation from the Phosphido - Adduct !

C	13.380569000	9.683176000	20.580206000
C	13.501339000	8.648258000	19.603469000
C	14.770542000	8.017253000	19.503492000

C	15.830962000	8.381855000	20.318071000
C	15.714901000	9.392551000	21.282649000
C	14.471844000	10.023897000	21.382988000
N	12.431531000	8.327141000	18.811746000
C	12.570185000	7.384455000	17.776790000
C	12.715295000	7.880150000	16.447513000
C	12.734186000	6.955650000	15.387967000
C	12.645949000	5.578911000	15.604082000
C	12.519317000	5.112650000	16.920504000
C	12.464538000	5.991894000	18.002584000
C	12.914149000	9.357327000	16.219991000
C	12.683732000	4.607370000	14.451390000
C	12.328785000	5.471774000	19.407081000
C	16.877197000	9.786469000	22.156307000
P	11.729685000	10.506823000	20.674305000
C	12.121283000	12.293977000	21.158089000
C	12.960371000	12.973561000	20.076510000
La	10.607450000	9.574410000	17.734427000
P	10.916707000	11.966274000	16.584346000
C	11.725863000	13.455342000	15.860696000
C	10.888086000	14.530650000	15.451226000
C	11.446953000	15.695386000	14.924498000
C	12.825792000	15.862593000	14.779620000
C	13.642757000	14.813595000	15.200052000
C	13.128570000	13.628234000	15.732743000
C	9.391905000	14.447727000	15.589953000
C	13.404055000	17.115309000	14.174854000
C	14.092103000	12.561657000	16.167211000
N	8.111470000	9.069270000	18.148465000
C	7.794290000	9.347786000	19.499242000
C	7.526237000	10.671231000	19.927717000

C	7.222801000	10.908925000	21.271887000
C	7.160287000	9.881002000	22.215204000
C	7.411459000	8.579272000	21.775469000
C	7.725090000	8.296819000	20.444168000
C	7.490757000	11.801367000	18.934904000
C	6.848405000	10.167750000	23.661578000
C	7.928060000	6.874920000	19.996576000
C	7.042643000	8.862555000	17.313408000
C	7.217737000	8.565018000	15.925273000
C	6.107549000	8.420282000	15.085473000
C	4.789235000	8.519584000	15.531921000
C	4.615568000	8.764213000	16.900672000
C	5.689062000	8.927126000	17.759554000
P	8.941970000	8.363645000	15.307203000
C	9.074955000	6.497992000	14.938726000
C	8.145922000	5.945374000	13.860388000
C	3.618726000	8.387448000	14.593449000
C	8.914002000	9.136215000	13.578325000
C	8.502741000	10.605810000	13.650498000
C	10.290237000	8.980782000	12.927349000
C	10.994347000	9.779005000	22.280550000
C	10.990716000	8.253717000	22.174144000
C	11.662597000	10.222966000	23.580418000
C	10.812965000	13.053825000	21.389042000
C	8.907134000	5.728494000	16.248933000
H	12.870188000	7.322017000	14.373952000
H	5.498209000	9.124042000	18.810023000
H	6.275958000	8.231805000	14.026783000
H	7.489602000	10.721672000	14.045150000
H	8.534409000	11.053148000	12.648435000
H	9.185810000	11.165094000	14.306386000

H	12.692816000	12.272905000	22.094952000
H	3.606594000	8.836522000	17.307082000
H	7.095592000	6.053544000	14.149381000
H	8.338186000	4.873643000	13.717000000
H	8.286086000	6.431949000	12.889812000
H	10.116245000	6.386653000	14.612390000
H	10.779057000	16.501551000	14.620009000
H	10.500231000	7.915648000	21.258473000
H	10.454345000	7.814487000	23.024430000
H	12.013101000	7.862065000	22.172889000
H	12.454847000	4.041177000	17.105775000
H	9.953188000	10.124156000	22.269831000
H	7.350720000	7.755738000	22.486298000
H	14.724847000	14.918601000	15.117650000
H	8.446206000	11.942449000	18.413363000
H	7.235941000	12.743494000	19.430352000
H	6.743790000	11.609261000	18.156737000
H	7.008211000	11.930353000	21.584304000
H	9.638798000	6.044773000	16.997445000
H	9.053397000	4.653859000	16.082867000
H	7.903011000	5.873974000	16.661538000
H	13.912789000	12.458937000	19.920557000
H	13.177076000	14.010412000	20.364531000
H	12.421754000	12.991708000	19.122118000
H	8.174611000	8.587139000	12.981249000
H	13.250929000	9.510066000	15.186023000
H	13.715595000	9.707845000	16.885718000
H	12.235296000	10.131841000	16.267172000
H	14.360615000	10.830730000	22.105576000
H	13.241797000	5.649731000	19.988274000
H	12.123712000	4.396768000	19.412139000

H	11.523734000	5.987078000	19.940379000
H	11.053309000	9.506376000	13.515674000
H	10.285324000	9.420873000	11.922214000
H	10.592227000	7.932560000	12.829677000
H	2.870434000	7.678034000	14.969286000
H	3.939630000	8.033483000	13.607987000
H	3.100251000	9.343965000	14.440454000
H	16.785671000	7.870442000	20.194555000
H	7.172588000	6.588001000	19.256703000
H	7.864310000	6.182737000	20.841840000
H	8.899113000	6.735412000	19.510404000
H	14.083835000	11.708163000	15.475099000
H	13.823568000	12.167568000	17.153355000
H	15.116561000	12.946950000	16.207144000
H	12.814242000	18.000232000	14.439785000
H	13.430207000	17.065349000	13.077308000
H	14.432019000	17.285196000	14.513154000
H	14.906132000	7.244307000	18.751650000
H	6.311624000	9.334915000	24.128357000
H	6.232067000	11.066616000	23.767280000
H	7.762082000	10.331470000	24.247886000
H	12.718647000	9.932753000	23.600232000
H	11.174468000	9.737871000	24.436445000
H	11.601499000	11.303752000	23.741279000
H	10.220928000	13.082697000	20.468247000
H	11.022906000	14.090319000	21.682089000
H	10.194783000	12.603688000	22.172732000
H	13.044530000	5.087752000	13.536511000
H	11.688513000	4.196951000	14.236276000
H	13.340655000	3.756255000	14.665133000
H	16.604704000	10.605391000	22.830302000

H	17.739922000	10.123464000	21.566739000
H	17.225803000	8.952936000	22.780715000
H	8.912543000	15.357739000	15.212168000
H	8.987396000	13.585390000	15.048381000
H	9.101286000	14.303754000	16.636984000

! Internal C-H activation from the Phosphido - Transition State !

C	13.409670	9.669542	20.547414
C	13.512249	8.630155	19.572510
C	14.776124	7.992309	19.458237
C	15.848083	8.351617	20.261027
C	15.748639	9.362324	21.226352
C	14.511231	10.004488	21.337368
N	12.431364	8.316437	18.797955
C	12.544764	7.367394	17.761562
C	12.687248	7.859639	16.426765
C	12.678309	6.919206	15.373144
C	12.588044	5.548658	15.598794
C	12.479141	5.090973	16.919238
C	12.442826	5.976811	17.997134
C	12.880509	9.305198	16.193052
C	12.601135	4.571325	14.450445
C	12.325573	5.464985	19.406234
C	16.912181	9.729651	22.109828
P	11.767260	10.508931	20.653229
C	12.179860	12.294885	21.124472
C	13.015974	12.961349	20.032475
La	10.601645	9.574953	17.736724
P	10.918953	11.962986	16.582333
C	11.731041	13.443723	15.845527

C	10.897232	14.527938	15.449265
C	11.458842	15.686505	14.913615
C	12.837550	15.839952	14.746847
C	13.649991	14.782750	15.153111
C	13.132474	13.602068	15.694572
C	9.402694	14.459225	15.611653
C	13.416971	17.091209	14.140068
C	14.092148	12.525529	16.112668
N	8.107280	9.085267	18.172216
C	7.806326	9.368699	19.525622
C	7.550979	10.695216	19.953768
C	7.265176	10.938228	21.300462
C	7.207846	9.912788	22.247367
C	7.445946	8.608784	21.808224
C	7.742071	8.320815	20.473734
C	7.510764	11.822626	18.958108
C	6.914851	10.207034	23.696212
C	7.932079	6.896608	20.027637
C	7.028562	8.886818	17.348034
C	7.187978	8.589199	15.958019
C	6.068758	8.452626	15.129181
C	4.755504	8.560623	15.588728
C	4.597010	8.804589	16.959292
C	5.680107	8.959463	17.807762
P	8.904799	8.375546	15.323012
C	9.020076	6.508383	14.957159
C	8.065110	5.957035	13.901085
C	3.575119	8.441063	14.660995
C	8.863387	9.144485	13.592624
C	8.462541	10.616948	13.666527
C	10.231223	8.979204	12.926539

C	11.041843	9.795312	22.270541
C	11.021299	8.269687	22.171413
C	11.727996	10.237952	23.561511
C	10.881038	13.068438	21.363617
C	8.876882	5.744562	16.273589
H	12.807615	7.283924	14.355136
H	5.500836	9.155450	18.860461
H	6.225582	8.262973	14.068902
H	7.454260	10.740170	14.071241
H	8.487115	11.062648	12.663541
H	9.155666	11.172799	14.309625
H	12.759222	12.272901	22.056504
H	3.592595	8.882578	17.375824
H	7.022010	6.069645	14.213493
H	8.250325	4.884355	13.755479
H	8.184901	6.441313	12.926603
H	10.053458	6.390631	14.608672
H	10.793908	16.499000	14.619489
H	10.513127	7.932117	21.265283
H	10.493326	7.840067	23.031798
H	12.039494	7.867528	22.156668
H	12.413797	4.020833	17.111631
H	10.004179	10.151016	22.269312
H	7.389031	7.787639	22.522075
H	14.731487	14.876398	15.051909
H	8.460813	11.955805	18.424727
H	7.267979	12.767814	19.453741
H	6.753305	11.633008	18.189563
H	7.060321	11.961755	21.612646
H	9.628076	6.058060	17.003805
H	9.011408	4.668274	16.108329

H	7.883556	5.898756	16.708651
H	13.963284	12.438487	19.872895
H	13.242632	13.998269	20.312471
H	12.470428	12.977616	19.081945
H	8.114059	8.598953	13.004647
H	13.156512	9.499983	15.153152
H	13.651804	9.703637	16.858203
H	11.995181	10.554449	16.269926
H	14.414134	10.815513	22.057326
H	13.251948	5.631268	19.969562
H	12.104149	4.393304	19.420253
H	11.538848	5.995536	19.951697
H	11.004048	9.496872	13.504540
H	10.217322	9.416731	11.920358
H	10.526021	7.929040	12.827958
H	3.089624	9.410157	14.480328
H	2.804909	7.770963	15.063255
H	3.877078	8.045498	13.685411
H	16.799220	7.836599	20.125864
H	7.172645	6.615097	19.289854
H	7.864370	6.206211	20.874071
H	8.901045	6.747825	19.539856
H	14.064381	11.672404	15.425536
H	13.835436	12.133760	17.102909
H	15.120944	12.900497	16.136311
H	12.953089	17.994799	14.553531
H	13.266123	17.125582	13.052332
H	14.495080	17.158578	14.319892
H	14.900310	7.221408	18.702362
H	6.238302	11.061758	23.802664
H	7.829814	10.449217	24.252493

H	6.452519	9.347970	24.193540
H	12.781231	9.937073	23.572008
H	11.243704	9.761391	24.424461
H	11.679460	11.319954	23.718338
H	10.282805	13.102985	20.447026
H	11.103888	14.102911	21.654242
H	10.263906	12.625391	22.152167
H	13.041659	5.016277	13.552512
H	11.586957	4.242365	14.187980
H	13.175768	3.671294	14.696592
H	17.857844	9.731016	21.554808
H	17.036224	9.029448	22.948270
H	16.783859	10.727886	22.542108
H	8.926147	15.374036	15.241994
H	8.981472	13.600922	15.076447
H	9.122448	14.322533	16.663178

! Internal C-H activation from the Phosphido - Product !

C	13.380569000	9.683176000	20.580206000
C	13.501339000	8.648258000	19.603469000
C	14.770542000	8.017253000	19.503492000
C	15.830962000	8.381855000	20.318071000
C	15.714901000	9.392551000	21.282649000
C	14.471844000	10.023897000	21.382988000
N	12.431531000	8.327141000	18.821720755
C	12.560210245	7.384455000	17.776790000
C	12.735244510	7.890124755	16.447513000
C	12.734186000	6.945675245	15.387967000
C	12.645949000	5.578911000	15.604082000
C	12.519317000	5.112650000	16.920504000

C	12.464538000	5.991894000	18.002584000
C	12.914149000	9.307453225	16.229965755
C	12.683732000	4.607370000	14.451390000
C	12.328785000	5.471774000	19.407081000
C	16.877197000	9.786469000	22.156307000
P	11.729685000	10.506823000	20.674305000
C	12.121283000	12.293977000	21.158089000
C	12.960371000	12.973561000	20.076510000
La	10.607450000	9.574410000	17.734427000
P	10.916707000	11.966274000	16.584346000
C	11.725863000	13.455342000	15.860696000
C	10.888086000	14.530650000	15.451226000
C	11.446953000	15.695386000	14.924498000
C	12.825792000	15.862593000	14.779620000
C	13.642757000	14.813595000	15.200052000
C	13.128570000	13.628234000	15.732743000
C	9.391905000	14.447727000	15.589953000
C	13.404055000	17.115309000	14.174854000
C	14.092103000	12.561657000	16.167211000
N	8.111470000	9.069270000	18.148465000
C	7.794290000	9.347786000	19.499242000
C	7.526237000	10.671231000	19.927717000
C	7.222801000	10.908925000	21.271887000
C	7.160287000	9.881002000	22.215204000
C	7.411459000	8.579272000	21.775469000
C	7.725090000	8.296819000	20.444168000
C	7.490757000	11.801367000	18.934904000
C	6.848405000	10.167750000	23.661578000
C	7.928060000	6.874920000	19.996576000
C	7.042643000	8.862555000	17.313408000
C	7.217737000	8.565018000	15.925273000

C	6.107549000	8.420282000	15.085473000
C	4.789235000	8.519584000	15.531921000
C	4.615568000	8.764213000	16.900672000
C	5.689062000	8.927126000	17.759554000
P	8.941970000	8.363645000	15.307203000
C	9.074955000	6.497992000	14.938726000
C	8.145922000	5.945374000	13.860388000
C	3.618726000	8.387448000	14.593449000
C	8.914002000	9.136215000	13.578325000
C	8.502741000	10.605810000	13.650498000
C	10.290237000	8.980782000	12.927349000
C	10.994347000	9.779005000	22.280550000
C	10.990716000	8.253717000	22.174144000
C	11.662597000	10.222966000	23.580418000
C	10.812965000	13.053825000	21.389042000
C	8.907134000	5.728494000	16.248933000
H	12.880162755	7.322017000	14.373952000
H	5.498209000	9.124042000	18.810023000
H	6.275958000	8.231805000	14.026783000
H	7.489602000	10.721672000	14.045150000
H	8.534409000	11.053148000	12.648435000
H	9.185810000	11.165094000	14.296411245
H	12.692816000	12.272905000	22.094952000
H	3.606594000	8.836522000	17.307082000
H	7.095592000	6.053544000	14.149381000
H	8.338186000	4.873643000	13.717000000
H	8.286086000	6.431949000	12.889812000
H	10.116245000	6.386653000	14.612390000
H	10.779057000	16.501551000	14.620009000
H	10.500231000	7.915648000	21.258473000
H	10.454345000	7.814487000	23.024430000

H	12.013101000	7.862065000	22.172889000
H	12.454847000	4.041177000	17.105775000
H	9.953188000	10.124156000	22.269831000
H	7.350720000	7.755738000	22.486298000
H	14.724847000	14.918601000	15.117650000
H	8.446206000	11.942449000	18.413363000
H	7.235941000	12.743494000	19.430352000
H	6.743790000	11.609261000	18.156737000
H	7.008211000	11.930353000	21.584304000
H	9.638798000	6.044773000	16.997445000
H	9.053397000	4.653859000	16.082867000
H	7.903011000	5.873974000	16.661538000
H	13.912789000	12.458937000	19.920557000
H	13.177076000	14.010412000	20.364531000
H	12.421754000	12.991708000	19.122118000
H	8.174611000	8.587139000	12.981249000
H	13.161156204	9.559939775	15.195997755
H	13.625822204	9.757718775	16.925617020
H	11.796406776	11.009619447	16.317045775
H	14.360615000	10.830730000	22.105576000
H	13.241797000	5.649731000	19.988274000
H	12.123712000	4.396768000	19.412139000
H	11.523734000	5.987078000	19.940379000
H	11.053309000	9.496401245	13.515674000
H	10.285324000	9.420873000	11.922214000
H	10.592227000	7.932560000	12.829677000
H	2.870434000	7.678034000	14.969286000
H	3.939630000	8.033483000	13.607987000
H	3.100251000	9.343965000	14.440454000
H	16.785671000	7.870442000	20.194555000
H	7.172588000	6.588001000	19.256703000

H	7.864310000	6.182737000	20.841840000
H	8.899113000	6.735412000	19.510404000
H	14.083835000	11.708163000	15.485073755
H	13.823568000	12.167568000	17.153355000
H	15.116561000	12.946950000	16.207144000
H	12.814242000	18.000232000	14.439785000
H	13.430207000	17.065349000	13.077308000
H	14.432019000	17.285196000	14.513154000
H	14.906132000	7.244307000	18.751650000
H	6.311624000	9.334915000	24.128357000
H	6.232067000	11.066616000	23.767280000
H	7.762082000	10.331470000	24.247886000
H	12.718647000	9.932753000	23.600232000
H	11.174468000	9.737871000	24.436445000
H	11.601499000	11.303752000	23.741279000
H	10.220928000	13.082697000	20.468247000
H	11.022906000	14.090319000	21.682089000
H	10.194783000	12.603688000	22.172732000
H	13.044530000	5.087752000	13.536511000
H	11.688513000	4.196951000	14.236276000
H	13.340655000	3.756255000	14.665133000
H	16.604704000	10.605391000	22.830302000
H	17.739922000	10.123464000	21.566739000
H	17.225803000	8.952936000	22.780715000
H	8.912543000	15.357739000	15.212168000
H	8.987396000	13.585390000	15.048381000
H	9.091311245	14.313728755	16.636984000

! H abstraction by HMDS on the adjacent methyl group - Adduct !

C	-0.380186000	-5.237164000	1.613583000

C	0.094947000	-4.687347000	0.395554000
C	-0.121847000	-5.412572000	-0.802104000
C	-0.786474000	-6.639052000	-0.767218000
C	-1.252321000	-7.194942000	0.424206000
C	-1.036768000	-6.470032000	1.597563000
P	1.025562000	-3.104032000	0.281697000
La	0.801161000	-0.316272000	-0.681916000
P	-2.321103000	-0.338115000	-1.189568000
C	-3.458141000	-1.726633000	-0.601726000
C	-3.625858000	-1.641101000	0.916825000
C	0.353795000	-4.867961000	-2.119260000
C	-1.938439000	-8.535652000	0.449590000
C	-0.211685000	-4.533904000	2.932731000
C	0.675216000	2.151232000	0.935695000
C	0.568056000	3.460012000	0.397896000
C	-0.541754000	4.235742000	0.727424000
C	-1.555410000	3.765552000	1.572919000
C	-1.449281000	2.473574000	2.093266000
C	-0.349450000	1.661592000	1.783098000
C	1.675122000	4.029894000	-0.446491000
N	1.810433000	1.340461000	0.649241000
C	2.958119000	1.542821000	1.390507000
C	4.141577000	0.806753000	1.107735000
C	5.287709000	0.991889000	1.890711000
C	5.340160000	1.895325000	2.952414000
C	4.172734000	2.623984000	3.218932000
C	3.018143000	2.458216000	2.471155000
C	-0.215442000	0.319205000	2.462796000
C	-2.734510000	4.621901000	1.950896000
P	4.064420000	-0.388215000	-0.294568000
C	5.127294000	-1.843355000	0.292082000

C	5.200181000	-2.904041000	-0.808623000
C	6.586491000	2.077141000	3.778343000
N	0.138910000	0.030234000	-2.987302000
C	-1.015442000	-0.294366000	-3.690089000
C	-2.251335000	-0.540724000	-3.026594000
C	-3.377906000	-0.924812000	-3.763511000
C	-3.372696000	-1.061110000	-5.152240000
C	-2.163528000	-0.789145000	-5.802385000
C	-1.024454000	-0.421211000	-5.102940000
C	-4.602856000	-1.479602000	-5.913779000
C	5.167362000	0.412567000	-1.631653000
C	6.655887000	0.514202000	-1.305262000
C	4.594166000	1.784835000	-1.981368000
C	1.255459000	0.428968000	-3.770325000
C	2.264027000	-0.504069000	-4.104860000
C	3.350983000	-0.095615000	-4.886404000
C	3.473967000	1.210529000	-5.358284000
C	2.464769000	2.119585000	-5.028379000
C	1.364365000	1.758665000	-4.250850000
C	2.136918000	-1.949609000	-3.698370000
C	4.658847000	1.634788000	-6.185670000
C	0.280551000	2.759574000	-3.967186000
C	-3.358222000	1.233043000	-0.924094000
C	-2.668980000	2.410851000	-1.609775000
C	-4.823981000	1.141346000	-1.341483000
C	-2.920947000	-3.090405000	-1.027243000
C	4.604272000	-2.441287000	1.597367000
N	-3.520766000	2.306215000	4.527634000
Si	-2.756718000	2.837375000	5.968064000
C	-3.410867000	4.520721000	6.679309000
Si	-5.090192000	1.632697000	4.417878000

C	-5.202033000	-0.271944000	4.770503000
C	-5.797793000	1.840558000	2.630218000
C	-6.474792000	2.379794000	5.556892000
C	-2.822128000	1.637874000	7.494546000
C	-0.870898000	3.139649000	5.684043000
H	-0.940938000	0.247027000	3.277249000
H	-4.524473000	-0.829909000	4.114878000
H	1.180823000	-2.803280000	1.669186000
H	-2.199761000	2.155165000	2.834953000
H	-0.105318000	-0.235523000	-5.649839000
H	-4.302482000	-1.133475000	-3.230218000
H	-2.844049000	-3.179282000	-2.114493000
H	-3.587481000	-3.883383000	-0.668502000
H	-1.933377000	-3.275364000	-0.593802000
H	6.132793000	-1.442983000	0.471008000
H	-2.106016000	-0.876500000	-6.886710000
H	-4.923832000	0.977994000	-2.419864000
H	-5.326728000	2.085539000	-1.101320000
H	-5.367870000	0.352347000	-0.815069000
H	-3.302897000	1.390003000	0.159858000
H	-0.944016000	-7.173385000	-1.703620000
H	3.560262000	1.715070000	-2.329015000
H	5.178729000	2.246391000	-2.785867000
H	4.622969000	2.454117000	-1.115558000
H	-0.607983000	5.248081000	0.329208000
H	5.035283000	-0.242511000	-2.502472000
H	2.531367000	3.143090000	-5.394630000
H	-1.400507000	-6.873253000	2.542050000
H	1.134855000	-2.331204000	-3.912750000
H	2.327695000	-2.119029000	-2.629091000
H	2.862427000	-2.566990000	-4.236300000

H	4.108848000	-0.830953000	-5.153311000
H	-1.650690000	2.558312000	-1.240394000
H	-3.222385000	3.335125000	-1.408476000
H	-2.633460000	2.266854000	-2.694792000
H	4.544441000	-1.695052000	2.394162000
H	5.276254000	-3.241809000	1.931698000
H	3.612323000	-2.880192000	1.451765000
H	-4.434695000	-1.564554000	-1.074585000
H	0.789992000	0.172845000	2.869834000
H	-0.430227000	-0.546420000	1.809375000
H	-0.130452000	-3.910960000	-2.354479000
H	0.138714000	-5.560621000	-2.938508000
H	1.434713000	-4.677047000	-2.099843000
H	6.173613000	0.397285000	1.676683000
H	2.575052000	4.206792000	0.154961000
H	1.374147000	4.982323000	-0.892504000
H	1.970522000	3.347286000	-1.249059000
H	-2.665817000	-1.784849000	1.423786000
H	-4.301058000	-2.431718000	1.263552000
H	-4.042988000	-0.686586000	1.249258000
H	-5.453355000	-1.628916000	-5.241660000
H	-4.445233000	-2.419707000	-6.457262000
H	-4.898090000	-0.727245000	-6.655736000
H	4.160891000	3.332388000	4.045813000
H	-0.663720000	2.454227000	-4.431331000
H	0.548596000	3.747116000	-4.353143000
H	0.084494000	2.849177000	-2.895247000
H	0.845909000	-4.415710000	3.199109000
H	-0.697386000	-5.094373000	3.736887000
H	-0.646058000	-3.527643000	2.912490000
H	-2.707486000	-8.577930000	1.228253000

H	-1.229890000	-9.349958000	0.652620000
H	-2.419411000	-8.757385000	-0.508758000
H	2.127456000	3.023156000	2.728604000
H	5.420887000	2.128382000	-5.569219000
H	4.368172000	2.344962000	-6.966825000
H	5.136809000	0.777356000	-6.669393000
H	6.825187000	1.139484000	-0.422998000
H	7.185570000	0.983227000	-2.144455000
H	7.122740000	-0.460091000	-1.132339000
H	4.205280000	-3.320707000	-1.000717000
H	5.850390000	-3.729949000	-0.495073000
H	5.599294000	-2.508445000	-1.748953000
H	-2.431390000	5.658035000	2.141120000
H	-3.218548000	4.207348000	2.844155000
H	-3.477230000	4.646969000	1.142332000
H	7.370362000	1.376561000	3.473400000
H	6.393951000	1.912237000	4.845390000
H	6.996388000	3.090688000	3.681475000
H	-2.860287000	4.820557000	7.580075000
H	-3.306703000	5.316885000	5.933720000
H	-4.472944000	4.445302000	6.936496000
H	-2.277069000	2.054511000	8.350954000
H	-3.855602000	1.453692000	7.809435000
H	-2.374622000	0.670016000	7.242948000
H	-0.398524000	3.541766000	6.588516000
H	-0.360866000	2.206709000	5.420903000
H	-0.707137000	3.849528000	4.866660000
H	-6.219314000	-0.655149000	4.619435000
H	-4.907829000	-0.485755000	5.804065000
H	-6.753955000	1.316979000	2.511268000
H	-5.955715000	2.899843000	2.400143000

H	-5.095726000	1.443715000	1.888922000
H	-7.442595000	1.897553000	5.370260000
H	-6.228941000	2.244496000	6.616217000
H	-6.587034000	3.454650000	5.377199000

! H abstraction by HMDS on the adjacent methyl group - Transition State !

C	8.850269	5.463865	15.359350
C	10.140585	5.851415	14.874698
C	10.290753	5.828443	13.458309
C	9.286981	5.396194	12.607824
C	8.047734	4.954993	13.087710
C	7.866118	5.014839	14.468860
N	11.170277	6.223378	15.720273
C	12.309721	6.783601	15.073023
C	13.364275	5.976200	14.583593
C	14.452288	6.569475	13.934020
C	14.547628	7.947534	13.749969
C	13.496586	8.734611	14.224082
C	12.383997	8.183851	14.863582
C	13.319708	4.477046	14.703058
C	15.743237	8.567948	13.075995
C	11.245247	9.075644	15.269402
C	6.975941	4.438935	12.164334
P	8.491963	5.639903	17.161716
C	7.382774	4.160179	17.573037
C	6.960442	4.233353	19.041591
La	11.494796	5.917026	18.221725
P	11.045237	3.520475	19.754319
C	10.985342	1.682766	19.793859
C	11.302692	0.952585	18.619503

C	11.268013	-0.440375	18.619741
C	10.923823	-1.174733	19.756204
C	10.607688	-0.449349	20.910056
C	10.631009	0.942451	20.958790
C	11.671248	1.724757	17.392802
C	10.918185	-2.681468	19.751426
C	10.279908	1.665414	22.230376
P	14.701868	5.452113	18.831442
C	15.390477	3.902037	19.673117
C	15.462696	2.738714	18.681559
C	16.072928	5.920426	17.588253
C	17.510978	5.746107	18.073428
C	14.852634	6.747420	20.138872
C	13.804185	7.708955	20.218570
C	13.933143	8.707828	21.218970
C	15.021857	8.746009	22.074297
C	16.052177	7.797697	22.006069
C	15.932087	6.810221	21.027713
N	12.727361	7.631194	19.372688
C	11.724327	8.626893	19.392644
C	10.433319	8.293289	19.893687
C	9.408654	9.258156	19.784167
C	9.622717	10.518499	19.245125
C	10.908256	10.831667	18.776185
C	11.950577	9.912664	18.827800
C	10.150608	7.022490	20.608702
C	8.515341	11.537875	19.173234
C	13.302187	10.271316	18.275155
C	17.217344	7.832005	22.959879
C	7.261800	7.099260	17.260412
C	7.886460	8.327682	16.603311

C	5.860929	6.846982	16.705848
C	15.831501	7.354209	17.116369
C	14.544876	3.539287	20.894328
C	8.060437	2.828168	17.260841
N	8.978902	7.497497	23.217977
Si	10.136189	7.764372	24.479544
C	11.785675	6.858398	24.096350
Si	7.262936	7.472558	23.405077
C	6.518823	8.954427	24.401068
C	6.562121	5.887941	24.261685
C	6.377483	7.538437	21.694955
C	10.585404	9.623302	24.744464
C	9.605062	7.119825	26.224138
H	9.588236	7.279487	21.864764
H	6.846430	4.993353	23.697359
H	10.710336	4.019112	21.041021
H	8.436531	9.011076	20.201222
H	11.233618	6.152477	13.030381
H	6.907955	4.692770	14.871706
H	8.388281	2.772298	16.218865
H	7.356927	2.004837	17.437017
H	8.924572	2.657421	17.908540
H	16.408153	4.140654	20.006706
H	9.477442	5.395212	11.534839
H	5.892828	6.624190	15.634335
H	5.250163	7.749698	16.833773
H	5.339611	6.031021	17.214607
H	7.187363	7.286526	18.339632
H	11.515408	-0.966601	17.697607
H	14.831458	7.482131	16.694638
H	16.555497	7.622995	16.338038

H	15.946587	8.058502	17.946432
H	11.097100	11.816660	18.350661
H	15.900438	5.245149	16.739327
H	13.529566	9.812914	14.074012
H	10.329793	-0.990826	21.814690
H	12.301198	4.096487	14.601058
H	13.699889	4.140094	15.674237
H	13.944427	4.010157	13.934873
H	15.243775	5.925973	13.551193
H	8.860452	8.567249	17.035296
H	7.238924	9.201255	16.744999
H	8.011797	8.169902	15.527086
H	14.566942	4.331604	21.647253
H	14.924524	2.618869	21.354893
H	13.502157	3.369134	20.609117
H	6.489507	4.251494	16.943145
H	11.044994	6.438695	20.849297
H	9.352097	6.410269	20.169308
H	10.843371	2.355498	17.035558
H	11.961433	1.073745	16.562909
H	12.522600	2.389890	17.598945
H	16.708283	6.049653	20.971181
H	14.068778	10.285388	19.058435
H	13.279256	11.257383	17.801270
H	13.629405	9.537540	17.531343
H	7.834594	4.171853	19.698112
H	6.301242	3.392355	19.288682
H	6.422243	5.155230	19.282009
H	6.015713	4.347274	12.682292
H	7.222281	3.447644	11.760457
H	6.825301	5.103960	11.305318

H	15.063633	9.526956	22.832267
H	10.309086	8.743436	14.810932
H	11.432635	10.108411	14.960934
H	11.088369	9.078125	16.352358
H	11.111785	2.280615	22.599231
H	10.019129	0.959916	23.024305
H	9.426009	2.343542	22.100951
H	10.842604	-3.076212	18.732550
H	10.075586	-3.084681	20.325256
H	11.833399	-3.100288	20.192791
H	13.138019	9.440146	21.323511
H	16.481346	8.914628	13.810581
H	15.458317	9.436311	12.472501
H	16.249054	7.852464	12.419746
H	17.717855	6.396873	18.928858
H	18.208488	6.026635	17.273364
H	17.742992	4.716001	18.361326
H	14.460907	2.418818	18.378412
H	15.948337	1.874090	19.150595
H	16.031632	2.986323	17.778719
H	8.808429	12.479870	19.651690
H	7.611473	11.178228	19.672768
H	8.252451	11.774070	18.134322
H	17.943785	7.046975	22.726028
H	16.898003	7.683411	23.999349
H	17.747866	8.792018	22.923640
H	11.366143	9.745555	25.505079
H	10.943870	10.062499	23.807799
H	9.704593	10.191874	25.061942
H	10.388899	7.330348	26.961814
H	8.680386	7.591043	26.573671

H	9.442671	6.037159	26.200301
H	12.514704	7.020765	24.898846
H	11.612143	5.780761	24.006574
H	12.233730	7.209143	23.162154
H	5.467509	5.921196	24.325775
H	6.960355	5.781397	25.275791
H	5.309053	7.321339	21.807504
H	6.471616	8.529086	21.238200
H	6.804735	6.801884	21.007657
H	5.424684	8.889489	24.443295
H	6.894323	8.978560	25.429667
H	6.789521	9.903496	23.926356

! H abstraction by HMDS on the adjacent methyl group - Product !

C	-0.177572000	3.886846000	-0.052002000
C	-0.064638000	2.558827000	0.429399000
C	-1.222378000	1.864241000	0.913434000
C	-2.460977000	2.553478000	0.856321000
C	-2.571921000	3.862461000	0.408626000
C	-1.418108000	4.522124000	-0.044503000
La	0.294553000	-0.083424000	-0.752673000
C	-1.112578000	0.487185000	1.354690000
N	1.165733000	1.853789000	0.416058000
C	2.119611000	2.142793000	1.357553000
C	3.346487000	1.413481000	1.386360000
C	4.321761000	1.711956000	2.341565000
C	4.161275000	2.710476000	3.305992000
C	2.947636000	3.410124000	3.288677000
C	1.956327000	3.139808000	2.356960000
P	3.528952000	0.079378000	0.121320000

C	4.733930000	0.870988000	-1.136590000
C	4.174512000	2.221924000	-1.581245000
C	5.240695000	3.023663000	4.308910000
C	-3.903884000	4.569088000	0.397201000
C	1.041774000	4.613602000	-0.548731000
N	0.146991000	-0.066471000	-3.301898000
C	1.424760000	0.207251000	-3.855497000
C	2.403085000	-0.809225000	-3.970723000
C	3.648513000	-0.506932000	-4.531694000
C	3.964003000	0.769527000	-4.999461000
C	2.983617000	1.758454000	-4.896533000
C	1.730878000	1.503903000	-4.335213000
C	2.086212000	-2.225634000	-3.574292000
C	5.320564000	1.074085000	-5.580042000
C	0.693936000	2.590965000	-4.282656000
C	-0.813779000	-0.455521000	-4.209317000
C	-2.172976000	-0.664075000	-3.821393000
C	-3.109543000	-1.136802000	-4.747120000
C	-2.802941000	-1.395807000	-6.083798000
C	-1.483812000	-1.138957000	-6.477750000
C	-0.525854000	-0.685795000	-5.585741000
P	-2.625053000	-0.253055000	-2.081379000
C	-3.694671000	1.314685000	-2.255280000
C	-5.003879000	1.157116000	-3.024506000
C	-3.829166000	-1.933748000	-7.045969000
C	-3.888569000	-1.579530000	-1.614463000
C	-3.243499000	-2.962384000	-1.676512000
C	-4.456637000	-1.291246000	-0.223240000
P	0.888960000	-2.955649000	0.203030000
C	-0.434595000	-4.220509000	0.471487000
C	-0.642438000	-5.175643000	-0.558222000

C	-1.576191000	-6.199258000	-0.395746000
C	-2.336080000	-6.332625000	0.767559000
C	-2.130712000	-5.388556000	1.774412000
C	-1.205816000	-4.347203000	1.656352000
C	0.136159000	-5.089658000	-1.841325000
C	-3.314783000	-7.465079000	0.940320000
C	-1.062938000	-3.386553000	2.804825000
C	4.631568000	-1.210938000	0.965546000
C	3.985737000	-1.768697000	2.233884000
C	4.943903000	-2.332071000	-0.029554000
C	6.179407000	1.026978000	-0.667313000
C	-2.842163000	2.432631000	-2.852631000
N	-1.819588000	0.851617000	5.346569000
Si	-3.528219000	0.855130000	5.808376000
C	-4.562601000	1.107273000	4.225397000
Si	-0.357530000	1.004024000	6.342184000
C	-0.616575000	0.071431000	7.994310000
C	1.103967000	0.236194000	5.394808000
C	0.050739000	2.829195000	6.753741000
C	-3.904556000	2.274842000	7.038627000
C	-4.056961000	-0.789259000	6.634551000
H	-1.649166000	0.839110000	4.344747000
H	-3.872689000	-1.629856000	5.958699000
H	0.845775000	-2.342403000	1.499861000
H	-3.345878000	2.042772000	1.233625000
H	0.484308000	-0.512440000	-5.942838000
H	-4.127971000	-1.320008000	-4.410260000
H	-2.876958000	-3.190386000	-2.681202000
H	-3.969116000	-3.735202000	-1.396172000
H	-2.401793000	-3.045860000	-0.981892000
H	5.566761000	-0.709192000	1.243346000

H	-1.192668000	-1.306590000	-7.514697000
H	-4.818848000	0.891121000	-4.070144000
H	-5.551882000	2.108621000	-3.020710000
H	-5.665031000	0.400909000	-2.589682000
H	-3.913574000	1.580161000	-1.214046000
H	-1.712281000	-6.913709000	-1.207820000
H	3.148930000	2.136189000	-1.945833000
H	4.782162000	2.632836000	-2.396175000
H	4.182951000	2.936282000	-0.751743000
H	-1.491403000	5.546595000	-0.406820000
H	4.703077000	0.189160000	-1.995426000
H	3.196925000	2.760738000	-5.266540000
H	-2.714659000	-5.460043000	2.692208000
H	1.172298000	-2.570819000	-4.068481000
H	1.926056000	-2.344081000	-2.495844000
H	2.903100000	-2.897325000	-3.855360000
H	4.384681000	-1.304604000	-4.625663000
H	-1.957683000	2.633447000	-2.242647000
H	-3.421173000	3.362802000	-2.908394000
H	-2.518027000	2.177072000	-3.866906000
H	3.729887000	-0.977846000	2.944332000
H	4.679788000	-2.459576000	2.729990000
H	3.077706000	-2.330175000	1.994490000
H	-4.705883000	-1.537317000	-2.345619000
H	-0.250867000	0.278734000	1.999633000
H	-2.032580000	0.045276000	1.736753000
H	-0.084048000	-4.159701000	-2.380907000
H	-0.096890000	-5.927916000	-2.505756000
H	1.216836000	-5.085555000	-1.647422000
H	5.242948000	1.132219000	2.350871000
H	1.713078000	4.881310000	0.276640000

H	0.764779000	5.532937000	-1.073907000
H	1.625807000	3.982562000	-1.225012000
H	-3.658302000	-1.286348000	0.525730000
H	-5.176002000	-2.069482000	0.059964000
H	-4.973131000	-0.326754000	-0.172887000
H	-4.833861000	-1.903183000	-6.611426000
H	-3.628257000	-2.977507000	-7.323437000
H	-3.856594000	-1.356876000	-7.978931000
H	2.768396000	4.185359000	4.033325000
H	-0.180381000	2.327370000	-4.887807000
H	1.097958000	3.536787000	-4.656253000
H	0.328212000	2.751230000	-3.263803000
H	-0.062143000	-3.439140000	3.252214000
H	-1.792918000	-3.605393000	3.590919000
H	-1.204650000	-2.349376000	2.480924000
H	-4.113105000	-7.200915000	1.642303000
H	-2.828837000	-8.369920000	1.331156000
H	-3.784210000	-7.740063000	-0.010886000
H	1.020187000	3.689883000	2.391118000
H	6.013180000	1.443108000	-4.812344000
H	5.260789000	1.843954000	-6.356637000
H	5.775779000	0.182485000	-6.023592000
H	6.239403000	1.657878000	0.226274000
H	6.771540000	1.516911000	-1.451665000
H	6.662802000	0.070723000	-0.446276000
H	4.022871000	-2.848240000	-0.321834000
H	5.610125000	-3.072717000	0.430927000
H	5.435661000	-1.963583000	-0.936631000
H	-3.831993000	5.567774000	0.844072000
H	-4.659384000	4.006567000	0.954456000
H	-4.279453000	4.703359000	-0.625345000

H	5.762838000	3.962249000	4.076445000
H	5.997051000	2.232269000	4.336946000
H	4.835787000	3.128325000	5.322747000
H	0.941898000	2.894644000	7.388066000
H	0.245382000	3.389201000	5.834261000
H	-0.780227000	3.312274000	7.277100000
H	0.278439000	0.163500000	8.619003000
H	-1.461756000	0.469249000	8.565058000
H	-0.797657000	-0.991481000	7.809602000
H	2.020933000	0.289601000	5.991162000
H	0.904749000	-0.813897000	5.161841000
H	1.287940000	0.768183000	4.456382000
H	-5.124521000	-0.772658000	6.881380000
H	-3.496906000	-0.969930000	7.556829000
H	-5.630866000	1.147713000	4.462906000
H	-4.282868000	2.039912000	3.726856000
H	-4.402710000	0.285364000	3.520938000
H	-4.956975000	2.251000000	7.342248000
H	-3.293909000	2.197738000	7.943913000
H	-3.700878000	3.244886000	6.575237000

6. Literature

1 a) M. E. Garner, J. Arnold, Reductive Elimination of Diphosphine from a Thorium–NHC–Bis(phosphido) Complex, *Organometallics*, **2017**, 36, 4511–4514. b) M.E. Garner, B.F. Parker, S. Hohloch, R.G. Bergman, J. Arnold, Thorium Metallacycle Facilitates Catalytic Alkyne Hydrophosphination, *J. Am. Chem. Soc.*, **2017**, 139, 12935–12338. c) F. A. Watt, A. Krishna, G. Golovanov, H. Ott, R. Schoch, C. Wölper, A. G. Neuba and S. Hohloch, Monoanionic Anilidophosphine Ligand in Lanthanide Chemistry: Scope, Reactivity, and Electrochemistry, *Inorg. Chem.*, 2020, **59**, 2719–2732.

2 S. Kundu, S. Sinhababu, M. M. Siddiqui, A. V. Luebben, B. Dittrich, T. Yang, G. Frenking and H. W. Roesky, Comparison of Two Phosphinidenes Binding to Silicon(IV)dichloride as well as to Silylene, *J. Am. Chem. Soc.*, 2018, **140**, 9409–9412.

3 G. M. Sheldrick, Crystal structure refinement with SHELXL, *Acta Cryst. C,* 2015, **71**, 3–8.

4 G. M. Sheldrick, SHELXT - integrated space-group and crystal-structure determination, *Acta Cryst. A,* 2015, **71**, 3–8.

5 O. V. Dolomanov, L. J. Bourhis, R. J. Gildea, J. A. K. Howard and H. Puschmann, OLEX2 : a complete structure solution, refinement and analysis program, *J Appl Crystallogr*, 2009, **42**, 339–341.

6 Gaussian 09, Revision D.01, M. J. Frisch, G. W. Trucks, H. B. Schlegel, G. E. Scuseria, M. A. Robb, J. R. Cheeseman, G. Scalmani, V. Barone, G. A. Petersson, H. Nakatsuji, X. Li, M. Caricato, A. Marenich, J. Bloino, B. G. Janesko, R. Gomperts, B. Mennucci, H. P. Hratchian, J. V. Ortiz, A. F. Izmaylov, J. L. Sonnenberg, D. Williams-Young, F. Ding, F. Lipparini, F. Egidi, J. Goings, B. Peng, A. Petrone, T. Henderson, D. Ranasinghe, V. G. Zakrzewski, J. Gao, N. Rega, G. Zheng, W. Liang, M. Hada, M. Ehara, K. Toyota, R. Fukuda, J. Hasegawa, M. Ishida, T. Nakajima, Y. Honda, O. Kitao, H. Nakai, T. Vreven, K. Throssell, J. A. Montgomery, Jr., J. E. Peralta, F. Ogliaro, M. Bearpark, J. J. Heyd, E. Brothers, K. N. Kudin, V. N. Staroverov, T. Keith, R. Kobayashi, J. Normand, K. Raghavachari, A. Rendell, J. C. Burant, S. S. Iyengar, J. Tomasi, M. Cossi, J. M. Millam, M. Klene, C. Adamo, R. Cammi, J. W. Ochterski, R. L. Martin, K. Morokuma, O. Farkas, J. B. Foresman, and D. J. Fox, Gaussian, Inc., Wallingford CT, 2016.

7 (a) A. D. Becke, Density-functional thermochemistry. III. The role of exact exchange. *J. Chem. Phys.*, 1993, **98**, 5648-5652, and references cited therein; (b) K. Burke, J. P. Perdew, W. Yang, Electronic Density Functional Theory: Recent Progress and New Directions. (Plenum, New York, 1998).

8 M. Dolg, U. Wedig, H. Stoll, H. Preuss, Energy-adjusted *ab initio* pseudopotentials for the first row transition elements, *J. Chem. Phys.,* 1987, **86**, 866-872.

9 A. W. Ehlers et al., A set of f-polarization functions for pseudo-potential basis sets of the transition metals Sc-Cu, Y-Ag and La-Au. *Chem. Phys. Lett.*, 1993, **208**, 111-114.

10 (a) P. C. Hariharan, J. A. Pople, The influence of polarization functions on molecular orbital hydrogenation energies. *Theor. Chem. Acc.*, 1973, **28**, 213-222; (b) W. J. Hehre, R. Ditchfield, J. A. Pople, Self—Consistent Molecular Orbital Methods. XII. Further Extensions of Gaussian—Type Basis Sets for Use in Molecular Orbital Studies of Organic Molecules. J. Chem. Phys. 1972, **56**, 2257-2261.

Supporting Information
for
Chapter 4

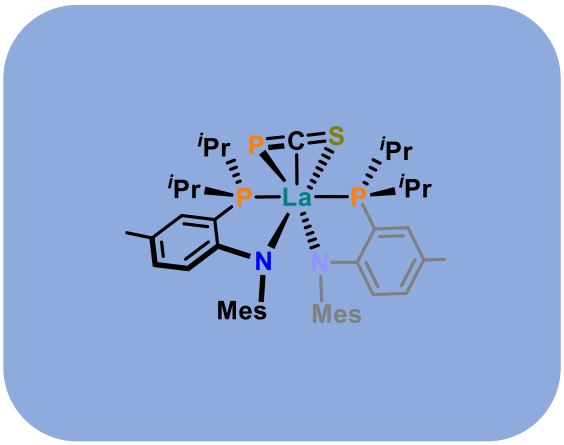

Angewandte Chemie
Eine Zeitschrift der Gesellschaft Deutscher Chemiker

Supporting Information

η^3-Coordination and Functionalization of the 2-Phosphaethynthiolate Anion at Lanthanum(III)**

Fabian A. Watt, Lukas Burkhardt, Roland Schoch, Stefan Mitzinger, Matthias Bauer, Florian Weigend, Jose M. Goicoechea,* Frank Tambornino,* and Stephan Hohloch**

anie_202100559_sm_miscellaneous_information.pdf

WILEY-VCH

SUPPORTING INFORMATION

Table of Contents

WILEY-VCH

SUPPORTING INFORMATION

1. Experimental Procedures

General Remarks.
If not otherwise mentioned, all transformations were carried out under inert conditions using an argon filled glovebox. All glassware (including glass-fibre filters) was stored in an oven at 150 °C for at least 12 h prior to use. Solvents (toluene, *n*-pentane, *n*-hexane, THF, acetonitrile, dichloromethane) were dried by a MBraun SPS system, degassed and stored over activated molecular sieves (3 Å) for at least 24 h prior to use. Pyridine, benzene and hexamethyldisiloxane (HMDSO) were degassed and stored over activated molecular sieves (3 Å) for at least 48 h prior to use. C_6D_6 was dried by storage over activated molecular sieves (3 Å) for at least 24 h prior to use. IR spectra were recorded at room temperature under inert conditions using a Bruker Vertex 70 with ATR equipment. If not otherwise stated, the NMR spectra were collected at 303 K on a Bruker AV-500 or an Ascent 700 spectrometer using a J-Young NMR tube. All chemical shifts (δ) are reported in ppm and coupling constants are given in Hz. ^{1}H and ^{13}C chemical shifts were calibrated to residual solvent peaks. ^{15}N chemical shifts (obtained by ^{1}H–^{15}N HMBC NMR spectroscopy) were calibrated externally to liquid ammonia (NH_3). ^{31}P chemical shifts were calibrated externally to phosphoric acid (H_3PO_4, 85% in water). Elemental analyses were performed using an Elementar vario microcube instrument at the Paderborn University. Starting materials **1-Cl**,[1] **1-I**,[1] **Na(diox)$_{2.3}$SCP**,[2] **^{Ad}CAAC**[3] and **^{Me}CAAC**[4] were synthesized following literature known procedures. **KSCN** and **KN_3** were used as received.

Synthetic Procedures.
Preparation of (PN)$_2$La(SCP) (2). Solid **NaSCP(diox)$_{2.3}$** (210 mg, 700 µmol, 1.4 eq.) was added to a solution of **1-Cl** (428 mg, 500 µmol, 1 eq.) in toluene (8 mL) at room temperature. The reaction mixture was stirred at room temperature for 26 h and then filtered through a glass-fibre filter. All volatile components of the orange-colored filtrate were removed *in vacuo*. The dark orange-colored residue was triturated by repeated addition of *n*-pentane (3 x2 mL) and subsequent removal *in vacuo* to give **2** as an amber microcrystalline solid. Single crystals suitable for X-ray structure determination were obtained by slow evaporation of solvent under reduced pressure from a concentrated toluene solution of **2** during work-up. Yield: 440 mg (490 mmol, 98%); ^{1}H NMR (C_6D_6, 700 MHz, in ppm): δ = 6.91–6.89 (m, C*H*$_{Ar}$, 2 H), 6.85 (br. s, C*H*$_{Ar}$, 4 H), 6.78 (dd, $^3J_{HH}$ = 8.5 Hz, $^4J_{HH}$ = 1.89 Hz, C*H*$_{Ar}$, 2 H), 5.66 (m, C*H*$_{Ar}$, 2 H), 2.28–2.10 (two s at 2.17 & 2.14 & br. s, C*H*$_{3Ar}$ & C*H*$_{iPr}$, 28 H), 1.23–0.92 (two br. s, C*H*$_{3iPr}$, 24 H); ^{13}C{^{1}H} NMR (C_6D_6, 176 MHz, in ppm): δ = 191.8 (d, $^1J_{CP}$ = 20.6 Hz, S*C*P$^-$), 160.6 (*pseudo*-t, J_{CP} = 12.0 Hz, C_{qAr}), 138.7 (s, C_{qAr}), 135.3 (s, C_{qAr}), 133.4 (s, *C*H$_{Ar}$), 133.3 (s, *C*H$_{Ar}$), 131.3 (s, *C*H$_{Ar}$), 123.9 (s, C_{qAr}), 114.1 (d, J_{CP} = 6.5 Hz, C_{qAr}), 114.08 (d, J_{CP} = 6.5 Hz, C_{qAr}), 113.5 (*pseudo*-t, J_{CP} = 3.7 Hz, *C*H$_{Ar}$), 24.2 (br. s, *C*H$_{iPr}$), 21.0 (s, *C*H$_{3Ar}$), 20.6 (s, *C*H$_{3Ar}$), 20.4 (br. s, *C*H$_{3Ar}$), 19.7 (br. s, *C*H$_{3iPr}$), 17.9 (br. s, *C*H$_{3iPr}$); ^{31}P{^{1}H} NMR (C_6D_6, 283 MHz, in ppm): δ = 9.6 (br. s, *P*N$^-$, 2 P), –44.9 (br. s, [SC*P*]$^-$, 1 P); IR (ATR, in cm^{-1}) = 2956(m), 2918(m), 2865(M), 1597(s), 1461(s), 1371(s), 1301(s), 1274(s), 1243(s), 1214(s), 1188(s), 1152(s), 1029(s), 884(s), 854(s), 825(s), 808(s), 710(s), 657(s), 611(s), 543(s), 490(s), 466(s), 435(s), 407(s), 387(s), 364(s), 307(s); elemental analysis (in %): $C_{45}H_{62}LaN_2P_3S$: calcd.: C 60.40, H 6.98, N 3.13; found: C 60.74, H 7.02, N 3.39.

Conversion of 2 into 1-Cl. A solution of **2** (153 mg, 171 µmol) in dichloromethane (4 mL) was stirred outside the glovebox in a pressure Schlenk tube at 45 °C and the reaction monitored by means of ^{31}P{^{1}H} NMR spectroscopy (see Figure S10). For this purpose, the slightly turbid reaction solution was allowed to cool down at the specified reaction times and a sample of 0.6 mL was then transferred to a J-Young NMR tube equipped with a C_6D_6 capillary inside the glovebox. The sample was transferred back to the pressure Schlenk tube after measurement and heating at 45 °C resumed until full conversion was reached (after 68 h). The dark brown precipitate (21 mg) was filtered off and the filtrate concentrated *in vacuo* to about 0.5 mL and then layered with *n*-pentane (ca. 3 mL). Colorless crystals formed within 5 min at room temperature and could be identified as **1-Cl** by X-ray diffraction analysis.[1] After washing with *n*-pentane and drying *in vacuo* **1-Cl** could be isolated in ca. 80% yield (117 mg, 137 µmol). The small amounts of dark brown precipitate were found to be essentially insoluble in other commonly used non-polar (alkanes, arenes) as well as polar (acetonitrile, pyridine, THF) solvents; and elemental analyses did not point to an obvious (defined) co-product of the reaction.

Preparation of (PN)$_2$La(μ-1,3-SCN)$_2$La(PN)$_2$ (3). Solid **KSCN** (23 mg, 240 µmol, 1.2 eq.) was added to a solution of **1-I** (189 mg, 200 µmol, 1 eq.) in THF (3 mL) at room temperature. Within 30 min a fine, colorless precipitate formed and the solution took on a yellow color. After the reaction mixture was stirred for additional 21 h at room temperature, the solvent was removed *in vacuo*. The remaining solid was extracted with toluene (3 mL), centrifuged and the solution filtered through a glass-fibre filter. The filtrate was concentrated under reduced pressure to a volume of about 1 mL and allowed to rest at room temperature for 1 h, during which yellow-colored crystalline blocks formed. The mother liquor was removed with a pipette and the crystals were washed with *n*-hexane (2 x 1.5 mL). After drying *in vacuo* **3** was obtained as a pale yellow microcrystalline solid (57 mg, first batch). By storing the combined toluene mother liquor and *n*-hexane washing solution at –40 °C for 2 d a second batch of the product was obtained as a fine, pale yellow precipitate (52 mg after washing with *n*-hexane and drying *in vacuo*). Single crystals suitable for X-ray structure determination were obtained by gas diffusion of *n*-hexane into a C_6D_6 solution of **3** (20 mg in 0.6 mL C_6D_6) at room temperature overnight. Yield: 109 mg (124 µmol, 62%); ^{1}H NMR (C_6D_6, 700 MHz, in ppm): δ = 6.86–6.84 (m, C*H*$_{Ar}$, 2 H), 6.83 (br. s, C*H*$_{Ar}$, 4 H), 6.79 (dd, $^3J_{HH}$ = 8.4 Hz, $^4J_{HH}$ = 1.7 Hz, C*H*$_{Ar}$, 2 H), 5.59–5.53 (m, C*H*$_{Ar}$, 2 H), 2.15 (s, C*H*$_{3Ar}$, 6 H), 2.13 (br. s, C*H*$_{3Ar}$, 12 H), 2.09 (br. s, C*H*$_{3Ar}$, 6 H), 1.89 (br. s, C*H*$_{iPr}$, 4 H), 1.18–1.12 (br. m, C*H*$_{3iPr}$, 12 H), 0.94–0.86 (br. m, C*H*$_{3iPr}$, 12 H); ^{13}C{^{1}H} NMR (C_6D_6, 176 MHz, in ppm): δ = 159.9 (*pseudo*-t, J_{CP} = 11.2 Hz, C_{qAr}), 142.6 (br. s, [S*C*N]$^-$), 138.2 (br. s, C_{qAr}), 136.8 (br. s, C_{qAr}), 135.8 (br. s, C_{qAr}), 133.8 (s, *C*H$_{Ar}$), 133.4 (s, *C*H$_{Ar}$), 131.9 (s, *C*H$_{Ar}$), 123.7 (s, C_{qAr}), 114.4 (*pseudo*-t, J_{CP} = 7.7 Hz, C_{qAr}), 112.7 (*pseudo*-t, J_{CP} = 3.3 Hz, *C*H$_{Ar}$), 23.1 (br. s, *C*H$_{iPr}$), 21.0 (s, *C*H$_{3Ar}$), 20.6 (s, *C*H$_{3Ar}$), 19.5 (*pseudo*-t, J_{CP} = 5.7 Hz, *C*H$_{3iPr}$), 18.9 (br. s, *C*H$_{3Ar}$), 17.4 (br. s, *C*H$_{3iPr}$); ^{31}P{^{1}H} NMR (C_6D_6, 283 MHz, in

ppm): δ = 10.1 (s, *P*N$^-$, 2 P); IR (ATR, in cm^{-1}) = 2957(m), 2917(m), 2867(m), 2008(s), 1598(s), 1462(s), 1392(s), 1382(s), 1300(s), 1277(s), 1263(s), 1250(s), 1215(s), 1191(s), 1154(s), 1036(s), 1029(s), 890(s), 881(s), 858(s), 815(s), 730(s), 706(s), 666(s), 620(s), 543(s), 490(s), 467(s), 432(s), 388(s), 364(s), 305(s); elemental analysis (in %): $C_{45}H_{62}LaN_3P_2S$: calcd.: C 61.57, H 7.12, N 4.79; found: C 61.01, H 6.78, N 4.79.

Preparation of (PN)$_2$La(μ-1,3-N$_3$)$_2$La(PN)$_2$ (4). Solid **KN$_3$** (36 mg, 450 µmol, 1.5 eq.) was added to a solution of **1-I** (285 mg, 300 µmol, 1 eq.) in THF (10 mL) at room temperature. The reaction mixture was stirred at room temperature for 14 h. After allowing the precipitate to settle, the solution was filtered through a glass-fibre filter. The yellow filtrate was concentrated *in vacuo* to an oily residue. After extraction with toluene (2 x 3 mL) and filtration through a glass-fibre filter, the yellow solution was concentrated to a volume of ca. 1 mL. The concentrated extract was stored at room temperature for 24 h, during which colorless crystals were formed. The mother liquor was removed with a pipette. The crystals were washed with *n*-pentane (3 x 2 mL) and left to dry in the glovebox atmosphere, since prolonged drying *in vacuo* resulted in significant decomposition. Even with these precautions, the crystalline material was not completely pure according to ^{1}H NMR spectroscopy and did not yield satisfying elemental analyses, wherefore we can only determine a crude yield and give ^{1}H NMR, ^{31}P{^{1}H} NMR and IR spectroscopic data for this complex. Single crystals of **4** suitable for X-ray structure determination were obtained during work-up as described above. Yield: 211 mg (245 mmol, 82%, crude); ^{1}H NMR (C_6D_6, 700 MHz, in ppm): δ = 6.92–6.88 (m, C*H*$_{Ar}$, 6 H), 6.78 (dd, $^3J_{HH}$ = 8.5 Hz, $^4J_{HH}$ = 1.8 Hz, C*H*$_{Ar}$, 2 H), 5.65–5.61 (m, C*H*$_{Ar}$, 2 H), 2.26–2.20 (two overlapping br. s, C*H*$_{3Ar}$, 18 H), 2.16 (s, C*H*$_{3Ar}$, 6 H), 2.09–1.93 (br. s, C*H*$_{iPr}$, 4 H), 1.13–1.02 (br. s, C*H*$_{3iPr}$, 24 H); ^{31}P{^{1}H} NMR (C_6D_6, 283 MHz, in ppm): δ = 5.1 (br. s, *P*N$^-$, 2 P); IR (ATR, in cm^{-1}) = 2956(m), 2918(m), 2867(m), 2729(m), 2113(s), 1599(s), 1537(s), 1494(s), 1463(s), 1390(s), 1300(s), 1276(s), 1239(s), 1213(s), 1191(s), 1157(s), 1137(s), 1060(s), 1032(s), 1009(s), 957(s), 928(s), 883(s), 859(s), 821(s), 813(s), 730(s), 714(s), 692(s), 661(s), 612(s), 576(s), 543(s), 502(s), 489(s), 468(s), 434(s), 389(s), 341(s), 346(s), 303(s), 268(s), 231(s).

Preparation of (PN)$_2$La{SPC(^{Ad}CAAC)} (5a). A solution of **^{Ad}CAAC** (57 mg, 151 151 µmol, 1 eq.) in *n*-hexane (2 mL) was added dropwise to a solution of **2** (135 mg, 151 µmol, 1 eq.) in *n*-hexane (2 mL) at room temperature. The initially yellow solution first became dark red and within 30 s brightened up to yellow again. After 10 min the reaction solution was filtered through a glass-fibre filter. The filtrate was concentrated under reduced pressure to a volume of about 0.3 mL and allowed to rest at room temperature for 3 d, during which yellow-colored crystalline blocks formed. The mother liquor was removed with a pipette, after which the crystalline material was washed with *n*-pentane (2 x 1.5 mL) and left to dry in the glovebox atmosphere, since prolonged drying *in vacuo* resulted in significant decomposition. Single crystals of **5a** suitable for X-ray structure determination were obtained during work-up as described above. Yield: 154 mg (121 µmol, 80%); ^{1}H NMR (C_6D_6, 700 MHz, in ppm): δ = 7.23 (t, $^3J_{HH}$ = 7.6 Hz, C*H*$_{Ar,Dipp}$, 1 H), 7.17–7.16 (resonance partly obscured by C_6D_6 peak, m, C*H*$_{Ar,Dipp}$, 1 H), 7.15 (dd, $^3J_{HH}$ = 7.6 Hz, $^4J_{HH}$ = 1.5 Hz, C*H*$_{Ar,Dipp}$, 1 H), 6.91–6.89 (m, C*H*$_{Ar}$, 2 H), 6.88–6.85 (m, C*H*$_{Ar}$, 4 H), 6.78 (dd, $^3J_{HH}$ = 8.6 Hz, $^4J_{HH}$ = 1.9 Hz, C*H*$_{Ar}$, 2 H), 5.65–5.61 (m, C*H*$_{Ar}$, 2 H), 3.54–3.49 (m, C*H*$_{2Ad}$, 1 H), 3.48–3.43 (m, C*H*$_{2Ad}$, 1 H), 3.36 (sept, $^3J_{HH}$ = 6.8 Hz, C*H*$_{iPr,Dipp}$, 1 H), 3.27 (sept, $^3J_{HH}$ = 6.8 Hz, C*H*$_{iPr,Dipp}$, 1 H), 2.30 (br. s, C*H*$_{3Ar}$, 6 H), 2.29 (br. s, C*H*$_{3Ar}$, 6 H), 2.22–2.21 (m, C*H*$_{Ad}$, 1 H), 2.17–2.16 (m, C*H*$_{Ad}$), 2.15 (s, C*H*$_{3Ar}$, 6 H), 2.14 (s, C*H*$_{3Ar}$, 6 H), 2.13 (d, $^2J_{HH}$ = 13.0 Hz, C*H*$_2$, 1 H), 2.09 (d, $^2J_{HH}$ = 13.0 Hz, C*H*$_2$, 1 H), 2.04–2.01 (m, C*H*$_{Ad}$, 1 H), 2.01–1.96 (m, C*H*$_{2Ad}$, 2 H), 1.90–1.80 (br. m, C*H*$_{2Ad}$, C*H*$_{Ad}$ & C*H*$_{iPr}$, 7 H), 1.71–1.68 (m, C*H*$_{2Ad}$, 1 H), 1.67–1.64 (m, C*H*$_{2Ad}$, 1 H), 1.64–1.60 (m, C*H*$_{2Ad}$, 1 H), 1.57 (d, $^3J_{HH}$ = 6.8 Hz, C*H*$_{3iPr,Dipp}$, 3 H), 1.54–1.51 (m, C*H*$_{2Ad}$, 1 H), 1.36 (br. d, $^3J_{HH}$ = 6.8 Hz, C*H*$_{3iPr,Dipp}$, 3 H), 1.31 (d, $^3J_{HH}$ = 6.8 Hz, C*H*$_{3iPr,Dipp}$, 3 H), 1.27 (d, $^3J_{HH}$ = 6.8 Hz, C*H*$_{3iPr,Dipp}$, 3 H), 1.18–1.15 (br. s, C*H*$_{3iPr}$, 6 H), 1.14 (s, C*H*$_3$, 3 H), 1.14–1.10 (br. s, C*H*$_{3iPr}$, 6 H), 1.08 (s, C*H*$_3$, 3 H), 1.01–0.91 (br. s, C*H*$_{3iPr}$, 12 H); ^{13}C{^{1}H} NMR (C_6D_6, 176 MHz, in ppm): δ = 237.3 (d, $^1J_{CP}$ = 34.9 Hz, $^-$SP*C*CR$_2$), 160.6 (*pseudo*-t, J_{CP} = 11.5 Hz, *C*$_{qAr}$), 152.2 (d, $^2J_{CP}$ = 6.1 Hz, $^-$SPC*C*R$_2$), 150.1 (s, *C*$_{qAr}$), 149.8 (s, *C*$_{qAr}$), 138.6 (s, *C*$_{qAr}$), 138.6–138.0 (br. s, *C*$_{qAr}$), 135.0 (s, *C*$_{qAr}$), 134.8 (s, *C*$_{qAr}$), 133.6 (s, *C*H$_{Ar}$), 133.3 (s, *C*H$_{Ar}$), 131.7 (s, *C*H$_{Ar}$), 131.6 (s, *C*H$_{Ar}$), 128.0 (resonance obscured by C_6D_6 peak, only identifiable by ^{1}H–^{13}C HSQC NMR spectroscopy, s, *C*H$_{Ar,Dipp}$), 124.8 (s, *C*H$_{Ar,Dipp}$), 124.2 (s, *C*H$_{Ar,Dipp}$), 122.9 (s, *C*$_{qAr}$), 114.2 (d, J_{CP} = 6.5 Hz, *C*$_{qAr}$), 114.1 (d, J_{CP} = 6.5 Hz, *C*$_{qAr}$), 112.9 (*pseudo*-t, J_{CP} = 4.0 Hz, *C*H$_{Ar}$), 63.2 (s, *C*$_q$(CH$_3$)$_2$), 53.0 (d, $^3J_{CP}$ = 3.8 Hz, *C*$_{qAd}$), 52.2 (s, *C*H$_2$), 39.9 (s, *C*H$_{2Ad}$), 39.1 (s, *C*H$_{Ad}$), 38.4 (s, *C*H$_{Ad}$), 35.6 (s, *C*H$_{2Ad}$), 35.3 (s, *C*H$_{2Ad}$), 34.0 (s, *C*H$_{2Ad}$), 33.3 (s, *C*H$_{2Ad}$), 30.1 (s, C$_q$(*C*H$_3$)$_2$), 29.9 (s, C$_q$(*C*H$_3$)$_2$), 29.2 (s, *C*H$_{iPr,Dipp}$), 28.8 (s, *C*H$_{iPr,Dipp}$), 28.3 (s, *C*H$_{3iPr,Dipp}$), 28.2 (s, *C*H$_{Ad}$), 27.5 (s, *C*H$_{Ad}$), 27.0 (d, $^{TS}J_{CP}$ = 9.8 Hz, *C*H$_{3iPr,Dipp}$), 24.6 (s, *C*H$_{3iPr,Dipp}$), 24.4 (s, *C*H$_{3iPr,Dipp}$), 22.8 (br. s, *C*H$_{iPr}$), 22.7 (br. s, *C*H$_{iPr}$), 21.0 (s, *C*H$_{3Ar}$), 20.6 (s, *C*H$_{3Ar}$), 20.9–19.9 (several broad, overlapping resonances, *C*H$_{3Ar}$ & *C*H$_{3iPr}$), 17.9 (br. s, *C*H$_{3iPr}$); ^{31}P{^{1}H} NMR (C_6D_6, 283 MHz, in ppm): δ = 139.4 (s, $^-$S*P*CCR$_2$, 1 P), 9.4 (s, *P*N$^-$, 2 P); IR (ATR, in cm^{-1}) = 2952(m), 2916(m), 2864(m), 1674(s), 1596(s), 1537(s), 1461(s), 1382(s), 1330(s), 1300(s), 1277(s), 1265(s), 1223(s), 1202(s), 1193(s), 1154(s), 1099(s), 1031(s), 927(s), 882(s), 858(s), 812(s), 784(s), 710(s), 660(s), 618(s), 608(s), 542(s), 463(s), 433(s), 390(s), 365(s), 294(s), 249(s). elemental analysis (in %): $C_{72}H_{101}LaN_3P_3S$: calcd.: C 67.96, H 8.00, N 3.30; found: C 68.15, H 8.06, N 3.09.

NMR scale reaction of 2 with ^{Me}CAAC to prepare (PN)$_2$La{SPC(^{Me}CAAC)} (5b). C_6D_6 (0.6 mL) was added to a mixture of solid **2** (18 mg, 20 µmol, 1 eq.) and **^{Me}CAAC** (6 mg, 20 µmol, 1 eq.) at room temperature. The resulting solution was red-brown and then turned to yellow within 1 min. The reaction solution was transferred to a J-Young NMR tube and analyzed by means of ^{1}H, ^{13}C{^{1}H} and ^{31}P{^{1}H} NMR spectroscopy, which indicated the formation of **5b** in analogy to **5a**. Attempts to obtain a pure powder or crystalline material from concentrated solutions of **5b** in C_6D_6, toluene, *n*-pentane, *n*-hexane, HMDSO or combinations thereof at room temperature or –40°C failed, since the raw product was very well soluble in all of these solvents. Only a crude solid could be obtained after complete removal of solvents *in vacuo*. Larger scaled reactions (up to 400 µmol) carried out in benzene, *n*-pentane, *n*-hexane or HMDSO did not give better results. Even though in each case the raw product was not completely pure after careful removal of solvent *in vacuo* and therefore no useful yield, IR spectrum or elemental analyses could be obtained, the NMR spectroscopic features of **5b** could be assigned quite well by comparison with **5a** (see Figures S34–S44). ^{1}H NMR (C_6D_6, 700 MHz, in ppm): δ = 7.23 (t, $^3J_{HH}$ = 7.5 Hz, C*H*$_{Ar,Dipp}$, 1 H), 7.17–7.16 (resonance partly obscured by C_6D_6 peak, m, C*H*$_{Ar,Dipp}$, 1 H), 7.12–7.10 (m, C*H*$_{Ar,Dipp}$, 1 H), 6.92–6.90 (m, C*H*$_{Ar}$, 2 H), 6.88–6.87

(m, CH_{Ar}, 2 H), 6.85–6.84 (m, CH_{Ar}, 2 H), 6.78 (dd, $^{3}J_{HH}$ = 8.4 Hz, $^{4}J_{HH}$ = 1.9 Hz, CH_{Ar}, 2 H), 5.66–5.64 (m, CH_{Ar}, 2 H), 3.43 (sept, $^{3}J_{HH}$ = 6.8 Hz, C$H_{iPr,Dipp}$, 1 H), 3.27 (sept, $^{3}J_{HH}$ = 7.0 Hz, C$H_{iPr,Dipp}$, 1 H), 2.34–2.21 (2 br. s at 2.29 & 2.26, CH_{3Ar}, 12 H), 2.16 (s, CH_{3Ar}, 6 H), 2.15 (s, CH_{3Ar}, 6 H), 2.08–1.93 (br. s, CH_{iPr}, 4 H), 1.85 (d, $^{2}J_{HH}$ = 12.7 Hz, CH_{2}, 1 H), 1.82 (d, $^{2}J_{HH}$ = 12.7 Hz, CH_{2}, 1 H), 1.54 (br. d, $^{3}J_{HH}$ = 6.8 Hz, CH_{3iPr}, 3 H), 1.52 (s, CH_{3}, 3 H), 1.35 (br. s, CH_{3}, 3 H), 1.31–1.26 (m, C$H_{3iPr,Dipp}$, 9 H), 1.21–1.16 (br. s, CH_{3iPr}, 6 H), 1.15 (s, CH_{3}, 3 H), 1.12–1.07 (br. s, CH_{3iPr}, 6 H), 1.07 (s, CH_{3}, 3 H), 1.06–0.90 (br. s, CH_{3iPr}, 12 H); ^{13}C{^{1}H} NMR (C_6D_6, 176 MHz, in ppm): δ = 224.5 (d, $^{1}J_{CP}$ = 23.5 Hz, $^{-}$SP*C*CR$_2$), 160.7 (*pseudo*-t, J_{CP} = 11.3 Hz, C_{qAr}), 155.8 (d, $^{2}J_{CP}$ = 3.4 Hz, $^{-}$SPC*C*R$_2$), 150.5 (s, C_{qAr}), 149.6 (s, C_{qAr}), 138.7 (s, C_{qAr}), 138.3 (br. s, C_{qAr}), 134.9 (s, C_{qAr}), 134.7 (s, C_{qAr}), 133.7 (s, *C*H$_{Ar}$), 133.2 (s, *C*H$_{Ar}$), 131.52 (s, *C*H$_{Ar}$), 131.45 (s, *C*H$_{Ar}$), 128.3 (resonance obscured by C_6D_6 peak, only identifiable by ^{1}H–^{13}C HSQC NMR spectroscopy, s, *C*H$_{Ar,Dipp}$), 124.7 (s, *C*H$_{Ar,Dipp}$), 124. 2(s, *C*H$_{Ar,Dipp}$), 122.9 (s, C_{qAr}), 114.2 (*pseudo*-t, J_{CP} = 6.6 Hz, C_{qAr}), 113.0 (m, *C*H$_{Ar}$), 65.2 (s, C_q(CH$_3$)$_2$), 53.7 (s, *C*H$_2$), 42.4 (s, C_q(CH$_3$)$_2$), 31.6 (s, C_q(*C*H$_3$)$_2$), 30.7 (s, C_q(*C*H$_3$)$_2$), 29.8 (s, C_q(*C*H$_3$)$_2$), 29.5 (s, C_q(*C*H$_3$)$_2$), 29.4 (s, *C*H$_{iPr,Dipp}$), 29.0 (s, *C*H$_{iPr,Dipp}$), 28.1 (s, *C*H$_{3iPr,Dipp}$), 27.1 (s, *C*H$_{3iPr,Dipp}$), 24.0 (s, *C*H$_{3iPr,Dipp}$), 23.9 (s, *C*H$_{3iPr,Dipp}$), 23.8 (br. s, *C*H$_{iPr}$), 23.3 (br. s, *C*H$_{iPr}$), 21.0 (s, *C*H$_{3Ar}$), 20.6 (s, *C*H$_{3Ar}$), 20.1 (s, *C*H$_{3Ar}$), 19.9 (br. s, *C*H$_{3iPr}$), 19.8 (br. s, *C*H$_{3iPr}$), 18.2 (br.s, *C*H$_{3iPr}$), 17.7 (br. s, *C*H$_{3iPr}$); ^{31}P{^{1}H} NMR (C_6D_6, 283 MHz, in ppm): δ = 145.2 (s, $^{-}$S*P*CCR$_2$, 1 P), 8.9 (s, *P*N^{-}, 2 P).

X-ray Crystallography

Single crystals for X-ray diffraction experiments were measured at the analytical facility of the Paderborn University using a Bruker Smart AXS or a Bruker D8 Venture instrument. All crystals were kept at 130(2) K or 120(2) K throughout data collection. Data collection was performed using either the APEXIII or the Smart software package. Data refinement and reduction were performed with Bruker Saint (V8.34A). All structures were solved with SHELXT[5] and refined using the OLEX 2 software package.[6] All non-hydrogen atoms were refined anisotropically, and hydrogen atoms were included at the geometrically calculated positions and refined using a riding model. All structures have been submitted to the CCDC and can be obtained under the numbers presented in Table S1. For further crystallographic details regarding crystal measurements, please check Tables S1 and S2.

2. NMR Spectra

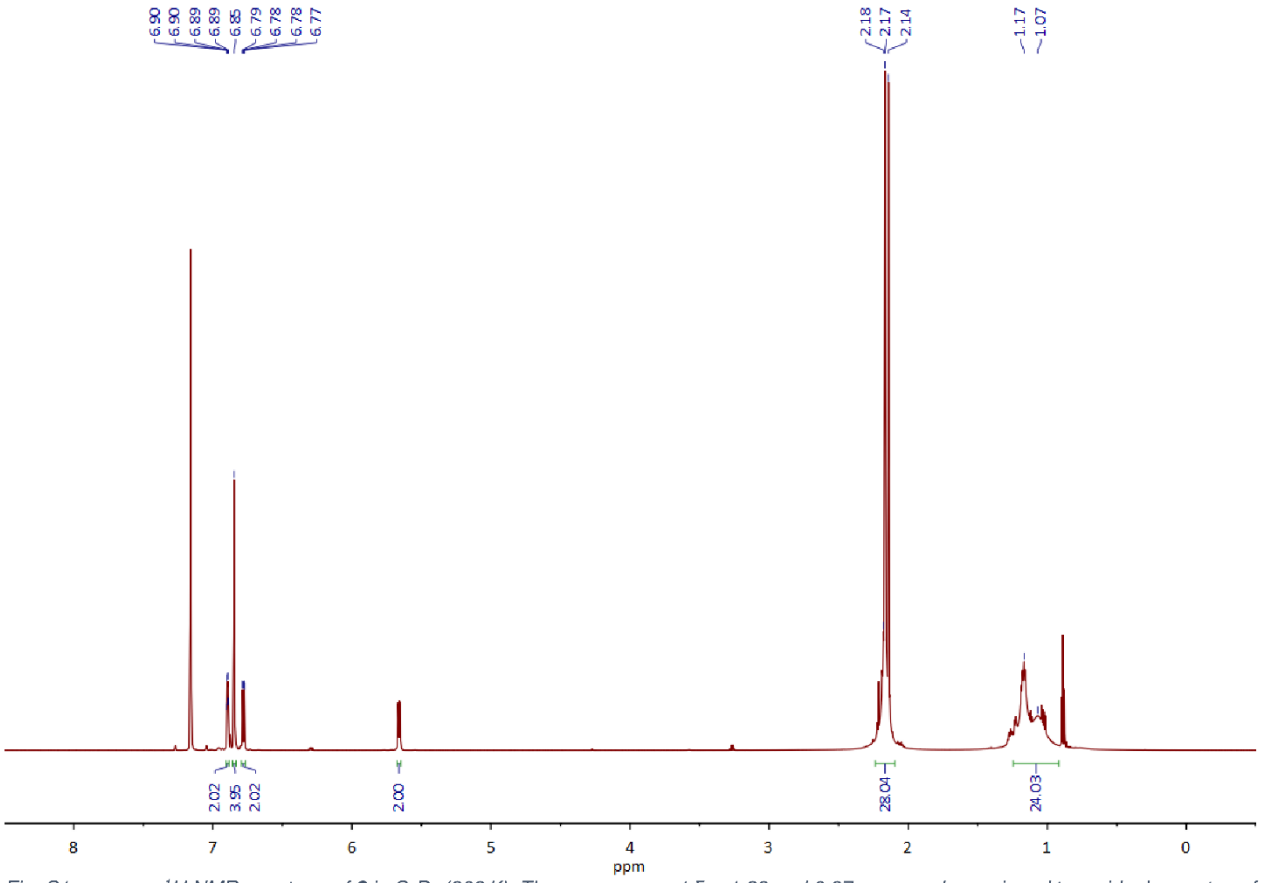

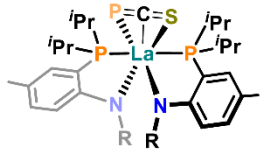

R = Mes

Fig. S1: *^{1}H NMR spectrum of **2** in C_6D_6 (303 K). The resonances at δ = 1.23 and 0.87 ppm can be assigned to residual n-pentane from work-up.*

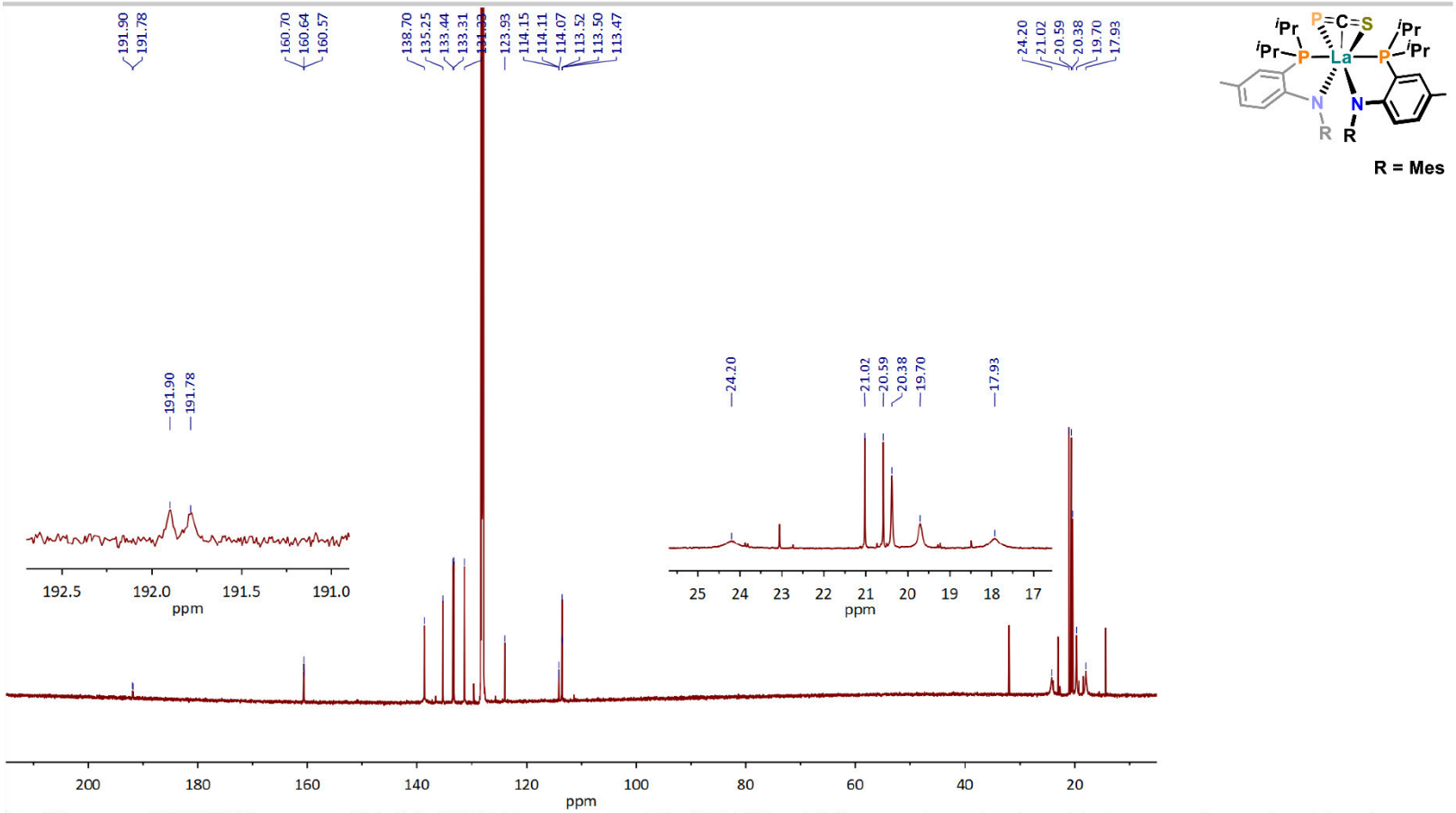

Fig. S2: *$^{13}C\{^1H\}$ NMR spectrum of **2** in C_6D_6 (303 K). The resonances at δ = 34.5, 22.7 and 14.3 ppm can be assigned to residual n-pentane from work-up. The enlargement on the left shows the characteristic doublet splitting ($^1J_{CP}$ = 20.6 Hz) of the [SCP]⁻ resonance, the enlargement on the right shows the resonances of **2** in the aliphatic region between δ ≈ 25 and 17 ppm.*

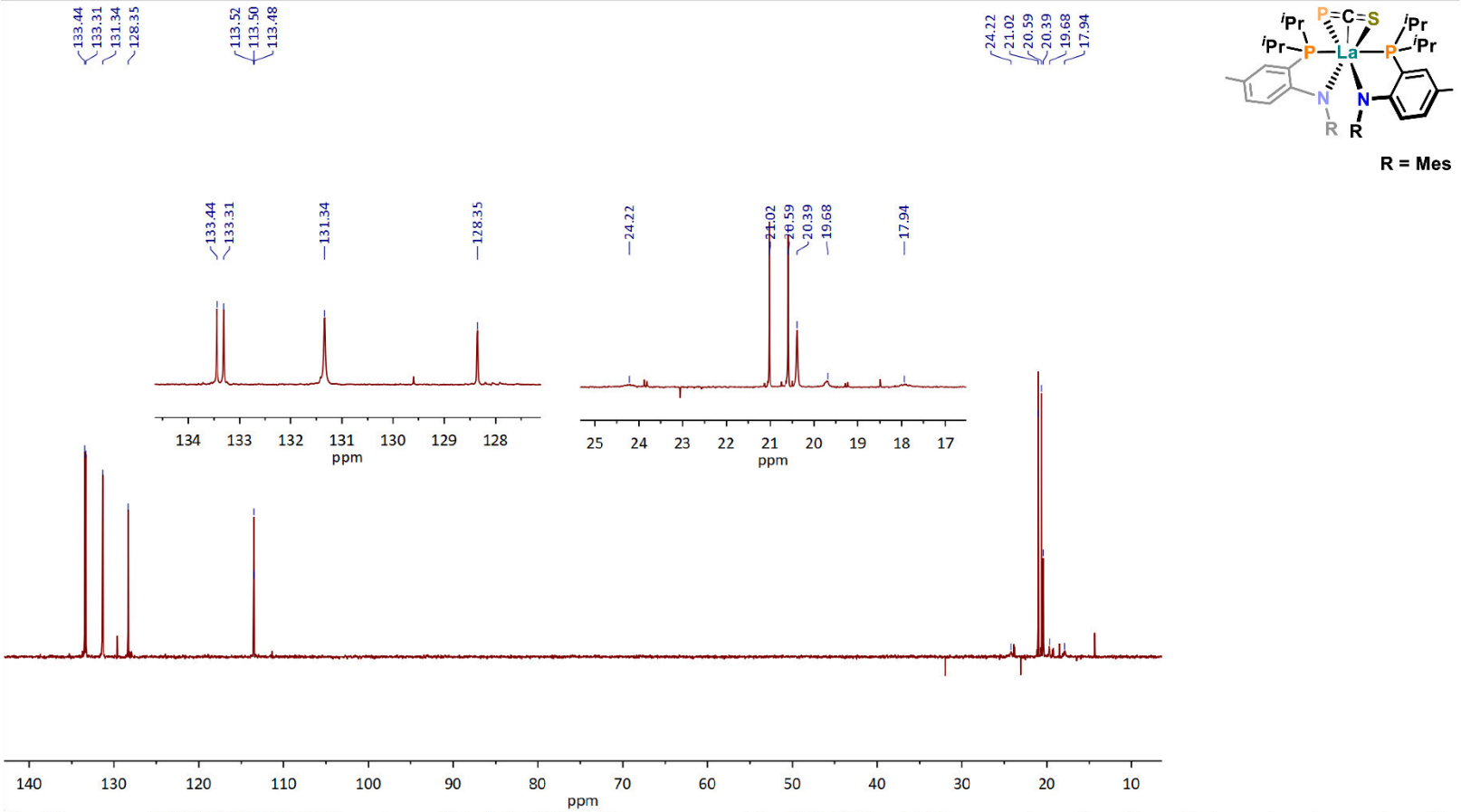

Fig. S3: *$^{13}C\{^1H\}$ DEPT135 NMR spectrum of **2** in C_6D_6 (303 K). The resonances at δ = 34.5, 22.7 and 14.3 ppm can be assigned to residual n-pentane from work-up. The two enlargements show the resonances of **2** in the aromatic region between δ ≈ 135 an 127 ppm (left) and the aliphatic region between δ ≈ 25 an 17 ppm (right).*

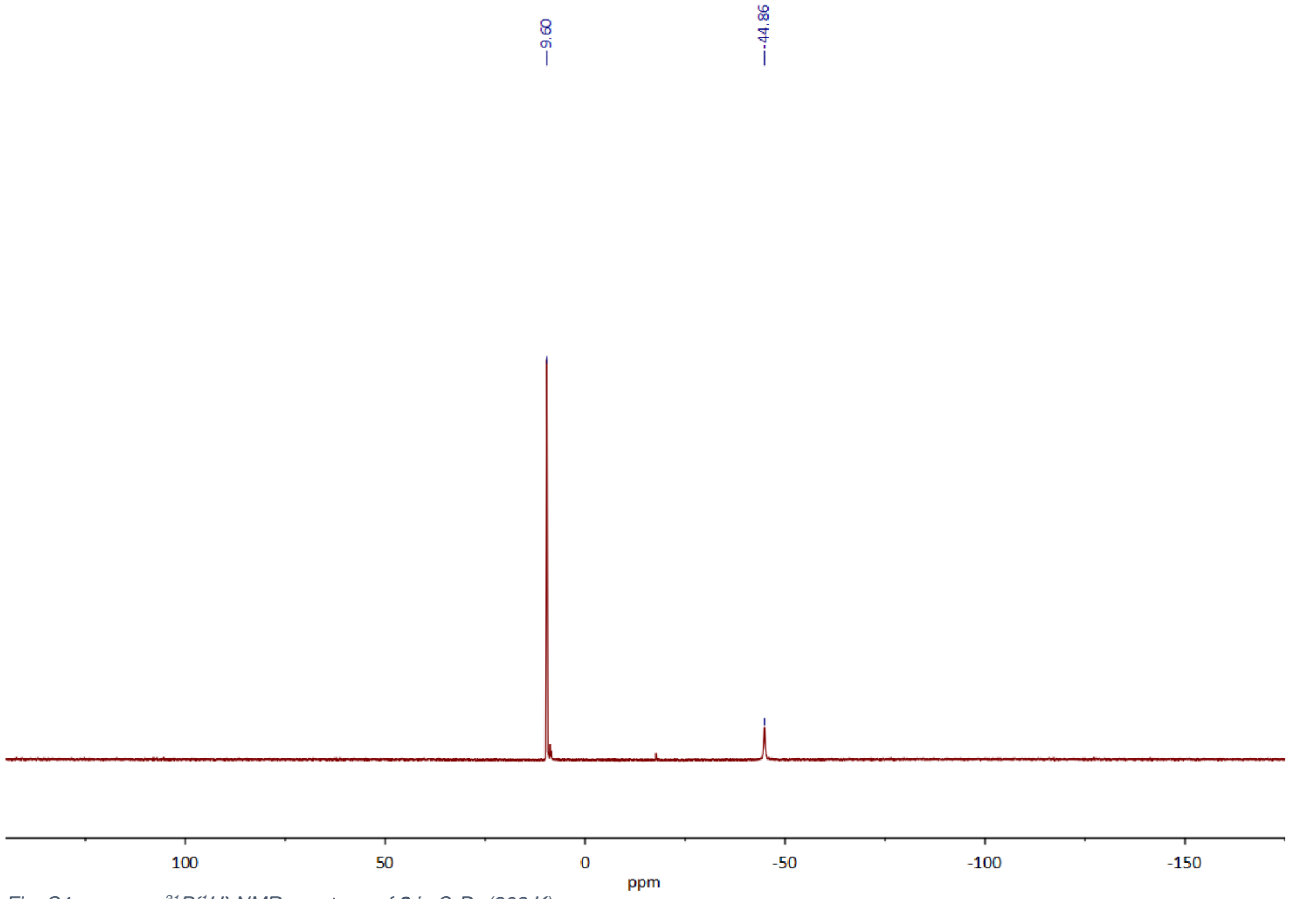

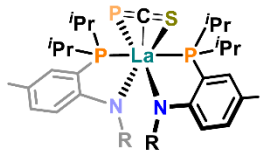

R = Mes

Fig. S4: *$^{31}P\{^{1}H\}$ NMR spectrum of **2** in C_6D_6 (303 K).*

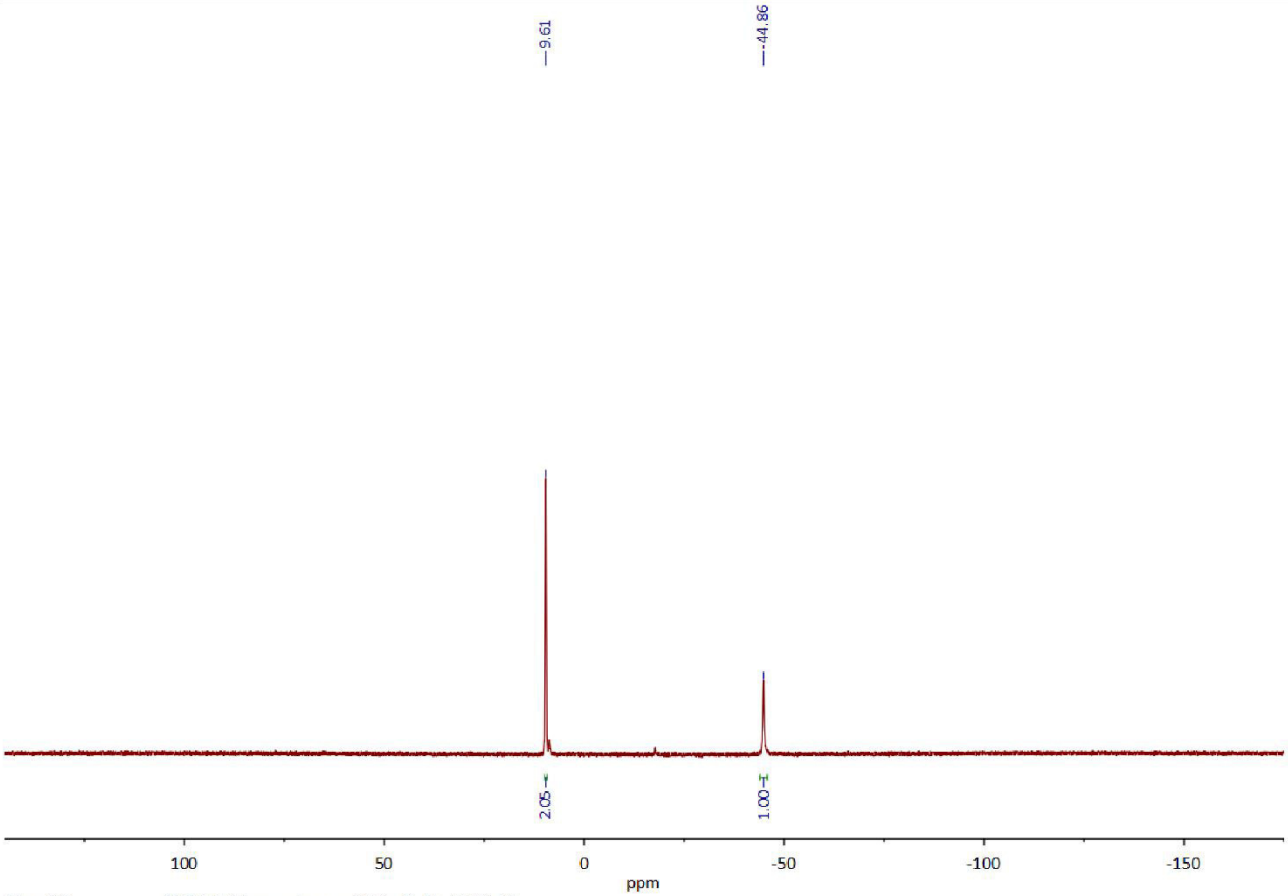

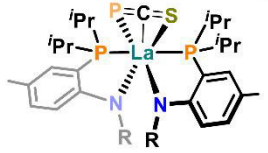

R = Mes

Fig. S5: *^{31}P NMR spectrum of **2** in C_6D_6 (303 K).*

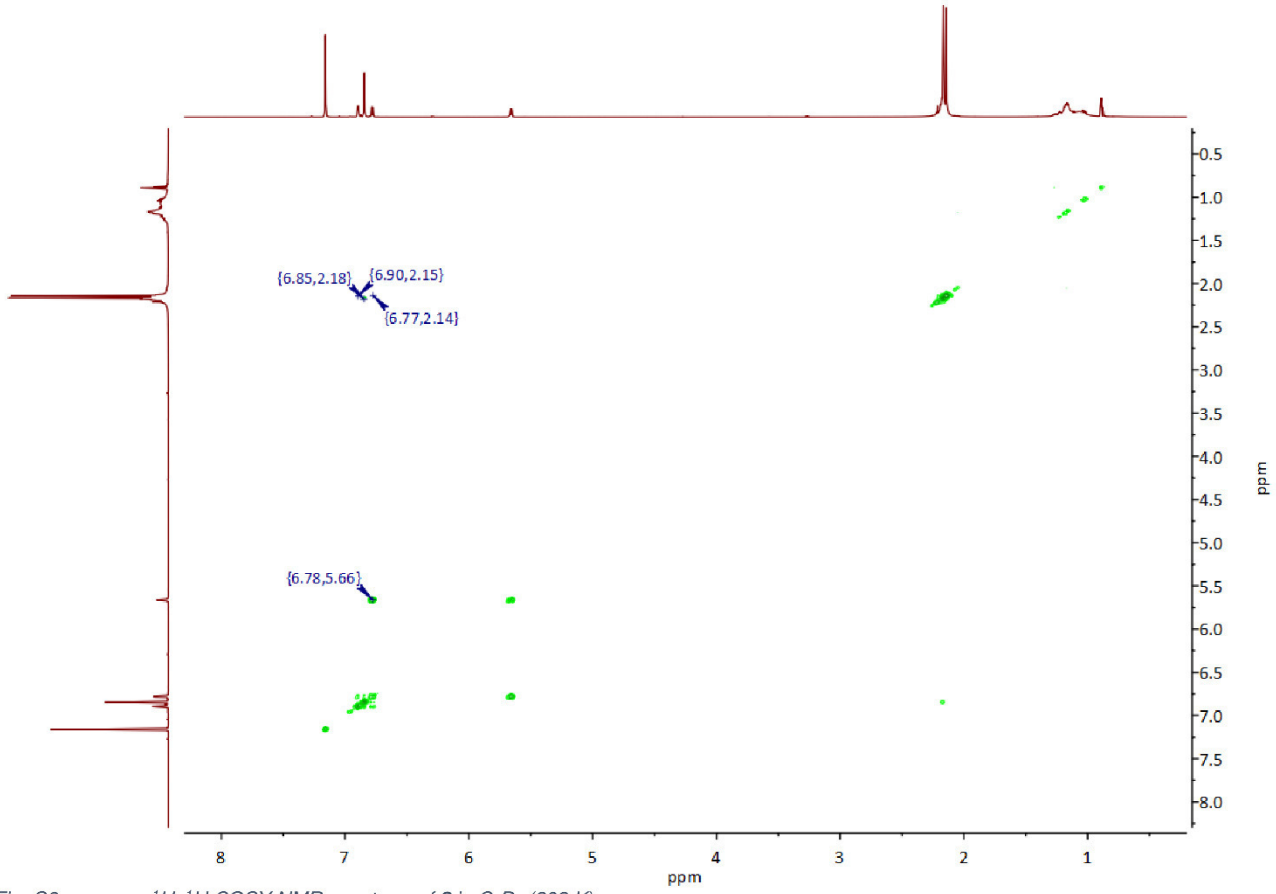

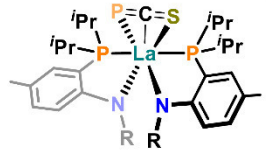

R = Mes

Fig. S6: *^{1}H–^{1}H COSY NMR spectrum of **2** in C_6D_6 (303 K).*

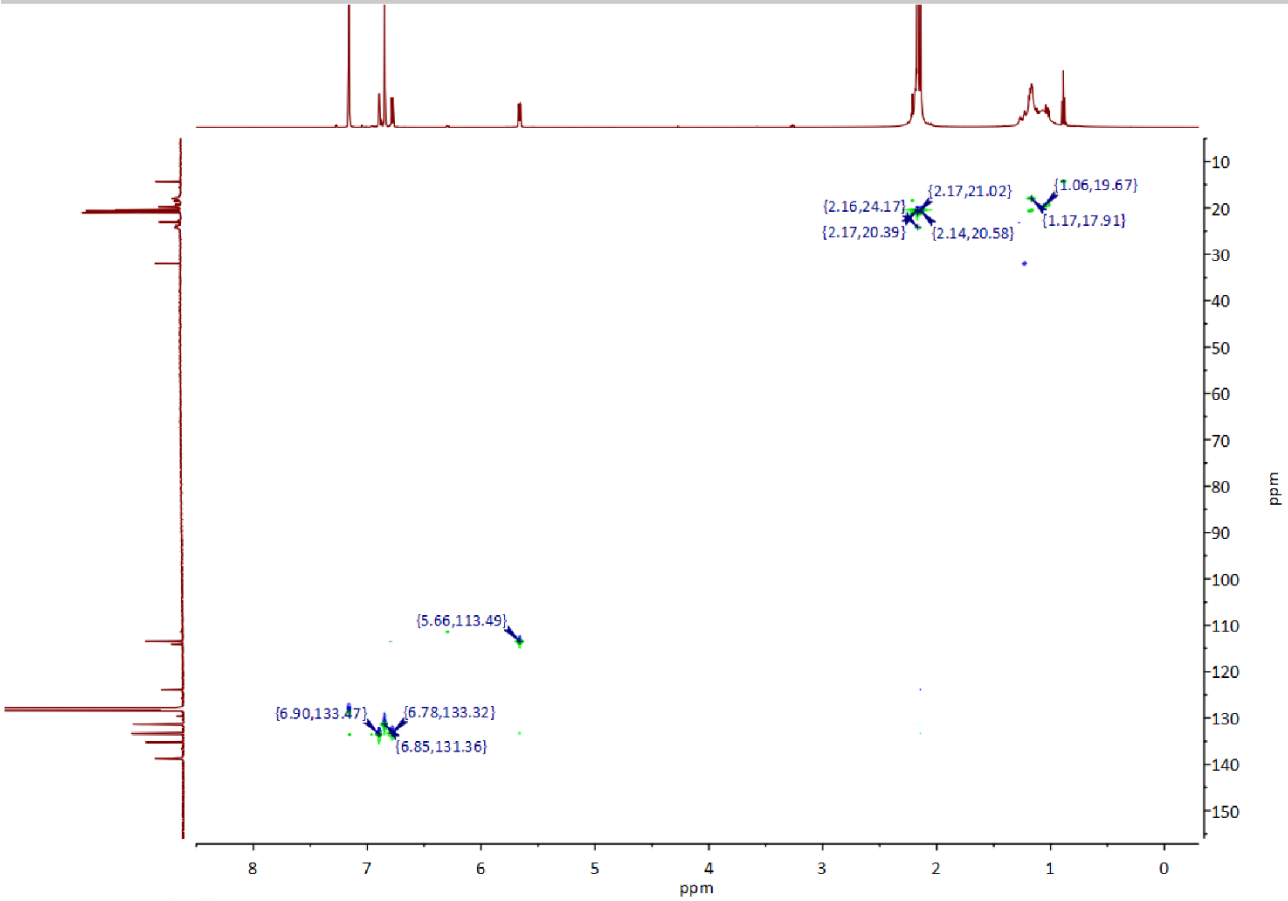

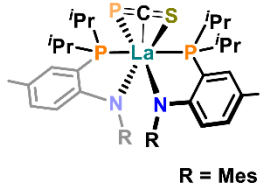

Fig. S7: *^{1}H–^{13}C HSQC NMR spectrum of **2** in C_6D_6 (303 K).*

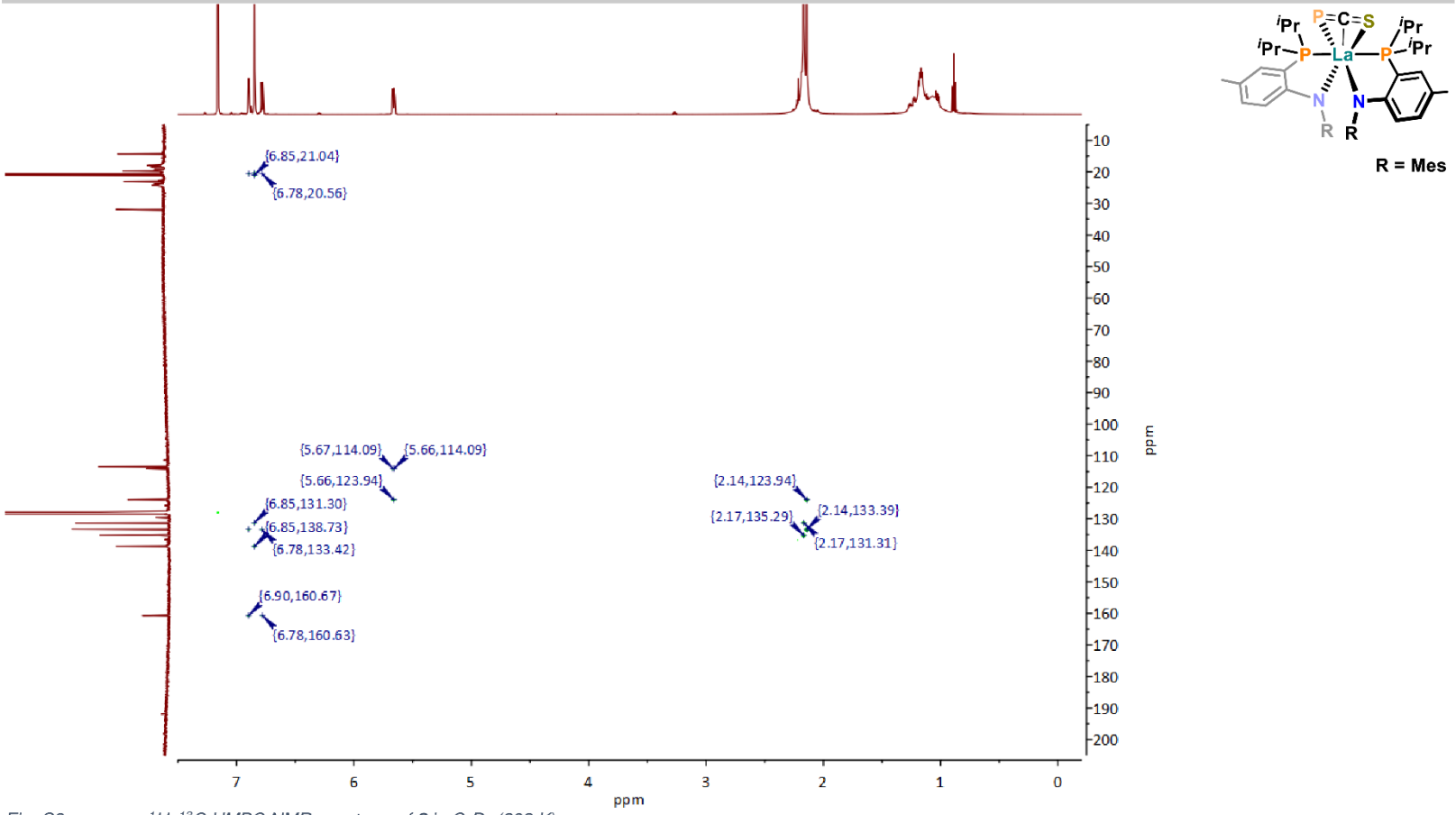

Fig. S8: *^{1}H–^{13}C HMBC NMR spectrum of **2** in C_6D_6 (303 K).*

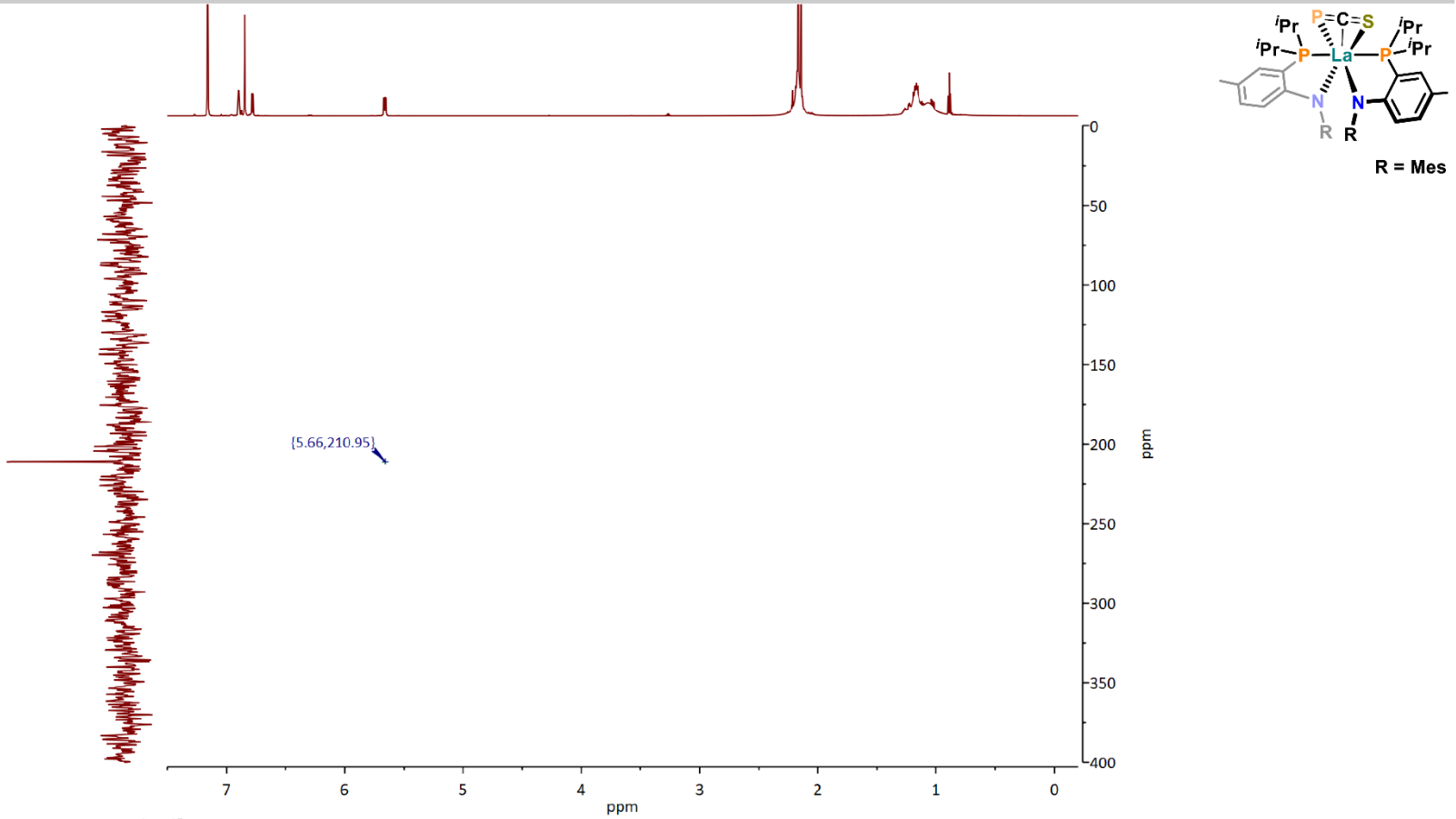

Fig. S9: *^{1}H–^{15}N HMBC NMR spectrum of **2** in C_6D_6 (303 K).*

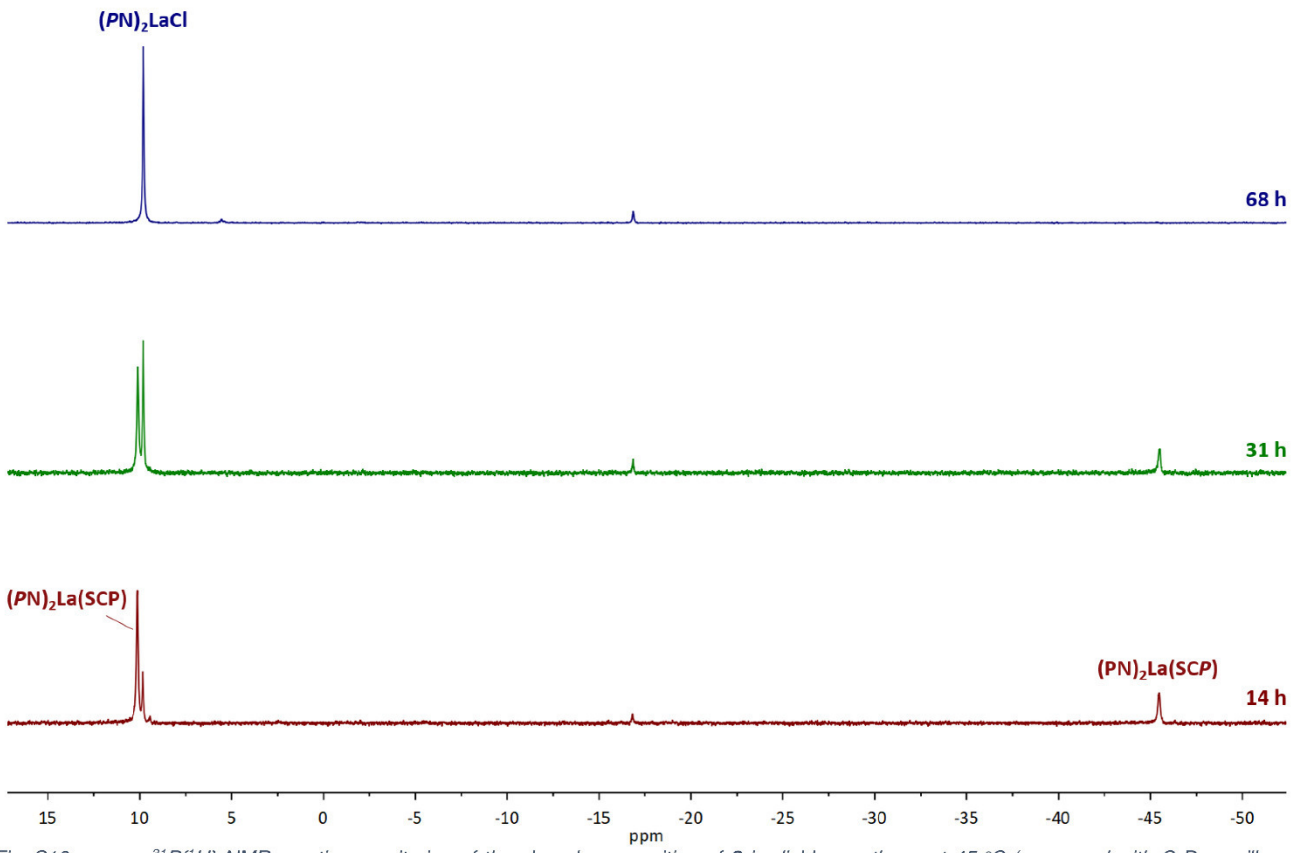

Fig. S10: *$^{31}P\{^{1}H\}$ NMR reaction monitoring of the slow decomposition of **2** in dichloromethane at 45 °C (measured with C_6D_6 capillary at 303 K). The reaction times are specified on the right. The product complex (top spectrum) was identified as **1-Cl** by X-ray diffraction analysis of suitable crystals which were grown after complete consumption of starting material **2**. The crystals were obtained within 5 min at room temperature after the reaction solution was filtered, concentrated in vacuo and layered with n-pentane.*

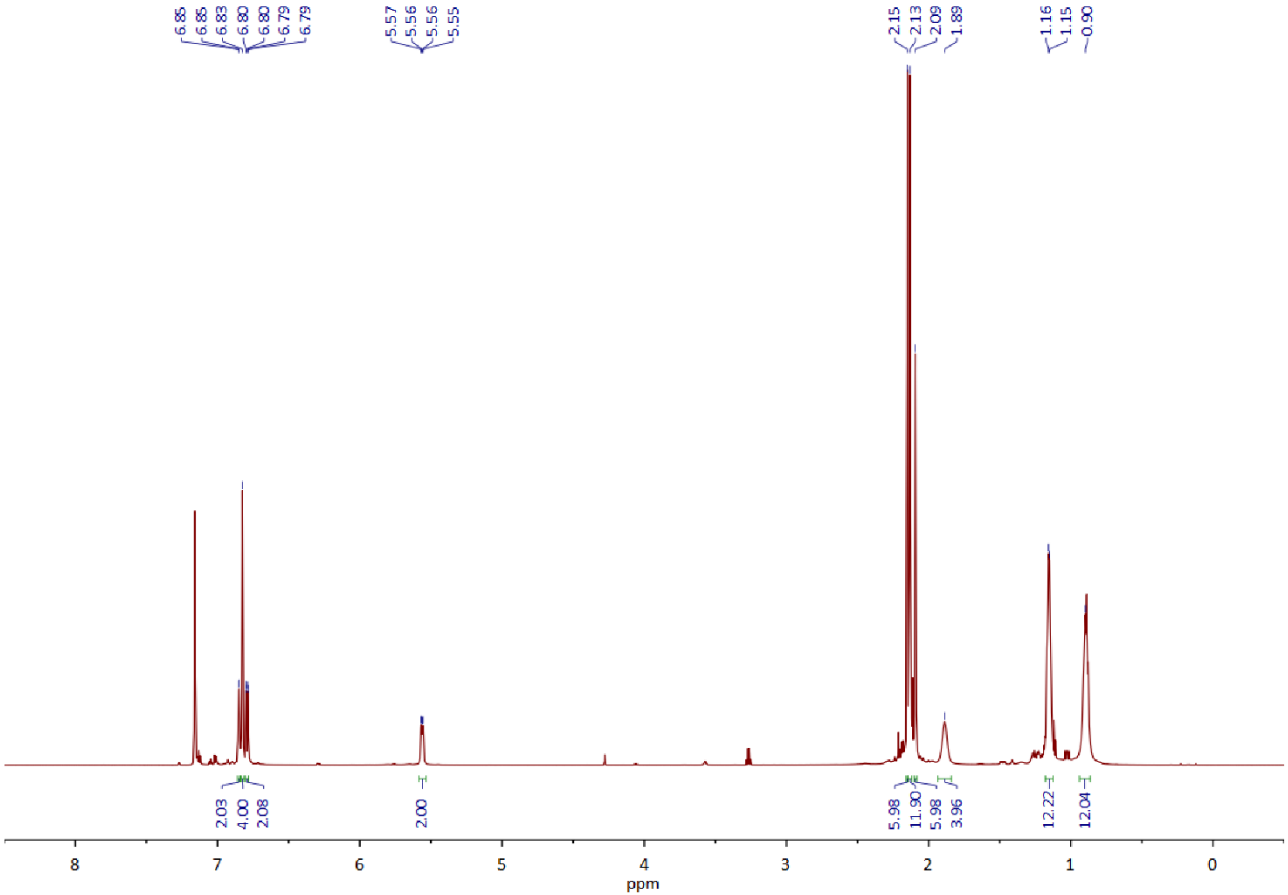

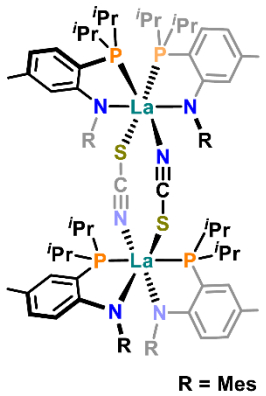

Fig. S11: *^{1}H NMR spectrum of **3** in C_6D_6 (303 K). Traces of solvents from the reaction and work-up can be assigned as the following: δ = 3.57 and 1.40 ppm (THF), δ = 7.13, 7.02 and 2.11 ppm (toluene), δ = 1.24 ppm (n-hexane). The peaks at δ = 3.26 and 1.11 ppm belong to traces of diethyl ether.*

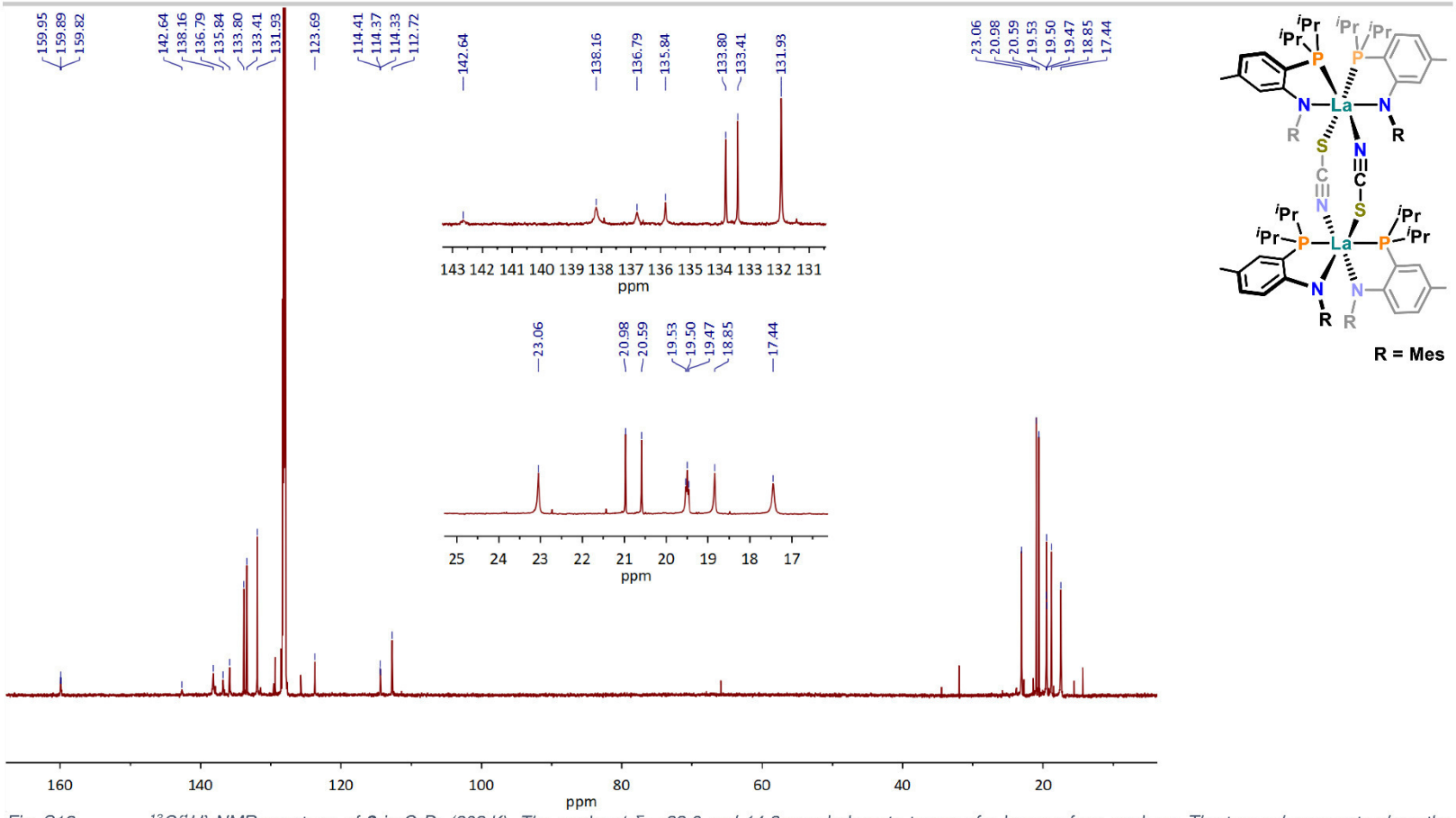

Fig. S12: *$^{13}C\{^1H\}$ NMR spectrum of **3** in C_6D_6 (303 K). The peaks at δ = 32.0 and 14.3 ppm belong to traces of n-hexane from work-up. The two enlargements show the resonances of complex **3** in the aromatic region between δ ≈ 143 and 131 ppm (top) and the aliphatic region between δ ≈ 25 and 17 ppm (bottom).*

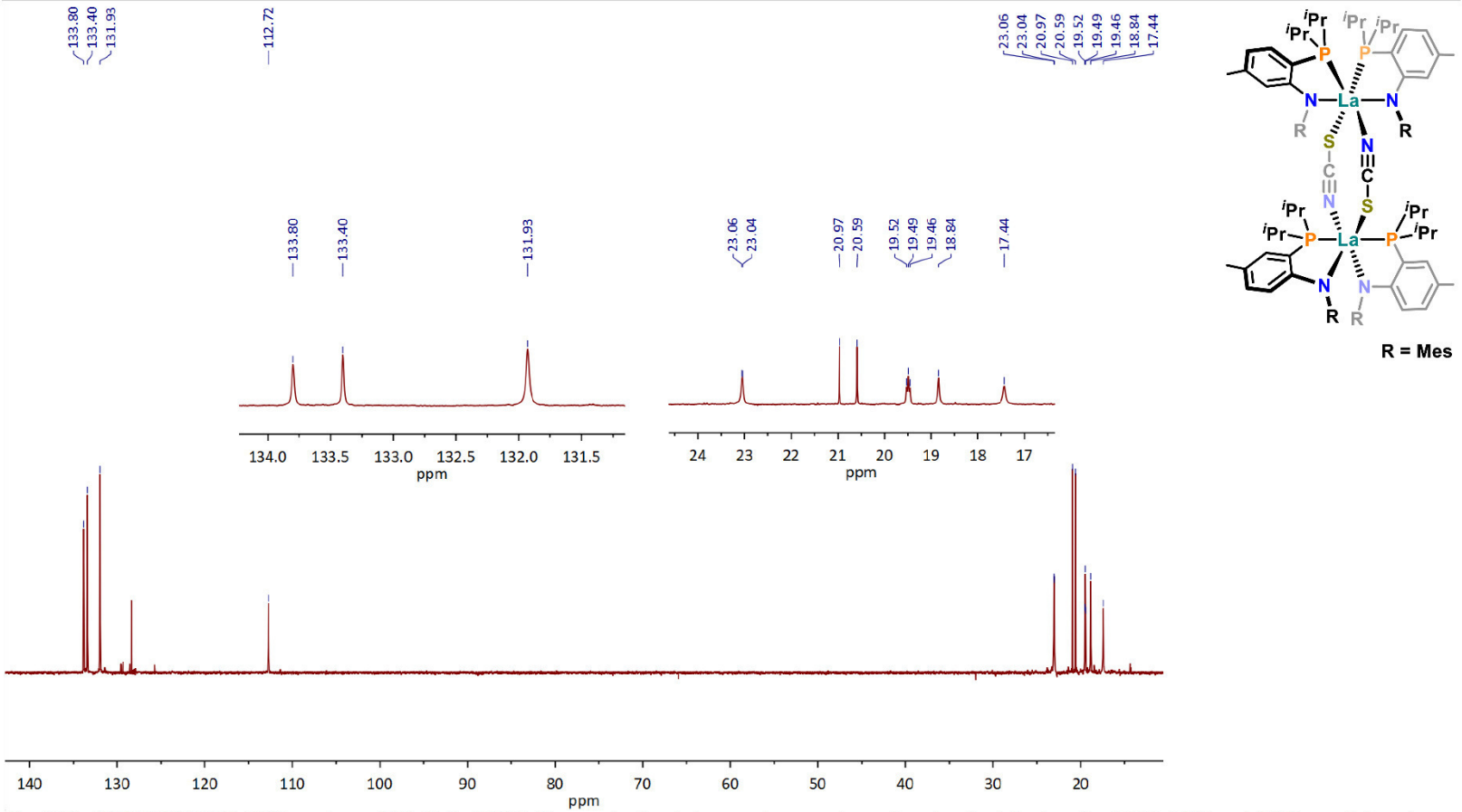

*Fig. S13: $^{13}C\{^{1}H\}$ DEPT135 NMR spectrum of **3** in C_6D_6 (303 K). Traces of solvents from work-up can be assigned as the following: δ = 129.3, 128.5 and 125.7 ppm (toluene), δ = 32.0 and 14.3 ppm (n-hexane). The two enlargements show the resonances of complex **3** in the aromatic region between δ ≈ 134 and 131 ppm (left) and the aliphatic region between δ ≈ 24 and 17 ppm (right).*

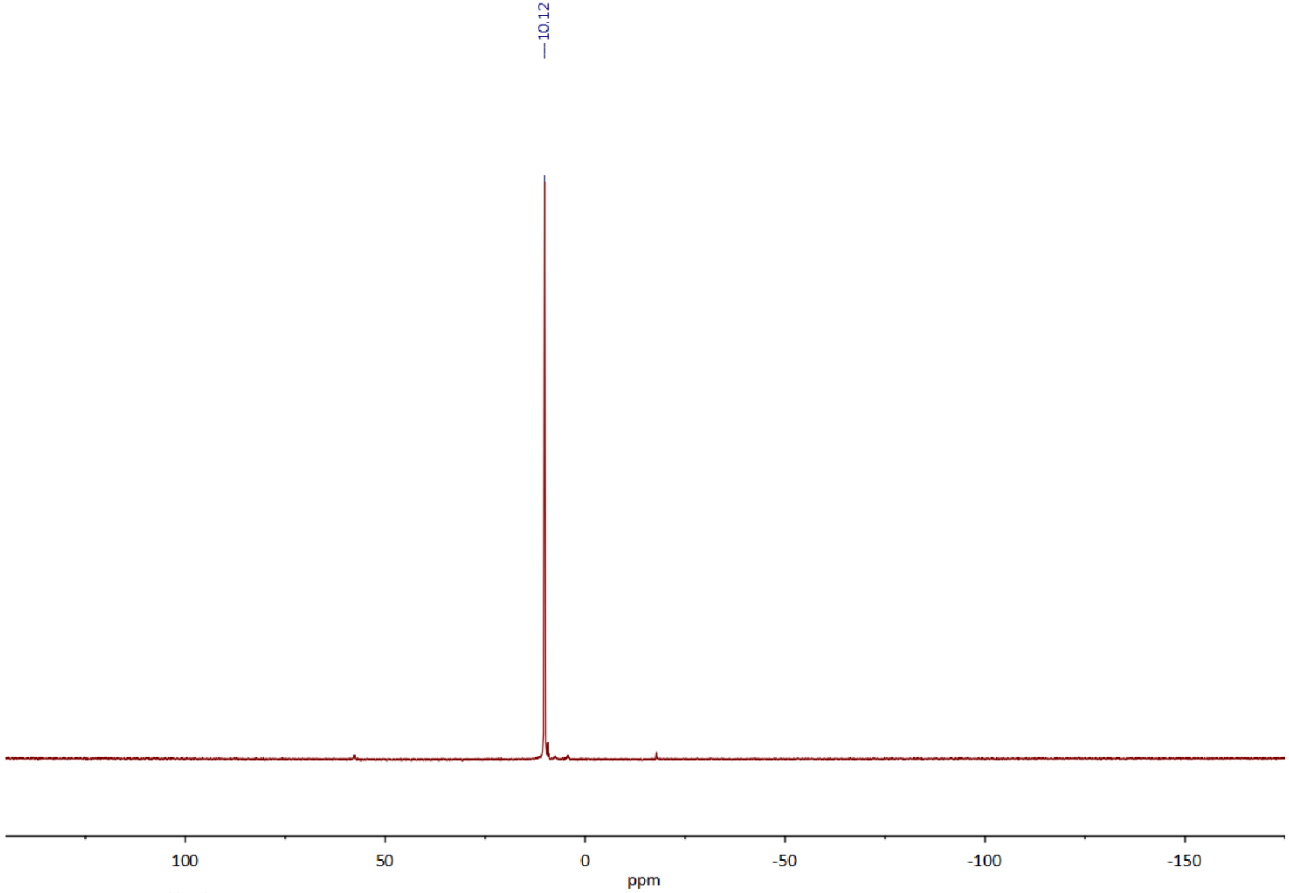

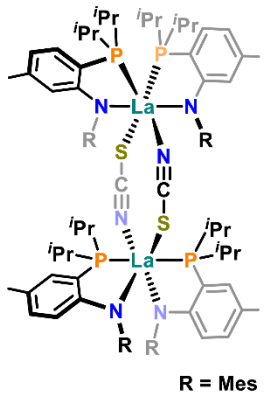

Fig. S14: $^{31}P\{^{1}H\}$ NMR spectrum of ***3*** in C_6D_6 (303 K).

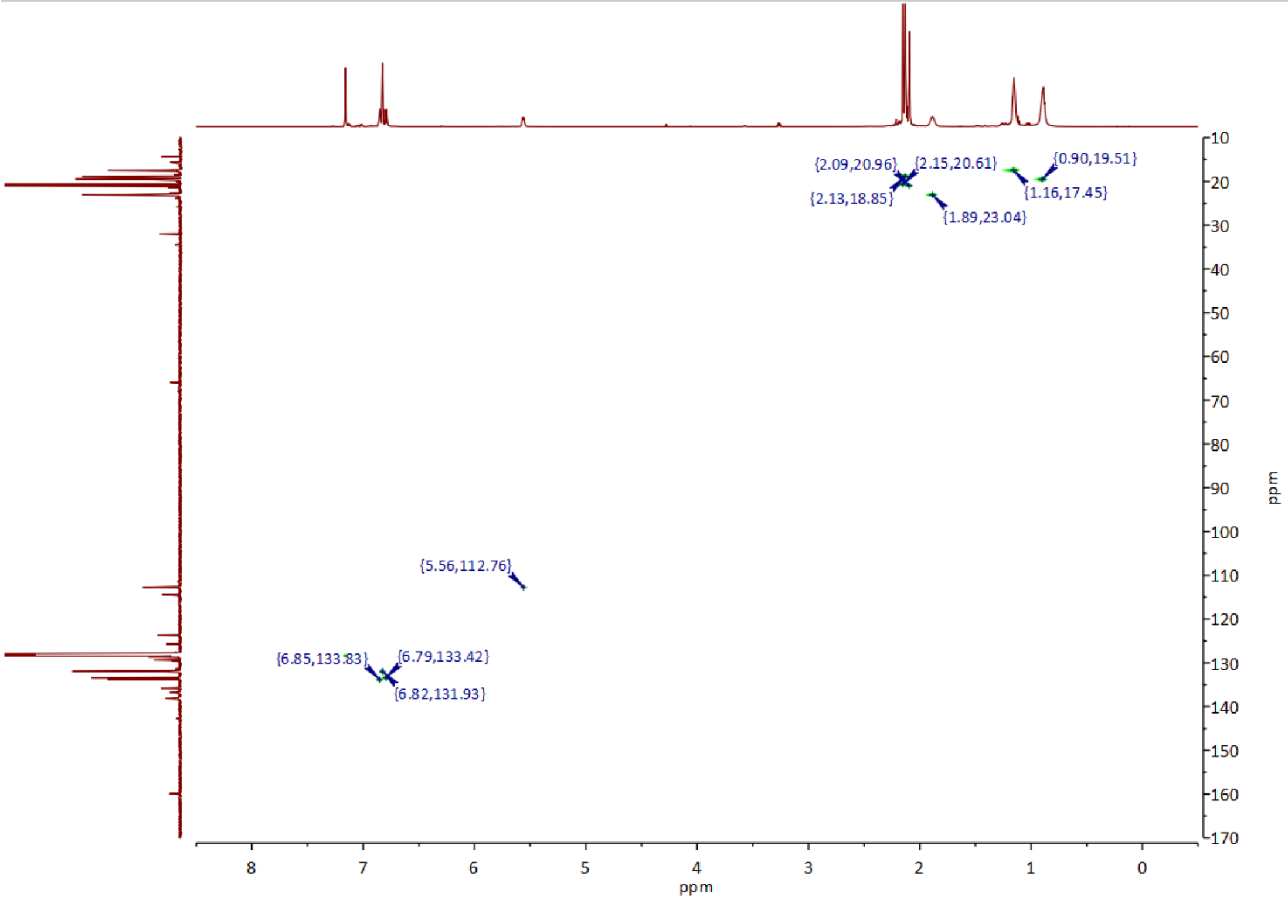

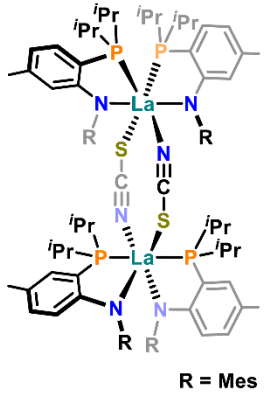

Fig. S15: *^{1}H–^{13}C HSQC NMR spectrum of **3** in C_6D_6 (303 K).*

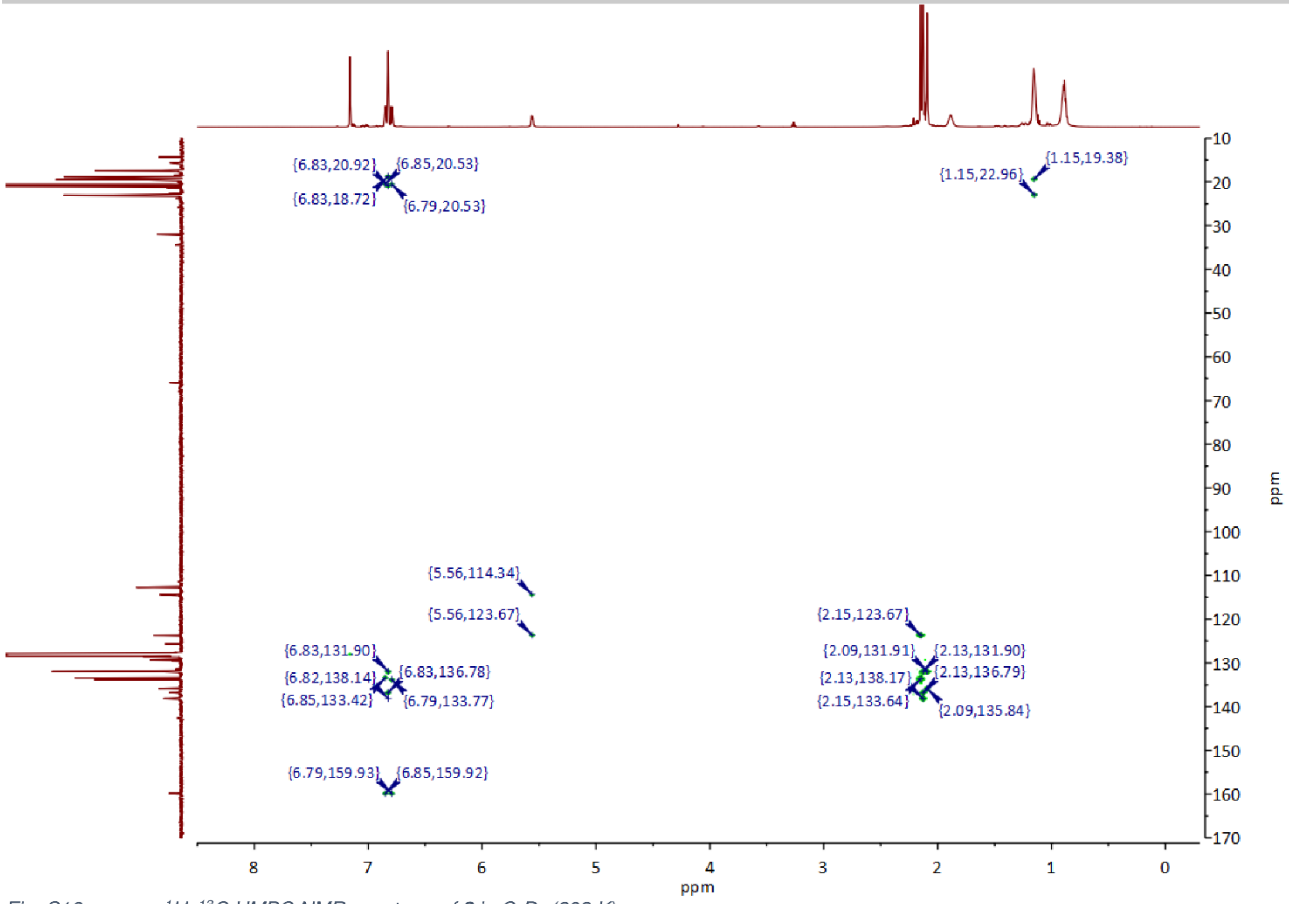

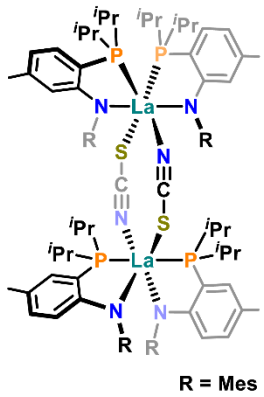

Fig. S16: *^{1}H–^{13}C HMBC NMR spectrum of **3** in C_6D_6 (303 K).*

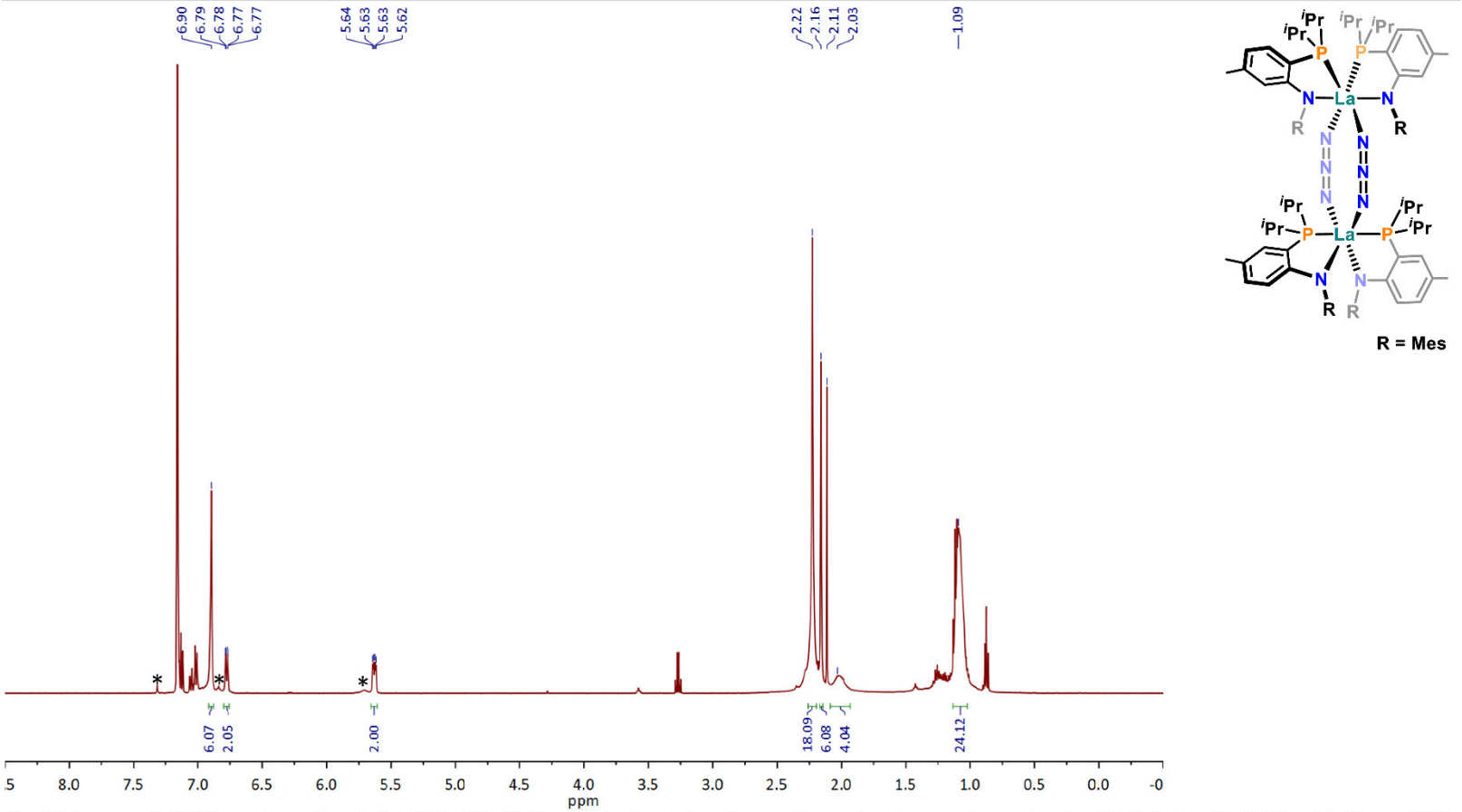

Fig. S17: *^{1}H NMR spectrum of crude **4** in C_6D_6 (303 K). Traces of solvents from the reaction and work-up can be assigned as the following: δ = 3.58 and 1.42 ppm (THF), δ = 7.13, 7.02 and 2.11 ppm (toluene), δ = 1.23 and 0.87 ppm (n-pentane). The peaks at δ = 3.26 and 1.11 ppm belong to traces of diethyl ether from the glovebox atmosphere. Resonances of an unknown impurity are marked by asterisks (*).*

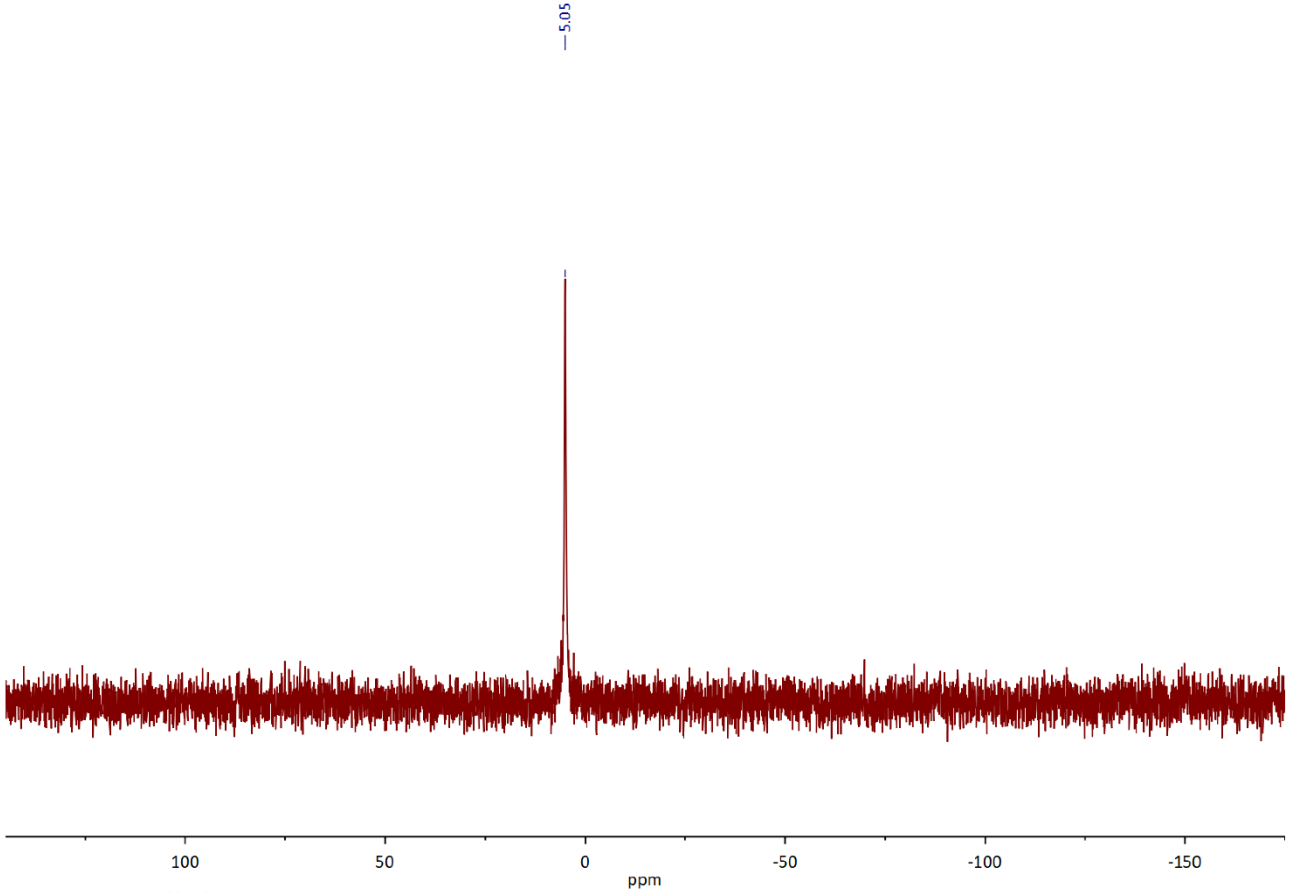

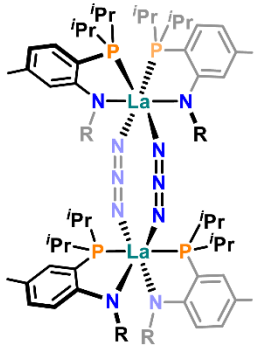

Fig. S18: $^{31}P\{^{1}H\}$ NMR spectrum of crude **4** in C_6D_6 (303 K).

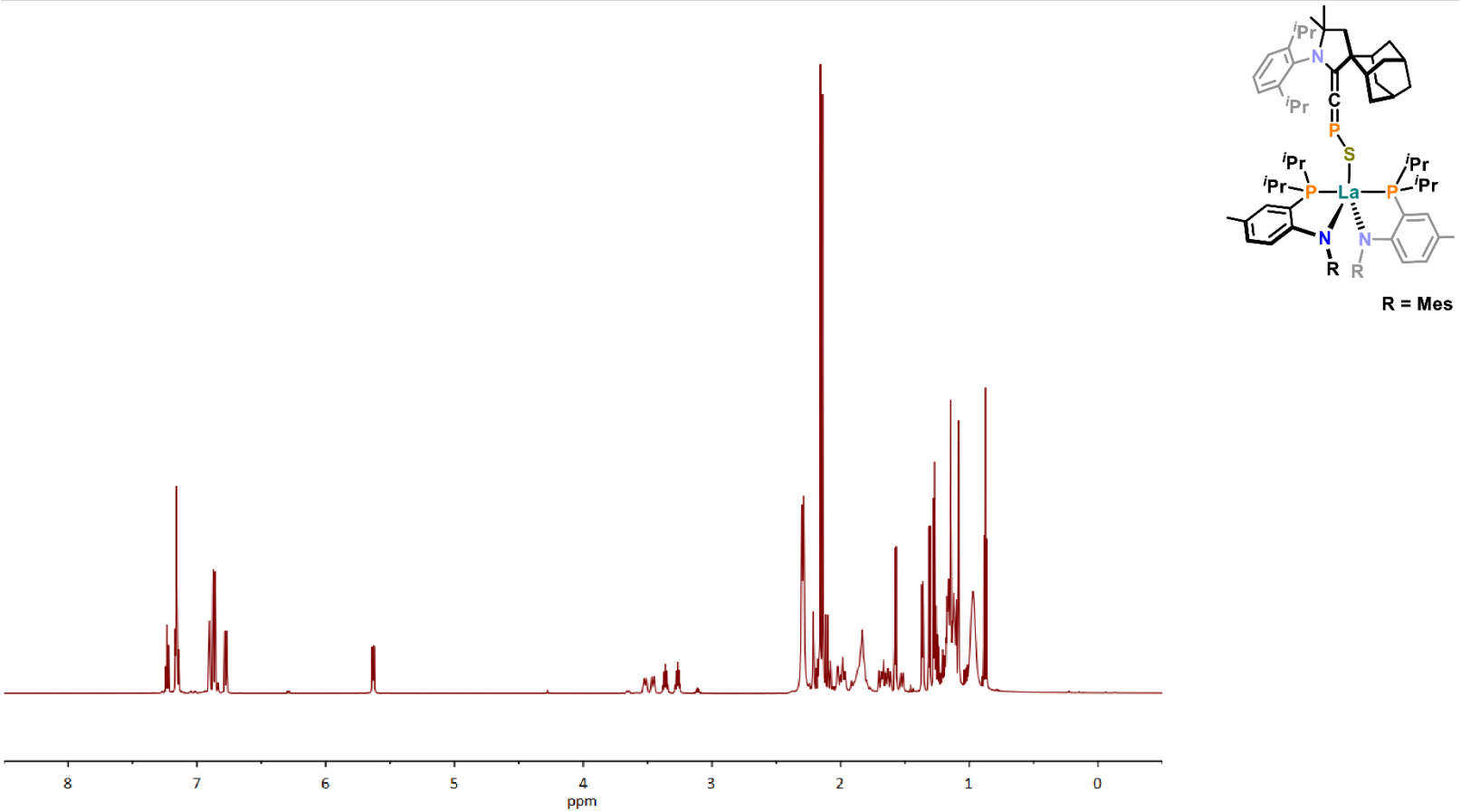

Fig. S19: *^{1}H NMR spectrum of **5a** in C_6D_6 (303 K). For chemical shifts and integrals please see Fig. S20–S22.*

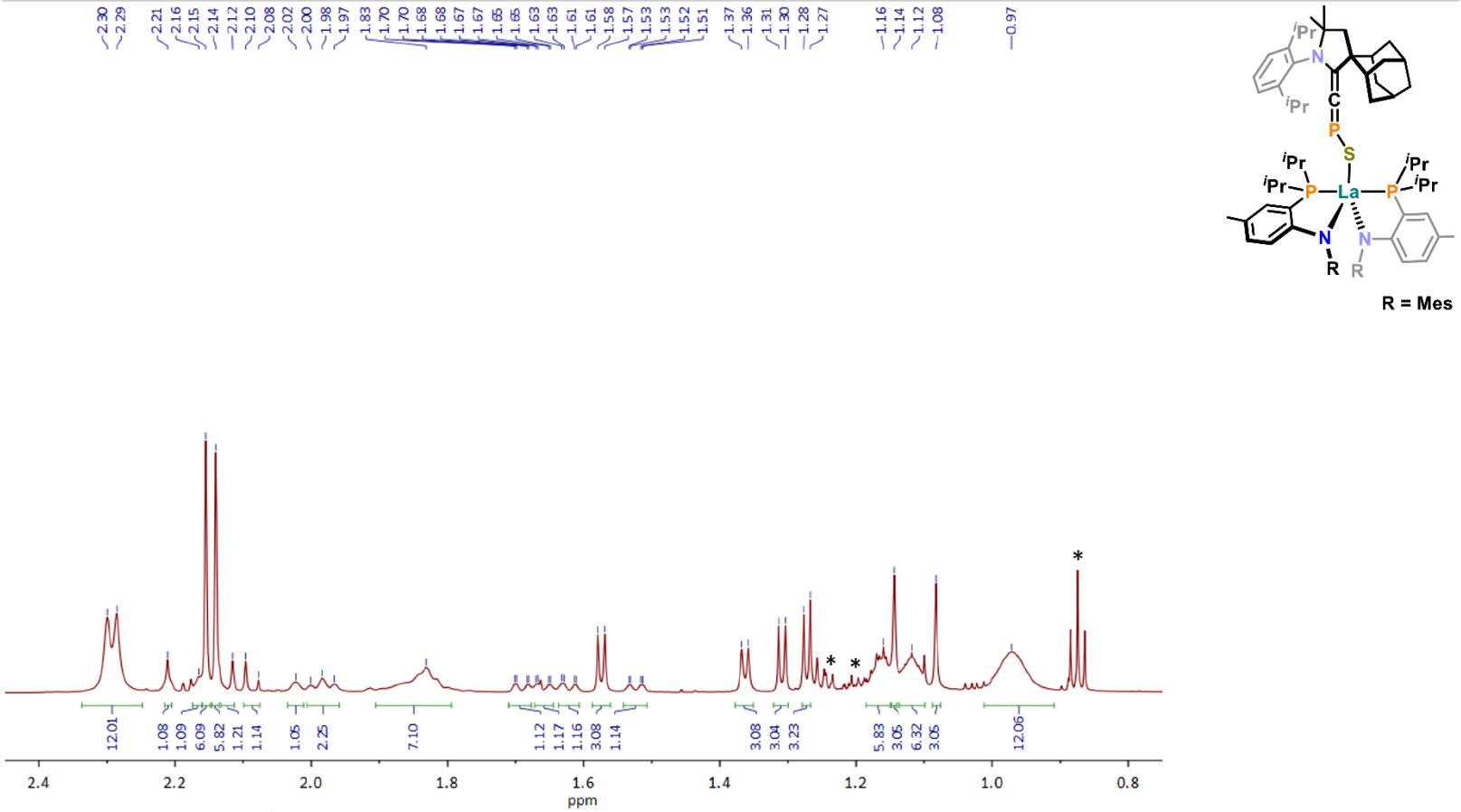

Fig. S20: *Section of the ^{1}H NMR spectrum (δ = 2.45 – 0.75 ppm) of **5a** in C_6D_6 (303 K). Residual n-pentane from work-up is marked by asterisks (*).*

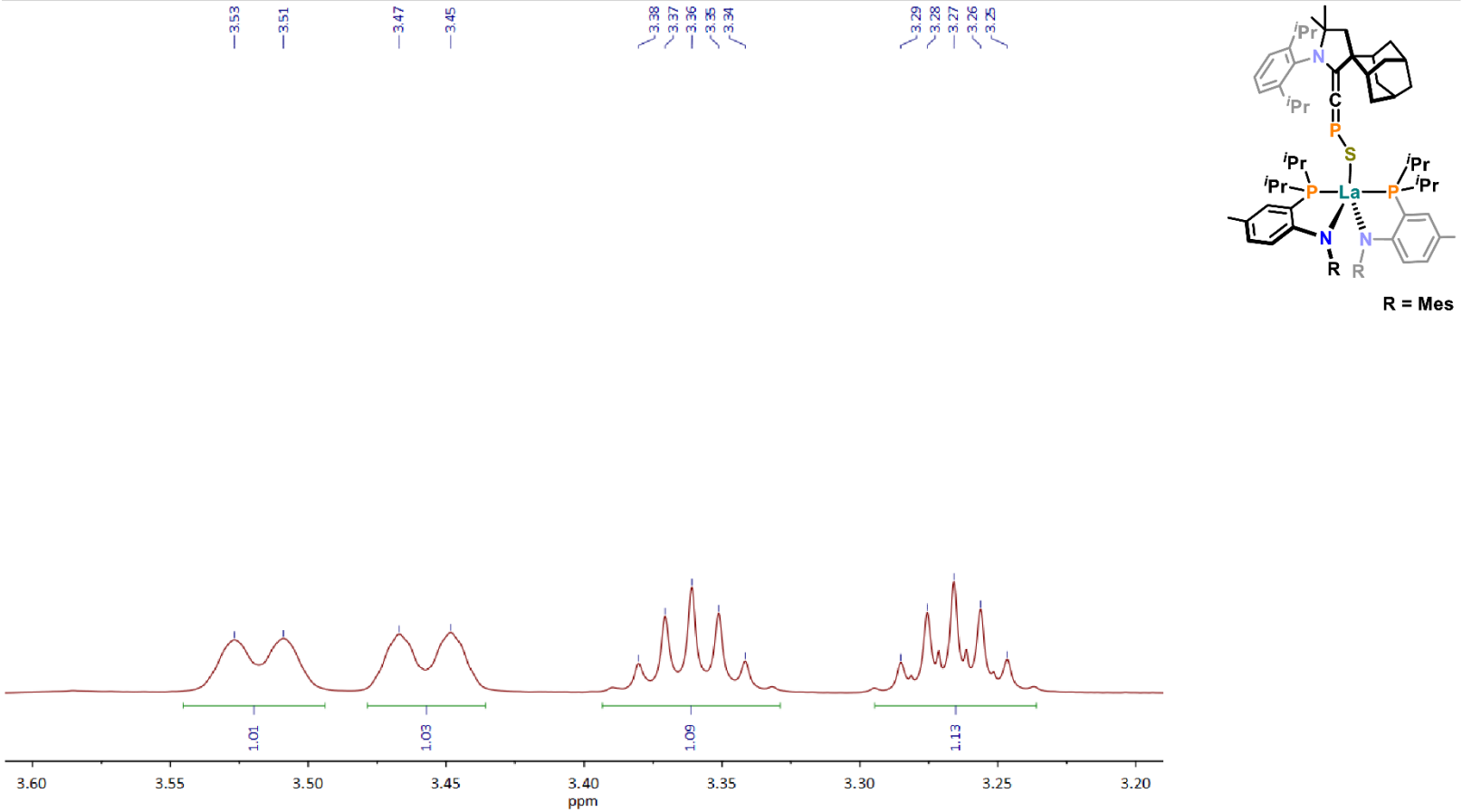

Fig. S21: *Section of the ^{1}H NMR spectrum (δ = 3.6 – 3.2 ppm) of **5a** in C_6D_6 (303 K).*

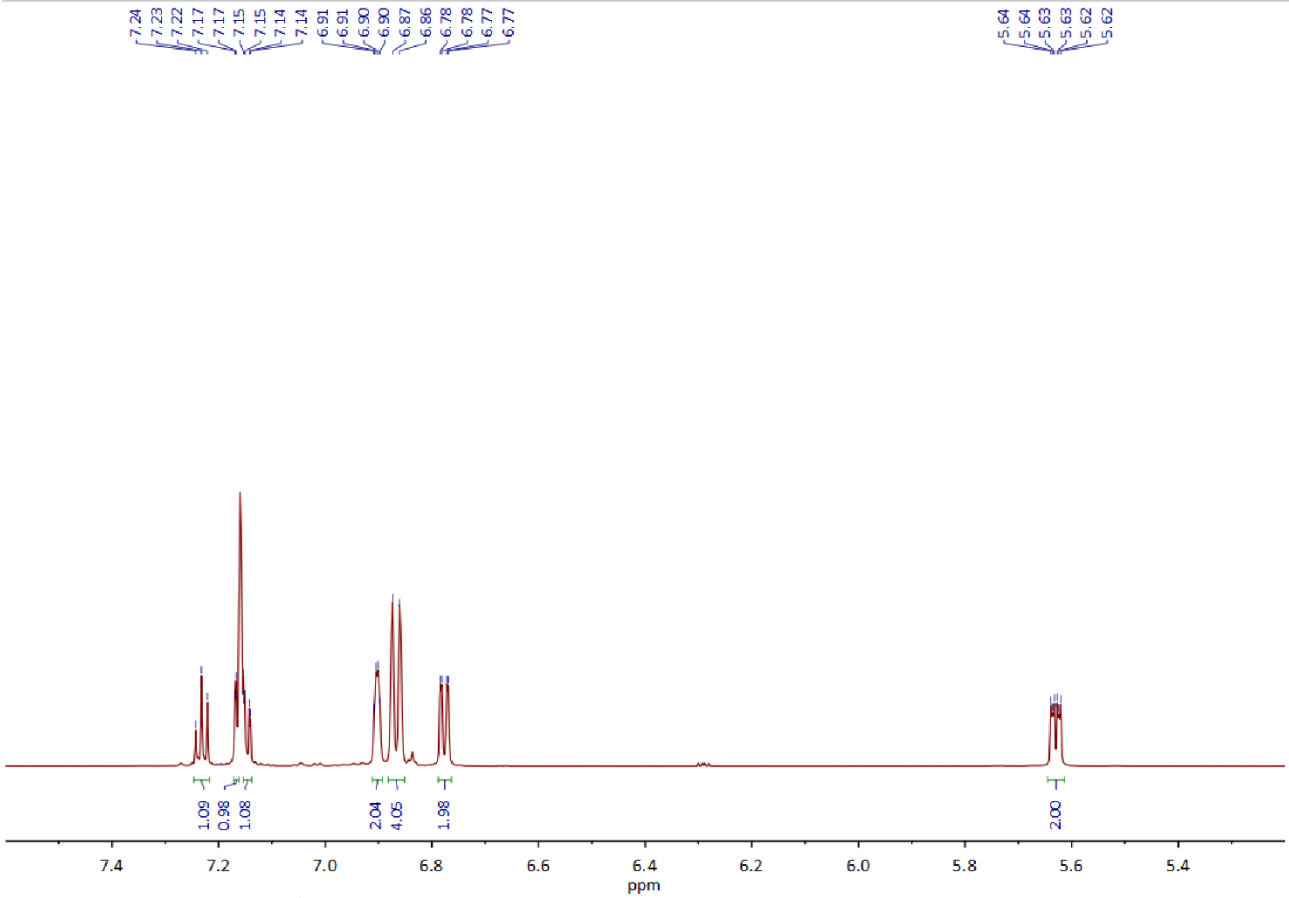

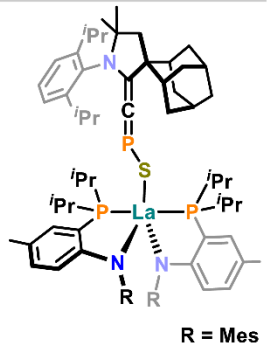

R = Mes

Fig. S22: *Section of the ^{1}H NMR spectrum (δ = 7.6 – 5.2 ppm) of **5a** in C_6D_6 (303 K).*

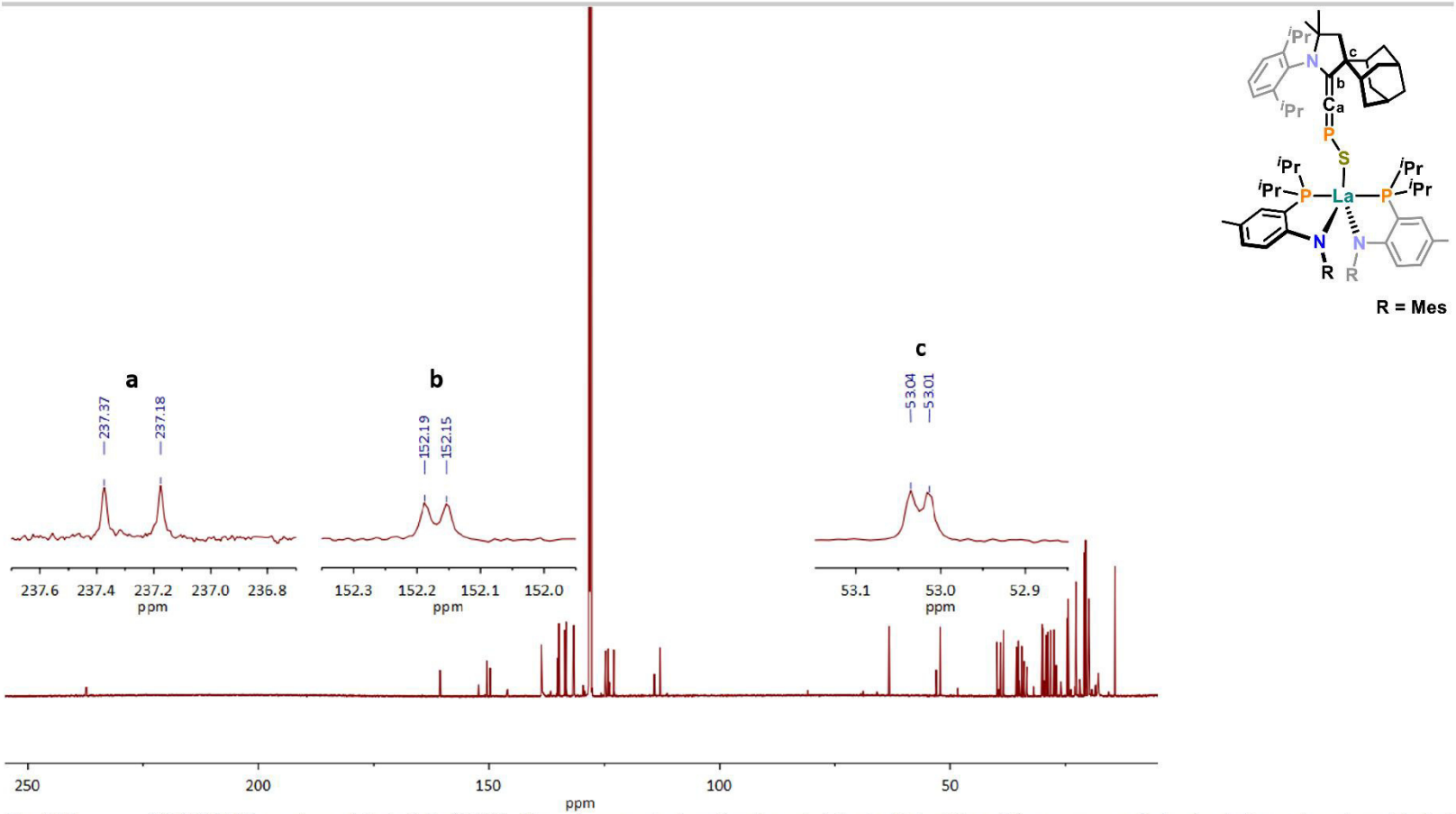

Fig. S23: *$^{13}C\{^1H\}$ NMR spectrum of **5a** in C_6D_6 (303 K). The enlargements show the characteristic doublet splitting of the resonances belonging to the carbon atoms labelled **a** (δ = 237.3 ppm, $^1J_{CP}$ = 20.6 Hz), **b** (δ = 152.2 ppm, $^2J_{CP}$ = 6.1 Hz) and **c** (δ = 53.0 ppm, $^3J_{CP}$ = 3.8 Hz), respectively. For a complete list of chemical shifts please see Fig. S24 and Fig. S25.*

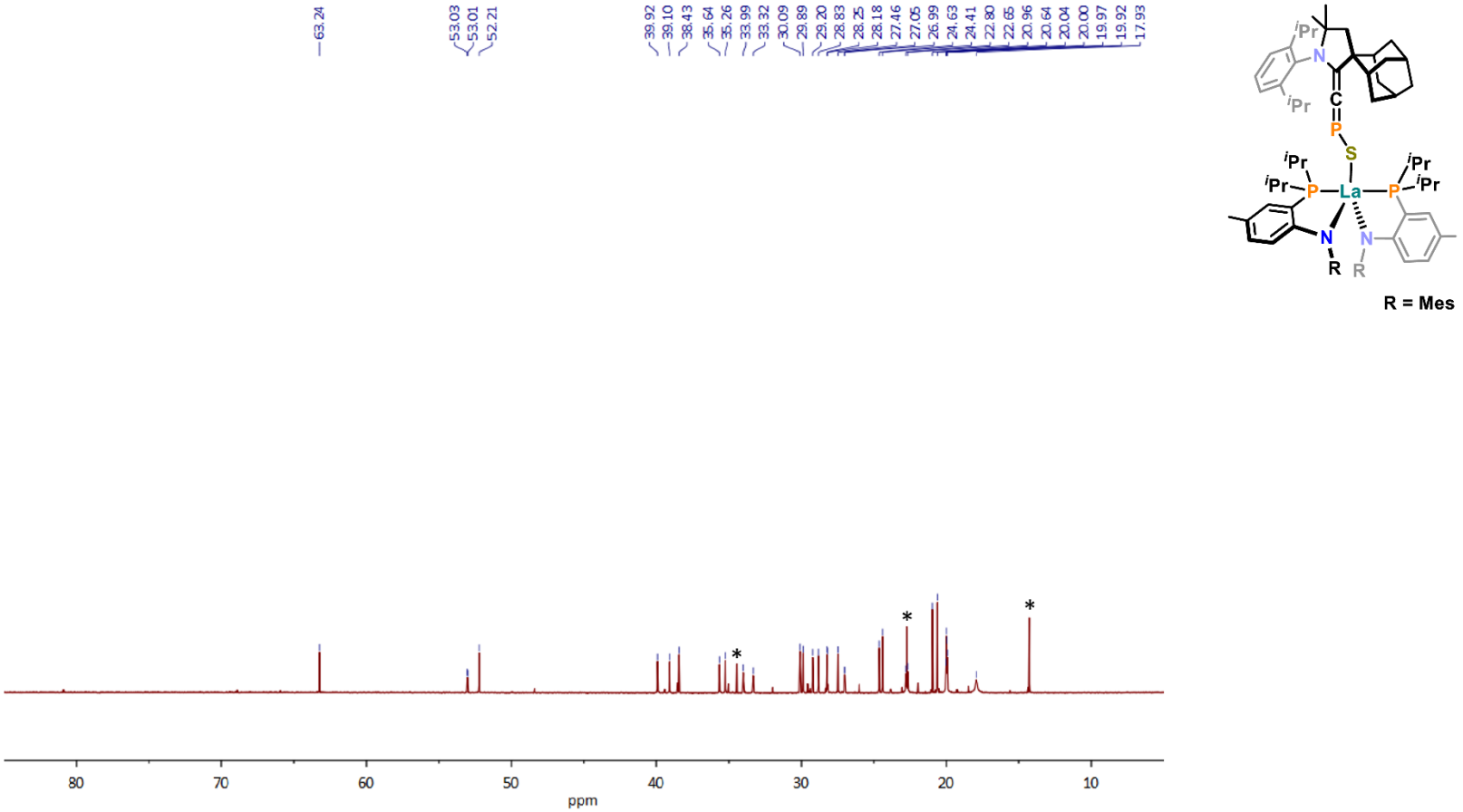

Fig. S24: *Section of the $^{13}C\{^{1}H\}$ NMR spectrum (δ = 85.0–5.0 ppm) of **5a** in C_6D_6 (303 K). Residual n-pentane from work-up is marked by asterisks (*).*

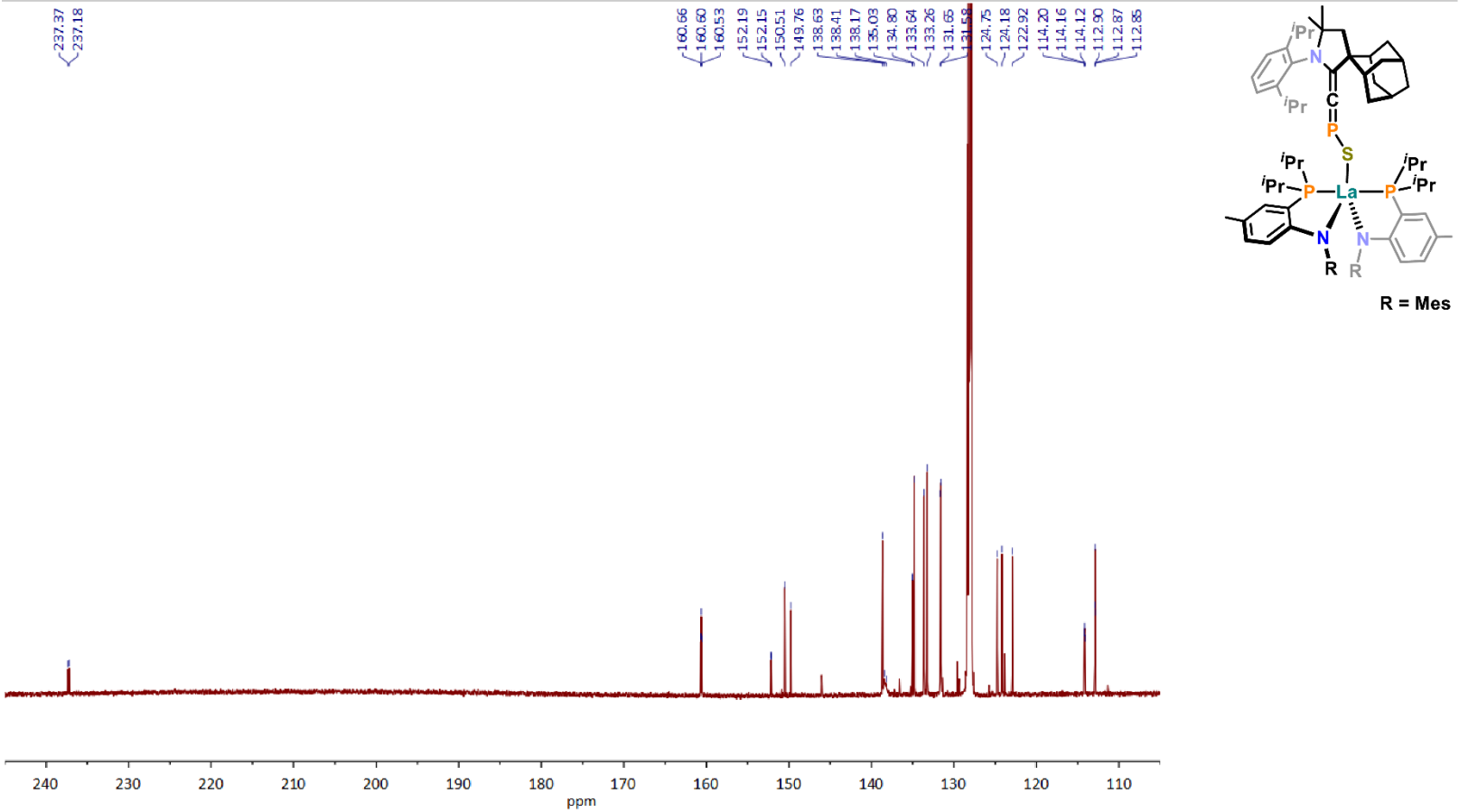

Fig. S25: *Section of the $^{13}C\{^{1}H\}$ NMR spectrum (δ = 245.0–105.0 ppm) of **5a** in C_6D_6 (303 K).*

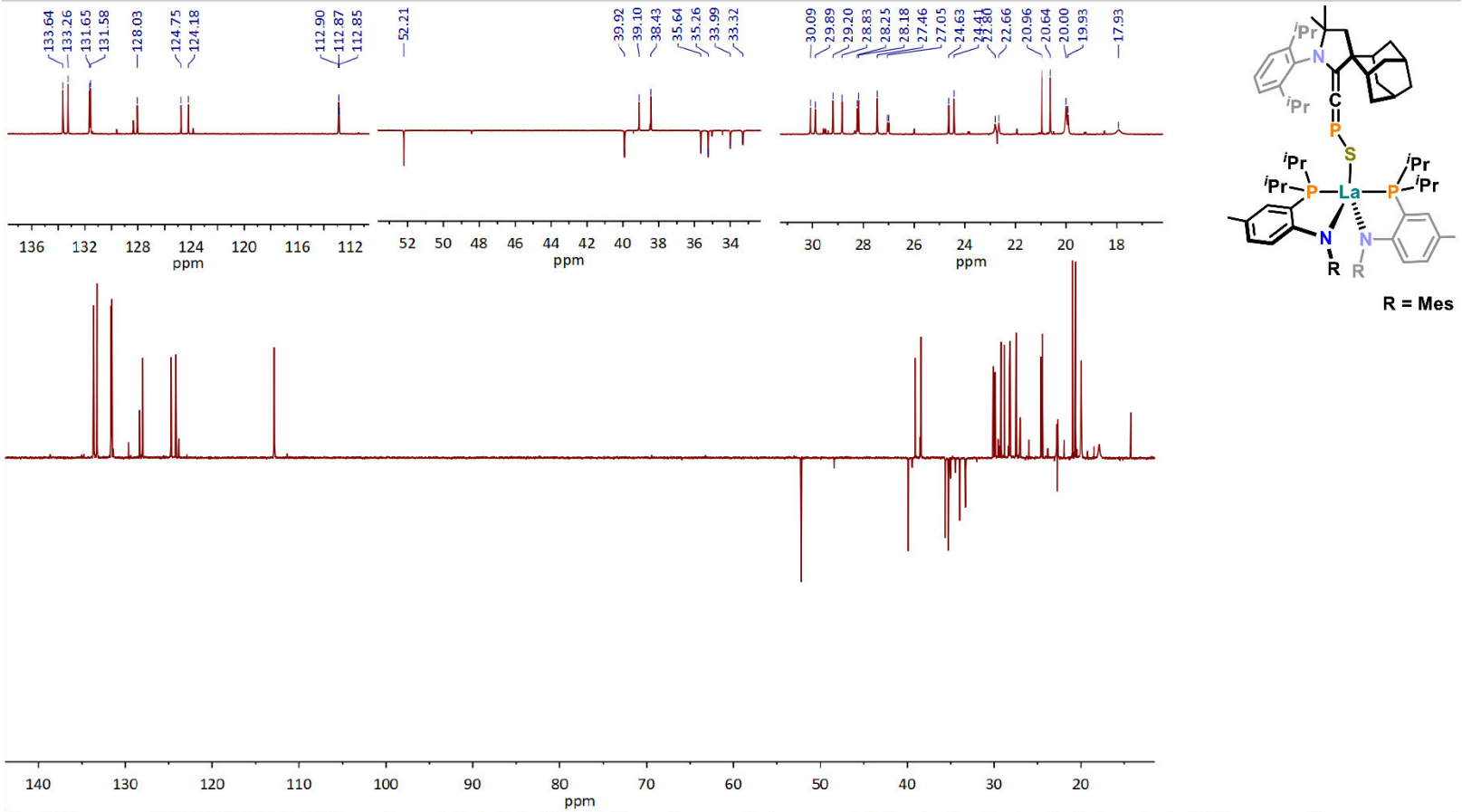

Fig. S26: *$^{13}C\{^1H\}$ DEPT135 NMR spectrum of **5a** in C_6D_6 (303 K). The enlargement gives a peak listing for the six chemically inequivalent CH_2 groups. The resonances at δ = 34.5, 22.7 and 14.3 ppm can be assigned to residual n-pentane from work-up. The three enlargements at the top show the resonances of complex **5a** in the aromatic region between δ ≈ 136 and 112 ppm (left) and the aliphatic regions between δ ≈ 53 and 32 ppm (middle) as well as δ ≈ 31 and 16 ppm (right).*

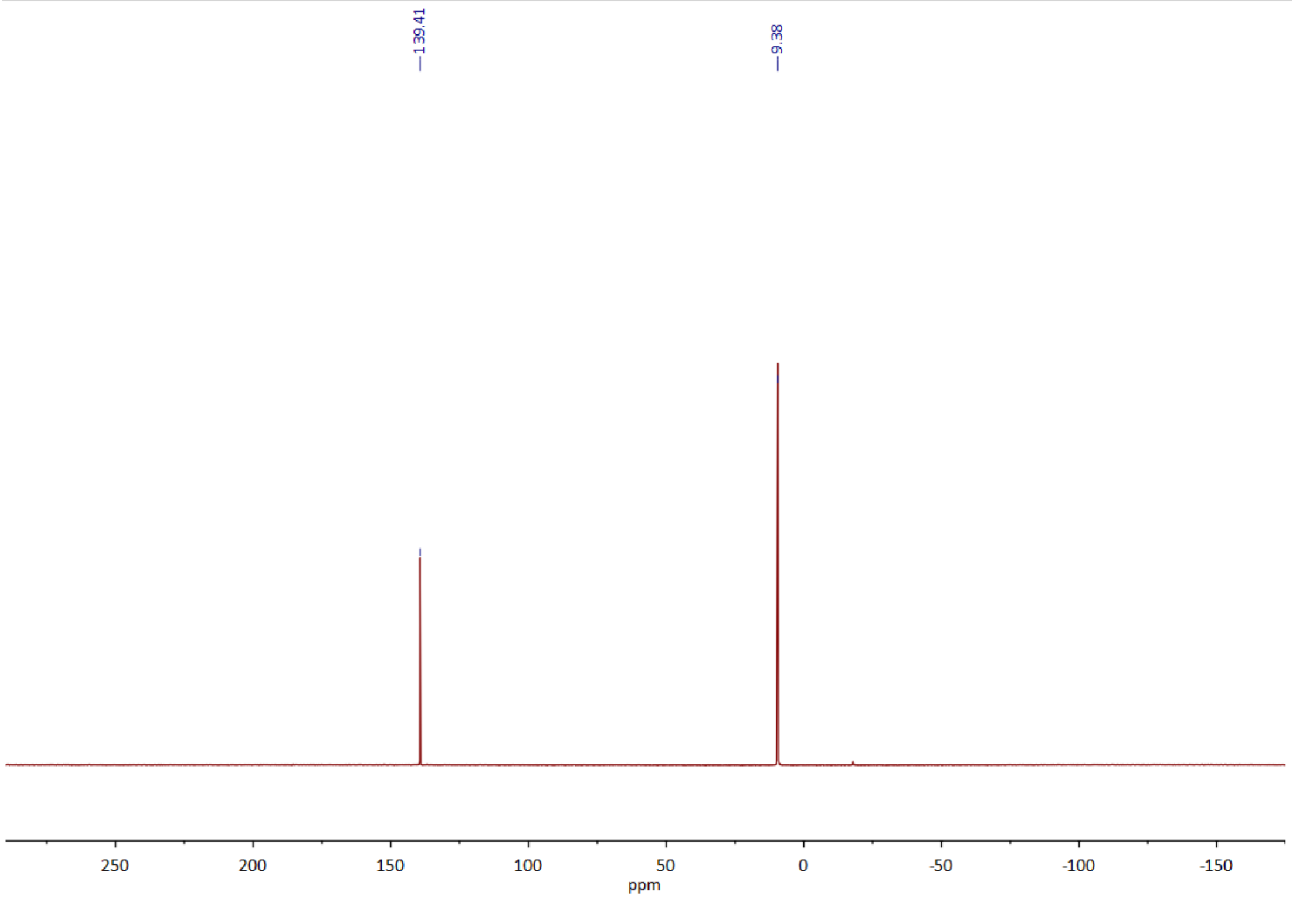

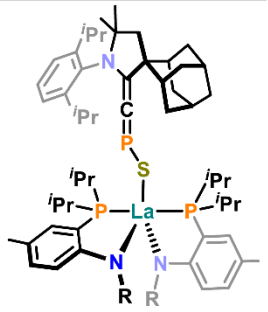

R = Mes

Fig. S27: $^{31}P\{^{1}H\}$ NMR spectrum of **5a** in C_6D_6 (303 K).

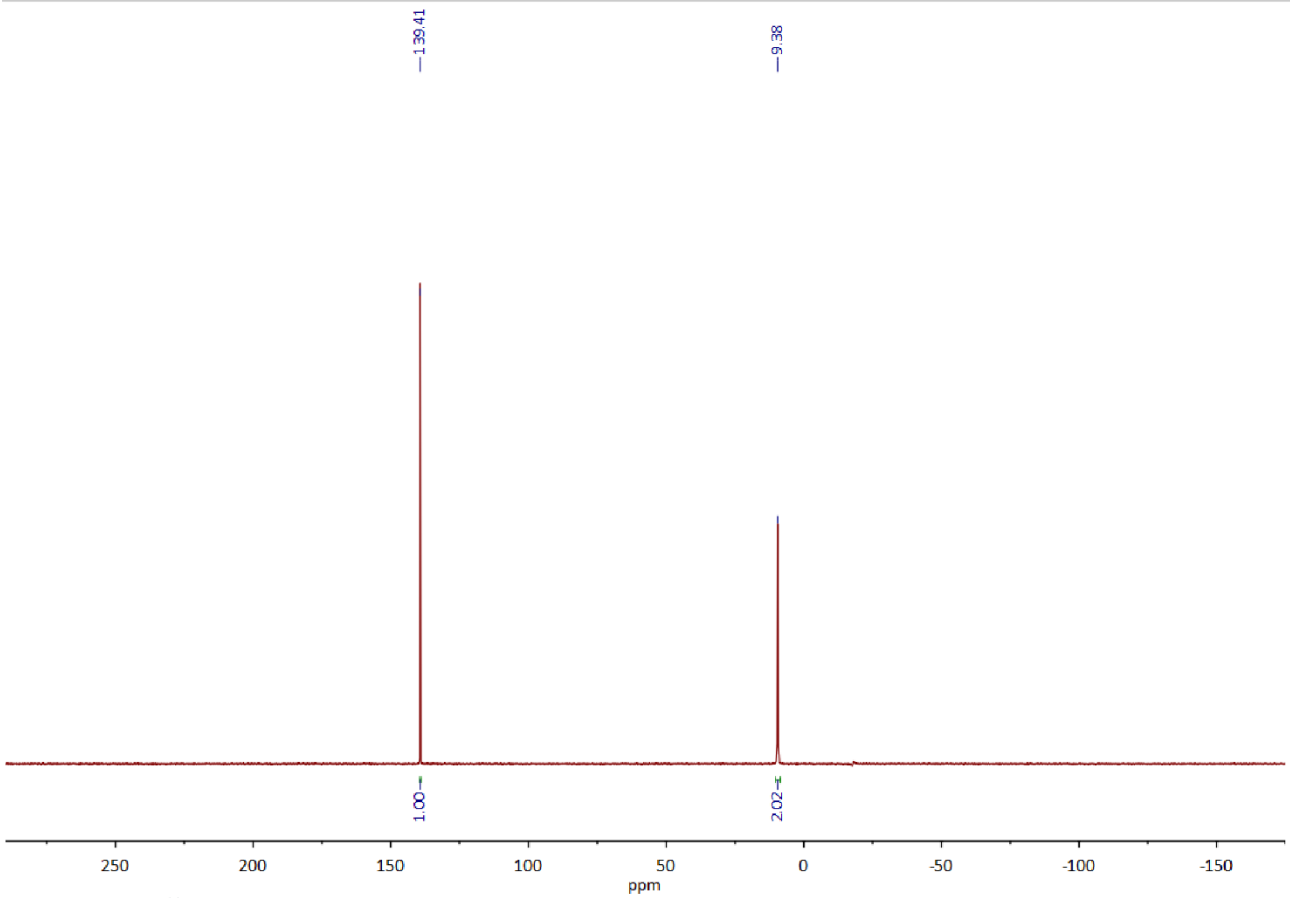

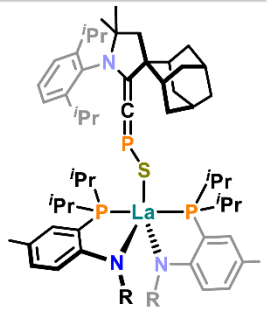

R = Mes

Fig. S28: *^{31}P NMR spectrum of **5a** in C_6D_6 (303 K).*

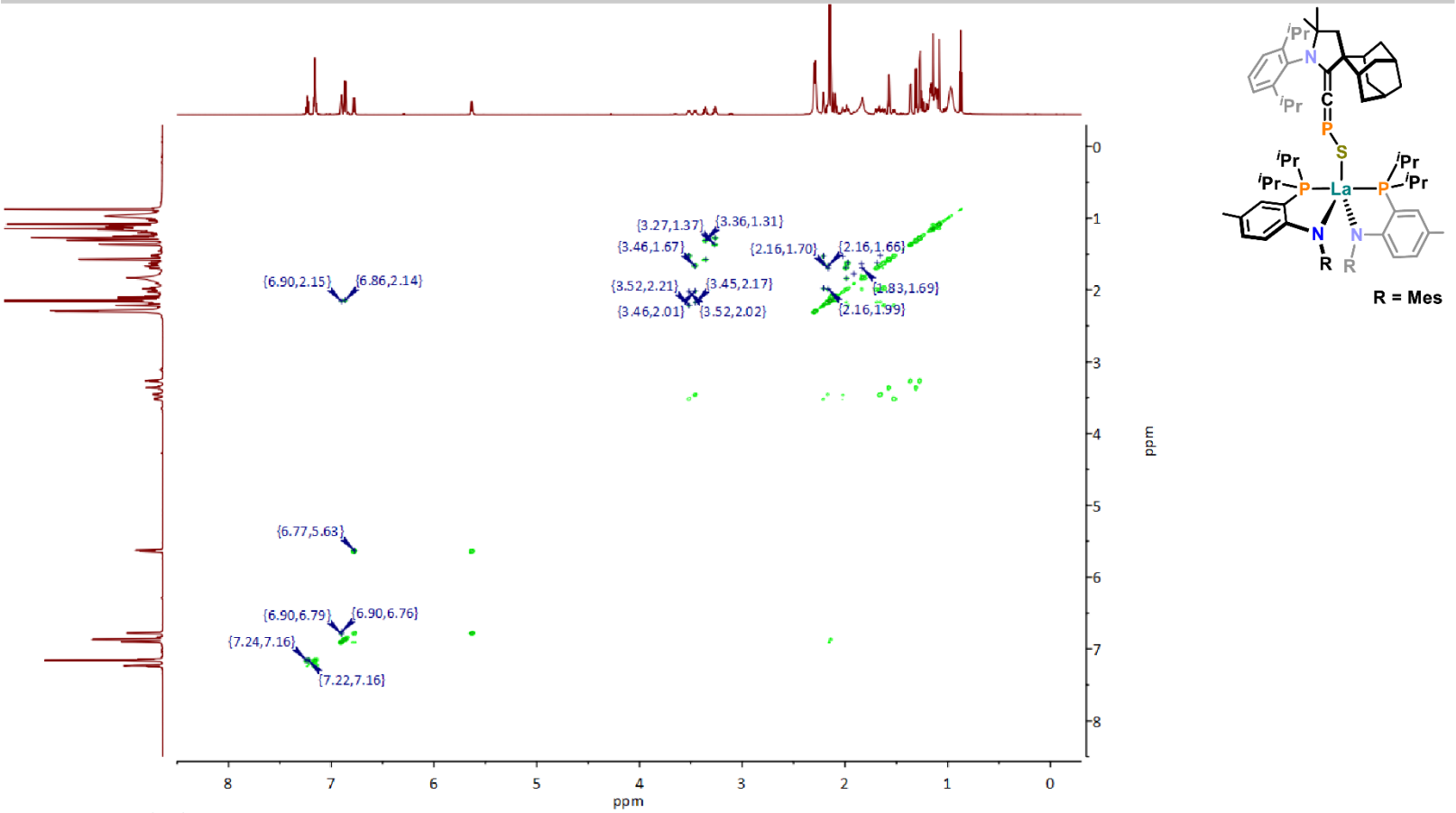

Fig. S29: *^{1}H–^{1}H COSY NMR spectrum of **5a** in C_6D_6 (303 K).*

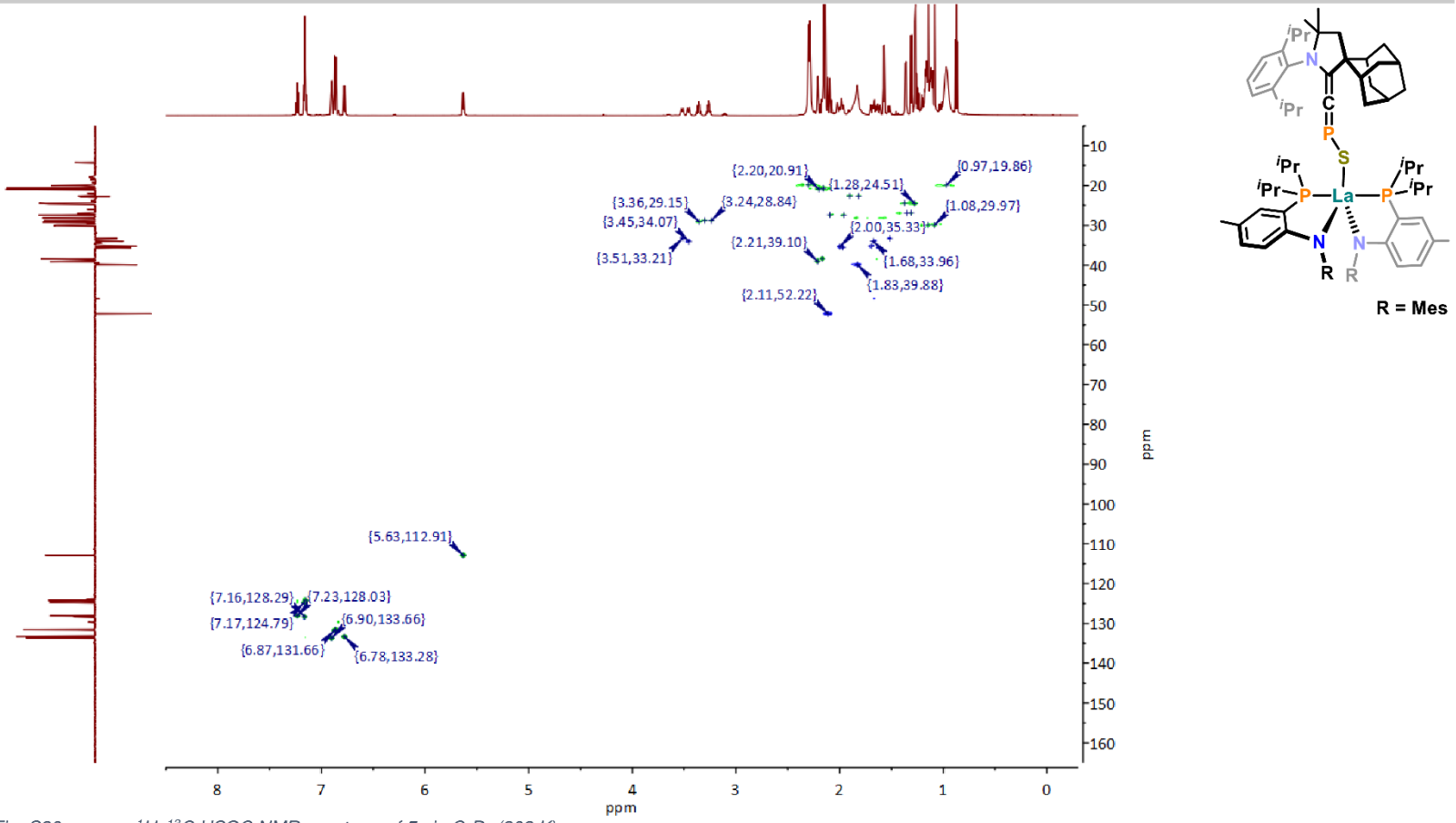

Fig. S30: *^{1}H–^{13}C HSQC NMR spectrum of **5a** in C_6D_6 (303 K).*

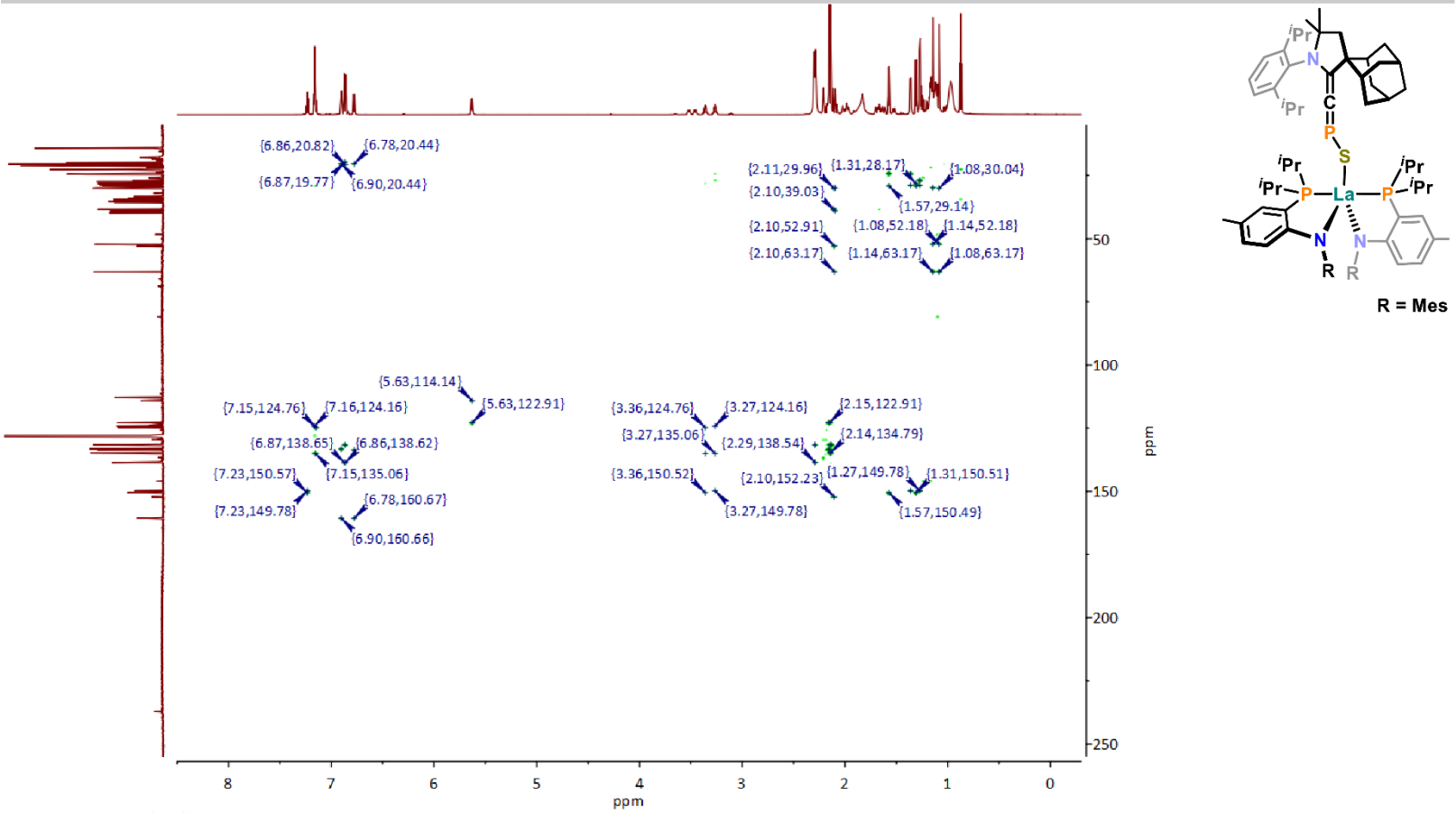

R = Mes

Fig. S31: *^{1}H–^{13}C HMBC NMR spectrum of **5a** in C_6D_6 (303 K).*

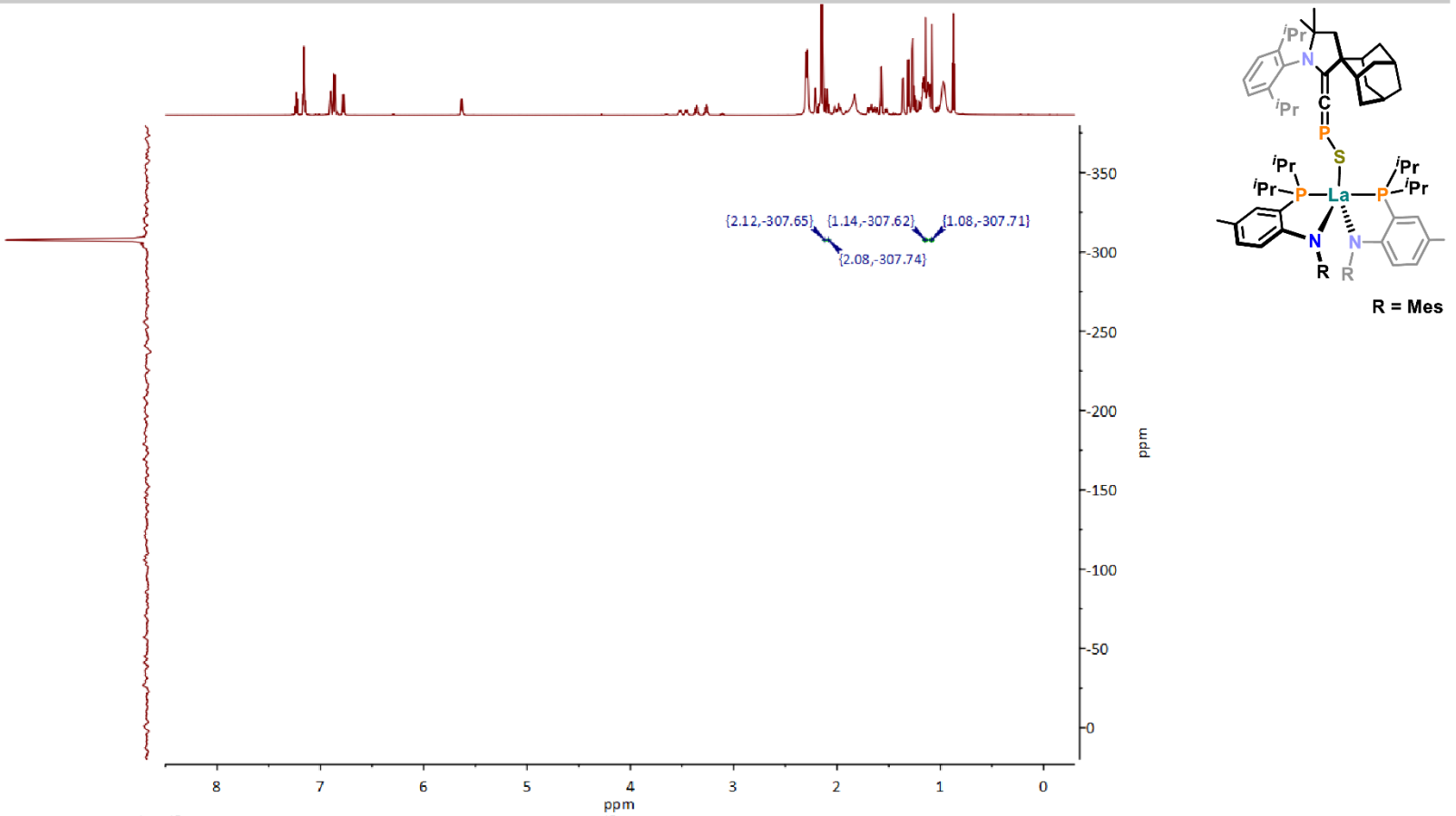

Fig. S32: *^{1}H–^{15}N HMBC NMR spectrum of **5a** in C_6D_6 (303 K). The ^{15}N resonance can be confidently assigned to the pyrrolidin N atom, due to the correlation peaks with the CH_2 backbone group and the adjacent two geminal CH_3 groups. No clearly visible and therefore unambiguously assignable correlation peak for the PN ligands (typically at $\delta(^{15}N)$ >0 ppm) could be found.*

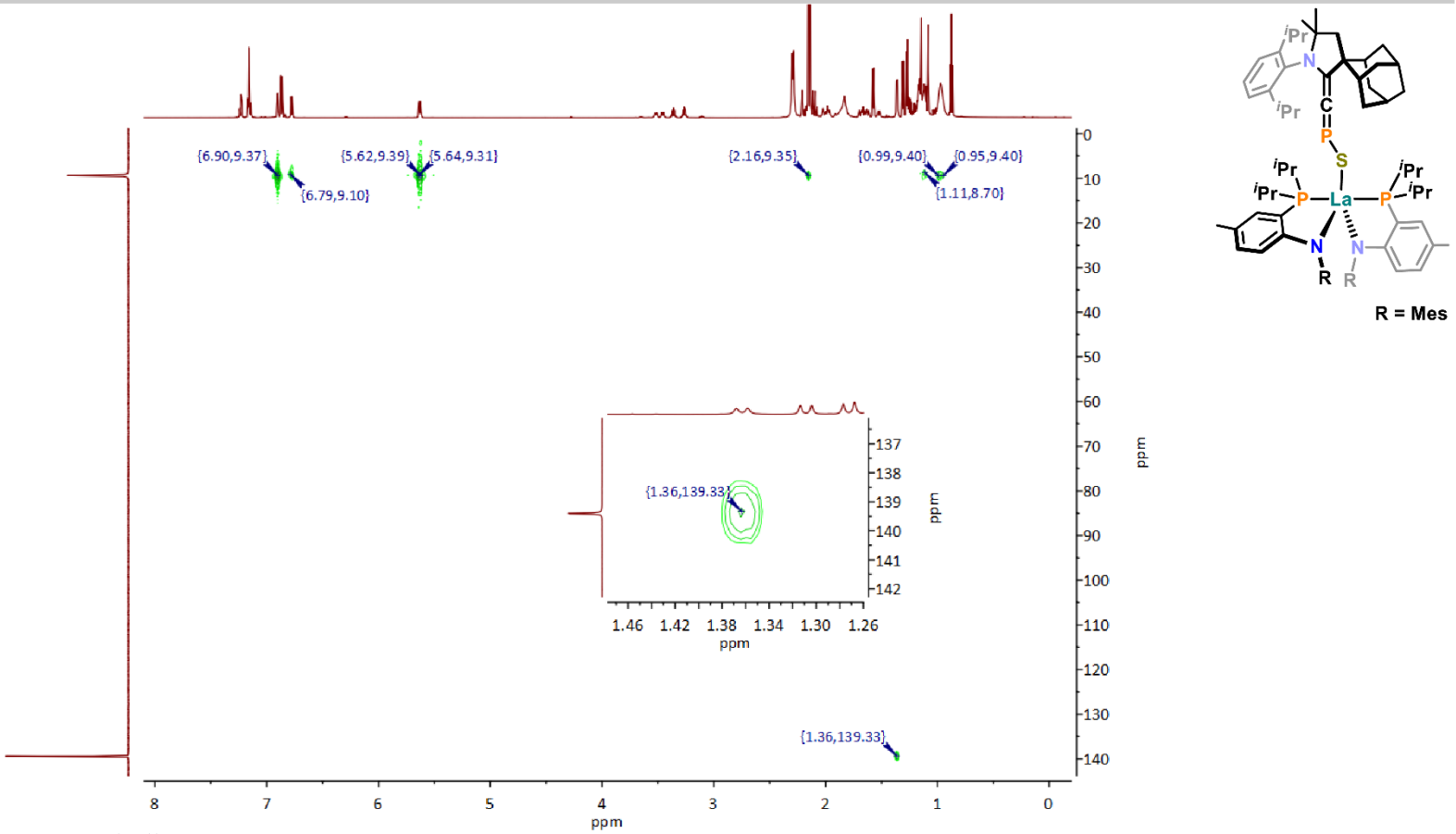

Fig. S33: *^{1}H–^{31}P HMBC NMR spectrum of **5a** in C_6D_6 (303 K). The enlargement shows the correlation peak between the P atom of the $^{-}SPCCR_2$ ligand and one of the CH_3 groups of the Dipp substituent, possibly due to an interaction through space.*

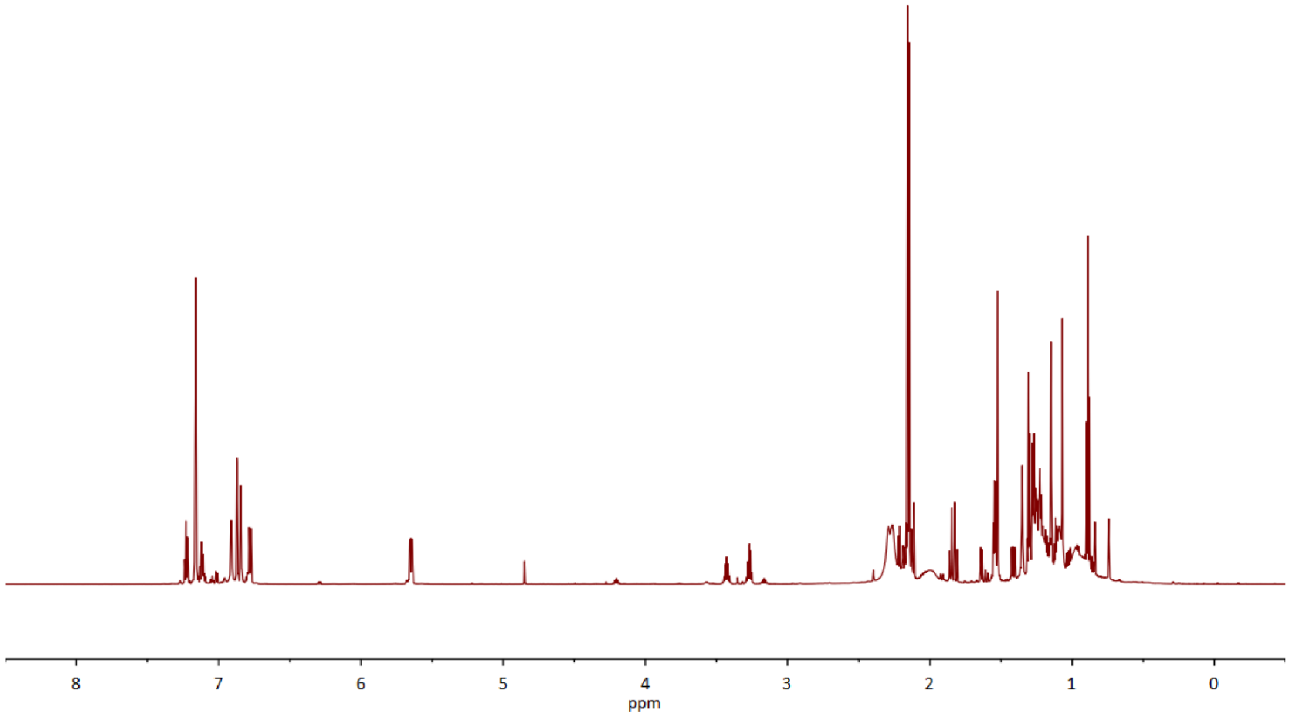

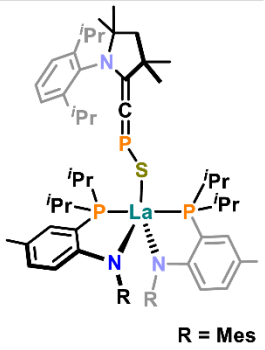

Fig. S34: *^{1}H NMR spectrum of crude **5b** (from NMR scale reaction of **2** with ^{Me}**CAAC**; not isolated) in C_6D_6 (303 K). For chemical shifts and integrals please see Fig. S35–S37.*

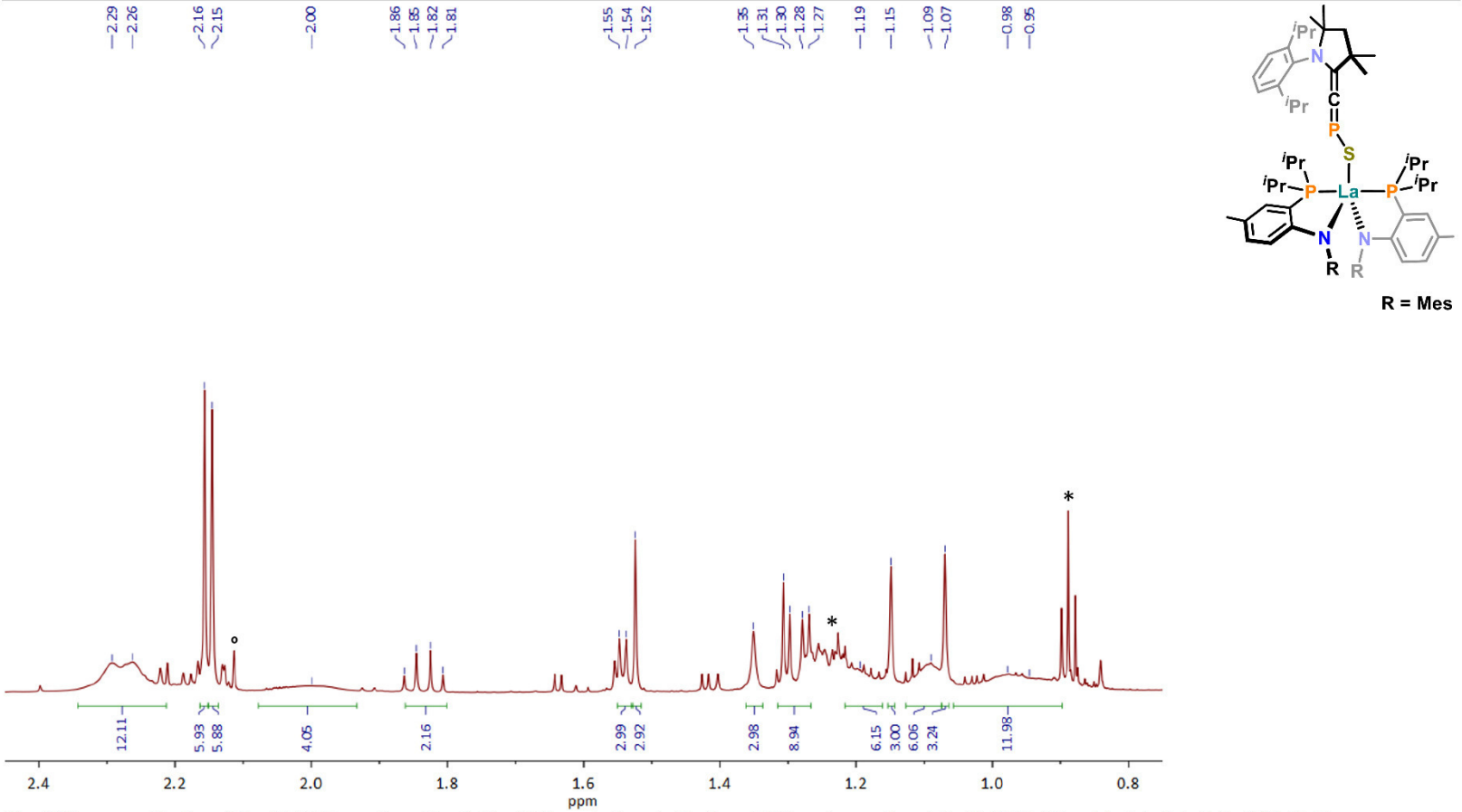

Fig. S35: *Section of the ^{1}H NMR spectrum (δ = 2.45 – 0.75 ppm) of crude **5b** (from NMR scale reaction of **2** with ^{Me}**CAAC**; not isolated) in C_6D_6 (303 K). Resonances of n-hexane are marked by asterisks (*), one resonance of toluene by °.*

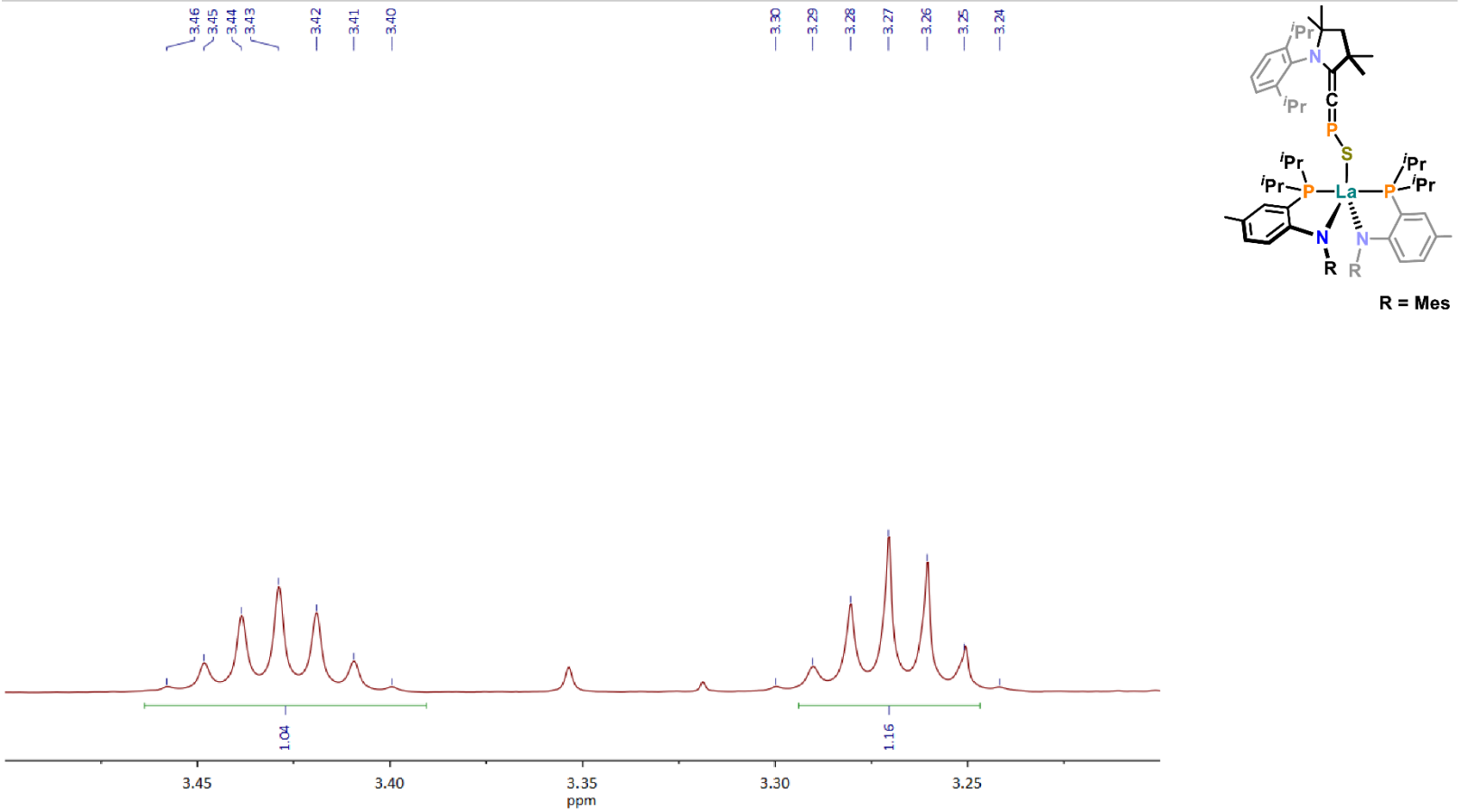

Fig. S36: *Section of the ^{1}H NMR spectrum (δ = 3.5 – 3.2 ppm) of crude **5b** (from NMR scale reaction of **2** with **^{Me}CAAC**; not isolated) in C_6D_6 (303 K).*

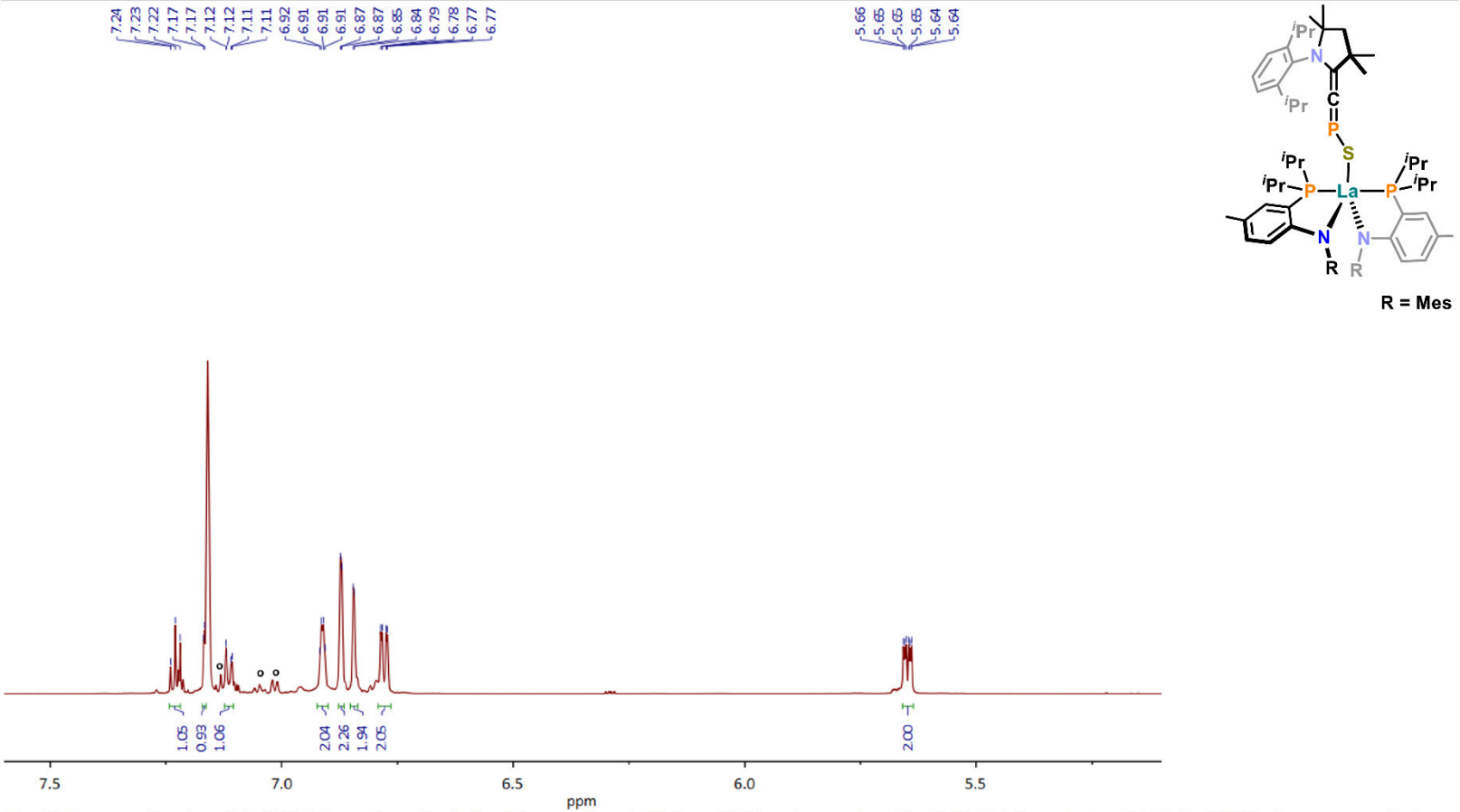

Fig. S37: *Section of the ^{1}H NMR spectrum (δ = 7.6 – 5.1 ppm) of crude **5b** (from NMR scale reaction of **2** with **^{Me}CAAC**; not isolated) in C_6D_6 (303 K). Resonances of toluene are marked by °.*

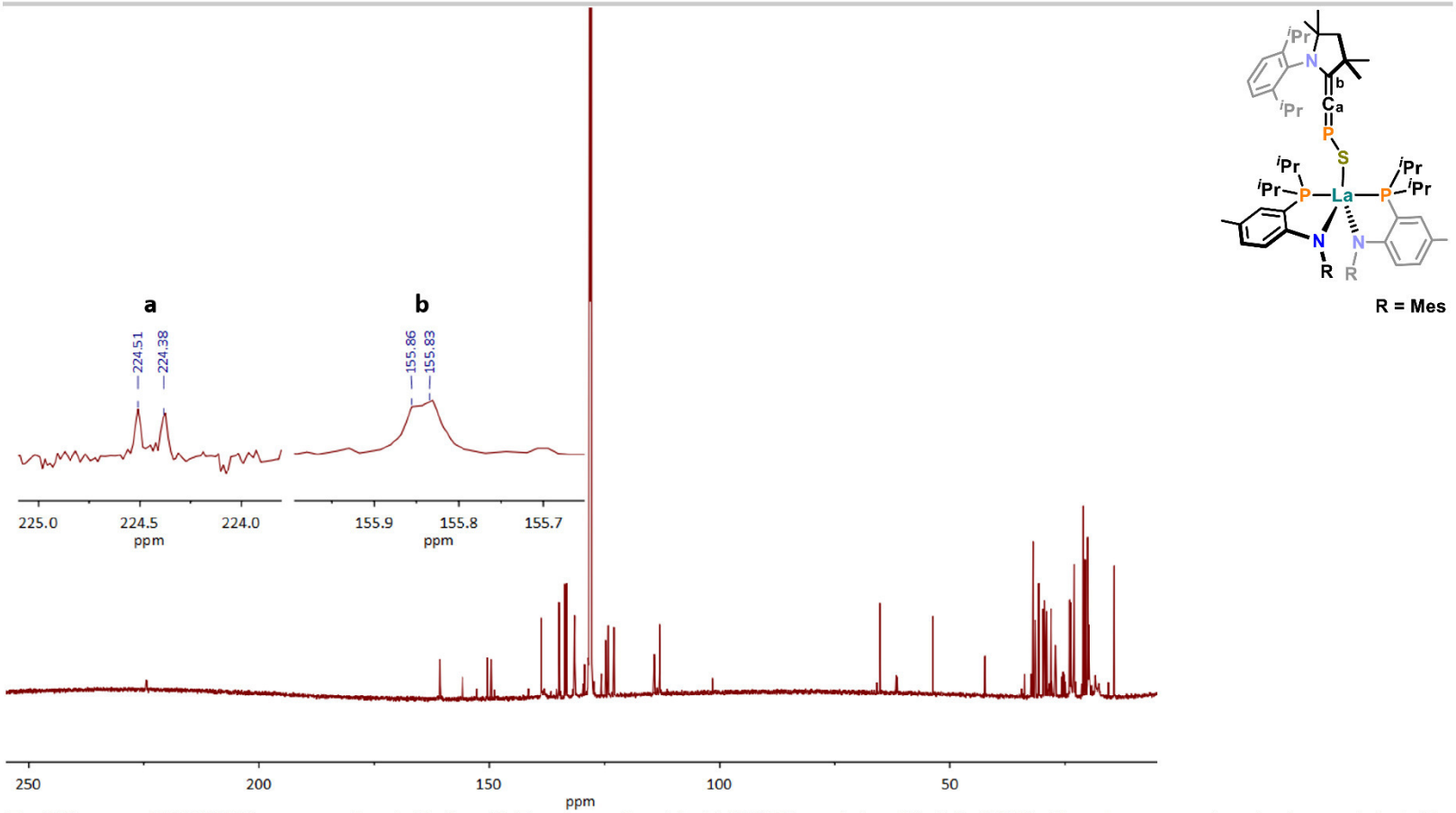

Fig. S38: *$^{13}C\{^1H\}$ NMR spectrum of crude **5b** (from NMR scale reaction of **2** with ^{Me}**CAAC**; not isolated) in C_6D_6 (303 K). The enlargements show the characteristic doublet splitting of the resonances belonging to the carbon atoms labelled **a** (δ = 224.5 ppm, $^1J_{CP}$ = 23.5 Hz) and **b** (δ = 155.8 ppm, $^2J_{CP}$ = 3.4 Hz), respectively. For a complete list of chemical shifts please see Fig. S39 and Fig. S40.*

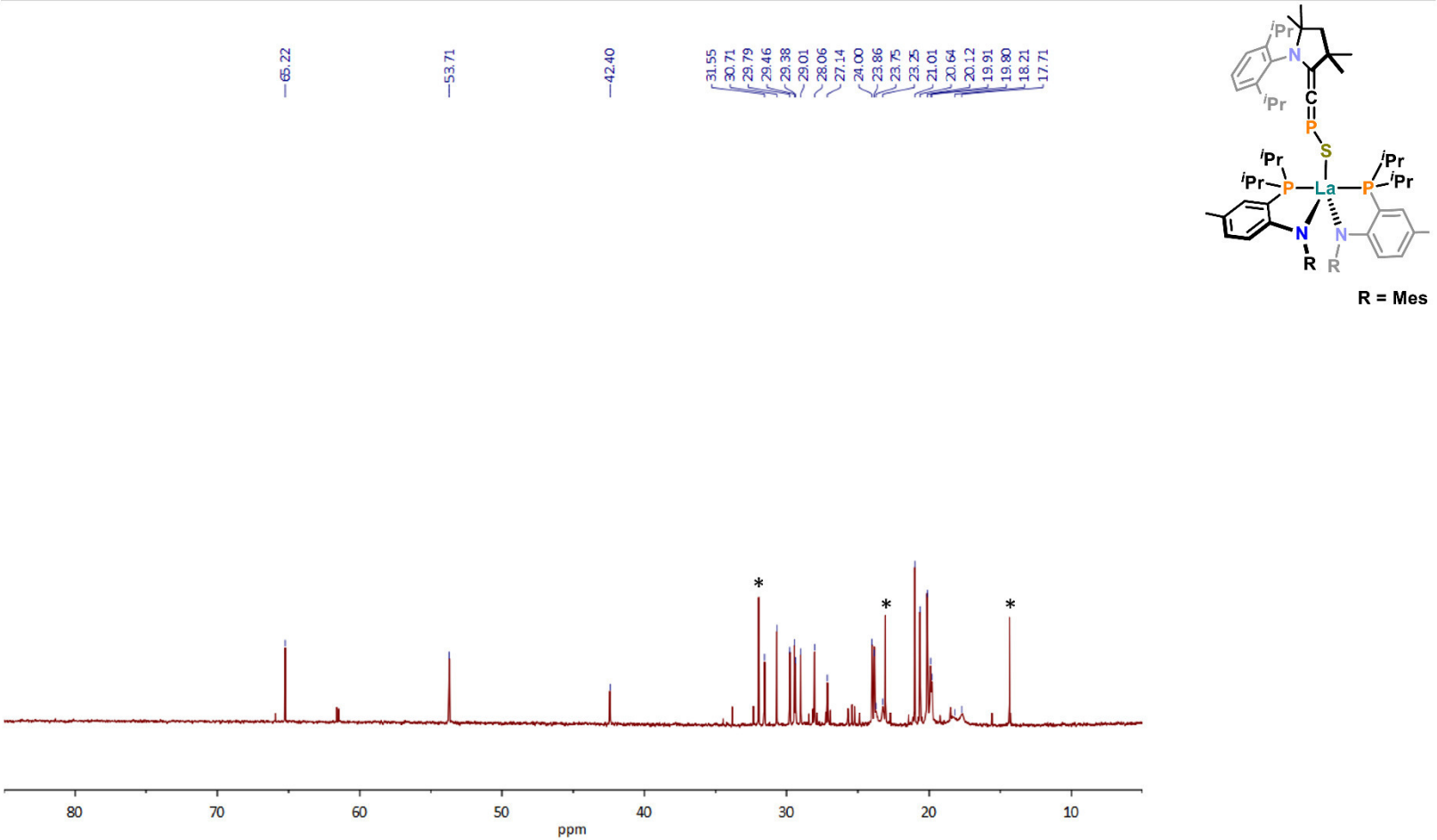

Fig. S39: *Section of the $^{13}C\{^{1}H\}$ NMR spectrum (δ = 85.0–5.0 ppm) of crude **5b** (from NMR scale reaction of **2** with ^{Me}**CAAC**; not isolated) in C_6D_6 (303 K). Resonances of n-hexane are marked by asterisks (*).*

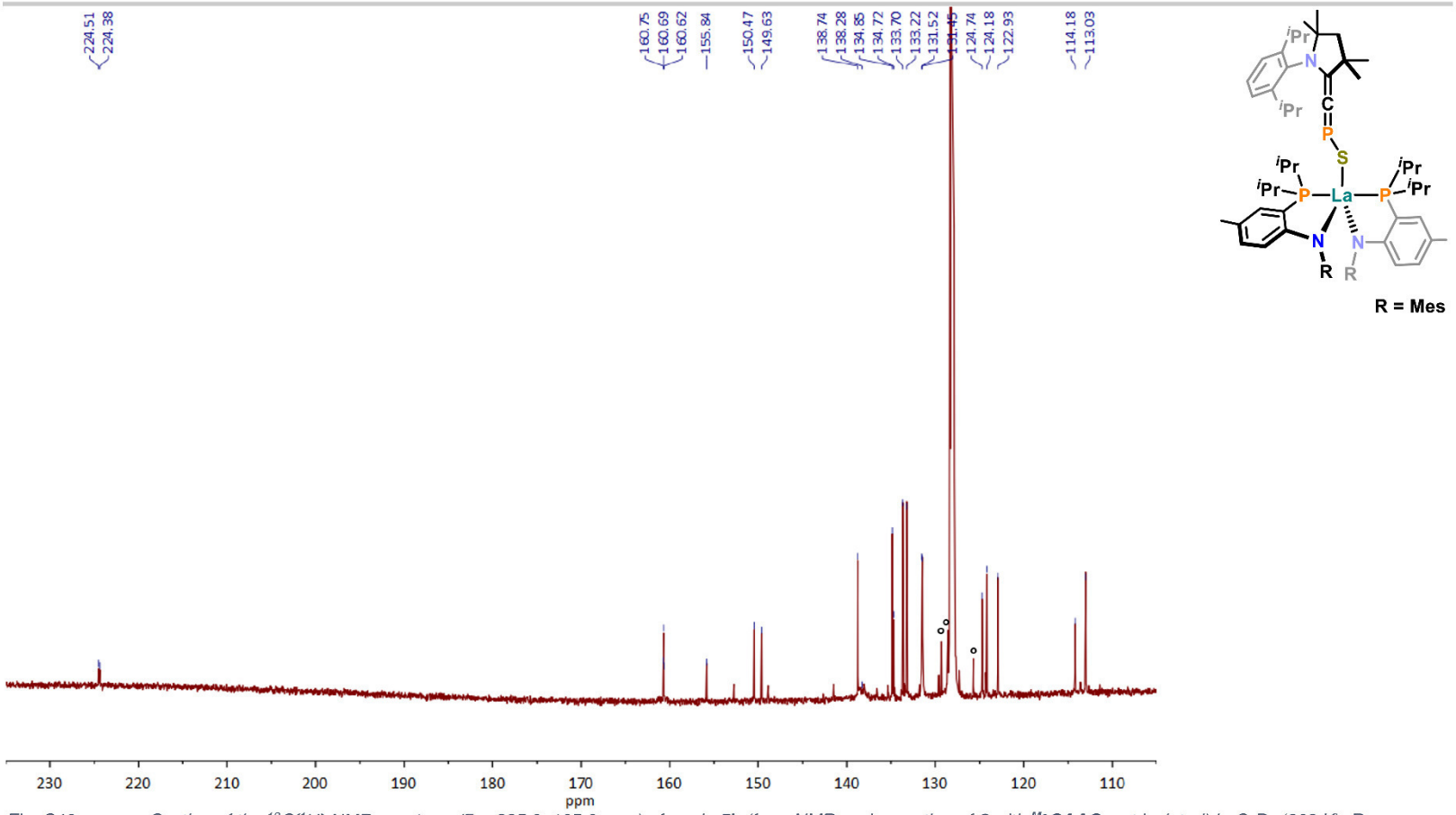

Fig. S40: *Section of the $^{13}C\{^1H\}$ NMR spectrum (δ = 235.0–105.0 ppm) of crude **5b** (from NMR scale reaction of **2** with **^{Me}CAAC**; not isolated) in C_6D_6 (303 K). Resonances of toluene are marked by °.*

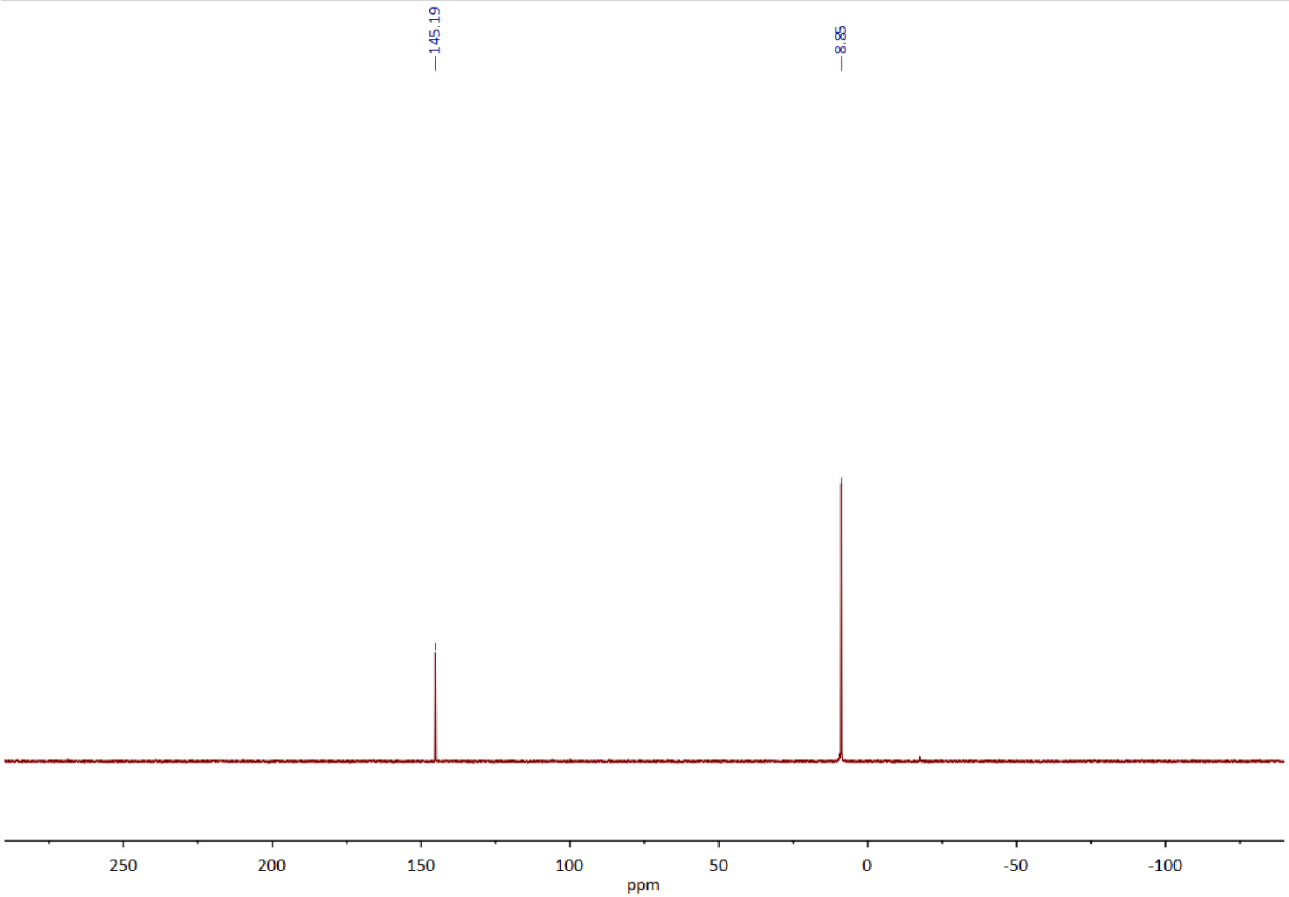

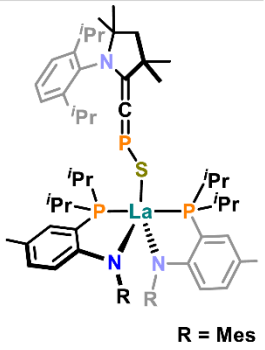

Fig. S41: $^{31}P\{^{1}H\}$ NMR spectrum of crude ***5b*** *(from NMR scale reaction of* ***2*** *with* ^{Me}***CAAC****; not isolated) in* C_6D_6 *(303 K).*

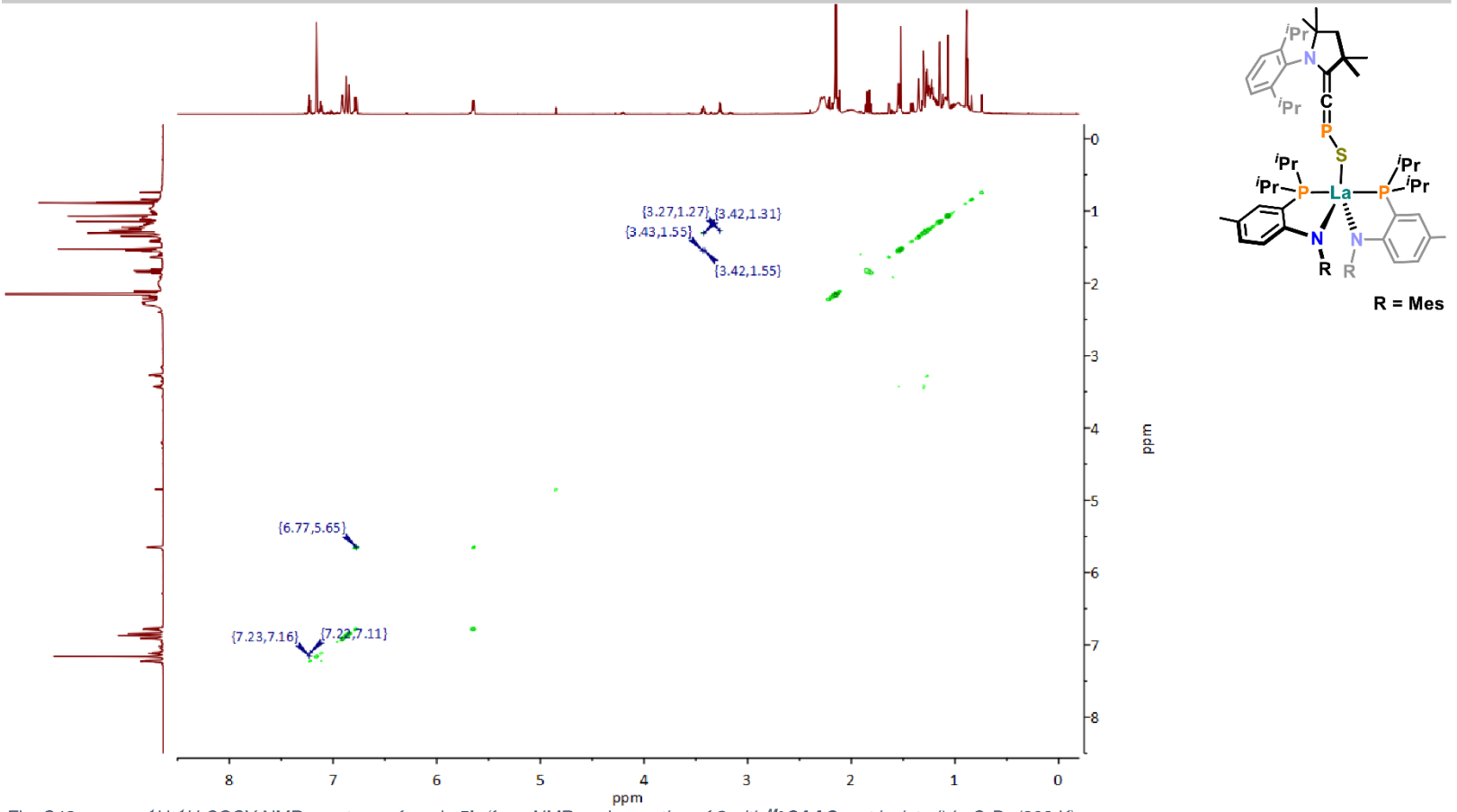

Fig. S42: *^{1}H–^{1}H COSY NMR spectrum of crude **5b** (from NMR scale reaction of **2** with ^{Me}**CAAC**; not isolated) in C_6D_6 (303 K).*

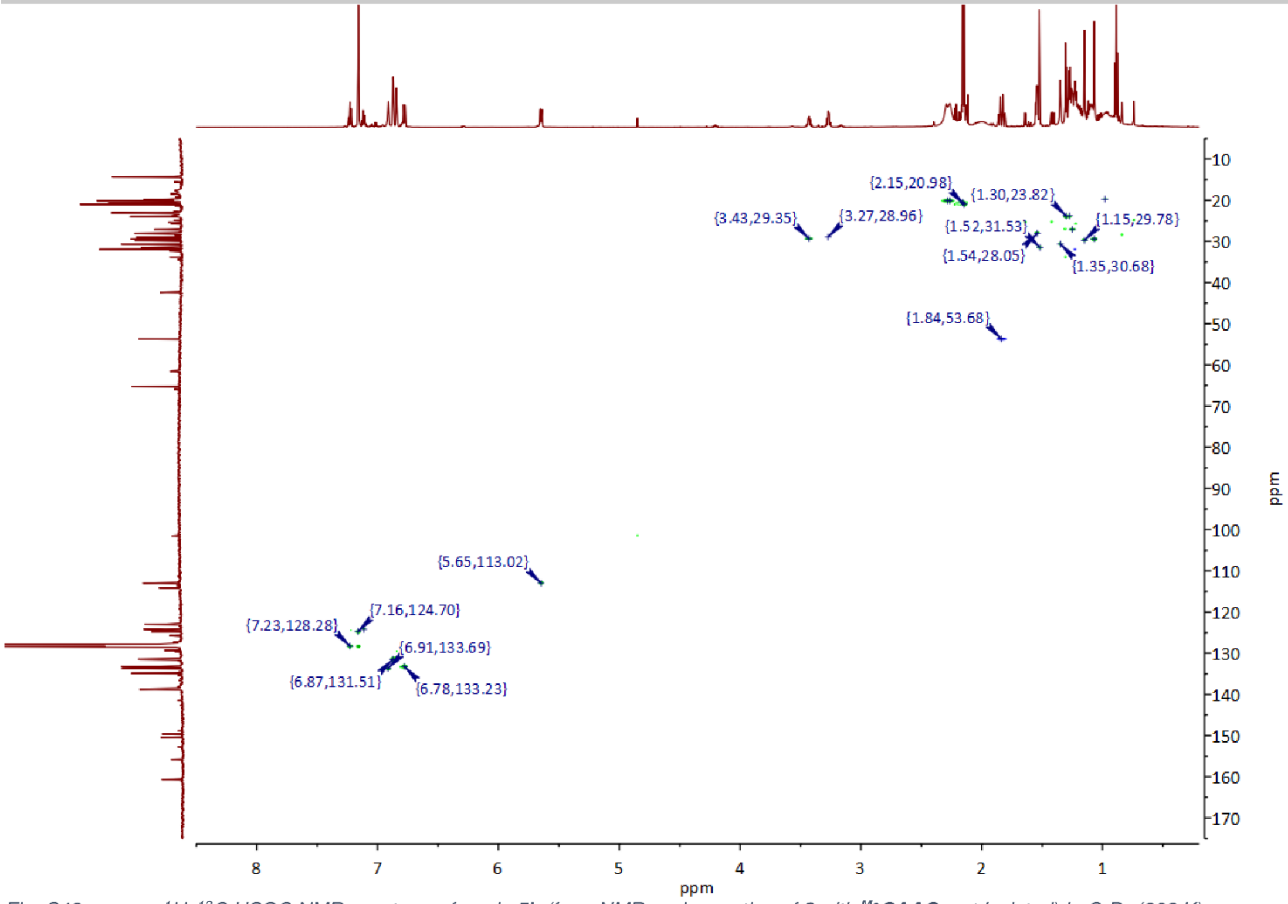

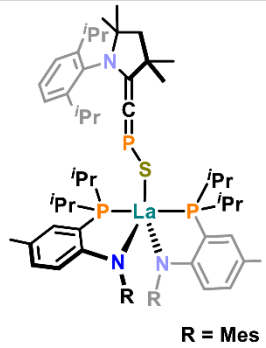

Fig. S43: *^{1}H–^{13}C HSQC NMR spectrum of crude **5b** (from NMR scale reaction of **2** with ^{Me}**CAAC**; not isolated) in C_6D_6 (303 K).*

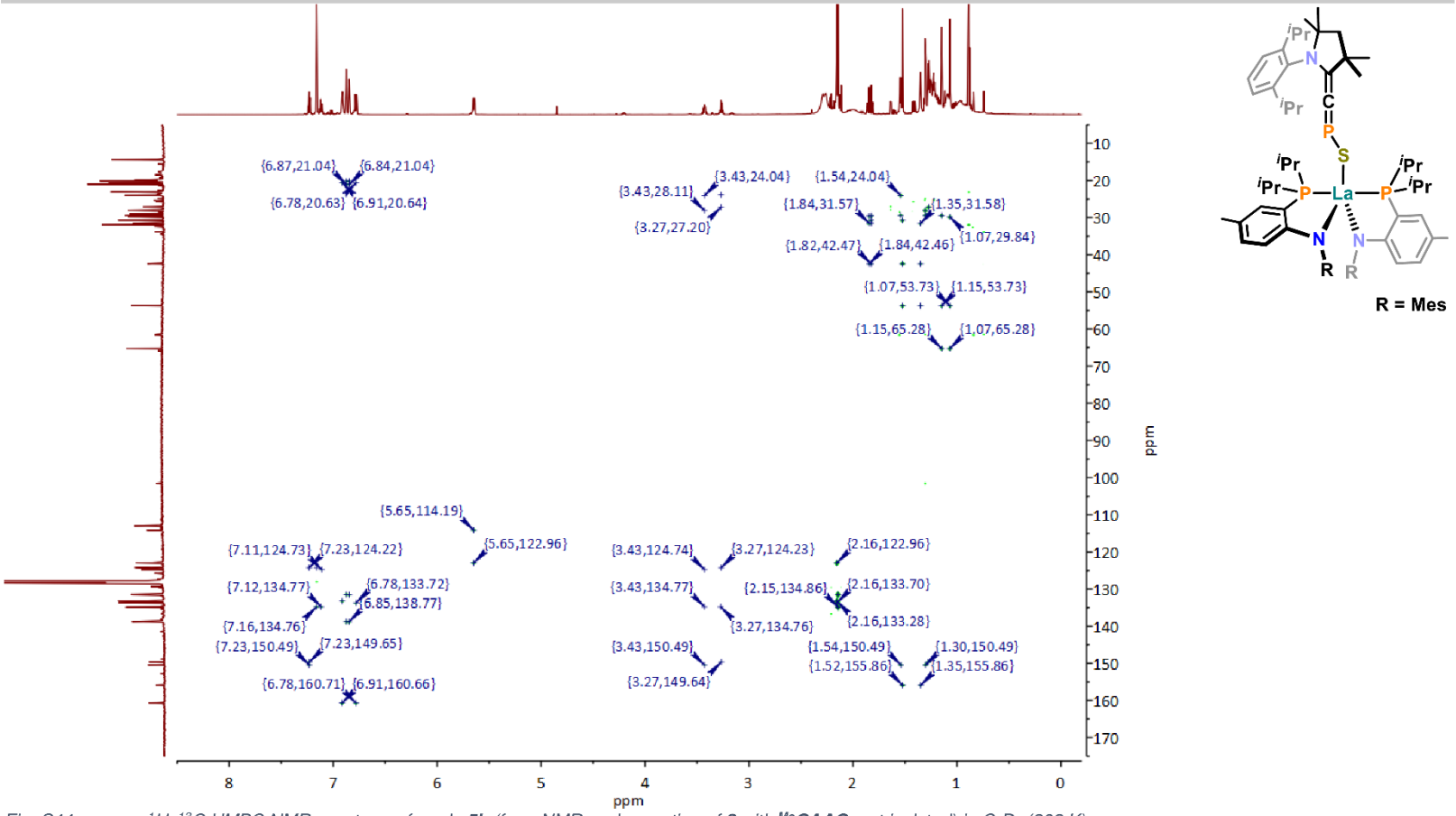

Fig. S44: *^{1}H–^{13}C HMBC NMR spectrum of crude **5b** (from NMR scale reaction of **2** with ^{Me}**CAAC**; not isolated) in C_6D_6 (303 K).*

3. IR Spectra

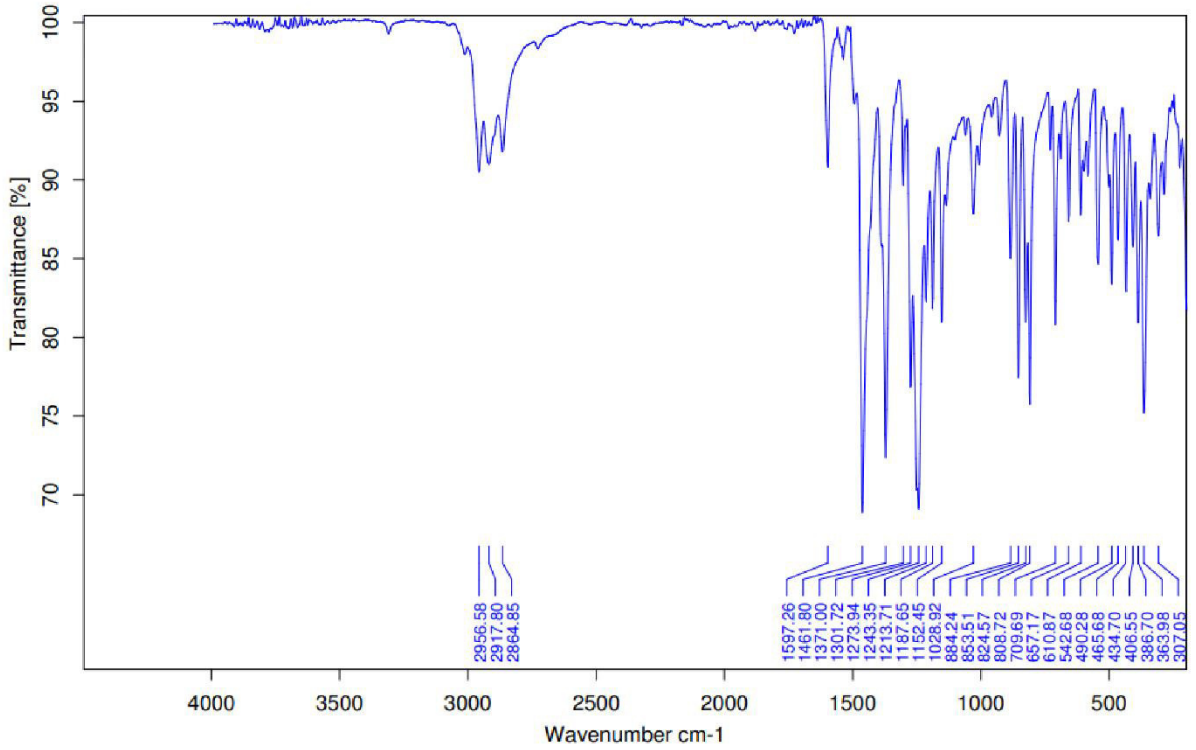

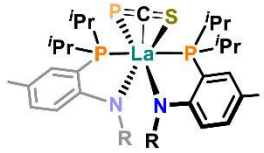

R = Mes

*Fig. S45: IR spectrum (ATR) of **2**.*

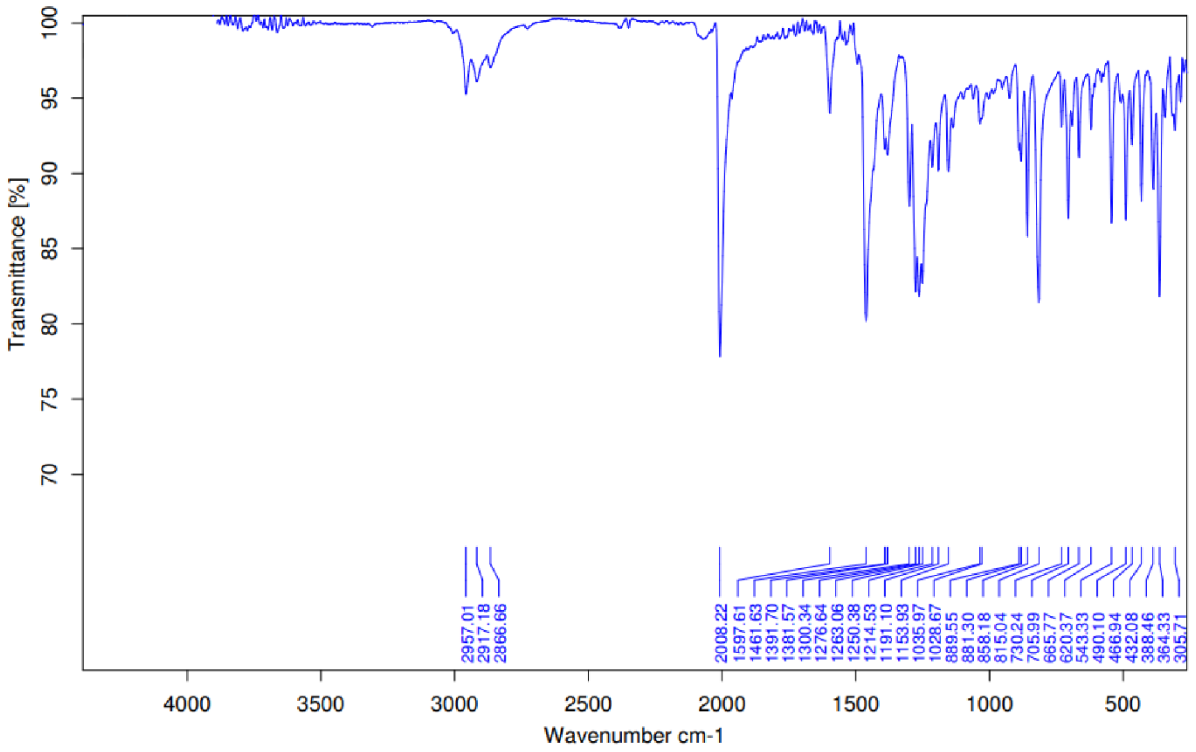

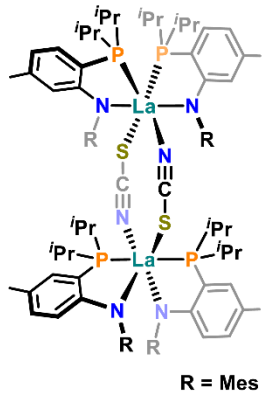

*Fig. S46: IR spectrum (ATR) of **3**.*

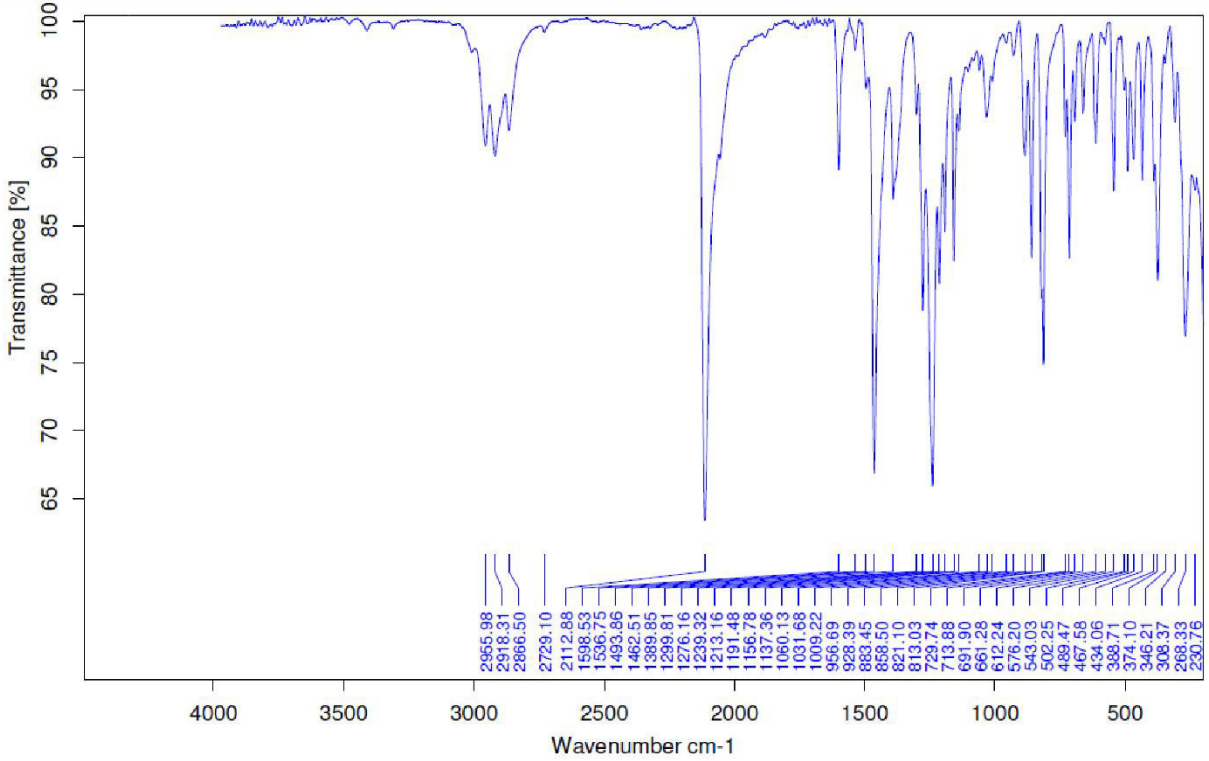

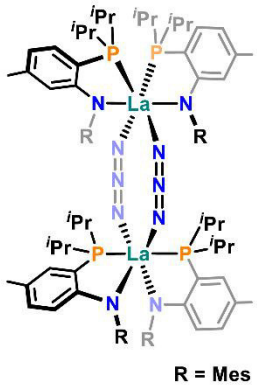

*Fig. S47: IR spectrum (ATR) of crude **4**.*

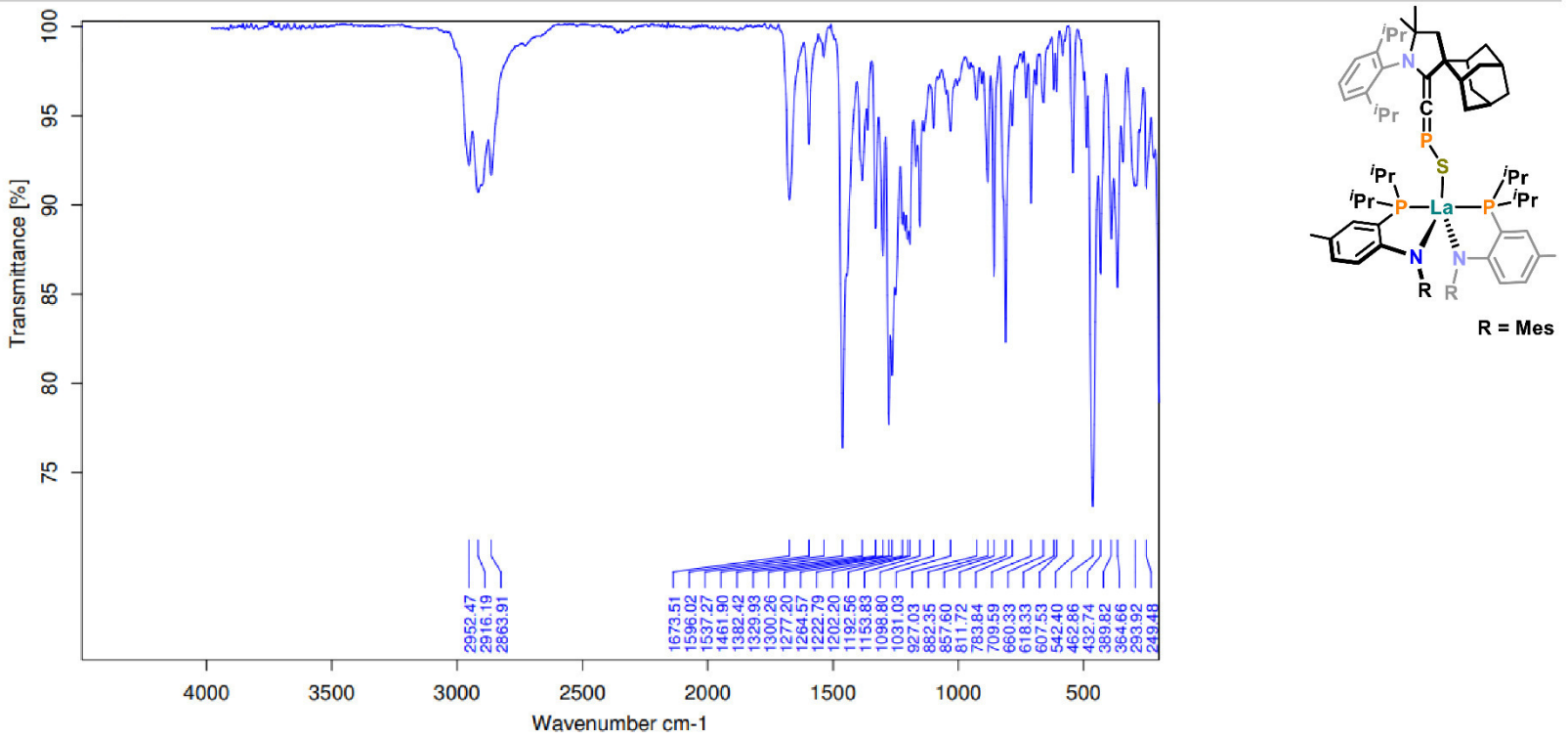

*Fig. S48: IR spectrum (ATR) of **5a**.*

4. Crystallographic Details

*Table S1: Crystallographic details on complexes **2**, **3**, **4** and **5a**.*

	2*	**3**	**4**	**5a**
Chemical Formula	$C_{45}H_{62}N_2P_3SLa$	$C_{90}H_{124}N_6P_4S_2La_2$	$C_{88}H_{124}N_{10}P_2La_2$	$C_{72}H_{101}N_3P_3SLa$
M_r	894.84	1755.76	1723.66	1272.43
Crystal System	Monoclinic	Orthorhombic	Monoclinic	Triclinic
Space Group	$P2_1/c$	$Fdd2$	$C2/c$	$P\bar{1}$
a (Å)	21.070(6)	20.749(2)	15.643(2)	15.165(1)
b (Å)	12.958(4)	61.552(5)	21.289(2)	15.506(1)
c (Å)	16.927(5)	16.151(1)	30.321(3)	16.340(1)
α (°)	90	90	90	63.477(2)
β (°)	104.103(5)	90	97.792(2)	84.201(2)
γ (°)	90	90	90	79.949(2)
V (Å^3)	4482(2)	20626(3)	10004(2)	3384.0(5)
Z	4	8	4	2
Density (g cm^{-3})	1.326	1.131	1.144	1.249
F(000)	1856	7296	3584	1344
Radiation Type	MoKα	MoKα	MoKα	MoKα
μ (mm^{-1})	1.138	0.959	0.949	0.775
Crystal Size	0.1x0.09x0.08	0.3x0.25x0.2	0.42x0.36x0.24	0.15x0.12x0.09
Meas. Refl.	26818	221463	33931	280227
Indep. Refl.	8163	10152	9289	13246
Obsvd. [$I > 2\sigma(I)$]	4171	9737	6741	12610
R_{int}	0.1534	0.0462	0.0747	0.0330
R_1 [$F^2 > 2\sigma(F^2)$]	0.0491	0.0539	0.0620	0.0274
$wR_2(F^2)$	0.1288	0.1442	0.1661	0.0648
S	0.776	1.029	1.021	1.074
$\Delta\rho_{max}$	1.489	1.826	1.355	1.770
$\Delta\rho_{min}$	–1.314	–1.537	–1.165	–1.509
CCDC	2039082	2039084	2039140	2039085

*The high R_{int} and low S values for **2** result from moderately good crystal quality and an unresolvable position disorder (<5%) in the SCP fragment.

*Table S2: Selected bond lengths in Å and angles in ° of complexes **2**, **3**, **4** and **5a**.*

	2	**3**	**4**	**5a**
La1 – S1	3.036(2)	3.131(3)	-	2.950(2)
La1 – P1	3.172(2)	3.203(3)	3.157(2)	3.1494(5)
La1 – P2	3.150(2)	3.164(2)	3.175(2)	3.1298(6)
La1 – P5	3.343(2)	-	-	-
La1 – N1	2.397(5)	2.443(7)	2.449(5)	2.402(2)
La1 – N2	2.361(5)	2.370(7)	2.407(5)	2.396(2)
La1 – N10 / N20	-	2.469(8)	2.536(5) / 2.560(5)	-
La1 – C1	2.837(7)	-	-	-
S1 – P5	-	-	-	2.081(3)
S1 – C1	1.607(7)	1.59(1)	-	-
C1 – P5	1.568(7)	-	-	1.63(2)
C1 – N10	-	1.22(1)	-	-
C1 – C100	-	-	-	1.36(2)
N10 – N11	-	-	1.163(6)	-
N20 – N21	-	-	1.160(5)	-
S1 – La1 – P1	85.79(5)	116.52(8)-	-	74.83(5)
S1 – La1 – P2	93.50(6)	69.86(7)	-	119.72(5)
S1 – La1 – P5	59.42(6)	-	-	-
S1 – La1 – N10	-	77.9(2)	-	-
P1 – La1 – P2	179.13(5)	172.06(6)	167.55(5)	165.43(2)
P5 – La1 – P1	93.22(6)	-	-	-
P5 – La1 – P2	86.84(5)	-	-	-
N1 – La1 – P1	64.3(1)	61.7(2)	63.0(1)	63.07(4)
N1 – La1 – N2	118.1(2)	126.6(2)	128.3(2)	125.78(6)
N2 – La1 – P2	64.0(1)	63.7(2)	62.4(1)	63.82(4)
N10 – La1 – P1	-	74.1(2)	114.7(1)	-
N10 – La1 – P2	-	112.8(2)	74.5(1)	-
S1 – C1 – P5	175.4(5)	-	-	-
S1 – C1 – N10	-	168(2)	-	-
S1 – P5 – C1	-	-	-	111.1(5)
P5 – S1 – La1	-	-	-	101.9(1)
P5 – C1 – C100	-	-	-	173.8(1)
C1 – S1 – La1	67.4(2)	100.8(5)	-	-
C1 – P5 – La1	57.8(3)	-	-	-
C1 – N10 – La1	-	171(1)	-	-
N10 – N11 – N10	-	-	178.1(9)	-
N20 – N21 – N21	-	-	178.3(9)	-

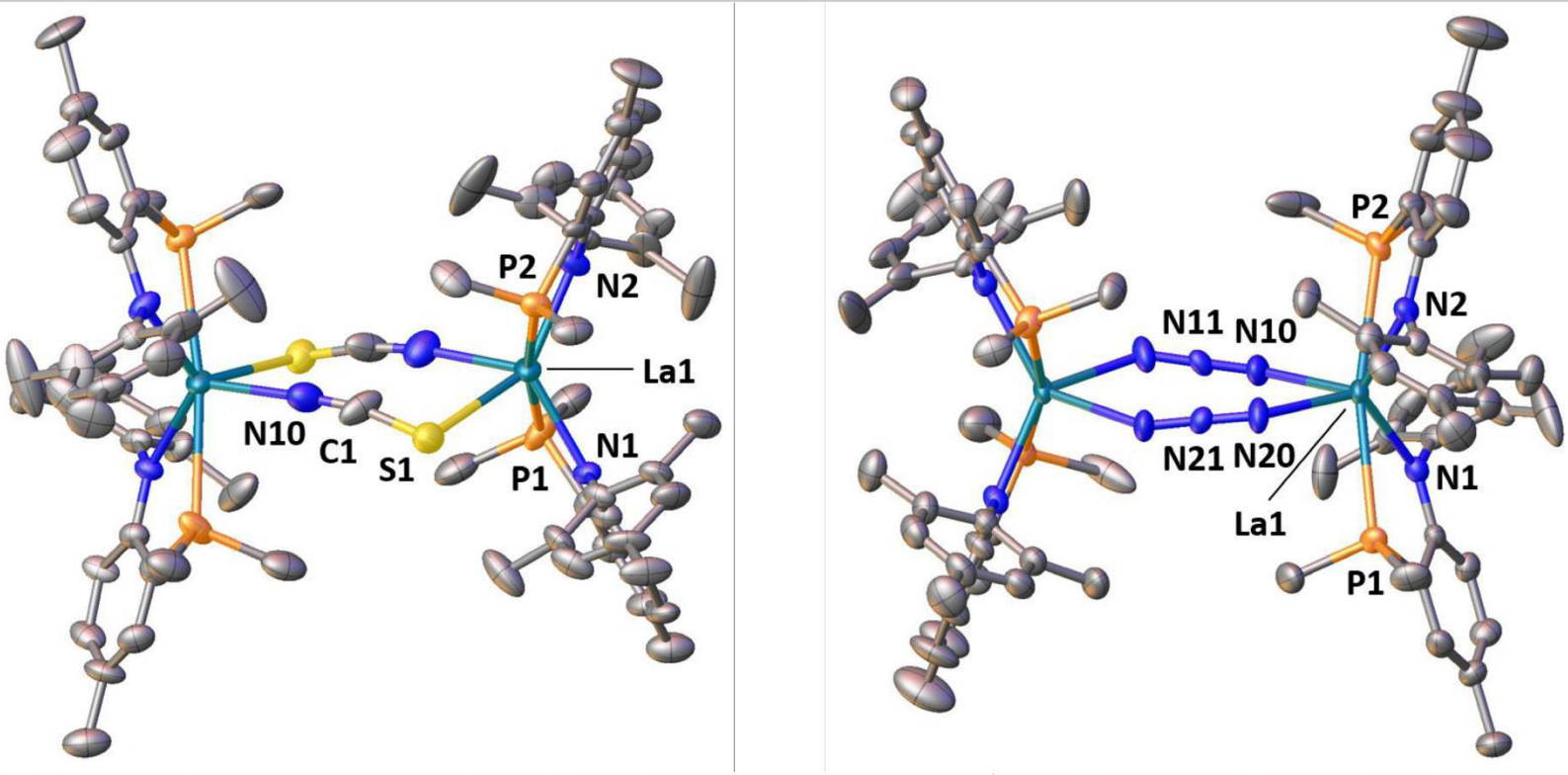

*Fig. S49: Thermal ellipsoid plots of the complexes **3** (left) and **4** (right). Hydrogen atoms have been omitted and ^{i}Pr groups truncated for clarity. Thermal ellipsoids are shown at a probability level of 50%. Both structures are centro-symmetric with an inversion center in the between the two lanthanum(III) ions.*

5. Theoretical and Mechanistic Investigations

Preliminary optimizations and single-point calculations were conducted with the ORCA quantum chemistry package (version 4.0.1).[7] Unconstrained geometry optimizations were performed with the PBEh-3c method.[8] The optimized structure of complex **2** (see supporting information file 2opt.xyz) was confirmed to be a minimum by numerical frequency calculations and the absence of negative frequencies. Energies and Kohn-Sham orbitals were computed using the PBE0 functional[9] in conjunction with the ZORA-def2-TZVP basis set on all atoms, except SARC-ZORA-TZVP[10,11] on La. Kohn-Sham orbitals were visualized using IQmol (version 2.14.0)[12] with an isosurface value of 0.03 au. All preliminary calculations were performed using the VeryTighSCF convergence criteria of orca (energy change of 10-9 au), with a grid of 5 (Lebedev434 and IntAcc = 5.01 for the SCF) and a Finalgrid of 6 (Lebedev590 and IntAcc = 5.34 in the final energy evaluation) on all atoms except on La, with an overall grid of 7 (Lebedev770 and IntAcc = 5.67).
Density functional calculations shedding light on the "angular stability" of the SCP fragment and the mechanism of the SCP to SPC rearrangement were done with TURBOMOLE.[13] Structural optimization of the complex reproduced the values of the X-ray structure very well. The La–E–C angles differ by less than ~2° from the crystallographically determined numbers of 57.8(3)° (for E = P) and 67.4(2)° (for E = S). For clarity we note that for none of the structures shown in Figure 2 significant covalent interactions between $[SCP]^-$ anion and the cation are observed. The dependence of the energy on the La–S–C or the La–P–S angle, respectively, was obtained by keeping this angle fixed and optimizing all other parameters. This was done at levels (functional/basis set) PBE[14]/def2-SV(P)[10], PBE0[9]/def2-SV(P), PBE/def2-TZVP[10]. Further, PBE0/def2-SV(P), PBE/def2-TZVP as well as PBE/X2C[15]/x2c-TZVPall[16] single point calculations were done for the structure parameters obtained with PBE/def2-SV(P), denoted PBE0/SV(P)@PBE/SV(P) etc. Energies for a series of La–P–C angles (P-connected species, Table S3) and La–S–C angles (S-connected species, Table S4) relative to the optimized structure show a rather small dependence on the functional and the method. Further, for both PBE0/def2-SV(P) and PBE/def2-TZVP single point energies at the PBE/def2-SV(P) structure parameters are almost identical to those for the structure parameters optimized at the corresponding level.

Table S3. Energies in kJ·mol^{-1} for fixed La–P–C angle relative to the fully optimized system. For the latter, the La–P–C angle α amounts to 57.8° for PBE/SV(P), to 56.7° for PBE0/SV(P) and to 58.2° for PBE/def2-TZVP (X-ray structure: 57.8°).

α/°	PBE/ SV(P)	PBE0/ SV(P)	PBE0/SV(P)@ PBE/SV(P)	PBE/TZVP	PBE/TZVP@ PBE/SV(P)	PBE/X2C/TZVP@ PBE/SV(P)
61.0	0.6	1.1	1.1	0.5	0.5	0.6
64.0	2.5	3.4	3.4	2.3	2.3	2.5
67.0	5.5	7.1	7.1	5.6	5.5	5.7
70.0	9.6	11.8	11.8	9.8	9.8	9.8
73.0	13.9	16.9	16.9	14.5	14.4	14.2
76.0	17.4	21.2	21.2	18.6	18.3	17.8
79.0	20.1	24.5	24.5	21.6	21.3	20.7
82.0	22.3	27.0	27.0	23.8	23.6	22.8
85.0	24.0	28.9	28.9	25.5	25.3	24.4
88.0	25.4	30.6	30.6	27.0	26.7	25.8
91.0	26.8	32.1	32.1	28.2	27.9	27.0
94.0	28.1	33.6	33.6	29.4	29.0	28.1
97.0	29.4	35.1	35.1	30.6	30.2	29.3
100.0	30.8	36.8	36.8	31.8	31.4	30.5
103.0	32.2	38.5	38.5	33.1	32.7	31.7
106.0	33.8	40.3	40.3	34.6	34.1	33.1
109.0	35.5	42.3	42.3	36.1	35.7	34.7
112.0	37.3	44.3	44.3	37.7	37.4	36.3
115.0	39.3	46.5	46.5	39.4	39.1	38.0
120.0	42.5	50.2	50.2	42.2	42.0	40.9
125.0	45.6	53.7	53.7	45.1	44.9	43.8
130.0	48.5	56.9	56.9	47.7	47.5	46.5
135.0	51.3	59.9	59.9	50.2	50.0	48.9
140.0	53.8	62.6	62.6	52.5	52.3	51.2
150.0	58.3	67.7	67.7	56.7	56.3	55.1
160.0	62.1	72.0	72.0	59.7	59.5	58.2
170.0	64.7	74.6	74.6	62.0	61.6	60.1
180.0[1)]	65.8	75.7	75.7			

[1)] Structure was obtained from that of α = 170° by adjusting the angle without further optimization.

Table S4. Energies in kJ·mol^{-1} for fixed La–S–C angle relative to the fully optimized system. For the latter, the La–S–C angle α amounts to 68.7° for PBE/SV(P), to 69.1° for PBE0/SV(P) and to 67.0° for PBE/def2-TZVP (X-ray-structure: 67.4°).

α/°	PBE/ SV(P)	PBE0/ SVP	PBE0/SVP@ PBE/SV(P)	PBE/TZVP	PBE/TZVP@ PBE/SV(P)	PBE/X2C/TZVP@ PBE/SV(P)
70.0	0.5	0.0	-.1	0.7	0.7	0.5
73.0	2.2	1.0	.8	2.8	2.9	2.3
76.0	4.7	3.1	2.9	6.0	5.9	5.1
79.0	7.7	5.8	5.6	9.5	9.3	8.1
82.0	10.8	8.7	8.5	13.0	12.9	11.4
85.0	13.8	11.6	11.4	16.4	16.2	14.6
88.0	16.6	14.3	14.1	19.4	19.2	17.4
91.0	19.1	16.6	16.4	22.0	21.8	19.9
94.0	21.3	18.7	18.5	24.3	24.1	22.1
97.0	23.2	20.6	20.4	26.3	26.1	24.1
100.0	25.0	22.3	22.1	28.1	27.8	25.7
103.0	26.6	24.0	23.8	29.7	29.4	27.4
106.0	28.2	25.6	25.4	31.2	30.9	28.8
109.0	29.8	27.3	27.1	32.6	32.3	30.3
112.0	31.3	28.9	28.7	34.1	33.8	31.7
115.0	32.9	30.7	30.5	35.6	35.2	33.1
118.0	34.6	32.6	32.4	37.1	36.9	34.7
121.0	36.5	34.6	34.4	38.7	38.5	36.3
124.0	38.4	36.7	36.5	40.4	40.2	38.0
127.0	40.3	38.9	38.7	42.2	41.9	39.7
130.0	42.3	41.1	40.9	43.9	43.7	41.5
135.0	45.5	44.6	44.4	46.7	46.5	44.2
140.0	48.4	47.9	47.7	49.4	49.1	46.9
145.0	51.0	50.8	50.6	51.8	51.5	49.2
150.0	53.8	53.3	53.1	53.8	54.4	52.1
160.0	58.4	58.6	58.4	57.9	57.9	55.1
170.0	62.3	62.7	62.5	60.9	60.8	57.5
180.0[1)]	63.3	64.7	64.5			

1) Structure was obtained from that of α = 170° by adjusting the angle without further optimization.

The optimization of the pathway at level PBE/SV(P) was done as follows. First, a pre-optimization was done with the (nudge-band-type) method proposed by Plessow[17] between the initial structure and the final structure. The latter was obtained by full structure optimization, the former was optimized with keeping the distance between La and the C atom in the pyrrolidine ring fixed at 1 157 pm. This pre-optimized path allowed us to identify two maxima and two intermediate local minima, which were optimized, indeed yielding two local minima (no imaginary frequency) and two transition states (one imaginary frequency) amounting to 167i cm^{-1} for the first and to 244i cm^{-1} for the second one. For the optimizations and frequency calculations the grid for the evaluation of the DFT-functional values was set to 4 and the calculation of weight derivatives was employed. The final path was obtained by optimizing the five segments separately (initial structure to first transition state, first transition state to first local minimum, first local minimum to second local minimum, second local minimum to second transition state, second transition state to final state). The two local minima are separated by a flat barrier, which was not further optimized. In the end, these segments were combined to yield the entire path. The path at PBE0 level was calculated without further structure optimization, which is justified according to the results shown in Tables S3 and S4. The pathways for both calculations are shown in Fig. S50.

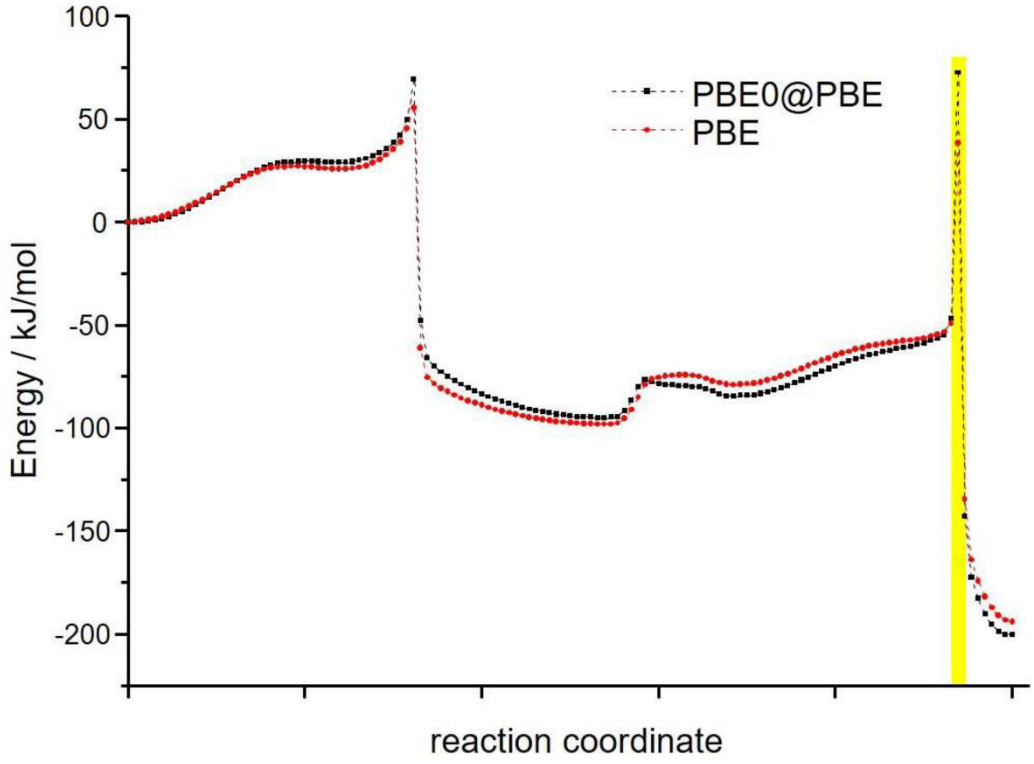

Fig. S50: Reaction pathway optimized at level PBE/def2-SV(P), red, and single-point calculations at level PBE(0)/def2-SV(P) for each structure along the path. The electronic situation of the area highlighted in yellow is investigated in detail in Fig. S52.

For the initial and the final structure as well as for the two local minima, excitation spectra were calculated with PBE0/def2-SV(P), which are shown in Fig. S51 together with plots of the difference in electron density of the ground state and the excited states for the first excitation band obtained with a tool described previously.[18] For 1, mainly HOMO and LUMO are involved, for 3 and 4 also HOMO–1 and/or LUMO+1 significantly contribute to the transition. For these three structures, excitation energies are similar and electrons are always transferred from the phenyl rings (of the $(PN)_2La$ part) to the La(d) orbitals, in case of 1 also to the anti-bonding π-orbital of the SCP unit, which forms the LUMO together with the former. For 2, the excitation energy is lower by ca. 0.5 eV and the character is different; here, electrons are transferred from the p-orbitals of P and S to the pyrrolidine ring. Cartesian coordinates for 1 – 4 as well as for the two transition states are listed in file structures.xyz.

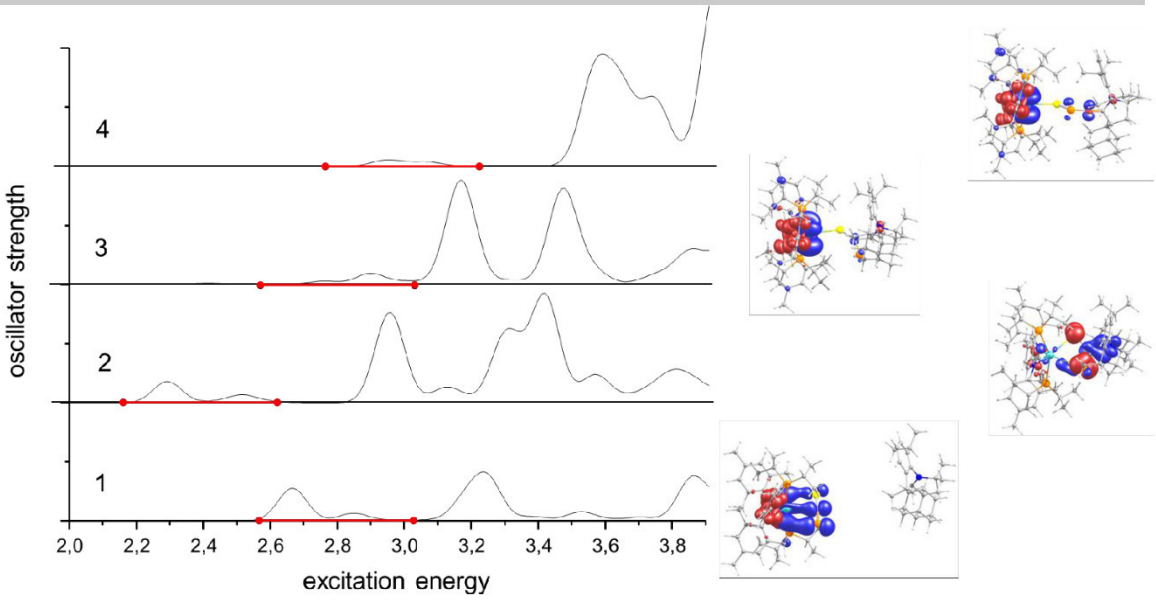

*Fig. S51: Computed excitation spectra of the four minima for the reaction coordinate leading from **2** to **5a**. Peaks are broadened by 0.1 eV. Red marked areas in the spectra show the band of lowest lying excitations. The images on the right show the differences in electron density of ground state and excited states within the band; red areas indicate a surplus for the ground state electron density, blue areas a surplus for the excited states (thus the electron flux upon excitation is from red to blue). Contours are drawn at 0.001 a.u.*

For the investigation of the electronic situation around the second transition state, the number of structures in the area marked in yellow in Fig. S50 was increased from 3 to 17 (by interpolation, without further optimization). For each structure, atomic partial charges and shared electron numbers (SEN) were calculated with a population analysis based on occupation numbers, as suggested by Heinzmann and Ahlrichs[19] for the three atoms S, P and C indicated in Fig. S52. They are shown in Fig. S52, together with the Coulomb energy calculated from the partial charges of these three atoms. At the transition state (middle structure in Fig. S52), the SENs between S and both C and P are close to zero, thus covalent interactions are very small, ionic interactions are present instead; the Coulomb interaction between the three atoms amounts to ca. -0.5 eV (ca. -50 kJ/mol). The reason for this is the positive partial charge of P at the transition structure leading to attractive interactions between P and the two other atoms. This is different from the structure at the left, where all partial charges are negative. The resulting repulsive interaction in this case is overcompensated by a strong covalent bond between S and C.

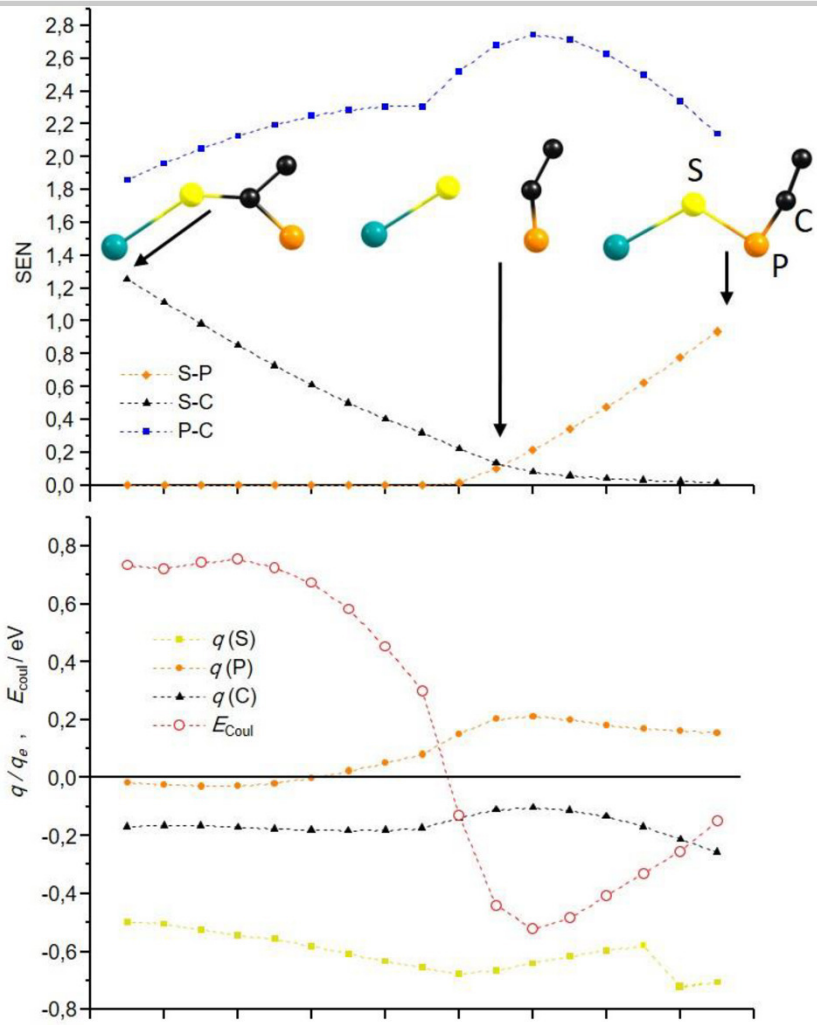

Fig. S52: Upper part: Shared electron number[19] between S, P and C in the vicinity of the second transition state shown in Figure S50. Lower part: Partial charges[19] for S, P and C and Coulomb energy resulting from these partial charges

6. References

[1] F. A. Watt, A. Krishna, G. Golovanov, H. Ott, R. Schoch, C. Wölper, A. G. Neuba, S. Hohloch, *Inorg. Chem.* **2020**, *59*, 2719.
[2] F. Tambornino, A. Hinz, R. Köppe, J. M. Goicoechea, *Angew. Chem. Int. Ed.* **2018**, *130*, 8230. Please note that the Na(diox)$_{2.3}$SCP adduct can be obtained following the exact same procedure as described for Na(diox)$_3$SCAs.
[3] V. Lavallo, G. D. Frey, S. Kousar, B. Donnadieu, G. Bertrand, *Proc. Natl. Acad. Sci. U.S.A.* **2007**, *104*, 13569.
[4] A. Grünwald, S. J. Goodner, D. Munz, *Journal of visualized experiments : JoVE* **2019**. DOI: 10.3791/59389.
[5] G. M. Sheldrick, *Acta Crystallogr.. C Struct. Chem.* **2015**, *71*, 3.
[6] O. V. Dolomanov, L. J. Bourhis, R. J. Gildea, J. A. K. Howard, H. Puschmann, *J. Appl. Crystallogr.* **2009**, *42*, 339.
[7] a) F. Neese, *WIREs Comput. Mol. Sci.* **2012**, *2*, 73; b) F. Neese, *WIREs Comput. Mol. Sci.* **2018**, *8*. DOI: 10.1002/wcms.1327.
[8] a) J. Hostaš, J. Řezáč, *J. Chem. Theory Comput.* **2017**, *13*, 3575; b) J. G. Brandenburg, C. Bannwarth, A. Hansen, S. Grimme, *J. Chem. Phys.* **2018**, *148*, 64104; c) S. Grimme, J. G. Brandenburg, C. Bannwarth, A. Hansen, *J. Chem. Phys.* **2015**, *143*, 54107.
[9] J. P. Perdew, M. Ernzerhof, K. Burke, *J. Chem. Phys.* **1996**, *105*, 9982.
[10] F. Weigend, R. Ahlrichs, *Phys. Chem. Chem. Phys.* **2005**, *7*, 3297.
[11] D. A. Pantazis, X.-Y. Chen, C. R. Landis, F. Neese, *J.Chem. Theory Comput.* **2008**, *4*, 908.
[12] http://iqmol.org/.
[13] TURBOMOLE V7.5 2020, a development of University of Karlsruhe and Forschungszentrum Karlsruhe GmbH, 1989-2007, TURBOMOLE GmbH, since 2007, available from http://www.turbomole.com.
[14] Perdew, Burke, Ernzerhof, *Phys. Rev. Lett.* **1996**, *77*, 3865.
[15] D. Peng, N. Middendorf, F. Weigend, M. Reiher, *J. Chem. Phys.* **2013**, *138*, 184105.
[16] P. Pollak, F. Weigend, *J. Chem. Theory Comput.* **2017**, *13*, 3696.
[17] P. Plessow, *J. Chem. Theory and Comput.* **2013**, *9*, 1305.
[18] Michael Kühn, Florian Weigend, *J. Chem. Phys.* **2014**, *141*, 224302.
[19] Heinzmann, R.; Ahlrichs, R., *Theor. Chim. Acta* **1976**, 42, 33–45.

7. Author Contributions

The project was designed by FT and SH. Experimental work was performed by FAW, SH, SM and FT. X-Ray diffraction analysis was performed by SH and RS. Theoretical calculations were performed by LB and FW. The manuscript was written by FAW, MB, JMG, FW, FT, and SH. All authors have given approval to the final version of the manuscript.

Appendix:
Additional Experimental Data

A.1 Experimental Section

This appendix contains additional data and a few other compounds of the doctoral research study, which have not been published prior to the submission of this dissertation.

A.1.1 General Remarks

If not otherwise mentioned, all transformations were carried out under inert conditions using the Schlenk technique or an argon filled glovebox. All glassware (including glass-fibre filters) was stored in an oven at 150 °C for at least 12 h prior to use. Solvents were dried by a MBraun SPS system, degassed and stored over activated molecular sieves (3 Å) for at least 24 h prior to use. The deuterated solvents C_6D_6, and toluene-d_8 were dried by storage over activated molecular sieves (3 Å) for at least 24 h. IR spectra were recorded at room temperature under inert conditions using a Bruker Vertex 70 with ATR equipment. UV-Vis and fluorescence data were recorded in THF at room temperature under inert conditions using a Cary 50 scan instrument or a Jasco FP-8300 spectrometer, respectively. If not otherwise stated, the NMR spectra were collected at 303 K on a Bruker AV-500 or an Ascent 700 spectrometer using a J-Young NMR tube. All chemical shifts (δ) are reported in ppm and coupling constants are given in Hz. ^{1}H and ^{13}C chemical shifts were calibrated to residual solvent peaks. ^{15}N chemical shifts (obtained by ^{1}H–^{15}N HMBC NMR spectroscopy) were calibrated externally to liquid ammonia (NH_3). ^{19}F chemical shifts were calibrated externally to trichlorofluoromethane (CCl_3F). ^{31}P chemical shifts were calibrated externally to phosphoric acid (H_3PO_4, 85% in water). Elemental analyses were performed using an Elementar vario microcube instrument at the Paderborn University. Starting materials **(PN)$_2$LaX** (X = Cl, I),[1] **KPHPh**[2] and **KBn**[3] were synthesized following literature known procedures. **KNH(C$_6$H$_3$-3,5-(CF$_3$)$_2$)** was prepared in analogy to other primary aryl amide potassium salts.[4] **Benzophenone** and **Michler's ketone** were used as received.

A.1.2 Synthetic Procedures

Preparation of (PN)$_2$La{NH(C$_6$H$_3$-3,5-(CF$_3$)$_2$)}. Solid **(PN)$_2$LaI** (383 mg, 400 µmol, 1 eq.) and **KNH(C$_6$H$_3$-3,5-(CF$_3$)$_2$)** (124 mg, 470 µmol, 1.15 eq.) were combined and toluene (12 mL) was added to this mixture. The resulting suspension was stirred for 14 h at room temperature. After centrifugation the supernatant was filtered through a glass-fibre filter and all volatiles were removed *in vacuo*. The residue was redissolved in *n*-hexane (2 mL) and stored at room temperature for 4 h, during which pale yellow crystals formed. The crystalline material was separated from the mother liquor, washed with *n*-hexane (2 x 1 mL) and dried *in vacuo* to give a first batch of pure material (141 mg). The mother liquor was combined with the *n*-hexane washing solution. Further concentrating of the combined solutions *in*

vacuo and storing at –40 °C overnight yielded additional crystals, which were washed with –40 °C cold *n*-hexane (2 x 1 mL) and dried *in vacuo* to give a second batch of crystalline material (147 mg). Single crystals of **(PN)$_2$La{NH(C$_6$H$_3$-3,5-(CF$_3$)$_2$)}** suitable for X-ray structure determination were also obtained in this way (prior to washing and drying). Yield: 288 mg (275 µmol, 69%); ^{1}H NMR (C$_6$D$_6$, 303 K, 700 MHz, in ppm): δ = 7.10 (s, C*H*$_{Ar}$, 1 H), 6.95 (s, C*H*$_{Ar}$, 2 H), 6.88–6.83 (several overlapping m, C*H*$_{Ar}$, 8 H), 5.75–5.70 (m, C*H*$_{Ar}$, 2 H), 5.40 (s, N*H*, 1 H), 2.21 (br. s, C*H*$_{3Ar}$, 12 H), 2.17 (s, C*H*$_{3Ar}$, 6 H), 2.13 (s, C*H*$_{3Ar}$, 6 H), 1.76 (br. s, C*H*$_{i\text{Pr}}$, 4 H), 0.99–0.93 (br. m, C*H*$_{3i\text{Pr}}$, 12 H), 0.82–0.74 (br. m, C*H*$_{3i\text{Pr}}$, 12 H); ^{13}C{^{1}H} NMR (C$_6$D$_6$, 303 K, 176 MHz, in ppm): δ = 159.9 (*pseudo*-t, J_{CP} = 11.4 Hz, *C*$_{qAr}$), 157.8 (s, *C*$_{qAr}$), 138.5 (s, *C*$_{qAr}$), 137.5 (br. s, *C*$_{qAr}$), 135.1 (s, *C*$_{qAr}$), 133.8 (s, *C*H$_{Ar}$), 133.7 (s, *C*H$_{Ar}$), 132.2 (q, $^1J_{CF}$ = 31.9 Hz, *C*F$_3$), 131.8 (s, *C*H$_{Ar}$), 125.6 (s, *C*$_{qAr}$), 124.0 (s, *C*$_{qAr}$), 123.4 (s, *C*$_{qAr}$), 116.5 (m, *C*H$_{Ar}$), 112.7 (*pseudo*-t, J_{CP} = 4.0 Hz), 112.6 (d, J_{CP} = 6.1 Hz, *C*$_{qAr}$), 112.55 (d, J_{CP} = 6.1 Hz, *C*$_{qAr}$), 107.1 (sept, $^4J_{CF}$ = 3.6 Hz, *C*H$_{Ar}$), 23.0 (br. s, *C*H$_{i\text{Pr}}$), 20.9 (s, *C*H$_{3Ar}$), 20.6 (s, *C*H$_{3Ar}$), 19.9 (*pseudo*-t, $^2J_{CP}$ = 5.6 Hz, *C*H$_{3i\text{Pr}}$), 19.5 (s, *C*H$_{3Ar}$), 17.6 (br. s, *C*H$_{3i\text{Pr}}$); ^{19}F{^{1}H} NMR (C$_6$D$_6$, 303 K, 659 MHz, in ppm): δ = –63.0 (s, C*F*$_3$, 6 F); ^{31}P{^{1}H} NMR (C$_6$D$_6$, 303 K, 283 MHz, in ppm): δ = 10.5 (s, *P*N$^–$, 2 P); elemental analysis (in %): C$_{52}$H$_{66}$F$_6$LaN$_3$P$_2$: calcd.: C 59.60, H 6.35, N 4.01; found: C 59.51, H 6.32, N 3.97.

Preparation of (PN)$_2$La(PHPh). Solid **(PN)$_2$LaCl** (342 mg, 400 µmol, 1 eq.) and **KPHPh** (71 mg, 480 µmol, 1.2 eq.) were combined and toluene (6 mL) was added to this mixture. The resulting yellow suspension was stirred for 12 h at room temperature. After centrifugation the supernatant was filtered through a glass-fibre filter and all volatiles were removed *in vacuo* to yield the crude product. This solid was resuspended in *n*-pentane (4 mL) and stirred for 3 h at room temperature. The suspension was then centrifuged and the supernatant was separated from the solid with a pipette. The yellow solid was washed with additional *n*-pentane (3 x 2 mL) and dried *in vacuo*. *(Caution: The product complex and the phosphanide starting material are very malodorous as well as potentially pyrophoric and should therefore be quenched carefully and only in small quantities with sodium hypochlorite solution before disposal.)* Single crystals suitable for X-ray structure determination were obtained as thin, pale yellow plates by storing a concentrated *n*-hexane solution of **(PN)$_2$La(PHPh)** at –40 °C for five weeks. No satisfying elemental analyses could be obtained for this compound. Yield: 224 mg (240 µmol, 60%); ^{1}H NMR (C$_6$D$_6$, 303 K, 700 MHz, in ppm): δ = 7.44–7.39 (m, C*H*$_{Ar}$, 2 H), 7.00–6.96 (m, C*H*$_{Ar}$, 2 H), 6.89–6.86 (m, C*H*$_{Ar}$, 2 H), 6.85–6.79 (s at 6.85 & m, C*H*$_{Ar}$, 7 H), 5.69–5.64 (m, C*H*$_{Ar}$, 2 H), 4.06 (d, $^1J_{PH}$ = 194.8 Hz, P*H*Ph, 1 H), 2.27–2.22 (br. s, C*H*$_{3Ar}$, 12 H), 2.16 (s, C*H*$_{3Ar}$, 6 H), 2.11 (s, C*H*$_{3Ar}$, 6 H), 1.80–1.67 (br. s, C*H*$_{i\text{Pr}}$, 4 H), 1.21–1.15 (br. m, C*H*$_{3i\text{Pr}}$, 12 H), 0.94–0.85 (br. m, C*H*$_{3i\text{Pr}}$, 12 H); ^{13}C{^{1}H} NMR (C$_6$D$_6$, 303 K, 176 MHz, in ppm): δ = 160.3 (*pseudo*-t, J_{CP} = 11.7 Hz, *C*$_{qAr}$), 148.6 (s, J_{CP} = 26.8 Hz, *C*$_{qAr}$), 138.3 (br. s, *C*$_{qAr}$), 138.0 (s, *C*$_{qAr}$), 135.3 (s, *C*$_{qAr}$), 133.8 (s, *C*H$_{Ar}$), 133.5 (s, *C*H$_{Ar}$), 131.8 (s, *C*H$_{Ar}$), 130.54 (s, *C*$_{qAr}$), 130.47 (s, *C*H$_{Ar}$), 127.9 (resonance obscured by C$_6$D$_6$ peak, only

identifiable by ^{1}H–^{13}C HSQC NMR spectroscopy, s, CH$_{Ar}$), 123.5 (s, C_{qAr}), 121.9 (s, CH$_{Ar}$), 113.9 (d, J_{CP} = 6.8 Hz, C_{qAr}), 113.8 (d, J_{CP} = 6.4 Hz, C_{qAr}), 112.7 (*pseudo*-t, J_{CP} = 3.8 Hz, CH$_{Ar}$), 22.4 (s, CH$_{i\text{Pr}}$), 20.9 (s, CH$_{3Ar}$), 20.6 (s, CH$_{3Ar}$), 19.9 (*pseudo*-t, J_{CP} = 5.4 Hz, CH$_{3i\text{Pr}}$), 19.7 (d, J_{CP} = 3.6 Hz, CH$_{3Ar}$), 17.7 (br. s, CH$_{3i\text{Pr}}$); $^{31}P\{^{1}H\}$ NMR (C_6D_6, 303 K, 283 MHz, in ppm): δ = 10.3 (s, PN^{-}, 2 P), –10.2 (s, PHPh, 1 P); ^{31}P NMR (C_6D_6, 303 K, 283 MHz, in ppm): δ = 10.3 (s, PN^{-}, 2 P), –10.2 (d, $^{1}J_{PH}$ = 194.8 Hz, PHPh, 1 P).

Preparation of [K(18-crown-6)][(PN)(PN$_{cyclo}$)LaCl]. Solid **(PN)$_2$LaCl** (257 mg, 300 µmol, 1 eq.) and **18-crown-6** (79 mg, 300 µmol, 1 eq.) were combined and 1,2-dimethoxyethane (7 mL) was added to this mixture. A solution of **KBn** (39 mg, 330 µmol, 1.1 eq.) in 1,2-dimethoxyethane (2 mL) was then added dropwise at room temperature. After 10 min the reaction mixture was filtered through a glass-fibre filter and the filtrate concentrated *in vacuo* to about 1 mL. The concentrated filtrate was stored at –40 °C overnight, which caused the formation of yellow, crystalline blocks. The crystals were separated from the mother liquor, washed with –40 °C cold diethyl ether (2 x 1 mL) and dried *in vacuo* to give **[K(18-crown-6)][(PN)(PN$_{cyclo}$)LaCl]** as a yellow microcrystalline solid. Single crystals suitable for X-ray structure determination were also obtained in this way (prior to washing and drying). Yield: 311 mg (269 µmol, 90%); ^{1}H NMR (C_6D_6, 303 K, 700 MHz, in ppm): δ = 7.13 (dd, J = 5.3 Hz, J = 2.0 Hz, CH_{Ar}, 1 H), 7.03–7.00 (m, CH_{Ar}, 2 H), 6.89 (dd, J = 5.0 Hz, J = 2.1 Hz, CH_{Ar}, 1 H), 6.83 (dd, J = 8.5 Hz, J = 2.1 Hz, CH_{Ar}, 1 H), 6.81–6.80 (m, CH_{Ar}, 1 H), 6.75 (dd, J = 8.5 Hz, J = 2.0 Hz, CH_{Ar}, 1 H), 6.63–6.60 (m, CH_{Ar}, 1 H), 3.10 (s, C$H_{2(18\text{-crown-6})}$, 24 H), 2.71 (s, CH_{3Ar}, 3 H), 2.69 (dd, $^{2}J_{HH}$ = 3.9 Hz, J = 1.6 Hz, C$H_{2Mes(PNcyclo)}$, 1 H), 2.60–2.54 (m, C$H_{i\text{Pr}}$, 1 H), 2.43 (s, CH_{3Ar}, 3 H), 2.40–2.35 (s & m, CH_{3Ar} & C$H_{i\text{Pr}}$, 4 H), 2.27 (s, CH_{3Ar}, 3 H), 2.26 (s, CH_{3Ar}, 3 H), 2.25 (s, CH_{3Ar}, 3 H), 2.22 (s, CH_{3Ar}, 3 H), 2.21–2.18 (m, C$H_{i\text{Pr}}$, 1 H), 1.63–1.59 (m, C$H_{3i\text{Pr}}$, 6 H), 1.58–1.54 (m, C$H_{i\text{Pr}}$, 1 H), 1.46–1.41 (m, C$H_{3i\text{Pr}}$, 6 H), 1.25 (t, J = 7.2 Hz, C$H_{3i\text{Pr}}$, 3 H), 1.15–1.13 (m, C$H_{2Mes(PNcyclo)}$, 1 H), 1.09–1.05 (m, C$H_{3i\text{Pr}}$, 6 H), 0.83 (dd, J = 16.8 Hz, J = 7.1 Hz, C$H_{3i\text{Pr}}$, 3 H); $^{13}C\{^{1}H\}$ NMR (C_6D_6, 303 K, 176 MHz, in ppm): δ = 162.9 (d, J_{CP} = 24.6 Hz, C_{qAr}), 161.4 (d, J_{CP} = 21.8 Hz, C_{qAr}), 144.5 (d, J_{CP} = 2.8 Hz, C_{qAr}), 144.1 (s, C_{qAr}), 139.8 (s, C_{qAr}), 138.7 (s, C_{qAr}), 136.9 (s, C_{qAr}), 133.5 (s, C_{qAr}), 133.4 (d, J_{CP} = 2.9 Hz, CH$_{Ar}$), 132.9 (d, J_{CP} = 3,5 Hz, CH$_{Ar}$), 132.9 (s, CH$_{Ar}$), 132.4 (s, C_{qAr}), 132.0 (s, CH$_{Ar}$), 131.9 (d, J_{CP} = 3.0 Hz, C_{qAr}), 131.2 (s, CH$_{Ar}$), 130.5 (s, CH$_{Ar}$), 128.4 (s, CH$_{Ar}$), 124.0 (s, CH$_{Ar}$), 120.8 (s, CH$_{Ar}$), 119.0 (d, J_{CP} = 2.7 Hz, C_{qAr}), 118.0 (d, J_{CP} = 2.7 Hz, C_{qAr}), 115.0 (d, J_{CP} = 10.3 Hz, C_{qAr}), 113.8 (d, J_{CP} = 10.5 Hz, C_{qAr}), 112.1 (d, J_{CP} = 6.6 Hz, CH$_{Ar}$), 112.0 (d, J_{CP} = 7.5 Hz, CH$_{Ar}$), 70.0 (s, CH$_{2(18\text{-crown-6})}$), 60.7 (s, CH$_{2Mes(PNcyclo)}$), 25.5 (d, J_{CP} = 2.7 Hz, CH$_{i\text{Pr}}$), 23.7 (d, J_{CP} = 3.7 Hz, CH$_{i\text{Pr}}$), 22.4 (d, J_{CP} = 3.6 Hz, CH$_{i\text{Pr}}$), 22.0 (s, CH$_{3Ar}$), 21.2–21.1 (d, J_{CP} = 8.2 Hz, CH$_{3i\text{Pr}}$, & s, CH$_{3Ar}$), 21.0 (s, CH$_{3Ar}$), 20.9 (s, CH$_{3Ar}$), 20.7 (d, J_{CP} = 10.3 Hz, CH$_{i\text{Pr}}$), 20.6 (s, CH$_{3i\text{Pr}}$), 20.1 (d, J_{CP} = 1.4 Hz, CH$_{3Ar}$), 20.0 (s, CH$_{3Ar}$), 19.9 (d, J_{CP} = 20.9 Hz, CH$_{3i\text{Pr}}$, & d, J_{CP} = 1.6 Hz, CH$_{3Ar}$), 19.8 (d, J_{CP} = 14.3 Hz, CH$_{3i\text{Pr}}$), 19.3 (s, CH$_{3Ar}$), 19.0 (d, J_{CP} = 17.0 Hz, CH$_{3i\text{Pr}}$), 16.3 (d, J_{CP} = 6.0 Hz, CH$_{3i\text{Pr}}$), 15.9 (d, J_{CP} = 6.7 Hz, CH$_{3i\text{Pr}}$); ^{31}P NMR (C_6D_6, 303 K, 283 MHz, in ppm):

δ = 4.6 (d, $^2J_{PP}$ = 40.7 Hz, $P(^i Pr)_2$, 1 P), 3.1 (d, $^2J_{PP}$ = 40.7 Hz, $P(^i Pr)_2$, 1 P); elemental analysis (in %): $C_{56}H_{85}ClKLaN_2O_6P_2$: calcd.: C 58.10, H 7.40, N 2.42; found: C 57.42, H 7.34, N 2.49.

Preparation of $(PN)_2La\{OCPh_2(PHMes)\}$. *(Note: The product is light-sensitive and partially decomposed solids or solutions thereof may appear slightly rose-colored or wine red.)* To a –40 °C cold solution of **$(PN)_2La(PHMes)$** (291 mg, 300 µmol, 1 eq.) in toluene (4 mL) was added dropwise a solution of **benzophenone** (57 mg, 312 µmol, 1.04 eq.) in toluene (2 mL) under the exclusion of light. The resulting reaction mixture was allowed to warm up to room temperature under stirring in the dark overnight. The slightly wine red solution was evaporated to dryness. The residue was washed with *n*-pentane (2 x 1 mL) and dried *in vacuo* to give a slightly beige-colored solid which was stored in the dark at –40 °C. Single crystals suitable for X-ray structure determination were obtained by diffusion of *n*-pentane into a toluene solution of **$(PN)_2La\{OCPh_2(PHMes)\}$** in the dark at –40 °C for two days. *(Note: Preliminary tests point to a greater solubility and stability of the isolated material in toluene than in benzene. In one particular case a batch of isolated material showed only partial solubility and immediate coloration (i.e., beginning of decomposition) in C_6D_6, whereas the same batch of material gave a clear solution in toluene-d_8 and stayed colorless for days, as long as the sample was shielded from light. The ^1H and ^{31}P resonances are broad in a lot of cases, which makes the integration and assignment more difficult and might point to different isomers in solution. The ^{13}C resonances did not have sufficient intensities for a proper comprehensive assignment. However, a very characteristic resonance for the phosphahemiketal carbon atom could be identified unambiguously.)* Yield: 328 mg (282 µmol, 94%); ^{1}H NMR (toluene-d_8, 303 K, 700 MHz, in ppm): δ = 7.89 (br. s, CH_{Ar}, 2 H), 7.66 (d, J = 7.6 Hz, CH_{Ar}, 1 H), 7.19–7.12 (br. m, CH_{Ar}, 2 H), 1.06–1.03 (br. m, CH_{Ar}, 2 H), 6.93–6.79 (several overlapping m, CH_{Ar}, 9 H), 6.79–6.67 (br. m, CH_{Ar}, 2 H), 6.59 (br. s, CH_{Ar}, 2 H), 5.83–5.77 (m, CH_{Ar}, 2 H), 4.79 (d, $^1J_{PH}$ = 224.4 Hz, P*H*Mes, 1 H), 2.35 (br. s, CH_{3Ar}, 6 H), 2.26–2.16 (several broad overlapping s & m, CH_{3Ar} & C$H_{i Pr}$, 16 H), 2.04 (s, CH_{3Ar}, 3 H), 1.88 (br. s, CH_{3Ar}, 6 H), 1.22–1.11 (br. m, C$H_{3i Pr}$, 6 H), 1.10–1.04 (br. m, C$H_{3i Pr}$, 6 H), 0.96-0.83 (br. m, C$H_{3i Pr}$, 12 H); $^{13}C\{^1H\}$ NMR (toluene-d_8, 303 K, 176 MHz, in ppm, only one characteristic resonance listed): δ = 91.9 (d, $^1J_{CP}$ = 8.7 Hz, O*C*Ph$_2$(PHMes)); $^{31}P\{^1H\}$ NMR (toluene-d_8, 303 K, 283 MHz, in ppm): δ = 9.2 (br. s, *P*N$^-$, 2 P), –17.1 to –21.6 (br. s at –18.4, with br. should at –20.0, *P*HMes, 1 P); ^{31}P NMR (toluene-d_8, 303 K, 283 MHz, in ppm): δ = 9.2 (br. s, *P*N$^-$, 2 P), –17.1 to –21.6 (br. d at –18.4, $^1J_{PH}$ = 232.6 Hz, with br. shoulder at –20.0 , *P*HMes, 1 P); elemental analysis (in %): $C_{66}H_{84}LaN_2OP_3$: calcd.: C 68.74, H 7.34, N 2.43; found: C 68.35, H 7.49, N 2.82.

Preparation of $(PN)_2La\{OC(C_6H_4\text{-}4\text{-}NMe_2)_2(PHMes)\}$. *(Note: This reaction was carried out only once and the following procedure does therefore not contain optimized reaction conditions. Exclusion of light (like in the preparation of* ***$(PN)_2La\{OCPh_2(PHMes)\}$****) is strongly recommended, since the product seems to be also light-sensitive to some extent.)* To a mixture of solid **$(PN)_2La(PHMes)$** (194 mg, 200 µmol, 1 eq.) and **Michler's ketone** (4,4'-bis(dimethylamino)benzophenone, 54 mg, 200 µmol, 1 eq.) was added toluene (5 mL) at room temperature. The resulting yellow-brown reaction mixture was stirred for 5 h at room temperature. The mixture was then filtered, and the filtrate evaporated to dryness. To the residue was added *n*-hexane (3 mL) and the resulting suspension was centrifuged. The dark *n*-hexane extract was separated from the solid and the washing / centrifugation / separation steps were repeated two more times. A batch of beige-colored solid (64 mg) was isolated and dried *in vacuo*. However, NMR spectroscopy did not point to a defined material. Crystals were therefore grown from the *n*-hexane extract at room temperature over a period of two days. After isolation and drying *in vacuo* a yellow, microcrystalline product was obtained. Single crystals suitable for X-ray structure determination of **$(PN)_2La\{OC(C_6H_4\text{-}4\text{-}NMe_2)_2(PHMes)\}$** were also obtained in this way (prior to isolation and drying). *(Note: A first test suggests that the product shows a better solubility and higher stability in C_6D_6 than* ***$(PN)_2La\{OCPh_2(PHMes)\}$****. However, the ^1H and ^{31}P resonances are also broad in a lot of cases, which makes the integration and assignment more difficult and might again point to different isomers in solution.)* Yield: 81 mg (65 µmol, 33%); ^{1}H NMR (C_6D_6, 303 K, 700 MHz, in ppm): δ = 7.95–7.73 (br. s, C*H*$_{Ar}$, 2 H), 7.29–7.12 (br. s, C*H*$_{Ar}$, 2 H), 6.96–6.93 (br. m, C*H*$_{Ar}$, 2 H), 6.90 (br. s, C*H*$_{Ar}$, 2 H), 6.89–6.87 (br. m, C*H*$_{Ar}$, 2 H), 6.86–6.80 (br. m, C*H*$_{Ar}$, 2 H), 6.70 (br. s, C*H*$_{Ar}$, 2 H), 6.56–6.39 (br. m, C*H*$_{Ar}$, 2 H), 6.28–6.10 (br. m, C*H*$_{Ar}$, 2 H), 5.96–5.90 (m, CHAr, 2 H), 2.59–2.49 (several br. s, with two prominent br. s at 2.56 & 2.54, C*H*$_{3NMe2}$ & C*H*$_{3Ar}$, 15 H), 2.31–2.19 (br. s at 2.24 & s at 2.21, C*H*$_{3Ar}$, 12 H), 2.19–2.00 (two br. s at 2.16 & 2.08, s at 2.07, C*H*$_{3Ar}$ & C*H*$_{i\text{Pr}}$, 16 H), 1.38–1.26 (br. m, C*H*$_{3i\text{Pr}}$, 6 H), 1.14–1.08 (br. m, C*H*$_{3i\text{Pr}}$, 6 H), 1.06–0.90 (br. m, C*H*$_{3i\text{Pr}}$, 12 H); ^{13}C{^{1}H} NMR (C_6D_6, 303 K, 176 MHz, in ppm): δ = 161.7 (br. s, C_{qAr}), 149.4 (s, C_{qAr}), 148.9 (s, C_{qAr}), 143.8 (br. s, C_{qAr}), 142.5 (br. s, C_{qAr}), 139.5 (br. s, C_{qAr}), 137.7 (br. s, C_{qAr}), 136.5 (br. s, C_{qAr}), 135.2 (br. s, C_{qAr}), 134.1 (s, *C*H$_{Ar}$), 133.3 (s, C_{qAr}), 133.1 (s, *C*H$_{Ar}$), 131.7 (br. s, *C*H$_{Ar}$), 131.2 (s, *C*H$_{Ar}$), 130.6 (br. s, *C*H$_{Ar}$), 129.2 (s, *C*H$_{Ar}$), 128.8 (br. s, *C*H$_{Ar}$), 121.7 (s, C_{qAr}), 113.5 (br. s, *C*H$_{Ar}$), 113.1 (*pseudo*-t, J_{CP} = 5.9 Hz, C_{qAr}), 111.7 (s, *C*H$_{Ar}$), 111.3 (br. s, *C*H$_{Ar}$), 91.8 (d, $^1J_{CP}$ = 6.0 Hz, O*C*(C_6H_4-4-NMe_2)$_2$(PHMes)), 40.6 (s, *C*H$_{3NMe2}$), 40.5 (s, *C*H$_{3NMe2}$), 24.0 (br. s, *C*H$_{i\text{Pr}}$), 22.0 (br. s, *C*H$_{3i\text{Pr}}$), 21.4 (br. s, *C*H$_{3i\text{Pr}}$), 21.2 (s, *C*H$_{3Ar}$), 20.9 (s, *C*H$_{3Ar}$), 20.7 (s, *C*H$_{3Ar}$), 19.4 (br. s, *C*H$_{3i\text{Pr}}$), 16.0 (br. s, *C*H$_{3i\text{Pr}}$); ^{31}P{^{1}H} NMR (C_6D_6, 303 K, 283 MHz, in ppm): δ = 9.1 (br. s, with br. shoulder at 8.2, *P*N$^-$, 2 P), –18.8 and –20.2 (two br. s, *P*HMes, 1 P); ^{31}P NMR (C_6D_6, 303 K, 283 MHz, in ppm): δ = 9.1 (br. s, with br. shoulder at 8.2, *P*N$^-$, 2 P), –18.8 and –20.2 (two br. d, $^1J_{PH}$ = 224.8 Hz for both, *P*HMes, 1 P); elemental analysis (in %): $C_{70}H_{94}LaN_4OP_3$: calcd.: C 67.84, H 7.65, N 4.52; found: C 67.87, H 8.07, N 4.45.

UV-Vis and Fluorescence Spectroscopy. UV-Vis and fluorescence data of analytically pure heterobimetallic complexes **5**, **6** and **7** (see Results and Discussion of Chapter 2) were recorded in THF at room temperature under inert conditions using a Cary 50 scan instrument or a Jasco FP-8300 spectrometer, respectively. The stock solutions were prepared in the glovebox: Ca. 4.9 mg (**5** and **6**) or ca. 4.6 mg (**7**) of the respective heterobimetallic complex were dissolved in 20 mL THF and diluted by a factor of four (using volumetric flasks), giving final concentrations of $c \approx 40\ \mu mol \cdot L^{-1}$ (**5** and **7**) or $37\ \mu mol \cdot L^{-1}$ (**6**). The solutions were freshly prepared before the measurements and the same THF solvent batch was used in blank measurements for background subtraction.

X-ray Crystallography. Single crystals for X-ray diffraction experiments were measured at the analytical facility of the Paderborn University using a Bruker Smart AXS or a Bruker D8 Venture instrument. All crystals were kept at 130(2) K or 120(2) K throughout data collection. Data collection was performed using either the APEXIII or the Smart software package. Data refinement and reduction were performed with Bruker Saint (V8.34A). All structures were solved with SHELXT[5] and refined using the OLEX 2 software package.[6] All non-hydrogen atoms were refined anisotropically, and hydrogen atoms were included at the geometrically calculated positions and refined using a riding model. For further crystallographic details regarding crystal measurements, please check Table A1 and Figures A51–A55.

A.2 NMR Spectra

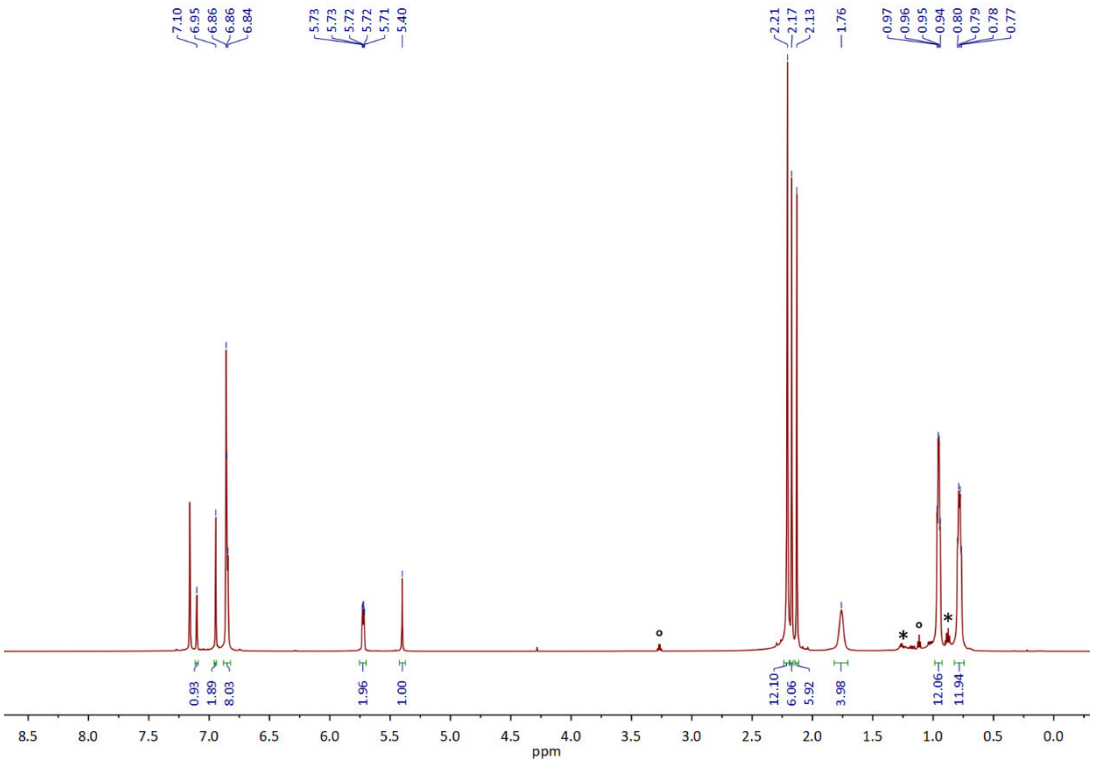

Figure A1. ^{1}H NMR spectrum of **(PN)$_2$La{NH(C$_6$H$_3$-3,5-(CF$_3$)$_2$)}** in C_6D_6 (303 K). Traces of *n*-hexane from work-up are marked by *, traces of diethyl ether from the glovebox atmosphere by °.

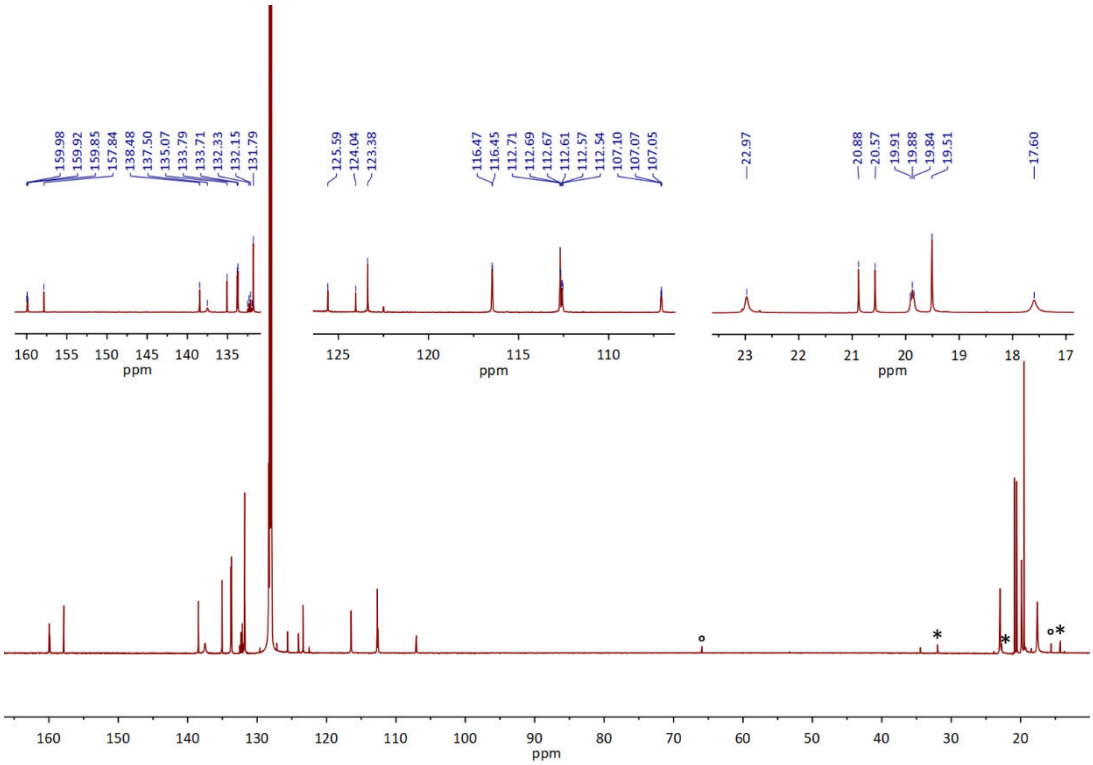

Figure A2. ^{13}C{^{1}H} NMR spectrum of **(PN)$_2$La{NH(C$_6$H$_3$-3,5-(CF$_3$)$_2$)}** in C_6D_6 (303 K). The peak listing is given in the three enlargements of the relevant aromatic and aliphatic regions of the spectrum. Traces of *n*-hexane from work-up are marked by *, traces of diethyl ether from the glovebox atmosphere by °.

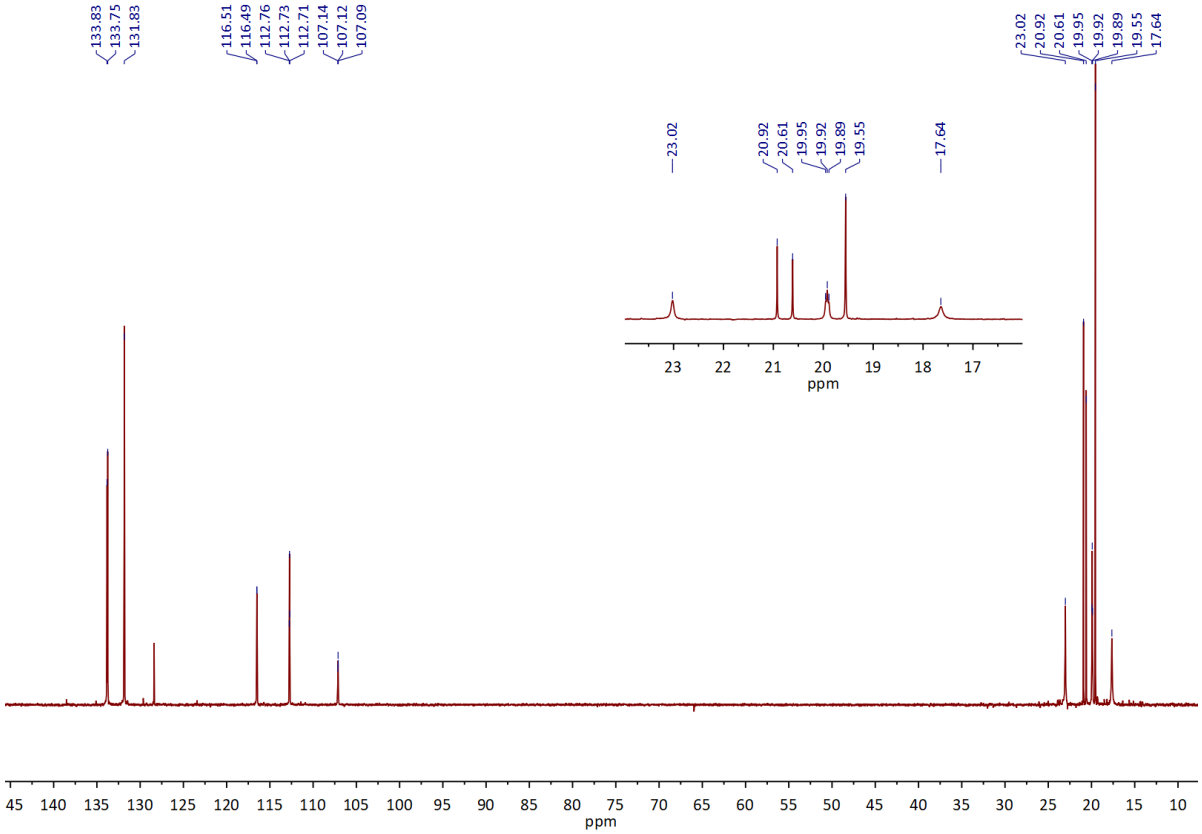

Figure A3. $^{13}C\{^{1}H\}$ DEPT135 NMR spectrum of **(PN)$_2$La{NH(C$_6$H$_3$-3,5-(CF$_3$)$_2$)}** in C_6D_6 (303 K). The enlargement shows the resonances in the aliphatic region.

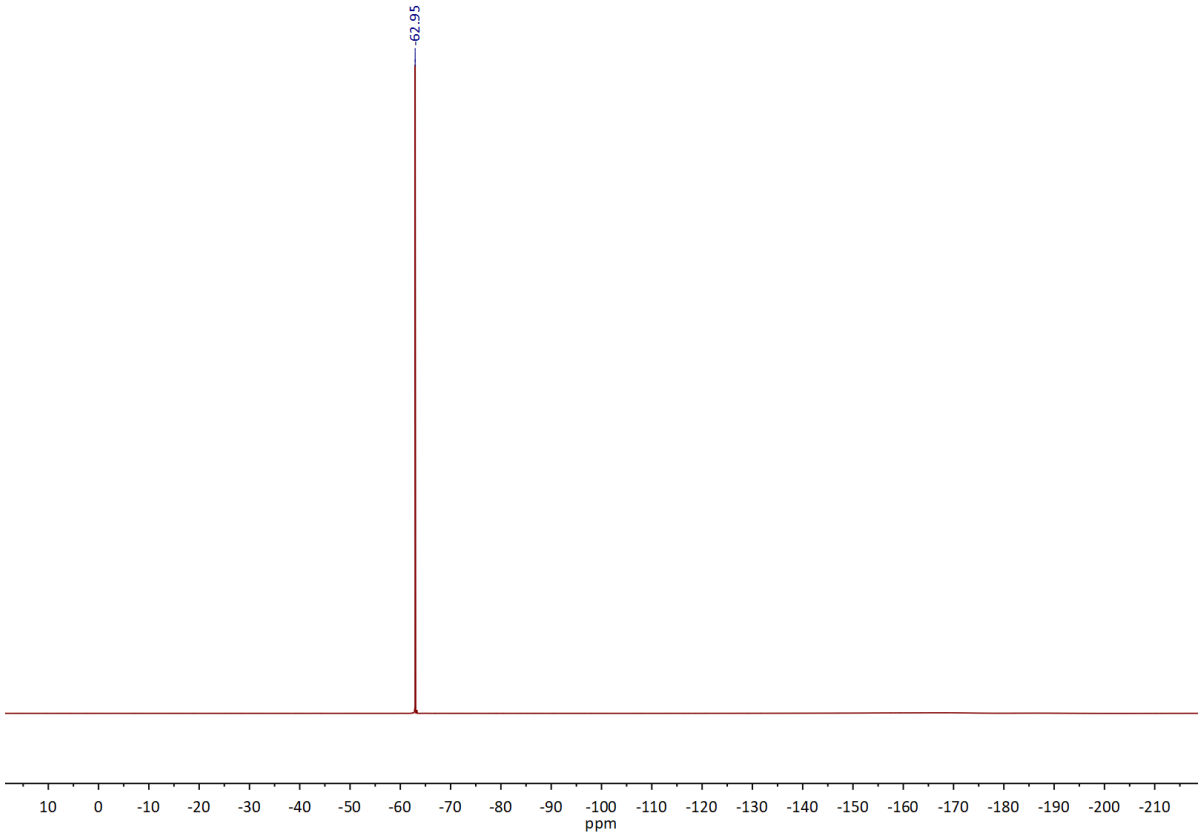

Figure A4. $^{19}F\{^{1}H\}$ NMR spectrum of **(PN)$_2$La{NH(C$_6$H$_3$-3,5-(CF$_3$)$_2$)}** in C_6D_6 (303 K).

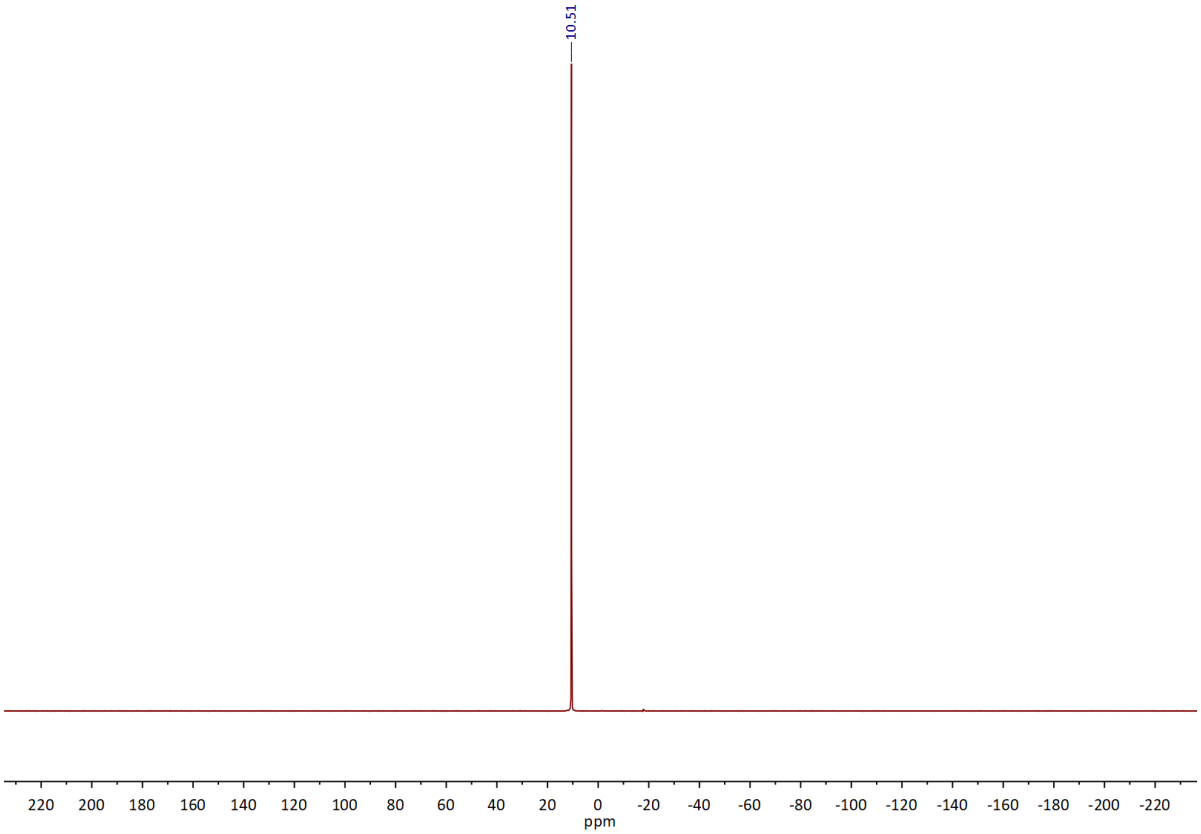

Figure A5. $^{31}P\{^{1}H\}$ NMR spectrum of **(PN)$_2$La{NH(C$_6$H$_3$-3,5-(CF$_3$)$_2$)}** in C_6D_6 (303 K).

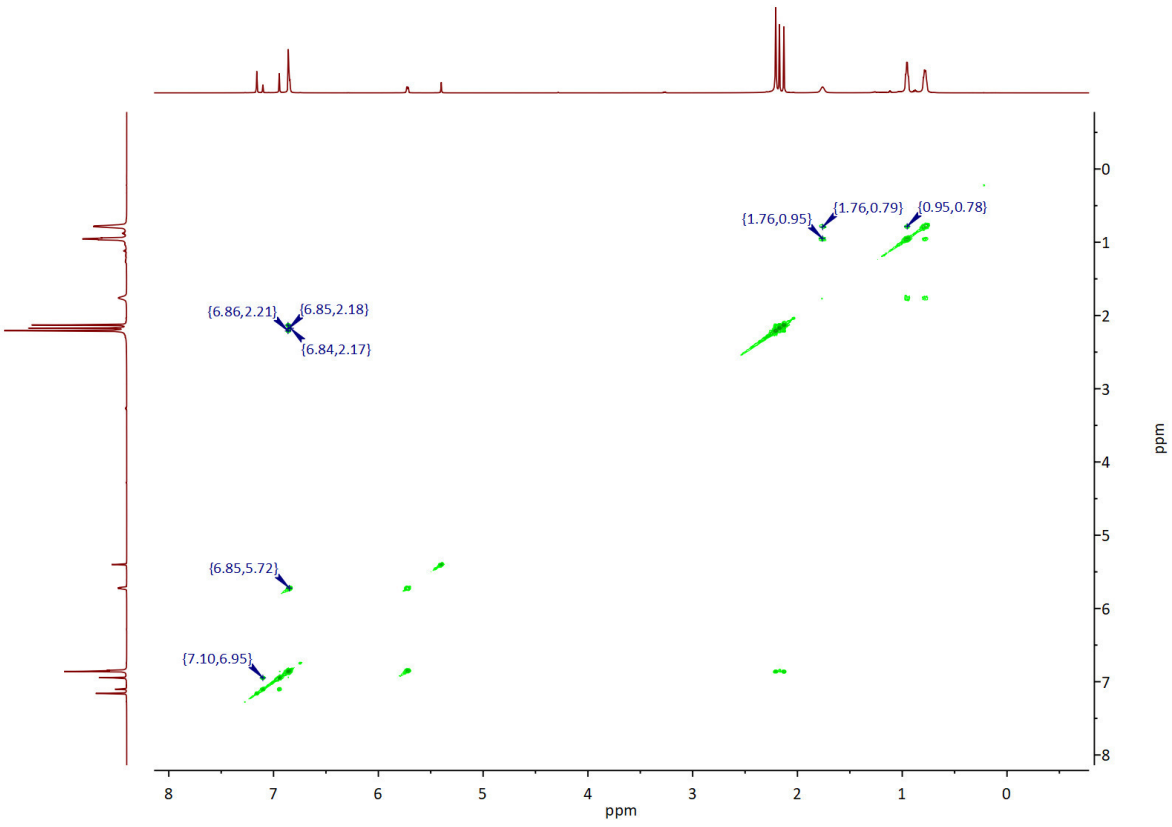

Figure A6. $^{1}H–^{1}H$ COSY NMR spectrum of **(PN)$_2$La{NH(C$_6$H$_3$-3,5-(CF$_3$)$_2$)}** in C_6D_6 (303 K).

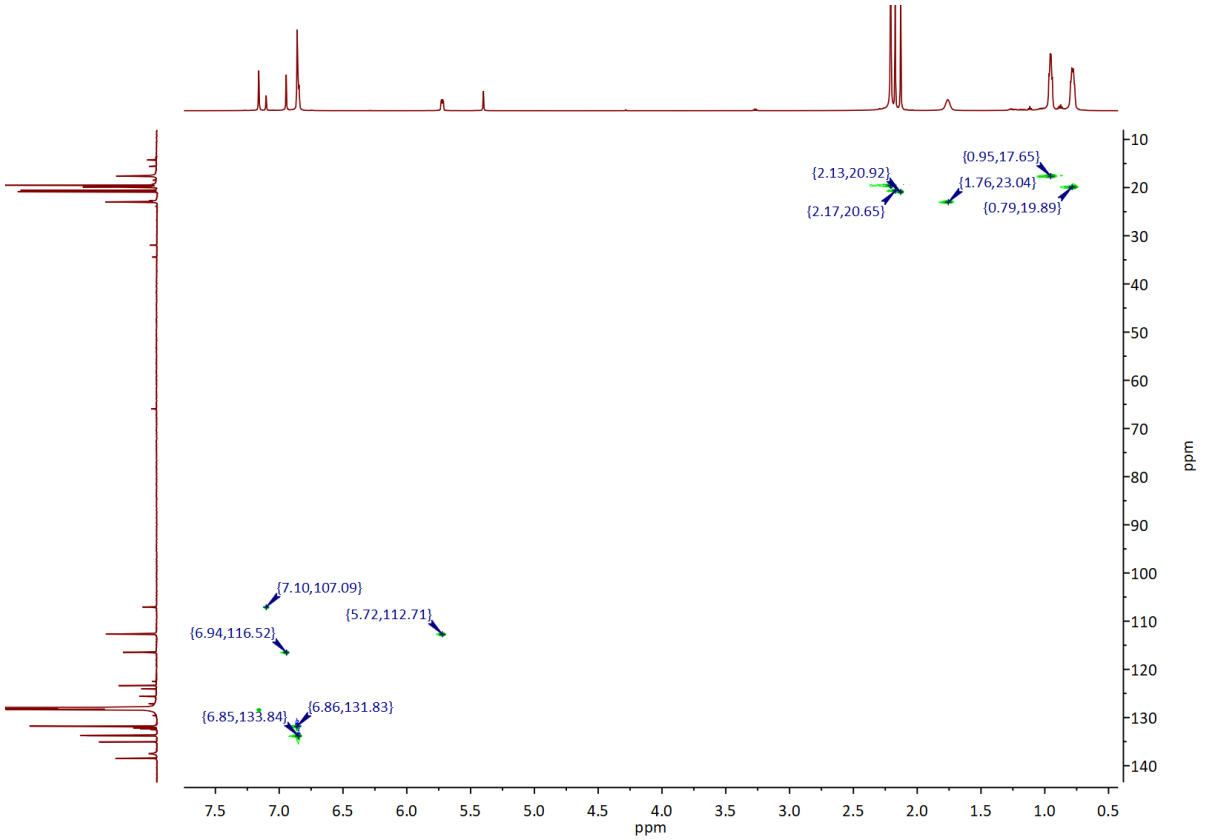

Figure A7. $^{1}H–^{13}C$ HSQC NMR spectrum of **(PN)$_2$La{NH(C$_6$H$_3$-3,5-(CF$_3$)$_2$)}** in C_6D_6 (303 K).

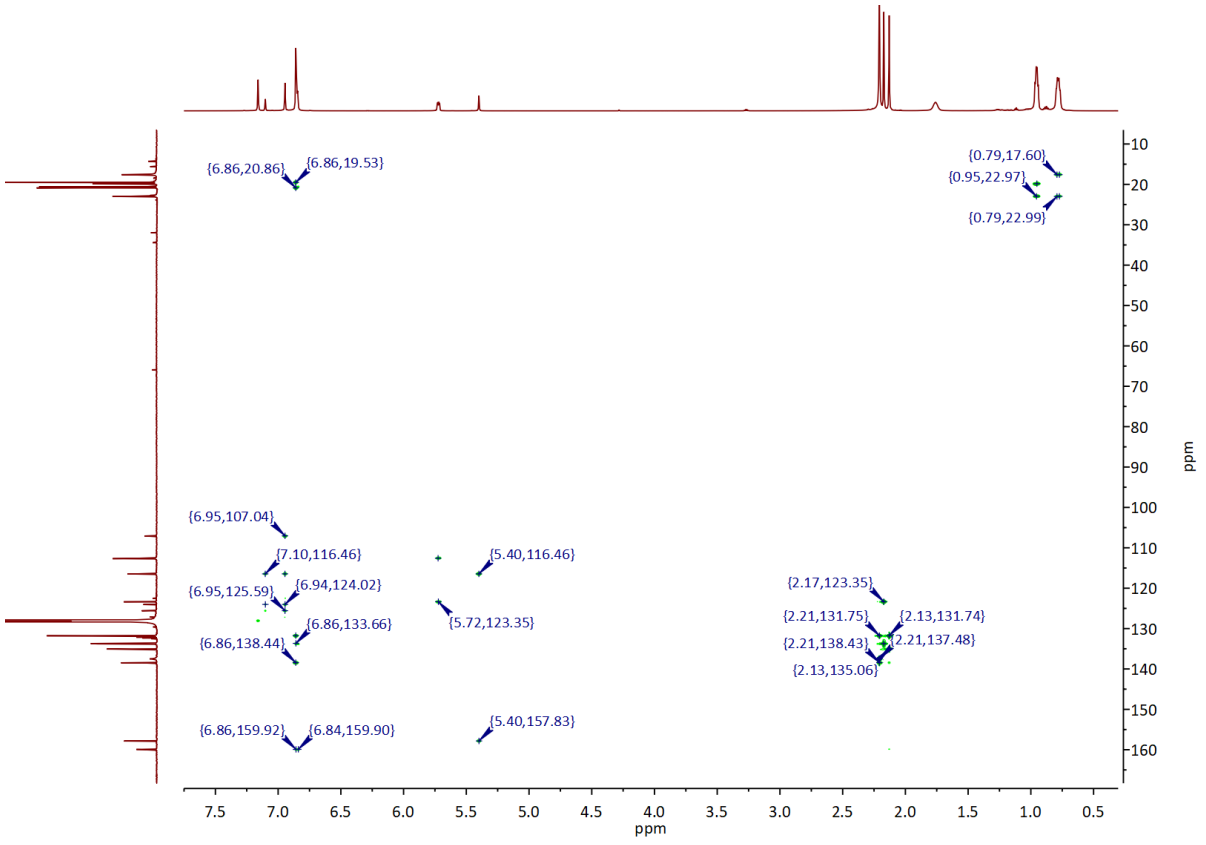

Figure A8. $^{1}H–^{13}C$ HMBC NMR spectrum of **(PN)$_2$La{NH(C$_6$H$_3$-3,5-(CF$_3$)$_2$)}** in C_6D_6 (303 K).

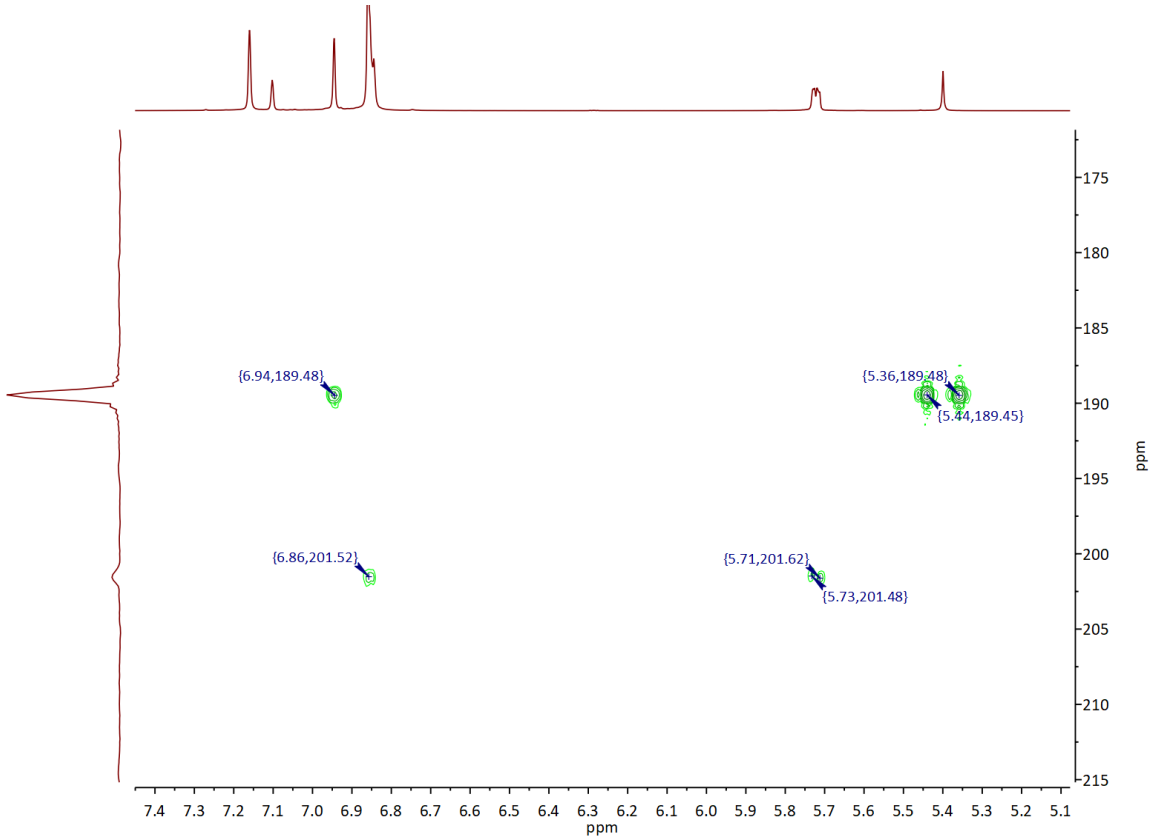

Figure A9. $^{1}H–^{15}N$ HMBC NMR spectrum of **$(PN)_2La\{NH(C_6H_3\text{-}3,5\text{-}(CF_3)_2)\}$** in C_6D_6 (303 K).

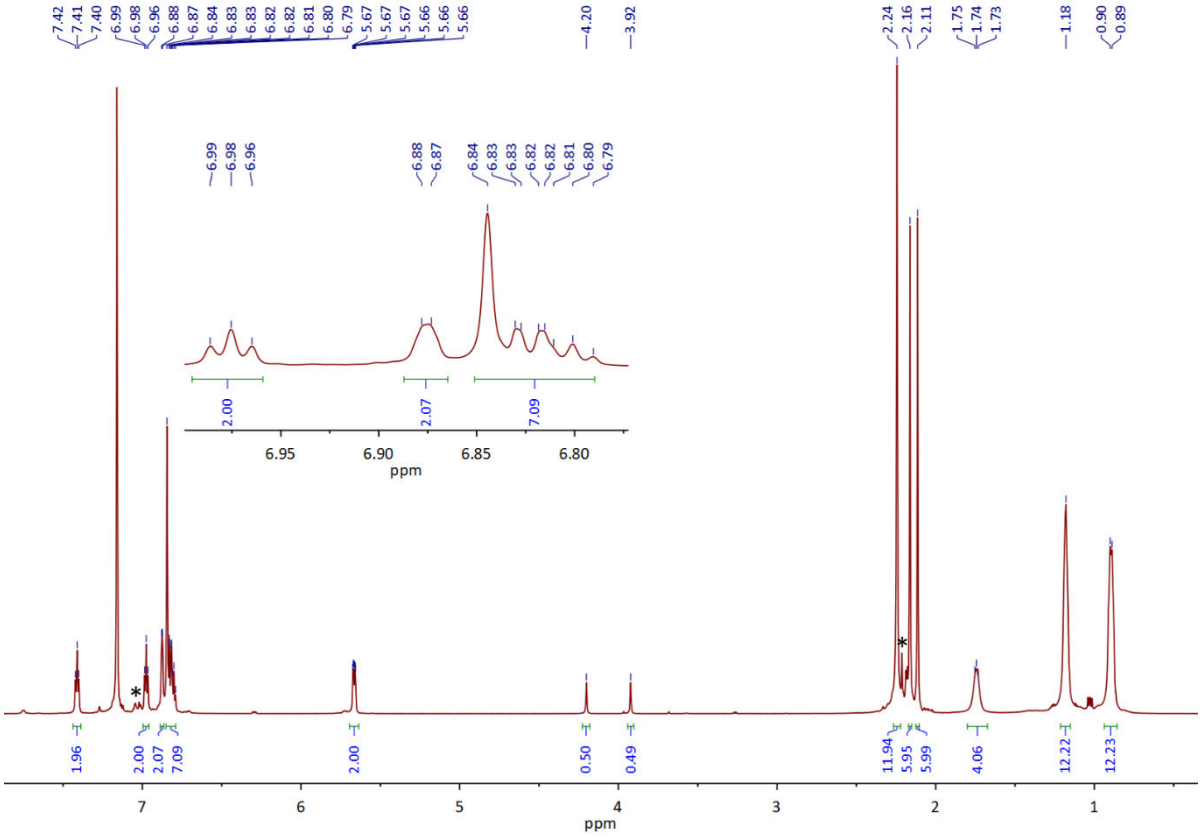

Figure A10. ^{1}H NMR spectrum of **$(PN)_2La(PHPh)$** in C_6D_6 (303 K). The enlargement shows the crowded resonances in the aromatic region. Traces of toluene from work-up are marked by *.

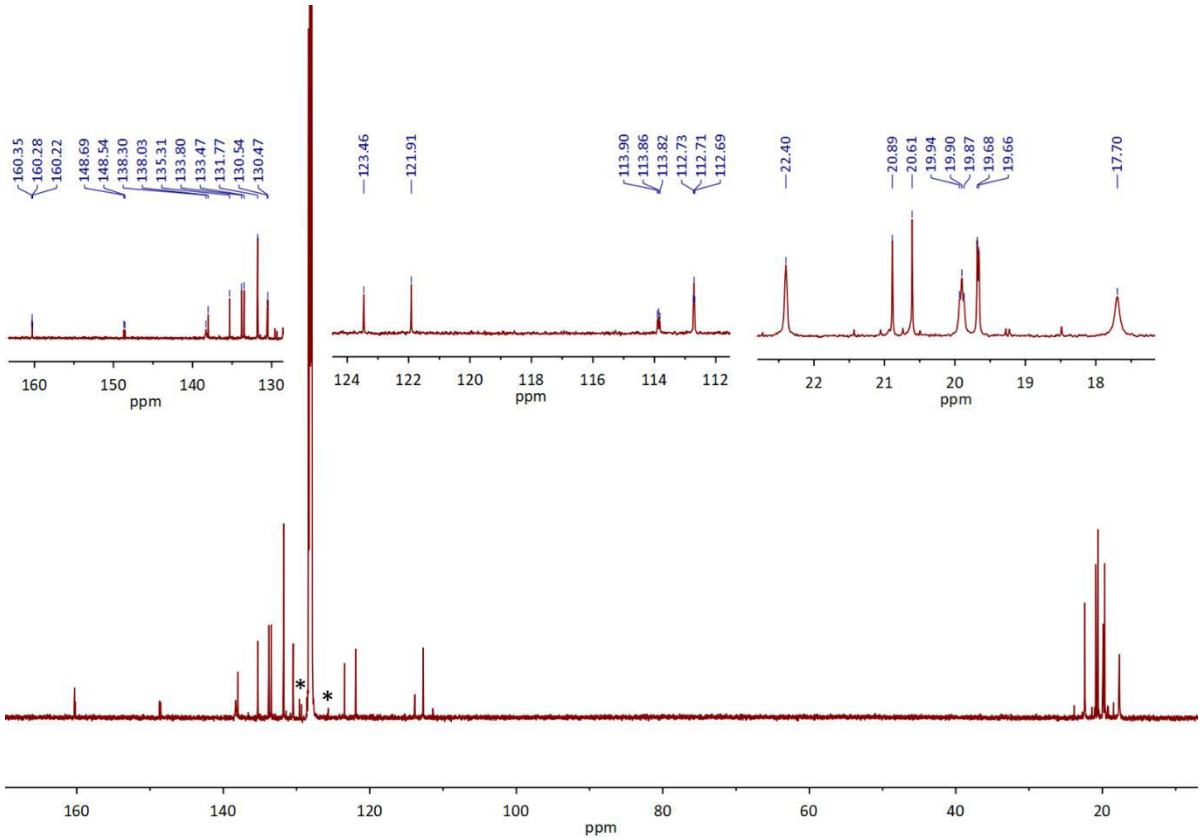

Figure A11. $^{13}C\{^{1}H\}$ NMR spectrum of **$(PN)_2La(PHPh)$** in C_6D_6 (303 K). The peak listing is given in the three enlargements of the relevant aromatic and aliphatic regions of the spectrum. Traces of toluene from work-up are marked by *.

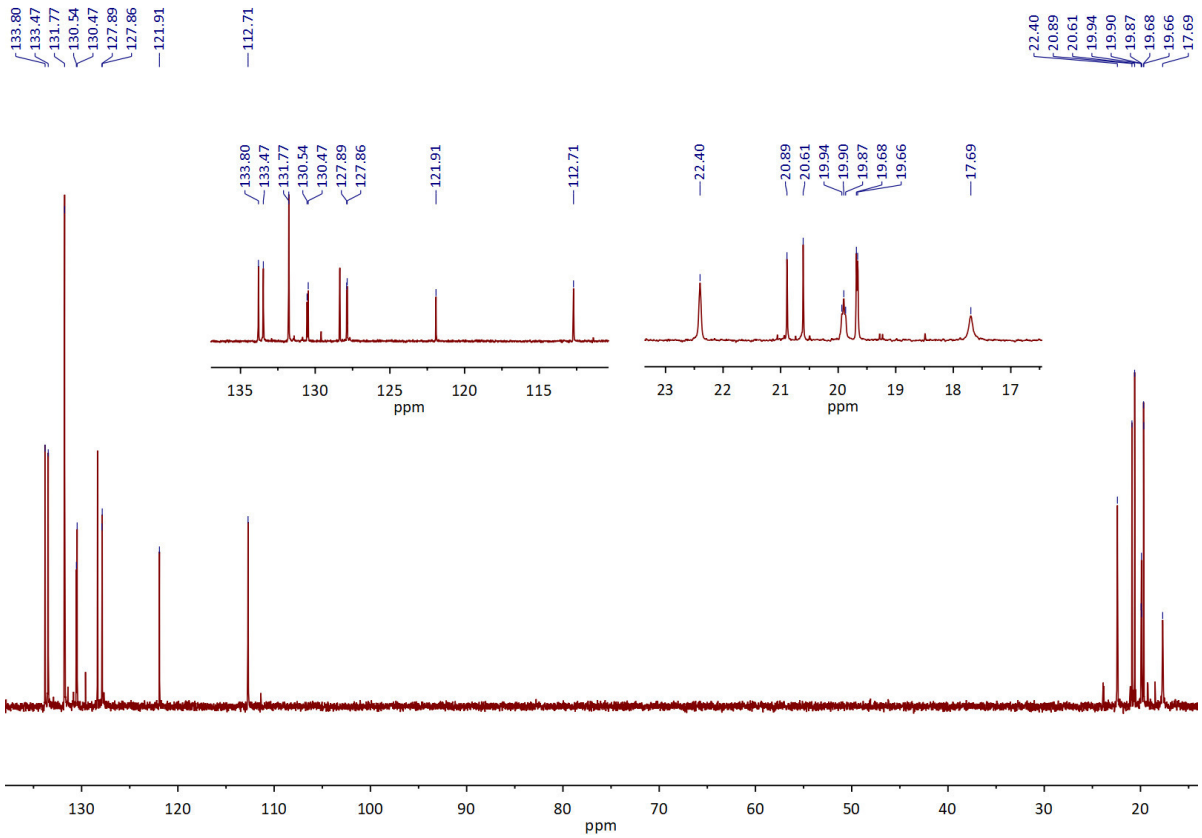

Figure A12. $^{13}C\{^{1}H\}$ DEPT135 NMR spectrum of **$(PN)_2La(PHPh)$** in C_6D_6 (303 K). The two enlargements show the resonances in the aromatic and aliphatic region.

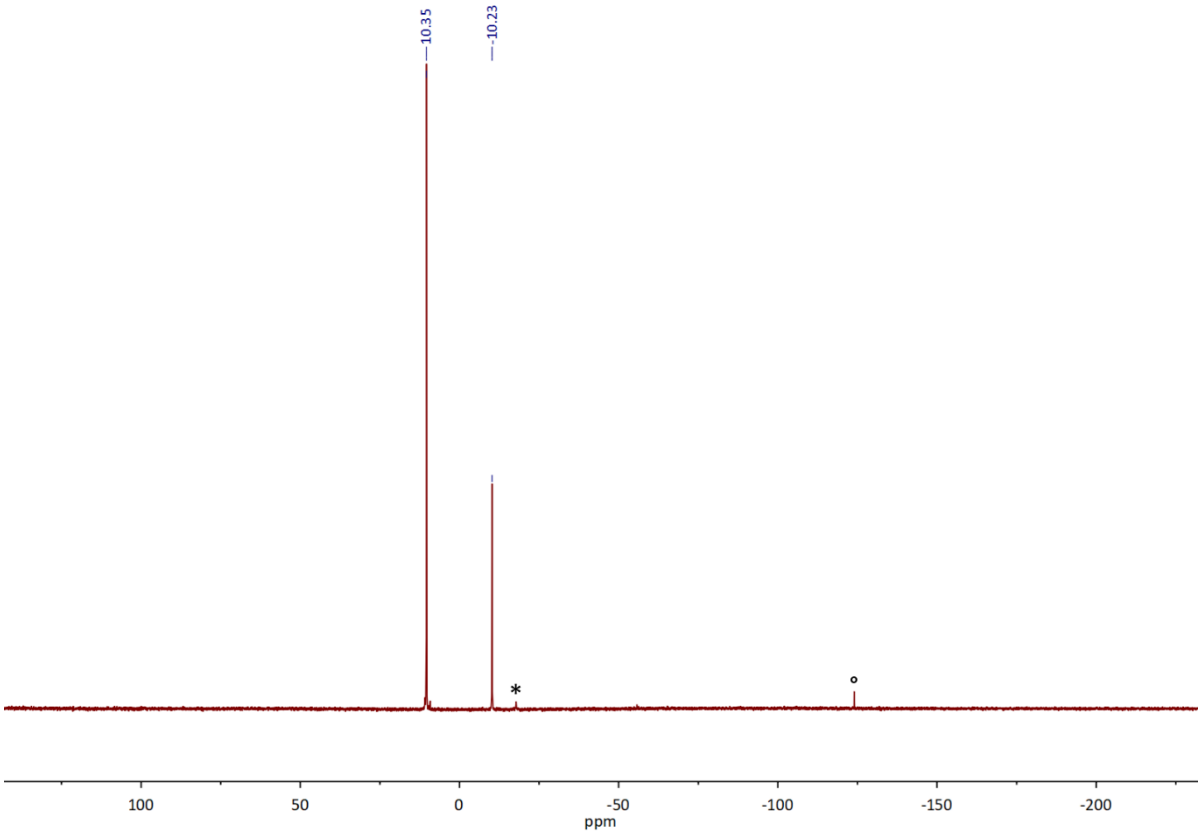

Figure A13. $^{31}P\{^{1}H\}$ NMR spectrum of **(PN)$_2$La(PHPh)** in C_6D_6 (303 K). Traces of protonated supporting ligand are marked by *, traces of phenylphosphine by °.

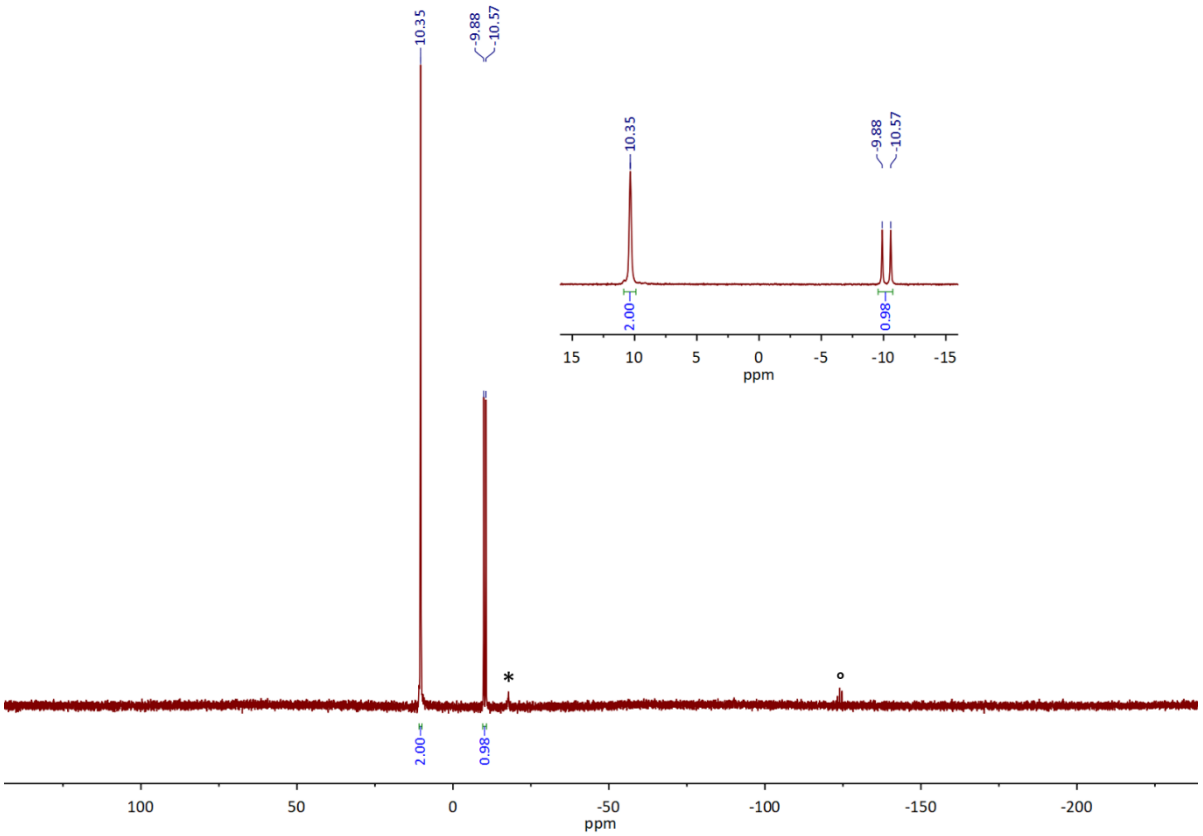

Figure A14. ^{31}P NMR spectrum of **(PN)$_2$La(PHPh)** in C_6D_6 (303 K). The enlargement shows the doublet splitting of the *P*HPh resonance. Traces of protonated supporting ligand are marked by *, traces of phenylphosphine by °.

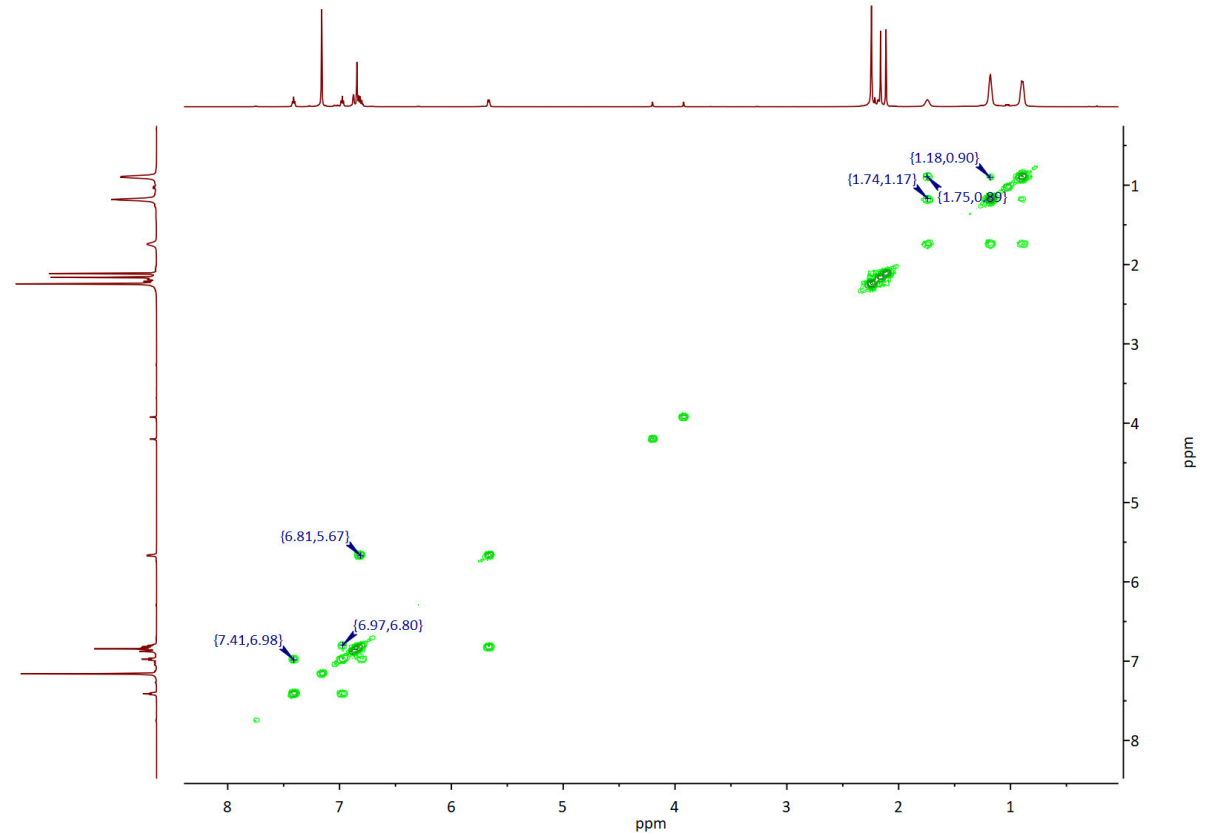

Figure A15. $^{1}H–^{1}H$ COSY NMR spectrum of **$(PN)_2La(PHPh)$** in C_6D_6 (303 K).

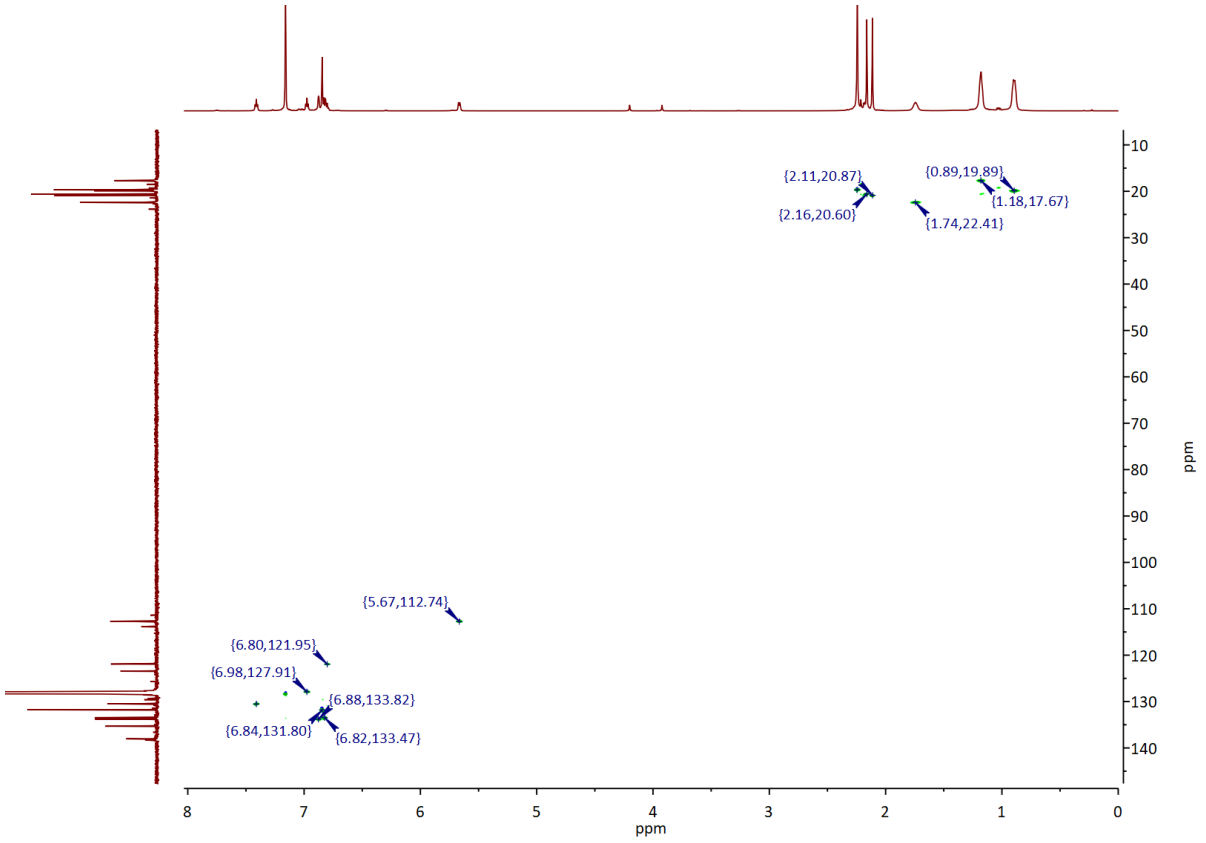

Figure A16. $^{1}H–^{13}C$ HSQC NMR spectrum of **$(PN)_2La(PHPh)$** in C_6D_6 (303 K).

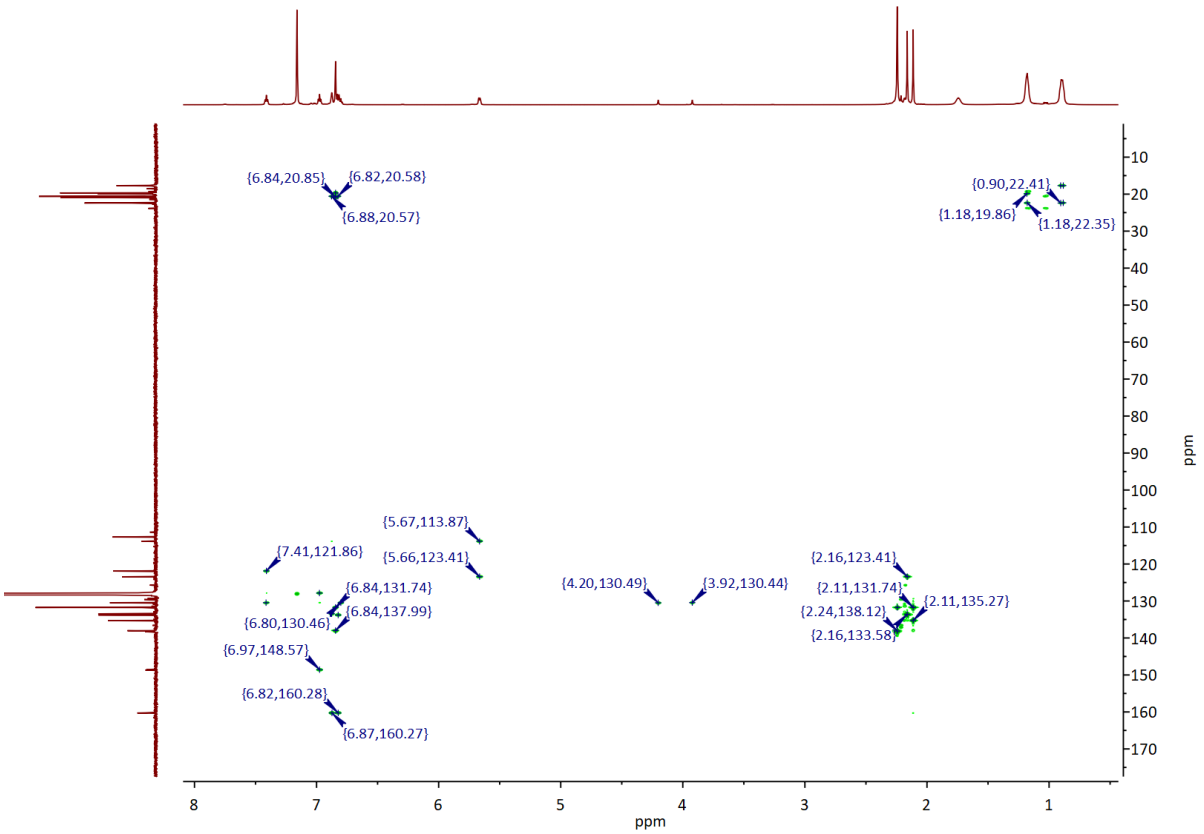

Figure A17. ^{1}H–^{13}C HMBC NMR spectrum of **$(PN)_2La(PHPh)$** in C_6D_6 (303 K).

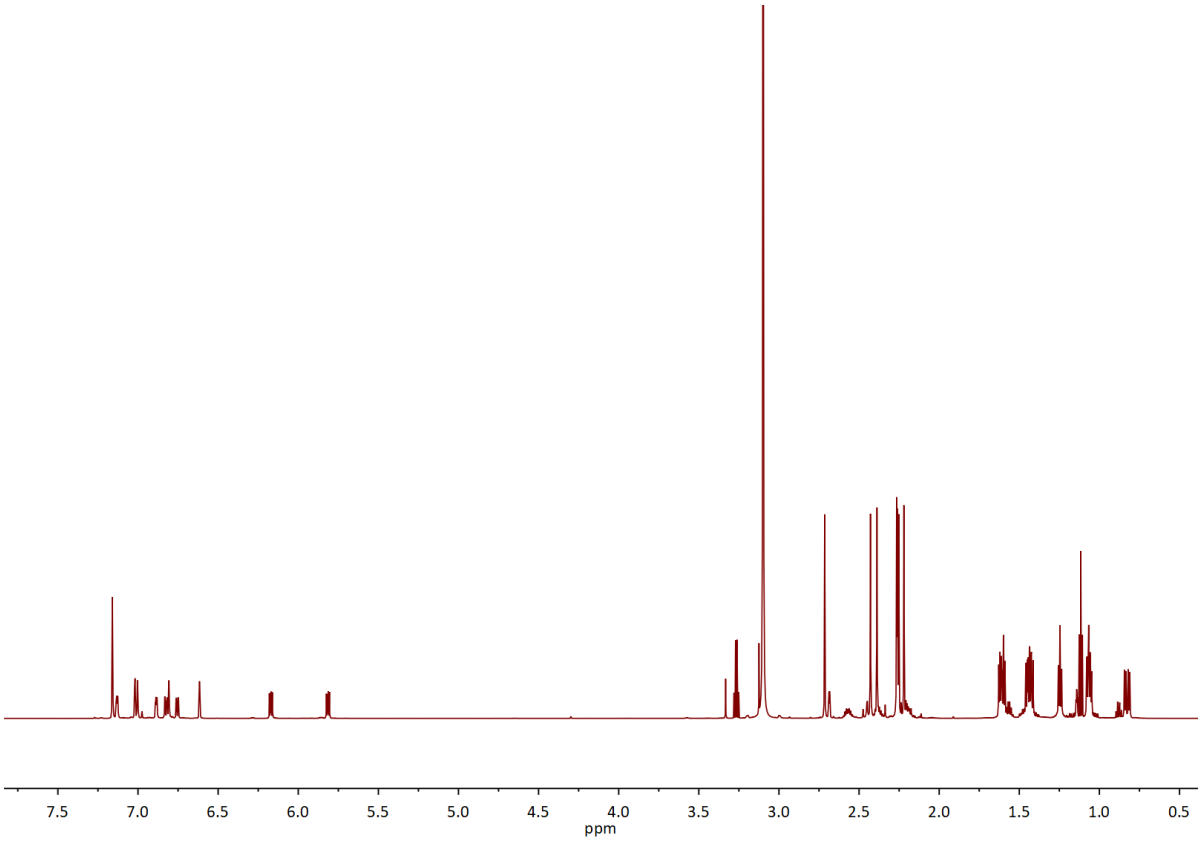

Figure A18. ^{1}H NMR spectrum of **[K(18-crown-6)][(PN)(PNcyclo)LaCl]** in C_6D_6 (303 K). For peak listing and integrals see Figures A19–21.

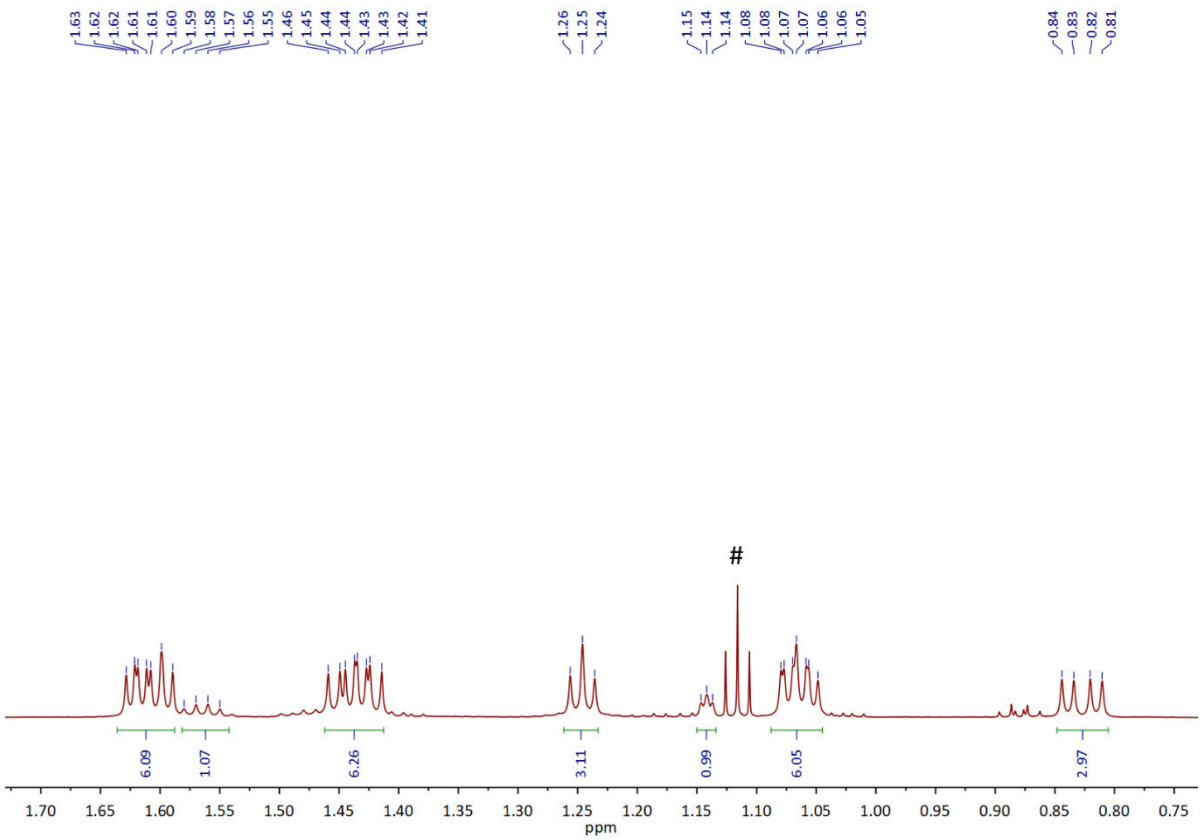

Figure A19. Section of the ^{1}H NMR spectrum (δ = 1.73 – 0.73 ppm) of **[K(18-crown-6)][(PN)(PNcyclo)LaCl]** in C_6D_6 (303 K). Residual diethyl ether from work-up is marked by #.

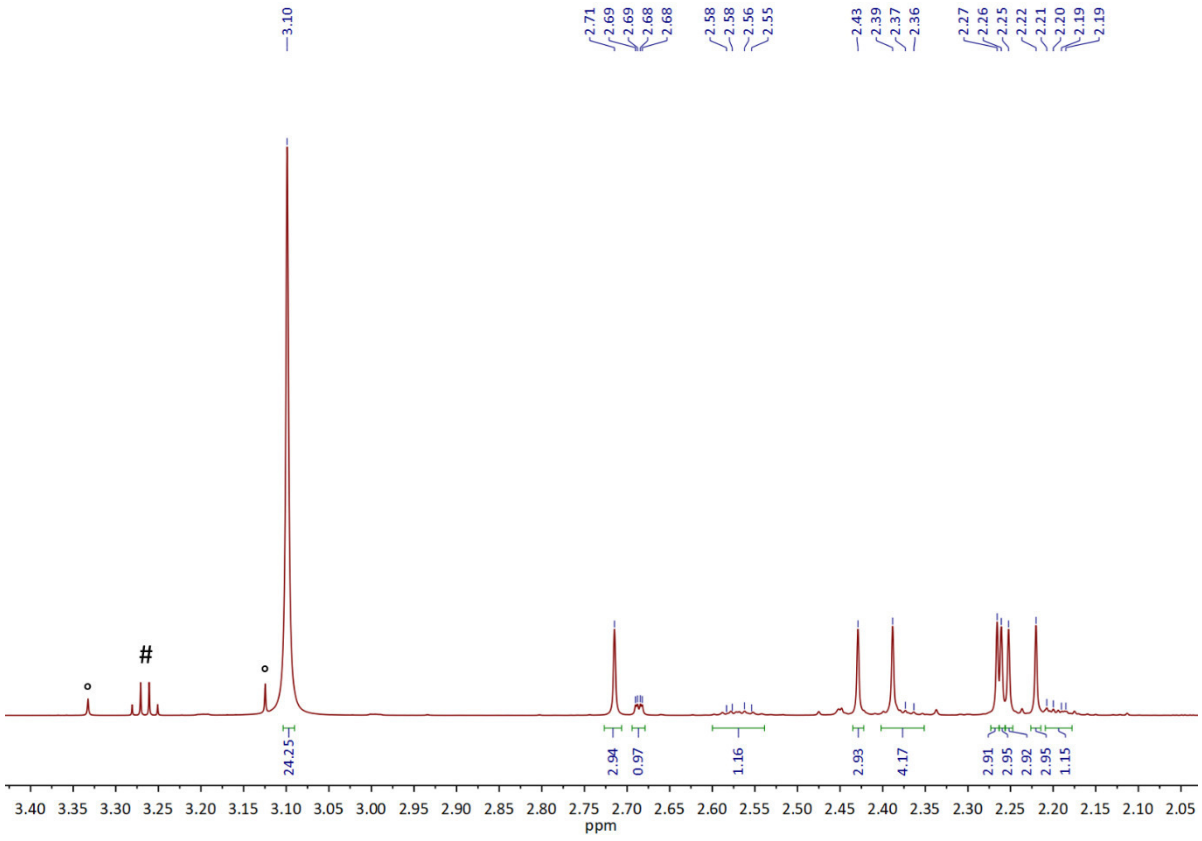

Figure A20. Section of the ^{1}H NMR spectrum (δ = 4.43 – 2.03 ppm) of **[K(18-crown-6)][(PN)(PNcyclo)LaCl]** in C_6D_6 (303 K). Residual diethyl ether from work-up is marked by #, residual 1,2-dimethoxyethane by °.

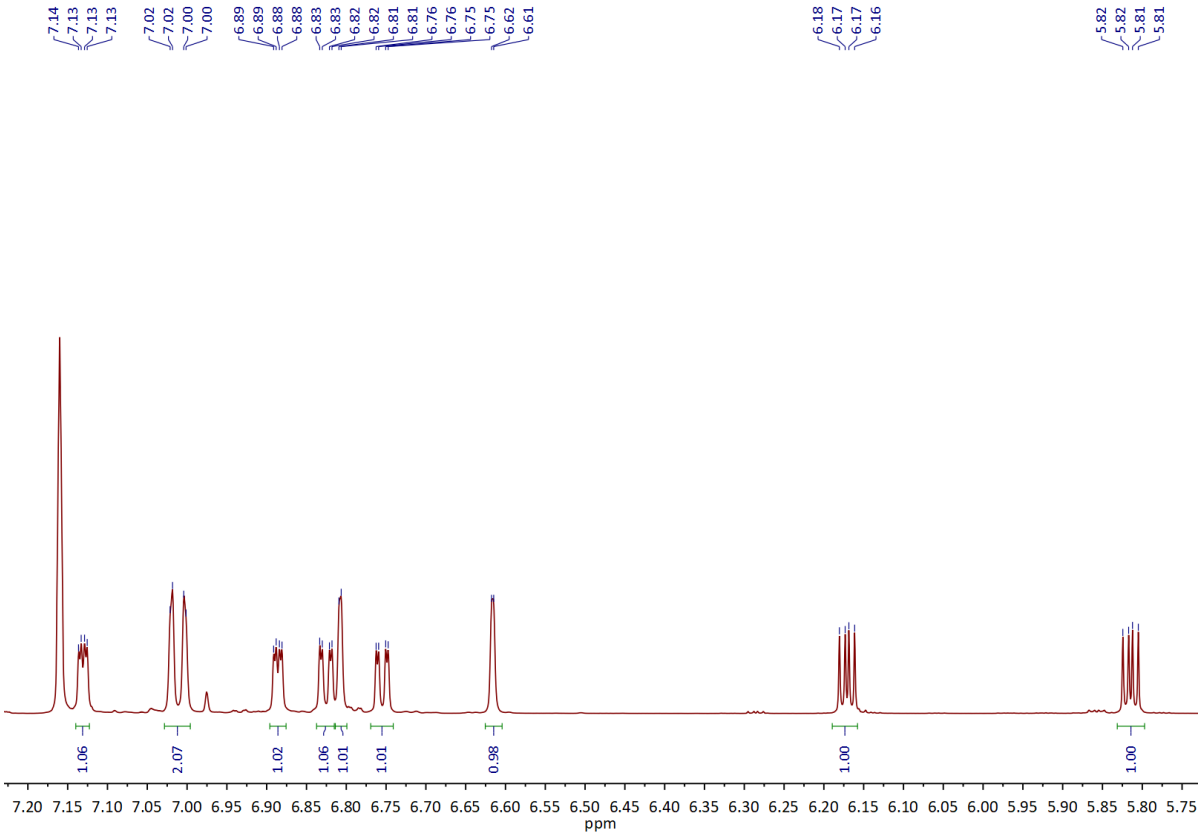

Figure A21. Section of the ^{1}H NMR spectrum (δ = 7.23 – 5.73 ppm) of **[K(18-crown-6)][(PN)(PNcyclo)LaCl]** in C_6D_6 (303 K).

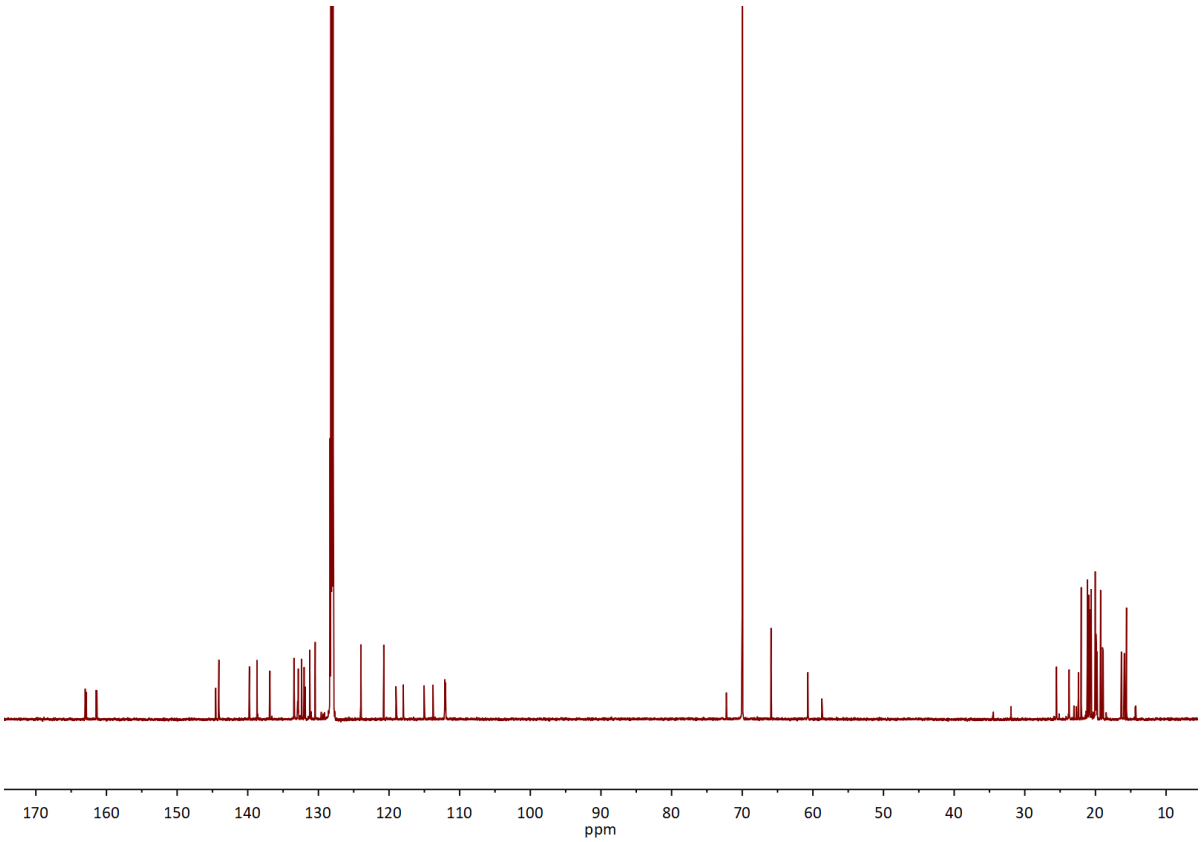

Figure A22. ^{13}C{^{1}H} NMR spectrum of **[K(18-crown-6)][(PN)(PNcyclo)LaCl]** in C_6D_6 (303 K). For peak listing see Figures A23–A26.

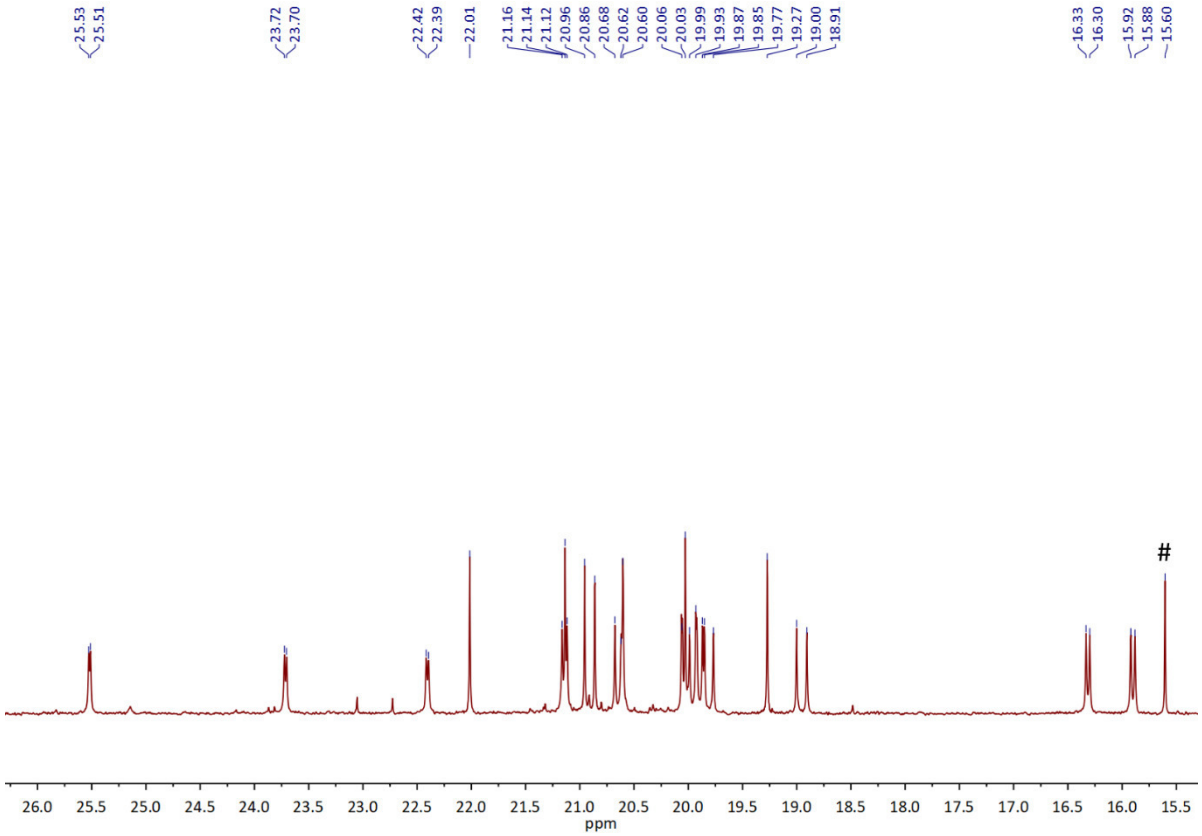

Figure A23. Section of the $^{13}C\{^{1}H\}$ NMR spectrum (δ = 26.3 – 15.3 ppm) of **[K(18-crown-6)][(PN)(PNcyclo)LaCl]** in C_6D_6 (303 K).

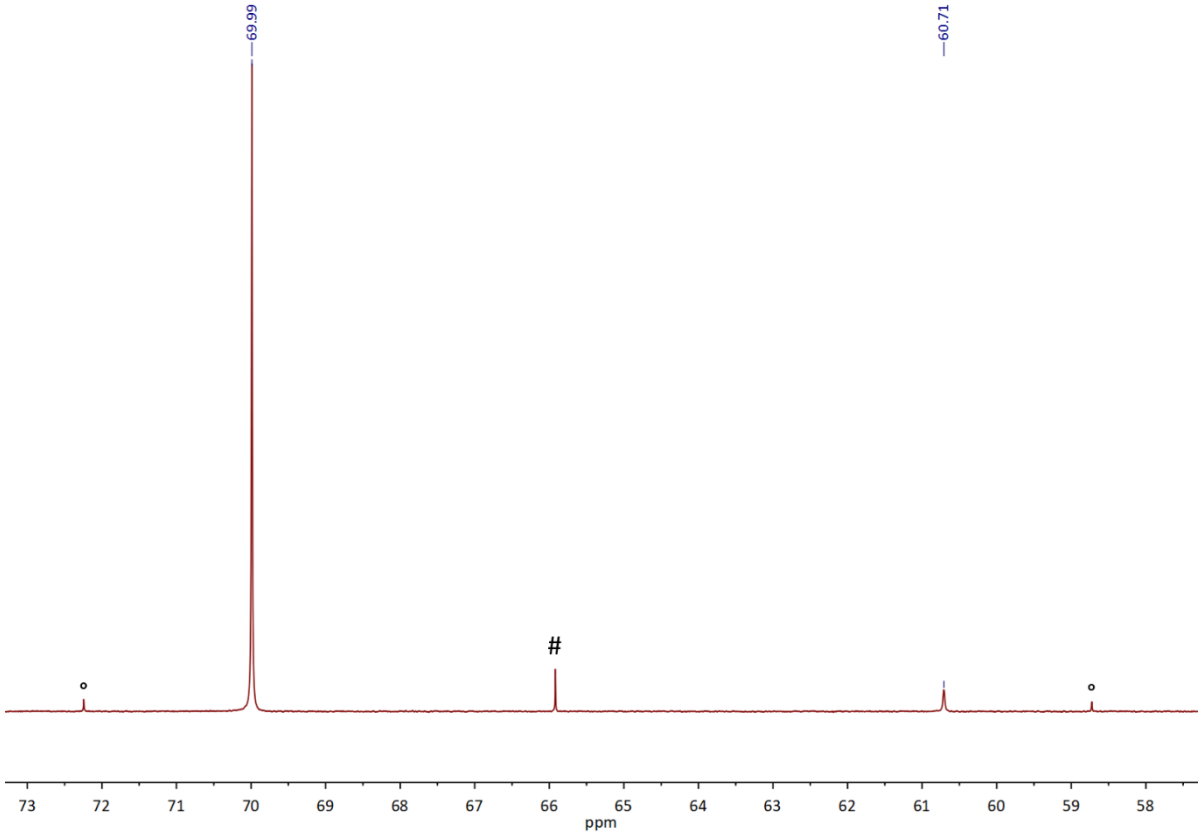

Figure A24. Section of the $^{13}C\{^{1}H\}$ NMR spectrum (δ = 73.3 – 57.3 ppm) of **[K(18-crown-6)][(PN)(PNcyclo)LaCl]** in C_6D_6 (303 K). Residual diethyl ether from work-up is marked by #, residual 1,2-dimethoxyethane by °.

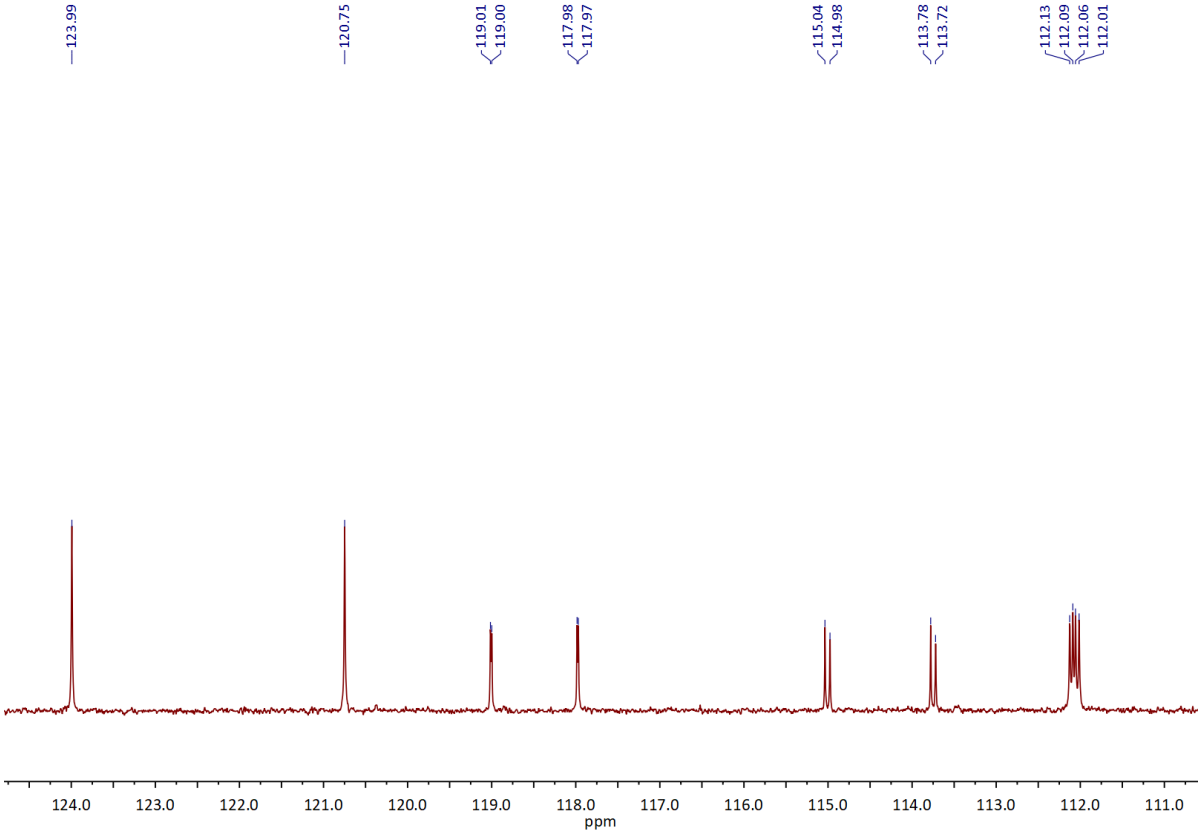

Figure A25. Section of the $^{13}C\{^{1}H\}$ NMR spectrum (δ = 124.8 – 110.6 ppm) of **[K(18-crown-6)][(PN)(PNcyclo)LaCl]** in C_6D_6 (303 K).

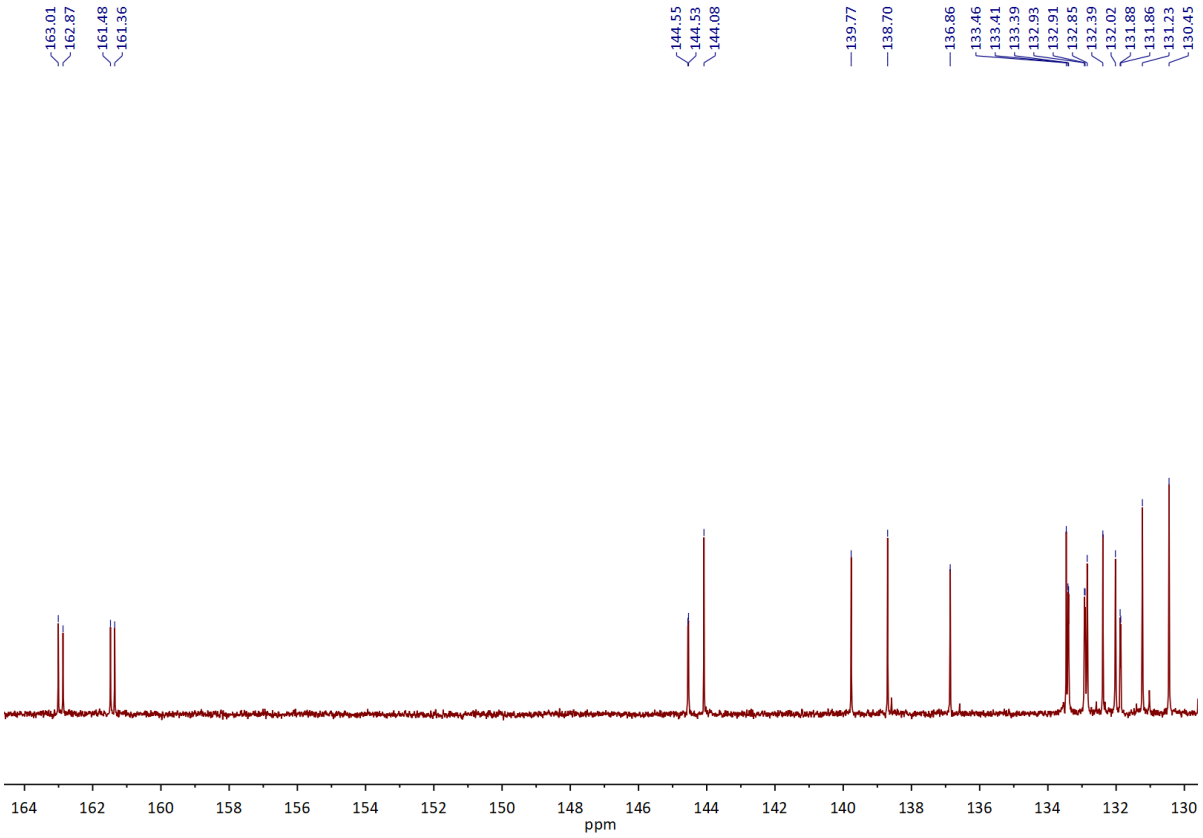

Figure A26. Section of the $^{13}C\{^{1}H\}$ NMR spectrum (δ = 164.6 – 129.6 ppm) of **[K(18-crown-6)][(PN)(PNcyclo)LaCl]** in C_6D_6 (303 K).

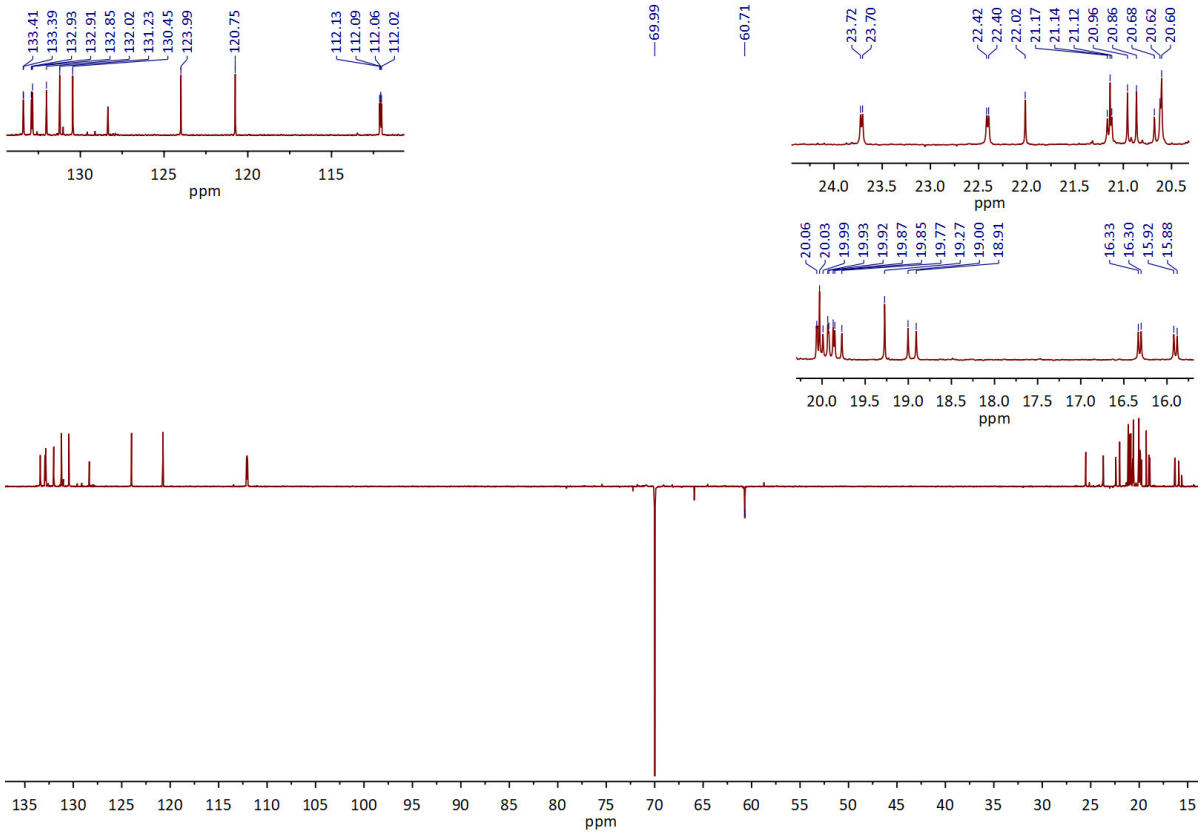

Figure A27. $^{13}C\{^{1}H\}$ DEPT135 NMR spectrum of **[K(18-crown-6)][(PN)(PNcyclo)LaCl]** in C_6D_6 (303 K). The three enlargements show the resonances in the aromatic (left) and aliphatic region (right).

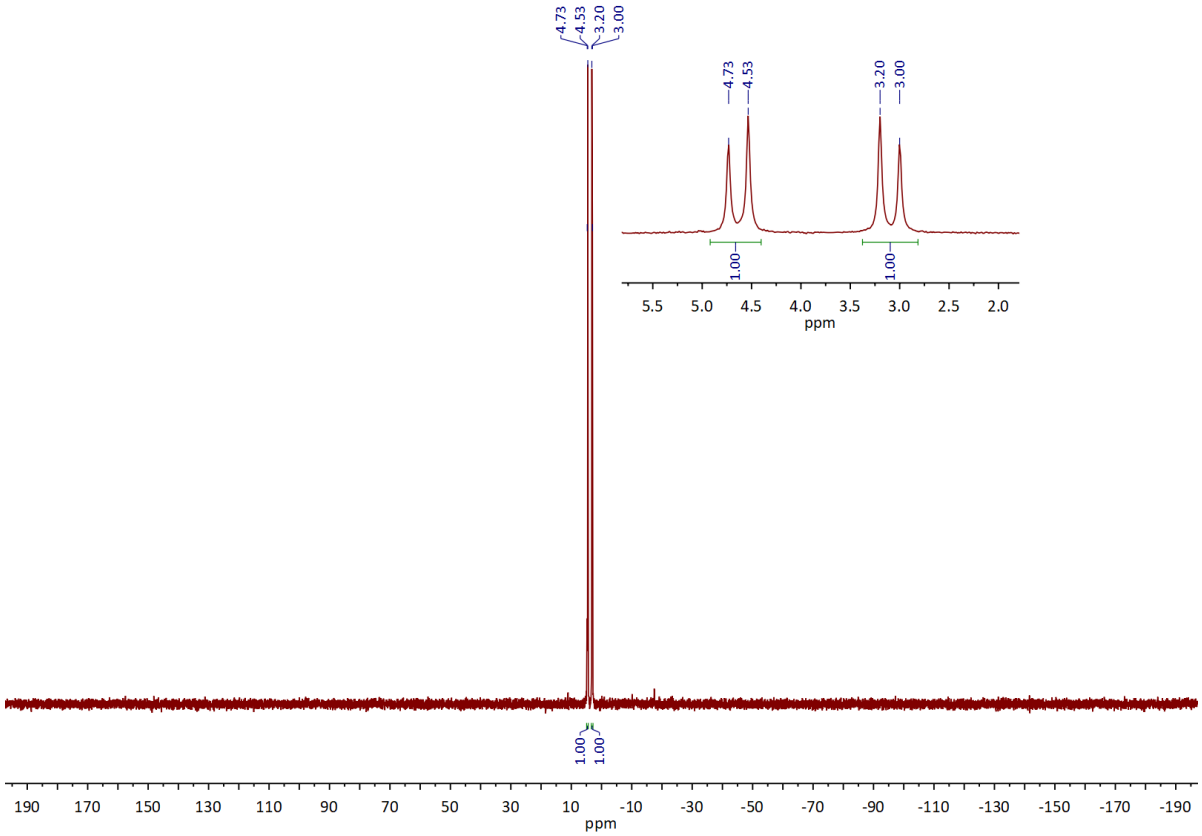

Figure A28. $^{31}P\{^{1}H\}$ NMR spectrum of **[K(18-crown-6)][(PN)(PNcyclo)LaCl]** in C_6D_6 (303 K). The enlargement shows the doublet splittings of the PN^{-} & PN_{cyclo}^{-} resonances.

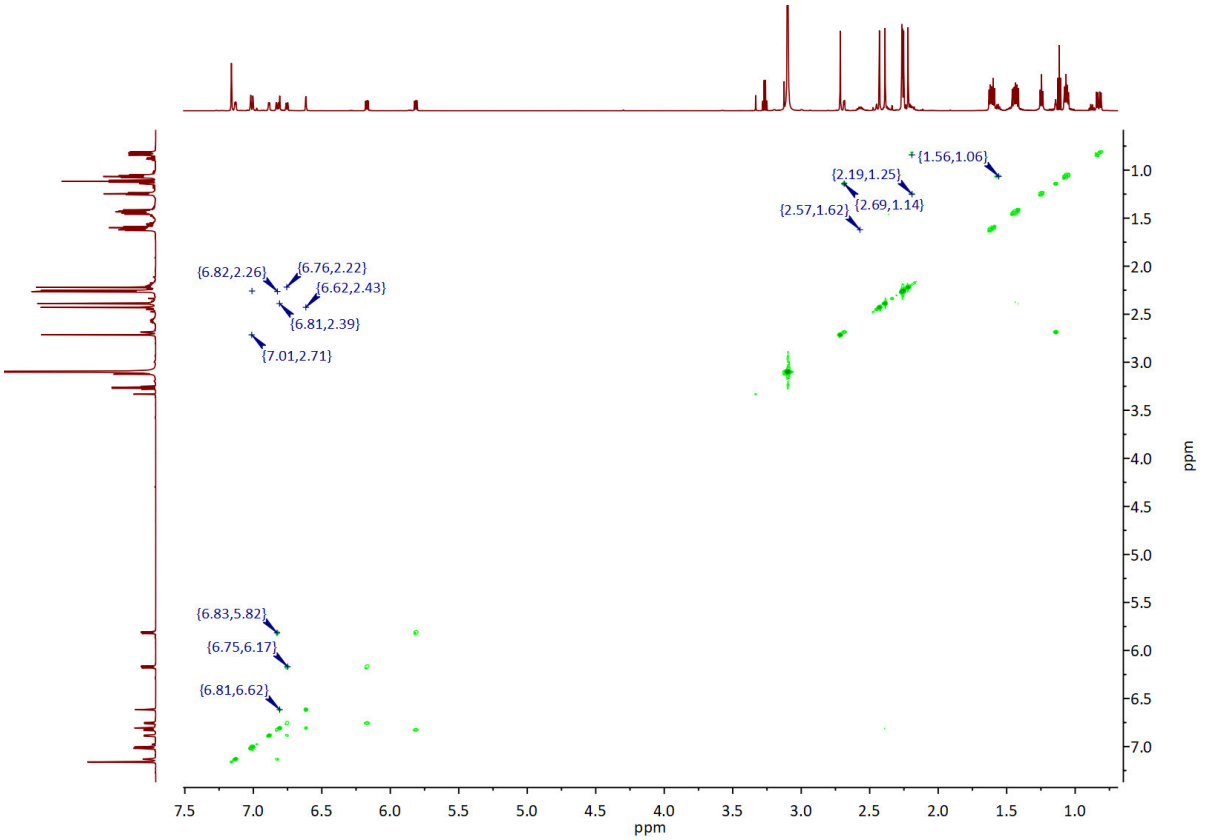

Figure A29. ^{1}H–^{1}H COSY NMR spectrum of **[K(18-crown-6)][(PN)(PNcyclo)LaCl]** in C_6D_6 (303 K).

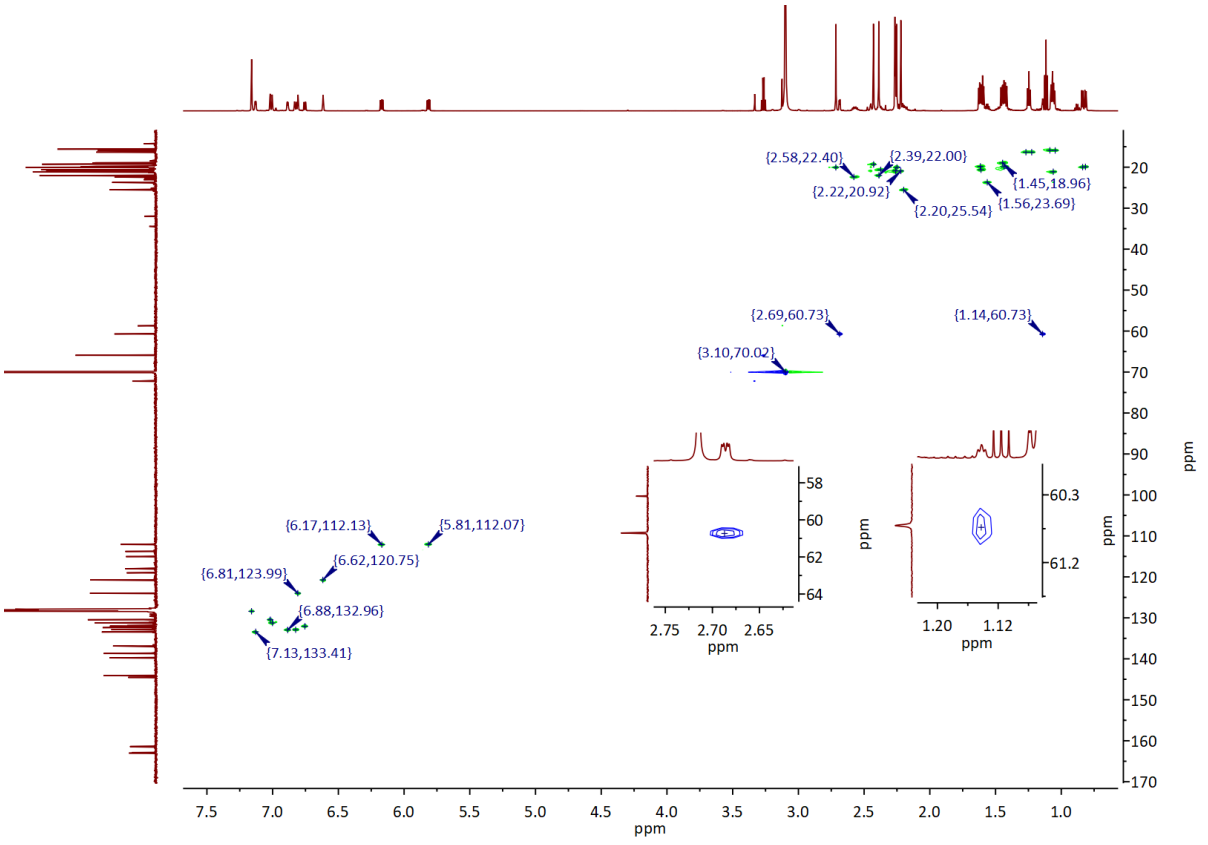

Figure A30. ^{1}H–^{13}C HSQC NMR spectrum of **[K(18-crown-6)][(PN)(PNcyclo)LaCl]** in C_6D_6 (303 K). The enlargements show the two cross peaks for the $CH_{2Mes(PNcyclo)}$ methylene protons.

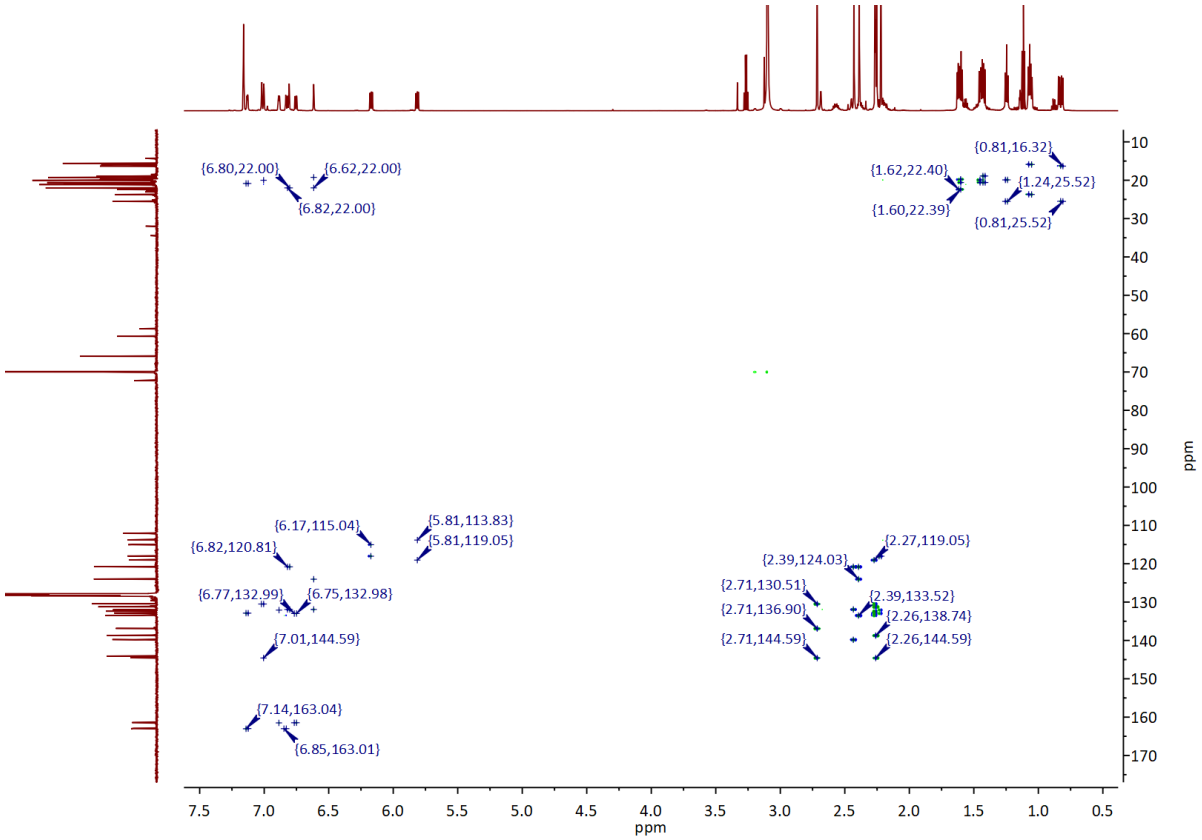

Figure A31. $^{1}H–^{13}C$ HMBC NMR spectrum of **[K(18-crown-6)][(PN)(PNcyclo)LaCl]** in C_6D_6 (303 K).

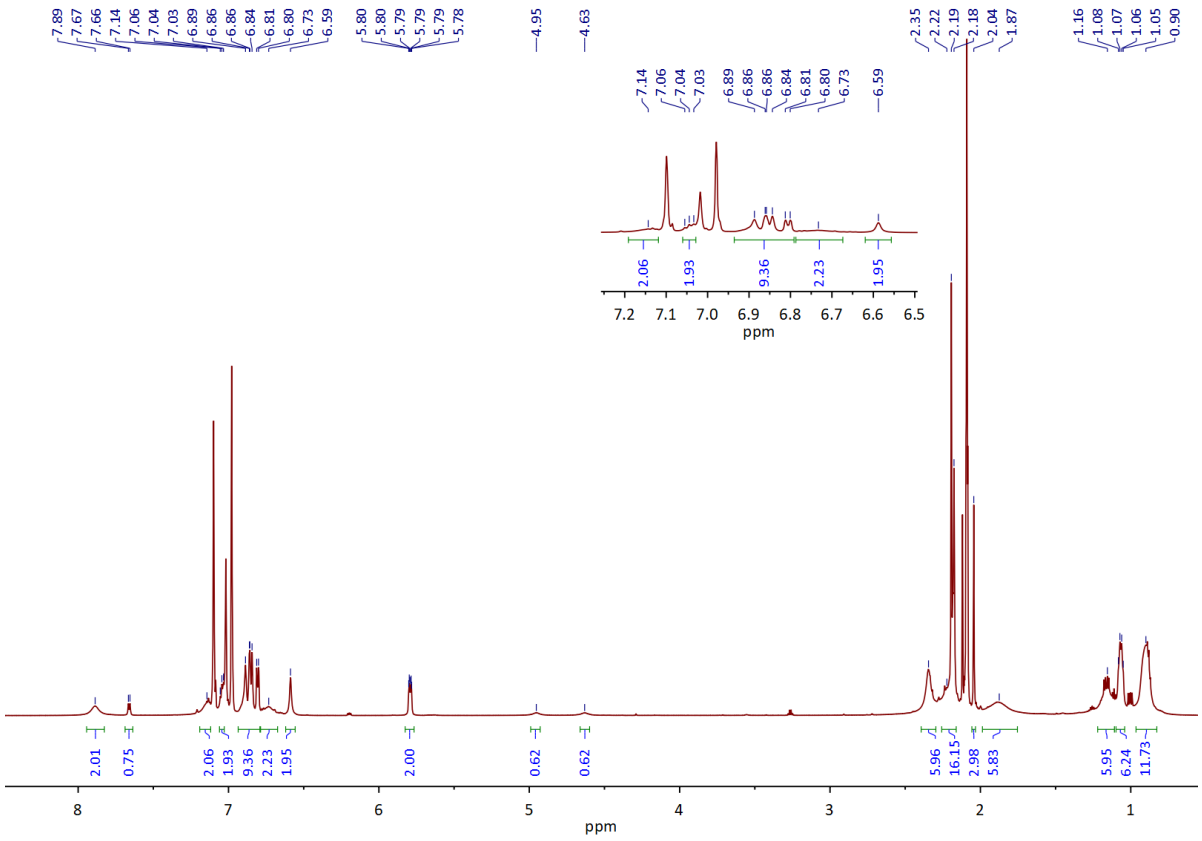

Figure A32. ^{1}H NMR spectrum of **$(PN)_2La\{OCPh_2(PHMes)\}$** in toluene-$d_8$ (303 K). The enlargement shows the crowded and broad resonances in the aromatic region.

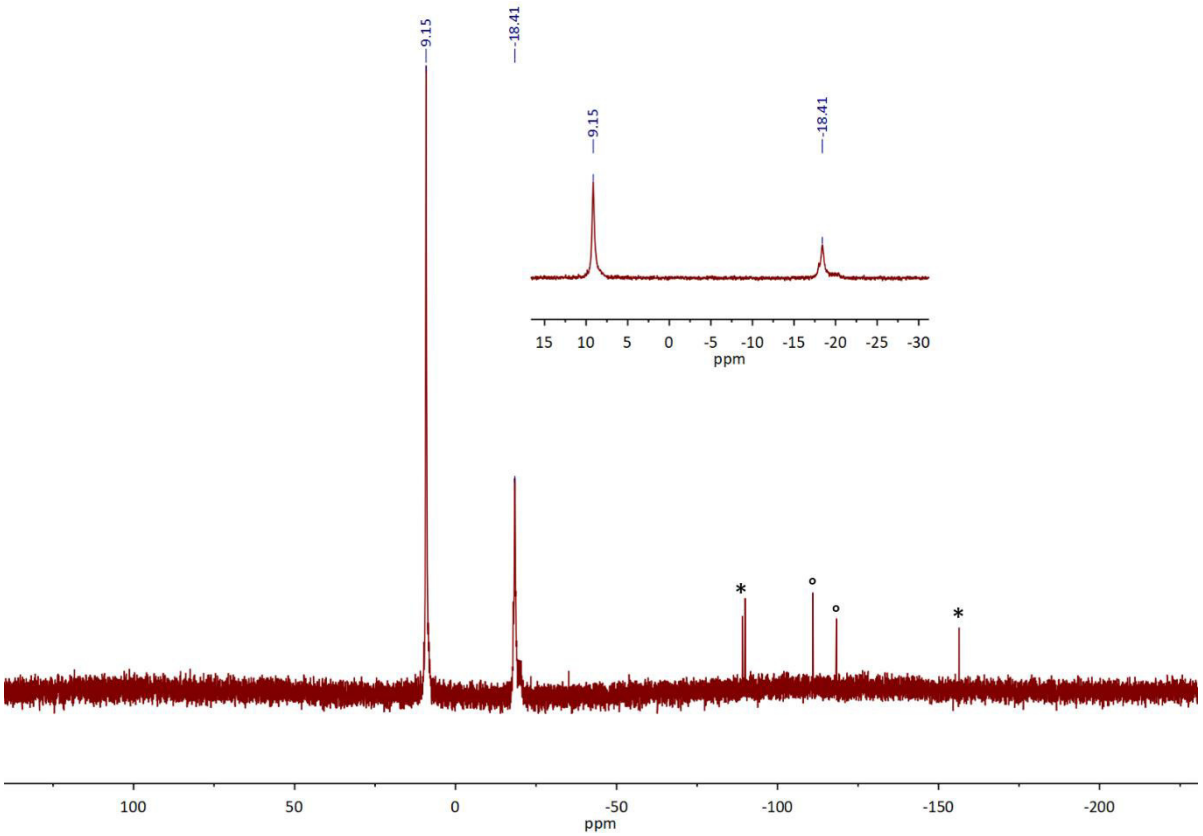

Figure A33. $^{31}P\{^{1}H\}$ NMR spectrum of **$(PN)_2La\{OCPh_2(PHMes)\}$** in toluene-$d_8$ (303 K). The enlargement reveals the broad shoulder on the right of the resonance at δ = –18.4 ppm. Traces of 1,2-dimesityldiphosphine are masked by °, traces of unknown impurities by *.

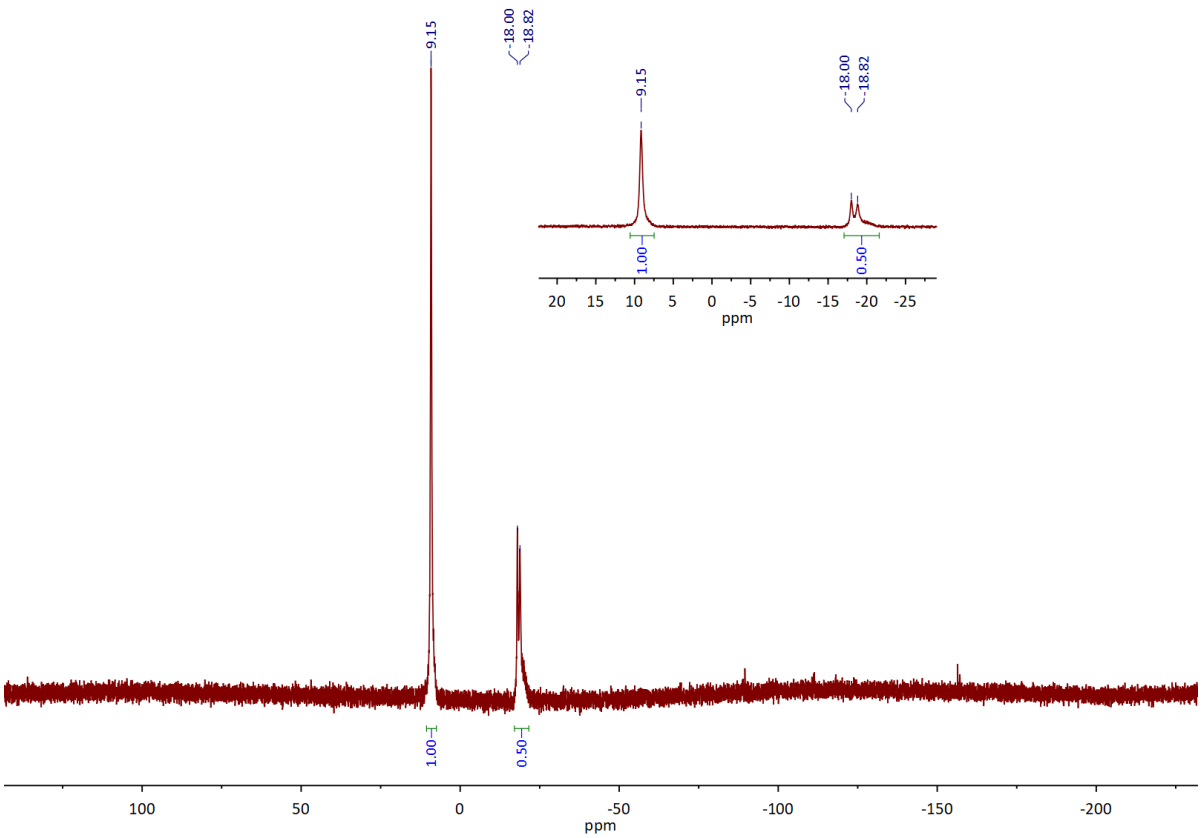

Figure A34. ^{31}P NMR spectrum of **$(PN)_2La\{OCPh_2(PHMes)\}$** in toluene-$d_8$ (303 K). Same enlargement as in Figure A33.

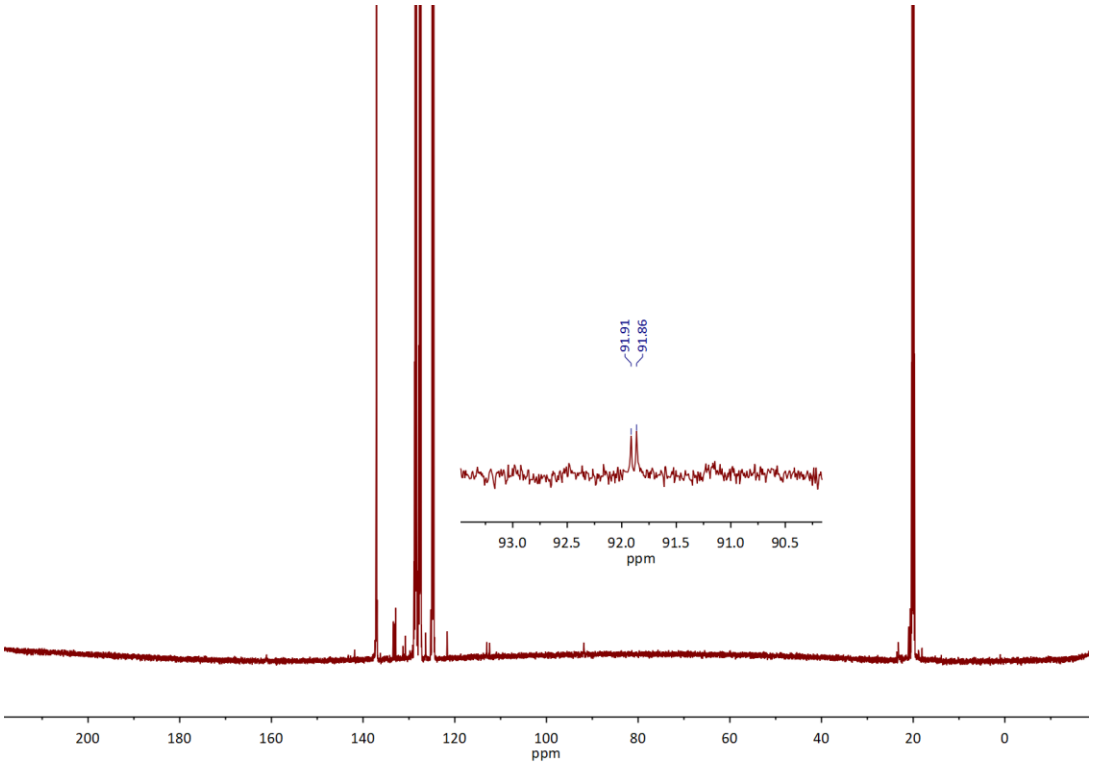

Figure A35. $^{13}C\{^{1}H\}$ NMR spectrum of **(PN)$_2$La{OCPh$_2$(PHMes)}** in toluene-d_8 (303 K). Note that, due to the low intensities, the spectrum cannot be used for an unambiguous, full assignment. However, the characteristic $^{-}OCPh_2$(PHMes) resonance can be identified (see enlargement).

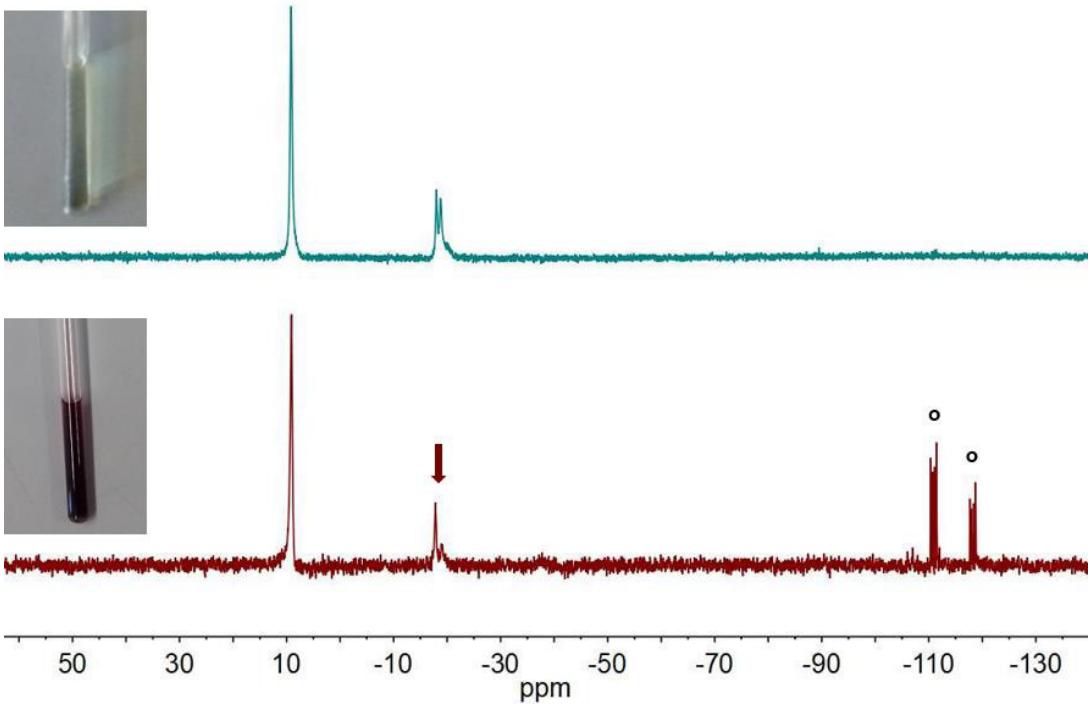

Figure A36. Stacked details of the $^{31}P\{^{1}H\}$ NMR spectra of **(PN)$_2$La{OCPh$_2$(PHMes)}** in C_6D_6 (303 K) before (top) and after irradiation with light (bottom). Irradiation at λ = 254 nm for 4 h and 4 W (standard bench UV lamp). The resonances of 1,2-dimesityldiphosphine are marked by °. The dark red arrow points to the starting material's resonance at δ = –18.4 ppm, which has decreased in intensity.

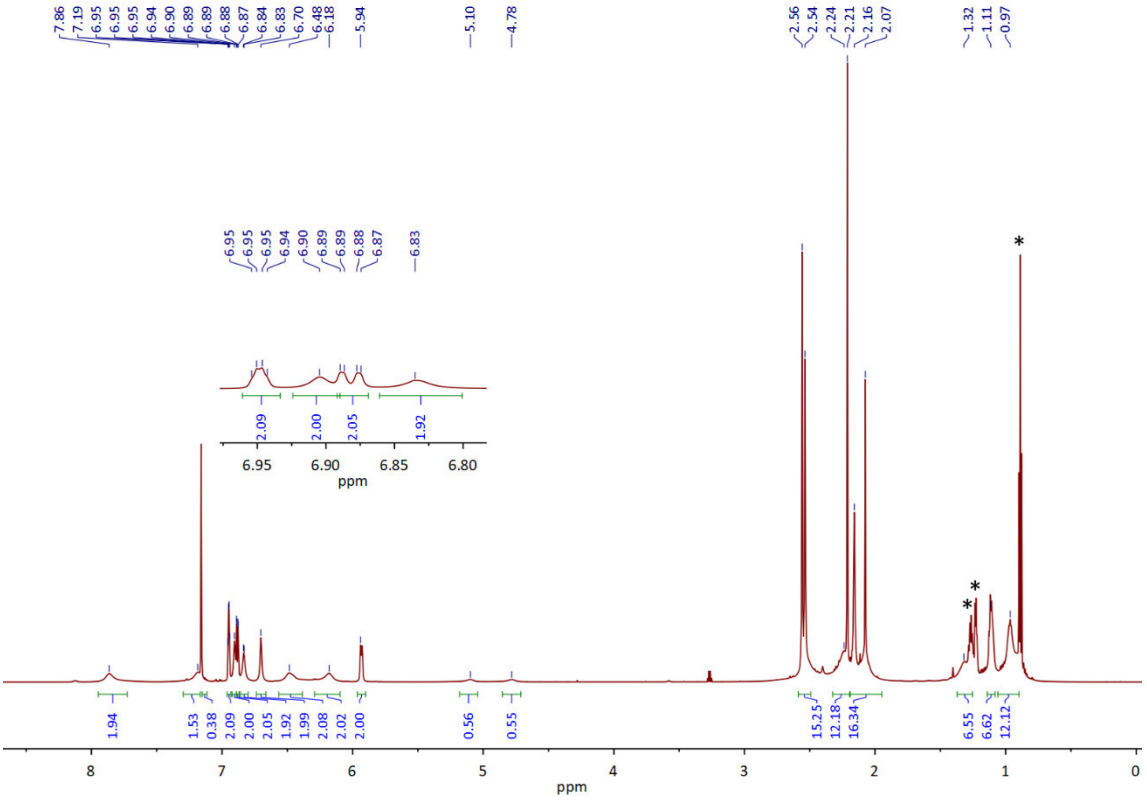

Figure A37. ^{1}H NMR spectrum of **(PN)$_2$La{OC(C$_6$H$_4$-4-NMe$_2$)$_2$(PHMes)}** in C_6D_6 (303 K). The enlargement shows the crowded and broad resonances in the aromatic region.

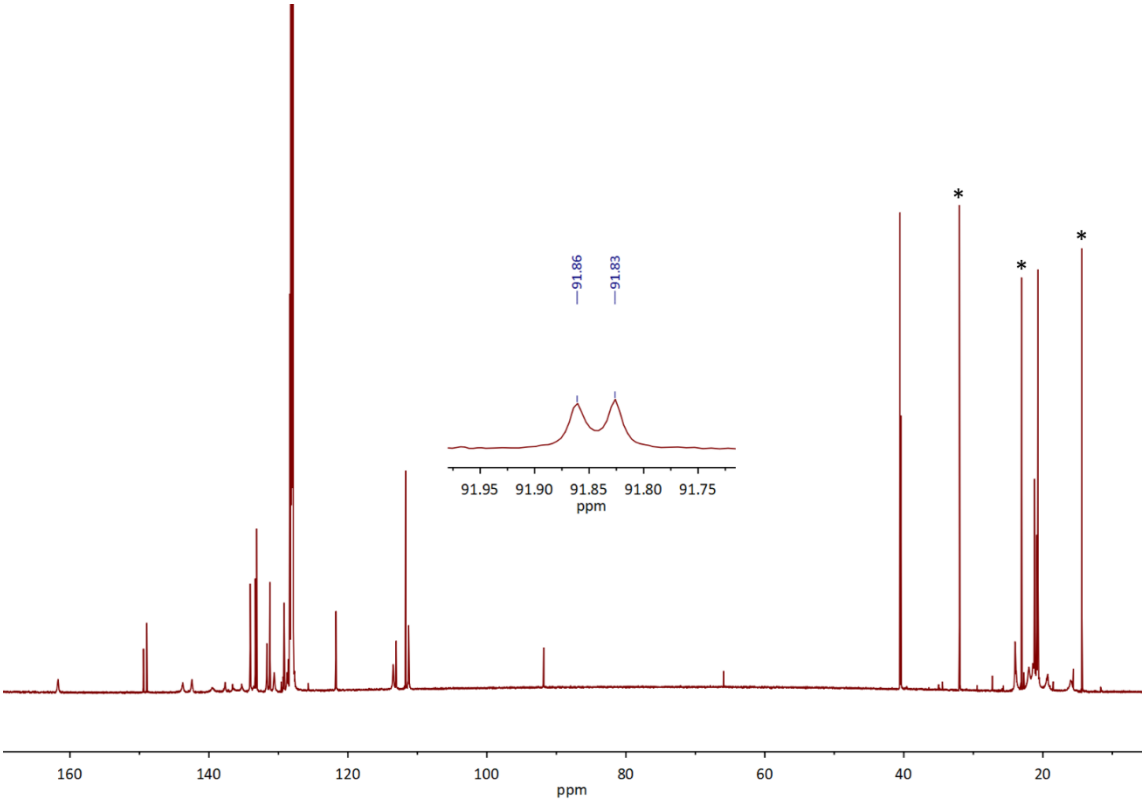

Figure A38. ^{13}C{^{1}H} NMR spectrum of **(PN)$_2$La{OC(C$_6$H$_4$-4-NMe$_2$)$_2$(PHMes)}** in C_6D_6 (303 K). The enlargement shows the characteristic $^{-}$O*C*R$_2$(PHMes) resonance. Residual *n*-hexane from work-up is marked by *. For a full peak listing see Figures A39–A41.

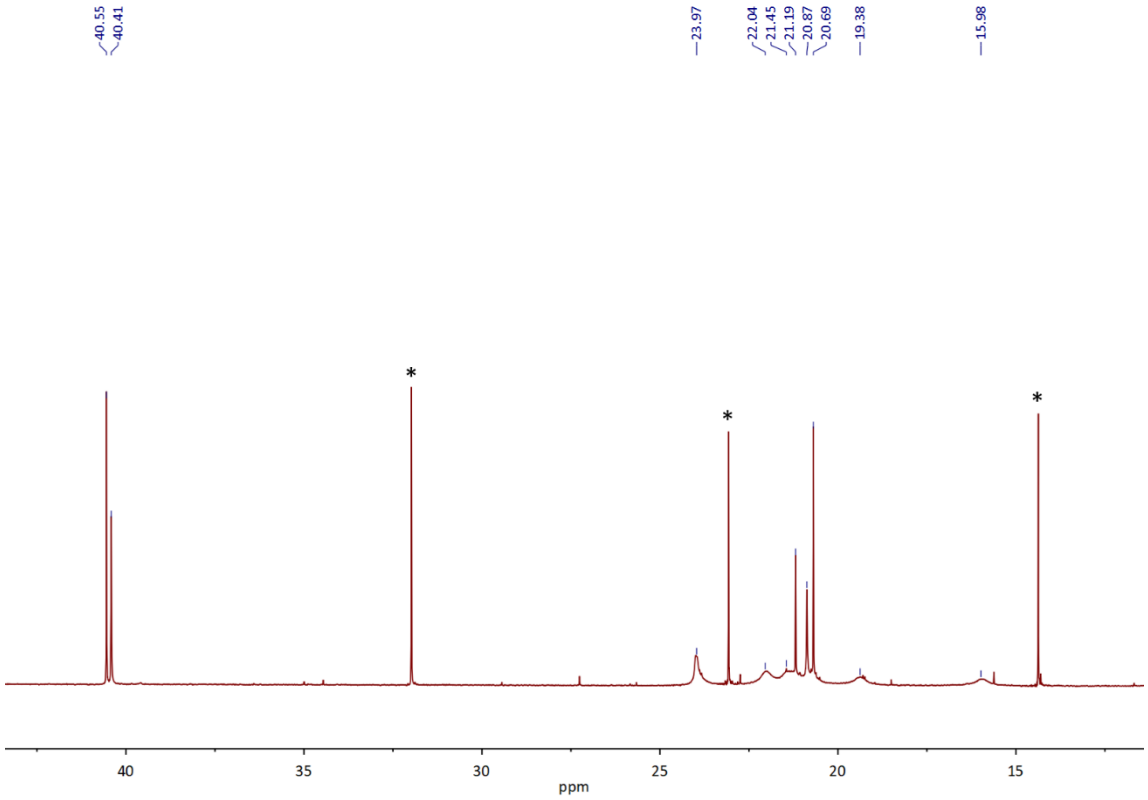

Figure A39. Section of the $^{13}C\{^{1}H\}$ NMR spectrum (δ = 43.4 – 11.4 ppm) of **(PN)$_2$La{OC(C$_6$H$_4$-4-NMe$_2$)$_2$(PHMes)}** in C_6D_6 (303 K). Residual *n*-hexane from work-up is marked by *.

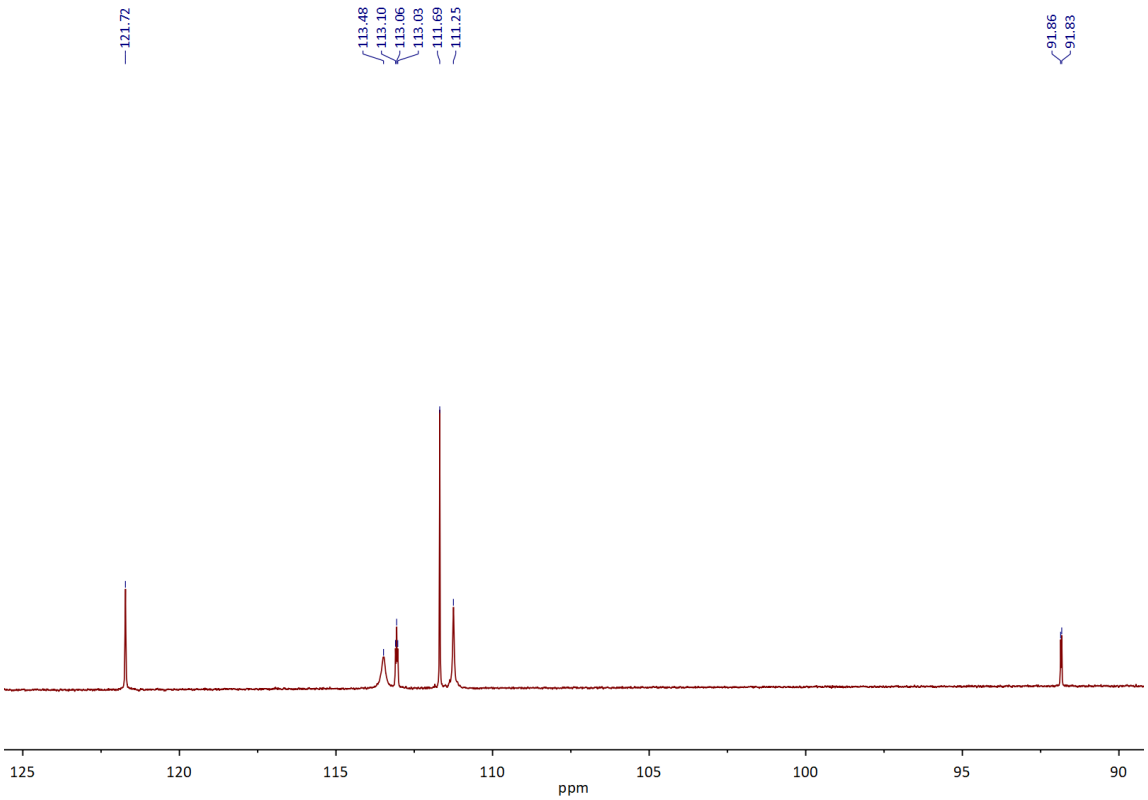

Figure A40. Section of the $^{13}C\{^{1}H\}$ NMR spectrum (δ = 125.6 – 89.2 ppm) of **(PN)$_2$La{OC(C$_6$H$_4$-4-NMe$_2$)$_2$(PHMes)}** in C_6D_6 (303 K).

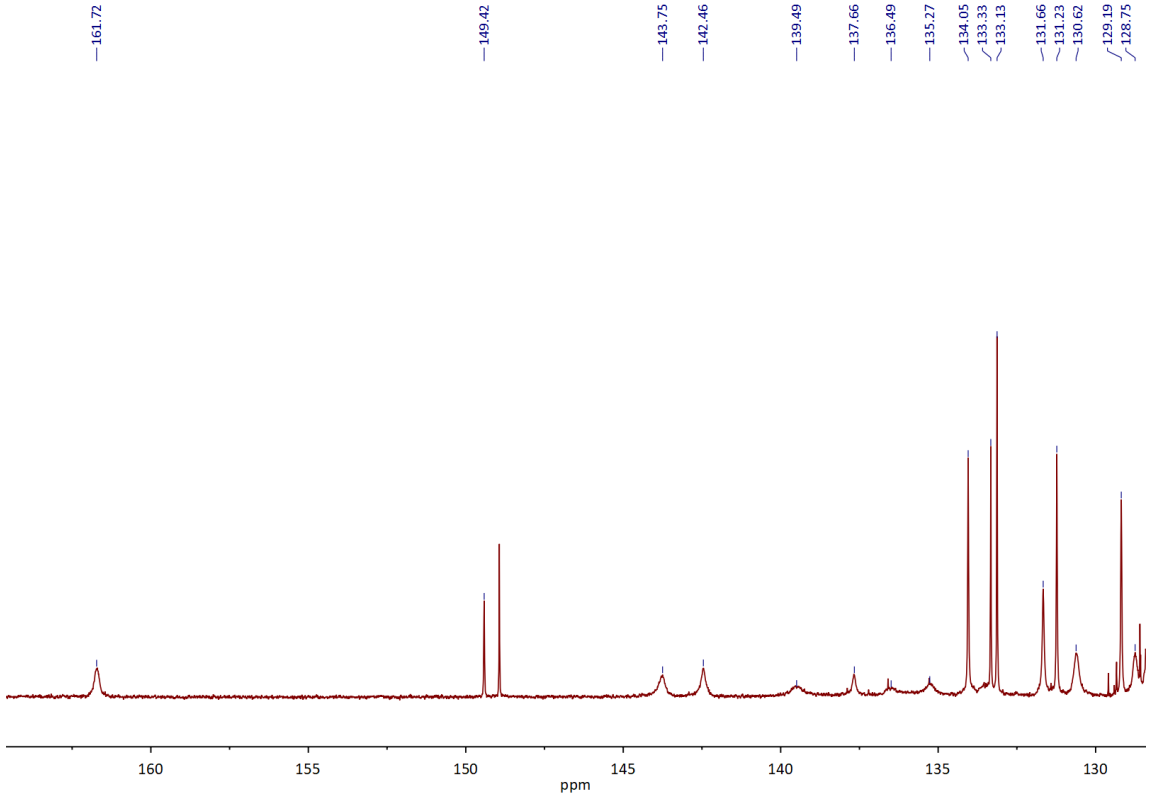

Figure A41. Section of the $^{13}C\{^{1}H\}$ NMR spectrum (δ = 164.6 – 128.4 ppm) of **(PN)$_2$La{OC(C$_6$H$_4$-4-NMe$_2$)$_2$(PHMes)}** in C_6D_6 (303 K).

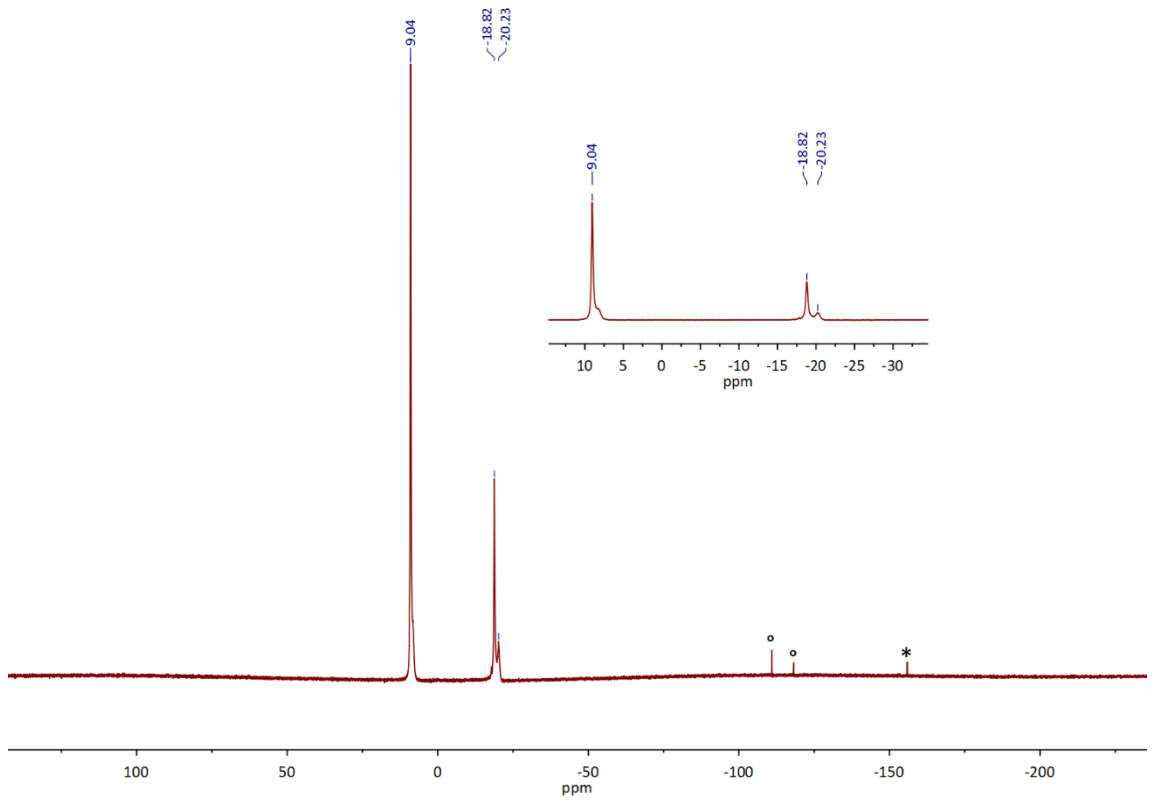

Figure A42. $^{31}P\{^{1}H\}$ NMR spectrum of **(PN)$_2$La{OC(C$_6$H$_4$-4-NMe$_2$)$_2$(PHMes)}** in C_6D_6 (303 K). The enlargement reveals the broads shoulder on the right of the resonance at δ = 9.0 ppm. Traces of 1,2-dimesityldiphosphine are masked by °, traces of unknown impurities by *.

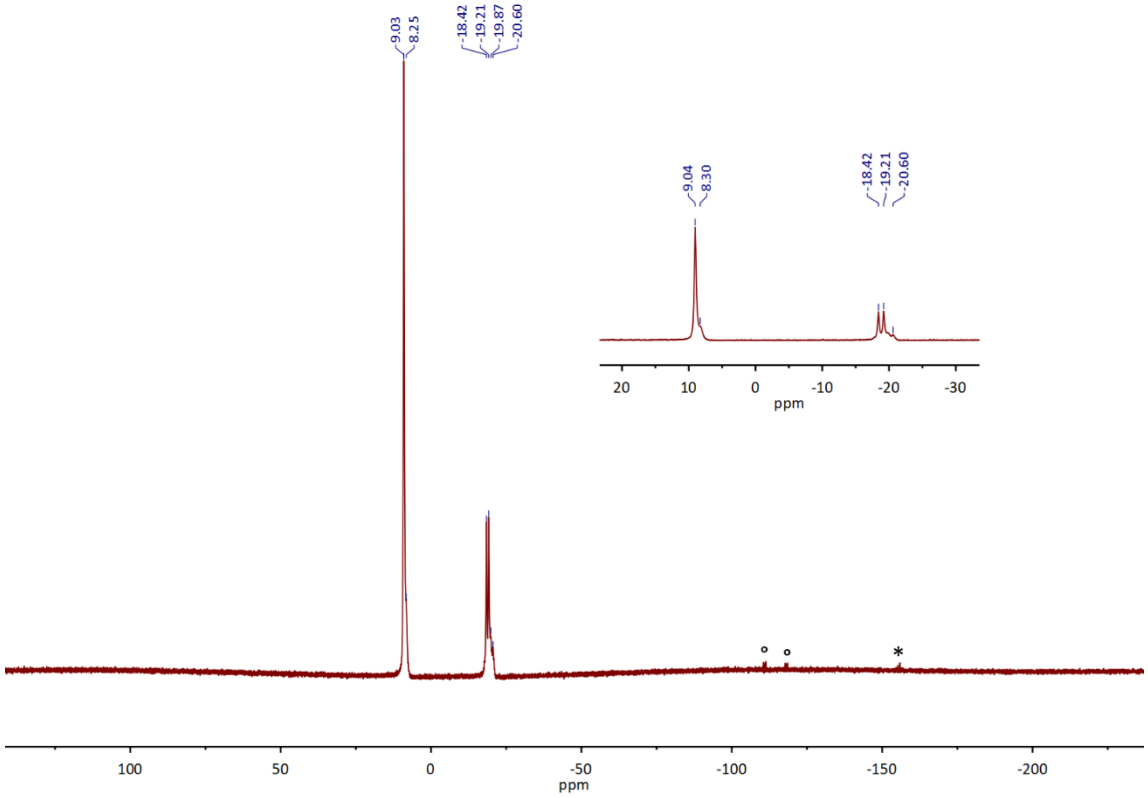

Figure A43. ^{31}P NMR spectrum of **(PN)$_2$La{OC(C$_6$H$_4$-4-NMe$_2$)$_2$(PHMes)}** in C$_6$D$_6$ (303 K). Same enlargement as in Figure A42. Traces of 1,2-dimesityldiphosphine are masked by °, traces of unknown impurities by *.

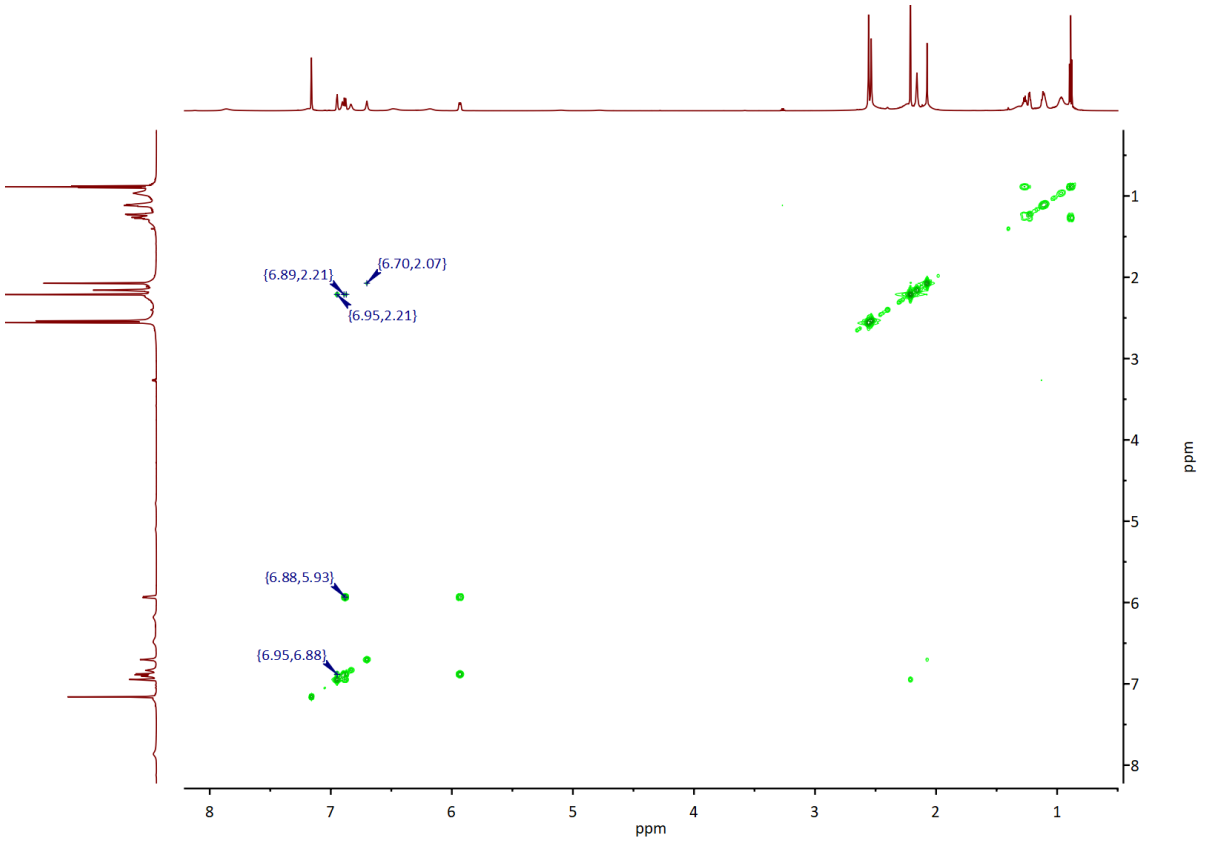

Figure A44. ^{1}H–^{1}H COSY NMR spectrum of **(PN)$_2$La{OC(C$_6$H$_4$-4-NMe$_2$)$_2$(PHMes)}** in C$_6$D$_6$ (303 K).

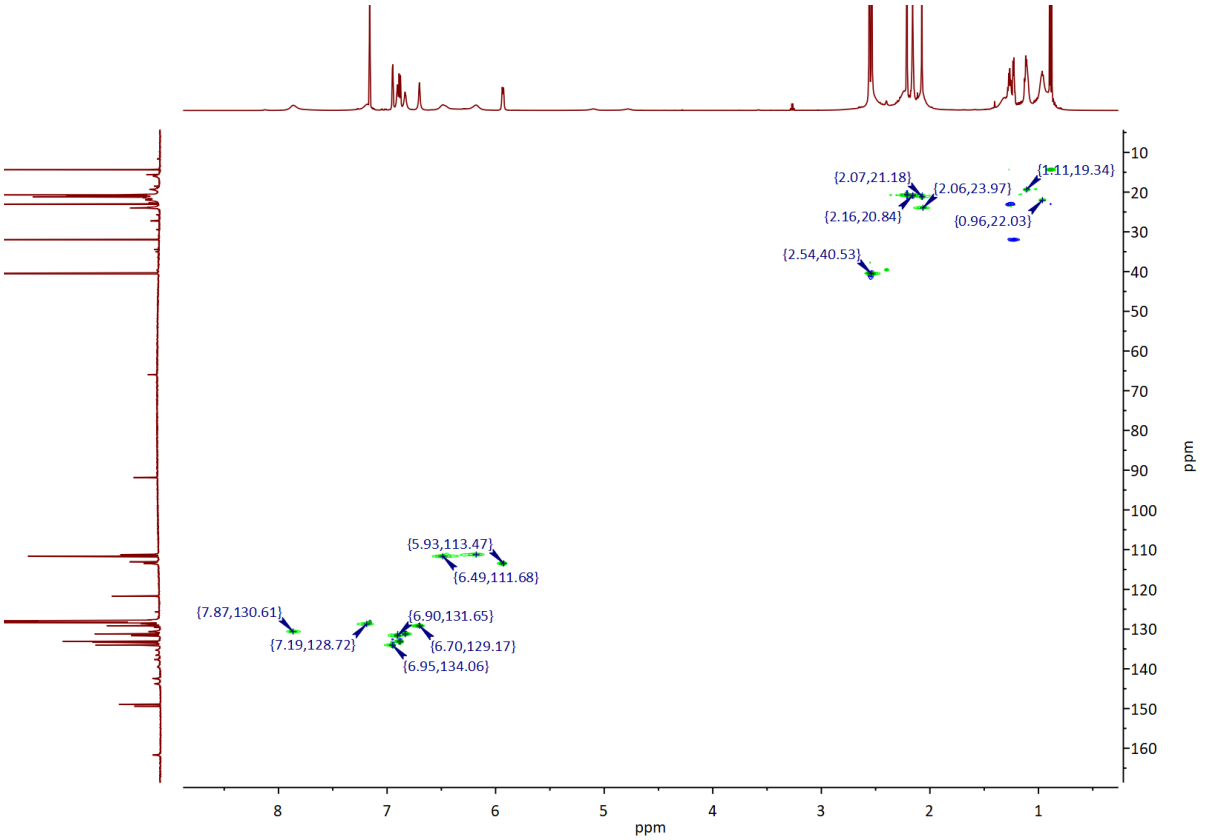

Figure A45. ^{1}H–^{13}C HSQC NMR spectrum of **(PN)$_2$La{OC(C$_6$H$_4$-4-NMe$_2$)$_2$(PHMes)}** in C_6D_6 (303 K).

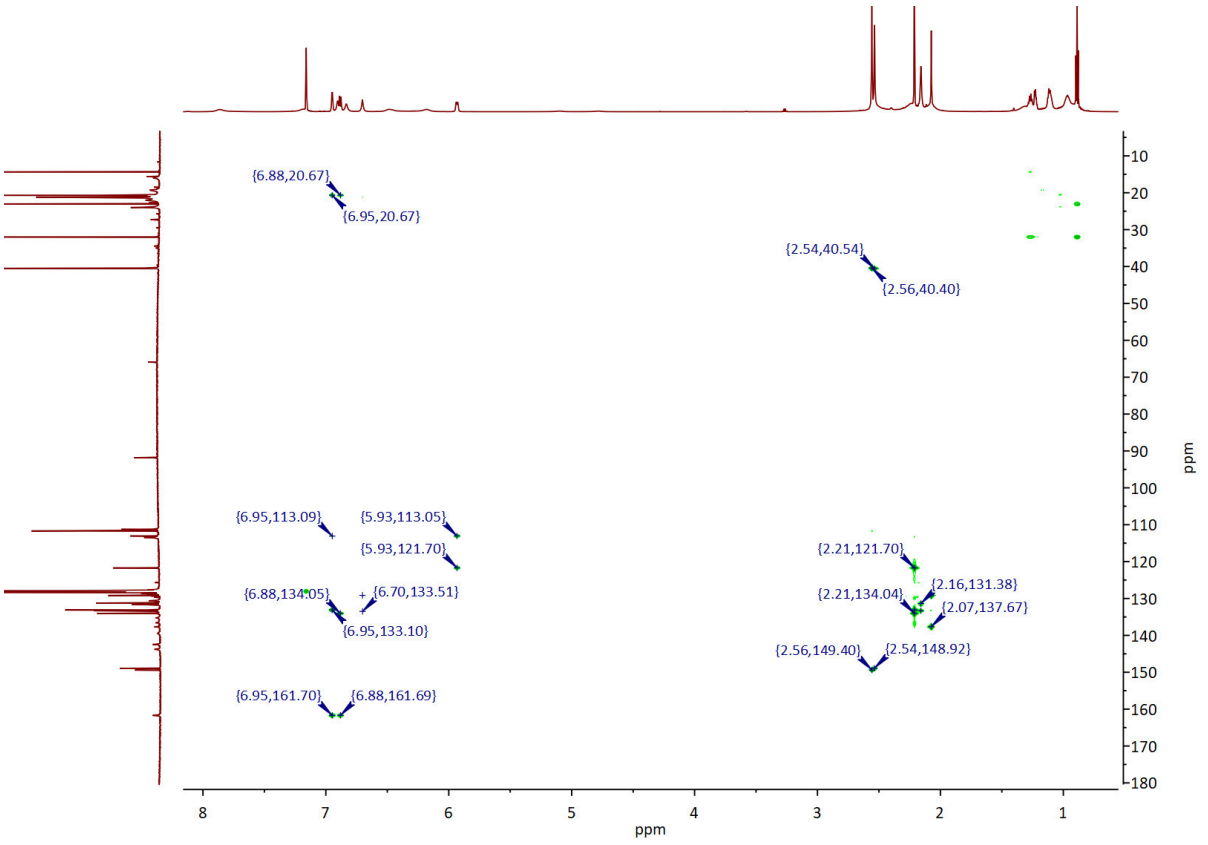

Figure A46. ^{1}H–^{13}C HMBC NMR spectrum of **(PN)$_2$La{OC(C$_6$H$_4$-4-NMe$_2$)$_2$(PHMes)}** in C_6D_6 (303 K).

A.3 IR Spectra

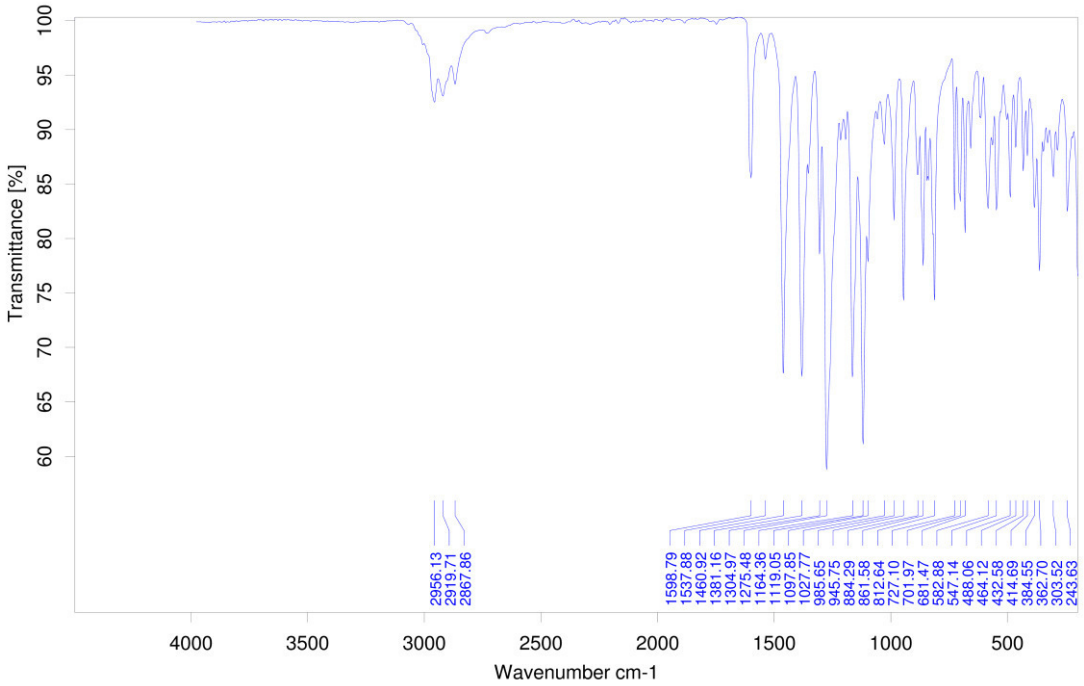

Figure A47. IR spectrum (ATR) of **$(PN)_2La\{NH(C_6H_3\text{-}3,5\text{-}(CF_3)_2)\}$**.

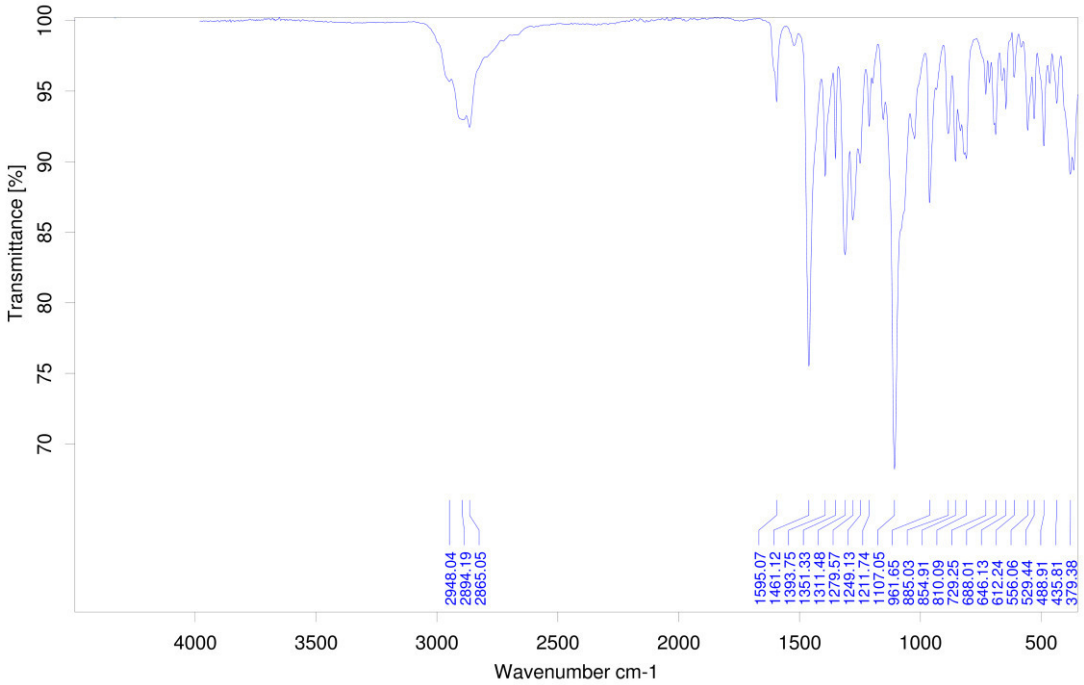

Figure A48. IR spectrum (ATR) of **[K(18-crown-6)][(PN)(PNcyclo)LaCl]**.

A.4 UV-Vis and Fluorescence Spectra

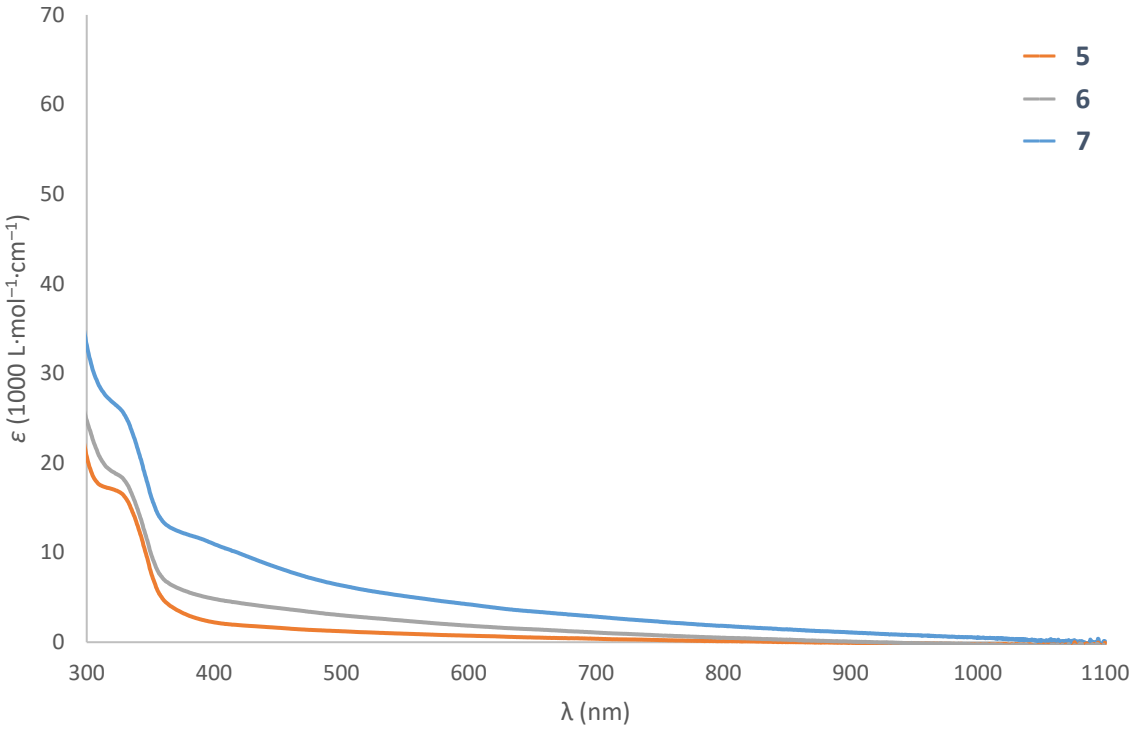

Figure A49. Stacked UV-Vis spectra of **5** (orange), **6** (grey) and **7** (blue) in THF at room temperature. See Results and Discussion of Chapter 2 for the structures of the assigned compounds.

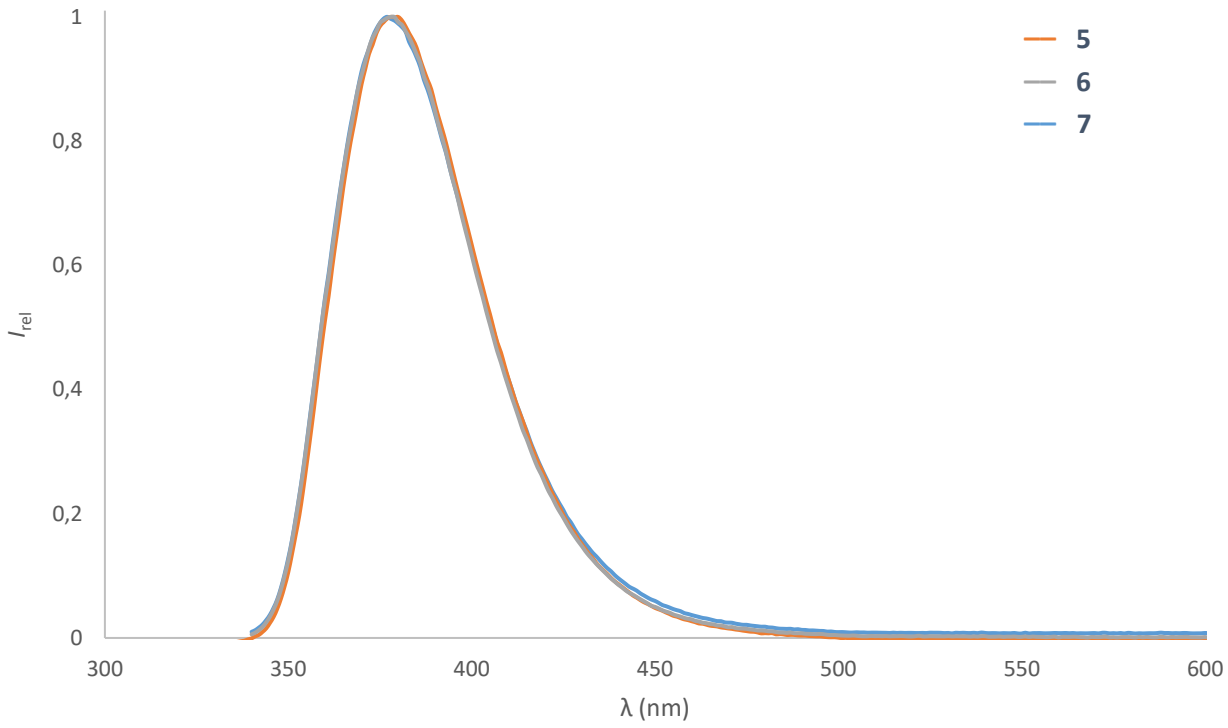

Figure A50. Stacked fluorescence spectra of **5** (orange, λ_{ex} = 318 nm), **6** (grey, λ_{ex} = 326 nm) and **7** (blue, λ_{ex} = 327 nm) in THF at room temperature. See Results and Discussion of Chapter 2 for the structures of the assigned compounds.

A.5 Crystallographic Details

Table A1. Crystallographic details on additional complexes obtained during this doctoral research study.

	$(PN)_2La\{NH(C_6H_3$-3,5-$(CF_3)_2)\}$	**$(PN)_2La(PHPh)$**	**[K(18-crown-6)] $[(PN)(PN_{cyclo})LaCl]$**	**$(PN)_2La\{OCPh_2$ (PHMes)}**	**$(PN)_2La\{OC(C_6H_4$-4-$NMe_2)_2$(PHMes)}**
Chemical Formula	$C_{52}H_{66}F_6LaN_3P_2$	$C_{50}H_{68}LaN_2P_3 \cdot C_6H_{14}$	$(C_{56}H_{85}ClKLaN_2O_6P_2)_2 \cdot C_7H_8$	$C_{66}H_{84}LaN_2OP_3 \cdot C_7H_8 \cdot C_5H_{12}$	$C_{70}H_{94}LaN_4OP_3 \cdot C_6H_{14}$
M_r	1047.92	1015.05	2407.44	1317.45	1325.48
Crystal System	Triclinic	Monoclinic	Triclinic	Monoclinic	Triclinic
Space Group	*P*–1	$P2_1/c$	*P*–1	$P2_1/c$	*P*–1
a (Å)	11.619(2)	17.744(2)	12.2789(8)	15.94(1)	13.184(1)
b (Å)	14.058(3)	11.872(1)	22.537(2)	13.42(1)	13.751(1)
c (Å)	16.233(4)	25.871(3)	23.301(2)	34.24(3)	21.523(2)
α (°)	84.75(1)	90	85.693(2)	90	100.872(2)
β (°)	79.28(1)	100.603(2)	82.784(2)	98.81(1)	105.488(2)
γ (°)	79.877(9)	90	74.761(2)	90	102.163(2)
V ($Å^3$)	2560.0(9)	5356.9(9)	6166.2(7)	7240(10)	3549.3(5)
Z	2	4	2	4	2
Density (g cm^{-3})	1.359	1.259	1.297	1.209	1.240
F(000)	1080	2136	2524	2784	1404
Radiation Type	MoKα	MoKα	MoKα	MoKα	MoKα
μ (mm^{-1})	0.955	0.923	0.903	0.700	0.715
Crystal Size	0.42x0.38x0.35	0.45x0.38x0.01	0.10x0.09x0.08	0.10x0.09x0.02	0.26x0.24x0.21
Meas. Refl.	192700	51208	285148	44792	41202
Indep. Refl.	11697	11410	22657	13087	13544
Obsvd. [$I > 2\sigma(I)$]	10562	8701	18688	7428	11072
R_{int}	0.744	0.0701	0.0718	0.1799	0.0571
R_1 [$F^2 > 2\sigma(F^2)$]	0.0287	0.0414	0.0558	0.0844	0.0384
$wR_2(F^2)$	0.0779	0.1327	0.1359	0.2044	0.0941
S	1.210	0.887	1.028	1.018	1.023
$\Delta\rho_{max}$	0.495	1.891	2.877	0.810	1.013
$\Delta\rho_{min}$	–0.494	–0.835	–1.674	–1.793	–0.531

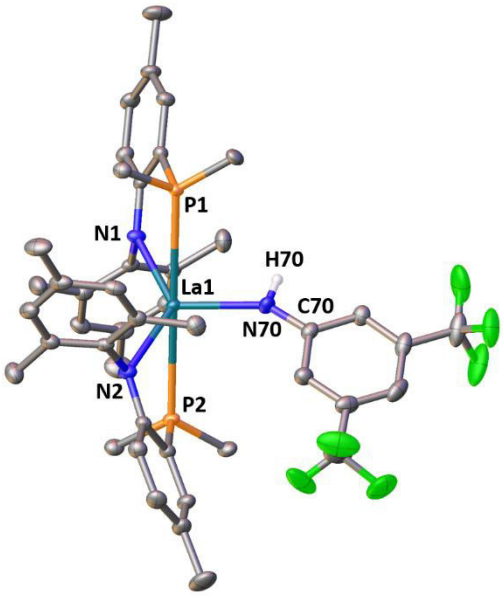

Figure A51. Thermal ellipsoid plot of **(PN)$_2$La{NH(C$_6$H$_3$-3,5-(CF$_3$)$_2$)}**. Thermal ellipsoids are shown at a probability of 50%. Hydrogen atoms (except for H70) have been omitted and ^{i}Pr groups truncated for clarity. Selected bond lengths (Å) and angles (°): La1–P1/P2 3.2158(8)/3.1797(8), La1–N1/N2 2.385(2)/2.402(2), La1–N70 2.391(2), N70–H70 0.84(3), N70–C70 1.347(3); P1–La1–P2 178.85(1), N1–La1–N2 127.31(6), N1/N2–La1–N70 114.32(7)/118.34(7), P1/P2–La1–N70 87.86(5)/92.02(5), La1–N70–C70 144.2(2).

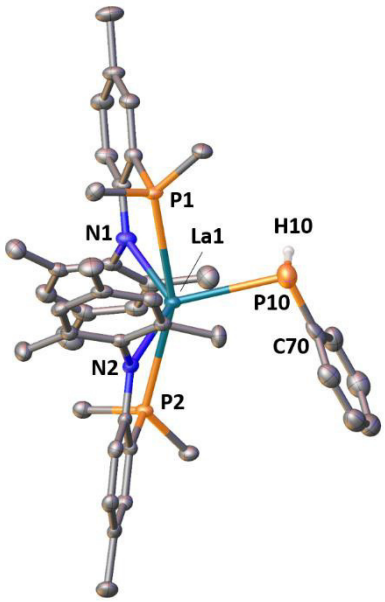

Figure A52. Thermal ellipsoid plot of **(PN)$_2$La(PHPh)**. Thermal ellipsoids are shown at a probability of 50%. Hydrogen atoms (except for H10) have been omitted and ^{i}Pr groups truncated for clarity. Selected bond lengths (Å) and angles (°): La1–P1/P2 3.126(1)/3.1400(9), La1–N1/N2 2.414(3)/2.392(3), La1–P10 3.009(1), P10–H10 1.32(2), P10–C70 1.763(5); P1–La1–P2 157.86(3), N1–La1–N2 124.2(1), N1/N2–La1–P10 112.23(8)/121.67(7), P1/P2–La1–P10 85.14(3)/117.01(3), La1–P10–C70 101.3(1).

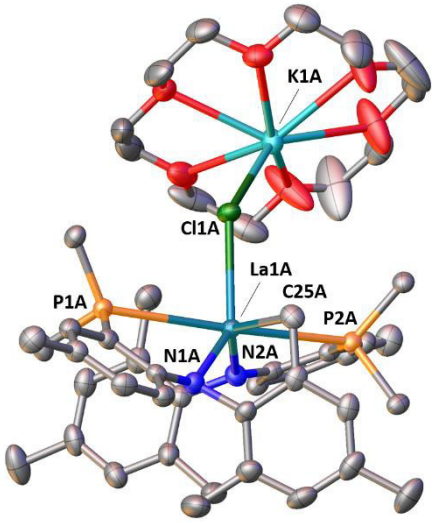

Figure A53. Thermal ellipsoid plot of **[K(18-crown-6)][(PN)(PN$_{cyclo}$)LaCl]**. Only one of the crystallographically independent molecules in the unit cell is shown. Thermal ellipsoids are shown at a probability of 50%. Hydrogen atoms have been omitted and ^{i}Pr groups truncated for clarity. Selected bond lengths (Å) and angles (°): La1A–P1A/P2A 3.207(1)/3.166(1), La1A–N1A/N2A 2.404(4)/2.469(4), La1A–C25A 2.644(6), La1A–Cl1A 2.816(1), Cl1A–K1A 3.246(2); P1A–La1A–P2A 172.16(3), N1A–La1A–N2A 117.66(1), N1A/N2A–La1A–C25A 67.9(1)/139.6(1), P1A/P2A–La1A–C25A 104.6(1)/82.3(1), N1A/N2A–La1A–Cl1A 134.1(1)/102.5(1), P1A/P2A–La1A–Cl1A 85.08(3)/90.39(3), C25A–La1–Cl1A 96.0(1), La1A–Cl1A–K1A 133.58(4).

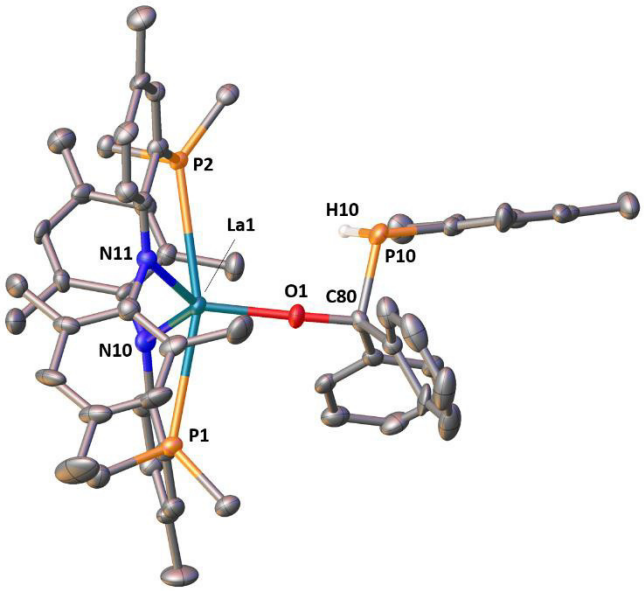

Figure A54. Thermal ellipsoid plot of **(PN)$_2$La{OCPh$_2$(PHMes)}**. Thermal ellipsoids are shown at a probability of 50%. Hydrogen atoms (except for H10) have been omitted and ^{i}Pr groups truncated for clarity. Selected bond lengths (Å) and angles (°): La1–P1/P2 3.133(3)/3.206(2), La1–N10/N11 2.463(6)/2.419(6), La1–O1 2.187(5), O1–C80 1.419(8), C80–P10 1.966(8), P10–H10 1.21(8); P1–La1–P2 161.63(5), N10–La1–N11 124.1(2), N10/N11–La1–O1 110.5(2)/125.3(2), P1/P2–La1–O1 94.4(1)/103.4(1), La1–O1–C80 174.7(5), O1–C80–P10 98.7(4).

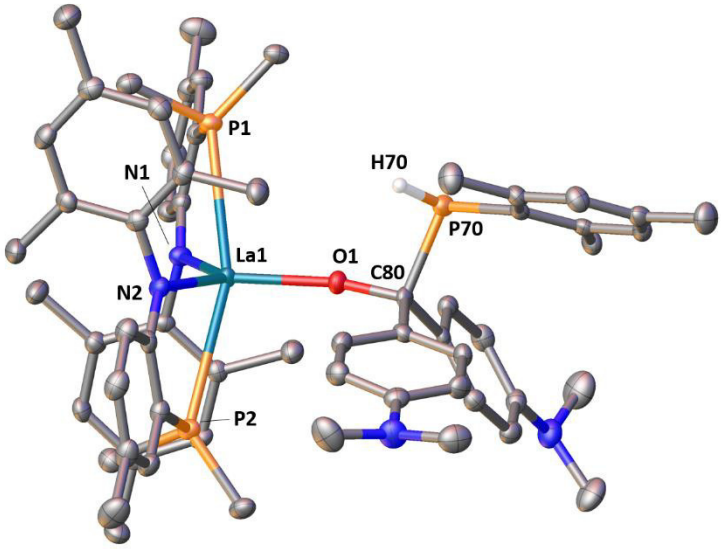

Figure A55. Thermal ellipsoid plot of **$(PN)_2La\{OC(C_6H_4\text{-}4\text{-}NMe_2)_2(PHMes)\}$**. Thermal ellipsoids are shown at a probability of 50%. Hydrogen atoms (except for H70) have been omitted and ^{i}Pr groups truncated for clarity. Selected bond lengths (Å) and angles (°): La1–P1/P2 3.1413(8)/3.1509(8), La1–N1/N2 2.447(2)/2.452(2), La1–O1 2.171(2), O1–C80 1.410(3), C80–P70 1.931(3), P70–H70 1.25(3); P1–La1–P2 160.50(2), N1–La1–N2 125.78(8), N1/N2–La1–O1 121.90(8)/112.19(8), P1/P2–La1–O1 101.08(6)/98.29(6), La1–O1–C80 166.9(2), O1–C80–P70 101.0(2).

A.6 References

(1) Watt, F. A.; Krishna, A.; Golovanov, G.; Ott, H.; Schoch, R.; Wölper, C.; Neuba, A. G.; Hohloch, S. Monoanionic Anilidophosphine Ligand in Lanthanide Chemistry: Scope, Reactivity, and Electrochemistry. *Inorg. Chem.* **2020**, *59*, 2719–2732.
(2) Garner, M. E.; Arnold, J. Reductive Elimination of Diphosphine from a Thorium–NHC–Bis(phosphido) Complex. *Organometallics* **2017**, *36*, 4511–4514.
(3) Kundu, S.; Sinhababu, S.; Siddiqui, M. M.; Luebben, A. V.; Dittrich, B.; Yang, T.; Frenking, G.; Roesky, H. W. Comparison of Two Phosphinidenes Binding to Silicon(IV)dichloride as well as to Silylene. *J. Am. Chem. Soc.* **2018**, *140*, 9409–9412.
(4) Bell, N. L.; Maron, L.; Arnold, P. L. Thorium Mono- and Bis(imido) Complexes Made by Reprotonation of *cyclo*-Metalated Amides. *J. Am. Chem. Soc.* **2015**, *137*, 10492–10495.
(5) Sheldrick, G. M. Crystal structure refinement with *SHELXL*. *Acta Cryst. C, Struct. Chem.* **2015**, *71*, 3–8.
(6) Dolomanov, O. V.; Bourhis, L. J.; Gildea, R. J.; Howard, J. A. K.; Puschmann, H. *OLEX2*: a complete structure solution, refinement and analysis program. *J. Appl. Crystallogr.* **2009**, *42*, 339–341.